University of Nevada, Reno

Influence of Mixture Characteristics on the Oxidative Aging of Asphalt Binders

A dissertation submitted in partial fulfillment of the requirements for the degree of Doctor of Philosophy in Civil Engineering

by

Nathaniel E. Morian

Dr. Peter E. Sebaaly, P.E.
Dissertation Advisor

May, 2014

ProQuest LLC.
789 East Eisenhower Parkway
P.O. Box 1346
Ann Arbor, MI 48106 - 1346

Influence of Mixture Characteristics on the Oxidative Aging of Asphalt Binders

University of Nevada, Reno
Statewide • Worldwide

THE GRADUATE SCHOOL

We recommend that the dissertation
prepared under our supervision by

NATHANIEL E. MORIAN

entitled

Influence of Mixture Characteristics on the Oxidative Aging of Asphalt Binders

be accepted in partial fulfillment of the
requirements for the degree of

DOCTOR OF PHILOSOPHY

Dr. Peter E. Sebaaly, Advisor

Dr. Elie Y. Hajj, Committee Member

Dr. Raj. V. Siddharthan, Committee Member

Dr. Gary M. Norris, Committee Member

Dr. Tomasz J. Kozubowski, Graduate School Representative

Marsha H. Read, Ph. D., Dean, Graduate School

May, 2014

ABSTRACT

The objective of this research effort focused on the evaluation of asphalt mixtures with respect to thermal cracking. Preliminary investigations soon indicated that a fundamental evaluation of thermal cracking was highly dependent upon the more complicated understanding of asphalt binder oxidation. The oxidation of asphalt binders within an asphalt mixture were understood to potentially be influenced by the mixture characteristics (i.e. air void levels, binder content, etc.) and aggregate properties (i.e. aggregate absorption, gradation, etc.). Therefore, this study was conducted in order to investigate and quantify the effects different aggregate sources and mixture properties may have on the oxidation and thermal cracking performance of asphalt mixtures.

The investigation specifically focused on quantifying the oxidation of the asphalt binder alone and as part of the asphalt mixture when subjected to isothermal oven aging. The oxidation parameters of pan-aged asphalt binders were quantified, according to the standard of practice in the industry. These parameters were then compared to extracted and recovered mixture-aged asphalt binders to examine the influence of the main aggregate and mixture factors on the binder oxidation. The study observed differences between the pan-aged and mixture-aged asphalt binders in terms of oxidation kinetics, rheological measures, and the combined effect represented as the hardening susceptibility.

Further evaluation of the binder oxidation based upon the dynamic modulus measures indicated marked influences of the mixture characteristics, the individual component materials, and the interactions between the investigated factors.

Differentiation of the experimental factors was further identified by the newly developed low-temperature evaluation method, Uniaxial Thermal Stress and Strain Test (UTSST). The UTSST provides a fundamental approach to characterize the thermo-viscoelastic properties of asphalt mixtures permitting the pragmatic evaluation of changes in the stiffness and overall behavior of mixtures as a function of oxidative aging. Five distinct stages in the UTSST modulus were identified as thermo-viscoelastic properties, which are identified as a function of temperature: viscous softening, viscous-glassy transition, glassy hardening, crack initiation, and fracture stages.

Through consideration of the thermo-viscoelastic properties, marked differences in the binder oxidation were noted between the experimental factors. Typically, decreases in the viscous response of the mixtures as well as increases in both the stiffness and brittle behavior were observed with aging. The evaluation method provides definitive measures to monitor multiple aspects of the performance of asphalt mixtures subjected to thermal loading.

DEDICATION

To my wife, my sons,

and all of my parents,

for all of their love, patience, and support.

I praise and thank the LORD for each of them.

ACKNOWLEDGEMENTS

First, I would like to express my gratitude to Dr. Peter Sebaaly for all of his guidance and persistence regarding my study program over the long term.

I would also like to express my great appreciation to Dr. Elie Hajj for all of his guidance and assistance over the duration of this research effort.

I also extend many thanks to Dr. Raj Siddharthan for the continued evaluation of material mechanics and providing valuable input to the foundation of this research effort.

I also wish to show my appreciation to Dr. Gary Norris for the support and continued willingness to participate in pavement related studies.

I would like to extent my appreciation to Dr. K for the guidance and direction during the initial exploration and final statistical analyses used in this research effort.

Lastly, I would like to express my appreciation to all of those who provided invaluable contributions from their own perspective of academic, research, agency, and private industry fields. I must also express my sincere gratitude to all of the faculty, staff, and students who contributed countless hours during the execution of this study.

TABLE OF CONTENTS

LIST OF TABLES

LIST OF FIGURES

1 INTRODUCTION

In this day in age, the asphalt pavement community is quickly becoming more technologically advanced in terms of analysis, design, and material characterization. This is a continuous process which is part of an overall effort to fully measure and comprehend the complexity of the asphalt.

The complexities begin with the nature and behavior of the asphalt binder. At a given point in time or aging condition, asphalt binders can be characterized with varying levels of appropriateness as linear elastic, linear viscoelastic, nonlinear viscoelastic, viscoplastic, etc. depending upon the measurement conditions and the level of detail desired in the characterization.

The aggregates typically exhibit linear elastic behavior over the range of loading conditions experienced within an asphalt pavement. However, when the aggregate are combined into a particular gradation, the bulk properties are highly influenced by many characteristics that are not easily modeled. Factors such as gradation, aggregate angularity, surface texture, surface coatings, and others have all been shown to influence the stiffness, flexibility, brittleness, resistance to rutting and many other performance measures considered in asphalt mixtures.

The situation becomes increasingly more complicated when the two components (i.e. asphalt binder and aggregate) are combined together into an actual mixture. Each component retains many of the complex characteristics of the parent material, in addition to exhibiting complex interactions. These interactions may be as simple as portions of

the binder being absorbed into the aggregate surface rendering it unavailable to the overall function of the mixture. On the other hand, complicated chemical interactions on the molecular level may significantly alter the overall behavior of the mixture. Additional influences from mineral fillers, chemical additives, and the compacted density of the material, and the entire system quickly becomes much more difficult to accurately characterize.

With all of these factors contributing to the characteristic behavior of a given mixture at a single point in time, it starts to become clear why the underlying changes in these characteristics are not fully understood as mixtures age and oxidize under variable conditions. Practical applications of damage from traffic, moisture, and freeze-thaw cycling continue to add to the highly variable environment where engineers need to design and analyze pavement structures and performance.

With those real-world conditions in mind, this study was initiated to quantify a few of the material unknowns that dictate mixture performance characteristics as a function of time. The overall research effort was supported by the Federal Highway Administration (FHWA) Contract DTFH61-07-H-00009, the Asphalt Research Consortium (ARC) beginning in 2007. The efforts included in this manuscript are a portion of the overall effort described under Work Element E2d.3 entitled Thermal Cracking Resistant Mixtures.

A significant portion of the overall effort put forth as part of the ARC included the development of a database to electronically store the reports, publications, materials characterization, and testing data produced as part of the research. Developed under the direction of Dr. Elie Hajj and colleagues at the University of Nevada, Reno, the database

may be found at http://www.arc.unr.edu/Outreach.html#ARC_Database. This database provides not only the measures and reports from the research discussed in this manuscript, but all of the reports, materials properties, produced measures, and publications prepared by all of the partners over the duration of the ARC contract.

1.1 Objective of the Study

Underlying the overall objective focused on thermal cracking, lies a much more complicated understanding of the true behavior of asphalt binder oxidation as it is influenced by the mixture characteristics (i.e. air void levels, binder content, etc.) and aggregate properties (i.e. aggregate absorption, quantitative gradation, etc.). This study was conducted in an effort to thoroughly investigate and quantify the effects different aggregate sources and mixture properties may have on the thermal cracking performance of asphalt mixtures. Once the asphalt binder oxidation process relative to the mixture characteristics is properly identified, its implication on other mixture properties and behaviors can be assessed. The results of this process will be applicable not only to thermal cracking, but also to numerous other properties that depend upon asphalt mixture characterization over time or at any aging condition where actual material testing is not practical or possible.

1.2 Problem Statement

This investigation is specifically focused on quantifying the oxidative aging characteristics of the asphalt binder by itself and as part of the asphalt mixture when both are subjected to controlled isothermal oven aging in the laboratory. The initial quantification will establish the oxidation parameters of the asphalt binder as has been the standard of practice in the industry. The next stage will determine the relationships among the properties and characteristics of the asphalt binder aged alone and within the asphalt mix. Once a solid foundation has been laid by determining these influences under a controlled laboratory setting, the methodology and principles may be applied to analyses of field conditions, which are inherently much more variable and unpredictable.

The current state of practice as will be discussed in detail in later sections, focuses almost exclusively on the characterization of the asphalt binder alone, completely blind to any influences of the aggregate or the majority of the mixture properties. This has been logically justified by acknowledging that the aggregates should not, under normal circumstances change significantly over time, i.e. that aggregate will not oxidize or otherwise age over time. While this fact cannot necessarily be argued, there have been many studies conducted that report direct and significant influences of mineral fillers, mastics, and aggregates on the physical and chemical properties of the associated binders. Certain fillers, such as lime, have long been known to improve the adhesion and thus moisture susceptibility characteristics of the asphalt mixture, with a catalytic stiffening effect on the mastic itself. Therefore, it stands to reason that it would be highly unlikely

that such influences would have a negligible influence on the oxidation process and resulting measurement of oxidation parameters of asphalt binders.

If the oxidation parameters are found to differ, then efforts will be put forth to quantify those differences utilizing phenomenological parameters as much as practical. These quantifiable parameters will become significant to the overall effort of the ARC, to quantify parameters to the extent that predictive models can be utilized to predict the performance of asphalt pavements in regards to specific conditions and distress modes, such as thermal cracking.

2 BACKGROUND

The study of asphalt binder aging is not a new concept by any means. Investigations have been ongoing for at least a century focusing on changes in asphalt material behavior as a function of age (Hubbard and Reeve, 1913). As can be expected, many of the efforts came from diverse viewpoints with specific objectives. Therefore, full comprehension of the subject by the asphalt community has remained elusive to this day.

2.1 General Overview

Many of the earlier studies were limited by technological advancements that simply were not available during the conduct of the research. Others were plagued by the common issue of limited time and resources to fully explore the findings and develop robust examination procedures.

A significant effort was put forth during the Strategic Highway Research Program, (SHRP). Much of the work by Bell et al. and others (Bell, 1989; Von Quintus et al., 1991; Bell et al., 1994; and Bell and Sosnovske, 1994) ultimately led to what exists today as the standard of practice for short and long-term aging of asphalt mixtures for mix design and mechanical testing. This standard is published as AASHTO R30 (AASHTO, 2013). Essentially, the aging was quantified by viscosity and penetration measurements at a single temperature of the binders extracted and recovered from mixtures aged in laboratory under various conditions. Limited resilient modulus testing was also

completed on the lab compacted samples. Unfortunately the long term aging properties, simulating five to ten years in service, had to be extrapolated from two year data available and using penetration estimation equations developed previously (Bell et al., 1994). To compound these issues, limitations on the project did not permit comparisons of the binder and mixture test results.

The most significant drawback of these early studies is that neither the binder penetration nor the viscosity are robust or strong enough links to adequately relate the mixture aging to the numerous binder aging studies, i.e. these tests are not sensitive enough to adequately differentiate oxidative aging. That is not to say penetration and viscosity are not affected by aging, but merely they are not powerful enough tools for adequate aging characterization.

Other studies began to incorporate not only the stiffness measures but also chemical characterization of the aged binders (Chari, 1988). These studies included variants of oxidation measurement by investigating carbonyl ratio and ketone factor. However, these studies included a limited scope of mixtures, but did include multiple aging durations, mixture resilient modulus, indirect tensile strength, and an estimated fracture energy parameter.

While these efforts have stood as the standard for some time, they have unfortunately been shown to be inadequate. Therefore, two new projects through the National Cooperative Highway Research Program, NCHRP, have been initiated and are currently underway. NCHRP Project 9-52 is focused on addressing the appropriate procedures to simulate short-term aging to adequately replicate batching, mixing, and placement of the asphalt mixtures in the field. Similarly, NCHRP Project 9-54 is

intended to characterize and produce a method to appropriately long-term age asphalt mixtures in the lab to replicate in-service aging in the field. These two projects are anticipated to be completed in 2014 and 2016, respectively. Therefore, the standard methods as they exist today are likely to either be validated or modified in the near future as a result of these research efforts.

2.2 Summary of State of Practice

Other research efforts provided a comprehensive literature review including a summary of a more appropriate measure of asphalt binder aging (Glover et al., 2009). Based on the numerous studies reviewed, oxidation was identified as the most influential hardening parameter on binder aging. Previous work by Liu et al. indicated that carbonyl area, CA, is a direct measure of binder oxidation (Liu et al., 1998). Other investigations further conclude that CA relates directly to binder physical properties or rheology, such as the low shear rate limiting viscosity (Martin et al., 1990 and Lau et al., 1992). Extensive studies of binder oxidation kinetics also have been reported (Lau et al., 1992).

In summary, these studies consider the binder kinetics as the relationship between CA and aging time as function of temperature and oxygen pressure or concentration. The other major determination with this technique is the hardening susceptibility (HS). While these parameters will be discussed at length in the methodology section, the HS parameter is essentially the relationship between the binder viscosity and the corresponding CA measures over a range of aging conditions.

In the majority of current aging procedures, the most common method of aging the binders is in some type of pan or metallic vessel. Commonly these are small laboratory pans that allow the binder to be aged in a thin film, to reduce limitations of the oxidation related to diffusion of the oxygen through the binder. The most common procedures keep the film thickness around 1 mm (Han, 2011; Morian et al., 2011, and Morian et al., 2013) and down to 0.3 mm (Farrar et al., 2012) in some instances. The standard practice is to age a given asphalt binder under atmospheric air supply and pressures over different durations at multiple temperatures that must be very tightly controlled. The selection of the temperatures and durations is somewhat subjective; however there are logical and practical limitations on each.

It stands to reason that it would be desirable to keep the aging duration as short as possible. The shorter the duration, the more samples may be tested and early results can be obtained within a given evaluation period. However, there must be sufficient time to permit the oxidation reactions to take place within the asphalt binders. Those reaction rates are significantly increased when the aging temperature is increased. So it is logical to increase the temperature and decrease the aging time. However, caution must be observed in these considerations since it has been shown that usage of temperatures that are too high will produce different oxidation products from a chemical species standpoint (Petersen, 2009). These differences in the chemical species or functional group may cause significant changes in the measurements being conducted in these types of experiments.

Essentially, the aging protocol needs to balance the temperatures, durations, oxidation reaction rates, and oxygen diffusion rates with sample geometry and oxygen

pressure as significant inputs into the process. To further complicate the situation, the determination of which process is limiting the oxidation of the binder, the oxidation reaction or the oxygen diffusion through the binder, is definitely not an easy or straight forward consideration. Often, very specific kinetics studies of the exact materials at hand are necessary to make these determinations, but such considerations are fairly outside the scope of this research effort and thus are not considered directly.

Additional asphalt binder aging measurements are also considered from field samples. Typically, these materials are obtained from cores cut from the pavements in the field. The binder is then extracted from the mixture before tested by the various aging protocols being used. Some of the measures are conducted on the binder as-is, and some binders may undergo additional aging in the laboratory to establish the kinetics and HS relationships for the binder obtained from the field mixture. These types of measurement provide aging information on the exact mixture and binder in the field.

In summary, the vast majority of oxidation studies on asphalt materials are conducted on asphalt binders aged in metallic pans, either steel or aluminum, over a range of temperatures and durations. Unless field samples are involved, these studies typically do not include the interaction of aggregates or mixture characteristics, which have proven to be significantly influential.

3 PROPOSED METHODOLOGY

An investigation into a subject as comprehensive as oxidative aging of asphalt mixtures will definitely necessitate the application of comprehensive theories, each with its own corresponding test methodologies and measures. These measures vary greatly depending upon the material characteristics being investigated as well as the conditions under which the material behavior is being evaluated. In general, the applied methodologies can be grouped by the material, namely; asphalt mixtures or asphalt binders. Further consideration of the oxidation models currently available in the industry and their relevance to this study are presented in the following sections.

This chapter is intended to present the methodologies utilized throughout this research effort. The tests and analysis methods used will be discussed at length to enable the later chapters to focus on the results and more importantly on the interpretations of those results without having the method development issues cluttering those discussions.

3.1 Mixture Characterization Procedures

Since this investigation is focused on oxidation and its impact on the properties of asphalt mixtures, a significant amount of effort will be spent on the quantification of the mixture stiffness. As such, the majority of the mixture characterization efforts will emphasize the different measures of the stiffness or modulus values of asphalt mixtures.

One method of characterizing the stiffness of asphalt mixtures that is becoming increasingly more popular is the determination of the dynamic modulus, |E*|. While the dynamic modulus measures the stiffness of asphalt mixtures in the complex domain under mechanical loading, a relatively new procedure known as the Uniaxial Thermal Stress and Strain Test, UTSST, establishes a modulus of the mixtures under thermal loading. Similar stiffness measures of the asphalt binders were also measured through the dynamic shear modulus.

Since these stiffness measures are all relative to each other at various aging stages of the asphalt binders, a chemical characterization has also been conducted through measures with Fourier-Transform Infrared Spectroscopy, FT-IR to chemically quantify the aging of asphalt binders. Additional measures of the complex interactions of the asphalt binders and the associated aggregates have also been explored through fractional composition measures of the asphalt binders combined with the respective aggregates used in the study.

Further details regarding each of these measures, has been provided in the following sections, with detailed analyses and results presented in subsequent chapters.

3.1.1 Dynamic Modulus

Stiffness measures have been utilized for many years to quantify the stress-strain relationship of materials. The notation, E, for modulus values are typically reserved for cases where axial loading is applied. In this particular instance the asterisk is added to

denote the complex domain or time dependent measure as opposed to the time independent measure, E or Young's modulus, such as a static load case.

The measure of dynamic modulus, |E*|, is becoming an increasingly useful tool for asphalt mixture characterization. One reason for the gained popularity of E*extends from the availability of more advanced pavement evaluation methods that incorporates the dynamic or time dependent nature of the load and material properties. These factors are becoming increasingly relevant given the fact that asphalt mixtures exhibit some degree of viscoelastic behavior.

The need for the viscoelastic characterization of asphalt mixtures is based on the fact that the moduli of these mixtures are highly influenced by both the loading rate (frequency) and the temperature at which the test is conducted. These characteristics are generally quantified in the dynamic modulus test by applying a compressive sinusoidal (Haversine) load in the axial direction and measuring the corresponding recoverable axial strain on the specimen. The applied load is composed of a frequency sweep repeated under multiple isothermal conditions. Because the asphalt mixture will respond in a viscoelastic manner, the applied stress and corresponding strain will be out of phase, i.e. there is a time lag between the load and response. This phase lag (ϕ) is depicted in Figure 3.1.

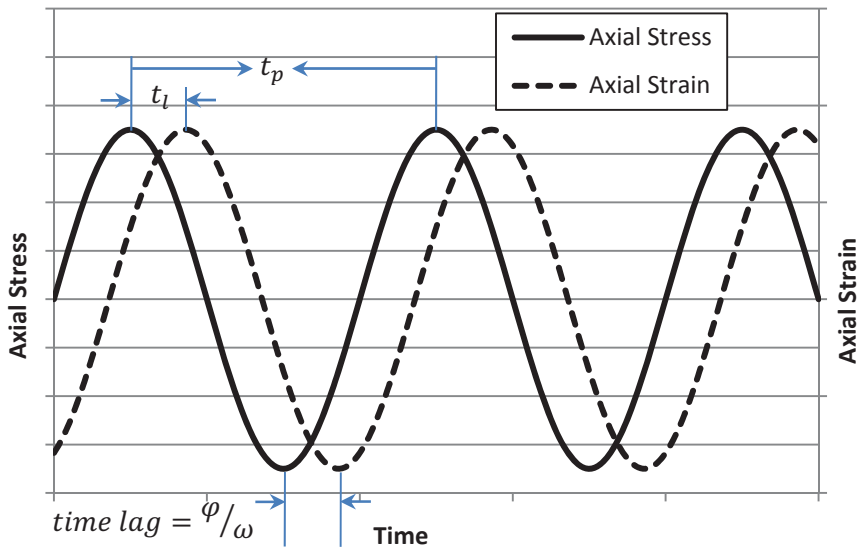

Figure 3.1 Typical Stress and Strain from Dynamic Modulus Testing

The determination of the dynamic modulus in the complex domain is represented by Equation 3.1.

$$E^* = \frac{\sigma_0 \sin \omega t}{\varepsilon_0 \sin(\omega t - \varphi)} = |E^*|(\cos \varphi + i \sin \varphi) = E' + iE'' \qquad \textbf{Equation 3.1}$$

where,
- E^* - complex dynamic modulus, psi (kPa);
- σ_0 - maximum amplitude of stress, psi (kPa);
- ε_0 - maximum amplitude of strain, in./in. (mm/mm);
- ω - angular frequency, Hz or rad/s;
- φ - phase angle, degrees;
- t - time; sec.;
- i - complex number, $i = \sqrt{-1}$;
- E' - storage or elastic modulus, psi (kPa);
- E" - loss or viscous modulus, psi (kPa).

Commonly, the absolute value of complex modulus, |E*|, is reported and utilized rather than the full complex form. Mathematically, |E*| is calculated as presented in Equation 3.2 with the accompanying phase angle calculated as depicted in Equation 3.3.

$$|E^*| = \frac{\sigma_0}{\varepsilon_0}$$ **Equation 3.2**

$$\varphi = \tan^{-1}\frac{E''}{E'} = \frac{t_l}{t_p}(360°)$$ **Equation 3.3**

One form of graphical representation of the contribution of E' and E" specific to E* is depicted by the vector addition shown in Figure 3.2.

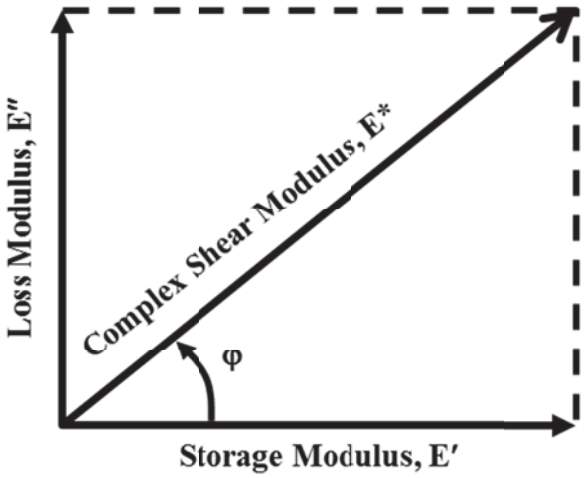

Figure 3.2 Vector Diagram of Dynamic Modulus Values

Chronologically speaking, dynamic modulus testing has existed for quite some time. Earlier versions of the method were prescribed in the American Association of State Highway Transportation Officials (AASHTO) provisional test method TP62-03 (AASHTO, 2006), which has been revised and now exists as a full test method T342. Essentially, this method established the testing protocol utilizing five temperatures and six frequencies with a rest period between each frequency sweep. Difficulties in conducting stress-controlled testing coupled with somewhat complicated software

operations available at the time, and extensive testing durations led to additional research efforts.

The additional efforts conducted through NCHRP Project 9-29 resulted in a modified testing protocol that eventually led to several equipment manufacturers producing what was known as the Simple Performance Tester (SPT). The major modifications to the SPT method included conducting the designated frequency sweeps in a strain controlled mode, reducing the protocol to four temperatures, recommending quality control limits on the applied load and resulting material response, and inducing a maximum limit on the total permanent strain (Bonaquist et al,. 2003). The selected temperatures stem from the recommendations of NCHRP 9-19 suggesting 4.4 and 21.1°C were related to the fatigue performance of mixtures and the high temperatures 37.8 and 54.4°C showed a relationship with rutting resistance. Based on these recommendations the dynamic modulus testing for this research was conducted under the following conditions:

- Temperatures: 4.4, 21.1, 37.8, and 54.4°C (40, 70, 100, and 130°F)
- Frequencies: 25, 10, 5, 1, 0.5, 0.1 Hz

In order to maintain consistency during the study period, the dynamic modulus test protocol was held consistent even though continued research efforts on dynamic modulus testing had continued elsewhere and suggested modifications. Some of the revisions reduced the number of temperatures and frequencies at the extreme ends of the testing conditions and applied binder's specific conditions. For example, a recent change requires four test frequencies at the highest test temperature which is dependent upon the Performance Grade (PG) of the asphalt binder in the mixture. This methodology is

commonly referred to as the Asphalt Mixture Performance Tester (AMPT) method and is currently addressed in AASHTO PP79-12 (AASHTO, 2012).

To clarify, the dynamic modulus testing during this research effort remained at the same four temperatures and six frequencies listed above and was not changed over the duration for the project in light of new developments in the method.

3.1.2 Dynamic Modulus Master Curve

The dynamic modulus measures described in the previous section typically generates a data set that is rationally organized into a six by four matrix. Since 24 data points from each data set are difficult to comprehend and thus make meaningful comparisons strenuous, it is a common practice to construct a dynamic modulus master curve utilizing the principles of time-temperature superposition commonly applicable to viscoelastic materials.

Graphically, an example of the measured dynamic modulus data is presented in Figure 3.3. From a practical standpoint, the master curve is created by shifting each respective isothermal frequency sweep groups along the horizontal axis until a single line or master curve is formed as presented in Figure 3.4.

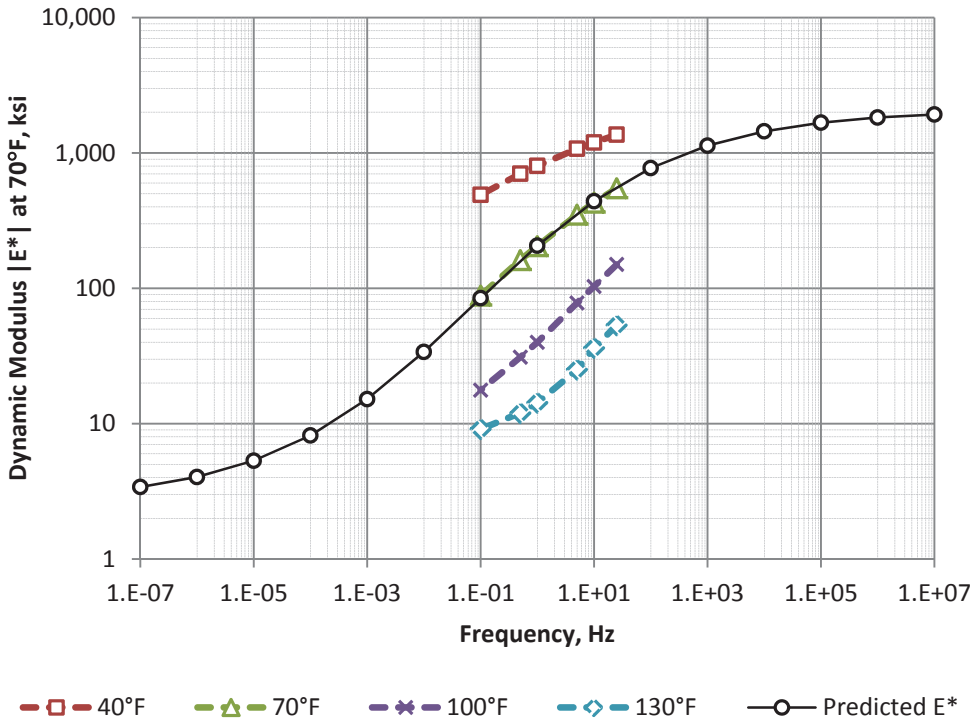

Figure 3.3 Example of Dynamic Modulus Measures

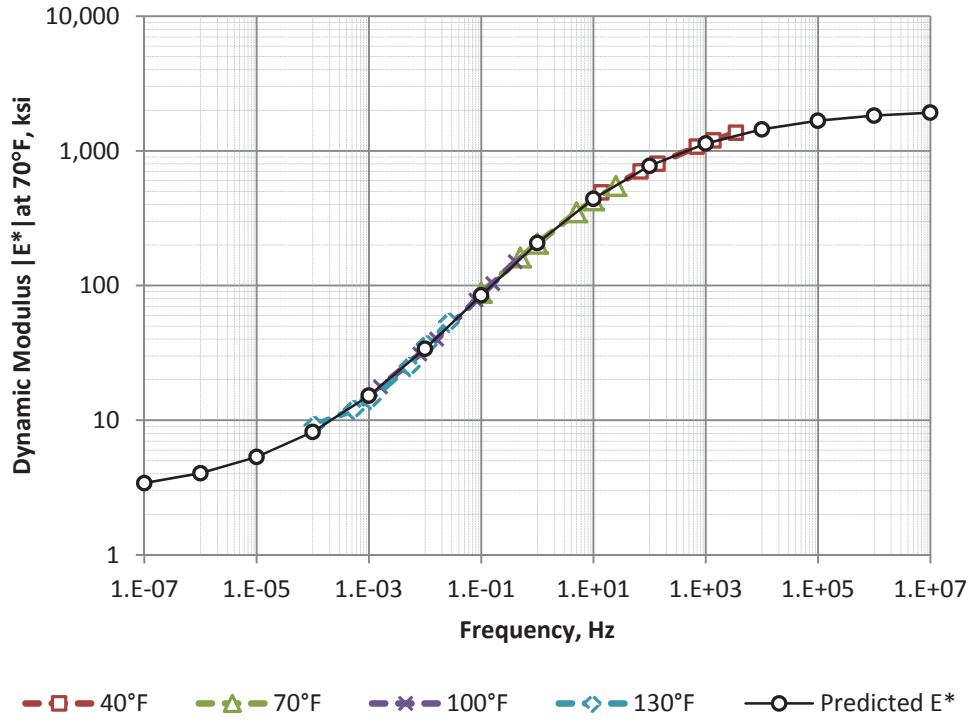

Figure 3.4 Example of Shifted Dynamic Modulus Master Curve

It is acknowledged that for some materials such as certain polymers, vertical shifting is also applied (i.e. vertical adjustment of the modulus values). The vertical adjustments are generally attributed to changes in the volume, typically quantified as density, of a given sample due to the temperature changes during testing (Mezger, 2011; Shaw and MacKnight, 2005). These adjustments are typically quite minor in comparison to the frequency shifting (i.e. horizontal) and typically are not applied to mixture evaluations. Generally following industry practice, the master curve shifting methods utilized in this study have only included horizontal shifting (i.e. shift factors applied to the reduced frequency only).

In Figure 3.4, each of the frequency sweep groups measured at the same temperature, isotherms, have been shifted by different amounts until they converge to the single master curve relationship at a reference temperature (T_r). The amount each isotherm is shifted is known as the shift factor (a_T) such that each isotherm will have one respective shift factor. Figure 3.5 presents each of the respective shift factors for each of the measured isothermal frequency sweeps as a function of temperature.

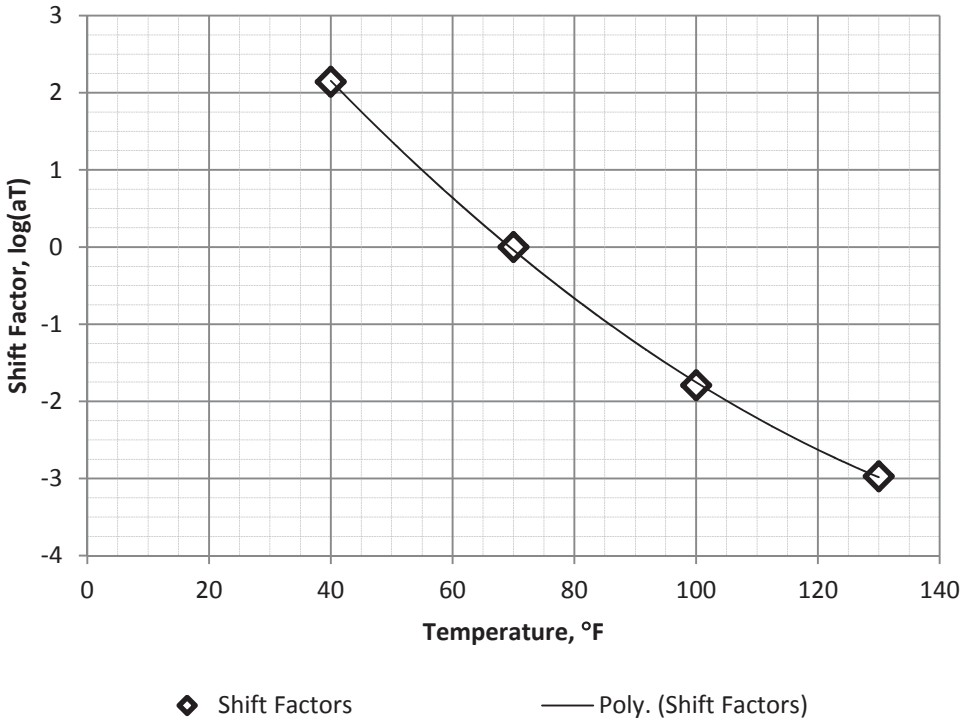

Figure 3.5 Example of Dynamic Modulus Shift Factors, a_T at T_r of 70°F

It should be clear that time-temperature superposition is only applicable to thermo-rheologically simple materials, that do not change their structural character within the temperature range being considered (Mezger, 2011). In other words, simple lateral shifting along the frequency axis yields a single master curve relationship. Another method which can be utilized to determine thermo-rheologically simple behavior is to consider the vector components, i.e. E' and E", of the complex modulus (E^*) in this instance. If the vector components are shifted and the respective shift factors are plotted in a manner similar to Figure 3.5, the two shift factor relationships as a function of temperature should overlap or become one a_T curve. If convergence does not occur, then a master curve cannot be legitimately created without more sophisticated analyses (e.g.

vertical shifting and thus the materials have not exhibited thermo-rheologically simple behavior (Ferry, 1980)).

The method of shifting just described is often referred to as free shifting, meaning that the shape of the master curve itself and the form of the shift factors are largely dictated by the measured data directly. Another way to consider this point is to acknowledge that neither the master curve nor the shift factors are confined by models, equations, or other predetermined restrictions other than convergence to a single relationship. While this type of shifting may be desired in many instances, it does require many data points to assume a reliable relationship and dependable master curve. Certainly more data than the dynamic modulus protocol utilized in this study could provide.

In such cases when free shifting is not appropriate, other methods are typically utilized and are often generalized as restricted shifting (Rowe et al., 2011). These methods, including the free shifting method, are generally described as follows.

- Free shifting – the shifting conducted on multiple sets of isothermal data to form a smooth master curve with the master and the shift parameters determined independently.
- Functional form – the shifting is conducted in such a manner so that the master curve, the shift function, or both are forced to fit a certain function form or predefined equation.
- Shift function - the shifting is conducted in such a manner so that the shift function is forced to fit a certain function form or predefined equation.

- Functional form with descriptive function – shifting is completed similar to the functional form method, except the parameters of the model or functions, either for the master curve or the shift functions, have specific meaning often phenomenological or similar physical significance.

As mentioned previously, the free shifting methods are generally preferred although likely the most difficult to actually perform and require the greatest amount of measured data as inputs. However, some of the functional form methods, especially those with phenomenological structures, can sometimes aid in mild extrapolation of data for the master curve construction.

Irrespective of the shifting protocol followed, once the shifting has been completed, many different model forms and functions may be fit to the data. These forms are largely complete during the so called restrictive shifting operations, but this practice also applies to free shifted data as well.

The Standard Logistic Sigmoidal Function

Some of the more common master curve models are generally labeled as sigmoidal functions. One of the most common versions is the symmetric sigmoidal function incorporated into the Mechanistic Pavement Design Guide (MEPDG) (ARA, 2004). This methodology, currently available in the AASHTOWare Pavement ME Design (AASHTOWare, 2013) software package is presented in Equation 3.4. This function is available from AASHTO PP61 (AASHTO, 2013) to accompany dynamic modulus data

obtained from the Asphalt Mixture Performance Tester (AMPT) method of AASHTO TP79 (AASHTO, 2013).

$$\log|E^*| = \delta + \frac{(Max - \delta)}{1 + e^{\beta + \gamma log f_r}} \quad \textbf{Equation 3.4}$$

where, |E*| - magnitude of complex dynamic modulus, psi (kPa);
δ - fitting parameter, signifying the lower asymptote of the master curve;
β - fitting parameter; influencing the frequency of the inflection point,
γ - fitting parameter; characterizing the slope of transition (center) region of the sigmoidal;
Max - the limiting maximum modulus estimated by the Hirsch model (Christensen et al., 2003), psi (kPa);
f_r - reduced or shifted frequency, Hz.

This model, along with the previous version presented in Equation 3.5 from AASHTO PP62 (AASHTO, 2013), are likely the most common forms of sigmoidal functions utilized for dynamic modulus master curve construction. It can be readily seen from Figure 3.6 that this form is a symmetric form of a sigmoid function and is often referred to as the standard logistic sigmoidal form. Note that the frequency of the inflection point of the master curve can be found mathematically as $10^{(\beta/\gamma)}$.

$$\log|E^*| = \delta + \frac{\alpha}{1 + e^{\beta + \gamma log \omega f_r}} \quad \textbf{Equation 3.5}$$

where, α - fitting parameter; signifying the maximum difference between δ and Max in Equation 3.4, numerically $\alpha = (Max - \delta)$.

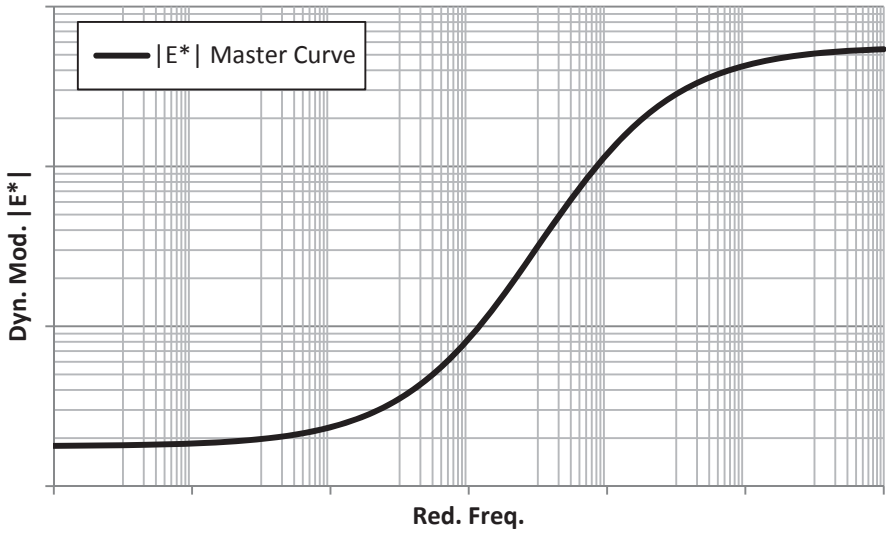

Figure 3.6 Example of Symmetric Sigmoidal Function

The symmetric sigmoidal function was chosen for the development of E^* master curves produced in this research since it is currently the most commonly used method.

The Non-Symmetric Sigmoidal Function

It has been suggested that a more appropriate fit of the dynamic modulus data may be obtained by allowing the measured data to have a stronger influence on the shape of the master curve, as opposed to forcing the shifting of the data to fit the shape of the symmetric sigmoidal function. Thus, an alternate form of the sigmoidal function has been proposed which can take on a non-symmetric form (Rowe et al., 2009) as depicted in Equation 3.6 and presented in Figure 3.7.

$$\log E^* = \delta + \frac{\alpha}{[1 + \lambda e^{\beta+\gamma log f_r}]^{1/\lambda}}$$ **Equation 3.6**

where, λ- fitting parameter which induces a non-symmetric shape to the sigmoidal by controlling the height of the inflection point on the master curve.

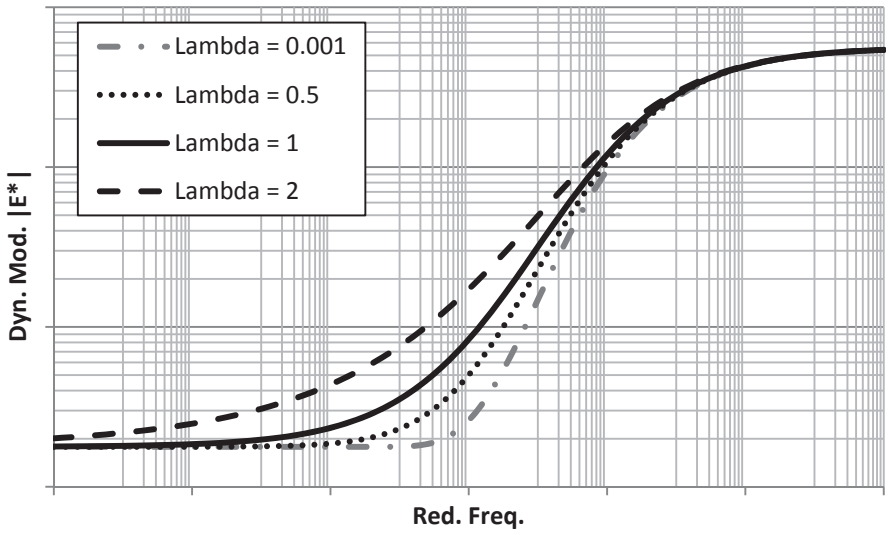

Figure 3.7 Example of Non-Symmetric Sigmoidal Functions

Note from Figure 3.7 that when lambda, λ, is equal to unity, the non-symmetric sigmoidal function is numerically equal to the standard logistic sigmoidal form. On the other hand, when the value of λ is zero or below, the model itself begins to dramatically decay and no longer provides realistic forms.

The 2S2P1D Model

A function that will be used in the analysis has been referenced previously as the Modified Huet-Sayegh analogical model. The Huet-Sayegh model has been modified by

adding a linear dashpot to two parabolic elements in series along with another spring as depicted in Figure 3.8. Recent assessments of this model have further defined it as the General 2S2P1D model following a shorthand notation of the mechanical elements utilized in the model (Olard and Di Benedetto, 2003) as presented in Figure 3.7.

$$E^*(i\omega\tau) = E_0 + \frac{E_\infty - E_0}{1 + \delta(i\omega\tau)^{-k} + (i\omega\tau)^{-h} + (i\omega\beta\tau)^{-1}} \qquad \textbf{Equation 3.7}$$

where, : i - complex number, $i = \sqrt{-1}$;
ω - angular frequency, $\omega = 2\pi f$;
E_0 - static modulus when $\omega \rightarrow 0$;
E_∞ - maximum limit of complex modulus when $\omega \rightarrow \infty$;
h, k - exponents such that $1>h>k>0$;
δ - dimensionless constant,
β - dimensionless constant, $\beta = {}^{\eta}/_{\tau(E_\infty - E_0)}$; when $\omega \rightarrow 0$, then $E^*(i\omega t) \sim E_0 + i\omega\eta$
η - dashpot coefficient or Newtonian viscosity;
τ - characteristic time, which varies only with temperature.

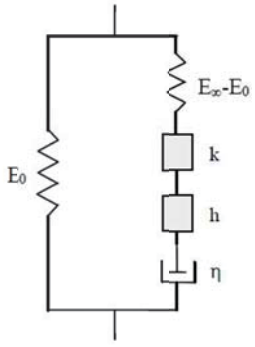

Figure 3.8 Mechanical Elements of 2S2P1D Model

Olard and Di Benedetto (Olard and Di Benedetto, 2003) and Dave (Dave, 2009) credit Huet with the proposal of parabolic relationship for the viscoelastic response of hydrocarbon based materials (Huet, 1963), i.e. asphalts. The addition of the other

mechanical elements soon followed, creating the Huet-Sayegh model (Sayegh, 1965). Practically speaking, the parabolic elements represent a peculiar dashpot with a constitutive relationship that follows a parabolic shape with time as represented in Equation 3.8.

$$\varepsilon(t) = \frac{\sigma}{A} t^k$$ **Equation 3.8**

where, : $\varepsilon(t)$ - parabolic dashpot strain as a function of time;
σ - applied stress;
A, k - experimental parameters with $0<k<1$,
t - time of applied loading.

A convenient method to display the parameters utilized in the 2S2P1D model is to consider the results in the Cole-Cole plane, or E' vs E" (Di Benedetto et al., 2004) as depicted in Figure 3.9.

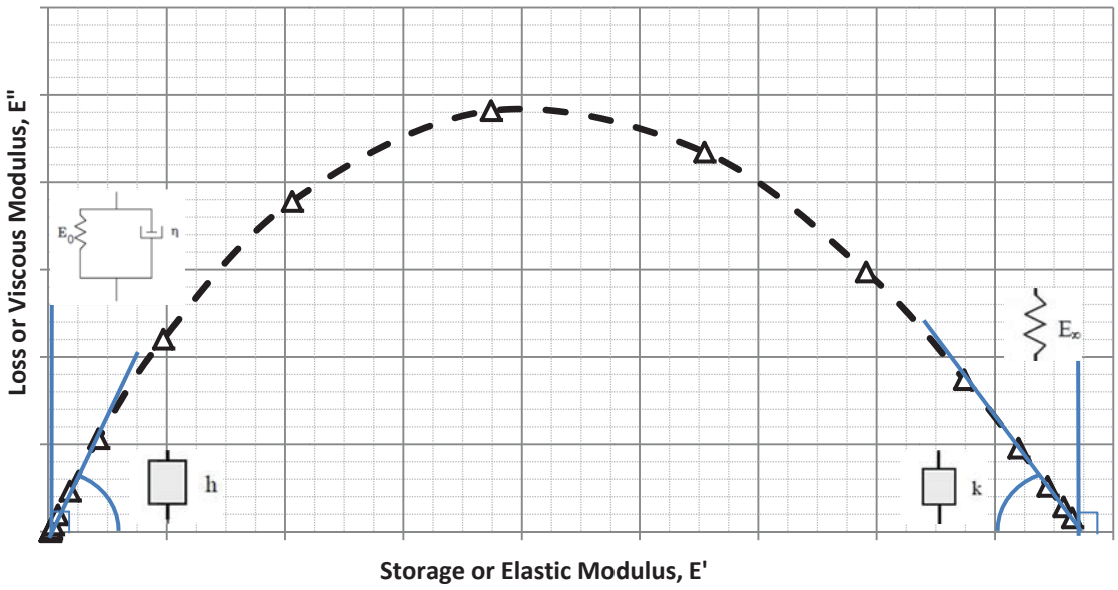

Figure 3.9 Example Cole-Cole plot for Dynamic Modulus of Mixtures

The Christensen-Andersen Models

A master curve function that is traditionally used with the asphalt binder shear modulus values was developed by as Christensen and Anderson, known as the "CA model" (Christensen and Anderson, 1992). However, if measurements of shear modulus are obtained for asphalt mixtures, the same functional form may apply (Zeng et al., 2001). The CA model is presented in Equation 3.9 and Equation 3.11.

$$G^* = \frac{G_g^*}{\left[1 + \left(f_c/f\right)^k\right]^{1/k}} \qquad \textbf{Equation 3.9}$$

$$\delta = \frac{90}{1 + \left(f/f_c\right)^k} \qquad \textbf{Equation 3.10}$$

where, G^*- complex dynamic shear modulus, kPa;
G_g^* - glass complex modulus, kPa;
f_c - crossover frequency, degrees;
f - reduced frequency, Hz or rad/s;
k - shape parameter, dimensionless;
δ - reduced phase angle, degrees.

The CA model was generally understood to be a restricted form of the more general equation proposed by Christensen, Anderson, Sharrock, and Bouldin, CASB (Rowe et al., 2001). This general equation included additional shape parameters which provided better data fitting abilities of G^* especially when the phase angle was considered. The general forms are depicted in Equation 3.11 and Equation 3.12.

$$G^* = \frac{G_g^*}{\left[1 + \left(f_c/f\right)^k\right]^{m_e/k}}$$ **Equation 3.11**

$$\delta = \frac{90 m_e}{1 + \left(f/f_c\right)^k}$$ **Equation 3.12**

where, m_e, k - shape parameters.

From this base model it has been shown that the Christensen-Anderson-Marasteanu, CAM model (Marasteanu and Anderson, 1999) can be generalized with a modified power law to apply to asphalt mixtures as well as asphalt binders (Zeng et al., 2001). Through this modification, the CAM model is adjusted to include non-symmetric parameters as shown in Equation 3.13 which is also presented in Figure 3.10. To simplify, the modified CAM model may be applied to asphalt binders by setting G_e^* equal to zero, which will return the original CAM model of Equation 3.11.

$$G^* = G_e^* + \frac{G_g^* - G_e^*}{\left[1 + \left(f_c/f\right)^k\right]^{m_e/k}}$$ **Equation 3.13**

To provide further clarification of the shape parameters, m_e and k, additional equations have been derived to accompany Figure 3.10 as described in Equation 3.14, Equation 3.15, and Equation 3.16.

$$f_c' = f_c \left(\frac{G_e^*}{G_g^*} \right)^{1/m_e}$$ **Equation 3.14**

$$R = \log \frac{2^{m_e/k}}{1 + \left(2^{m_e/k} - 1\right)\left(G_e^* / G_g^* \right)}$$ **Equation 3.15**

$$R' = \log \left\{ 1 + \left(\frac{G_g^*}{G_e^*} - 1 \right) \left[1 + \left(\frac{G_g^*}{G_e^*} \right)^{k/m_e} \right]^{-m_e/k} \right\}$$ **Equation 3.16**

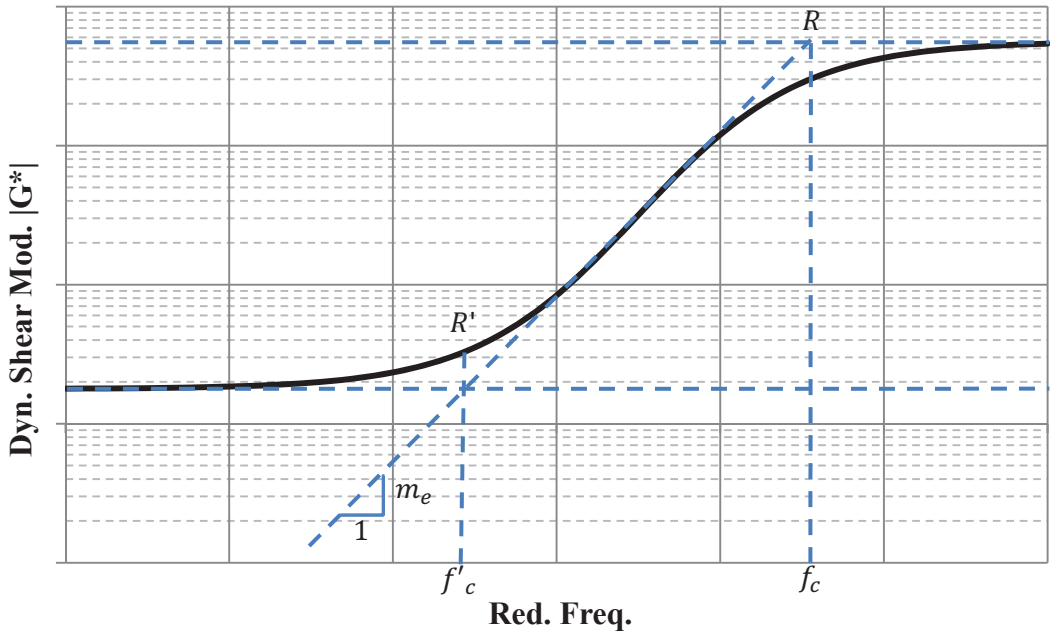

Figure 3.10 Christensen-Anderson-Marasteanu Model Parameters

It should be noted that Figure 3.10 generally includes the parameter names associated with the CAM model as other forms have been used elsewhere.

Several other versions of the CASB model have been utilized and deemed appropriate for a number of applications. The two most commonly referenced versions of the CASB model are known as the Christensen-Anderson-Sharrock, CAS model, (Rowe et al., 2001) and the previously noted Christensen-Anderson-Marasteanu, CAM model (Marasteanu and Anderson, 1999). Table 3.1 presents a summary of the overall model parameters, Equation 3.13, relative to their naming convention as well as their usage in the model fitting procedure.

Table 3.1 Christensen-Anderson-Sharrock-Bouldin Model Parameters

Model Name	Assumed Parameter	Number of Fitted Parameters	Fitted Parameters
Asphalt Mixtures			
Mod. CAM	N/A	5	G_e^*, G_g^*, k, m_e, f
Asphalt Binders $G_e^* = 0$			
CASB	$G_e^* = 0$	4	G_g^*, k, m_e, f
CA	$G_e^* = 0$ $G_g^* = 3 * 10^3 MPa$ $m_e = 1$	2	k, f
CAS	$G_e^* = 0$ $m_e = 1$	3	G_g^*, k, f
CAM	$G_e^* = 0$ $G_g^* = 3 * 10^3 MPa$	3	k, m_e, f

It should be noted that the most robust model is the modified CAM and the CASB due to their enhanced flexibility and widest range of material response. However, the more simplified models have been found useful for certain circumstances where the full form is not necessary. The simplified models generally can be utilized with less material properties as some parameters of the full model are assumed. The appropriateness of the reduced models largely depends on how valid each respective assumption may be to the data set under consideration.

The Prony Series

In keeping with the mechanical element modeling procedures, two more commonly used representations of viscoelastic behaviors; generalized Maxwell-Weichert and generalized Kelvin-Voigt models, are collectively referred to as Prony series equations (Park and Schapery, 1998).

The generalized Maxwell-Wiechert model consists of a spring and $\boldsymbol{m}$ number of Maxwell mechanical elements connected in parallel as shown by Equation 3.17. The Maxwell elements consist of a spring and a dashpot connected in series as in Figure 3.11.

$$E(t) = E_e + \sum_{i=1}^{m} E_i \, e^{-\left(t/\rho_i\right)} \qquad \textbf{Equation 3.17}$$

where, : $E(t)$ - relaxation modulus as a function of time;
E_e - equilibrium modulus;
E_i- relaxation strength,
ρ_i- relaxation time;
m- number of Maxwell elements;
t - time of applied loading.

Figure 3.11 Schematic of Maxwell Element

Similarly, the creep compliance can be represented by the Kelvin-Voigt model, which consists of a spring and a dashpot in series with $\boldsymbol{n}$ number of Voigt elements depicted by Equation 3.18. The Kelvin-Voigt element consists of a spring and a dashpot connected in parallel as presented in Figure 3.12.

$$D(t) = D_g + \frac{t}{\eta_0} + \sum_{j=1}^{n} D_j \left(1 - e^{-\left(t/\tau_j\right)}\right) \qquad \textbf{Equation 3.18}$$

where, : $D(t)$ - creep compliance as a function of time;
D_g - glassy compliance;
η_0 - zero shear or long time viscosity;
D_j- retardation strength,
τ_j- retardation time;
n- number of Voigt elements;
t - time of applied loading.

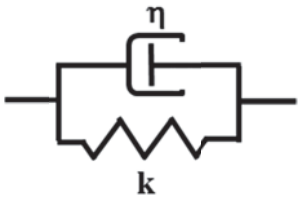

Figure 3.12 Schematic of Voigt Model Element

It should be noted that other representations of the Kelvin-Voigt model have been utilized with the viscosity term, η_0, excluded from Equation 3.18 (Hu and Zhou, 2010). As a matter of convenience, it has been shown that the relaxation spectra, e.g. Maxwell-Wiechert model, and the creep compliance curve, e.g. Kelvin-Voigt models can be interconverted with each other, which may prove a useful tool for certain circumstances (Park and Schapery, 1998; Hu and Zhou, 2010).

Many other representations of these same models components have also been suggested as model for asphalt materials. As an example the Burgers model is generally described as a Maxwell element in series with a number of Kelvin-Voigt elements. Since, these model forms are not explicitly used in this study, no further consideration of these models merits further discussion. However, the Prony series relationships are provided as a reference and will also be utilized in discussions specific to the master curve relationships noted specifically with the asphalt binder measures.

The previous discussions of available master curve models and the following section pertaining to proposed shift functions is not intended to be a comprehensive record of all models available, but rather an exemplary compilation of the varied forms most commonly available.

Viscosity-Temperature Susceptibility Shift Function

For the most part, the specific master function used does not necessarily dictate the shift function used to obtain the master curve. However, certain shift functions are commonly paired to certain master curve functions which are sometimes specified together. For instance, AASHTO PP62 (AASHTO, 2012) specifies two options for the shift functions

to accompany the standard logistic sigmoidal form of Equation 3.5 by utilizing data produced according to AASHTO T342 (AASHTO, 2012). Those two options are presented as the MEPDG shift factors and the second-order polynomial function. The MEPDG shift factors, also referred to as the A-VTS or viscosity-temperature susceptibility method, utilizes the measured viscosity of the asphalt binder to dictate the shifting function as provided in Equation 3.19.

$$\log f_r = \log f + c\left(log\eta - log\eta_{T_R}\right) \qquad \textbf{Equation 3.19}$$

where, : f_r - reduced or shifted frequency, Hz.;
f - loading frequency at the test temperature, Hz.;
c - fitting coefficient;
η - viscosity of the binder at the test temperature, cP;
η_{T_R} - viscosity of the binder at the reference temperature, cP;
T_R - reference temperature in Rankin, °R.

The viscosity, η, used in Equation 3.19 can be found using the A-VTS parameters found in Equation 3.20 and depicted in Figure 3.13.

$$\log \eta = 10^{[A+VTS \log T]} \qquad \textbf{Equation 3.20}$$

where, : η - viscosity of the binder at the desired temperature T, cP;
A - intercept of the viscosity-temperature relationship, cP;
VTS - viscosity-temperature susceptibility or slope of A-VTS plot;
T - test temperature of interest in °R = (°F + 459.67).

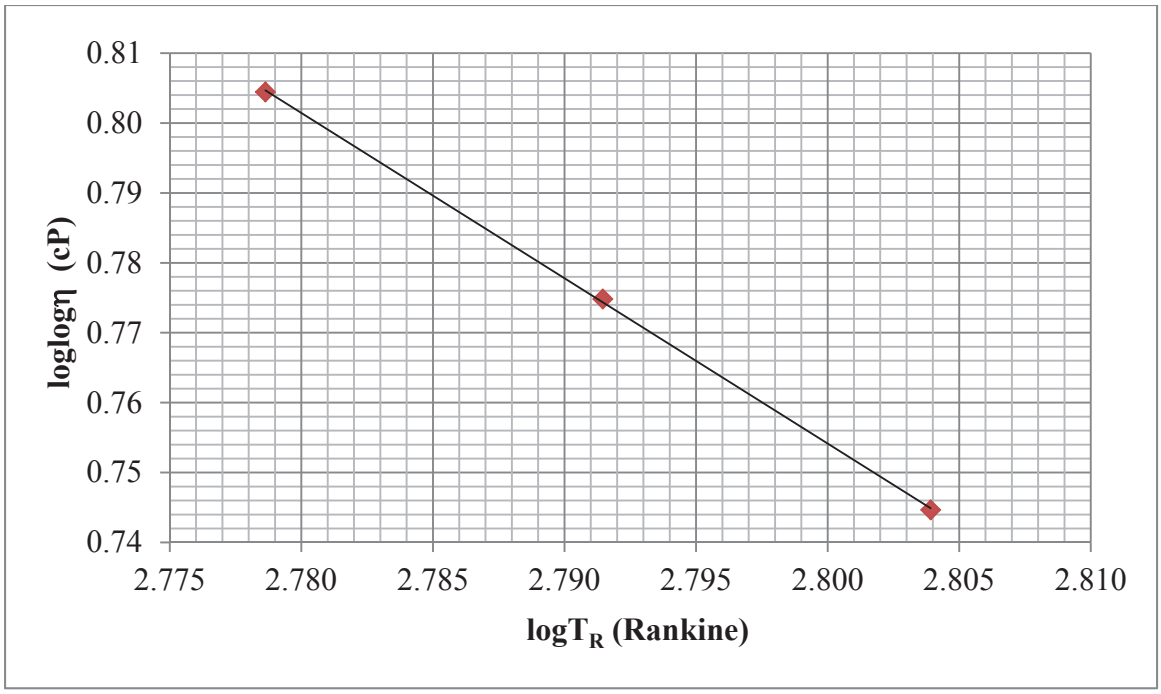

Figure 3.13 Example A-VTS relationship

A relatively convenient method for determining the asphalt binder viscosity can be conducted using the dynamic shear rheometer (DSR) following ASSHTO T315 (AASHTO, 2012) and inputting the results into Equation 3.21 (Witczak, 2005).

$$\eta = \frac{G^*}{10}\left(\frac{1}{\sin\delta}\right)^{4.8628} = \frac{G^*}{10}\left(\frac{1}{\sin\delta}\right)^{4.8628} \qquad \textbf{Equation 3.21}$$

where, : η - viscosity of the binder, cP;
G^*- binder complex shear modulus, Pa;
δ - phase angle of binder complex shear modulus, degrees;
10 - represents the testing frequency of 10 rad/s.

Thus the relationship for the shift factors (a_T) from the A-VTS method takes the form of Equation 3.22.

$$\log a_T = c\left(10^{[A+VTS\log T]} - 10^{[A+VTS\log T_R]}\right)$$ **Equation 3.22**

where, : a_T - shift factor as a function of temperature, T;
c - fitting coefficients;

Second-Order Polynomial Shift Function

The other shift function available in AASHTO PP62 (AASHTO, 2012) is the second-order polynomial. While other polynomial functions of different exponential orders may be used AASHTO PP62 recommends the second-order function shown in Equation 3.23. The relationship for the shift factors, a_T, from the second-order polynomial function takes the form of Equation 3.24 (Witczak, 2005).

$$log f_r = \log f + a_1(T_R - T) + a_2(T_R - T)^2$$ **Equation 3.23**

where, : f_r - reduced or shifted frequency, Hz.;
f - loading frequency at the test temperature, Hz.;
a_1, a_2 - fitting coefficients;
T_R - reference temperature in Rankin, °R;
T - test temperature of interest in °R.

$$\log a_T = aT^2 + bT + c$$ **Equation 3.24**

where, : a_T - shift factor as a function of temperature, T;
a, b, c - fitting coefficients;
T - test temperature of interest in °F or °R.

Arrhenius Shift Function

AASHTO PP61 utilizes data from AASHTO TP79 (AASHTO, 2012) following the AMPT method to fit the modified symmetric sigmoidal function presented in Equation 3.4 by conducting the shifting with an Arrhenius function presented in Equation 3.25.

Thus the relationship for the shift factors, a_T, from the Arrhenius function takes the form of Equation 3.26.

$$log f_r = \log f + \frac{\Delta E_a}{19.14714}\left(\frac{1}{T} - \frac{1}{T_r}\right) = \log f + \frac{\Delta E_a}{R(\ln 10)}\left(\frac{1}{T} - \frac{1}{T_r}\right) \qquad \textbf{Equation 3.25}$$

where, : f_r - reduced or shifted frequency, Hz.;
f - loading frequency at the test temperature, Hz.;
ΔE_a - activation energy, here treated as a fitting coefficient;
T - test temperature of interest in °K. Kelvin;
T_R - reference temperature, °K;
R - ideal gas constant, 8.314 J/(°K mol).

$$\log a_T = \frac{\Delta E_a}{19.14714}\left(\frac{1}{T} - \frac{1}{T_r}\right) = \frac{\Delta E_a}{R(\ln 10)}\left(\frac{1}{T} - \frac{1}{T_r}\right) \qquad \textbf{Equation 3.26}$$

It should be noted that the Arrhenius form should only be considered for low-viscosity fluids or when the temperatures for the material of interest are above $T > T_g + 100°K$ (Mezger, 2011.). However, others have reported the usage of Arrhenius at much colder temperatures, even below T_g (Rowe et al., 2009).

Williams, Landel, and Ferry Shift Function

One of the more classic shift functions commonly used for the shifting of rheological data is typically referenced by the original authors' names Williams, Landel, and Ferry or the WLF equation (Williams et al., 1955). This function as depicted in Equation 3.27, has been commonly used and is generally viewed as an empirical relationship.

$$\log a_T = \frac{-c_1(T - T_g)}{c_2 + (T - T_g)} \qquad \textbf{Equation 3.27}$$

where, : a_T - shift factor as a function of temperature, T;
c_1, c_2 - fitting coefficients;
T - test temperature of interest, °C, valid for $T_g < T < T_g + 100°C$;
T_g - glassy transition temperature often taken as the reference temp., °C.

However, the original WLF manuscript based upon polymer materials, as well as others (Ferry, 1980), have suggested that the fitting parameters are related to the fractional free volume of the molecular structure of the material at hand. Recognizing that free molecular volume is not easy to measure, the parameters are typically used as fitting coefficients. However, it has been suggested that c_1 determines the location of the inflection point and the c_2 parameter can be an indication of the temperature susceptibility of a binder, which also increases with binder aging (Rowe, 2012; and Yusoff et al., 2011). It has also been noted that the WLF relationship is valid for temperatures near T_g to $T_g + 100°K$ (Rowe et al., 2009).

Kaelble Shift Function

As a result of often questionable shifting at lower temperatures with the WLF function, a slight modification made by adding the absolute value of the temperature difference in the denominator of the WLF function has been proposed (Kaelble, 1985) and is presented by Equation 3.28.

$$\log a_T = \frac{-c_1(T - T_g)}{c_2 + |T - T_g|} = \frac{-c_1(T - T_d)}{c_2 + |T - T_d|} \qquad \textbf{Equation 3.28}$$

where, : a_T - shift factor as a function of temperature, T;
c_1, c_2 - fitting coefficients;
T - test temperature of interest, °C, valid for $T_g < T < T_g + 100°C$;
T_g - glassy transition temperature often taken as the reference temp., °C.
T_d - defining temperature °C.

However, the form referencing T_g specifically requires that the inflection point of the sigmoidal function described by Kaelble must occur at the glass transition temperature (Rowe et al., 2009). Thus, it may be more appropriate to consider the right hand version of Equation 3.28 and replace T_g with a defining temperature noted as T_d (Rowe and Sharrock, 2011). However, this still requires that the defining temperature, T_d, and the reference temperature be the same. This occurrence may be negated by introducing another term to separate the defining and reference temperature (Rowe and Sharrock, 2011) as presented in Equation 3.29.

$$\log a_T = -c_1 \left(\frac{T - T_d}{c_2 + |T - T_d|} - \frac{T_r - T_d}{c_2 + |T_r - T_d|} \right) \qquad \textbf{Equation 3.29}$$

where, : a_T - shift factor as a function of temperature, T;
c_1, c_2 - fitting coefficients;
T - test temperature of interest, °C or °K;
T_g - glassy transition temperature;
T_d.- defining temperature, sets the location of the inflection point in the shift function.

The ability to distinguish between the shape defining term and the reference temperature term, makes the modified Kaelble function more useful when shifting data at both above and below the glassy transition temperatures.

A graphical example of the differences between the Arrhenius, WLF, and Kaelble shift functions was provided by Rowe, Baumgardner, and Sharrock (Rowe et al., 2009) and is presented in Figure 3.14.

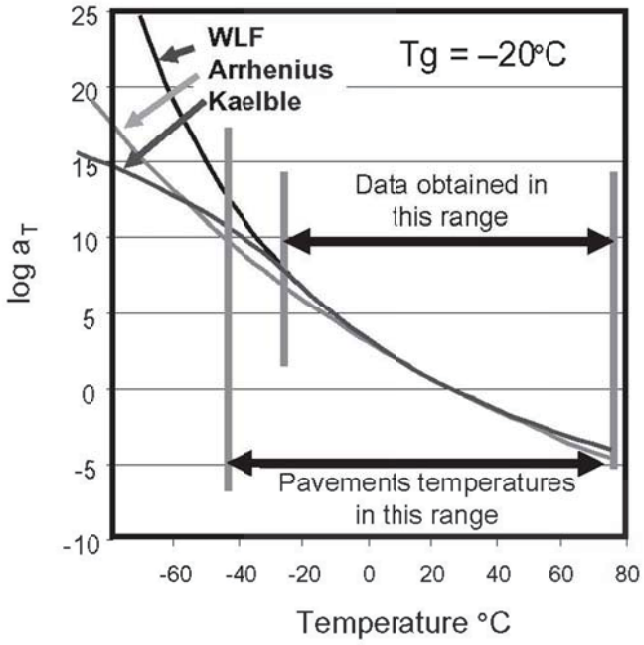

Figure 3.14 Example Common Shift Functions (Rowe et al., 2009)

Log-Linear Shift Function

The log-linear shift function is one that has been proposed but has not seen as wide of usage as the previous methods discussed, but still has seen some applicability to asphalt

mixtures (Yusoff et al., 2011). However, due to its simplicity it will be briefly described as presented in Equation 3.30.

$$\log a_T\left(\frac{T}{T_r}\right) = \beta(T - T_r) \qquad \textbf{Equation 3.30}$$

where, : a_T - shift factor as a function of temperature, T;
β - slope of linear relationship between $\log a_T$ and temperature;
T - test temperature of interest, °C or °K;
T_r.- reference temperature.

Selected Master Curve Forms

Of all the methods discussed in this section, this study largely utilized the symmetric sigmoidal and the 2S2P1D functions fitted to the measured dynamic modulus data discussed in later sections. The shifting for the symmetric sigmoidal form typically followed the second-order polynomial shift function as did the fitting of the 2S2P1D master curves. Even though the Kaelble shift function is recommended due to the increase in fitting capability, it was deemed not necessary for this research largely due to the lack of measurement above and below the glassy transition temperature.

3.1.3 Uniaxial Thermal Stress Specimen Test

The Uniaxial Thermal Stress Specimen Test (UTSST) has recently been developed at the Pavements/Materials program of the University of Nevada, Reno in collaboration with the University of Wisconsin-Madison (UWM). Strictly speaking, a separate method is being developed at each university with the collaboration yielding a single proposed AASHTO test method. The UWM method, known commonly as the Asphalt Thermal

Cracking Analyzer (ATCA) uses a slightly different sample and preparation method along with minor differences in the test protocol as described by Method B in the most current proposed method found in Appendix A. In general, the UTSST and the ATCA methods produce comparative data and thus the calculation methods may be applied to both methods. The UTSST will be presented followed by a discussion of the data analysis.

The origin of the UTSST method stems from the Thermal Stress Restrained Specimen Test (TSRST) (AASHTO, 1995). The TSRST test was originally developed as a part of Strategic Highway Research Program (Jung and Vinson, 1994). In the TSRST, an asphalt mixture specimen is started at an initial temperature, typically five or 20°C, then subjected to a temperature drop until fracture while the height of the specimen is kept constant. The TSRST test has been successfully utilized in pavement research to evaluate low temperature cracking properties of asphalt mixtures through measurements of fracture stress and fracture temperature. The TSRST test method had been initially published as AASHTO standard TP10. However, it has since been dropped from the current AASHTO standards, but recently has been included in European standard to characterize asphalt mixtures for thermal cracking resistance EN12697-46 (European Standard, 2012).

TSRST tests conducted over many years at the University of Nevada, Reno led to the observation that the thermal stress build-up often varied between replicate samples of the same asphalt mixture with prismatic specimens while the variability of the test results, both the fracture stress and temperature, were at an acceptable level. In order to proceed with viable calculations of a modulus value and other thermo-viscoelastic properties of

the asphalt mixtures, the thermal stress and strain development curves needed to be highly repeatable between replicates of a given mixture. After a lengthy investigation into sample geometry, preparation methods, epoxy type selection, and gluing techniques, the final recommended test procedure outlined in Method A of the draft AASHTO procedure was developed and is listed in Appendix A.

The use of cylindrical specimens from Superpave gyratory-compacted (SGC) mixtures were found to improve the repeatability of thermal stress and strain development curves as a function of temperature when compared to prismatic specimens traditionally used in the TSRST. It should be clearly noted that the ability to conduct the TSRST method on either prismatic or cylindrical specimen was supported by previous researchers (Jung and Vinson, 1994; Marasteanu et al., 2007). The SGC method of compaction was sought in order to reduce the overall variability of the mixture volumetrics, specifically the bulk air void content. By compacting the mixtures volumetrically, i.e. to a specific height, much better control over the overall air void level and much more repeatable sample production is possible compared to previously used compaction methods, i.e. beam specimens from modified kneading compactors.

In order to maintain consistency with actual field conditions, cored specimens for the UTSST were cut from the SGC samples perpendicular to the axis of compaction as depicted in Figure 3.15 (Cortez et al., 2011). This was supported by several studies clearly demonstrating the anisotropic nature of compacted asphalt mixtures (Zhang et al. 2012; Wagoner and Braham, 2008; Christensen and Bonaquist, 2004). This effort was further supported by the practical fact that asphalt mixtures placed in the field are

compacted in the vertical direction, but the expected geometry of a developed thermal crack will be a horizontal separation, i.e. perpendicular to the axis of compaction.

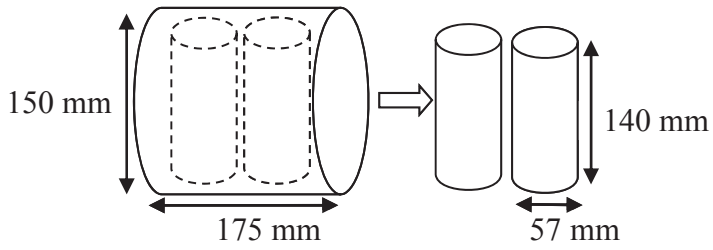

Figure 3.15 UTSST Specimen Geometry

Stemming from the change in geometry of the TSRST specimens, a significant effort was put forth to assure the proper alignment of the specimen, platens, and loading frame during the TSRST and subsequently the UTSST procedures. The end result of several modifications on a trial and error basis yielded the positive pedestal machined into the end platens as depicted in the draft AASHTO standard and Figure 3.16.

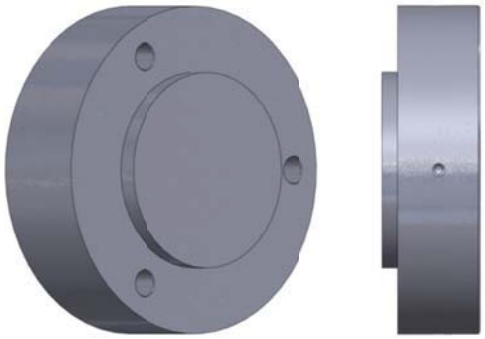

Figure 3.16 UTSST Platen Geometry

The platen modification, when coupled with the additional axis alignment modification to the gluing jig and procedure, produced UTSST specimens with attached load patens that were satisfactorily in axial alignment. The modification to the gluing jig included additional axial restraints to limit the lateral movement noted with threaded connections on the current connecting rod used to fix the bottom platen. An additional restraint was added to the top connecting rod similarly to prevent lateral displacement even though this rod was manufactured with a smooth shaft and associated bushing. Further, refinement was added by means of lateral contact plates (i.e. hinges fixed to the back of the jig that the restraint screws pressed upon), to provide a larger bearing surface to restrain the cylindrical specimen during gluing. These modifications are outlined in Figure 3.17.

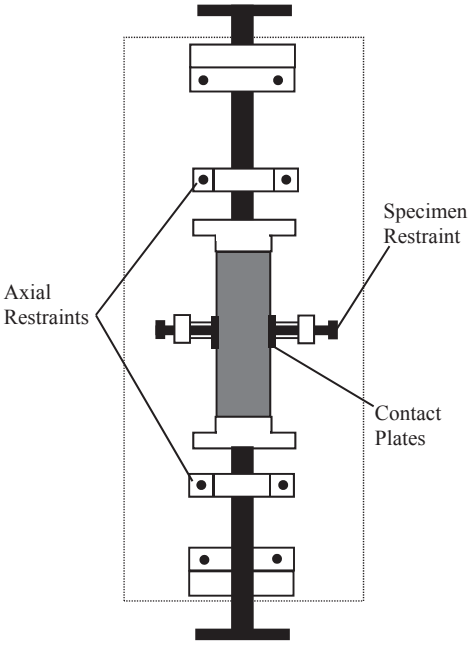

Figure 3.17 Modified UTSST Restrained Specimen Gluing Jig

A significant improvement to the previous TSRST method was the addition of a modular feature allowing the direct measurement of the resulting thermal strain developed within an unrestrained specimen concurrently with the stress development measurements from the restrained specimen during the temperature reduction or thermal loading of the test. The unrestrained specimen was constructed of two 57 mm diameter cylindrical specimens glued together using a thin layer of an appropriate epoxy, Devcon® 10110. The two specimens were chosen to have similar volumetric properties and physical dimensions and thus act nearly as one uniform specimen. The two specimens were fixed, end to end, to provide a longer gauge length for the unrestrained specimen adding to the reliability of the measurement while permitting the sample compaction using the SGC and perpendicular specimen coring as previously discussed. The retention of the same specimen geometry as the restrained specimen was a matter of convenience for the preparation time and equipment as well as to provide the same physical properties as the restrained specimen, which is an important characteristic to maintain for later calculations.

As part of the development of the unrestrained specimen, it became apparent that the location of the measurements, i.e. location of the linear variable differential transformers (LVDTs), may potentially influence the measurements. This was found to be the result of a limited temperature range of commonly available LVDTs. Other measurement devices were also investigated, such as clip gauges and extensometers. However, the appropriate thermal range of those devices did not readily prove sufficient either. As a result, it was determined to be advantageous to perform the unrestrained measurements outside of the temperature controlled chamber as depicted in Figure 3.18.

To physically be able to place the LVDTs outside the temperature chamber, extension rods were affixed to the outer ends of the unrestrained conglomerate specimen. These rods were specifically manufactured out of invar, a high-nickel steel, resulting in a thermally stable material, i.e. low coefficient of thermal expansion/contraction. The invar rods were attached to the unrestrained specimen with the same epoxy utilized throughout the remainder of the UTSST procedure. A separate gluing jig for the unrestrained specimen was also designed specifically for this purpose and is shown schematically in Figure 3.19.

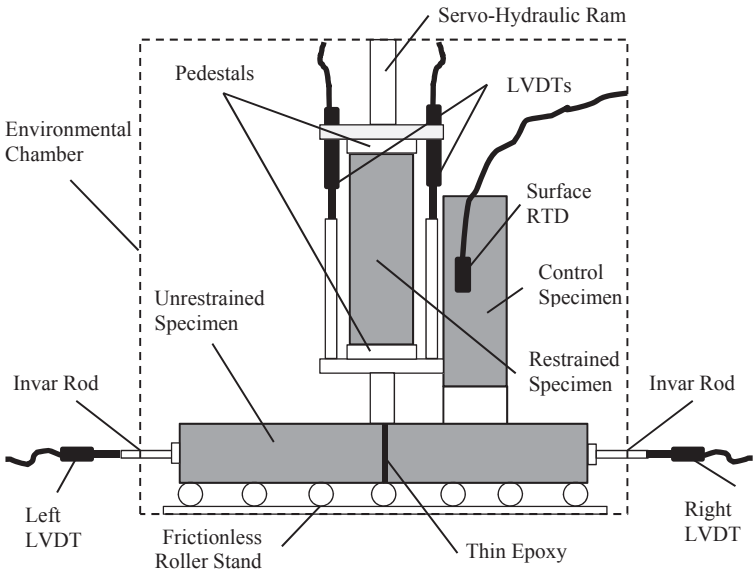

Figure 3.18 Schematic of Uniaxial Thermal Stress and Strain Test (UTSST)

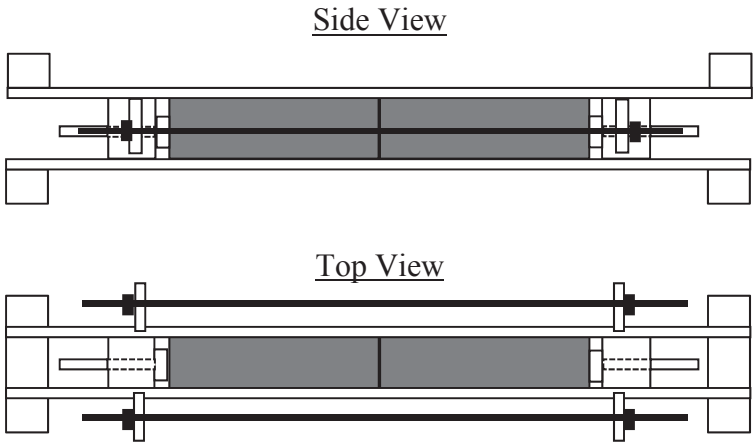

Figure 3.19 UTSST Unrestrained Specimen Gluing Jig

During the execution of the UTSST, the restrained specimen is restricted from movement as determined through the associated LVDTs which are held to a zero net displacement by the measured load applied by the servo-hydraulically controlled ram. Concurrently, the LVDTs mounted outside the chamber and in direct contact with the unrestrained specimen record the deflection from both ends of the unrestrained specimen. The environmental control unit is set to the desired rate of temperature reduction of 10°C per hour in this study. The internal specimen temperature determined by recording the temperature at the surface of the control specimen using a surface resistance temperature detector (RTD) temperature probe as depicted in Figure 3.18.

Previous thermally controlled measures of this type often utilize temperature measurements from the interior or center of control or dummy specimens. During the development of the current procedure, it was realized that such measurements may not be the most appropriate for such loading conditions. It stands to reason, similar to the UTSST procedure that the actual initiation of a thermal crack occurs at or very near the

surface of the pavement and consequently the outer surface of UTSST specimen. Several factors contribute to this conclusion including consideration of the thermal loading as a function of depth in a pavement section. It is generally understood that the largest temperature fluctuation occurs at the interface between the pavement and ambient atmosphere, i.e. the pavement surface. Since it is either the low overall temperature or large fluctuations in temperature that induce the highest thermal loading, it is logical to deduce that thermal cracks initiate at the pavement surface which corresponds to the surface of the UTSST specimen. Therefore, the change in temperature near the expected point of failure should be determined at that location as well. Further, the temperature difference, or lag, between the actual chamber temperature, control specimen surface temperature, and the center of a control specimen varies with the cooling rate. Typical measures in the laboratory vary from almost no lag for a cooling rate of 2.5°C/hr., up to almost 2 to 2.5°C for a rate of 17.5°C/hr., with a common temperature lag of about 0.3 to 0.6°C for a cooling rate of 10°C/hr.

It has been stated that a potential concern with TSRST and thus UTSST methods is that the fracture of the restrained specimen ideally should occur in the middle of the specimen (Jung and Vinson, 1994; Bolzan and Huber, 1993). Further, some suggest that any fracture outside the middle one-third of the sample length may be suspect and thus may not be considered a valid measurement. While many UTSST specimens do break within the desired middle third of the specimen length as depicted in Figure 3.20. It has also been observed that a significant number of UTSST specimens obtained from SGC specimens do ultimately fracture outside the desired middle third of the specimen as depicted in the Figure 3.21.

Figure 3.20 UTSST Middle Specimen Fracture

Figure 3.21 UTSST Asymmetrical Specimen Fracture

Several aspects specific to the methods of specimen preparation are suspected to contribute to this asymmetrical fracture pattern. The main contributor is suspected to be the non-uniform air void distribution within the parent SGC samples. It has been shown that typical samples compacted by SGC have up five or even ten percent higher air voids

at the top as compared to the bottom of the sample (Masad et al., 1999). Similar, although lesser magnitude, air void differentials were directly measured along the length of UTSST specimens as depicted in Figure 3.22. To clarify, the length dimension of the UTSST specimen would run along the horizontal direction of the SGC sample, i.e. perpendicular to the axis of compaction as in Figure 3.15.

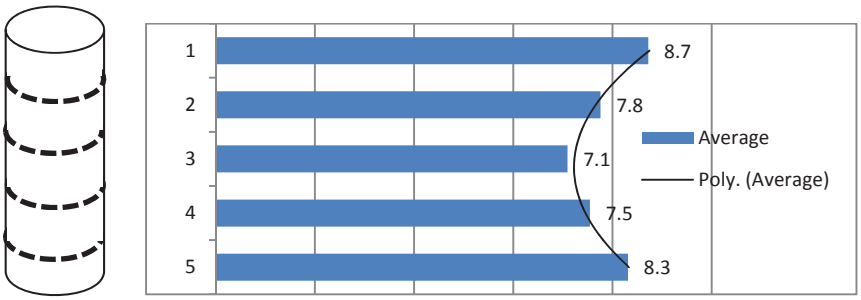

Figure 3.22 Longitudinal Air Void Distribution of UTSST Specimen

As can be seen in Figure 3.22, there is a definite air void gradient between the middle and the ends of the specimen. It is a logical conclusion that the fracture will occur at the weakest location along the longitudinal axis of the UTSST sample. This is likely to occur closer to the ends of the specimen rather than at the center simply as a result of the higher air void content. Simply put, the higher the air void content of a particular cross section, the lower the density leading to a reduction in strength.

Additional justification for the fracture near the end of the specimen could be related to differential aging within the test specimens. This controversial topic will be discussed at length in later sections, however there is a possibility that the material in closer proximity to the exterior of the specimen, in this case the ends of the longitudinal UTSST specimens, will be more oxidized and thus more prone to cracking. To be clear,

this aspect of differential oxidation with pavements depth is arguable, however the potential for such occurrences do exist.

To further validate the compaction and differential aging of the specimens as the potential source of asymmetrical fracture, several UTSST specimens obtained in the perpendicular to compaction from field cores were tested. Although direct comparisons of the same mixtures compacted in the field and in the SGC were not available, all the field cores that were tested (around six specimens) did result in ultimate fracture within the center third of the specimen length.

Due to the increased popularity of the UTSST or even TSRST methods, many new developments in equipment and software are beginning to become available on the open market. Some of the proposed devices have certain aspects which cause concern to both the method and the results produced from such devices. Most of the devices on the market propose to have some sort of closed-loop control system to monitor and adjust to maintain the constant height of the restrained specimen. Whether the system is servo-hydraulic, mechanical step motors, or pneumatic may or may not make a significant difference as long as the data acquisition and adjustments are made in a sufficiently fast and smooth manner to prevent jumps in the measured load of more than a few pounds or kilograms.

To avoid this potential jump in the applied load, some devices have been proposed which do not use a closed loop or controlled restrained specimen setup but rather a fixed or otherwise rigid frame to lock the restrained specimen and thus retain its height. The majority of these types of restraint systems use a load cell between the restrained specimen and the rigid frame to electronically measure the load developed, a necessary

measurement. Concern arises from the usage of such restraint systems due to the fact that a load cell is little more than a calibrated spring following Hooke's law as presented in Equation 3.31.

$$F = K(\delta)$$

Equation 3.31

where, : F - Force or load applied to the load cell;
K - spring constant, essentially the elastic modulus of the load cell;
δ - deflection measured within the load cell.

This requires, by definition, that any load measured in the restrained system must be accompanied by a measured deflection. While most load cells are designed to keep the overall deflection small, there still needs to be some physical displacement. This potential movement becomes an item of concern when measuring the load developed within a restrained specimen such as in UTSST measurements because very small deflections will generally result in significant reductions in the produced load developed by contraction of the mixture. This load reduction may be considered in the analysis as a relaxation or viscous response of the material, when it really is an artifact of the test setup. A simple consideration of the unrestrained or CTC measures indicate very small movements in the system with temperature, such that any movement permitted in the restrained specimen can logically be viewed as misinformation. This does not explicitly state that the closed loop system do not have any deflection themselves, it merely suggests that attempts should be made to limit such deflections as much as possible in all systems.

This realization is attributed, for the most part, to developmental experiments in which a threaded pedestal was added as a matter of convenience between the restrained specimen and the load platens. Referencing Figure 3.16, the external pedestals were attached to the load platens, and thus to the constant height LVDTs, through a threaded connection. This threaded connection was initially torqued to very tight levels, though not to measurable amounts with a pipe wrench. When a sample was glued and tested in the UTSST setup, enough deflection resulted from the threaded connections that the sample did not fracture. The same mixture was previously determined to fracture at approximately -22°C, but the test with the threaded connections did not fracture even when the temperature was reduced below -40°C. These measures led to the conclusion that very small deflections can yield sufficient relaxation of the stress, which can significantly affect the overall response of the restrained specimen.

Additional caution is advised when testing cooling rates that are too far above practical pavement temperature drops. Although a matter of great convenience, applying cooling rates that are too fast may not permit the mixture to behave appropriately (Bolzan and Huber, 1993). After much study and consideration of the UTSST results, the test conditions can be simplified to the basic idea of competing effects between the thermal contraction and relaxation of the mixture over time. The cooling rate effectively applies the thermal loading to the restrained specimen, while at the same time the mixture itself will relax those same induced stresses. Under a slow enough cooling rate a tremendous amount of thermal contraction can be expected to relax out of the specimen. Of course, this is dependent upon the actual temperature, with less relaxation occurring at colder temperatures especially below the glassy transition temperature (T_g). Considering the

opposite end of the spectrum, too high of cooling rates would artificially reduce the effects of relaxation with the thermal contraction quickly becoming the dominant response.

A secondary concern specific to overly fast cooling rates is to consider the thermal gradient within the sample itself. It is understood that the restrained specimen is cooled based on thermal conduction, i.e. being in direct contact with the temperature conditioned air within the cooling chamber. This necessitates that the surface of the specimen will be cooled faster than the interior, which is also dependent upon the thermal conductive properties of the mixture relative to the cooling rate applied. If extreme cooling rates are applied without considering these effects or verifying the validity of the results, the resulting calculations may be unknowingly skewed. Further consideration of cooling rates on UTSST results have been considered as part of this overall research effort and are discussed elsewhere (Alavi et al., 2013; Hajj et al., 2013; Morian et al., 2014; Alavi and Hajj, 2014).

UTSST Calculation and Data Processing

While the UTSST is being conducted, the data acquisition system records; (at regular intervals over the test duration) ram displacement, applied load, displacement of the restrained LVDTs, displacement of both unrestrained LVDTs, and the temperature of the surface RTD on the control specimen. These measures are directly input into the data analysis and calculation methods that follow. This calculation procedure and further background information has been published elsewhere with the expressed

acknowledgement of the contribution of Zia Alavi (Alavi et al., 2013; Hajj et al., 2013; Morian et al., 2014; Alavi and Hajj, 2014).

The measured thermally-induced stress in the UTSST restrained specimen can be related to the corresponding measured strain in the unrestrained specimen using the uniaxial constitutive equation for linear viscoelastic materials, i.e., Boltzmann equation (Christensen, 2003). The Boltzmann equation can be written in terms of thermal stress, thermal strain, and the UTSST modulus as in Equation 3.32. In the discrete form, Boltzmann's superposition integral can be written as depicted in Equation 3.33.

$$\sigma(t) = \int_0^t E_r(t - t') \frac{\partial \varepsilon(t')}{\partial t'} dt' \qquad \textbf{Equation 3.32}$$

where, : $\sigma(t)$ - thermal stress;
$E_r(t)$ - relaxation modulus;
$\varepsilon(t)$ - thermal strain;
t'.- variable of integration.

$$\sigma(t_n) = \sum_{i=1}^{n} E(t_n - t_i) \times (\varepsilon(t_i) - \varepsilon(t_{i-1})) \qquad \textbf{Equation 3.33}$$

where, : n - time index;
$\sigma(t_0)$ - initial stress condition, set to zero;
$\varepsilon(t_0)$ - initial strain condition, set to zero.

By considering the synchronized measurements of thermal stress and thermal strain, the UTSST modulus at each temperature can be derived from the discrete form of Boltzmann's superposition principle according to Equation 3.34.

$$E(T(t_n)) = \frac{\left(\sigma(t_{n+1}) - \sum_{i=2}^{n+1} E(t_{n+1} - t_i)\left(\varepsilon(t_i) - \varepsilon(t_{i-1})\right)\right)}{\varepsilon(t_1)} \qquad \textbf{Equation 3.34}$$

Figure 3.23(a) presents an example of the UTSST modulus curve derived from the thermal stress and strain measurements of an asphalt mixture based on Equation 3.34. The modulus of the mixture as a function of temperature follows similar trends as that of linear amorphous polymer materials, as depicted in Figure 3.23(b). Five characteristic stages were defined based on the response of the calculated modulus as a function of temperature for amorphous polymeric materials. Those stages are: glassy, glassy transition, rubbery, rubbery flow and liquid flow stages (Sperling, 2006).

From Figure 3.23, it can be readily observed that the characteristic shape of the asphalt mixture, Figure 3.23(a), closely resembles that of the polymer, Figure 3.23(b). There are some noted differences between the two, mostly near the limits of the data in each case. It appears from the figure that the polymer was not tested to complete failure, or much past the onset of the glassy response. On the other hand, the asphalt mixture exhibits another region which is related to crack initiation within the asphalt specimen as the testing progresses toward ultimate fracture and failure of the sample. Furthermore, due to the physical limitations of the material, the asphalt mixtures were not fully characterized in the region known as liquid flow for the polymer. Due to these slight discrepancies and the fundamental differences between homogeneous materials (i.e. polymers) and heterogeneous (i.e. asphalt mixtures) the characteristic points of the modulus as a function of temperature curve have been renamed to the five properties noted in Figure 3.23(a) discussed below. Figure 3.24 presents an example of the

measured thermal stress and strain during the UTSST. Figure 3.25 identifies the various characteristic properties of the thermal relaxation modulus derived from those measures.

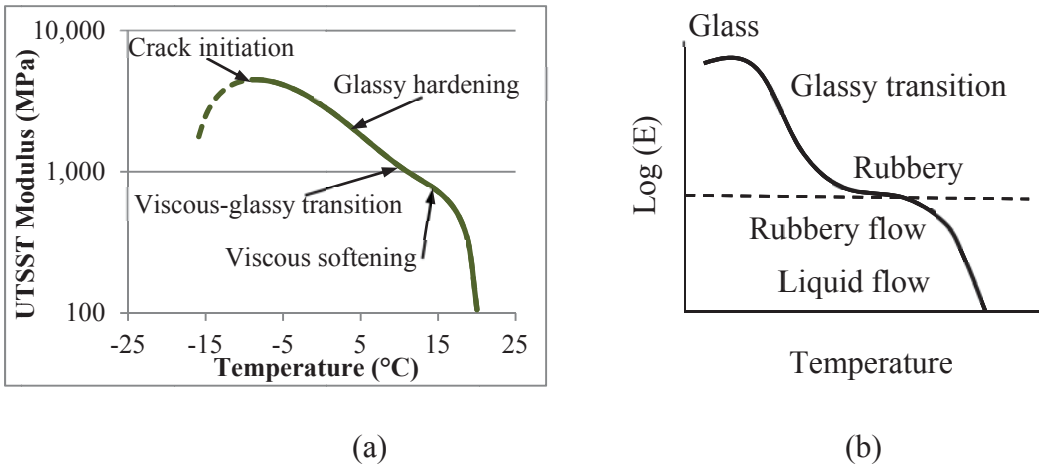

Figure 3.23 (a) Example UTSST Modulus of an Asphalt Mixture and (b) Typical Modulus-Temperature Curve for Linear Amorphous Polymer

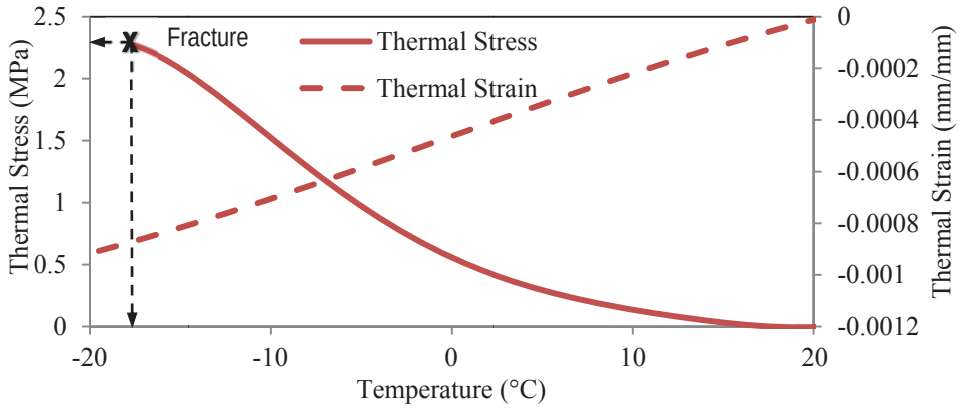

Figure 3.24 Example of Stress and Strain Measured During UTSST

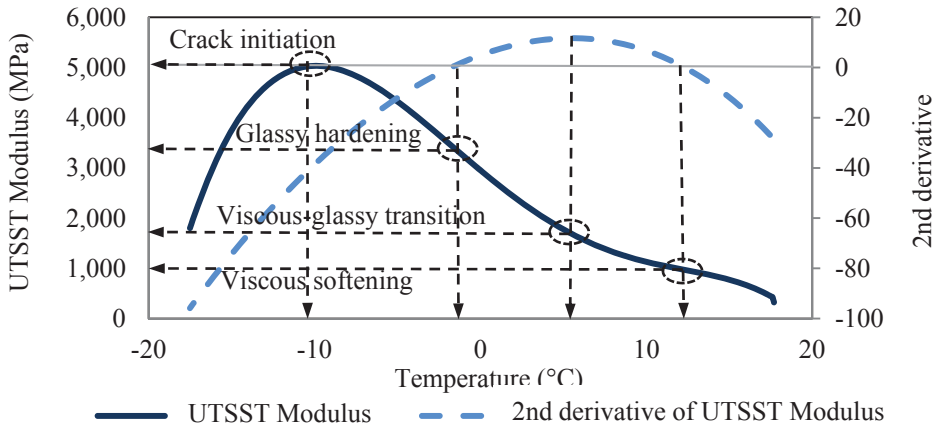

Figure 3.25 Example of Derived UTSST Modulus

After conducting the UTSST procedure and performing the associated calculations, a plot of the UTSST modulus as a function of temperature can be prepared as shown in Figure 3.25. Considering the second derivative of that relationship yields further information including the thermo-viscoelastic properties also depicted in Figure 3.25. Those five properties are determined as discussed in the following sections.

- **Viscous Softening:** At this stage the UTSST modulus of the asphalt mixture increases rapidly, mostly in a linear fashion, with decreasing temperature. The point of viscous flow can be identified as the temperature at which the second derivative of the UTSST modulus with respect to temperature reaches zero on the warmer temperature side.
- **Viscous-glassy Transition:** At this stage the glassy properties of the material become more dominant over the viscous properties. The transition stage can be detected as the point at which the second derivative of the UTSST modulus with respect to temperature reaches a maximum.

- **Glassy hardening:** At this stage the behavior of the asphalt material is almost completely glassy. The glassy hardening stage can be identified as the point at which the second derivative of UTSST modulus with respect to temperature reaches zero on the colder temperature side.
- **Crack initiation:** In this stage micro cracking occurs in the specimen due to the induced thermal stresses when the material behavior is glassy or brittle. This stage is identified as the maximum value of the UTSST modulus as seen in Figure 3.25. An instantaneous decrease in the calculated UTSST modulus reveals that the asphalt mixture specimen is no longer uniform as a result of initiation of micro cracks in the specimen, i.e. discontinuities with in the cross section of the specimen.
- **Fracture:** At this stage the asphalt mixture specimen breaks due to the propagation of micro cracks as a result of the induced thermal stresses as depicted in Figure 3.24 and Figure 3.25. It should be noted that other researchers have also observed that mixture failures in the TSRST do not always exhibit clear brittle fracture (Pucci et al., 2004). They observed a reduction in the slope of thermal stress curve prior to ultimate fracture. This behavior was referred to as the initiation of micro cracks.

Further discussion on the specific interpretation of the thermo-viscoelastic properties measured utilizing the UTSST will be reserved for the relevant portions of the test results and data analyses sections.

3.2 Asphalt Binder Characterization Procedures

Similar to the varied techniques used to characterize the asphalt mixtures, testing methodologies for the asphalt binder characterization also exhibit different forms and functions for distinctly different purposes. In this study, the physical properties of the asphalt binders are categorically limited to stiffness measures, while chemical characterization included portions of composition as well as information on the chemical structure of the asphalt binders.

The asphalt binder stiffness has been characterized by the dynamic shear modulus (G^*) as opposed to dynamic modulus measures (E^*) conducted on the mixtures. These measures were likewise combined into shear modulus master curves that enabled the calculation of the low shear viscosity (LSV) values.

The chemical characterization included measurements of the composition of the asphalt binder, i.e. binder component separations based upon the molecular weight, molecular polarity, and/or adsorption characteristics of the fractions, as well as quantification of the changes in certain functional groups apparent through Fourier-Transform Infrared (FT-IR) Spectroscopy determinations. On a limited basis, certain materials were examined for specific elemental components to provide a background upon which many of the comparisons in this study are founded.

3.2.1 Dynamic Shear Modulus

Dynamic shear modulus (G*) measures were conducted using the dynamic shear rheometer (DSR) as generally outlined in AASHTO T315 (AASHTO, 2013). The measurements were conducted utilizing parallel plate geometry as is the standard of practice for asphalt binder testing in the industry. A schematic of the parallel plate geometry and functional operation of the DSR is presented in Figure 3.26.

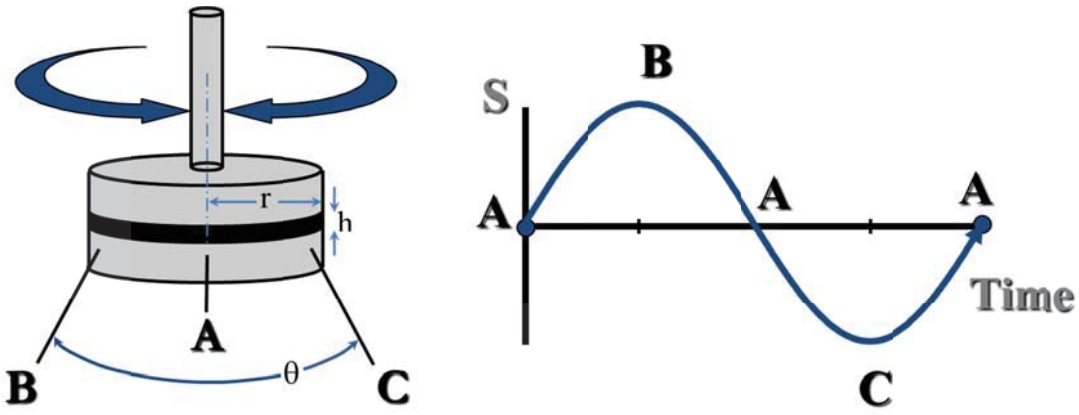

(a) (b)

Figure 3.26 (a) Dynamic Shear Rheometer Parallel Plate Geometry and (b) Parallel Plate Spindle Location

During the operation of the DSR, the bottom plate remains in a fixed position, while the top plate begins at position A, progresses to location B, then back to location A. From there the top plate continues in the same direction to position C, then back to the original position A. This action would complete one oscillatory cycle of the parallel plate geometry with the angle of displacement (θ) being determined by the preset shear strain value. As depicted in Figure 3.26(b) the speed of rotation is adjusted such that the

rotational displacement (S) occurs in a sinusoidal fashion. The overall speed or time for one full oscillation is described by the test frequency either in cycles per second (Hz) or radians per second (ω).

Further consideration of the DSR results requires the calculation of the shear stress (τ) and shear strain (γ). These are determined as shown in Figure 3.26(a) and by Equation 3.37 and Equation 3.36, respectively (SP-1, 1994).

$$\tau = \frac{2T}{\pi r^3}$$ **Equation 3.35**

where, τ - shear stress, kPa;
T - maximum applied torque on spindle;
r - plate radius, mm.

$$\gamma = \frac{\theta r}{h}$$ **Equation 3.36**

where, γ - shear strain;
θ - rotation angle of spindle, radians;
h - specimen height, mm.

In a manner very similar to the dynamic modulus (E^*) in the complex domain, the dynamic shear modulus (G^*) is represented by Equation 3.37 below.

$$G^* = \frac{\tau_0 \sin \omega t}{\gamma_0 \sin(\omega t - \delta)} = |G^*|(\cos\delta + i \sin\delta) = G' + iG''$$ **Equation 3.37**

where, G* - complex dynamic shear modulus, kPa;
τ_0 - maximum amplitude of stress, kPa;
γ_0 - maximum amplitude of strain;
ω - angular frequency, Hz or rad/s;
δ - phase angle, degrees;
t - time; sec.;
i - complex number, $i = \sqrt{-1}$;
G' - storage or elastic shear modulus, kPa;
G" - loss or viscous shear modulus, kPa.

Commonly, the absolute value of complex modulus, |G*|, is reported and utilized rather than the full complex form. Mathematically, |G*| is calculated as presented in Equation 3.38 with the accompanying phase angle calculated as depicted in Equation 3.39.

$$|G^*| = \frac{\tau_0}{\gamma_0} = \frac{2hT}{\pi r^4 \theta}$$ **Equation 3.38**

$$\delta = \tan^{-1}\frac{G''}{G'}$$ **Equation 3.39**

A common form of graphical representation displaying the contribution of G' and G" to G^* is depicted by the vector addition shown in Figure 3.27.

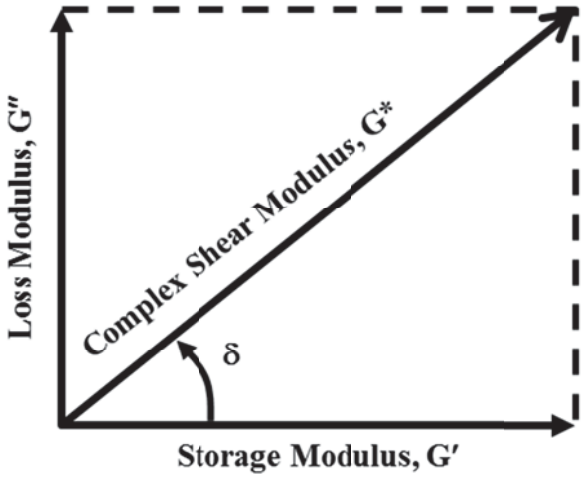

Figure 3.27 Vector Diagram of Dynamic Modulus Values

Similar to AASHTO T315, two parallel plate dimensions were used during the DSR measures for the majority of this study, namely 25 and 8 mm for high and intermediate temperatures, respectively. Contrary to AASHTO T315 method, the DSR measures were

not solely conducted with a loading frequency of 10 rad/sec. In fact, each binder was tested over multiple frequencies as well as temperatures. However, the shear strain was kept at a low value of 1 percent for all testing to presumably stay well within the linear viscoelastic (LVE) range of the binder. Multiple samples were tested to verify the testing was within the LVE range, but practical limitations prevented each binder at each condition from being verified.

The testing temperatures varied according to the binder grade or stiffness of the binder and was adjusted depending upon whether or not the binder was polymer modified or not. Although not every binder investigated was tested at all temperatures, the test conditions utilized are presented in Table 3.2. More specific information on each of the evaluated binders and their respective protocols will be included in the results section.

Table 3.2 Dynamic Shear Rheometer Test Conditions

DSR Test Temperature, °C	Parallel Plate Diameter, mm	Gap Setting, mm	Tested Frequencies, Hz	Tested Frequencies, rad/s	Data Points per Decade
85, 95, 100	25	0.5	0.00159-15.9	0.01-100	2.25
52, 60, 64, 70, 80	25	1.0	0.00159-15.9	0.01-100	2.25
46, 40, 34, 28, 22, 16	8	2.0	0.1-100	0.628-628	10

3.2.2 Shear Modulus Master Curves

Even though the last section showed the form of dynamic shear modulus measures closely follow a similar mathematical form and similar rheological comparisons can be made with either E^* or G^*, much less effort has been expended on binder master curves of G^*. This is not at all to suggest that research has not been conducted and methodologies have not been developed, but specifically to point out that asphalt binder master curve development has not experienced the refining efforts that the comparative mixtures have undergone. As such, no set AASHTO or ASTM standard exists comparable to what have been published for E^* measures. As a result, binder master curves are developed in a more research oriented fashion, thus requiring an approach on a much more investigative basis and less procedural or standardized testing.

Nonetheless, even when there are not strict standards for testing protocol there are established models commonly utilized from the calculation and development of the binder master curves. Largely due to the overall similarities in the form of the data, nearly all the E^* master curve models previously discussed may also be applied to G^* master curve construction efforts. To summarize, the following master curve models may also be applicable to binder master curves:

- Standard logistic sigmoidal form, Equation 3.4 and Equation 3.5;
- Nonsymmetrical sigmoidal form, Equation 3.6;
- 2S2P1D model, Equation 3.7; and
- Christensen-Anderson or variations, Equation 3.13
- Prony series, Equation 3.17 and Equation 3.18

This summary is by no means a complete or exhaustive list, but is focused more on the different forms of models used as well as those most commonly used.

Similar to the master curve models being for the most part common between the mixture and binder measurements, the majority of the shift functions are commonly used for binder measurements as well. A summary of those already discussed in the E* section are as follows:

- A-VTS shifting, is essentially mixture shifting based upon the viscosity-temperature susceptibility of the binder, Equation 3.22;
- 2nd order polynomial, Equation 3.24;
- Arrhenius, Equation 3.26;
- WLF, Equation 3.27;
- the original Kaelble, Equation 3.28;
- the modified Kaelble, Equation 3.29, and
- limited usage of the log-linear shift function, Equation 3.30.

Certainly, each of these have been used and are deemed acceptable for some data sets and materials, while others may not be as appropriate for certain measurement conditions. A general procedure that has been readily utilized in a rheological software package (RHEA, 2011) has proven to be quite robust by providing fairly reliable results for a wide variety of rheological data. In the software package RHEA, the shifting is essentially conducted utilizing a procedure detailed by Gordon and Shaw (Gordon and Shaw, 1994). This procedure incorporates several steps of increasing accuracy to the shifting methods

to provide a more thorough shifting technique and an overall improved fit to whatever master curve form and shift function is ultimately chosen.

This procedure has been summarized in the literature (Rowe and Sharrock, 2011), but largely takes place within the software package RHEA and is, for the most part, invisible to the user. However, the method is summarized as follows:

- Each pair of isotherms is initially estimated using a linear fit which is contrasted to a modified WLF equation using the original universal constants. These values are presumably 8.86 and 101.6 for factors c_1 and c_2, respectively from Equation 3.27.
- Those initial shifts are further refined using the benefit of weighted least square polynomial fit calculations. The order of the polynomial and thus some influence on the shape are determined by the number of data points and the frequency range of the measures though an undisclosed proprietary empirical equation.
- The shift factors are produced for each successive pairs of isotherms, which are then numerically subtracted from the shift at T_r. This is done so that the shift factor at T_r becomes the origin and all other temperatures are taken with respect to the reference temperature (T_r).
- The software employs a cubic spline fit for the final shift to T_r.

This method, reportedly (Rowe and Sharrock, 2011) has the advantage of being able to sufficiently shift data sets that do not overlap once the isotherms are shifted. Typically, data sets that do contain such gaps cause difficulties in master curve construction due to

insufficient measures to provide direct fitting comparisons among the isotherms. In the present form, it has been reported that the method utilized in RHEA can overcome gaps in a given data set of up to four decades (Rowe and Sharrock, 2011), which represents a significant gap in the initial measurements.

In the current form of these calculations vertical shifting is not conducted, with the exception of a density correction applied to the modulus values as a function of temperature. The density correction which is widely used in the polymer industry, but is less common in the asphalt community is conducted according to Equation 3.40 which is originally attributed to Rouse (Rouse, 1953).

$$G_r = \frac{T_r \rho_r G_{T,t}}{T \rho_T} \qquad \textbf{Equation 3.40}$$

where, G_r - transient shear modulus at loading time and reference temperature, T_r;
T_r - reference temperature;
ρ_r - material density at the reference temperature;
$G_{T,t}$ - shear modulus at the shifted loading time and measured temperature;
T - temperature of stiffness measurement;
ρ_T - density of material at measurement temperature, T.

3.2.3 Low Shear Viscosity

The concept of low shear viscosity (LSV) which is sometimes referred to as the low shear rate limiting viscosity (Martin et al., 1990; Lau et al., 1992), originated from practical limitations not permitting measurements sufficient to determine the zero shear viscosity (ZSV) (Anderson et al., 2002).

Several methods to determine ZSV or LSV exist in the literature. Certain models, such as the Burgers and Carreau models are traditionally utilized with creep test

measurements as depicted in Equation 3.41 and Equation 3.42, respectively (Biro et al., 2008).

$$\gamma(t) = \frac{\tau_0}{G_0} + \frac{\tau_0}{G_1}\left(1 - e^{\frac{-tG_1}{\eta_1}}\right) + \frac{\tau_0}{\eta_0}t \qquad \textbf{Equation 3.41}$$

where, γ - deformation as a function on time, t;
τ_0 - shear stress;
G_0, G_1 - shear modulus of spring elements;
η_1 - shear viscosity of an individual Maxwell or Kelvin-Voigt element;
η_0 - zero shear viscosity;
t - testing time.

$$\eta^* = \frac{\eta_0 - \eta_\infty}{[1 + (K\omega)^2]^{m/2}} + \eta_\infty \qquad \textbf{Equation 3.42}$$

where, η^* - complex viscosity;
η_0 - first Newtonian viscosity, absolute viscosity;
η_∞ - infinite shear viscosity;
ω - loading frequency, very slow on the order of 4 hour loading time;
K, m - fitted material parameters.

It is clear to see how these viscosity relationships have stemmed from flow curve models commonly used in more traditional rheology measures. For instance, the Carreau model in Equation 3.42 can easily be transferred into the form of a flow curve utilizing rotational shear loading of a specific shear rate, , in a cup and bob or concentric cylinder geometry (Sybilski, 1993; Sybilski, 1996; Mezger, 2011). In these terms the Carreau model takes for the form of Equation 3.43.

$$\eta(\dot{\gamma}) = \frac{\eta_0 - \eta_\infty}{[1 + (c_1\dot{\gamma})^2]^p} + \eta_\infty$$ **Equation 3.43**

where, $\eta(\dot{\gamma})$ - complex viscosity as a function of rotational shear rate, $\dot{\gamma}$;
η_0 - first Newtonian viscosity, absolute viscosity;
η_∞ - infinite shear viscosity;
$\dot{\gamma}$ - shear rate, s^{-1};
c_1 - fitted material parameter, Carreau constant;
p - fitted material parameter, Carreau exponent.

Indeed, there are far too many flow curve viscosity functions of this type to be listed here, thus are likewise left as a reference (Mezger, 2011). However, this form of the viscosity flow curve equation can be represented by Equation 3.44 and as summarized in Table 3.3. Of course, the more variables included in the model, the more complicated but potentially improved fit to the measured data is possible.

$$\eta(\dot{\gamma}) = \frac{\eta_0 - \eta_\infty}{[1 + (c\dot{\gamma})^{p_2}]^{p_1}} + \eta_\infty$$ **Equation 3.44**

where, $\eta(\dot{\gamma})$ - complex viscosity as a function of rotational shear rate, $\dot{\gamma}$;
η_0 - first Newtonian viscosity, absolute viscosity;
η_∞ - infinite shear viscosity;
$\dot{\gamma}$ - shear rate, s^{-1};
c - fitted material constant, see Table 3.3;
p, p_1, p_2 fitted material exponents, see Table 3.3.

Table 3.3 Cross and Carreau Viscosity Flow Curve Model Parameters

Model Name	Assumed Parameters	Number of Fitted Parameters	Fitted Parameters
Cross	$p_1 = 1$	3	c, η_∞, p_2
Cross/Sybilski	$\eta_\infty \to 0$ $p_1 = 1$	2	$c,\ p_2$
Carreau	$p_2 = 2$	3	c, η_∞, p_1
Carreau/Gahleitner	N/A	4	c, η_∞, p_1, p_2
Carreau/Yasuda	$p_1 = \frac{1-p}{p_2}$ $c = \lambda$, relaxation time	4	c, η_∞, p, p_2

Over the course of this research effort it was decided that the potential for erroneous ZSV or LSV predictions as a result of data extrapolated to fit the model forms was not desirable. Therefore, rather than using the mentioned predictive models, it was decided to perform the necessary rheological measures to construct sufficient master curves which would permit the determination of the desired complex viscosity values.

In this investigation, a minimum of two replicate binders were tested in the DSR to determine the LSV at their respective aging states. The LSV values were determined by conducting frequency sweeps at different temperatures creating isotherms ranging from 16 to 100°C. The isotherms were then shifted into master curves of |G*| and phase angle (δ) utilizing the Rhea software package (RHEA, 2011). The master curves were converted into the components of complex viscosity (η' and η"). Likewise, these are

readily used to compute the complex viscosity (η^*) utilizing the vector addition shown in Equation 3.45.

$$|\eta^*| = \sqrt{(\eta')^2 + (\eta'')^2} \qquad \textbf{Equation 3.45}$$

To determine LSV, the complex viscosity (η^*) is plotted as a function of testing frequency similar to the methodology used by Anderson (Anderson et al., 2002) to determine ZSV. For unmodified binders, this plot creates a clear plateau in complex viscosity with lower frequencies. The definition of ZSV is essentially when the response is purely viscous, i.e. the elastic response is zero. The concept of LSV is introduced so that η^* can be considered from the master curves without additional modeling to determine the ZSV, i.e. the elastic response is very small, but not exactly zero.

Traditionally, problems arise if LSV values are attempted for polymer-modified asphalt binders due to the highly elastic nature of the polymers. By definition, LSV can only be determined in the plateau region of η^* versus frequency plot. However, LSV and ZSV are commonly measured in the polymer industry by increasing the test temperatures and/or reducing the test frequencies until the plateau develops. In this study, equipment and time limitations prevented the use of frequencies lower that 0.01 rad/s for each isotherm. Further limitations on the maximum testing temperatures were due to sample flow from between the parallel DSR plates. To remedy this issue, the higher temperatures required for the polymer-modified binders (85 to 100°C) were tested with a 0.5 mm gap setting rather than the typical 1 mm gap, which was used up to 80°C.

To assure the LSV values being determined were reliable and not just a random point along the η^* curve, the percent difference between η^* and the viscous component (η') was determined according to Equation 3.46.

$$\%\, Difference = 100\frac{\eta * - \eta'}{\eta *} \qquad \textbf{Equation 3.46}$$

This type of calculation does not explicitly follow the LSV determinations used for oxidation studies in the literature. The standard measure for LSV is usually directly measured at 0.1 rad/s at 60°C with the 25 mm parallel plate geometry and a 0.5 mm gap on the DSR (Martin et al., 1990; Lau et al., 1992). However, issues arise with certain materials not truly representing low shear viscosity behavior under those measurement conditions. Examination of the example vector components just discussed from the complex viscosity plot in Figure 3.28.

Figure 3.28 reveals that an LSV determination of this particular binder at 0.1 rad/s is not very representative of the LSV plateau behavior intended. In this example, the arrow highlights that neither vector component has exhibited the type of plateau behavior that is desired for the accurate determination of LSV. As a result, the master curve determinations and thus the selected LSV values were determined at 60°C and 0.001 rad/s, with and a maximum permissible limit of 5% difference from Equation 3.46.

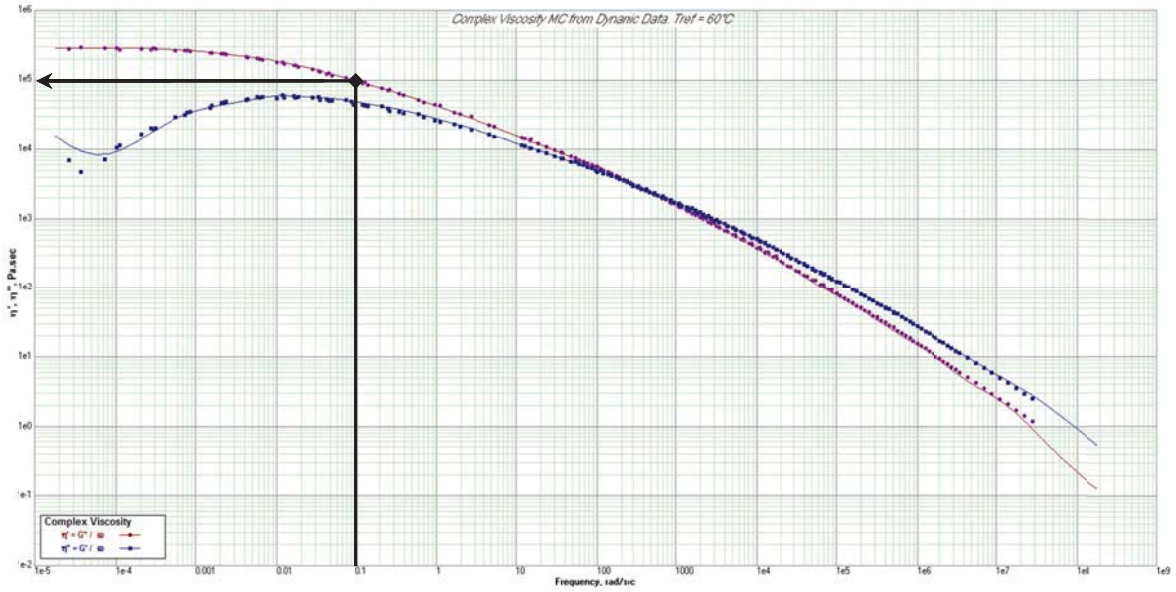

Figure 3.28 Example of Low Shear Viscosity Determination

3.2.4 Comparison of Methods for Mixture and Binder Master Curves

Due to the similarities in the form of the rheological measures of mixtures and binders, it is logical to draw conclusions from a comparison between the two. In fact, a basic differentiation between viscoelastic solids, i.e. mixtures, and viscoelastic fluids, i.e. binders, is whether the material in question will retain any non-zero stress after a simple shear deformation is maintained over a sufficient duration (Christensen, 2003). The stress state in the viscoelastic solid will retain a non-zero value, while the stress in the viscoelastic fluid will eventually decay to zero or completely relax the resulting stress.

This type of behavior can be quantified as discussed previously in the modification of the CAM model shown in Equation 3.11 by a power law function which resulted in the modified master curve of Equation 3.13 that can be used for mixture or binder characterization (Zeng et al., 2001). Using this type of master curve function permits the

nearly direct comparison of the mixture master curve to that of an appropriate binder. Adjustment of the G_e^* and G_g^* term will differentiate the mixture or binder measurements, while the $m_e, k,$ and f_c terms can exhibit marked changes in the material behavior.

From a slightly different approach, consideration of the 2S2P1D model of Equation 3.7 can likewise be fit to rheological measures of asphalt mixture as well as binders. This type of consideration reveals that the tau (τ) parameter in the model can be viewed as the characteristic time, which only varies with temperature for a given mixture. As such, consideration of the τ parameter as a function of the reference temperature may be obtained (Olard et al., 2003). Such a comparison yields the relationship between the developed master curves of the asphalt mixture and corresponding binders through the relationship presented in Equation 3.47.

$$\tau(\theta)_{mix} = 10^{\alpha} * \tau(\theta)_{binder} \qquad \textbf{Equation 3.47}$$

where, $\tau(\theta)_{mix}$- characteristic time of the mix which varies only with temperature, θ;
$\tau(\theta)_{binder}$ - characteristic time of the binder at temperature, θ;
α - correlation parameter, varies with mixture characteristics and aging;
θ- temperature.

The determination of the α parameter in this manner permits comparisons to be made between the asphalt mixture and the asphalt binder master curves according to Equation 3.48 with the input value for the binder coming from Equation 3.7.

$$E^*_{mix}(\omega,T) = E_{0,mix} + \left[E^*_{binder}(10^{\alpha}\omega,T) - E_{0,binder}\right]\frac{E_{\infty,mix} - E_{0,mix}}{E_{\infty,binder} - E_{0,binder}} \quad \textbf{Equation 3.48}$$

where, $E_{0,mix}$- minimum asymptote of mix modulus as very low frequencies;
$E_{\infty,mix}$- maximum asymptote of mix modulus as high frequencies.

According to Olard and Di Benedetto (Olard et al., 2003) Equation 3.48 is independent of the 2S2P1D model, presumably once the α parameter is established.

3.2.5 Fourier-Transform Infrared Spectroscopy

Typically, the applications of Fourier-Transform Infrared (FT-IR) Spectroscopy measurements are focused on the identification of certain molecules or functional groups and the concentration of those molecules within a sample (Smith, 2011). This is largely accomplished by observation of the interaction of certain molecules with certain energy levels of light. In the case of FT-IR spectra, the interaction is noted as the electromagnetic energy absorbance or vibrational resonance with a certain wavelength or frequency that is specific to a certain chemical bond, molecule, or functional group. A basic requirement necessary for absorption of infrared radiation is that these resonant vibrations cause a net change in the dipole moment of the functional group or molecule (Coates, 2000).

Simply put, light travels in a sinusoidal wave form. The distance travelled by the light over the duration of one cycle is referred to as the wavelength, often given in centimeters. FT-IR spectra are usually presented by a plot with the horizontal axis, i.e. x-axis, in the units of wavenumber, which have the relationship to wavelength as shown in Equation 3.49.

$$W = {}^{1}/_{\lambda}$$ **Equation 3.49**

where, W- wavenumber of light, cm^{-1};
λ- wavelength of light, cm.

Most FT-IR considerations are limited to the mid-infrared range of about 4,000 to 400 cm^{-1}. Practically, the term wavenumber signifies the number of cycles of light within a given length or distance, cm in this case. Therefore, a wavenumber of 1,800 cm^{-1}, indicated 1,800 cycles over a one cm measurement length.

Physically, the FT-IR spectrometer produces and thus measures an FT-IR spectra over a range of wavenumbers, e.g. 4,000 to 400 cm^{-1}. This is produced through a scanning operation of a device known as an interferometer which entails what is known as an IR beam splitter, typically made of potassium bromide (KBr). What effectively happens in the interferometer is that an initial source or IR light is passed through the beam splitter, which splits the light into two separate beams. Essentially, part of the beam is reflected and part is transmitted though the KBr prism with both beams known to be of the same wavelength. However, one beam is reflected off a fixed mirror which gives it a certain path length (A_1). The other portion of the beam is reflected of a moving mirror which provides for a variable path length of light (A_2). Both beams are again passed through a beams splitter which recombines them into a single beam of light.

When the two path lengths are equal, the amplitude of both beams are in-phase with each other and they undergo what is known as constructive interference, i.e. they are additive components. When the moving mirror changes the path length of one of the beams the amplitude of the peak of the light waves are out of phase with each other and

undergo destructive interference or part of one wave cancels a part of the other. In this manner, the FT-IR creates what is known as an interferogram, which is defined as the infrared detector output as a function of the difference in optical path length just described. Finally, the Fourier transform is applied to the interferogram, which converts it into the infrared spectrum to be used for analysis purposes, thus the reference to the Fourier transform in the FT-IR nomenclature.

By the process just summarized, the FT-IR device provides the mid-infrared range of the IR spectra with the final amplitude of the input light as shown in Equation 3.50 (Smith, 2011).

$$A_f = A_1 + A_2$$ **Equation 3.50**

where, A_f- final amplitude of recombined light beam;
A_1- amplitude of stationary mirror beam;
A_2 amplitude of moving mirror beam.

With the intensity of a light wave proportional to amplitude of the wave, or energy level, it can be seen how an FT-IR spectrometer can subject a test specimen to a range of wavenumbers and light intensity levels. Since the FT-IR spectrometer is measuring the interference of light waves with matter travelling through some ambient medium based on the reflection of the light beam from a series of mirrors, it can be expected that the exact output beam and energy level will not be retained throughout the entire measurement system.

As such, it becomes important to frequently measure the influence of these factors on a regular basis, particularly if the ambient or environmental conditions change around

the device. These base measurements are known as background scans, which are effectively subtracted from the sample measurement. This subtraction process produces the final output of the FT-IR spectra and represents the influence of the test specimen as an absorbance value as depicted in Equation 3.51 (Smith, 2011).

$$A = \log\left(I_0/I\right) \qquad \textbf{Equation 3.51}$$

where, A- sample absorbance, arbitrary units;
I_0- intensity of the background scan at a certain wavenumber;
I intensity of the specimen scan at the same wavenumber.

Therefore a plot of the absorbance as a function of the wavenumber yields the typical FT-IR relationship shown in Figure 3.29, which presents an example background scan along with the corresponding measure of the toluene and ethanol solution used in the extraction and recovery process.

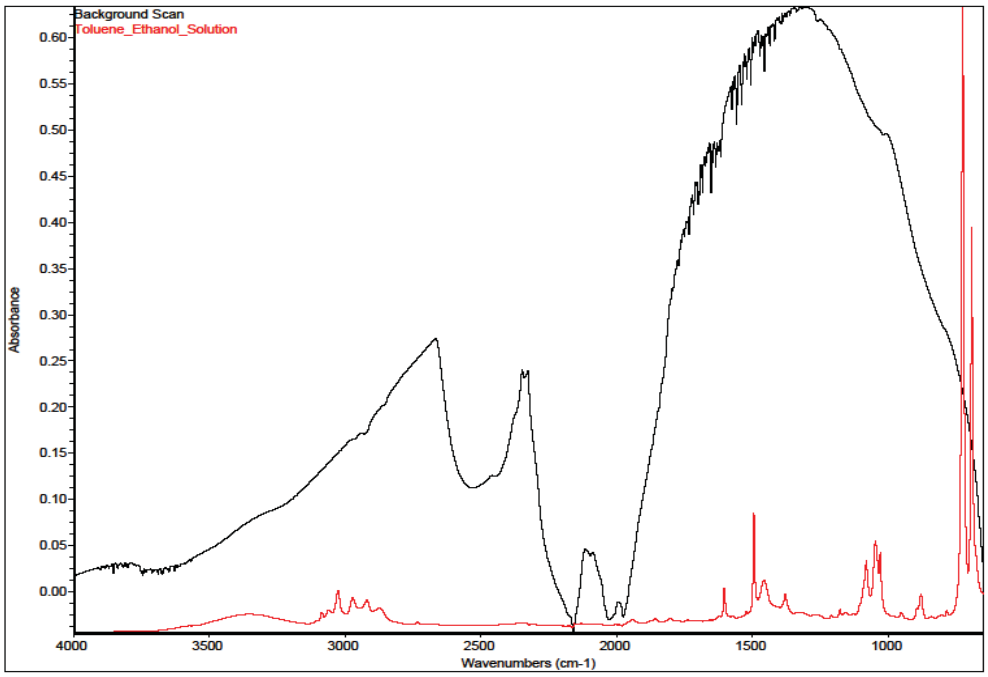

Figure 3.29 FT-IR Spectra of Toluene and Ethanol Solution and Background Scan

From the spectra shown in Figure 3.29, a great deal of information can be interpreted. Certain molecules or functional groups tend to exhibit absorbance at certain characteristic wavenumbers. As an example, Figure 3.29 exhibits a strong absorbance peak around 730 wavenumbers, which has been shown to be indicative of out-of-plane bending of the carbon hydrogen bond (C-H). This peak is important as it was used to detect residual solvent in the extracted and recovered binders as will be discussed in later sections.

These types of behaviors from each respective molecular group are largely the result of net change in the dipole moment of the functional group (Coates, 2000). As a result, there are many materials which are invisible to FT-IR spectral analyses. As an example, inert singular gases are known to not show absorbance in the mid-infrared range. In general, this is the main justification for using nitrogen gas to purge the FT-IR

system and reduce background interference on the measures. Nitrogen gas (N_2) does not exhibit the necessary change in polarity with a resonance at any mid-infrared frequencies, thus nitrogen gas is invisible to FT-IR analyses. In this study, a constant nitrogen purge was used in the FT-IR to reduce the influences of moisture and carbon dioxide on the measured spectra.

Fourier Transform Infrared Spectroscopy Sample Preparation and Measurement Techniques

In basic terms, there are two categories of FT-IR sample preparation and accompanying measurement technique. The first is what is known as transmission testing, where the IR beam is passed directly through the investigated sample before being read by the detector. The other method is generally known as reflectance testing, where the IR beam is reflected or bounced off of the specimen surface then measured by the detector.

In transmission measurements, the sample of interest is frequently contained within an IR transparent cell, between IR transparent windows, or is mixed with an IR transparent powder as applicable to the physical state of the sample (Smith, 2011). By far the most common material used for the cells, windows and powders is potassium bromide (KBr) which is likely used due to the relatively low cost and high transparency in IR range. One significant drawback to using KBr is that it is fairly hydroscopic, meaning it will readily absorb moisture from the atmosphere and could potentially dissolve.

The actual preparation of the sample for measurement varies somewhat with each sample, but in general is either cast, squeezed, or diluted into a solution sufficiently thin enough to pass the IR beam.

Solid samples are sometimes squeezed into sufficiently thin films in high pressure IR cells. Or they can be ground into a powder mixed with KBr powder which is pressed into what is known as a KBr pellet for measurement. Some polymers or other soft solids or highly viscous fluids can be pressed into appropriately thin films for transmission measurements.

Some solids are readily dissolved and some fluids are pressed between two windows to create a sufficiently thin specimen for IR measurements. Additional sample preparation has been conducted by placing droplets of the solution on an infrared compatible window and allowing the solvent to evaporate (Smith, 2011). Diluted specimens have also been spun on a rotating samples window in a process referred to as spin casting to obtain sufficiently thin sample path-lengths.

Another option is to prepare a mull sample by grinding the sample into a powder and mixing it typically with a mineral oil or mulling agent until a paste is formed which may be squeezed between two KBr windows.

It is imperative to quantify the concentration of the measured specimen or analyte when conducting transmission measurements. If the sample is too thick or the concentration is too high, measurement quality can suffer due to opacity issues not permitting enough IR light through the specimen for measurement. This condition is described by Beer's law as given in Equation 3.52.

$$A = \varepsilon lc$$

Equation 3.52

where, A- sample absorbance, arbitrary units;
ε- Absorptivity of the specimen;
l- pathlength, or thickness of the specimen;
c- concentration of the analyte.

As can be seen from Equation 3.52, if the product of the concentration and the path-length are too great, the absorbance measured will be too high and the sample will effectively block the measurable IR light. If the product were too low, then the absorbance would be too small and there would not be enough information in the signal to make meaningful measures, i.e. it would be very similar to a background measurement. As such, careful attention should be paid to the path-length and concentration with trial and error sometimes being the best approach to obtain a useable sample.

Another category of FT-IR measurement techniques that are conducted include reflectance testing. One form of reflectance measurement reflects the IR beam off the surface of a powdered sample that has been mixed with ground KBr material is known as diffuse reflectance Infrared Fourier Transform Spectroscopy (DRIFTS). DRIFTS preparations are somewhat similar to the preparation of a KBr pellet, only compression into the pellet is not required. The use of additional mirrors in the DRIFTS accessory make it possible to measure the IR spectra by reflecting the beam off the surface of the powdered mixture composed of the sample and KBr.

Another common type of reflectance measurement is known as attenuated total reflectance (ATR). This type of measurement is conducted by passing the IR beam

through a crystal of high refractive index (n_c) on to the surface of the sample with a lower index (n_s). Figure 3.30 presents a schematic of how the IR beam travels through the ATR attachment.

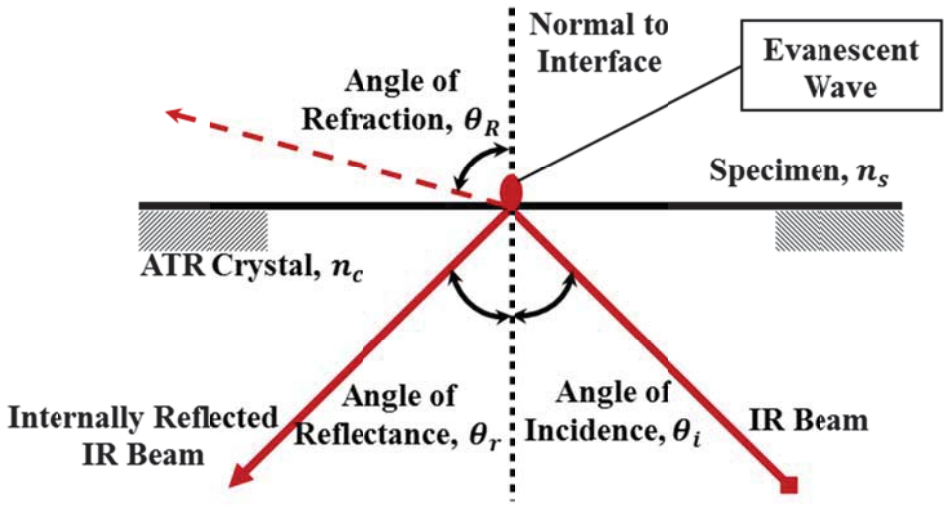

Figure 3.30 Path of Infrared Beam with Refraction and Reflection (Smith, 2011)

In order for ATR to function sufficiently, the angle of incidence (θ_i) must be at or below what is known as the critical angle (θ_c) which will cause all the infrared light to be reflected within the ATR crystal, i.e. total internal reflectance. The critical angle is based upon the relationship between the respective refractive indices of the sample and the ATR crystal as depicted by Equation 3.53.

$$\theta_c = \sin^{-1}\left({}^{n_s}/_{n_c}\right) \qquad \textbf{Equation 3.53}$$

where, θ_c- critical angle of incidence to cause total internal reflectance;
n_s- refractive index of specimen;
n_c- refractive index of ATR crystal.

It is logical to deduce that no measurement of the sample would take place if all of the IR beam were reflected internally, however this is not strictly the case. What actually happens is that the IR beam immediately around the point of reflectance, incident and reflected beam, must occupy the same physical space. Since these beams are in-phase with each other they experience constructive interference and the wave amplitude is increased or attenuated, thus the name attenuated total reflectance. Since the beam itself occupies the space within the crystal, the attenuated wave has nowhere to go but upward presenting as an evanescent wave.

Typically, the evanescent wave is on the order of ten microns or less in height depending on the experiment at hand (Smith, 2011). Specific determination of the depth of penetration (Dp) for an ATR measurement is a function of both the geometry of the measurement and refractive indices of both the crystal and the specimen as depicted in Equation 3.54.

$$Dp = \frac{1}{2\pi W n_c \sqrt{\sin^2\theta - \left({}^{n_s}/_{n_c}\right)^2}} \qquad \textbf{Equation 3.54}$$

where, Dp - Depth of penetration;
W - Wavenumber;
θ - critical angle of incidence to cause total internal reflectance;
n_s - refractive index of specimen;
n_c - refractive index of ATR crystal.

With wavenumber (W) in the denominator of Equation 3.54, it is readily acknowledged that the depth of penetration (Dp) and thus the measured IR path-lengths should be different for different wavenumbers. Specifically, as the wavenumber increases to high frequencies, the Dp should decrease with all other parameters being constant for a given

IR measure. At first, this may seem to be a negligible observation, but it may potentially cause some concern with certain types of analyses and therefore will be discussed in the section on measurement quantification techniques.

Depending upon the specimen being measured and material the crystal is comprised of ATR measurements can sometimes suffer from a weak signal due to the limited depth of penetration. To overcome this issue, some ATR crystals are constructed to include more than one evanescent wave, thus increasing the overall path-length within the sample. An example of such a "multi-bounce" ATR attachment is presented schematically in Figure 3.31.

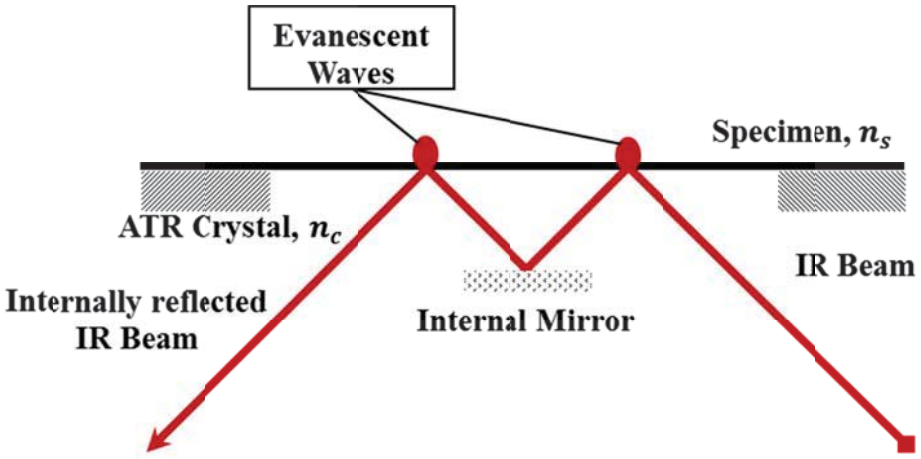

Figure 3.31 Path of Infrared Beam with "Multi-Bounce" ATR Crystal

The majority of multi-bounce ATR crystals are made of either zinc selenide (ZnSe), silicon, or germanium. Special care must typically be given to these crystals as they are easily damaged and some are water soluble. As a result, many "single-bounce" attachments are being manufactured with a ZnSe backing placed behind a diamond

surface crystal. This configuration provides the very inert and durable surface of the diamond, while retaining the IR clarity with the ZnSe. As a general rule, overall cost prohibits most users from purchasing multi-bounce diamond ATR prisms, due to the larger surface area.

Nearly all the FT-IR measurements conducted as part of this study were conducted with ATR attachments. Early on, measurements were conducted with the collaborative effort of Dr. Charles Glover and his group at Texas A&M University with a multi-bounce ATR attachment using a zinc selenide prism. As the study progressed, the FT-IR measures were conducted at the University of Nevada, Reno with an ATR attachment containing a single-bounce prism with a diamond surface and zinc selenide backing.

Quantification of Fourier Transform Infrared Spectra

Once adequate FT-IR spectra are obtained, the overall spectra can be observed to identify many functional groups and often some interactions between adjacent molecular groups. A great deal of study has been conducted in this area and is a highly developed branch of chemistry. While these types of analyses can yield a great deal of information regarding the molecular structure, how those structures are arranged, and information regarding the interaction of different molecules or functional groups, such observations are not directly the focus of this research effort. The objective of the FT-IR measurements in this effort are focused more on the quantity or concentration of certain functional groups.

One of the most common methods to quantify a functional group is what is known as the peak height method. Essentially, IR spectra is quantified by measuring the height of the peak of interest either from the absolute bottom of the graph, i.e. zero absorbance,

or from an imposed baseline relative to the absorbance peak at hand. As depicted in Figure 3.32 the peak height of the hydroxyl group in hydrated lime $Ca(OH)_2$ mixed with an asphalt binder has been determined as a wavenumber of approximately 3,640 cm^{-1} (Arnold et al., 2006).

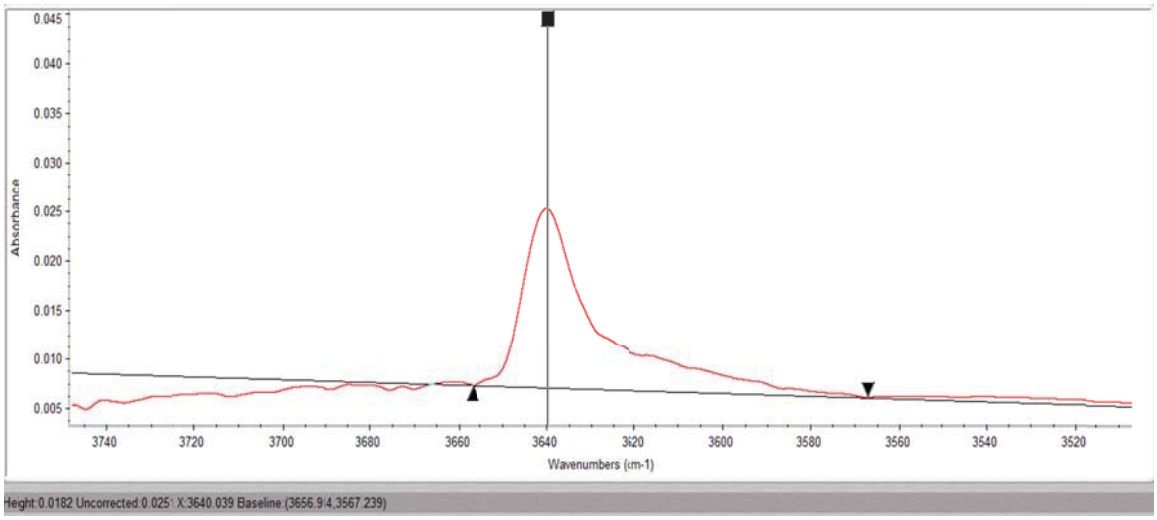

Figure 3.32 Example of Peak Height Quantification

The peak height method is likely one of the most common quantification methods for IR spectra, especially when paired with the direct transmission method of measurement. However, the method may be subject to some sources of error that are unique to its application. For instance, by definition the peak height is selected and measured at a single wavenumber which could experience a shift if influenced by another functional group that is present at similar wavenumbers. In other words, changes in nearby peaks may influence the overall shape of a particular peak of interest and these types of fluctuations may be problematic with the peak height method. Another potential drawback of the peak height method is that no information is provided on the width or

shape, only the height of a particular peak. This may cause some changes in the width of the peak to be missed, particularly if the functional group of interest presents a broad band as opposed to a sharp and well defined peak.

There are some advantages to the peak height method specifically in the actual quality of the measured data. When only considering the peak of a certain spectral feature, only the highest signal is considered in the analysis. This can be beneficial since this will by necessity provide the best signal to noise ratio in the region of interest. This can be beneficial is the analysis in exhibiting low overall energy levels as which will produce a weak signal and thus noisy spectral features. Nevertheless, the peak height method is commonly used by many researchers and some who study asphalt binder oxidation and kinetics measurements.

It has been stated that as a result of variable path-length (Dp) as a function of wavenumber as depicted in Equation 3.54, that ATR spectra should not be used for quantitative analysis techniques (Smith, 2011). Beer's law, Equation 3.52, essentially necessitates that both the path-length, and absorptivity of the specimen be constant in order to investigate or predict the concentration of a certain chemical species. However, many successful measurements and quantitative analyses have been conducted utilizing ATR measurements. In fact, AASHTO T302 (AASHTO, 2013) establishes the determination of polymer content within a modified asphalt binder sample recommends both transmission and ATR as valid methods of quantitative FT-IR measurements.

As an example Figure 3.33 presents the same peak depicted in Figure 3.32, only the peak area method is presented. The value of the measurement will be quite different, however in certain circumstances the relative difference between the two may remain the

same throughout an analysis, though not always. There are certain influences that may cause systematic shifting of the data with the peak height method compared to quantification measures using the peak area method and vice versa.

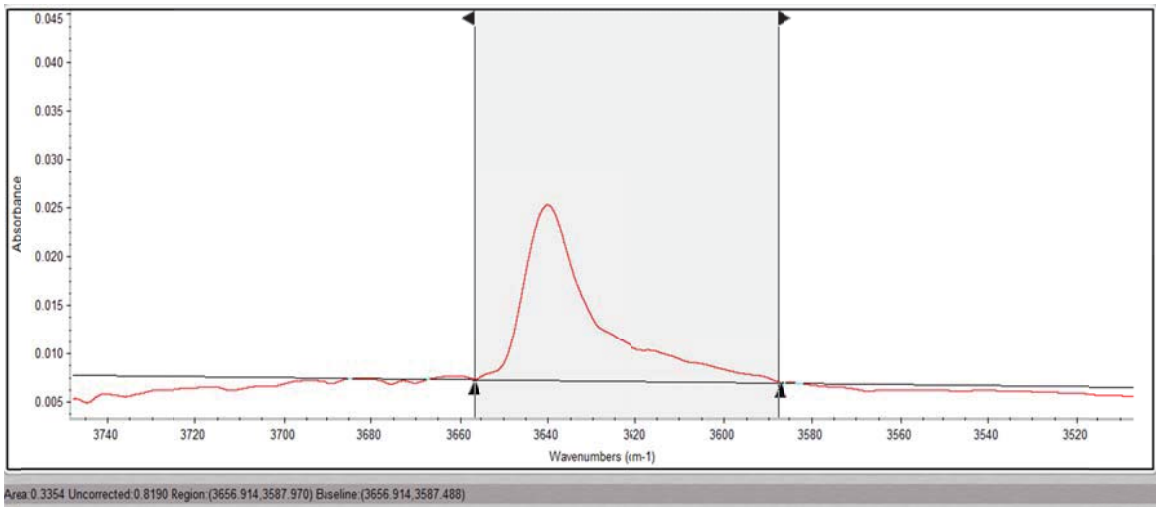

Figure 3.33 Example of Peak Area Quantification

Although the peak area method may appear to be the preferred method due to potential issues with the peak height method mentioned previously. However, the peak area method has certain limitations as well. For instance, significant changes in adjacent peaks to the one specifically being measured may cause erroneous changes in either the peak of interest directly, or may potentially change portions of the spectra that may be used to determine the baseline for the area calculation. Depending upon the circumstances, these errors may or may not be present in peak height measures.

All of the IR quantification measures utilized in this study were based upon the peak area method. This was consistent with both Texas A&M data as well as measures conducted at the University of Nevada, Reno. In both cases the peak area in the carbonyl

region referred to as the carbonyl area, CA, was computed as the area, in arbitrary units, between the absorption spectrum and the magnitude of the absorption at 1,820 cm^{-1} as the baseline and between the wavelengths of 1,650 and 1,820 cm^{-1}. This area was calculated utilizing the FT-IR software, Omnic, following a macro written specifically to determine the peak area within this region.

To be precise, the carbonyl functional group can sometimes be separated into further fractions based upon the specific molecular orientation with carbonyl as the main component. The base chemical structure for carbonyl is an oxygen atom double bonded to a carbon atom. A carbonyl can, in turn, be bonded to other atoms or functional groups. A depiction of carbonyl and a carbonyl functional group are presented in Figure 3.34, where A and B can be different atoms or atom groups.

(a) **(b)**

Figure 3.34 (a) Carbonyl Molecule and (b) Carbonyl Functional Group

As a result of the general definition of the carbonyl functional group, i.e. inclusion of the nonspecific A and B functional groups, several more specific definitions are readily defined to provide more specific characterization of the molecular structures commonly observed in the proximity of carbonyl functional groups. Some typical definitions are provided in Figure 3.35 (Petersen, 2009; Odian and Blei, 1994).

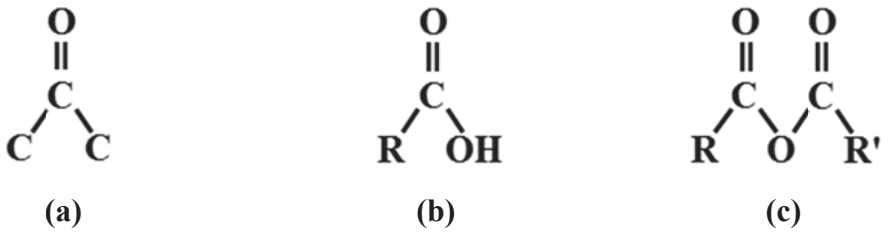

Figure 3.35 (a) Ketone, (b) Carboxylic Acid, and (c) Anhydride Functional Groups

In Figure 3.35(a), ketones are defined as a carbonyl group where the attached atoms are strictly carbon, as can be visualized in through the mid-portion of over the length of a long hydrocarbon chain. Figure 3.35(b) presents a carboxylic acid where one of attached functional groups to the carbonyl group is a hydroxide, OH^- and the other, R, is an undefined functional group. Figure 3.35(c) presents a slightly different orientation including an oxygen atom between the carbonyl functional groups and including the two other undefined monovalent functional groups, R and R'.

In general, the definitions of Figure 3.35 are provided as a reference point to aid in the comprehension of some common literature that discusses the carbonyl function groups in terms of the more stringent definitions. As a general overview, discussions of ketones and carbonyl measures are closely related to one another, with the majority of carbonyl groups logically occurring as ketones along what can be simplified to long hydrocarbon chain structures in asphalt binders.

3.2.6 Asphalt Binder Composition

In-depth studies of asphalt binder behavior, especially those considering the chemical signature and evolution of the molecular structure, often include characterization of the

composition of the asphalt binders being studied. Although not necessarily directly relatable to the FT-IR characterization of the functional groups discussed in the previous sections, the composition separation of asphalt binders into distinct fractions augment each other in a productive manner.

One of the most common methodologies used in the fractional characterization of asphalt is attributable to Corbett (Corbett, 1969) and thus bears his name. The Corbett methodology combined with subsequent efforts (Corbett and Petrossi, 1978) have led to the method being standardized as ASTM D4124-09 (ASTM, 2010). In general, this methodology separates the asphalt binder into four fractions based largely upon differential levels of polarity and adsorption of the respective fractions, with secondary effects of molecular weight. With a certain amount of variation in terminology, the most common naming convention applied to the four fractions leads to the acronym SARA, which are derived from each respective fraction: saturates, aromatics, resins, and asphaltenes. Other terminology used to represent essentially the same components are termed saturates, naphthene aromatics (NA), polar aromatics (PA), and asphaltenes.

While the details of the method are left to ASTM D4124 (ASTM, 2010), a brief outline will discuss the method of separation, which may not necessarily seem to follow the most logical progression. To summarize, the asphalt binder of interest is thoroughly mixed into a solution with iso-Octane so that the undissolved portion, the asphaltenes, may be left after filtration under vacuum and decanting of the soluble liquid phase, termed the maltenes. The maltenes are then distilled to remove the iso-Octane and are then brought into solution with *n*-heptane. The solution is then brought into contact with calcined alumina in a chromatographic column where the saturate fraction passes quickly

through the column. After a short rinse with toluene, the clear solution that has passed through the column is rotary evaporated (rotovap) to yield the saturate fraction.

The column is then further flushed with toluene followed by a 50:50 mixture of toluene and methanol to yield a yellow solution containing the naphthene aromatic (NA) fraction after a rotovap procedure. Separation of the saturate and NA fractions are verified utilizing a UV-detector and noting changes in the absorbance near 350 or 366 nm.

The polar aromatic (PA) fraction is obtained by switching the eluent, solution, to trichloroethylene and monitoring the dark band migrating up the column, which also corresponds to a change in the UV absorbance at 400 nm.

All three solutions are then distilled in a rotovap assembly, followed by a heated nitrogen gas-stream evaporator, followed by a final rotary evaporation process to obtain the final dried fractions of the binder. Thus, with each of the four fractions separated, the composition of the binder is reported as the percentage of each fraction by mass.

As a result of the separation process, it becomes clearer why the definition of the components is not a clear-cut fractionation measurement. The separation is somewhat dependent upon the reactivity of the different fractions to the solvent used in each step relative to the adsorption tendencies to the alumina medium in the column. Despite the actual mechanisms acting during the separation, there are some generalities of each fraction that yield some useful information, particularly in regards to oxidative aging (Liu et al., 1998).

- **Saturates:** typically the fraction with the lightest molecular weight and are generally the most stable component with aging.
- **Aromatics (naphthene aromatics):** typically are a little heavier molecular structures which tend to grow in molecular size upon oxidation largely transforming into polar aromatics, but rarely into asphaltenes (Liu et al., 1999).
- **Resins (polar aromatics):** the second heaviest in terms the molecular sizes. Polar aromatics often migrate into asphaltenes upon oxidation, though they are typically smaller and thus less reactive than the asphaltenes found in the original asphalt binder.
- **Asphaltenes:** The heaviest fraction in terms of the molecular sizes. Asphaltenes tend to be brittle and increase concern over cracking resistance as a binder oxidizes with age. Asphaltenes are generally considered the most polar component of asphalt binders and therefore are typically responsible for increases in stiffness and viscosity of the asphalt binder.

Polar Organic Fractions of Asphalt Binder

Using the same basic procedure as the SARA analysis, previous research (Robertson et al., 2006) conducted similar chromatographic separations utilizing cyclohexane as the initial eluent in a column of mineral aggregate fines or filler and Celite, diatomaceous earth, to effectively separate out the lighter ends or weakly polar components of the asphalt binder. A second eluent composed of a 10:1 blend of toluene and ethanol was then used to remove the strongly polar components of the asphalt binder that were adsorbed onto the mineral aggregates in the column. Again, recovery of each

representative fraction gave an indication of the asphalt-aggregate, mineral filler, interaction taking place. This methodology was conducted on all eight of SHRP binders and seven SHRP aggregates (Robertson et al., 2006). As an illustration of the potential significance of this interaction, a summary of the results from those measurements are presented in Table 3.4.

Table 3.4 Average Mass Percent of Polar Organic Components Adsorbed on Aggregate-Celite Columns (Robertson et al., 2006)

SHRP Asphalt Id	Strongly Adsorbed Polar Organic Components, Ave Mass Percent									
	SHRP Aggregate Id									
	RA	**RB**	**RC**	**RD**	**RH**	**RK**	**RL**	Min	Max	Diff
AAB-1	4.3	8.0	12.1	6.8	15.4	9.3	9.7	4.3	15.4	11.1
AAC-1	7.1	8.9	9.2	6.4	8.8	7.3	7.1	6.4	9.2	2.8
AAD-1	4.0	12.4	13.7	6.5	17.3	12.0	17.0	4.0	17.3	13.3
AAF-1	5.7	9.1	10.4	7.8	12.2	8.4	9.0	5.7	12.2	6.6
AAM-1	2.8	7.3	11.7	3.8	12.5	7.5	9.1	2.8	12.5	9.7
AAW	10.4	11.4	13.4	10.4	14.1	9.9	13.2	9.9	14.1	4.3
AAY	12.4	13.3	15.9	14.8	19.4	12.6	12.2	12.2	19.4	7.3
ABD	5.1	6.7	8.6	6.3	9.5	7.4	7.9	5.1	9.5	4.4
Min	2.8	6.7	8.6	3.8	8.8	7.3	7.1	2.8		
Max	12.4	13.3	15.9	14.8	19.4	12.6	17.0		19.4	
Diff	9.6	6.6	7.4	11.0	10.6	5.3	9.9			16.6

The most significant contribution of these measurements is noted by the overall magnitude of the variation between the different asphalt binders and aggregate sources, even though these are average values of two replicate measures. As shown by the shaded cells in Table 3.4, indicating the minimum, maximum, and difference between the two for each respective row or column, there is a significant difference in the measured adsorption depending upon the combined materials.

Considering all the materials tested, the minimum adsorbed polar components were 2.8 % and the maximum of all materials measured at 19.4 %. The maximum difference for the entire data set was 16.6 % difference in adsorbed polar components, depending on which of the tested materials are being considered. Within a given binder, the maximum difference was 13.3 % for the aggregates measured. Within a given aggregate, the maximum difference based upon which binder was selected was 11.0 %.

These rather significant differences indicate a potentially important interaction between the asphalt binder and the aggregates used to make a particular asphalt mixture. If such significant portions of the asphalt are effectively adsorbed, i.e. bound to the aggregates, the overall quantity of binder effective in the mix performance may be significantly altered. Not only may this affect the oxidative aging of the binder, but it may also play a role in moisture susceptibility, rutting, fatigue, and thermal cracking performance of the mixtures with mixed results for each depending upon the distress and conditions at hand.

It is because of this potentially significant influence, that this chromatographic measure has been considered as one of the significant parameters to consider with the influence of the mixture characteristics on oxidative aging of the asphalt binders. Further discussions of this topic will be considered in the data analysis sections.

3.3 Asphalt Binder Extraction and Recovery

Many of the binders evaluated by the methods established in previous sections were obtained from mixtures aged to various conditions either in the laboratory or otherwise noted. The mixtures aged in the laboratory were typically mixed, short-term aged, compacted in the Superpave gyratory compactor (SGC) then aged by their respective protocol prior to preparation and mixture testing. After the respective mixture testing, replicate samples were processed to extract and recover the binder in order proceed to with the respective binder testing and evaluation methods. The specifics of this extraction and recovery process are detailed in Appendix B. However, a general discussion is executed here to highlight some of specific evaluation efforts that took place during the development of the final procedure.

The basis for the extraction procedure was founded upon the procedure outlined in AASHTO T164, Method A Centrifuge Extraction (AASHTO, 2012). The method requires the placement a mixture sample of known mass in a centrifuge bowl with a filter paper between the lid and the bowl containing the mixture. The asphalt binder in the mixture is soaked in an appropriate solvent to extract it from the mixture and remove it from the aggregate surface. At regular intervals, the centrifuge bowl is spun to a maximum speed of 3,600 revolutions per minute (rpm) extruding the solvent and dissolved binder through the filter paper to effectively remove the binder from the mixture, leaving the aggregate behind. The filter paper retains the majority of the fines that may be suspended in the solution of binder and solvent. The solution is then retained for further processing.

The mixture is repeatedly soaked with fresh solution which is centrifuged through the same filter paper. AASHTO T164, Method A (AASHTO, 2012) specifies that the process be continued until the solution being extruded is a light straw color. However, one of the major modifications to the extraction method was the ending color of the solution to indicate a complete extraction. In this study the extraction process was continued well past the stated straw color and was carried out until the solution was nearly as clear as fresh solvent. To assure consistency in the level of extraction a small flask of the final solution was retained as a blank for comparison with each individual extraction process.

The extraction process was carried out to this extent to alleviate some of the potential issues that had been noted with this procedure, specifically inferences of partial or incomplete removal of the binder from the mixture. Questions had been raised early in the process development regarding the partial removal and thus phase or other systematic segregation of the binder due to the extraction and recovery process.

Another significant alteration of the process in AASHTO T164 was the solvent used during the extraction process. The method specifically states that trichloroethylene, methylene chloride, *normal*-propyl bromine, or terpene may be used as the extraction solvent. However, this study used a mixture of toluene and ethanol in a blend of 85 and 15% by volume, respectively as the extracting solvent. This modification was largely based upon the recommendations Dr. Charles Glover and collaboration of Texas A&M University (Burr et al., 1991).

The procedure developed to recover the asphalt binder from the extracted solution likewise included modification and verification from the method published as AASHTO

T319 (AASHTO, 2012). The first modification was the extraction procedure as previously discussed in the modification of AASHTO T164, Method A not the method and apparatus described in T319.

Additional changes were applied to the rotary evaporator bath temperature and vacuum level due to measured and previously noted difficulties in complete removal of the toluene/ethanol solvent. After a rather lengthy and laborious investigative process, the temperature of the bath was finally settled upon 150°C (302°F) for the entire recovery procedure.

The evacuation pressures were also modified from the published AASHTO T319, due to the change in solvent to the toluene/ethanol blend. To sufficiently remove the solvent from the recovered binder, an initial vacuum of approximately 150 to 200 mbar was applied to remove the bulk of the solvent from the recovered binder. In practice, this was done by applying the absolute pressure within the rotovap flask of approximately 650 mbar, down from the ambient measurement of approximately 850 mbar which fluctuated due to passing weather patterns etc.

Once the majority of the solvent had been removed from the binder and all necessary iterations of the solution had been run through the system, a second lower pressure was applied to drive-off the last remaining bit of solvent. The vacuum was set to 0 mbar absolute pressure, but due to the nitrogen purge and other small imperfections in the system, 20 to 30 mbar was the level of vacuum achieved. This resulted in a total vacuum of approximately 820 to 830 mbar gauge depending upon the ambient barometric pressure at the time. The overall duration of this high vacuum stage was increased to four hours duration to assure the adequate removal of the solvent.

Due to the large mixture sample size, relatively low efficiency of the toluene/ethanol blend the extraction portion of the process took place over a period of 4-8 hours. Since the recovery process largely overlapped the extraction efforts, the recovery time spanned a similar duration. However, the secondary high vacuum phase added a significant amount of time and thus increased the overall duration for the combined extraction and recovery procedure to 8-12 hours, with a few samples periodically extending to 14 hours total duration.

Extraction and Recovery Process Validation

Since it has been well documented that many extraction and recovery processes cause an unknown level of influence on the material properties of asphalt binders (Burr et al., 1990; Burr et al, 1991; Cipione et al., 1991, Abu-Elgheit et al., 1960), initial samples used in the development of the procedure were validated for significant influences due to the extraction and recovery process. Initial efforts focused on the complete removal of the toluene/ethanol solvent. Several binders were tested in collaboration with Texas A&M University to verify the complete removal of toluene from the recovered binder. Gel permeation chromatography (GPC) techniques were utilized and interpreted by Dr. Charles Glover to verify the complete solvent removal. A summary of some of the GPC results are presented in Figure 3.36.

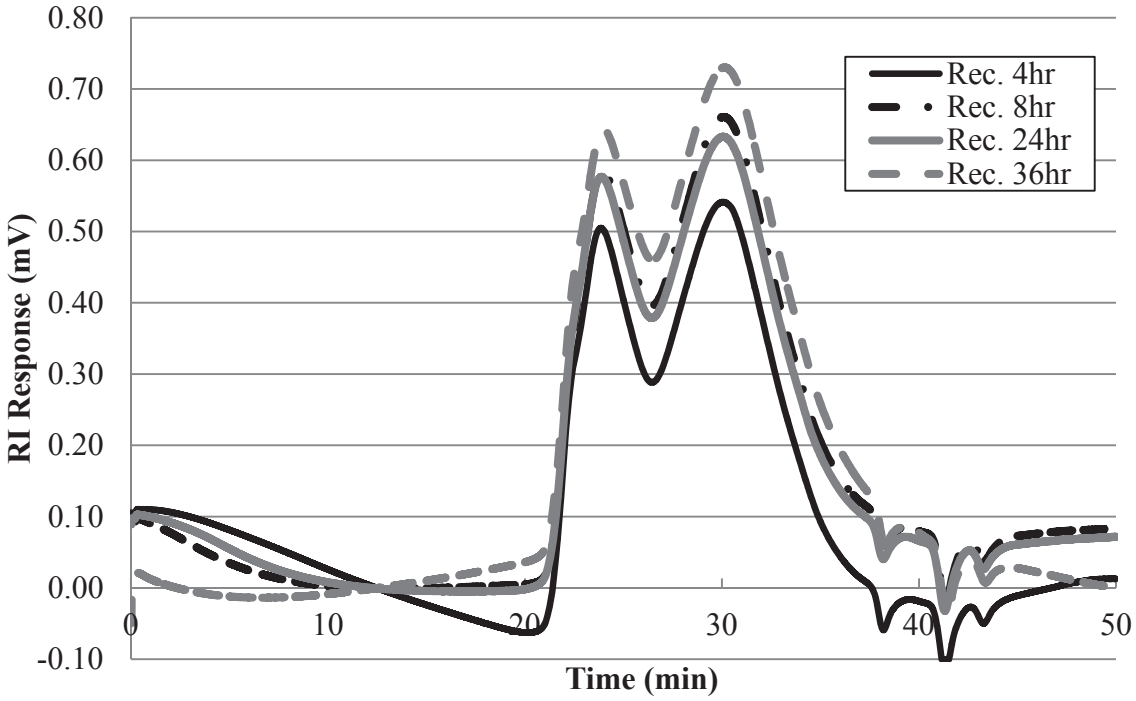

Figure 3.36 Example of Gel Permeation Chromatography with Recovery Time

As presented in Figure 3.36, the GPC response is reported as an RI Response or refractive index, which is quantification of light passing capability of the eluent or solvent used in the test. While GPC results can provide information regarding the molecular weight distribution of the evaluated sample, such information is not the focus of this effort (Martin et al., 1990).

The focus of this effort in regard to the GPC measures is to note that there are not new or disappearing peaks noted with changes in the rotovap recovery time, Figure 3.36, for the example binder shown. It is expected that the toluene/ethanol blend would be depicted to the right or with longer elution time since it should have a lower molecular weight and thus a longer retention time through the porous media when compared to the asphalt binder. The figure does not show a significant difference in the location, not

necessarily the magnitude, but the location of the peaks with respect to the elution time, even after the extreme case of 36 hours of high vacuum distillation. This has been interpreted to signify that the toluene/ethanol blend is not present in the recovered binder and thus has been sufficiently removed by the four hour high vacuum recovery time.

To further validate the procedure, two of the binders included in the study, a neat PG 64-22 and a styrene-butadiene-styrene (SBS) modified PG 64-28, were further tested to quantify the effect of the extraction and recovery procedure. The binders were essentially run through a blank extraction and recovery process, where the original binder was subjected to the extraction and recovery process without having been otherwise aged or blended into a mixture. The comparison was made on both binders in an original state and after the extraction and recovery process. The specific comparisons included evaluations of the FT-IR spectra as well as rheological measures represented as the dynamic shear modulus (G*) master curves. The FT-IR spectra of the original and blank extracted and recovered binders are presented in Figure 3.37 and Figure 3.38 for the PG 64-22 and PG 64-28 binders, respectively.

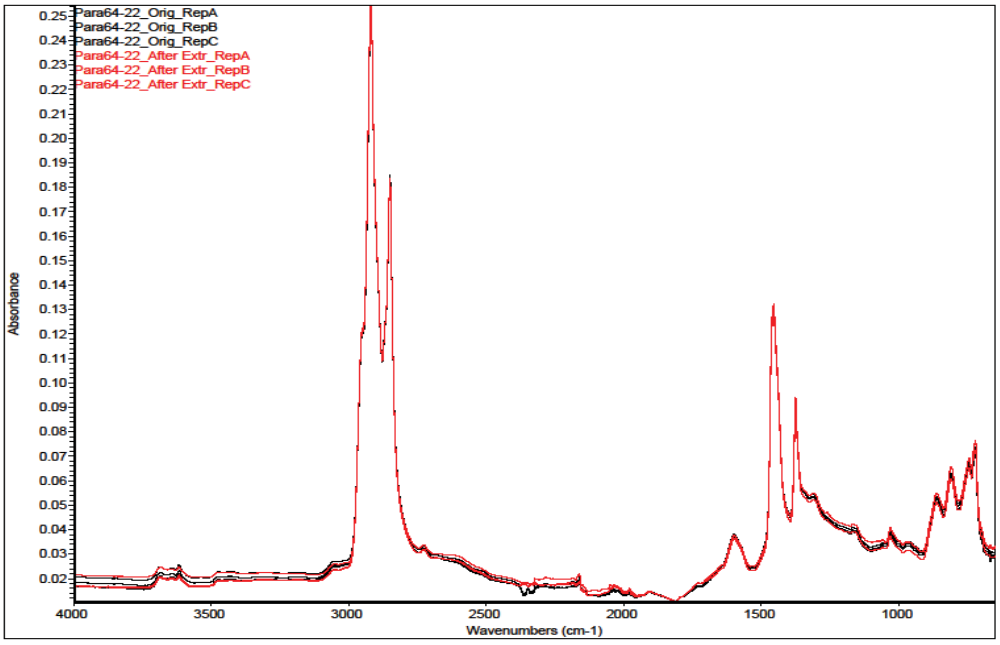

Figure 3.37 PG 64-22 Blank Extraction and Recovery FT-IR Spectra

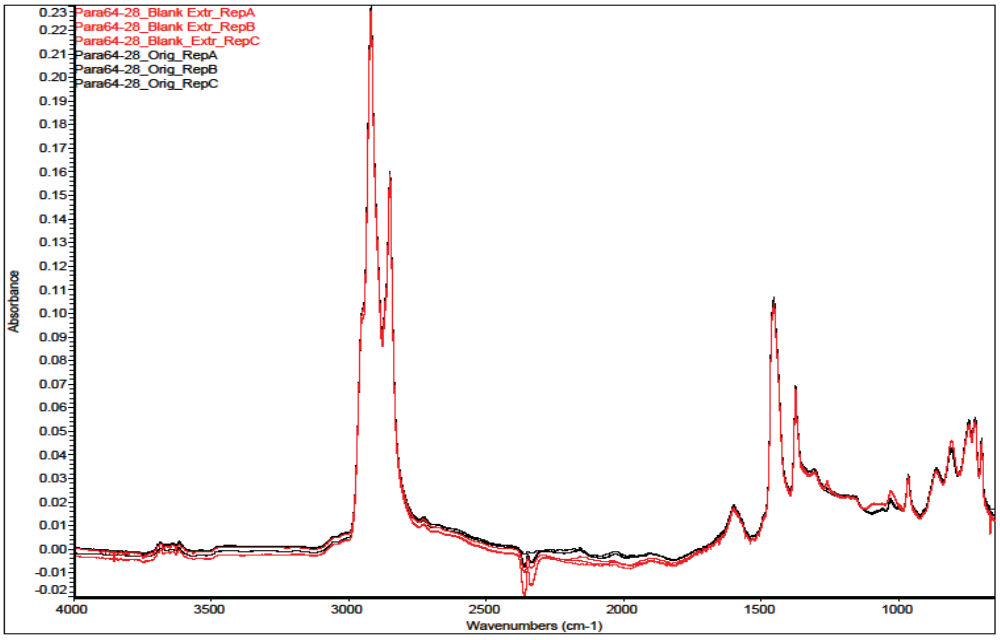

Figure 3.38 PG 64-28 Blank Extraction and Recovery FT-IR Spectra

In both Figure 3.37 and Figure 3.38, replicate FT-IR spectra of the original binder are shown as the black plots and the blank extracted and recovered binder are shown as red.

As mentioned previously, a great deal of information about the molecular structure can be obtained from IR spectra when observed by individuals who specialize in this type of analyses. However, this is not the focus of this research, but a few general comments on the FT-IR interpretation will be noted to increase familiarity on the topic.

From both Figure 3.37 and Figure 3.38, it is observed that the largest peaks occur around 2,950 and 2,860 cm^{-1} or so. These are known to be the stretching response of the carbon-hydrogen bonds CH_2 and CH_3 respectively. The next most influential peak occurs near 1,425 cm^{-1} which is due to the bending of the CH molecules. The next molecular structure of interest is the peak located at a wavenumber of 1,600 cm^{-1}, which is typically attributed to the carbon double bond (C=C). Again, no drastic influence was noted due to the extraction and recovery process.

It is not a coincidence that a material basically classified as a hydrocarbon chain would exhibit absorbance in these regions. Further, it is quite important that these peaks remain nearly identical before and after the extraction and recovery process. If these functional groups were altered even by a small amount, that would signify a drastic change in the overall molecular structure of the asphalt binder, thus creating substantial cause for concern.

Another region where very little change is observed is on the side of the C=C peak. The wavenumber region from 1,650 to 1,820 cm^{-1} is what has been defined as the carbonyl region which represents the molecular bonding of oxygen to carbon atoms creating the carbonyl functional groups as previously discussed. It is critical that the

extraction and recovery process did not generate changes in the carbonyl area as this is the main functional group used to measure and quantify aging of the asphalt binders in this study.

Another region of interest in oxidation studies are the sulfoxides (S=O) which typically occur near a wavenumber of 1,030 cm^{-1}. It has been observed that sulfoxide growth may significantly influence the stiffness or other rheological measures on asphalt binders largely dependent upon the available sulfur content of the binder (Robertson et al., 2006). In more simplistic terms, the more sulfur that is available for an oxidation reaction within a binder, the more influential it becomes on the physical properties of the aged binder. As a result of the generally low sulfur content of these two binders, approximately 3.9% by weight for both the PG 64-22 and PG 64-28 binders, the sulfoxide region of the IR spectra will be observed, but not necessarily taken into account for calculation purposes.

Figure 3.37 depicts the unmodified PG 64-22 binder which does not show significant changes in the sulfoxide region due to the extraction and recovery process within reasonable repeatability limits of the measurements. However, Figure 3.38, depicting the SBS modified PG 64-28 binder does indicate some influence of the extraction and recovery process as growth of the sulfoxide functional group.

Further consideration of Figure 3.38 with the PG 64-28 binder indicates a slight peak developing near approximately 1,260 cm^{-1} wavenumbers. Although not confirmed by any other measurements, this peak could be attributed to an increase in a methyl group, i.e. CH_3. While this occurrence should be noted, it is advantageous that this anomaly occurs outside the carbonyl region which is the true functional group of interest.

Additional deviation is noted as a doublet centered around 2,350 cm^{-1}. This region and potentially the broad band extending nearly to 1,900 or 2,000 cm^{-1} is presumably evidence of carbon dioxide, CO_2 in the system at the time of the IR measurement. Being that the extraction and recovery process, sample tins during storage, and the FT-IR system either received or is under constant nitrogen, N_2, purge, the CO_2 is presumably an artifact of the ambient environmental conditions at the time the IR measurements were taken. Again, this alteration should be noted, but is not expected to significantly affect the carbonyl area measures between 1,650 and 1,820 cm^{-1}.

As mentioned in the discussion regarding Figure 3.29, the toluene and ethanol solution exhibits a strong absorbance near 730 cm^{-1}. Neither Figure 3.37 nor Figure 3.38 show any difference in the absorbance after the extraction and recovery process, suggesting the un-measurable amount of the solvent is left after the recovery process. This is a significant finding, since frequent concerns with other recovery methods were primarily based upon incomplete removal of the extraction solvent.

Since practically insignificant influences of the extraction and recovery process were observed on the molecular structure as measured by the FT-IR, further exploration into the potential effects on the physical properties were also considered. To this end, multiple frequency sweeps at several isothermal conditions were conducted on the DSR as previously discussed on each asphalt binder before and after the blank extraction and recovery process. These rheological measures were shifted to dynamic shear modulus masters curves at a reference temperature of 60°C (140°F) utilizing the RHEA software package outlined previously. Those binder master curves are presented in Figure 3.39.

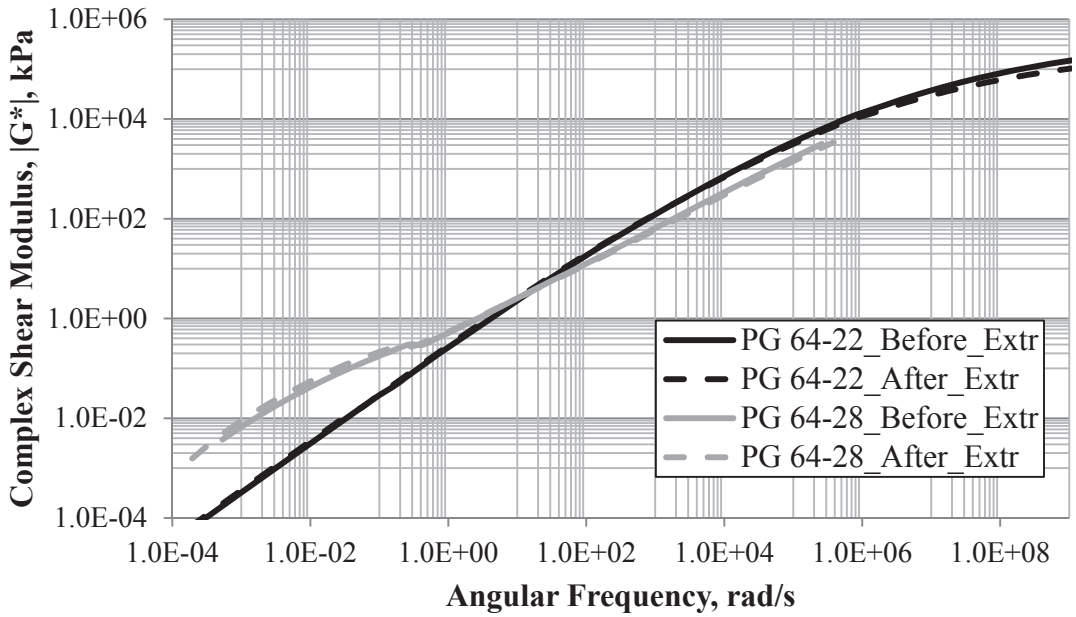

Figure 3.39 Blank Extraction and Recovery Complex Shear Modulus Master Curve

As depicted in Figure 3.39, the developed binder master curves are very close to the same before and after the extraction and recovery process, within each respective binder. Caution is advised when interpreting master curve relationships such as Figure 3.39 since they are represented in a log-log plot. What may seem like very small deviations, may actually be more significant depending upon the location on the log scale. However, given the truly replicate nature of the measurements including independent shifting of each master curve, Figure 3.39 is generally interpreted as yielding the same master curve relationship before and after the extraction and recovery process for both binders.

The slight deviation noted on the higher G^* end of the unmodified PG 64-22 master curves is of little concern especially when characterizing the binder stiffness as the low shear viscosity, LSV, which is highly dependent upon the low end of the G^* relationship.

As will be seen quite frequently, the SBS modified PG 64-28 binder shows slightly more variation as compared to the unmodified binder. The variation noted here does have some level of importance since the deviation between the two are noted at the low end of the G^* master curve, which will influence the LSV relationship. However, the deviation is apparently fairly slight and is expected to be a constant offset when considering the extracted binders over different ages since the extraction and recovery process remained constant irrespective of the age of the mixture. Additional observations of the PG 64-28 binder from Figure 3.39 also indicated measureable differences in the overall behavior of the binder at higher temperatures which are represented by the lower frequencies in the plot. The discontinuity or bump that occurs near 0.5 rad/s is presumably the separate behavior in the binder and SBS polymer. With these binders being almost completely unaged the asphalt phase of the binder is relatively soft and very fluid at the low frequencies and high temperatures that lead to that portion of the master curve. Under those same test conditions, the SBS polymer still retains a significant amount of elasticity and stiffness, therefore presumably creating the inflection point noted. As will be seen in further binder master curve data presented in later sections, this effect is relatively evident with the softer unaged binders but becomes less prominent as the binders are aged and the relative difference in stiffness is reduced. Further discussion on this matter will resume in the test results section of the binder measurements.

As an overall summary of the influence of the extraction and recovery process, these measures have suggested that the influence is relatively insignificant for the unmodified PG 64-22 binder. However, some slight influences were noted with the SBS modified PG 64-28 binder, both in the IR spectra representing the molecular structure of

the binder and the rheological measures representing the physical properties of the binder.

It should be noted that some of the samples left a very small amount of what appeared to be a light oil on the inside of the recovery flask as has previously been noted in previous research (Burr et al., 1990). Because of the limited amount of this material available, only preliminary measures were conducted which identify it as some type of light petroleum oil. Presumably these are lighter oils that were pulled out of the binder during the recovery process. However, because of the small volume of material observed, the inconsistency of which samples created it, ease of removing during the transfer from the recovery flask and storage tins, and the apparent lack of significant influence on the results, no further effort was extended to identify or prevent the creation of the residue. Presumably a lower recovery temperature or less severe vacuum would prevent the residue production, however solvent removal then may become problematic.

3.4 Aggregate Mineralogy

To provide a more in-depth characterization of the aggregates petrographic analysis were conducted following ASTM C295 in conjunction with the nomenclature defined in ASTM C294 (ASTM, 2010).

Although specifically related to Portland cement concrete aggregates, the petrographic analysis quantifies by visual observation, the mineralogical composition of the aggregate. The different mineral compositions are observed following the techniques

outlined in those procedures, but in general are conducted by visual observation, microscopic inspection, physical hardness estimations, and some limited chemical interactions. While a robust description of the petrographic examination protocol is much too lengthy and far outside the scope of this research effort, a general description of the major aspects will be provided for reference. Due to the specialized nature of these types of analyses, the petrographic analyses were conducted by Mr. Thomas J. Adams and Dr. Gretchen C. Schmauder with Terracon Consulting at the time.

Initial inspections of so called hand samples include observations of the color, texture, mineral grain size, fracture characteristics, relative hardness, acid solubility, or any other distinguishing features. Often times, with ample experience, mineral identification can be decided solely based upon visual observation of hand samples which provide the bulk aggregate properties. These observations are typically conducted using the unaided eye and some low power, up to x50 magnification, microscopic observations (Ingham, 2010).

A portion of the aggregates can then be fixed to a microscope slide and finely ground to a thin section which permits passable light. These thin sections may then be further analyzed with higher magnification microscopes and quantify the relative composition of the various mineralogical features contained within the aggregate. The thin sections may be on the order of 30 μm in thickness, which can vary depending upon the minerals being observed (Demange, 2012). The microscopic inspections often convey a great deal of information about the mineral composition of the aggregate sample being observed due to the different light sources used in that evaluation.

First, the sample is viewed under white, or normal, light conditions to observe certain crystalline features and observe the overall structure of mineral composition. Then, polarized light may be used to identify certain minerals. Initially, two polarizing films are oriented such that in-plane polarization of the light is applied and referred to as plane-polarized light (PPL).

Observations are then made of the thin sections by crossing the two polarizing films to create what is known as cross-polarized light (CPL). Certain minerals exhibit clearly identifying characteristics, such as color or a range of colors, under these optical conditions. Changing the direction of the polarized light, may permit the clear identification of other minerals in a process commonly termed preferential orientation of the mineral crystals, such quartz. Figure 3.40 presents an example of the preferential orientation of the quartz crystals (ISU, 2013) Each of the three crystals shown in the center of Figure 3.40 are quartz, however they are oriented in different directions relative to the plane of the applied CPL.

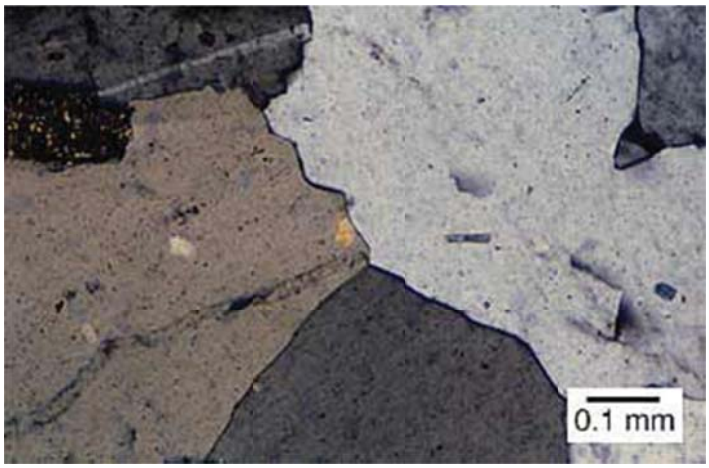

Figure 3.40 Example of Preferential Crystal Orientation, Quartz (ISU, 2013)

Additional features may be identified by contrasting the response of different minerals between PPL and CPL. An example presented in Figure 3.41, presents a clinopyroxene crystal in basalt under; (a) CPL and (b) PPL. It is clear how such techniques can readily identify certain minerals once their behaviors under these conditions have been documented.

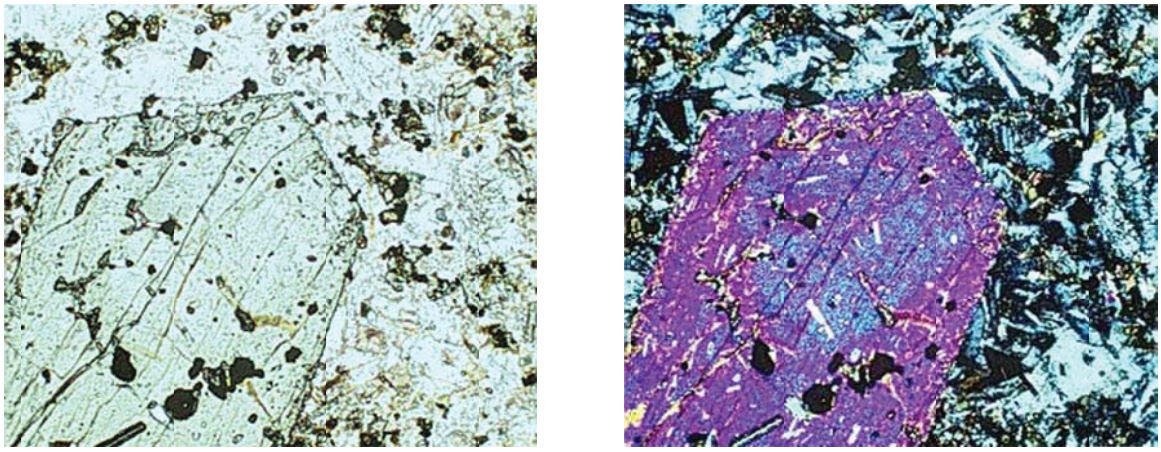

(a) **(b)**

Figure 3.41 Example of Clinopyroxene Crystal in Basalt Under (a) CPL and (b) PPL (ISU, 2013)

Another common characteristic trait noted with CPL called twinning, aids in the identification of certain minerals such as feldspar as depicted in Figure 3.42.

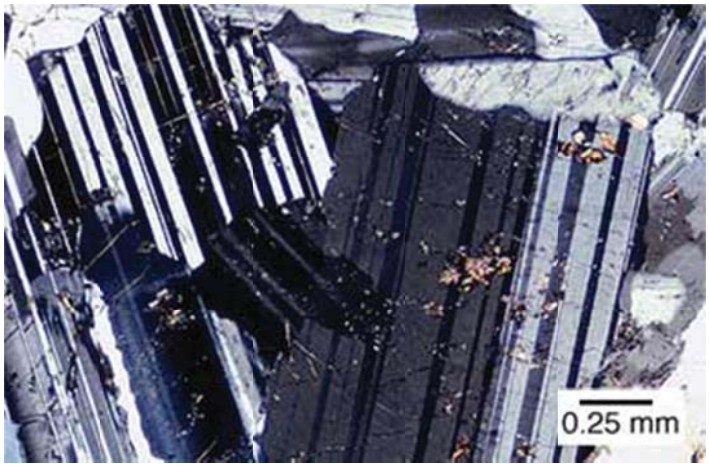

Figure 3.42 Example of Twinning, Plagioclase (ISU, 2013)

To be certain, many more observational techniques are utilized during the identification of each mineral component within a given sample. These are merely some of the most common identifiers which support the necessity for specialized personnel when conducting these measures.

After the identification of the various minerals within an aggregate specimen, each is quantified as the percentage of the two-dimensional area of the thin section to establish the composition of the entire specimen. In the case of mixed mineralogies within a given aggregate, such as a gravel source, the composition of each fraction is reported in conjunction with the overall percentage of each fraction.

3.5 Aggregate Image Measurement System Procedures

The Aggregate Image Measurement System (AIMS) was utilized to quantify the shape, angularity, and surface texture of aggregates used in this study. The AIMS acquisition

system makes use of a camera, microscope, back and top lighting, and an aggregate rotation tray to collect data which is then analyzed by the integrated software system (Pine, 2011). Since the AIMS was used as-is and no additional development of the method was conducted as part of this research, only a review of the procedure and a summary of the outputs will be discussed here. More in depth analysis of the functions and formulas utilized can be found in the referenced documentation (Pine, 2011).

Measurements are made on washed and dried aggregates from the maximum aggregate size through the full gradation down to material retained on the 0.075 mm (# 200) sieve. Materials smaller than the 0.075 mm (# 200) sieve are typically not included in the analysis, largely due to optical resolution limitations of the device. As a result of some measurements interacting with each other, particularly with the fine aggregate sizes, the quantitative measures are adjusted based upon the size of the material being measured. The differentiation between coarse and fine material is made on the 4.75 mm (# 4) sieve. Therefore the analysis of the data will vary according to coarse or fine aggregate measures.

3.5.1 AIMS Coarse Aggregate Analyses

The coarse aggregate measures are conducted by measuring each of 150 to 500 aggregate particle three times. The first scan used back lighting to achieve a high contrast image of the profile of each particle. The second scan utilizes top lighting to focus on the surface of the aggregate to measure the height or thickness of each individual particle. The third scan zooms in closely to quantify the surface micro-texture of each particle capturing

features on approximately 0.5 mm (0.02 in.) or less. From those three measures, four properties are calculated and presented for each aggregate size measured and are summarized below.

Coarse Aggregate Angularity

The Coarse Aggregate Angularity is calculated as a Gradient Angularity (GA) which is the quantification of the sharpness of two-dimensional images of the particles. The higher the GA, the more angular or sharper the corners are in the two-dimensional image of the aggregate. Strict calculation of the Gradient Angularity is presented in Equation 3.55.

$$GA = \frac{1}{\frac{n}{3} - 1} \sum_{i=1}^{n-3} |\theta_i - \theta_{i+3}| \qquad \textbf{Equation 3.55}$$

where, GA - Gradient Angularity;
n- total number of measured points on the particle;
θ_i- angle of orientation of the edge point, i.

Utilizing Equation 3.55, which sums the Gradient Angularity for each individual particle, the result has a relative scale of zero to 10,000. Following this method of calculation a perfect circle will have a small but non-zero value. The Gradient Angularity can be used as a metric of its own or may be combined with other measures to further characterize the aggregates as will be discussed further in later sections.

Coarse Aggregate Texture

The aggregate texture (TX) is a quantification of the relative smoothness of the particle surface, again only on the micro scale. Utilizing the wavelet method for quantification, the texture term exhibits a relative scale from zero to 1,000 with smoother surfaces depicted by smaller calculated texture index values. The TX is calculated from three separate images representing the horizontal, vertical, and diagonal directions, respectively. At a given decomposition level, TX is the arithmetic mean of the squared values of the wavelet coefficients for all three directions (Pine, 2011). The TX is presented in Equation 3.56, except for the proprietary decomposition function, which has necessarily been omitted.

$$TX = \frac{1}{3N}\sum_{i=1}^{3}\sum_{j=1}^{N}\left(D_{i,j}(x,y)\right)^2 \qquad \textbf{Equation 3.56}$$

where, TX - texture index;
N - total number of wavelet coefficients in an image;
i - 1, 2, or 3 for detailed images;
j - wavelet index;
$D_{i,j}$ - proprietary decomposition function;
x, y - location of coefficients in transformed domain.

Similar to the Gradient Angularity, the Texture Index can be used as a metric of its own or may be combined with other measures for further characterization.

Sphericity

Sphericity is a quantity that describes the overall three-dimensional shape of a particle. With a relative scale of zero to one, a value of one indicates equal dimensions in each

direction of an orthogonal space, i.e. a cubical shape. Sphericity is calculated for each particle as presented in Equation 3.57.

$$SP = \sqrt[3]{\frac{d_S d_I}{d_L^2}} \qquad \textbf{Equation 3.57}$$

where, SP - Sphericity measure;
d_S - the shortest dimension of the particle;
d_I - the intermediate dimension of the particle;
d_L - the longest dimension of the particle.

Coarse Aggregate Flatness, Elongation, Flat and Elongated, and Flat or Elongated Ratios

The flat and elongated measures of the AIMS are quite similar to those prescribed in ASTM D4791 (ASTM, 2010). In the procedure, a flat particle is defined as one where the width, or intermediate dimension (d_I) of the particle is greater than the thinnest portion (d_S) multiplied by the specified ratio factor. Typically, this factor is one, three or five. As an example, given a specified factor of three, a particle that is wider than three times its thickness will be considered flat for that analysis. By a similar calculation, one that is longer than three times its width will be considered elongated. Determinations of flat and elongated will quantify, usually as a percentage of the total mass or particle count, the portion of a certain sieve size where the maximum length exceeds the thickness multiplied by the given ratio factor. Particles of the flat or elongated designation will be determined by summing the representative percentages that are either flat or elongated.

Critically speaking, it is unlikely that AIMS flat and elongation measures will be exactly the same as manual measures (ASTM, 2010), due to the manual method appropriately seeking the absolute thinnest and absolute longest dimensions of a given particle. The automated and optical nature of the AIMS measures will not possess this directional orientation. However, the automatic measurement and strict calculation rules should presumably lead to more consistent results over time with the AIMS methodology.

The calculation methods for the AIMS measures of the flat and elongation parameters are similar to those of the ASTM, even though the procedures to obtain the inputs are quite different. Mathematically, the calculations are performed according to Equation 3.58 through Equation 3.61.

$$F = \frac{d_S}{d_I} \qquad \textbf{Equation 3.58}$$

$$E = \frac{d_I}{d_L} \qquad \textbf{Equation 3.59}$$

$$L/S = \frac{d_L}{d_S} \qquad \textbf{Equation 3.60}$$

$$ForE = \frac{d_I}{d_S} \; or \; \frac{d_L}{d_I} > R \qquad \textbf{Equation 3.61}$$

where, F - Flatness Ratio;
E - elongation ratio;
L/S - flat and elongation ratio;
$ForE$ - flat or elongated ratio;
R - specified ratio factor, e.g. 1, 3, or 5.

Coarse Aggregate Angularity Texture Value

As mentioned in previous sections, some of the terms can be combined to provide more of an overall assessment of the coarse aggregate characteristics in a single value. The proposed combined factor includes the coarse aggregate texture and the angularity gradient as presented in Equation 3.62.

$$CAAT = 10 * TX + 0.5 * GA$$

Equation 3.62

The combined $CAAT$ factor can provide an indication of the contribution of the aggregate texture and angularity on the internal friction of the aggregate. Indeed, it has been shown that this factor may be a significant parameter to the rutting resistance of asphalt mixtures (Ulloa, 2013).

Together, these coarse aggregate measures can provide quantitative information regarding the shape and texture of the coarse aggregate particles. These can be compared in side by side analysis or included in more detailed analysis which combines measures from certain sieve sizes into a combined characterization of some specific size distribution or aggregate gradation.

3.5.2 AIMS Fine Aggregate Analyses

Similar to the coarse aggregate measures, several characteristics are also determined from the fine aggregates. The measurement of angularity is basically measured in the same manner as the coarse aggregate fractions. However, surface texture and flat and elongation determination are no longer practical. Due to smaller aggregate sizes

considered in the fine aggregate measurements, an opaque or dark colored tray is used on materials retained on the 0.3 mm (# 50) sieve and smaller material. This is needed to enhance the contrast between the aggregate particles and the container.

Fine Aggregate Angularity

The fine aggregate angularity is measured by the same procedure as the coarse aggregate. Calculations are conducted in the same manner as presented in Equation 3.55.

Fine Aggregate Form 2D

As a consequence of the size of the fine aggregate beginning to approach or even becoming smaller than the measures being made, e.g. 0.5 mm micro-texture used to determine aggregate texture, some modification of the quantitative results are necessary. In the fine aggregate size range, complex interactions can occur with sphericity and flat and elongated measures becoming close in magnitude to texture determinations, thus causing unwanted error in those calculations. Specifically when trying to quantify the three dimensional shape of such small particles, these interactions are commonly multiplied by resolution limits or other logistic constraints of the equipment.

As a result, a modified calculation is utilized to characterize the shape of the fine aggregate which somewhat combines these parameters into a single Form 2D calculation. This parameter has a relative scale of zero to 20, with a perfect two-dimensional circle having a value of zero. Form 2D is computed solely on the two-dimensional or profile images of the fine aggregate and is presented in Equation 3.63.

$$Form\ 2D = \sum_{\theta=0}^{\theta=360-\Delta\theta} \left[\frac{R_{\theta+\Delta\theta} - R_{\theta}}{R_{\theta}}\right] \qquad \textbf{Equation 3.63}$$

where, $Form\ 2D$ – relative two-dimensional form of fine aggregate;
θ - angle of the particular measure of interest;
R_{θ} - radius of the particle at the angle θ;
$\Delta\theta$ - incremental difference in the angle θ.

Once the appropriate measures have been conducted, the information can be analyzed and processed for different purposes. Largely depending upon how the original materials were measured, the analysis can be conducted in several developed workbooks including those named: stockpile, shape, degradation, surface, or blend which are discussed as follows.

- **Stockpile:** The stockpile analysis method considers each of the measured sieve sizes and combines them into a single measurement value for the entire gradation. The measurements are combined based upon the relative contribution of each size compared to the whole, i.e. the measures are weighted according to the aggregate gradation for the stockpile.
- **Shape:** The shape calculations compare measurements of the same sieve size obtained from different material sources. Generally, this sheet was designed to compare different aggregate sources by comparing the same particle size for each.
- **Degradation:** The degradation format is established specifically for measurements before and after the Micro-Deval test procedure described in AASHTO T327 (AASHTO, 2012). The sheet essentially quantifies the

breakdown of the aggregate during the test into more specific measures compared to the standard percent loss.

- **Surface:** The surface calculation sheet is prepared to measure the surface characteristics of an asphalt pavement typically from a core specimen. The measures generally provide information on the surface height macro-texture as well as the surface texture measures, i.e. micro-texture for analysis purposes.
- **Blend:** The blend sheet enables established measures accumulated in the stockpile sheets to be compiled into complete gradations according specified blend percentages. In this manner, measures may be conducted on individual stockpiles so that the properties resulting from changes in the bin percentages during the design process may be estimated without having to rerun the individual measurements.

AIMS measurements conducted as a part of this study were performed using the stockpile sheets, but the material tested was the complete gradation used in the mix design. This method was utilized so each gradation could be evaluated as used in the design and as were used in the aged mixtures.

3.6 Asphalt Binder Oxidation Models

A great deal of the research efforts spent on oxidation measurements and characterization ultimately results in some type of modeling application. While the modeling of material

behavior is not a necessity, it is a highly sought after application for such measures. If the asphalt industry can accurately characterize the aging characteristics of a given mixture and appropriately model the change in those properties over time, remarkable improvements in pavement design procedures could be realized.

Clearly, attempts have been made to accomplish this and several aging models exist. Some are more comprehensive and therefore more complicated, but also tend to be more accurate in their predictions. Many of these models have been developed by researchers conducting the oxidation studies, which is a logical step for such investigations. Therefore, as a consequence of such development efforts, many of the models end up being strictly tied to the adopted measurement technique conducted during a particular research effort. This creates some ambiguity in regards to the appropriateness of one model compared to another. Since the input measurements for the respective models are often different, the resulting calculations are then different, it is difficult to compare the results and determine the most effective method to use.

A select few of the more common models will be discussed in the following sections.

3.6.1 Global Aging System

The Global Aging System, or GAS model, as it commonly termed is the aging model currently utilized by the Pavement ME Design software (AASHTOWare, 2013). The models are essentially a system of consecutive models that when used in succession are intended to adequately address the aging and thus stiffening effect of asphalt binders

within a pavement section. These models, being developed to function congruently with the A-VTS shifting function given in Equation 3.20, Equation 3.21, and Equation 3.22 are likewise presented in terms of the binder viscosity.

The first model estimates the binder viscosity after the mixing and laydown operations to simulate the initial stiffness of the binder immediately after construction and is presented in Equation 3.64 (Mirza and Witczak, 1995). This formula can be used to estimate the binder viscosity immediately after construction, unless actual measurements of binder viscosity after aging in rolling thin film oven (RTFO) or extracted and recovered binders after mixing and laydown are available for use.

$$\log(\log(\eta_{t=0})) = a_0 + a_1 \log\big(\log\big(\eta_{orig}\big)\big) \qquad \textbf{Equation 3.64}$$

where, $a_0 = 0.054405 + 0.004082 * code$
$a_1 = 0.972035 + 0.010886 * code$
$\eta_{t=0}$ – binder viscosity after mixing and laydown, cP, at the ref. temp., T_r °R;
η_{orig} - viscosity of original binder, cP, at the ref. temp., T_r °R;
$code$ - hardening resistance, takes on a value of -1, 0, 1 or 2 depending on a ratio of the $\log\log \eta_{RTFO}$ and $\log\log \eta_{orig}$;
η_{RTFO} - viscosity of RTFO aged binder, cP, at the ref. temp., T_r °R.

The next equation in the system predicts the viscosity of the binder at what is called the surface of the pavement at any desired time in the service life of the pavement. The surface is defined as approximately 6 mm (0.25 in.) below the actual surface of the pavement, largely due to this model being developed from field core samples. As a result, the so called surface measurements of the cores were assumed to include the very surface as well as some small depth into the core (Mirza and Witczak, 1995).

$$\log\log\eta_{t>0} = \frac{\log(\log(\eta_{t=0})) + A * t}{1 + B * t}$$ **Equation 3.65**

where, $A = -0.004166 + 1.41213 * C + C * \log(Maat) + D * \log(\log(\eta_{t=0}))$
$B = 0.197725 + 0.068384 * \log(C)$
$C = 10^{274.4946 - 193.831 * \log(T) + 33.9366 * \log(T)^2}$
$D = -14.5521 + 10.47662 * \log(T) - 1.88161 \log(T)^2$
$\eta_{t=0}$ – binder viscosity after mixing and laydown, cP, at temperature, T °R;
$\eta_{t>0}$ - binder viscosity at time t, cP, at temperature, T, °R;
$Maat$ - mean annual air temperature, °F;
T - temperature, °R;
t - time in months.

Additional model equations of the same form are also included in the GAS to represent changes in the air void level and the viscosity as a function of depth in the asphalt concrete layer.

As can be seen by Equation 3.64 and Equation 3.65 summarizing the GAS aging models relevant to this discussion, these models are regression models fit to a database of viscosity measures based largely upon unmodified binders tested at the time of development. Based on this background information, it is fairly clear that these predictions are valid for the set of conditions that are included in the fitting data set. Specifically, if the binder characteristics, environmental conditions, or any other conditions inherently built into these models change, the predicted binder viscosities may no longer be accurate and should be considered suspect.

To improve upon the limitations of empirical models, more materials based inputs into more fundamentally based models are being developed.

3.6.2 Western Research Institute Procedure

A much more fundamentally based approach has recently been under development by Mr. Ron Glaser of the Western Research Institute (WRI) in Laramie, Wyoming. This model is founded largely upon the dual oxidation mechanism of asphalt binders that had previously been developed at WRI by Dr. J. Claine Petersen and his colleagues (Petersen and Harnsberger, 1998). Sparing much of the discussion on the actual chemical processes proposed, the dual oxidation mechanism rationalizes the oxidation process to describe the two main products of asphalt binder oxidation as sulfoxides and later in the oxidation process ketones.

Both of these functional groups have previously been discussed in the section on the FT-IR spectroscopy measures. Recall, the sulfoxides are the functional groups created upon oxidation including sulfur molecules. These were identified in the FT-IR measures as the peak developing near 1,034 cm^{-1}. The ketone structure was identified in the FT-IR measures as the peak developing near 1,693 cm^{-1}. Ketones as identified in Figure 3.35(a), is presented as one of the molecular groups categorized in the larger functional group of carbonyl. The carbonyl function group presents itself as a band developing between about 1,820 and 1,650 cm^{-1}, with happens to be located on the side of the carbon double bond peak located near 1,600 cm^{-1}.

With these oxidation products in mind as the final result of the aging process of asphalt binder, an oxidation model was formulated based on extensive laboratory studies (Petersen and Glaser, 2011). The proposed asphalt binder oxidation rate equation is depicted in Equation 3.66 (Glaser et al., 2012).

$$[P(t)] = M\left(1 - \frac{k_2}{k_1}\right)\left(1 - e^{-k_1 P_{O_2}^n t}\right) + k_2 P_{O_2}^m M t + [S = O + C = O]_{rtfo} \quad \textbf{Equation 3.66}$$

where, $[P(t)] = [S = O + C = O]_t$,
oxidation pressure or sulfoxide and carbonyl contents over time, t;
$k_1 = e^{18.78} e^{\frac{-7164}{T}}$,
fast reaction rate coefficient;
$k_2 = e^{10.95} e^{\frac{-5207}{T}}$
slow or constant reaction rate coefficient;
$P_{O_2}^m = \left({P_{tot}}/{0.74}\right)^m$
$P_{O_2}^n = \left({P_{tot}}/{0.74}\right)^n$
P_{tot} - atmospheric pressure applied during aging, 0.74 atm for Laramie, Wyo.
m, n pressure exponents, determined experimentally for constant and fast rate atmospheric pressure, respectively;
M - time zero concentration of sulfoxide and carbonyl, fitted parameter indicative of the aging rate of the binder;
T - temperature;°K
t - time, days;
$[S = O + C = O]_{rtfo}$,
sulfoxide and carbonyl content of binder after RTFO aging.

Although still under development to achieve the final form, Equation 3.66 is proving to be quite effective in the laboratory assessment of asphalt binder oxidation measurements. These relationships provide a much better fundamental understanding of the oxidation kinetics of asphalt binders.

To clarify, the carbonyl and sulfoxide measurements utilized in this model were obtained utilizing the peak height measures with direct transmission method of FT-IR spectroscopy. These measurements were made utilizing 50 mg of asphalt binder per milliliter of carbon tetrachloride (CCl_4,) as the solvent with a 1 mm path-length in the measurement cell.

This protocol is mentioned in regards to the increase in popularity of FT-IR measurements, specifically those measured with attenuated total reflectance attachments. It is important to note that the appropriateness of this method has not been validated with ATR measurements. There is the potential for concern in with ATR measurements since the quantification measures are conducted two different wavenumbers. This can be problematic depending upon the change in the depth of penetration (DP) between the measurements of carbonyl, 1,693 cm^{-1}, and the sulfoxide, 1,034 cm^{-1}, functional groups. This is not to state that ATR measures nor utilizing peak area determinations are not applicable to this method, only to clarify that such assessments have not been conducted to date and thus are unverified in terms of accuracy.

3.6.3 Texas A&M Methodology

The methodology specific to the Artie McFerrin Department of Chemical Engineering at Texas A&M University has been developed over the course of many years under the direction of Dr. Charles J. Glover and his research team. These models are much more complicated when compared to the previous regression type relationships on viscosity, but are much more applicable in the general sense of providing a clearer depiction of the actual interactions and processes taking place during the oxidative aging of an asphalt binder.

Although there are a few different versions of the overall process available in the literature based upon the level of complexity in the analysis, the method essentially comes down to a partial differential equation to represent the partial pressure of oxygen

present in an asphalt binder film. The partial pressure of the oxygen may be likened to the oxygen concentration, or amount of oxygen, within the asphalt binder through Equation 3.67 (Han, 2011).

$$C_{O_2} = h\left(\frac{P_{O_2}}{RT}\right) \qquad \textbf{Equation 3.67}$$

where, C_{O_2} – oxygen concentration of asphalt binder phase;
h - Henry's Law constant, temperature dependent and dimensionless;
P_{O_2} - partial pressure of oxygen gas phase;
R - ideal gas constant, 8.3144621 J/mol•°K ;
T - temperature, °K.

It is well established that Henry's Law constant is temperature dependent, thus suggesting it should be a coefficient rather than a constant. As such, it is often represented by the relationship found in Equation 3.68 with the h_0 and T_r parameters specific to the substance in question. For asphalt binders h_0 has been found to be 0.0076 at 30°C, thus modifying Equation 3.68 to the formula on the right (Han, 2011).

$$h = h_0[1 + 0.00215(T - T_r)] = 1.634 * 10^{-5}(T) - 2.647 * 10^{-3} \qquad \textbf{Equation 3.68}$$

where, h - Henry's Law constant, dimensionless;
h_0 - h at the reference temperature, 0.0076 at 303.15°K;
T - temperature, °K.
T_r - reference temperature, 30°C or 303.15°K in this case;

Based on these developed relationships, the overall equation driving the oxidation growth within an asphalt binder film is represented by the partial differential equation presented as Equation 3.69 in the cylindrical coordinate system.

$$\frac{\partial P}{\partial t} = \frac{1}{r}\frac{\partial}{\partial r}\left(r D_{O_2}\frac{\partial P}{\partial r}\right) - \left(\frac{cRT}{h}\right) r_{CA} \qquad \textbf{Equation 3.69}$$

where, P – partial pressure of oxygen in the asphalt binder film;
t - time, days;
r - radial distance in calculation, relative to pore and binder shell radii;
D_{O_2} – diffusivity of asphalt binder, m^2/s;
c - experimental constant, range from 2.75 to $4.59*10^{-4}$ with an average value of $3.71*10^{-4}$ used in most calculations;
R - ideal gas constant, 8.3144621 J/mol•°K ;
T - temperature, °K;
h - Henry's Law constant, dimensionless;
r_{CA} – rate of carbonyl area, CA, growth;

Due to the complex nature and significant dependency and interrelationships among many input parameters contained within Equation 3.69, a closed form solution is not currently available to solve the partial differential equation. Therefore, the actual solution must be determined numerically, most easily accomplished using a mathematical software package available for such purposes. Currently, a Matlab ® code has been developed and is available to produce carbonyl predictions utilizing this protocol.

Some parameters included within Equation 3.69 require several additional relationships and parameters that should be determined experimentally. One of the most significant material inputs result from kinetics measures of the asphalt binder aged over different durations at different temperatures. Kinetics measurements are conducted by quantifying the oxidation of the asphalt binder at hand over the range of aging temperatures and durations. The oxidation measures associated with this methodology are again obtained through FT-IR spectroscopy measures to determine the carbonyl area (CA) which was computed as the area, in arbitrary units, between the absorption spectrum and the magnitude of the absorption at 1,820 cm^{-1} as the baseline and between

the wavelengths of 1,650 and 1,820 cm^{-1}. This area was calculated utilizing the FT-IR software, Omnic, following a macro written specifically to determine the peak area within this region. An example of the data produced by such measures is presented in Figure 3.43.

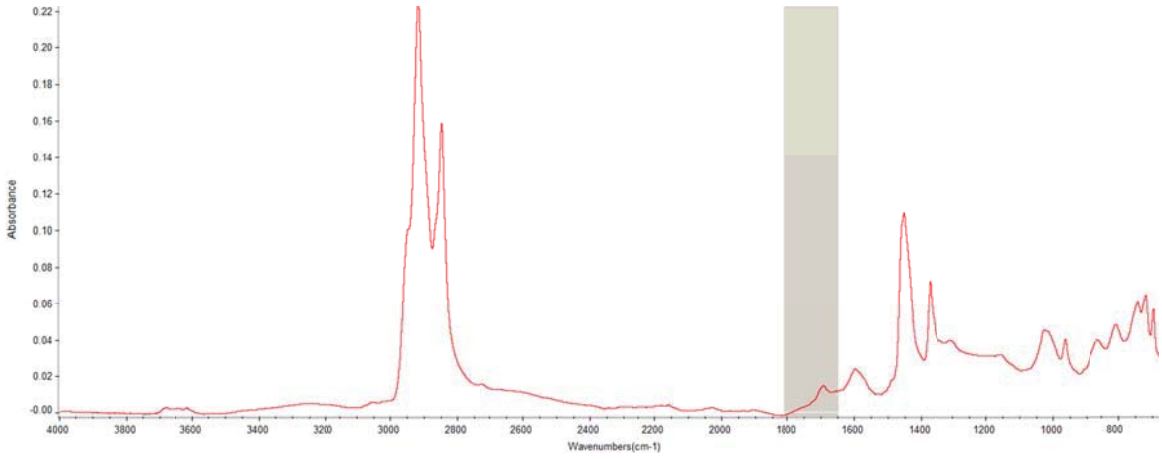

Figure 3.43 Example of Carbonyl Area Measurements

Equation 3.69 includes the kinetics measures in the form of the r_{CA} term. This term is aptly termed the constant rate kinetics parameter representing the constant or slower rate of oxidation as is presented in Figure 3.44, and Equation 3.70.

$$r_{CA} = AP^{\alpha} e^{-E_a/RT}$$ **Equation 3.70**

where, r_{CA} – rate of carbonyl area, CA, growth;
A - pre-exponential factor;
P - absolute oxygen pressure during oxidation, atm;
α reaction order with respect to oxidation pressure;
E_a - activation energy, J/mol;
R - ideal gas constant, 8.3144621 J/mol•°K ;
T - temperature, °K.

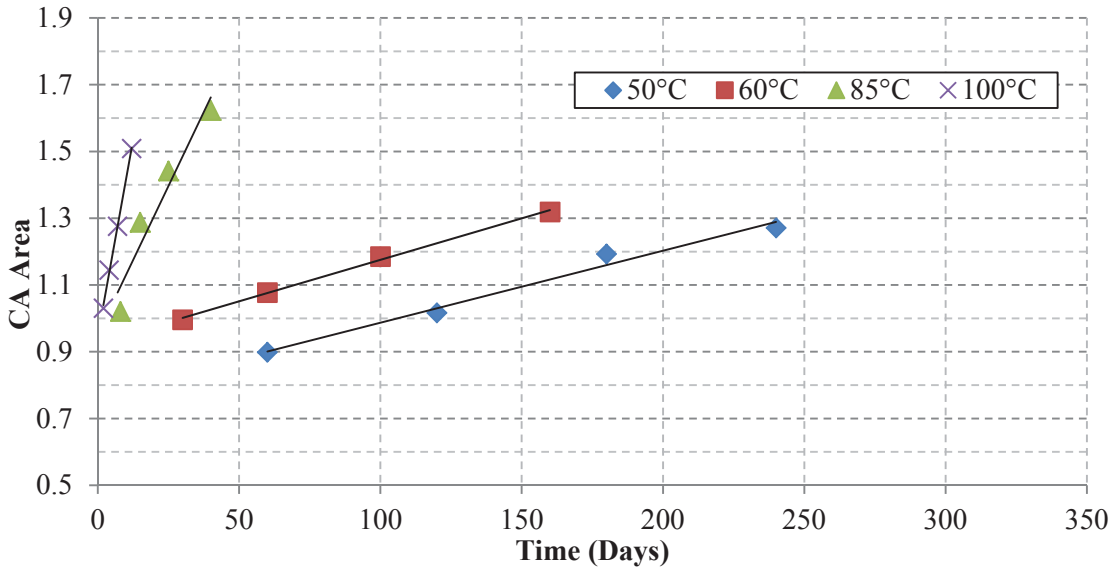

Figure 3.44 Example of Constant Rate Kinetics Measurements

The measures exemplified in Figure 3.44 are considered constant rate kinetics due to each aging temperature exhibiting a linear relationship with time. These measures are fit to the form of Equation 3.70 by considering the oxidation rate for each isothermal aging condition as a function of temperature, specifically the inverse of temperature and the ideal gas constant, $^{1}/_{RT}$. By taking the slope of each linear temperature condition and plotting with the $^{1}/_{RT}$ term, the relationship may be determined by the Arrhenius form of Equation 3.70 as presented in Figure 3.45.

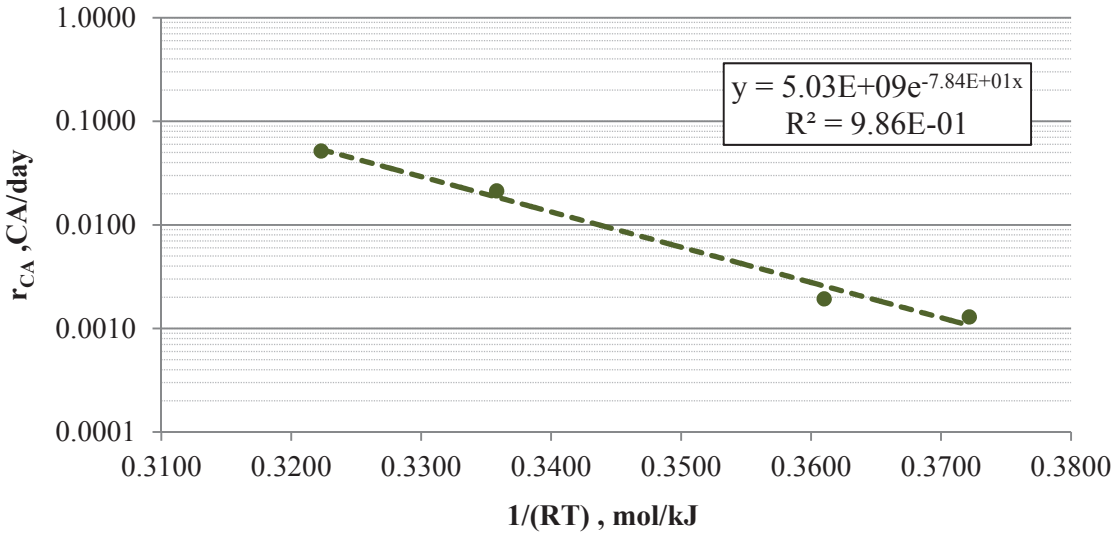

Figure 3.45 Example of Constant Rate Kinetics Measurements

The oxidation kinetics of the asphalt binders are reported in this format and will be included in further considerations of the aged binder properties. Additional developments at Texas A&M produced kinetics measures although chronologically preceding, but very similar in form to those discussed with the previous WRI model. The methodology utilized in the Texas A&M model retained the emphasis of oxidation measures on the carbonyl area and deemed the considerations of the sulfoxide functional group unnecessary.

To capture the oxidation behavior of the binder in the fast rate region of the kinetics measurements, shorter aging durations are necessary for each respective aging temperature. Graphically, the additional measures represented by Figure 3.46.

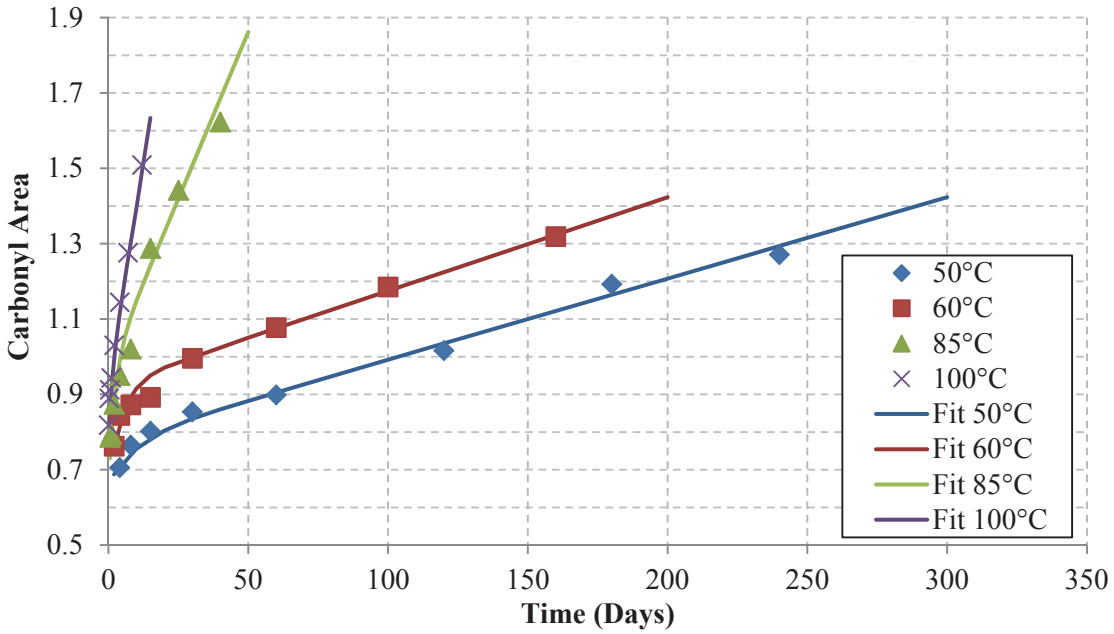

Figure 3.46 Example of Fast and Constant Rate Kinetics Measurements

Similar to the fast rate and constant rate measures, k_1 and k_2 from the WRI model, the Texas A&M version includes k_f and k_c determined from the initial fast rate and the slower constant rate terms, respectively. These two can generally be combined into one relationship for carbonyl area as depicted in Equation 3.71.

$$CA = CA_0 + (IJ - CA_0) * \left(1 - e^{-k_f t}\right) + k_c t \qquad \textbf{Equation 3.71}$$

where,
- CA - carbonyl area, CA;
- CA_0 - original or tank CA measurement;
- IJ - initial jump, magnitude of fast rate reaction in terms of CA;
- k_f fast rate of CA growth;
- k_c slow or constant rate of CA growth;
- t time, days.

During the initial planning stages of this research, it was not fully recognized if the fast rate kinetics measurements provide significant benefit to kinetics measurements and the resulting binder characterization. At that time, it was suggested to improve the efficiency of laboratory testing, initial or fast rate kinetics may be excluded. Therefore, the main focus of this research and the vast majority of the laboratory determinations associated with it are commensurate with the slow or constant rate kinetics measures.

In fact, the majority only include the constant rate measures as these are the characteristics that are expected to control the oxidation process over the majority of pavement aging. Therefore, the vast majority of the measurement and analyses included in the study are based upon the constant rate kinetics measures depicted in Figure 3.44, and Equation 3.70. Significant effort has been put forth to assure the time periods utilized for the respective aging temperatures would result in the constant rate period of each asphalt binder. Therefore, the majority of the measures produced during this study are intentionally past the fast rate response period.

The second most significant factor that must be determined through laboratory measures is termed the hardening susceptibility (HS). The HS term specifically relates the binder stiffness, here represented as LSV, η_0^* as a function of aging, again using the carbonyl area. The HS relationship is defined mathematically by Equation 3.72.

$$\ln \eta_0^* = HS * CA + m$$

Equation 3.72

where, η_0^* - low shear viscosity of the asphalt binder, Poise;
HS - hardening susceptibility, Poise/CA;
CA - carbonyl area, CA;
m - intercept of $\log \eta_0^*$ and CA relationship, Poise.

The HS relationship is typically unique to each binder. However, it has been observed through coincidence that many binder of similar composition often have similar HS relationships. Using the same aging protocol as the kinetics studies, measurement of η_0^* can be determined with each CA measurement to develop HS relationships. Typically the HS relationship for a given binder is constant with aging temperature and may be represented as one relationship as presented in Figure 3.47 as an example.

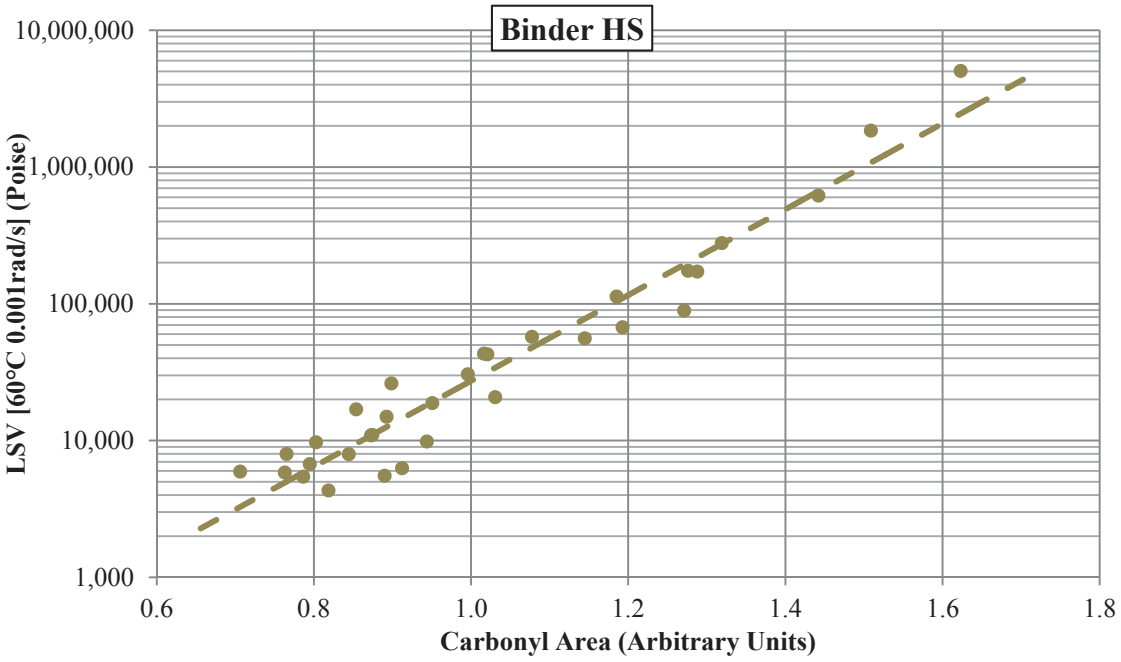

Figure 3.47 Example of Hardening Susceptibility Determinations

Utilizing the binder kinetics relationship, CA vs. time, and the hardening susceptibility, LSV vs. CA, will permit many observations and studies to be conducted on the aging of different asphalt binders and mixture configurations. Based on these capabilities, a significant portion of this study will focus on these types of analyses. However, other

material and environmental inputs are necessary to utilize the full oxidation predictions available through Equation 3.69.

Other necessary inputs are derived from the results of another relationship used with the overall model. One example of this ii the oxygen diffusivity (D_{O_2}), term attributable to work published by Reid (Reid et al., 1984). Throughout the development efforts of the carbonyl growth model, a correlation between the diffusivity and the viscosity of the asphalt binder has been established (Lunsford, 1994). Further refinements of more detailed experimentation have since been conducted and are presented in Equation 3.73 (Han, 2011).

$$D_{O_2} = T * 5.21 * 10^{-12}(\eta_0^*)^{-0.55}$$ **Equation 3.73**

where, D_{O_2} – diffusivity of asphalt binder, m^2/s;
T - binder temperature, °K;
η_0^* - shear rate limiting viscosity, LSV, Pa•s.

In order for the carbonyl growth model, Equation 3.69, to adequately predict the aging of an asphalt binder, the analysis also needs sufficient temperature inputs typically utilized as a thermal profile. A thermal profile may be as simple as isothermal conditions (i.e. constant temperature) or they may be as complicated as hourly temperature fluctuations from various depths in a pavement section from the field. While the isothermal conditions are very simplistic, the hourly field temperatures a much more complicated and generally require predictive modeling to obtain sufficient data to support the carbonyl predictive model. Such a model for the surface temperature, Equation 3.74, has been developed in conjunction with the carbonyl growth model at Texas A&M University

(Han, 2011) and has also been developed into a software package at the University of Nevada, Reno (Alavi et al., 2014).

$$\rho C \frac{\Delta x}{2} \frac{\partial T_s}{\partial t} = Q_s(1 - \tilde{\alpha}) + \varepsilon_a \sigma T_a^4 - \varepsilon \sigma T_s^4 - h_c(T_s - T_a) + k\left(\frac{\partial T_s}{\partial x}\right) \quad \textbf{Equation 3.74}$$

where, ρ – material density;
C - heat capacity;
ρC – volumetric heat capacity of the pavement;
x - depth into the pavement layer;
T_s – surface temperature, °K;
T_a – air temperature, °K;
t – time;
Q_s – heat flux due to solar radiation;
$\tilde{\alpha}$ – albedo of pavement surface (fraction of reflected solar radiation);
ε_a – absorption coefficient of the pavement;
ε – emissivity of the pavement;
σ – Stefan-Boltzman constant, $5.68*10^{-8}\ {}^{W}/_{m^2K^4}$;
h_c – heat transfer, a function of temperature and wind speed, ${}^{W}/_{m^2K}$;
k – thermal conductivity of the asphalt mixture;

Once the temperature has been determined at the surface, heat transfer through the pavement layers can be modeled by the more classical thermal diffusion relationship shown in Equation 3.75.

$$\frac{\partial T}{\partial t} = \kappa\left(\frac{\partial^2 T}{\partial x^2}\right) = \frac{k}{\rho C}\left(\frac{\partial^2 T}{\partial x^2}\right) \quad \textbf{Equation 3.75}$$

where, T – pavement temperature, °K;
κ - thermal diffusivity.

While these descriptive equations are far from a robust explanation of pavement temperature profile modeling, further development and analysis discussions are included elsewhere (Han, 2011; Alavi et al., 2014). These models are significant to this research effort by combining the weather data from field measures and historical air temperature inputs into the temperature profile models to provide accurate temperature predictions at multiple locations within a pavement section as a function of time. These temperature profiles can then be used by the carbonyl prediction model to assess the expected oxidation within the pavement structure as described by the protocol outlined by the Texas A&M procedures. These methods will be the basis for many of the research efforts that have been conducted in this study.

Modifications to the Texas A&M Procedure

The previous section presented what is typically referred to as the state of practice of oxidation modeling and characterization readily available to the asphalt pavement community. This research was not conducted merely to provide data within the standard practice methodology, although some of the measures will provide this benefit. During the course of this study, a few aspects of the standard methodology were reviewed and subsequently revised.

One such modification to the traditional methodology focused on the growth of the CA measurement rather than considering the CA measurement itself in certain instances. The growth is represented as the difference between the measured CA at a given aging condition and the CA measurement of the original binder otherwise known as CA_{Tank}. By considering the CA measurements in this manner any influences of the magnitude of

the CA measures on statistical significance determinations will be nulled by CA_{Tank}. For simplicity, the oxidation will be represented as carbonyl growth (CAg), which is defined by Equation 3.76.

$$CAg = CA_i - CA_{Tank}$$ **Equation 3.76**

where, CA_i - carbonyl area measured at specific aging condition i;
CA_{Tank} - carbonyl area of the binder at the original or unaged condition.

Another aspect of this study that has received a significant amount of investigation contributed to modifications in the determination of the low shear viscosity. The established method traditionally utilized dynamic shear rheometer measures at 0.1 rad/s at 60°C as the LSV determination. It was noted that some materials were not within the desired low shear plateau region under those testing conditions such as the example in Figure 3.28, particularly polymer modified asphalt binders. Therefore, the protocol using the master curves represented by the complex viscosity was developed and used for this effort.

As a natural consequence of the proposed improvements to the LSV determinations, it is logical to expect some slight modifications to the hardening susceptibilities of the measured binders. While some influence may be noted, both the aged asphalt binders and the binder recovered from aged mixtures were evaluated using the same protocol. Therefore, the two are still considered to be valid comparisons, although the actual LSV determinations with the modified method are expected to be more technically sound from a rheological standpoint.

3.7 Statistical Evaluation Methods

While a great deal of information may be obtained by observing tables of data along with plots or figures of the same information, there are certain circumstances which require a more detailed analysis to clearly differentiate and interpret data sets. In these instances a wide range of available statistics tools and analysis techniques are readily available to further analyze and distinguish significant similarities and differences.

Of the many available options, a select few statistical tools have been utilized as part of this research effort. Those more common techniques are discussed in the following sections.

3.7.1 Analysis of Variance

The analysis of variance, ANOVA, can be utilized within the Minitab software to test the statistical significance of noted differences between measures or other characteristic parameters. ANOVA provides methods to compare the mean of two or more (MANOVA) data sets by analyzing the variance of the input data and uses the F-statistic to determine significance of the input factors between the respective data sets. Significance detection in this study was determined at an α value of 0.05 confidence level, which is defined as a 5% percent chance that the determination if significance is untrue. Specifically, if the probability term, i.e. P-value, is less than or equal to the α value, the F-statistic is understood to be significantly influential at that confidence

interval. Thereby finding the particular parameter used to determine the F-statistic to be statistically significant to the analysis.

In order for these analyses to be statistically valid, several assumptions of the data sets must be verified. The basic assumption required for ANOVA or MANOVA statistical evaluations state that the data set must not exhibit multicollinearity among the predictor variables which should result in random experimental errors with normal distribution and a mean of zero and the variance of each statistical grouping should exhibit homogeneity of variance, i.e. equal variance (Kuehl, 2000; Fernandez, 2003). Verification of the necessary assumptions are made through visual observations of residual calculations presented in Figure 3.48, as an example.

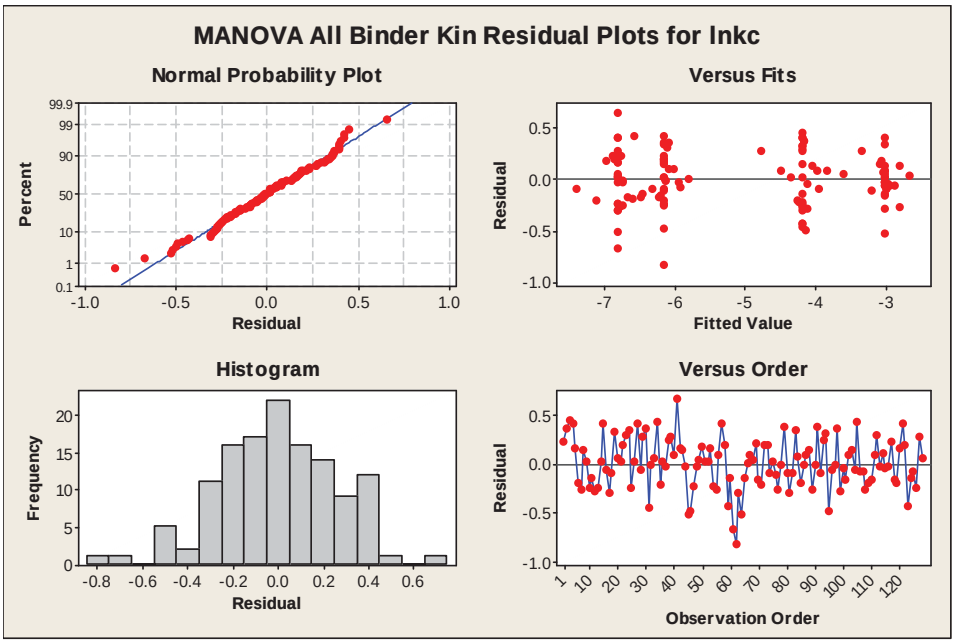

Figure 3.48 Example of Visual Verification of Statistical Assumptions

The statistical assumptions are verified by observing each of the plots contained in Figure 3.48. First, the normal probability plots should be verified to be a relatively straight line, otherwise the error distribution is not considered normal (Kutner et al., 2004). The frequency histogram is utilized to verify the mean of the residual errors generally follow a normal distribution with the mean near zero. The residual plots as a function of the fit and order can be assessed to verify the is no collinearity of the error terms with either fitted values, i.e. magnitude of the predicted value, the order by which the data is presented, e.g. either time or sampling order effects. These two plots can also be observed to verify that the residual error occurs in a random fashion and is of relatively equal magnitude, such as not dependent upon the sampling order etc.

3.7.2 Multivariate Linear Regression Techniques

Further statistical analyses were conducted utilizing multivariate linear regression techniques. While many statistical comparisons quite similar to the ANOVA analyses are used internal to the software calculations, linear regression modeling is used in a fairly different fashion.

The basic assumptions required for multivariate linear regression evaluations are quite similar to the ANOVA conditions and state that the data set must not exhibit multicollinearity among the predictor variables which should result in random experimental errors with normal distribution and the variance of each statistical grouping should exhibit homogeneity of variance, i.e. equal variance (Kutner et al., 2004).

The model function utilized in these comparisons was based upon the general linear regression model (GLM) with some additional considerations including transformed variables, qualitative predictor variable, and interaction terms. An example of the form with two input variable is depicted by Equation 3.77.

$$Y_i = \beta_0 + \beta_1 X_{i1} + \beta_2 X_{i2} + \beta_3 X_{i1} X_{i2} + \varepsilon_i \qquad \textbf{Equation 3.77}$$

where, Y_i – dependent variable in the analysis;
β_0 - intercept of the base equation (condition A);
β_1 - slope of the base equation (condition A);
β_2 - modification to the intercept of the base equation due to condition B;
β_3 - modification to the slope of the base of the equation due to condition B;
X_{i1} - independent predictor variable (quantitative in this example);
X_{i2} - qualitative predictor variable (dummy variable);
$X_{i2} = 0$, for condition A,
$X_{i2} = 1$, for condition B,
ε_i - independent error term of normal distribution and equal variance;
$i = 1, \ldots, n$ as the number of input data points.

The response function can be considered to follow to form of Equation 3.78, with X_2 as either a qualitative or dummy variable used to distinguish between the two data sets or a quantitative variable which would adjust the intercept by the value of β_2 and the slope of the regression by the product of $\beta_3 X_2$.

$$E\{Y\} = \beta_0 + \beta_1 X_1 + \beta_2 X_2 + \beta_3 X_1 X_2$$ **Equation 3.78**

where, $E\{Y\}$ – predicted dependent variable in the analysis;
β_0 - intercept of the base equation (condition A);
β_1 - slope of the base equation (condition A);
β_2 - modification to the intercept of the base equation due to condition B;
β_3 - modification to the slope of the base of the equation due to condition B;
X_1 - independent predictor variable (quantitative in this example);
X_2 - qualitative predictor variable (dummy variable);
$X_2 = 0$, for condition A,
$X_2 = 1$, for condition B.

Interpretation of this response function was used extensively in this study by noting the significance of the β_2 term as the significance of condition B on the intercept (β_0) of regression equation based on condition A. Similarly, the influence of the interaction term is determined by the significance of that respective coefficient (i.e. β_3). Physically, the interaction is noted as the adjustment of the slope due to condition B on the overall or base model slope (β_1) noted as condition A. To summarize, if both influences of condition B are found to be significant, the respective response functions for condition A and condition B are given by Equation 3.79 and Equation 3.80, respectively.

$$E\{Y_A\} = \beta_0 + \beta_1 X_1$$ **Equation 3.79**

$$E\{Y_B\} = (\beta_0 + \beta_2) + (\beta_1 + \beta_3) X_1$$ **Equation 3.80**

Following this form, the various material factors (e.g. binder types) mixture characteristic, aggregate sources, etc., were analyzed to detect the significance of these factors on the various relationships considered. In this particular study, the significance of the potentially different relationships were investigated using regression fitting and

significance tests using the Minitab 15 software (Minitab, 2006) by analyzing the variance of the input data and using the t-statistic to determine significance of the input factors between the respective data sets. Significance detection was determined at an α value of 0.05 significance level, which is defined as a 5% percent chance that the determination if significance is untrue. Specifically, if the probability term, i.e. P-value, is less than or equal to the α value, the t-statistic is understood to be significantly influential at that confidence interval. Thereby finding the particular parameter used to determine the t-statistic to be statistically significant to the analysis. It should be noted that for a given α value the F-statistic is numerically equivalent to a two-tailed t-statistic (Kutner et al., 2004).

Clearly, not all the regression analyses conducted in this study will contain only one quantitative predictor variable given all the mixture characteristics parameters to be investigated. In these instances, there is a significant potential for the independent predictive factors to exhibit collinearity between them, which violates the assumptions of the statistical analysis methods. To detect these potentials, correlation matrix plots and tables were analyzed similar to the examples provided in Figure 3.49 and Table 3.5, respectively.

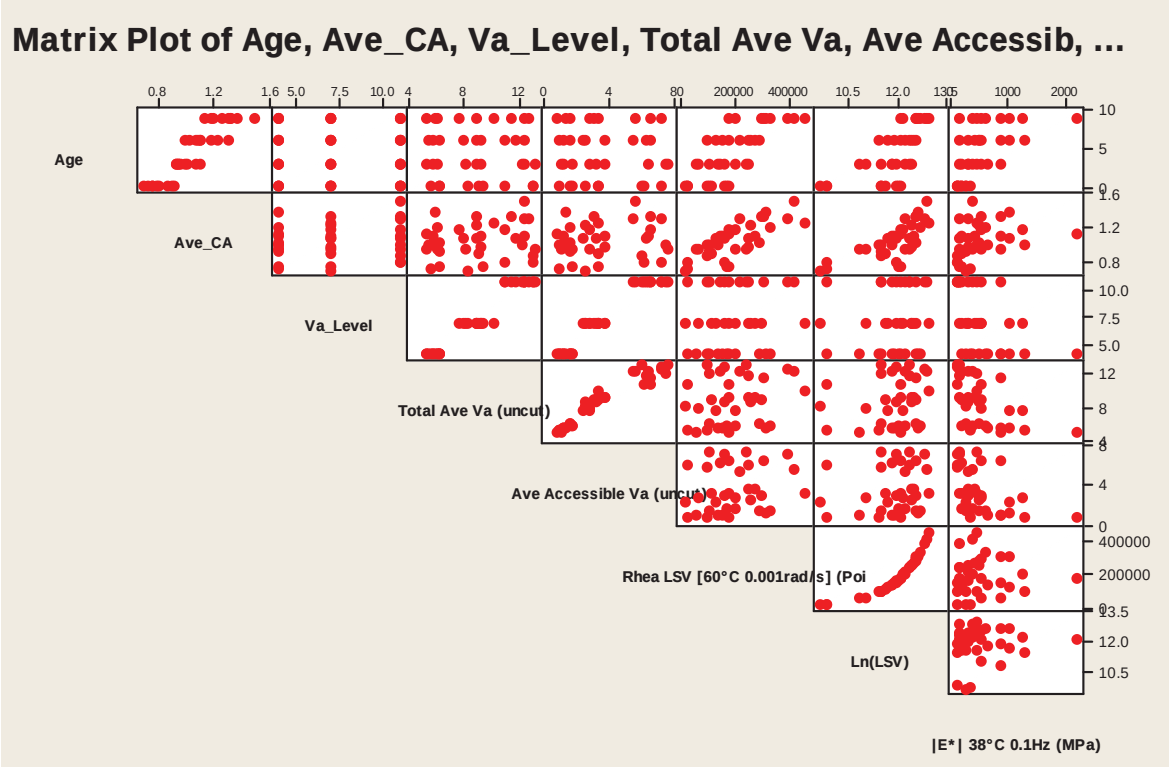

Figure 3.49 Example of Correlation Matrix Plots

Table 3.5 Example Correlation Matrix[a]

	Ave_CA	Va_Level	Total Ave_Va (uncut)	Ave Accessible Va	Ln(LSV)	|E*| 38°C 0.1Hz
Age	0.904 0.000	0.000 1.000	-0.025 0.886	-0.029 0.869	0.669 0.000	0.546 0.001
Ave_CA		0.188 0.271	0.182 0.288	0.144 0.401	0.720 0.000	0.322 0.055
Va_Level			0.972 0.000	0.970 0.000	0.108 0.531	-0.447 0.006
Total Ave_Va (uncut)				0.963 0.000	0.210 0.220	-0.543 0.001
Ave Accessible Va					0.171 0.318	-0.491 0.002
Ln(LSV)						0.086 0.617

a – Each cell contains the Pearson Correlation on the top and the associated P-value on the bottom.

If two input variable were found to exhibit significant collinearity, such as the first cell showing the correlation between the Age and Ave_CA, one of the two variables was removed from the analysis. First, the most logically appropriate parameter would be retained. Lacking any logical difference between the two parameters, the most influential parameter would be determined and retained. This was conducted by first removing one of the parameters to detect the influence associated with that parameter on the overall regression equation. Then, the first parameter was returned to the analysis and the second was removed. The final model included whichever parameter was found to be most influential to the overall fitted function, while the other was omitted from the final model form.

In more complicated portions of the analyses where more than one independent variable were found to exhibit collinearity issues, the addition and removal of the input parameters into the respective models were partially automated utilizing a stepwise regression function available through the Minitab software package. Essentially, the stepwise regression function methodically adds an input variable to a base regression equation one at a time from a predetermined list and examines the influence of that parameter on the overall fit of the regression equation. In a similar fashion, input variables may also be removed from the fitted regression equation to determine their respective influence on the overall regression analysis. In this study a method termed forward and backward was utilized which alternatingly added and removed select input variables from the analysis if the parameter exhibited a significant influence determined by an alpha value of 0.15.

Specifically in this analysis, a correlation matrix was first constructed of the input variables to determine which exhibited significant collinearity within a given data set. Then, logically different sets of independent variables were selected for the optional input into the stepwise regression analyses. Following the several sets of analyses utilizing the stepwise regression, the final model was selected based upon the overall R^2 value for the model utilizing the most relevant input parameters.

3.7.3 Microsoft® Excel Regression Methods

Nearly all of data sets analyzed throughout this study were organized and initially assessed utilizing Microsoft® Excel. As part of this initial analysis, many of the relationships were fitted to the data sets utilizing the trend line function available as part of the standard Excel package. Due to the large number of functions readily available, these functions were often utilized to explore the best fit functions to representative data sets prior to the more detailed analyses conducted with the Minitab software. In general, this procedure aided in applying any necessary transformations necessary to conduct the most appropriate statistical comparisons in Minitab.

In general, the trend line options determine the best fit functions for a particular dataset utilizing sum of squares error (Microsoft, 2013). In the specific instance of logarithmic, power, and exponential trend lines, Excel utilizes a transformed regression model for the analyses (Microsoft, 2013). Unfortunately, the majority of these operations are not visible to the user, which are only permitted to see the final regression model coefficients and the calculated coefficient of determination or R^2 value, not R^2 adjusted.

Despite the lack of comprehensive statistical analyses tools, Excel has been utilized in this study to perform many of the calculations and prepare many of the figures used in this study. As an example, in a spreadsheet originally developed by Dr. Elie Hajj and further modified over the duration of this study, the dynamic modulus master curves were developed by simultaneously fitting the master curve input parameters, i.e. $\delta, \alpha, \beta, and\ \gamma$, and the second-order polynomial shift function coefficients utilizing a recorded macro available in the Excel software package.

4 MATERIALS AND MIX DESIGNS

Initially, the thermal cracking subtask E2d.3 of the ARC effort focused on the intermountain region of the United States. Later in the progression of the study, it was decided to not limit the analysis specifically to this region. As a result, majority of the materials used in this study came from the intermountain region, with a few additions from outside the area. A similar situation was realized with the asphalt binder sources, but to a lesser extent, largely due to the ARC Core materials being added to later phases of the study.

The majority of the materials were obtained unmixed from the field, that is aggregate stockpiles and virgin asphalt binders. This was largely done to enhance the control of the binder aging and exposure so that these conditions could be closely monitored and maintained constant throughout the project, i.e. without the unknown aging conditions of the mixing process in the plant. However, a few additional field mixtures were included for portions of this study to initiate a future field validation effort, to be carried out at a later time.

4.1 Aggregates

At the initial planning stages, the aggregate sources were selected from various locations throughout the western U.S. As a result, the majority of the aggregate measurements are based on those materials. A portion of the ARC Core aggregates were included at a later

stage, therefore a correspondingly less comprehensive assessment was made on those materials specific to this task of the overall ARC research effort.

The main portion of this task, thermal cracking, included aggregate sources from California, Colorado, Nevada, and Utah. In actuality, there were three sources from Nevada including one currently available source and both aggregate sources from the WesTrack project that took place approximately 60 miles southeast of Reno, NV in the mid-1990s. The WesTrack materials used in this study were the original materials that had been used during the two paving operations of the project, the first in 1995 and the second in 1997. Both aggregates and binder samples, were obtained from the FHWA Materials Reference Library (MRL), where they have been stored in a warehouse since construction.

The laboratory validation samples were obtained from local paving projects in the Reno area. These materials were not sampled as virgin aggregates and binders, but were obtained from plant produced mixtures sampled during the paving operations of each respective project. Although the aggregates were not exclusively tested for this project, they are included here as background information for the aging studies in later sections. Two of aggregates sources were obtained from the ARC core materials list and were obtained from the Ohio test section and one from Texas A&M University. Further discussion of these field mixtures will be reserved for the mixture section.

General information regarding the aggregate identification and source identification are presented in Table 4.1. Note that a general notation has been included which identifies each aggregate source as either a mixed gravel or a single hard-rock source. These terms are intended to provide a general indication as to whether the source is a

mixed gravel composed of alluvial and/or fluvial deposits, or if they were a more consistent hard-rock aggregate source of one general aggregate type.

Table 4.1 Aggregate Source Identification

Aggregate Source ID	ARC Database ID	Source Location	Source Type	General Geologic Name	Sample Year
CAL	AGS 0051	Gardner, CA	Mixed Gravels	Mudstone, Sandstone, Gneiss, Chert, and Volcanic Ash	2009
CO	AGS 0052	Morrison, CO	Single Hard-Rock	Mica Gneiss, Mica Schist, Quartz	2007
NV	AGS 0053	Lockwood, NV	Single Hard-Rock	Complex Volcanic Sequence, including Basalt, Andesite, and Rhyolite	2009
WT95	AGS 0055	Dayton, NV	Mixed Gravels	Weathered Andesite, Decomposing Granite Sand	1995
WT97	AGS 0056	Lockwood, NV	Single Hard-Rock	Weathered Andesite	1997
UT	AGS 0054	Utah	Mixed Gravels	Quartzite, Limestone, Granodiorite, and Basalt	2008
Moana Lane	AGS 0053	Lockwood, NV	Single Hard-Rock	Complex Volcanic Sequence, including Basalt, Andesite, and Rhyolite	2006
Sparks Blvd.	AGS 0053	Lockwood, NV	Single Hard-Rock	Complex Volcanic Sequence, including Basalt, Andesite, and Rhyolite	2008
OH	AGS 0004	Ostrander, OH	Single Hard-Rock	Limestone[a]	2012
TX	AGS 0002	New Braunfels, TX	Single Hard-Rock	Limestone[a]	2010

a – Reported mineralogy values, not determined as part of this study.

From Table 4.1, it is apparent that some of the sources are common between mixtures. The Lockwood, NV location is a presently active aggregate source just east of Reno, NV which is operated by Granite Construction, Co. Generally, this was the same source used for the Nevada, Moana Lane, and Sparks Boulevard mixtures. However, due to the chronological differences these aggregates are slightly different from those noted as WesTrack 1997, WT97. While these three Nevada sources and WT97 aggregates are from the same aggregate source by name, a change in the physical location has resulted in the noted change in mineralogy found in Table 4.1.

4.1.1 Stockpiles

As can be expected, each of the sources included several different stockpiles as were used in the production of the mixtures from each respective location. Each of the stockpiles that were eventually used to produce mixtures in the lab were tested to determine their respective grain size distribution in accordance with AASHTO T27 (AASHTO, 2006). Further, each respective stockpile was tested to determine their respective specific gravities and absorptions, of water, in accordance with AASHTO T84 and T85 (AASHTO, 2006) for the coarse and fine measurements, respectively. In the tables that follow, the specific gravity and absorption values reported are either the coarse or the fine measurements depending on which size fraction made up the majority of each respective stockpile, separated by the 4.75 mm (No. 4) sieve. In this manner, the measures of gradation, specific gravity, and absorption for each respective stockpile from each source, as measured in this particular study are reported in Table 4.2 through Table 4.8.

Table 4.2 Measured California Stockpile Gradations and Specific Gravities

AGC 0051	Gardner 19 mm	Gardner 12.5 mm	Gardner 9.5 mm	Gardner Crusher Fines	Bee Rock Crusher Fines	Gardner Sand
Sieve Size	**Gradation, Percent Passing (200x)**					
25.0 mm (1")	100.0	100.0	100.0	100.0	100.0	100.0
19.0 mm (3/4")	51.5	100.0	100.0	100.0	100.0	100.0
12.5 mm (1/2")	3.1	67.0	100.0	100.0	100.0	100.0
9.5 mm (3/8")	2.0	12.3	92.1	100.0	100.0	100.0
4.75 mm (No. 4)	1.5	2.5	17.9	98.9	98.9	99.9
2.36 mm (No. 8)	1.4	2.3	3.8	63.6	73.9	88.8
2.00 mm (No. 10)	1.4	2.3	3.6	56.5	67.2	84.3
1.18 mm (No. 16)	1.4	2.2	3.4	41.1	51.7	70.5
0.6 mm (No. 30)	1.3	2.1	3.2	29.2	38.8	57.2
0.425 mm (No. 40)	1.3	2.1	3.1	24.7	34.1	31.6
0.3 mm (No. 50)	1.3	2.0	3.0	20.7	29.8	17.5
0.15 mm (No. 100)	1.2	1.9	2.8	15.0	23.4	4.2
0.075 mm (No. 200)	0.9	1.5	2.2	11.1	18.3	1.9
Specific Gravity and Absorption						
Bulk SG	2.463	2.362	2.302	2.214	2.625	2.435
SSD SG	2.537	2.472	2.421	2.378	2.645	2.520
Apparent SG	2.661	2.654	2.613	2.650	2.680	2.659
Abs. (%)	3.02	4.67	5.18	7.43	0.79	3.46

Table 4.3 Measured Colorado Stockpile Gradations and Specific Gravities

AGC 0052	Morrison 3/4"	Morrison Classified Sand	Platte Valley Processed Fines	Thornton Concrete Sand
Sieve Size	**Gradation, Percent Passing**			
25.0 mm (1")	100.0	100.0	100.0	100.0
19.0 mm (3/4")	90.6	100.0	100.0	100.0
12.5 mm (1/2")	42.1	100.0	100.0	100.0
9.5 mm (3/8")	24.3	100.0	100.0	100.0
4.75 mm (No. 4)	5.4	88.4	94.8	100.0
2.36 mm (No. 8)	3.3	60.3	64.9	98.4
2.00 mm (No. 10)	3.1	55.5	57.0	94.9
1.18 mm (No. 16)	2.8	44.8	38.9	76.0
0.6 mm (No. 30)	2.5	36.0	23.9	46.3
0.425 mm (No. 40)	2.4	31.9	18.6	30.6
0.3 mm (No. 50)	2.3	27.6	14.4	16.0
0.15 mm (No. 100)	1.9	18.7	8.7	2.6
0.075 mm (No. 200)	1.5	12.0	5.5	1.1
Specific Gravity and Absorption				
Bulk SG	2.628	2.604	2.581	2.694
SSD SG	2.659	2.619	2.600	2.715
Apparent SG	2.714	2.644	2.630	2.750
Abs. (%)	1.21	0.57	0.73	0.75

Table 4.4 Measured Nevada Stockpile Gradations and Specific Gravities

AGC 0053	3/4"	1/2"	3/8"	Crusher Fines	Wadsworth Sand
Sieve Size	**Gradation, Percent Passing**				
25.0 mm (1")	100.0	100.0	100.0	100.0	100.0
19.0 mm (3/4")	99.7	100.0	100.0	100.0	100.0
12.5 mm (1/2")	43.5	99.1	100.0	100.0	100.0
9.5 mm (3/8")	9.7	50.6	99.6	100.0	100.0
4.75 mm (No. 4)	1.4	1.2	28.3	94.5	99.2
2.36 mm (No. 8)	1.0	1.0	1.8	65.9	98.1
2.00 mm (No. 10)	0.9	0.9	1.5	59.2	97.6
1.18 mm (No. 16)	0.9	0.9	1.1	42.6	95.0
0.6 mm (No. 30)	0.8	0.8	1.0	29.5	80.6
0.425 mm (No. 40)	0.8	0.8	0.9	24.9	62.3
0.3 mm (No. 50)	0.8	0.8	0.9	21.6	39.9
0.15 mm (No. 100)	0.8	0.8	0.8	17.4	11.6
0.075 mm (No. 200)	0.7	0.8	0.7	14.0	3.2
Specific Gravity and Absorption					
Bulk SG	2.597	2.582	2.577	2.521	2.540
SSD SG	2.650	2.641	2.637	2.606	2.611
Apparent SG	2.742	2.744	2.741	2.755	2.733
Abs. (%)	2.04	2.29	2.32	3.38	2.78

Table 4.5 Measured Utah Stockpile Gradations and Specific Gravities

AGC 0054	3/4"	7/16"	1/4"	T3
Sieve Size	**Gradation, Percent Passing**			
25.0 mm (1")	100.0	100.0	100.0	100.0
19.0 mm (3/4")	100.0	100.0	100.0	100.0
12.5 mm (1/2")	54.4	100.0	100.0	100.0
9.5 mm (3/8")	11.5	89.6	100.0	100.0
4.75 mm (No. 4)	1.3	2.4	73.4	81.8
2.36 mm (No. 8)	1.2	1.7	8.7	57.5
2.00 mm (No. 10)	1.2	1.7	5.6	53.0
1.18 mm (No. 16)	1.2	1.6	3.1	42.5
0.6 mm (No. 30)	1.1	1.5	2.6	33.5
0.425 mm (No. 40)	1.1	1.5	2.5	29.5
0.3 mm (No. 50)	1.1	1.5	2.4	25.5
0.15 mm (No. 100)	1.0	1.4	2.0	18.0
0.075 mm (No. 200)	0.8	1.2	1.8	12.8
Specific Gravity and Absorption				
Bulk SG	2.660	2.664	2.639	2.671
SSD SG	2.679	2.683	2.674	2.690
Apparent SG	2.712	2.714	2.733	2.722
Abs. (%)	0.73	0.68	1.31	0.70

Table 4.6 Measured WesTrack 1995 Stockpile Gradations

AGS 0055	3/4"	1/2"[a]	3/8"	Crusher Dust	Wadsworth Sand
Sieve Size	**Gradation, Percent Passing (2008)**				
25.0 mm (1")	100.0	100.0	100.0	100.0	100.0
19.0 mm (3/4")	99.8	100.0	100.0	100.0	100.0
12.5 mm (1/2")	63.5	99.9	100.0	100.0	100.0
9.5 mm (3/8")	33.7	82.6	97.5	100.0	100.0
4.75 mm (No. 4)	10.8	19.5	27.5	99.1	100.0
2.36 mm (No. 8)	5.0	4.3	5.1	76.6	99.4
1.18 mm (No. 16)	4.3	3.2	4.2	54.1	96.4
0.6 mm (No. 30)	4.0	2.9	3.8	39.2	79.6
0.3 mm (No. 50)	3.7	2.6	3.5	28.7	39.8
0.15 mm (No. 100)	3.4	2.4	3.1	20.3	10.6
0.075 mm (No. 200)	3.0	2.0	2.5	13.9	2.5

a – Stockpile was not available and was manufactured from cold feed samples as a replacement.

Table 4.7 Measured WesTrack 1997 Stockpile Gradations and Specific Gravities

AGS 0056	3/4"	1/2"	3/8"	Crusher Dust
Sieve Size	**Gradation, Percent Passing (2008)**			
25.0 mm (1")	100.0	100.0	100.0	100.0
19.0 mm (3/4")	89.9	100.0	100.0	100.0
12.5 mm (1/2")	19.7	94.0	100.0	100.0
9.5 mm (3/8")	5.7	18.4	98.9	100.0
4.75 mm (No. 4)	2.5	2.1	30.8	97.8
2.36 mm (No. 8)	2.1	1.7	5.7	66.7
1.18 mm (No. 16)	2.0	1.5	3.4	58.6
0.6 mm (No. 30)	2.0	1.5	3.4	39.7
0.3 mm (No. 50)	1.8	1.3	2.5	18.7
0.15 mm (No. 100)	1.8	1.3	2.4	14.7
0.075 mm (No. 200)	1.7	1.2	2.2	11.9

Table 4.8 Measured Texas Stockpile Gradations and Specific Gravities

AGC 0002	Type C	Type F	Washed Screenings	Field Sand
Sieve Size	**Gradation, Percent Passing (2012)**			
25.0 mm (1")	100.0	100.0	100.0	100.0
19.0 mm (3/4")	98.5	100.0	100.0	100.0
12.5 mm (1/2")	68.1	100.0	100.0	100.0
9.5 mm (3/8")	28.9	99.7	100.0	100.0
4.75 mm (No. 4)	6.2	57.6	96.9	99.0
2.36 mm (No. 8)	3.4	7.9	87.7	87.6
2.00 mm (No. 10)	3.2	6.0	85.0	84.1
1.18 mm (No. 16)	3.0	3.6	76.5	70.6
0.6 mm (No. 30)	2.8	2.9	62.0	52.3
0.425 mm (No. 40)	2.8	2.8	43.3	43.3
0.3 mm (No. 50)	2.7	2.7	15.9	33.7
0.15 mm (No. 100)	2.6	2.6	1.7	17.7
0.075 mm (No. 200)	2.5	2.5	0.9	8.5

To be clear, the stockpile gradations, specific gravity, and absorption measures provided in Table 4.2 through Table 4.8 were measured in the lab directly, as part of this investigation. The year the samples were obtained and tested has been provided as a reference to help differentiate these particular measures from previously determined ones. Specifically, both WesTrack and the Texas stockpile gradations had been determined as part of the initial sampling of those materials upon their establishment as part of the ARC study.

However, some of the mixtures used were not necessarily prepared in the laboratory and were mixed by plant production in the field. These mixtures already have established stockpile information, all of which may or may not have been determined after the fact. For example, both WesTrack mixtures have had extensive measures reported during the

original WesTrack experiment, but the mixtures used in this study were prepared from the raw materials obtained from the MRL, as previously discussed. Conversely, some of the mixture gradations utilized were obtained solely from the plant produced mixtures and thus the individual raw materials were no longer available or not retained for testing. This occurred with materials from the Moana Lane, the Sparks Blvd., and the Ohio section. In these instances, the mix design or other previously published stockpile information has been provided in Table 4.9 through Table 4.14, again with the publication date in the second row of the table. As is common practice for mix design reporting, the specific gravity and absorption measures are only reported for the combined gradation and not the stockpiles. Therefore, they have been omitted from the summary tables.

Table 4.9 Established WesTrack 1995 Stockpile Gradations (Epps et al., 2002)

AGS 0055	3/4"	1/2"	3/8"	Crusher Dust	Wadsworth Sand
Sieve Size	**Gradation, Percent Passing (1994)**				
25.0 mm (1")	100.0	100.0	100.0	100.0	100.0
19.0 mm (3/4")	99.8	100.0	100.0	100.0	100.0
12.5 mm (1/2")	63.5	99.9	100.0	100.0	100.0
9.5 mm (3/8")	33.7	82.6	97.7	100.0	100.0
4.75 mm (No. 4)	10.8	19.5	29.8	99.8	99.7
2.36 mm (No. 8)	5.0	4.3	6.4	76.3	99.0
1.18 mm (No. 16)	4.3	3.2	5.0	53.3	96.0
0.6 mm (No. 30)	4.0	2.9	4.4	38.3	79.9
0.3 mm (No. 50)	3.7	2.6	3.9	26.3	40.1
0.15 mm (No. 100)	3.4	2.4	3.4	17.6	11.0
0.075 mm (No. 200)	3.0	2.0	2.8	11.3	3.3

Table 4.10 Established WesTrack 1997 Stockpile Gradations (Epps et al., 2002)

AGS 0056	3/4"	1/2"	3/8"	Crusher Dust
Sieve Size	**Gradation, Percent Passing (1997)**			
25.0 mm (1")	100.0	100.0	100.0	100.0
19.0 mm (3/4")	96.8	100.0	100.0	100.0
12.5 mm (1/2")	29.4	99.5	100.0	100.0
9.5 mm (3/8")	7.4	49.7	99.5	100.0
4.75 mm (No. 4)	3.0	1.8	31.3	98.5
2.36 mm (No. 8)	2.0	1.3	4.7	73.0
1.18 mm (No. 16)	1.6	1.1	2.4	47.9
0.6 mm (No. 30)	1.5	1.0	2.0	33.6
0.3 mm (No. 50)	1.3	0.9	1.8	24.8
0.15 mm (No. 100)	1.2	0.8	1.6	19.4
0.075 mm (No. 200)	1.0	0.7	1.5	15.6

Table 4.11 Established Texas Stockpile Gradations

AGS 0002	Type C	Type F	Washed Screenings	Field Sand
Sieve Size	**Gradation, Percent Passing (2003)**			
25.0 mm (1")	100.0	100.0	100.0	100.0
19.0 mm (3/4")	98.7	100.0	100.0	100.0
9.5 mm (3/8")	21.5	93.0	100.0	100.0
4.75 mm (No. 4)	3.4	65.3	99.4	97.4
2.36 mm (No. 8)	1.4	29.0	74.8	85.3
0.6 mm (No. 30)	1.3	8.9	40.0	64.5
0.3 mm (No. 50)	1.3	3.8	20.0	15.0
0.075 mm (No. 200)	1.0	3.6	3.6	2.5

Table 4.12 Established Moana Stockpile Gradations[a] Both PG64-22 and PG64-28 Designs

PL 0016-PG64-22 PL 0017-PG64-28	3/4"	1/2"	3/8"	Rock Dust	Wadsworth Sand	Lime
Sieve Size	**Gradation, Percent Passing (2006)**					
19.0 mm (3/4")	100.0	100.0	100.0	100.0	100.0	100.0
12.5 mm (1/2")	39.2	100.0	100.0	100.0	100.0	100.0
9.5 mm (3/8")	4.2	53.6	100.0	100.0	99.8	100.0
4.75 mm (No. 4)	0.7	1.2	18.0	94.5	98.7	100.0
2.36 mm (No. 8)	0.7	1.1	1.6	63.3	97.1	100.0
2.00 mm (No. 10)	0.7	1.1	1.4	56.4	96.5	100.0
1.18 mm (No. 16)	0.7	1.0	1.3	39.9	93.2	100.0
0.6 mm (No. 30)	0.7	0.9	1.1	26.8	77.2	99.7
0.425 mm (No. 40)	0.7	0.9	1.0	22.7	59.5	99.7
0.3 mm (No. 50)	0.7	0.8	1.0	19.7	39.0	99.7
0.15 mm (No. 100)	0.7	0.8	0.9	15.4	11.3	99.7
0.075 mm (No. 200)	0.6	0.7	0.7	12.2	3.2	83.0

a – Values reported from project mix design found in Figure 16.3 and Figure 16.4.

Table 4.13 Established Sparks Blvd. Stockpile Gradations[a]

PL 0018	3/4"	1/2"	3/8"	Rock Dust	Wadsworth Sand	Lime
Sieve Size	**Gradation, Percent Passing (2008)**					
19.0 mm (3/4")	100.0	100.0	100.0	100.0	100.0	100.0
12.5 mm (1/2")	38.1	100.0	100.0	100.0	100.0	100.0
9.5 mm (3/8")	6.7	50.0	99.9	100.0	100.0	100.0
4.75 mm (No. 4)	0.9	1.0	19.0	97.4	98.5	100.0
2.36 mm (No. 8)	0.7	1.0	1.2	72.3	96.4	100.0
2.00 mm (No. 10)	0.7	0.7	1.0	63.8	95.6	100.0
1.18 mm (No. 16)	0.7	0.6	0.8	44.8	91.4	100.0
0.6 mm (No. 30)	0.7	0.6	0.8	29.7	72.1	99.7
0.425 mm (No. 40)	0.7	0.6	0.8	25.0	52.4	99.7
0.3 mm (No. 50)	0.7	0.6	0.7	21.3	32.1	99.7
0.15 mm (No. 100)	0.6	0.6	0.7	16.8	8.3	99.7
0.075 mm (No. 200)	0.5	0.5	0.5	13.5	2.1	83.0

a – Values reported from project mix design.

Table 4.14 Established Ohio Stockpile Gradations[a]

AGC 0004	Limestone #8	Mod. Limestone	Natural Sand
Sieve Size	**Gradation, Percent Passing (2012)**		
25.0 mm (1")	100.0	100.0	100.0
19.0 mm (3/4")	100.0	100.0	100.0
12.5 mm (1/2")	100.0	100.0	100.0
9.5 mm (3/8")	95.0	100.0	100.0
4.75 mm (No. 4)	20.0	99.0	100.0
2.36 mm (No. 8)	6.0	67.0	86.0
1.18 mm (No. 16)	4.0	37.0	61.0
0.6 mm (No. 30)	4.0	21.0	37.0
0.3 mm (No. 50)	4.0	12.0	10.0
0.15 mm (No. 100)	4.0	7.0	4.0
0.075 mm (No. 200)	3.5	5.2	3.2

a – Values reported from project mix design.

As occasionally happens with different time periods or even different production runs for a given material, some of the measured properties of the stockpiles did not exactly match those previously established from the source during the design processing. These comparisons were only possible with the WesTrack and the Texas aggregate sources.

Table 4.15 Difference in Established and Measured WesTrack 1995 Stockpile Gradations

AGS 0055	3/4"	1/2"[a]	3/8"	Crusher Dust	Wadsworth Sand
Sieve Size	**Differences in Gradation, Percent Passing**				
25.0 mm (1")	0.0	0.0	0.0	0.0	0.0
19.0 mm (3/4")	0.0	0.0	0.0	0.0	0.0
12.5 mm (1/2")	0.0	0.0	0.0	0.0	0.0
9.5 mm (3/8")	0.0	0.0	0.2	0.0	0.0
4.75 mm (No. 4)	0.0	0.0	2.3	0.7	-0.3
2.36 mm (No. 8)	0.0	0.0	1.3	-0.3	-0.4
1.18 mm (No. 16)	0.0	0.0	0.8	-0.8	-0.4
0.6 mm (No. 30)	0.0	0.0	0.6	-0.9	0.3
0.3 mm (No. 50)	0.0	0.0	0.4	-2.4	0.3
0.15 mm (No. 100)	0.0	0.0	0.3	-2.7	0.4
0.075 mm (No. 200)	0.0	0.0	0.3	-2.6	0.8

a – Stockpile was not available, thus was manufactured from cold feed samples as a replacement.

Table 4.16 Difference in Established and Measured WesTrack 1997 Stockpile Gradations

AGS 0056	3/4"	1/2"	3/8"	Crusher Dust
Sieve Size	**Differences in Gradation, Percent Passing**			
25.0 mm (1")	0.0	0.0	0.0	0.0
19.0 mm (3/4")	6.9	0.0	0.0	0.0
12.5 mm (1/2")	9.7	5.5	0.0	0.0
9.5 mm (3/8")	1.7	31.3	0.6	0.0
4.75 mm (No. 4)	0.5	-0.3	0.5	0.7
2.36 mm (No. 8)	-0.1	-0.4	-1.0	6.3
1.18 mm (No. 16)	-0.4	-0.4	-1.0	-10.7
0.6 mm (No. 30)	-0.5	-0.5	-1.4	-6.1
0.3 mm (No. 50)	-0.5	-0.4	-0.7	6.1
0.15 mm (No. 100)	-0.6	-0.5	-0.8	4.7
0.075 mm (No. 200)	-0.7	-0.5	-0.7	3.7

Table 4.17 Difference in Established and Measured Texas Stockpile Gradations

AGS 0002	Type C	Type F	Washed Screenings	Field Sand
Sieve Size	**Differences Gradation, Percent Passing**			
25.0 mm (1")	0.0	0.0	0.0	0.0
19.0 mm (3/4")	0.2	0.0	0.0	0.0
9.5 mm (3/8")	-7.4	-6.7	0.0	0.0
4.75 mm (No. 4)	-2.8	7.7	2.5	-1.6
2.36 mm (No. 8)	-2.0	21.1	-12.9	-2.3
0.6 mm (No. 30)	-1.5	6.0	-22.0	12.2
0.3 mm (No. 50)	-1.4	1.1	4.1	-18.7
0.075 mm (No. 200)	-1.5	1.1	2.7	-6.0

As can be seen in Table 4.15 through Table 4.17, some of the gradations varied considerably from the established values. The maximum difference was found to be 22 percent as determined by subtracting the measured values from the established gradations. However, in an effort to not alter the mix design based upon the current gradation measures and thus lose the historical or reference value of the mixtures, the overall combined gradations were compared to those in the established design documents. If appreciable deviations between the combined gradations existed, as determined by allowable measure between two laboratory measures (d2s) available from AASHTO T27 (AASHTO, 2006), the combined gradation was adjusted and checked again. Through this iterative method of batching and gradation verification, the combined gradation of each produced mixture matched those of the established gradation within practical limits. For some of the more problematic sources, this required hand batching each specimen on each sieve in the measured gradation, i.e. all 12 sieve sizes for the 19 mm (3/4 inch) NMAS gradations.

4.2 Asphalt Binders

Similar to the aggregates utilized in this study, the asphalt binder were initially concentrated around sources in the western U.S. This initial plan was soon expanded to eventually include a total of fifteen asphalt binders from seven sources or suppliers, including the four ARC Core binders.

A summary of the nomenclature used in this study along with information regarding the continuous performance grade, binder supplier, binder modification, and sampling date is summarized in Table 4.18. The continuous performance grade (PG) of the asphalt binders were determined in accordance with AASHTO M320 (AASHTO, 2006) which preceded and did not include measures of the Multi-Stress Creep Recovery test (MSCR).

Table 4.18 Asphalt Binder Source Identification

Asphalt Binder ID	ARC Database ID	Continuous Performance Grade	Binder Supplier	Binder Modification	Sample Year
PG64-22	BI 0052	PG66.8-25.3	Paramount Petroleum	None	2007
PG64-22 + 3% SBS	BI 0050	PG77.1-25.1	Paramount Petroleum	3% Styrene-butadiene-styrene, SBS	2007
PG64-22 +10% Lime	BI 0052 FI 0011	N/A	Paramount Petroleum	10% Hydrated Lime	2007
PG64-22 +20% Lime	BI 0052 FI 0011	N/A	Paramount Petroleum	20% Hydrated Lime	2007
PG64-28	BI 0051	PG70.0-31.4	Paramount Petroleum	Styrene-butadiene-styrene, SBS	2007
Base Stock	BI 0046	N/A	Paramount Petroleum	None	2010
WT95-22	BI 0053	PG66.2-20.7	West Coast Refinery	None	1995
WT97-22	BI 0054	PG67.8-20.8	Idaho Asphalt	None	1997
Moana 22	BI 0047	PG64-22[a]	Paramount Petroleum	None	2006
Moana 28	BI 0048	PG64-28[a]	Paramount Petroleum	Styrene-butadiene-styrene, SBS	2006
Sparks 28	BI 0049	PG64-28[a]	Paramount Nevada	Styrene-butadiene-styrene, SBS	2008
BI1 PG67-22	BI 0001	PG69.6-28.2[b]	PDVSA, Venezuelan	None	2010
BI2 PG64-16	BI 0002	PG68.3-17.2[b]	Valero	None	2010
BI3 PG58-28	BI 0003	PG60.7-29.6[b]	Holly Frontier	None	2012
BI4 PG70-22	BI 0004	PG74.3-24.3[b]	Shelly Materials	Styrene-butadiene-styrene, SBS	2012

a – Specified binder grades reported from project mix design.
b – Binder grading conducted by the University of Wisconsin-Madison in collaboration with the ARC.

As presented in Table 4.18, several binders have been supplied by Paramount Petroleum from their terminal in Fernley, NV. In fact, the first four binders listed have the same asphalt binder components, only the latter few have had styrene-butadiene-styrene, SBS polymer, or differing amounts of hydrated lime added to the PG 64-22.

Additional binder were aged with hydrated lime was added to the PG 64-22 binder in proportions of 10 and 20 percent by mass of binder. The binders that were aged with lime additions were not fully graded due to the focus of this study being on the aging characteristics of the binders and not strictly the influence of lime on the binder grade. The addition of the lime technically made these materials a mastic rather than a binder, thus they were not PG graded.

Another companion set of binders were also tested with the PG 64-28 and Base Stock binders. Base Stock was the representative unmodified base binder that was then modified with SBS to achieve the PG 64-28 grade. As the base binder, it was requested that Base Stock not be graded, therefore those tests were not conducted.

Although the two WesTrack binders were initially reported as PG64-22, they were two different binders from two different sources with fairly significant different material properties, especially aging characteristics as will be seen in later sections. Further observation of the WesTrack binders reveals that their measured continuous grade temperatures do not fully meet the reported grade of PG 64-22. This is presumably due to the extended storage time of the binders at ambient temperatures. The binder samples were obtained from the FHWA MRL in Sparks, NV where they had been stored since the original paving operations in 1995 and 1997, respectively. Apparently, ten to twelve years of storage unfrozen may permit some aging of the asphalt binders in spite of being

stored in sealed containers. This is of fairly little consequence to this project, since all measures and calculations have been determined from that point forward. It would have been preferred that the binders still met their original grades, however it was determined that having the same binders would be a better long-term comparison to field validation effort to follow this particular study.

The Moana Lane and Sparks Boulevard binders were not graded since they were obtained from the plant produced mixtures, the same as the aggregates from those mixtures. Rather than relying on the rolling thin film oven (RTFO) to simulate the production aging at the plant as is currently under investigation by NCHRP Project 9-52, the binders were reported according to the specified PG grade on their respective mix designs. This was further compounded by the limited supply of these binders due to the fact that were obtained by extracting and recovering the binder from the sampled plant produced mixtures.

The mixture designs comprised of the individual stockpiles presented in Table 4.2 through Table 4.8 and the asphalt binders provided in Table 4.18 will be discussed in the following mixture design section.

4.3 Mix Designs of Laboratory Mixtures

Utilizing the aggregate stockpiles defined in Table 4.2 through Table 4.8 were combined in the specific proportions provided in Table 4.19 through Table 4.23 to create the combined gradations presented in Table 4.24 which were used in the individual mix

designs. These combined gradations were utilized along with the asphalt binders defined in Table 4.18, to produce the several mixtures that were designed in the laboratory. Two levels of qualitative gradations were used for many of the aggregate sources, intermediate and fine, with the exception of the WesTrack materials which were defined as coarse and fine as determined by the Superpave design method found in AASHTO M323 (AASHTO, 2006).

Table 4.19 Bin Percentages for Laboratory Determined Mix Designs, California

Aggregate Source	Stockpile	Stockpile Percentages
California Intermediate	Gardner 19 mm	13.0
	Gardner 12.5 mm	25.0
	Gardner 9.5 mm	12.0
	Gardner Crusher Fines	40.0
	Bee Rock Crusher Fines	0.0
	Gardner Sand	10.0
California Fine	Gardner 19 mm	8.0
	Gardner 12.5 mm	6.0
	Gardner 9.5 mm	18.0
	Gardner Crusher Fines	59.0
	Bee Rock Crusher Fines	0.0
	Gardner Sand	9.0

Table 4.20 Bin Percentages for Laboratory Determined Mix Designs, Colorado

Aggregate Source	Stockpile	Stockpile Percentages
Colorado Intermediate	Morrison 3/4”	58.0
	Morrison Classified Sand	12.0
	Platte Valley Processed Fines	0.0
	Thornton Concrete Sand	30.0

Table 4.21 Bin Percentages for Laboratory Determined Mix Designs, Nevada

Aggregate Source	Stockpile	Stockpile Percentages
Nevada Intermediate	3/4”	20.0
	1/2”	15.5
	3/8”	24.0
	Crusher Fines	21.0
	Wadsworth Sand	20.0
Nevada Fine	3/4”	17.7
	1/2”	5.5
	3/8”	26.5
	Crusher Fines	26.8
	Wadsworth Sand	24.4

Table 4.22 Bin Percentages for Laboratory Determined Mix Designs, Utah

Aggregate Source	Stockpile	Stockpile Percentages
Utah Intermediate	3/4”	9.5
	7/16”	23.6
	1/4”	40.4
	T3 Fines	4.3
	Wadsworth Sand	22.2
Utah Fine	3/4”	11.5
	7/16”	18.2
	1/4”	26.4
	T3 Fines	9.0
	Wadsworth Sand	34.9

Table 4.23 Bin Percentages for Mix Designs, WesTrack

Aggregate Source	Stockpile	Stockpile Percentages
WesTrack 1995 Fine	3/4”	31.0
	1/2”	19.0
	3/8”	10.0
	Crusher Dust	13.5
	Wadsworth Sand	25.0
	Hydrated Lime	1.5
WesTrack 1997 Coarse	3/4”	24.0
	1/2”	15.5
	3/8”	27.5
	Crusher Dust	31.5
	Hydrated Lime	1.5

The intermediate and fine design gradations noted in Table 4.24 are depicted in Figure 4.1 and Figure 4.2, respectively. The specific gravity and absorption values reported are the combined coarse and fine measurements combined in proportion of the percent retained and passing the 4.75 mm (No. 4) sieve, respectively.

To clarify, the Utah aggregate gradations were 12.5 mm (1/2 inch) NMAS gradations, with the remainder of the blend gradations, both intermediate and fine, meeting the requirements for 19 mm (3/4 inch) NMAS. Further, the Max Density Line plots in both Figure 4.1 and Figure 4.2 correspond to the 19 mm (3/4 inch) NMAS gradations and not the 12.5 mm (1/2 inch). For a direct comparison, additional plots including both the intermediate and fine gradations, coarse and fine for WesTrack, for each respective aggregate source have also been provided in Figure 4.3 through Figure 4.6.

Table 4.24 Laboratory Determined Combined Gradations and Specific Gravities

Aggregate Source	California		Colorado	Nevada		Utah		WesTrack	
Gradation	Int.	Fine	Int.	Int.	Fine	Int.	Fine	1997 Coarse	1995 Fine
ARC Database ID	AGC 0051F	AGC 0051G	AGC 0052D	AGC 0053F	AGC 0053G	AGC 0054G	AGC 0054F	AGC 0056F	AGC 0055E
Sieve Size	Blend Gradation, Percent Passing								
25.0 mm (1")	100.0	100.0	100.0	100.0	100.0	100.0	100.0	100.0	100.0
19.0 mm (3/4")	93.7	96.1	94.6	99.9	99.9	100.0	100.0	99.2	99.9
12.5 mm (1/2")	79.2	90.3	66.4	88.6	89.9	95.7	94.8	82.8	88.5
9.5 mm (3/8")	64.4	85.5	56.1	74.4	81.2	89.1	87.9	69.5	75.4
4.75 mm (No. 4)	52.5	70.8	43.7	46.9	57.1	55.9	61.9	41.4	48.9
2.36 mm (No. 8)	35.5	46.5	38.6	34.2	42.3	28.3	42.1	25.6	38.4
2.00 mm (No. 10)	32.2	41.8	36.9	32.6	40.3	26.7	40.8	-	-
1.18 mm (No. 16)	24.6	31.5	29.8	28.5	35.1	24.7	38.2	16.8	33.9
0.60 mm (No. 30)	18.5	23.2	19.7	22.8	28.0	20.8	32.2	12.1	27.6
0.425 mm (No. 40)	14.1	18.2	14.4	18.2	22.3	16.6	25.4	-	-
0.30 mm (No. 50)	11.1	14.6	9.5	13.0	15.9	11.4	17.2	9.1	15.7
0.15 mm (No. 100)	7.4	9.9	4.2	6.4	7.9	4.6	6.6	7.2	6.8
0.075 mm (No. 200)	5.4	7.3	2.6	4.0	4.9	2.5	3.0	5.8	3.5
Specific Gravity and Absorption									
Bulk SG	2.308	2.276	2.600	2.557	2.564	2.644	2.616	2.592	2.545
Abs. (%)	5.44	5.97	0.90	2.71	2.45	1.48	1.66	2.66	2.48

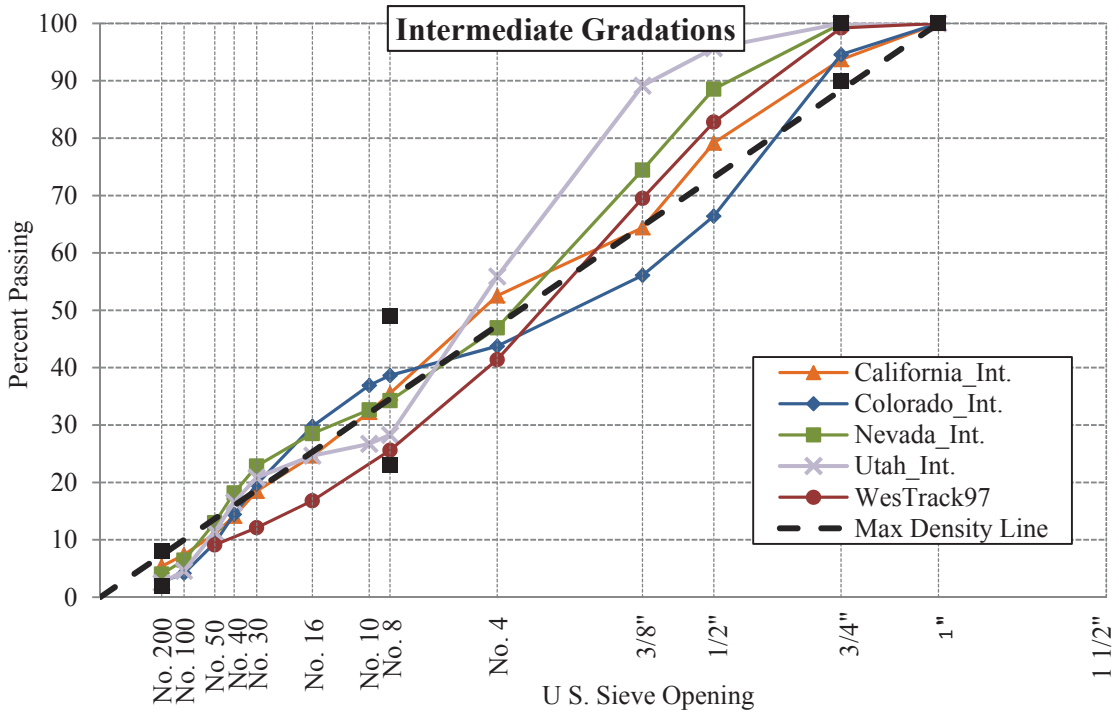

Figure 4.1 Intermediate Laboratory Gradations

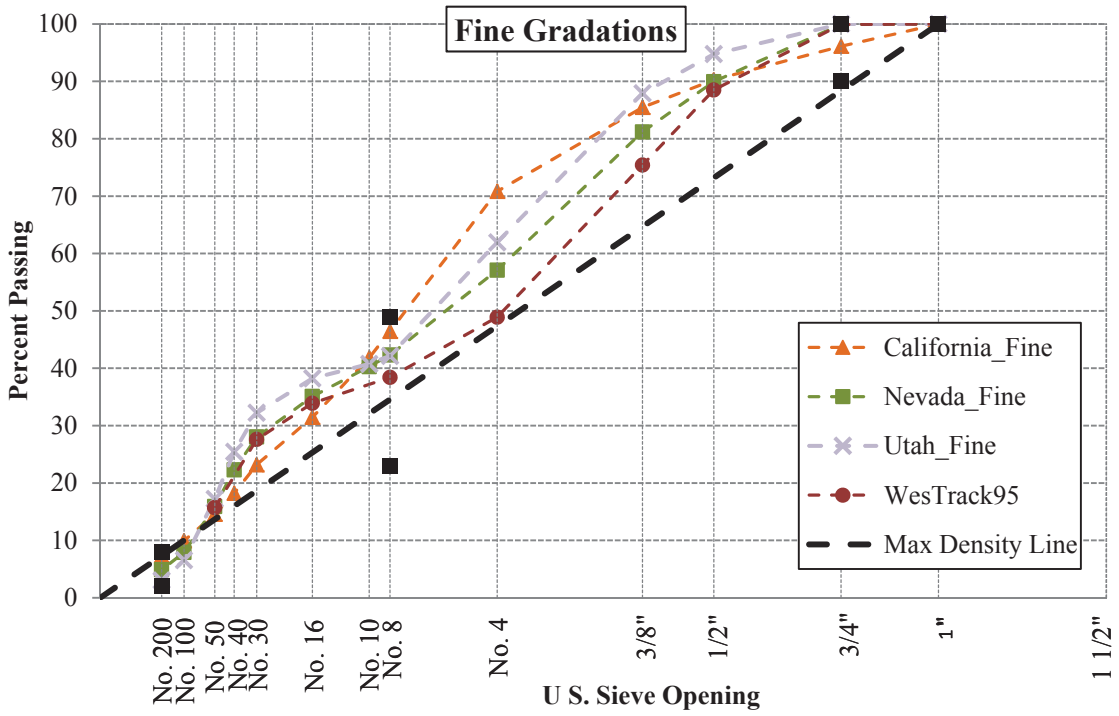

Figure 4.2 Fine Laboratory Gradations

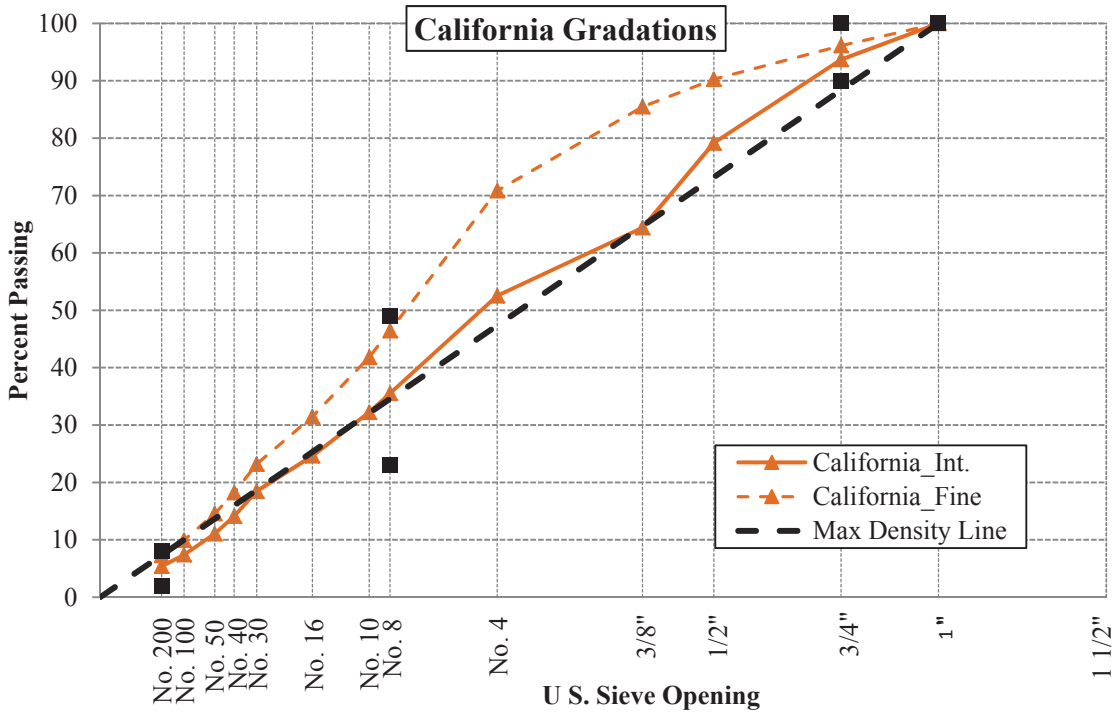

Figure 4.3 California Intermediate and Fine Laboratory Gradations

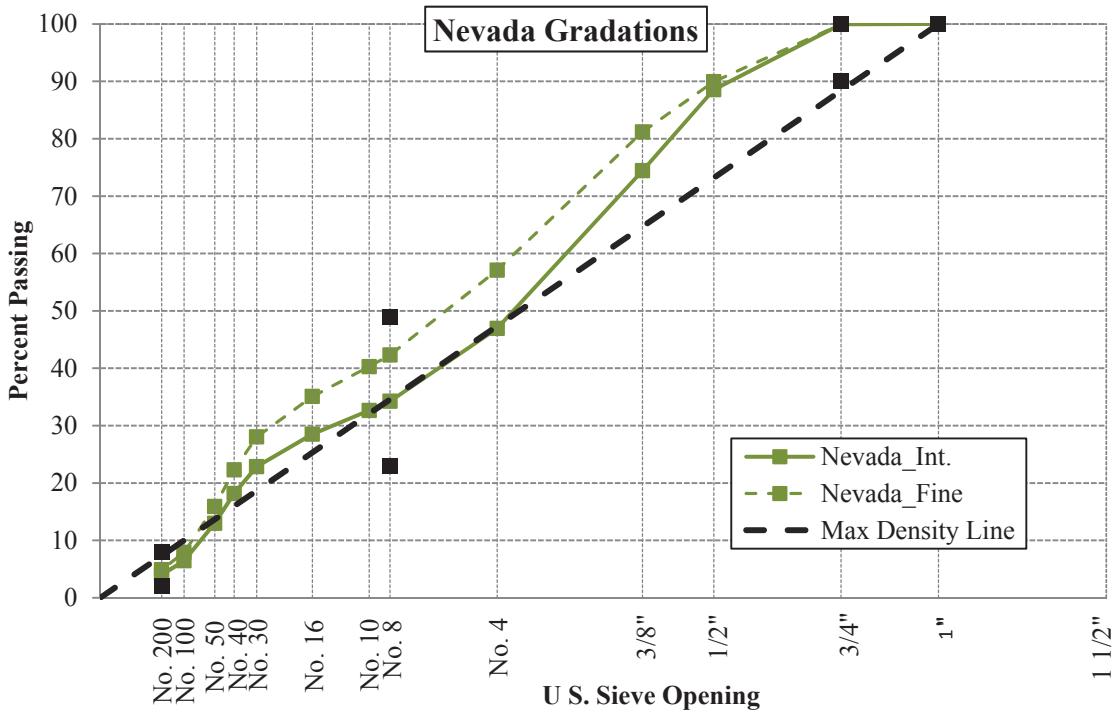

Figure 4.4 Nevada Intermediate and Fine Laboratory Gradations

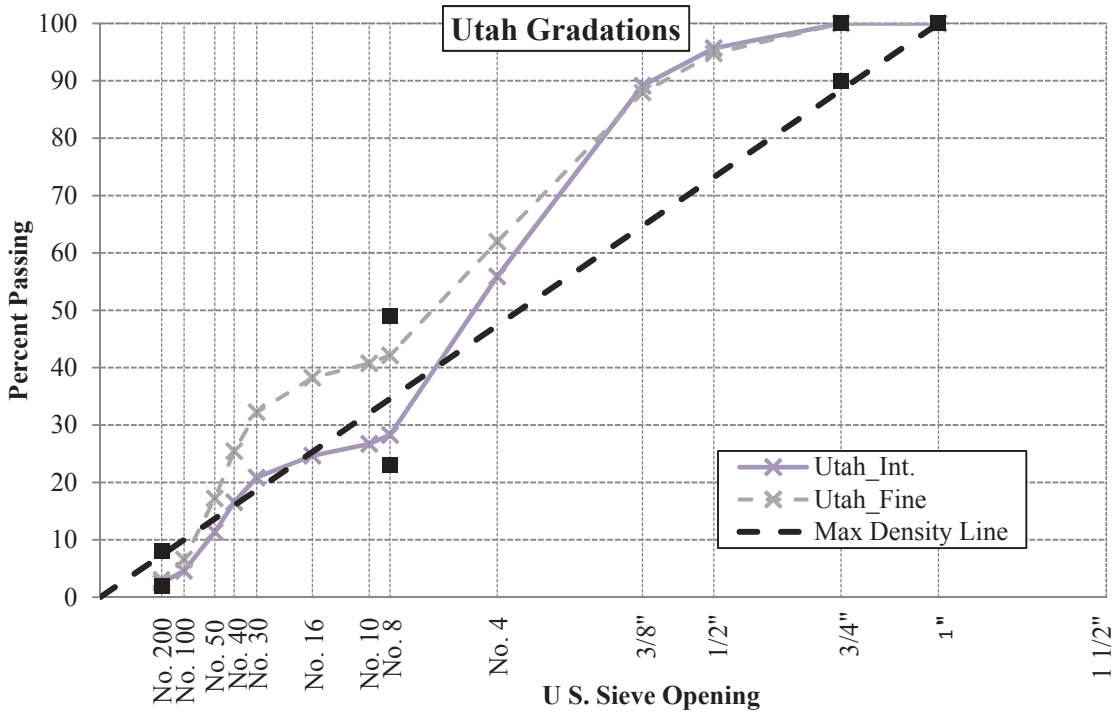

Figure 4.5 Utah Intermediate and Fine Laboratory Gradations

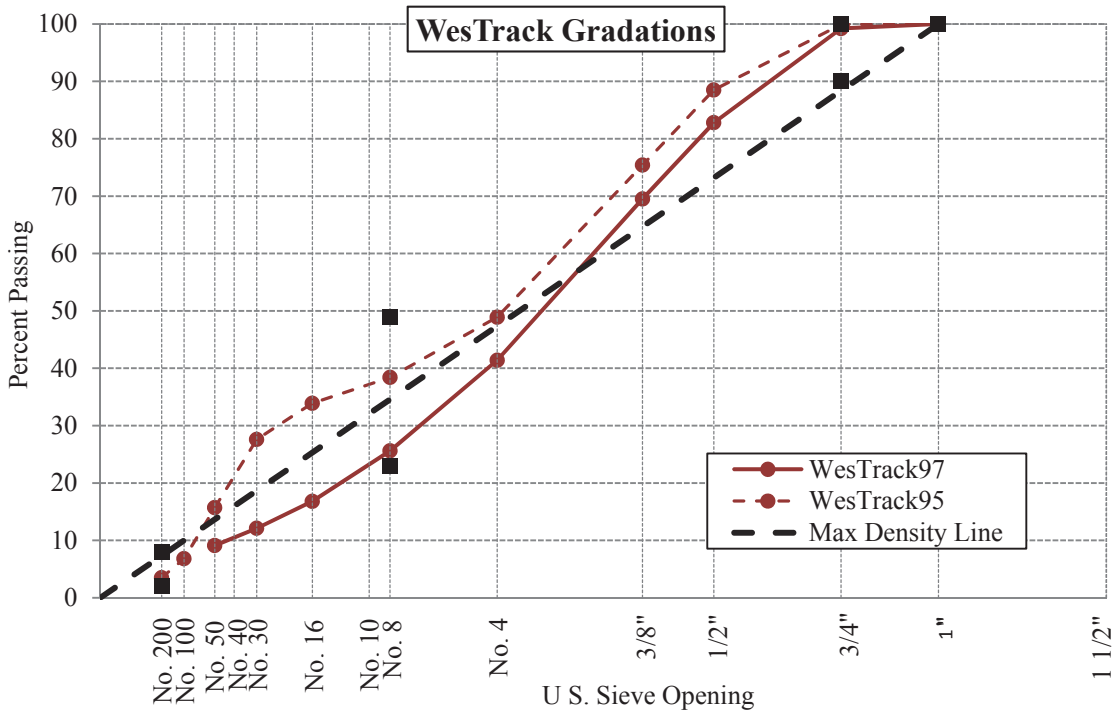

Figure 4.6 WesTrack Coarse and Fine Laboratory Gradations

Once the combined gradations were defined, it became necessary to establish the base mix design of each respective mixture. In practicality, the gradations were determined as part of the mix design process, as is the current state of practice for mix design methodology. The base mix designs were conducted following the Superpave design method in general accordance with AASHTO M323 (AASHTO, 2006). In an effort to conserve materials, not all the consensus properties of all the aggregate sources were determined since each source was actively producing hot mix asphalt mixtures and thus general compliance was assumed. A summary of each mix design for the laboratory mixtures used in the study are presented in Figure 15.1 through Figure 15.10, which can be found in Appendix C.

Each of the designs was conducted with 100 gyrations as the design compaction effort, with the optimum binder content determined at the 4% air void level. All other relevant volumetric properties were verified for compliance at the optimum binder content. Moisture susceptibility, in the form of the tensile strength ratio (TSR) was also measured as part of the mix design process in accordance with AASHTO T283 (AASHTO, 2006). However, changes to the mixtures were not made solely based upon failing TSR measures. As such, only the two WesTrack mixtures contained hydrated lime and none of the other laboratory mixtures contained lime or any other anti-stripping agents, despite several designs not meeting the minimum criteria for tensile strength ratio.

4.4 Field Mixtures

The field mixtures were a part of the larger field validation efforts that are not directly a part of this manuscript, but will be included in the model development and validation efforts which are being completed by Zia Alavi and other colleagues at the University of Nevada, Reno.

Three samples were obtained from two active projects being administered by the Regional Transportation Commission (RTC) of Washoe County, NV. The two samples identified as Moana Lane were obtained from the top, PG 64-28, and bottom lifts, PG 64-22, of the Moana Lane Extension project in Reno, NV constructed in 2006. The extension project can now be identified as Airway Drive. The project limits extended Moana Lane from Neil Road to Louie Lane under RTC contract 5309. The Moana Lane Extension was constructed with an SBS modified PG 64-28 binder for a minimum thickness of two inches placed on top of the binder course containing the unmodified PG 64-22 utilizing the same aggregate gradation in both 75 blow Marshall mix designs.

The Sparks Boulevard samples were obtained from the reconstruction efforts on Sparks Boulevard from Springland Drive to Baring Boulevard in Sparks, NV in 2008. The Sparks Boulevard project was constructed with seven inches of a 75 blow Marshall mix design containing Lockwood aggregates and an SBS modified PG 64-28 binder.

Mixtures from both the Moana Lane extension and the Sparks Blvd. projects were Type II gradations, 19 mm (3/4 inch) NMAS in accordance with the Standard Specification for Public Works Construction (SSPWC, 2006). By coincidence, all three

mixtures were produced by Granite Construction Co. with aggregates from their Lockwood facility combined with asphalt binders from Paramount Petroleum.

The fourth material being considered as a field mixture was obtained from the overlay project on US-23 southbound in Delaware County Ohio constructed utilizing ARC Core materials and associated with the Long-Term Pavement Performance (LTPP) field section 390901. The asphalt binder, an SBS modified PG 70-22 supplied by Shelly Materials is referenced as BI 0004 CORE in the ARC Database. The mixture was likewise produced by Shelly Materials with AGC 0004 aggregates, resulting in the plant produced mixture PL 0004. The BI4 binder was obtained as virgin binder which was tested for the binder kinetics and hardening susceptibility (HS) determinations. The mixture-aging studies were conducted on the plant produced mixtures samples from the paving operations of the Ohio test section conducted in 2012.

For reference all four sample locations are provided in Table 4.25. All four field mixtures were utilized for both the binder aging studies as well as validation of the laboratory aging studies to be completed as part of the oxidation modeling efforts being conducted by others.

Table 4.25 Field Mixture Sample Locations

Mixture ID	ARC Database ID	Asphalt Binder Grade[a]	Sample Location	Sample Year
Moana 22	PL 0016	PG64-22	Northbound Inside Lane at Sta. 75+80, Second 3 inch Lift	2006
Moana 28	PL 0017	PG64-28	Intersection of Neil and Moana, Top Lift	2006
Sparks 28	PL0018	PG64-28	Northbound at Intersection of Springland Drive and Sparks Bld., Top Lift	2008
OH	PL 0004	PG70-22	LTPP Section 390901	2012

a – Specified binder grades reported from project mix design.

5 EXPERIMENTAL MATRIX

The objective of this research effort was investigated through the execution of a partial factorial experimental plan utilizing the materials and gradations discussed in Chapter 4. The experiment was conducted with a partial factorial design due to the high number of conducted measures and the long aging durations necessary to characterize the oxidative aging behavior of both the asphalt mixtures and the accompanying asphalt binders.

To accomplish these analyses, many of the exploratory measures described in the methodology sections of Chapter 3 were applied to their respective material types, namely aggregates, binders, mixtures, or mastics over a range of aging conditions. To clarify the experimental factors being investigated, the overall experimental matrix will be based upon the respective aging conditions for each respective material, as discussed in the following sections.

5.1 Asphalt Mixture Evaluation

Initial considerations of the asphalt mixtures were focused on capturing the effects of the mixture characteristics on the aging of the mixtures. This was addressed by varying the characteristics of the mixture and the components used to create the mixture, i.e. the aggregate and asphalt binder, to adequately explore the main factors in the experimental design as a function of aging or time. The main factors evaluated in the laboratory investigation are as follows:

- Aggregate Factors
    - Qualitative Gradation
    - Aggregate Absorption
    - Aggregate Mineralogy
- Asphalt Binder Factors
    - Unmodified Binder
    - Modified Binder
- Mixture Characteristic Factors
    - Asphalt Binder Content
    - Mixture Density or Air Voids

To address each of these in the partial factorial experimental design, the laboratory mixture experimental matrix has been organized into two tables. Table 5.1 was initiated by the ARC subtask E2d.3-b and was intended to investigate the influence of the aggregate absorption, a portion of the aggregate mineralogy, the asphalt binder type, and the asphalt binder content on the aging of the incorporated asphalt binders. Table 5.2 originated from ARC subtasks E2d.3-b and c which were intended to investigate the experimental factors described as the qualitative gradation, additional aggregate mineralogy, and mixture density or air voids and decipher their influence on the aging of the asphalt binder component.

The mixture identification nomenclature used for the mixtures consists of NV19I28_5.22_60C_4%_3mo indicated: **N**e**v**ada aggregates with a 19 mm (3/4 inch) NMAS **I**ntermediate gradation mixed with PG64-**28** binder at **5.22**% binder content by total weight of mix (TWM) was aged in a **60°C** forced draft oven, after being compacted

to the **4%** total air void level after cutting, for the prescribed time period (0, **3**, 6, or 9 **mo**nths).

Table 5.1 Subtask E2d.3-b Laboratory Mixture Experimental Matrix

Aggregate Source	Gradation	Binder Grade	Optimum Binder (% TWM)	Tested Binder Content (% TWM)	Binder Film Thickness (µm)	Air Void (%)	ARC Database ID
CAL	Int.	64-22	6.65 LL0051Fa				
				7.44	9.0	7	LL 0051Fd
	Int.	64-28	7.04 LL0051Fb				
				7.51	9.0	7	LL 0051Ff
CO	Int.	64-22	4.36 LL0052Da	4.5	11.7	7	LL 0052Dd
				3.61	9.0	7	LL 0052Dc
	Int.	64-28	4.40 LL0052Da	4.5	11.6	7	LL 0052De
				3.65	9.0	7	LL 0052Df
NV	Int.	64-22	5.18 LL0053Fa	4.5	7.0	7	LL 0053Fc
				5.38	9.0	7	LL 0053Fd
	Int.	64-28	5.11 LL0053Fb	4.5	7.4	7	LL 0053Fe
				5.22	9.0	7	LL 0053Fg

Table 5.2 Subtask E2d.3-b&c Laboratory Mixture Experimental Matrix

Aggregate Source	Gradation	Binder Grade	Tested Binder Content (% TWM)	Film Thickness (µm)	Air Voids (%)	ARC Database ID
CAL	Int.	64-22	7.44	9.0	4	LL 0051Fc
					7	LL 0051Fd
					11	LL 0051Fe
	Fine	64-22	9.14	9.0		
					7	LL 0051Gb
NV	Int.	64-28	5.22	9.0	4	LL 0053Ff
					7	LL 0053Fg
					11	LL 0053Fh
	Fine	64-28	6.00	9.0		
					7	LL 0053Gb
UT	Int.	64-28	3.79	9.0	4	LL 0054Gb
					7	LL 0054Gc
					11	LL 0054Gd
	Fine	64-28	5.22	9.0		
					7	LL 0054Fb
WT	Coarse	WT97 64-22	5.10	9.2	4	LL 0056Fb
					7	LL 0056Fc
					11	LL 0056Fd
	Fine	WT95 64-22	5.20	9.0		
					7	LL0055Eb

Evaluated Mixtures

To clearly define the experimental design relative to the aggregate absorption, i.e. subtask E2d.3-b, as depicted in Table 5.1, the aggregates are composed of those defined in Table 4.24 along with the asphalt binders as defined in Table 4.18. To reiterate, the PG 64-22 binder identified in Table 5.1 and Table 5.2 is the unmodified asphalt binder BI 0052.

Similarly, the PG 64-28 binder identified in Table 5.1 and Table 5.2 is the SBS modified asphalt binder BI 0051. Further, the two PG 64-22 binders noted in the WesTrack mixes are the WT95 (BI 0053) for the fine gradation design and the WT97 (BI 0054) for the coarse design, respectively. Each of the mixtures described in Table 5.1 and Table 5.2 were evaluated as a function of oxidative aging induced by different durations in laboratory ovens.

A discrepancy is clearly evident between the optimum binder content established in the mix designs in Appendix C and the asphalt binder contents utilized in this study as presented in Table 5.1 and Table 5.2. Close observation will reveal that almost none of the mixtures were prepared or evaluated at the optimum binder content, except for the WesTrack95 fine mixture. The WesTrack mixtures were prepared following the same mix design proportions used during the two respective construction cycles of the field experiment, i.e. 1995 and 1997. As a comparison, the two mixtures evaluated replicated the field mixtures from the original WesTrack sections 1 and 15 for the WesTrack95 mixtures and sections 38 and 56 for the WesTrack97 mixtures, respectively.

For the other mixtures. the binder contents utilized in this investigation were 4.5% by TWM and a variable binder content that resulted in a calculated 9 μm apparent film thickness (AFT). The 4.5% TWM binder content was selected as a rough average of the optimum binder contents that did not necessarily match any particular mixture. This method was applied to the Nevada and Colorado mixtures for both the PG 64-22 and PG 64-28 binders, but was not used with the California aggregates. This was largely due to the optimum binder content for the California mixtures being more than two percent

above the 4.5% target binder content. As a result, the California mixtures were investigated only at the binder content which resulted in a calculated AFT of 9 μm.

The inclusion of the constant binder content into the investigation was intended to isolate and explore the influence of the aggregates on the aging characteristics of the asphalt binder. The different aggregate sources present variations of the absorption, mineralogy, and surface characteristics on the aggregates themselves. Perhaps not the most ideal experimental design to have more than one variable change at a time, this was the most practical approach to use actual aggregates from active aggregate sources. Although more fundamental studies would include more exact isolations of each aggregate characteristic, but this would yield impractical and necessarily manufactured aggregate materials. This particular effort was intended to include more natural aggregate sources that were currently being used in production facilities.

With a constant binder content, changes in the aggregate present different levels of absorption, which directly necessitate changes in the absorbed binder content that have a direct effect on the effective binder content. The variations in the effective binder content, in turn, create differences in the apparent film thickness. By maintaining a constant air void level and presumably a similar pore structure within the mixture, it is logical to assume the evaluation will practically isolate the binder film thickness, with some potential influence of the aggregate surface adsorption and chemistry. Further consideration of the potential influence of the aggregate adsorption will be discussed further with the analyses of those measured results.

The other mixtures included in the experimental matrix of Table 5.1 and all the mixtures included in Table 5.2 were those created with a calculated apparent film

thickness of 9 μm. These binder contents were determined by calculating the AFT of each of the binder contents used in the mix design determinations and selecting the binder content that corresponded to 9 μm under the design conditions.

There have been arguments made as to the accuracy and even the relevance of film thickness calculations. However, they are still quite common in the asphalt industry since film thickness calculations tend to provide relevant information on the useable binder content within a given mixture. Therefore, the binder film thickness was one of the controlling parameters in this particular study on mixture aging characteristics.

While there are a few different methods available to calculate the binder film thickness in a given mixture (Radovskiy, 2003), most of them provide a strictly calculated value. Since it is quite difficult to actually measure the thickness of an asphalt binder film on even a single aggregate, the asphalt industry is left to rely on calculated values based on a few reasonable assumptions. Attempts have been made to quantify the actual binder film using scanning electron microscopy and visual microscopy (Elseifi et al., 2008). However, complications occur with fine materials creating mastic rather than an aggregate with a finite asphalt binder film thickness.

Even though the physical representation of the calculated values may not be as direct as desired, film thickness determinations have been found to be linked to both short and long-term aging rates of asphalt mixtures based on measures of viscosity, penetration, and complex modulus of asphalt binders recovered from mixtures using the Abson method (Kandhal and Chakraborty, 1996). Prior studies found the hardening of asphalt binders in a mixture correlated with air voids, permeability, and film thickness (Goode and Lufsey, 1965). Additional studies has suggested that calculated film

thickness values combined with mixture permeability were relevant to predictions of the hardening resistance of a given asphalt mixture (Kumar and Goetz, 1977).

As such, this particular investigation utilized the binder film calculation methodology that determined the apparent film thickness following the procedures outlined in the NCHRP manual on hot mix asphalt design (Christensen, 2010). The fact that such a significant number of the mixtures were tested at the 9 μm AFT binder content warrants further discussion of the determination of the apparent film thickness.

From the design manual (Christensen, 2010), a series of volumetric calculations permit the determination of the apparent film thickness as depicted by Equation 5.1 through Equation 5.6, which were used to determine the AFT for the mixtures included in this study. Essentially, the determination of the AFT for a particular mixture requires the specific gravity of the aggregate, the combined gradation of the aggregate, the asphalt binder content, and the maximum theoretical specific gravity of the mixture as presented in Equation 5.8.

$$AFT = \frac{1{,}000VBE}{S_s P_s G_{mb}} \qquad \textbf{Equation 5.1}$$

where, AFT – apparent film thickness, μm;
VBE - volume of effective binder, % total volume of mixture;
S_s - specific surface of the aggregate gradation, m^3/kg;
P_s - aggregate content, % by total weight of mixture, $100 - P_b$;
G_{mb} - bulk specific gravity of the mixture.

The specific surface of the aggregate is essentially represented by the surface area of the entire aggregate gradation. The specific surface is based upon the aggregate gradation as presented in Equation 5.2. An abbreviated version of Equation 5.2 has been developed

and is presented in Equation 5.3, however, the long form of the determination, Equation 5.2, has been utilized in this study. The percent stone (P_s) may be determined by subtracting from 100 the value of the binder content (P_b) as the percentage by total weight of the mixture, which is a common input parameter for asphalt mixtures. The bulk specific gravity of the mixture (G_{mb}) is also a common measure utilized to characterize the density of a compacted mixture.

$$S_s = \left(\frac{1}{1{,}000G_{sb}}\right)[1.4(P_{50} - P_{37.5}) + 2.0(P_{37.5} - P_{25}) + 2.8(P_{25} - P_{19}) + 3.9(P_{19} - P_{12.5}) + 5.5(P_{12.5} - P_{9.5}) + 8.9(P_{9.5} - P_{4.75}) + 17.9(P_{4.75} - P_{2.36}) + 36.0(P_{2.36} - P_{1.18}) + 71.3(P_{1.18} - P_{0.60}) + 141(P_{0.60} - P_{0.30}) + 283(P_{0.30} - P_{0.15}) + 566(P_{0.15} - P_{0.075}) + 1{,}600(P_{0.075})] \quad \textbf{Equation 5.2}$$

$$S_s \cong \frac{P_{0.30} + P_{0.15} + P_{0.075}}{5} \quad \textbf{Equation 5.3}$$

where, S_s - specific surface of the aggregate gradation, m^3/kg;
G_{sb} - bulk specific gravity of the aggregate;
P_{50} - percent passing the 50 mm (2 inch) sieve;
P_i - percent passing the i^{th} mm sieve from 50 to 0.075mm
as depicted by Equation 5.2 and Equation 5.3, respectively.

Once the aggregate component of the AFT calculation has been determined, the next significant contribution is the volume of effective binder (VBE). The VBE can be understood to represent the volume of asphalt binder added to a mixture which has not been absorbed into the aggregate and is thus available to influence the overall

performance of the mixture. The calculation of VBE is presented by Equation 5.4 with each of the corresponding inputs as determined by Equation 5.5 and Equation 5.6.

$$VBE = VB - VBA$$ **Equation 5.4**

where, VBE - volume of effective binder, % total volume of mixture;
VB - total volume of asphalt binder, % total volume of mixture;
VBA - volume of absorbed binder, % total volume of mixture.

$$VB = \frac{P_b G_{mb}}{G_b}$$ **Equation 5.5**

where, VB - total volume of asphalt binder, % total volume of mixture;
P_b - percent of asphalt binder, % total weight of the mixture;
G_{mb} - bulk specific gravity of the mixture;
G_b - specific gravity of the asphalt binder.

$$VBA = G_{mb}\left[\frac{P_b}{G_b} + \frac{P_s}{G_{sb}} - \frac{100}{G_{mm}}\right]$$ **Equation 5.6**

where, VBA - volume of absorbed binder, % total volume of mixture;
G_{mb} - bulk specific gravity of the mixture;
P_b - total percent of asphalt binder, % total weight of the mixture;
G_b - specific gravity of the asphalt binder;
P_s - total percent of stone or aggregate, % total weight of the mixture;
G_{sb} - specific gravity of the aggregate;
G_{mm} - theoretical maximum specific gravity of the mixture or Rice value.

As stated previously, the determination of the AFT for a particular mixture requires much fewer inputs than the previous three equations. This reduction in input parameters is accomplished by substituting Equation 5.5 and Equation 5.6 into Equation 5.4, which yields Equation 5.7.

$$VBE = G_{mb}\left[\frac{P_s}{G_{sb}} - \frac{100}{G_{mm}}\right]$$ **Equation 5.7**

By substituting Equation 5.7 back into the original calculation of Equation 5.1, AFT can be found for a particular mixture by the specific gravity of the aggregate, the combined gradation of the aggregate, the asphalt binder content, and the maximum theoretical specific gravity of the mixture, as stated previously. Equation 5.8 is a much simpler equation to calculate and does not involve all the potential errors in measurement of G_{mb} or G_b etc.

$$AFT = \frac{1{,}000}{S_s(100 - P_b)}\left[\frac{(100 - P_b)}{G_{sb}} - \frac{100}{G_{mm}}\right]$$ **Equation 5.8**

The formula for AFT presented in Equation 5.8 makes logical sense by the G_{mm} establishing the absorbed binder in terms of specific gravity of the aggregate (G_{sb}) modified by the applied P_b spread over the surface of the aggregate (S_s).

Therefore, two sets of mixtures were produced in the laboratory; those with 4.5% TWM and those with a mix-specific binder content to yield the 9 μm apparent film thickness. These laboratory produced mixtures were then aged in the laboratory ovens for their respective durations prior to the evaluation testing procedures.

Due to the varied mixture components and compaction levels utilized in this study, photographs of representative laboratory prepared specimens can be found in Figure 17.1 through Figure 17.16 of Appendix E. Those figures present the uncut sample as they were aged in the ovens, the dynamic modulus specimens and the side-cut UTSST

specimens as a visual reference of the aggregate orientation, visual porosity, and overall structure of each mixture.

Additional mixtures, as mentioned in the laboratory validation section, were also compacted in the laboratory and subjected to different aging conditions prior to the evaluation testing be conducted. These field mixtures included in the laboratory validation efforts were prepared from plant produced mixtures and compacted in the laboratory, with the exception being the Texas mixture which was mixed in the laboratory rather than in an HMA plant. The laboratory validation mixtures were all compacted to a nominal air void level of 7% in the cut specimen.

Laboratory Aging of Mixtures

Each of the laboratory prepared mixtures depicted in of Table 5.1 and Table 5.2 were short term aged in a loose condition at 135°C (275°F) for four hours prior to compaction to their respective air void levels. The same mixtures are compacted and aged in an uncut condition in a forced draft oven at 60°C (140°F) for durations of 0, 3, 6, and 9 months, with a month representing 28 days.

As the result of a few curiosities with the binder aging studies that will be discussed later, two of the mixtures were aged under a different set of oven conditions. The two mixtures were the Lockwood aggregates mixed with the PG64-28 binder and the California aggregates mixed with the PG64-22 binder. Both mixtures were compacted to all three air void levels (i.e. 4, 7, and 11%). These mixtures were then aged for 0.5, 1 and 3 month durations at 85°C (185°F) prior to the evaluation testing.

It was suspected, and soon confirmed, that the oven aging could distort and even cause gross shear failure of some of the compacted sample, especially those with higher asphalt binder contents and higher air void levels, i.e. lower overall mix stability. As a result, many of the mixtures that were suspected to exhibit this instability at the aging temperatures were wrapped in an expanded wire shell to restrict any potential movement, but still permit the free flowing conditions for air circulation around and into the specimens. Any mixtures that did distort or were noted to have any damage due to the aging duration were excluded from testing and replaced by additionally prepared and aged specimens as applicable. Figure 5.1 presents an example of samples that failed during aging along with the reproduced specimens secured in wire mesh wrapping.

(a) **(b)**

Figure 5.1 WesTrack 1997 Coarse Aging Samples (a) Top View without and (b) Side View with Wire Mesh

Even though the height or sample diameter were not determined before or after the application of the oven aging, careful visual observations were made to determine if any noticeable deformations were present. Further, of all the measurements made on all of the aged specimens, only the 3 month samples aged at 85°C (185°F) exhibited any signs of aggregate disruption or other significant influence traceable back to the aging conditions. Further discussion of those results will follow in the appropriate section relevant to that topic.

Once the mixture specimens completed their respective aging durations, they were cut to the appropriate test specimen geometry and were tested for bulk specific gravity to determine the air void of the cut specimens, utilizing the same theoretical maximum specific gravity (G_{mm}) as determined by the mix design procedure. Specifically, the same G_{mm} value was used for all aging conditions of the mixtures; thereby necessitating the G_{mm} determination was not specifically of the same aging condition as the bulk specimen. This was done for practical reasons, namely that it would have been unreasonable to age the G_{mm} specimen for the prolonged durations that the specimens were exposed to, nor could those aging conditions be expected to be the same for compacted and loose mixtures.

Following the underwater and saturated surface dry portions of the G_{mb} determination, the cut specimens were dried for 48 hours in front of high capacity fans under ambient conditions to dry the specimens and determine the dry mass as needed for the air void calculation. The specimens were then immediately wrapped in plastic cling wrap and placed in a freezer at -18°C (0°F) at least overnight or until the remainder of the testing could be conducted. This was done for three main reasons. The first is that the

oxidation of the samples is much reduced by placing the specimen in low-temperature environments, especially when the flow of replenishing oxygen is minimized with the plastic wrap. Second, not all of the samples could be tested immediately upon the conclusion of their respective aging duration, especially early on in the project when a large number of specimens were being prepared at the same time. Lastly, all the specimens were placed in the freezer overnight to maintain that all the specimens had run through a single cooling cycle to -18°C only once. Thus, any steric or other physical hardening that may have been instilled in the frozen specimens would be a constant influence applied to all specimens, for consistency sake.

Asphalt Mixture Evaluation Testing

Once the respective aging had been applied and the specimens were prepared, frozen once, then thawed at ambient temperatures, they were ready to proceed with the scheduled testing protocol composed of the measures discussed in the methodology sections of Chapter 3. Referencing those details, the mixtures were tested for dynamic modulus measures and evaluation by the Uniaxial Thermal Stress and Strain Test.

Upon completion of the E^* testing, those samples were broken down in general accordance with the preparation method for the determination of the theoretical maximum specific gravity outlined in AASHTO T209 (AASHTO, 2006), before being sealed in a snap closure plastic bag and returned to the -18°C (0°F) freezer for a minimum duration of overnight. The loose mixtures were then ready to proceed through the extraction and recovery operations discussed previously and outlined in Appendix B to retain the aged asphalt binder for further testing as outlined in the following section.

5.2 Asphalt Binder Evaluation

The asphalt binder evaluation was primarily focused on aging the asphalt binders to different oxidation levels in open pans exposed to atmospheric air pressure and oxygen concentrations over a range of aging temperatures. The samples were aged in pressure aging vessel (PAV) pans however no additional air or oxygen pressure was applied to the samples during aging. The PAV pans were aged in specialized forced draft ovens, which were selected to provide precise and consistent temperature control, generally within 0.7°C.

The aging samples were prepared in standard PAV pans with the dimensions of 140 mm (5.5 inch) diameter by 9.5 mm (3/8 inch) deep as specified in AASHTO R28 and T179 (AASHTO, 2006). Utilizing the specific gravity of each asphalt binder, an appropriate mass of asphalt binder was added to each pan to result in an asphalt film thickness of 1 mm (~0.04 inches) according to Equation 5.9, which generally resulted in about 15.7 grams of binder in each PAV pan.

$$M_b = \frac{G_b \rho_w \pi d^2 h}{4} \qquad \textbf{Equation 5.9}$$

where, M_b - mass of asphalt binder, gram;
G_b - specific gravity of the asphalt binder;
ρ_w - density of water, 1 g/cm^3;
d - diameter of PAV pan, cm;
h - thickness of the asphalt binder film, 1 mm = 0.1 cm.

The sample pans were placed on multiple racks, with eight samples per rack as standard practice. At each of the prescribed intervals, the sample pans were removed from the aging, a minimum of two at a time. This was exercised so that a normalized rate of aging of the binder could be maintained by strategically selecting the location of the pans included with each sample interval throughout the aging duration. Initially, concern was expressed that different locations within a given aging oven may yield slightly different temperatures and differing amounts of air flow, and thus a variable oxygen supply. Differences in these parameters critical to the oxidation of the asphalt binder led to careful planning to alternate the location of the paired aging pans.

Essentially, the systematic selection of the pan locations by alternating between the top and bottom racks and front and backs rows of a given column within a particular oven. As an example, for the first aging duration in a given column, the pan from the front row of the top rack would be combined with the pan from the back row of the bottom rack. The second sampling would combine the back row of the top rack with the front row of the bottom rack, and so on toward the center racks of the oven. When combined in this manner, it was found that the given asphalt binders did not receive differential aging, but were aged in a repeatable fashion and were not dependent upon the sample location within the ovens.

In this fashion, the aging pans containing the asphalt binders were aged for different durations at the temperatures levels presented in Table 5.3. As presented in the table, a few different aging protocols were followed in this study. Initially, the duration of the 50°C aging ranged from 60 to 320 days as were utilized with the first six binders evaluated. Further exploration in this study highlighted the necessity to reduce the

overall duration of the laboratory aging in an effort to expedite these types of long term aging studies. Therefore, the longer durations at 50°C were reduced to 180 and 240 days for both WesTrack and the binders extracted and recovered from the field produced mixtures. As previously discussed in the methodology of section 3.6.3, these aging durations at their respective temperatures were specifically designed as part of the experimental matrix to yield kinetics measures previously described as constant rate kinetics relationships. As discussed in these previous sections, it was decided as part of the original experimental design, that the constant rate kinetics were likely sufficiently precise to characterize the oxidative aging characteristics of the relevant asphalt binders and mixtures included as part of this overall research effort.

The final set of conditions for the asphalt binder aging and kinetics studies were conducted on the ARC Core materials. Clearly, double the number of measures were conducted on as many aging conditions as were included in the constant rate kinetics measures of the other binders. Observation of these additional aging conditions notes that these durations were much shorter in length as the previous two evaluations. The reason for this was to evaluate the early or fast rate kinetics parameters of the four core binders. It was decided that even if this particular study were based solely on the constant rate kinetics measures, including the associated modeling efforts being conducted in parallel to this study, it would still be a valuable asset to the overall research effort to record in the ARC Database both the fast and constant rate kinetics data for future use, if desired.

As a result, the asphalt binder aging temperatures and their corresponding durations are presented in Table 5.3.

Table 5.3 Binder Kinetics Aging Conditions

Asphalt Binders	Aging Temperature			
	50°C (122°F)	**60°C (140°F)**	**85°C (185°F)**	**100°C (212°F)**
PG64-22, PG64-28, Base Stock, PG64-22+3%SBS, PG64-22+10%Lime, PG64-22+20%Lime	60, 120, 200, 320 days	30, 60, 100, 160 days	7.5, 15, 25, 40 days	1.83, 3.75, 6.25, 10 days (44, 90, 150, 240 hours)
WT97-22, WT95-22, Moana 22, Moana 28, Sparks 28	60, 120, 180, 240 days	30, 60, 100, 160 days	7.5, 15, 25, 40 days	1.83, 3.75, 6.25, 10 days (44, 90, 150, 240 hours)
BI 0001 BI 0002 BI 0003 BI 0004	4, 8, 15, 30, 60, 120, 180, 240 days	2, 4, 8, 15, 30, 60, 100, 160 days	0.5, 1, 2, 4, 8, 15, 25, 40 days	0.083, 0.25, 0.5, 1, 2, 4, 7, 12 days (2, 6, 12, 24, 48, 96, 168, 288 hours)

As a consequence of Reno being at a significantly higher elevation than sea level, the atmospheric pressure in the laboratory was not quite one atmosphere (atm) of pressure. In the laboratory where the binders were aged, it has been estimated that the atmospheric pressure was closer to 0.83 atm. As a result the partial pressure of the applied oxygen for the oven aged samples was approximately 0.168 atm as opposed to more commonly used values of 20% near sea level. This adjustment may need to be considered when utilizing the kinetics measures from these materials relative to other elevations and oxygen pressures.

As a result of these aging conditions, several different aging levels were created that permitted the evaluation of the aging characteristics of these binders by the methods previously discussed in Chapter 3 and summarized in the following section.

Asphalt Binder Evaluation Testing

As previously discussed in Chapter 3, the evaluation of the asphalt binders included quantification of both the changes in the chemical structure and the physical behavior of the asphalt binder as a result of the induced oxidation. The chemical structure was determined through measurements made with the Fourier-Transform Infrared Spectroscopy and quantified as calculations of the carbonyl area. The physical measures were largely based upon rheological measurements conducted on the dynamic shear rheometer and the resulting calculations based on those measures.

5.3 Laboratory Validation

The portion of this study being termed the laboratory validation testing, was generally intended to utilize the evaluation methods used with the laboratory prepared mixtures and apply those methods to field produced mixtures. Further, the results of these efforts were intended to provide a separate set of measures to aid in the statistical validation efforts being conducted after this evaluation phase of the overall effort had been completed.

As a result, the asphalt binders were evaluated in a nearly identical fashion as outlined in section 5.2 previously. The kinetics and hardening susceptibility measures were conducted on the respective asphalt binders. Specifically, the Moana Lane and Sparks Blvd. asphalt binders were extracted and recovered from the mixtures to obtain the necessary materials for the binder kinetics and hardening susceptibility measures.

Conversely, the binders used in the Texas and Ohio mixtures were readily available as the ARC core materials and were thus tested as virgin binders. The Ohio mixtures evaluated were the plant produced loose mixtures that were compacted in the laboratory for the appropriate aging in the laboratory ovens and subsequent testing. Being that the Ohio materials were obtained from an actual field project, relevant field samples are anticipated to be included in the evaluation once they have been allotted varied levels of time to age in-situ to aid in the overall validation effort of this study.

On the other hand, the Texas materials did not directly have field sections associated with them. Therefore, those mixtures were prepared in the laboratory and aged in the laboratory ovens as well, resulting in the term laboratory validation.

These materials with the specific focus to establish a more practical and user friendly evaluation system, these mixtures were aged in laboratory ovens at 85°C (185°F) for 0, 0.5, and 1 month (28 day) durations. This was to reduce the overall time requirement for this type of evaluation coupled with the noted issues of the samples aged for 3 months at 85°C (185°F) previously in the study. Some of the longer asphalt binder aging duration were also reduced as noted in the previous asphalt binder aging section.

As a result, shorter duration aging conditions for both the asphalt binder and the mixtures aged in the laboratory were examined in an effort to provide a more time efficient strategy, founded upon the experience and measured results of the more rigorous laboratory mixture evaluation phase.

5.4 Summary of Mixture and Asphalt Binder Testing

An abbreviated summary of the mixture and asphalt binder testing processes is depicted in flowchart of Figure 5.2. Beginning in the upper left of the figure, the process is initiated with the development of the relevant aggregate selection and gradation, which were then mixed with the selected asphalt binder creating the mixture. The mixture was then subjected to the appropriate short-term aging conditioning prior to compaction of the mixture to the desired density or air void level. The compacted mixtures were then subjected to varied levels of oxidative aging in laboratory ovens over different durations as the chart proceeds to the left. After the aging was complete and the specimens were trimmed to the appropriate geometry, they were evaluated with either E^* or UTSST measurements, in the upper right of the figure. Continuing through the center of the figure, the binders were then extracted and recovered lending to the completion of the asphalt binder measurements of partial kinetics and the hardening susceptibility measures with the FT-IR and the DSR on the bottom right of the figure.

The asphalt binder kinetics and hardening susceptibility determinations are also depicted by the asphalt binder sample shown, again in the upper left of the figure. The binder evaluation then proceeded to the PAV pan-aging over their respective temperatures and duration along the bottom of the figure, which ultimately ended up with the same FT-IR and rheological measures as the binders recovered from the mixtures.

The succinct objective of this study revolves around the comparison of these material measures and calculated oxidation parameters. Specifically, the influence of the aggregates, i.e. absorption, adsorption, mineralogy and qualitative gradation, as well as

the mixture properties, i.e. air voids and binder content, on the overall aging performance of the evaluated mixtures and their respective asphalt binders were the main evaluations conducted.

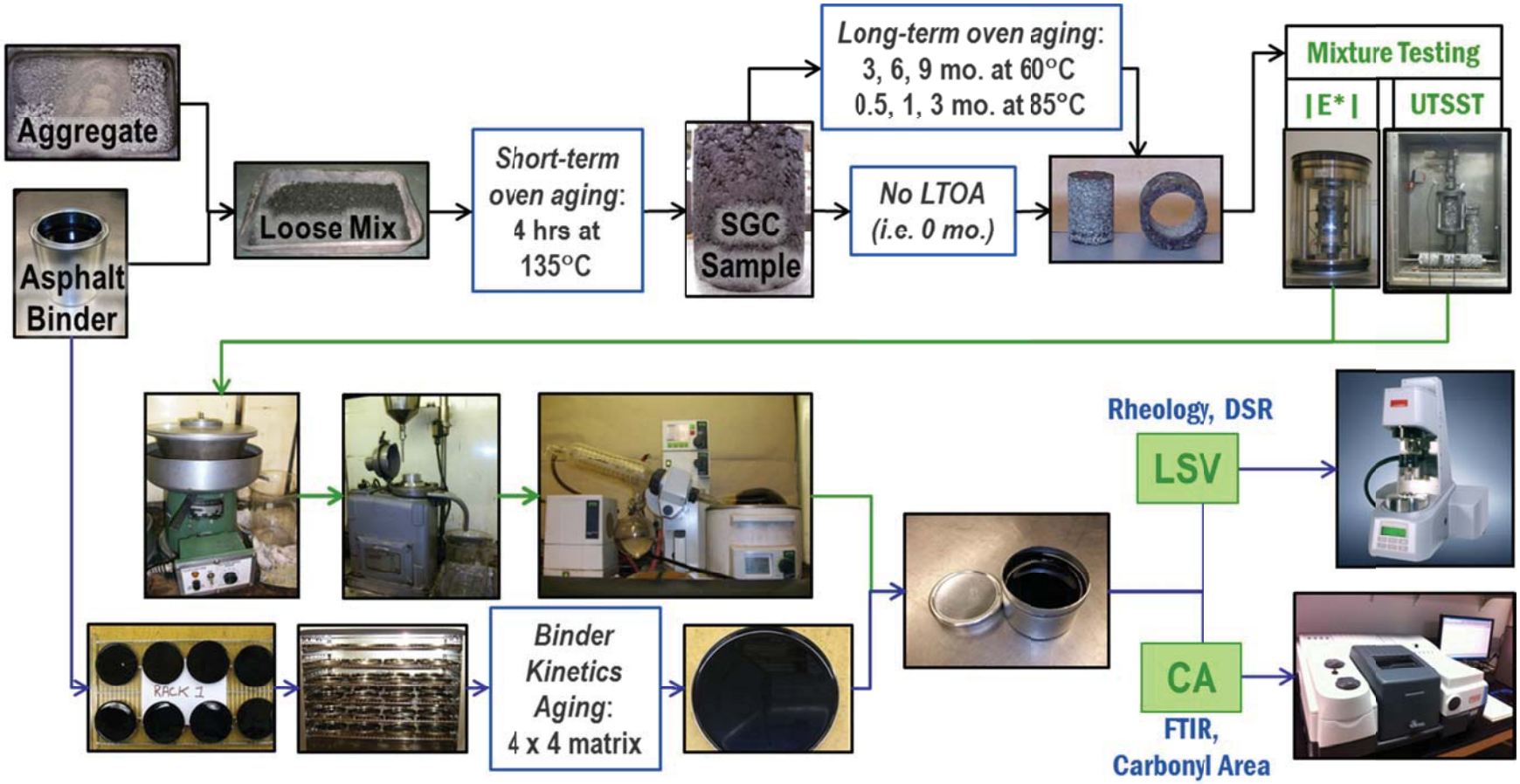

Figure 5.2 Flowchart of Mixture and Binder Evaluation

5.5 Asphalt Binder-Aggregate Interaction

Further attempts were made on an exploratory basis, i.e. not on all the relevant aggregate and asphalt combinations, to directly quantify the complex interaction between the asphalt binder and the aggregate on the aging of asphalt mixtures and binders. The analysis termed saturates, aromatic, resins, and asphaltenes (SARA) separates the asphalt binder into those four fractions based upon the combined effect of molecular weight, solubility of the asphalt binder in certain solvents presenting differences in molecular polarity, and adsorption characteristics of the asphalt binder to the medium placed in the separation column.

Measures on the California, Nevada, and Texas aggregate sources were conducted by what is termed a modified SARA analysis. In these measures, the standard alumina based medium had been replaced by a sand fraction from the respective aggregate gradations. The fraction of the gradation used was sized by passing through the 0.60 mm (No. 30) sieve and washed over the 0.30 mm (No. 50) sieve. The fractions used from the Nevada and California aggregates were both the intermediate gradation while the Texas aggregates only had a single reported combined gradation. This aggregate fraction was selected based on the characteristics of the gradations being considered.

The SARA analysis requires a fairly clean and relatively single-sized material of diameter nominally smaller than 1 mm (~0.04 inch) as the separation medium. The 0.30 mm (No. 50) sieve size was particularly selected due to the suspected influence of the Wadsworth sand used in a few of the analyzed mixtures. Previous explorations of this

type (Robertson et al., 2006) suggested that silica content of the aggregates had a significant influence on the adsorption characteristics of the asphalt-aggregate interaction with a given binder. There was also a somewhat lesser effect of calcium content of the aggregate noted as well. The mineralogy of Wadsworth sand is primarily quartz, which has significant silica content. The gradation of Wadsworth sand stockpile shows a significant proportion of that stockpile is retained on the 0.30 mm (No. 50) sieve. By combining these two effects, it was anticipated that this particular sand size would provide the clearest indication of any significant effects of the gradation on the binder separations. The Texas aggregates were also examined to specifically exclude the silica content, but also to include the high calcium content of the limestone.

The binders used for these separations were both the PG 64-22 and PG 64-28 binders with the intermediate gradations of both the Nevada and California aggregates, a 4x4 matrix to correspond to the mixtures prepared within this study. Similarly, the Texas aggregates were combined with the Venezuelan BI 0001 PG 67-22 binder, just as in the mixture aging evaluation.

These analysis techniques were initiated and conducted by a collaborative effort with P. Michael Harnsberger and A. Troy Pauli at the Western Research Institute in Laramie, Wyoming.

6 AGGREGATE TEST RESULTS AND DISCUSSION

In addition to the standard test methods to determine the gradation and specific gravity of the aggregates, each of the aggregate sources was also examined by the Aggregate Image Measurement System (AIMS) along with an analysis based on visual petrography. Each of those determinations are discussed in the following respective sections.

6.1 Petrographic Analysis

As discussed in the methodology section, the petrographic analysis was conducted to identify the mineralogical constituents of each aggregate source in accordance with ASTM C295 (ASTM, 2010). To conserve resources, the petrographic analyses were limited to a reasonable number where only the main component of each aggregate source was analyzed. Typically, the majority of the coarse aggregate stockpiles within a given aggregate source exhibited fairly consistent mineralogical characteristics based upon inspections of hand sample. As a result, for most of the aggregate sources only a representative selection of the coarse aggregate stockpiles were submitted for petrographic analysis. However, if a certain sand or fines portion of one of the stockpiles varied significantly, it was also considered in the mineralogical consideration.

Petrographic analysis provides details on the individual minerals components found within the aggregate. Considering the amount and specific combinations of the observed

minerals combined with other physical observation of the specimens, i.e. weathering, layering, alterations, etc., the classification and thus official name of the rock can be identified as previously discussed in the material description of Chapter 4. The thin sections are prepared by gluing a section of each specimen to a microscope slide and grinding it thin enough to pass visible light though it. As discussed previously, the light used during petrographic analyses focused on polarized and cross-polarized light.

Presentation of the results are provided in Table 6.1 through Table 6.6, and visual representation of the overall aggregate gradation along with photographs of the thin sections under the appropriate lighting conditions are provided in Appendix F.

Table 6.1 Petrographic Examination of California Aggregates

Properties	Gardner Aggregate					Bee Rock Crusher Fines
	Mudstone	**Sandstone**	**Gneiss**	**Chert**	**Volcanic Ash**	**Limestone**
Constituent Percent (%)	48	33	12	5	2	100
Particle Shape	Sub-Angular, Sub-Round	Sub-Angular to Round	Sub-Angular	Angular to Sub-Round	Round	Very Angular
Surface Texture	Smooth	Smooth	Smooth	Smooth where fractured	Smooth	Sugary Crystalline
Grain Size	<<1 mm	1 mm	< 1 mm	<<1 mm	< 1 mm	< 1 mm
Color	Dark grey with green tint	Light tan	Light tan	Red to dark gray	White	Light tan
Mineral Composition	Too fine grained to identify, Serpentine	Quartz, Feldspar, mica	Quartz veining	Silica	Quartz	Calcite
General Condition	Moderately weathered	None noted	Moderately weathered	Fresh, Dense	Fresh, Porous	Fresh
Coating/ Incrustations	Iron Oxide	Weakly cemented with calcium carbonate	Iron Oxide	Stained on weathered edge	Manganese dioxide (dendrites)	Powdery coating on weathered edges, Manganese dioxide (dendrites)
Deleterious Constituents	None noted	None noted	None noted	Unit possibly deleterious	None noted	Potentially

The California aggregate source largely consisted of a blend of marine sediments, siliceous flows, and ash flows. The open and somewhat porous textures gave rise to the atypically high absorption rates noted. Because of this high absorption, the Gardner material was included in this analysis.

Table 6.2 Petrographic Examination of Colorado Aggregates

Properties	Colorado Aggregate		
	Morrison Mica Gneiss	**Morrison Mica Schist**	**Morrison Quartz**
Constituent Percent (%)	50	47	3
Particle Shape	Angular, Sub-Angular	Angular, Sub-Angular	Sub-Angular
Surface Texture	Medium to Coarse Grain	Medium Grain	Smooth
Grain Size	2 mm	1 mm	1 mm
Color	Pink to red and dark grey to black	Dark grey with round pink tints	Powdery white with light link tint
Mineral Composition	Quartz – 40% Orthoclase – 35% Biotite – 25%	Biotite – 25% Quartz – 30%	Quartz
General Condition	Moderately weathered	Moderately weathered	Fresh
Coating/ Incrustations	Iron Oxide staining	None noted	None noted
Deleterious Constituents	Biotite	Biotite mica with foliation	Vein quartz

The Colorado coarse aggregate is the crushed and angular material summarized in Table 6.2. However, the blended gradation also included the clean silica sand from the Thornton concrete sand stockpile. Similarly, the Platte Valley processed fines were a washed, but not as clean, siliceous sand material.

Table 6.3 Petrographic Examination of Nevada Aggregates

Properties	Nevada Aggregate			
	Complex Volcanic Sequence	**Wadsworth Sand**		
	Basalt, Andesite, Rhyolite	**Quartz**	**Lithic Clasts**	**Plagioclase Feldspar**
Constituent Percent (%)	100	50	45	5
Particle Shape	Angular, Sub-Angular	Sub-Angular to Sub-Rounded	Sub-Angular to Sub-Rounded	Sub-Angular to Sub-Rounded
Surface Texture	Fine grained	Crystalline	Aphanitic	Crystalline
Grain Size	< 1 mm	1-2 mm	1-2 mm	1-2 mm
Color	Grey	White to Grey	Grey to Brown	Pinkish Grey
Mineral Composition	Quartz: <10%, Biotite Mica: <10%, Plagioclase Feldspar (microscopic): 80% Minor Clay alteration minerals and Lithic Clasts: <10%	Quartz	Basalt, Andesite, and Rhyolite exhibiting minor clay alteration minerals	Plagioclase Feldspar
General Condition	Minor weathering	Sound	Minor weathering	Minor weathering
Coating/ Incrustations	Minor iron staining, minor sandy coating, likely broken rock fragments	None noted	None noted	None noted
Deleterious Constituents	None noted	None noted	Presence of minor clay minerals	Presence of minor clay minerals

The Nevada aggregates included the highly crushed and angular volcanic complex mineralogy; basalt, andesite, and rhyolite, with some weathering as noted. These aggregates were nearly always combined with the Wadsworth Sand, which is a clean alluvial siliceous sand including some complex volcanic sequence mineralogy.

Table 6.4 Petrographic Examination of Utah Aggregates

Properties	Utah Aggregate[a]			
	Quartzite	**Limestone**	**Granodiorite**	**Basalt**
Constituent Percent (%)	45	22	17	16
Particle Shape	Angular, Sub-Angular, Sub-Round	Sub-Angular	Angular, Sub-Angular	Angular, Sub-Angular
Surface Texture	Fine grained	Fine grained	Fine-Med.-Coarse grained	Fine grained
Grain Size	< 1 - < 2 mm	< 1 mm	< 2 - < 3 mm	< 1 mm
Color	Light green, light pink, to white	Grey	Dark grey, grey, to white with grey crystals	Med. Grey, minor yellow/orange coating
Mineral Composition	Quartz, minor pyrite, and trace iron oxide	Calium carbonate	Plagioclase and sodium feldspar, quartz, biotite mica, horneblende, trace magnetite	Quartz, mica, fine groundmass with quartz, minor secondary pyrite
General Condition	Fresh	Fresh	Fresh to minor weathering	Fresh
Coating/ Incrustations	Minor oxide staining	Minor oxides on weathered surface	None noted	Minor iron staining
Deleterious Constituents	None noted	None noted	None noted	Possible slight foliation

a – Petrographic descriptions are the summary of ten individual sample units which resulted in the four rock classifications noted in the table.

The Utah material is a mixed partially crushed gravel source with a wide range of mineralogical components. The 1/4" stockpile was made up of very rounded nearly single sized coarse sand material, while the other stockpiles were fairly similar in mineralogical measures to the examined materials included in Table 6.4 for each respective stockpile size.

Table 6.5 Petrographic Examination of WesTrack 1995 Aggregates

Properties	WesTrack 1995 Aggregate		
	Andesite to Basalt	**Rhyolite**	**Granite**
Constituent Percent (%)	95	3	2
Particle Shape	Angular, Sub-Angular	Sub-round to round	Angular
Surface Texture	Fine grained	Fine grained with glassy quartz grains	Granitic texture
Grain Size	< 5 mm	< 1 mm	< 5 mm
Color	Dark grey to light pink	Light pink	White to green
Mineral Composition	Fine groundmass, magnetite, plagioclase feldspar, quartz	Fine groundmass, quartz	Quartz, feldspar, chloritized amphiboles
General Condition	Moderately weathered	Fresh, porous	Moderately weathered
Coating/ Incrustations	Iron and manganese oxide staining	None noted	Iron oxide
Deleterious Constituents	None noted	Very porous	None noted

The WesTrack 1995 aggregates included the crushed and angular volcanic complex mineralogy, basalt, andesite, and some rhyolite, with some Granitic materials as well. These aggregates were combined with the Wadsworth Sand, which is a clean alluvial siliceous sand including some complex volcanic sequence mineralogy.

Table 6.6 Petrographic Examination of WesTrack 1997 Aggregates

Properties	WesTrack 1997 Andesite to Basalt
Constituent Percent (%)	100
Particle Shape	Sub-Angular, Sub-Round
Surface Texture	Porphyritic, very fine groundmass
Grain Size	< 5 mm
Color	Dark grey with greenish hue
Mineral Composition	Biotite Mica, Quartz, magnetite, pyrite, Plagioclase Feldspar
General Condition	Fresh to Mod. weathered
Coating/ Incrustations	Iron and manganese oxide coatings on weather edges
Deleterious Constituents	None noted

Aggregate mineralogy has been found to substantially affect the interaction with asphalt binders. Specifically, the silica content and to a lesser extent calcium have been shown to exhibit higher levels of influence on the adhesion bonding with the polar components of an asphalt binder. Unfortunately, as can be observed in the tables of mineralogical data, the majority of the aggregate sources initially selected for this project contain a substantial proportion of silica, whether added as a sand stockpile or as a component of the aggregate itself. This is not an unexpected finding, given the fact that the vast majority of the rock and mineral deposits on the earth contain significant amounts of

silica. It does however, present an underlying factor that should not be neglected during the analyses conducted as part of this research.

6.2 AIMS Results

The Aggregate Image Measurement System (AIMS) was utilized to quantify the shape, angularity, and surface texture of aggregates used in this study. The specific measurement techniques and calculations were presented in Chapter 3. A summary of the measurements conducted with the AIMS software on the individual combined gradations utilized in this study are presented in Table 6.7.

Table 6.7 Summary of AIMS Measurements

AIMS Parameters		Aggregate Gradations								
		CAL		CO	NV		UT		WT95	WT97
		Int.	Fine	Int.	Int.	Fine	Int.	Fine	Fine	Coarse
Coarse Aggregate	Angularity	2,433	2,435	2,897	3,062	3,055	2,552	2,562	3,204	2,947
	Texture	309	248	559	366	358	277	272	369	335
	Sphericity	0.61	0.63	0.61	0.63	0.62	0.69	0.69	0.67	0.65
	Flat & Elongated 1:1	47.5	29.2	56.3	53.0	42.8	44.1	38.1	51.0	57.8
	F&E 2:1	34.3	20.6	44.3	35.0	34.1	29.9	26.7	31.1	41.5
	F&E 3:1	14.3	9.1	12.1	15.5	14.8	10.5	11.1	12.2	13.2
	F&E 4:1	6.2	4.4	1.4	5.9	4.7	3.6	4.7	3.2	4.6
	F&E 5:1	3.2	1.7	0.2	0.8	2.1	2.4	2.1	0.5	1.1
	Flat or Elongated 1:1	47.5	29.2	56.3	53.0	42.8	44.1	38.1	51.0	57.8
	F or E 1:2	18.1	11.7	19.9	21.8	19.5	13.0	13.9	16.6	19.5
	F or E 1:3	5.1	2.5	0.2	4.9	5.4	4.2	2.7	1.1	2.9
	F or E 1:4	1.8	0.6	0.0	0.2	1.0	0.4	0.9	0.0	0.6
	F or E 1:5	0.0	0.2	0.0	0.0	0.5	0.1	0.2	0.0	0.0
	CAAT	4,294	3,680	7,033	5,195	5,111	4,049	4,000	5,293	4,818
Coarse and Fine Angularity		3,151	3,177	3,326	2,973	3,178	2,729	2,840	3,004	3,053
Fine Aggregate	Angularity	3,185	3,197	3,346	2,968	3,183	2,739	2,848	2,995	3,065
	2D Form	8.59	8.40	8.00	8.04	8.29	7.66	7.87	8.26	8.29

Since each of the AIMS measurements are calculated values of representative measurements on the numerous sieve sizes, performing replicate measurements necessary for statistical analyses was not conducted. However, some general observations of the finding are readily possible.

There are some noted differences in the coarse angularity noted between the different aggregate sources varying from 2,433 for the CAL intermediate gradation to 3,204 with the WesTrack fine gradation. Although numerically quite different, the two

likely are extremely different given the overall scale of 10,000 for the angularity measurements. Fairly similar values were noted between the intermediate and fine gradations within the same aggregate source. This is not necessarily an unexpected result considering the coarse fraction largely should not change for the majority of the gradations utilized in this study. The reported variations in Table 6.7 are likely the results of the differences in the respective gradations used as part of the calculation process for the coarse angularity parameter. Further deviations are noted between the two WesTrack aggregates, however it is important to recall that they are actually two separate aggregate sources. Therefore, noted deviations reflect the change in source as well as the combined gradation.

Considering the coarse aggregate texture, the majority of the aggregate blends exhibit fairly similar values. However, relatively greater deviations are noted between the intermediate and fine gradations with the California aggregate source as compared to the others in the table. In addition, an increased roughness in the texture is noted for the Colorado aggregate source.

The coarse aggregate angularity and texture (CAAT) parameter, which is a calculated value based upon the coarse angularity and the coarse aggregate texture, presents a parameters that shows some potential to clearly differentiate among the aggregate gradations as well as aggregate sources. With an overall range of the CAAT parameter from a low of 3,680 with the California fine gradation to the highest value of 7,033 with the intermediate gradation from Colorado, the CAAT parameter has some potential to characterize the aggregate properties in the forthcoming analyses in spite of the overall scale of zero to 15,000. Logically, this parameter provides an overall general

characterization of the aggregate surface by combining the roughness of the texture measurement with a parameter characterizing the external surface of the aggregate into a single measure. Therefore the CAAT parameter will be considered as a characteristic input for the respective aggregate properties in future analyses.

The sphericity parameter does not show an overly large variation between the gradations or aggregate sources with this particular data set. This does not necessarily mean that the parameter does not hold some significance, only that the statistical influence of this parameter relative to these analyses may be limited due to the relative similarity between all the sources.

Some degree of differentiation is apparent in the flat and elongated (F & E) and the flat or elongated (F or E) parameters between the intermediate and fine gradations of the California aggregate source. However, only limited differences were noted with the other aggregate sources.

Similar comparisons showed limited relative differences between the coarse and fine angularity parameter, especially considering the overall range of the measured data of less than 600 compared to the total scale of the measure. Unfortunately, both the fine angularity and the 2D form parameters also showed fairly limited relative differentiation between the aggregate sources and thus were expected to have limited influences on the statistical comparisons in the following sections.

It should be noted that just because some of the measured parameters do not show a large difference between the mixtures in this study, by no means makes the measurement invalid. It simply indicates that the parameter may not be significantly influential to the oxidation and interaction of the asphalt binder in a given mixture. However, these

measurements do provide a more robust characterization of the materials utilized in this study.

It is important to recognize that the parameters are strictly based upon the optical measurement of physical characteristics of the aggregates. Nevertheless, these measurements will be examined in later sections that focus on the quantifiable differentiation of numerous mixture measurements and the resulting changes with oxidative aging that have been determined by other efforts in this investigation. Clearly, these measurements have a finite scale which is generally limited to the level of surface texture measurements. However, they still may prove useful in characterizing the absorption tendencies of each respective aggregate source.

7 ASPHALT BINDER TEST RESULTS AND DISCUSSION

By applying the test methodologies of Chapter 3 to the materials discussed in Chapter 4 through the experimental matrix of Chapter 5, the overall objective of this study has been explored. In short, the objective of the study was to establish the aging characteristics of the asphalt binders aged without the effect of the aggregate or mixtures. Similar characteristics were also determined for the binders aged in the asphalt mixtures, then the two were compared to quantitatively determine what were the most influential characteristics of the aggregate and mixtures on the oxidation of the asphalt binders aged in the mixtures.

The following sections address each of separate material inputs, measures, and analyses of this investigation.

7.1 Pan-Aged Asphalt Binder Test Results

The protocol for the pan-aged asphalt binder, i.e. the standard of practice, has been previously presented in the applicable sections of Chapter 3 describing the aging temperatures and durations. Also discussed in that section were the tests conducted on the aged binders and analysis procedures conducted on the produced data. The first of the quantifiable measures were conducted by Fourier-transform infrared (FT-IR) spectroscopy to establish the level of oxidation within the samples as a function of time

and temperature otherwise known as oxidation kinetics determinations. Second, the dynamic shear modulus (G^*) master curves were developed for the aged binders based upon frequency sweep measures using the dynamic shear rheometer (DSR). Lastly, these two measurements were combined to establish the low shear viscosity (LSV) as a function of oxidation to establish the hardening susceptibility (HS) of the asphalt binders.

These test procedures and analysis methods were discussed previously, therefore the following sections focus on the presentation of the measured data and the material characteristics derived from them.

7.1.1 Fourier-Transform Infrared Spectroscopy

As previously established, the measurement of the oxidation level of the asphalt binders were measured by Fourier-transform infrared FT-IR spectroscopy. The actual quantification of the oxidation was determined by measuring the peak area of the carbonyl functional group, in this case defined as area under the absorbance band bound between 1,650 and 1,820 cm^{-1}, with the absorbance at 1,820 cm^{-1} as the baseline. This numeric value termed the carbonyl area (CA) in arbitrary units represents the quantification of the absorbed oxygen into the molecular structure of the asphalt molecules as a whole, i.e. the separate fractions of the binder are not differentiated. To be clear, the oxygen being measured in this manner is effectively the oxygen double-bonded to carbon atoms (C=O) creating a net increase in the amount of carbonyl functional groups.

As such, the CA measures, as representation of the oxygen absorbed, is expected to increase with additional aging time or harshness of the aging conditions, i.e. either temperature, pressure, or both. Since all of the oxidative aging conducted as part of this study were applied at ambient atmospheric pressure, the variation of the aging conditions were focused on the aging temperatures and durations. As an example, Figure 7.1 presents a series of FT-IR measures from the Paramount PG 64-28 binder, aged over four durations at 85°C in the oven. Note that there is a slight increase in the carbon to carbon double bond (C=C) occurring at 1,600 cm^{-1} as the binder ages from 7.5 through 40 days of aging. This is not really a concern, since the CA is measured along the side of this band, and is centered around 1,700 cm^{-1}. This very occurrence is the main reason for the baseline of the peak area being calculated at the absorbance value occurring at 1,820 cm^{-1} or wavenumbers. This effectively normalized the data to unforeseen changes in the magnitude of the CA peak. Simply put, if the overall absorbance curve increases, the baseline does by a similar amount, thus making the CA a more consistent measurement with changes resulting from the increase in oxygen and not artifacts of the measurements.

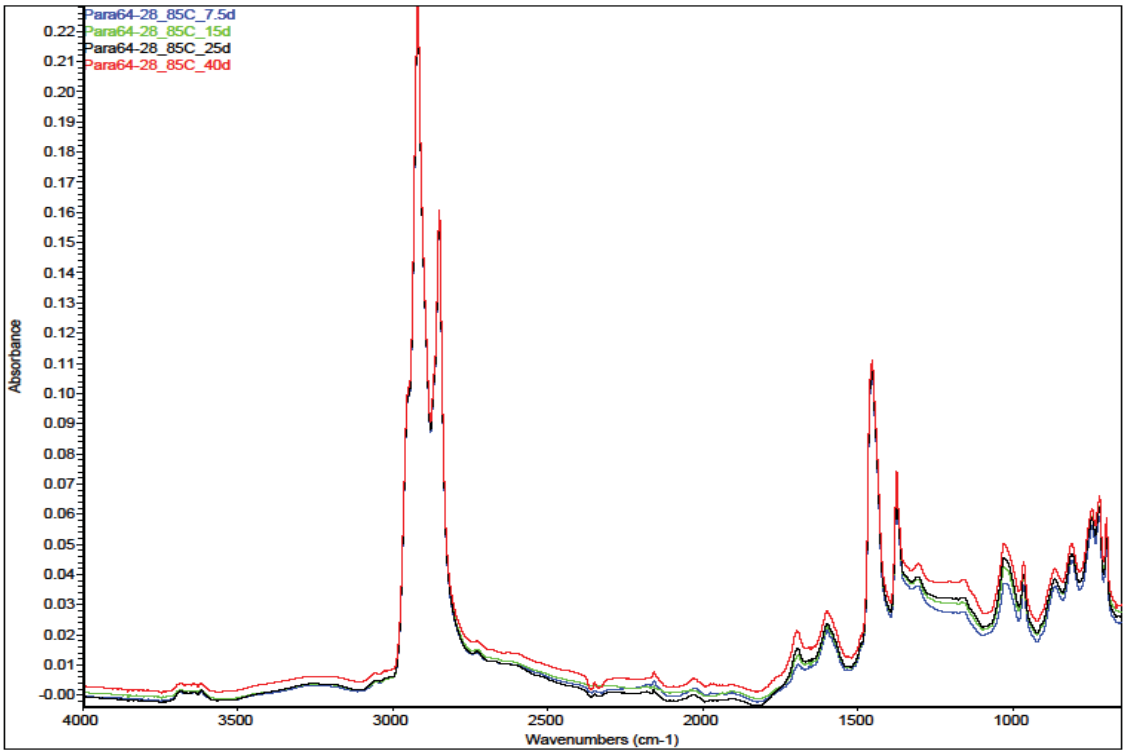

Figure 7.1 Example of FT-IR Spectra with Age, Paramount PG 64-28

Figure 7.1 also provides the opportunity to notice the sulfoxide peaks presented as the wider peak just to the left of 1,000 cm^{-1}, centered around 1,034 cm^{-1}. This also represents the absorption of oxygen, or oxidation of sulfur components within the asphalt binder. However, as discussed in the methodology of Chapter 3, the protocol followed in this study does not account for sulfoxide growth and assumes it is a relatively short-lived oxidation process and thus may be appropriately neglected in long-term aging and oxidation considerations. Further support of this decision resulted from the relatively low sulfur content of the majority of the asphalt binders utilized in this study, approximately 3.9% by weight for both the PG 64-22 and PG 64-28 binders, thus making the

contribution of the sulfoxide growth to both kinetics and rheological measures negligible from a practical standpoint.

7.1.2 Pan-Aged Asphalt Binder Kinetics

Utilizing the CA determinations as the quantitative measure of the oxidation of the asphalt binders as a function of the aging time and temperature, according to the binder testing matrix previously established, permits the determination of the binder kinetics parameters. The kinetics parameters of the asphalt binders are one of the key inputs into the asphalt oxidation models described in the methodology discussions of Chapter 3. The determination of the CA as measured in the FT-IR was established by averaging a minimum of two, but typically three individual CA measures.

In this instance, a single CA measure is defined as one reported value according to the testing protocol followed by Texas A&M University. Since the measurements they provided were conducted on a multi-bounce ATR attachment, a single measurement was effectively the physical average of multiple measures. These individual measures typically did not vary by more than 0.05, but on average within 0.03.

Conversely, the measurements conducted at the University of Nevada, Reno were obtained with a single bounce ATR attachment. Therefore, a single CA measurement was defined as the average of several actual CA determinations, thereby effectively creating a similar level of confidence in the produced CA measures. Following this procedure, typically produced individual CA determinations within 0.02, and the variability of the CA measures within about 0.03 for the pan-aged asphalt binders.

Recognizing the fairly sensitive nature of these measurements, some of the resulting CA measurements appeared to be outliers based upon 12 to 14 other binder measurements within the same relative kinetics evaluations. In some instances the arithmetic average of all the measurements were not utilized in the overall kinetics relationships. Under the least ideal circumstances, the average of two or very rarely, one repeated CA measurement, i.e. either one multi-bounce determination, or several single-bounce determinations were used. However, these were only a few conditions throughout the entire data set of over six-hundred FT-IR measurements. Due to the extensive handling during aging, processing, storage, and measurements activities ample opportunity for external influences may occur, so while a specific single cause may not have been available for each excluded data point, the infrequent occurrence of such conditions supports sufficient reliability in the measurements. However, summary plots of the average CA measures utilized during further analysis in this study are presented in Figure 19.1 through Figure 19.15 found in Appendix G, according to the respective aging durations noted in Table 5.3.

A summary of the average carbonyl area measurements for the pan-aged binders is provided in the following Table 7.1 through Table 7.3 for the three respective sets of pan-aged binders.

Table 7.1 Summary of Average Carbonyl Area Measurements

Aging Conditions		Asphalt Binders					
Temp.	**Duration (days)**	**PG64-22[a]**	**PG64-28[b]**	**Base Stock[a]**	**PG64-22 +3% SBS[a]**	**PG64-22 +10% Lime[a]**	**PG64-22 +20% Lime[a]**
Orig.	**CA_{Tank}**	0.496	0.704	0.434	0.778	0.710	0.595
50°C	**60**	0.776	1.072	0.677	1.024	1.057	0.793
	120	0.908	1.134	0.709	1.121	1.134	0.815
	200	0.975	1.159	0.832	1.281	1.213	0.894
	320	1.154	1.295	0.960	1.245	1.293	0.994
60°C	**30**	0.802	1.133	0.706	1.072	1.069	0.864
	60	0.926	1.173	0.752	1.177	1.121	0.932
	100	1.038	1.285	0.867	1.273	1.230	0.981
	160	1.210	1.373	1.035	1.361	1.289	1.087
85°C	**7.5**	0.899	1.017	0.840	1.141	1.133	0.905
	15	1.105	1.153	1.058	1.383	1.277	0.941
	25	1.352	1.351	1.311	1.538	1.393	1.140
	40	1.684	1.705	1.515	1.912	1.528	1.311
100°C	**1.83**	0.817	1.045	0.690	1.068	0.902	0.802
	3.75	1.005	1.155	0.857	1.313	1.074	0.939
	6.25	1.177	1.295	1.030	1.363	1.210	1.000
	10	1.424	1.466	1.260	1.485	1.374	1.122

a – Carbonyl Area measurements determined by Texas A&M University.
b – Carbonyl Area measurements determined by the University of Nevada, Reno.

Table 7.2 Summary of Average Carbonyl Area Measurements

Aging Conditions		Asphalt Binders[a]				
Temp.	**Duration (days)**	**WT95 PG64-22**	**WT97 PG64-22**	**Moana PG64-22**	**Moana PG64-28**	**Sparks PG64-28**
Orig.	**CA_{Tank}**	0.810	0.656	0.844	0.631	1.130
50°C	**60**	1.058	1.306	1.039	1.177	1.221
	120	1.113	1.333	1.127	1.247	1.250
	180	1.256	1.406	1.219	1.366	1.284
	240	1.305	1.517	1.273	1.475	1.325
60°C	**30**	0.974	1.205	1.059	1.196	1.295
	60	1.117	1.304	1.124	1.384	1.298
	100	1.254	1.482	1.194	1.481	1.313
	160	1.378	1.624	1.281	1.559	1.415
85°C	**7.5**	1.133	1.333	1.113	1.467	1.232
	15	1.247	1.470	1.197	1.574	1.408
	25	1.326	1.582	1.343	1.649	1.495
	40	1.460	1.745	1.486	1.802	1.623
100°C	**1.83**	0.952	1.250	1.047	1.336	1.303
	3.75	1.125	1.377	1.087	1.447	1.315
	6.25	1.229	1.561	1.268	1.560	1.391
	10	1.361	1.650	1.459	1.685	1.529

a – Carbonyl Area measurements determined by the University of Nevada, Reno.

Table 7.3 Summary of Average Carbonyl Area Measurements

Aging Conditions		ARC Core Binders[a]			
Temp.	**Duration (days)**	**BI 0001**	**BI 0002**	**BI 0003**	**BI 0004**
Orig.	**CA_{Tank}**	0.581	0.663	0.760	0.583
50°C	**4**	0.905	0.706	0.844	0.717
	8	0.917	0.765	0.894	0.756
	15	0.966	0.803	0.965	0.849
	30	1.006	0.854	0.975	0.880
	60	1.097	0.899	1.020	0.935
	120	1.112	1.016	1.059	1.008
	180	1.163	1.193	1.112	1.074
	240	1.296	1.271	1.136	1.146
60°C	**2**	0.952	0.763	0.882	0.602
	4	0.957	0.844	0.888	0.634
	8	0.962	0.873	0.972	0.713
	15	1.024	0.892	0.990	0.746
	30	1.125	0.996	1.043	0.807
	60	1.157	1.077	1.133	0.972
	100	1.358	1.185	1.176	1.074
	160	1.451	1.319	1.227	1.155
85°C	**0.5**	0.866	0.786	0.816	0.615
	1	0.880	0.795	0.871	0.636
	2	0.907	0.874	0.892	0.655
	4	0.928	0.951	0.987	0.732
	8	0.989	1.021	1.086	0.813
	15	1.201	1.288	1.198	0.906
	25	1.446	1.442	1.393	1.115
	40	1.642	1.623	1.469	1.300
100°C	**0.083**	0.824	0.819	0.813	0.622
	0.25	0.848	0.890	0.881	0.626
	0.5	0.859	0.912	0.838	0.645
	1	0.898	0.944	0.902	0.729
	2	0.955	1.031	1.028	0.774
	4	1.049	1.145	1.080	0.838
	7	1.192	1.276	1.249	0.972
	12	1.484	1.509	1.486	1.267

a – Carbonyl Area measurements determined by the University of Nevada, Reno.

While clear and direct comparisons of all the measures provided in Table 7.1 through Table 7.3 may not be practical, highlighting a few of the key measures within each group could provide some useful comparisons.

First, it is fairly clear that all of the evaluated binders did not age at the same rate as indicated by the wide range of the CA values at the more aged conditions, e.g. the CA measures of the binders aged at 85°C for 40 days and those aged at 100°C for 10 days. The direct comparison of the values must take into consideration the original CA measures of the asphalt binder, here represented as CA_{Tank}. For simplicity, the oxidation will be represented as carbonyl growth (CAg), which is defined by Equation 7.1.

$$CAg = CA_i - CA_{Tank} \qquad \textbf{Equation 7.1}$$

where, CA_i - carbonyl area measured at specific aging condition i;
CA_{Tank} - carbonyl area of the binder at the original or unaged condition.

It is generally accepted that asphalt binders themselves, do not necessarily oxidize in the same fashion or at the same rate, therefore, general considerations of the relative aging of these binders are separated according to those meaningful comparisons, rather than grouping all the binders together. Thus, the general considerations of the unmodified binders and their comparative binder measures are considered in the following Figure 7.2, with the modified binders and their respective counterparts considered in Figure 7.3.

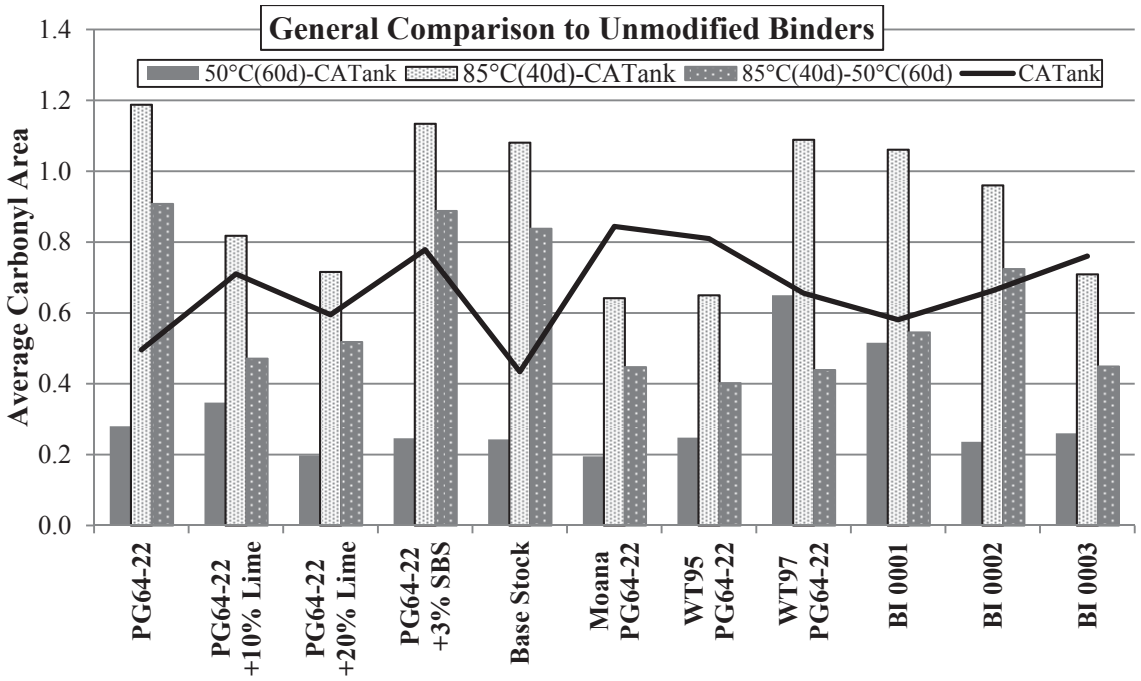

Figure 7.2 Carbonyl Area Measures for Associated Unmodified Binders at Select Aging Levels

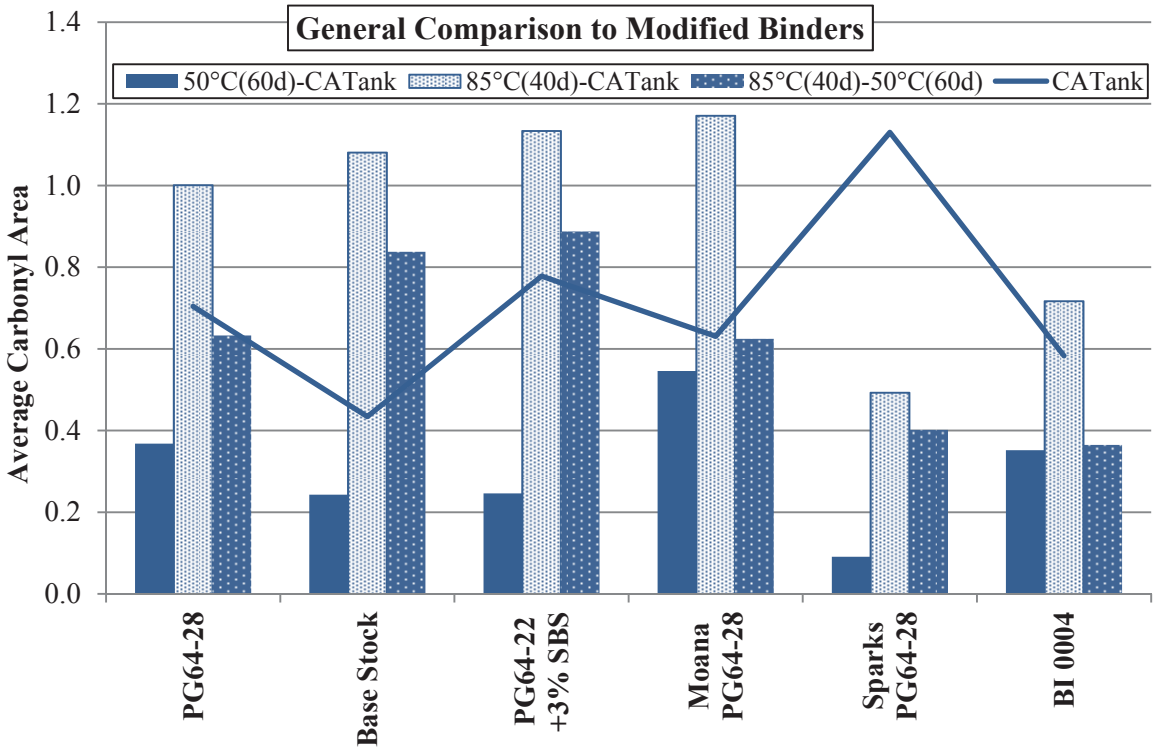

Figure 7.3 Carbonyl Area Measures for Associated Modified Binders at Select Aging Levels

To get a simple overview of the relative aging characteristics of the pan-aged binders, the overall aging protocol was summarized by the least severe aging condition, 50°C for 60 days, and one of the most severe conditions, 85°C for 40 days, relative to the original binder CA measures (CA_{Tank}). Initially, it is logical to assume that the most sever aging conditions would be the highest temperature and the longest duration, however there is a balance between the temperature and duration. Thus, the longest duration chosen for the 100°C did not provide as severe aging conditions as the longest duration of the 85°C aging based upon the protocol containing four temperatures aged over four durations. As a result, the aging durations were modified for the four ARC Core binders, to provide longer durations at 100°C. However, for this brief analysis, all the aging durations have been limited to 50°C for 60 days and 85°C for 40 days, so direct comparisons may be made.

Beginning with the PG 64-22 as the basis for comparison, the initial aging at 50°C for 60 days resulted in somewhat similar, but variable, aging levels for the binder which contained added components to the PG 64-22 binder. The addition of lime appeared to reduce the initial aging level with higher lime concentrations, although the 10% lime addition exhibited slightly more than the PG 64-22 itself. These variations are quite small in comparison to the overall magnitude of the CA measures noted in Table 7.1. Reductions in the overall CA growth levels are noted when comparing the overall oxidation growth from the tank measurements through the 85°C for 40 days when comparing the PG 64-22 to the two binders aged with increasing concentrations of lime. However, this reduction with lime content is not continued when observing the difference between the 85°C for 40 day and the 50°C for 60 day aging levels. Here the lime seems

to reduce the carbonyl growth to a similar level for both lime contents, both of which are well below the unmodified PG 64-22 binder.

Similar comparisons can be made between the PG 64-22 binder and the resulting binder when 3% SBS was added to it. Quite similar results are noted between the two binders with the modified version exhibiting slightly lower CA measures at all three aging conditions.

It has been suggested that the noted reductions in carbonyl growth under conditions such as these solely result from the contribution of the asphalt binder component of the overall blend (Woo et al., 2007a,b). Essentially, the lime and the polymer are not suspected to oxidize, or not expected to create carbonyl functional groups upon aging, so any resulting growth in carbonyl measures are suspected to be the result of the asphalt binder alone. This understanding seems to be generally supported with the reported measures, with the exception of the growth from the tank to the 50°C at 60 day CA measurements, which do not.

The Base Stock binder was added to Figure 7.2 as a mere overall comparison of the unmodified binders. Although not specifically the base binder for any of other binders in Figure 7.2, it does convey similar aging behavior as the PG 64-22, which contains the same base binders, but in different proportions.

The remainder of the binders included in Figure 7.2, are generally for observations of the relative magnitude of the different binders. They are not expected to oxidize in the same manner since they are not at all from the same binder or crude supply. Thus they are presented to make general observation of the overall variability in different binders

used in production. However, some information may be interpreted, without having to make direct comparisons.

For instance, the generally low magnitude of the CA changes for the Moana PG 64-22 and WesTrack 1995 binders could potentially suggest that binders obtained after the fact, either extracted and recovered or stored from initial construction sampling, may appear to age at a slower rate than those measured on fresh or recently sampled materials. This somewhat supports the general theory of oxygen saturation, specifically stating that there may be a point where the oxidation process may slow or even stop once the asphalt binder has reached the point of saturation or all the available bonding sites for oxygen molecules are full or otherwise bound. While this may be a possibility, the WesTrack 1997 data seem to suggest quite the opposite exhibiting the highest initial aging from the CA_{Tank} measurement to the 50°C for 60 day measurement, followed by rather average carbonyl growth measurements after that. Further, the WesTrack 1997 binder seems to exhibit similar conditions to that of the Venezuelan based BI 0001 binder, while the WesTrack 1995 measurements seem to more closely match those of the Holly Frontier blend of BI 0003.

Overall, these comparisons seem to suggest a lack or pointed shifting in the aging characteristics of the evaluated asphalt binders based upon the respective method by which they were sampled. Specifically, the extraction and recovery procedure used on the Moana 64-22 binder and the extended time period between the sampling and testing of the two WesTrack binders did not systematically influence this simplified analysis. This suggests that the oxidative aging of these asphalt binders are best described as being binder or source specific.

Now considering the measurements summarized in Figure 7.3 presenting the comparisons relative to the modified asphalt binders, there initially appears to be a similar trend noted between the Base Stock and the PG 64-28 produced from it as that observed with the unmodified and lime treated binders discussed previously. In general the modified PG 64-28 binder exhibits a reduced rate of carbonyl growth over the specific aging conditions when compared to its Base Stock, again with the exception of the initial aging from the CA_{Tank} measurement and the 50°C for 60 days determination.

However, comparisons of the other modified binders present varied responses. The PG 64-22 + 3% SBS generally presents higher CA measures than the PG 64-28 at all conditions except for the initial CA_{Tank} measurement to the 50°C for 60 days determination. The Moana PG 64-28 binder is fairly similar to the PG 64-28 when comparing the growth from the 50°C for 60 day to 85°C for 40 days aging levels, however the other measures are higher for the Moana PG 64-28 binder. In contrast, the Sparks PG 64-28 binder exhibits the lowest overall CA measures even though it is from the same supplier as the Moana and the PG 64-28 binders. The PG 70-22 BI 0004 binder supplied by Shelly Materials is quite different from all the other binders considered exhibiting fairly high CA growth initially, but relatively low CA growth from the 50°C for 60 days to 85°C for 40 days aging levels.

This simple comparison illustrated that each binder should be expected to exhibit its own specific oxidation rate and even materials composed of the same base materials may not necessarily age in the same manner. Thus it becomes highly important to consider the aging of a particular system individually, and gross generalizations should be made

with caution. Unfortunately, this makes studies of oxidation and asphalt binder aging all the more complex, time consuming, and costly.

Nonetheless, additional considerations are warranted to establish the oxidation properties of the asphalt binders themselves, in order to comparatively investigate the influence of the aggregate and mixture characteristics on the overall aging of the mixture. To better characterize the binder aging and specifically its rate of aging, a common approach is to examine the rate of oxidation, represented here by the growth of the carbonyl area. This rate (r_{CA}) is generally described by the Arrhenius relationship defined by Equation 3.70. In this particular study, which focused primarily on the long-term or constant rate kinetics measurements, also considers the determination of the r_{CA} term analogous to the k_c term noted in Equation 3.71. For reference, Equation 3.70 has been provided below as Equation 7.2.

$$r_{CA} = AP^{\alpha} e^{-E_a/RT}$$ **Equation 7.2**

where, r_{CA} – rate of carbonyl area, CA, growth;
A - pre-exponential factor;
P - absolute oxygen pressure during oxidation, atm;
α reaction order with respect to oxidation pressure;
E_a - activation energy, J/mol;
R - ideal gas constant, 8.3144621 J/mol•°K ;
T - temperature, °K.

To determine these parameters, reference is made to each of the isothermal aging relationships presented in Appendix G with each respective temperature creating a rate of oxidation determined from the four aging durations. When these rates are plotted as a function of the reciprocal of the product of the gas constant multiplied by the

temperature, the measures may be characterized by the relationship provided by Equation 7.2 and presented in Figure 7.4 through Figure 7.8 for the respective asphalt binder comparisons. Due to the close proximity of the data in these figures, they have been reduced to only show specific comparisons rather than creating complex figures with too much information to be deciphered. For clarity, the activation energy term (E_a) and the pre-exponential factors with and without the oxygen pressure term (P^{α}) from the fitted relationships are provided in Table 7.4.

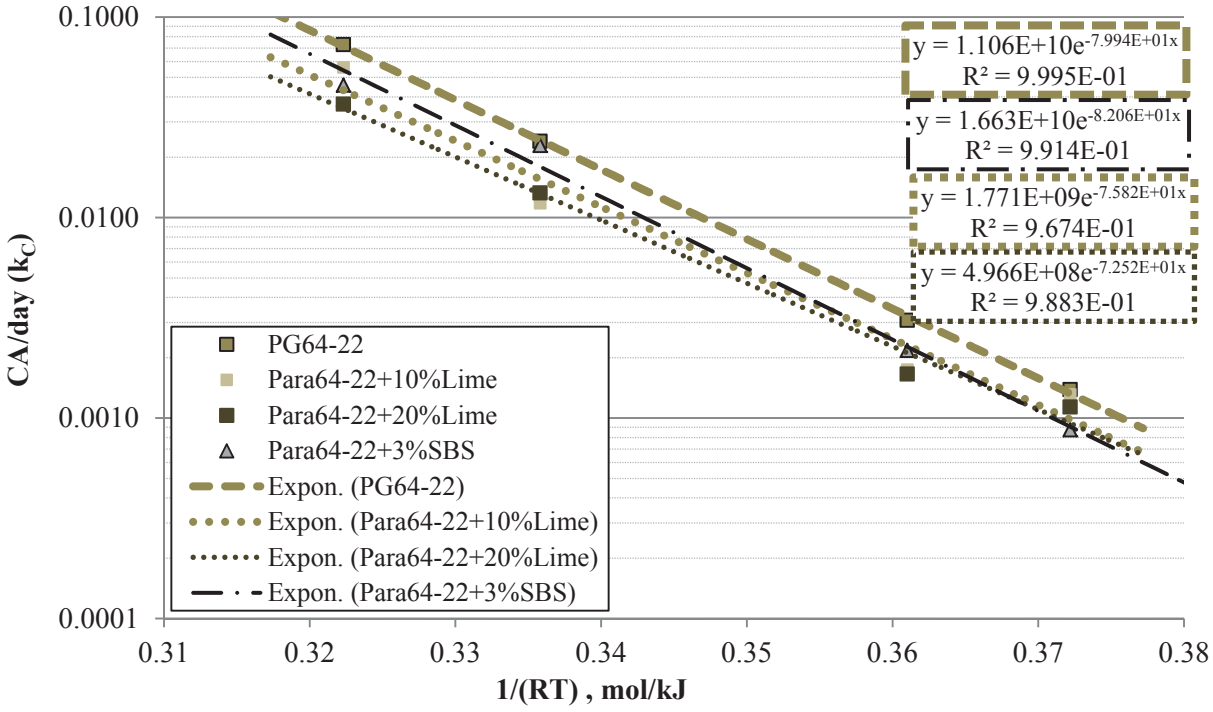

Figure 7.4 Constant Rate Binder Kinetics Relationships for PG 64-22 and Associated Binders

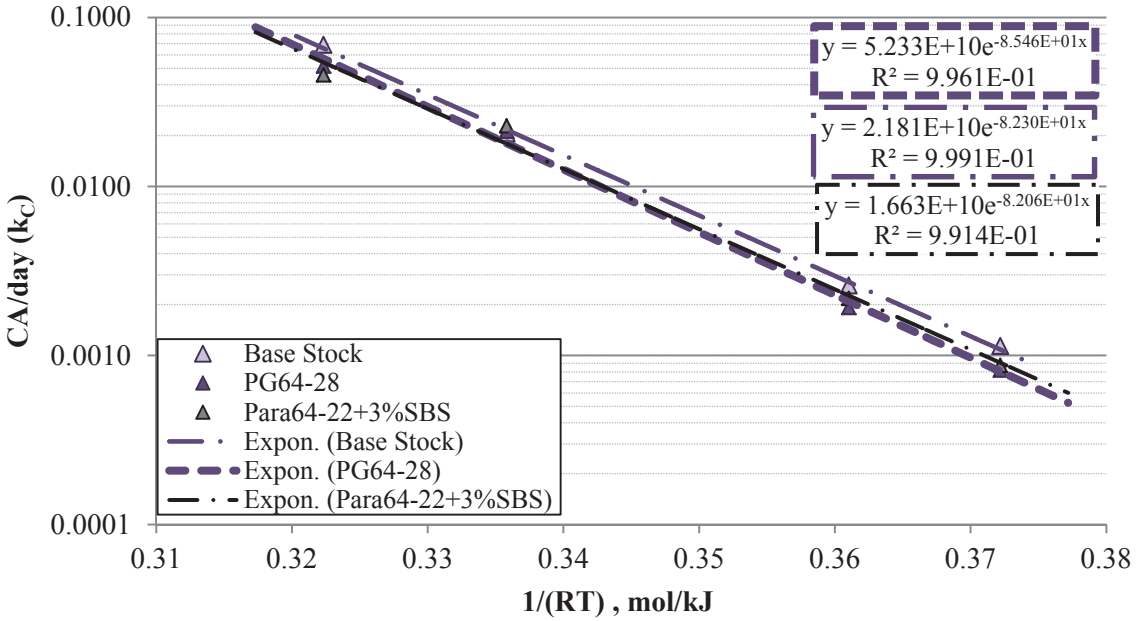

Figure 7.5 Constant Rate Binder Kinetics Relationships for PG 64-28 and Associated Binders

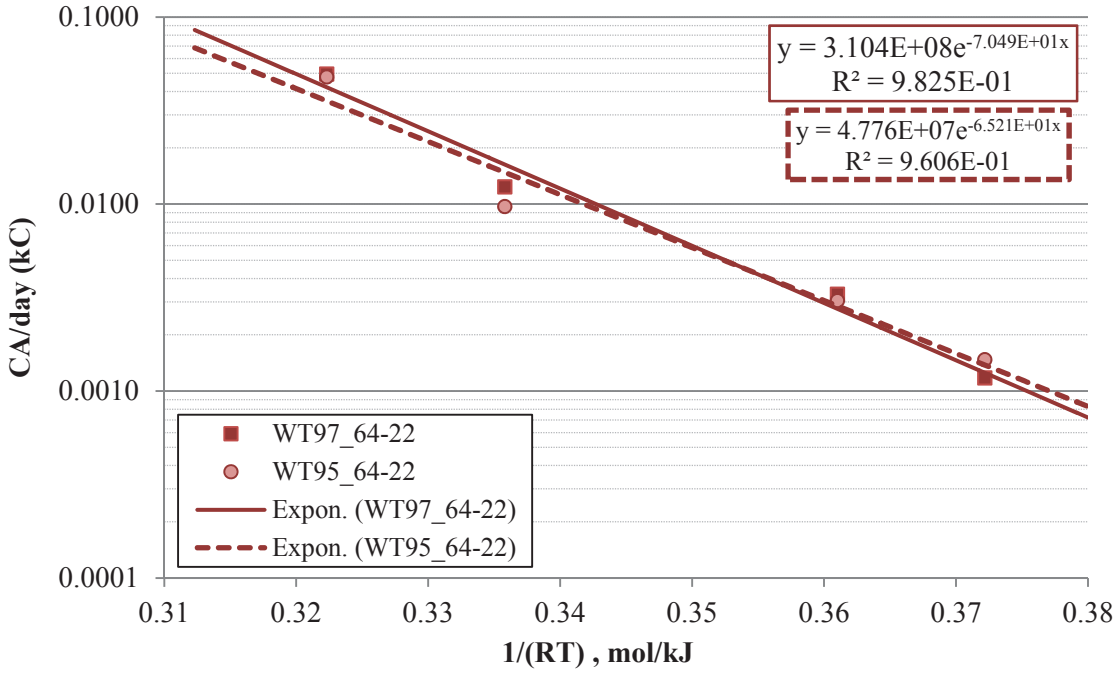

Figure 7.6 Constant Rate Binder Kinetics Relationships for WesTrack PG 64-22 Binders

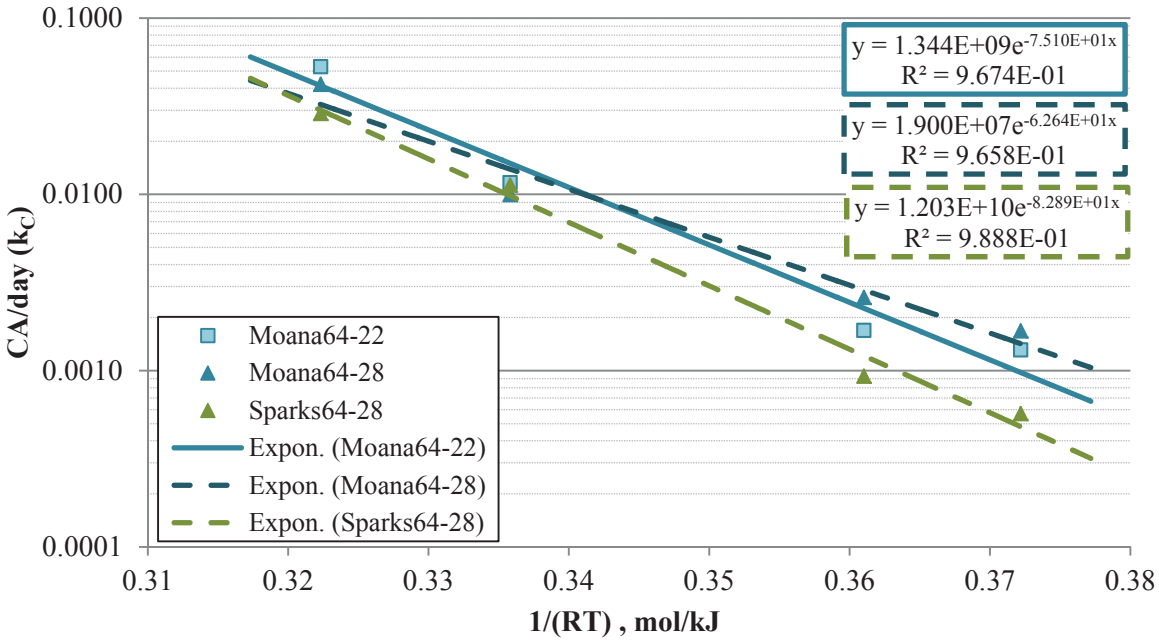

Figure 7.7 Constant Rate Binder Kinetics Relationships for Moana Lane and Sparks Blvd. Binders

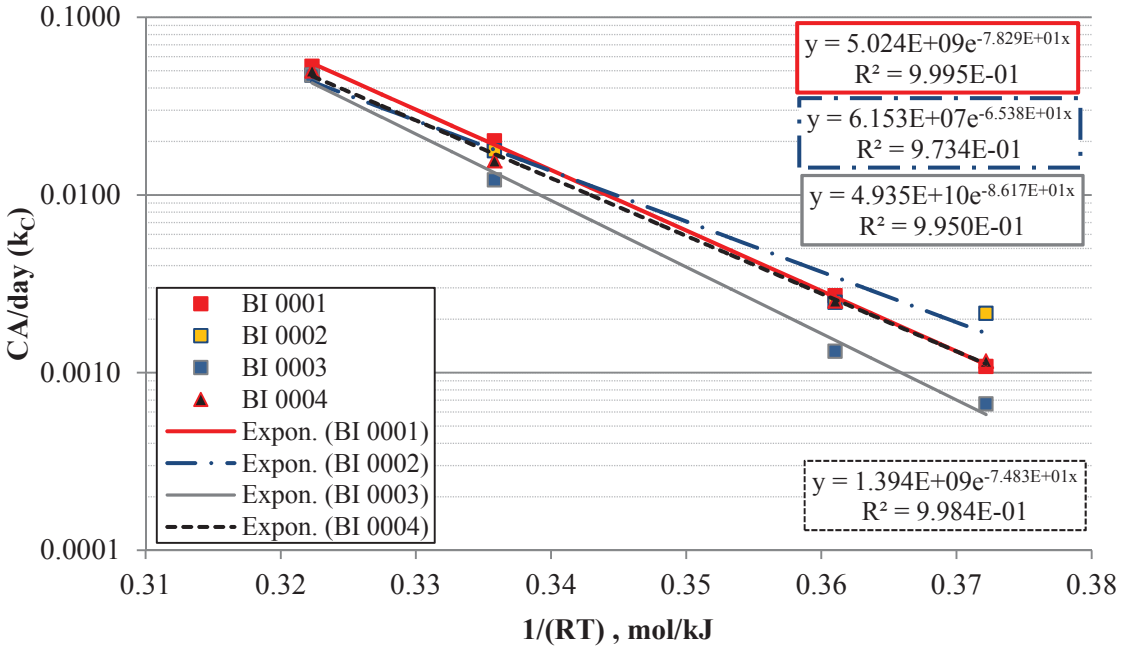

Figure 7.8 Constant Rate Binder Kinetics Relationships for ARC Core Binders

Table 7.4 Summary of Fitted Relationships for Asphalt Binder Kinetics[a]

Asphalt Binder ID	Pre-exponential, AP^{α}	Activation Energy, E_a	Pre-exponential[b], A
PG64-22	1.106E+10	79.94	1.802E+10
PG64-22 +10% Lime	1.771E+09	75.82	2.885E+09
PG64-22 +20% Lime	4.996E+08	72.52	8.140E+08
PG64-22 + 3% SBS	1.663E+10	82.06	2.709E+10
PG64-28	5.233E+10	85.46	8.526E+10
Base Stock	2.181E+10	82.30	3.553E+10
WT95-22	3.104E+08	70.49	5.057E+08
WT97-22	4.776E+07	65.21	7.781E+07
Moana 22	1.344E+09	75.10	2.190E+09
Moana 28	1.900E+07	62.64	3.096E+07
Sparks 28	1.203E+10	82.89	1.960E+10
BI1 PG67-22	5.024E+09	78.29	8.185E+09
BI2 PG64-16	6.153E+07	65.38	1.002E+08
BI3 PG58-28	4.935E+10	86.17	8.040E+10
BI4 PG70-22	1.394E+09	74.83	2.271E+09

a –Reference is made to Equation 7.2, $r_{CA} = AP^{\alpha}e^{-E_a/RT}$

b – Noting that in these studies, α=0.27 and $P = 0.164$ atm in Reno, A can be found specifically.

General observations from Figure 7.4 provide support for the previous simplified analysis which indicated that the addition of either the lime or the SBS polymer reduced the rate of oxidation noted as the r_{CA} or $k_C$term for this particular asphalt binder as noted by the lower k_C term at a given temperature. In general, this reduction is also suggested by the pre-exponential terms for the given relationships, however there is also a noted influence of the slope as noted with the PG 64-22 + 3% SBS binder. The temperature dependency

of the CA growth rate is largely represented by the activation energy (E_a) noted in the exponent of Equation 7.2. From the relationships provided in the figure, it was also observed that the addition of lime also reduced the E_a term, but not with the 3% SBS binder measurements.

The noted reduction in the oxidation due to the addition of lime into the binder during aging has been previously observed by others (Wisneski et al., 1996; Petersen et al., 1987a, b) and many more as noted (Lesueur and Little, 1999). It has been suggested that the overall influence of the lime addition can be associated with the strong interaction of certain chemical functional groups with the surface of the hydrated lime (Petersen et al., 1987a, b). At times the adhesion is with hydrated lime is even stronger than interactions with silica fines (Lesueur and Little, 1999). This suggests a much more in-depth analysis with the adhesion measurements of the modified SARA analysis in later sections.

Despite the visual and calculated differences in the kinetics relationships noted in Figure 7.4, all four of the binders were found to exhibit statistically similar relationships between k_C and temperature. In other words, all four plots were statistically the same, as determined by the transformed multi-linear regression analysis conducted with Minitab at the 0.05 significance level.

Further, observations from Figure 7.5 initially yield quite similar relative comparisons as the PG 64-22 binder and the corresponding modified versions of that binder. Specific to Figure 7.5, the Base Stock binder exhibits a higher k_C values at each respective temperature interval, however the slope or E_a term is lower for the Base Stock than the modified PG 64-28. The PG 64-22 + 3% SBS has been added to the figure as a

general comparison to the PG 64-28 binder even though they were produced from different base binders, i.e. the PG 64-22 and the Base Stock, respectively. Further, the transformed multi-linear regression analysis conducted with Minitab at the 0.05 significance level also confirmed no statistically significant difference between the kinetics parameters of all three binders.

Figure 7.6 depicts the binder kinetics measurements for both the WesTrack binders. Although they are from different dates and different suppliers, there appears to be only slight difference between the kinetics parameters between the two. The transformed multi-linear regression analysis conducted with Minitab at the 0.05 significance level also confirmed no statistically significant difference between the two.

Figure 7.7 presents the kinetics relationships for the binders extracted and recovered from the field produced mixtures used in the Moana Lane Extension and Sparks Boulevard reconstruction projects. Although by coincidence, these three binders were provided by the same supplier and were combined with the same aggregate source, the measured kinetics parameters appear to be somewhat different from each other. These differences do not appear to be the result of polymer modification since the binder that presents the largest deviation is the Moana PG 64-28, which is dissimilar from the Sparks PG 64-28. However, the transformed multi-linear regression analysis conducted with Minitab again confirmed no statistically significant difference between the three binders at the 0.05 significance level.

Figure 7.8 presents the kinetics measurements for the four ARC Core binders. Even though they are not from the same supplier or crude source and are thus not necessarily expected to exhibit the same kinetics relationship, they do appear to be somewhat similar

as with the other comparisons. The transformed multi-linear regression analysis again did not find the measures statistically significantly different at the 0.05 significance level, but the BI 0002 binder was found to be significantly different at the 0.10 significance level for both the slope, i.e. activation energy, and the intercept, i.e. defined by the pre-exponential term (AP^{α}).

The lack of statistically significant differences noted in these measures is likely due in part to the variability of the measurements coupled with the relatively small magnitude of the measures being considered. This should not be too disconcerting given the fact that these measures are only a part of the overall characterization of the asphalt binder oxidation process as a whole. Additional consideration may be given to assess whether or not all of the binders considered as a whole may be determined statistically similar or not. This is accomplished by considering all of the data points discussed thus far as the base or overall regression relationship, then each of the different binders may individually be compared statistically to this overall average regression equation. The outcome of this analysis determined that the kinetics relationships for each of the respective binders were statistically similar at the 0.05 significance level. However, the Moana PG 64-28 did show significant differences in both kinetics terms at the 0.10 significance level.

As a result of the noted similarities, it may prove useful to further explore the overall relationship between the kinetics parameters of the investigated asphalt binders. Therefore, Figure 7.9 was prepared to compare both pre-exponential factor and the calculated activation energies between all the investigated pan-aged binders.

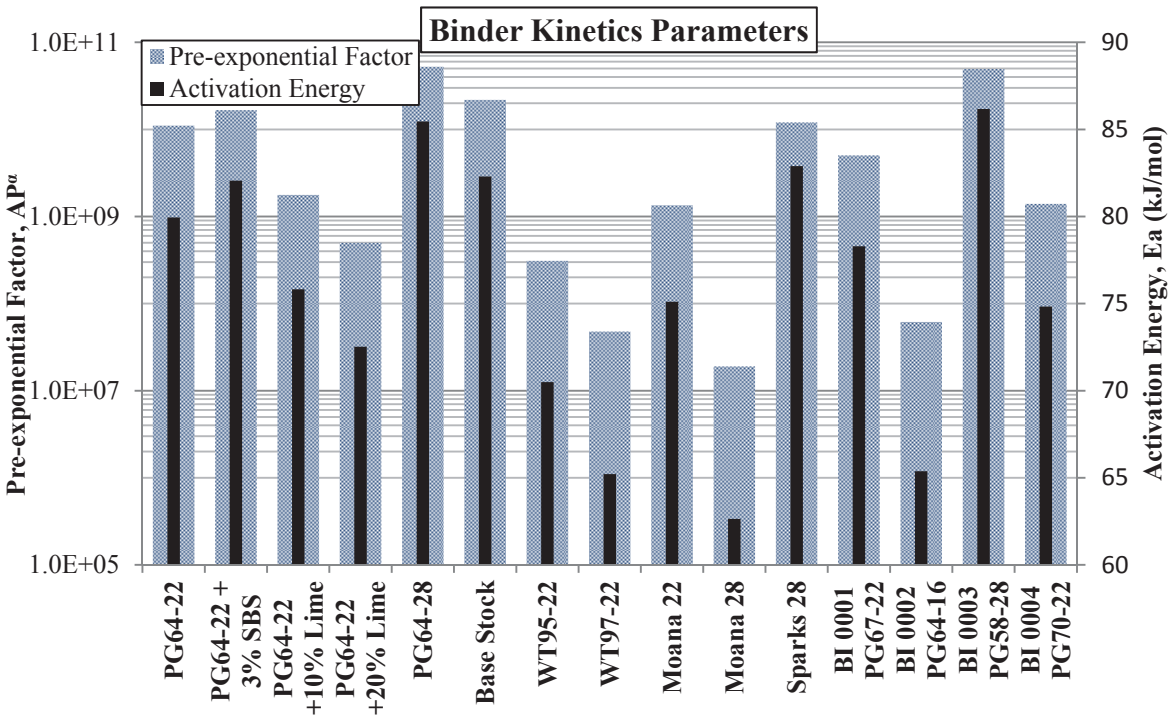

Figure 7.9 Constant Rate Binder Kinetics Parameters for Pan-Aged Binders

With the kinetics information presented in this form, the overall change in the magnitude of the determined value is evident as the pre-exponential factor ranges from 10^7 up into the 10^{10} as the order of magnitude. Although of much reduced order of magnitude, the activation energy exhibits a similar level of variability ranging from about 62 to 85 as depicted in Figure 7.9 and Table 7.4. Further observation of the figure seems to suggest that there may be a correlation between the two factors, e.g. when the pre-exponential factor decreases so does the activation energy within its own respective scale. Therefore, a plot of the pre-exponential factor as a function of the activation energy is considered in Figure 7.10.

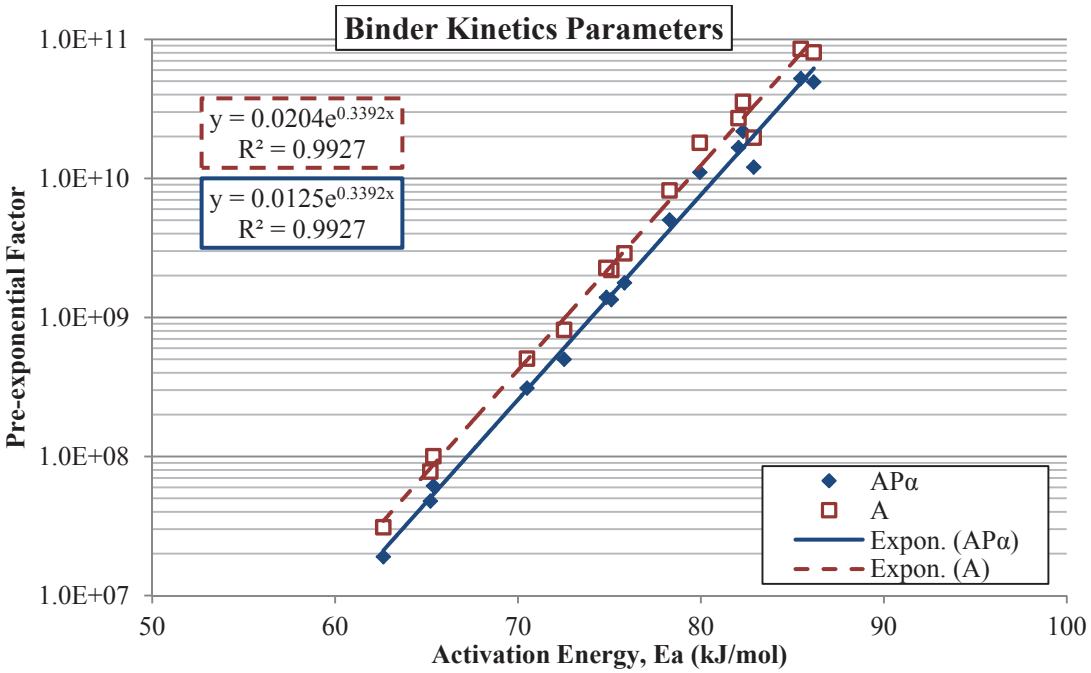

Figure 7.10 Constant Rate Binder Kinetics Relationship for Pan-Aged Binders

As Figure 7.10 clearly indicates there is a distinct relationship between the pre-exponential factor, both including and without the effect of the oxygen pressure (P^{α}) and the calculated activation energy as has been observed by others (Glover and Cui, 2013). In fact, their reported data which spanned over a 17 year time period, 1996 through 2013, reported nearly the same relationship with a pre-exponential factor of 0.0266 and the exponent of 0.3347. These values are practically the same as those determined in this study, i.e. pre-exponent factor of 0.0204 and the exponent of 0.3392.

While this finding may be of academic interest, it has not proven overly useful from a practical standpoint. It may have some potential benefit with respect to oxidation rate calculations specific to aging prediction modeling. However, in the current evaluation methodology, the two factor as determined simultaneously. The measurements need to

find one factor and directly produces the other. It may be possible to determine the activation energy term from some other evaluation tool, maybe some correlation with Arrhenius shift factors may provide additional information, but at this point in the overall research effort, such relationships have not been developed or thoroughly analyzed.

For sure, the kinetics parameters of the asphalt binders are a useful component in the consideration of the oxidative aging of asphalt binder. However, additional physical characterization measures of the asphalt binders are also necessary and are thus discussed in the following sections.

7.1.3 Pan-Aged Asphalt Binder Rheological Measurements

To accompany the chemical characterization provided by the FT-IR measures, physical measurements of the aged asphalt binders were also conducted to determine the rheological behavior and changes of that behavior with oxidative aging. The rheological measures are typified by the dynamic shear modulus (G^*) and the phase angle measured on the respective binders with the dynamic shear rheometer (DSR). From these two components in the complex domain, many other rheological parameters can be determined and assessed.

Table 7.5 presents a summary of the test conditions applied to each respective asphalt binder during the DSR measurements, with more specific details of the DSR test parameters referenced in Table 3.2. After the frequency sweep testing at each of the specified test conditions, the rheological data was transferred to the Rhea software package to calculate the G^* master curves as described in previous sections.

Table 7.5 Dynamic Shear Rheometer Test Conditions

Asphalt Binder ID	DSR Test Parameters			
	60, 70, 80, 85, 95, 100°C	60, 64, 70°C	52, 60, 64°C	46, 40, 34, 28, 22, 16°C
PG64-22		X		X
PG64-22 +10% Lime		X		X
PG64-22 +20% Lime		X		X
PG64-22 + 3% SBS	X			X
PG64-28	X			X
Base Stock[a]			X	X
WT95-22		X		X
WT97-22		X		X
Moana 22		X		X
Moana 28	X			X
Sparks 28	X			X
BI1 PG67-22		X		X
BI2 PG64-16		X		X
BI3 PG58-28			X	X
BI4 PG70-22	X			X

a – The Base Stock binder was tested at the high temperatures of 52, 60, and 70°C.

The first rheological parameter to be considered were the G^* master curves constructed from the isothermal frequency sweep measurements conducted on the pan-aged binders at each of their respective aging conditions, specifically aging temperature and duration. As previously described in the methodology section, the shifting of the frequency sweep data was conducted using the Rhea software package. This software utilizes the robust shifting techniques to obtain more reliable shifting and thus more appropriate master curves at each respective condition. However, the tradeoff for the technical merit is realized in the presentation of the data. While Rhea presents master curve information on

one or maybe two binders in a very precise format, it becomes quite difficult to present more functions on the same plot. Since the vast majority of the considerations in this study include a minimum of three up to eight different master curve relationships for a given aging set, alternative presentation styles are necessary.

Therefore, example plots of the G^* master curves produced for the full range of pan-aged conditions for one binder, PG 64-22, are presented in Figure 7.11 through Figure 7.14 for the respective aging temperatures. This binder along with the remaining measurements on pan-aged binders will be summarized into plots that exhibit the original or the unaged condition of a given binder as well as the longest duration of the aging temperatures. Examples of the summary plots for the PG 64-22 binder are provided in Figure 7.15.

In addition to the G^* master curve plots, black space plots, G^* as a function of the phase angle, were also prepared for each of the respective summary plots for each respective pan-aged asphalt binder. Examples of the summary black space plots for the PG 64-22 binder are provided in Figure 7.16.

The summary of the G^* master curves and the black space plots are provided in Figure 20.1 through Figure 20.24 found in Appendix H for all fifteen pan-aged binders considered in this study. It is relevant to point out that these figures present the fitted model forms as determined with the Rhea software. Some deviation from the actual discrete spectra used to define the master curves in Rhea should be expected, particularly with the polymer modified binders.

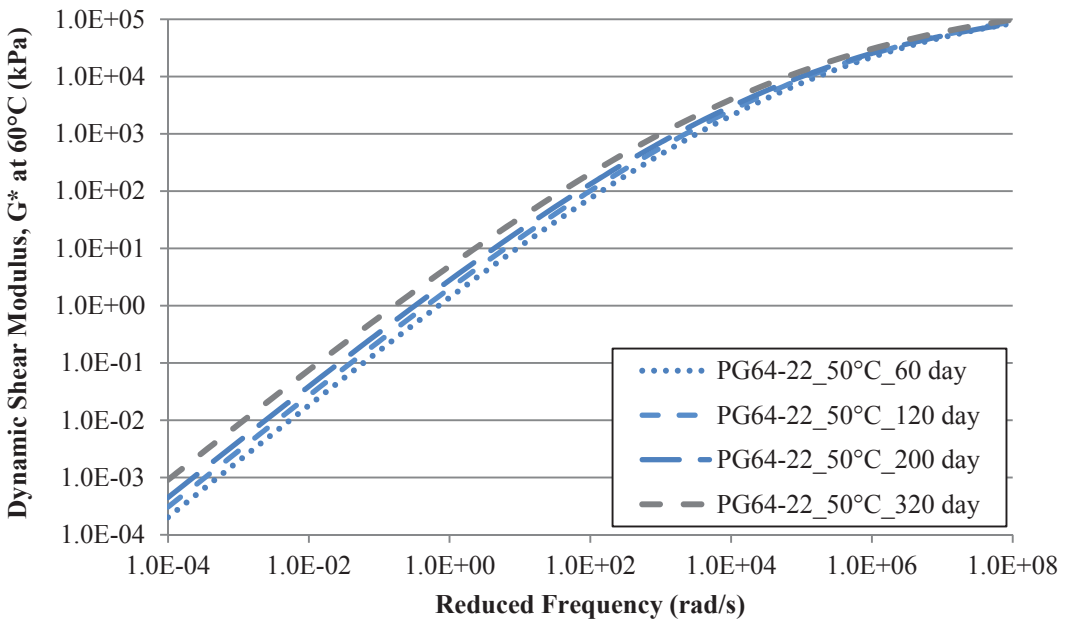

Figure 7.11 PG 64-22 Pan-Aged at 50°C Dynamic Shear Modulus Master Curves

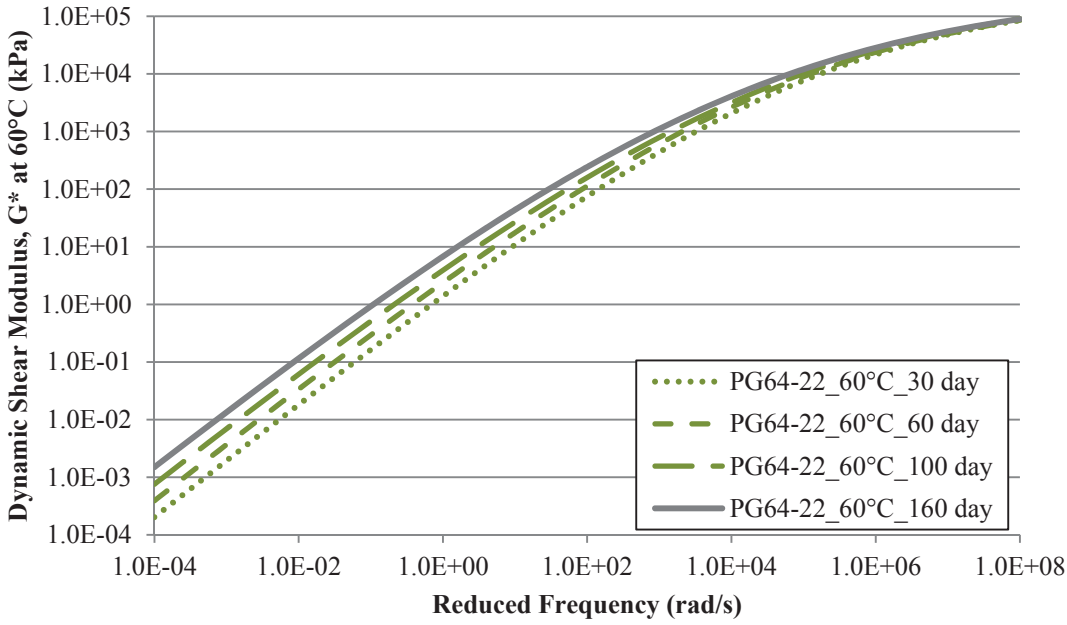

Figure 7.12 PG 64-22 Pan-Aged at 60°C Dynamic Shear Modulus Master Curves

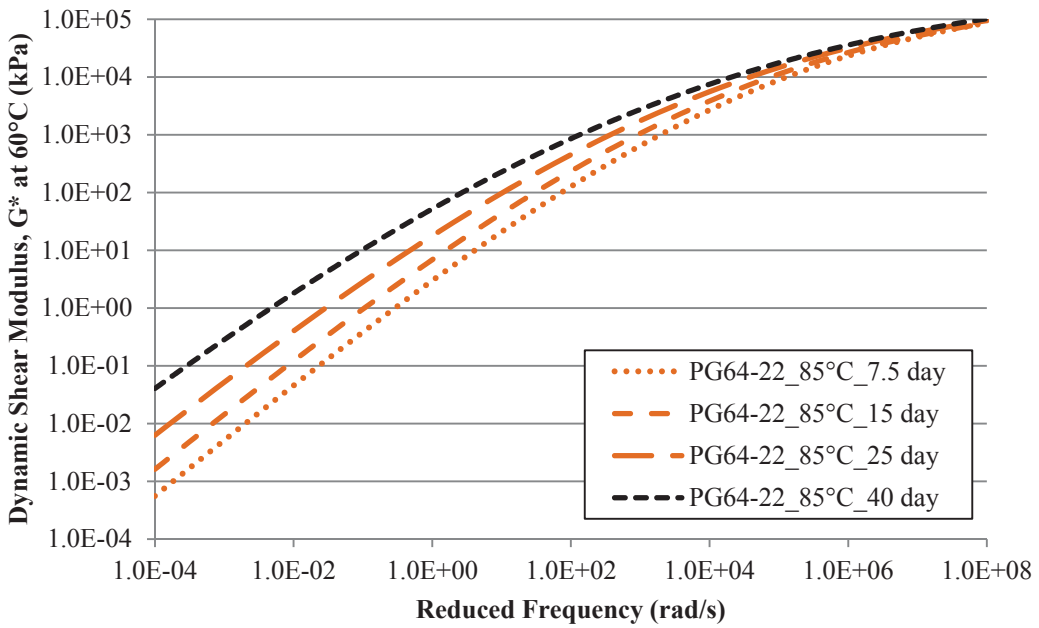

Figure 7.13 PG 64-22 Pan-Aged at 85°C Dynamic Shear Modulus Master Curves

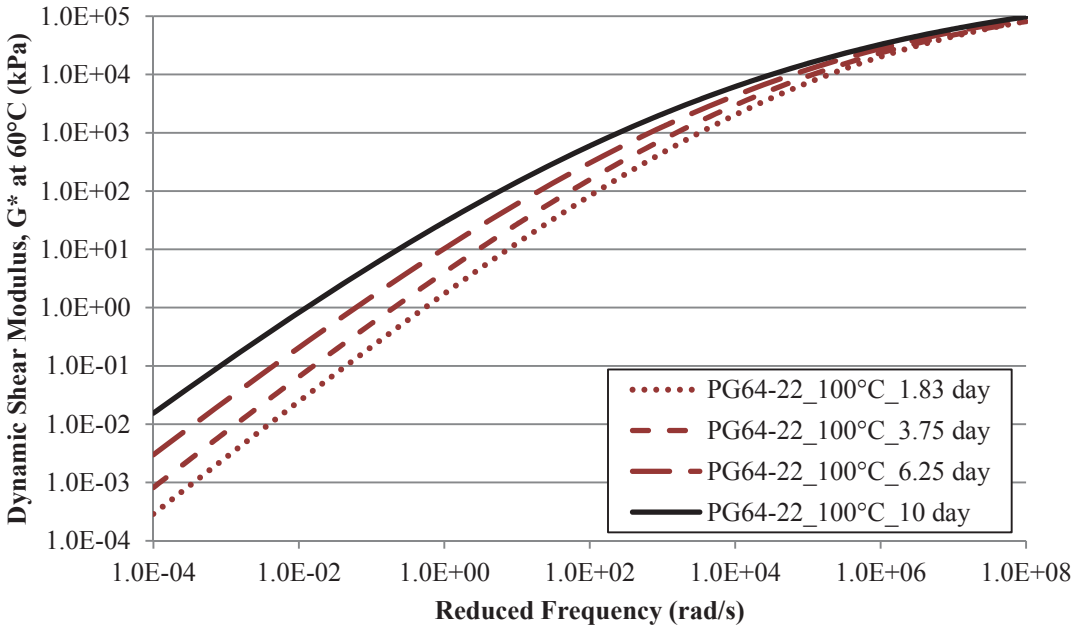

Figure 7.14 PG 64-22 Pan-Aged at 100°C Dynamic Shear Modulus Master Curves

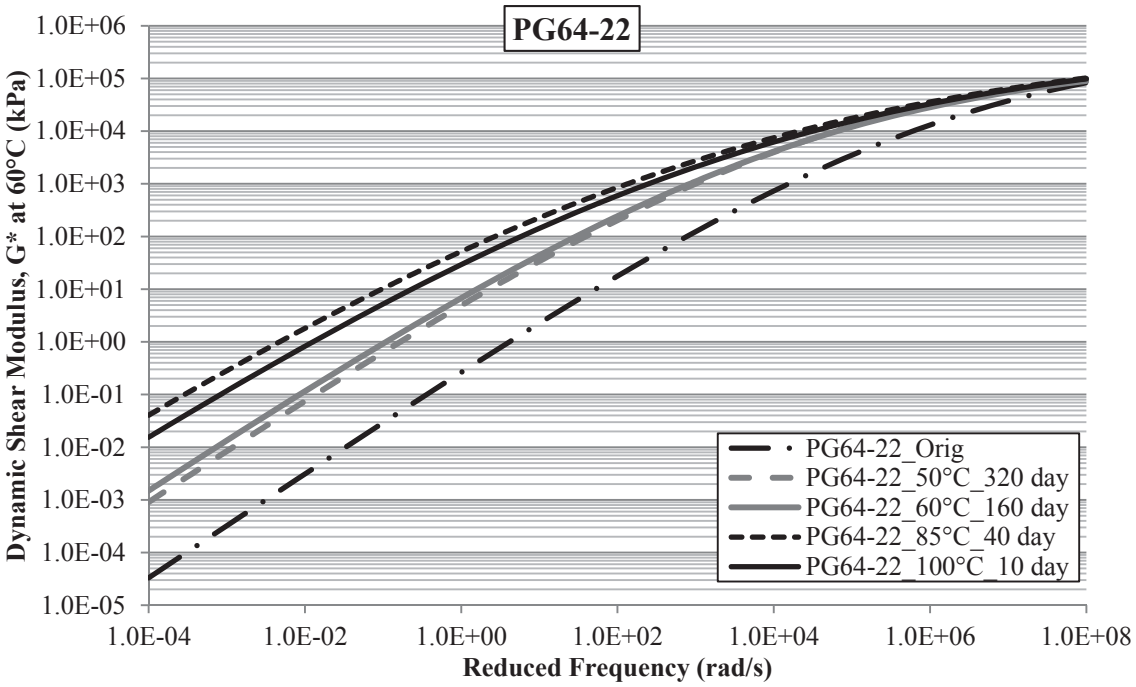

Figure 7.15 Summary of PG 64-22 Dynamic Shear Modulus Master Curves

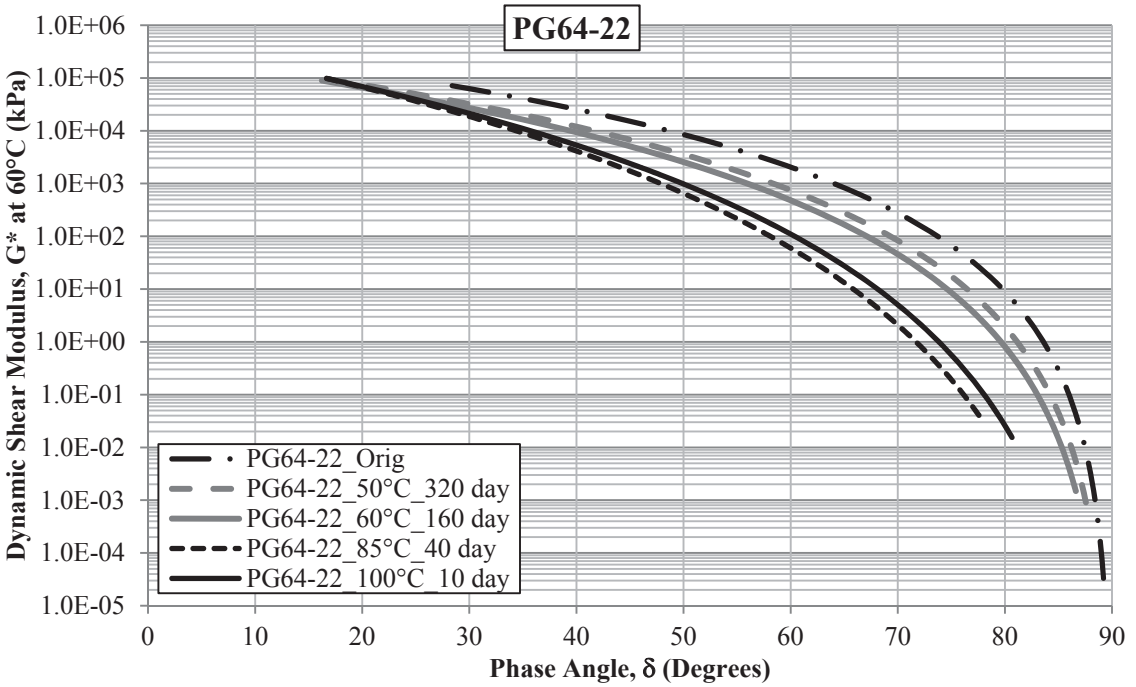

Figure 7.16 Summary of PG 64-22 Black Space Plots

These figures were prepared by exporting the shifted master curve function parameters into an Excel spreadsheet where the plots were produced based upon the function parameters produced with the Rhea software package. The master curve function utilized by Rhea has the form of the Christensen-Anderson-Sharrock, CAS model, which is also provided in Equation 7.3 along with Equation 7.4 presenting the associated phase angle, for reference. Table 21.1 through Table 21.12 found in Appendix I provide a summary of the master function parameters respective to each aged condition of the asphalt binders.

$$G^*(\omega) = G_0\left[1 + \left({}^{\omega_0}/_{\omega}\right)^{\beta}\right]^{-\kappa/\beta} \qquad \textbf{Equation 7.3}$$

$$\delta(\omega) = {}^{90}\Big/\left[1 + \left({}^{\omega}/_{\omega_0}\right)^{\beta}\right] \qquad \textbf{Equation 7.4}$$

where, G^* – complex shear modulus, Pa;
ω - oscillation frequency, rad/s;
G_0 - Glassy shear modulus, Pa;
ω_0 crossover frequency, rad/s;
κ asymptote gradient, -log:log;
β - width parameter;

$$\beta = \ln\left({}^{G_0}/_{2^{\kappa}}\right)\Big/\ln\left(G^*(\omega_0)\right)$$

General observations of the master curve figures found in Appendix H present results which are quite expected. As the severity of the aging increased, so did the measured shear modulus of the asphalt binders at a given reduced frequency. Within any given figure, it is clear that the softest, i.e. lowest modulus measurements occur in the unaged or original binder. It should not be overlooked that the actual modulus level is a function

of both the temperature and the duration of aging. Clearly this is evidenced by the 85°C master curves, typically yielding higher measured modulus values at 40 days duration, as compared to the 100°C aging for 10 days. Certainly, the large disparity in the aging durations at the respective temperatures has led to the coincidental similarity of these two conditions.

It is curious to note that for nearly all the pan-aged binders, the 50 and 60°C aging levels tend to be similar to each other and the 85 and 100°C seem to be comparable. Again, the aging duration at each respective temperature plays a significant role in these relative comparisons. However, the relative similarities between these measurements may prove useful in later considerations resulting from these measurements.

The shear modulus master curves for a given asphalt binder also appear to converge to nearly the same glassy modulus value at the higher reduced frequencies over the various stages of oxidation presented in the figures. While this occurrence is not rare, it often is the result of the glassy modulus being an assumed value, such as the CA and CAM models. Indeed, these measurements seem to support such practice, however the actual value of the glassy modulus is different for each of the binders and does actually vary within each asphalt binder as presented in the tables found in Appendix I. Further, these master curves were not produced with an assumed glassy shear modulus, but with the CAS model allowing the glassy modulus to be a variable parameter adjustable to improve the fit with the measured data.

General observations of the black space plots also provide some overall trends that are worth noting. Care must be given in the interpretation of the black space, since they are not as common as the traditional modulus compared to reduced frequency plots. For

instance, the more aged a given binder becomes, the lower on the modulus scale it appears in the black space diagram. This by no means indicates the binder became softer, it merely indicates a shift to the left with respect to phase angle. Therefore, a more meaningful interpretation is that for a given shear modulus, the aged binders exhibit a lower phase angle, thus representing a reduction in the viscous response, or otherwise known as an increase in the brittleness of the asphalt binder. The later interpretation of course more follows the expected material behavior, again noting that the presented relationships are based upon the fitted CAS model from the Rhea software program.

In general, the unmodified asphalt binders tended to exhibit the horizontal shift just discussed, with typically minor adjustments to the shape and curvature. The polymer modified binders on the other hand, seem to exhibit larger modifications to the overall shape of the black space plots and even converge upon each other toward the higher phase angles in some instances. This deviation for the unmodified binders has been suggested to be the combined effect of the oxidative stiffening of the asphalt binder phase and the congruent breakdown of the polymer modifier when aged through the standard RTFO (163°C) and PAV (90-110°C) aging conditions (Airey and Brown, 1998). These findings have been further supported by High-Pressure Gel Permeation Chromatography, HP-GPC (Airey and Brown, 1998) as well as Size Exclusion Chromatography, SEC, analyses (Ruan et al., 2003a). However, further studies based upon force ductility measurements have suggested that the degradation of the modified binder may be more appropriately linked to the base binder embrittlement as opposed to breakdown of the SBS polymer based on aging studies ranging from 60 to 135°C (Woo et al., 2007a,b).

More specific observations of the three master curve plots representing the fitting shear modulus master curves for the PG 64-22 and the two binders aged with lime, suggest some influence of the hydrated lime on the oxidation of the asphalt binders. To be clear, the original PG 64-22 binder was mixed with the hydrated lime, then aged in the respective ovens, and tested as a mastic, i.e. without removal of the lime.

Consideration of these binders are summarized in Figure 7.17 below. Rather than considering all the black space plots together, only the least aged, i.e. original, and the most aged, i.e. 85°C aged for 40 days are presented for clarity. Initial observations not the quite similar black space diagrams for all three binders in the original condition. The slight differences in the original plots can likely be attributed to small increases in stiffness with the addition of lime without detrimentally affecting the phase angle or viscous response as has been noted by others (Huang et al., 2002).

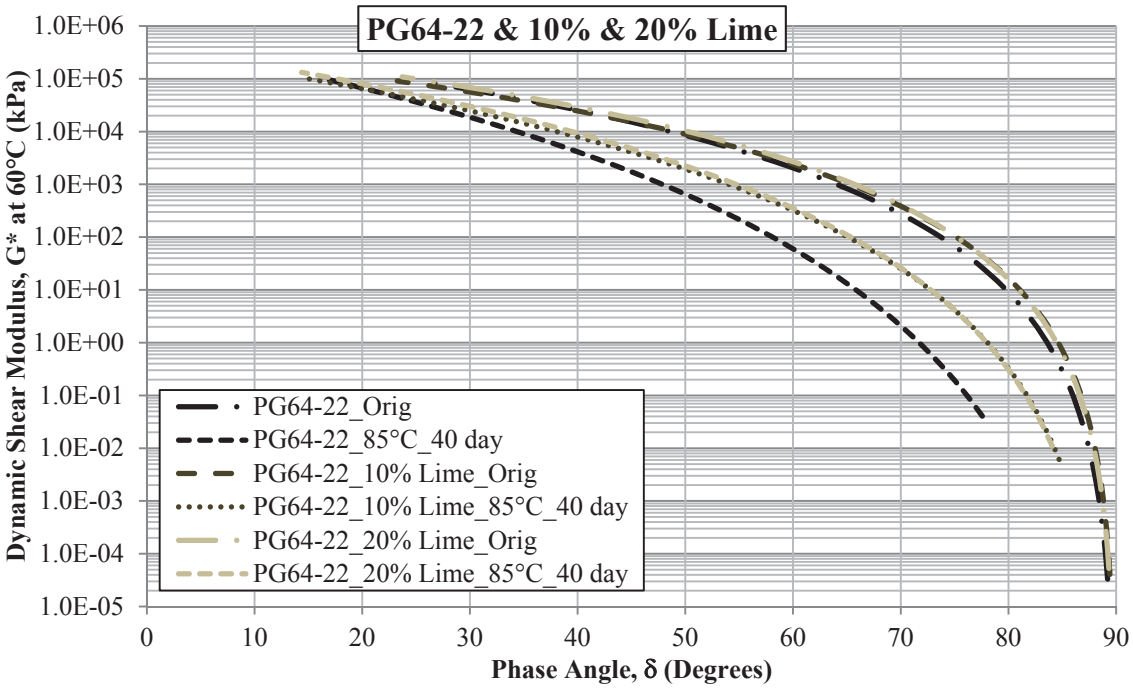

Figure 7.17 Summary of PG 64-22 and 10% and 20% Lime Black Space Diagrams

When the black space diagrams of the binder aged at 85°C for 40 days was considered, the lime modified binders were again very similar, but the unmodified PG 64-22 binder exhibited a significant reduction in the viscous response presented as the phase angle here. Thus, the unmodified binder can presumably be considered more brittle than those aged and tested with lime.

However, when the relative aging condition of the binders were compared it became clearer that the oxidation level may also be playing a role in the response. If the carbonyl area measured for each of the binders is also considered a more thorough understanding of the material behavior comes to light. The data in Table 7.1 indicates that the overall CA measurement for each of these aging conditions are quite different as summarized in Table 7.6. If the original carbonyl measurements respective to each binder are subtracted from the binder aged at 85°C for 40 days, it becomes evident that the lime modified binders have not aged nearly as much as the unmodified PG64-22. This clearly supports previous findings that the addition of lime reduces the overall oxidation of asphalt binders (Huang et al., 2002). Further, if a similar level of aging as determined by the CAg metric were sought for the PG 64-22 binder, the 85°C at 15 days aging condition comes close, as does the 60°C aging for 160 days. Additional considerations are possible when these black space diagrams are also included as presented in Figure 7.18.

Table 7.6 Select Average Carbonyl Area Measurements for PG 64-22 and 10% and 20% Lime

Asphalt Binder	Aging Conditions						
	Orig.	85°C				60°C	
	CA_{Tank}	40 days	40 days (CAg)	15 days	15 days (CAg)	160 days	160 days (CAg)
PG 64-22	0.496	1.684	1.188	1.105	0.609	1.210	0.714
PG 64-22 +10% Lime	0.710	1.528	0.818				
PG 64-22 +20% Lime	0.595	1.311	0.716				

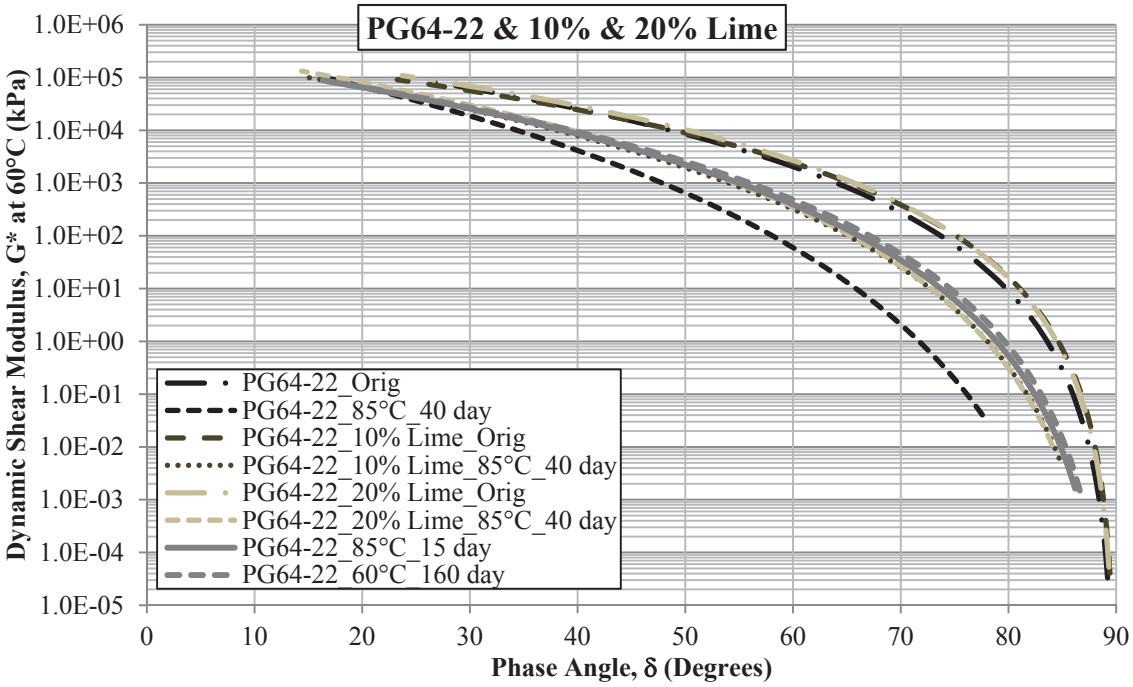

Figure 7.18 Summary of PG 64-22 and 10% and 20% Lime Black Space Diagrams

This comparison indicated much closer agreement between the black space diagrams of all three asphalt binders when the level of aging is taken into consideration, in this case irrespective of the aging temperature. This highlights the importance of making comparisons between physical properties of asphalt materials at relatively comparable

aging states, otherwise any noted differences may potentially be due to the aging as opposed to the treatment under consideration. Similarly, any agreement between such comparisons should be viewed as the combined effect of both the treatment under consideration and the aging level. These results also support previous studies showing the reduction in oxidation with the inclusion of hydrated lime (Huang et al., 2002) and by extension the potential for a similar effect with aggregates in mixtures.

A similar comparison can also be made between the PG 64-22 binder and the PG 64-22 + 3% SBS as well as the PG 64-28 and the Base Stock binder. These comparisons will also be made at a relative oxidation state defined by an arbitrary target value for the CAg metric of 0.70, for consistency between the binders. Figure 7.19 depicts these comparisons in terms of the black space diagrams.

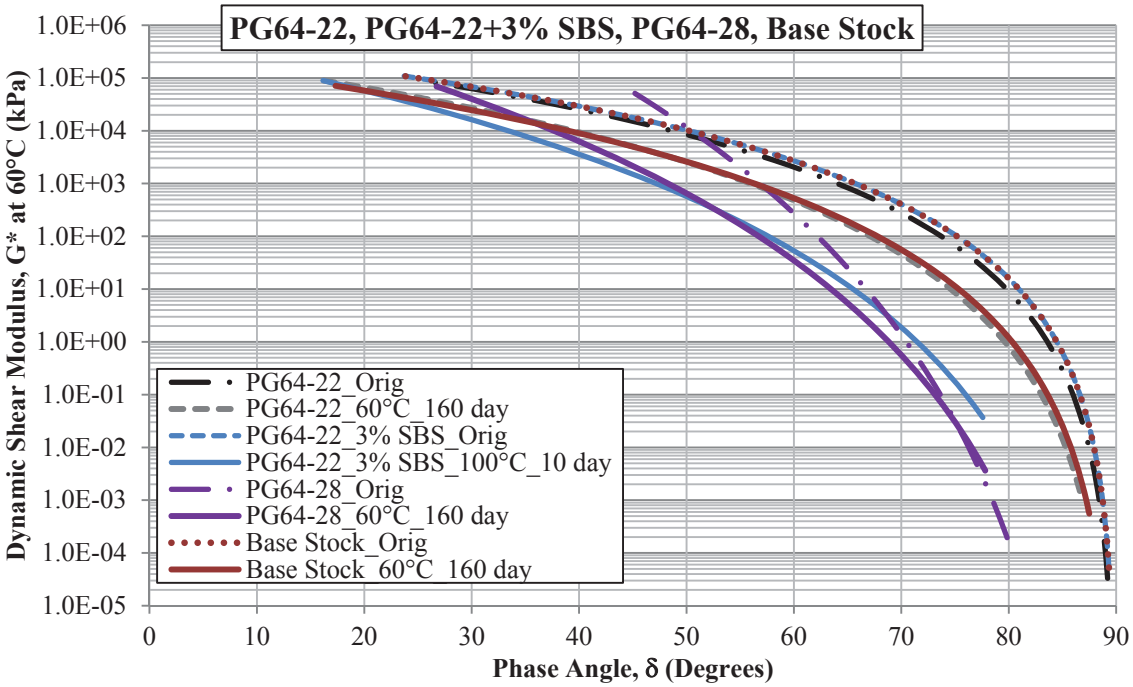

Figure 7.19 Summary of PG 64-22, PG 64-22 + 3% SBS, PG 64-28, and Base Stock Binder Black Space Diagrams

In spite of being a fairly busy plot, Figure 7.19 does serve a particular purpose in presenting the base binders and their modified counterparts in both their original and aged condition. Initial observations indicate the PG 64-22, PG 64-22 + 3% SBS, and the Base Stock exhibiting quite similar black space diagrams in their original conditions, despite their respective CA_{Tank} levels. However, the PG 64-28 exhibited significantly different properties represented by a large shift to the left at the original aging level. This behavior seems to suggest that the mere existence of the SBS polymer does not necessarily provide significant improvement to the performance of the binder, as evidenced by the lack of improvement in the rheological properties of the PG 64-22 + 3% SBS compared to the base PG 64-22. However, this particular binder was not formulated or specifically designed by the asphalt binder supplier. It was produced by special request for this study to simply add the 3% SBS to the PG 64-22 binder without specific modification or preparation of the base. Specifically, no special efforts were expended on the blending operations such as cross-linking the polymer etc… This finding highlights the benefit of having properly formulated asphalt binder particularly when polymer modification is involved. Simply adding the polymer without proper assessment and digestion of the polymer do not always yield the expected benefits that are known to accompany polymer modification.

Quite the opposite result was noted with the PG 64-28 compared to the respective Base Stock binder. In this case, the polymer modification process has dramatically improved the rheological performance of the asphalt binder resulting in much lower phase angle measures as a result of the much increased efficiency of the elastic component provided by the SBS.

It should be clearly differentiated that the reduction in phase angle with the polymer modification is expected to be the result of the added elastic component due to the polymer. This is in contrast to the unmodified binders which also show a reduction in the phase angle with aging, however these changes are suspected to be the result of a loss in the viscous component, i.e. a more brittle behavior. As a result, the general assumption of lower phase angle indicating more brittle behavior does not necessarily apply to modified asphalt binders. In summary, a lower phase angle as a function of aging typically indicates an increase in the brittleness or loss of ductility of the asphalt binder which is an undesirable occurrence. But a reduction in phase angle due to polymer modification adds to the elasticity of the system without the corresponding loss in ductility, i.e. the binder has not been damaged by the addition of the polymer, which is a positive influence on the asphalt binder as a whole.

For the aged conditions defined as an arbitrary CA value of 0.70 above the CA_{Tank} measures, the two unmodified binders, i.e. PG 64-22 and the Base Stock exhibit a similar reduction in the phase angle as the other unmodified binders and those with lime. For the PG 64-22 + 3% SBS binder the initial black space diagram nearly matched the PG 64-22. However, the aged condition of the PG 64-22 + 3% SBS binder exhibits a similar behavior to that of the PG 64-28. Based upon the black space diagrams of the PG 64-22 + 3% SBS and the PG 64-28, it is not clear whether the reduction of the phase angle is due to the embrittlement of the asphalt binder phase, the added effectiveness of the SBS polymer over time, i.e. the efficiency of the polymer improved with time of digestion, or a combination of both.

While comparisons between the other pan-aged binders may be possible, it is generally accepted that these properties are binder specific. As such, the other comparisons are not truly valid comparisons and are therefore left to later analyses such as the hardening susceptibility comparisons.

7.1.4 Low Shear Viscosity Determination

A great deal of very descriptive information is provided by the dynamic shear modulus master curves produced at different aging durations as discussed in the previous section. While these measures provide great information regarding the actual behavior of the asphalt binders as a function of oxidation, there is too much information provided to efficiently incorporate this level of detail into oxidation rate studies and prediction modeling. Therefore, the rheological measures on the asphalt binders need to be logically reduced to a more useable form.

In this study, the reduction was made by shifting all the dynamic shear modulus master curves on the binder to 60°C and considering the complex viscosity (η^*) master curve to determine the low shear viscosity (LSV) as discussed previously in Chapter 3. In an effort to consider all the binders evaluated within this study at both unaged and highly oxidized states, the LSV determination was evaluated at the shifted 60°C and at a frequency of 0.001 rad/s. This condition generally fit well with the majority of the asphalt binders evaluated with some of the unaged binders requiring minor extrapolation of the complex viscosity relationship and some of the more aged materials have data

points capable of extending to much lower frequencies. However, consistency was maintained throughout the evaluation at 0.001 rad/s.

The extrapolation of the LSV determination on the lesser oxidized measurements were by necessity limited to minor extrapolations. Specifically, Rhea limits the range of data extrapolation based upon the shifted data used to construct the master curves and does not permit the calculation of information outside the reliable limits based upon the shifted rheological inputs.

The actual determination of LSV can be viewed either as a function of aging time and temperature or as a function of the measured oxidation level, i.e. carbonyl area. Since the comparison with time show markedly different results with respect to temperature, these comparisons are of limited usefulness. However, when LSV is compared to the oxidation level, very practical information is obtained. This comparison is termed the hardening susceptibility which will be used in the oxidation parameter determinations and so the data will be presented and discussed in that particular section.

7.1.5 Pan-Aged Asphalt Binder Hardening Susceptibility

The hardening susceptibility (HS) as next step in the progression of data analysis is highly significant since it does not only combine the major aspects of the binder kinetics and the LSV determinations, but it is also utilized as one of the main comparative tools between the pan-aged asphalt binders and those aged in the mixtures. As discussed in the methodology section of Chapter 3, HS is defined as the slope of the LSV determination as a function of aging, here represented as the carbonyl area. In the constant rate region

of the total kinetics relationships, the HS parameter is determined by fitting the LSV and CA measurements to the relationship depicted in Equation 3.72 which has also been provided in Equation 7.5 for reference.

$$\ln \eta_0^* = HS * CA + m$$ **Equation 7.5**

where, η_0^* - low shear viscosity of the asphalt binder, Poise;
HS - hardening susceptibility, with η_0^* in Poise;
CA - carbonyl area, arbitrary units - unit less;
m - intercept of $\log \eta_0^*$ and CA relationship, with η_0^* in Poise.

Utilizing the form of Equation 7.5, the HS of the pan-aged asphalt binders may be established according to the traditional methodology (Martin et al., 1990; Lau et al., 1992). However, over the course of this study it became necessary to standardize the carbonyl measurements based upon the CA measurement of the original binder. This modifies the CA term in Equation 7.5 to CAg determination as depicted in Equation 7.6.

$$\ln \eta_0^* = HS * (CAg) + m_{Tank}$$ **Equation 7.6**

where, η_0^* - low shear viscosity of the asphalt binder, Poise;
HS - hardening susceptibility, with η_0^* in Poise;
$CAg = CA - CA_{Tank}$ - carbonyl area standardized by original binder, CA_{Tank};
m_{Tank} - intercept of $\log \eta_0^*$ and CAg relationship, with η_0^* in Poise.

Note that the HS parameter in the relationship will remain unchanged and only the abscissa, i.e. x-axis, and correspondingly the intercept of that plot on the ordinate, i.e. y-axis, will be altered. To differentiate between the two systems, the subscript Tank will be

included for considerations based upon CAg, while those based upon CA directly will retain the CA and m designations.

While this initially may seem like an unnecessary complication, it becomes quite important when considering the model inputs discussed in Section 3.6.3, discussing the oxidation modeling inputs. Specifically, Equation 3.73 provides the oxygen diffusivity (D_{O_2}) through the binder based upon the measured viscosity of that asphalt binder. If the HS relationship were calculated in the standard format only utilizing the CAg data, the viscosity may potentially be an order of magnitude higher than reality, thus making the calculated diffusivity extremely low thereby falsely limiting the amount of oxygen present in the aging system. However, the CAg standardization is also necessary in order to make relevant comparisons between the different FT-IR measurement devices utilized over the course of this study.

This modification can be simplified overall by combining Equation 7.5 with Equation 7.6 as depicted in **Error! Reference source not found.**. In this form, both form of the HS relationship can be presented congruently. When the CAg modification is included, all the terms are necessary, with the true m parameter necessary as an input to the diffusivity relationship in oxidation modeling. When the CA_{Tank} term was not utilized, it simply collapsed the equation back to the original form of Equation 7.5. The actual fitted values of the exponential form from the Excel regression function noted in the figures yields the format presented in **Error! Reference source not found.** which are also presented in the HS plots to follow.

$$\ln \eta_0^* = HS * (CAg) + \left(m + HS(CA_{Tank})\right)$$ **Equation 7.7**

$$\eta_0^* = e^{HS*(CAg)} e^{\left(m+HS(CA_{Tank})\right)}$$ **Equation 7.8**

where, η_0^* - low shear viscosity of the asphalt binder, Poise;
HS - hardening susceptibility, with η_0^* in Poise;
$CAg = CA - CA_{Tank}$ - carbonyl area standardized by the original binder, CA_{Tank};
m_{Tank} - intercept of $\log \eta_0^*$ and CAg relationship, with η_0^* in Poise.

As a result, the calculated HS parameters based upon the standardized CAg will be discussed in the text, while the HS parameters necessary for prediction modeling according to Section 3.6.3 based upon CA directly will be included in Appendix J. Figure 7.20 though Figure 7.24 present the HS plots for the pan-aged asphalt binders based upon the summary data presented in Table 7.7.

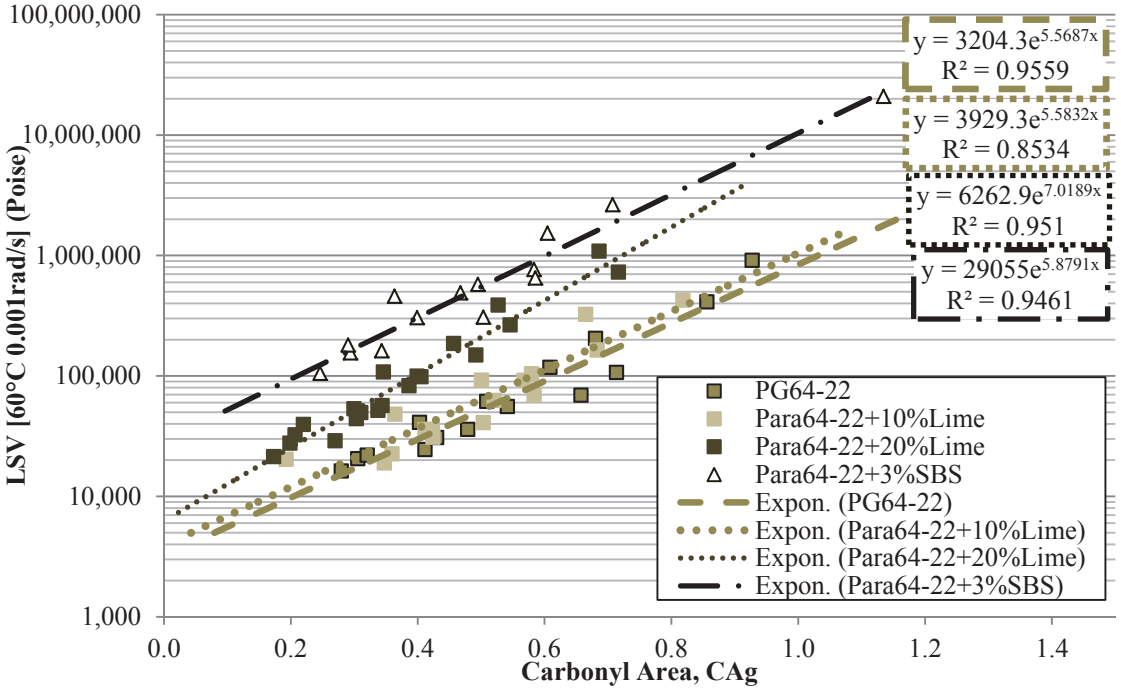

Figure 7.20 Hardening Susceptibility Relationships for PG 64-22 and Associated Binders

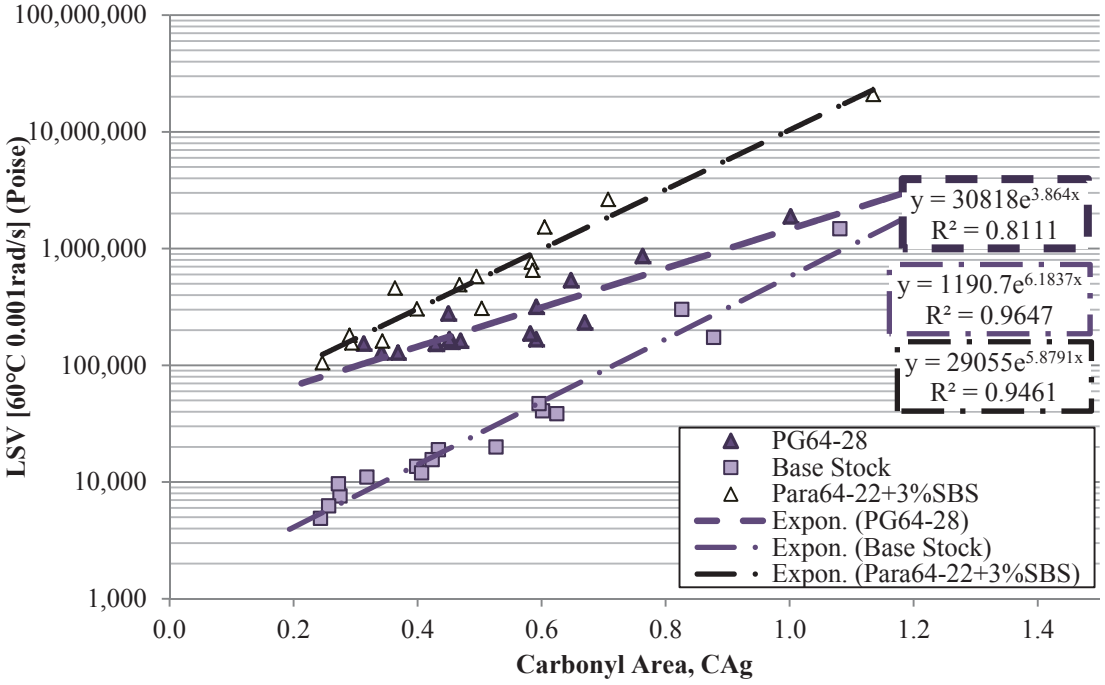

Figure 7.21 Hardening Susceptibility Relationships for PG 64-28 and Associated Binders

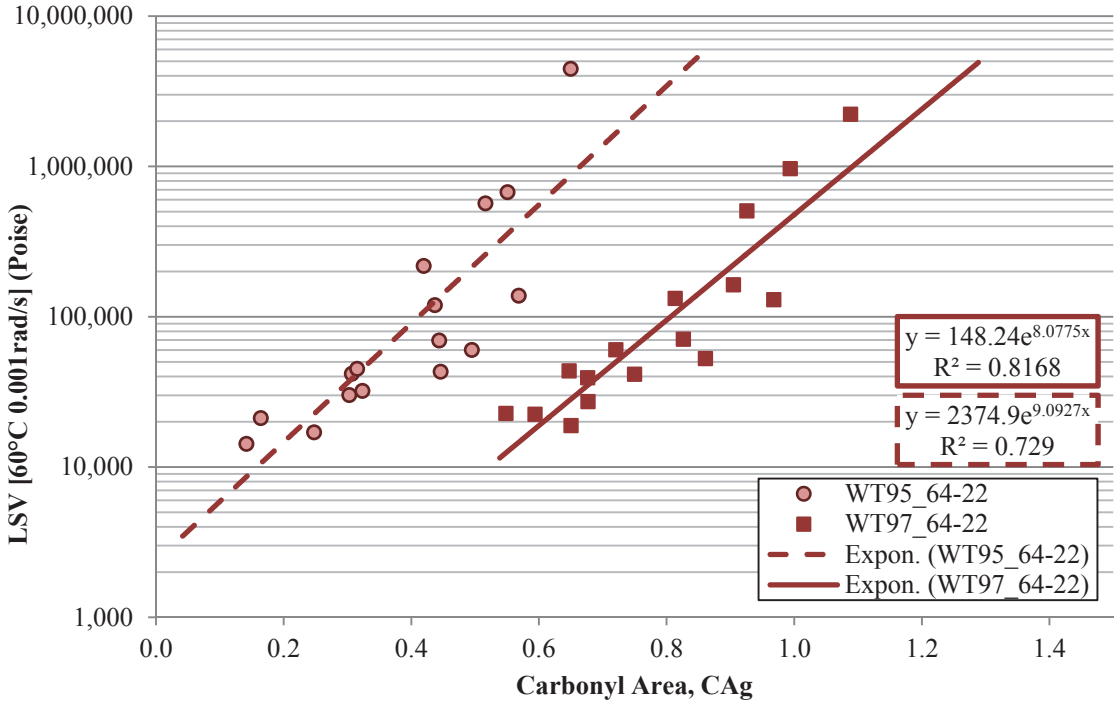

Figure 7.22 Hardening Susceptibility Relationships for WesTrack PG 64-22 Binders

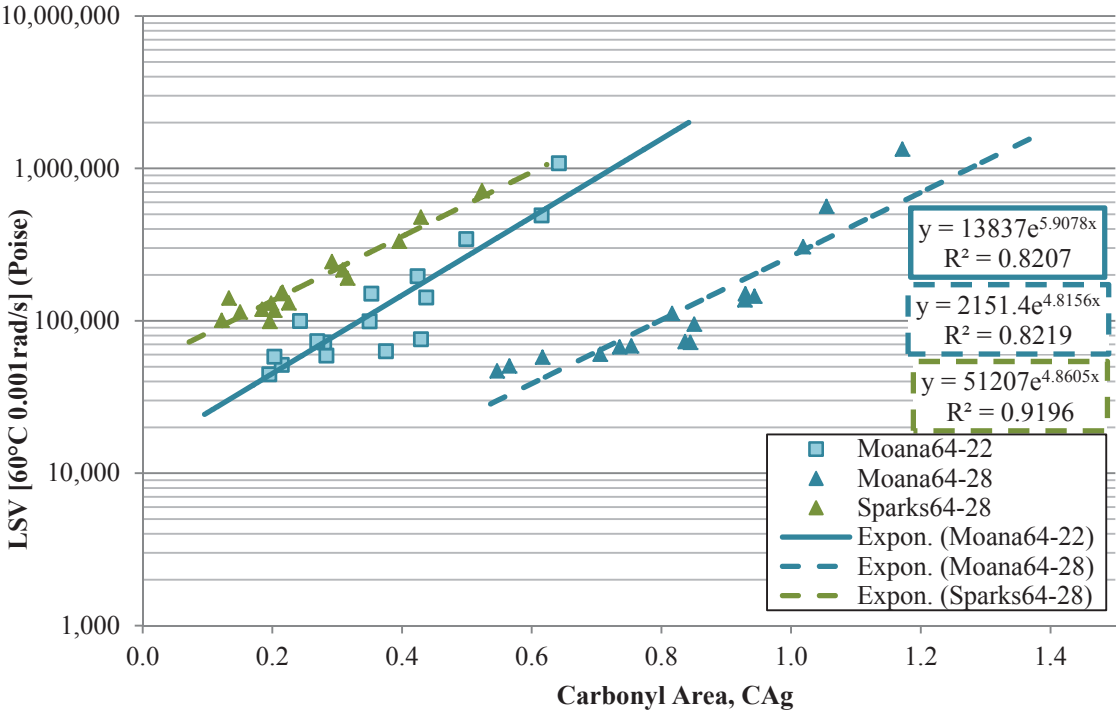

Figure 7.23 Hardening Susceptibility Relationships for Moana Lane and Sparks Blvd. Binders

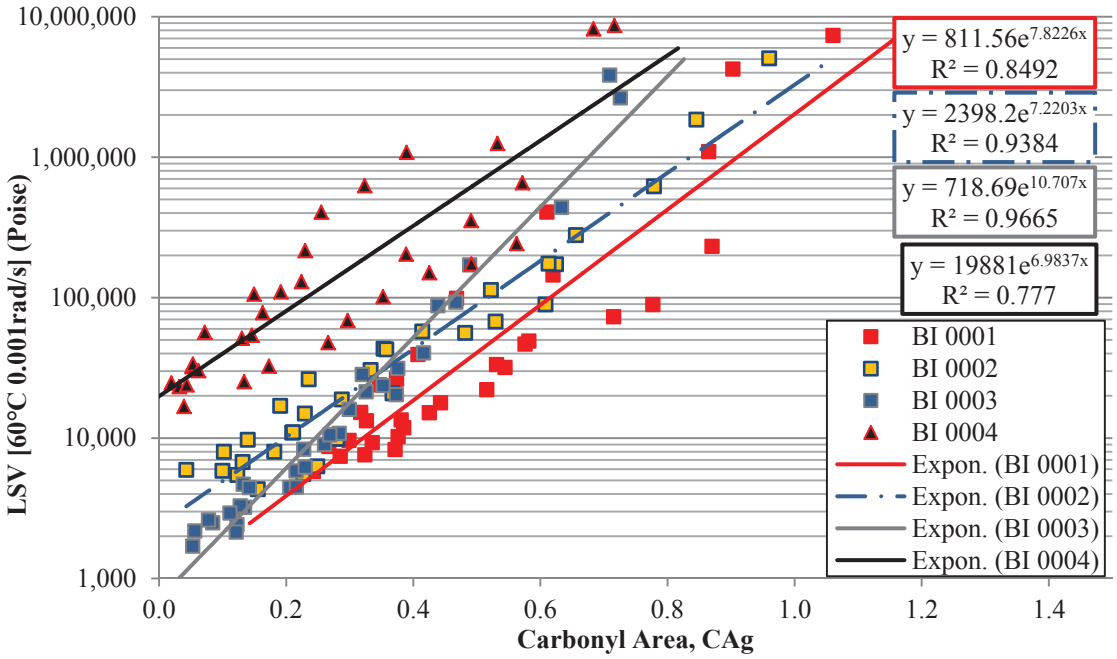

Figure 7.24 Hardening Susceptibility Relationships for ARC Core Binders

Table 7.7 Hardening Susceptibility Relationships for Pan-Aged Asphalt Binders

Asphalt Binder ID	Hardening Susceptibility[a], HS	Intercept[a], m_{Tank}	Intercept[a], m
PG64-22	5.5687	8.0722	5.3102
PG64-22 +10% Lime	5.5832	8.2762	4.3150
PG64-22 +20% Lime	7.0189	8.7424	4.5685
PG64-22 + 3% SBS	5.8791	10.2769	5.7030
PG64-28	3.8640	10.3359	7.6175
Base Stock	6.1837	7.0823	4.4016
WT95-22	9.0927	7.7727	0.4107
WT97-22	8.0775	4.9988	-0.3000
Moana 22	5.9078	9.5351	4.5489
Moana 28	4.8156	7.6739	4.6376
Sparks 28	4.8605	10.8436	5.4995
BI 0001 PG67-22	7.8226	6.6990	2.1541
BI 0002 PG64-16	7.2203	7.7825	2.9954
BI 0003 PG58-28	10.707	6.5774	-1.5564
BI 0004 PG70-22	6.9837	9.8975	5.8260

a – Reported values are based upon η_0^* reported in Poise.

Figure 7.20 presents the hardening susceptibility relationships for the PG 64-22 binder along with its associated modified versions, i.e. with 10% lime, 20% lime, and 3% SBS polymer. Basing the comparison on the influence of the lime and the SBS polymer to the influence on the PG 64-22 itself, the general trends indicate that the addition of either component increases the viscosity of the binder. In the case of the 10% lime, the increase is quite marginal and present statistically the same relationship from the transformed linear regression analysis. This finding is not all that unexpected, especially when noting

the increased variability of the relationship with the 10% lime added. The PG 64-22 +20% lime presents a more drastic increase not only in the intercept (*m*) of the relationship, but also in the slope (HS). From the transformed linear regression analyses, the PG 64-22 + 20% lime was found to fit an intercept that was statistically significantly different, but the slope was found marginally the same, p-value of 0.142. The PG 64-22 + 3% SBS relationship exhibited notably higher viscosity values as can be expected with the addition of SBS polymer. The intercept of the PG 64-22 + 3% SBS was statistically greater than that of the PG 64-22 based upon the transformed linear regression analyses, while the slope was determined to be statistically similar. Consideration of the HS relationships of the same binders only considering the actual CA measures rather than those modified by CA_{Tank} as depicted in Figure 22.1, all the relationships become substantially closer together with the 3% SBS and the 20% lime relationships presenting the highest viscosities for a given CA measurement level.

Figure 7.21 presents the SBS modified PG 64-28, its associated Base Stock binder and as a general comparison, the PG 64-22 + 3% SBS. Considering the Base Stock binder and the PG 64-28, a reduction in the HS is noted due to the addition of the SBS polymer. However, consideration of both the general influence of the polymer when added to the PG 64-22 binder compared to that of the Base Stock suggests that the addition of SBS polymer into the asphalt binder may not necessarily decrease the HS of a given binder. Given the relative similarities of the PG 64-22 and the Base Stock binder, this result suggests the formulation processing, e.g. cross-linking operations, polymer digestion time, etc. can have a significant influence on the overall behavior of the modified asphalt binder. Based upon the transformed linear regression analysis, the Base Stock binder was

found to be statistically significantly different from the PG 64-28 asphalt binder, both intercept (*m*) and slope (*HS*). However, the PG 64-22 + 3% SBS binder was found to fit a similar intercept (*m*) but have a significantly different slope (HS) when compared to the PG 64-28 relationship. Additional consideration of Figure 22.2 based upon the actual CA measurements show general similarities in the relationships. However, the discrepancy in the HS measurements between the Base Stock and the PG 64-28 were still evident.

Relative comparisons between the two WesTrack binders found in Figure 7.22 and Figure 22.3 are not truly valid given that the two binders are not from the same supplier, base stock, or crude source. However, general observations indicate the HS of the two are fairly similar, despite the relatively high variability of both binders. Statistical significance between the two were likewise not relevant and thus not considered as part of this analysis.

Similar to the WesTrack binders, relative comparisons of the HS parameters are not completely valid. Even though they were all produced from the same supplier, they were not necessarily produced from the same asphalt binder components and were sample a couple of years apart. The combination of those factors made direct comparisons of the HS measurements from the Moana Lane and Sparks Blvd. binders statistically invalid. However, simple observations seem to follow the general trends noted with the other asphalt binders. In general, the HS of the SBS modified binders, i.e. Moana 64-28 and Sparks 64-28, were typically lower than that of the unmodified Moana 64-22 binder. The time separation between the sampling of the two modified binders made the difference in the magnitude of the CA measurements of little consequence. Interestingly enough, considerations of Figure 22.4 indicate the two modified binders appear closer than with

the CAg methodology. Again, their relative differences are of little consequence at this point in the evaluation.

Observation of the ARC Core binders found in Figure 7.24 are again not statistically valid. But it is worth noting the general increase in the variability of the HS relationship with the polymer modified BI 0004 asphalt binder when compared to the other ARC Core binders.

7.1.6 Pan-Aged Temperature Dependency of Hardening Susceptibility

Over the course of measuring and determining the HS parameters for the pan-aged asphalt binders, systematic variations in the HS measurements (slopes) were observed with certain asphalt binders. Even though the established methodology (Lunsford, 1990; Martin et al., 1990, Lau et al., 1992, Al-Azri et al., 2006) and some measurements contained within this study support considerations of slope of the HS relationship independently from the aging temperature, some of the asphalt binders showed a systematic increase in the HS slope as a function of aging temperature. This typically occurred with the binders that exhibited relatively lower R^2 values as presented in Figure 7.25, which present the HS relationships of the PG 64-28 binder corresponding to each individual aging temperature along with the standard HS relationship developed independently from the aging temperature for reference.

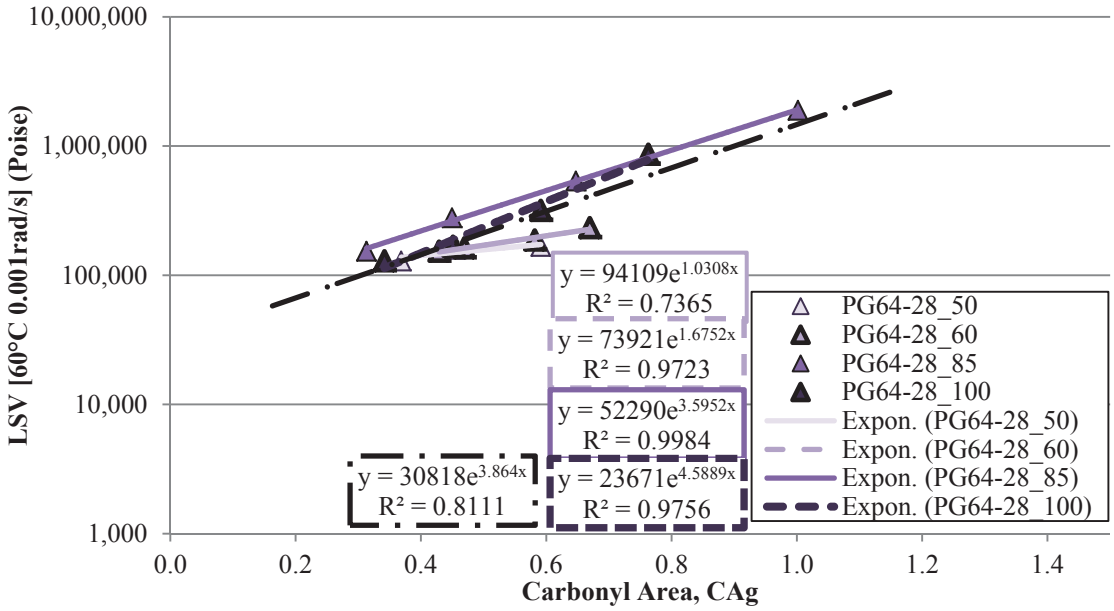

Figure 7.25 Temperature Dependent Hardening Susceptibility Relationships for PG 64-28 Binder

As can be observed from the figure, the HS relationship generally increases with a fairly large range of HS varying from slightly greater than 1 for the 50°C aging to a maximum of over 4.5 for the 100°C aging results. It is further noted that the HS of the PG 64-28 independently exhibits an HS slope of roughly 3.9, which happens to be close to the HS of the binder aged at 85°C. However, the overall R^2 value of the HS relationships was substantially lower than the HS of each aging temperature, except for the binders aged at 50°C.

This finding contradicts the HS of the PG 64-22+20% Lime binder, which generally follows a single HS independent of temperature as presented in Figure 7.32

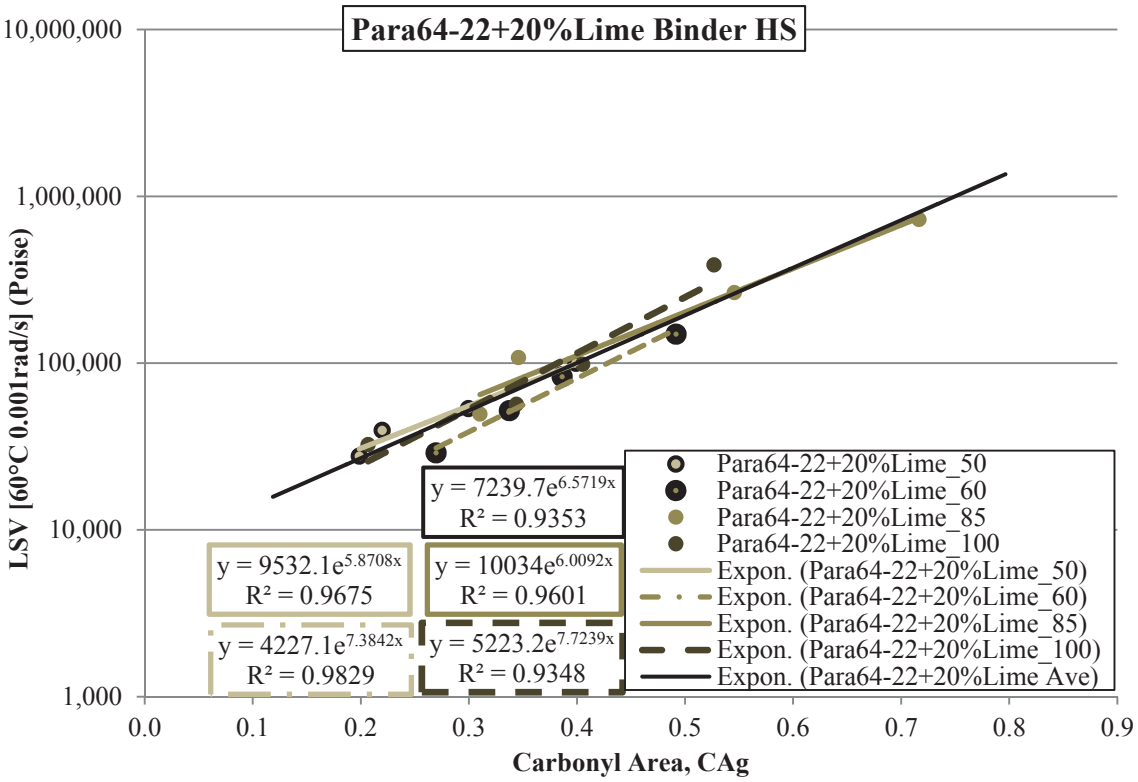

Figure 7.26 Temperature Dependent Hardening Susceptibility Relationships for PG 64-22 + 20% Lime Binder

From a visual perspective it is clear that the PG 64-28 binder exhibited substantially more variation in the HS term as a function of temperature as compared to the example PG 64-22 + 20% Lime. This observation is likewise supported by the differences in the calculated coefficient of determination for each binder, R^2 = 0.8111 and 0.9348 for the PG 64-28 and PG 64-22 + 20% Lime binders, respectively. As a result of these noted variations, it became a point of interest to make note of the potential consistency of the temperature dependency of the HS term with the remainder of the tested pan-aged asphalt binders. Therefore, Figure 7.27 through Figure 7.30 were prepared to clearly identify the temperature dependency of the initial eleven tested asphalt binders, excluding the ARC Core binders at this time.

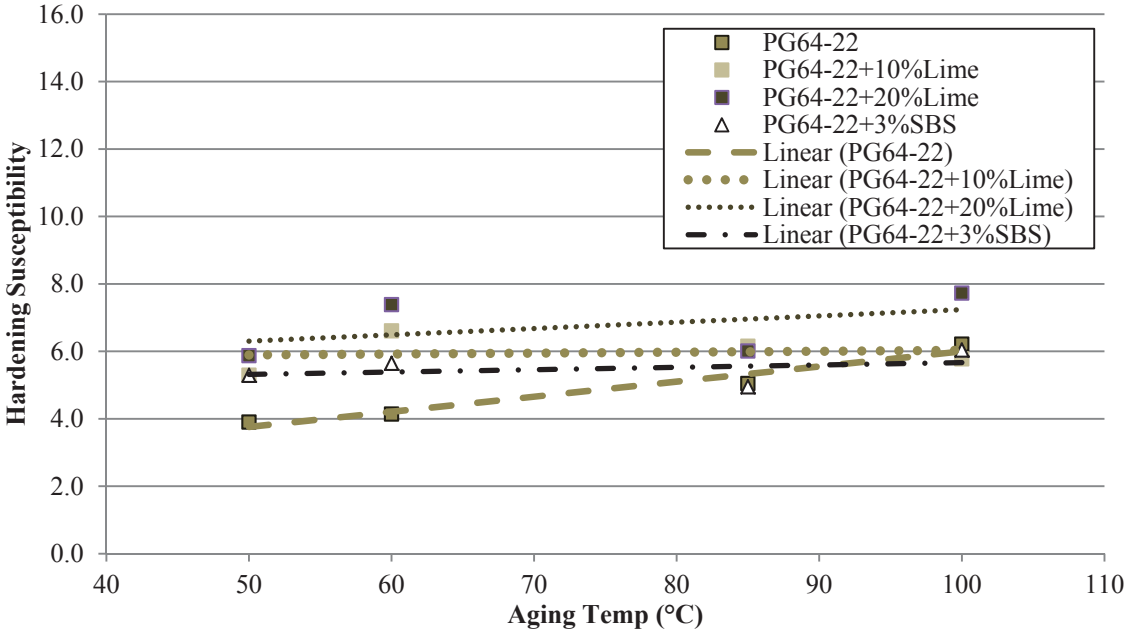

Figure 7.27 Temperature Dependent Hardening Susceptibility Relationships for PG 64-22 and Associated Binders

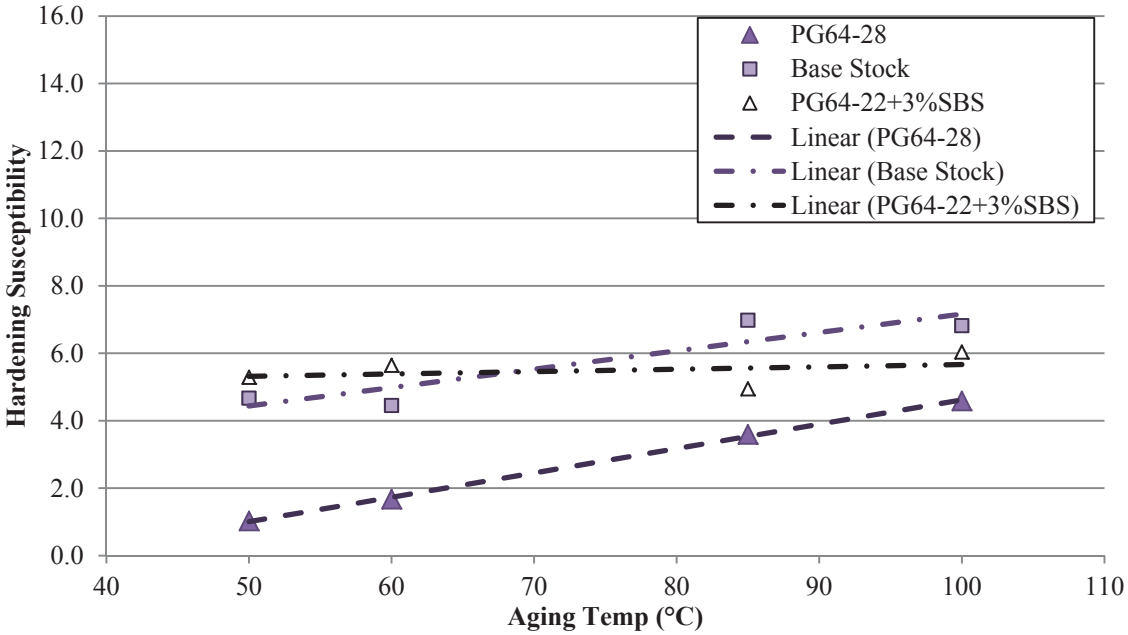

Figure 7.28 Temperature Dependent Hardening Susceptibility Relationships for PG 64-28 and Associated Binders

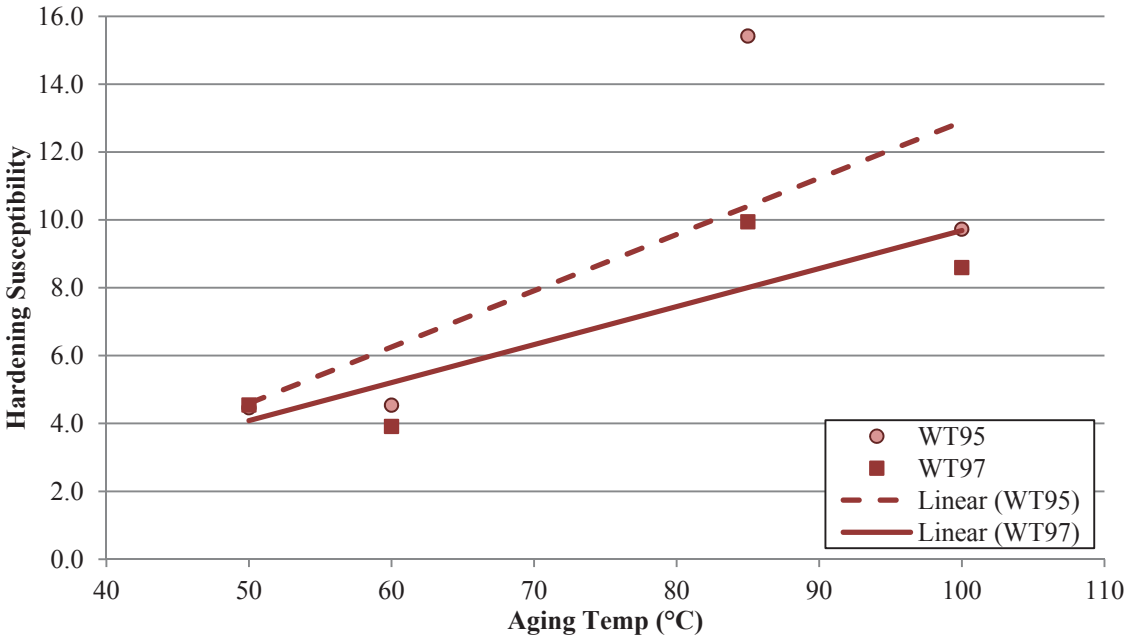

Figure 7.29 Temperature Dependent Hardening Susceptibility Relationships for WesTrack Binders

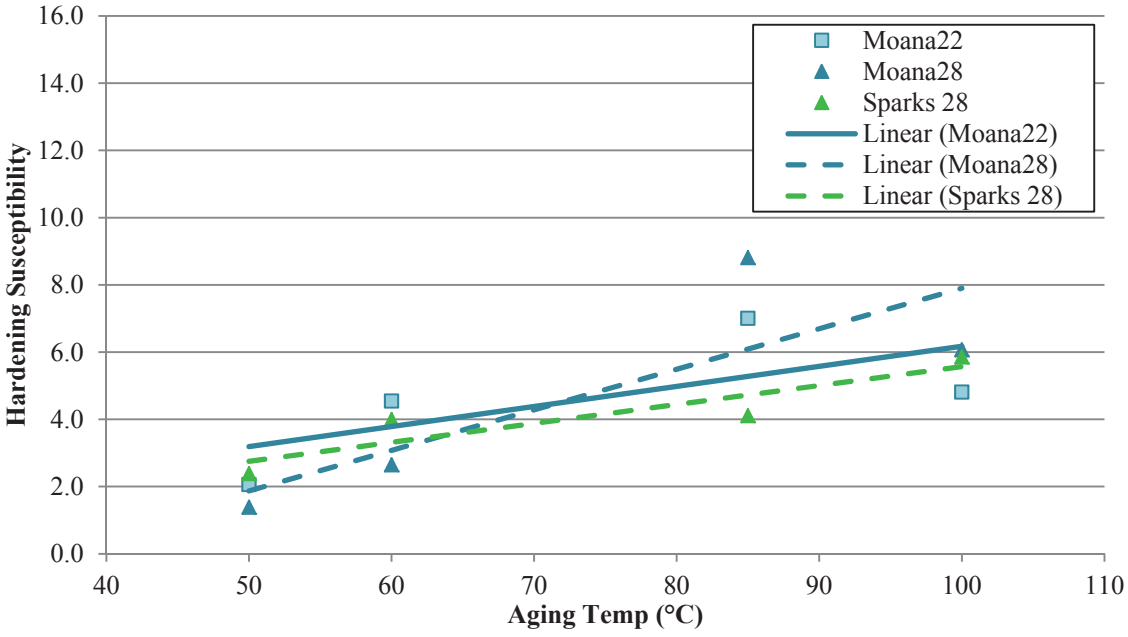

Figure 7.30 Temperature Dependent Hardening Susceptibility Relationships for Moana Lane and Sparks Blvd. Binders

When observing Figure 7.27 through Figure 7.30, a flat or horizontal relationship is interpreted to indicate that the HS of that particular binder is independent of the aging temperature. If the slope is not horizontal, then the HS parameter is understood to be influenced by the aging temperature with the steepness of the relationship representing the overall influence of the aging temperature. The steeper the relationships in Figure 7.27 through Figure 7.30, the more susceptible the particular binder is to the aging temperature.

With that understanding, Figure 7.27 presents the temperature dependency of the HS relationships for the PG 64-22 and associated binders. In general, the majority of these particular binders exhibit relatively low sensitivity to the oxidation temperature. The PG 64-22 binder itself shows the greatest temperature dependency, however the R^2 value of the overall HS relationship neglecting the different temperatures was determined to be above 0.93, thus generally supporting the independent nature of the HS term on aging temperature as is the standard of practice currently.

Consideration of Figure 7.28 presents the HS temperature dependency of the PG 64-28 and related Base Stock along with the PG 64-22 + 3% SBS binder as a relative comparison. As seen previously the PG 64-22 + 3% SBS is relatively unaffected by the aging temperature. However both the PG 64-28 and its Base Stock binder exhibited a fairly substantial temperature dependency with the HS term. This variability was noted in the R^2 value of 0.81 for the PG 64-28 binder, however the Base Stock binder exhibited a much improved value of over 0.96.

Similar observations of Figure 7.29 representing the two different PG 64-22 binders from WesTrack, indicate that these binders are substantially affected by the aging

temperature. There is also a higher level of variability noted in these binders as observed with the WT95 asphalt binder. On a relative scale, both WesTrack binders are also noted to have some of the highest HS levels included in this study. The R^2 values of the HS parameters calculated from both WesTrack binders also suggest an increased variability of the HS determination with these particular binders with calculated R^2 values of nearly 0.73 and 0.82 for the WT95 and WT97 binders, respectively.

Figure 7.30 presents the temperature dependency of the extracted and recovered binders from the field mixed samples from Moana Lane and Sparks Blvd. projects. It is curious to note the relative similarities between the Moana22 and Sparks28 binders compared to the generally high level of temperature dependency of the Moana28 asphalt binder. The R^2 values of the Moana Lane binders are quite similar to one another despite the increased dependency on temperature noted with the Moana28 binder. The flatter slope of the temperature dependency of the Sparks28 HS relationship does seem to be supported by the improved R^2 value of nearly 0.92 for that binder. This suggests that the temperature dependency of the HS term may not be the only variable influencing the HS parameters determinations, but it does seem to answer for a large portion of it.

Overall, based upon Figure 7.27 through Figure 7.30, it appears that the temperature dependency of the HS term is not necessarily based upon whether the asphalt binder had been modified with a polymer or not. This justification has been suggested as an overall systematic error in the revised LSV determination, i.e. using the entire master curve to obtain a rheologically more appropriate LSV value. However, any potential issues with the LSV determination were largely limited to the modified binders. The unmodified

binders typically exhibited very clear and distinct plateau behaviors in the complex viscosity plots at the frequency and temperature of interest.

Due on large part to the establishment of the state of practice dictating that the HS parameter is represented as being independent of temperature, the majority of this study will continue to represent them as such. A good deal of effort has been put forth to verify the rheological measures and thus the determination of the LSV values are valid while some inherent flaw in the testing methodology has caused the temperature dependency of these measure. However, since all of the oxidation modeling and the majority of the analyses that result from those efforts are based upon a single HS value for a given asphalt binder, that will be the approach followed in this manuscript while still remaining conscious of the variations noted in this section.

7.2 Mixture-Aged Asphalt Binder Oxidation Results

Since the overall objective of this study was to investigate the influence of the aggregate and mixture characteristics on the oxidation parameters of asphalt binders aged in compacted mixtures, the same binder testing protocol as was used with the pan-aged asphalt binders was conducted on the binders extracted and recovered from mixtures aged to varied conditions. Due to the significant increase in logistical demands that are associated with mixture aging (e.g. preparation time, physical size of the samples, stability of the mixture specimens at elevated temperature, etc.), the mixtures were not aged over the full temperature and duration range of the pan-aged asphalt binders.

Rather, the majority of the specimens were aged at 60°C over four durations, with a select few mixture also aged at 85°C to further investigate the potential temperature dependency of the HS term observed with the pan-aged binder evaluations.

Relevant to this portion of the investigation, the mixture identification nomenclature for these mixtures is for example, NV19I28_5.22_60C_4%_3mo would indicate **N**e**v**ada aggregates with a 19 mm (3/4 inch) NMAS **I**ntermediate gradation mixed with PG 64-**28** binder at **5.22**% binder content by total weight of mix (TWM) was aged in the **60**°**C** forced draft oven, after being compacted to the **4%** total air void level after cutting, for the prescribed time period (0, **3**, 6, or 9 **mo**nths).

Specifically, the main factors being explored in this portion of the evaluation are:

- Aggregate Factors
    - Qualitative Gradation
    - Aggregate Absorption
    - Aggregate Mineralogy
- Asphalt Binder Factors
    - Unmodified Binder
    - Modified Binder
- Mixture Characteristic Factors
    - Asphalt Binder Content
    - Mixture Density or Air Voids

However, each of the factors will be discussed in the order which makes the analysis logistically simpler to comprehend. For instance, the air void levels will be analyzed first, so that any relevance noted may be clearly addressed in the later discussions.

7.2.1 Statistical Analysis Methods of Mixture-Aged Binder Oxidation

The response functions utilized in these analyses can be considered to follow the form of the previously referenced Equation 3.78 which has also been restated as Equation 7.9. In these analyses, X_2 can either be a qualitative or dummy variable used to distinguish between the two data sets or a quantitative variable which would adjust the intercept by the value of β_2 and the slope of the regression by the product of $\beta_3 X_2$.

$$E\{Y\} = \beta_0 + \beta_1 X_1 + \beta_2 X_2 + \beta_3 X_1 X_2 \qquad \textbf{Equation 7.9}$$

where, $E\{Y\}$ – predicted dependent variable in the analysis;
β_0 - intercept of the base equation (condition A);
β_1 - slope of the base equation (condition A);
β_2 - modification to the intercept of the base equation due to condition B;
β_3 - modification to the slope of the base of the equation due to condition B;
X_1 - independent predictor variable (quantitative in this example);
X_2 - qualitative predictor variable (dummy variable);
$X_2 = 0$, for condition A,
$X_2 = 1$, for condition B.

This method of utilizing quantitative input variables based upon physical measurements is much preferred over the initial analyses utilizing qualitative categorical variables that only determine significant differences or similarities between the modeled relationships. In this manner, the input variables may be tested for true significance with information suggesting whether or not the particular variable of interest may be expected to have a true influence on the aging of the binder. The categorical variables, while useful for differentiation purposes are not always applicable to materials other than those strictly examined in the analysis from which they were derived.

In this set of analyses, it was common for more than one input variable to exhibit co-linearity issues, therefore the stepwise regression function available through the Minitab software package was utilized. Specifics of the forward and backward stepwise regression function have been previously discussed in Section 3.7.

In these analyses a correlation matrix was first constructed of the input variables to determine which ones exhibit significant co-linearity within a given data set. Then logically different sets of independent variables were selected for the optional input into the stepwise regression analyses. Following the several sets of analyses utilizing the stepwise regression, the final model was selected based upon the overall R^2 value for the model utilizing the most relevant input parameters. Although each of the input parameters may not be appropriate for every statistical analysis conducted, Table 7.8 presents the full list of potential input variables used in the statistical analysis of the aged mixtures.

Table 7.8 Potential Statistical Input Variables for Asphalt Mixtures

Aggregate Properties		Asphalt Binder Content (% TWM)		Mixture Characteristics		Asphalt-Aggregate Interaction[a]	
Aggregate Absorption	Abs	Total binder content	Pb	Air Voids, % TM	Va	Weight of material from 2nd and 3rd peaks	2-3wt
Coarse Aggregate Angularity and Texture	CAAT	Effective Asphalt Binder Content	Pbe	Voids Filled with Asphalt, %	VFA	Height of 2nd UV peak	2ht
Coarse and Fine Angularity	C&F_ Ang			Dust Proportion	DP	Height of 3rd UV peak	3ht
Qual. Gradation	Grd			Apparent Film Thickness, μm	AFT		

a – Measurements conducted as part of the modified SARA analysis.

Not all of the parameters listed in Table 7.8 were applicable to each statistical consideration. Many of the factors typically exhibited some degree of co-linearity (e.g. Abs and Pb typically) and were therefore not included in the same regression equation simultaneously. However, the stepwise regression analysis technique made exploration of the most appropriate inputs variables a much more practical method compared to searching for the best regression equations by hand.

7.2.2 Air Void Level of Compacted Mixtures

The factor to be considered was the effect of the compacted air void level in the mixtures during the oven aging. These mixtures were compacted at the asphalt binder content

which produced a calculated apparent film thickness (AFT) of 9 µm. Specifically these mixtures were compacted to three different ranges in the air void level measured on the cut E* specimens, i.e. 4, 7, and 11% voids in total mix.

After their respective aging durations at the appropriate temperatures, the mixtures were tested for E* measurements, then the binders were extracted and recovered in the process already discussed. Those measurements resulted in the CA measures presented in Figure 7.31 and Figure 7.32 for the mixtures prepared with PG 64-22 and PG 64-28 asphalt binders, respectively. Recall that the PG 64-22 binder utilized in the WesTrack mixtures were not the same as with the California mixtures, even though they have the same PG grade.

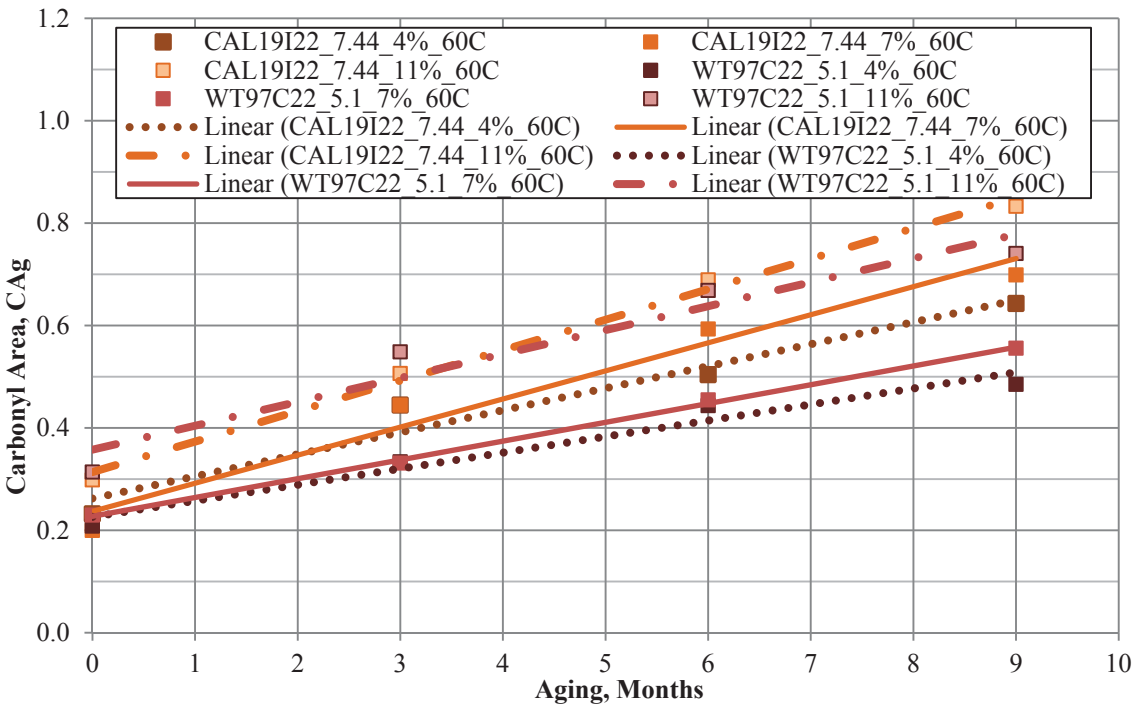

Figure 7.31 Carbonyl Growth Relationships for Mixtures Containing PG 64-22 Asphalt Binders

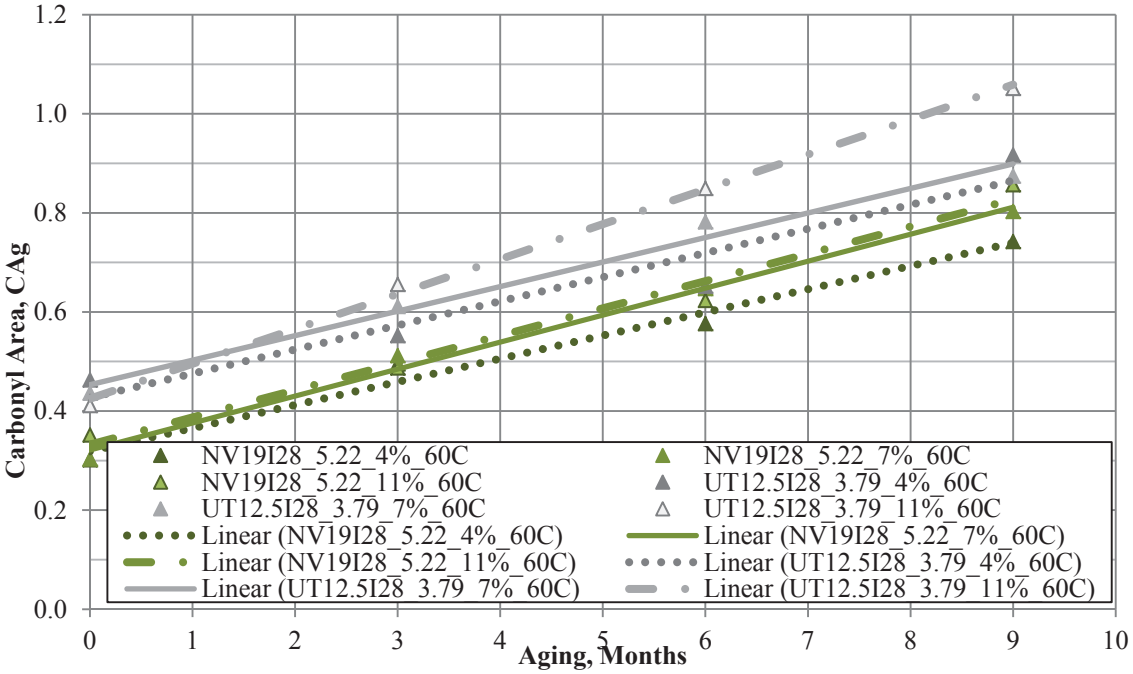

Figure 7.32 Carbonyl Growth Relationships for Mixtures Containing PG 64-28 Asphalt Binders Aged at 60°C

Observations of Figure 7.32 and Figure 7.33 present a rather systematic variation in the CA measurements as a function of the air void level of the mixtures during the oven aging. In these figures, the CA measurements derived from the mixtures aged with 4% air voids exhibit not only the lowest relative values of CA, but also present the lowest rate of CA growth depicted as the slope of the CA measurements as a function of the aging duration. The systematic variation is also realized with the mixtures prepared with 7% air voids as they present generally higher CA measures over the 4% air void mixtures. Typically the slope of the 7% air void mixtures is higher than those of the 4% air void mixtures, with the Utah mixture being the exception. Similar general increased are further noted with the mixtures containing 11% air voids over the aging duration, with the Nevada aggregates being the exception.

Statistical considerations conducted through linear regression on these mixtures in particular, generally resulted in no statistically significant difference between the air void levels within each aggregate source with a few exceptions. Statistically significant differences were noted between the slope of the 4 and 11% air void mixtures for all of the mixtures except NV19I28_5.22. The difference between the 7 and 11% of the Utah mixtures were not quite statistically significant at the 0.05 significance level. Additionally, the intercepts of the WT97C22_5.1 mixtures with 4 and 7% air voids were statistically different from the 11% air void mixture. A summary of the statistical regression parameters are presented in Table 7.9 though Table 7.12.

Table 7.9 Statistical Significance of Air Void Level on Carbonyl Area with Aging Time at 60°C for CAL19I22_7.44

Statistical Significance							
Intercept		CAL19I22		Slope		CAL19I22	
Mix	Air Voids	7%	11%	Mix	Air Voids	7%	11%
CAL19I22	4%	NS	NS	CAL19I22	4%	NS	SH[a]
	7%		NS		7%		NS
	11%				11%		
Regression P-values							
Intercept		CAL19I22		Slope		CAL19I22	
Mix	Air Voids	7%	11%	Mix	Air Voids	7%	11%
CAL19I22	4%	0.584	0.213	CAL19I22	4%	0.174	0.028
	7%		0.126		7%		0.581
	11%				11%		

a – SH indicates the CAL19I22_7.44_11% mixture regression slope was significantly higher than the CAL19I22_7.44_4% at the 0.05 significance level.

Table 7.10 Statistical Significance of Air Void Level on Carbonyl Area with Aging Time at 60°C for NV19I28_5.22

Statistical Significance							
Intercept		NV19I28		Slope		NV19I28	
Mix	Air Voids	7%	11%	Mix	Air Voids	7%	11%
NV19I28	4%	NS	NS	NV19I28	4%	NS	NS
	7%		NS		7%		NS
	11%				11%		
Regression P-values							
Intercept		NV19I28		Slope		NV19I28	
Mix	Air Voids	7%	11%	Mix	Air Voids	7%	11%
NV19I28	4%	0.909	0.563	NV19I28	4%	0.127	0.168
	7%		0.633		7%		0.950
	11%				11%		

Table 7.11 Statistical Significance of Air Void Level on Carbonyl Area with Aging Time at 60°C for WT97C22_5.1

Statistical Significance							
Intercept		WT97C22		Slope		WT97C22	
Mix	Air Voids	7%	11%	Mix	Air Voids	7%	11%
WT97C22	4%	NS	NS	WT97C22	4%	NS	SH[a]
	7%		SH[b]		7%		NS
	11%				11%		
Regression P-values							
Intercept		WT97C22		Slope		WT97C22	
Mix	Air Voids	7%	11%	Mix	Air Voids	7%	11%
WT97C22	4%	0.863	0.009	WT97C22	4%	0.457	0.034
	7%		0.005		7%		0.134
	11%				11%		

a – SH indicates the WT97C22_5.1_11% mixture regression slope was significantly higher than the WT97C22_5.1_4% at the 0.05 significance level.

b – SH indicates the WT97C22_5.1_11% mixture regression intercept was significantly higher than the WT97C22_5.1_7% at the 0.05 significance level.

Table 7.12 Statistical Significance of Air Void Level on Carbonyl Area with Aging Time at 60°C for UT12.5I28_3.79

Statistical Significance							
Intercept		UT12.5I28		Slope		UT12.5I28	
Mix	Air Voids	7%	11%	Mix	Air Voids	7%	11%
UT12.5I28	4%	NS	NS	UT12.5I28	4%	NS	SH[a]
	7%		NS		7%		NS
	11%				11%		
Regression P-values							
Intercept		UT12.5I28		Slope		UT12.5I28	
Mix	Air Voids	7%	11%	Mix	Air Voids	7%	11%
UT12.5I28	4%	0.797	0.787	UT12.5I28	4%	0.825	0.044
	7%		0.624		7%		0.073
	11%				11%		

a – SH indicates the UT12.5I28_3.79_11% mixture regression slope was significantly higher than the UT12.5I28_3.79_4% at the 0.05 significance level.

It should be noted that some of the statistical significance determinations may have been limited based upon the limited range of the measurements included in the analysis. Clearly, if the apparent trends continued as expected from these data, additional aging durations would be expected to eventually detect more significant differences among the different air void levels. From a physical standpoint, the observed differences in these measure though orderly and systematic, are simply too close to each other at these aging conditions to detect statistically significant differences.

Utilizing the form for the regression equations presented in Equation 7.9 and including the air voids as an additional independent variable, Table 7.13 and Table 7.14 present the regression relationships derived for the CA measurements on the binders extracted and recovered from their respective mixtures as a function of aging time.

Table 7.13 Statistical Significance of Air Void Level on Carbonyl Area with Aging Time at 60°C for Mixtures with PG 64-22 Binders

	CAL19I22_7.44			WT97C22_5.1		
Regression Parameter	Coefficient	P-value	Significance	Coefficient	P-value	Significance
Intercept, β_0	0.2204	0.000	Sig.	0.1254	0.045	Sig.
Age (Slope, β_1)	0.0349	0.000	Sig.	0.0215	0.075	NS
Air Voids, Va	0.0077	0.162	NS	0.0194	0.013	Sig.
Va*Age	0.0023	0.026	Sig.	0.0024	0.103	NS
R^2 (%)	95.6			91.3		
Adj. R^2 (%)	94.8			89.4		

Table 7.14 Statistical Significance of Air Void Level on Carbonyl Area with Aging Time at 60° C for Mixtures with PG 64-28 Binder

	NV19I28_5.22			UT12.5I28_3.79		
Regression Parameter	Coefficient	P-value	Significance	Coefficient	P-value	Significance
Intercept, β_0	0.2980	0.000	Sig.	0.4470	0.000	Sig.
Age (Slope, β_1)	0.0444	0.000	Sig.	0.0361	0.001	Sig.
Air Voids, Va	0.0025	0.561	NS	-0.0013	0.854	NS
Va*Age	0.0012	0.164	NS	0.0029	0.040	Sig.
R^2	98.1			95.5		
Adj. R^2	97.6			94.4		

For the mixtures considered with the three levels of air voids during aging, three of the four mixtures showed a significant difference either in the slope or intercept with the change in air void level. Only the NV19I28_5.22 mixture was not significantly affected by the range of air voids. Therefore, in general the level of air voids are expected to have an influence on the rate of CA growth or oxidation of a given mixture. This also suggests that the oxidation of the binders aged in mixtures may potentially be different from those of the pan-aged binders, otherwise the air void level would not have shown any

significant influence (i.e. the mixture properties would not have an influence on the aging rate of the asphalt binder).

7.2.3 Asphalt Binder Content

The next factor to be considered was the influence of the asphalt binder content of the mixtures during the aging process. By maintaining a constant gradation and air void level, changes in the asphalt binder content also by definition varied the AFT measured for the respective mixtures.

Recall that the overall experimental matrices found in Table 5.1 and Table 5.2 describe two levels for the binder content factor. The first level examined contained the same 4.5% TWM binder content for each mixture, excluding the California aggregate source. The other level included mixtures that were produced with a binder content that would yield a calculated AFT of 9 μm, which necessitated variable total asphalt binder contents. Figure 7.33 though Figure 7.39 present the oxidation growth measures for the mixtures used to evaluate changes in the asphalt binder content and also those considered in the AFT evaluation as well. Beginning with the mixtures containing the 4.5% TWM binder contents presented in Figure 7.33 through Figure 7.35.

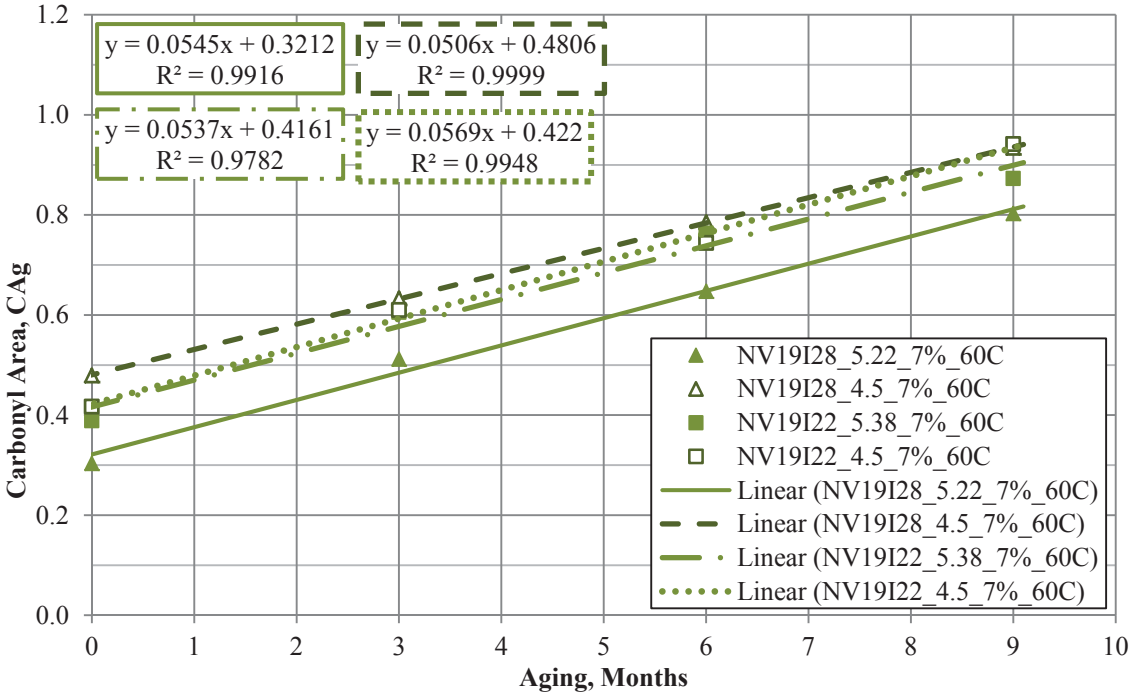

Figure 7.33 Carbonyl Growth Relationships for the Nevada Mixtures with Different Binder Contents Aged at 60°C

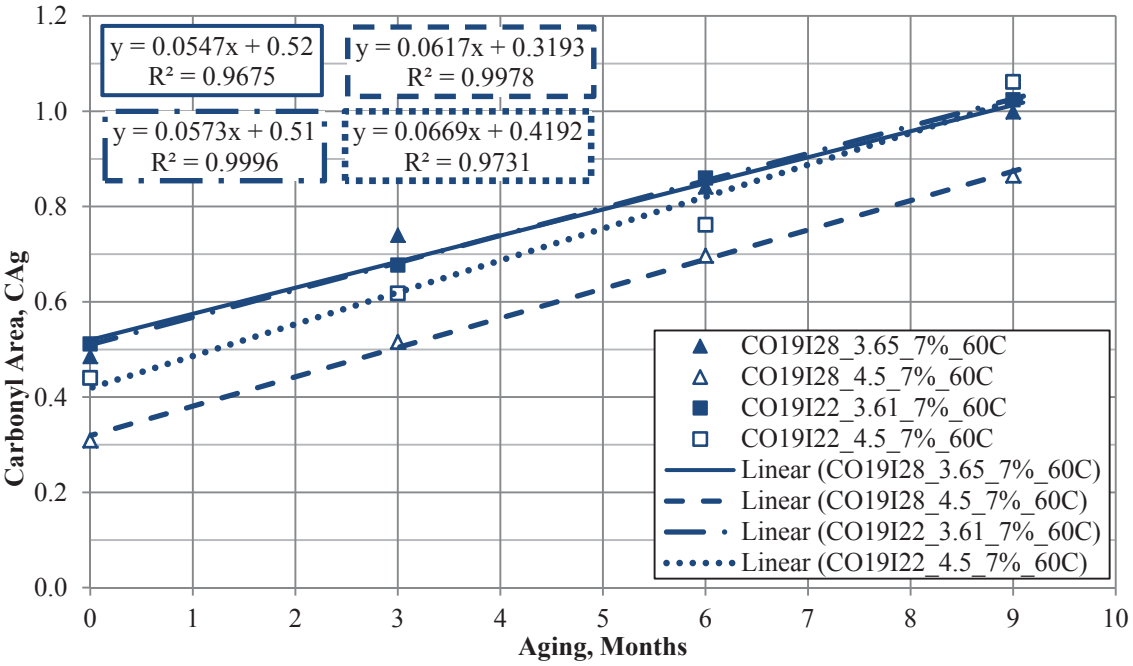

Figure 7.34 Carbonyl Growth Relationships for the Colorado Mixtures with Different Binder Contents Aged at 60°C

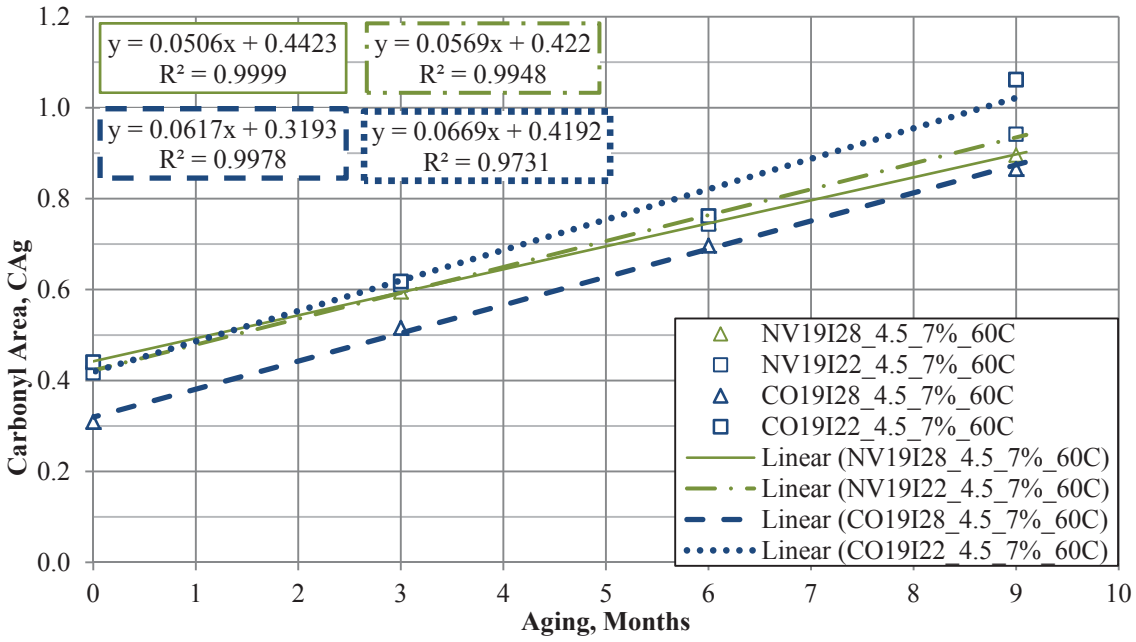

Figure 7.35 Carbonyl Growth Relationships for Mixtures Aged with 4.5% Asphalt Binder Content Aged at 60°C

General observations of Figure 7.33 suggest that changes in the asphalt binder content of up to 0.7% TWM may not influence the rate of CA growth for the mixtures containing the PG 64-28 binder and the Nevada aggregates with the intermediate gradation. However, an increase of almost 0.9% possibly can reduce the CA level, but not the growth rate with the PG 64-22 binder and the Nevada intermediate aggregate source.

Specific to these analyses related to Figure 7.33 and Figure 7.34 are the aggregate properties. Given that each of the figures represents measurements made from binders extracted and recovered from aged mixtures from a single aggregate source, any aggregate factors will necessarily be same within each of these two figures. Specifically, any terms including the aggregate absorption, gradation measures, or AIMS parameters will only yield a single value for each figure respectively, thus must be omitted from the analyses. By a similar circumstance, considerations of Figure 7.35 yield a single value

for the total asphalt binder content of 4.5% TWM, and thus were eliminated from this particular analysis.

The stepwise regression analysis for the Nevada aggregates presented in Figure 7.33 which resulted in the highest R^2 value after accounting for co-linearity concerns was initiated with nine parameters (Age, Pbe, VFA, 2ht, BI, and the interaction terms of the four variables with Age). The final regression equation from this input is presented in Table 7.15. It should be noted that quite similar regression equations were also developed utilizing Pb and AFT terms in place of the Pbe input. Although they resulted in very similar R^2 values these particular inputs were selected to aid in consistency with additional analyses of other mixture-aged binders to be discussed shortly.

Table 7.15 Stepwise Regression on Carbonyl Area with Aging Time at 60°C for Nevada Mixtures

NV19I Binder Content Analysis			
Regression Parameter	Coefficient	P-value	Significance
Intercept, β_0	0.4769	0.001	Sig.
Age (Slope, β_1)	0.0543	0.000	Sig.
Pbe	-0.1434	0.000	Sig.
VFA	0.0105	0.011	Sig.
R^2 (%)	94.30		
Adj. R^2 (%)	93.75		

The lack of significance of any interaction terms (e.g. Pbe*Age) indicates that the slope of all four evaluated mixtures were statistically the same. Further, the lack of significance of the categorical BI term indicates that both the slope and the intercepts were not strictly influenced by the SBS modification of the binder when mixed with the Nevada aggregates. However, other aspects such as the Pbe and VFA were found significant indicating that the quantity of binder not absorbed into the aggregates is influential to the level of binder oxidation when mixed with the Nevada aggregates.

Similar considerations of Figure 7.34 also suggest minimal influence of an almost 0.9% TWM decrease in the asphalt binder content produced a fairly minimal effect on the CA level with the PG 64-22 asphalt binder and the Colorado aggregates with the intermediate gradation. However, the same aggregates with the PG 64-28 did produce potentially lower CA measures due to a 0.85% TWM increase in the binder content with the PG 64-28 asphalt binder and the Colorado intermediate gradation. The final equation from the stepwise regression analysis conducted on the Colorado aggregates is illustrated in Table 7.16 with almost the same input variables as were used in the Nevada mixtures (Age, Pbe, VFA, BI, and the interaction terms of the three variables with Age) excluding the modified SARA parameter (2ht). Note that the 2ht parameter from the Colorado mixtures was not available for inclusion in this analysis and thus had no input into the regression analysis.

Table 7.16 Stepwise Regression on Carbonyl Area with Aging Time at 60°C for Colorado Mixtures

CO19I Binder Content Analysis			
Regression Parameter	Coefficient	P-value	Significance
Intercept, β_0	1.1456	0.000	Sig.
Age (Slope, β_1)	0.0617	0.000	Sig.
BI	-0.0764	0.000	Sig.
VFA	-0.0143	0.000	Sig.
R^2 (%)	95.08		
Adj. R^2 (%)	94.65		

The regression analysis with the Colorado aggregates overall provided a slightly better R^2 value indicating the input parameters explain a little more of the variation noted in the CA growth in the respective mixtures. The final equation is fairly similar except the Pbe term has been replaced with the categorical BI term in the final model. This is not a surprising finding since the previous analysis of the pan-aged binders demonstrated fairly significant differences between the unmodified PG 64-22 and the SBS modified PG 64-28 asphalt binders. This does not necessarily indicate that the effective binder content does not play a role in the oxidation characteristics of the mixtures, but merely that with this limited data set, the categorical variable showed a stronger statistical influence, both of which make sense logically. Further analyses in this section which include more variations in the binder content and the BI term may help to clarify the overall influence of these parameters. Similar to the Nevada analysis, the VFA term still proved to be statistically significant, thus supporting the previous finding that the amount of asphalt binder not absorbed into the aggregate has an effect on the aging of the mixture.

Considerations of the mixtures containing 4.5% TWM asphalt binder in Figure 7.35, suggest that with the Nevada aggregates, the polymer modification did not highly influence the CA growth within the mixture. There were slight differences noted with the Colorado aggregate source between the two binders, however the slopes are fairly consistent within each respective aggregate source. When comparing within the two asphalt binder grades, the aggregate source did tend to exhibit slight variations in the level of CA measured over time, although the differences are relatively minor.

The stepwise regression analysis based upon the mixtures aged with 4.5% TWM binder content enable the inclusion of some of the aggregate properties that were singular inputs to the previous two considerations. As a result of maintaining the gradation of each aggregate source largely the same, most of the AIMS parameters ended up being highly correlated to each other as well as other mixture characteristic measures, such as the absorption. Without multiple gradation levels utilizing the same aggregate source, much of the statistical power of such measures has been masked by too few data points into the analysis. Thus, only a few of the AIMS parameters have been included in the statistical comparisons out of logistical necessity.

Through the course of the stepwise regression analyses conducted utilizing the AIMS parameters, it became evident that the CAAT parameter was highly significant to certain regression considerations. However, the actual degree of that influence was often masked by the magnitude of the CAAT parameter (usually measured in 1,000s) compared to the CA measures with a relative magnitude in the tenths (0.1) or hundredths (0.01) as a relative magnitude. Thus, a reduced CAAT parameter was determined by dividing the actual measured CAAT parameter by 1,000, thus producing the CAAT2

parameter with a magnitude close to the ones place (1.0). The CAAT2 parameter was utilized with the majority of the stepwise analyses conducted.

The stepwise evaluation of the Nevada and Colorado mixtures aged with 4.5% TWM binder content resulted in the final regression model based upon nine input predictor variables (Age, Pbe, VFA, BI, CAAT2, and the interaction terms of the four variables with Age) as presented in Table 7.17.

Table 7.17 Stepwise Regression on Carbonyl Area with Aging Time at 60°C for Mixtures with 4.5% TWM Asphalt Binder

4.5% TWM Binder Content Analysis			
Regression Parameter	Coefficient	P-value	Significance
Intercept, β_0	-0.5675	0.030	Sig.
Age (Slope, β_1)	N/A	N/A	NS
Pbe	0.7478	0.000	Sig.
CAAT2	-0.2823	0.000	Sig.
BI	-0.0565	0.014	Sig.
Age*Pbe	0.0171	0.000	Sig.
Age*BI	-0.0069	0.096	NS[a]
R^2 (%)	96.7		
Adj. R^2 (%)	96.1		

a – Statistically not significant for alpha = 0.05, but exclusion dramatically influenced the other coefficients.

Initially, concern arose from the Age term not being statistically significant in the 4.5% TWM Pb analyses, but further observation noted the Age term being highly significant in the interaction term with Pbe and moderately significant in the BI interaction term. The combined effect of those two terms have adequately addressed the overall influence of

the aging duration (Age term), which is part of the reason why the Age*BI term was retained even though it was found not to be significant at the 0.05 significance level.

Other input parameters that were found to be highly significant were the Pbe and BI terms as noted in the Nevada and Colorado analyses collectively. The influence of the aggregate was also determined to influence the oxidation as represented by the significance of the CAAT2 term.

7.2.4 Qualitative Gradation

The influence of the quantitative gradations (i.e. intermediate and fine) on the aging of the asphalt binders in mixtures were considered in Figure 7.36 and Figure 7.37 for PG 64-22 and the SBS modified PG 64-28 asphalt binders, respectively. Recall that the WesTrack binders are not the same as the Paramount Petroleum PG 64-22 binder utilized with the other mixtures. Therefore, interpretations of Figure 7.36 must keep that in perspective.

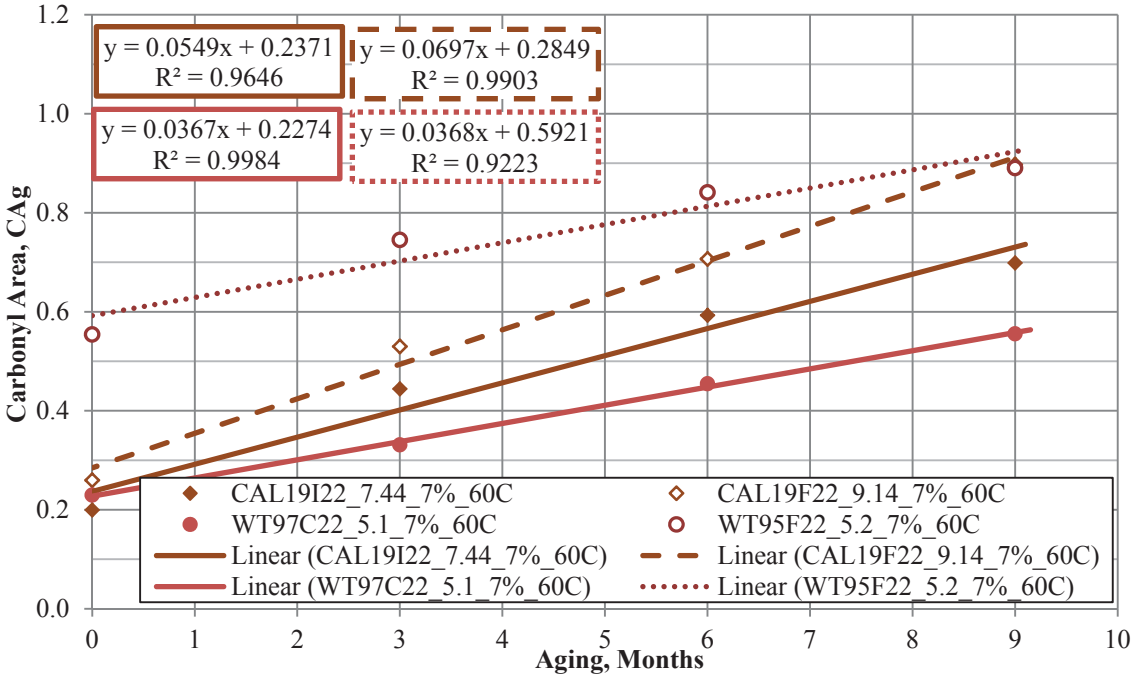

Figure 7.36 Carbonyl Growth Relationships for the Mixtures with PG 64-22 Binders with Different Gradations Aged at 60°C

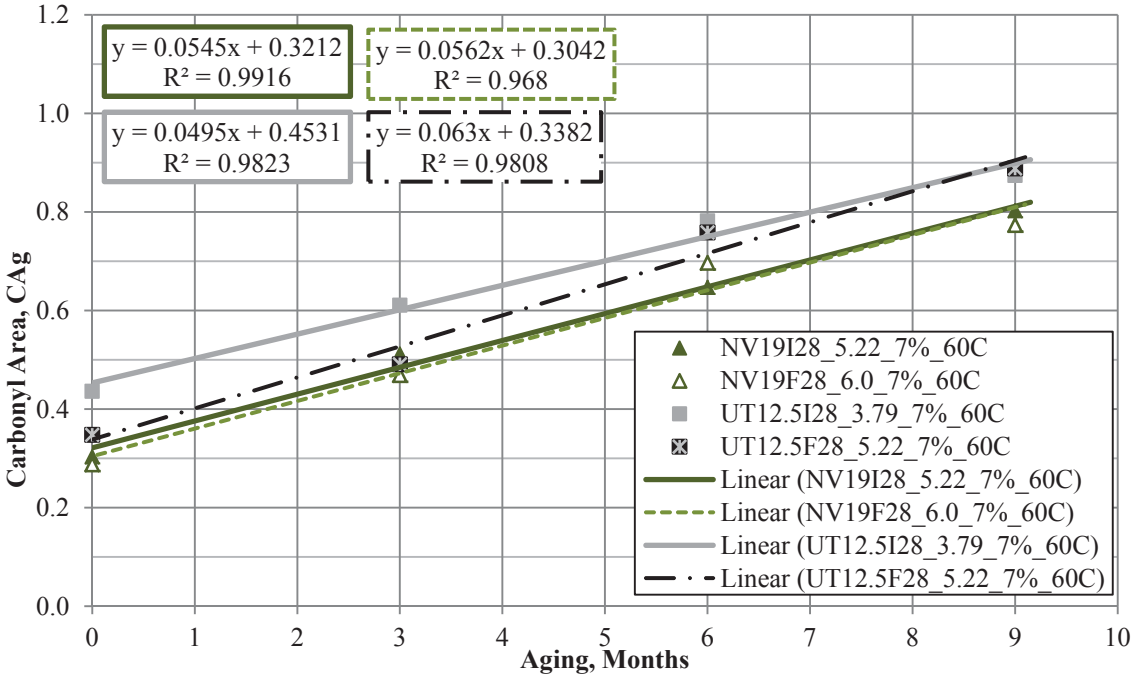

Figure 7.37 Carbonyl Growth Relationships for the Mixtures with PG 64-28 Binder with Different Gradations Aged at 60°C

General observations of Figure 7.36 and Figure 7.37 suggest that the fine gradations tend to increase the rate of CA growth for a given aggregate source with the California and Utah aggregates, but not with the Nevada mixtures. Again note that the WesTrack mixtures were composed of different asphalt binders and different aggregates, so thus are not compared directly. The noted increase in the growth of the CA measures is potentially significant to the practical application of this study. Specifically, the considerations previously investigated with the varied binder content compared to the 4.5% TWM mixtures presented in Figure 7.33 and Figure 7.34 suggest that an increase in the asphalt binder content of 0.85% or greater may reduce or not affect the CA growth for a given mixture at the 7% air void level. The measures based on the intermediate and fine gradations propose an increase in the CA growth with the fine gradations, despite an increase in the asphalt binder content of 0.78 to 1.7 between the two gradations. This becomes more significant when the optimum binder contents of the intermediate and fine gradations are considered.

As an extreme example, the CAL19I22 mixture has an optimum binder content of 6.65% TWM, while the CAL19F22 mixture has an optimum of 7.04% TWM, with a difference of 0.39% TWM. Therefore, expected binder contents for field produced mixtures based on these designs are assumed to target levels that are much closer to one another as opposed to the 1.7% difference utilized in this study. Despite the drastic increase in the binder content of the California fine mixture, it still exhibited a higher level of CA growth compared to the intermediate gradation. It can be expected that the difference would be even more pronounced had the fine gradation been mixed at an even

lower binder content as was indicated by the optimum design. The noted differences exist despite the counteracting effect of the higher binder content.

These results also suggest that the calculated AFT of the mixtures does not directly control the oxidation rate of the asphalt binder contained within a given mixture. This is not to state that the calculation method for the AFT is correct or not. The fact is that a substantial increase in the binder content did not overcome the increase in fine material, and presumably the increased surface area of the fine gradations in two of the three cases considered here.

The stepwise evaluation of the California, Nevada, and Utah mixtures aged with a binder content that corresponded to the 9 μm AFT for each respective mixture developed the final regression model based upon thirteen input predictor variables (Age, Abs, Pbe, VFA, DP, BI, CAAT2, and the interaction terms of the six variables with Age) as presented in Table 7.18.

Table 7.18 Stepwise Regression on Carbonyl Area with Aging Time at 60°C for Mixtures over Qualitative Gradation

Qualitative Gradation Analysis			
Regression Parameter	Coefficient	P-value	Significance
Intercept, β_0	0.9327	0.000	Sig.
Age (Slope, β_1)	0.0320	0.002	Sig.
Abs	-0.0933	0.000	Sig.
DP	0.6883	0.003	Sig.
VFA	-0.0048	0.008	Sig.
CAAT2	-0.1593	0.000	Sig.
Age*Pbe	0.0057	0.005	Sig.
R^2 (%)	96.1		
Adj. R^2 (%)	95.4		

While running the multiple stepwise regression function on the mixture-aged results with a specific interest in the qualitative gradation, it became apparent that there was no need for a categorical or qualitative dummy variable to distinguish the different levels in the gradation so far as the CA growth measures were concerned. Specifically, the changes in the aggregate properties (i.e. Abs and indirect changes to Pbe, VFA, etc.) were statistically significant enough to detect the modification to the gradation without the addition of the empirical categorical variable.

Therefore, the final regression model was based upon the aggregate characteristics (Abs and CAAT2), the asphalt binder content (Pbe), and the interaction between the two components (VFA and DP) in the compacted aggregate structure.

7.2.5 Constant Film Thickness

Additional mixtures were produced and aged with an asphalt binder content that corresponded to the 9 μm AFT for each respective mixture as presented in Figure 7.38 and Figure 7.39. These mixtures were designed to investigate the influence of the aggregate effects while maintaining the binder content and air void levels constant within the mixtures.

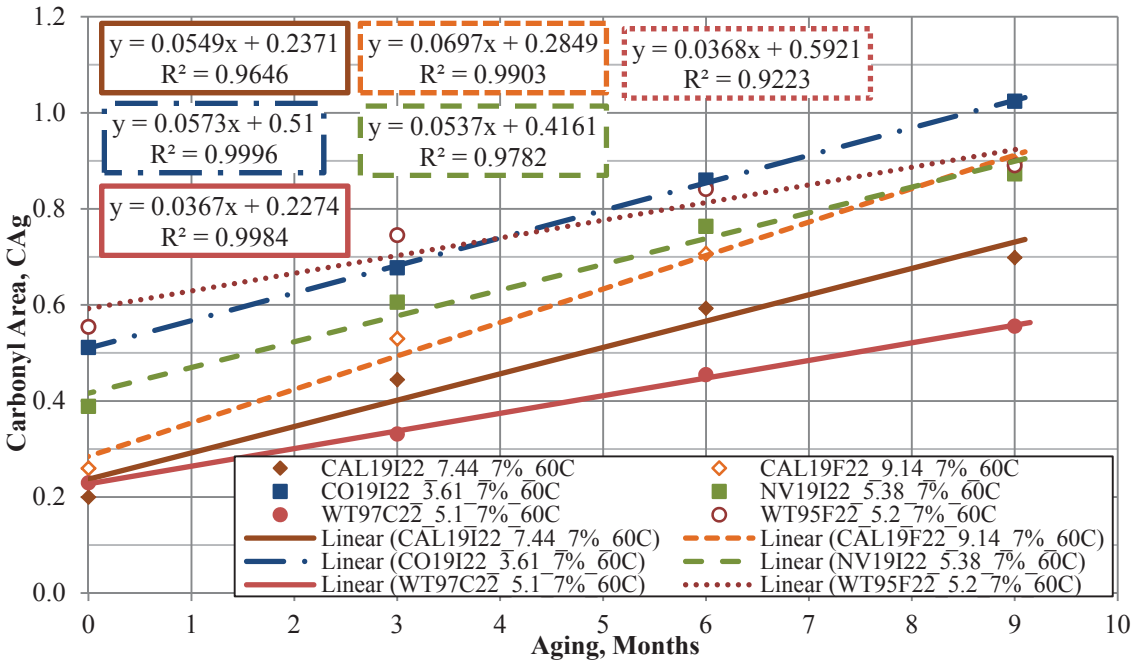

Figure 7.38 Carbonyl Growth Relationships for PG 64-22 Mixtures Aged with 9µm Film Thickness Aged at 60°C

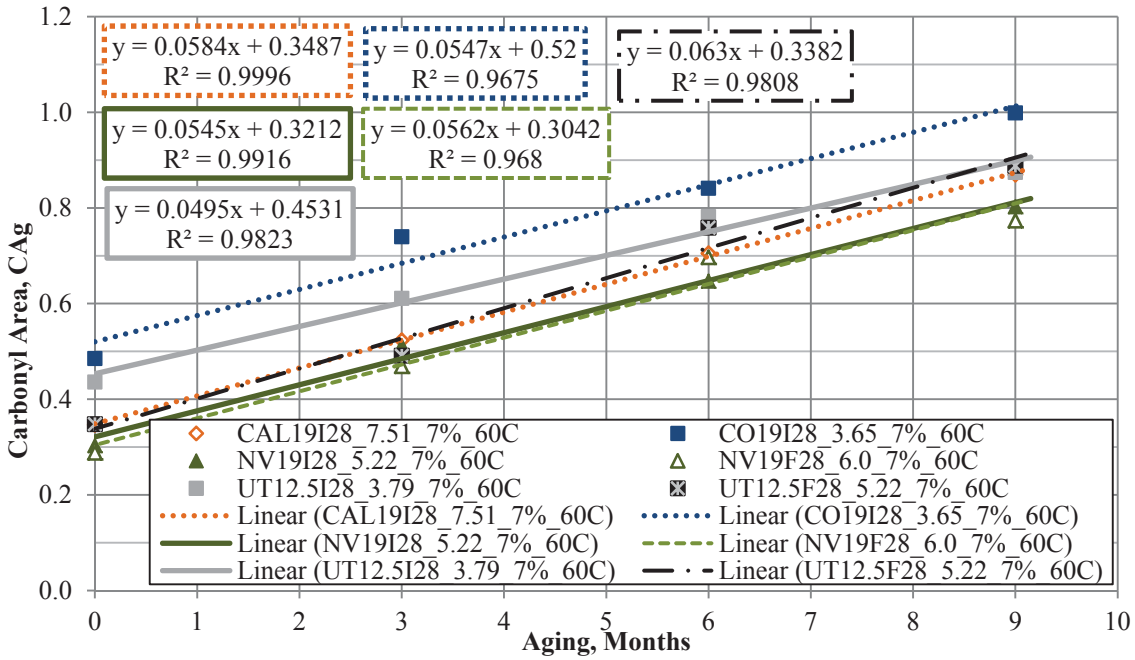

Figure 7.39 Carbonyl Growth Relationships for PG 64-28 Mixtures Aged with 9µm Film Thickness Aged at 60°C

The stepwise evaluation of the California, Colorado, Nevada, and Utah mixtures aged with a binder content that corresponded to the 9 μm AFT for each respective mixture developed the final regression model based upon eleven input predictor variables (Age, Pbe, VFA, DP, BI, CAAT2, and the interaction terms of the five variables with Age) as presented in Table 7.19.

Table 7.19 Stepwise Regression on Carbonyl Area with Aging Time at 60°C for Mixtures with 9μm Apparent Film Thickness

9μm Apparent Film Thickness Analysis			
Regression Parameter	Coefficient	P-value	Significance
Intercept, β_0	0.7937	0.000	Sig.
Age (Slope, β_1)	0.0395	0.002	Sig.
BI	-0.0544	0.000	Sig.
DP	-0.3809	0.000	Sig.
VFA	-0.0039	0.042	Sig.
CAAT2	0.0308	0.000	Sig.
Age*Pbe	0.0043	0.016	Sig.
R^2 (%)	93.4		
Adj. R^2 (%)	92.9		

It is interesting to note that nearly all the same input parameters that were incorporated into the final regression model based upon the qualitative gradations also were included into this analysis to observe the influence of the overall aggregate effect with a constant 9 μm AFT. In this model the BI term has replaced the Abs term used in the gradation analysis, however the remainder of the terms are the same. The overall magnitude of the coefficients may have slightly changed, however, the significance of each parameter remained largely intact. The overall R^2 was also reduced slightly, but not by a large

amount especially when considering the 9 µm AFT model includes ten total mixtures as opposed to the six utilized to develop the gradation regression model.

Therefore, the final regression model was based upon the aggregate characteristics (CAAT2), the asphalt binder content (Pbe), the interaction between the two components (VFA and DP) in the compacted aggregate structure, and the categorical separation (BI) between the SBS modified and unmodified asphalt binders.

7.2.6 Mixture-Aging Temperature

Similar to the pan-aged binders, the CA growth levels of the mixture-aged binders were also expected to vary with the aging temperature. Largely stemming from the temperature dependency of the HS terms noted with several of the pan-aged binders, additional mixtures were prepared and aged in in the oven in the same manner as the first set of mixtures which were aged at 60°C, only these additional specimens were aged at 85°C. The increase in temperature was suspected to increase the potential for specimen deformation as was noted with some of the mixtures aged at 60°C. Therefore all of the mixtures prepared for the 85°C aging were wrapped in the wire mesh prior to their placement in the aging ovens. Following the respective aging duration of 0.5, 1, or 3 months in the 85°C ovens, the specimens were removed from the ovens, cooled and trimmed to the correct geometry for mixture testing, either E^* or UTSST. Following the mixture testing, the binder from the E^* specimens were extracted and recovered to be tested for CA measures on the FT-IR and rheological measures with the DSR.

Due to the significant amount of resources required to age additional mixtures, only two mixtures (California and Nevada) were selected for the 85°C aging. However, each

of the mixtures were aged with all three levels of air voids (i.e. 4, 7, and 11%) over each of the respective durations (0.5, 1, and 3 months). This would not only permit the calculation of the CA growth as was previously discussed, but would also enable the determination of the oxidation kinetics parameters (E_a and the pre-exponential term) and the HS parameters as a function of temperature for later comparison to the pan-aged binders.

Initial analyses of these mixtures started with the evaluation of the CA growth of the binder extracted and recovered from the respective mixtures as a function of temperature and aging time which are presented in Figure 7.40 and Figure 7.41.

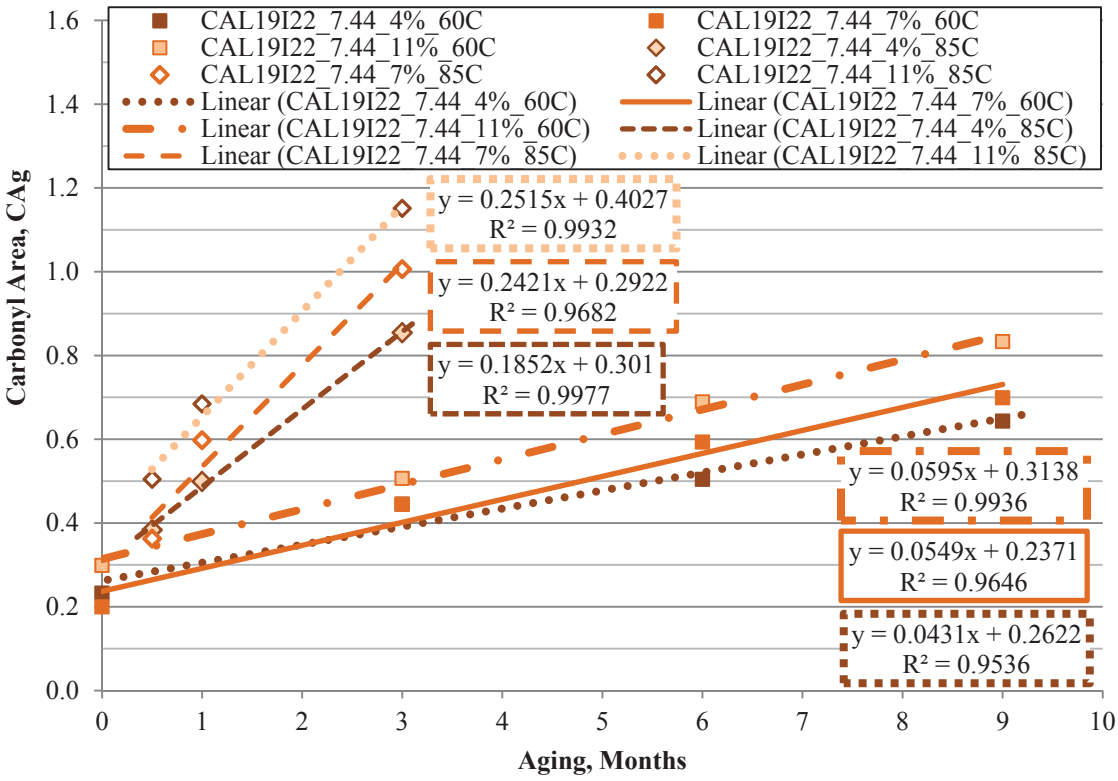

Figure 7.40 Carbonyl Growth Relationships for the CAL19I22_7.44 Mixtures Aged at 60 and 85°C

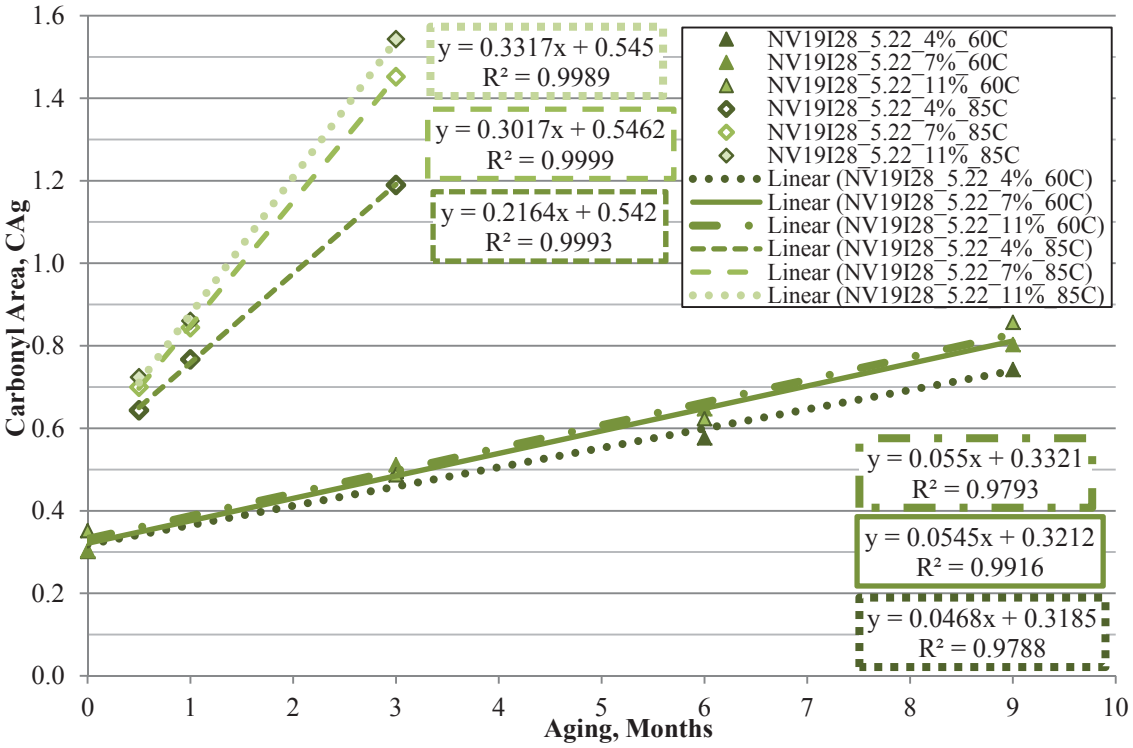

Figure 7.41 Carbonyl Growth Relationships for the NV19I28_5.22 Mixtures Aged at 60 and 85°C

General observations of the two figures clearly indicate the dramatic influence of the aging temperature on the growth rate of the CA measures as can be expected. The statistical analysis on the 60°C aged samples determined that the air void level did not significantly affect the intercept for either the California or Nevada mixtures. However, the slope was significantly influenced with the California mixtures. In contrast, general observations of the influence of the air void level seem to exhibit a more substantial influence when the mixtures were aged at 85°C. Indeed, when the regression analysis was repeated including both the 60 and 85°C aging on the California and Nevada mixtures separately as depicted in Table 7.20, both mixtures were significantly influenced by the level of air voids. Additionally, the slopes of the CA growth for both

mixtures were significantly affected by the aging temperature. The oxidation rate was not significantly influenced by the level of air as determined by the lack of statistical significance of the Age*Va term. However, similar to the analysis with the 60°C aging, this is suspected to be an inherent limitation of the data set. If the current trends (i.e. CA growth rates) continue as expected, then the significance of the discrepancy with air void level would continue to increase to the point where it would become statistically significant. Further, no information has been found to date to suggest that the oxidation rate of the asphalt binder should deviate from the current trends for reasonable levels of oxidation in the asphalt binder. It has been theoretically suggested that there should be an oxidation saturation point where the oxidation rate slows down. However, physical measurements during laboratory and field experiments have not yet supported such theories.

Table 7.20 Stepwise Regression on Carbonyl Area with Aging Time at 60 and 85°C for Mixtures with 9μm Apparent Film Thickness

	CAL19I22_7.44_60 & 85°C			NV19I28_5.22_60 & 85°C		
Regression Parameter	Coefficient	P-value	Significance	Coefficient	P-value	Significance
Intercept, β_0	0.1364	0.000	Sig.	-0.3441	0.002	Sig.
Age (Slope, β_1)	-0.4034	0.000	Sig.	-0.4918	0.000	Sig.
Air Voids, Va	0.0225	0.000	Sig.	0.0171	0.000	Sig.
Age*Temp	0.0075	0.000	Sig.	0.0091	0.000	Sig.
Temp.	N/A	N/A	NS	0.0090	0.000	Sig.
R^2 (%)	93.9			96.9		
Adj. R^2 (%)	93.3			96.6		

It should be noted that the stepwise regression analysis on the California mixtures found the aging temperature not to be a significant parameter (P-value = 0.089) at the 0.05 significance value. As a result, the omission of the aging temperature from that analysis resulted in minimal reduction in the overall R^2 (i.e. about 0.4%) producing the final statistical model presented in Table 7.20.

7.2.7 Summary of Mixture-Aged Asphalt Binder Oxidation Results

The previous sections presented the investigation into which aggregate and mixture properties proved most influential to rate of oxidation of the asphalt binders aged in an asphalt mixture aged at two temperatures (i.e. 60 and 85°C). This analysis was largely based upon quantification of the oxidation level by the carbonyl area (CA) measured through Fourier-transform infrared spectroscopy on extracted and recovered binders from the aged mixtures.

A summary of the included aggregate and mixture parameters considered in this analysis is provided in Table 7.8. The following Table 7.21, presents a summary of which parameters were found to be significant in any of the statistical analyses. The table also includes a reference to which section of this chapter was used to make the significance determination for each respective input parameter.

Table 7.21 Summary of Influential Mixture Factors on Carbonyl Area as Function of Aging Time

Input Variable	CA value (Intercept)	CA Rate (slope)	Analysis Reference
Abs	Sig.	NS	7.2.4
Pbe	Sig.	Sig.	7.2.3, 7.2.4, 7.2.5
VFA	Sig.	NS	7.2.3, 7.2.5
DP	Sig.	NS	7.2.4, 7.2.5
CAAT	Sig.	NS	7.2.3, 7.2.5
BI	Sig.	NS	7.2.3, 7.2.5
Va	Sig.	Sig.	7.2.2, 7.2.6
Temp.	Sig.	Sig.	7.2.6

The results of Section 7.2 as summarized in Table 7.21 indicate that rate of oxidation of asphalt binders can be significantly influenced by the effective asphalt binder content (Pbe), the air void (Va) level of the asphalt mixture during aging, and the temperature during the oxidation of the evaluated asphalt mixtures.

The magnitude or overall level of oxidation was, in certain circumstances, affected by those parameters as well as the aggregate absorption (Abs), the calculated voids filled with asphalt (VFA), the calculated dust proportion (DP), the coarse aggregate angularity and texture (CAAT) measured with the AIMS device, and the asphalt binder grade (BI). In this particular instance, the BI term differentiates between the PG 64-22 and PG 64-28 asphalt binders. Due to their relative similarities, the majority of the noted differences are assumed to be appropriately attributed to the polymer modification of the PG 64-28 binder.

7.3 Mixture-Aged Asphalt Binder Rheological Measurements

Similar to the pan-aged asphalt binders, the extracted and recovered mixture-aged binders were subjected to the frequency sweep testing which were used to develop the binder master curves as part of the rheological assessment of the asphalt binders. This assessment will be conducted in a similar manner as with the pan-aged asphalt binders specifically referencing the test conditions found in Table 7.5. Recalling that the main focus of the mixture-aged analysis was conducted with the PG 64-22 and PG 64-28 asphalt binders, with a select few from WesTrack included, the rheological test conditions noted in Table 7.5 were maintained with respect to each asphalt binder grade. Further, the rheological measures were shifted into master curves at a reference temperature of 60°C which were fit to the CAS model with Rhea software package. The fitted CAS model parameters were then utilized to create the black space plots considered in this analysis.

Similar to the pan-aged binder analysis, the black-space plots will be considered to present the rheological measures of the extracted and recovered asphalt binders. Certain comparisons will be made in the following sections, while a summary of the dynamic shear modulus (G^*) master curves and the associated black space plots are provided in Appendix K. Additionally, a summary of the CAS model parameters for the respective measures is provided in Appendix L.

7.3.1 Mixture Air Void Level

Since significant changes were noted in the mixture-aged oxidation measurements of the asphalt binders due to variations in the air void level, the influence of the air void level on the rheological measurements will be assessed. Similar to the pan-aged analyses, the rheological measures of the mixture-aged and subsequently extracted and recovered asphalt binders will generally be considered in terms of the black space plots.

The first comparison will be made with the California aggregate source mixed with the PG 64-22 asphalt binder aged at 60°C with 4, 7, and 11% air voids. General reference is made to Figure 23.1 through Figure 23.6 of Appendix K for the full set of master-curve and black space plots which are summarized by the black space plot of Figure 7.42.

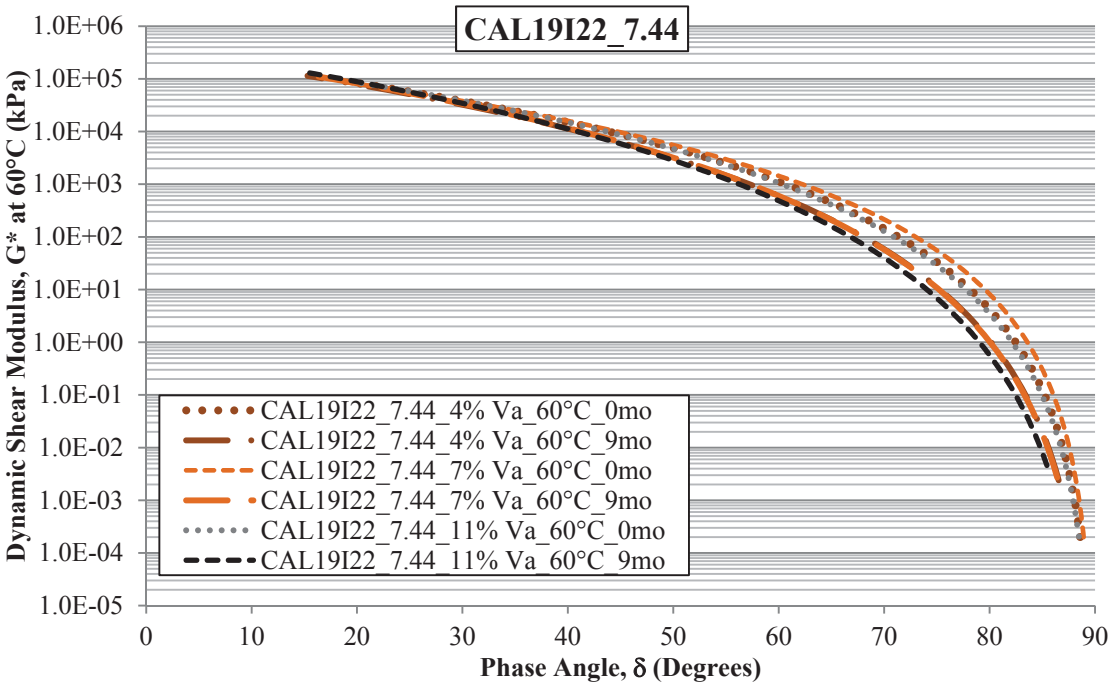

Figure 7.42 Black Space Plots for CAL19I22_7.44 Mixtures Aged at 60°C with 4, 7, and 11% Air Voids

For ease of data presentation, only the measurements from the extracted and recovered binders of the zero and nine month aged specimens are presented in Figure 7.42. Figure 23.1 through Figure 23.6 also show a general shift in the black space plot, generally toward lower phase angles as a function of aging duration with each of the air void levels. Figure 7.42 presents a relative comparison of all three air void levels, noting the general similarities in the black space relationships of the zero month aged mixtures. The relative similarities continue with the measurements of the nine month mixture-aged binders. Recall from the oxidation kinetics measurements that the oxidation levels of the respective mixtures were noticeably different relative to the air void level. However, the binder rheological measures exhibited much less variation as a function of the air void level over the same aging durations. This is not to state that each of the asphalt binders were not aged or stiffened over the nine month duration in the 60°C oven, but merely their black space representation did not shift significantly. As indicated in Figure 7.43, the G^* master curves as a function of frequency to clearly display the overall differences in the shear modulus values of the respective binders.

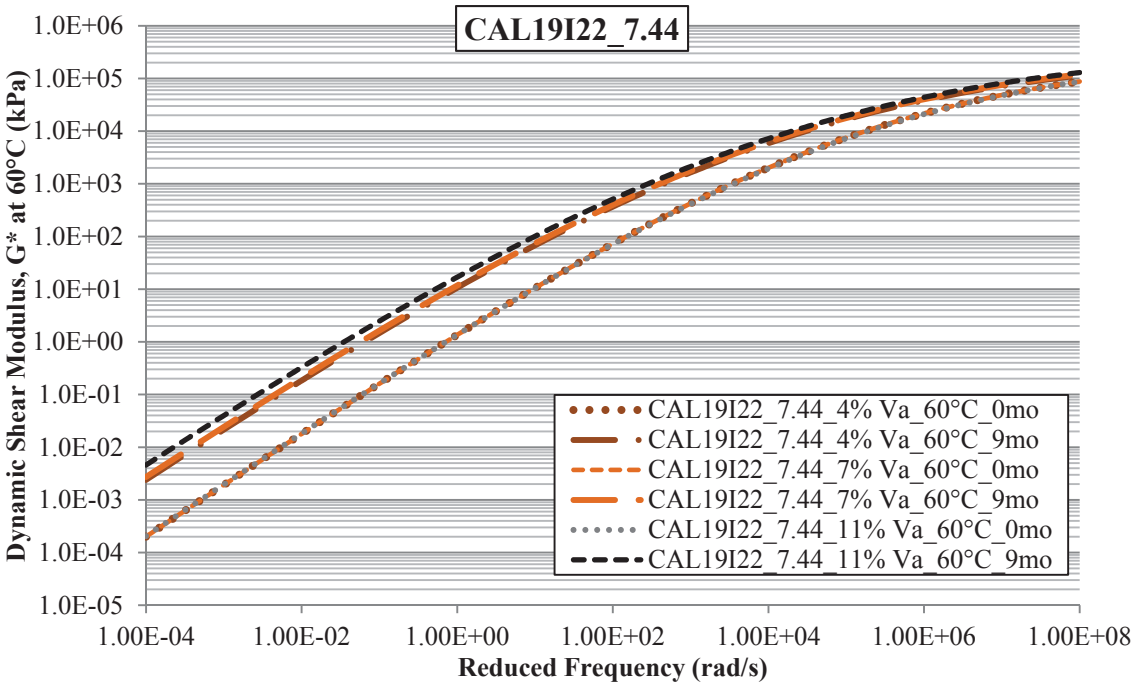

Figure 7.43 Summary of Dynamic Shear Modulus Master Curves for CAL19I22_7.44 Mixtures Aged at 60°C with 4, 7, and 11% Air Voids

The comparative data presented in Figure 7.43 show that the binders do, in fact age appreciably in the mixtures. Further, the example G^* master curve relationships presented in Figure 7.43 also indicate the similarities in the zero month aged samples (i.e. short term aged only), as compared to the systematic increase in the G^* master curve with aging as a function of the respective air void level of the mixtures.

Therefore, the oxidation of the PG 64-22 binder generally led to a reduction in the phase angle for a given stiffness value (G^*) as a function of aging with some increase in the stiffness noted with the air void level at a given aging duration. In other words, oxidation caused the binder to increase in stiffness and loses some of the measured flexibility with oxidation.

Figure 7.44 presents the black space plots of the Nevada aggregates mixed with the PG64-28 asphalt binder as a function of aging time at 60°C and air void level.

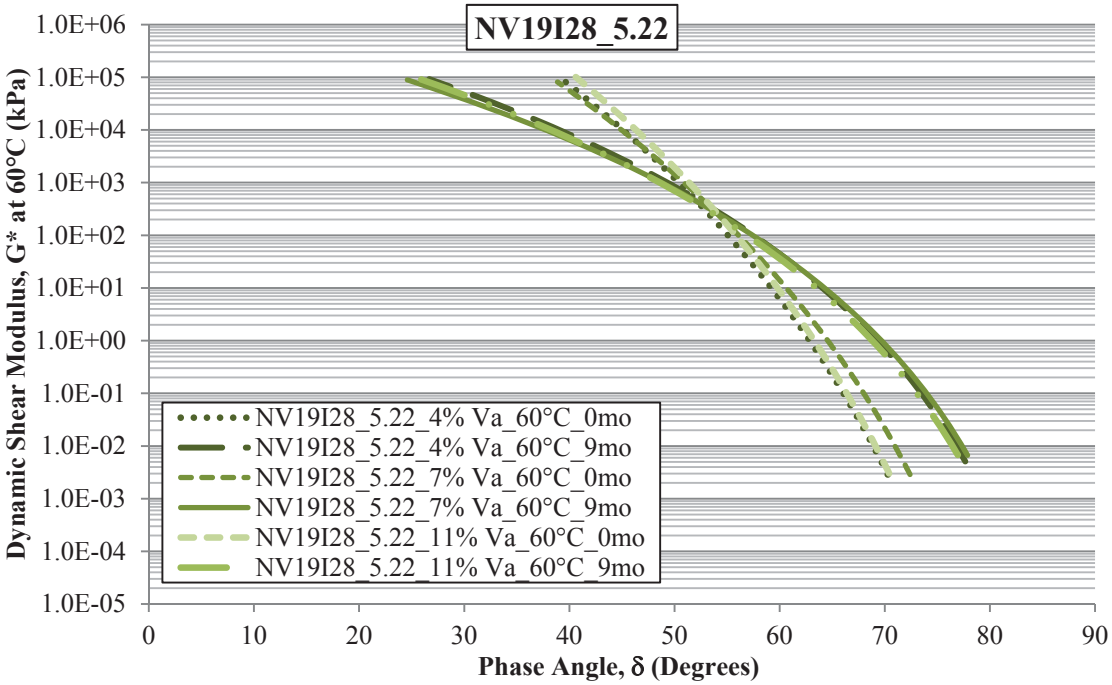

Figure 7.44 Black Space Plots for NV19I28_5.22 Mixtures Aged at 60°C with 4, 7, and 11% Air Voids

From the figure it is clear that the polymer modification has some influence on the aging of the binder, particular in the black space representation. Similar to the measurements of the polymer modified pan-aged binders, the mixture-aged SBS modified binders also exhibits a rotation not just the lateral translation as was the case for the PG 64-22 binder previously. Referencing Figure 23.31 through Figure 23.36 found in Appendix K, the black space representation of the shifted master curves all exhibit the same rotation with increased levels of aging. This is accompanied by the clear increase in the G^* master curves as a function of reduced frequency. However, not only does the measured value

of G^* increase with aging, the curvature of the master curves also increase. The increase in the curvature in this case signifies the initiation of glassy or more brittle behavior at lower reduced frequencies. This is evidenced by the general decrease in both the fitted glassy modulus (G_0) and the crossover frequency (ω_0) presented in Table 24.3 of Appendix L. While the decrease in G_0 may initially seem to indicate a softening of the binder, it should be clarified that this is the result of the combined effect of the reduced curvature and the higher ω_0 indicating much higher frequencies are necessary to produce similar glassy behaviors with the lesser aged binders. Thus, the increased curvature (i.e. at the reference temperature of 60°C) and the general reduction in the phase angle produce the combined effect of the rotation of the black space representation of the respective master curves.

There are some subtle differences noted in the final black space representation noted with the variation in air void level. However, it is important to recall the dramatic differences noted in the level of oxidation observed as a function of the air void level in the mixtures during aging. Thus, the combined effect will be considered in the following section relative to the measured hardening susceptibility of the respective mixture-aged asphalt binders.

Figure 7.45 presents the rheological measurements of the mixture with Utah aggregates and the PG 64-28 asphalt binder aged with different air void levels at 60°C.

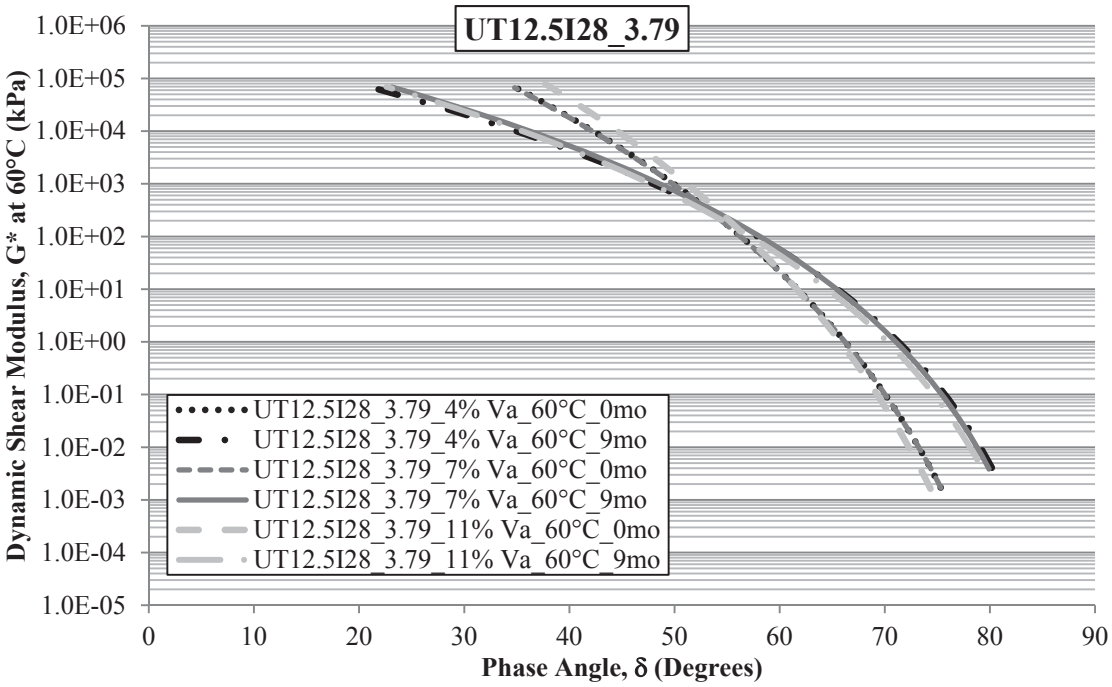

Figure 7.45 Black Space Plots for UT12.5I28_3.79 Mixtures Aged at 60°C with 4, 7, and 11% Air Voids

The Utah aggregates in Figure 7.45 present nearly the same overall behavior as the Nevada mixtures. The same rotation of the black space representation is observed again with the similar magnitude of the black space plots relative to the air void level. The binders extracted and recovered from the Utah mixtures did tend to have a more systematic variation compared to the Nevada mixtures. Specifically the 11% air void mixtures are consistently the furthest in terms of a clockwise rotation of the black space representation of the master curves for a given aging condition. Similarly, the measurements from the 4% air void mixtures are the furthest in a counter-clockwise rotation for a given aging condition. Thus, placing the measurements from the 7% air voids partially in between with the overall rotation of the black space representations moving in a counter clockwise rotation.

Figure 7.46 presents the rheological measurements of the WesTrack aggregates mixed with the respective WesTrack PG64-22 asphalt binder, both from 1997 aged with different air void levels at 60°C.

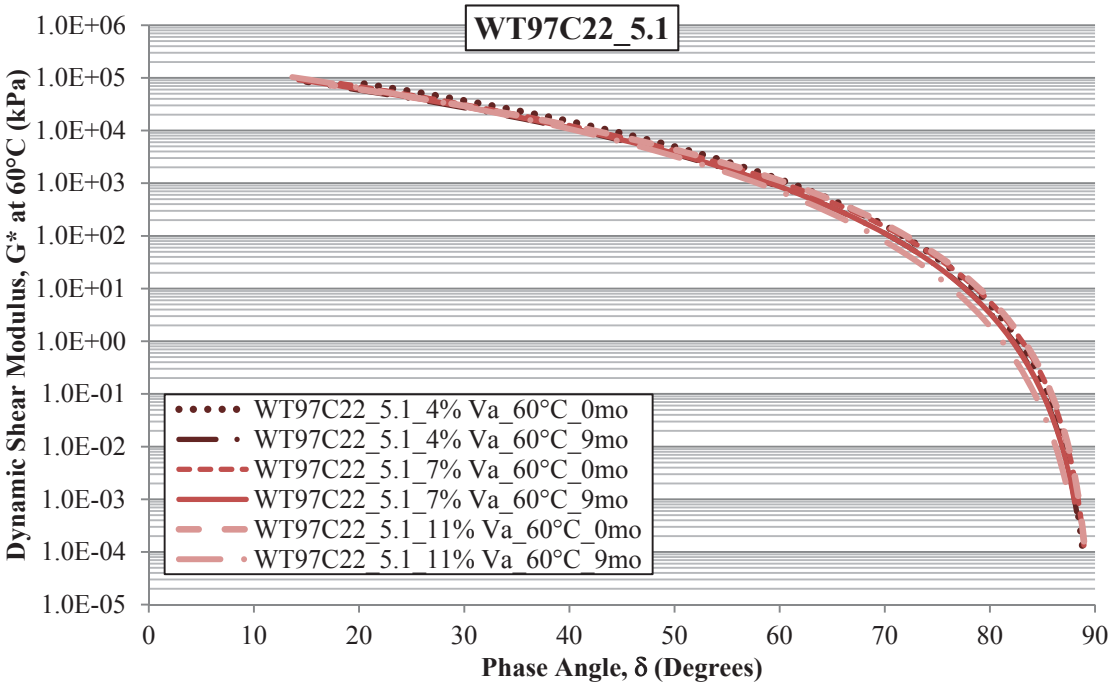

Figure 7.46 Black Space Plots for WT97C22_5.1 Mixtures Aged at 60°C with 4, 7, and 11% Air Voids

Observations of the binder master curves of the extracted and recovered binders obtained from the WesTrack mixtures from 1997 aged at different air void levels at 60°C in the black space representation present nearly identical relationships for all mixtures regardless of the aging or air void level. This clearly does not suggest that the binders have not been oxidized as indicated by the G^* master curves presented in Figure 23.53 though Figure 23.58 of Appendix K. In those figures, observations of the G^* plots readily indicate the increase in the stiffness of the binder by the increase in the measured

G^* values as a function of the reduced frequency. So clearly, the binder are becoming more oxidized with aging time as should be expected. Figure 7.47 presents the G^* master curve relationships as a function of reduced frequency.

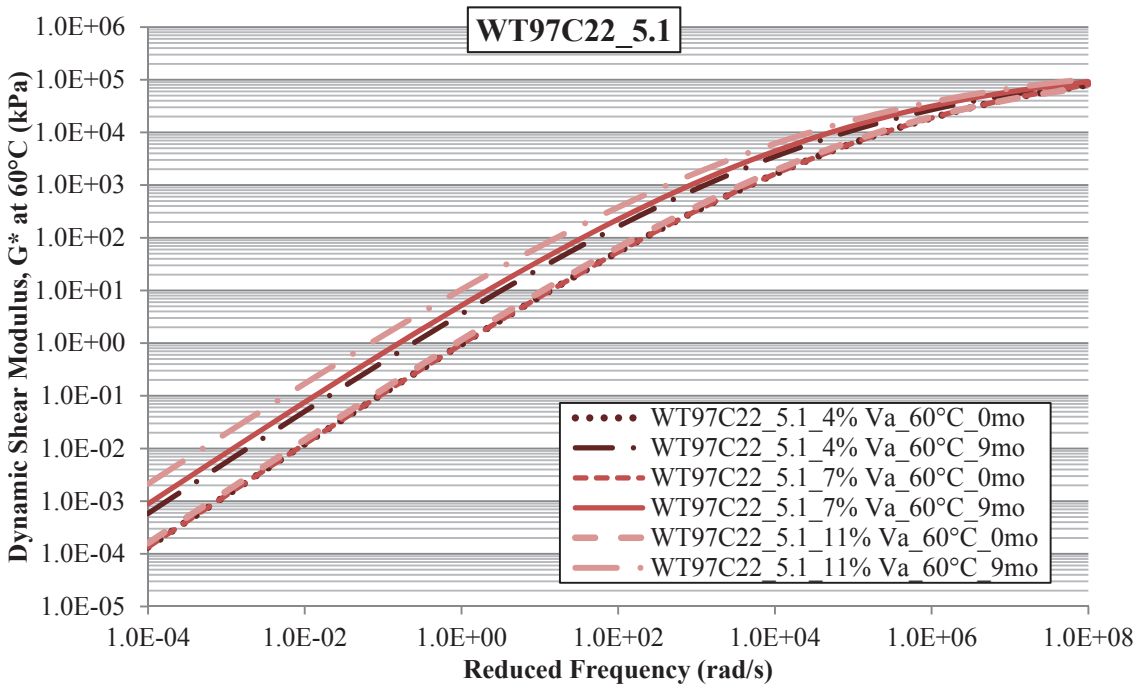

Figure 7.47 Summary of Dynamic Shear Modulus Master Curves for WT97C22_5.1 Mixtures Aged at 60°C with 4, 7, and 11% Air Voids

Figure 7.47 clearly shows that the mixtures are indeed stiffening in a systematic order with the air void level of the mixtures. Therefore, the black space representation should not be interpreted as a lack of stiffening in the mixture-aged binders, but should serve to highlight the fact that solely observing the master curves in the black space plots do not directly indicate the influence of the tested or shifted (i.e. reduced) frequencies. They do however, provide information regarding the stiffness (i.e. G^*) in relation to a representation of flexibility or viscous response (i.e. phase angle).

In general, the influence of the air void level was not dramatically evident in the black space plots measured on the extracted and recovered binders from mixtures with different air void levels aged at 60°C. However, some systematic variations were noted with most of the measured binders particularly when the G^* master curves as a function of the reduced frequency found in Appendix K are considered. It is important to recall the significant differences noted in the level of oxidation observed in the previous section 7.2. Therefore, the combined effect of the variations noted in the oxidation levels and minor differences observed with the rheological measures will be combined in the respective section focusing on the hardening susceptibilities of the respective mixture-aged asphalt binders.

7.3.2 Asphalt Binder Content

The evaluation of the influence of the asphalt binder content on the rheological measures of the extracted and recovered asphalt binders was again considered directly with the Colorado and Nevada mixtures produced with two asphalt binder contents using both the PG 64-22 and PG 64-28 asphalt binders.

Figure 7.48 and Figure 7.49 present the rheological measures of the extracted and recovered binder from the Nevada mixtures for the constant binder content of 4.5% TWM and the binder content to obtain the calculated 9μm AFT for the zero and nine month aging durations with the PG 64-22 and PG 64-28 asphalt binders, respectively.

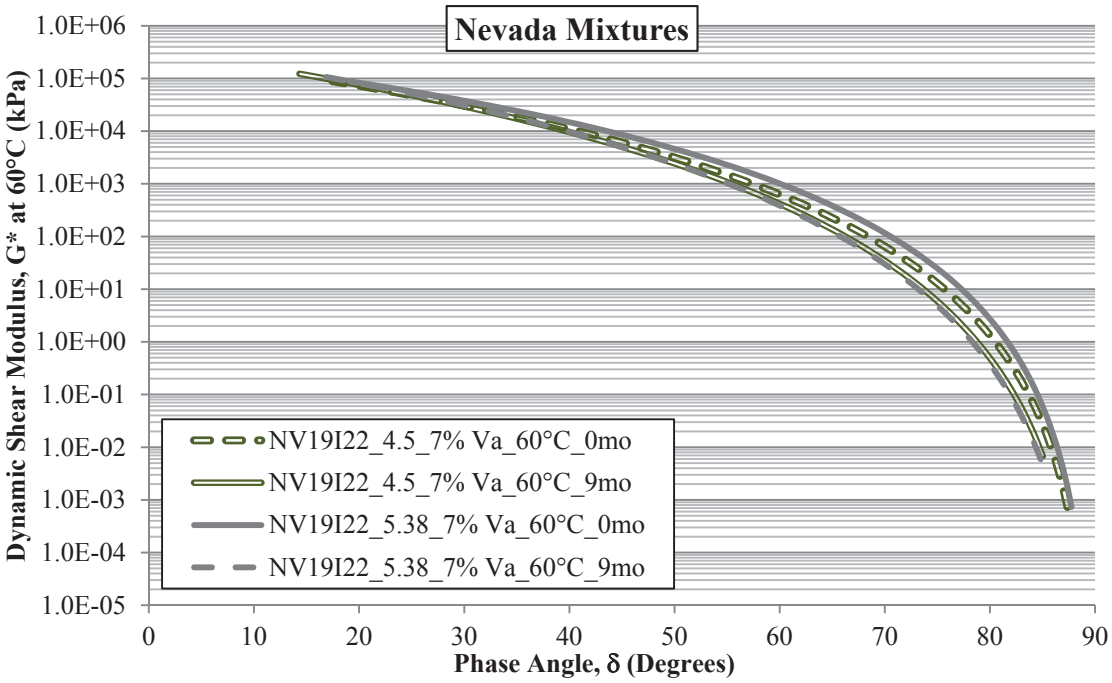

Figure 7.48 Black Space Plots for Nevada Mixtures with PG 64-22 Binder Different Binder Contents Aged at 60°C

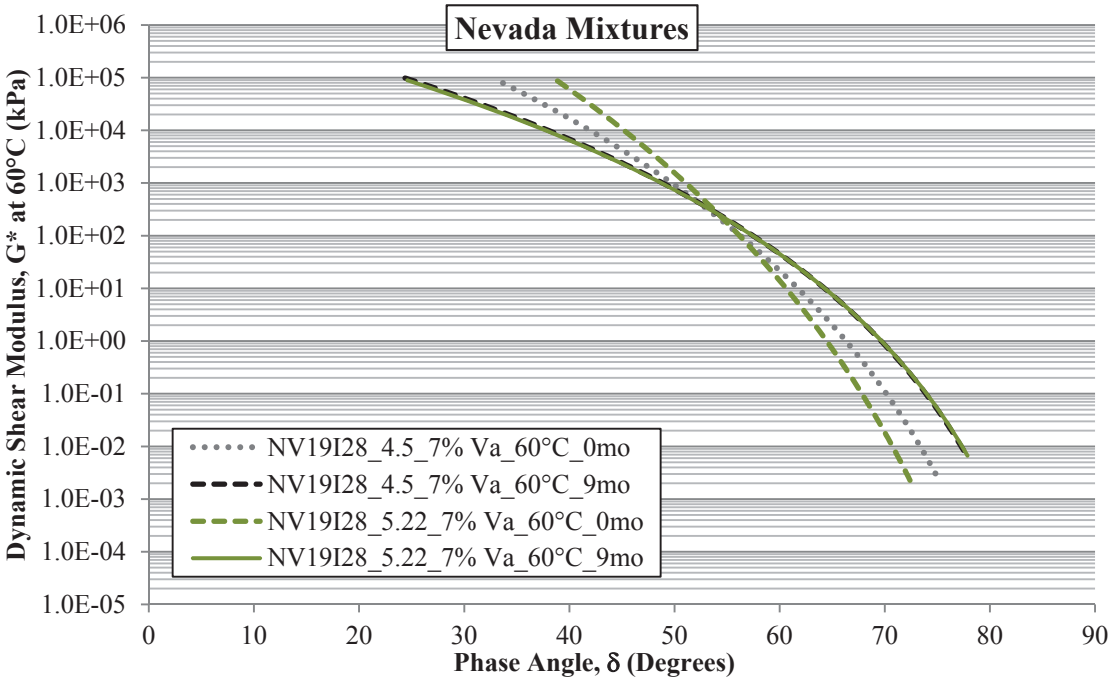

Figure 7.49 Black Space Plots for Nevada Mixtures with PG 64-28 Binder Different Binder Contents Aged at 60°C

Similar trends to those already noted in the air void evaluation are noted for the respective asphalt binders mixed with the Nevada aggregates. Specifically, the mixtures containing either of the binder contents with the PG 64-22 binder generally exhibits the lateral translation of the black space plot to the left with increases in the oxidation level of the binder. Though they appear quite similar in magnitude, the shift of the mixture with the higher binder content (i.e. 5.38% TWM) appears to be a little larger than that of the lower binder content (i.e. 4.5% TWM).

Considerations of the Nevada mixtures with the PG 64-28 binder presented in Figure 7.49 show similar trends to those noted previously with the modified binder. The same counter-clockwise rotation of the black space representation of the measured binder master curves from the mixture-aged binders was observed, again with the higher binder content showing the largest movement in the black space representation as was noted with the mixtures containing the unmodified PG 64-22 binder.

Figure 7.50 and Figure 7.51 present the rheological measures of the extracted and recovered binders from the Colorado mixtures aged with the constant binder content of 4.5% TWM and the binder content to obtain the calculated 9μm AFT for the zero and nine month aging durations with the PG 64-22 and PG 64-28 asphalt binders, respectively.

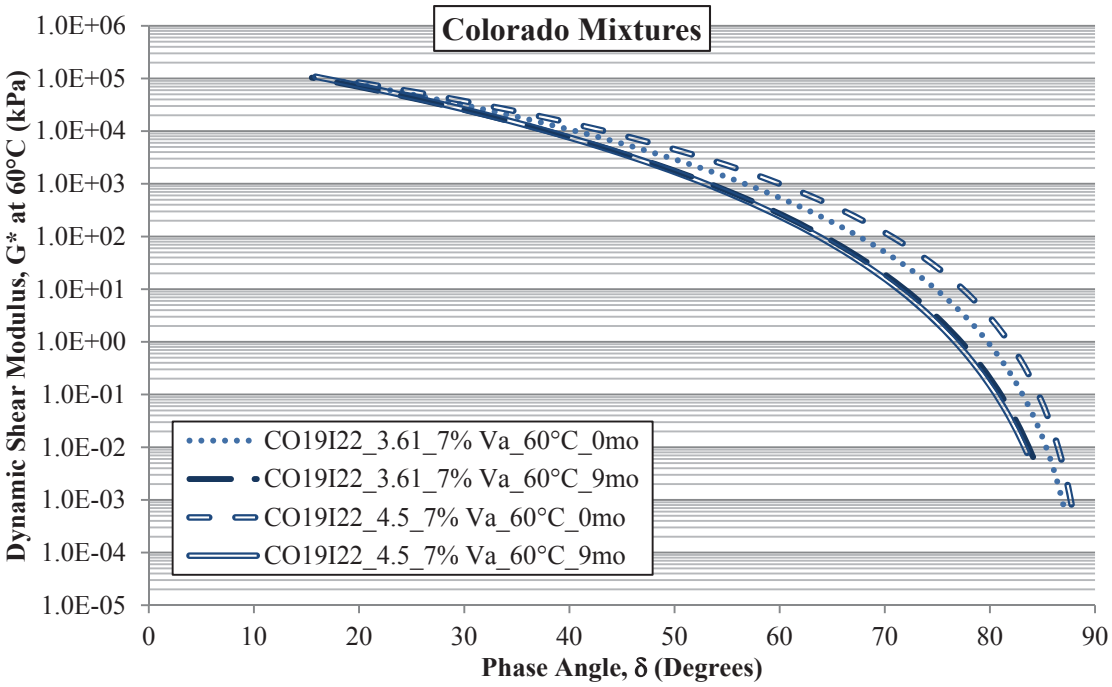

Figure 7.50 Black Space Plots for Colorado Mixtures with PG 64-22 Binder Different Binder Contents Aged at 60°C

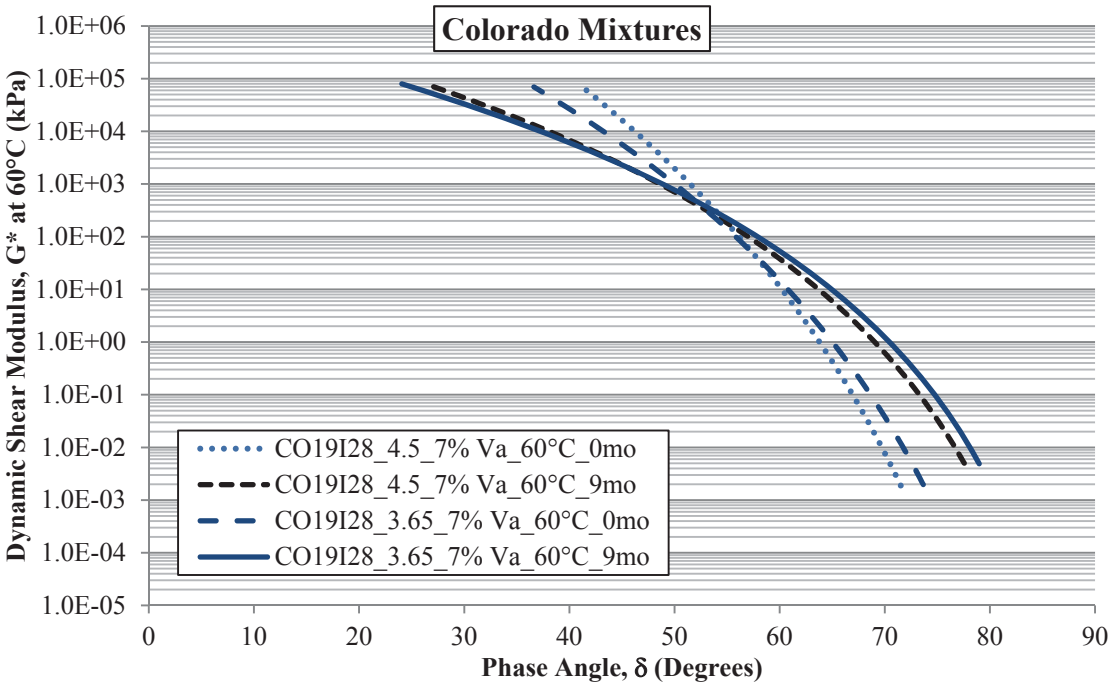

Figure 7.51 Black Space Plots for Colorado Mixtures with PG 64-28 Binder Different Binder Contents Aged at 60°C

Considering the black space plots of the Colorado mixtures with the unmodified PG 64-22 binder of Figure 7.50, gives rise to an aging behavior very similar to what has been observed with the previous rheological measures of the mixture-aged binders in this section. The same leftward translation is noted as well as the magnitude of the shift remained the greatest with the mixture containing the higher binder content (i.e. 4.5% TWM).

Similar considerations of the black space plots of the Colorado mixtures with the modified PG 64-28 binder of Figure 7.51 also indicate a generally similar response to the aging with a counter-clockwise rotation of the black space representations. Due to the initial offset between the two binder contents at the zero month aging condition, it is difficult to accurately assess which binder content presents the largest overall shift, but there are some slight indications that the higher binder content (i.e. 4.5% TWM) may again exhibit the largest shift, at least by a slight margin.

Figure 7.52 through Figure 7.55 present the rheological measures of the extracted and recovered binders from the Colorado and Nevada mixtures aged with the constant binder content of 4.5% TWM at the zero and nine month aging durations with both the PG 64-22 and PG 64-28 asphalt binders including within aggregate source and within binder source comparisons.

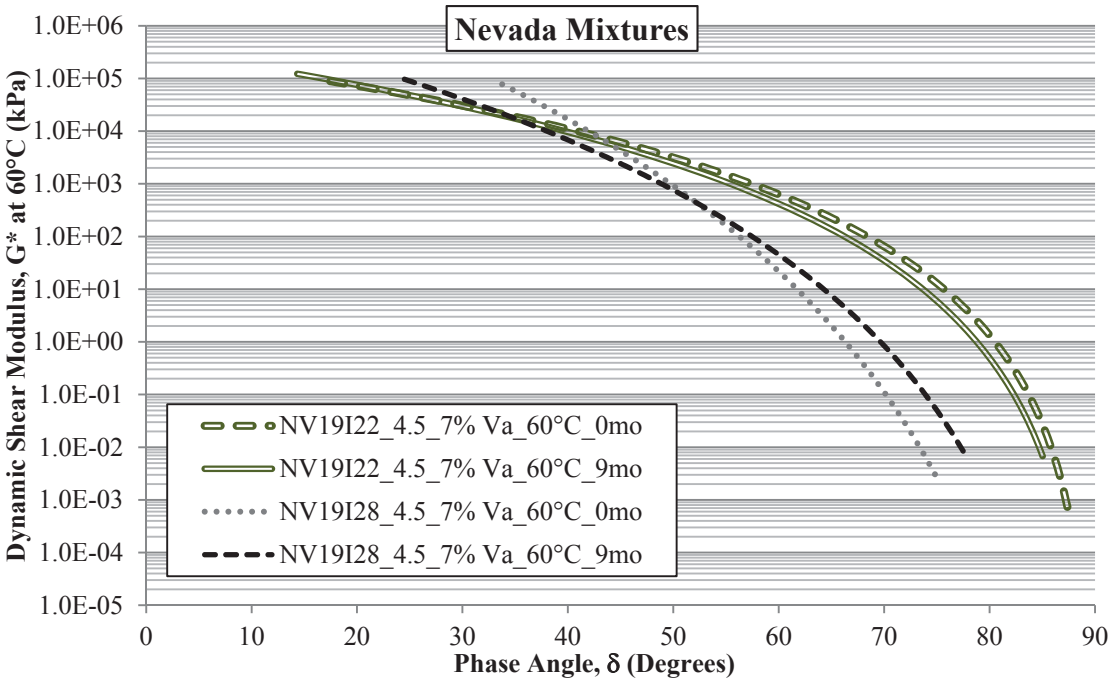

Figure 7.52 Black Space Plots for Nevada Mixtures with 4.5% TWM Asphalt Binder Content Aged at 60°C

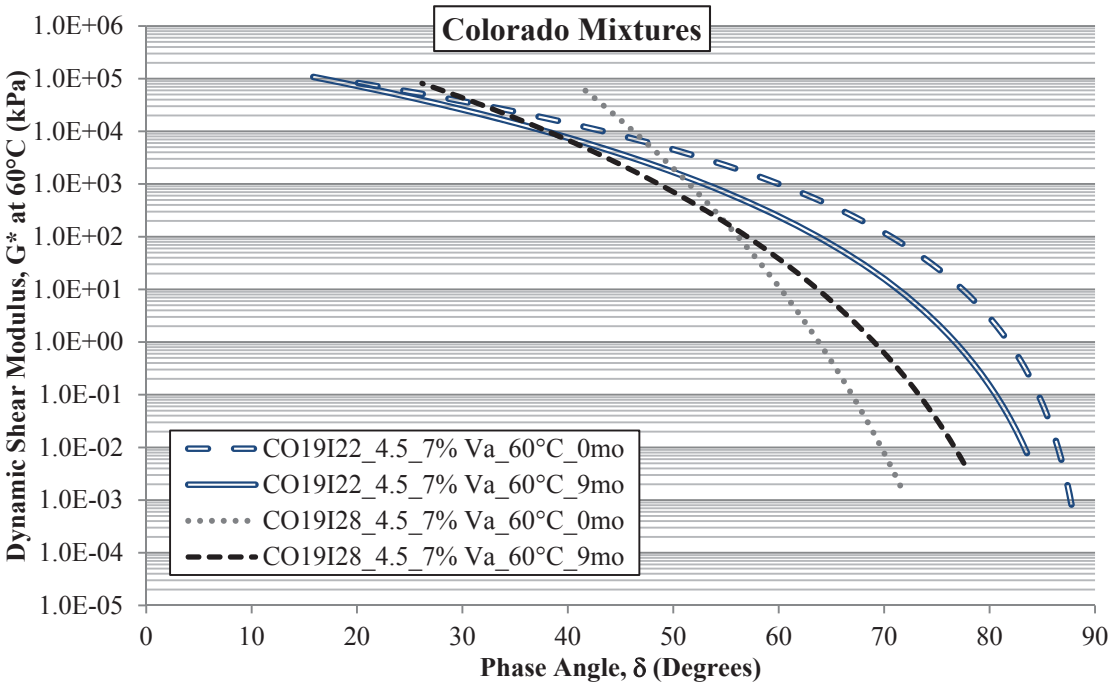

Figure 7.53 Black Space Plots for Colorado Mixtures with 4.5% TWM Asphalt Binder Content Aged at 60°C

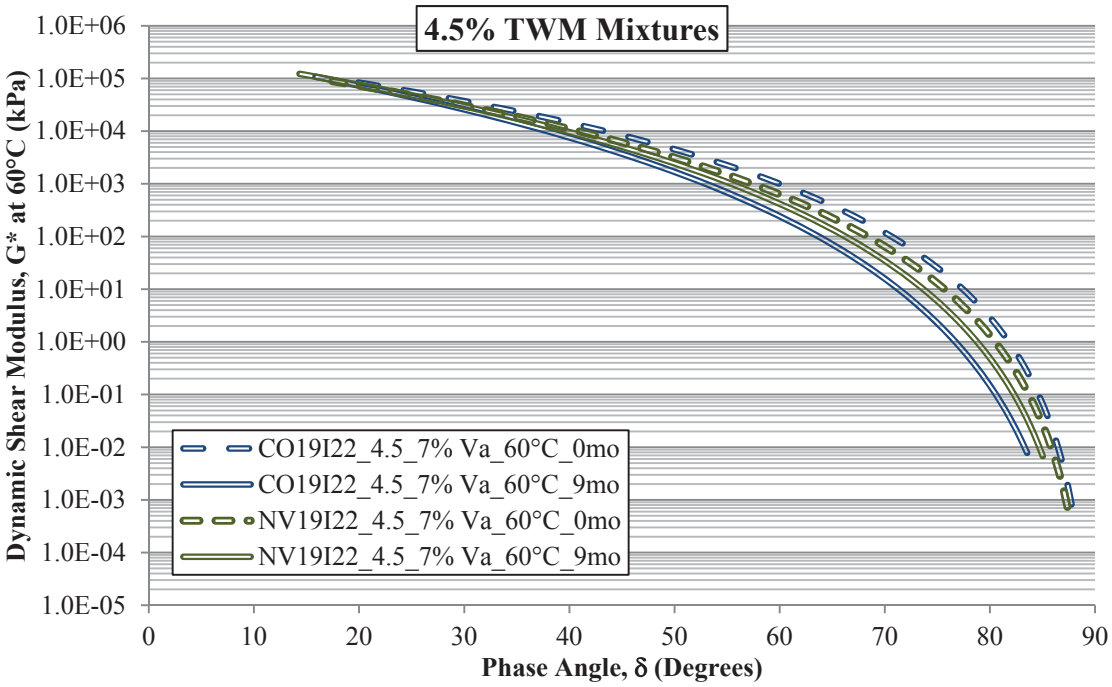

Figure 7.54 Black Space Plots for Mixtures with 4.5% TWM with PG 64-22 Asphalt Binder Aged at 60°C

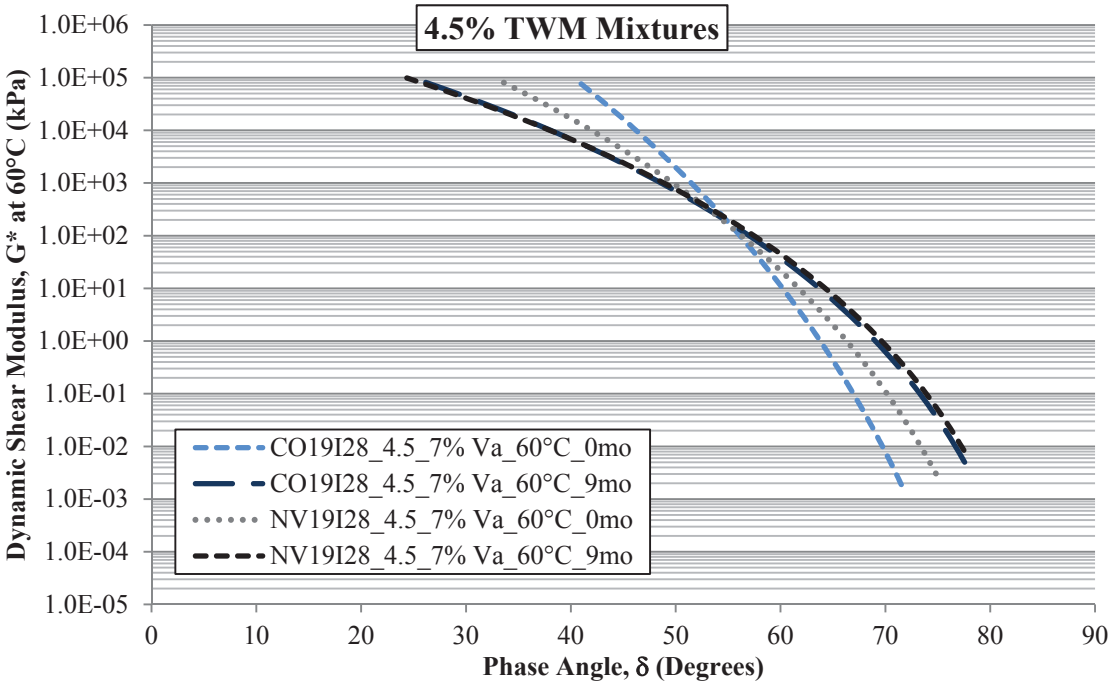

Figure 7.55 Black Space Plots for Mixtures with 4.5% TWM with PG 64-28 Asphalt Binder Aged at 60°C

Figure 7.52 and Figure 7.53 provide evidence that while the properties of the asphalt binder may be the most significant factor influencing the oxidation process of asphalt mixtures, there is also some influence introduced by the mixtures or aggregates as well. Considering the magnitude of the leftward shifting of the PG 64-22 binder curves in Figure 7.54 indicates that the exact same binder at the same binder content within the mixture does not necessarily produce the same rheological measures of the extracted and recovered binders. Again, this particular assessment has intentionally excluded the chemical measures of the oxidation level (i.e. FT-IR measures), but was focused on the rheological and stiffness measures. It is generally noted that the magnitude of the shift in the black space plots with the Colorado aggregates is substantially larger than that of the Nevada mixtures.

By a similar comparison in Figure 7.55, a similar observation is made with the mixtures containing the PG 64-28 asphalt binder. Though the final measures of the nine month aged specimens are relatively the same, the measures from the two aggregate sources initially did not exhibit the same relationship (i.e. zero month aging). This observation necessitates that the changes during the aging process differ from each other as well. Similar to the mixtures containing the unmodified PG 64-22 binder, this comparison also indicates that the smaller change in the black space representation of the binder master curve occurred with the Nevada mixtures.

In general, the influence of the asphalt binder type (i.e. unmodified compared to polymer modified) was again found to significantly influence the rheological measures on the asphalt binder as a function of the oven aging duration. Additional considerations also found the binder content to be a contributing factor to the overall change in the

rheological measures of the extracted and recovered binders from different mixtures. The aggregate sources themselves were also noted to exhibit discrepancies between mixtures with the same asphalt binder content. However, this portion of the investigation only included two aggregate sources (i.e. Colorado and Nevada), thus exploration into the specific cause of this variation was not plausible.

7.3.3 Qualitative Gradation

The investigation into the influence of the qualitative gradation was conducted on the California aggregates with the PG 64-22 asphalt binder and on the Nevada and Utah aggregates with the PG 64-28 asphalt binder. These mixtures were prepared at the respective asphalt binder contents to yield the 9 μm AFT determined from the respective mix design for each mixture. This produced different total asphalt binder contents for each mixture dependent upon the influence of the aggregate gradation, the respective surface characteristics calculated for each mixture, as well as the changes in the absorption of each aggregate source.

Figure 7.56 presents a summary of the black space plot of the binders extracted and recovered from the California aggregates for the intermediate and fine gradations after aging at 60°C for zero and nine month durations.

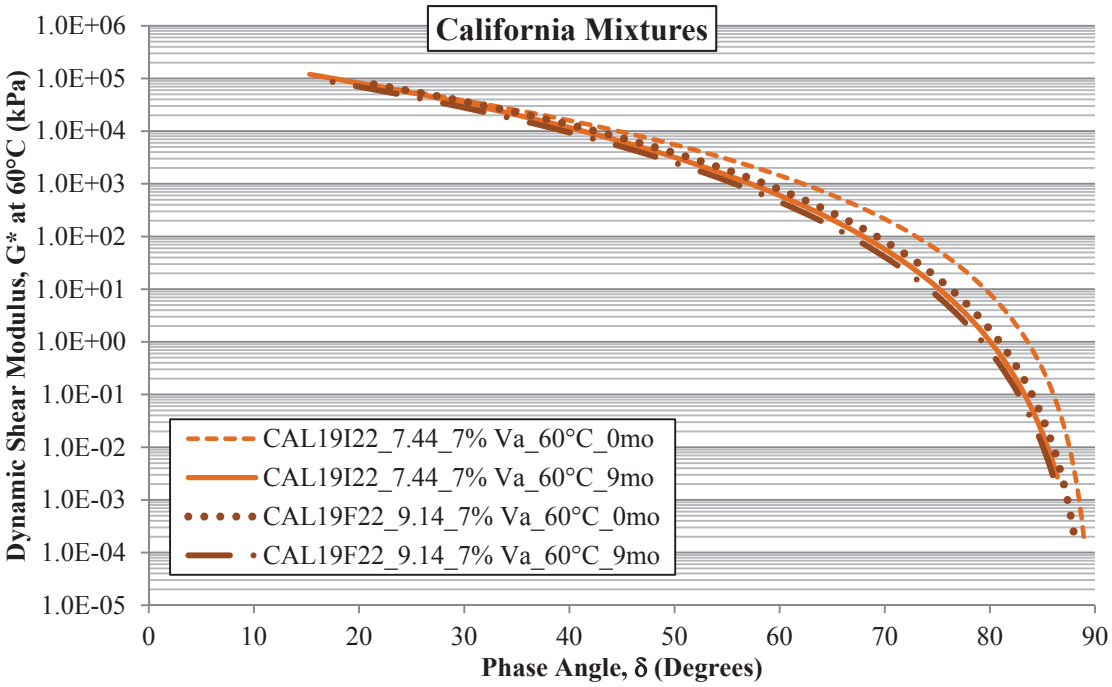

Figure 7.56 Black Space Plots for California Mixtures with Different Qualitative Gradations Aged at 60°C

The relative comparison between the intermediate and fine gradation of the California aggregates with the PG 64-22 asphalt binder presented in Figure 7.56, indicates a general shift in the black space representation between the respective mixtures. From this representation, it appears that the fine gradation was not as influenced by the aging duration compared to the intermediate gradation. However, Appendix K provides reference to Figure 23.3 and Figure 23.4 compared to Figure 23.15 and Figure 23.16 suggests that the apparent difference noted here may not be as prominent as it appears. Figure 23.4 depicts the black space representation of all four aging durations of the intermediate gradation and notes that the zero month mixture is fairly different from the other three durations, which are quite similar to one another. By comparison, Figure 23.16 indicates that all of the relationships from the fine mixture are fairly similar, but

systematically vary with the aging duration. Further consideration of these relative differences is observed by comparing Figure 23.3 and Figure 23.15, which suggest as far as the G^* master curves are concerned, the aging level may be fairly similar. As a result, rather than provide judgment based upon one set of data, it may be prudent to observe the other mixtures for further clarification on this analysis.

Therefore, Figure 7.57 and Figure 7.58 present the relative comparisons between the intermediate and fine gradations with the Nevada and Utah aggregate sources mixed with the PG 64-28 asphalt binder.

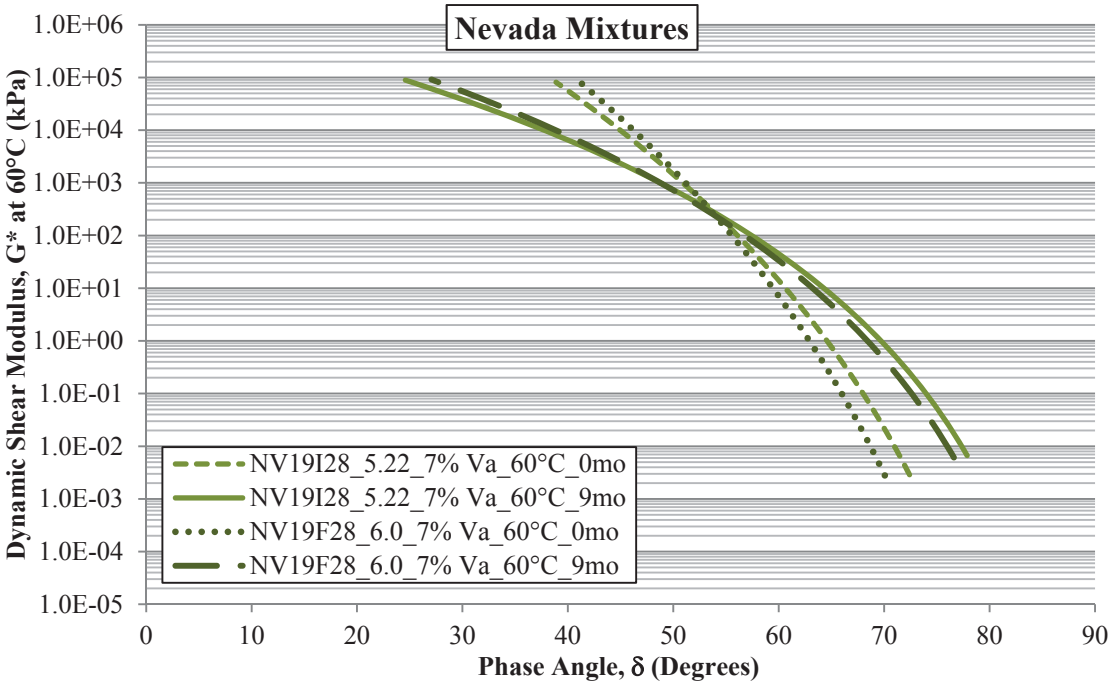

Figure 7.57 Black Space Plots for Nevada Mixtures with Different Qualitative Gradations Aged at 60°C

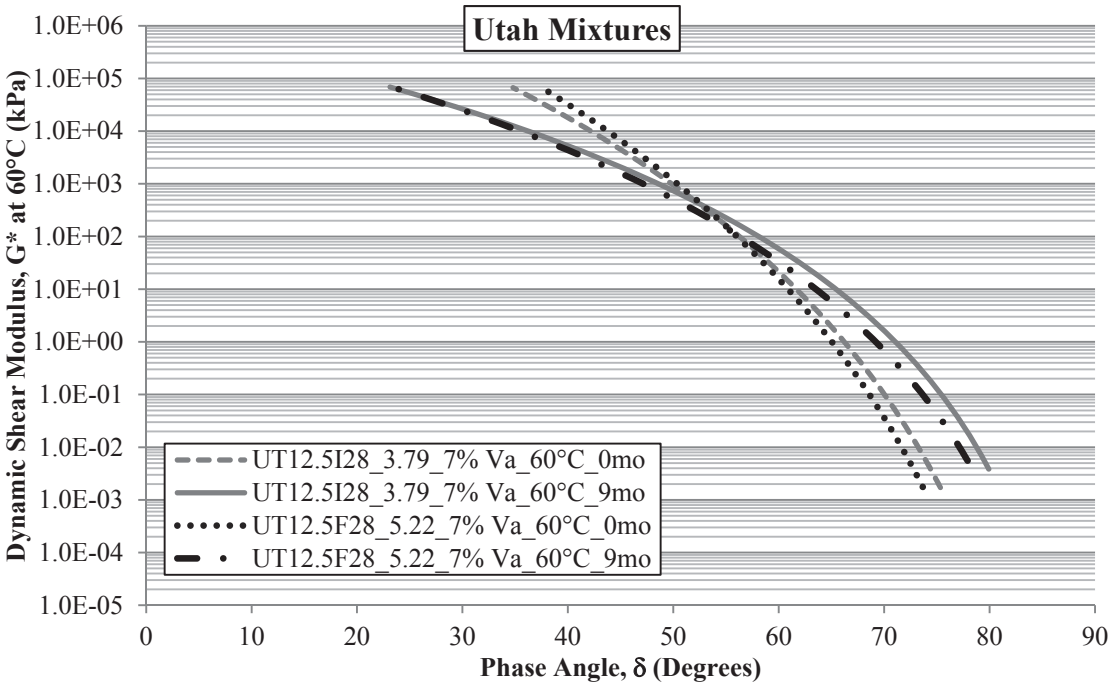

Figure 7.58 Black Space Plots for Utah Mixtures with Different Qualitative Gradations Aged at 60°C

Consideration of the qualitative gradation from the mixtures containing the PG 64-28 asphalt binder suggests that the overall magnitude observed in the shifting of the black space representations are fairly similar between the two gradation levels evaluated. It has been noted that the fine gradations typically exhibit a further clockwise rotation as compared to the intermediate gradation. However, the difference between the zero and nine month ageing durations is largely the same with respect to the qualitative gradation.

The additional rotation of the black space plots has also been observed as a function of the aging level with the PG 64-28 asphalt binder. In this regard, general observations of Figure 7.36 and Figure 7.37 from the mixture-aged oxidation analysis suggests that the fine gradations tend to increase the rate of CA growth for a given aggregate source with the California and Utah aggregates, but not with the Nevada mixtures. Thus the variation

in the rheological measures with the California and Utah mixtures may potentially be the result of differences in the oxidation level, however the Nevada mixtures suggest otherwise. Further consideration of this interaction will be considered in terms of the HS parameters in the coming sections.

7.3.4 Constant Film Thickness

Further investigations into the impact of the mixture and aggregate characteristics on the rheological measurements of the mixture-aged binders were performed with mixtures prepared at the total asphalt binder content determined to provide a constant AFT of 9 µm. Figure 7.59 through Figure 7.61 present the respective black space representation for those mixtures with the PG 64-22 and PG 64-28 asphalt binders.

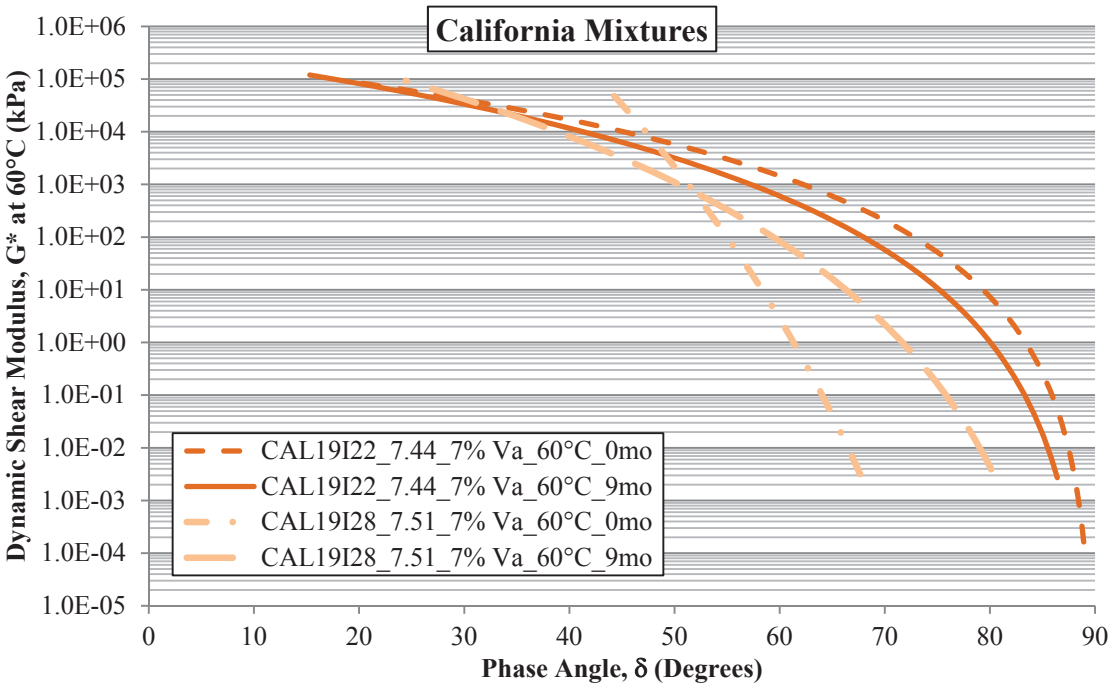

Figure 7.59 Black Space Plots for California Mixtures with Constant Apparent Film Thickness Aged at 60°C

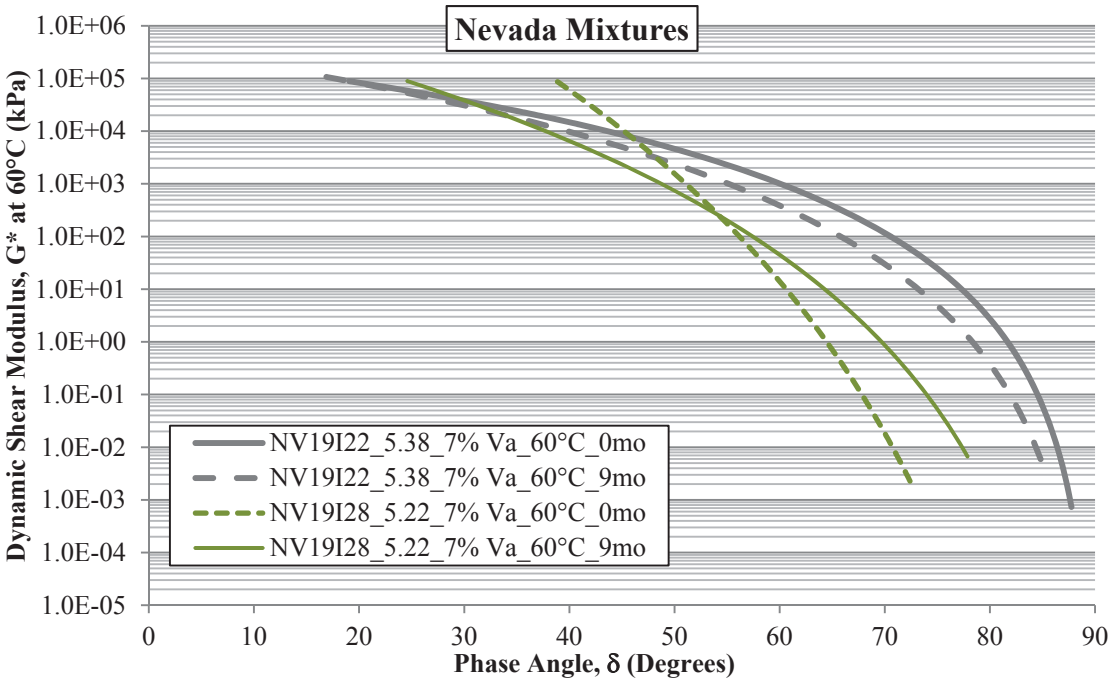

Figure 7.60 Black Space Plots for Nevada Mixtures with Constant Apparent Film Thickness Aged at 60°C

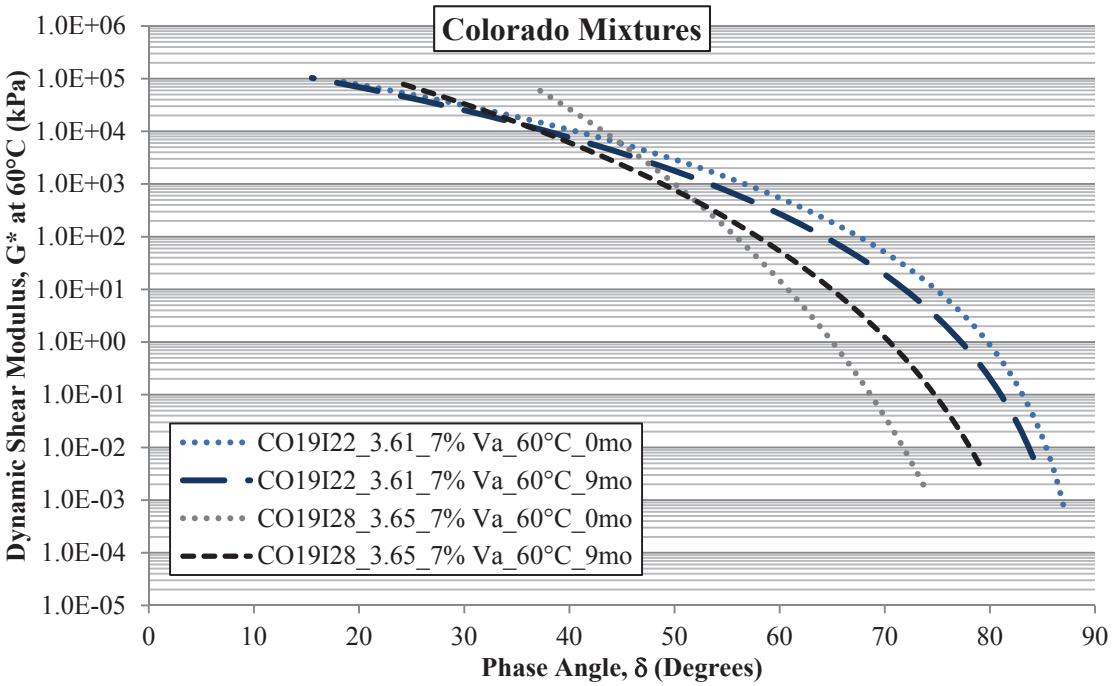

Figure 7.61 Black Space Plots for Colorado Mixtures with Constant Apparent Film Thickness Aged at 60°C

Consideration of Figure 7.59 through Figure 7.61 present similar deviations in the rheological measures noted previously between the two asphalt binder grades (i.e. PG 64-22 and PG 64-28). Within each respective aggregate source, the only factor that has changed in these comparisons was the asphalt binder grade. The aggregate gradation was held constant and the total binder content was adjusted so the AFT of 9 μm was also maintained. Thus, based upon the assumption of the AFT calculation being an accurate representation of the absorbed and effective asphalt binder contents, the only variable in these considerations was the asphalt binder grade.

Based on those conditions, it is readily apparent that the asphalt binder grade (i.e. specifically the polymer modification process) provided a significant contribution to the rheological measures as a function of aging duration in respective mixtures. It is further noted that the magnitude of the discrepancies between the different binders changes with the aggregate source as well. As an example from Figure 7.59, relative comparisons of the rheological changes exhibited over the nine month aging duration are vastly different between the two binder grades. This relative difference is not replicated with either the Colorado or Nevada mixtures, and even they exhibit a noticeable discrepancy between each other.

Due to the dramatic differences between the two asphalt binders, more conclusive observations of these mixtures are provided by considering each of the respective aggregate sources specific to one binder type at a time. Therefore, the mixtures containing the unmodified PG 64-22 binder are presented in Figure 7.62 and the mixtures containing the SBS modified PG 64-28 are provided in Figure 7.63.

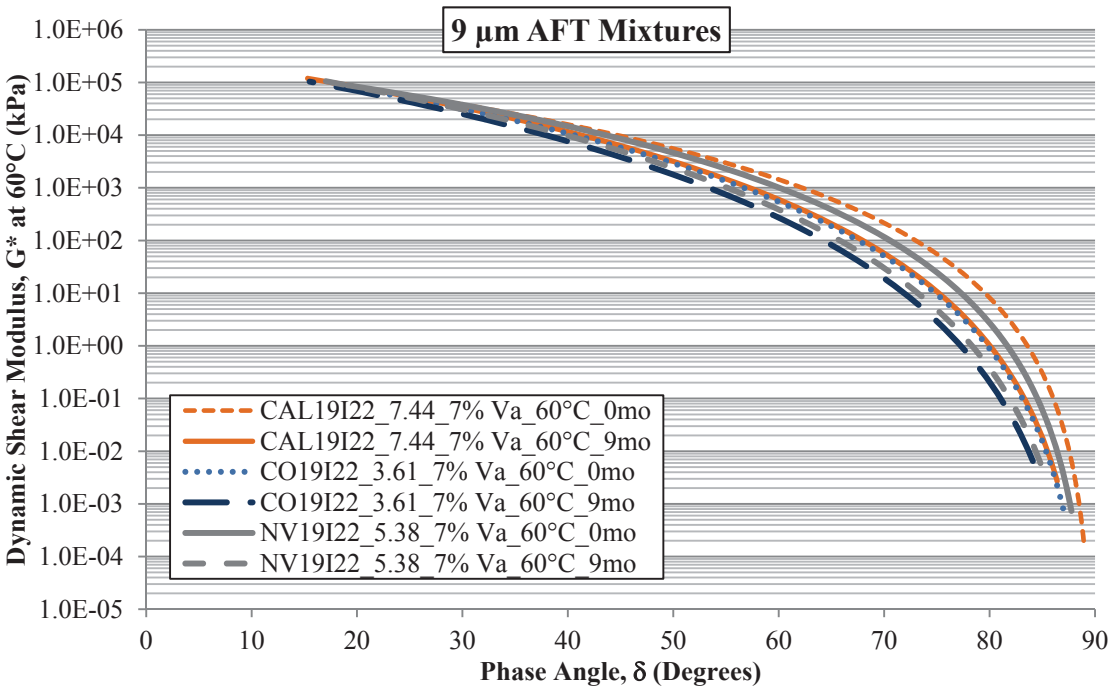

Figure 7.62 Black Space Plots for Select Mixtures with Constant Apparent Film Thickness Aged at 60°C with PG 64-22 Binder

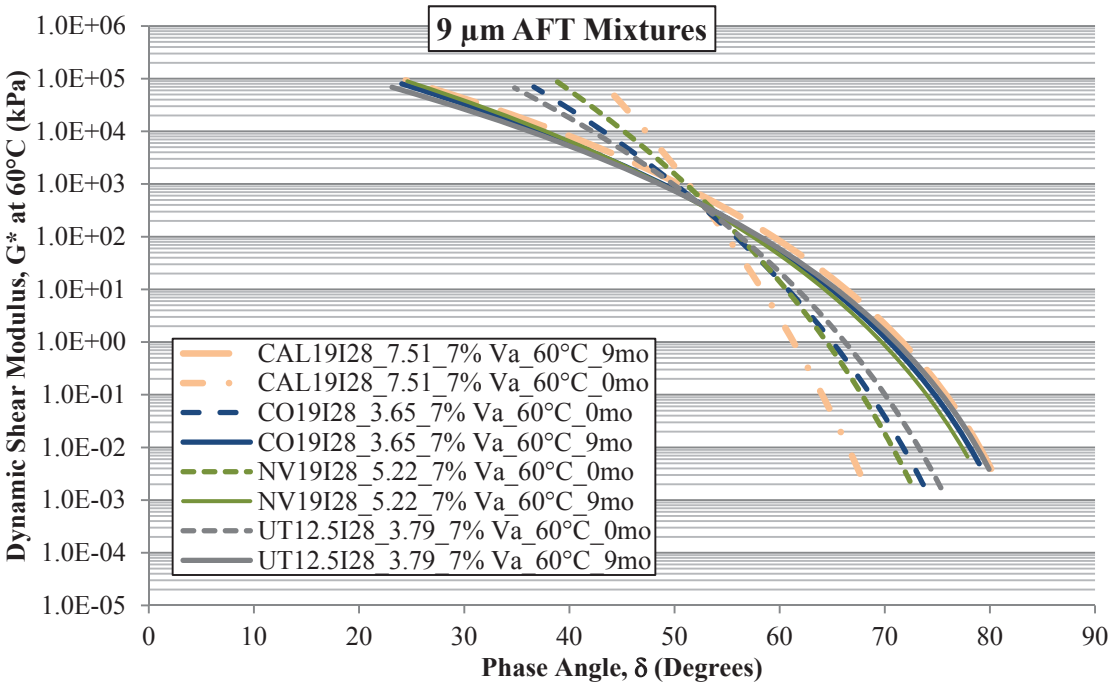

Figure 7.63 Black Space Plots for Select Mixtures with Constant Apparent Film Thickness Aged at 60°C with PG 64-28 Binder

Observations of the mixtures containing the PG 64-22 binder in Figure 7.62 indicate a fairly similar deviation in the black space representation over the nine month aging duration between the respective mixtures. However, the initial measurements (i.e. zero month aging condition) exhibited larger discrepancies between the respective aggregate sources.

Similar variations due to the nine month aging duration are observed between the different aggregate sources in Figure 7.63 with the Colorado, Nevada, and Utah mixtures, but not with the California mixture. In this instance, the California mixture was not only initiated at a different black space representation (i.e. zero month aging), but also exhibited a fairly different relationship after nine months of aging. This directly presents a substantial change in the black space due to the nine month aging duration at 60°C.

There were also systematic variations noted between the Colorado, Nevada, and Utah mixtures, though the overall change in the black space plots remained comparatively similar between those three mixtures.

7.3.5 Mixture Aging Temperature

Similar to the analysis of the oxidation growth of the mixture-aged asphalt binders, an additional aging temperature of 85°C has been considered in addition to the previous measures which were aged at 60°C. For the sake of clarity, the black space diagrams presenting the effects of aging temperature on the rheological measurements will be separated relative to the air void level of the mixtures during aging. Therefore, the California mixture with 7% air voids has been provided in Figure 7.64, while the

mixtures aged with 4 and 11% air voids were provided in Figure 7.65. Similarly, for the Nevada mixtures aged at 60 and 85°C, the 7% air voids mixtures were provided in Figure 7.66, while the mixtures aged with 4 and 11% air voids were presented in Figure 7.67.

In these figures it is important to note that the least aged mixtures with the 85°C aging were conditioned for 0.5 months (i.e. 2 weeks) as opposed to the 60°C aging sets which initially only experienced short-term oven aging (i.e. zero months).

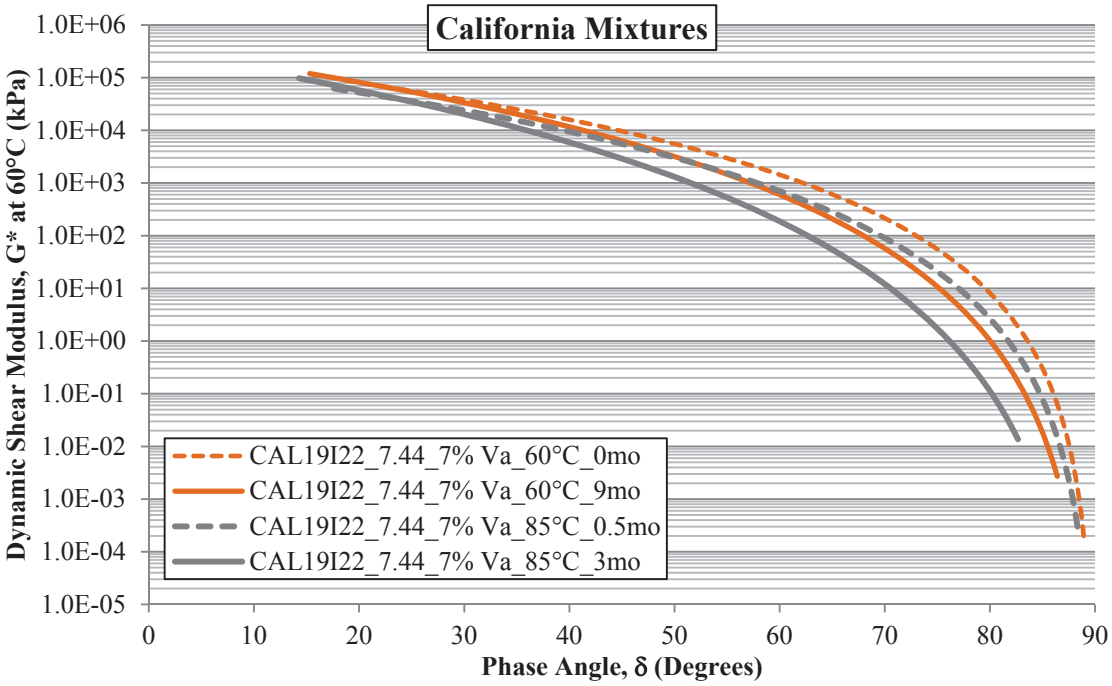

Figure 7.64 Black Space Plots for the CAL19I22_7.44_7% Va Mixtures Aged at 60 and 85°C

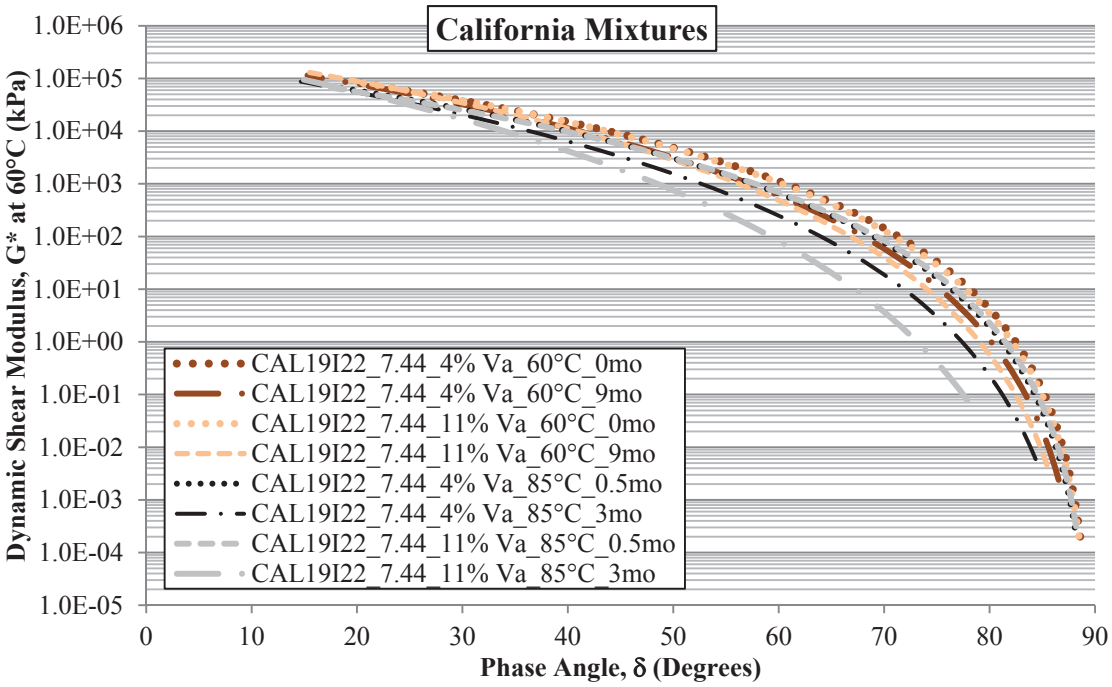

Figure 7.65 Black Space Plots for the CAL19I22_7.44_4 and 11% Va Mixtures Aged at 60 and 85°C

Consideration of the California mixtures with 7% air voids and the PG 64-22 binder in Figure 7.64, showed that the aging temperature had a fairly significant effect on rheological measures of the extracted and recovered binders. This is quite expected given the drastic influence the aging temperature had on the oxidation measures discussed previously.

Through the many mixtures presented in Figure 7.65, it is evident that there is a general migration of the black space relationships as a function of increased aging severity, whether due to duration or increased temperature. It is interesting to note the similarities in the black space representations of the binder master curves between the CAL19I22_7.44_11% Va_60°C_9mo measurement and that of the CAL19I22_7.44_4% Va_85°C_3mo. These two black space plots are similar to one another and also have

relatively close oxidation levels (i.e. CA measures) as depicted previously in Figure 7.40. This is an encouraging finding, although only a single point of consideration this suggests that the CA measures are appropriately correlating the chemical changes due to the oxidation process with the measured physical changes in terms of rheological measures. More comprehensive and robust correlations between these measurements are considered with the hardening susceptibility analyses found in section 7.4.6.

Considerations of the aging temperature on the Nevada mixtures containing the PG 64-28 asphalt binder with the 7% air void level are also provided in Figure 7.66. Similar consideration of the Nevada mixtures containing the PG 64-28 binder only aged with 4 and 11% air voids are provided in Figure 7.67.

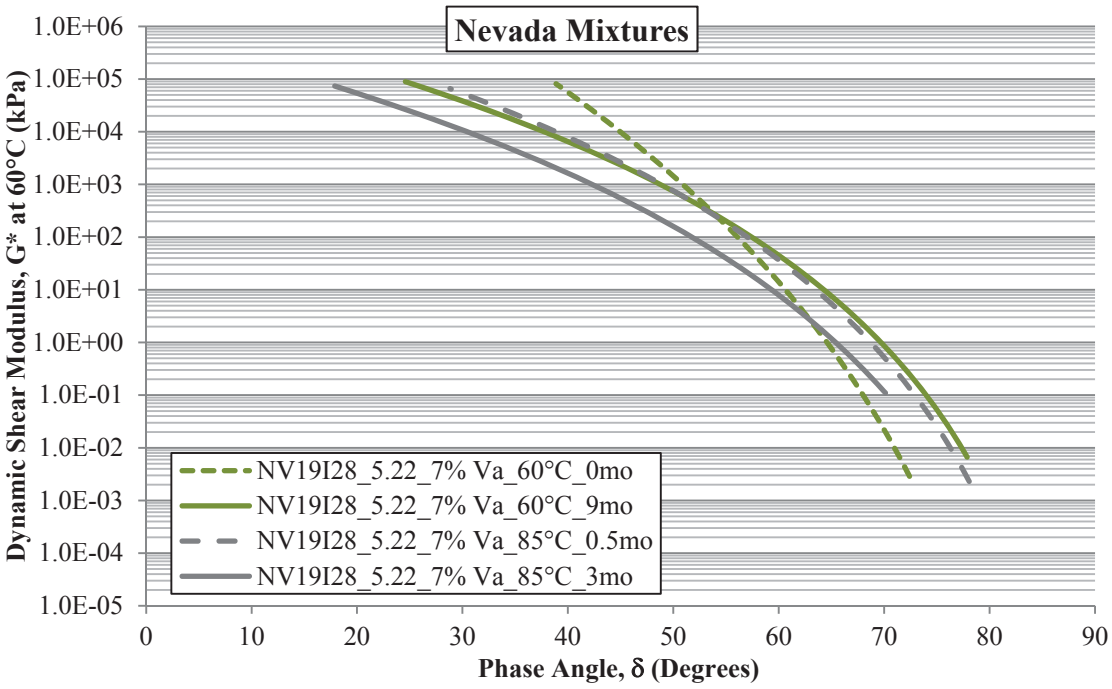

Figure 7.66 Black Space Plots for NV19I28_5.22_7% Va Mixtures Aged at 60 and 85°C

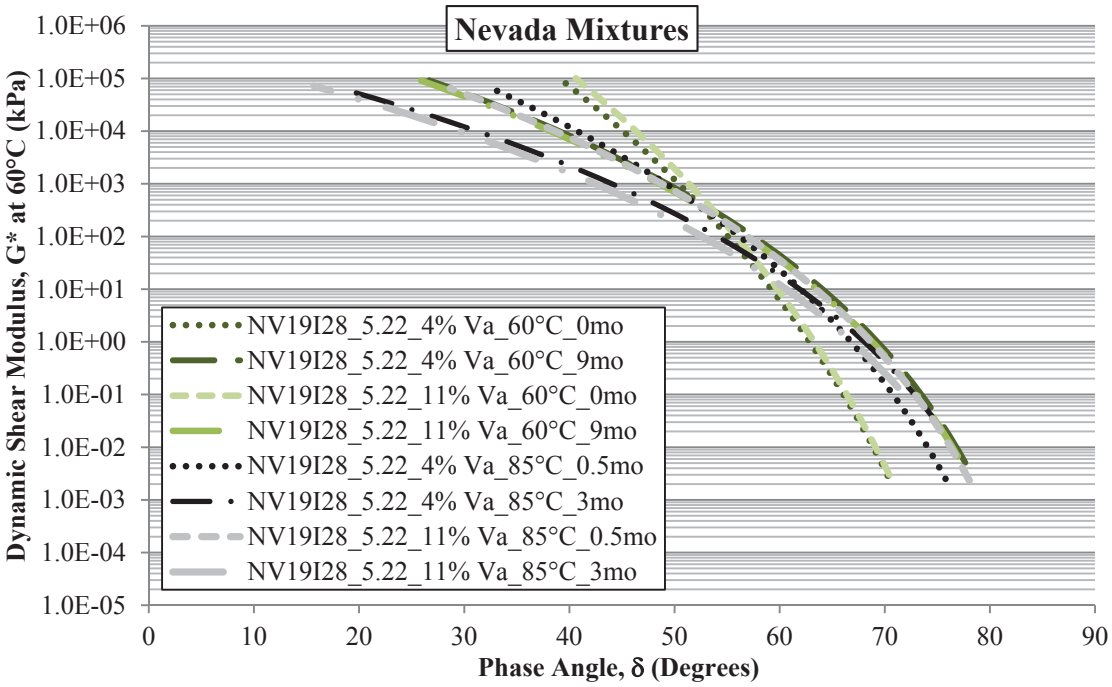

Figure 7.67 Black Space Plots for NV19I28_5.22_4 and 11% Va Mixtures Aged at 60 and 85°C

Similar commonalities as were noted with the California mixtures were also observed for the Nevada mixtures with the PG 64-28 asphalt binder. Specifically, very similar rheological measures were noted between the NV19I28_5.22_7% Va_60°C_9mo materials and the measurements of the NV19I28_5.22_7% Va_85°C_0.5mo presented in Figure 7.66. Again referencing Figure 7.41, the measured CA values are different by approximately 0.1, which is a fairly close comparison.

Observation of the 4 and 11% air void mixtures of Figure 7.67 begin to show some discrepancies between the overall rheological behavior as a result of the aging temperature. Specifically, the two mixtures aged for three months at 85°C are quite similar to each other and fairly similar to the mixtures aged for nine months at 60°C toward the higher end of the phase angle range. They exhibit a substantial discrepancy

from the 60°C aged mixtures at the lower end of the phase angle range (i.e. higher modulus values).

Thus, the general conclusions that can be drawn from these observations is that some of the measured rheological relationships of the mixtures were influenced by the temperature under which the mixtures were aged, typically with some marked difference in the oxidation level (i.e. CA level). Some of the rheological measures were relatively similar at the same levels of aging, based upon the limited point to point comparisons. However, a more robust analysis of the correlations between the rheological measures and the measured oxidation level with respect to the aging temperatures will be considered in section 7.4.6, which focuses on the hardening susceptibility relationships of the these mixture-aged binders.

7.3.6 Summary of Mixture-Aged Rheological Measurements

Considerations of the rheological measurements of the mixture-aged asphalt binders were conducted by producing mixtures with differing levels of the experimental factors under investigation (e.g. mixture air void level, asphalt binder content, asphalt binder type, qualitative gradation, and aging temperature). The mixtures were aged to different oxidation levels, extracting and recovering the binders which were then tested on the dynamic shear rheometer.

The systematic influence of the mixture air void level was observed with the mixtures containing the modified PG 64-28 asphalt binder, although the differences were

not overly substantial. Evidence of the same variation of mixture air void level was not as clear with the mixtures containing the unmodified PG 64-22 asphalt binder.

Considerations of the asphalt binder content indicated that the higher asphalt binder contents generally exhibited larger changes in the black space representation of the binder master curves (i.e. Colorado and Nevada mixtures). This was observed in mixtures containing both the unmodified PG 64-22 and the modified PG 64-28 asphalt binders.

The influence of the qualitative gradation on the rheological measures was somewhat inconsistent and thus inconclusive, largely due to potential influences by the overall oxidation level of the respective binders. More specific considerations combining these two factors will be addressed in the hardening susceptibility analyses.

Consideration of the mixtures containing the variable asphalt binder contents to maintain a 9 um AFT indicated that the aggregate sources had a potential influence on the black space representations of the asphalt binder master curves with the unmodified PG 64-22 binder. Although the magnitude of the change in the black space plots over the aging duration remained fairly consistent between the aggregate sources.

The black space plots of the mixtures containing the PG 64-28 binder were systematically ordered but relatively similar for three of the four aggregate sources considered. However, the California mixture exhibited a substantial variation both in terms of the initial black space relationship and the change in that representation due to the nine month oxidation period.

The influence of the aging temperature was observed to increase the binder stiffness represented by the black space curves. From the limited point-to-point considerations the data suggest that the increase in the aging temperature largely tended to progress the

black space plots along a similar path as was noted at lower aging temperature, only at a faster rate. However, more comprehensive analyses will be considered with all of the measures in section 7.4.6, not a simple point-to-point consideration presented in this section.

It is important to note that many of the rheological measures presented in this section generally exhibited fairly inconsistent results relative to the experimental factors being investigated (e.g. air void level, qualitative gradation, and constant film thickness evaluations). However, other factors were noted to have noticeable influences on the rheological measures of the extracted and recovered mixture-aged binders (i.e. asphalt binder content and type).

It is important to note that some of the very same factors were found to be highly influential on the relative levels of oxidation observed with the same mixtures. This directly highlights the limitations of many of the previous studies of binder oxidation which have been largely based upon mixture and/or asphalt binder stiffness or viscosity measurements. The stiffness measures of these materials do not completely describe their behavior and thus may inadequately describe the performance of these materials in service. Further considerations of this effect will be considered in the following chapters with respect to the measured characteristic behavior of the asphalt binders as well as the direct measures of the asphalt mixture properties as a function of oxidative aging.

7.4 Mixture-Aged Asphalt Binder Hardening Susceptibility

Similar to the pan-aged asphalt binders, the kinetics information was readily combined with the rheological measurements in the form of the low shear viscosity determinations to create the hardening susceptibility (HS) relationships for the respective mixtures based upon the binders extracted and recovered from the aged mixtures. Reference is made to Table 5.1 and Table 5.2 for the overall testing matrix and the corresponding naming convention of the recovered asphalt binders specific to the factors considered in this analysis. After a general analysis of the rheological measurements on the extracted and recovered asphalt binders, the HS of the mixture-aged binders will be assessed following the same order as kinetics determinations.

7.4.1 Statistical Analysis Methods of Mixture-Aged Hardening Susceptibility

The statistical analysis for the HS relationships were conducted in much the same manner as were previously utilized for the oxidation kinetics measurement utilizing multivariate linear regression techniques. However, the HS relationship is defined as the slope of the plot of LSV as a function of CA in a semi-log scale as has been previously defined by Equation 3.72. To permit the use of the linear regression techniques conducted previously, the dependent variable (LSV) had to be transformed in the log scale. Further, it was convenient to refer to the relationship in the exponential form, so the natural log form was utilized. Therefore, the same regression form of Equation 7.9 was maintained with the slight modification of the predicted response being ln(LSV), as indicated by

Equation 7.10. In this form, the statistical analyses were conducted with the Minitab software.

$$E\{Y\} = \beta_0 + \beta_1 X_1 + \beta_2 X_2 + \beta_3 X_1 X_2 \qquad \textbf{Equation 7.10}$$

where, $E\{Y\}$ – predicted dependent variable in the analysis, ln(LSV);
β_0 - intercept of the base equation (condition A);
β_1 - slope of the base equation (condition A);
β_2 - modification to the intercept of the base equation due to condition B;
β_3 - modification to the slope of the base of the equation due to condition B;
X_1 - independent predictor variable ($CA\text{-}CA_{Tank}$);
X_2 - qualitative predictor variable (dummy variable);
$X_2 = 0$, for condition A,
$X_2 = 1$, for condition B.

To find LSV directly, as opposed to finding ln(LSV) and taking it to a power of Euler's number (e), the regression expression may be restated to the form of Equation 7.11. In this revised form, the statistical coefficients (β values) retain the numeric value and LSV may be determined directly.

$$LSV = e^{\beta_0} e^{\beta_1 (CAg)} e^{\beta_2 X_2} e^{\beta_3 (CAg) X_2} \qquad \textbf{Equation 7.11}$$

In either the form of Equation 7.10 or Equation 7.11, the HS relationships for the mixture-aged binders are considered.

7.4.2 Mixture Air Void Level

Once the rheological measures have been calculated to yield the LSV values, the LSV and CA measurements from the extracted and recovered binders from each respective mixture aging condition for the appropriate set of mixture characteristics may be combined together to yield the HS relationship for that particular mixture. Similar to CA growth and rheological analyses already completed, Figure 7.68 and Figure 7.69 present the hardening susceptibility plots produced from the binder obtained by extraction and recovery from the mixtures aged at different air void levels aged at 60°C, differentiated by the asphalt binder type (i.e. polymer modified PG 64-28 or unmodified PG 64-22).

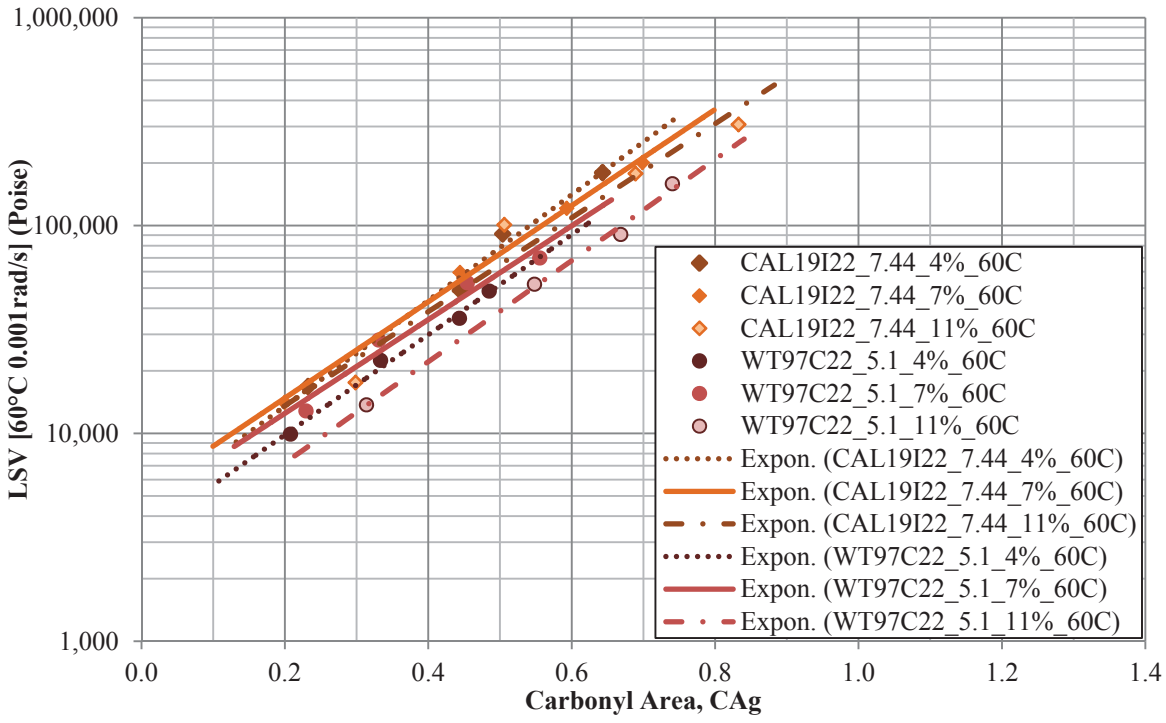

Figure 7.68 Hardening Susceptibility Relationships for Different Air Void Levels with PG 64-22 and WT97-22 Binders Aged at 60°C

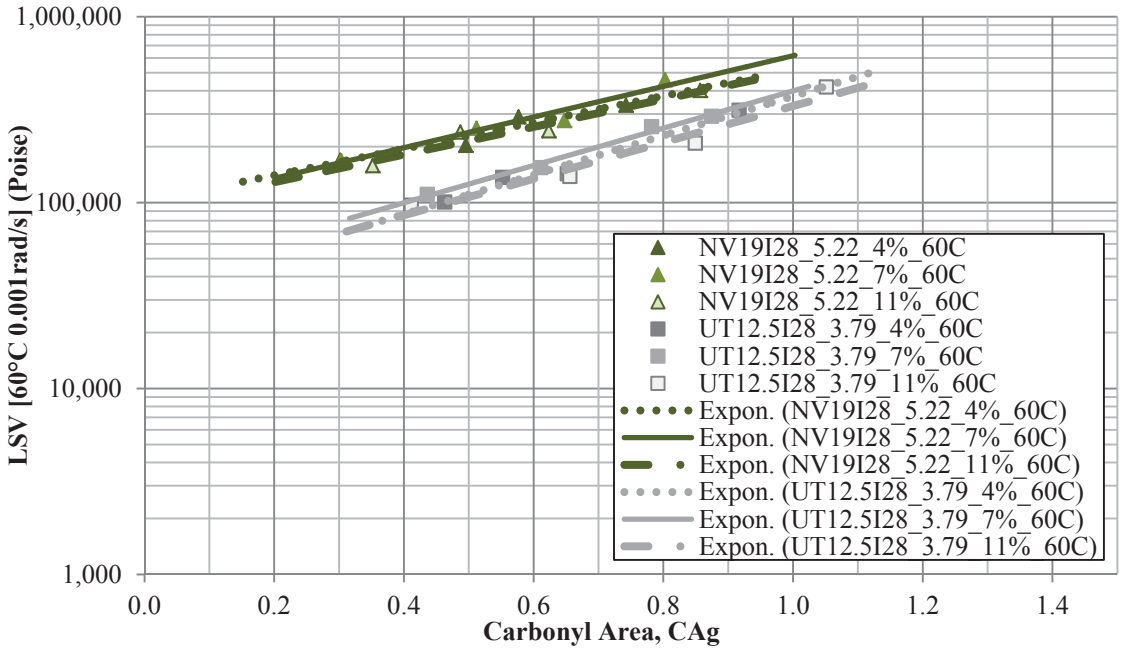

Figure 7.69 Hardening Susceptibility Relationships for Different Air Void Levels with PG 64-28 Binders Aged at 60°C

Initial observations of these figures clearly indicate potential discrepancies between the mixture-aged binders. At first, the mixture-aged PG 64-22 measurements of Figure 7.68 seem to indicate there may be quite similar relationship for the unmodified binders. However, it is important to note the clear discrepancies that were observed with the pan-aged binder HS relationships. Therefore, based on these measures alone, it cannot be clearly determined if the HS relationship is dependent solely upon the asphalt binder, or if a significant interaction with aggregate source may have caused the similarity by coincidence.

Additional consideration of Figure 7.69 presents clear evidence that the influence of the aggregate may, with certain materials such as the PG 64-28 in this case, cause a significant difference in the HS relationships of mixture-aged asphalt binders. To be clear, the only differences between the HS relationships were the aggregate sources and

the total binder content. Further consideration of both cases will be considered with additional mixture-aged HS relationships.

Another significant finding noted in the mixture-aged asphalt binder measures with both the unmodified PG 64-22 binders and the SBS modified binders is that the relative difference between the air void levels of the mixtures during the aging process are either very small or non-existent, at least for these mixtures in particular. This finding was further supported by the stepwise regression and final regression models presented in Table 7.22 and Table 7.23.

Table 7.22 Statistical Significance of Air Void Level on Hardening Susceptibility at 60°C for Mixtures with PG 64-22 Binders

	CAL19I22_7.44			WT97C22_5.1		
Regression Parameter	Coefficient	P-value	Significance	Coefficient	P-value	Significance
Intercept-m, β_0	8.5340	0.000	Sig.	8.3259	0.000	Sig.
CAg (HS, β_1)	5.2766	0.000	Sig.	4.9098	0.000	Sig.
R^2 (%)	96.6			94.8		
Adj. R^2 (%)	96.3			94.3		

Table 7.23 Statistical Significance of Air Void Level on Hardening Susceptibility at 60°C for Mixtures with PG 64-28 Binder

	NV19I28_5.22			UT12.5I28_3.79		
Regression Parameter	Coefficient	P-value	Significance	Coefficient	P-value	Significance
Intercept-m, β_0	11.4630	0.000	Sig.	10.5172	0.000	Sig.
CAg (HS, β_1)	1.7489	0.000	Sig.	2.2745	0.000	Sig.
R^2 (%)	91.4			94.5		
Adj. R^2 (%)	90.6			94.0		

Table 7.22 and Table 7.23 both confirm the lack of significance of the air void level on the HS relationship with both the unmodified (PG 64-22 and WT64-22) and modified asphalt binders (PG 64-28). This is an important finding by indicating that the HS relationship is independent of the air void level or density of the asphalt mixture during aging. As a result, the HS relationship for a given mixture, with a given gradation and binder content can be represented by a single HS determination as shown in Figure 7.70.

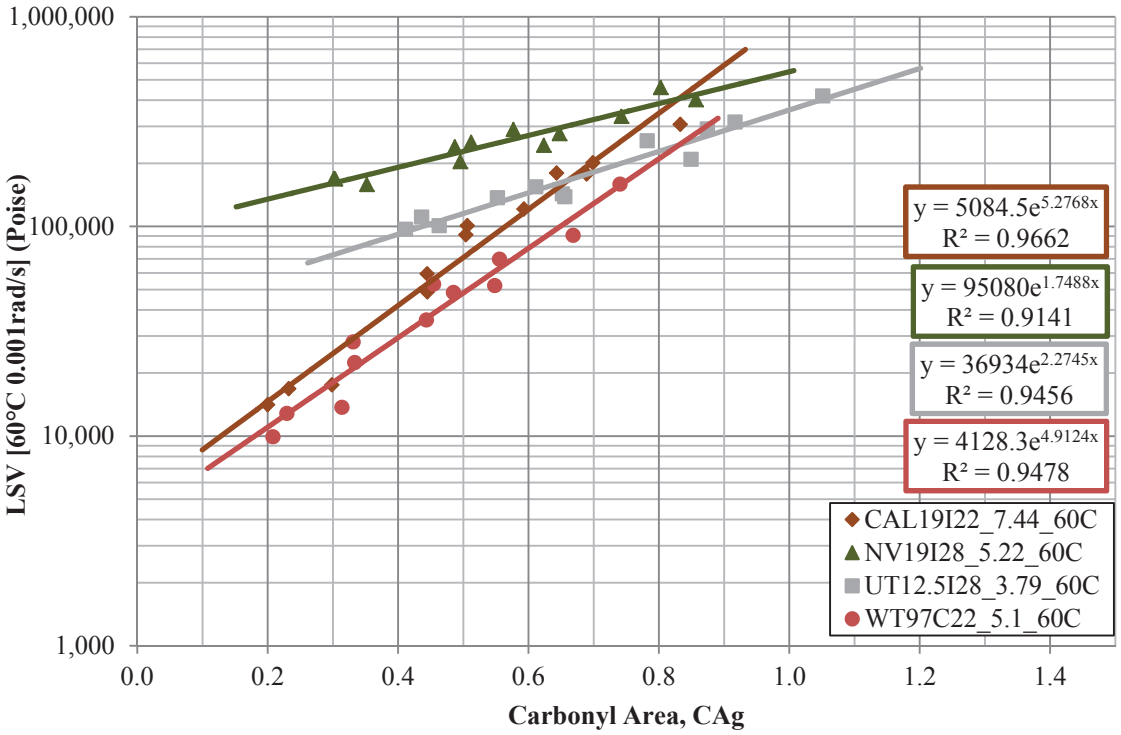

Figure 7.70 Combined Hardening Susceptibility Relationships for Mixtures with Different Air Void Levels Aged at 60°C

Based upon visual observation of the HS plots, the calculated coefficient of determination (R^2) presented in Figure 7.70, and the statistical evaluation provided in Table 7.22 and Table 7.23, it has been generally accepted that the HS of the mixture-aged binders may appropriately be represented by a single relationship. This is a significant benefit in terms of the overall reduction in the quantity of testing required to perform these types of analyses. Therefore, the determination of the HS relationship for a particular mixture of a given gradation and binder content may be determined by a single air level, thus reducing the number of tested specimens by two thirds in this investigation. Unfortunately, the kinetics measurements (i.e. CA growth) did not follow this convenient similarity. Therefore the kinetics is still dependent upon the air void level of the mixture, while the HS parameters may be considered independent of the air void level.

7.4.3 Asphalt Binder Content

The next experimental factor considered was the variation in the asphalt binder content. By keeping the aggregate gradation the same and varying the asphalt binder content also caused noted changes in the apparent film thickness (AFT) of the asphalt binder in the mixture.

Figure 7.71 and Figure 7.72 consider the HS relationships between the different asphalt binder contents of mixtures utilizing the Colorado and Nevada aggregates with both the PG 64-22 and PG 64-28 binders.

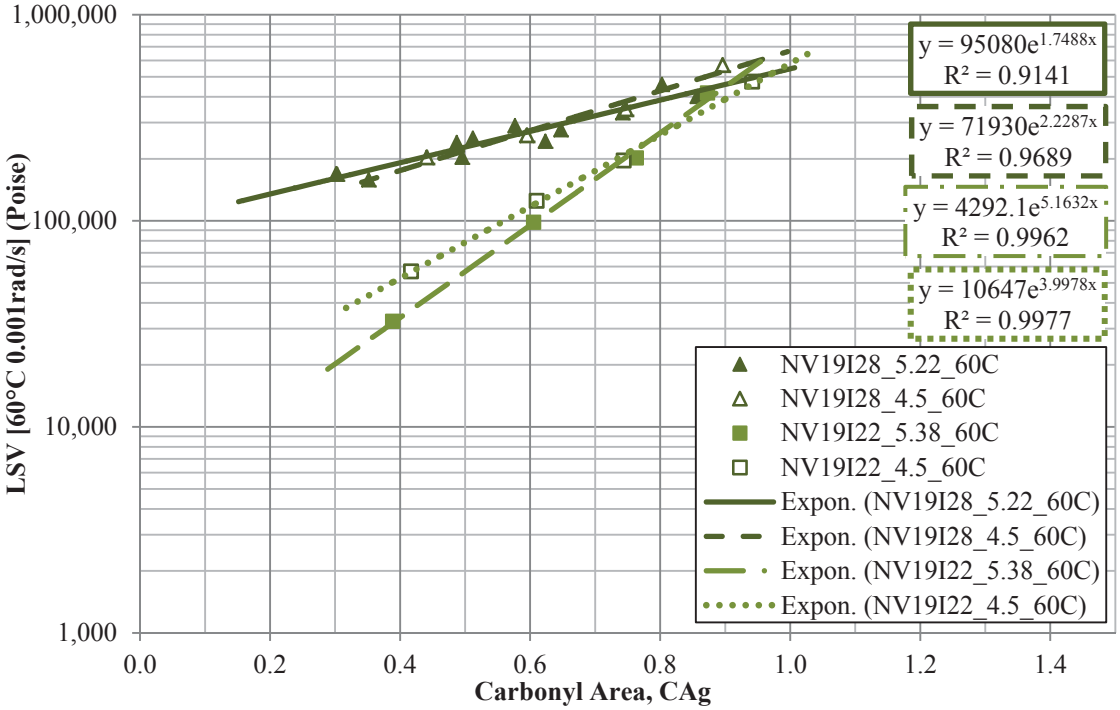

Figure 7.71 Hardening Susceptibility Relationships for the Nevada Mixtures with Different Binder Contents Aged at 60°C

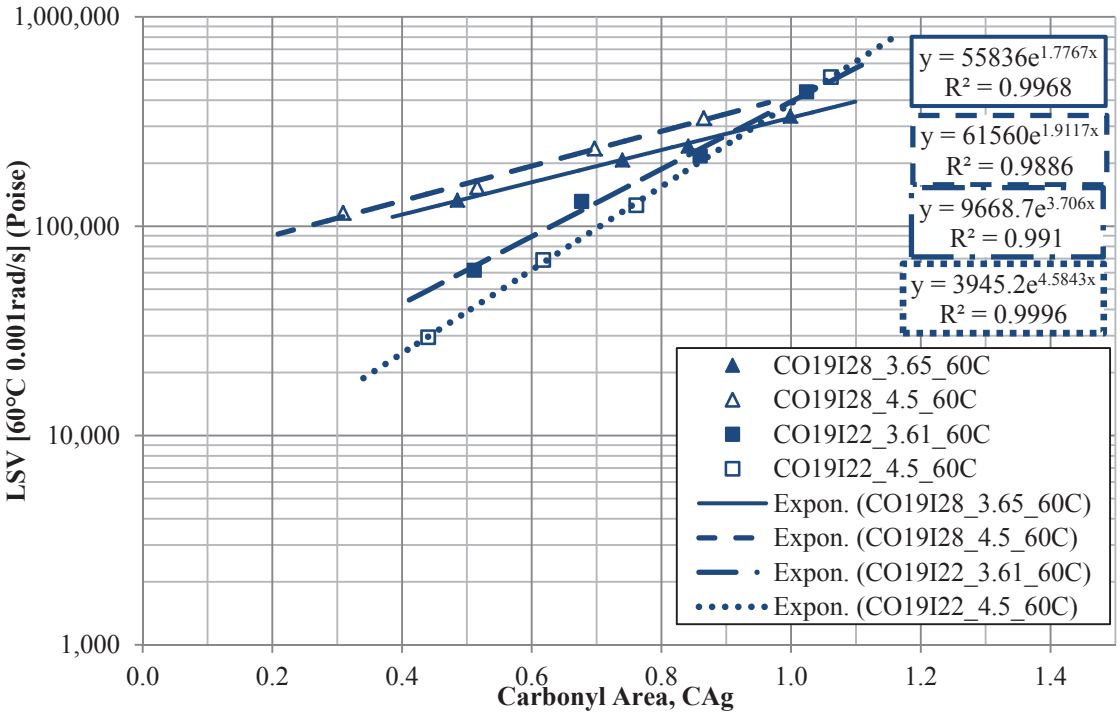

Figure 7.72 Hardening Susceptibility Relationships for the Colorado Mixtures with Different Binder Contents Aged at 60°C

General observations of Figure 7.71 indicate that there is a fairly minor difference between the two binder contents with the Nevada aggregates and the PG 64-28 asphalt binder. There is a slight difference noted between the two binder contents with the Nevada aggregates and the PG 64-22 binder, with a clear separation between the binder grades.

Figure 7.72 presents a similar comparison but with the Colorado aggregates. A similar deviation is noted between the two asphalt binder grades as was noted with the Nevada aggregates. However, a slight deviation is noted between the two binder contents in the Colorado mixtures. Unfortunately, the deviation with binder content does not follow a consistent pattern between the binder grades. Specifically, the HS relationship plots lower on the figure with CO19I22 mixture with an increase in binder content (i.e. 3.61 to 4.5% TWM). However, the opposite is true for the HS of CO19I28 mixtures (i.e. the 4.5% plots higher than the 3.65% TWM mixture). By comparison, a relatively similar reduction was noted with both the Nevada and Colorado aggregates with PG 64-22 asphalt binder, although the HS of the NV19I22 mixtures do cross each other making this assessment dependent upon the CA level in the consideration.

To clearly identify if these relationships are significantly different within the general groupings noted by visual observation, the stepwise linear regression analysis was conducted to produce the final regression relationships for each respective aggregate source. The results of those analyses are presented in Table 7.24 and Table 7.25 with the categorical variable (BI) set to a value of unity for the SBS modified PG 64-28 and a value of zero for the unmodified PG 64-22 asphalt binders, respectively.

Table 7.24 Statistical Significance of Hardening Susceptibility at 60°C for Nevada Mixtures

NV19I Binder Content Analysis			
Regression Parameter	Coefficient	P-value	Significance
Intercept-m, β_0	8.8169	0.000	Sig.
CAg (HS, β_1)	4.5704	0.000	Sig.
BI	2.5449	0.000	Sig.
(CAg)*BI	-2.6416	0.000	Sig.
R^2 (%)	97.6		
Adj. R^2 (%)	97.0		

Table 7.25 Statistical Significance of Hardening Susceptibility at 60°C for Colorado Mixtures

CO19I Binder Content Analysis			
Regression Parameter	Coefficient	P-value	Significance
Intercept-m, β_0	8.6164	0.000	Sig.
CAg (HS, β_1)	4.2817	0.000	Sig.
BI	2.4725	0.000	Sig.
(CAg)*BI	-2.6062	0.000	Sig.
R^2 (%)	96.9		
Adj. R^2 (%)	96.1		

The statistical analyses presented in in Table 7.24 and Table 7.25 generally follow the observations made from Figure 7.71 and Figure 7.72. The significance of the BI term and the interaction term (CAg)*BI indicate that the asphalt binder grade, or more importantly in this case the effect of the polymer modification, significantly affects the intercept (m-value) and the slope (HS) with both the Colorado and Nevada aggregates.

With these being the only modification to the base HS equation (e.g. CO19I22 when BI = 0 for the Colorado mixtures), further indicates that the slight differences in the HS parameter noted due to the change in asphalt binder content were not statistically significant in the regression analysis. It should be noted that the majority of the aggregate factors noted in Table 7.8 are necessarily blind to these particular calculations since each were conducted within an aggregate source (i.e. Nevada or Colorado), therefore each analysis would have exactly the same value for these properties thus providing no significant benefit to the overall model.

To assess the potential influence of the aggregate properties on the HS relationship, those input parameters must exhibit some variation in the experimental design. Thus, Table 7.26 provides the final regression model for the HS relationships with the Colorado and Nevada mixtures all containing 4.5% TWM asphalt binder content with both the unmodified PG 64-22 and the SBS modified PG 64-28 asphalt binders.

Table 7.26 Statistical Significance of Hardening Susceptibility at 60°C for Mixtures with 4.5% Asphalt Binder Content

4.5% TWM Binder Content Analysis			
Regression Parameter	Coefficient	P-value	Significance
Intercept-m, β_0	8.8442	0.000	Sig.
CAg (HS, β_1)	4.2033	0.000	Sig.
BI	2.1176	0.001	Sig.
(CAg)*BI	-1.9635	0.012	Sig.
R^2 (%)	91.4		
Adj. R^2 (%)	89.3		

In these particular analyses, all the aggregate factors noted in Table 7.8 were included, though not all at one time to avoid unacceptable co-linearity issues with the input variables. Nevertheless, the only significant factors found aside from the main effects of the HS and m terms were again the BI and (CAg)*BI terms, noting that the binder grade or modification in this case significantly influences the HS relationship (i.e. both the HS and m parameters).

7.4.4 Qualitative Gradation

The effect of the aggregate gradation was investigated on a qualitative basis by considering one intermediate and one fine gradation for the California, Nevada, and Utah aggregate sources. Note that the two WesTrack mixtures were also included, but only as a general reference. Although they are composed of different gradations (coarse and fine), the WesTrack mixtures should not compared directly or through statistical means as they were produced from different aggregates and different binder sources. Therefore, the WesTrack mixtures have been included in Figure 7.73 as a general observation. However, since so many factors were changed at one time, the WesTrack mixtures have been excluded from the further statistical analyses. Further, the qualitative gradation analysis for the mixtures containing the PG 64-28 binders with the Nevada and Utah aggregates are presented in Figure 7.74.

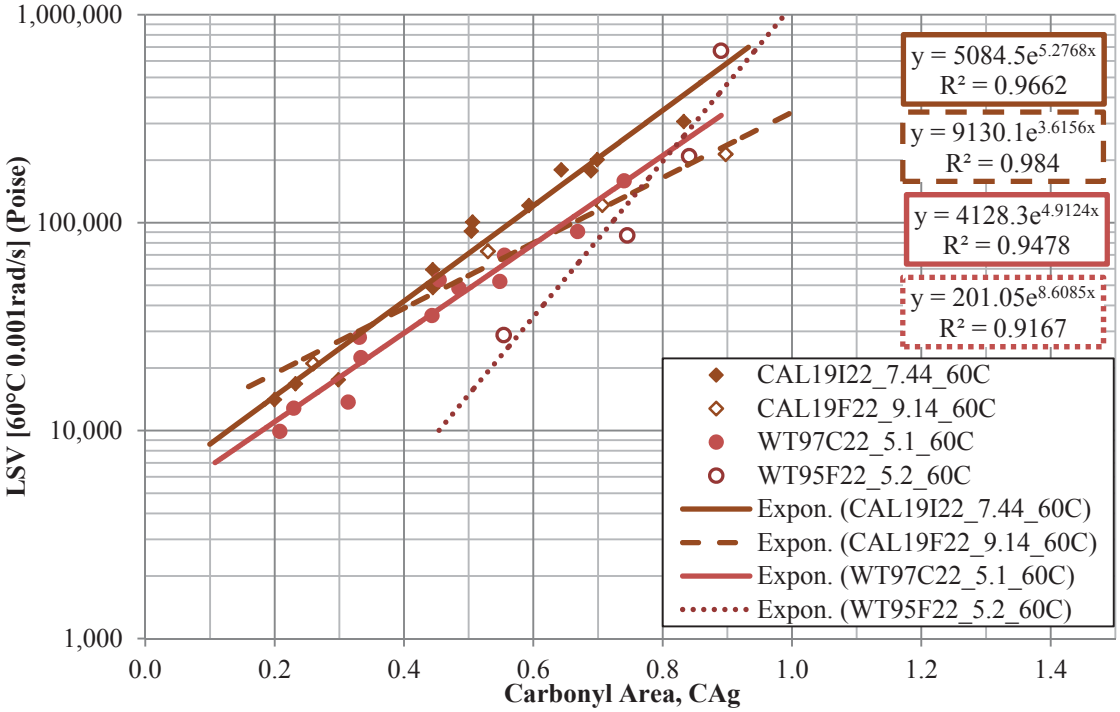

Figure 7.73 Hardening Susceptibility Relationships for the Mixtures with PG 64-22 Binders with Different Gradations Aged at 60°C

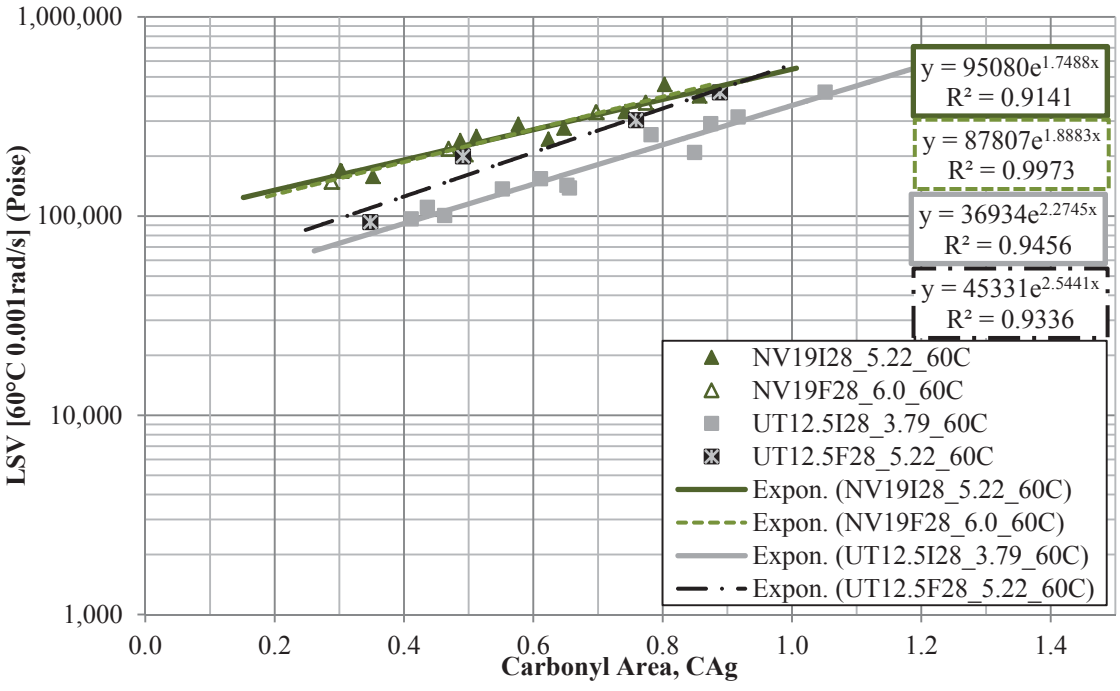

Figure 7.74 Hardening Susceptibility Relationships for the Mixtures with PG 64-28 Binder with Different Gradations Aged at 60°C

General observations of Figure 7.73 indicate potential differences in the HS between the two gradations of the California aggregate with the PG 64-22 binder. There are also differences noted in the WesTrack mixtures, but the two are not a valid comparison as mentioned previously. It is curious to note the apparent similarity between the CAL19I22 and WT97C22 HS relationships, however these are understood to be more coincidental than true similarities.

The Utah intermediate and fine mixtures appear to follow generally the same HS (slope), but have fairly different m values (intercept) in Figure 7.74. The Nevada mixtures on the other hand appear nearly indiscernible so far as the gradation is concerned. To identify the significance of these noted deviations the stepwise linear regression analysis was again conducted on the HS relationships between the respective mixtures.

Rather than simply including a categorical or dummy variable to test the significance between the qualitative gradation levels, physical properties measured from the aggregates themselves were the preferred input variables. The categorical variables would only show significant differences between the two mixtures being considered by that analysis, thus making it more of an empirical indication of those particular set of conditions. However, having common material properties as the differentiation variable should increase the application of these findings to additional mixtures not particularly evaluated in this study. Therefore, the HS parameters presented in Figure 7.73 and Figure 7.74 were analyzed according to the stepwise linear regression analysis to develop the final regression model for the HS parameters relative to the qualitative gradation analysis presented in Table 7.27, again omitting the WesTrack mixtures.

Table 7.27 Statistical Significance of Hardening Susceptibility at 60°C for Mixtures over Qualitative Gradation

Qualitative Gradation Analysis			
Regression Parameter	Coefficient	P-value	Significance
Intercept-m, β_0	9.1022	0.000	Sig.
CAg (HS, β_1)	N/A	N/A	NS
BI	1.8823	0.000	Sig.
(CAg)*Abs	0.9638	0.001	Sig.
(CAg)*DP	-4.950	0.027	Sig.
(CAg)*CAAT2	0.9802	0.004	Sig.
R^2 (%)	95.2		
Adj. R^2 (%)	94.2		

The regression model provided in Table 7.27, indicates several points to consider. The first is the lack of significance of the actual HS parameter (CAg). Initially, this seems to suggest that the LSV is not influenced by changes in the measured CA values, an obvious error in the interpretation by a general reference to both Figure 7.73 and Figure 7.74. However, more careful consideration of the developed regression model provides a strong influence of three interaction terms, all of which provide the overall model with a direct dependency of the LSV term on the measured CA level. The dependency was merely found to correlate to additional parameters in the model as well. Those other parameters generally are direct measures of the aggregate properties (i.e. Abs and the AIMS CAAT parameter) as well as the combined aggregate and effective binder content (i.e. DP). Recall that the dust proportion (DP) is the ratio of the percent passing the 75

μm (No. 200) sieve, divided by the effective asphalt binder content (Pbe), thus including an aggregate measure and a binder quantity measure in one variable.

These results also support the general observations that the HS parameters (HS and m value) are influenced by both the characteristics of the asphalt binder as well as the aggregate utilized in a given mixture.

7.4.5 Constant Film Thickness

Additional considerations of the influence of the aggregates on the HS of the extracted and recovered binders were continued by investigating mixtures with a constant AFT of 9 μm. The 9 μm AFT was calculated utilizing the methods outlined in Section 5.1 which necessarily led to variable asphalt binder contents for each respective aggregate source following the experimental matrix outlined in Table 5.1 and Table 5.2.

In an effort to single-out and control as many variables as possible to isolate and examine the effect of the main factors in the experiment, the WesTrack mixtures have been excluded from the present statistical considerations since both WesTrack binders were from different sources than the main PG 64-22 and PG 64-28 asphalt binders. Therefore, in the statistical evaluation presented in this section, the categorical variable (BI) only differentiates the PG 64-22 (BI=0) from the PG 64-28 (BI=1).

The HS relationships for the mixtures compacted to 7% air void level with respective binder contents corresponding to the AFT of 9 μm are presented in Figure 7.75 and Figure 7.76 for the PG 64-22 and PG 64-28 asphalt binders, respectively.

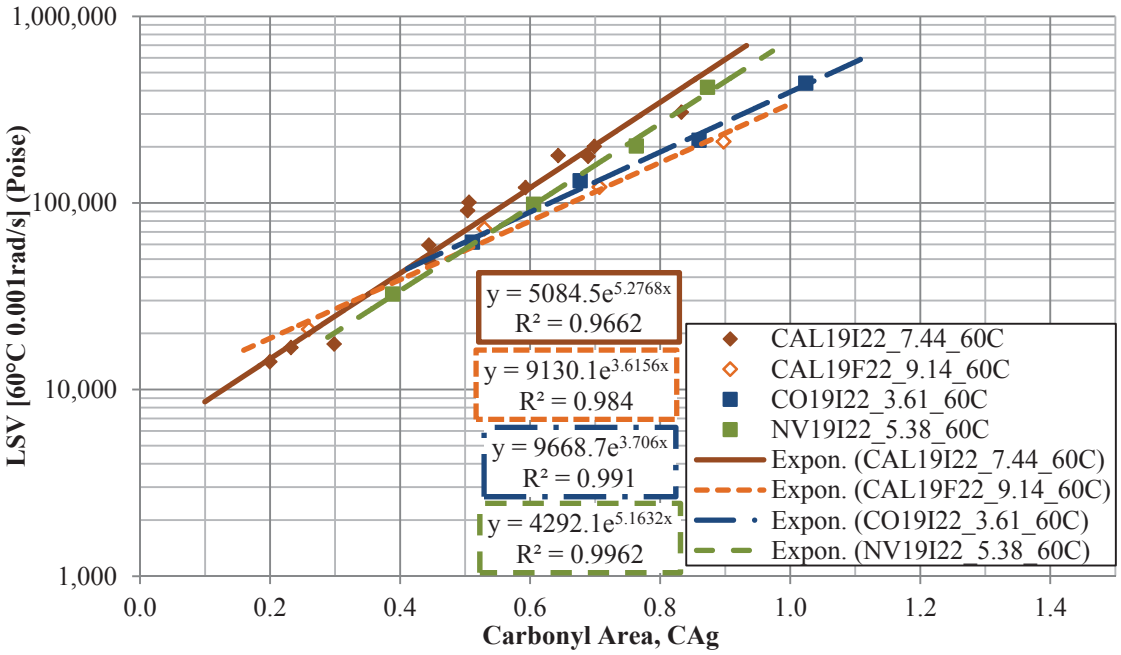

Figure 7.75 Hardening Susceptibility Relationships for PG 64-22 Mixtures Aged with 9µm Film Thickness Aged at 60°C

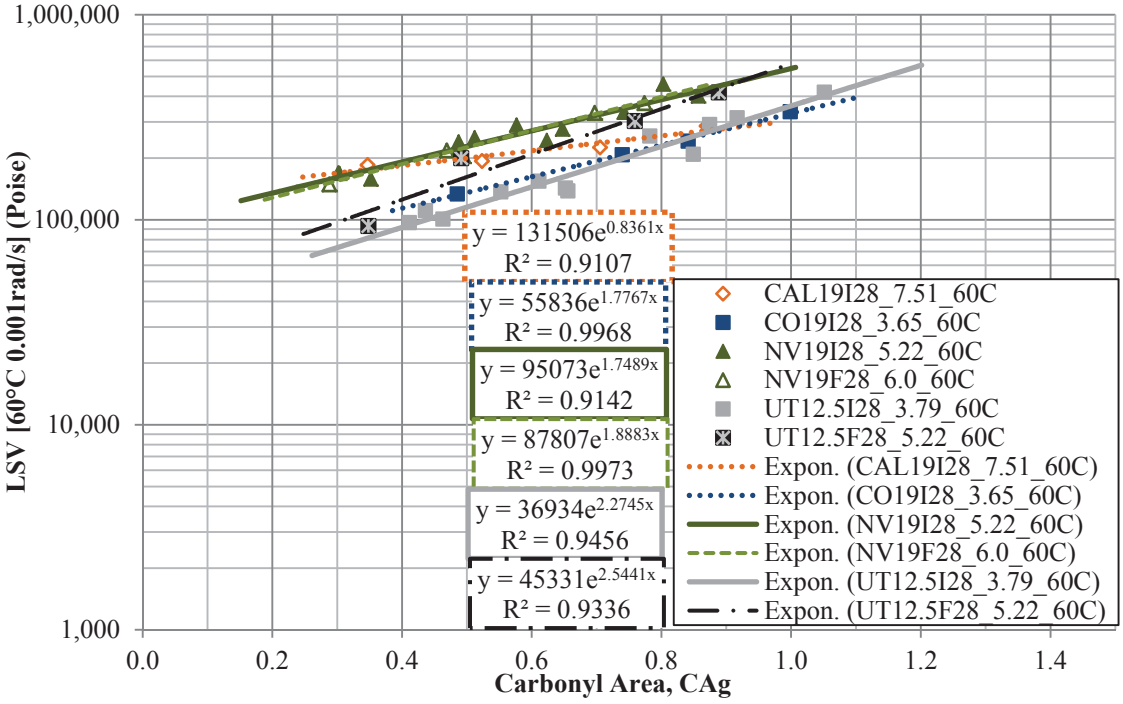

Figure 7.76 Hardening Susceptibility Relationships for PG 64-28 Mixtures Aged with 9µm Film Thickness Aged at 60°C

General observations of Figure 7.75 presenting the mixtures with the PG 64-22 asphalt binder note reasonable similarities between the HS relationships with an AFT of 9 μm. There is a general decrease in the HS (slope) noted with decreases in the total asphalt binder content (Pb) noted with the intermediate gradations of the California, Nevada, and Colorado, respectively. However, the fine gradation of the California aggregates does not follow this trend. A similar trend is also observed with the mixtures containing the PG 64-28 presented in Figure 7.76, however the separation between the mixtures appears to be more closely related to the m value (intercept) than the HS (slope).

To adequately identify the most influential factors in these noted deviations the stepwise regression analysis was conducted on all ten mixtures presented in Figure 7.75 and Figure 7.76 collectively. The final form of the regression model from this analysis is presented in Table 7.28.

Table 7.28 Statistical Significance of Hardening Susceptibility at 60°C for Mixtures with 9μm Apparent Film Thickness

9μm Apparent Film Thickness Analysis			
Regression Parameter	Coefficient	P-value	Significance
Intercept-m, β_0	7.9777	0.000	Sig.
CAg (HS, β_1)	4.3415	0.000	Sig.
BI	2.5973	0.000	Sig.
DP	0.8498	0.010	Sig.
(CAg)*BI	-2.7191	0.000	Sig.
R^2 (%)	92.3		
Adj. R^2 (%)	91.4		

The stepwise regression analysis indicated that in addition to the main effects (i.e. the m value, β_0 and the HS, β_1), the binder type was significantly influential to both the slope and the intercept, as was expected by the previous general observations. The DP was also found to decipher between the aggregate sources better than any of the other evaluated input parameters. While the adjusted coefficient of determination was not overly high (0.91), it was considered sufficient given that at least one of the mixtures alone had an R^2 of that same level.

Therefore, as an overall summary of the HS of the mixtures with the constant film thickness of 9 μm, the binder grade and the influence of the interaction of the effective binder content and the aggregate fines portion (i.e. DP) were found influential to the HS relationship of the binder extracted and recovered from those respective mixtures.

7.4.6 Mixture Aging Temperature

Similar to the noted discrepancies with the pan-aged HS relationships between binders aged at 60 and 85°C, a similar evaluation of the aging temperature on the HS of mixture-aged binders was also conducted. Following the respective aging duration of 0.5, 1, or 3 months in the 85°C ovens, the specimens were removed from the ovens, cooled and trimmed to the correct geometry for mixture testing, either E* or UTSST. Following the mixture testing, the binder from the E* specimens was extracted and recovered to be tested for CA measures on the FT-IR and rheological measures with the DSR.

Due to the significant amount of resources required to age additional mixtures, only two mixtures (California and Nevada) were selected for the 85°C aging. However, each

of the mixtures was aged with all three levels of air voids (i.e. 4, 7, and 11%) over each of the respective durations (0.5, 1, and 3 months). This permitted the calculation of the CA growth and rheological comparisons previously discussed, but also enabled the consideration HS relationship as a function of temperature for later comparison to the pan-aged binders.

Therefore, Figure 7.77 and Figure 7.78 present the HS relationships determined on the extracted and recovered binders from the California with the PG 64-22 and the Nevada aggregates with the PG 64-28 asphalt binder including all three air void levels at both 60 and 85°C, respectively.

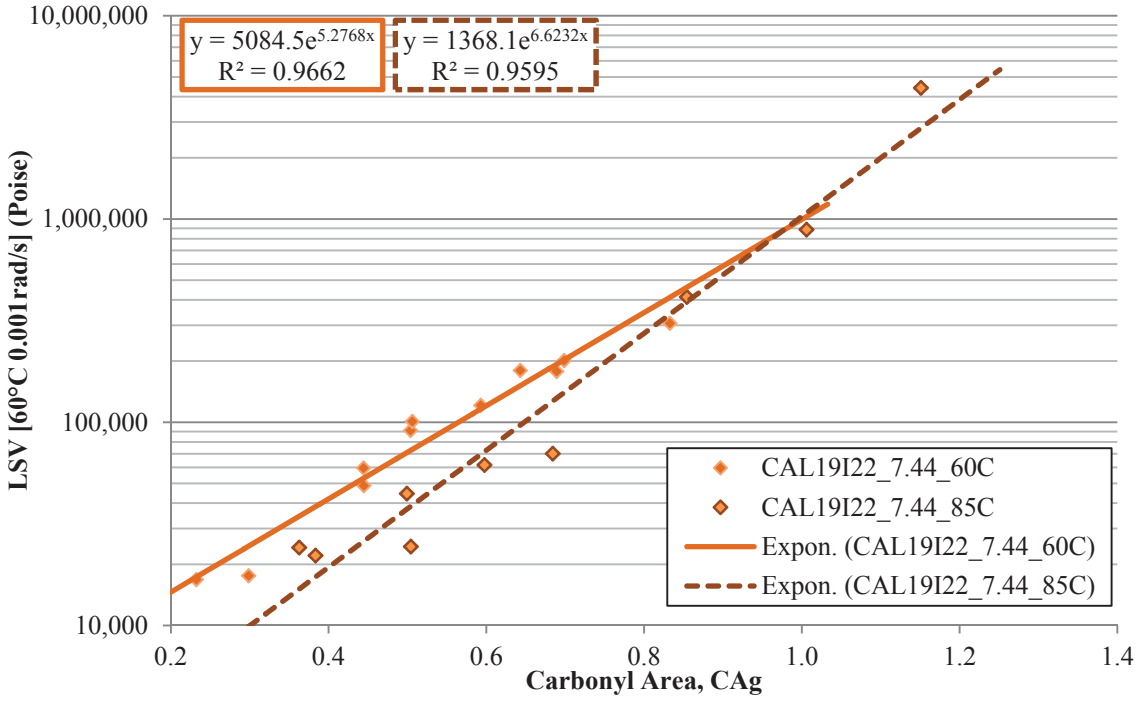

Figure 7.77 Hardening Susceptibility Relationships for the CAL19I22_7.44 Mixtures Aged at 60 and 85°C

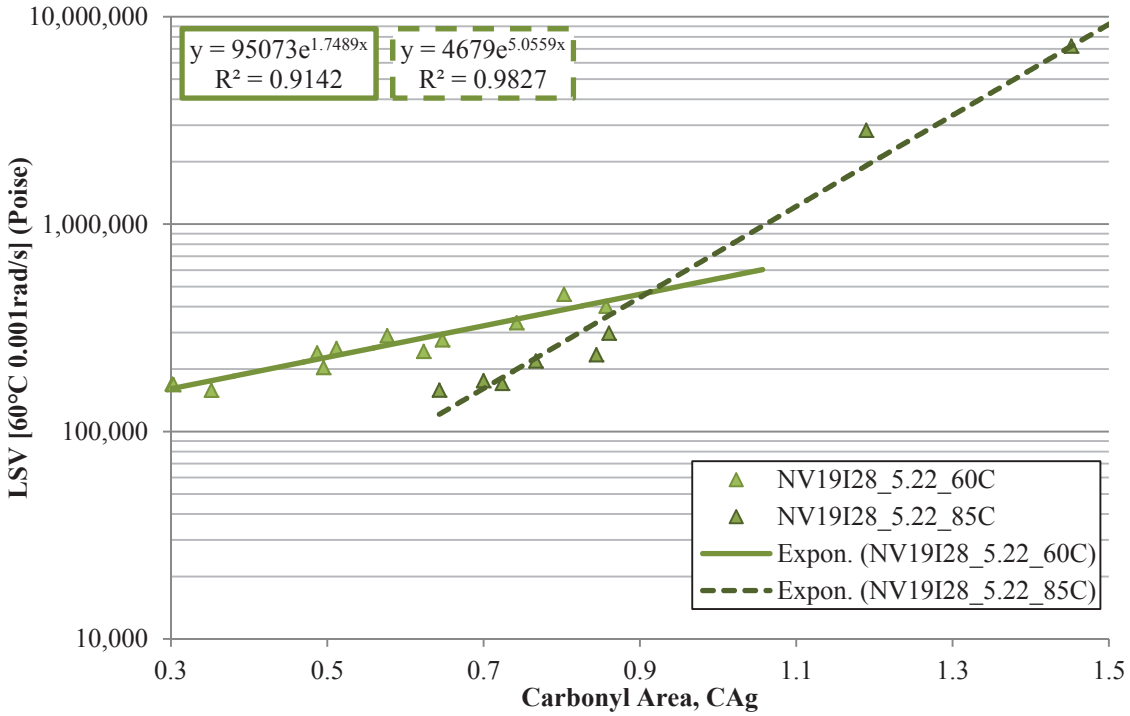

Figure 7.78 Hardening Susceptibility Relationships for the NV19I28_5.22 Mixtures Aged at 60 and 85°C

General observations of both Figure 7.77 and Figure 7.78 indicate a potential change in the HS relationship due to the temperature of the oven over the respective aging durations applied to the mixtures. In general, a trend very similar to pan-aged asphalt binders was observed generally indicating a noticeable increase in the HS parameter (slope) with the increase in the temperate during oxidation with both mixtures including both asphalt binders. By similar observations, the m value (intercept) also appears to be influence by temperature of the mixture aging. Interestingly enough, the intercept appears to decrease with increased aging temperature while the slope was noted to increase with temperature.

The stepwise transformed linear regression analysis was also preformed to statistically differentiate these noted observations with a summary of final model presented in Table 7.29.

Table 7.29 Statistical Significance Hardening Susceptibility at 60 and 85°C for Mixtures with 9μm Apparent Film Thickness

	CAL19I22_7.44_60 & 85°C			NV19I28_5.22_60 & 85°C		
Regression Parameter	Coefficient	P-value	Significance	Coefficient	P-value	Significance
Intercept-m, β_0	11.6850	0.000	Sig.	18.6842	0.000	Sig.
CAg (HS, β_1)	2.0450	0.280	NS	-6.187	0.000	Sig.
Temp.	-0.0525	0.003	Sig.	-0.1204	0.000	Sig.
(CAg)*Temp.	0.0539	0.039	Sig.	0.1323	0.000	Sig.
R^2 (%)	96.2			98.2		
Adj. R^2 (%)	95.6			97.9		

The statistical evaluation summarized in Table 7.29 indicates that the aging temperature was influential to the measures HS relationships from the mixture-aged binders. With both of the evaluated mixtures, the HS (slope) and the m value (intercept) were found to be statistically influenced by the differences in aging temperature.

It should be noted that the air void level was also found to be statistically influential with the HS measures over the two aging temperatures with the Nevada mixtures. However, removing the Va parameter from the analysis only reduced the overall R^2 by 0.5%, both of which were above the R^2 of the California mixture with the same analysis. To remain consistent throughout all the air void analyses with the mixture-aged binders, the Va term has been omitted while retaining acceptable HS relationships.

7.4.7 Summary of Mixture-Aged Asphalt Binder Hardening Susceptibility

In summary, this section has provided evidence that the hardening susceptibility relationships of the mixture-aged asphalt binder have been influenced by the aggregate and mixture parameters with which they were aged.

Specifically, in nearly all the evaluations, the air void level was found to have an insignificant influence on the HS relationship of the extracted and recovered asphalt binders. The one exception was the NV19I28_5.22 mixtures when compared at 60 and 85°C aging temperature. However, omission of the air void level in this particular analysis still provided a very acceptable regression relationship (i.e. Adj. R^2 of 97.9%), thus the analysis continued without Va as an input parameter.

Additional considerations of the mixture variables indicated that the asphalt binder grade (e.g. polymer modified or unmodified) was significantly influential to the HS relationships overall. This occurrence was noted with both slope (e.g. HS) and the intercept (m value) of the respective relationships.

Further, the influence of the gradation and aggregate properties were found to be influential to the HS parameters and indicated the aggregate absorption (Abs), dust proportion (DP), and AIMS measurement combining the coarse aggregate angularity and texture measurements (CAAT) were adequate in describing these influences.

The aging temperature was also found to be influential to the HS measurements over the range of evaluated air void levels with both the modified PG 64-28 and the unmodified PG 64-22 binders with two evaluated mixtures.

A summary of the statistical evaluations conducted on the HS parameters has been provided in Table 7.30 including references to the particular sections presenting more specific information on those evaluations.

Table 7.30 Summary of Influential Mixture Factors on Hardening Susceptibility Relationships

Input Variable	m value (Intercept)	Hardening Susceptibility (slope)	Analysis Reference
Abs	NS	Sig.	7.4.5
DP	Sig.	Sig.	7.4.5, 7.4.6
CAAT	NS	Sig.	7.4.5
BI	Sig.	Sig.	7.4.4, 7.4.5, 7.4.6
Va	NS	NS	7.4.3
Temp.	Sig.	Sig.	7.4.6

Overall, the influence of the aggregate and mixture properties were both observed to be significantly influential to the HS relationships of the mixture-aged asphalt binders observed in this evaluation.

7.5 Asphalt Binder-Aggregate Interaction

In addition to the physical property measurements, i.e. dynamic shear modulus, and the chemical characterization, i.e. FT-IR determinations of the chemical functional groups, the previous findings have suggested complex interactions between the aggregate sources and the asphalt binder included in this analysis. As a result, efforts to quantify these complicated physiochemical interactions became a useful endeavor. The quantification

of these interactions were determined by the combined effects of the binder adhesion to the aggregate surface, with secondary influences from the asphalt binder molecular weight and relative levels of polarity in the modified SARA analysis conducted at WRI.

Although discussed in further detail previously, the method essentially dissolves a known amount of asphalt binder in a relatively weak solvent, cyclohexane. The solution is then introduced to saturate a column of fine aggregate, i.e. passing the 0.60 mm (No. 30) and retained on the 0.30 mm (No. 50) sieve in this case. In this solution the asphalt binder is higher mobile permitting the most polar molecules of the asphalt binder to chemically adhere to the aggregate as the interaction chemistry would dictate. Upon removal of the solution, the relatively less and non-polar fractions of the binder are flushed out of the column. The fraction of binder that was removed in this step is somewhat analogous to the saturates and aromatic fractions in the ASTM standard D4124, after which this testing was modeled (ASTM, 2010).

Purging the system with a stronger solvent, toluene, then removed the asphalt binder fraction that had a midrange chemical bond with the packed aggregate column. This fraction would be somewhat analogous to the resin fraction determined in ASTM D4124 (ASTM, 2010).

One final purge with the strongest solvent, a 50:50 blend of toluene and methanol, essentially removes remainder of the asphalt binder from the column. This fraction then represents the asphaltenes component defined specifically as the most polar and thus the component exhibiting the strongest adhesion to the aggregate.

Each of the three fractions was then evaporated to remove their respective solvents and the weight determined the relative percentage of each fraction. To be specific, the

fractions determined in this manner do not necessarily correspond to the defined fractions found in ASTM D4124 (ASTM, 2010). Clearly, the expected influence of the interaction between the asphalt binder and the aggregate column would cause noted variations in the relative quantity of the fractions defined during this testing. Thereby, necessitating deviation from defined terms of saturates, aromatics, resins, and asphaltenes as defined in ASTM D4124 (ASTM, 2010).

This characterization was investigated on an exploratory basis with the Nevada and California aggregates combined with both the PG 64-22 and PG 64-28 asphalt binders. The Texas AGC 0002 aggregate was also evaluated, but with the relevant Venezuelan BI 0001 PG67-22 asphalt binder. Figure 7.79 through Figure 7.81 present the chromatograms of retention peaks with respect to the UV measures at the 450 nm wavelength conducted during the test procedure for each of the respective asphalt binder-aggregate pairs tested in this fashion. The UV absorbance is measured on the eluted solution flowing out of packed column to aid in the verification of the removal of each respective binder fraction.

A summary of the retained mass of each respective binder fraction for each of the measures is included in Table 7.31, except for the Texas aggregate, which was only evaluated by the peak height. Table 7.31 also includes an estimation of the different fractions based upon the relative peak heights of each binder fraction. Specifically, these percentages were calculated as a percentage of the summation of all three peak heights, two in the case of the BI1 and Texas aggregate measure. Figure 7.82 presents a visual representation of the same information to more clearly show the relative differences between the measurements both between the asphalt binders and the aggregate sources.

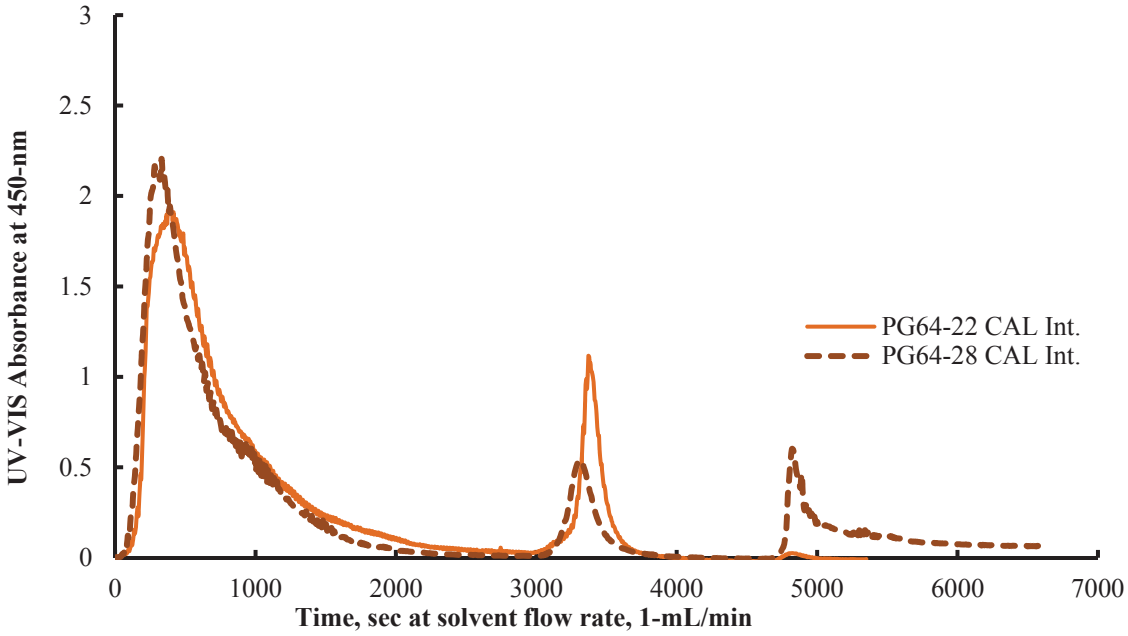

Figure 7.79 Chromatogram of Retention Peaks with California Aggregate

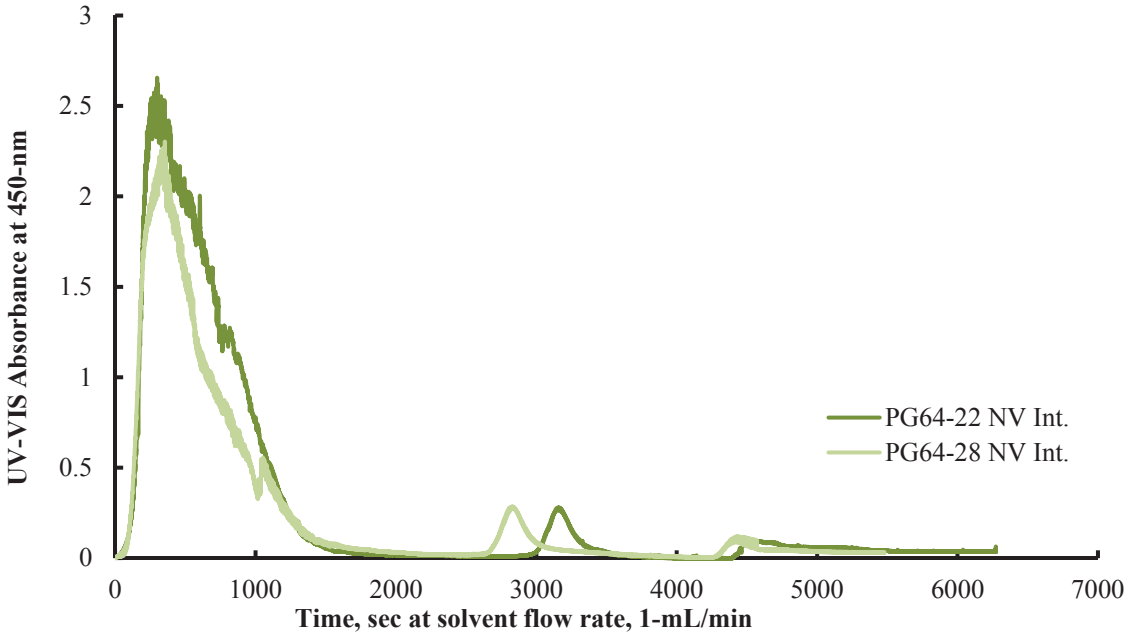

Figure 7.80 Chromatogram of Retention Peaks with Nevada Aggregate

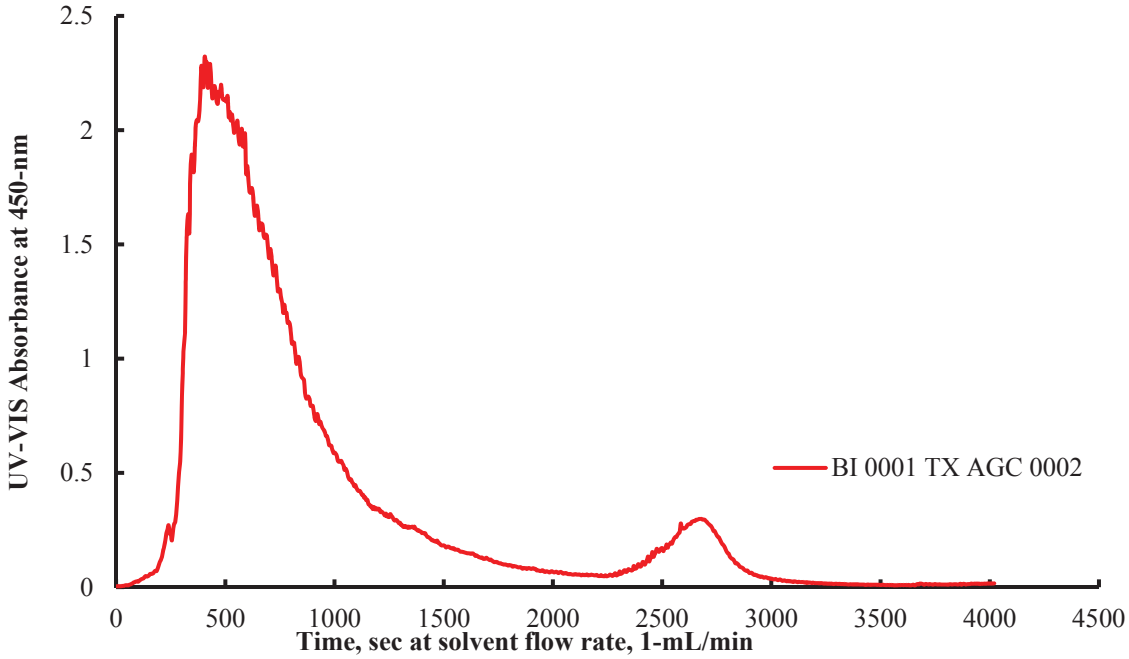

Figure 7.81 Chromatogram of Retention Peaks with Texas Aggregate

Table 7.31 Modified SARA Analysis of Select Asphalt Binders

Aggregate Source Aggregate Source	Asphalt Binder ID Asphalt Binder ID	Asphalt Binder Fractions, Percent by Mass		Asphalt Binder Fractions, Percent by UV Peak Height		
		1st Fraction, Cyclohexane	2nd Fraction, Toluene – Tol./Meth.	1st Fraction, Cyclohexane	2nd Fraction, Toluene	3rd Fraction, Tol./Meth.
California Intermediate	PG64-22	84	16	63	36	1
	PG64-28	85	15	66	16	18
Nevada Intermediate	PG64-22	96	4	85	11	4
	PG64-28	96	4	88	9	3
Texas	BI 0001 PG67-22	N/A[a]	N/A[a]	89	11	0

a – Mass fractions were not determined for the Texas aggregate measurements.

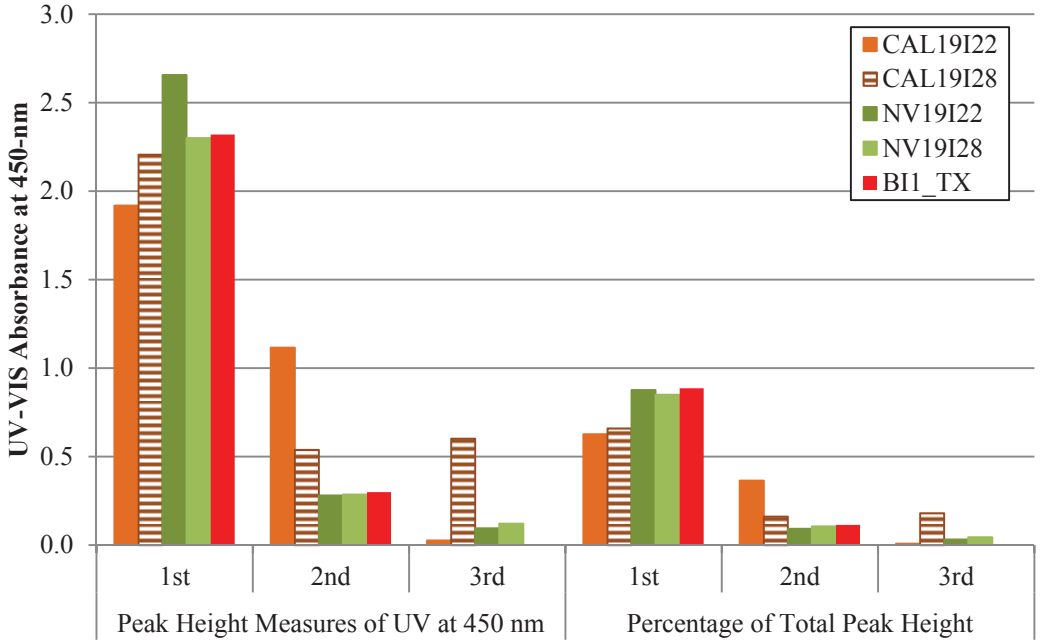

Figure 7.82 Summary of Retention Peaks for Exploratory Asphalt-Aggregate Blends

Initial observations of Table 7.31 when considering only the California aggregate source, suggest that the interaction between the PG 64-22 and PG 64-28 binders with the California aggregate are nearly identical based upon the calculated mass percentages. However, further observations of Figure 7.79 and Figure 7.82 suggest quite a different behavior between these materials. While the total percentage of the mass may be similar between the PG 64-22 and PG 64-28 measures, the distribution of the eluted material between the toluene wash and the toluene:methanol blend are expected to be quite different. Assuming the peak height is an acceptable representation of the eluted mass of binder, in actuality it likely is a representation of the concentration of the asphalt binder in solution, which can be expected to correlate to the mass, then there appears to be a large difference in the adhesion between the second and third peaks. Interpretation of the

second peak as mild to moderate adhesion of the binder to the aggregate, and considering the third peak as strongly adhered material, presents a fair distinct difference between the two binders when combined with the California aggregates. If this interpretation is correct, then the expectation is that the PG 64-28 binder should be expected to exhibit a much stronger bond with the aggregate which may influence oxidation characteristics of the combined mixture. If this noted difference does now follow the mixture oxidation measures and the two binders behave in a similar fashion upon aging, this may possibly suggest that the mild to moderate adhesion is sufficiently strong to influence the oxidation of the asphalt binder within a given mixture.

Consideration of the Nevada aggregates in Figure 7.81 and the information provided in Table 7.31 led to fairly different results from the California aggregate source. These measures suggested that the interaction between the Nevada aggregates and the PG 64-22 and the PG 64-28 asphalt binders utilized in this study are fairly similar to each other. This does not limit the value of the information, since there are marked differences between both binders mixed with the Nevada aggregates and the noted differences with the California aggregates. These noted variations will be considered at length in the respective sections devoted to the comparison of the pan-aged and mixture-aged asphalt binders.

As a matter of completeness, observation of the BI 0001 binder combined with the Texas aggregate seem to present similar adhesion properties as the Nevada aggregates, with the exception of the third peak with the BI1/TX blend. This finding presents a rather expected result, suggesting by the lack of a strongly adhered binder fraction that the calcareous nature of the Texas limestone does not possess the strong attraction of the

siliceous material noted with the other two aggregate blends. As such, the influence of the potential effect of only the mild to moderate interactions may be examined to further differentiate the effect of the stronger interactions noted with the siliceous materials.

7.6 Sulfur Content of Asphalt Binder

The sulfur content of the asphalt binders used for the majority of this investigation, i.e. PG 64-22 and PG 64-28, were determined on original or tank binders samples by Wyoming Analytical Laboratories, Inc. of Laramie, Wyoming according to ASTM D2622 which is the Standard Test Method for Sulfur in Petroleum Products by Wavelength Dispersive X-ray Fluorescence Spectrometry. Details of the method are left to the published standard test method. The results of the measures are presented in Table 7.32 for the PG 64-22 and PG 64-28 asphalt binders utilized for a significant portion of this evaluation.

Table 7.32 Sulfur Content of Select Asphalt Binders

Asphalt Binder ID	ARC Database ID	Total Sulfur, % by weight
PG 64-22	BI 0052	3.94
PG 64-28	BI 0051	3.85

These measurements were conducted from a reference standpoint, to assure that the majority of the kinetics measurements were not significantly influenced by the total sulfur content of the asphalt binders, which would present a significant stiffening of the binders as a function of sulfoxide growth. The generally accepted level to determine

significant influence on the rheological and kinetics measures has been stated to be closer to 5 or 6% of the binder weight (Robertson et al., 2006).

Given that both of these measured asphalt binders are at least one percent below that level, it has been generally assumed that the utilized carbonyl measurements satisfactorily describe the oxidation process in this investigation and the sulfoxide growth may appropriately be neglected.

8 INFLUENCE OF MIXTURE CHARACTERISTICS ON ASPHALT BINDER AGING

The previous chapter established measurements of the binder oxidation, physical properties (i.e. rheology), and their combined properties (i.e. HS parameters) for both pan and mixture-aged binders. Previous analyses contrasted the different responses between the respective aging conditions of the materials (i.e. mixture-aged or pan-aged binders). Those results will now be considered to explore the differing effects of the mixture aging as compared to the aging conducted in the laboratory pans. The following sections will present the influence of the aggregate and mixture characteristics on the oxidation and HS parameters as those have been identified to have the most significant influence on oxidation modeling efforts described in chapter 3.

8.1 Oxidation Kinetics of Pan-Aged and Mixture-Aged Binders

Comparisons of the oxidation growth between the pan-aged and mixture-aged binders were considered initially with the aging temperature held constant. Since each of the respective aging conditions (i.e. pan-aged and mixture-aged) utilized the 60°C aging temperature over different durations, the analysis will initially consider those measurements. The oxidation (i.e. CA) measurements are presented in Figure 8.1 and Figure 8.3 for the pan and mixture-aged PG 64-22 and PG 64-28 binders, respectively.

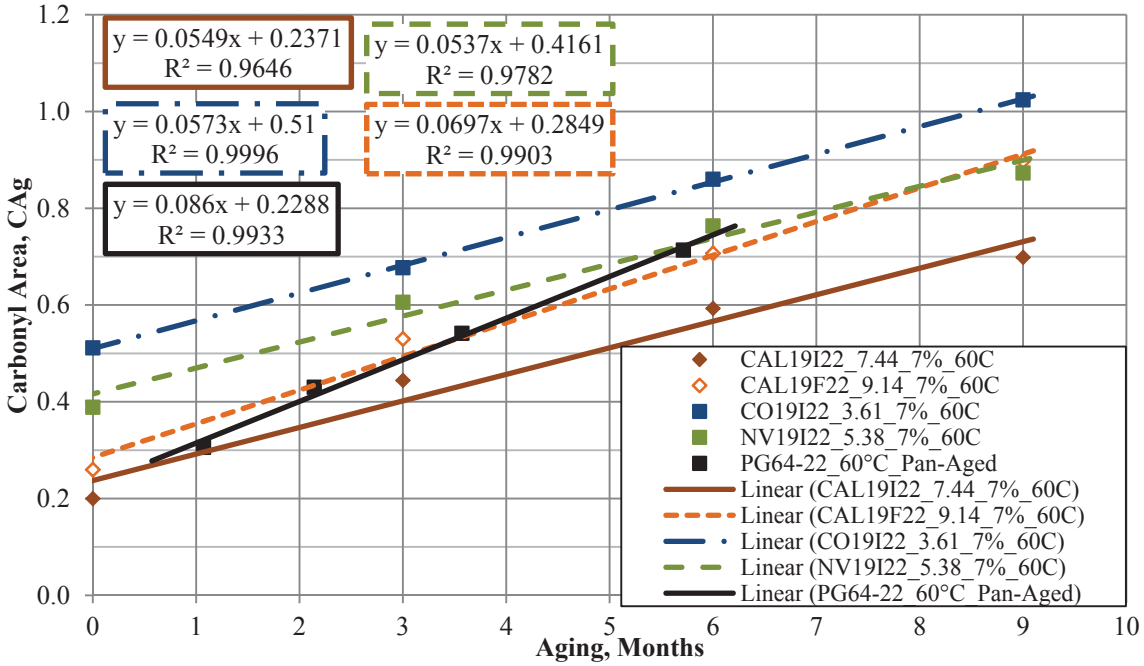

Figure 8.1 Pan-Aged and Mixture-Aged Oxidation Measurements of the PG 64-22 Binder Aged at 60°C

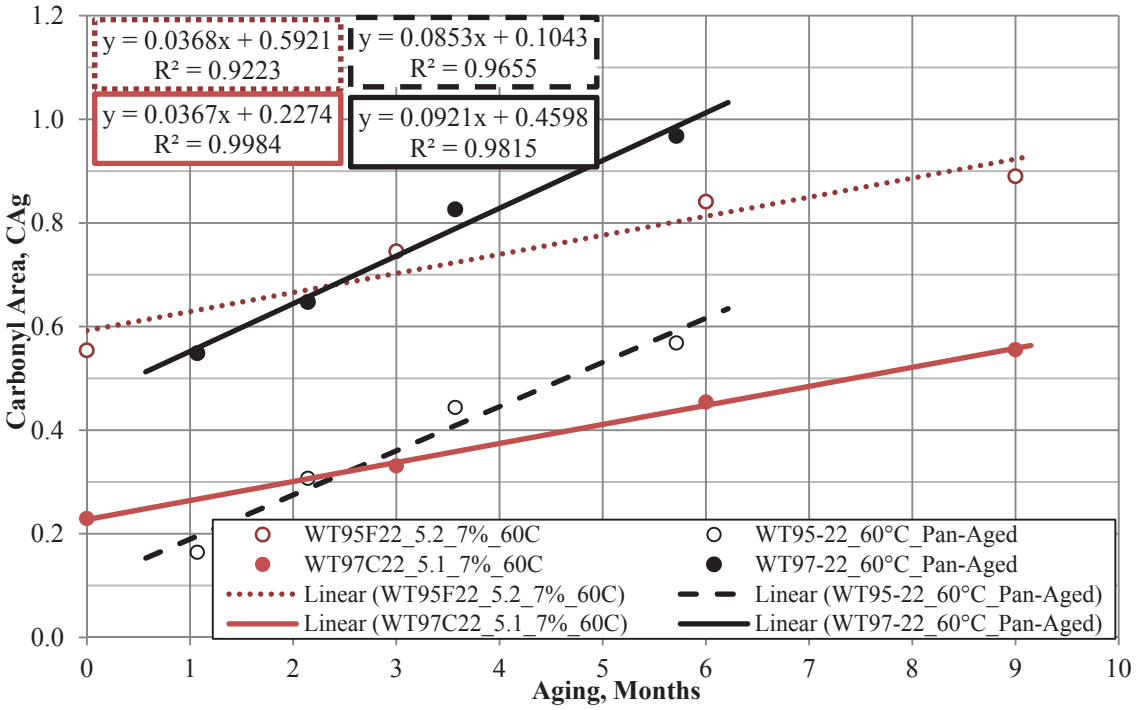

Figure 8.2 Pan-Aged and Mixture-Aged Oxidation Measurements of the WesTrack Binders Aged at 60°C

Considering the rate of aging represented as the slope of the CAg measures as a function of time for the pan-aged PG 64-22 binder compared to the other aging rates of the same binder aged in the mixtures in Figure 8.1, it is clear that the rate of aging was reduced in the mixture-aged binder for the same 60°C aging temperature. Although the overall oxidation measurement (magnitude of CAg) may be relatively similar, the slope of the pan-aged binder was clearly higher than the mixture-aged binders regardless of the aggregate used or the binder content of the mixture.

By simple observation and consideration of the slope of the fitted trend lines the mixture with the slope closest to the pan-aged binder was the CAL19F22 which also had the highest asphalt content (i.e. 9.14% TWM). However, the other mixtures presented in Figure 8.1 were not systematically ranked according to the binder content.

The two WesTrack binders and two mixtures presented in Figure 8.2 also indicate a noticeable increase in the rate of oxidation with the pan-aged binder compared to those of the mixture-aged binders. The magnitude of the measured CA values are notably different, with the CA measures of the pan-aged binders plotting below the mixture-aged binders for the WT95 and the opposite noted for the WT97, again with both aged at 60°C.

These measures indicated that unmodified binders aged in mixtures with the 9 μm AFT, the mixture-aged CA growth was lower (i.e. occurred at a slower rate) than the comparative pan-aged binders at the same 60°C. Consideration of the SBS modified materials, again with the 9 μm AFT mixture-aged and the pan-aged binders aged at 60°C are presented in Figure 8.3.

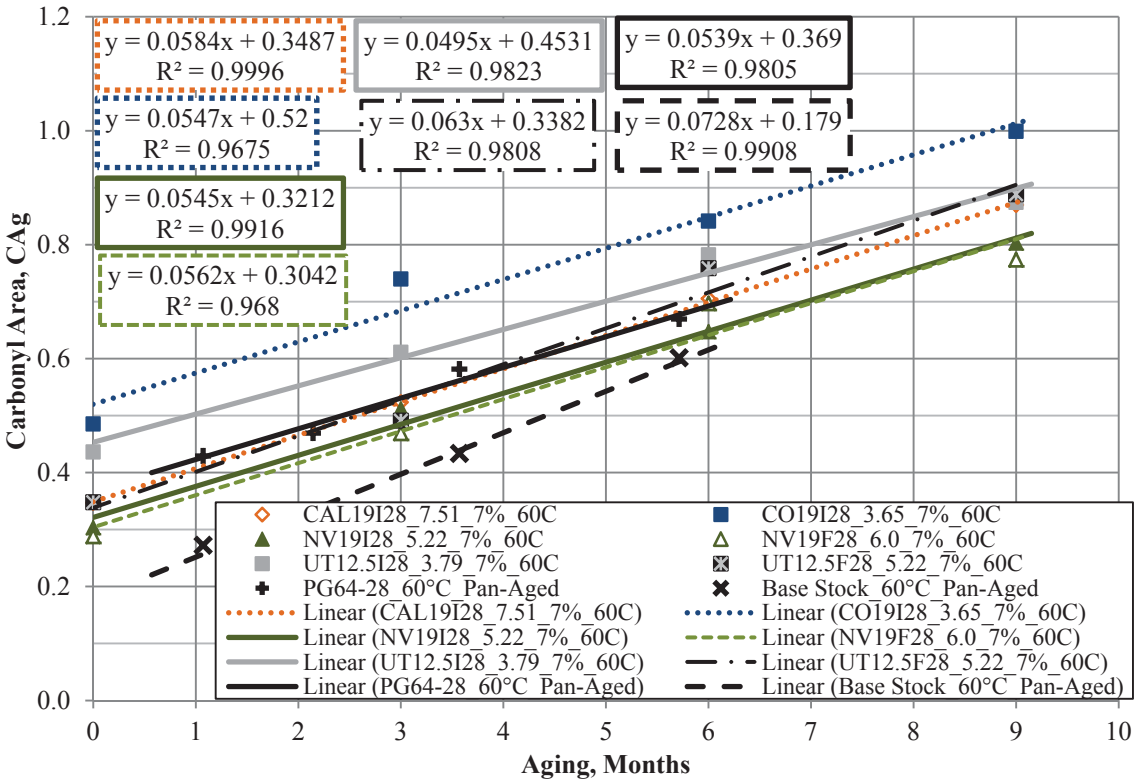

Figure 8.3 Pan-Aged and Mixture-Aged Oxidation Measurements of the PG 64-28 Binder Aged at 60°C

Comparison of the modified binders in Figure 8.3 indicates a different conclusion from the previous consideration of the unmodified binders. With the SBS modified materials, the rate of the oxidation is nearly the same for the pan and mixture-aged binders. In fact most of the mixture-aged materials numerically present a slightly faster oxidation rate compared to the pan-aged binder at 60°C. Figure 8.3 also presents the oxidation rate of the Base Stock binder used to produce all the SBS modified PG 64-28 binders shown in the figure. The Base Stock binder exhibited the highest rate of oxidation among the binders presented in this figure. This finding suggests that the influence of the aggregate and/or mixture characteristics resulted in a reduction of the oxidation rate as did the polymer modification of this particular asphalt binder. This may not be the case for every

asphalt binder and polymer combination, but the same trend also occurred with the 3% SBS added to the PG 64-22 binder by referencing Figure 7.4 of the previous chapter.

Statistical differentiation of these measures was not conducted since these measures lend directly to the kinetics parameters E_a and AP^{α} of the kinetics relationships presented previously as Equation 7.1. In order to develop these full relationships, the aging must be conducted over multiple temperatures (i.e. a minimum of two). Therefore, initial considerations of this type will be considered with the California and Nevada mixtures as they were aged at both 60 and 85°C as presented in Figure 8.4 and Figure 8.5, respectively.

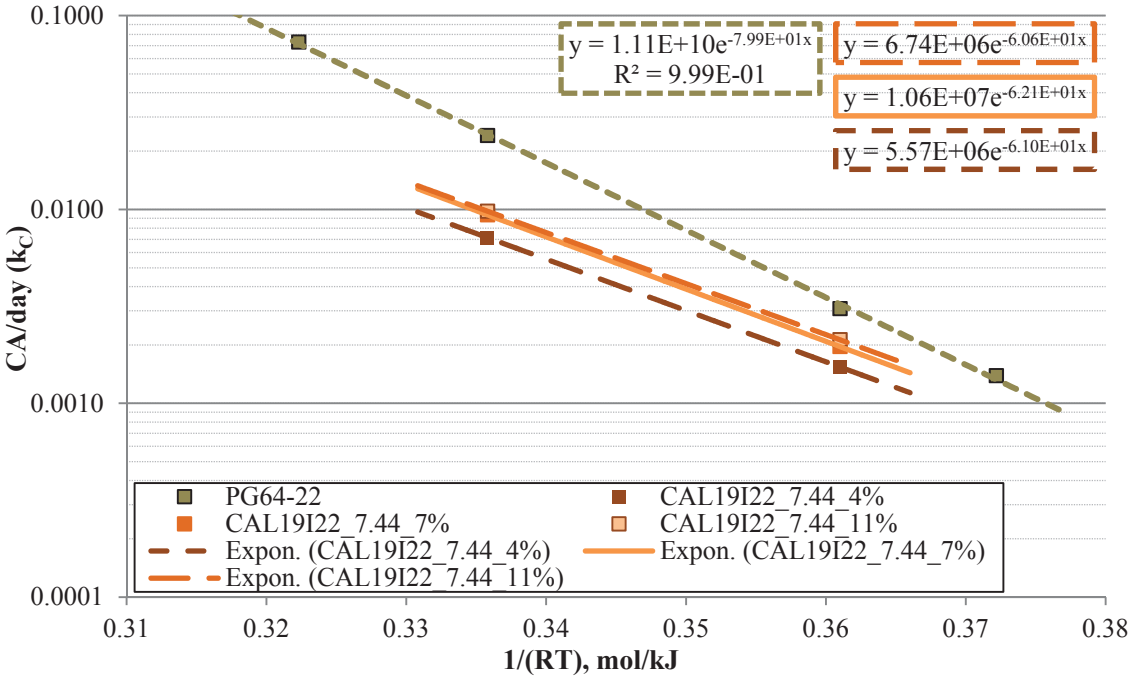

Figure 8.4 Pan-Aged and Mixture-Aged Oxidation Kinetics of the PG 64-22 Binder Aged at 60 and 85°C

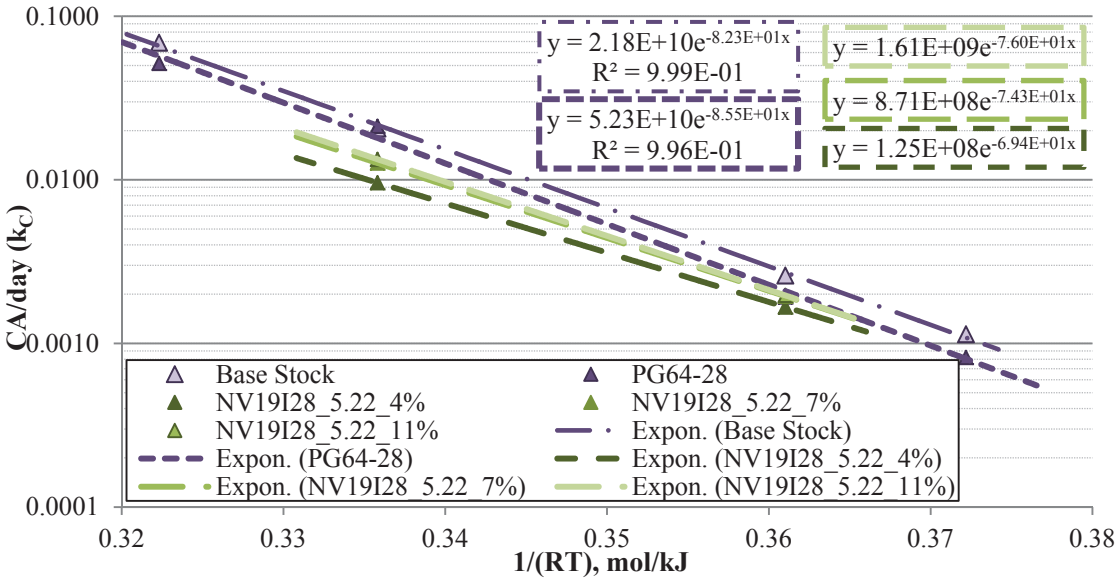

Figure 8.5 Pan-Aged and Mixture-Aged Oxidation Kinetics of the PG 64-28 Binder Aged at 60 and 85°C

By adding the mixture-aged kinetics determination to those of the corresponding pan-aged binders presented in Figure 7.4 and Figure 7.5, the present comparisons indicate a clear differentiation between the mixture-aged and pan-aged binders. Specifically, the measurements of the pan-aged materials with both the PG 64-22 and the PG 64-28 binders exhibit higher rates of oxidation at the measured aging temperatures noted by the k_C term which is equivalent to the r_{CA} term noted in Equation 7.1.

More detailed observations note the consistent decrease in the slope (E_a) and the intercept (AP^{α}) of the mixture-aged binders compared to the corresponding pan-aged binders. Further, there is a systematic decrease in the AP^{α} term with increased air void level of the mixture-aged binders for both asphalt binders. The Nevada mixtures containing the PG 64-28 binder also has a systematic decrease in the E_a term with increases in the air void level. However, this same trend was not numerically present

with California mixtures containing the PG 64-22 asphalt binder, though they are relatively close to one another.

It is also worth mentioning that the mixture-aged measurements only included two aging temperatures as opposed to the four temperatures utilized to produce the pan-aged binder kinetics parameters. This is not to suggest the mixture-aged data are not valid, but to highlight the fact that the slight variations in the mixture-aged relationships may be significantly influenced by slight variation in a single measured data point. Whereas, the pan-aged binder relationships are not as sensitive being developed from four aging temperatures. However, the trends still exhibit a clear differentiation between the oxidation kinetics parameters (i.e. E_a and AP^{α}) of the mixture-aged and pan-aged asphalt binders.

To summarize, these findings indicate that the oxidation kinetics parameters (i.e. E_a and AP^{α}) which would represent a significant input into the oxidation prediction modelling are reduced by the influence of aggregate and mixture characteristics with both the unmodified PG 64-22 and the SBS modified PG 64-28 asphalt binders based upon the selected mixtures evaluated here.

To further analyze this occurrence, reference is made to Figure 7.10, which presented the relationship between the kinetics parameters (i.e. E_a and AP^{α}) of the fifteen pan-aged binders included in this investigate. This relationship between the kinetics parameters is summarized in Figure 8.6, which also includes the mixture-aged kinetics parameters from the California and Nevada mixtures for comparative purposes. This figure has also highlighted which of the previous fifteen data pint correspond to the asphalt binders being evaluation with the mixture kinetics measurements.

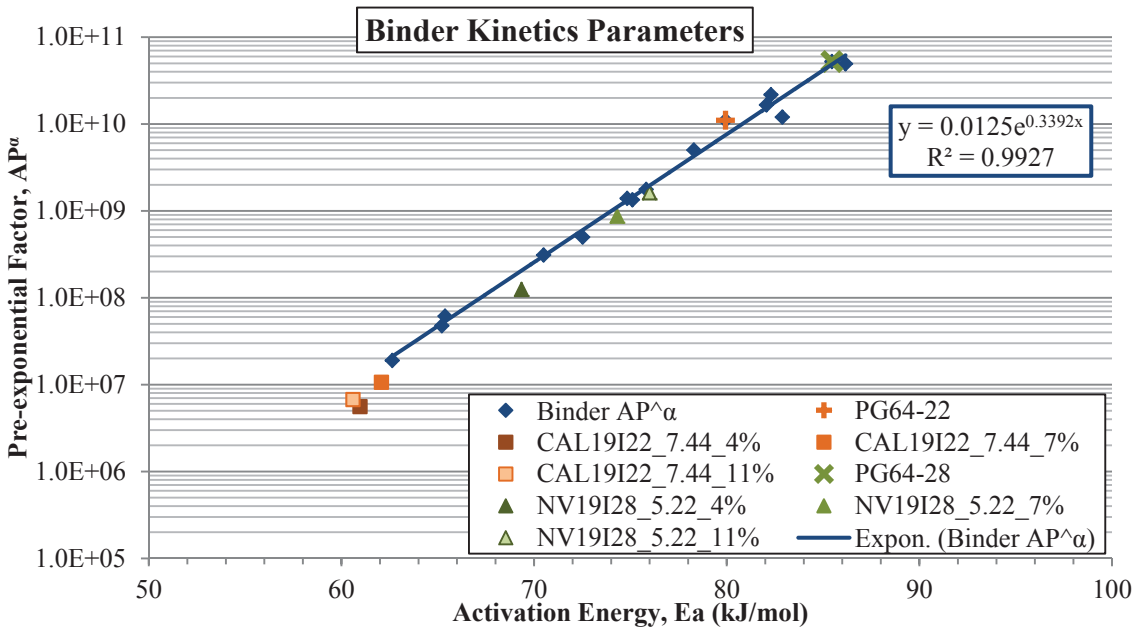

Figure 8.6 Pan-Aged and Mixture-Aged Oxidation Kinetics

Observation of the kinetics parameters from the perspective given in Figure 8.6, clearly indicates the differences between the mixture-aged and pan-aged asphalt binders. Although they still generally follow the same overall relationship, the relative position along that relationship has been affected with the mixture-aged binders. For instance, considering the pan-aged PG 64-28 located in the far upper right of the plot, in contract to the mixture-aged measures with the Nevada aggregates, which are more centrally located on the plot, clearly show the influence of the either aggregate or mixture characteristics. In fact, the air void level also exhibits a systemic variation in the kinetics parameters with the 11% Va measures being the closest to the pan-aged measures followed by the 7% and finally the 4% Va measures.

Similar observations are noted among the California mixtures with the PG 64-22 binder, although the ordering of the air void levels are not as clear as was noted in the

previous Figure 8.4 as well. Nevertheless, there is a definite separation between the location of the pan-aged PG 64-22 binder and the mixture-aged CAL19I22_7.44 measurements along the kinetics parameter relationship developed through this investigation and others (Glover and Cui, 2013).

8.2 Temperature Dependency of Hardening Susceptibility

With the oxidation kinetics parameters being the first material specific input into the oxidation modeling procedure described in chapter 3, the second material input to consider is logically the hardening susceptibilities (HS) of the mixture-aged and pan-aged asphalt binders. Being that the HS parameters are determined by the relationship between the oxidation and rheological measures, these considerations incorporate influences from both of those parameters into one combined relationship.

Since only the California and Nevada mixtures were aged at more than one temperature, the influence of the aging temperature on the HS parameters will be considered only on those mixtures. Previous discussions in sections 7.1.6 and 7.4.6 noted significant differences between the HS parameters of certain binders aged at 60 and 85°C. Thus, the relative comparisons of the California and Nevada mixture-aged and corresponding pan-aged PG 64-22 and PG 64-28 binders were considered by combining all three air void levels for each mixture in Figure 8.7 and Figure 8.8, respectively

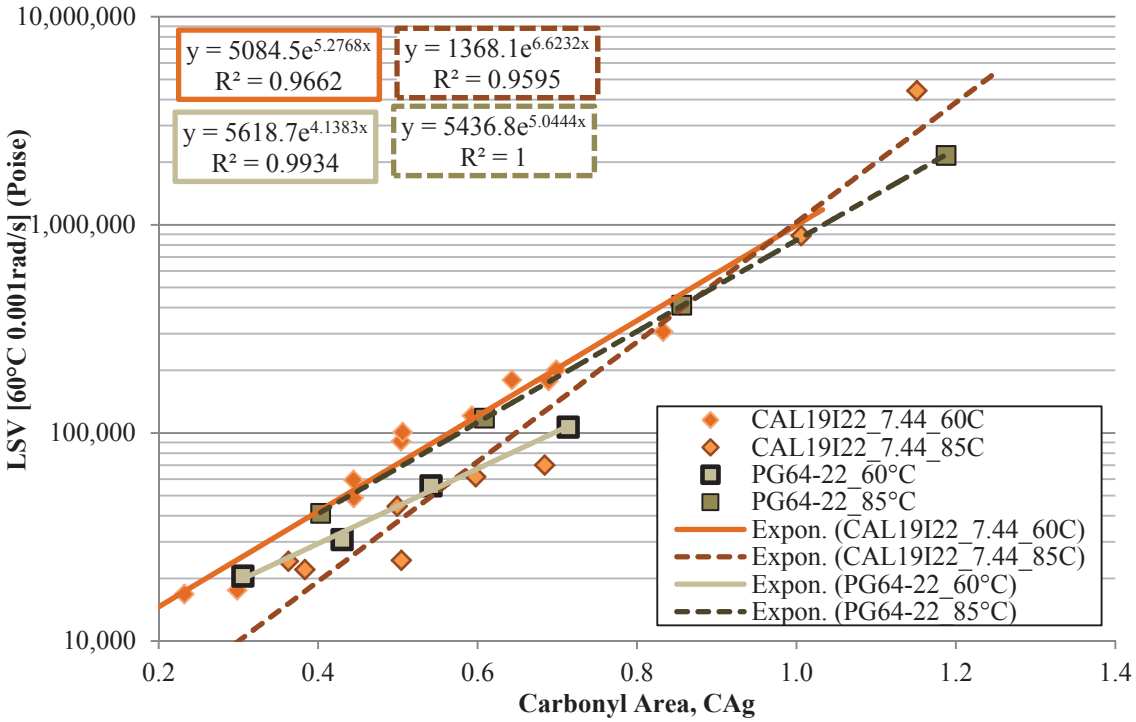

Figure 8.7 Hardening Susceptibility Relationships for the CAL19I22_7.44 Mixtures Aged at 60 and 85°C

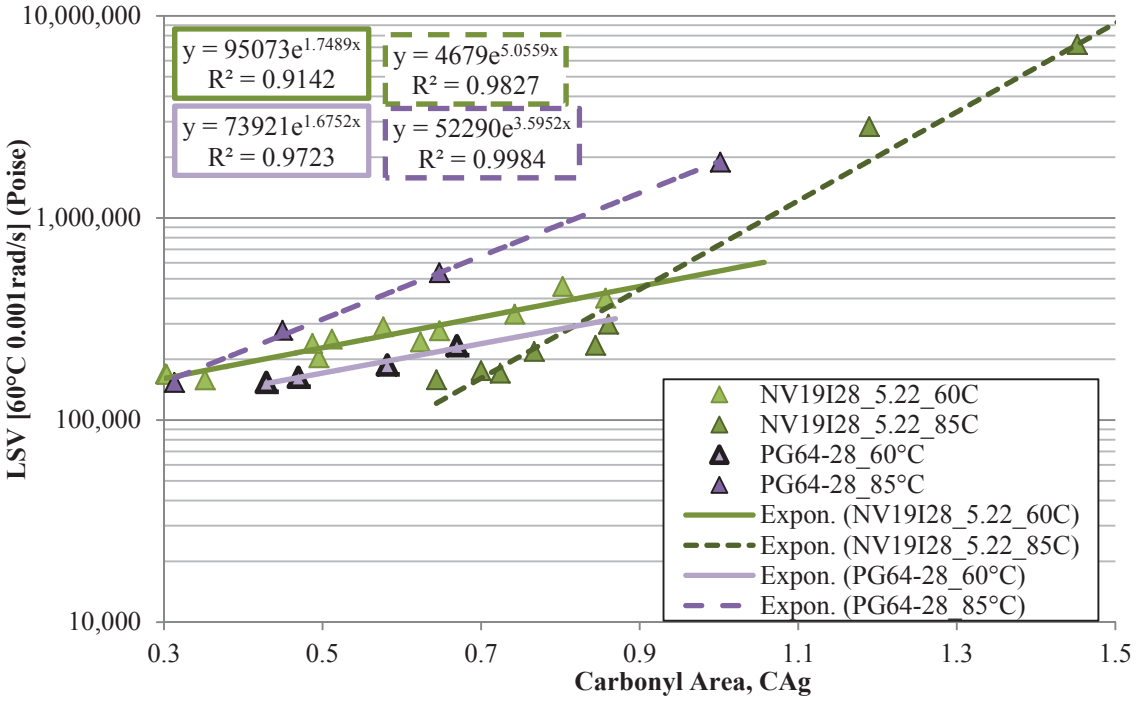

Figure 8.8 Hardening Susceptibility Relationships for the NV19I28_5.22 Mixtures Aged at 60 and 85°C

Examination of the PG 64-22 binder of Figure 8.7 shows the relative insensitivity of the unmodified binder to the aging temperature (i.e. the influence is not drastic). However, reference to Figure 7.27 and Figure 7.77, the PG 64-22 binder does show some degree of dependency on the aging temperature with the unmodified binder. Comparison of both the mixture-aged and pan-aged binders suggests that a very similar influence of the aging temperature is noted with the mixture-aged binder measures as well. The difference is clearly presented as an increase in the HS measurement itself (exponential term) with aging temperature for both the mixture-aged and pan-aged relationships.

Similar considerations of the Nevada mixtures with the PG 64-28 binder in Figure 8.8, present very similar but more profound differences between the aging temperatures. The relative increase in the temperature dependency of the modified binder noted previously in Figure 7.28 and Figure 7.78, was also observed in the measurements of the mixture-aged binders from the Nevada mixtures. In addition, it is interesting to note the general similarities between the HS measurements (i.e. slope) of the mixture-aged and pan-aged binders.

In summary, both asphalt binders exhibit marked differences in the HS relationships between different aging temperatures with the extent of the difference being binder dependent. This was noted with both the pan-aged as well as the mixture-aged asphalt binders.

8.3 Hardening Susceptibility of Pan-Aged and Mixture-Aged Binders

In addition to the California and Nevada mixtures aged at two temperatures, the majority of the mixtures were aged at 60°C for the appropriate durations. To provide a summary of these considerations, the HS of the mixtures aged at 60°C with the calculated 9 µm AFT are presented in Figure 8.9 through Figure 8.11, with respect to the different asphalt binder grades, which were also included. Thus, Figure 8.9 presents the HS of the PG 64-22 binder and the relevant mixtures that contain that particular asphalt binder. Figure 8.10 presents the pan-aged and mixture-aged HS relationships for the WesTrack binders. Figure 8.11 present the relevant mixture-aged and pan-aged measures for the PG 64-28 asphalt binder as well as its Base Stock binder.

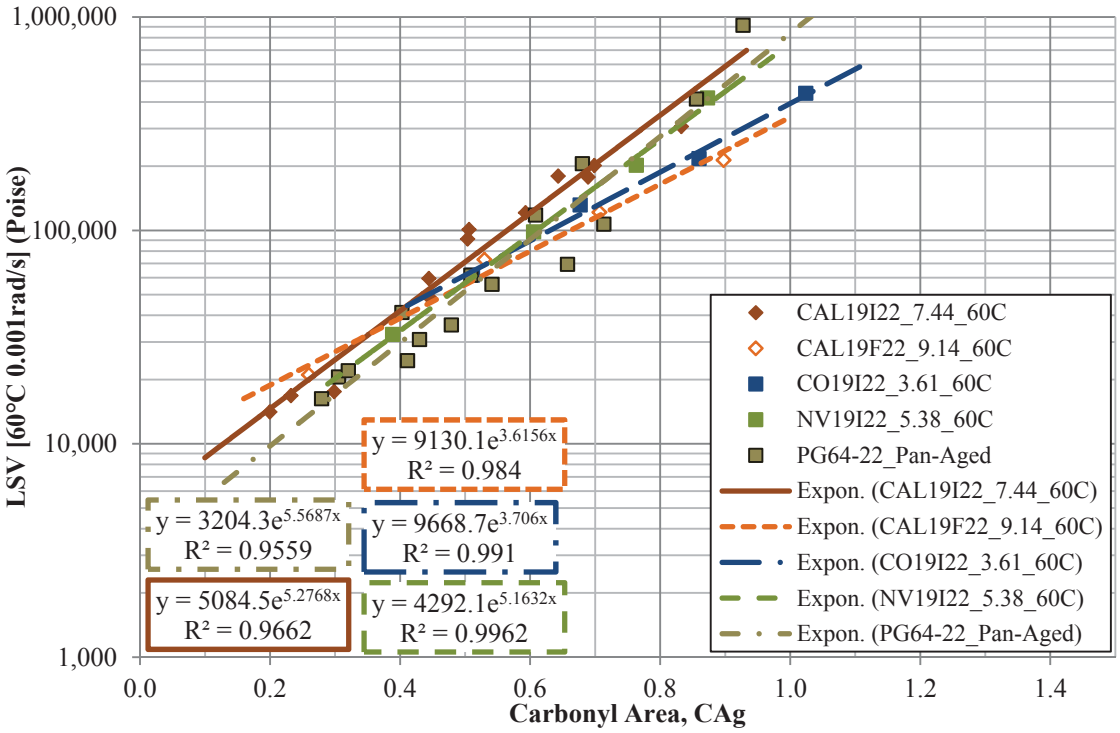

Figure 8.9 Hardening Susceptibility Relationships for Pan-Aged and Mixtures-Aged PG 64-22 Binder

The HS relationships found in Figure 8.9 suggest that there was a larger variation in the HS parameters between the mixture-aged binders than for the same binder aged in the pan and in the mixture. The variability of the mixture-aged HS relationships has already been discussed in section 7.4, but generally found that the observed variability can statistically be explained with a combination of the aggregate (i.e. absorption and CAAT), mixture (i.e. dust proportion), and binder grade (i.e. the categorical BI factor).

In general, the HS measurements of the pan-aged binder considered here are generally thought to fit within the range of mixture-aged binders. However, no valid statistical evaluation was conducted since the variation in the mixture measurements has already been statistically explained, thus any significant parameter observed between the pan and mixture-aged binders would essentially be a categorical or dummy variable, and thus viewed with limited practical significance. Essentially, any mixture variable used to describe the difference between the two aging systems could provide a value for the mixtures (i.e. absorption, film thickness, dust proportion, air voids, etc.) would by necessity either be a value of zero or unity for the pan-aged binders. This occurrence essentially reduces each of those input parameters from a continuous input variable to a less practical categorical or dummy variable which is not overly useful in this evaluation.

Similar consideration of additional unmodified binders utilized in the WesTrack project are considered in the Figure 8.10 for both the 1995 and 1997 materials aged both in pans and in their respective mixtures. The WT95F22 mixtures were only aged with 7% air voids, while the WT97C22 mixtures included all three air void levels (i.e. 4, 7, and 11%). Further, both mixtures were prepared at binder contents used in the field, but also with nearly the same AFT of 9 μm.

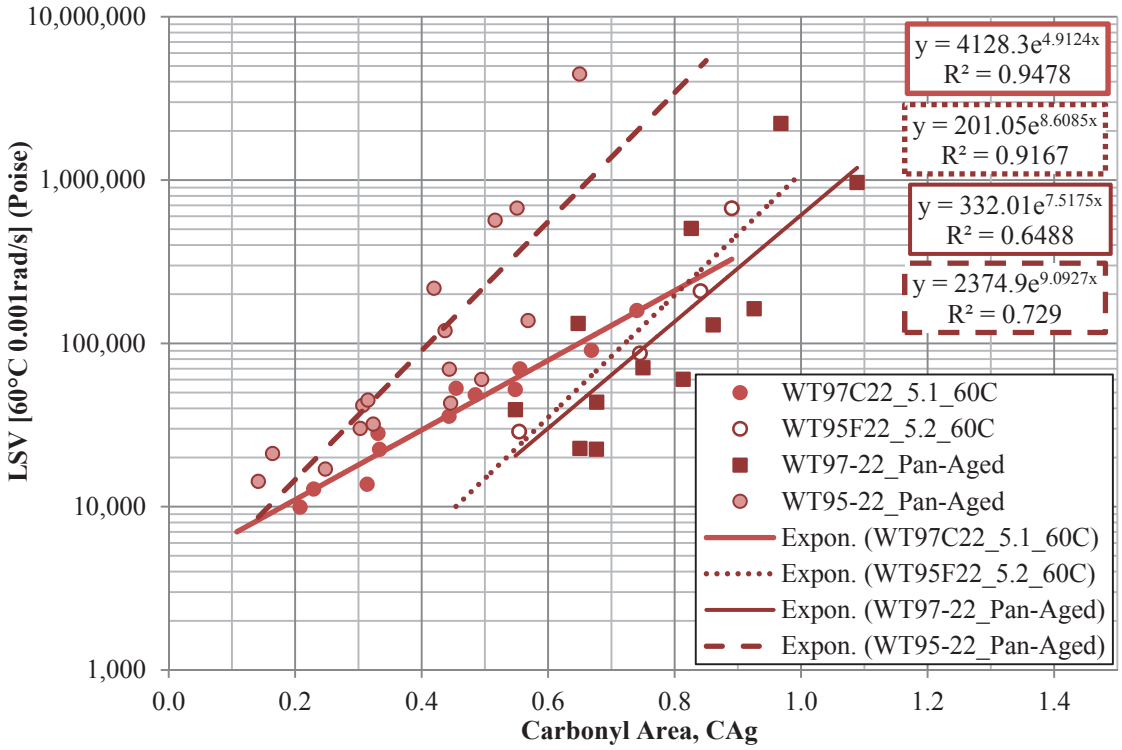

Figure 8.10 Hardening Susceptibility Relationships for Pan-Aged and Mixtures-Aged WesTrack Binders

Observation of the pan-aged and mixture-aged WesTrack binders from 1995 generally support the findings of the PG 64-22 binder previously by exhibiting nearly the same slope with the mixture-aged and pan-aged binder measurements. Even though the HS (slope) is nearly the same the m-value (intercept) was noted to be substantially different between the aging conditions. Further consideration of these binders highlighted the significant increase in the variability of the pan-aged WT95F22 binders indicated by the comparatively lower R^2 near 0.73. Reference to Figure 7.29 indicated the high level of sensitivity of the HS measures with both of the WesTrack pan-aged binders, but especially the HS of the WT95-22 binder aged at 85°C. This increased level of temperature dependency is understood to directly influence the overall variability of the

pan-aged HS for the binder due to the fact that the HS of all four aging temperatures are combined for the final HS of the binder. Quite similar observations are noted with the pan-aged WT97-22 HS measures which exhibited an even lower R^2 of less than 0.65. The slopes of the HS parameters of the mixture-aged and pan-aged WesTrack 1997 binders are noticeably different. However, such generalizations between the aging conditions should be viewed with caution due to the drastic differences between the variability of the measured HS values. In spite of these precautions, the HS of the mixture-aged binder were numerically reduced compared to the pan-aged binder for both WesTrack materials.

The comparison of the HS parameters is continued with the mixture-aged PG 64-28 and associated pan-aged PG 64-28 and the corresponding Base Stock binder in Figure 8.11.

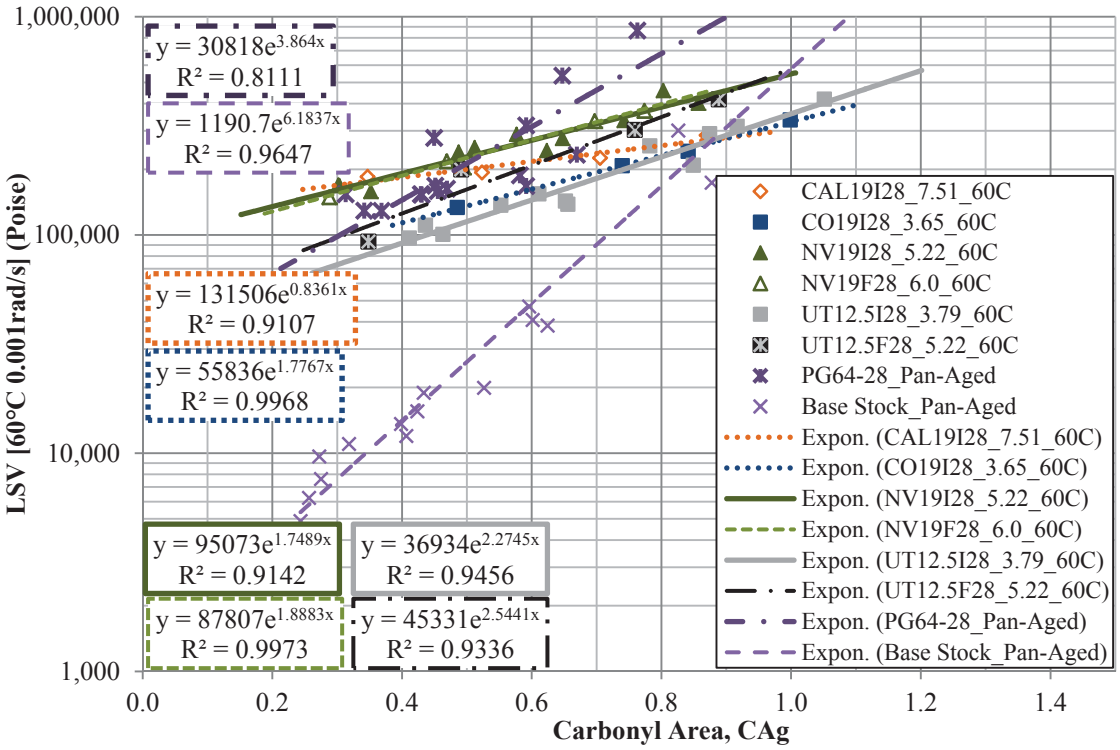

Figure 8.11 Hardening Susceptibility Relationships for Pan-Aged and Mixtures-Aged PG 64-28 and Base Stock Binder

Somewhat unlike the kinetics parameters presented in Figure 8.3, the HS parameters of the mixture-aged and pan-aged binder are notably different with the PG 64-28 binders. The HS of the pan-aged PG 64-28 more closely matched that of the Base Stock binder, however the Base Stock exhibited the highest HS measurement shown in the figure. However, there is also a clear difference between the HS of the mixture-aged and pan-aged PG 64-28 asphalt binders.

Similar to previous considerations with the PG 64-22 binder, the variations in the mixture-aged HS measures has been discussed in section 7.4. Similar to the WesTrack binders, there is a noted increase in the variability of the pan-aged PG 64-28 asphalt binder represented by the R^2 value slightly higher than 0.81. In very much the same

manner as the WesTrack binders, some portion of this variation is attributed to the temperature dependency of the HS measures as presented in Figure 7.25 and Figure 7.28. However, the differences in the HS of the Base Stock, pan-aged PG 64-28, and the mixture-aged PG 64-28 asphalt binders are fairly distinct in spite of the differences in the overall variability.

Thus, an overall assessment of the comparison of the pan-aged and mixture-aged binders has determined the comparison to be inconsistent overall. Similarities were noted with the unmodified PG 64-22 binder, but noted differences were also observed with other unmodified binders (i.e. WesTrack). Additional deviations were also noted between the pan-aged and mixture-aged HS parameters with the modified PG 64-28 asphalt binder, including comparisons with the accompanying Base Stock asphalt binder.

As a result of these findings, efforts to clearly differentiate the significance of these parameters in relation to one another have led to consideration of the relationship between the HS and m parameters, similar to the relationship noted between the kinetics parameters (i.e. E_a and AP^{α}) in section 8.1. Thus, Figure 8.12 presents the m value (intercept) and measured HS (slope) of all 15 pan-aged binders and 21 of the mixture-aged binder relationships collectively. Recognizing that Figure 8.12 presents a large number of data points in a limited space, the overall trend will be established followed by more detailed considerations based upon the abbreviated figures that follow.

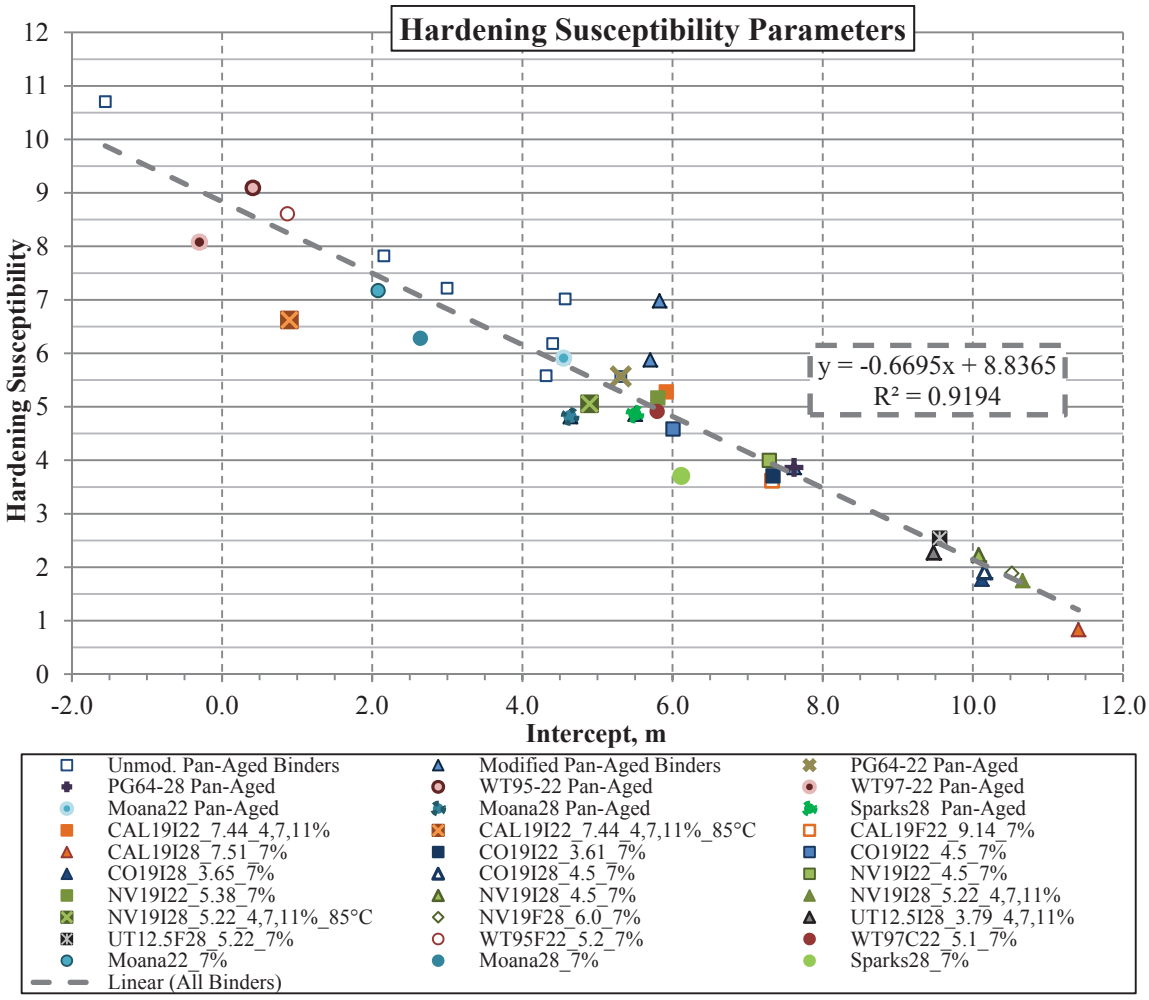

Figure 8.12 Hardening Susceptibility Relationships for the Pan-Aged and Mixture-Aged Asphalt Binders

Initial observations of Figure 8.12 indicate a fairly reliable relationship between the HS and m parameters considering the 36 total data points, which are each composed of three to twelve individual measurements and still resulting in an overall R^2 of nearly 0.92.

Further observations of the figure indicate that there are general groupings of the data as a whole. In general the unmodified binders tend to be in the upper left of the relationship, while the polymer modified binders tend to occupy the lower right. This follows the general observation that the unmodified binders had a tendency to age at a

faster rate and exhibited a higher HS (slope) than the modified binders. Additionally, the pan-aged measurements were also typically noted to appear higher and to the left from the mixture-aged measures for most binders. More careful considerations of these observations will be conducted with the more focused relationships found in Figure 8.13 though Figure 8.15.

One observation to note is the couple of points on the far left that have negative m values (i.e. have an intercept below zero). Physically, this would indicate that the measured low shear viscosity (η_0^*) was negative at a CA measure of zero. Obviously, this is contrary to the logical understanding of viscosity. However, the m value is actually fitted to the data in log scale (i.e. the data are fitted as e^m) which is then calculated to a value of $m = \ln e^m$. Therefore, any e^m less than unity will yield a negative calculated m value. In addition, the measured CA value of zero does not physically have a practical meaning. Given the close proximity of the carbon double bond (i.e. C=C at 1,600 cm^{-1}) to the carbonyl functional group (i.e. C=O at approximately 1,690 to 1,700 cm^{-1}), it is logically not expected that the measured CA values would produce a value of zero. Therefore, these measures are viewed as defining values used to quantify the relationship in the more practical regions as noted in Figure 8.12.

To further investigate the relationship observed in Figure 8.12, the significance of each parameter will be considered by generalizing the relationship between HS and m as presented in Equation 8.1. Rearranging the referenced Equation 7.4 and Equation 7.10 enable the basic Equation 3.72 to be produced, which may be rearranged to same format as Equation 8.1 as presented in Equation 8.3, which further yields the descriptors presented in Equation 8.4 and Equation 8.5.

$$HS = Am + B$$ **Equation 8.1**

$$\ln \eta_0^* = HS(CA) + m$$ **Equation 8.2**

$$HS = \frac{\ln \eta_0^* - m}{CA} = \frac{\ln \eta_0^*}{CA} - \frac{m}{CA}$$ **Equation 8.3**

where, η_0^* - low shear viscosity of the asphalt binder, Poise;
HS - hardening susceptibility, with η_0^* in Poise;
CA - carbonyl area, arbitrary units - unit less;
m - intercept of $\log \eta_0^*$ and CA relationship, with η_0^* in Poise.

$$A = \frac{1}{CA}$$ **Equation 8.4**

$$B = \frac{\ln \eta_0^*}{CA}$$ **Equation 8.5**

Practical application of this type of equation would generally suggest that multiple levels of CA and $\ln \eta_0^*$ be utilized to fully observe the rate of change in these parameters (e.g. of CAg and associated η_0^*). Caution is advised in the un-restricted application of this relationship on HS measures due to the strict design of aging conditions of the binders used in the development of this relationship. Specifically, the aging temperatures and durations upon which this relationship was based were intentionally selected to assure the measured kinetics would be operating in the constant rate region (i.e. $k_C \; and \; r_{CA}$) as opposed to any of the fast rate or initial jump behaviors. At this point, it is unknown how universal the relationship may be or whether short term aging conditions (e.g. RTFO, PAV, or other shorter duration conditions) may produce sufficient HS relationships or if the constant rate kinetics conditions must be maintained. Until those aspects have been

further assessed, caution is advised in regards to the global application of this type of relationship between the HS and m parameters.

However, based upon the noted relationship between the HS and m values, more specific evaluations will proceed based upon the overall combined relationship developed in Figure 8.12, but with limited additional data points included in a systematic evaluations of specific sets of measures to be compared relatively. Therefore, Figure 8.13 considers the same overall relationship highlighting the PG 64-22 mixture-aged and pan-aged binders.

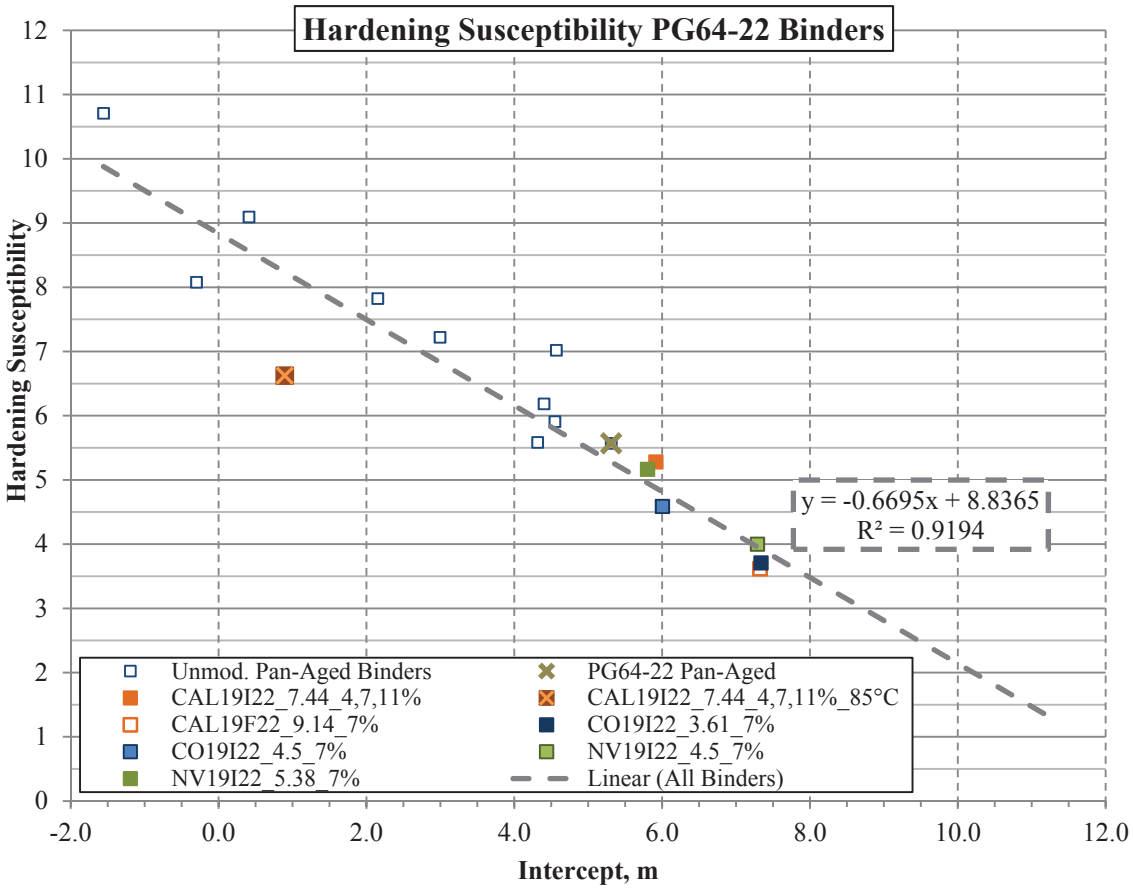

Figure 8.13 Hardening Susceptibility Relationships for the Pan-Aged and Mixture-Aged PG 64-22 Asphalt Binders

In the summarized view of Figure 8.13, the separation between the pan and mixture-aged binders has become more prevalent. In general, comparisons of the unmodified pan-aged binders (i.e. hollow blue squares) are generally concentrated higher and to the left compared to the individual mixture-aged binders. In this figure, the unmodified pan-aged binders are all of the unmodified binders included in this study. Certain specific binders that fall into this category (e.g. PG 64-22) have been specifically identified for direct comparisons, while the rest have remained part of the group as a whole for simplicity. Specifically, each of the mixture-aged binders are lower and to the right of both the PG 64-22 as well as nearly all of the other pan-aged unmodified binders. The only exception was the CAL19I22 mixture aged at 85°C, which was slightly offset from the remainder of the plot, but was generally located among the pan-aged binder values. To be clear, the pan-aged binder values were based upon the combined HS parameters from all four aging temperatures (i.e. 50, 60, 85, and 100°C).

Additional comparisons of the WesTrack binders along with the unmodified Moana22 binders are considered in Figure 8.14.

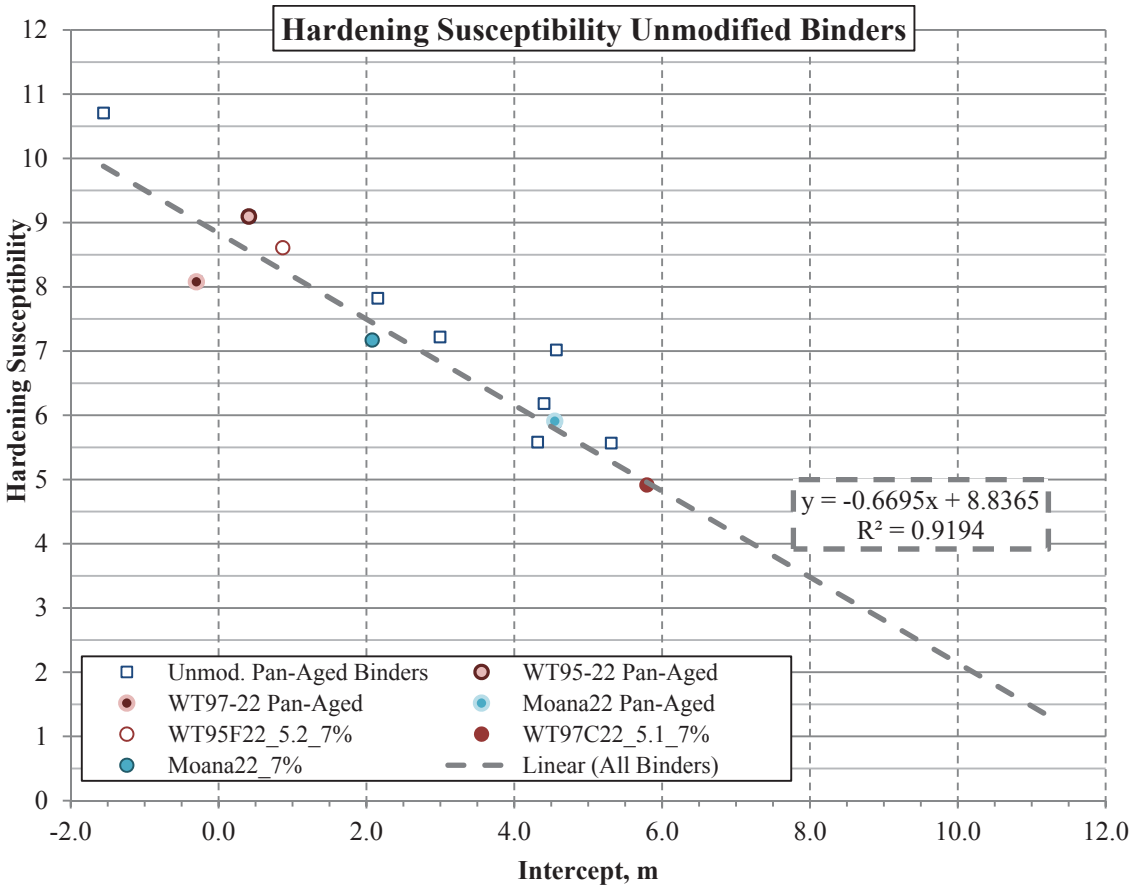

Figure 8.14 Hardening Susceptibility for the Pan-Aged and Mixture-Aged WesTrack, Moana Lane, and Sparks Blvd. Asphalt Binders

General observations of Figure 8.14 typically follow the same systematic variation of the HS and m relationship of the PG 64-22 binder noted previously. For most of the binders in the figure, the mixture-aged binders plot lower and to the right of the corresponding pan-aged binders with the exception being the Moana22 materials. The Moana22 pan-aged binders are substantially lower and further to the right than the mixture-aged binder from the same source. It is unknown whether or not the extraction and recovery of these binders prior to the pan-aging process influenced this behavior, but it is something to consider. The HS parameters for the WT95 pan-aged and mixture-aged binders are fairly

close to each other, while the parameters of the WT97 binder are fairly well separated as was noted in the other PG 64-22 comparisons.

Overall, the unmodified binders (i.e. those of Figure 8.13 and Figure 8.14) generally follow the overall fit of the HS and m relationship developed with all the binders from Figure 8.12. All of the pan-aged binders except the Moana22 typically exhibited higher measured HS values and correspondingly lower m values compared to the mixture-aged binders for the unmodified binders considered thus far in the analysis.

Further comparisons of the PG 64-28, modified pan-aged, Moana28, and Sparks28 binders are presented in the following Figure 8.15.

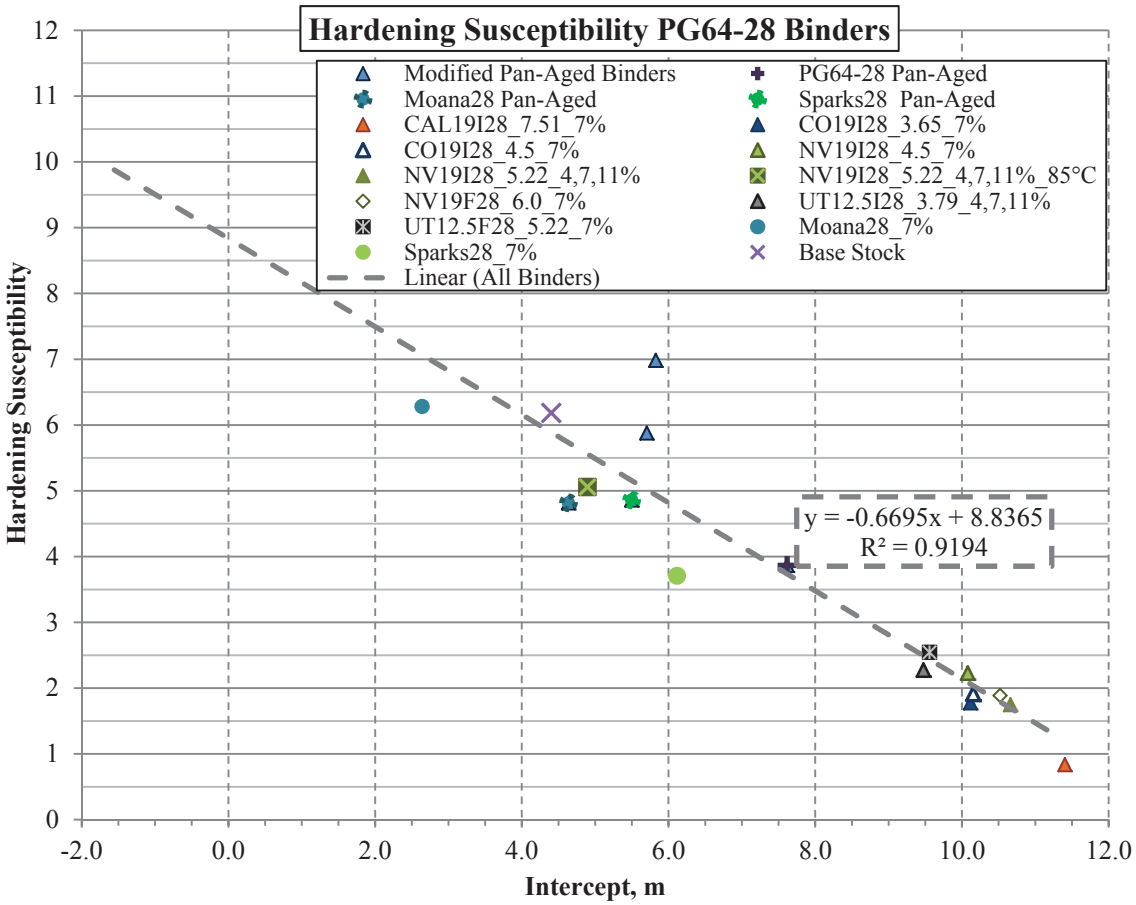

Figure 8.15 Hardening Susceptibility Relationships for the Pan-Aged and Mixture-Aged PG 64-28 Asphalt Binders

The modified binders presented in Figure 8.15 generally follow the same trends noted with the other asphalt binders with the exception being the Moana28 binders. The majority of the binders in the figure are graded to be PG 64-28. However, the Moana Lane and Sparks Blvd. binders are from a different chronological timeframe and thus have the potential to be from different crude sources. Aside from the Moana28 binders, the HS values of the modified pan-aged binders generally are higher and thus exhibit lower m values than the corresponding mixture-aged binders.

Further, the unmodified Base Stock binder also followed the previously noted shift to higher levels of the measured HS compared to the modified and pan-aged PG 64-28 binder. Similar to the PG 64-22 binder considerations, the HS of the 85°C aged NV19I28_5.22 binder exhibited a higher HS and lower m value than the pan-aged PG 64-28, while they all relatively follow the overall relationship developed from Figure 8.12.

8.4 Summary of Mixture-Aged and Pan-Aged Binder Oxidation Parameters

General conclusions of the comparisons between the pan-aged binders and the binder aged in different mixtures clearly show a distinct difference between the rate of oxidation for most binders, but not always with the PG 64-28. It was also observed that the polymer modification of a particular asphalt binder tended to reduce the oxidation rate in a similar fashion.

The comparison of the hardening susceptibility (HS) parameters between the pan-aged and mixture-aged binders were observed to be similar for the unmodified PG 64-22, variable for the unmodified WesTrack binders (i.e. one similar and one different), and

substantially different with the SBS modified PG 64-28 binders. In the comparisons that were different, the majority of the pan-aged HS parameters were higher in magnitude than the comparative mixture-aged binders, except for the two binders from the Moana Lane Extension, project (i.e. the unmodified Moana22 and the SBS modified Moana28).

The aging temperature was noted to influence both the oxidation rate and the HS parameters, though by varied amounts depending upon the binder. The influence was less prominent for the unmodified PG 64-22 binder as compared to the modified PG 64-28 asphalt binder.

By combining the measured oxidation kinetics parameters of all the investigated asphalt binders, a strong correlation was observed between the activation energy (E_a) and the pre-exponential factor (AP^{α}) utilized to describe the oxidation rate or the k_C term which is equivalent to the r_{CA} term noted in Equation 7.1.

In a similar manner, the combination of all the investigated binders resulted in a decent correlation between the HS (slope) and the m value (intercept) for the form presented by Equation 7.4.

To summarize these findings even further, Table 8.1 generalizes the findings of the evaluation of the pan-aged and mixture-aged oxidative aging parameters considered in this chapter. It should be noted that a few varied results from the field produced mixtures may not strictly agree with every consideration in the table.

Table 8.1 Comparison Summary of Pan-Aged and Mixture-Aged Binders

Oxidation Parameters		PG 64-22	PG 64-28
Oxidation Kinetics	r_{CA}	Pan > Mix.	Pan ≥ Mix.[a]
	E_a	Pan > Mix.	Pan > Mix.
	AP^{α}	Pan > Mix.	Pan > Mix.
Hardening Susceptibility	***HS***	Pan ≥ Mix.	Pan > Mix.
	m value	Pan < Mix.	Pan < Mix.

a – The overall trends indicated the pan-aged rates were higher than the mixture-aged, ref. Figure 8.5.

In general, these conclusions seem to follow the logical understanding of the interaction between asphalt binders and fillers or other blended mixtures. In fact, further studies have noted that the asphalt binder component irreversibly adsorbed onto hydrated lime particles consisted almost exclusively of carboxylic acids and 2-quinolone-type chemical functional groups (Little and Petersen, 2005). Being that these functional groups are either components of or readily turn into carbonyl groups, provides a significant validation that the hydrated lime, thereby a potential for aggregates, to significantly alter the oxidation characteristics of the asphalt binder within a given mixture. Also considering that lime is fairly chemically active, could also suggest the opportunity for the diminished effect, or possibly a variable level of influence of the adhesion interaction between asphalt binders and aggregates. This may potentially explain why some asphalt-aggregate combinations yield very different oxidation properties from the binder aged alone, and some are fairly similar.

9 ASPHALT MIXTURE TEST RESULTS AND DISCUSSION

As previously outlined in the experimental matrix discussed in Chapter 5, the influence of the aggregate and mixture characteristics on the oxidation properties of the evaluated asphalt binders were investigated by characterizing the mixtures over multiple aging conditions which varied in temperature and duration. The stiffness of the mixtures were evaluated through measurements of dynamic modulus (E^*) while the thermal and low temperature behavior of the mixtures were evaluated through uniaxial thermal stress and strain (UTSST) measurements.

9.1 Dynamic Modulus Results

As previously discussed in section 3.1, a portion of the mixture characterization focused on the E^* of the asphalt mixtures subjected to the varied oxidation levels previously described in the discussion of mixture aging results.

The selected testing protocol were based upon the recommendations of NCHRP 9-19 suggesting 4.4 and 21.1°C were related to the fatigue performance of mixtures and the high temperatures of 37.8 and 54.4°C showed a relationship with rutting resistance. Based on these recommendations, the dynamic modulus testing for this research was conducted under the following conditions:

- Temperatures: 4.4, 21.1, 37.8, and 54.4°C (40, 70, 100, and 130°F)
- Frequencies: 25, 10, 5, 1, 0.5, 0.1 Hz

In order to maintain consistency during the study period, the E^* test protocol was held consistent even though research efforts on dynamic modulus testing had continued elsewhere and suggested modifications.

In a manner very similar to the investigation conducted with the binder extracted and recovered from the mixtures after the E^* testing, the main factors being explored in this portion of the evaluation are:

- Aggregate Factors
    - Qualitative Gradation
    - Aggregate Absorption
    - Aggregate Mineralogy
- Asphalt Binder Factors
    - Unmodified Binder
    - Modified Binder
- Mixture Characteristic Factors
    - Asphalt Binder Content
    - Mixture Density or Air Voids

A summary of the E^* master curves are provided in Figure 25.1 through Figure 25.30 found in Appendix M for the laboratory prepared oven-aged mixtures considered in the laboratory portion of this study. It is relevant to point out that these figures present the fitted symmetric standard logistic sigmoidal form as discussed in section 3.1.1. The model parameters provided in Table 26.1 through Table 26.5 found in Appendix N present a summary of the master curve function parameters respective to each aged condition of the asphalt mixtures.

These master curves were developed utilizing an Excel spreadsheet to minimize the sums of squares error terms between the shifted measurements and the combined symmetric standard logistic sigmoidal formula. The master curve parameters were simultaneously fit with the second-order polynomial shift function parameters to develop the best fit relationships presented in Appendix M and Appendix N as a general reference.

For consistency, the influence of each of the experimental factors on the dynamic modulus master curves will be discussed in the same order as has been utilized in the mixture-aged binder oxidation, rheology, and hardening susceptibility sections.

9.1.1 Mixture Air Void Level

The air void level within the compacted mixtures was the first experimental factor to be evaluated with respect to the E^* measurements since it has long been understood to significantly influence the overall stiffness of a given mixture. Further, it has generally been accepted that the stiffening of a given mixture is also influenced by the air void level, logically deducing that the higher the air void level the more oxygen exposure is present to the asphalt binder within the interior of the mixture.

To evaluate these generalizations, the investigated mixtures were aged over the four durations at 60°C when compacted to three different air void levels (i.e. 4, 7, and 11%) as measured by the cut specimens after aging. Two unmodified binders (i.e. PG 64-22 and WT97-22) were evaluated with the California and WesTrack 1997 aggregates, respectively. Further, the modified PG 64-28 binder was evaluated with two aggregate

sources (i.e. Nevada and Utah) as well. The California mixtures are presented in Figure 9.1, with the short-term aged (i.e. zero month) and the longest aged (i.e. nine month) master curves presented for each of the air void levels. Similarly, the WesTrack materials are considered in Figure 9.2 with the modified binder presented in Figure 9.3 and Figure 9.4 for the Nevada and Utah aggregates, respectively.

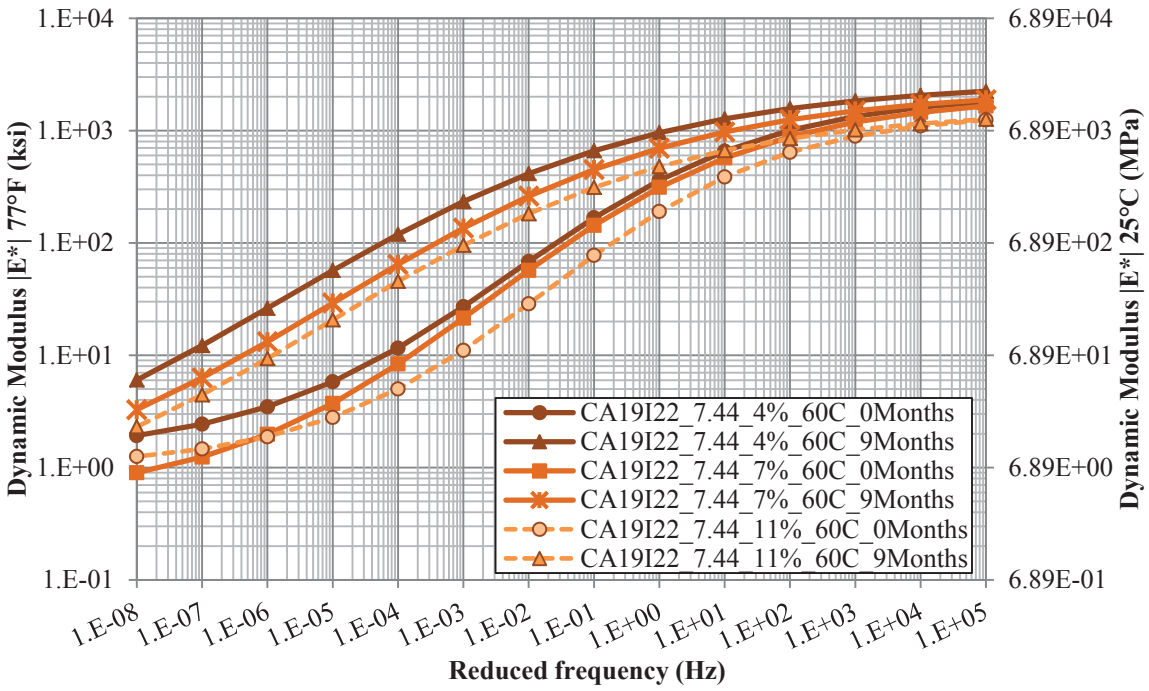

Figure 9.1 Dynamic Modulus Master Curves for the CAL19I22_7.44 Mixtures Aged at 60°C with Different Air Void Levels

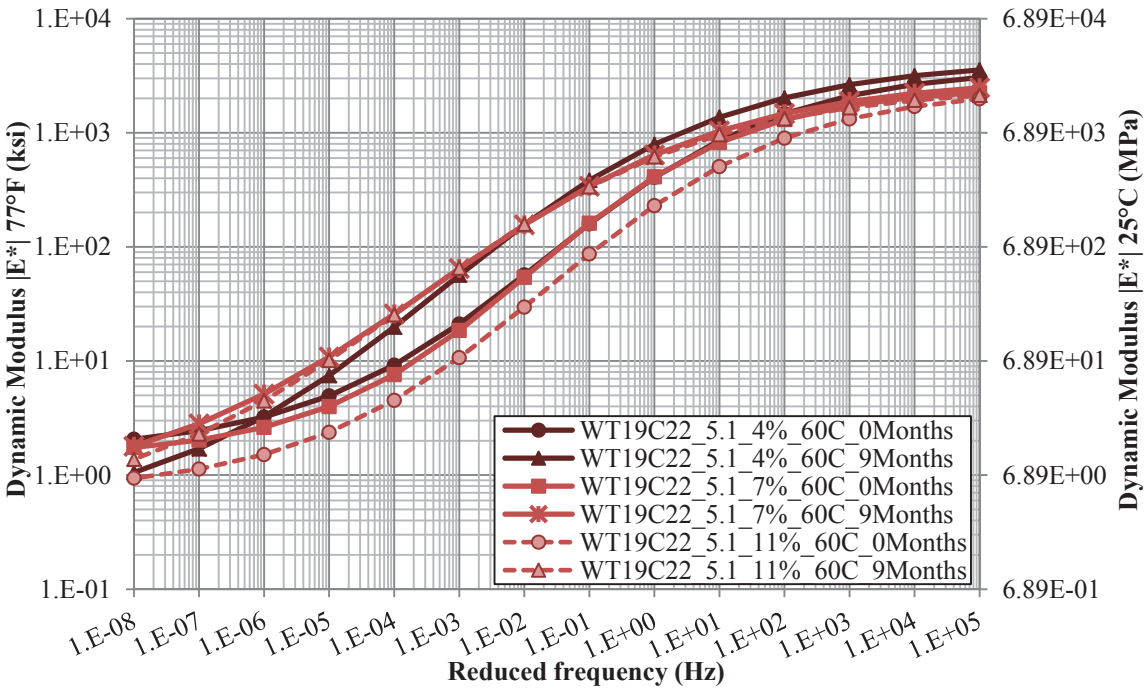

Figure 9.2 Dynamic Modulus Master Curves for the WT97C22_5.1 Mixtures Aged at 60°C with Different Air Void Levels

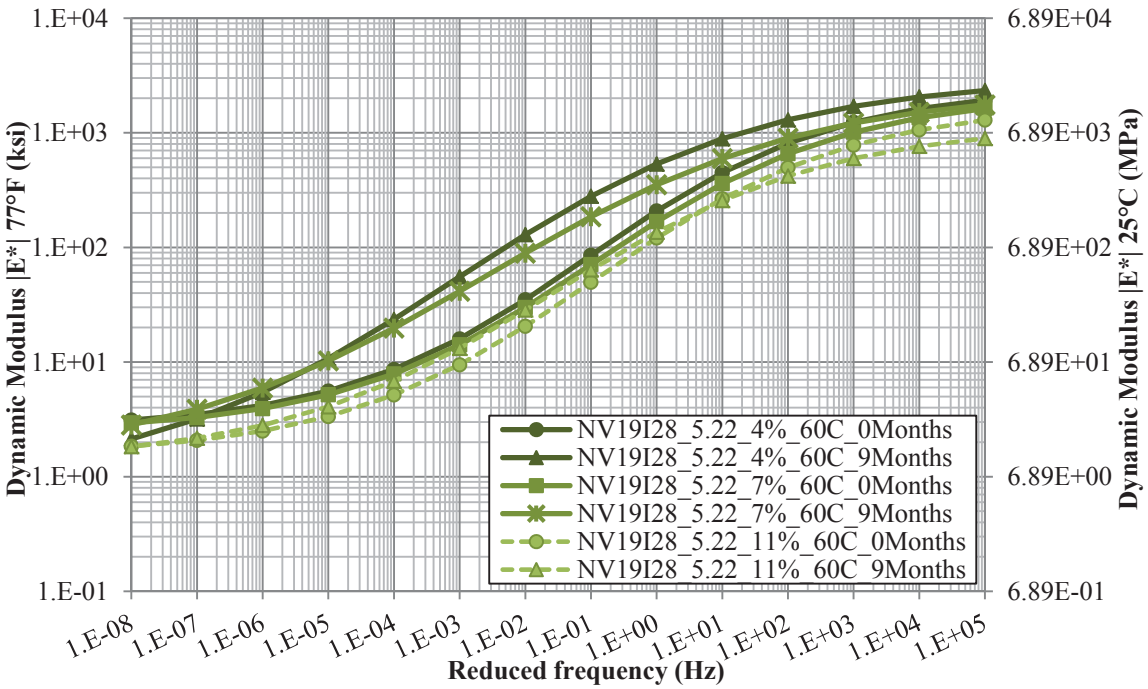

Figure 9.3 Dynamic Modulus Master Curves for the NV19I28_5.22 Mixtures Aged at 60°C with Different Air Void Levels

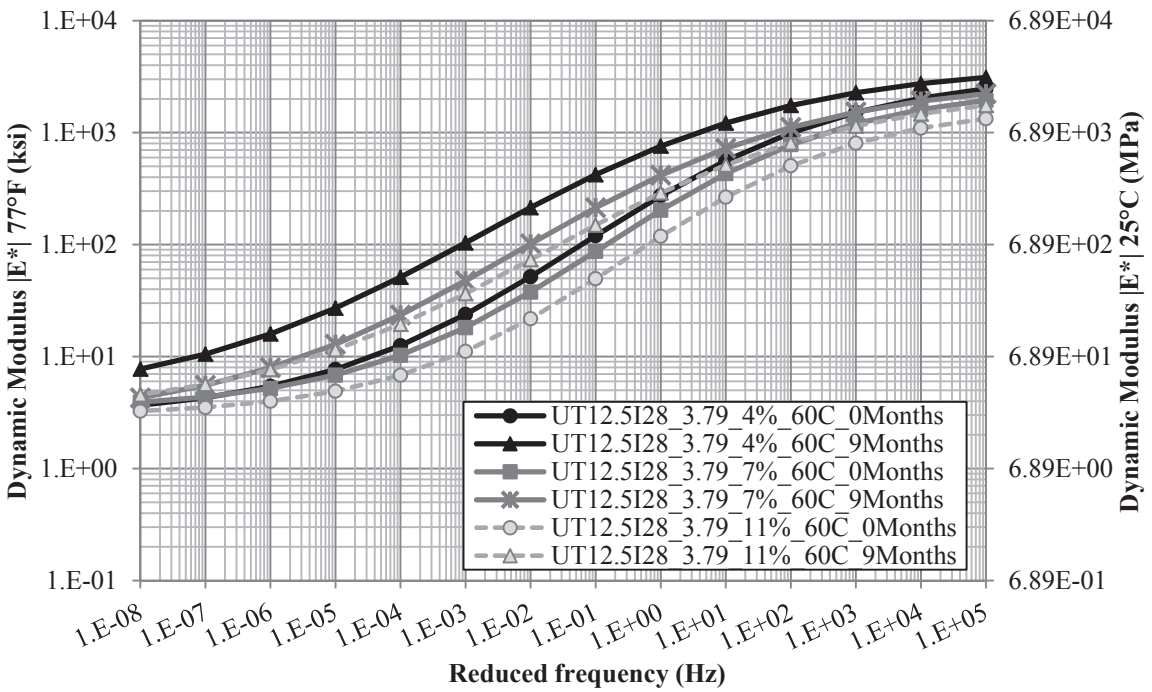

Figure 9.4 Dynamic Modulus Master Curves for the UT12.5I28_3.79 Mixtures Aged at 60°C with Different Air Void Levels

General observations of all four plots relative to the air void level (i.e. Figure 9.1 though Figure 9.4) clearly indicate the general increase in the measured stiffness of the mixtures as a function of the aging duration. In general terms, there was also a systematic shifting due to the air void level at both the zero and nine month aging durations, with a couple of exceptions. Further general comparisons also noted the loss of the lower asymptote (i.e. higher temperature or lower frequency measures) of most of the mixtures over the duration of oven aging. It was not fully evaluated whether this was a true loss of that plateau region in the material, or if it were simply a side effect of the stiffening of the material relative to the reference temperature. In other words, the overall shape of the fitted master curve (i.e. whether or not it has both asymptotes) can be dependent upon several factors including the actual temperatures and frequencies conducted during the

test, the reference temperature utilized for shifting, and the relative proximity of the two. To minimize these effects, the reference temperature was maintained well within the tested temperatures. However, the reduced frequencies (i.e. after shifting) often depend upon the material properties themselves (i.e. temperature and load rate dependencies) which are not always directly analyzed. Nevertheless, overall characteristics of the E^* master curves provide a fair amount of information regarding the characterization of the material behavior.

More specific observations of the CAL19I22 mixtures of Figure 9.1, indicate the clear separation of the master curves corresponding to both the aging duration as well as the air void level of the mixtures. The mixtures compacted to the 11% air void level exhibit the lowest E^* measures at nearly all the considered reduced frequencies and aging conditions. This differentiation was present through the intermediate and higher reduced frequency range. As indicated in the figure, the actual quantification of the discrepancies would highly depend upon the selected frequency and likely the shifted temperature for the evaluation. Therefore, more generalized considerations of this type will be conducted on the combined data followed by a discussion of the more specific observations of each.

Consideration of the WT97C22 mixtures in Figure 9.2, suggest a slightly different influence of the aging duration on the developed E^* master curves. These mixtures initially show a difference at the 11% air void level, but only minor differences between the 4 and 7% air void levels. There was a consistent differentiation between the air void levels in the higher frequency range. Similar, but less consistent separations were observed in the lower reduced frequency range, with the exception of the 4% air void mixture after nine months of oven aging. These mixtures were also noted to exhibit very

similar master curves after nine months of oven aging in the intermediate reduced frequency range, showing nearly identical value in some instances.

These findings suggest further observations may be warranted to help explain some of the contrasted results compared to the previous California mixtures. Recalling that the two mixtures were produced with completely different asphalt binders, in addition to the PG grade of 64-22, the aggregate structure of the mixtures were quite different. Referencing the photographs of the respective mixtures in Appendix E, suggests that the aggregate structure of the WesTrack mixture was much more open compared to the California mixture. This suggests that perhaps the open structure of the mixture may be more influential to the level of oxidation, which would be expected to correlate to the air void level for most mixtures. Further evaluations of these mixtures may provide additional information to better clarify the difference in the overall mixture properties.

Observations of the polymer modified PG 64-28 binder aging in the Nevada mixtures of Figure 9.3 show the aging behavior that is somewhat of a compromise of the first two evaluated mixtures. The NV19I28 mixture aged with 4% air void level seemed to follow the previous observations producing the stiffening effect and the loss of the lower asymptote after nine months of oven aging at 60°C. The mixture aged with 7% air voids, exhibited a slightly smaller magnitude in stiffening, but retained the asymptotic curvature in the lower reduced frequency range. Continuing the overall trend, the mixtures aged at the 11% air void level showed very little change in the magnitude of the E^* master curve after nine months of oven aging at 60°C. There was some slight variations noted between the two 11% air void mixtures, but not the systematic shifting observed with the other air void levels.

Additional observations of the modified PG 64-28 asphalt binder were conducted with the Utah aggregate as presented in Figure 9.4. These materials appear to exhibit a very ordered and systematic increase in the E^* master curves with respect to the air void level and oven aging duration. The figure presents very clear differentiation between the air void levels which is continued through to the nine-month oven-aged mixtures without a significant change to the master curve shape as was noted in some previous evaluations in this section.

The already presented results suggest that with certain mixtures, the air void level during aging has a very distinct influence on the level of oxidation, while others have exhibited quite minor influences, and some mixtures exhibited both behaviors. Therefore, to conduct a more robust evaluation of these findings, the actual rate of stiffness increase was considered. This comparison also included the mixtures aged at three and six month oven aging durations at 60°C for additional input into the analysis.

To accomplish these comparisons, E^* had to be represented by fewer values than the large data matrices often produced during master curve testing. To appropriately reduce the data, the fundamentals of viscoelastic theory were applied. It is generally accepted that HMA mixtures can be appropriately characterized as a viscoelastic solid. Specifically, this means that the material will not exhibit purely viscous behavior, most directly indicated by a phase angle approaching 90°. This has been demonstrated to be the case for HMA mixtures subjected to shear loading (Zeng et al., 2001). What makes HMA a viscoelastic solid is that the phase angle increases to a point, then decreases with increasing or decreasing load frequency. The same principle can be applied to the axial loading conditions applied during E^* testing. In the same report, it was shown that

asphalt binders could be considered viscoelastic liquids. This was evidenced by the increasing phase angle with slower loading frequencies, which essentially led to the low or zero shear viscosity concept (LSV or ZSV), respectively. Similar to LSV theory, it was preferred to conduct such analysis with actual measured data points rather than using responses from a fitted model, i.e. shifted master curves. Therefore the E^* analysis was limited to the temperatures and frequencies actually tested.

Since this investigation was interested in the aging of the asphalt binders and corresponding changes to the mixture properties, it was desired to capture as much of the viscous response of the mixture as possible. The most viscous response in an E^* test was determined by locating the highest phase angle, which would not necessarily occur at the lowest frequency or the highest temperature, i.e. viscoelastic solid behavior, as would be the case for binder testing, i.e. viscoelastic fluid behavior. After much consideration into the measured phase angle and the corresponding modulus values at each of the E^* testing conditions, it was decided that the best option would be to consider E^* at 37.8°C (100°F) at 0.1 Hz. In general, the decision was based upon lower phase angles at higher and lower temperatures. At the lower temperatures, the binder was too stiff to provide a good indication of its aging condition. At the higher temperatures the binder became too soft causing the majority of the mixture response to be dictated by the aggregate structure. Explorations also considered the elastic (E') and viscous (E") components of the measured E^* values, however their relationship to E^* through the phase angle (δ) resulted in very similar results as E^* directly. Even though this methodology was developed independently, it was later reinforced by the literature (AbWahab et al., 1993). Therefore, for the sake of simplicity E^* values at 37.8°C (100°F) and 0.1 Hz were

considered with respect to the measured CA values. Figure 9.5 and Figure 9.6 present the E^* plots for the previously evaluated mixtures containing the unmodified and modified binders at 37.8°C (i.e. 100°F) and 0.1 Hz, respectively. Generally keeping within the low shear viscosity presentation format, the air void evaluation has been produced in the semi-log scale as a function of the standardized CA measurements.

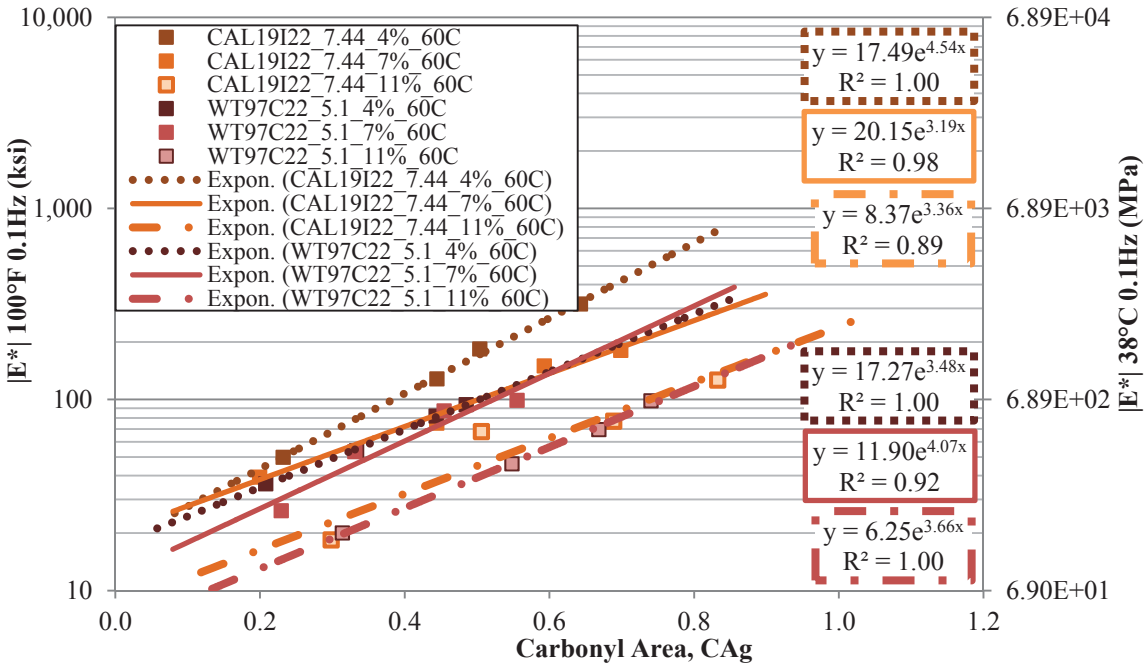

Figure 9.5 Select Dynamic Modulus Measures of Unmodified Mixtures with Different Air Void Levels Aged at 60°C

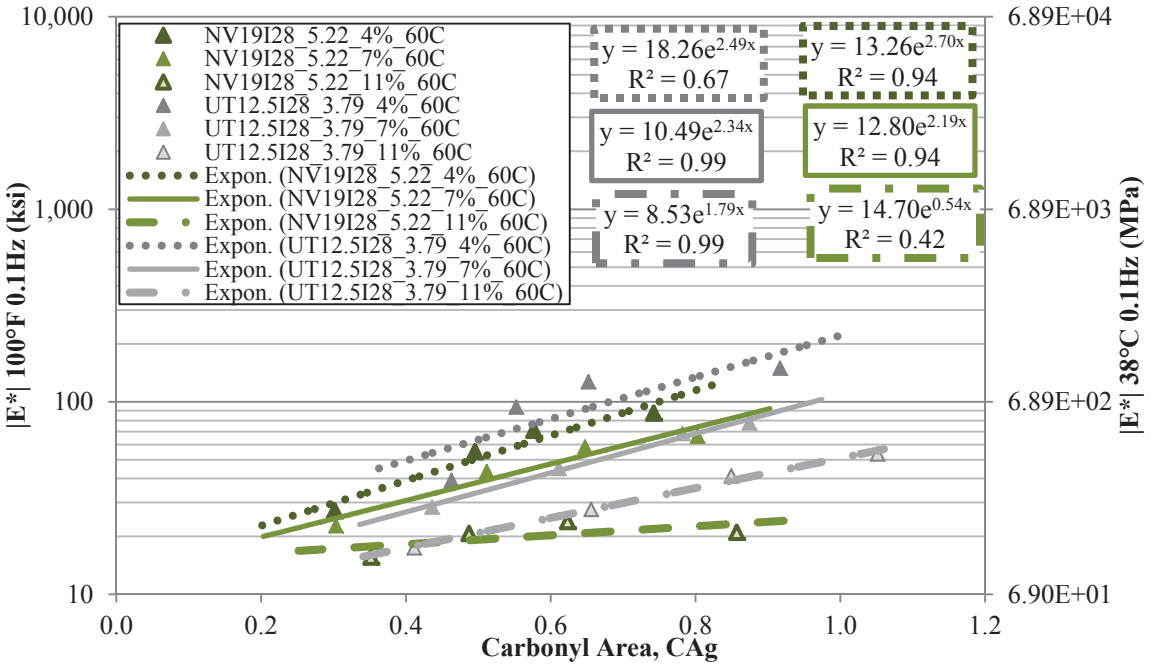

Figure 9.6 Select Dynamic Modulus Measures of Modified PG 64-28 Mixtures with Different Air Void Levels Aged at 60°C

As was suggested in the previous evaluations of the full master curves, this abbreviated consideration clearly presents the air void dependency of not only the measured E^* values, but also the increase in those measures under constant aging conditions (i.e. mixture oven aging at 60°C).

The mixtures with the two unmodified binders presented in Figure 9.5 show the well-expected behavior that the air void level or mixture density have a distinct influence on the overall stiffness of the mixtures. Although there is some overlap in the mixtures aged at the 7% air void level, but the 4 and 11% air void levels with the CAL19I22 mixtures generally showed a reduction in the rate of the measured increase in the E^* values under these aging conditions with increased air void levels. This trend does not

seem to be consistent with the WesTrack mixtures, which tend to exhibit more scatter in the aging rate overall.

Additional considerations of the polymer modified binder aged in the Nevada and Utah mixtures presented in Figure 9.6 suggest a much more systematic variation as the results of the air void level. These mixtures demonstrate a clear separation in not only the magnitude of the measured E^* values, but also a reduction in the rate of the measured increase in the E^* values under these aging conditions with increased air void levels. In other words, the higher the air void level of the mixture during aging, the slower the rate of increase in the overall measured E^* values.

Initially, this may appear as somewhat contrary to what would generally be expected. The expected result would seem to indicate that the higher the air void level, the higher the expected exposure to oxidation and thus the higher the rate of stiffening within the mixture. However, these results seem to indicate the opposite effect. There are two potential explanations to account for the influence of the air void levels on the results just discussed assuming there was no appreciable damage to any of the samples over the course of the oven aging durations. If there was appreciable creep or other deformation within the mixtures, then the aggregate structure would presumably be altered and produce erroneous results. However, this is not thought to be the case with these mixtures since the magnitude of the measured E^* values remained systematic and consistent with the general stiffening upon oxidative aging within each respective mixture.

The first possible explanation can be explained by considering the physical nature of the cross-sectional area of the mixtures. It stands to reason that the lower the air void

level, the more tightly packed the aggregate structure and thus the overall mixture (i.e. the less air voids present the more physical material in a given area) provided the other properties of the mixture remain constant (i.e. binder content, aggregate gradation, etc.). As the asphalt binder stiffens with oxidation, the sheer amount of material throughout the specimen can have a substantial influence on the overall stiffness of the conglomerate mixture. In other words, a slight increase in the oxidation of the 4% air void mixture will ultimately cause a greater increase in the mixture stiffness compared to an 11% air void mixture, despite the higher oxidation level of the less dense mixture as indicated in the oxidation kinetics of section 7.2.2. Thus, a reduction in the density (i.e. higher air voids) would effectively reduce the overall contribution of such binder influences, if the increased rate of oxidation of the binder due to the higher void level was not large enough to overcome the reduction in the overall aggregate contact points. Essentially, the increased oxidation of the binder itself was not sufficiently large to overcome the reduction in the stiffness due to the large volume of air voids found within a given test specimen with higher air void levels.

This explanation is somewhat supported by the previous evaluation of the mixture-aged asphalt binders. The kinetics evaluation of section 7.2.2 demonstrated the increased level of oxidation with increased air void levels of the mixture-aged binders over the same aging conditions. However, the hardening susceptibility plots discussed in section 7.4.2 indicated that the overall HS relationship of the mixture-aged binders was largely independent of the air void level, though the air void level did influence where on the relationship a particular aging condition would be present. Thus the reduced oxidation of the lower air void level mixtures were ultimately more influential than the higher rate of

oxidation with the higher air void levels on the measured E^* values of the mixtures in this analysis.

The second potential explanation for these results stems from the physical application of the kinetics modeling methodology. Specifically, the rate of oxidation reactions as were conducted here are typically either limited by the oxygen availability (i.e. oxygen depravity slowing the reaction) or by the rate of diffusion of oxygen through the binder into the interior of the film thickness. Without a detailed experimental evaluation designed specifically for one case or the other, it is quite difficult to determine which aspect is controlling the oxidation reaction or aging of the binder. Thus, without being able to clearly decipher which is the limiting factor in the aging of any of the evaluated mixtures, it becomes distinctly possible that the 4 and 11% air void cases may be controlled by different mechanisms.

Without specific measures focusing on this aspect, it cannot be determined for sure which is the controlling condition. However, it is important to note that the CA measures and the HS determinations were conducted on extracted and recovered binders from the respective aged mixtures. Evidence was provided in section 3.3 indicating that the actual extraction a recovery procedure was expected not to have a significant influence on these measures. However, it most certainly by necessity the process blends all of the extracted binder together, thus eliminating the necessary separation to evaluate partial penetration or diffusion limitations within the asphalt binder itself.

Taking into consideration all the above factors, it is feasible that the 11% air void mixtures effectively have full oxygen exposure at the interface of a given air void and the asphalt binder film. This may potentially enable the very outer surface of the air void to

oxidize at a rapid rate, nearly the same as the pan-aged binders. This rapid oxidation at the surface could potentially create a very stiff boundary which would in turn substantially decrease the rate of oxygen diffusion to the interior of the binder film. This oxidized barrier would serve to essentially protect the interior of the binder film and reduce the level of oxygen exposure, effectively creating a diffusion limited system. During the extraction and recovery process, nearly all the binder became blended together in the solution, thus yielding the increased CA growth as was observed in section 7.2.2. However, when the binder remained within the mixture, the relatively lesser aged binder would be located between the aggregate particles away from the air voids (i.e. at the aggregate contact points discussed previously), thereby producing a reduced stiffening effect from the mixture testing (i.e. measured E^* values).

Initially, this suggested occurrence may seem to directly contradict the findings of the pan-aged binders where full exposure is nearly completely assured. However, there is a significant difference in the area of the exposed surface of the pan-aged binders compared to those surrounding the pore (i.e. air void) and binder interface. Considering the cylindrical coordinate system discussed in the methodology section, the surface area of the inner surface of a pore is substantially smaller than that of a fully exposed pan-aged geometry. Therefore on a surface to volume comparative basis, the cylindrical pore system has a significant reduction in the surface area of the exposed surface compared to the volume of binder into which the oxygen would diffuse. Essentially, the concentration of the oxygen would be far greater at the pore interface compared to the surface area of a fully exposed pan-aged binder sample.

In the case of the 4% air void mixtures, it is conceivable that a quite different set of circumstances is controlling the reaction. Possibly, the replenishment of the oxygen within the pore space of the mixture would not be as fast or complete, thus depleting the overall quantity of available oxygen at the air void (i.e. pore) interface. This would directly decrease the oxidation level at the very interface, which in turn would permit the diffusion rate at that location to remain comparatively higher than the aged and stiffened interface with the 11% air void mixture. Although the overall oxygen level would be reduced, the amount of oxygen that was available would more readily diffuse into the interior regions of the asphalt binder film. In such an environment, the interior of the binder, such as would be present at the aggregate contact points would be at higher oxidation level than the so called protected 11% air void mixtures. Possibly, the combined effect of the higher quantity of the contact points and only minor increases in the oxidation of the binder would result in the higher rate of oxidation with the lower air void levels on the measured E^* values of the mixtures.

Again, validation of these potential explanations of the oxidation rates based upon the air voids in the aged mixtures would require a more focused investigation of these mixtures as well as the specific evaluation of the oxidation level at various locations within a given asphalt binder film. It is highly likely that some combination of the two interactions are responsible for the observed behaviors of the majority of the mixtures evaluated in this study. By similar logic, the aging rate of the 7% air void samples may potentially be the combined effect of both influences, each to their own relative extent as dictated by the actual conditions controlling the oxidation rate (i.e. either diffusion limitations or oxygen supply starvation).

9.1.2 Asphalt Binder Content

The evaluation of the asphalt binder content was conducted on both the unmodified PG 64-22 and the modified PG 64-28 with both the Colorado and Nevada aggregate sources. Figure 9.7 presents the mixtures aged for zero and nine months for the mixtures containing the unmodified PG 64-22 with the constant 4.5% TWM binder content and the binder content resulting in a calculated 9 µm AFT and compacted to 7% air voids.

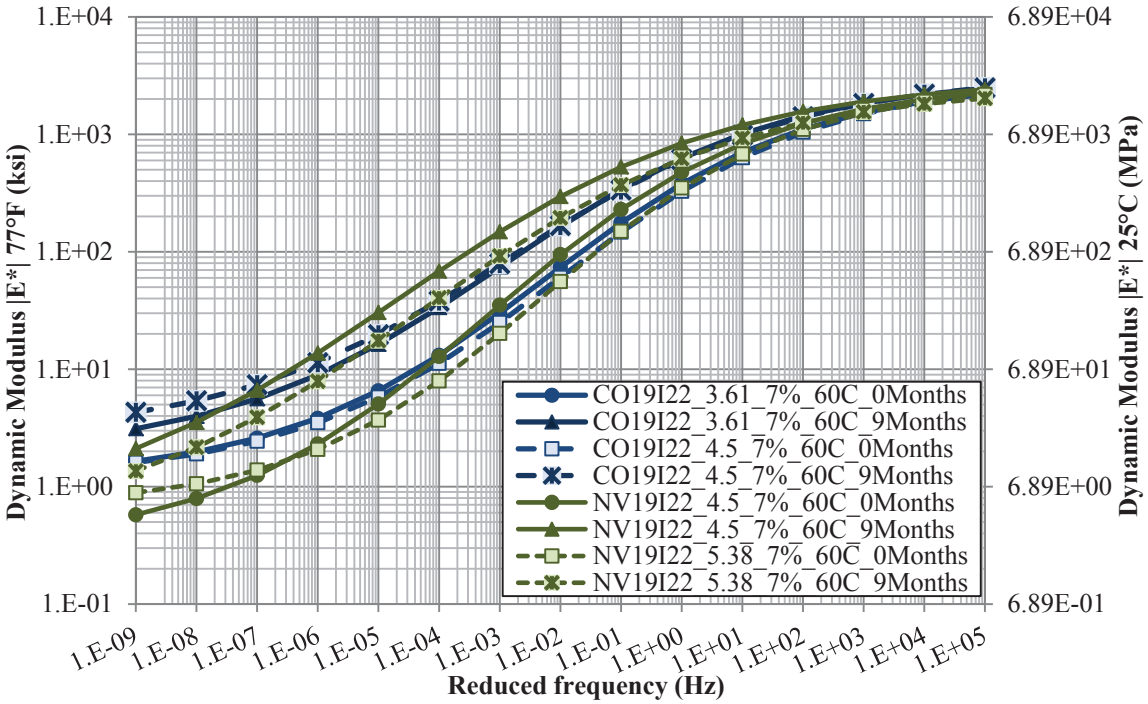

Figure 9.7 Dynamic Modulus Master Curves for the PG 64-22 Mixtures with Different Binder Contents Aged at 60°C

In Figure 9.7, the higher binder content of each aggregate source are indicated by the dashed lines, though they are not consistent between the 4.5% and 9 µm AFT binder contents for the two sources. However, with the zero month aged measures, the higher binder is typically lower in the figure as would be expected, although the Colorado

mixture are nearly the same for this aging condition. After nine months of aging the Nevada mixture with the higher binder content generally stayed below the 4.5% TWM mixture. Almost the reverse is true for the Colorado mixtures at the intermediate and lower reduced frequency ranges. Further, the higher reduced frequency range for the two Colorado mixtures are nearly the same, which is practically the case for all the mixtures presented in this figure.

The magnitude of the shift in the measured E^* master curves due to aging appears to be relatively consistent with each aggregate source. However, the shift in the Nevada mixtures appears to be slightly larger, particularly with the 4.5% TWM mixture.

Figure 9.8 presents the mixtures aged for zero and nine months for the mixtures containing the modified PG 64-28 with the constant 4.5% TWM binder content and the binder content resulting in a calculated 9 μm AFT and compacted to 7% air voids. Again, the higher binder content of each aggregate source are indicated by the dashed lines, though they still are not consistent between the 4.5% and 9 μm AFT binder contents for the two sources.

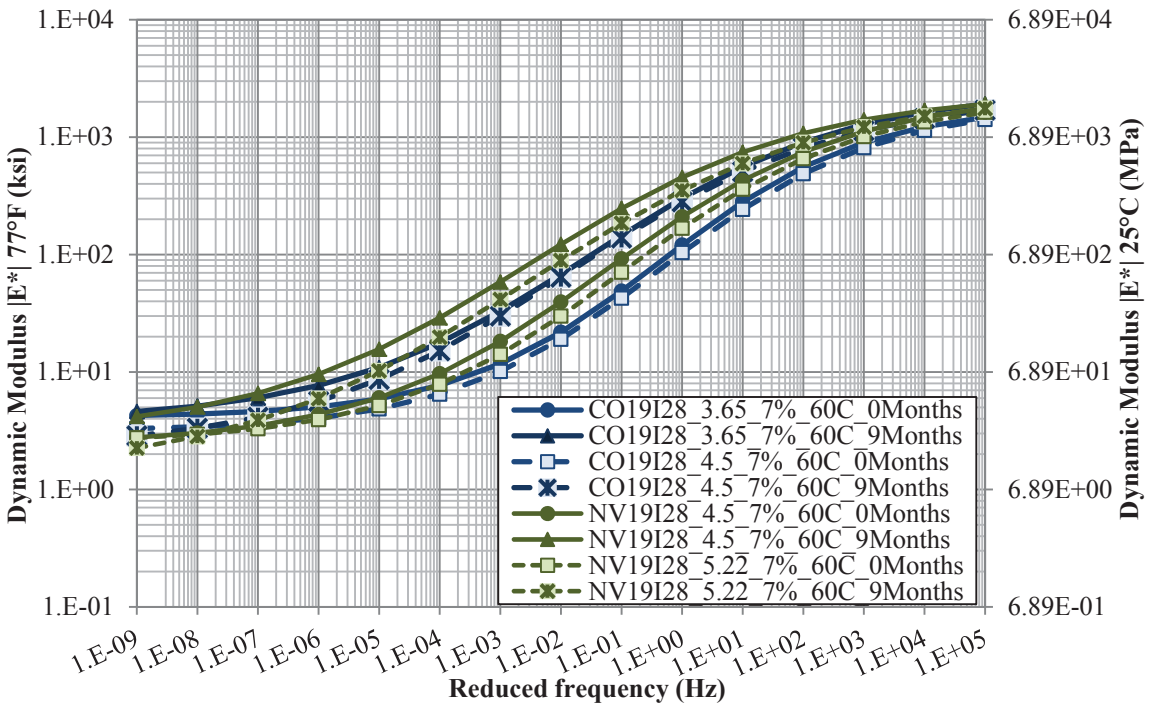

Figure 9.8 Dynamic Modulus Master Curves for the PG 64-28 Mixtures with Different Binder Contents Aged at 60°C

The polymer modified mixtures in Figure 9.8 present a more orderly and systematic variation of the measured E^* master curves compared to the unmodified mixtures. With the modified mixtures, the master curves of the higher binder contents plot just below the other mixture for a given aggregate source in nearly every comparison. The oxidation levels are relatively similar as well, as is evidenced by the same order of the mixtures at both the zero and nine month aged measures. Although the Colorado mixtures appear slightly closer to each other after the nine months aging, the Nevada mixtures exhibited a bit further separation when compared to the respective zero month aged master curves.

Figure 9.9 presents the mixtures containing the Colorado aggregates with both binders and for the two binder contents compacted to 7% air voids.

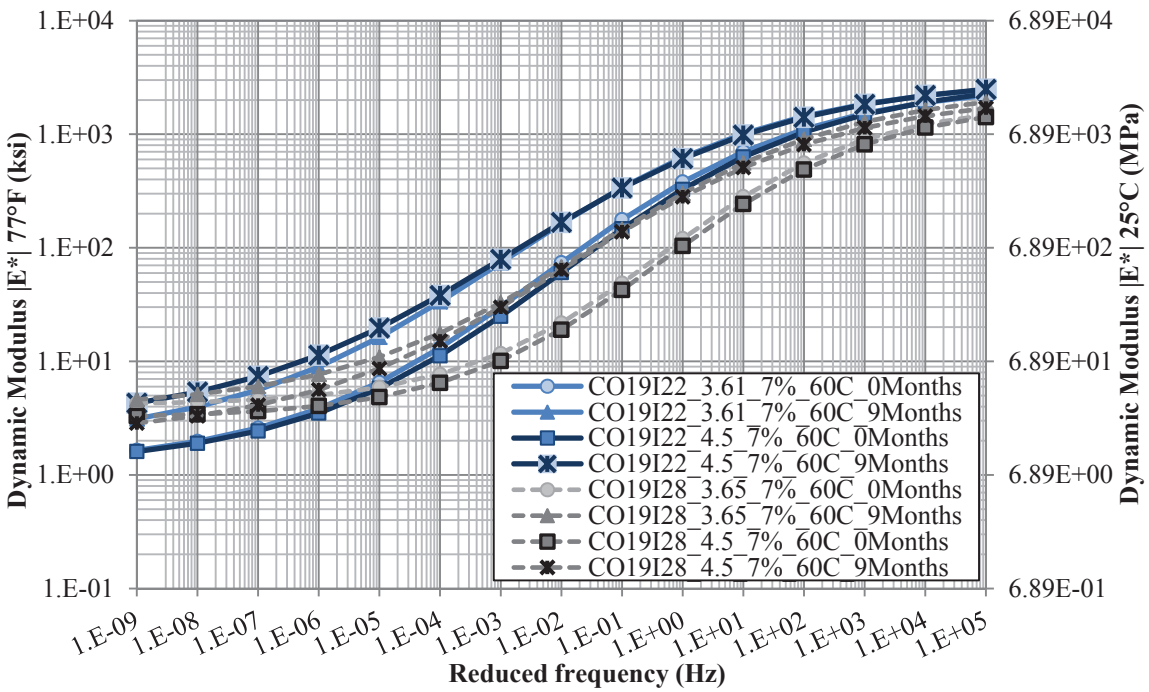

Figure 9.9 Dynamic Modulus Master Curves for the Colorado Mixtures with Different Binder Contents Aged at 60°C

Figure 9.9 demonstrates the relative similarities between the binder contents, but also presents the clear separation due to the binder grade or more specifically the polymer modification of the binder. The mixtures containing the unmodified PG 64-22 binder present a higher overall stiffness at each of the respective aging conditions, except at the lower reduced frequency range. The differences in the overall range of the E^* master curves are indicated by the increased stiffness of the lower asymptote and the reduced E^* values of the higher asymptote with the modified binder.

The magnitude of the shifting in the E^* master curves provides an indication of the influence of the nine month aging duration at 60°C. In the intermediate reduced frequency range, the modified PG 64-28 binder exhibited a slightly larger shift compared to the unmodified PG 64-22. However, in the lower range of reduced frequency the

mixtures with the PG 64-22 binder show a significant increase in the overall shift due to aging. Further, the mixtures with the modified PG 64-28 binder also appear to converge upon nearly the same asymptote values at both the high and low ranges of the sigmoidal curve. Conversely, the mixtures with the unmodified PG 64-22 binder are similar only at the higher asymptote, at least within the range of frequencies considered with these Colorado mixtures.

By a similar comparison, Figure 9.10 presents the mixtures containing the Nevada aggregates with both the PG 64-22 and PG 64-28 binders and both binder content levels, again compacted to 7% air voids for the aging durations.

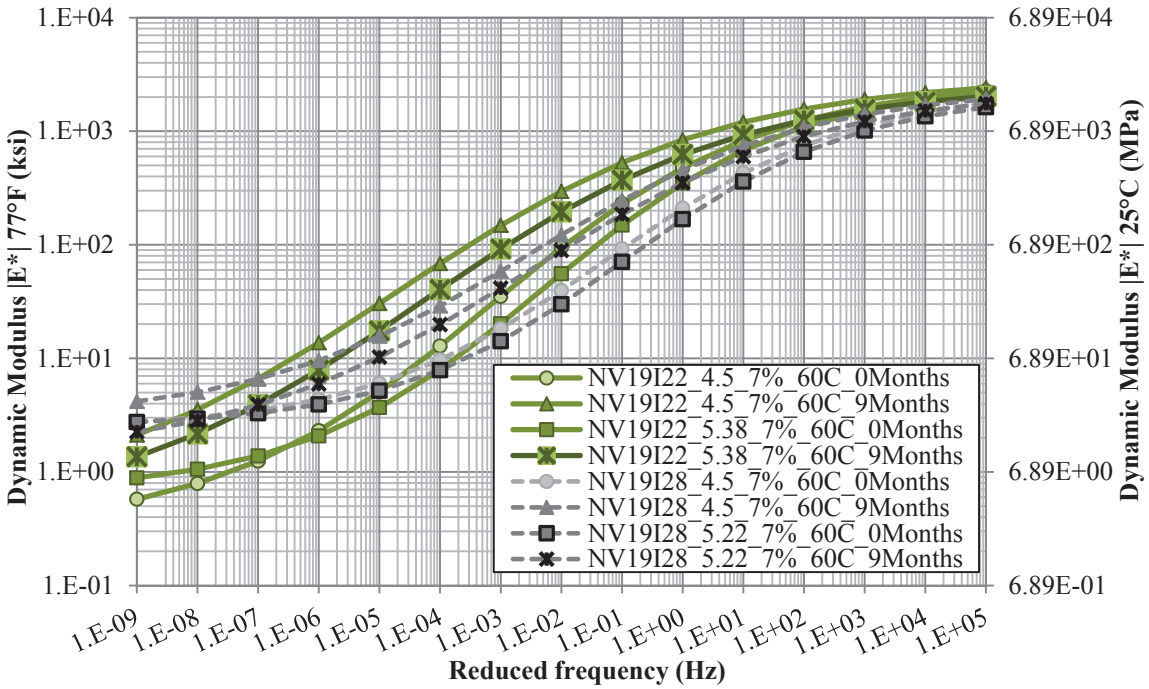

Figure 9.10 Dynamic Modulus Master Curves for the Nevada Mixtures with Different Binder Contents Aged at 60°C

Similar to the Colorado mixtures, the Nevada mixtures presented in Figure 9.10 also exhibit substantial differences between the two binder grades. The mixtures with the unmodified PG 64-22 binder are notably stiffer for the same test conditions at all but the lower asymptote of the sigmoidal relationship. Again, a similar convergence was noted for both the high and low E^* values with the mixtures containing the modified PG 64-28, but only on the stiffer asymptote with the mixtures containing the PG 64-22 binder within the reduced frequency range included in these observations. The increase in the influence of the nine months of aging is also noticeable with the mixtures containing the PG 64-22 binders compared to the modified binder.

In summary, the mixtures containing the unmodified PG 64-22 binder were stiffer (i.e. higher E^* values) than the comparative mixtures containing the modified PG 64-28, for all but the lower range or reduced frequencies. This finding also generally concurred with the lower range of E^* values (i.e. difference between the upper and lower asymptotes of the sigmoidal curve) noted for the modified binders. With both the Colorado and Nevada aggregates the influence of the aging was fairly similar within each binder type, although the mixtures containing the unmodified PG 64-22 binder were noted to result in larger increases in the E^* value due to the oven aging as compared to the modified binder. This finding generally agrees with the previous hardening susceptibility observations conducted on the extracted and recovered binders from these mixtures.

The close proximity of the E^* master curves obtained with the mixtures containing the PG 64-22 binder produced inconsistent rankings with respect to the measured E^* value as a function of the total asphalt binder content. However, the expected rankings

were observed with the mixtures containing the modified PG 64-28 binder with the mixtures containing the higher overall binder content behaving slightly softer (i.e. lower measured E^* values).

9.1.3 Qualitative Gradation

The qualitative gradation evaluation was conducted by adjusting the stockpile percentages of the intermediate gradations to provide a finer overall aggregate gradation utilizing the same aggregate components. Each of the same stockpiles were included in both the intermediate and fine gradations to keep the mineralogy the same, with possibly different proportions.

These evaluations were conducted with the unmodified PG 64-22 asphalt binder with the California aggregates and the modified PG 64-28 binder with the Nevada and Utah aggregate sources. Initially, the WesTrack mixtures were intended to provide additional comparisons between the relative gradation levels, however since both the asphalt binders and the aggregate sources were different between the two construction dates, and thus the two gradation levels, this comparison was considered invalid and thus has not been included here. However, the same comparison has been included in the constant film thickness discussions relevant to Figure 9.15.

Comparisons of the California mixtures with the PG 64-22 binder compacted to the 7% air void level are presented in Figure 9.11.

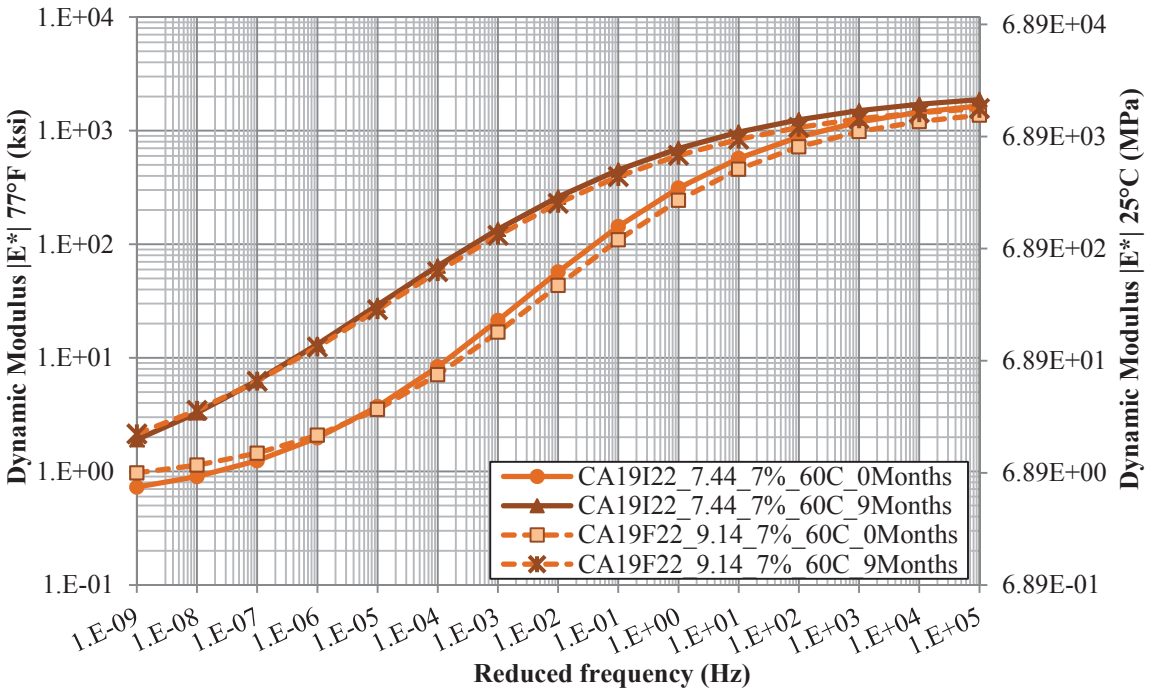

Figure 9.11 Dynamic Modulus Master Curves for the PG 64-22 and California Mixtures with Different Qualitative Gradations Aged at 60°C

Despite an increase of 1.7% in the total asphalt binder content corresponding to an increase of nearly 1.1% in the effective asphalt binder content (Pbe), the measured E^* values did not exhibit an appreciable change with the substantial change in the gradation with the California aggregates and the PG 64-22 asphalt binder as depicted in Figure 9.11. The masters curves developed at the zero month aging condition was slightly softer with the fine gradation as compared to the intermediate, but after nine months in the 60°C oven they were nearly identical. This suggests that the finer gradation may have stiffened by a marginal amount, or they were the same within the permissible test variation.

Additional considerations of the qualitative aggregate gradations are presented in Figure 9.12 and Figure 9.13 for the PG 64-28 binder with the Nevada and Utah aggregates, respectively.

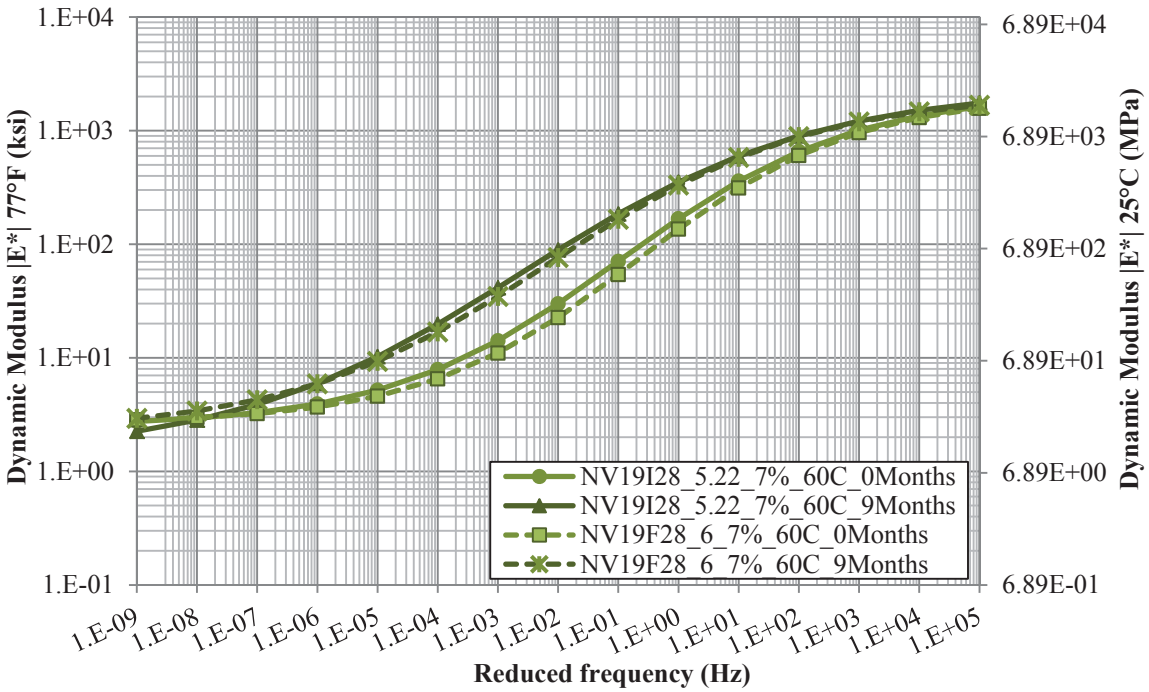

Figure 9.12 Dynamic Modulus Master Curves for the PG 64-28 and Nevada Mixtures with Different Qualitative Gradations Aged at 60°C

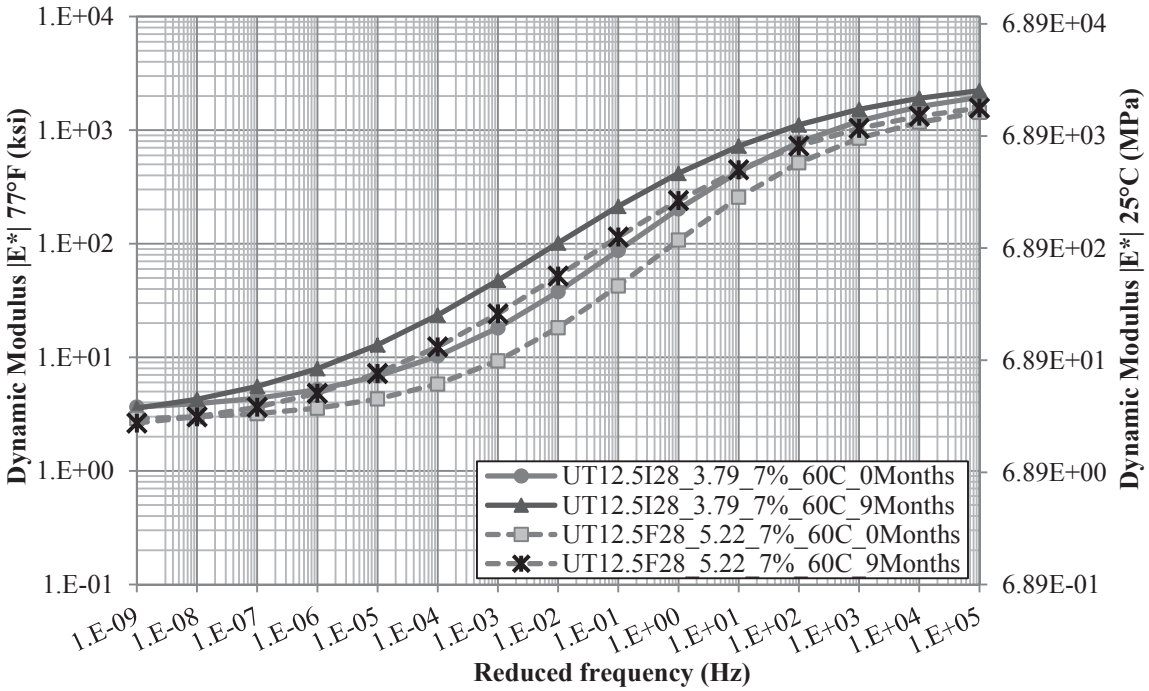

Figure 9.13 Dynamic Modulus Master Curves for the PG 64-28 and Utah Mixtures with Different Qualitative Gradations Aged at 60°C

Figure 9.12 indicates nearly the same behavior as the California and PG 64-22 mixtures. Only a slight reduction in the measured E^* values were noted with the fine gradation with only an increase in the total asphalt binder content of 0.78% (0.82% Pbe). The proximity of the two mixtures at each respective aging condition also agrees with the California mixtures, suggest a very slight increase in the stiffening of the fine gradation compared to the intermediate.

Initial observations of the Utah mixtures with the PG 64-28 binder presented in Figure 9.13 indicate that the intermediate mixtures were substantially stiffer than the fine mixtures at each of the aging conditions. The total binder content for the fine gradation with the Utah aggregates was 1.43% higher than the intermediate gradation, which corresponded to an increase of 1.15% Pbe. The increase in stiffness due to the nine months of oven aging at 60°C was notably higher with the intermediate gradation compared to the fine, a result somewhat contrary to those of the previous two aggregate sources.

In summary, the findings of the qualitative gradation evaluation were generally inconsistent. The California mixtures presented nearly the same behavior, despite large changes in the asphalt binder contents with the unmodified PG 64-22 binder. The Nevada mixtures with the PG 64-28 binder generally supported the same influence. However, the Utah mixtures behaved substantially different between the two gradation levels.

Therefore, it seems logical to explain why the responses were different and to identify what may be the underlying cause of these different behaviors. Due to the limited number of mixtures in the analysis, robust statistical considerations are not

practical. Therefore, considerations of the basic changes to the material properties are necessary. Recalling that the aggregate mineralogy has been shown to influence the adhesion of asphalt binders onto aggregate surfaces (Robertson et al., 2006), the interaction of the silica with the asphalt binder will be explored. Since the actual elemental analysis of the different aggregate sources has not been determined, the stockpile percentage of the Wadsworth sand will be utilized as a surrogate for the total silica content of each aggregate gradation as it was determined to be a substantial source of siliceous material. However, the California mixture did not contain the Wadsworth stockpile, but it was noted to contain a wide range of different mineralogies some of which contain quartz (i.e. SiO_2). Therefore, this abbreviated analysis will, by necessity neglect the California mixtures until the silica content can be approximated.

The stockpile percentages of the Wadsworth sand were assumed to represent the silica content of the Nevada and Utah aggregates. Numerically, the Wadsworth sand was determined to contain approximately 50% silica. Thus, in this simplified manner, the silica content was assumed numerically equivalent to half of the Wadsworth content. In this manner, the Wadsworth stockpile percentages for the intermediate and fine gradations for the Nevada aggregates were 20 and 24%, respectively. Thereby, indicating the silica content for the Nevada aggregates were 10 and 12%, respectively. Similarly, the Wadsworth stockpile percentages for the intermediate and fine gradations for the Utah aggregates were 22 and 35%, respectively. Thus, the silica content for the intermediate and fine gradations for the Utah aggregates were 11 and 17.5%, respectively. In this context, a relatively small difference in the silica content (i.e. 2% for Nevada) produced fairly similar changes in the E^* modulus values for a given aging

condition. Conversely, a substantial increase in the silica content (i.e. 6.5% for the Utah aggregates) resulted in a measurable reduction in the increase in stiffness (i.e. E^*) over the same aging duration. If this were the case, it would correspond to the increased adhesion of the binder to the aggregate, thereby reducing the relative quantity of polar fractions of the asphalt binder available to increase the stiffness and presumably brittleness of the binder and correspondingly the mixture as a whole.

It should be noted that two mixtures are not sufficient to validate this potential explanation. Unfortunately, the data from the modified SARA analyses are not available to further examine these findings. However, these results merely suggest that additional studies in this area may be warranted.

9.1.4 Constant Film Thickness

Additional considerations of the aggregate influence on the measured E^* values were conducted though evaluations of the mixtures produced with the asphalt binder content which corresponded to a 9 μm apparent film thickness (AFT). In these considerations each of the mixtures was compacted to the 7% air void level of the cut specimens with each mixture aged in a forced draft oven at 60°C for the prescribed duration. As with the previous sections, only the mixtures aged for zero and nine months are presented in the following figures for the sake of clarity in the figures.

Considerations of the unmodified binders are presented in Figure 9.14 for the mixtures containing the PG 64-22 asphalt binder. Both of the WesTrack mixtures with their respective PG 64-22 binders are depicted in Figure 9.15. Again, it is important to

note the differences in asphalt binders and aggregate sources between the WesTrack materials themselves, but also between the WesTrack and the other laboratory prepared PG 64-22 mixtures.

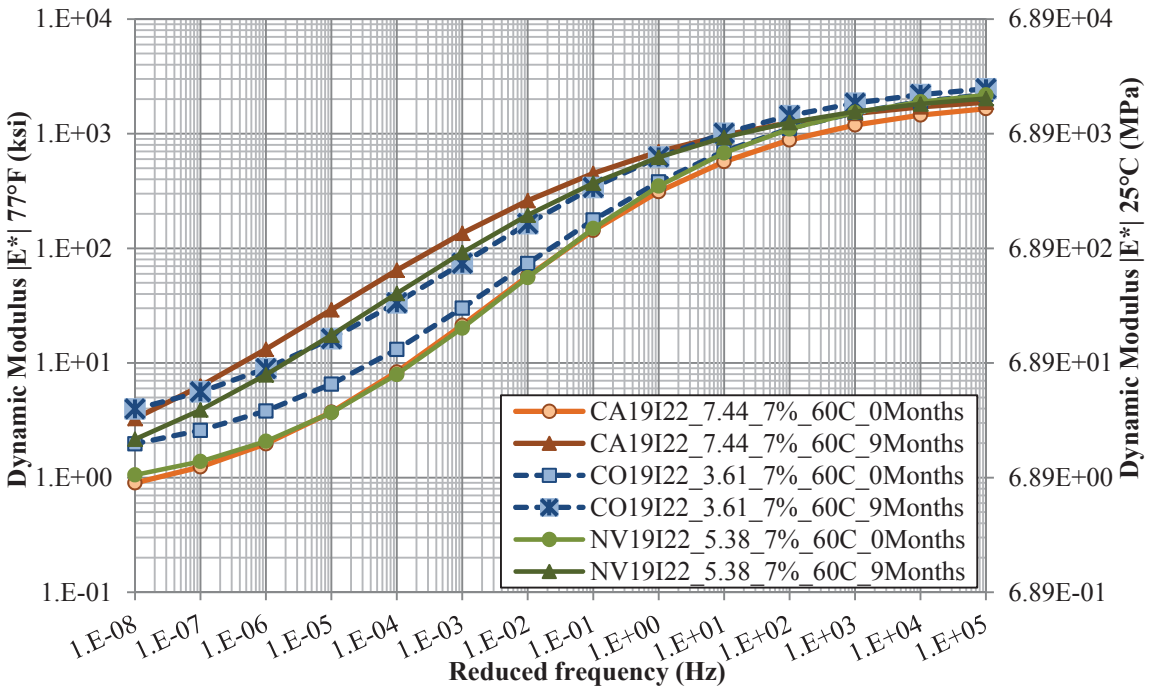

Figure 9.14 Dynamic Modulus Master Curves for the Mixtures with PG 64-22 and Constant Film Thickness Aged at 60°C

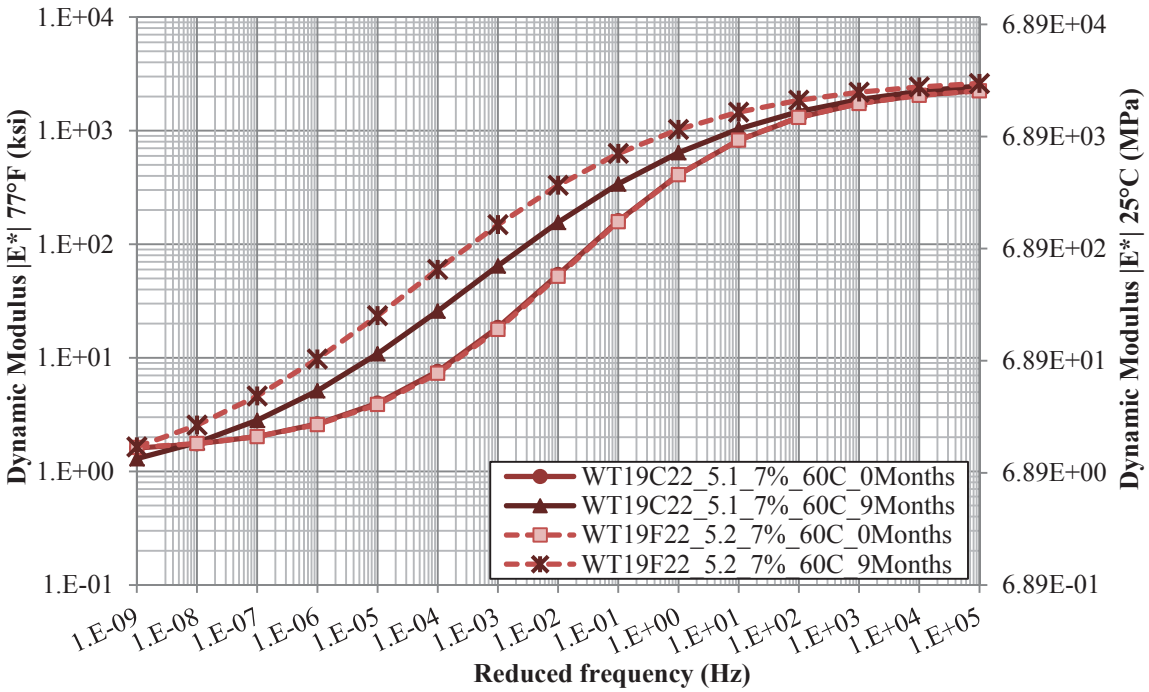

Figure 9.15 Dynamic Modulus Master Curves for the WesTrack Mixtures Aged at 60°C

Initial observations of Figure 9.14 indicate that the zero month aging condition, the California and Nevada mixtures have very similar E^* master curves, while the Colorado mixture is slightly stiffer. After nine months in the 60°C oven, portions of the Colorado and Nevada mixtures are quite similar while the California mixture was generally stiffer than both, except at extreme limits of the data where the Colorado mixture is the stiffest of the mixtures considered in Figure 9.14. Solely based upon the relative changes in the E^* master curves, it appears that the Colorado mixtures were the least influenced by the nine month oxidative aging duration. The California mixture was influenced the most, while the Nevada mixture was in between the other two mixtures. This corresponded very well with the total asphalt binder content, effective binder content (Pbe), as well as the measured water absorption of the aggregate.

Considerations of the two WesTrack mixtures presented in Figure 9.15 indicate nearly the same E^* master curves at the zero month aging condition. Despite the differences in gradation, aggregate source, and binder source, the E^* master curves of the two mixtures were nearly identical. After the nine month conditioning at 60°C, the two mixtures exhibited substantially different E^* master curves. Recognizing that the two mixtures should not be directly compared to each other; this information does indicate a significantly higher level of aging with the coarse WesTrack gradation from 1997. This creates some disagreement between the oxidation measures as well as the HS parameter discussed in chapter 8. However, it does tend to support the aggregate structure discussions previously presented in section 9.1.1 and referencing the mixture photographs in Appendix E.

Considerations of the modified binders are presented in Figure 9.16 for the mixtures containing the PG64-28 asphalt binder.

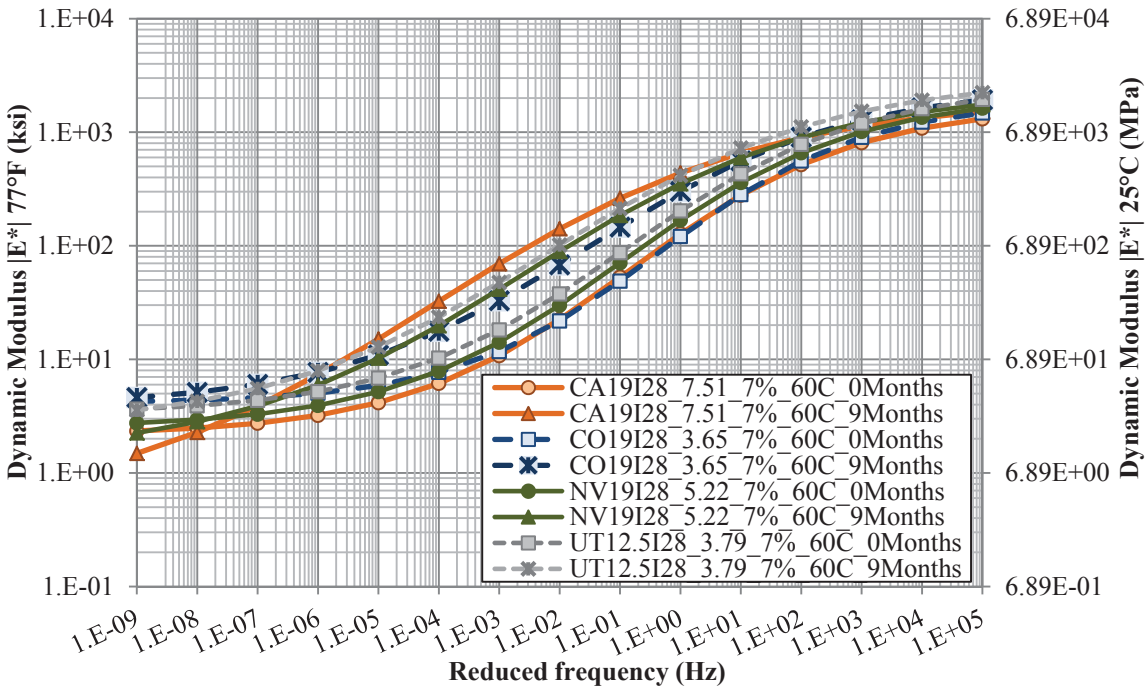

Figure 9.16 Dynamic Modulus Master Curves for the Mixtures with PG 64-28 and Constant Film Thickness Aged at 60°C

The E^* master curves for the mixtures containing the modified PG 64-28 binder and the 9 µm AFT presented in Figure 9.16 indicate fairly similar results to those of the unmodified mixtures. Again, the California mixture with the highest binder content generally exhibited the largest increase in E^*, though only in the intermediate range of the reduced frequency. At the lower end of the reduced frequency range presented, the Colorado aggregates exhibited the highest E^* values, similar to the unmodified binder results. In general, the majority of the intermediate frequencies suggest a similar degree of stiffening of the mixtures due to the nine month aging duration with the Colorado, Nevada, and Utah aggregates, although the upper and lower asymptotes of the E^* sigmoidal function were distinguishable among all the respective aggregate sources.

Similar to the considerations of the Colorado and Nevada mixtures prepared with both the PG 64-22 and PG 64-28 binders, Figure 9.17 presents the California intermediate gradation mixtures at the 9 µm AFT compacted to the 7% air void levels, with both asphalt binders.

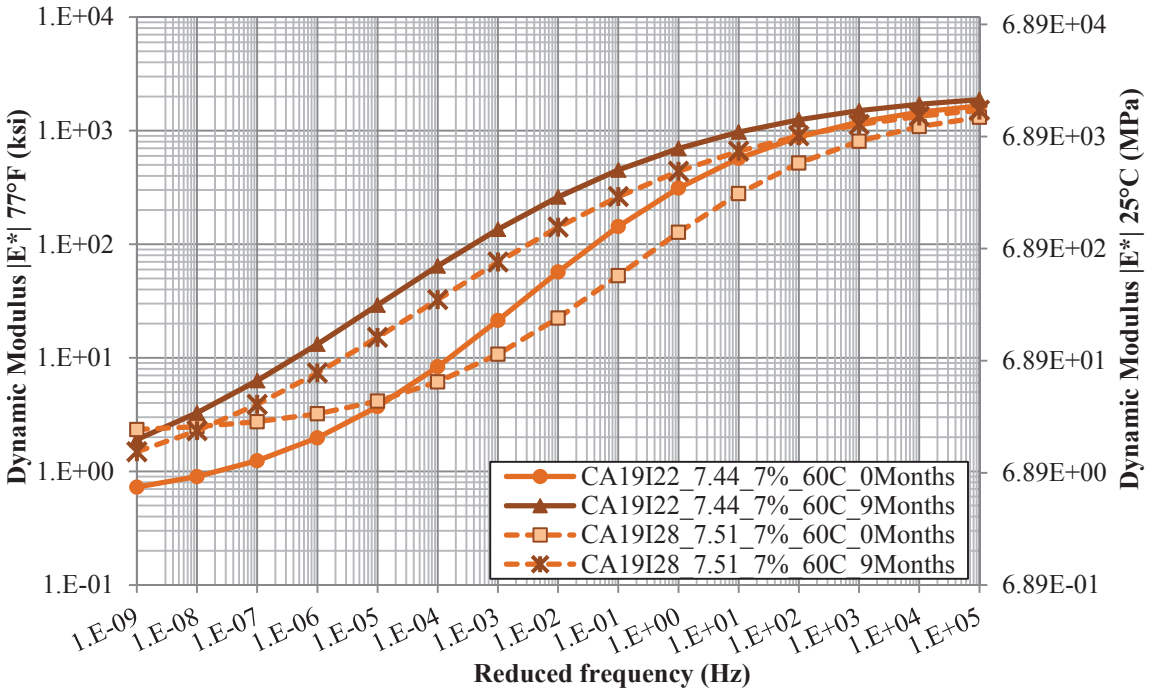

Figure 9.17 Dynamic Modulus Master Curves for the California Mixtures with Constant Film Thickness Aged at 60°C

Figure 9.17 indicates that the California aggregates exhibit similar behavior to the Colorado and Nevada mixtures discussed in the previous section 9.1.2. In all but the lower end of the reduced frequencies range, the mixtures containing the unmodified PG 64-22 exhibited higher E^* values compared to the modified PG 64-28 mixtures. The overall influence of the nine month oxidation duration did not appear to be appreciably different between the two binders, nor was it fully consistent over the reduced frequency

range. There was a further separation at the lower end of the reduced frequency range with the PG 64-22 binder, but again this may very well be the combined effect of the test temperatures and frequencies relative to the reference temperature and reported reduced frequency range, respectively.

Due to the mixed mineralogy of the California, Colorado, and Utah aggregates, it is impractical to estimate the silica content of these sources, even by the previous estimation of the Wadsworth sand content. Therefore, without the elemental analysis discussed previously, it becomes impossible to provide reliable input specific to the silica or other mineralogical content for these particular mixtures.

Overall, the mixtures aged with a constant 9 μm AFT indicate that the higher binder contents typically resulted in a greater degree of stiffening exhibited in the E^* master curve plots over a portion of the reduced frequency range. Further differences in the influence of the nine month aging duration were noted, but could not be fully explained by standard volumetric parameters (e.g. binder content, absorption, or specific gravity).

9.1.5 Mixture Aging Temperature

Further considerations of the influence of mixture oxidation on the E^* master curves were conducted by aging select mixtures at 85°C in addition to the 60°C aging temperature already analyzed. Due to the significant amount of resources consumed during mixture preparation, aging, and testing, only the CAL19I22_7.44 and NV19I28_5.22 mixtures were aged at both 60 and 85°C, at the three air void levels (4, 7, and 11%). Based upon considerations of the pan-aged binders evaluated in section 7.1.6, the aging durations for

the 85°C aging were reduced to 0.5, 1, and 3 months, as were presented in section 7.2.6 and elsewhere. As a result of the aging durations not being the same for both temperatures, Figure 9.18 though Figure 9.24 present all four aging conditions at 60°C along with the three conducted at 85°C for each mixture differentiated by the compacted air void level during the aging process. Figure 9.18 through Figure 9.20 present the California aggregates with the PG 64-22 binder, while Figure 9.22 through Figure 9.24 present the Nevada mixtures containing the modified PG64-28 asphalt binder.

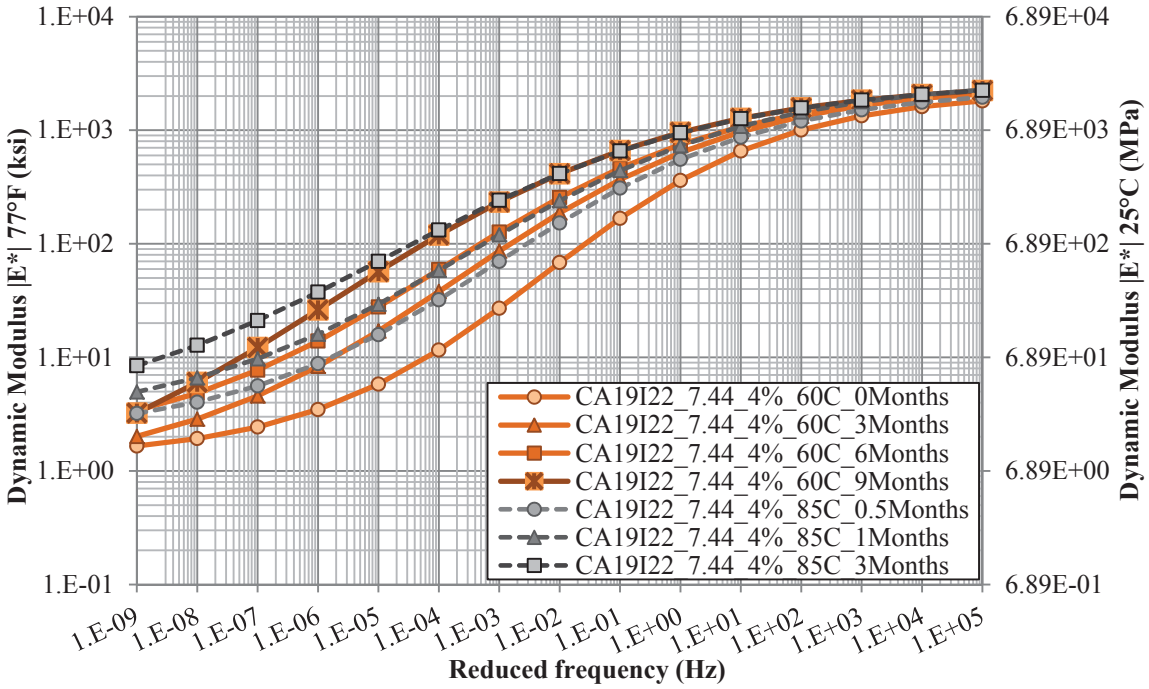

Figure 9.18 Dynamic Modulus Master Curves for the CAL19I22_7.44 4% Air Void Mixtures Aged at 60 and 85°C

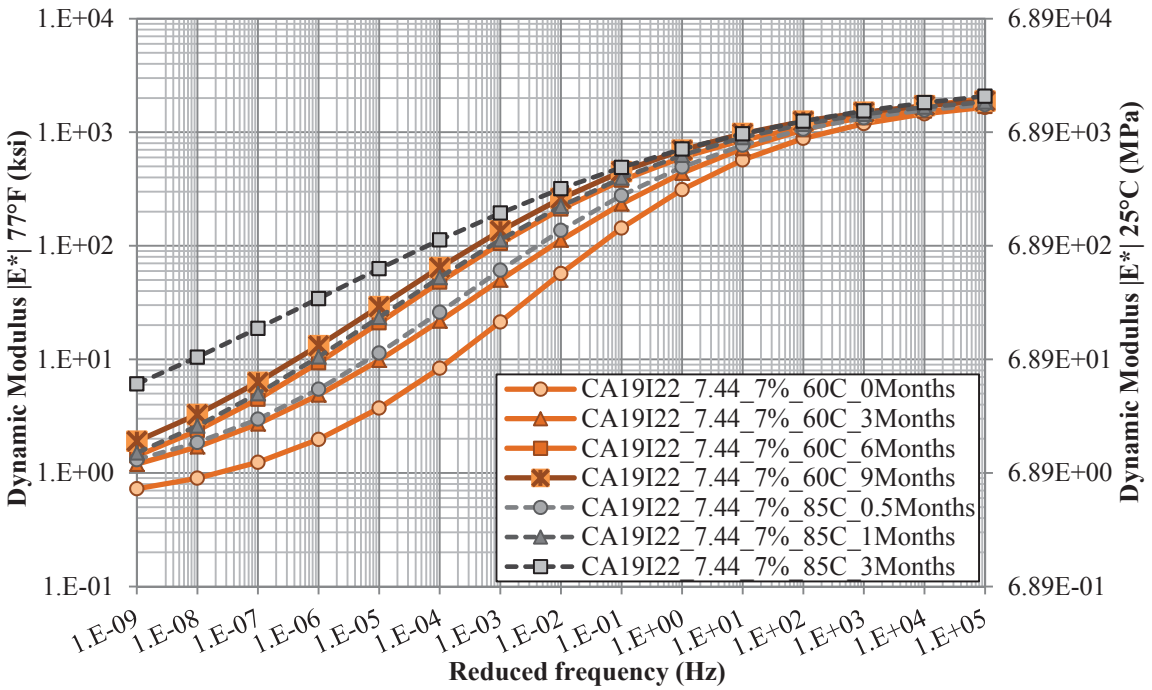

Figure 9.19 Dynamic Modulus Master Curves for the CAL19I22_7.44 7% Air Void Mixtures Aged at 60 and 85°C

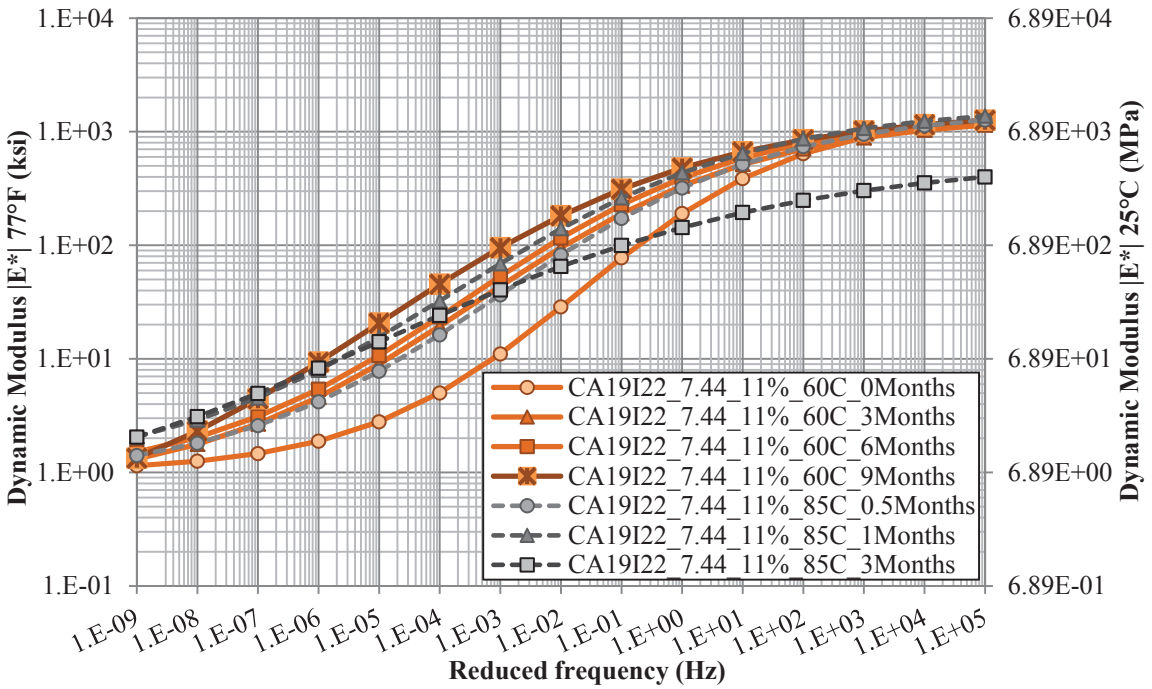

Figure 9.20 Dynamic Modulus Master Curves for the CAL19I22_7.44 11% Air Void Mixtures Aged at 60 and 85°C

Beginning with Figure 9.18, the California mixtures prepared with the PG 64-22 binder aged with 4% air voids definitely show increased E^* values with the 85°C aging conditions. The shift is substantial enough that the 0.5 month at 85°C aging measures are fairly similar to those of measured after three months at 60°C aging. The measures after three months at 85°C are similar to those after nine months at 60°C, except for some variation noted at the lower end of the reduced frequency range where the 85°C aged mixtures exhibits higher values of E^*. This comparison was quite expected after observations of the pan-aged binder analyses as well as the mixture-aged binder rheology measurements conducted in Chapter 7.

Consideration of the mixtures aged with 7% air voids presented in Figure 9.19 exhibit fairly similar relative behavior to the 4% air void mixtures, except the separation between the mixture aged for three months at 85°C and the mixture aged for nine months at 60°C are spaced further from each other. In general, this signifies the reduced magnitude of aging with the 7% air void level of the mixtures aged at 60°C. With the exception of the mixture aged for three months at 85°C, the 11% air void mixtures also exhibit a similar reduction in the overall spread due to different levels of oxidation applied through the various aging durations. In general, the influence of the higher aging temperature increased the stiffening of the binder over a given aging duration for a given air void level.

A substantially different behavior was noted for the 11% air void mixture aged at 85°C for the three month duration. Even though nearly all the other mixtures share a relatively common maximum E^* asymptote, this mixture was substantially lower. Further, the overall E^* master curve of this mixture was lower than even the one month

aged mixtures. These reductions were measured despite the substantial increase in the asphalt binder stiffness measured on the extracted and recovered binders in sections 7.2.6 and 7.3.5. It is suspected that perhaps the extended aging duration permitted the reorganization of the aggregate structure (i.e. creep) in the mixture, thus altering the overall stiffness of the mixture at this aging condition. It is unknown at this point why this influence was isolated to only the 11% air void mixture and only the 3 month duration sample. This behavior may be logically explained if creep displacement and subsequent aggregate reorientation were the cause of the significant deviation from the expected values, which was not observed in this case. Thus, further discussion of this occurrence will be delayed, depending on the outcome of the Nevada mixtures with the PG 64-28.

In general, the overall reduction in the magnitude of the measured E^* values is in general agreement with the previous air void analysis, which indicated the rate of the oxidation was higher with lower air void levels. To verify these general observations, Figure 9.21 presents the previous air void analysis from the 60°C aged mixtures and the E^* master curves developed from the companion mixtures aged at 85°C for the California mixtures containing the PG 64-22 asphalt binder.

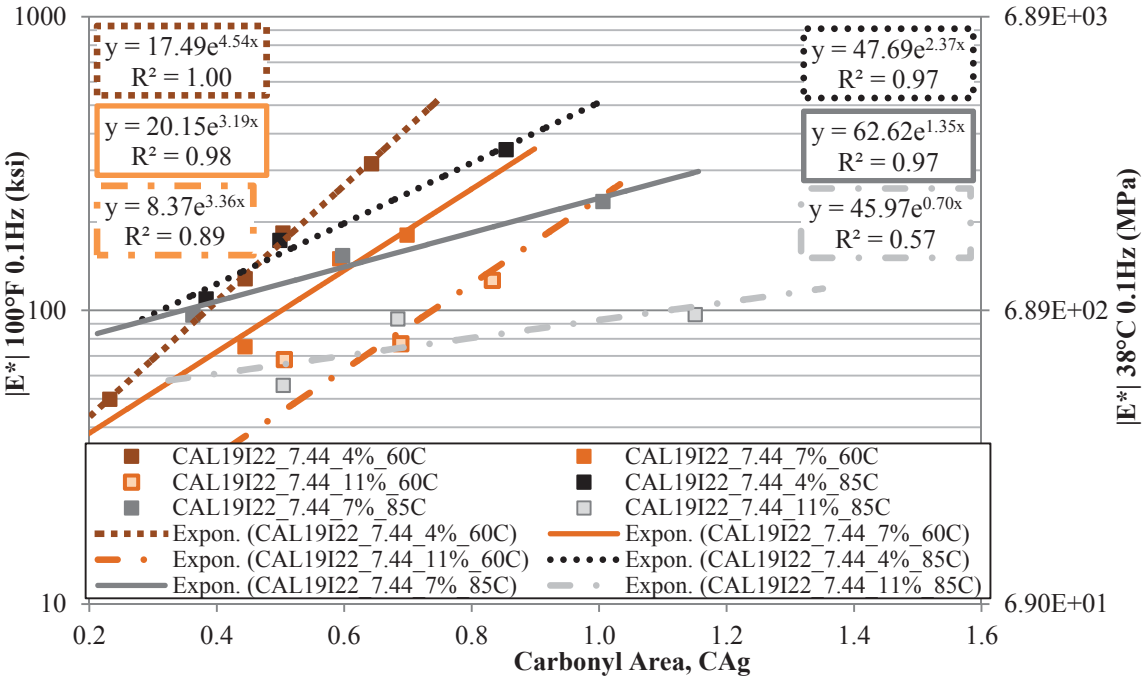

Figure 9.21 Select Dynamic Modulus Measures of California Mixtures with PG 64-22 and Different Air Void Levels Aged at 60 and 85°C

The data from the mixtures aged at 85°C presented in Figure 9.21 exhibited substantially different responses as a function of the air void level when compared to those aged at 60°C. However, there was still a clear separation between the air void levels within each respective aging temperature. Though not fully consistent with these particular mixtures aged at 60°C, the 85°C aged mixtures present the reduced increase in E^* with the increased air void level discussed in the previous section 9.1.1 as indicated by the exponential term of the developed relationships.

The temperature susceptibility evaluation of the mixtures also included the Nevada aggregates prepared with the SBS modified PG 64-28 asphalt binder. The developed E^* master curves of those mixtures compacted to 4, 7, and 11% air voids and aged at both 60 and 85°C are presented in Figure 9.22 through Figure 9.24, respectfully.

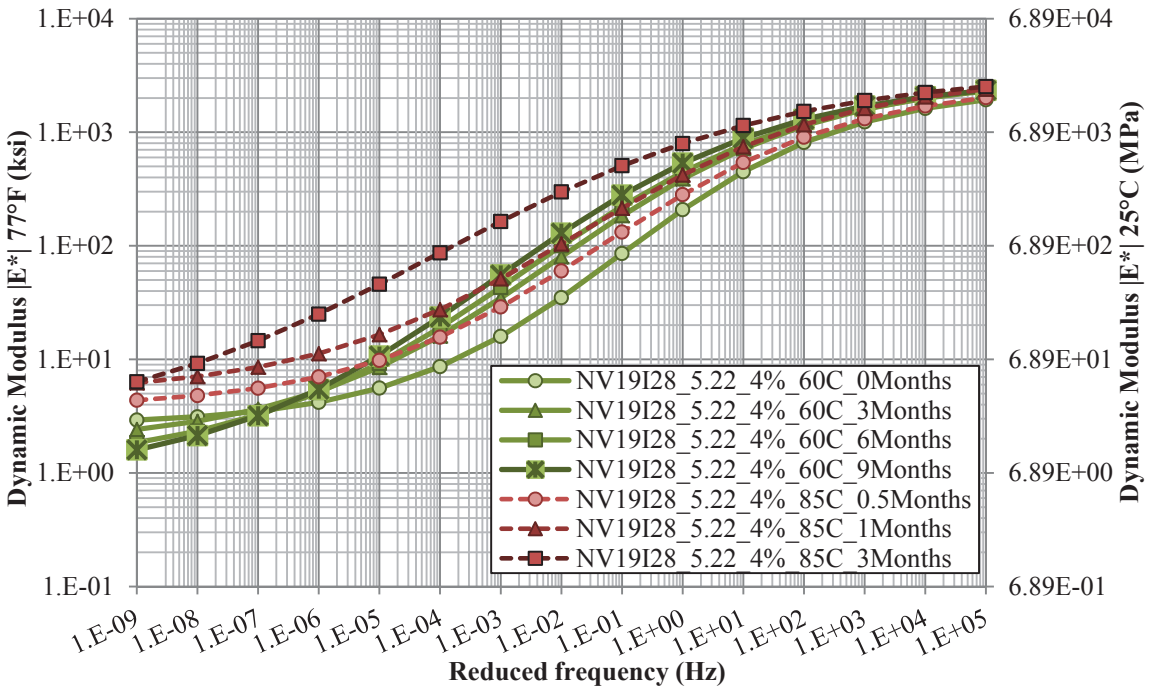

Figure 9.22 Dynamic Modulus Master Curves for the NV19I28_5.22 4% Air Void Mixtures Aged at 60 and 85°C

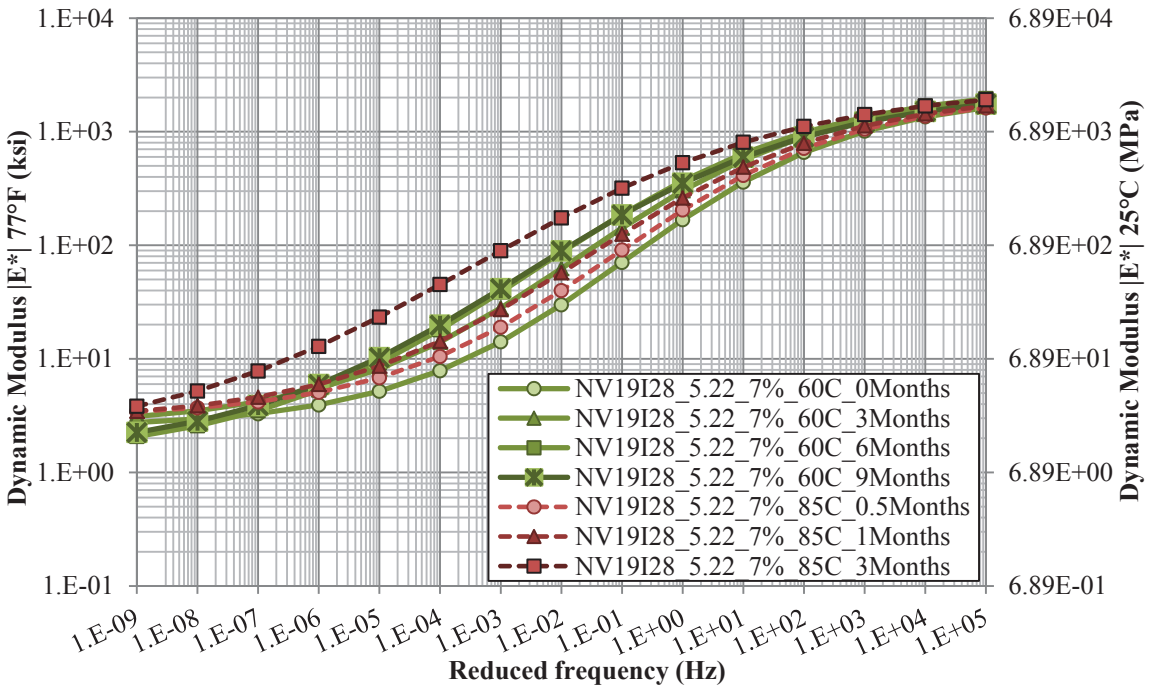

Figure 9.23 Dynamic Modulus Master Curves for the NV19I28_5.22 7% Air Void Mixtures Aged at 60 and 85°C

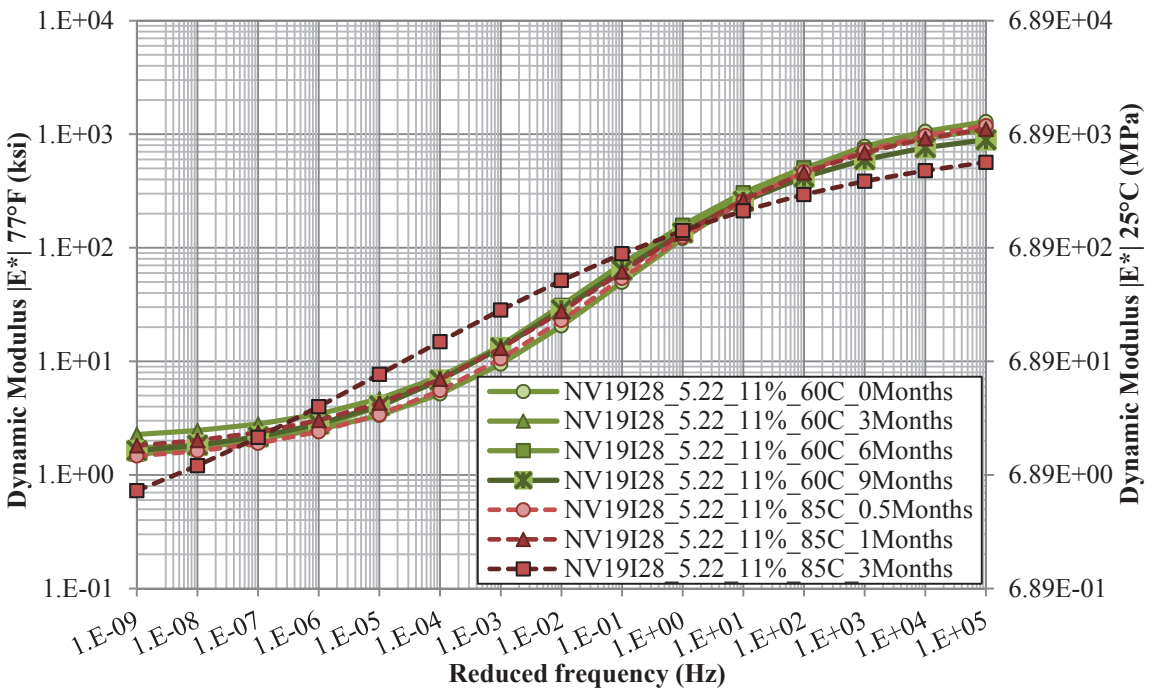

Figure 9.24 Dynamic Modulus Master Curves for the NV19I28_5.22 11% Air Void Mixtures Aged at 60 and 85°C

Initial observations of the Nevada mixture with the PG 64-28 binder compacted to 4% air voids presented in Figure 9.22 suggests a fairly similar behavior to that of the California mixtures with the PG 64-22 binder. Slight differences are noted in the typically reduced influence of the measured E^* master curves of the modified materials after the 60°C aging, thus giving the appearance of an increase influence of the temperature change to 85°C as compared to the unmodified mixtures. The Nevada mixtures aged at 85°C did exhibit a larger increase in the measured E^* master curves over the full three month aging duration compared to the same mixtures aged at 60°C for the nine month duration, contrary to the findings of the unmodified mixtures. However, the relative comparisons between the two will be carried out with all three air void levels. Similar to the unmodified mixtures, the Nevada mixtures with the modified PG 64-28 binder has started

to lose the lower asymptote on the E^* with the 85°C mixture aged for three months, while retaining more of the curvature compared to the unmodified mixtures. Again, this behavior is suspected to be due to the combined effect of the relation between the measured temperatures with respect to the reference temperature as well as the relative margin between the measured frequencies with respect to the presented reduced frequency range.

Consideration of the Nevada mixture with the PG 64-28 binder compacted to 7% air voids presented in Figure 9.23 shows a similar relative comparison noting the overall larger influence of the three month aging duration at 85°C compared to nine months at 60°C. Again, this observation differs from that of the California mixtures containing the PG 64-22 asphalt binder, where the overall magnitude of the E^* increase was more comparable.

The Nevada mixture with the PG 64-28 binder compacted to 11% air voids presented in Figure 9.24 show very little change in the measured E^* values as a function of either the 60° or the 85°C aging conditions, again with the exception of the mixture aged for three months at 85°C. For the mixtures aged at 85°C, the relatively minimal shift in the E^* values support that of the mixtures aged at 60°C previously discussed in Figure 9.3.

Additional considerations of the temperature influence are again represented by considering the measured E^* values at 37.8°C (100°F) at 0.1 Hz for the two respective aging temperatures. Figure 9.25 presents the previous air void analysis from the 60°C aged mixtures and also the E^* master curves developed from the companion mixtures aged at 85°C for the Nevada mixtures containing the PG 64-28 asphalt binder.

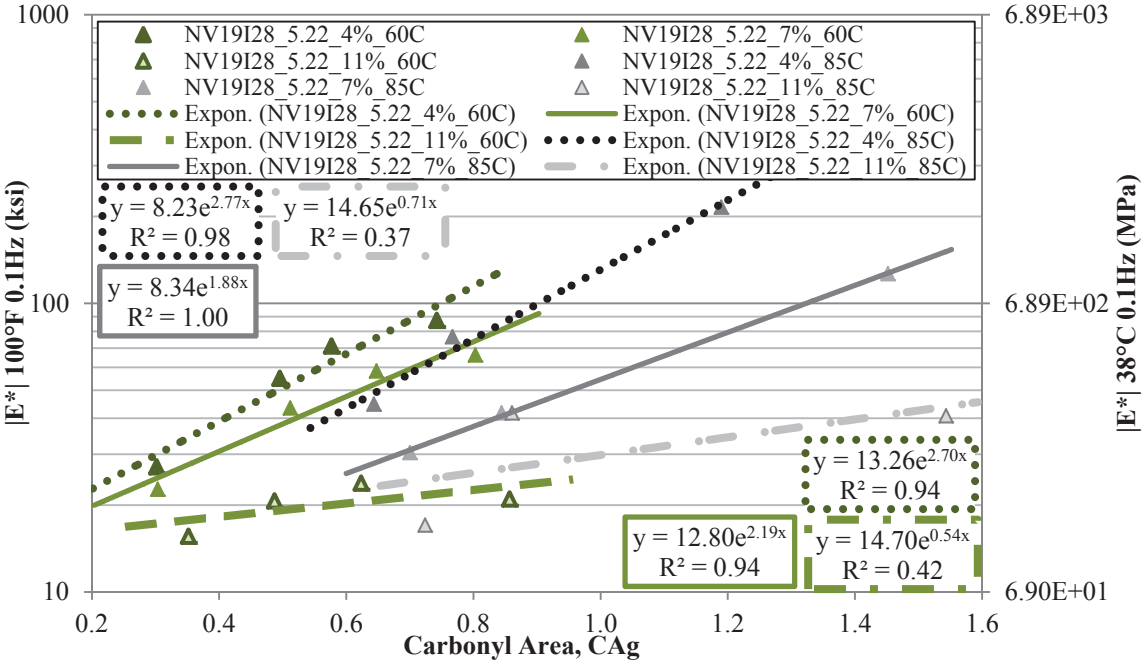

Figure 9.25 Select Dynamic Modulus Measures of Nevada Mixtures with PG 64-28 and Different Air Void Levels Aged at 60 and 85°C

Observations of the representative E^* values presented in Figure 9.25 indicate general similarity between the rates of increase in the E^* values between the two aging temperatures, within the same air void level. Clearly, each of the respective air void levels differ from one another. However, within each air void level, the slope or rate of increase in the E^* values as a function of CA remained fairly consistent as indicated by both visual observation and the similarity in the exponential term of the fitted relationships presented in the figure.

To further analyze the effect of the aging temperature Figure 9.26 through Figure 9.28 present the measured E^* values at 37.8°C (100°F) at 0.1 Hz for the two respective aging temperatures with both mixtures at a single air void level in each figure.

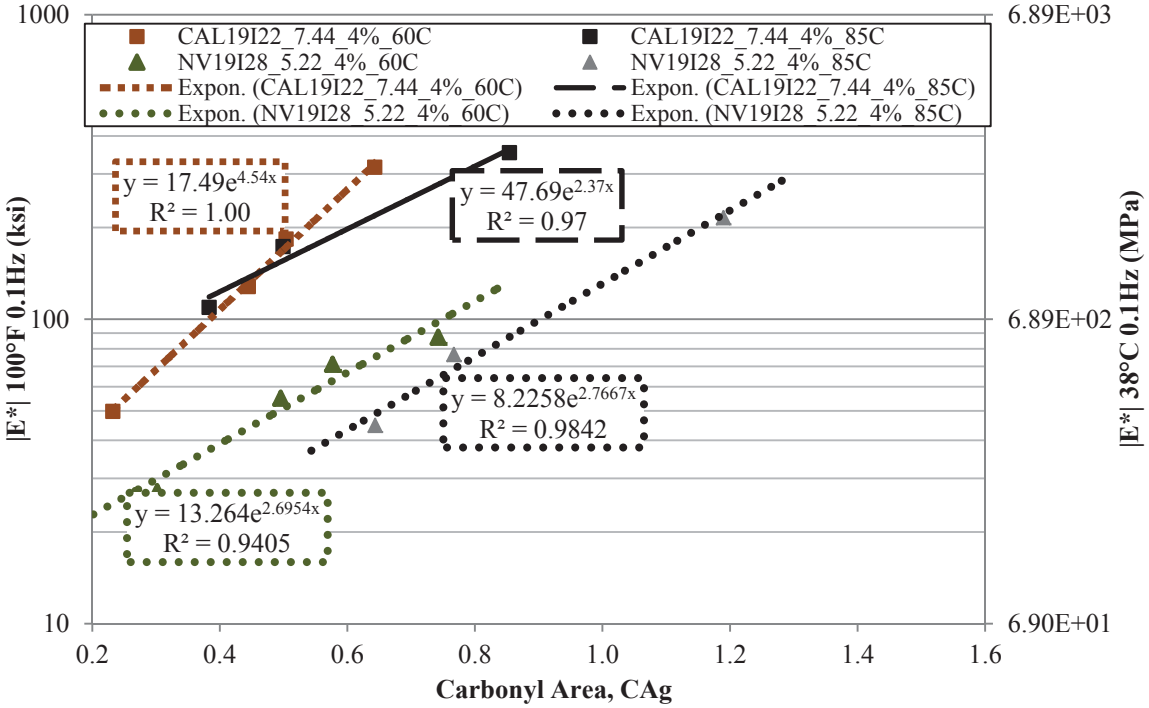

Figure 9.26 Select Dynamic Modulus Measures of California and Nevada Mixtures with 4% Air Void Level Aged at 60 and 85°C

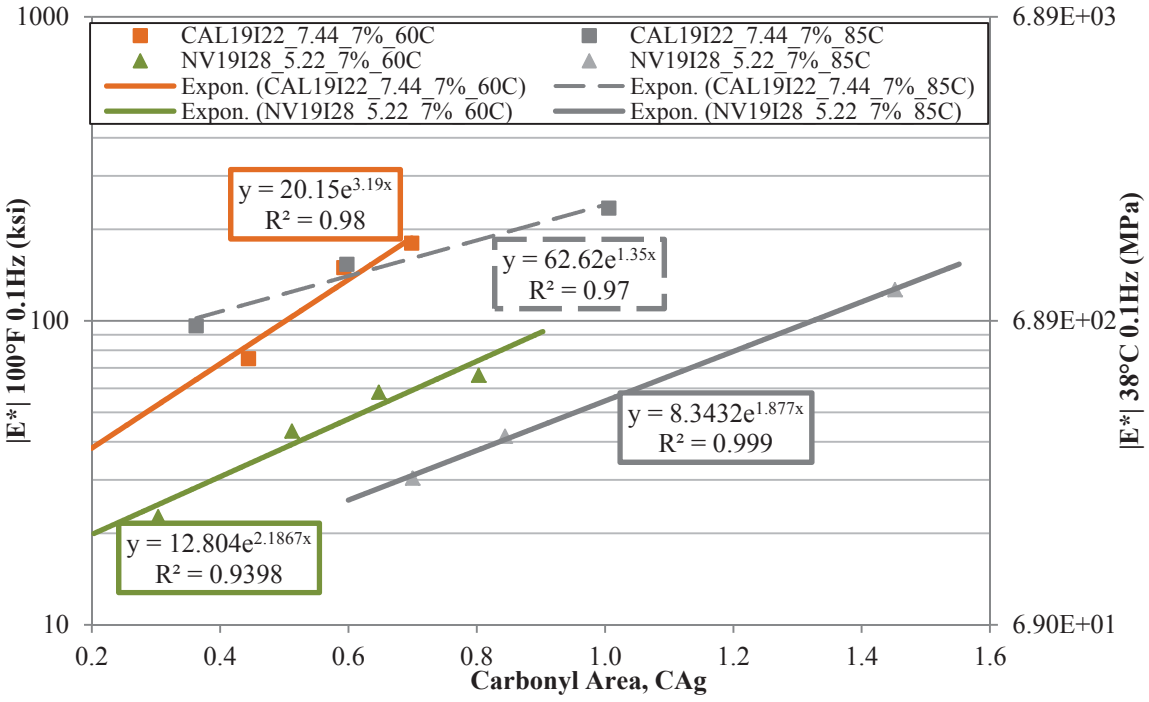

Figure 9.27 Select Dynamic Modulus Measures of California and Nevada Mixtures with 7% Air Void Level Aged at 60 and 85°C

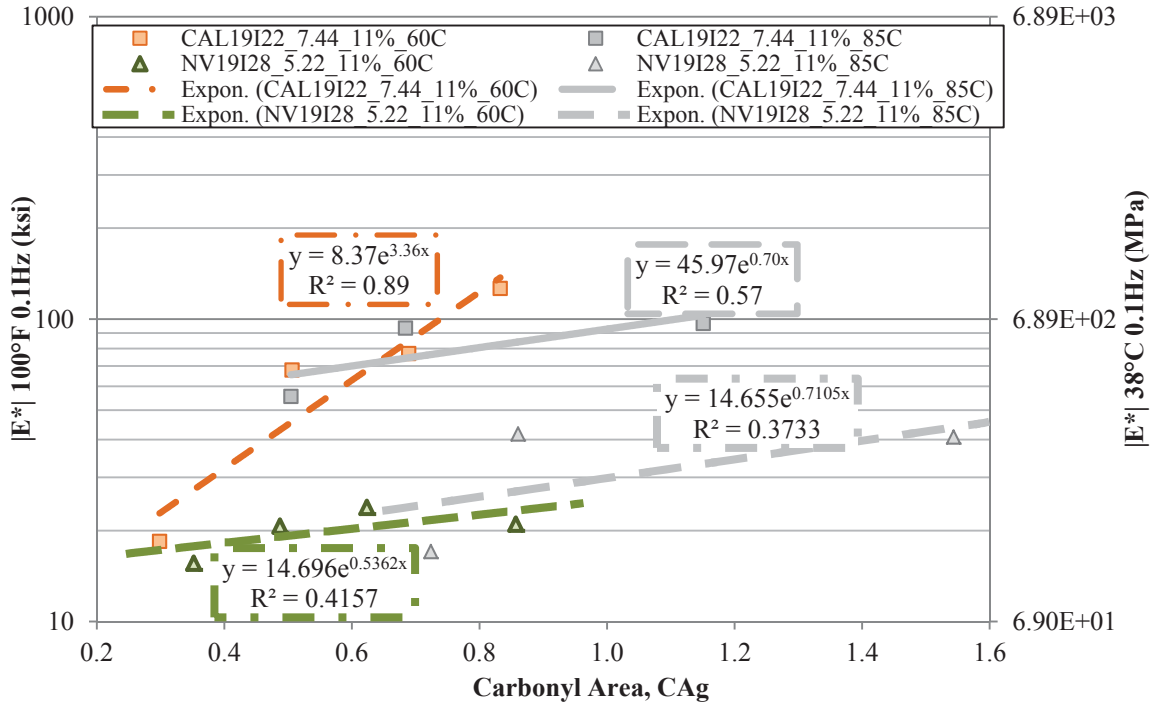

Figure 9.28 Select Dynamic Modulus Measures of California and Nevada Mixtures with 11% Air Void Level Aged at 60 and 85°C

Consideration of the mixtures aged at the 4% air void level in Figure 9.26, indicates some general similarities among several of the mixtures. Specifically, the slopes of both the Nevada mixtures and California mixture aged at 85°C exhibit fairly similar slopes or the rate of increase in the measured E^* value with carbonyl growth is similar. The California mixture aged at 60°C was determined to have a relatively higher slope. However, the first two 85°C measures (i.e. 0.5 and 1 month) for California fall nearly identically within the range of the 60°C aged mixtures, despite the overall fit (i.e. R^2 value) of both relationships being quite good. It is evident that the California mixtures with the unmodified PG 64-22 binder are substantially stiffer than the Nevada mixtures with the modified PG 64-28, even with lower carbonyl measures for the unmodified mixtures.

Observations of the mixtures aged with the 7% air void level presented in Figure 9.27 again suggest fairly similar stiffening rates with carbonyl growth for the two Nevada mixtures containing the modified PG 64-28 asphalt binder. A clear separation is shown between the two relationships, however the slope or rate of stiffening are relatively similar. The California mixtures with the unmodified binder present fairly different slopes between the two temperatures, with one slope less than and one greater than the Nevada mixtures. Again, the overall magnitude of the measured E^* values was higher for the unmodified California mixtures.

Representations of the measured E^* values for the mixtures aged with the 11% air void level are presented in Figure 9.28. Initial observations of this figure suggest that both Nevada mixtures and the California mixture aged at 85°C exhibit very similar rates of increase in the measured E^* values with carbonyl growth. Again, the California mixture aged at 60°C is substantially different. However, similar to 4% air void evaluation, the first two aging levels for the 85°C mixtures are substantially different from the overall trend including all three aging durations. The 0.5 and one month duration for the California mixture plots very similar to the California mixture aged at 60°C. The 0.5 and one month duration for the Nevada mixture presents a slope dissimilar to both California aging conditions and the Nevada mixture aged at 60°C.

Taking into consideration the overall behavior of the shifted master curves of the mixtures aged at 85°C for the three month duration, there is reason to question these values until further investigation can be conducted to either substantiate and verify the reported measures or to explain why they do not seem to follow the aging pattern observed with the other mixtures.

If the measured E^* values at 37.8°C (100°F) and 0.1 Hz were considered as a representative value of the low shear viscosity for mixtures as presented in section 9.1.1, it is possible that such a profound change in slope (i.e. representation of the hardening susceptibility of mixtures) could be caused by the fast rate or initial nonlinear behavior of the binder. Such speculation cannot readily be supported or refuted, since the relative level of linear or constant rate portion of the constant rate kinetics measures of pan-aged asphalt binders change relative to the aging temperature. In short, with the limited number of mixtures evaluated in this case, the true cause of the apparent discrepancy cannot be adequately determined.

Thus, whether these behaviors are the product of the aging condition, some level of damage or cracking within the structure of the mixture, or some other cause yet to be determined for these materials and will be recommended for additional evaluation as part of that relevant section of chapter 11. It is possible that an evaluation of the aggregate structure of these mixtures (e.g. two-dimensional imaging analysis of the aggregate orientation) may provide some useful justification for the observed behavior of the 11% air void mixtures aged for three months at 85°C. It is logical that some common unknown factor may explain these uncharacteristic behaviors. It is odd that even though the prior aging conditions did not yield the same response to aging between the two mixtures, this particular aging condition gave almost the same response.

Without further investigation it is difficult to decipher, however it is possible that perhaps the binders in these particular mixtures became so aged that they exhibited micro-cracks and were thus damaged yielding the much reduced E^* values noted. This type of cracking was noted with some initial pan-aged binder samples that were aged at

135°C and a few at lower temperatures. The damage was not evident in the pan-aged materials presumably due to the annealing effect during the heating and remolding processes required for the FT-IR and DSR measurements. The E^* measures were specifically not annealed or heated above ambient temperature in any way prior to the E^* testing process. In fact, they were kept at colder temperatures (i.e. -18°C), which very well may have increased the amount of damage to these particular specimens prior to testing. Therefore, their influence on the overall behavior of the mixtures at the other aged conditions should be tentatively accepted until further evaluation reveals the underlying cause of these behaviors.

However, if the measured E^* values at 37.8°C (100°F) and 0.1 Hz were considered as a representative value of the low shear viscosity thus lending the slope to be a representation of the hardening susceptibility (i.e. HS) of the mixture, the slope can be evaluated in a manner similar to the HS parameters evaluated previously in chapters 7 and 8.

In such a context, Figure 9.29 presents the determined slope from the measured E^* values as a function of carbonyl growth from each of California and Nevada mixtures that were aged at both 60 and 85°C.

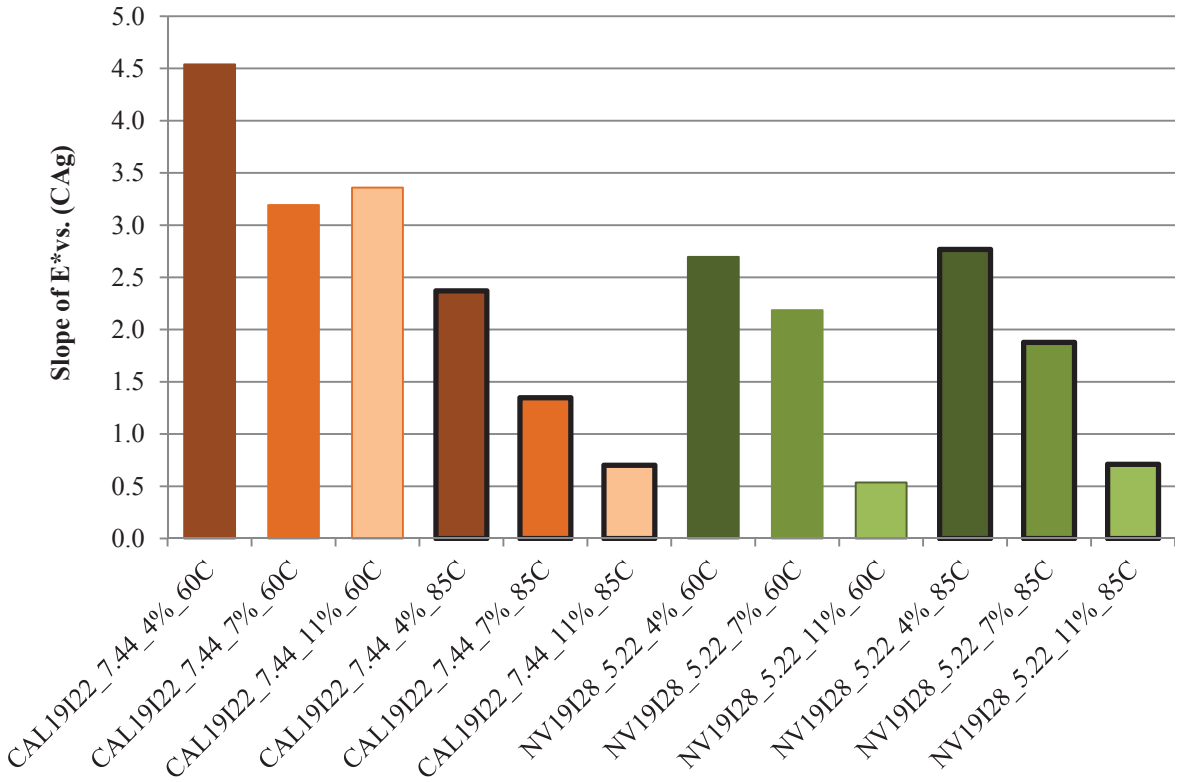

Figure 9.29 Rate of Increase in Dynamic Modulus Measures of Select Mixtures with Different Air Void Levels Aged at 60 and 85°C

Consideration of the rate of increase for the stiffness of the mixtures (i.e. E^*) in the format of Figure 9.29 presents a summary of the overall stiffening rate of the mixtures relative to one another. In this format, it is clearly shown that for nearly all the evaluated mixtures, the rate of increase in the E^* values due to the oven temperature decreases with increased air void levels under isothermal aging conditions. It is further determined that the magnitude of the rates were fairly similar for both aging temperatures with the mixtures containing the modified PG 64-28 binders. Additionally, the aging of the California mixture at 85°C was not too dissimilar from those of the Nevada mixtures. However, the 60°C aging of the California mixtures were not consistent with any of the

other three aging conditions. Thus, these findings can be interpreted such that the mixture characteristics may potentially influence the oxidation and subsequent stiffening of the mixtures. Clearly, the level of air voids or density of the mixture are expected to influence the overall stiffening of the mixtures as a function of oxidation, however the rate of the oxidation growth cannot be ignored in such considerations. The increased rate of oxidation of the mixtures with higher air voids may offset the reduced sensitivity of the measured E^* values as a function of oxidation, however the net effect of these two behaviors is expected to depend upon the actual aging conditions (i.e. not isothermal for pavements in the field).

As an initial evaluation of these isothermal aging conditions, Figure 9.30 presents the measured E^* values at 37.8°C (100°F) and 0.1 Hz with respect to the actual aging time over the respective aging temperatures and mixture air void levels.

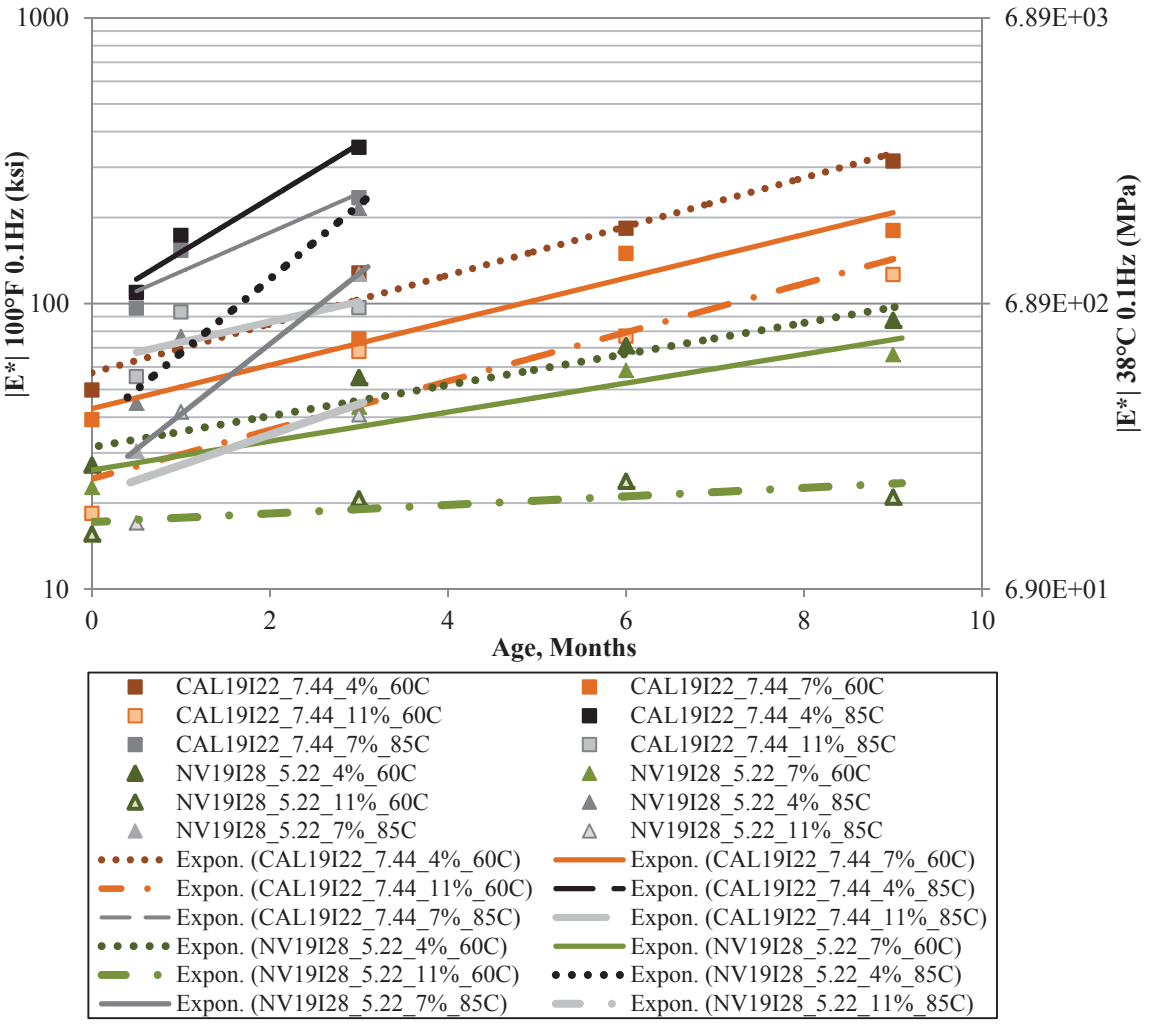

Figure 9.30 Dynamic Modulus Measures of Select Mixtures with Different Air Void Levels Aged at 60 and 85°C

Examination of the measured E^* values at 37.8°C (100°F) at 0.1 Hz presented in Figure 9.30 indicate the aging behavior that should be expected with respect to the actual time of aging for the majority of the mixtures. In nearly all the cases considered in the figure, the 85°C aging condition stiffened the mixtures (i.e. increase the measured E^* values) at a much faster rate compared to the 60°C aging durations, with the 11% air void mixtures at 85°C presenting the possible exception. Again, the 11% air void mixtures aged at 85°C

for the three month duration may have a substantial influence of the rate of those mixtures and should be carefully considered pending the additional evaluation efforts discussed previously.

9.1.6 Summary of Dynamic Modulus Data of Aged Mixtures

The general conclusions that can be drawn from the measured E^* values evaluated in this section indicate that many factors have potential and varied influences on the oxidation of asphalt mixtures based upon the isothermal oven aging conducted as part of this study. Some of the evaluated factors presented consistent influences on the measured E^* values and thus the shifted master curve equations following the standard logistic symmetric sigmoidal form. However, many of the evaluated factors did not always exhibit consistent influences. Further, some of the inconsistencies were accounted for while some are still to be determined upon further investigation.

The majority of the mixtures evaluated in this section were compacted Superpave gyratory specimens which were aged in forced draft ovens at 60°C for their respective durations. Following the prescribed aging duration, the specimens were trimmed to the proper geometry for dynamic modulus (E^*) testing which was presented in this chapter. Following the E^* determinations, these samples were prepared for the extraction and recovery process described in previous chapters to conduct the mixture-aged evaluations on the recovered asphalt binders.

Based upon the measured E^* values obtained from the mixtures aged at 60°C, it was observed that increases in the air void content of the mixture during the aging process,

typically yielded less significant influences of the aging duration on the measured E^* values. In other words, the 11% air void mixtures were not a sensitive to the oxidation procedure as were the 4 or 7% air void mixtures. This does not contradict the previous findings of the oxidation, rheological, and hardening susceptibility measures as these measures also inherently include influences of the internal structure of the mixtures.

Further observations indicate that, in general, the mixtures containing the unmodified asphalt binder produced mixtures of greater stiffness (i.e. higher measured E^* values) than the mixtures containing the SBS modified asphalt binder. Additionally, the mixtures containing the modified binder also typically exhibited smaller changes in the overall magnitude of the measured E^* values compared to the unmodified mixtures when all other mixture characteristics were held constant.

The evaluation of the changes in the qualitative gradation produced inconsistent results. In two of the three evaluated mixtures, the influence of the constant aging conditions produced similar results between the mixtures of the same aggregate sources only with different gradations. However, the third mixture exhibited a substantially different influence due to the same oxidation procedure. Although not fully verified, the quantity of silica in the aggregate gradation has been suggested as a potential explanation for the differences in the oxidation outcome. Potentially, the modified SARA analysis will also yield additional information relevant to differentiating these behaviors. However, limited tests results for these particular mixtures prohibited such determinations.

Increases in the total asphalt binder content (*Pb*) of a given mixture generally led to more substantial increases in the measured E^* values for a given set of aging conditions (i.e. temperature and duration).

Rather inconsistent findings were observed on the measured E^* values due to the oxidation temperature as determined by two mixtures; one with an unmodified and one with the SBS modified binder with different aggregate sources. For the majority of the aging conditions, the higher aging temperature increased the oxidation level of the mixtures. When the measured E^* values were considered as a function of the oxidation level (i.e. carbonyl measurements) rather than a time or duration scale, the results were not as consistent nor the deviations readily explained. Due to the complex interactions between the increased oxidation rates and the reduced sensitivity noted with increased air void levels, it is not clear what the overall effect the mixture density will have on the measured E^* values under non-isothermal aging conditions such as the exposure conditions expected in the field.

9.2 Uniaxial Thermal Stress and Strain Test Results

The evaluation of the significance of aging on the thermal cracking performance of asphalt mixtures considered in this analysis was conducted utilizing the Uniaxial Thermal Stress and Strain Test (UTSST) developed as a part of this study. The applicable methodology and actual procedure were previously discussed in section 3.1.2 and associated sub-sections. As a general overview, the UTSST measurement evaluated the

behavior of the tested mixtures when subjected to thermal loading (i.e. temperature reduction) by measuring the thermal stress development in restrained specimens and the thermal strain developed in unrestrained specimens throughout the test duration.

Similar to the traditional Thermal Stress Restrained Specimen Test (TSRST), the restrained specimen provided a direct measure of the stress induced within the test specimen. This stress is the net influence of the forces developed due to contraction of the specimen less the force reduction caused by the relaxation of the load within the specimen as a function of time. The physical combination of these two behaviors is expected to provide more fundamental characterization of actual low temperature properties of asphalt mixtures, as opposed to many other evaluation tools conducted through mechanical loading under isothermal conditions. Testing under isothermal conditions minimizes, if not eliminates the effect of thermal strain development within the tested mixture, thus making the test blind to such potentially significant influences upon the performance of the mixture.

The thermal strain determined from the unrestrained specimen not only provided information on the coefficient of thermal contraction, but also may be combined with the induced stress to yield the UTSST modulus ($E_{(UTSST)}$) of the mixture as a function of temperature for a given mixture. The coefficient of thermal contraction can be a highly significant input parameter into mechanistic evaluations which consider the influence of thermal loading on the state of stresses within a pavement layer. Thus, accurate measures of such mixture properties become increasingly important with more sophisticated evaluation methods.

Specific influences of particular mixture characteristics on the UTSST modulus curves will be considered in the following sections. Due to the substantial volume of results produced during these measurements (i.e. the multiple thermo-viscoelastic properties of each mixture over multiple oxidative levels), the following considerations will focus on the lower temperature measurements (i.e. crack initiation and fracture properties) with general observations of the behavior of the mixtures at warmer temperatures (i.e. the viscous properties of the mixtures). More specific information regarding any particular measurement for a given mixture may be found in the appropriate sections of Appendix O through Appendix Q.

9.2.1 Oxidation Level

General considerations of the UTSST modulus exhibit drastic changes in the calculated $E_{(UTSST)}$ values as a function of temperature when considering the effect of oxidative aging as can be observed by the figures presented in Appendix O. Overall, it is observed that the oxidative aging of asphalt binder significantly alters the UTSST modulus curves of the mixtures. Not only do the curves generally shift upward at warmer temperatures, indicating an increase in the stiffness of the material with age, but they also significantly change shape at many of the thermo-viscoelastic property temperatures as indicated in the tables presented in Appendix P as well as the figures of Appendix Q. In addition to the referenced information, the following sections contain figures presenting the UTSST modulus relationships, but also include the carbonyl measurements for the respective

mixtures at each aging condition. For simplicity, the oxidation will be represented as carbonyl growth (CAg), which is defined by Equation 9.1.

$$CAg = CA_i - CA_{Tank}$$ **Equation 9.1**

where, CA_i - carbonyl area measured at specific aging condition i;
CA_{Tank} - carbonyl area of the binder at the original or unaged condition.

Even though, nearly all of the UTSST modulus curves presented in Appendix O exhibit the same general behavior with respect to aging, there are a few exceptions. Specifically, the California mixtures aged at 85°C showed some discrepancies compared to the remainder of the UTSST measurements, particularly those aged at the 11% air void level as shown in Figure 27.6. Similar, but less dramatic effects were noted with the Nevada mixtures aged at 85°C. These discrepancies also substantially influenced the determination of the thermo-viscoelastic properties of these mixtures, which in turn altered the consistency of those values presented in Appendix Q. However, the apparent issues with the 85°C aging condition were also evident in the dynamic modulus measures of the previous sections. Therefore, it was generally suspected that the aging conditions may have influenced the measures in an unexpected manner, which is still under investigation to fully evaluate this occurrence.

Additionally, some of the Colorado mixtures containing the PG 64-28 asphalt binder (i.e. Figure 27.11 and Figure 27.12) did not fully exhibit the same systematic change in the UTSST modulus values as the majority of the other mixtures. Another minor discrepancy was noted with the NV19I28_5.22_4%_9mo_60°C mixture of Figure 27.16.

However, as a general consideration of the overall influence of aging on the UTSST modulus curves, these few mixtures should not necessarily detract from the consistent trends noted with the remainder of the nearly 30 mixtures aged to multiple oxidation levels. In addition, the variation of the these measurements was also considered to be very reasonable given the fact that the vast majority of these measurements were based upon only two replicate tests due to the arduous nature of the aging process. Nevertheless, the results were considered to exhibit acceptable levels of repeatability and provide a consistent evaluation of the low temperature properties of the aged mixtures. However, precision and bias statements have not been developed for the method.

General observations of the findings from the UTSST results were specifically focused on the UTSST modulus values defined as the four thermo-viscoelastic properties as well as the temperatures when they occurred during testing. In addition to the determined modulus values, the measured stress at fracture and the crack initiation stages were also considered. Therefore, the following six conditions were considered as an overview of the behavior of the evaluated mixtures in the UTSST as a function of aging and thermal loading conditions:

- Crack Initiation Modulus
- Glassy Hardening Modulus
- Viscous-Glassy Transition Modulus
- Viscous Softening Modulus
- Fracture Stress
- Crack Initiation Stress

Overall behaviors of these parameters as a function of oxidation have been considered in the following subsections.

Crack Initiation Modulus

The crack initiation modulus represents the highest peak of the UTSST modulus curves, where it is understood that the mixture has begun to exhibit substantial micro cracking or other micro damage. At this stage of the test, the thermally induced damage has begun to present larger scale macro cracks which are understood to exist as a true physical separation of the mixture (i.e. a true crack has developed in the mixture). Therefore, this parameter is highly important to thermal cracking analyses since it represents the fundament beginning or initiation of thermal cracks within the mixture.

A clear trend was observed as the overall decrease in the crack initiation modulus as a function of age within each respective mixture (i.e. CAg). Typically, the UTSST modulus values determined in the colder temperature regions of the test measurements significantly decrease with higher levels of oxidation in the mixtures. Initially, this may seem counterintuitive, as the stiffness is well known to increase with oxidative aging as was also noted in the warmer temperature region of the UTSST modulus curves. However, this brings to light some of the potential discrepancies between mechanical testing, at isothermal conditions, and restrained specimen testing under a temperature loading regime.

This observation tends to exemplify that while a given mixture may be stiff, it may not be as tolerant of applied loading without incurring some degree of damage (i.e. it has become more brittle and has lost some capacity to relax the induced thermal stresses). Essentially, the aged specimens present evidence of damage or brittle behavior earlier in the test (i.e. at warmer temperatures). In more traditional terms, it has lost its ability to relax (i.e. it is more brittle as it ages as can be expected).

It should be noted, that the reduction in the slope of the thermal stress build up curve prior to fracture has been observed by other researchers (Fortier and Vinson, 1998 and Pucci et al., 2004). This behavior was referred to as the initiation of micro-cracks in the TSRST specimen before fracturing. In general, the global fracture of the restrained specimen is understood to be the further development of previously formed micro-damage, e.g. cracks, dislocations, etc., which lead to the macro or global fracture of the specimen.

These findings quite clearly indicate the significance of the complex behavior of the interaction between the induced stresses from the thermally applied loading as compared to the ability of the mixture to relax and thus reduce those developed stresses as presented in the figures of Appendix Q. This is particularly evident by the changes in this interaction as the asphalt binders age and result in substantial changes in their characteristic behaviors as a result.

Glassy Hardening Modulus

The glassy hardening modulus is identified as the point where the behavior of the mixture is predominately glassy. It indicated a change in the material behavior where nearly all the viscous or relaxation properties of the mixtures no longer significantly contribute to the thermal response of the mixture.

General observations of the glassy hardening modulus values determined as a function of oxidation (i.e. CAg) continue along the same trend as that of the crack initiation modulus by typically decreasing with oxidation level. With very few exceptions this was observed for all mixtures, thus indicating that the increase in the

brittle behavior of the mixture has a clear influence on the overall behavior of the mixture under thermal loading. The decrease in the glassy hardening modulus further supports the understanding that the UTSST modulus is a type of damaged modulus and is thus influenced by not only the stiffness of the mixture but also the micro cracking damage that has been incurred within the specimen during testing.

Not only does the glassy hardening modulus decrease with oxidation, but the temperature at which this behavior is observed also occurs at warmer temperatures due to higher levels of oxidation within the mixture. Such observations indicate that not only did the specimens incur more damage as they aged and became more brittle, but the observed brittleness and damaged behavior occurred at warmer temperatures.

From a practical standpoint, this is generally supported through the observed thermal cracking performance of in-service mixtures. Many locations exhibit thermal cracking distresses even when the ambient temperature has not been lower than the low temperature value of the PG for the binder. Essentially, as the mixtures age, the damage is induced earlier and at warmer temperatures, thus leading to more prevalent thermal cracking with age.

The reduction in the glassy hardening modulus values were also generally supported by a reduction in the stress measured in the restrained specimen at these temperatures. In other words, the initiation of the brittle behavior was noted to occur at warmer temperatures and lower stress values as the mixtures were more severely oxidized, thus leading to the thermally induced damage, micro cracking, etc. as the result of significantly less severe thermal loading cycles.

Viscous-Glassy Transition Modulus

The viscous-glassy transition modulus represents the transformation of the viscous behavior of the mixture to more of a brittle or glassy response. At the transition point, the behavior of the mixture presented a significant brittle component but also retained portions of the viscous or relaxation properties. Further reduction in the temperature substantially increased the brittle response of the mixture as the material approached the glassy hardening point.

For the vast majority of the evaluated mixtures the viscous-glassy transition modulus increased with the oxidation level of the mixtures. This increase corresponded to a similar increase in the temperature at which the transition modulus was identified as the aging increased in the specimens. Similarly, the thermally induced stress of the restrained specimens also increased at the viscous-glassy transition temperature.

Contrary to the previously discussed thermo-viscoelastic properties, the viscous-glassy transition modulus values for a few mixtures did not follow the general trend of higher values with increased aging levels. Specifically, the California mixture aged at 85°C along with the Colorado mixtures containing the PG 64-28 asphalt binder, and the Nevada mixture with the fine gradation were all noted to deviate from the increasing viscous-glassy transition modulus with increased oxidation levels.

Interpretation of the general increase in the viscous-glassy transition modulus, temperature, and stress level was understood to result from the viscous component of the mixture. It was very clear that the stiffness of the mixtures significantly increased with increased oxidation severity as noted by the asphalt binder evaluations in Chapters 7 and 8 as well as the previous E^* measurements discussed in section 9.1. Therefore the end

result of the stiffening effect of the binder on the thermal behavior of the mixture resulted in an increase in the measured stress which led to increases in the modulus value all taking place at increasingly warmer temperatures. In this temperature range, this increase in stiffness was not counteracted by the damaging effects of the brittle components noted in the glassy hardening and crack initiation regions of the UTSST relationship, largely due to the corresponding viscous component retained by the asphalt binder.

Viscous Softening Modulus

The viscous softening modulus was identified as the rapid increase in the UTSST modulus resulting from the mixture no longer sufficiently capable of fully relaxing the thermally induced stress in the restrained specimen. The viscous softening point marked the initial buildup of thermally induced stresses indicating the rate of contraction had begun to compete with the permissible relaxation rate of the mixture all of which was understood to be partially dependent upon the thermal loading rate (i.e. cooling rate of the test). Since all of the mixtures tested as part of this study were evaluated at the constant cooling rate of 10°C per hour, the observed differences in the modulus, stress, and temperatures at which these occurred were understood to be a function of the mixture properties being evaluated, including the level of oxidation.

The viscous softening modulus values for each mixture were observed at warmer temperatures with increased aging (i.e. increasing CAg). Further examination into the cause of this shift revealed a subtle change in the stress development as a function of temperature. Through the initial stages of testing which occurred at warmer temperatures, the build-up stresses were lower for the lesser aged mixtures. The lesser

aged mixtures were softer and thus had a greater potential for viscous flow or in this case an increased ability to relax the induced stress. As the materials aged, the viscous component was reduced or stiffened, thus rendering the mixture less capable of relaxing the developed thermal stresses. This resulted in greater stress build-up, all of which yielded higher calculated modulus values at the warmer temperatures as a function of aging. While this behavior was noted for both the unmodified and modified binders, it had a less significant effect overall with the modified binder, as noted by the enhanced retention of the viscous characteristics with age.

Fracture Stress

The fracture stress was one of the original parameters reported from the TSRST methodology as was the temperature where the fracture of the test specimen occurred. These two values were the basis for the observed correlations dating back to the SHRP studies (Kanerva et al., 1994).

The TSRST data of the mixtures evaluated in this study showed a reduction in the stress magnitude as well as warmer fracture temperatures as the oxidation level of the mixtures was increased (i.e. CAg increased) with only a couple of exceptions. Of the nearly thirty mixtures evaluated in this study, only the Colorado mixtures with the 9 μm AFT with the unmodified PG 64-22 binder did not follow this trend. Given the limited number of replicates and the substantial time necessary to complete this type of aging evaluation, it should be of little concern that a select few of the mixtures were noted to vary from the otherwise very consistent trend. Overall, the fracture stress was noted to

substantially decrease and the fracture temperature became warmer with increased levels of aging.

Much earlier research reported a very similar behavior pattern as well. Results from traditional TSRST testing have shown that mixtures made with stiffer binders will develop thermally induced stresses more rapidly than softer binders, thus in general were expected to fracture at warmer temperatures (Jung and Vinson, 1994).

Crack Initiation Stress

The crack initiation stress was defined as the stress induced in the restrained specimen at the temperature where the crack initiation modulus was observed. Similar to the crack initiation modulus, the crack initiation stress was observed to consistently decrease with increased levels of oxidation. Contrary to the modulus values, the crack initiation stress was typically not the highest stress observed throughout the UTSST procedure. The fracture stress was nearly always of greater magnitude compared to the crack initiation stress. However, as noted in the previous sections the modulus values provide additional information through combined effect of both the thermally induced stress and the strain measured on the unrestrained specimen.

Therefore, as an overall summary of the collective influence of oxidative aging on the measured UTSST parameters based upon the general overview of the mixtures evaluated in this study, Table 9.1 presents a summary of the observed behavior of the UTSST modulus, temperature, and stress values observed throughout the test duration. The arrows indicate the general influence the oxidative aging will have on a given parameter. For instance, an arrow pointing up for the Fracture row in the Temperature

column indicates that the fracture temperature was observed to increase (i.e. became warmer) with increased levels of aging or oxidation.

Table 9.1 Summary of the Influence of Oxidative Aging on the Thermo-Viscoelastic Properties of Asphalt Mixtures

Thermo-Viscoelastic Property	$E_{(UTSST)}$	Temperature	Stress
Fracture	N/A	⇧	⇩
Crack Initiation	⇩	⇧	⇩
Glassy Hardening	⇩	⇧	⇩
Viscous-Glassy Transition	⇧	⇧	⇧
Viscous Softening	⇧	⇧	⇧

With these general observations, more specific influences of particular mixture characteristics on the UTSST modulus curves will be considered in the following respective sections. Many of the following considerations will focus on the lower temperature measurements (i.e. crack initiation and fracture properties) with general observations of the behavior of the mixtures at warmer temperatures (i.e. the viscous properties of the mixtures). More specific information regarding any particular measurement for a given mixture may be found in the appropriate sections of Appendix O through Appendix Q.

To reiterate, the characteristics being investigated throughout the observed UTSST results were focused around the main factors of the overall experiment as discussed in previous sections. Those main factors are listed below for convenience. However, they

will be discussed in the same order as in previous sections to maintain consistency throughout the analysis.

- Aggregate Factors
    - Qualitative Gradation
    - Aggregate Absorption
    - Aggregate Mineralogy
- Asphalt Binder Factors
    - Unmodified Binder
    - Modified Binder
- Mixture Characteristic Factors
    - Asphalt Binder Content
    - Mixture Density or Air Voids

9.2.2 Mixture Air Void Level

Similar to the previous mixture test evaluations, the mixture air void level was the first characteristic to be considered over the respective aging durations. The investigated mixtures were aged over the four durations at 60°C when compacted to three different air void levels (i.e. 4, 7, and 11%) measured on the cut specimens after aging. The two unmodified binders (i.e. PG 64-22 and WT97-22) were evaluated with the California and WesTrack 1997 aggregates, respectively. Similar to previous consideration, the modified PG 64-28 binder was evaluated with two aggregate sources (i.e. Nevada and Utah). The California mixtures are presented in Figure 9.31, with the short-term aged zero month and the longest aged (i.e. nine month) UTSST curves presented for each of the air void levels. Similarly, the WesTrack materials are presented in Figure 9.32 with the modified

binder presented in Figure 9.33 and Figure 9.34 for the Nevada and Utah aggregates, respectively.

For the sake of clarity, only the mixtures that were short-term aged (i.e. zero month) and the mixtures with the longest aging duration (i.e. nine months) were provided. The complete set of UTSST curves for all the respective aging durations can be found in the referenced Appendix O through Appendix Q. Further, the level of oxidation represented as the change in the measured carbonyl area (CAg) for each respective mixture has also been provided in the figures.

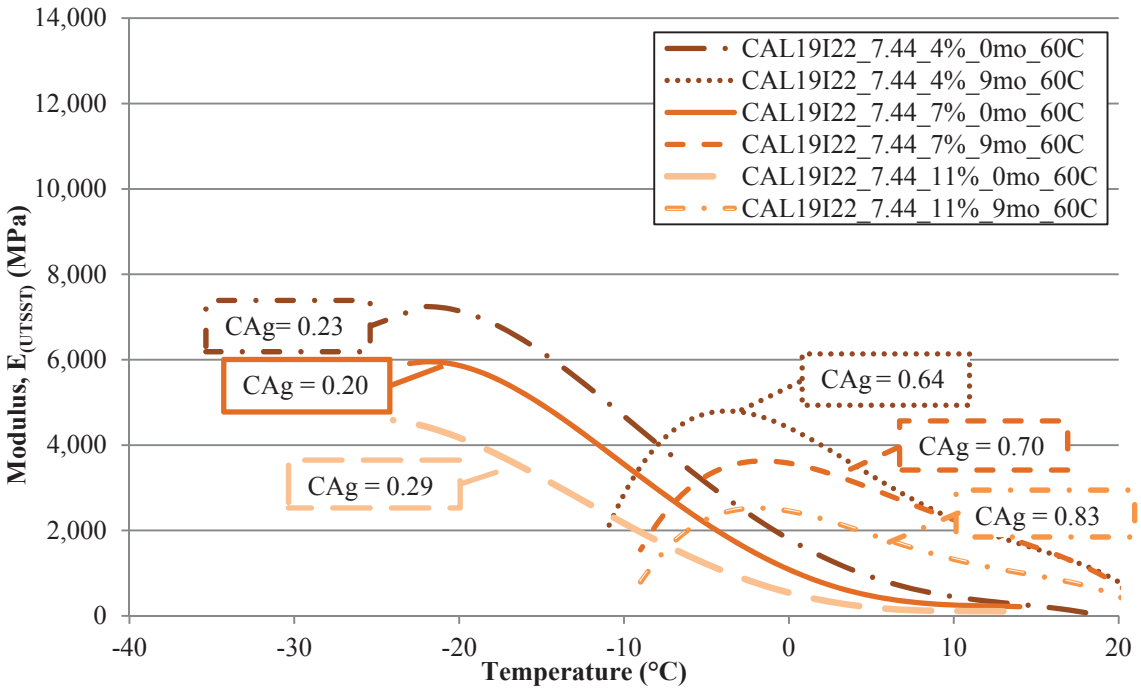

Figure 9.31 Summary of UTSST Modulus Curves for the CAL19I22_7.44 Mixtures Aged at 60°C with Different Air Void Levels

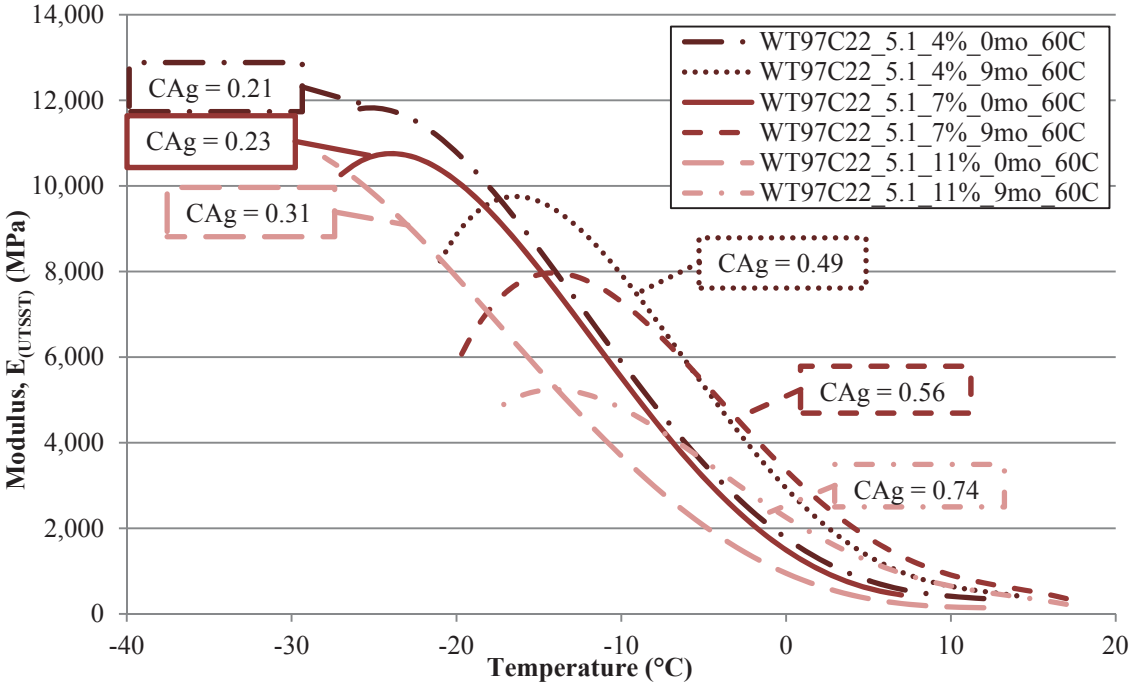

Figure 9.32 Summary of UTSST Modulus Curves for the WT97C22_5.1 Mixtures Aged at 60°C with Different Air Void Levels

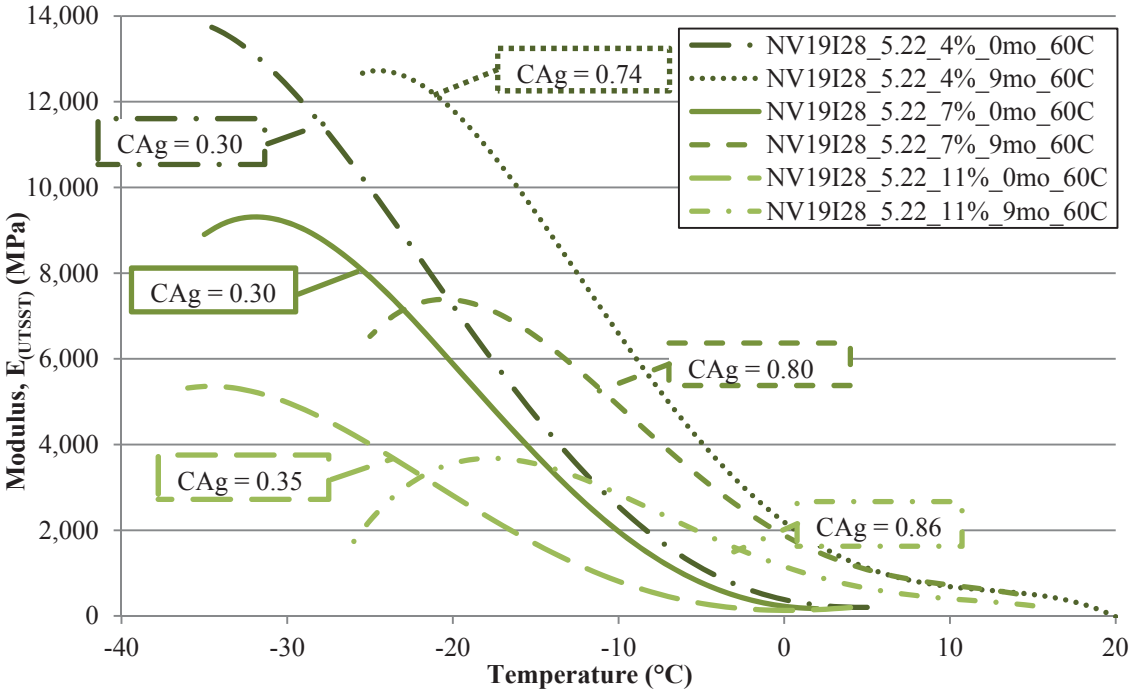

Figure 9.33 Summary of UTSST Modulus Curves for the NV19I28_5.22 Mixtures Aged at 60°C with Different Air Void Levels

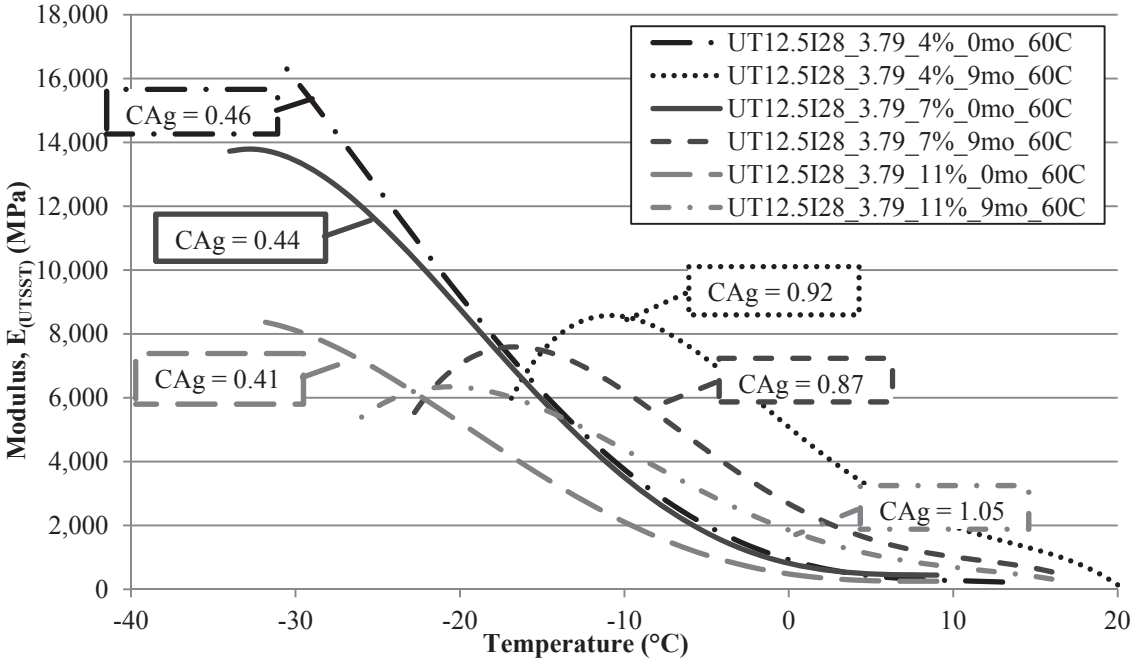

Figure 9.34 Summary of UTSST Modulus Curves for the UT12.5I28_3.79 Mixtures Aged at 60°C with Different Air Void Levels

Regardless of the aggregate source or binder type, it was evident that the oxidation process had a significant influence on the UTSST modulus curve as discussed in the previous section 9.2.1. In addition, the effect of the air void level was also very prevalent within each mixture. In each respective mixture, at each aging level observed in the figures, there was a clear separation with the 4% air void level indicating the highest UTSST modulus values, the 11% air void presenting the lowest measures, with the 7% air void level fell in between. With each of the mixtures, except WesTrack, the short-term aged zero month specimen with 11% air voids exhibited UTSST modulus values less than the 4% air void specimens after aging for nine months at 60°C despite the CAg values being nearly double values of the zero month specimens. After nine months of

aging at 60°C, the distinction between the UTSST modulus values was still substantial within each mixture (i.e. aggregate and binder combination).

The fracture and crack initiation temperatures were not highly influenced by the air void level for the zero month aged specimens, which was expected based upon the CAg measures. This was not overly expected based upon the density of the material, however the difference was noted in the stress and UTSST modulus values. After the nine month aging condition, a more systematic variation in the crack initiation temperatures within each mixture at the different air void levels was observed. In three of the four mixtures (Utah being the exception) the crack initiation temperature of the mixtures increased with increased air void levels. For the three mixtures displaying similar trends the CAg measures also increased in a regular manner with increased air void levels (i.e. the higher air void specimens had higher CAg values after the same aging duration within a given mixture). However, the exception to this pattern of CAg measures were noted in the Utah mixtures which did not follow a consistent pattern, nor did the Utah mixes follow the same pattern for the crack initiation temperature.

In summary, the air void level of the mixtures was found to have a profound influence on the thermal stress induced within the mixtures which led to a substantial decrease in the UTSST modulus at colder temperatures for mixtures with higher air void levels. The effect was not as substantial with the temperature of the thermo-viscoelastic properties. However, three of the four mixtures generally indicated increased crack initiation temperatures as well as increased oxidation measures within the same mixtures with increasing air void levels.

9.2.3 Asphalt Binder Content

Similar to the previous analyses, the influence of the asphalt binder content was conducted by aging mixtures at two asphalt binder contents, the first at 4.5% TWM and the second corresponding to the calculated AFT of 9 μm. This evaluation was conducted on both the unmodified PG 64-22 and the SBS modified PG 64-28 asphalt binders with both the Colorado and Nevada aggregates, all with the intermediate gradation.

Due to the significant number of mixtures to be evaluated in this section, several of the UTSST figures have been separated by the aging durations to improve the clarity of the figures under consideration. For a complete assessment of all the aging durations together for a given mixture, Appendix O through Appendix Q may be referenced. In this manner, Figure 9.35 and Figure 9.36 present the UTSST modulus relationships for the mixture containing the unmodified PG 64-22 asphalt binder. In a similar fashion, Figure 9.37 and Figure 9.38 present the modified PG 64-28 for both the Colorado and Nevada mixtures. All four figures differentiate the zero month and nine month aging durations for each respective set of mixtures. Again, the CAg measures are provided as an additional point of reference.

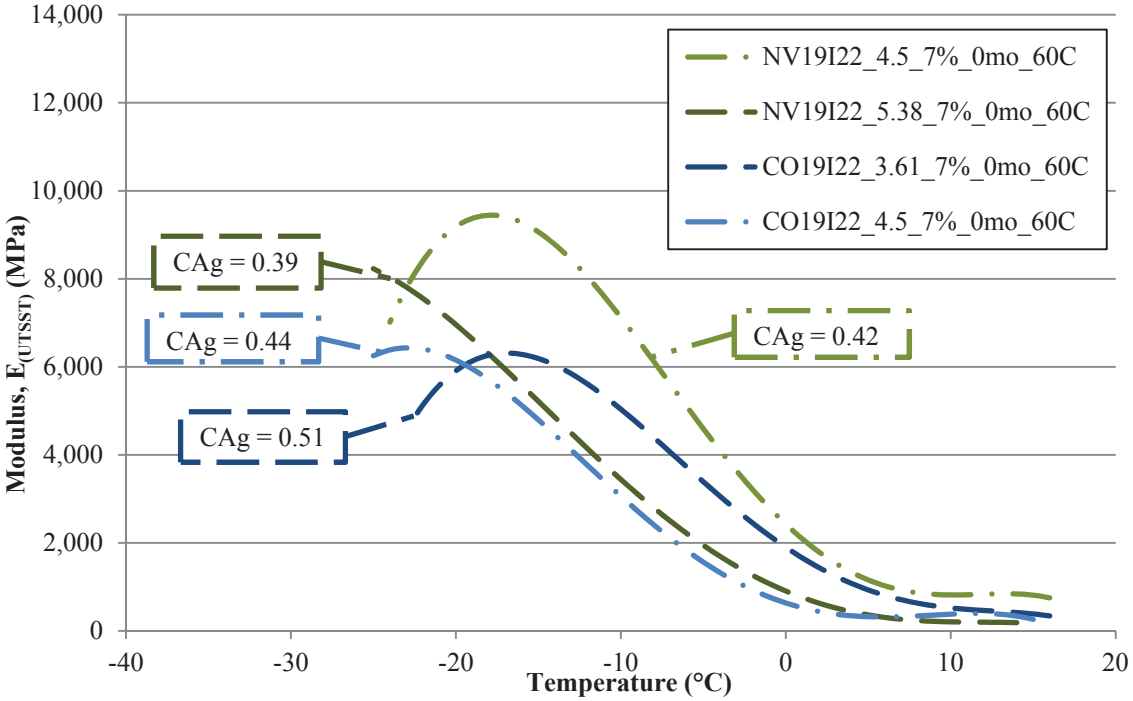

Figure 9.35 Summary of UTSST Modulus Curves for the PG 64-22 Mixtures with Different Binder Contents Aged for 0 Months

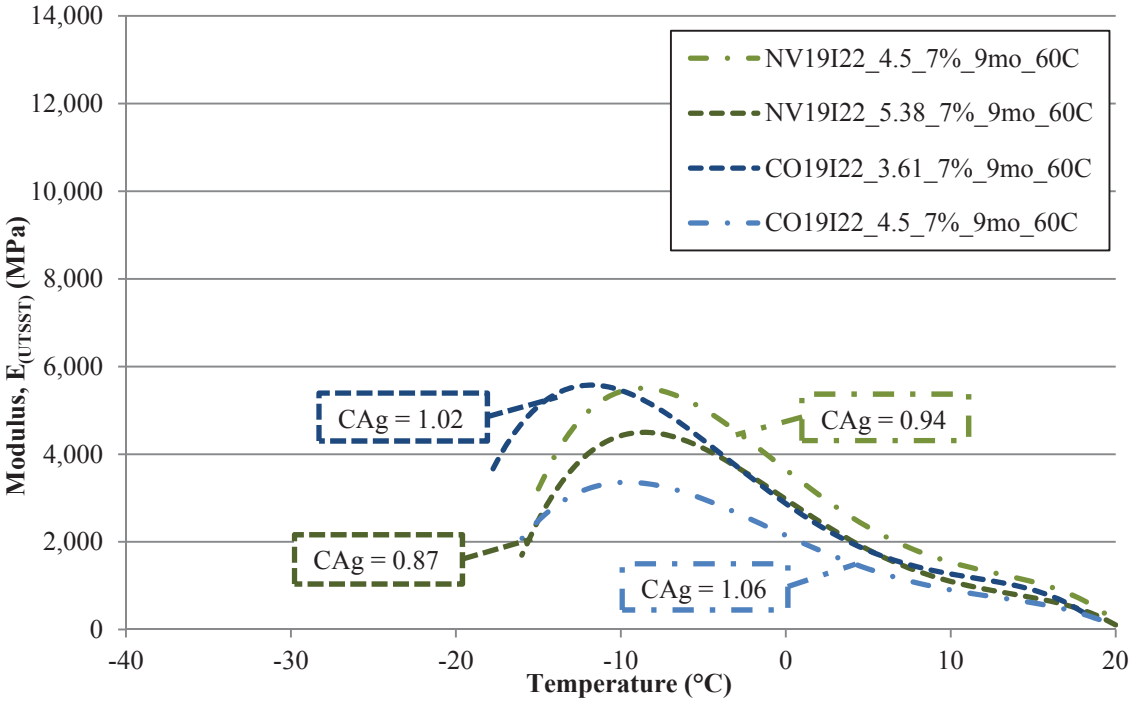

Figure 9.36 Summary of UTSST Modulus Curves for the PG 64-22 Mixtures with Different Binder Contents Aged at 60°C for 9 Months

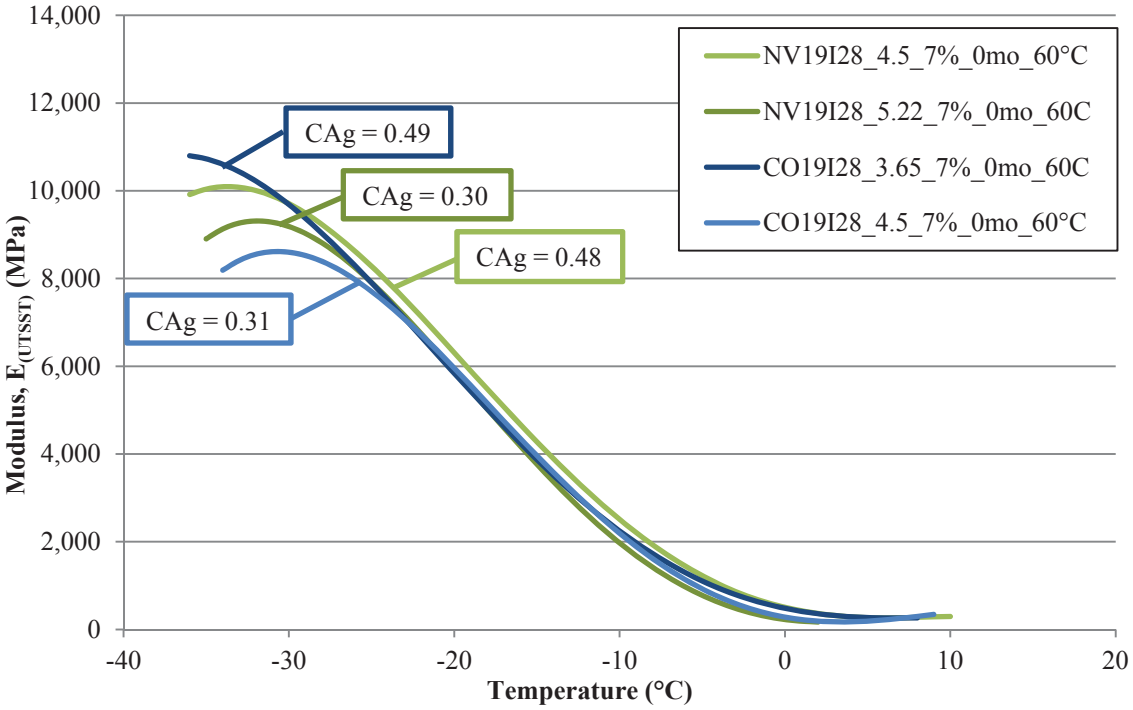

Figure 9.37 Summary of UTSST Modulus Curves for the PG 64-28 Mixtures with Different Binder Contents Aged for 0 Months

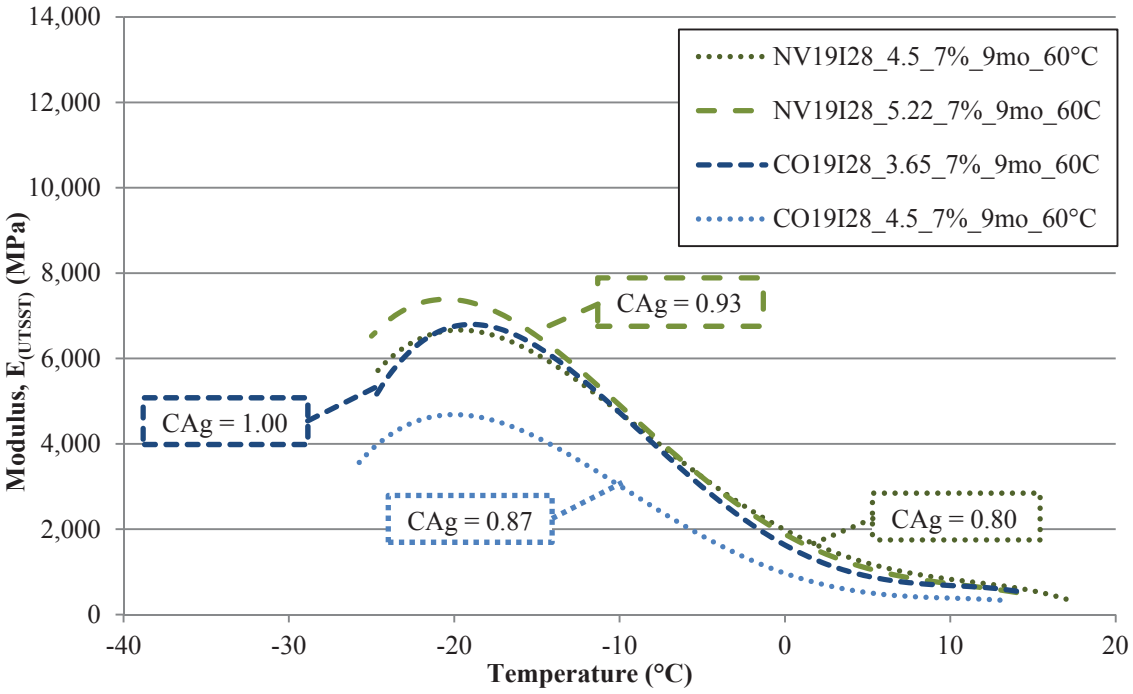

Figure 9.38 Summary of UTSST Modulus Curves for the PG 64-28 Mixtures with Different Binder Contents Aged at 60°C for 9 Months

Initial considerations based upon the zero month aged mixtures for both asphalt binders presented in Figure 9.35 and Figure 9.37 showed fairly different behaviors relative to one another. The mixtures containing the unmodified PG 64-22 binder generally exhibited better low-temperature properties with increased binder content for a given aggregate source. This was most notably indicated by the lower crack initiation and fracture temperatures for the mixtures with higher asphalt binder contents. The crack initiation modulus values were primarily dependent upon the aggregate source rather than the binder content.

The zero month aged mixtures for both aggregates with the modified PG 64-28 binder did not show the same overall trend. In these mixtures, the lower the binder content exhibited the higher observed crack initiation modulus values. However, the Colorado mixture exhibited the highest and the lowest crack initiation modulus values, with the Nevada mixtures falling in between. Despite the lack of systematic order in the crack initiation and fracture stages, the UTSST relationships of the mixtures containing the PG 64-28 binder were substantially more consistent from the initial 20°C starting temperature down though the viscous-glassy transition, regardless of binder content or aggregate source.

Consideration of the same mixtures after aging for nine months at 60°C (i.e. Figure 9.36 and Figure 9.38) indicate nearly the reverse for the relative trends as compared to the zero month aged specimens. At the nine month aging condition, the Colorado mixtures containing the PG 64-22 binder presented the highest and lowest crack initiation modulus values, with the lower binder content yielding the higher value even though the CAg measures were fairly close to one another. The Nevada mixtures with the PG 64-22

binder generally supported this finding with the lower binder content mixture presenting the higher crack initiation modulus of the two. Both UTSST modulus relationships for the Nevada mixtures were generally between the two Colorado mixtures despite a CAg range of almost 0.2 between all four mixtures. The crack initiation temperatures of the mixtures were relatively similar, with the Nevada mixtures indicating a slightly warmer temperature.

Observations of the mixtures containing the modified PG 64-28 binder and both the Colorado and Nevada aggregates after aging for nine months at 60°C (i.e. Figure 9.38) present very similar crack initiation and fracture temperatures, to a greater degree than the zero month aged mixtures with the modified binder. The crack initiation modulus values of the Nevada mixtures were generally higher than those of the Colorado mixtures. Although the Nevada mixture with 4.5% TWM binder and the Colorado with 3.65% TWM presented nearly identical UTSST modulus curves. The Nevada mixture with the higher total binder content exhibited a slightly higher UTSST modulus curve after the viscous-glassy transition stage. In contrast, the Colorado mixture with the lower binder content presented the higher UTSST modulus curve throughout the calculated temperature range, within the same aggregate source.

As an interim summary with respect to the asphalt binder content, the mixtures containing the higher binder content of PG 64-22 initially presented higher UTSST modulus values at the zero month aging condition. After nine months of aging at 60°C nearly the opposite trend was observed. Thereby indicating that the mixtures containing the higher binder content resulted in the largest shift in the UTSST modulus relationships after a given oxidation exposure level. This finding can logically be explained by

recognizing the mixture component most influenced by oxidation to be the asphalt binder, thus the greater the proportion of the mix the binder composes, the more significant its contribution to the overall aging behavior of the mixture. In other words, the portion of the mixture most susceptible to oxidation is the binder, thus the more binder there is in the mixture, the more susceptible the mixture will be to oxidative aging.

In contrast, the same overall trend based upon the asphalt binder content was not observed with the mixtures containing the modified PG 64-28 binder. The overall trend was much less consistent than the mixtures with the unmodified binder, but appeared to be more based upon the aggregate rather than the binder content with the Colorado mixtures exhibiting a slightly greater shift due to the nine month oxidation duration.

Further consideration of the influence of the binder content on the UTSST modulus relationships was undertaken by evaluating the different binder contents relative to the respective binder grades within each aggregate source. Again the zero and nine month aged specimens were considered separately. As such, the Colorado mixtures are presented in Figure 9.39 and Figure 9.40, while the Nevada mixtures are presented in Figure 9.41 and Figure 9.42 for the zero and nine month aging durations, respectively.

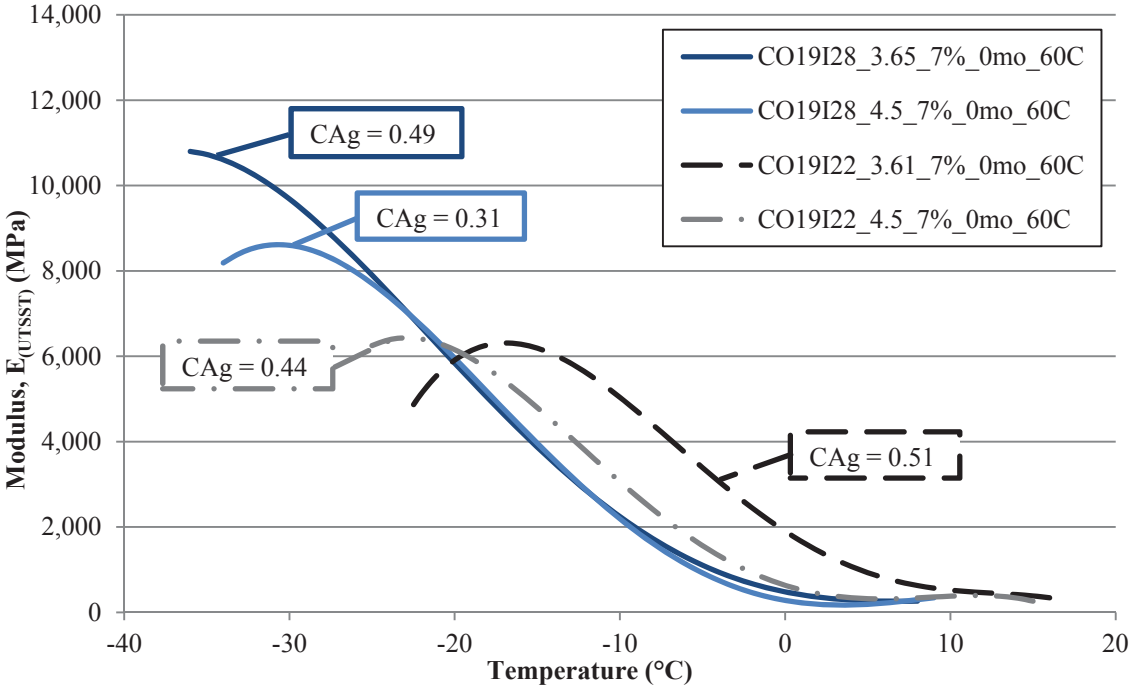

Figure 9.39 Summary of UTSST Modulus Curves for the Colorado Mixtures with Different Binder Contents Aged for 0 Months

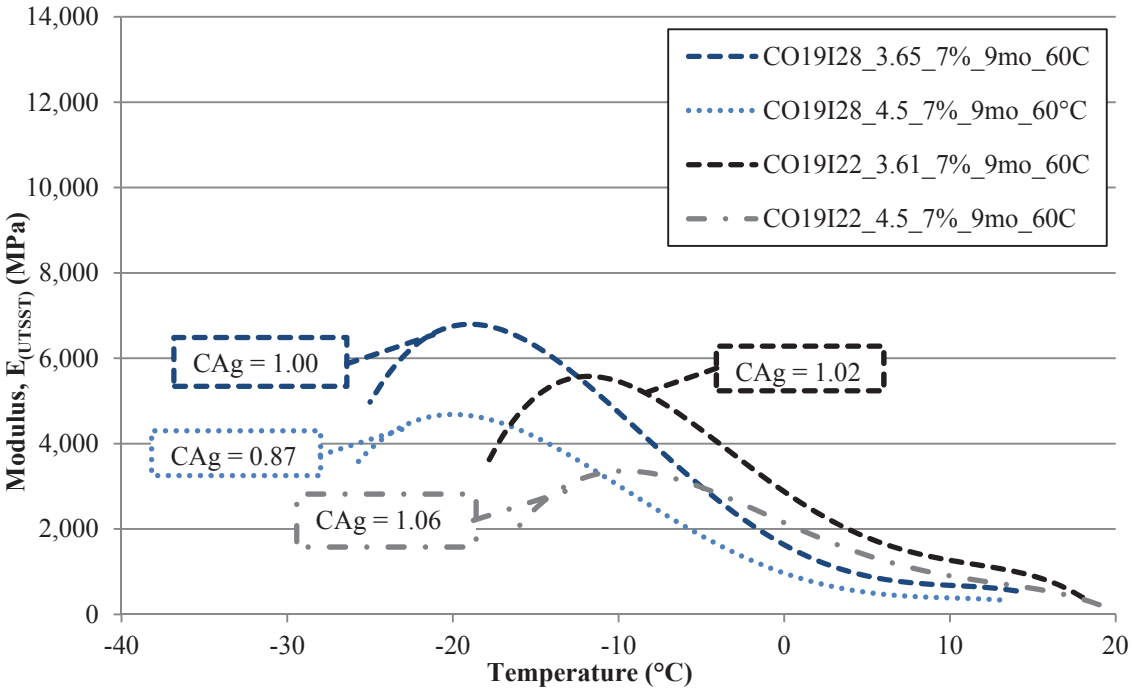

Figure 9.40 Summary of UTSST Modulus Curves for the Colorado Mixtures with Different Binder Contents Aged at 60°C for 9 Months

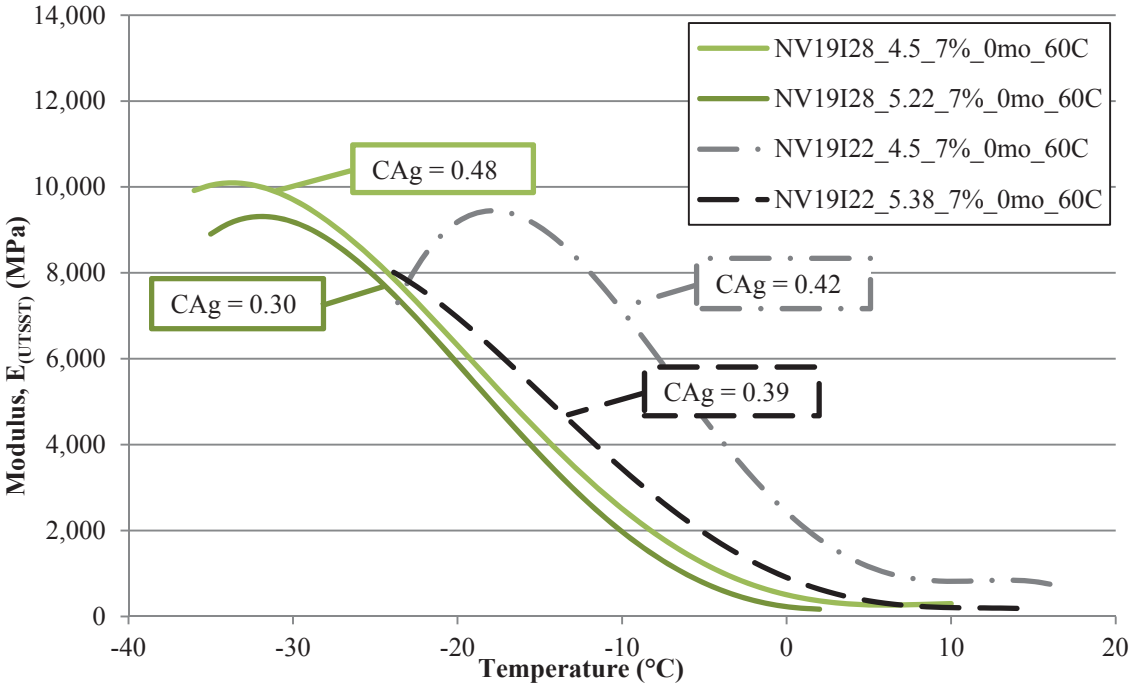

Figure 9.41 Summary of UTSST Modulus Curves for the Nevada Mixtures with Different Binder Contents Aged for 0 Months

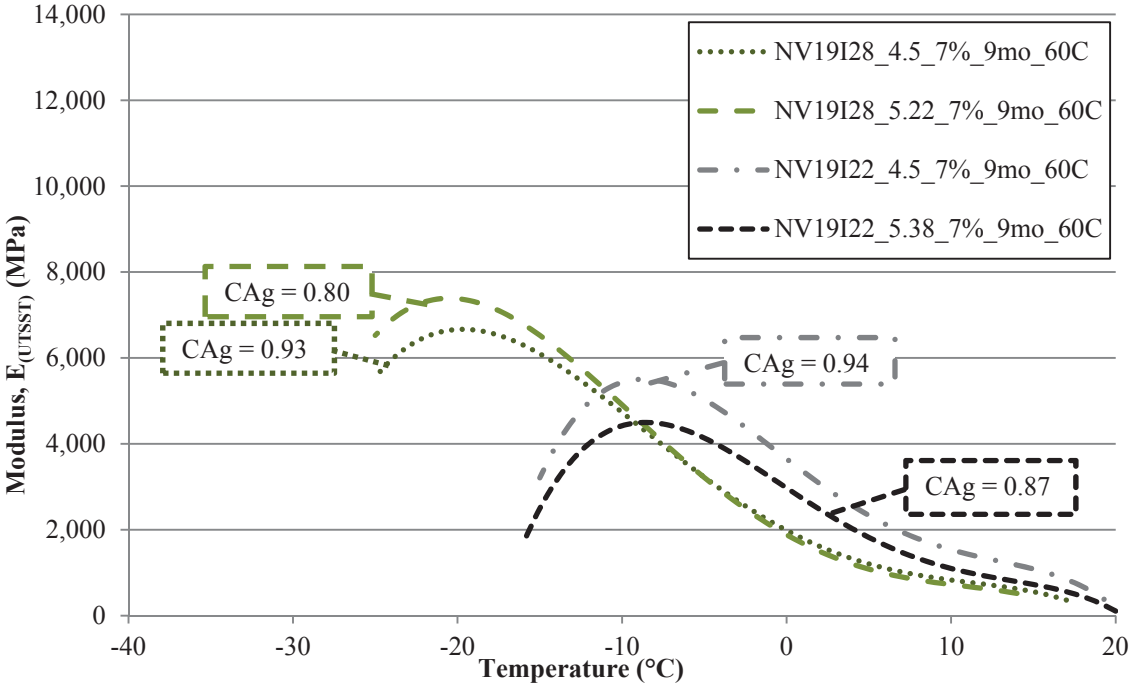

Figure 9.42 Summary of UTSST Modulus Curves for the Nevada Mixtures with Different Binder Contents Aged at 60°C for 9 Months

Initial considerations of the zero month aged specimens from Colorado indicated a clear distinction of the UTSST modulus curves between the two binders, as would be expected. The mixtures containing the unmodified PG 64-22 binder initially exhibited higher UTSST modulus relationships, but rapidly dropped below the modified mixtures at temperatures below -20°C or so. The crack initiation modulus values for the two unmodified mixtures were fairly similar, although they were of much lower magnitude than the modified mixtures.

After the nine month aging duration the UTSST modulus values were much closer to one another, however the modified mixtures were noted to have crack initiation and fracture temperatures well below those of the unmodified PG 64-22 mixtures with the Colorado aggregates. Further, the mixtures with the higher binder contents (i.e. 4.5% TWM) exhibited lower UTSST modulus values relative to the 9 μm AFT companion mixtures, again all with the Colorado aggregate source.

The UTSST modulus relationships with the Nevada aggregates also presented a difference in the two asphalt binder grades, but the distinction was not as clear as with the Colorado aggregates. The mixtures containing the modified PG 64-28 binders still yielded the highest crack initiation modulus and lowest temperatures at the crack initiation and fracture stages. However, the Nevada mixture with the 9 μm AFT binder content (i.e. 5.38% TWM) presented a similar overall UTSST modulus curve, but fractured well before (i.e. at warmer temperatures) the modified mixtures. Despite the different crack initiation temperatures with the NV19I22_4.5_7%_0mo_60C mixture, the mixtures were consistently ranked with the mixtures containing the 4.5% TWM binder

content exhibiting higher UTSST modulus curves compared to the 9 μm AFT mixture, within the same binder grade.

After the nine month aging duration with the Nevada aggregates, the ranking of the UTSST modulus relationships based on the binder content were not consistent. For the mixtures containing the modified PG 64-28 binder, the 9 μm AFT mixture exhibited the highest crack initiation modulus. But for the Nevada mixtures with the unmodified binder, the 4.5% TWM mixture presented the higher magnitude UTSST modulus curve. The clear distinction between the two binder grades was still maintained with the crack initiation modulus, but even more so with the crack initiation and fracture temperatures.

With both aggregate sources and over both aging conditions noted in these figures, the mixtures containing the modified PG 64-28 binder maintained lower UTSST modulus values at the warmer temperatures in the viscous regions of the relationship. At the colder temperatures, transitioning through the viscous-glassy transition and into the crack initiation and subsequently micro damage stages of the evaluation, the modified materials often resulted in higher modulus values as the result of less substantial damage. This is further evidenced by the glassy hardening and crack initiation temperatures of the mixtures containing the unmodified PG 64-22 occurring at substantially warmer temperatures compared to the modified mixtures.

Further evaluation of the influence of the aggregate on the UTSST modulus relationships are provided in Figure 9.43 and Figure 9.44 which present the mixtures containing the 4.5% TWM asphalt binder content separated by the aggregate source of the mixtures.

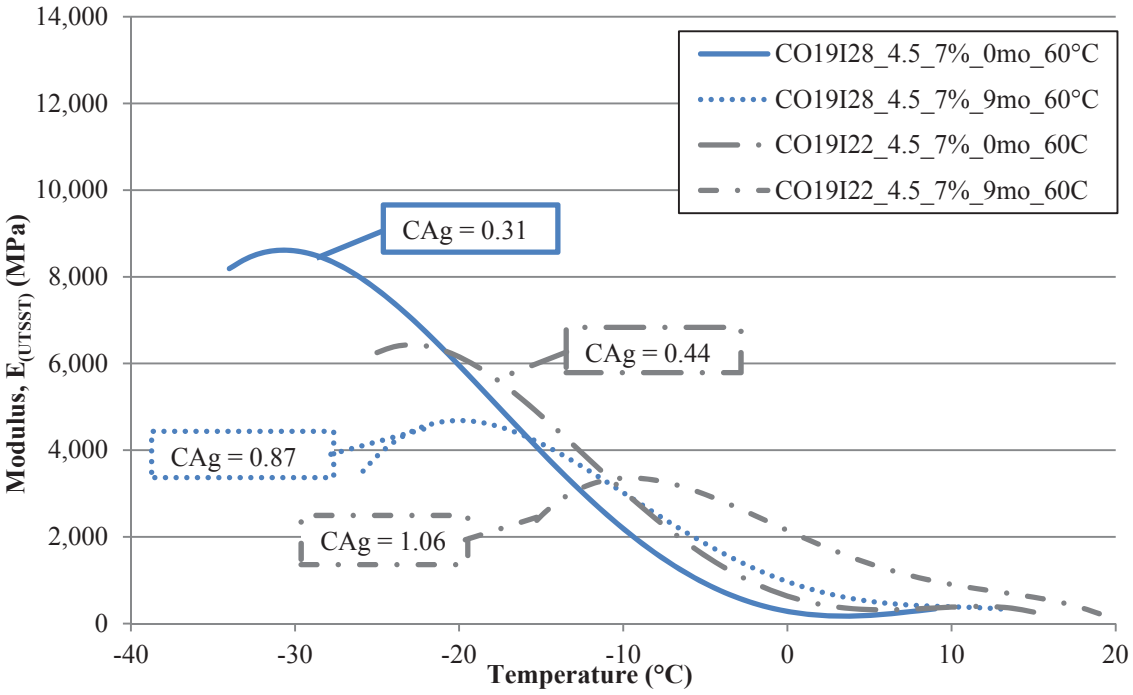

Figure 9.43 Summary of UTSST Modulus Curves for the Colorado Mixtures with 4.5% Binder Aged at 60°C

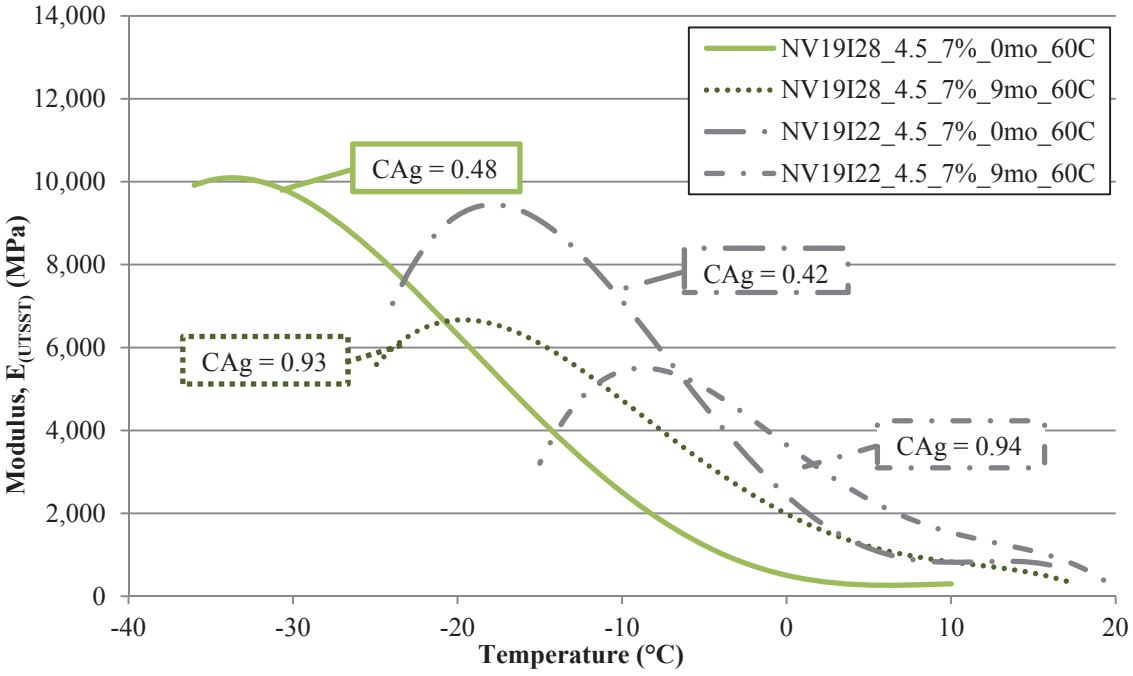

Figure 9.44 Summary of UTSST Modulus Curves for the Nevada Mixtures with 4.5% Binder Aged at 60°C

Observations of the Colorado mixtures in Figure 9.43 exemplify the previously noted changes in the UTSST modulus values between the two binder grades. With almost exactly a 6°C difference in the low temperature grade between the two binders based upon the true grade temperature provided in Table 4.18, the mixtures would be expected to indicate a similar temperature differential in the fracture and physical measurements of the mixtures according to traditional expectations. At the zero month aging duration, the fracture temperature of the Colorado mixtures differed by 8°C. The difference increased to almost 9°C after the nine month aging duration. The measurements of the Nevada mixtures at the zero month condition increased to 10.5°C and 10.7°C after the nine month aging duration as indicated in Figure 9.44. Similar comparisons based upon the crack initiation temperature indicated that the Colorado mixtures varied from almost 8 to more than 10°C with the zero and nine month aged specimens, respectively. The Nevada mixtures exhibited a differential of nearly 15°C at zero months and close to 11°C after the nine month aging duration at 60°C.

Recalling that these mixtures were produced with the same asphalt binders which only differed in their low temperature grade by 6.1°C. The changes in the temperature ranges of the mixtures varied by as little as a couple of degrees to as high as 15°C which was considered a substantial influence solely due to the aggregate and mixture properties. In certain instances (i.e. the Colorado mixtures) the binder grading may prove sufficient, or relatively close to the mixture temperatures. However, the actual modulus values, strain values leading to the coefficient of thermal contraction, and the stress levels remain undetermined with the binder grading alone. Moreover, in other instances such as with the Nevada mixtures, the binder grade did not adequately characterize the low

temperature properties of the mixtures. Therefore, the substantial influences in the mixture behavior clearly indicated the necessity for mixture testing of low temperature properties in order to reliably differentiate the actual behavior expected of the mixtures.

The analysis of the mixtures with specific binder contents and the influence of the aggregate on the UTSST modulus relationships are presented in Figure 9.45 and Figure 9.46, which contain the mixtures with the 4.5% TWM asphalt binder content separated by the binder type. Each of these respective figures were prepared with a single asphalt binder and only the aggregate source and associated gradation has been changed, within each figure. The binder content for each mixture was held constant at 4.5% TWM, which was not necessarily at the optimum binder content for either mixture.

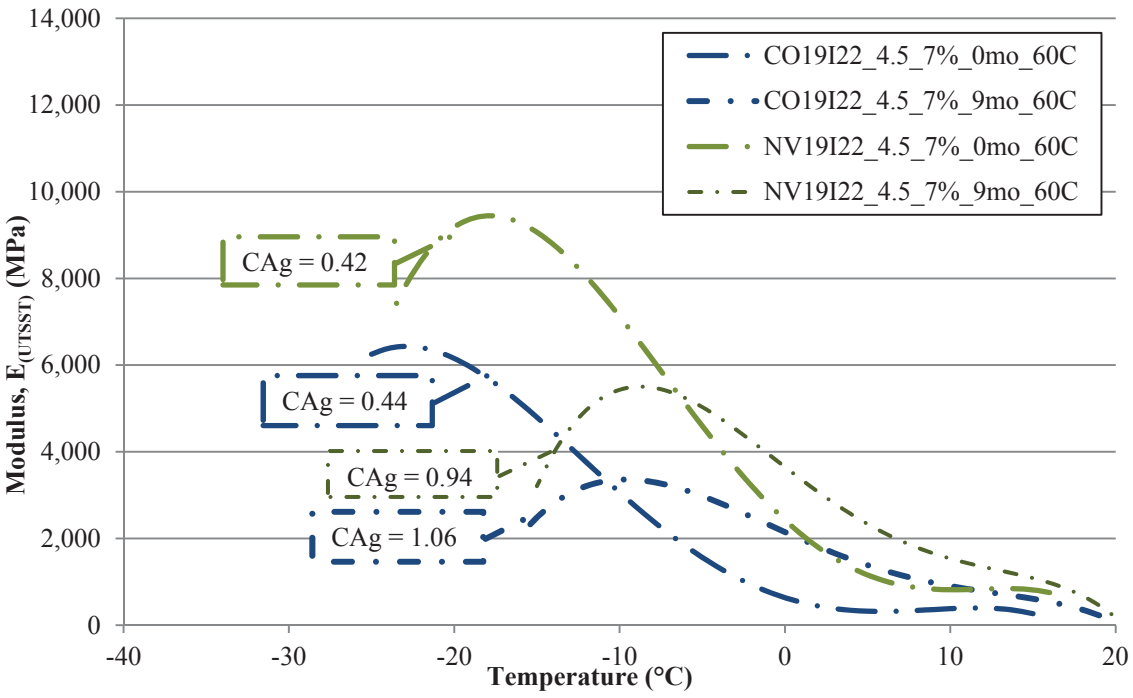

Figure 9.45 Summary of UTSST Modulus Curves for the Mixtures with 4.5% PG 64-22 Binder Aged at 60°C

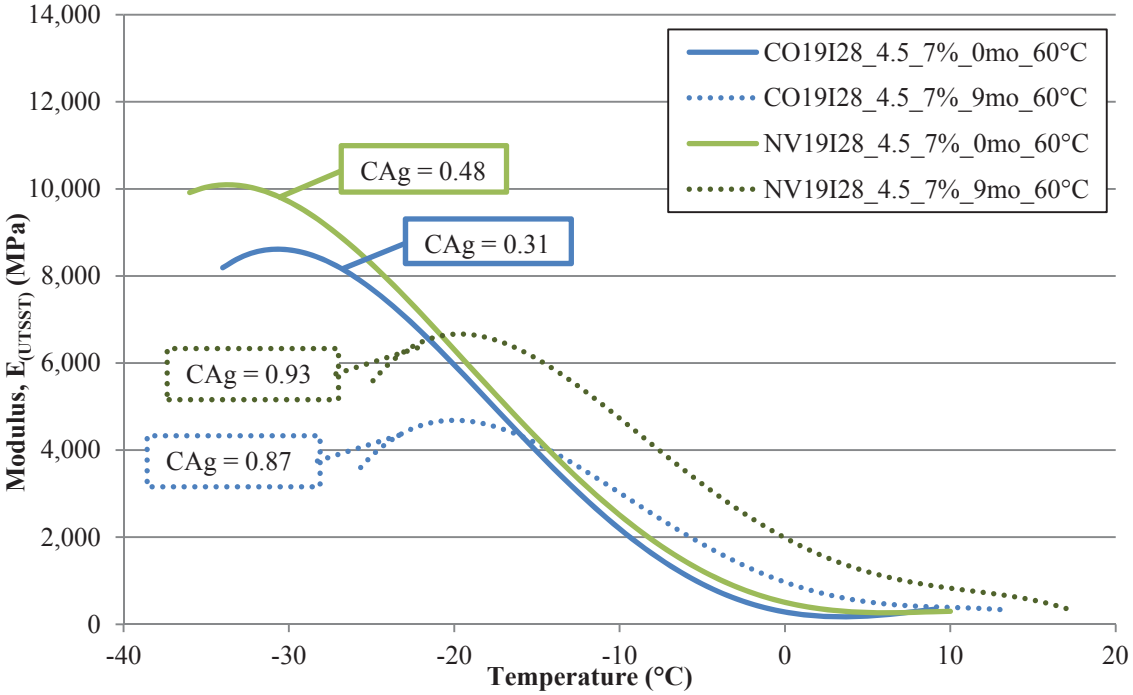

Figure 9.46 Summary of UTSST Modulus Curves for the Mixtures with 4.5% PG 64-28 Binder Aged at 60°C

With the binder content held to a constant 4.5% TWM, the influence of the aggregate properties and their influence were readily observed. Considering the mixtures with the unmodified PG 64-22 binder in Figure 9.45, it was noted that the temperatures of many of the thermo-viscoelastic properties occurred as fairly similar ranges within the same aging level of the mixtures. It appeared that the Nevada mixtures may have slightly warmer temperatures for nearly all the UTSST parameters, which was confirmed for nearly all the measures summarized in the referencing Appendix P.

These observations were accompanied by the distinct differences noted in the UTSST modulus values between the two mixtures containing the unmodified binder. The Nevada mixture exhibited substantially higher UTSST modulus values as compared to the Colorado mixture. This finding was accompanied by the higher water absorption

rates for the Nevada mixtures (i.e. 2.7 compared to 0.9), which led to a reduced effective binder content *Pbe* (i.e. 3.3 compared to 4.0), and finally resulted in an lower AFT (i.e. 7.0 compared to 11.7) for the Nevada mixture. This suggested that *Pbe* and or AFT may provide a significant influence on the thermal cracking behavior of asphalt mixtures. This observation was in general agreement with the commonly held view that increasing the asphalt binder content should improve the thermal cracking resistance of a given mixture, only these results indicate that the effective binder content should be the controlling factor not necessarily the total asphalt binder content. In this particular instance, improved thermal cracking performance was indicated by reduced UTSST modulus values, which indicated lower thermally induced stresses that coincided with the lower thermo-viscoelastic temperatures with the increase in *Pbe* and/or AFT.

These general findings were also somewhat supported by the mixture results presented in Figure 9.46 with the SBS modified PG 64-28 asphalt binder. These mixtures were noted to have similar physical properties with the same increased water absorption rates for the Nevada mixtures (i.e. 2.7 compared to 0.9), which led to a reduced effective binder content *Pbe* (i.e. 3.4 compared to 3.9), and finally resulted in an lower AFT (i.e. 7.4 compared to 11.6) for the Nevada mixture. However, with the modified binder in the zero month aging condition the Nevada mixture exhibited colder lower thermo-viscoelastic temperatures. After the nine month aging duration at 60°C, the Colorado mixture presents the cooler temperatures though by a slim margin, similar to the unmodified binders.

Further observations indicated that these relative comparisons were also coincided by higher changes in the oxidation level (i.e. CAg) with the Colorado mixture. For the

unmodified binder the Colorado mixtures presented a measured increase in CAg of 0.62 compared to 0.52 for Nevada. By similar comparison with the modified PG 64-28 binder, the Colorado mixtures indicated CAg change of 0.56 compared to 0.45 for Nevada after the nine month aging duration at 60°C.

Therefore as an overall summary, the asphalt binder has been shown to influence the UTSST modulus measures as well as the thermo-viscoelastic temperatures of asphalt mixtures. The binder content, specifically *Pbe* was found to be influential as it was also found significant in the oxidation evaluations of section 7.2. However, there were some potential influences attributable to the interaction of the aggregate with the binder, particularly with the rate of oxidation of the mixtures.

9.2.4 Qualitative Gradation

The qualitative gradation evaluation was conducted by adjusting the intermediate gradations to provide a finer overall gradation utilizing the same aggregate components. Each of the stockpiles were included in both the intermediate and fine gradations to keep the mineralogy the same, though possibly with different proportions. These evaluations were conducted with the unmodified PG 64-22 asphalt binder and the California aggregates as well as the modified PG 64-28 binder with the Nevada and Utah aggregate sources. The WesTrack mixtures were intended to provide additional comparisons between the relative gradation levels. However, both the asphalt binders and the aggregate sources were different between the two construction dates, and thus this comparison was considered invalid and has not been included here.

Comparisons of the California mixtures with the PG 64-22 binder compacted to the 7% air void level are presented in Figure 9.47.

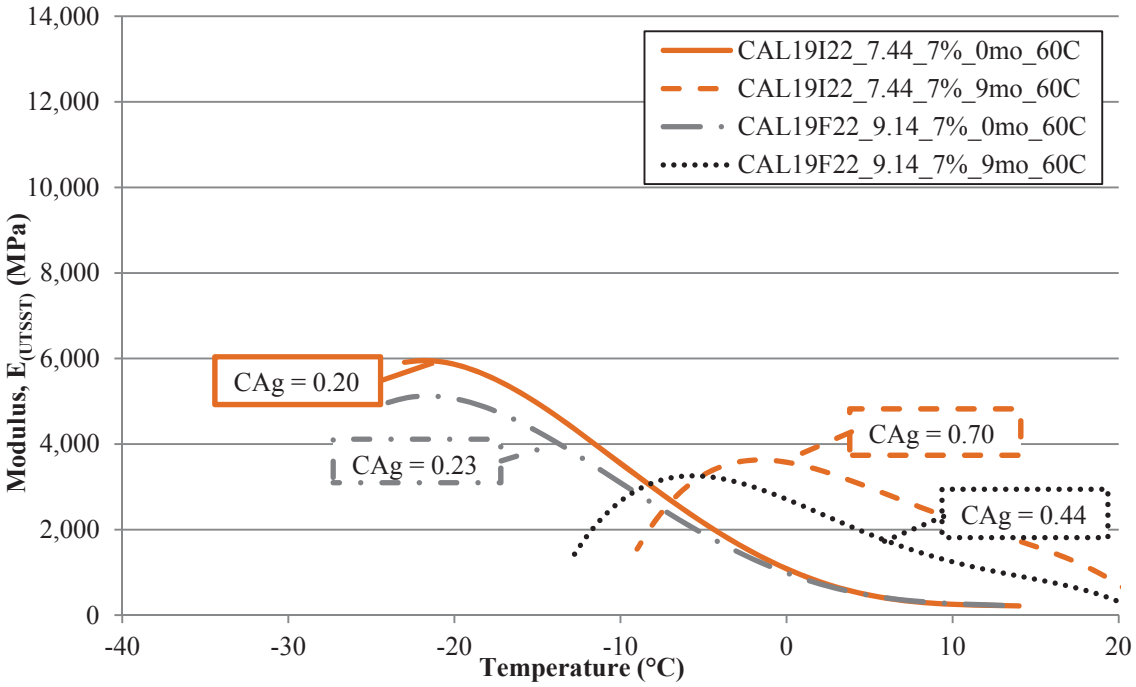

Figure 9.47 Summary of UTSST Modulus Curves for the PG64-22 and California Mixtures with Different Qualitative Gradations Aged at 60°C

Despite an increase of 1.7% in the total asphalt binder content corresponding to an increase of nearly 1.1% in the effective asphalt binder content (*Pbe*), the measured UTSST modulus relationship values exhibited only a moderate change with the substantial change in the gradation with the California aggregates and the PG 64-22 asphalt binder as depicted in Figure 9.47. The UTSST curve developed at the zero month aging condition was slightly lower with the fine gradation as compared to the intermediate. But after nine months in the 60°C oven they were fairly similar in terms of

the crack initiation modulus. However, the thermo-viscoelastic temperatures exhibited substantial differences with the fine mixture presenting clearly colder temperatures. This suggests that the fine gradation may have retained a considerable portion of the viscous properties, which was also supported by the significantly reduced change in the CAg measure of the fine gradation. This finding further supported the asphalt binder content evaluation conducted in section 9.2.3, which suggested increases in *Pbe* may exhibit potential benefits to the low temperature properties of asphalt mixtures.

Additional considerations of the qualitative aggregate gradations are presented in Figure 9.48 and Figure 9.49 for the PG 64-28 binder and the Nevada and Utah aggregates, respectively.

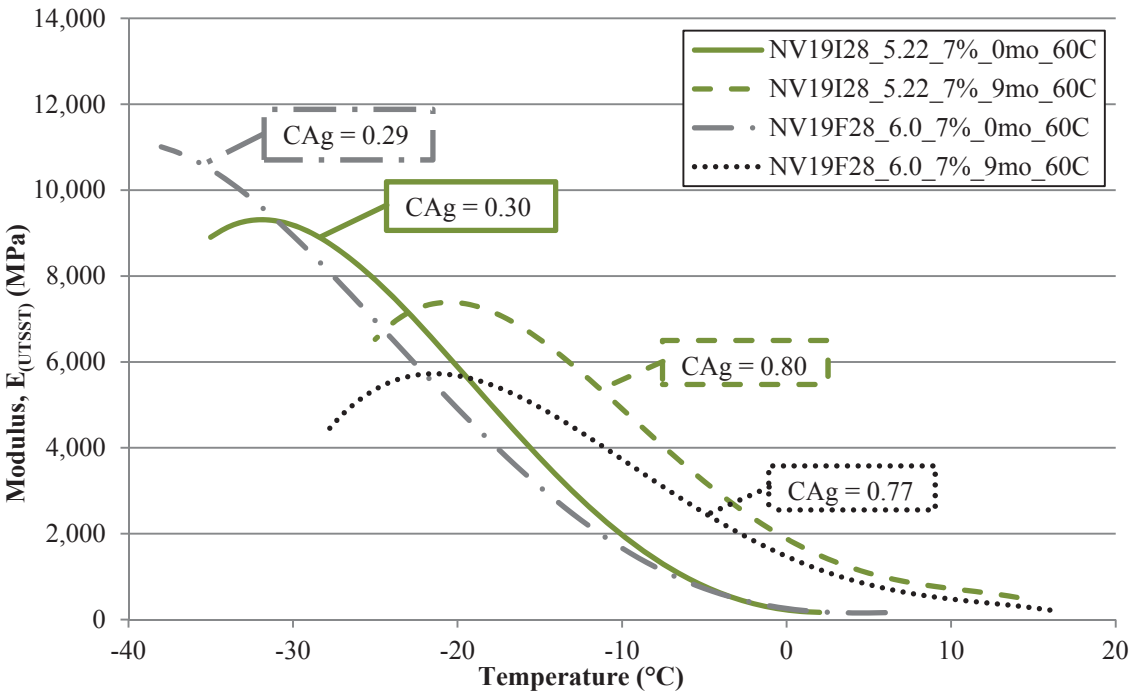

Figure 9.48 Summary of UTSST Modulus Curves for the PG 64-28 and Nevada Mixtures with Different Qualitative Gradations Aged at 60°C

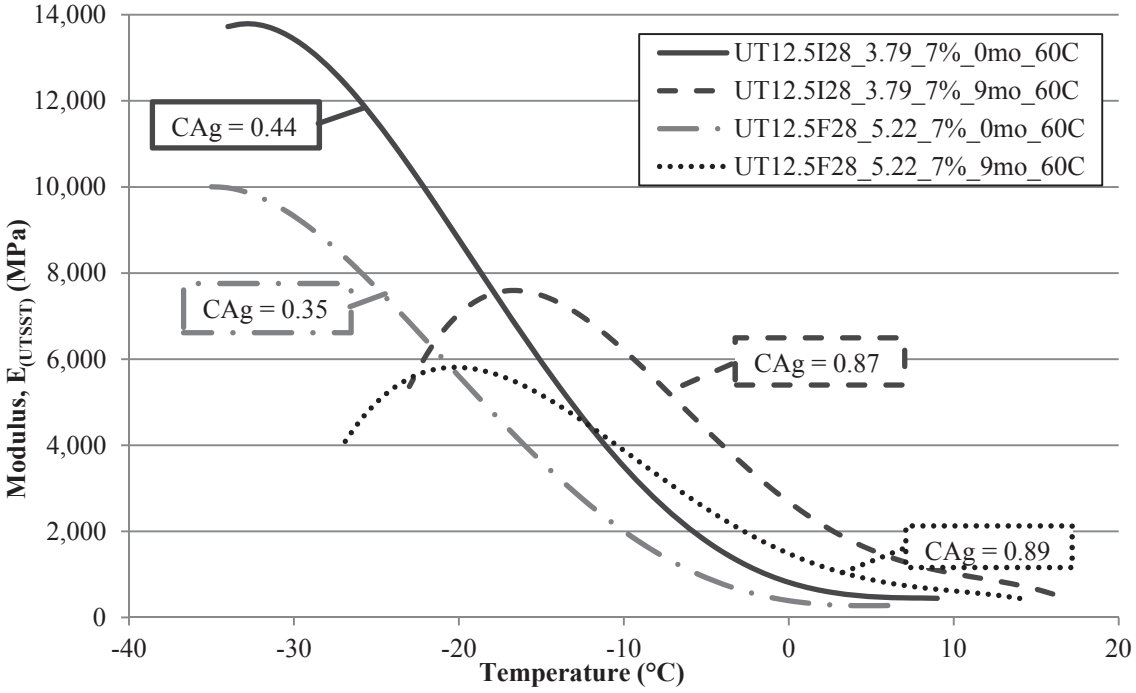

Figure 9.49 Summary of UTSST Modulus Curves for the PG 64-28 and Utah Mixtures with Different Qualitative Gradations Aged at 60°C

Figure 9.48 indicated substantially different UTSST behavior compared to the California PG 64-22 mixtures. The zero month aged specimens for the intermediate gradation presented a higher UTSST curve compared to the fine until approximately the glassy hardening region was reached. At that point, the increase in the total asphalt binder content of 0.78% (0.82% *Pbe*) evidently provided the fine mixture with improved low temperatures properties. Specifically, the improvements of the fine gradation were observed as increased crack initiation modulus and fracture stress noted at colder temperatures. These properties were not as influenced by the induced damage at the lower temperatures with the fine gradation and increased binder content, thus the stress

and modulus values remained at higher values and the fracture was delayed to colder temperatures.

After the nine month aging period at 60°C, the order of the crack initiation modulus and fracture stress levels were reversed, as the intermediate gradation maintained the higher values. However, the fine gradation still maintained the lower temperatures at the colder thermo-viscoelastic stages. This continues to support the influence of the binder content on the influence of oxidation on the thermal properties of the asphalt mixtures.

Initial observations of the Utah mixtures with the PG 64-28 binder presented in Figure 9.49 indicated nearly the same ranking of the UTSST modulus curves as the California and PG 64-22 mixtures. The UTSST modulus curves of the intermediate mixtures were substantially higher than the fine mixtures at both of the aging conditions considered in the figure, despite the larger increase in the CAg measures with the fine gradation. However, the fine gradation still maintained lower temperatures at the colder thermo-viscoelastic stages likely the result of the total binder content for the fine gradation being 1.43% higher than the intermediate gradation, which corresponded to an increase of 1.15% Pbe.

In summary, the findings of the qualitative gradation evaluation were somewhat inconsistent. The California and Utah mixtures presented nearly the same overall behavior, despite large changes in the asphalt binder contents in each mixture and the two utilizing different binder grades. The Nevada mixtures with the PG 64-28 binder exhibited a relatively higher influence of the oxidation level with the fine gradation and higher asphalt binder content.

Therefore, logical process would strive to definitively explain why the responses were different and to identify what may be the underlying cause of these different behaviors. Recalling that the aggregate mineralogy discussion in the prior section 9.1.3 the interaction of the silica with the asphalt binder will be explored. As mentioned previously, an elemental analysis of the different aggregate sources has not been determined. Therefore, the stockpile percentage of the Wadsworth sand will be utilized as a surrogate for the total silica content of each aggregate gradation as it was determined to be a substantial source of silica. However, the California mixture did not contain the Wadsworth stockpile, but it was noted to contain a wide range of different mineralogies some of which contain quartz (i.e. SiO_2). However, this abbreviated analysis will, by necessity neglect the California mixtures until the silica content can be approximated.

Therefore, the stockpile percentages of the Wadsworth sand were assumed to represent the silica content of the Nevada and Utah aggregates. Numerically, the Wadsworth sand was determined to contain approximately 50% silica. Thus, in this simplified manner, the silica content was assumed numerically equivalent to half of the Wadsworth content. In this manner, the Wadsworth stockpile percentages for the intermediate and fine gradations for the Nevada aggregates were 20 and 24%, respectively. Thereby, indicating the silica content for the Nevada aggregates were 10 and 12%, respectively. Similarly, the Wadsworth stockpile percentages for the intermediate and fine gradations for the Utah aggregates were 22 and 35%, respectively. Thus, the silica content for the intermediate and fine gradations for the Utah aggregates were 11 and 17.5%, respectively. In this context, a relatively small difference in the silica content (i.e. 2% for Nevada) produced fairly similar changes in the UTSST

modulus values for a given aging condition. Conversely, a substantial increase in the silica content (i.e. 6.5% for the Utah aggregates) resulted in a measurable but systematic deviation in the UTSST modulus values over the same aging duration. If this were the case, it would correspond to the increased adhesion of the binder to the aggregate, thereby reducing the relative quantity of polar fractions of the asphalt binder available to increase the stiffness and presumably brittleness of the binder and correspondingly the mixture as a whole.

By no means, should two mixtures be sufficient to validate this potential explanation. However, these results merely suggest that additional studies in this area may be warranted. Unfortunately, the additional data was not available to further examine these findings, but the potential for these influences still should be considered as potential explanations to enhance the more thorough understanding of the complex relationships and interactions taking place with asphalt mixtures.

9.2.5 Constant Film Thickness

Additional evaluations of the aggregate influence on the UTSST modulus relationships were conducted by consideration of the mixtures produced with the asphalt binder content specific to each mixture corresponding to a 9 μm apparent film thickness (AFT). In these considerations, each of the mixtures were compacted to the 7% air void level of the cut specimens with each mixture aged in a forced draft oven at 60°C for the prescribed duration. As with the previous sections, only the mixtures aged for zero and nine months are presented in the following figures for the sake of clarity in the plots.

Considerations of the unmodified binders are presented in Figure 9.50 for the mixtures containing the PG 64-22 asphalt binder and the California, Colorado, and Nevada aggregate sources with their respective intermediate gradations. Further, both the WesTrack mixtures with their respective PG 64-22 binders are depicted in Figure 9.51. Again, it is important to note that not only the differences in asphalt binders and aggregate sources between the WesTrack materials themselves, but also between the WesTrack and the other laboratory prepared PG 64-22 mixtures.

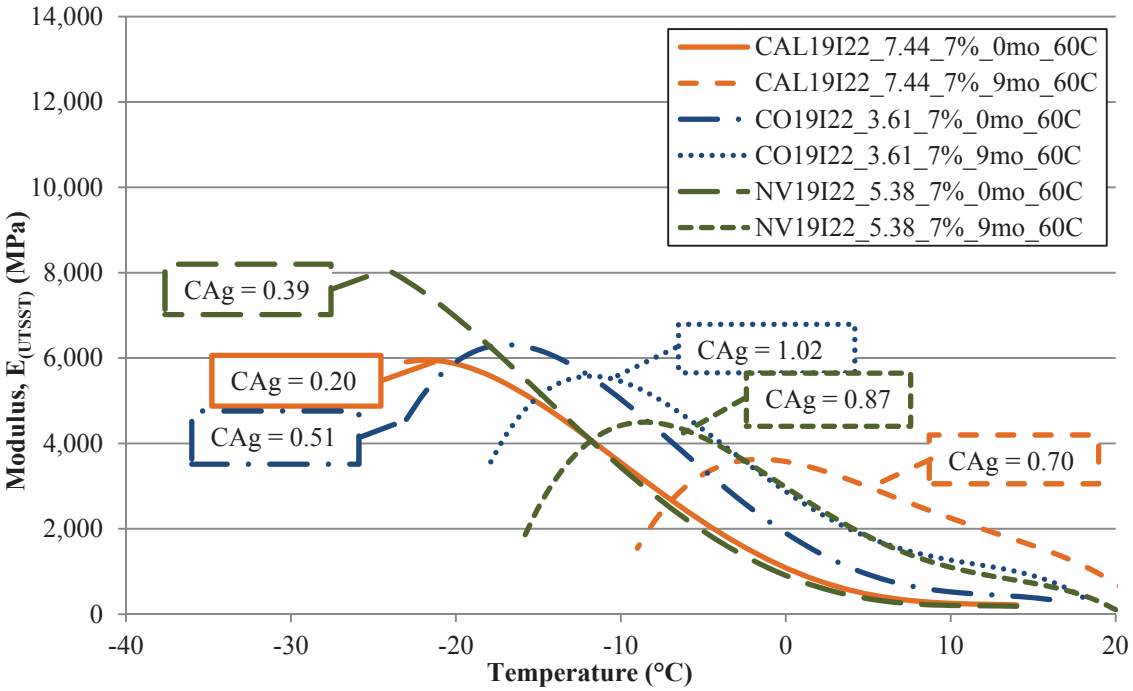

Figure 9.50 Summary of UTSST Modulus Curves for the Mixtures with PG 64-22 and Constant Film Thickness Aged at 60°C

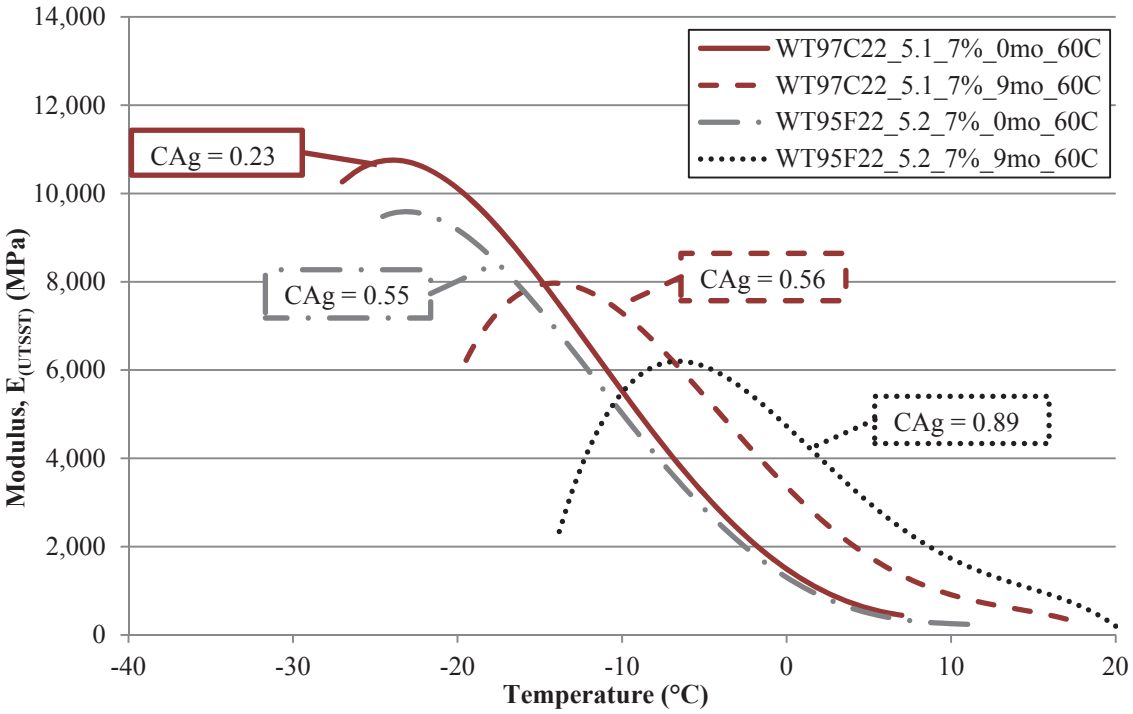

Figure 9.51 Summary of UTSST Modulus Curves for the WesTrack Mixtures Aged at 60°C

Initial observations of the mixtures containing the PG 64-22 binder with the calculated 9 µm AFT presented in Figure 9.50 clearly depict the influence of the mixture characteristics on the low temperature properties of the mixtures. These mixtures were prepared with exactly the same binder and were designed to be volumetrically as similar as possible. With all the gradations at the intermediate level, though not exactly same, the air voids all at the 7% level, and the asphalt binder content selected to provide the same calculated film thickness, the variation in these mixtures was limited to the aggregate mineralogy and the associated physical properties (i.e. texture, porosity, absorption, etc.) chemical properties, and unavoidable variations in the gradation, these mixtures were designed to isolate the aggregate effect as much as practical. For reference, the effective binder content (*Pbe*) with the PG 64-22 binder were determined

to be 4.9% for California, 3.1% for Colorado, and 4.2% for the Nevada mixtures, respectively.

With the volumetric similarities in the mixtures, Figure 9.50 indicated there were various levels of interactions not fully explained by the binder content, either total or effective binder content. Specifically, the zero month aged specimens of the California and Nevada mixtures at the warmer thermo-viscoelastic temperatures were nearly identical at temperatures down to the viscous-glassy transition region. At temperatures lower than that, the California mixture quickly transitioned through the glassy hardening, crack initiation, and on to fracture with relatively small changes in the UTSST modulus. Over the same behavioral range, the Nevada mixture exhibited similar temperature decrease, but presented nearly double the UTSST modulus increase up to the crack initiation modulus. The Colorado mixture exhibited a UTSST modulus curve quite similar in shape to that of the California mixture, but at appreciably warmer temperatures. The overall effect of this shift caused the UTSST modulus curve for the Colorado mixture to present substantially higher UTSST modulus values at a given temperature, again specific to the zero month aged specimens for each of the mixtures.

After the nine month aging duration at 60°C, the general similarities between the different mixtures changed. In the aged condition, the Colorado and Nevada mixtures resulted in very similar UTSST modulus curves at the warmer temperatures down through approximately the glassy hardening stage. As the temperature was further decreased, the Colorado mixture exhibited higher levels in the measured UTSST modulus and colder temperatures for the crack initiation and fracture stages. At the same aging condition, the California mixture exhibited a substantial shift to warmer temperatures,

which increased the modulus values at a given temperature until the region containing the glassy and brittle stages of the modulus relationship. In the glassy regions (i.e. at the colder temperatures) the California mixture rapidly transitioned through the viscous-glassy transition, glassy hardening, and crack initiation stages within a limited temperature and UTSST modulus range. All of these changes were noted with almost the same overall change in the oxidation caused by the nine-month aging duration as represented by changes in the measured CAg values all being near 0.5, again with the same PG 64-22 binder used in each of the mixtures.

Considerations of the WesTrack materials in Figure 9.51 must first recognize the differences in asphalt binders and aggregate sources between the two WesTrack materials themselves, and also between the WesTrack and the other laboratory prepared PG 64-22 mixtures just discussed. Despite those differences, it is curious to note the similarities in the relative change in the oxidation measures (CAg) with both of the WesTrack mixtures being 0.33 and 0.34 for the coarse and intermediate gradations, respectively. As an additional point of reference, the calculated *Pbe* values for the two mixtures were 4.3% and 4.4% for the coarse and intermediate gradations, respectively.

Consideration of the zero month aged mixtures from WesTrack indicated relatively similar UTSST modulus curves with the fine gradation presenting slightly lower crack initiation modulus and fracture stress measurements as well as slightly warmer temperatures. However, they were quite similar given the differences in the CAg measurements at the zero month aging condition and the fact that they were different aggregate and asphalt binder sources. The disparity in the CAg measures at this condition present a clear illustration that the carbonyl measurement alone may not be a

sufficient indicator of the mechanical behavior of a given binder or mixture, but highlights the fact that the CA measures are material specific. The usefulness of the CA measures result from the changes in CA (i.e. CAg), but must also be considered with respect to the oxidation properties of the specific binder itself. In other words, a CAg measurement of any arbitrary number is not overly useful from a practical standpoint, until it can be tied to physical measurements of the materials. Hence the previous efforts to establish the oxidation kinetics and hardening susceptibility parameters for the binder evaluated in this study.

After the nine month aging duration, the UTSST relationships were observed to be substantially different, despite nearly the same change in CAg between the two mixtures. The coarse gradation of the WT97 mixture exhibited substantially higher UTSST modulus in the colder regions of the modulus curve (i.e. glassy hardening, crack initiation, and fracture stress) compared to the WT95 mixture with the fine gradation. The fine gradation of the WT95 mixture also displayed the thermo-viscoelastic regions at warmer temperatures compared to the coarse mixture, which had a similar shifting effect on the overall modulus as was observed with the other PG 64-22 mixtures. This presented higher modulus values at a given temperature for the warmer temperature region of the UTSST modulus curve. However, the lower values of the glassy hardening and crack initiation modulus values with the WT95 rapidly decreased the overall modulus curve as the temperatures were decreased further. These findings generally agree with the oxidation rate determinations on these binders considered previously in chapter 7.

All of these comparisons present a clear example of the wide range of low temperature performance that can be observed with different asphalt binders that were

determined to have same low temperature PG grade. Specifically, the two WesTrack binders graded to within 2°C of each other on the high temperature side and to within 0.1°C on the low temperature side. The PG 64-22 binder was determined to have a high temperature grade between the two WesTrack binders, and a low temperature grade less than 5°C cooler. This provides measurable indication that much more activity is taking place within the mixture under low temperature conditions than can be described by binder testing alone.

Considerations of the mixtures containing the SBS modified binder are presented in Figure 9.52 and Figure 9.53 for the mixtures containing the PG 64-28 asphalt binder and the California, Colorado, Nevada, and Utah aggregate sources with their respective intermediate gradations.

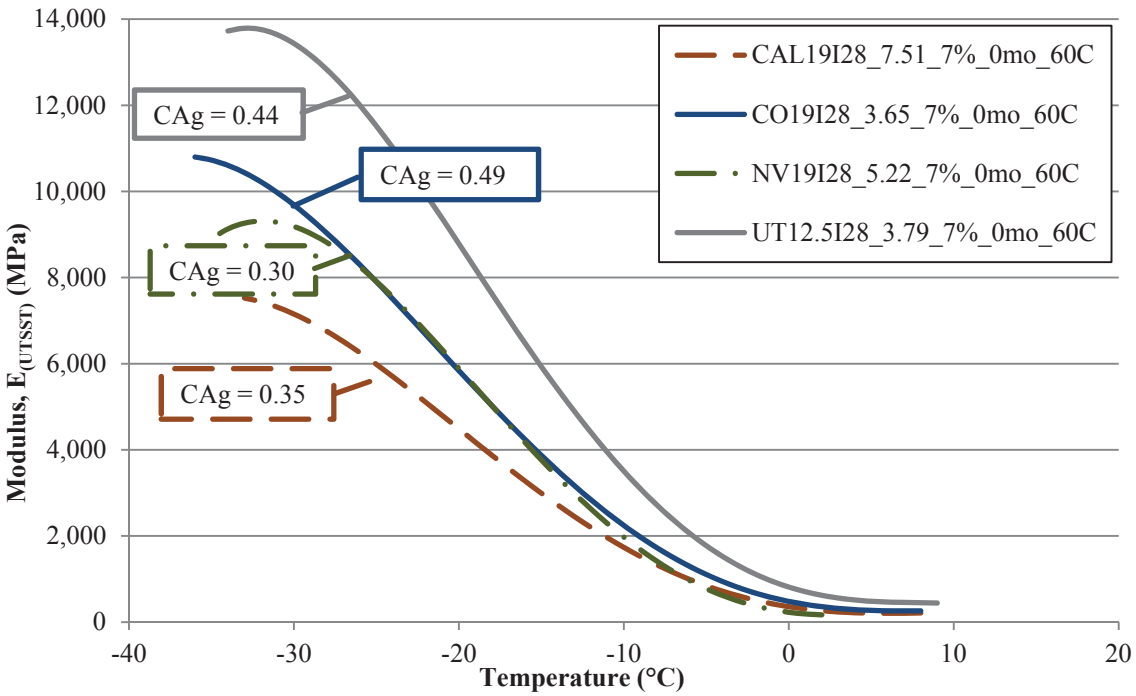

Figure 9.52 Summary of UTSST Modulus Curves for Mixtures with PG 64-28 and Constant Film Thickness Aged for 0 Months

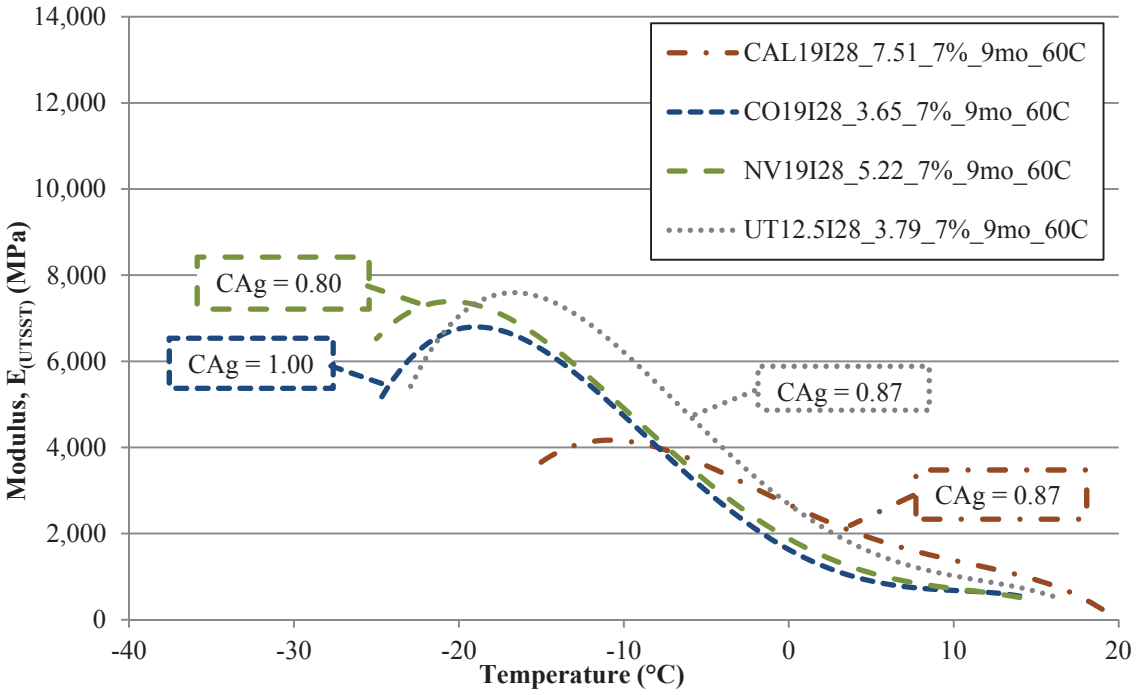

Figure 9.53 Summary of UTSST Modulus Curves for Mixtures with PG 64-28 and Constant Film Thickness Aged at 60°C for 9 Months

General observations of the zero month aging condition in Figure 9.52 note that the Utah mixture displayed the highest overall UTSST modulus relationship, even though it was not the highest or lowest of the total binder content (*Pb*), effective binder content (*Pbe*), or carbonyl measurement (CAg). As an additional point of reference, the effective binder contents (*Pbe*) with the PG 64-28 asphalt binder were determined to be 5.3% for California, 3.1% for Colorado, 4.2% for the Nevada, and 3.3% for the Utah mixtures, respectively. Previously observed similarities remain between the UTSST modulus measures of the Colorado and Nevada mixtures despite their differences in gradation, aggregate absorption, *Pb*, *Pbe*, and CAg measures. Referencing Figure 9.52 and Appendix P, it was observed that the Nevada mixture exhibited a lower magnitude crack initiation modulus but a higher fracture stress compared to the Colorado mixture. Again,

the California mixture exhibited the lowest UTSST modulus values of the group. Although, at the zero month aging condition, the mixtures presented in Figure 9.52 all generally displayed similar temperatures for the thermo-viscoelastic properties (i.e. generally within a few degrees).

Considerations of the same mixtures after the nine month aging duration at 60°C from Figure 9.53, indicate some similarities in the order of the UTSST modulus relationships of the mixtures. First, the Utah mixture retained the highest UTSST modulus curve after aging for the majority of the UTSST relationship, but by a much smaller margin compared to the zero month measures. In fact, the crack initiation modulus of the Utah and Nevada mixtures were fairly similar, although they appeared at different temperatures. The Utah mixture was also measured to exhibit the least change in the oxidation level (i.e. change in the CAg) over the nine month aging duration.

Similar to the zero month aging condition, the California mixture exhibited the lowest low-temperature modulus values, but were observed at substantially warmer temperatures after the nine month aging duration. In the warmer temperature regions of the UTSST modulus curve, the viscous properties of the California mixture presented much stiffer mixtures and thus higher UTSST modulus values.

In between the Utah and California mixtures, the UTSST modulus values of the Colorado and Nevada mixtures remained fairly similar to one another, although the order was reversed in terms of the crack initiation modulus values. The similarities were accompanied by nearly the same change in the measured CAg values between the two mixtures, but quite different levels of *Pbe*, as noted earlier.

In general, these findings provided additional support that the low temperature grade of the binder may provide a certain amount of information on the low temperature properties of similar mixtures (e.g. Colorado, Nevada, and to a certain extent Utah). However, there are clearly other factors that very well may prove influential to the low temperature properties of asphalt mixtures that are not always incorporated by the binder grading and standard volumetric measures on the mixtures (e.g. the California mixture).

The 9 μm AFT mixtures with both binders for the Colorado and Nevada mixtures were previously analyzed in section 9.2.3, but the comparative California mixtures were omitted from that section due to the lack of mixtures produced with 4.5% TWM binder content. Therefore, Figure 9.54 presents the comparison of the California aggregates with both the PG 64-22 and the PG 64-28 asphalt binders again limiting the comparison to the zero and nine month aging condition at 60°C. Both of these mixtures utilized the same intermediate gradation, targeted the calculated 9 μm AFT, and were compacted to the 7% air void level prior to aging. To reiterate, the effective binder content (*Pbe*) was determined to be 4.9% for the PG 64-22 mixture and 5.3% for the PG 64-28 mixture, both with the intermediate gradation of the California aggregates.

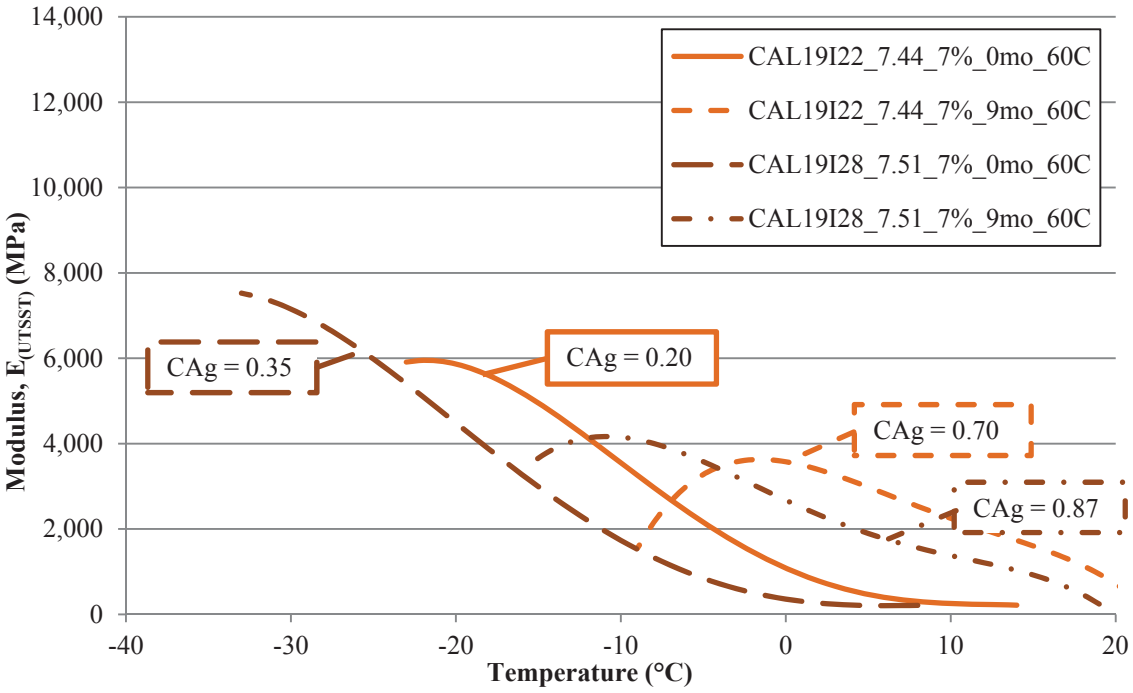

Figure 9.54 Summary of UTSST Modulus Curves for the California Mixtures with Constant Film Thickness Aged at 60°C

The comparison the California mixtures with the unmodified and modified binders presented in Figure 9.54 generally indicate similar findings to those of the Colorado and Nevada mixtures discussed in section 9.2.3. In general, those mixtures exhibited substantial differences in the UTSST modulus values as well as the temperatures at which they were observed. The California mixtures at the zero month aging condition presented here generally supported the same conclusions. However, after nine months conditioning at 60°C, the crack initiation modulus values appeared to be fairly close to one another. The most relevant observation from these two mixtures was the offset in the temperatures where the thermo-viscoelastic properties are observed due to the asphalt binder grade, which has been consistently observed and is quite the expected result.

Overall the UTSST measures on these mixtures clearly indicated the low temperature performance of a given asphalt mixture should be expected to be partially dependent upon the asphalt binder grade and the aging condition of the mixture. However, observations of the various aggregate sources provided additional support that in addition to the low temperature grade of the binder there are clearly other factors that very well may prove influential to the low temperature properties of asphalt mixtures which are not always incorporated by the binder grading and standard volumetric measures on the mixtures.

While the fundamental mechanisms of these influences may or may not be identifiable or measureable for an individual mixture, the result of the combination of the all the factors become increasingly clear through the appropriate mixture evaluation tools such as those of the UTSST methodology. From a practical standpoint, the end result of many unknown factors may be observed through such mixture tests as opposed to relying on assumption or generalizations, when is has been shown that many of the observed interactions are highly material specific.

9.2.6 Mixture Aging Temperature

Similar to the dynamic modulus evaluation, an evaluation of the influence of the aging temperature on the mixture properties was conducted by aging selected mixtures at 85°C in addition to the 60°C aging temperature already analyzed. Due to the significant amount of resources consumed during mixture preparation, aging, and testing, only the CAL19I22_7.44 and NV19I28_5.22 mixtures were aged at both 60 and 85°C, although

with each of the three air void levels (4, 7, and 11%). Based upon considerations of the pan-aged binders evaluated in section 7.1.6, the aging durations for the 85°C aging were reduced to 0.5, 1, and 3 months, which were presented in section 7.2.6 and elsewhere. As a result of the aging durations not being the same between temperatures, Figure 9.55 though Figure 9.60 present all four aging conditions at 60°C along with the three conducted at 85°C for each mixture differentiated by the compacted air void level during the aging process. Figure 9.55 through Figure 9.57 present the California aggregates containing the PG 64-22 binder, while Figure 9.58 through Figure 9.60 present the Nevada mixtures containing the modified PG 64-28 asphalt binder.

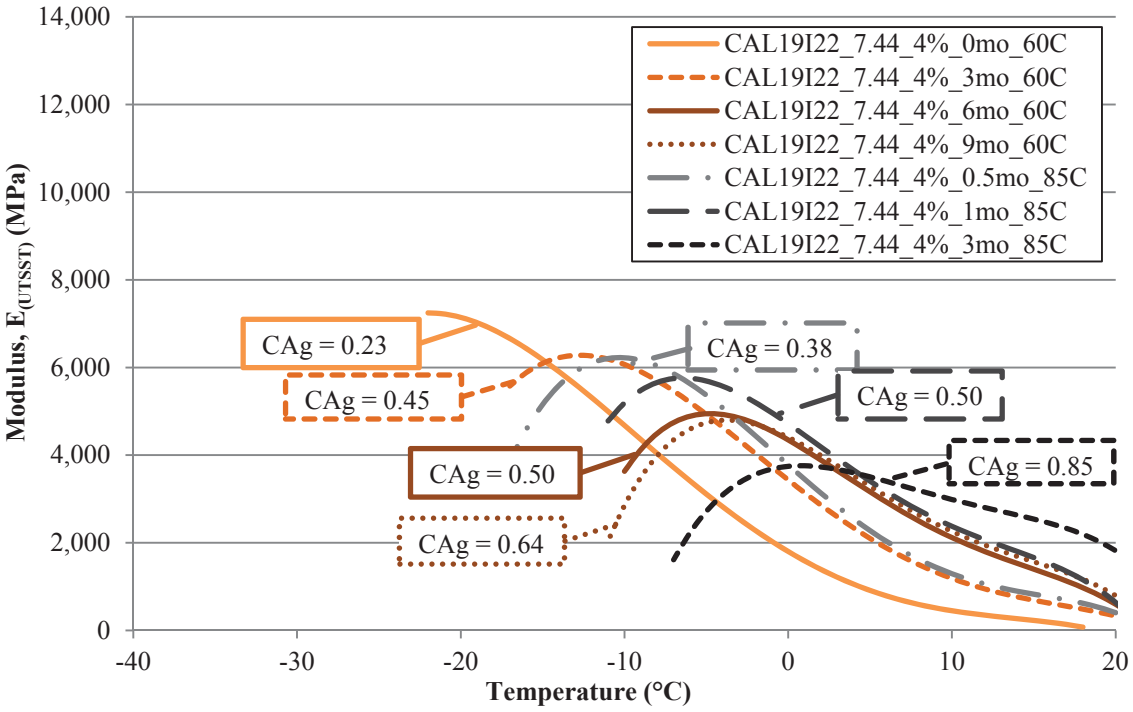

Figure 9.55 Summary of UTSST Modulus Curves for the CAL19I22_7.44 4% Air Void Mixtures Aged at 60 and 85°C

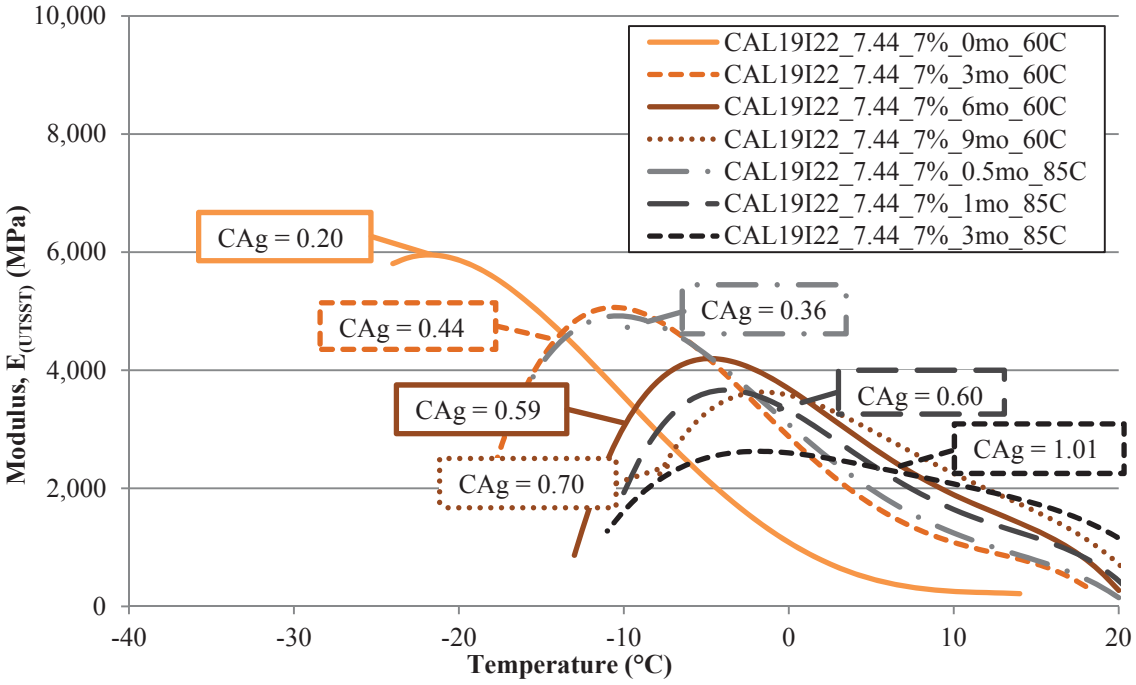

Figure 9.56 Summary of UTSST Modulus Curves for the CAL19I22_7.44 7% Air Void Mixtures Aged at 60 and 85°C

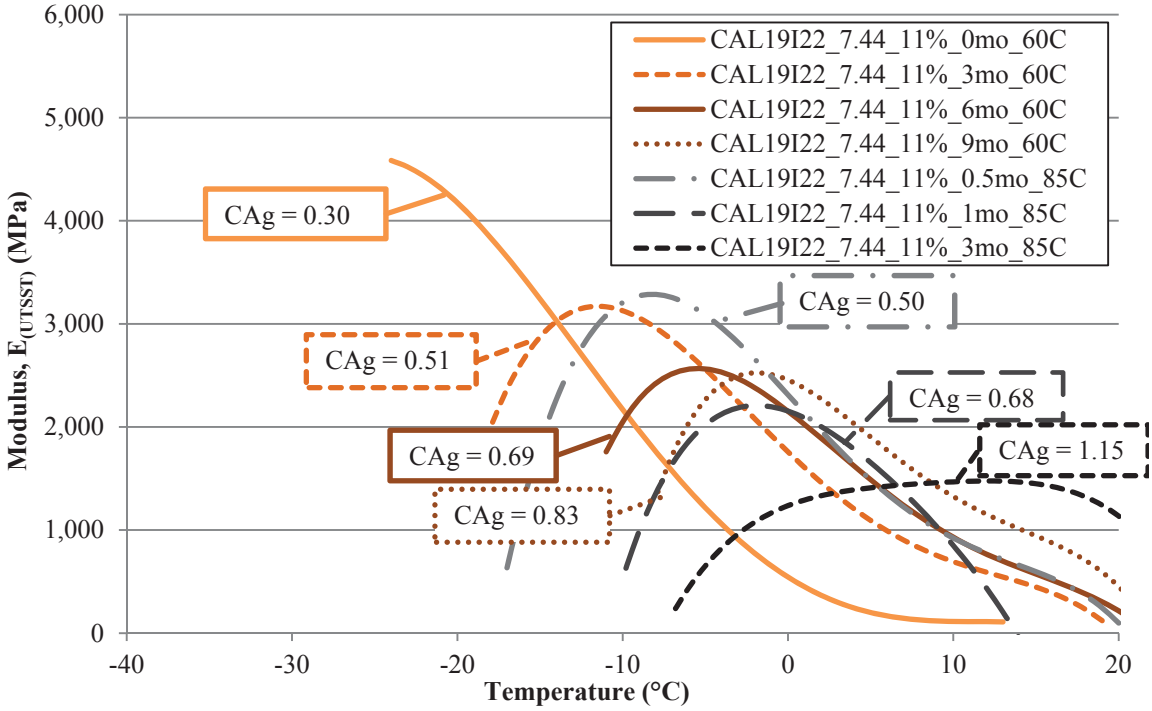

Figure 9.57 Summary of UTSST Modulus Curves for the CAL19I22_7.44 11% Air Void Mixtures Aged at 60 and 85°C

Beginning with a general overview of all three figures presenting the California mixtures containing the PG 64-22 binder, it was evident that the increase in the aging temperature did increase the rate of aging with respect to the aging time. In order to make this observation all of the aging conditions should be viewed at once, thus negating the desire to separate the UTSST modulus relationships according to age as was done with previous analyses. Although the figures become congested, the overall trends in the UTSST behavior may readily be observed. For instance, the general behavior of the UTSST modulus curves as a function of the increased oxidation, typically indicated a simultaneous shift and counter-clockwise rotation of the UTSST modulus curve. Specifically, increased aging reduced the modulus values in the brittle region (i.e. crack initiation, glassy hardening, and fracture stress) and shifted those properties to warmer temperatures. On the other end of the UTSST modulus curve (i.e. viscous-glassy transition and viscous softening), the modulus values typically increased with aging as well as shifted to warmer temperatures, as were previously summarized in Table 9.1.

Specific considerations of the California mixtures aged at the 4% air void level which were presented in Figure 9.55 indicated some degree of inconsistency between the measured oxidation level (i.e. CAg) and the temperature where brittle behavior and damage initiated within the samples. For instance, the mixture aged for 0.5 months at 85°C (i.e. CAg of 0.38) presented slightly warmer glassy hardening and crack initiation modulus values than the mixture aged for 3 months at 60°C (i.e. CAg of 0.45). Logically, the more aged mixture (i.e. the higher CAg value) would exhibit increased brittle behavior and fracture earlier or at warmer temperatures. Although these mixture were very similar to one another. Further observations of the 4% air void mixtures aged

at 85°C for 1 month compared to the 60°C mixture aged for 6 months indicated nearly the level of oxidation as determined by the CAg measures. The UTSST modulus relationships were quite similar in terms of the thermo-viscoelastic temperatures. However, the 85°C mixture did present slightly colder temperatures and higher modulus values in the glassy region at colder temperatures. The 4% air void mixture aged for 3 months at 85°C presented CAg measures substantially higher than any of the mixtures aged at 60°C. The UTSST modulus relationship for this mixture also indicated substantially stiffer materials at the warmer temperatures and decisively more brittle behavior at warmer temperatures as compared to those with lesser oxidation levels.

Similar findings were observed with the 7% air void mixtures aged at 85°C as indicated in Figure 9.56. Comparison of the 7% air void mixtures aged for 0.5 months at 85°C and the 60°C aged specimens after 3 months produced somewhat similar oxidation levels (i.e. CAg of 0.36 and 0.44, respectively) and presented nearly identical UTSST modulus relationships. By a similar comparison, the mixture aged for 1 month at 85°C and 6 months at 60°C also produced very similar oxidation measures (i.e. CAg of 0.60 and 0.59, respectively) at the 7% air void level. However, the 85°C mixture did exhibit slightly higher modulus values and correspondingly warmer thermo-viscoelastic property temperatures. Similar to the lower air void level comparison, the 7% air void mixture aged for 3 months at 85°C presented CAg measures substantially higher than any of the mixtures aged at 60°C. By a similar margin, the UTSST modulus relationship for this mixture also indicated substantially stiffer materials at the warmer temperatures and decisively more brittle behavior at warmer temperatures compared to lower oxidation levels.

Additional considerations of the California mixtures aged at 85°C at the 11% were based upon Figure 9.57. Comparison of the 11% air void mixtures aged for 0.5 months at 85°C and the 60°C aged specimens after 3 months produced nearly the same oxidation level (i.e. CAg of 0.50 and 0.51, respectively) and presented very similar UTSST modulus relationships. However, the 85°C mixture did exhibit slightly higher modulus values and correspondingly warmer thermo-viscoelastic property temperatures. By a similar comparison, the mixture aged for 1 month at 85°C and 6 months at 60°C also produced very similar oxidation measures (i.e. CAg of 0.68 and 0.69, respectively) at the 11% air void level. The brittle behavior of the mixtures indicated some degree of separation in both UTSST modulus values and the associated temperatures in the colder temperature region of the UTSST relationship. However, the viscous components of the UTSST modulus curve of the 3 month aged mixture at 85°C at the warmer temperatures showed a substantial deviation from the 60°C mixture. The California mixture aged for 3 months at 85°C at the 11% air void level presented a serious deviation from the expected UTSST modulus relationship. Not only was the oxidation level very high compared to the 60°C aged mixtures, the UTSST measures on the mixture indicated a very brittle mixture with minimal indication of the viscous component or relaxation potential remaining in the mixture. While this may in fact have been the behavior of the mixture after this aging condition, it did indicate a significant change in the behavior of the mixtures that was partially observed, but mostly inexplicably noted in the dynamic modulus measures.

More thorough discussion of this topic will be resumed after consideration of the Nevada mixtures with the modified PG 64-28 binder in Figure 9.58 through Figure 9.60.

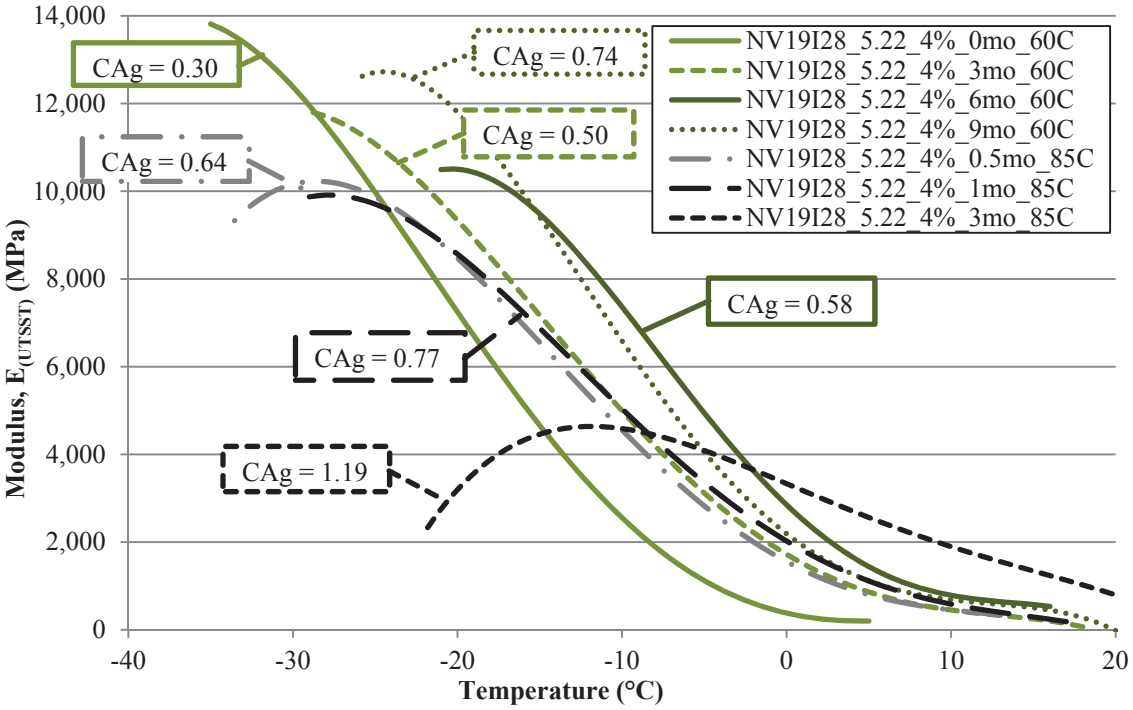

Figure 9.58 Summary of UTSST Modulus Curves for the NV19I28_5.22 4% Air Void Mixtures Aged at 60 and 85°C

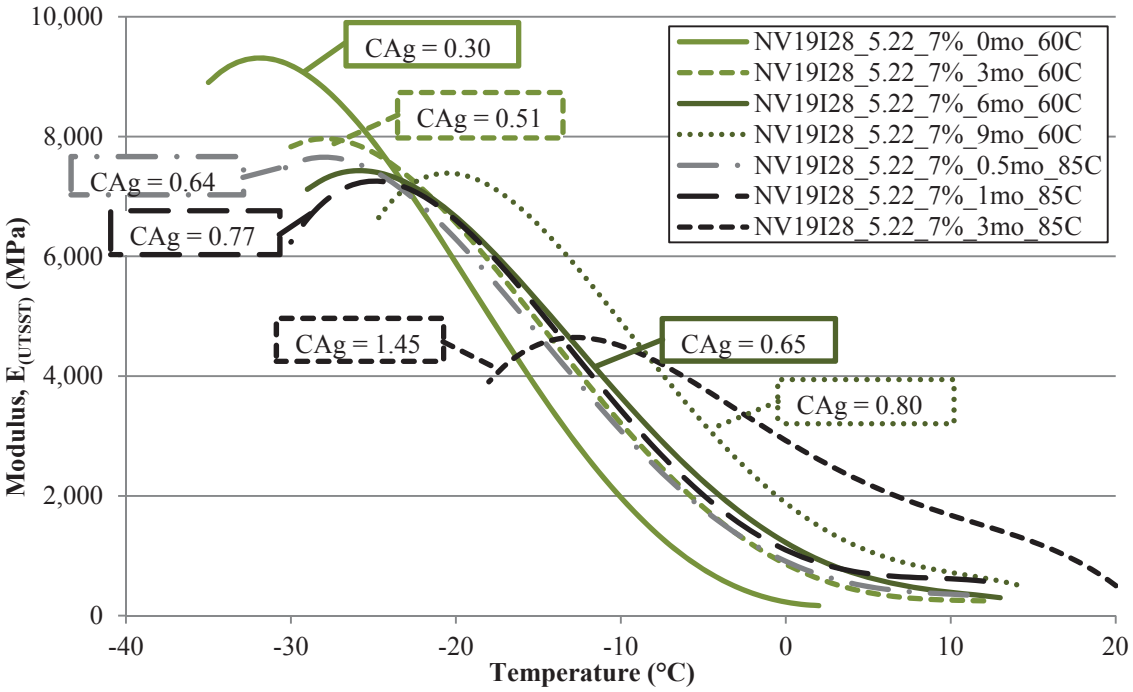

Figure 9.59 Summary of UTSST Modulus Curves for the NV19I28_5.22 7% Air Void Mixtures Aged at 60 and 85°C

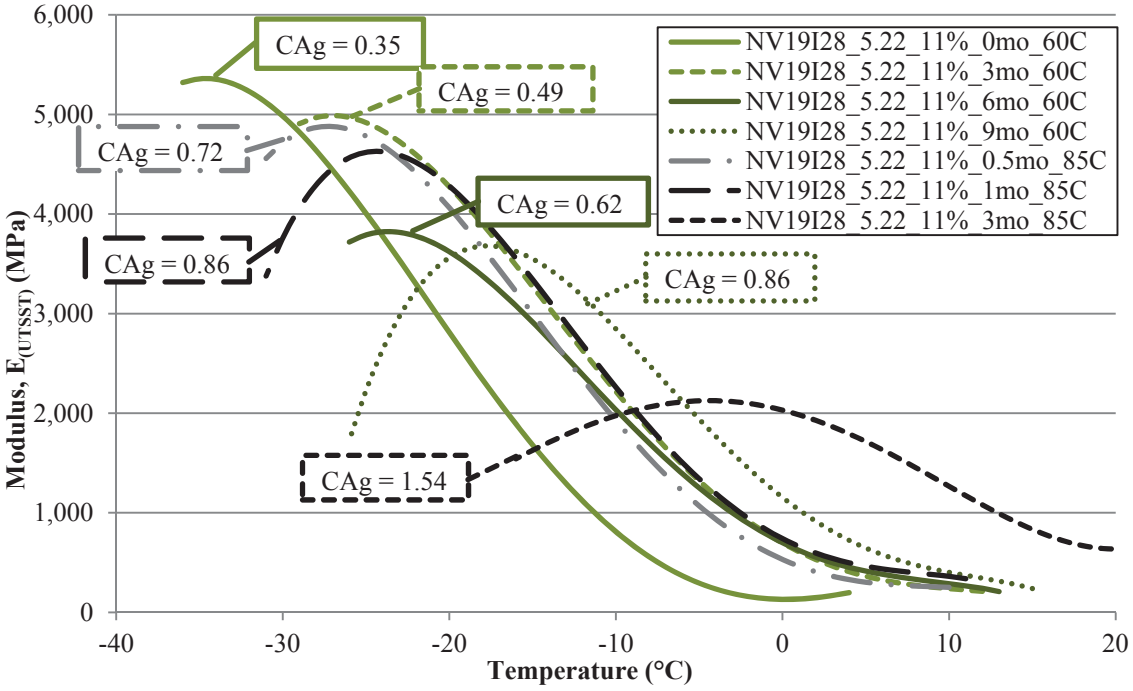

Figure 9.60 Summary of UTSST Modulus Curves for the NV19I28_5.22 11% Air Void Mixtures Aged at 60 and 85°C

In general, the overall behavior of the Nevada mixtures with the modified PG 64-28 binder presented in Figure 9.58 through Figure 9.60 were typically quite similar to the unmodified binder and the California mixtures when aged at 85°C. As an overview, the modified mixtures presented very similar reduction in the glassy and brittle regions of the UTSST modulus relationship, but typically did not exhibit the same degree of stiffening in the viscous region at warmer temperatures.

Observations of the Nevada mixtures with the PG 64-28 binders aged at the 4% air void level in Figure 9.58 initially identified an anomaly in mixture aged at 60°C for 9 months. As discussed in the air void analysis of section 9.2.1, this mixture, although verified with a third test specimen, was considered an outlier. Thus, the consistent and logical progression of the UTSST modulus relationships observed in the 0, 3, and 6

month-aged specimens were considered as the true behavior, largely excluding the 9 month specimen from the overall analysis. Therefore, further discussions on the 4% air void mixtures were based upon the remaining six mixtures presented in the figure.

As such, general observations of the 4% air void mixtures aged at 85°C for the 0.5 and 1 month durations showed very similar UTSST modulus relationships despite the measurable change in the oxidation level indicated by the CAg difference of 0.13. The mixture aged for 1 month did present very slightly higher modulus values at temperatures warmer than the glassy hardening region, but the margin was quite small. Continued aging of the mixture to a 3 month duration at 85°C produced the drastic change in the UTSST modulus relationship as was generally observed with the unmodified mixtures previously. Comparison of the 4% air void mixtures between the two aging temperatures indicated some discrepancy between the UTSST modulus relationships, particularly with respect to the measured oxidation level (i.e. CAg). Specifically, the measured CAg values did not correlate as well to the UTSST modulus relationships as with the unmodified binder. For instance, the viscous portions of both the 0.5 and 1 month mixtures aged at 85°C follow very closely with that of the mixture aged for 3 months at 60°C, until the glassy region of the curve where the 85°C mixture presented lower modulus values. This behavior was observed even though the CAg values were appreciably different noting difference of 0.14 and 0.27 between the two aging temperatures. Comparison of the same mixtures aged at 85°C for 0.5 and 1 month durations to the mixture aged for 6 months at 60°C indicated similar CAg measures, but the UTSST modulus curves for 85°C mixtures were lower in the modulus values or, in other words, the thermo-viscoelastic properties occurred at colder temperatures.

Consideration of the mixtures with the PG 64-28 binder and Nevada aggregates aged at the 7% air void level, presented in Figure 9.59, indicated similar but more systematic and orderly variations compared to the 4% air void mixtures. With the 7% air void level there were more systematic and expected UTSST modulus curves developed as a function of increased aging. Specifically, the mixtures aged for 0.5 and 1 month durations at 85°C were observed to exhibit the expected increase in CAg measures, but also followed the same basic trend of shifting and rotation noted with the unmodified mixtures. With increased aging, the glassy and brittle modulus values were reduced and occurred at warmer temperatures. Similarly, the viscous components of the UTSST modulus values increased with increased oxidation levels. The potential discontinuity between the CAg and UTSST measures was retained with considerations of mixture aged at 85°C for 1 month compared to the mixture aged at 60°C for the 9 month duration. Despite fairly similar CAg measures and UTSST modulus values, the mixture aged at 85°C reached the thermo-viscoelastic properties at noticeably colder temperatures. Continued aging of the 7% air void mixture to a 3 month duration at 85°C produced the drastic change in the UTSST modulus relationship as was generally observed with the other mixtures.

The analysis of the aging temperature on the UTST modulus measures was continued through observations of Figure 9.60 which contained the modified mixtures aged at the 11% air void level. The 11% air void mixtures generally supported the previously noted discrepancy between the UTSST measures and the CAg values, specifically when the mixture aged for 0.5 months at 85°C with the mixture aged for 3 months at 60°C were compared. These two mixtures exhibited fairly similar UTSST

modulus relationships, however their CAg values differ by more than 0.2. The trend continued with the mixture aged for 1 month at 85°C with the mixture aged for 9 months at 60°C. These two mixtures had the same measured CAg value, but exhibited substantially different UTSST modulus relationships. Continued aging of the 11% air void mixture to a 3 month duration at 85°C produced a similar change in the UTSST modulus relationship as was generally observed with the other mixtures, but again did not have a comparative 60°C mixture due to the high level of oxidation.

The noted discrepancies between the UTSST measures and the CAg measures quantifying the oxidation level were not interpreted as errors or inadequacies in either method. Rather, these findings were logically considered as further support of the differential observations with aging temperature noted in the hardening susceptibility measures presented in Figure 7.25 though Figure 7.30 discussed in section 7.1.6. Both of these evaluations suggest that there could sometimes be a change in the behavior of the binder, namely increased brittleness which was not always quantified, due to the temperature applied during the aging process of the mixtures. This finding has been observed previously with changes in the chemical structure of the oxidation products caused by overly high oxidation temperatures with certain asphalt binders (Petersen, 2009). As a consequence of such potential discrepancies, caution should be exercised in the selection of accelerated aging procedures so that the simulated aging may retain the basic properties of actual field aged mixtures which typically are exposed to substantially lower environmental temperatures.

The potential exists that the increased brittleness indicated in the UTSST measurements coupled with similar CAg levels, but at different aging temperatures would

not necessarily be displayed in the hardening susceptibility measures due to the blending of the binder that may occur during the extraction and recovery process as well as during the annealing process required during the sample loading on the dynamic shear rheometer. Building upon that concept, these findings further support valid but unconventional or unexpected measurements of E* under the extreme conditions provided by the long duration at 85°C. The general behavioral trend continued throughout the various aging levels with the UTSST measures, which logically supports the increased brittleness of the asphalt binder that may not have been fully characterized as with the UTSST measures. Further evaluation of the true mechanisms dictating these behaviors is likely warranted to achieve a more thorough comprehension of these results.

Thus, the overall behavior of the mixtures in terms of the UTSST measures at different temperatures indicated a general increase in the stiffness of the mixtures with a corresponding increase in the brittle components of the binder. The increased brittleness of the mixtures were generally exhibited in the lower temperature ranges of the material characterization (i.e. UTSST modulus relationship) at temperatures where the thermal cracking potential is examined. Some differences were observed between the overall behavior of the unmodified PG 64-22 binder compared to the modified PG 64-28, particularly with regard to the development of the brittle behavior corresponding to the level of oxidation measured in the respective mixtures.

9.2.7 Summary of Uniaxial Thermal Stress and Strain Test Measurements

In summary, the general influence of increased oxidation levels on the Uniaxial Thermal Stress and Strain Test (UTSST) results were summarized in Table 9.1. The primary influence of the increased oxidation levels were found to decrease the crack initiation and glassy hardening modulus values, which subsequently led to reductions in the fracture, crack initiation, and glassy hardening stress levels. By similar comparison, increased levels of aging led to increased viscous-glassy transition and viscous softening modulus values which were accompanied by increases in those corresponding stress levels as well. All of the thermo-viscoelastic properties were observed to occur at warmer temperatures with increased levels of oxidation within the evaluated mixtures. Thus, the general findings were understood to indicate a general stiffening of the mixtures at the warmer temperatures where the viscous properties were prevalent. Further, the low temperature portion of the test indicated a clear increase in the brittle behavior of the mixtures with increased oxidation levels.

The air void level of the mixtures was observed to have a substantial influence on the thermal stress induced within the mixture, which led to a substantial decrease in the UTSST modulus at colder temperatures for mixtures with higher air void levels. The effect did not have as profound of an influence on the temperature of the thermo-viscoelastic properties. Nonetheless, three of the four mixtures generally indicated increased crack initiation temperatures as well as increased oxidation measures within the same mixture corresponding to increased air void levels.

The evaluation focused on the influence of the asphalt binder content generally indicated that the mixtures containing the higher binder contents with the unmodified

binder initially presented higher UTSST modulus values at the zero month aging condition. However, at higher levels of oxidation nearly the opposite was observed. Thereby suggesting that the mixtures containing the higher binder content experienced the largest influence in the UTSST modulus relationships due to a given level of oxidation exposure. This finding was logically expected by considering the portion of the mixture most susceptible to oxidation as the binder, thus the more binder present the more susceptible the mixture will be to oxidative aging. In contrast, the same overall trend based upon the asphalt binder content was not noted with the mixtures containing the polymer modified binder. The overall trend was much less consistent than the mixtures with the unmodified binder, but appeared to be more based upon the aggregate source rather than the binder content. In addition, the asphalt binder itself was shown to influence the UTSST modulus measures as well as the thermo-viscoelastic temperatures of asphalt mixtures. The binder content, specifically *Pbe*, was found to be influential, just as it was in the oxidation evaluations of section 7.2. However, there were some potential influences attributable to the interaction of the aggregate with the binder, particularly with the rate of oxidation of the mixtures.

The findings of the qualitative gradation evaluation were somewhat inconsistent between the unmodified and modified binders. The mixtures containing the unmodified binder presented nearly the same overall behavior, despite large changes in the asphalt binder contents in each mixture and two different binder grades. The mixtures with the modified binder exhibited a relatively higher influence of the oxidation level with the fine gradation and correspondingly higher asphalt binder content.

Overall the UTSST measures on these mixtures clearly indicated that the low temperature performance of a given asphalt mixture should be expected to be partially dependent upon the asphalt binder grade and the aging condition of the mixture. However, observations of the various aggregate sources provided additional support that, in addition to the low temperature grade of the binder there are clearly other factors that very well may prove influential to the low temperature properties of asphalt mixtures that are not always incorporated by the binder grading and standard volumetric measures of the mixtures.

While the fundamental mechanisms of these influences may not be fully developed for an individual mixture, the result of the combination of the all the factors become increasingly clear through the appropriate mixture evaluation tools such as those of the UTSST methodology. From a practical standpoint, the end result of many unknown factors may be observed through such mixture tests as opposed to relying on assumption or generalizations, when it has been shown that many of the observed interactions are highly material specific.

The evaluation of the influence of the aging temperature identified discrepancies between the UTSST measurements and the determined oxidation level (i.e. CAg measures). However, these results were logically considered to be in support of the differential observations with aging temperature noted in the hardening susceptibility measures presented in section 7.1.6. Both of these evaluations suggested that sometimes increases in the aging temperature may lead to increased brittleness in the binder which may not always be quantified in every evaluation method. As a consequence of such potential influences, caution should be exercised in the selection of accelerated aging

procedures so that the simulated aging may retain the basic properties of actual field aged mixtures which typically are exposed to substantially lower environmental temperatures.

The general behavioral trend was continued throughout the aging levels with the UTSST measures, which logically supports the increased brittleness of the asphalt binder at lower temperatures. Further evaluation of the true mechanisms dictating these behaviors is likely warranted to achieve a more complete understanding of these results.

Thus, the overall behavior of the mixtures in terms of the UTSST measures at different temperatures indicates a general increase in the stiffness of the mixtures with a corresponding increase in the brittle components of the binder. The increased brittleness of the mixtures were generally exhibited in the lower temperature ranges of the material characterization (i.e. UTSST modulus relationship) at temperatures where the thermal cracking potential is examined. Some differences were observed between the inherent behavior of the unmodified binder compared to the modified binder, particularly with regard to the development of brittleness in the mixtures corresponding to increased levels of oxidation measured in the respective mixtures.

Finally, as an overall summary of the influence of the main experimental factors on the thermal cracking performance of the evaluated mixtures, Table 9.2 presents the generalized summary of the main factors on the determined UTSST parameters. Similar to the format of Table 9.1 which is also included, the arrows indicate the general influence increases in the specific factor will have on a given parameter. To provide a more concentrated summary, the results from the UTSST modulus, temperatures observed for the thermo-viscoelastic properties, and the accompanying stress levels have been provided in that order in a single table.

For instance, a hollow arrow pointing upward for the Fracture row in the Oxidation column indicates that the fracture temperature was observed to increase (i.e. become warmer) with increased levels of aging or oxidation, and so on for the remaining measures and input factors. Note that the air void analysis was conducted on only the 60°C aging conditions due to the potentially detracting variability observed with the mixtures aged at 85°C.

Further information has been provided indicating the previous sections focused on particular experimental factor. However, the majority of the observed trends noted in the figure were largely determined through careful observations of the numeric tables presented in Appendix P. Table 9.2 also presents the number of measures considered in the development of the overall trends indicated in the table. This provides an indication of the number of mixtures observed when the overall trends were determined. Specifically, a comparison was evaluated between two mixtures, here largely based up the same aging state of the mixtures. In other words, comparing the average UTSST results of one zero month aged mixture to the same mixture aged for 3 months at 60°C was counted as one mixture consideration for the oxidation comparison. Likewise the measures from the mixture after 3 months of aging compared to those after 6 months of aging at 60°C were counted as another.

The table also provides an indication by parentheses, of the variability of number of times comparisons were observed which opposed or did not agree with the overall trend noted with a factor. If too many oppositions were observed, then the factor was noted to have indeterminate or varied influences for that particular thermo-viscoelastic property.

Table 9.2 Summary of the Influence of Mixture Characteristics on the Thermo-Viscoelastic Properties of Asphalt Mixtures

Thermo-Viscoelastic Property	Oxidation	Aggregate Factors		Asphalt Binder	Mixture Characteristics	
	Aging Duration (Increase)	Qualitative Gradation (Finer)	Aggregate Absorption/ Mineralogy (Increase)	Polymer Modification (SBS Mod.)	Binder Content (Increase)	Air Void Level (Increase)
Fracture	N/A ⇧⇩	N/A ⇩(⇧)	N/A — —	N/A ⇩⇧	N/A(⇩) —	N/A —⇩
Crack Initiation	⇩⇧⇩	⇩(⇩) —	(⇩)(⇧) —	⇧⇩⇧	⇩ — —	⇩ —⇩
Glassy Hardening	⇩⇧⇩	⇩(⇩) —	(⇩)(⇧) —	⇧⇩⇧	⇩(⇧) —	⇩ —⇩
Viscous-Glassy Transition	⇧⇧⇧	⇩ — —	(⇧)⇧(⇧)	(⇩)⇩(⇩)	⇩ —⇩	⇩(⇩)⇩
Viscous Softening	⇧⇧⇧	⇩ — —	—(⇧) —	⇩⇩⇩	⇩ —⇩	(⇩)(⇩)(⇩)
Referenced Sections	9.2.1 9.2.6	9.2.4	9.2.5	9.2.3	9.2.3	9.2.2
Number of Measures Considered	114	12	40	20	16	48

⇧⇩ solid symbols indicate UTSST modulus

⇧⇩ hollow symbols indicate UTSST thermo-viscoelastic temperature

⇧⇩ bar symbols indicate UTSST stress

( ) parentheses indicate more than 20% variability or disagreement in the overall trend, but less than 33.3%

— indicates varied or indeterminate effects (i.e. more than 1/3 or 33% variation in findings)

10 SUMMARY AND CONCLUSIONS

The overall objective of this research effort focused on the performance and evaluation of asphalt mixtures with respect to thermal cracking. However, preliminary investigations soon indicated that a fundamental evaluation of the thermal cracking resistance of a given asphalt mixture was largely dependent upon a much more complicated understanding of the true behavior of asphalt binder oxidation. It was also acknowledged that the oxidation of asphalt binders aged within a pavement layer had the significant potential to be influenced by the mixture characteristics (i.e. air void levels, binder content, etc.) and aggregate properties (i.e. aggregate absorption, gradation, etc.). Therefore, this study was conducted in an effort to thoroughly investigate and quantify the effects different aggregate sources and mixture properties may have on the thermal cracking performance of asphalt mixtures. Once the asphalt binder oxidation process relative to the mixture characteristics was adequately identified, the results of this process will be applicable not only to thermal cracking, but also to numerous other properties that depend upon asphalt mixture characterization over time or at any aging condition.

The investigation specifically focused on quantifying the oxidative aging characteristics of the asphalt binder by itself and as part of the asphalt mixture when both are subjected to controlled isothermal oven aging in the laboratory. The initial quantification established the oxidation parameters of the asphalt binder, as has been the standard of practice in the industry. These parameters were then evaluated with mixture-aged asphalt binders under varying conditions to examine the influence of the main

aggregate and mixture factors included in the study. Because the oxidation parameters were found to differ between the pan-aged and mixture-aged binders, efforts were put forth to quantify those differences utilizing meaningful input parameters as much as possible.

To this end, these quantifiable parameters are summarized and discussed in the following sections based upon the main experimental factors in the overall experimental plan. Those main factors are listed below for convenience.

- Aggregate Factors
    - Qualitative Gradation
    - Aggregate Absorption
    - Aggregate Mineralogy
- Asphalt Binder Factors
    - Unmodified Binder
    - Modified Binder
- Mixture Characteristic Factors
    - Asphalt Binder Content
    - Mixture Density or Air Voids

Within each of the respective sections focusing on these experimental factors, a summary of the overall findings is discussed based upon the evaluations provided in previous chapters. Specific results regarding the oxidation kinetics, rheological measures, hardening susceptibility measures, dynamic modulus measurements, as well as the thermal cracking performance evaluated through the uniaxial thermal stress and strain test are the main objective of each section.

Many of the stated evaluations exhibit underlying components which evaluated the performance of the asphalt binder alone. However, since those measures were not a substantial research effort in this study, they will be omitted from this chapter and can be considered as state of the practice or background information.

10.1 Aggregate Factors

The aggregate factors evaluated concentrated on the potential influences on the binder aging that may be attributable to the aggregate material or source specifically. Namely, the qualitative gradation, aggregate absorption, and the aggregate mineralogy were the main factors under investigation.

Specifically with these factors, it was generally difficult to completely isolate the single factor effect under consideration. Therefore, in some instances more than one factor had to be adjusted and evaluated at one time. For example, changes in the aggregate gradation often adjusted the absorption of the combined gradation. Similarly, changes in the aggregate mineralogy or source typically affected both the gradation and absorption levels of the aggregate blend. Thus, the general conclusions which were drawn from the completed testing and subsequent evaluation will be considered simultaneously.

The evaluation of the qualitative gradation was conducted by comparing the varied behavior of the asphalt mixtures as a function of oxidation level between the intermediate and fine gradations for a given aggregate source. This was achieved by adjusting the

stockpile percentages of intermediate gradation to provide a finer overall gradation (i.e. greater percent passing the majority of the sieve sizes) utilizing the same aggregate components. Each of the same stockpiles were included in both the intermediate and fine gradations to keep the mineralogy the same, though with potentially different proportions. The intent was to maintain similar aggregate properties, but to compare different levels of the aggregate structure which necessarily led to changes in the aggregates absorption, surface area, and subsequently different asphalt binder contents.

10.1.1 Qualitative Aggregate Gradation

In this portion of the study, all the comparisons were made between mixtures which were prepared with an asphalt binder content that corresponded to a calculated apparent film thickness (AFT) for the asphalt binder of 9 μm respective to each mixture. The modifications to the gradation and resulting changes in the absorption and calculated surface area of the aggregate were theoretically negated through adjustments in the asphalt binder content respective to each aggregate source.

Conclusions drawn from changes in the gradation relative to the oxidation rate of the binder discussed in section 7.2.4 generally indicated that the mixtures aged with the finer aggregate gradations exhibited higher rates of oxidation in two out of three comparisons independently of the asphalt binder grade. These findings were generally supported by the rheological evaluation presented in section 7.3.3. The evaluation of the hardening susceptibility (HS) of the same mixtures presented rather mixed results as previously discussed in section 7.4.4. The HS measures of one mixture were clearly

different with the change in gradation, one was almost identically the same, and a third exhibited the same slope (i.e. HS value), but decidedly different intercept based upon the measurements of the extracted and recovered binders aged within the respective mixtures. Both of these findings generally indicated that the increased binder contents observed in the fine mixtures largely produced higher rates of oxidation within the respective mixtures.

The mixture stiffness as represented by the dynamic modulus (E^*) measurements presented in section 9.1.3 comparing the relative gradation within the mixtures, largely suggested that the findings based upon the qualitative gradation were generally inconsistent. One mixture with the unmodified asphalt binder and another with the polymer modified asphalt binder presented nearly the same E^* master curve for the two gradation types, despite a substantial increases in the total and effective asphalt binder contents. However, the third mixture produced with the modified asphalt binder exhibited dynamic modulus measures that were substantially different between the two gradation levels.

The thermal cracking analysis based upon the Uniaxial Thermal Stress and Strain Test (UTSST) discussed in 9.2.4 again observed variable influences due to the qualitative change in the aggregate gradation. Two of the mixtures, although not the same two as were noted in the E^* analysis, presented nearly the same overall response to the gradation change at low temperatures, despite a substantial difference in the binder contents and the two asphalt binder grades. The third comparison between mixtures with changes in the gradation produced with modified asphalt binder exhibited a relatively greater influence

to the oxidation level with the fine gradation and higher asphalt binder content compared to the corresponding intermediate mixture.

Therefore as an overall generalization, the unmodified asphalt binder aged in the mixtures were largely similar between the qualitative gradation adjustments. Thus, suggesting the volumetric calculations utilized to quantify the mixture characteristics provided similar mixture properties and performance. However, the same conclusion cannot be drawn for the evaluated mixtures containing the modified asphalt binder. Some of the modified mixtures exhibited similar performance while others did not. However, the discrepancies were not consistent between the two aggregate sources. In other words, one aggregate sources was not consistently the same or different when comparing the two the gradation levels.

10.1.2 Aggregate Absorption and Mineralogy

Unfortunately, it was not possible to completely isolate each factor in the considerations of the aggregate absorption level and the effect of different mineralogical composition of the aggregates. To a limited extent, the change in the aggregate gradation permitted the exclusion of the mineralogy, but out of necessity also presented changes in the surface area and other physical properties of the aggregates and could not solely isolate the absorption as an experimental factor. As a result, only portions of the absorption evaluation were obtained from the gradation analysis. Further considerations combined the influence of the absorption level and mineralogy of the aggregate out of necessity due to the physical limitations of the material.

General conclusions of the absorption and mineralogical effects upon the oxidation measurements provided in section 7.2.3 typically indicated that increased asphalt binder contents generally led to increased levels of oxidation as well as increased rates of oxidation products due to the greater amount of asphalt binder contained within the mixture. Further increased levels of the AIMS parameter CAAT generally supported a reduction in the level of oxidation, but not a strong influence on the oxidation rate with mixtures containing the same asphalt binder content. It was also acknowledged that these parameters have been shown to be influenced by aggregate absorption measures or aggregate mineralogy (e.g. increased absorption levels generally require increased asphalt binder contents for a given mix design methodology).

Additional findings based upon the mixtures with the constant film thickness of section 7.2.5 generally indicated a reduction in the oxidation level due to increases in both the calculated dust proportion (DP) and the voids filled with asphalt (VFA). However, increases in the AIMS CAAT parameter were observed to result in increased levels of oxidation for the mixtures with a constant film thickness and variable asphalt binder contents. Further, increased levels of the effective binder content in the mixtures were correlated to increased oxidation rates with the mixtures of constant film thickness.

The results of section 7.2 indicate that the magnitude or overall level of oxidation was, in certain circumstances, affected by the aggregate absorption (Abs), effective asphalt binder content (*Pbe*), the calculated voids filled with asphalt (VFA), the calculated dust proportion (DP), the coarse aggregate angularity and texture (CAAT) measured with the AIMS device, and the asphalt binder grade (BI). It was also observed that rate of oxidation of asphalt binders was significantly influenced by the effective

asphalt binder content (*Pbe*) of the asphalt mixture during aging, which is known to be influenced by the total binder content and a absorption rate (Abs) of the aggregate.

The combined effect of the aggregate absorption and mineralogy on the measured hardening susceptibility parameters presented in section 7.4.3 based upon the mixtures aged with the constant asphalt binder content did not show statistically significant interactions with the measured aggregate characteristics. However, the findings based upon the mixtures with a constant binder film thickness considered in section 7.4.5 indicated that the dust proportion (DP) was sufficient to statistically differentiate the influence of the four evaluated aggregate sources on the hardening susceptibility relationships.

The evaluation of the dynamic modulus (E^*) measurements evaluated in section 9.1.4 indicated that the oxidation level with unmodified binder corresponded very well with the total asphalt binder content, effective binder content (Pbe), as well as the measured water absorption of the aggregate (Abs) (i.e. increased binder content led to a greater influence of oxidation). Further considerations based upon the polymer modified binder indicated a distinction with the mixture containing the highest binder content, but the other three mixtures presented similar responses to oxidation as each other, independent of binder content, absorption, or distinguishable mineralogy. Thus suggesting that some indiscernible influence of the aggregate mineralogy on the oxidation of the mixtures thereby causing the variable results in the E^* analysis.

The influence of the aggregate properties on the thermal cracking performance of the mixtures presented in sections 9.2.3 considering the mixtures with the unmodified binder and constant binder content noted that the temperatures of many of the thermo-

viscoelastic properties occurred as fairly similar ranges within the same aging level of the mixtures. The mixture with the higher absorption and thus lower AFT and *Pbe* exhibited slightly warmer temperatures for nearly all the UTSST parameters. These observations were accompanied by the distinct differences noted in the UTSST modulus values between the two evaluated mixtures. The mixture with substantially higher UTSST modulus values were accompanied by the higher water absorption rates, which led to a reduced effective binder content *Pbe* that further resulted in an lower AFT. This suggested that *Pbe* and or AFT may provide a significant influence on the thermal cracking behavior of asphalt mixtures, which was in general agreement with the commonly held view that increasing the asphalt binder content should improve the thermal cracking resistance of a given mixture. Only these results indicate that the effective binder content should be the controlling factor not necessarily the total asphalt binder content. In this particular instance, improved thermal cracking performance was indicated by reduced UTSST modulus values, which indicated lower thermally induced stresses that coincided with the lower thermo-viscoelastic temperatures with the increase in *Pbe* and/or AFT.

These general findings were also somewhat supported by the mixture results with the polymer modified asphalt binder (SBS). The mixture noted to have the same increased water absorption rates, again led to reduced effective binder content *Pbe* and resulted in a lower AFT initially exhibited colder low thermo-viscoelastic temperatures. After aging, the same mixture presents warmer low-temperature thermo-viscoelastic temperatures though by a slim margin, similar to the unmodified binders. Further

observations indicated that these relative comparisons were also coincided by higher changes in the oxidation level with the increased *Pbe*, as was noted previously.

Therefore as an overall summary, the asphalt binder has been shown to influence the UTSST modulus measures as well as the thermo-viscoelastic temperatures of asphalt mixtures. The binder content, specifically *Pbe* was found to be influential as it was also found significant in the oxidation evaluations of section 7.2. However, there were some potential influences attributable to the interaction of the aggregate with the binder, particularly with the rate of oxidation of the mixtures.

The influence of the aggregate properties on the thermal cracking performance of the mixtures with the constant binder content presented in sections 9.2.5 generally indicated that despite the intentional volumetric similarities in the mixtures, there were various levels of interactions not fully explained by the aggregate absorption nor the binder content, either total or effective binder content. Further comparisons presented evidence of the wide range of low-temperature performance that can be observed with different asphalt binders that were determined to have same low temperature PG grade. Thus supporting the concept of increased asphalt-aggregate interaction within the mixtures as they age, which may directly influence the low temperature properties of asphalt mixtures. In general, these findings provided additional support that the low temperature grade of the binder may provide a certain amount of information on the low temperature properties of similar mixtures. However, there are clearly other factors that very well may prove influential to the low-temperature properties of asphalt mixtures that are not always incorporated by the binder grading and standard volumetric measures on the mixtures.

It is recognized that the fundamental mechanisms behind all of these influences may not be readily identifiable for all mixtures. It is further acknowledged that additional evaluation of the influence of the aggregate mineralogy specifically focused on the identification of root cause of the variability observed in these types of measures is warranted and thus will be discussed in the next chapter.

10.2 Asphalt Binder Modification

The influence of the polymer modification of the asphalt binder on the oxidation of the asphalt binder in mixtures was carried out as an additional component of several other main factor evaluations. The majority of the other considerations were conducted with both an unmodified and an SBS modified asphalt binder. These two binders were not strictly the same binder merely with and without modification, but they did contain the same base asphalts as their origin.

Evaluation of the oxidation properties of the two binders provided in section 7.2.3 presented lack of statistical significance of the categorical term indicating that both the slope and the intercepts were not significantly influenced by the SBS modification of the binder when mixed with the one aggregate source, but was found to significantly influence the oxidation characteristics of a second mixture. Considerations of the mixtures containing constant asphalt binder content again suggested that the overall influence on the polymer modification of the binder was aggregate dependent. Specifically, the polymer modification did not highly influence the oxidation growth

within one mixture, but there were slight differences noted with the other aggregate source between the two binders. Evaluations of the mixtures prepared with a constant asphalt film thickness presented in section 7.2.5 supported the statistical significance of the categorical influence of the SBS modification of the asphalt binder.

In general, the influence of the asphalt binder grade (i.e. unmodified compared to polymer modified) was found to significantly influence the rheological measures on the asphalt binder as a function of the oven aging duration as presented in section 7.3.2. Further considerations with mixtures of constant film thickness undertaken in section 7.3.4 observed similar deviations in the rheological measures between the two asphalt binder grades (i.e. PG64-22 and PG64-28). Within each respective aggregate source, the only factor that has changed in these comparisons was the asphalt binder grade. The aggregate gradation was held constant and the total binder content was adjusted so the AFT of 9 μm was also maintained. Thus, based upon the assumption of the AFT calculation being an accurate representation of the absorbed and effective asphalt binder contents, the only variable in these considerations was the asphalt binder grade. Under those conditions, it was readily apparent that the asphalt binder grade, specifically the polymer modification of the asphalt binder, resulted in a significant alteration of the rheological measures as a function of aging duration in the respective mixtures. Continued analysis of the hardening susceptibility determinations of section 7.4.3 and 7.4.5 indicated the binder significantly affected the intercept (m-value) and the slope (HS) with two aggregate sources.

Assessment of the binder type with respect to the dynamic modulus (E^*) found in section 9.1.2 and 9.1.4 presented a clear separation due to the binder grade or more

specifically the polymer modification of the binder. The mixtures containing the unmodified binder presented a higher overall stiffness at each of the respective aging conditions, except at the lower reduced frequency range. The differences in the overall range of the magnitude E^* master curves were indicated by the increased stiffness of the lower asymptote and the reduced E^* values of the higher asymptote with the modified binder. After extended aging, the mixture with the modified binder exhibited a slightly larger shift in the intermediate reduced frequency range compared to the unmodified mixture. However, in the lower range of reduced frequency the mixtures with the unmodified binder showed a significant increase in the overall shift due to aging. Further, the mixtures with the modified binder also appear to converge upon nearly the same asymptote values at both the high and low ranges of the sigmoidal curve. Conversely, the mixtures with the unmodified binder were similar only at the higher asymptote.

In summary, the mixtures containing the unmodified binder were stiffer (i.e. higher E^* values) than the comparative mixtures containing the modified asphalt binder, for all but the lower range or reduced frequencies. This finding generally agrees with the previous hardening susceptibility observations conducted on the extracted and recovered binder from these mixtures.

The evaluation of the low-temperature characteristics through the UTSST measures on the mixtures containing different binder grades found in section 9.2.3 and 9.2.5 initially indicated a clear distinction of the UTSST modulus curves between the two binders, as would be expected. The mixtures containing the unmodified binder initially exhibited higher UTSST modulus relationships, but rapidly dropped below the modified

mixtures at temperatures below a certain temperature. The crack initiation modulus values for the unmodified mixtures were of much lower magnitude than the modified mixtures.

After the extended aging duration the UTSST modulus values were much closer to one another, however the modified mixtures were noted to have crack initiation and fracture temperatures well below those of the unmodified mixtures. With both aggregate sources and over both short and long-term aging conditions, the mixtures containing the modified binder maintained lower UTSST modulus values at the warmer temperatures in the viscous regions of the relationship. At the colder temperatures, transitioning through the viscous-glassy transition and into the crack initiation and subsequently micro damage stages of the evaluation, the polymer modified mixtures often resulted in higher modulus values as the result of less substantial damage. This is further evidenced by the glassy hardening and crack initiation temperatures of the mixtures containing the unmodified binder occurring at substantially warmer temperatures compared to the modified mixtures.

These mixtures were produced with the similar asphalt binders except for the polymer modification of one binder which only differed in their low temperature grade by 6°C. However, the change in the UTSST temperature ranges of the mixtures varied by as little as a couple of degrees to as high as 15°C which was considered a substantial influence solely due to the aggregate and mixture properties. In certain instances the binder grading may prove sufficient, or relatively close to the mixture temperatures. However, the actual modulus values, strain values leading to the coefficient of thermal contraction, and the stress levels remain undetermined with the binder grading alone. In

other instances, the binder grade did not adequately characterize the low temperature properties of the mixtures. Therefore, the substantial influences in the mixture behavior clearly indicated the necessity for mixture testing of low temperature properties in order to reliably differentiate the actual behavior expected of the mixtures.

Continued observation of the influence on the binder grade presented in section 9.2.5 involved the addition of different asphalt binder sources from WesTrack. Initial consideration of the short-term aged mixtures from WesTrack indicated relatively similar UTSST modulus curves with the fine gradation presenting slightly lower crack initiation modulus and fracture stress measurements as well as slightly warmer temperatures. However, they were quite similar given the differences in the oxidation levels which are material specific and the fact that they were different aggregate and asphalt binder sources. After the long-term aging duration, the UTSST relationships were observed to be substantially different, despite nearly the same change in oxidation level between the two mixtures.

All of these comparisons present a clear example of the wide range of low temperature performance that can be observed with different asphalt binders that were determined to have same low temperature PG grade. Specifically, the two WesTrack binders graded to within 0.1°C for the low-temperature grade of the binders. The PG64-22 binder was determined to have a high temperature grade between the two WesTrack binders, and a low temperature grade less than 5°C cooler. This provides measurable indication that much more activity is taking place within the mixture under low temperature conditions than can be described by binder testing alone.

In general, these findings provided additional support that the low-temperature grade of the binder may provide a certain amount of information on the low temperature properties of similar mixtures. However, there are clearly other factors that very well may prove influential to the low temperature properties of asphalt mixtures that are not always incorporated by the binder grading and standard volumetric measures on the mixtures.

Overall the UTSST measures on these mixtures clearly indicated the low temperature performance of a given asphalt mixture should be expected to be partially dependent upon the asphalt binder grade and the aging condition of the mixture. However, observations of the various aggregate sources provided additional support that in addition to the low temperature grade of the binder there are clearly other factors that very well may prove influential to the low temperature properties of asphalt mixtures which are not always incorporated by the binder grading and standard volumetric measures on the mixtures.

Although not considered in the mixture evaluation in this study, some additional binder influences were investigated in the pan-aged binder study that have contributed to the evaluation of binder modification properties. General observations in section 7.1.2 indicated that the addition of either the lime or the SBS polymer reduced the rate of oxidation. Despite the visual and calculated differences in the kinetics relationships, the oxidation parameters of the evaluated modified and unmodified binder were found to be statistically similar.

When the black space diagrams of the binder at a highly aged condition was considered, the lime modified binders were fairly similar, but the unmodified binder

exhibited a significant reduction in the viscous response presented as the phase angle. Thus, the unmodified binder can presumably be considered more brittle than those aged and tested with lime.

However, when the relative aging condition of the binders were compared it became apparent that the oxidation level may also be playing a role in the response. It became evident that the lime modified binders had not been aged nearly as far as the unmodified binder. This clearly supports previous findings that the addition of lime reduces the overall oxidation of asphalt binders (Huang et al., 2002). Further evaluations of the influence of binder modification was considered in Figure 7.19 which presented black space diagrams of the base binders and their modified counterparts in both their original and aged condition. Initial observations found the PG 64-22, PG 64-22 + 3% SBS, and the Base Stock exhibiting quite similar black space diagrams in their original conditions, despite their respective oxidation levels. However, the PG 64-28 presented significantly different properties noted as a large shift to the left at the original aging level. This behavior seems to suggest that the mere existence of the SBS polymer did not necessarily provide significant improvement to the performance of the binder, as evidenced by the lack of improvement in the rheological properties of the PG 64-22 + 3% SBS compared to the base PG 64-22. However, this particular binder was not formulated or specifically designed by the asphalt binder supplier. It was produced by special request for this study to simply add the 3% SBS to the PG 64-22 binder without specific modification or preparation of the base to do so. Specifically, no special efforts were expended on the blending operations such as cross-linking the polymer etc. This finding highlights the benefit of having properly formulated asphalt binder particularly when

polymer modification is involved. Simply adding the polymer without proper assessment and digestion of the polymer do not always yield the expected benefits that are known to accompany polymer modification.

Quite the opposite result was noted with the PG 64-28 compared to the respective Base Stock binder. In this case, the polymer modification process has dramatically improved the rheological performance of the asphalt binder resulting in much lower phase angle measures as a result of the much increased efficiency of the elastic component provided by the SBS.

It should be clearly differentiated that the reduction in phase angle with the polymer modification is expected to be the result of the added elastic component due to the polymer. This is in contrast to the unmodified binders which also show a reduction in the phase angle with aging, however these changes are suspected to be the result of a loss in the viscous component (i.e. a more brittle behavior). As a result, the general assumption of lower phase angle indicating more brittle behavior does not necessarily apply to modified asphalt binders. In summary, a lower phase angle as a function of aging typically indicates an increase in the brittleness or loss of ductility of the asphalt binder which is an undesirable occurrence. But a reduction in phase angle due to polymer modification adds to the elasticity of the system without the corresponding loss in ductility (i.e. the binder has not been damaged by the addition of the polymer), which is a positive influence on the asphalt binder as a whole.

While comparisons between the other pan-aged binders may be possible, it is generally accepted that these properties are binder specific. As such, the other

comparisons are not truly valid comparisons and are therefore left to later analyses such as the hardening susceptibility comparisons.

Combining the observed similarities in the binder oxidation measures with those of the rheological measures permits the evaluation of the hardening susceptibility relationships as discussed in section 7.1.5 for the PG 64-22 binder along with the associated modified versions made from it (i.e. with 10% lime, 20% lime, and 3% SBS polymer). Basing the comparison on the influence of the lime and the SBS polymer of the influence to the PG 64-22 itself, the general trends indicate that the addition of either component increased the viscosity of the binder. In the case of the 10% lime, the increase is quite marginal and present statistically the same relationship from the transformed linear regression analysis. This finding is not all that unexpected, especially when noting the increased variability of the relationship with the 10% lime added. The PG 64-22 +20% lime presents a more drastic increase not only in the intercept (m) of the relationship, but also in the slope (HS). From the transformed linear regression analyses, the PG 64-22 + 20% lime was found to fit an intercept that was statistically significantly different. The PG 64-22 + 3% SBS relationship exhibited notably higher viscosity values as can be expected with the addition of SBS polymer. The intercept of the PG 64-22 + 3% SBS was statistically greater than that of the PG64-22 based upon the transformed linear regression analyses, while the slope was determined to be statistically similar.

Considering the Base Stock binder and the PG64-28, a reduction in the HS was noted due to the addition of the SBS polymer. However, consideration of both the general influence of the polymer when added to the PG 64-22 binder compared to that of the Base Stock suggested that the addition of SBS polymer into the asphalt binder may

not necessarily decrease the HS of a given binder. Given the relative similarities of the PG 64-22 and the Base Stock binder, this result suggests the formulation processing (e.g. cross-linking operations, polymer digestion time, etc.) can have a significant influence on the overall behavior of the modified asphalt binder. Based upon the statistical analysis, the Base Stock binder was found to be statistically significantly different from the PG 64-28 asphalt binder, both intercept (*m*) and slope (*HS*). However, the PG 64-22 + 3% SBS binder was found to fit a similar intercept (*m*) but have a significantly different slope (HS) when compared to the PG 64-28 relationship.

Therefore, as an overall summary of the influence of binder modification the analyses indicated that the polymer modification process may not necessarily reduce the rate of aging over and above material specific differences between different binders. However, the physical properties of the binder may be significantly influenced, particularly with proper formulation and sufficient digestion of the polymer into the asphalt binder. The end result is that the modified binders and resulting mixtures may experience improved physical characteristics that may overcome or better resist the detrimental effects due to the oxidation process.

10.3 Mixture Characteristics

Further evaluation of the influence of the general mixture characteristics were also considered. Specifically, variations in the asphalt binder content and the level of compaction or air void level were also evaluated to assess the influence of these factors

on the oxidative aging of the mixtures and the resulting changes in the measured physical properties of the mixtures.

10.3.1 Asphalt Binder Content

The influence of the asphalt binder content on the aging properties of the mixtures was conducted by keeping the aggregate gradation the same and varying the asphalt binder content. Accordingly, this results in changes in the apparent film thickness (AFT) of the asphalt binder in the mixture.

As such, the influence of the variations in the asphalt binder content of the mixtures during the aging process were evaluated in section 7.2.3. General observations suggested that changes in the asphalt binder content of up to 0.7% TWM may not influence the rate of oxidation for the mixtures containing the modified binder and the one aggregate source with the intermediate gradation. However, another aggregate source indicated potentially lower oxidation levels due to a 0.85% TWM increase in the binder content. Further, an increase of almost 0.9% possibly reduced the oxidation level, but not the growth rate with the unmodified binder and the one aggregate source, but indicated only a minor influence with the other aggregate source all with the intermediate gradation.

The stepwise regression analysis for one evaluated mixtures indicated a reduction in the oxidation level with *Pbe* and an increase in the oxidation level corresponding to increased VFA, with neither parameter significantly influencing the oxidation rate. It should be noted that quite similar regression equations were also developed utilizing *Pb* and AFT terms in place of the *Pbe* input. The evaluation of the oxidation level with a

second mixture was found to exhibit a significant reduction in the level of oxidation with the modified binder and a decrease with the VFA term, contrary to the first mixture. However, neither input parameter was found to highly affect the rate of oxidation.

Considerations of the mixtures containing the constant asphalt binder content indicated that *Pbe*, BI, and CAAT terms significantly influenced the oxidation measures. In addition, the interaction term between the aging duration and *Pbe* indicated that Pbe was significantly influential to both the level and the rate of oxidation in the mixture-aged binder. The age and BI term differentiating polymer modification of the binder was also observed to be moderately significant.

The evaluation of the influence of the binder content on the rheological measures of mixture-aged binders discussed in section 7.3.2 observed that although the plots were similar in magnitude, the leftward shift of the black space plot from the mixture with the higher binder content appeared to be larger than that of the lower binder content with the unmodified binder. Similar trends to those noted previously with the modified binders were also observed noting the same counter-clockwise rotation of the black space representation of the mixture-aged binder master curves. Again, the higher binder content showed the largest movement in the black space representation.

The evaluation of the binder content effect on the hardening susceptibility measures presented in section 7.4.3 generally noted slight but inconsistent deviations in the HS measures in relation to the asphalt binder content in the evaluated mixtures. The statistical analyses indicated that the slight differences in the HS parameters noted due to the change in asphalt binder content were not statistically significant to the overall regression analysis.

The evaluation of the asphalt binder content on the oxidation of asphalt mixture also included dynamic modulus (E^*) measures presented in section 9.1.2. The results from the unmodified mixtures indicated that with the short-term aged mixtures, those with the higher binder content typically presented lower E^* values at a given reduced frequency. After long-term aging the order of the mixtures did not consistently rank according to the asphalt binder content, nor were they consistent across the entire reduced frequency range. The polymer modified mixtures presented a more orderly and systematic variation of the measured E^* master curves compared to the unmodified mixtures. With the modified mixtures, the master curves of the higher binder contents plotted just below the other mixture for a given aggregate source in nearly every comparison. The oxidation levels were relatively similar as well, as is evidenced by the same order of the mixtures at both the short and long-term aging conditions.

The overall summary regarding the influence of the asphalt binder content on the low-temperature UTSST properties of the asphalt mixture has been presented in section 9.2.3. Initial considerations based upon the short-term aged mixtures for both asphalt binders exhibited fairly different behaviors relative to one another. The mixtures containing the unmodified binder generally exhibited better low-temperature properties with increased binder content for a given aggregate source. This was most notably indicated by the lower crack initiation and fracture temperatures for the mixtures with higher asphalt binder contents. The crack initiation modulus values were primarily dependent upon the aggregate source rather than the binder content.

Similar comparisons between the short-term aged mixtures with the modified binder did not present the same overall trend. In these mixtures, the lower the binder

content exhibited the higher observed crack initiation modulus values. Despite some discrepancies noted in the ranking of the mixtures in the crack initiation and fracture stages, the UTSST relationships of the mixtures containing the modified binder were substantially more consistent from the initial starting temperature down though the viscous-glassy transition, regardless of binder content or aggregate source.

As an interim summary with respect to the asphalt binder content, the unmodified mixtures containing the higher binder content initially presented higher UTSST modulus values at the short-term aging condition. After long-term aging at 60°C nearly the opposite trend was observed. Thereby indicating that the mixtures containing the higher binder content resulted in the largest shift in the UTSST modulus relationships after a given oxidation exposure level. This finding can logically be expected by recognizing the mixture component most influenced by oxidation to be the asphalt binder, thus the greater the proportion of the mix the binder composes, the more significant its contribution to the overall aging behavior of the mixture. In other words, the portion of the mixture most susceptible to oxidation is the binder, thus the more binder there is in the mixture, the most susceptible the mixture will be to oxidative aging. In contrast, the same overall trend based upon the asphalt binder content was not observed with the mixtures containing the modified asphalt binder. The overall trend was much less consistent that the mixtures with the unmodified binder, but appeared to be more based upon the aggregate rather than the binder.

Therefore as an overall summary, the binder content, specifically *Pbe* was found to be influential as it was also found significant in the oxidation evaluations of section 7.2.

However, there were some potential influences attributable to the interaction of the aggregate with the binder, particularly with the rate of oxidation of the mixtures.

10.3.2 Mixture Air Void Content

The compacted air void level in the mixtures was also evaluated to observe the effect on the oxidation of the binder during the oven aging. These mixtures were compacted at the asphalt binder content which produced a calculated apparent film thickness (AFT) of 9 μm. Specifically, these mixtures were compacted to three different ranges in the air void level measured on the cut E^* specimens (i.e. 4, 7, and 11% voids in total mix).

Observations of section 7.2.2 presented rather systematic variations in the binder oxidation measurements as a function of the air void level of the mixtures during the oven aging. The measurements of the mixtures aged at the 4% air void level exhibited not only the lowest oxidation values, but also present the lowest rate of oxidation growth depicted as the slope of the oxidation measures with respect to the aging duration. The systematic variation is also realized with the mixtures prepared with 7% air voids as they present generally higher oxidation measures compared to the 4% air void mixtures. Typically the slope of the 7% air void mixtures was higher than those of the 4% air void mixtures, with limited exceptions. Similar general increases are further noted with the mixtures containing 11% air voids over the aging duration, again with minor exceptions noted. However, statistical considerations conducted between the mixtures individually, generally resulted in no statistically significant difference between the air void levels, again with a few exceptions. It was noted that some of the statistical significance

determinations may have been limited based upon the limited range of the measurements included in the analysis. Clearly, if the apparent trends continued as expected from these data, additional aging durations would be expected to eventually detect more significant differences among the different air void levels.

Utilizing the more robust regression analysis presented in Equation 7.8 which included the air void level as an additional independent variable to investigate the oxidation measurements on the extracted and recovered binders from their respective mixtures as a function of aging time. In this manner, three of the four mixtures showed a significant difference either in the slope or intercept with the change in air void level. Therefore, in general the level of air voids were considered to have an influence on the rate or level of oxidation of a given mixture. This also suggests that the oxidation of the binders aged in mixtures may potentially be different from those of the pan-aged binders, otherwise the air void level would not have shown any significant influence (i.e. the mixture properties would not have an influence on the aging rate of the asphalt binder).

Additional evaluation of the air void level included observations of the different aging temperature on the oxidation measures. General observations of the influence of the air void level exhibited more substantial influence when the mixtures were aged at higher temperatures. When the regression analysis was repeated including both the 60 and 85°C aging on the two mixtures separately, both mixtures were significantly influenced by the level of air voids as well as significantly affected by the aging temperature. The oxidation rate was not highly influenced by the level of air voids as determined by the lack of statistical significance of the Age*Va term. However, similar to the analysis with the 60°C aging, this is suspected to be an inherent limitation of the

data set. If the current trends (i.e. oxidation growth rates) continue as expected, then the significance of the discrepancy with air void level would continue to increase to the point where it would become statistically significant.

The evaluation of the influence of the mixture air void levels on the rheological measures presented in section 7.3.1 observed a similar general shift in the black space plot, generally toward lower phase angles as a function of aging duration with each of the air void levels with the unmodified binder. A relative comparison of all three air void levels, noted the general similarities in the black space relationships of the short-term aged mixtures as well as the after the long-term aging duration. The G^* master curve relationships also indicated the similarities in the short-term aged samples. However, a clear and systematic increase in the G^* master curve was noted with aging duration as a function of the respective air void level of the mixtures. Therefore, the oxidation of the unmodified binder generally exhibits a reduction in the phase angle for a given stiffness value (G^*) as a function of aging with some increase in the stiffness noted with the air void level at a given aging duration. In other words, the binder increases stiffness and loses some of the measures flexibility with oxidation.

The mixture-aged SBS modified binders also exhibited a rotation in the black space representation not just the lateral translation as was observed with the unmodified binder previously. With a certain amount of inconsistency between all the mixtures collectively, some general trends were observed in the black space representation of the rheological measures. Specifically the 11% air void mixtures are consistently the furthest in terms of a clockwise rotation of the black space representation of the master curves for a given aging condition. Similarly, the measurements from the 4% air void mixtures are the

furthest in a counter-clockwise rotation for a given aging condition. Thus, placing the measurements from the 7% air voids partially in between with the overall rotation of the black space representations moving in a counter clockwise rotation. In other mixtures, the influence of the air void level was not dramatically evident in the black space plots measured on the extracted and recovered binders from mixtures with different air void levels aged at 60°C. However, some systematic variations were noted with most of the measured binders particularly when the G^* master curves as a function of the reduced. Therefore, the combined effect of the variations noted in the oxidation levels and minor differences observed with the rheological measures will be combined in the hardening susceptibilities of the respective mixture-aged asphalt binders.

Section 7.4.2 presented the evaluation of the mixture air void level on the hardening susceptibility of the aged mixtures. A significant finding clearly indicated that the relative difference between the HS relationships due to the air void levels of the mixtures during the aging process are either very small or non-existent, with both the unmodified and modified asphalt binders. This finding was further supported by the statistical regression analysis. Therefore, the determination of the HS relationship for a particular mixture of a given gradation and binder content may be determined by a single air void level.

It was further noted that the air void level was also found to be statistically influential to the HS measures between the two mixture aging temperatures with the one of the two mixtures. However, removing the Va parameter from the analysis caused only minimal adjustment to the final results. Therefore, to maintain consistency throughout all

the air void analyses with the mixture-aged binders, the Va term was omitted but still produced acceptable HS characterizations.

The influence of the air void level on the mixture stiffness indicated by the E^* measures were presented in section 9.1.1. General observations relative to the mixture air void level clearly indicated a systematic shifting due to the air void level at both the short and long-term aging conditions, with a couple of exceptions. The results have suggested with certain mixtures that the air void level of the mixtures during aging very distinctly influence the level of oxidation, while others have exhibited quite minor influences, and some mixtures exhibited both behaviors. Therefore, to conduct a more robust evaluation of these findings, the actual rate of stiffness increase was considered. To accomplish these comparisons, E^* had to be represented by fewer values than full master curves. To appropriately reduce the data, the fundamentals of viscoelastic theory were referenced. Since this investigation was interested in the aging of the asphalt binders and corresponding changes to the mixture properties, it was desired to capture as much of the viscous response of the mixture as possible. The most viscous response in an E^* test was determined by locating the highest phase angle. After much consideration into the measured phase angle and the corresponding modulus values at each of the E^* testing conditions, it was decided that the best option would be to consider E^* at 37.8°C (100°F) and 0.1 Hz. Generally keeping within the low shear viscosity presentation format, the air void evaluation was conducted in the semi-log scale as a function of the oxidation level. As was suggested in the previous evaluations of the full master curves, this abbreviated consideration clearly presents the air void dependency of not only the measured E^* values, but also the increase in those measures under constant aging.

The mixtures with different unmodified binders displayed the well-established expectation that the air void level or mixture density exhibited a distinct influence on the overall stiffness of the mixtures. Although there is some overlap in certain mixtures, the analysis generally showed a reduction in the rate of the measured increase in the E^* values with increased air void levels, with a few noted exceptions. Additional considerations of the polymer modified binder aged in the mixtures suggested a much more systematic variation as a result of the air void level. These mixtures demonstrated a clear separation in not only the magnitude of the measured E^* values, but also a reduction in the rate of the measured increase in the E^* values under these aging conditions with increased air void levels. In other words, the higher the air void level of the mixture during aging, the slower the rate of increase in the overall measured E^* values.

Interpretation of these findings suggests that the physical quantity of material in a given cross-sectional area of a given mixture will have a profound influence on the sensitivity of the mixture to binder oxidation. The expectation is that higher the air void level, the higher the expected exposure to oxidation and thus the higher the rate of stiffening within the mixture. However, as supported by these results, the lower quantity of air voids in the 4% air void mixture makes the overall mixture more sensitive to changes in the binder stiffness. Conversely, the increased air void area in a given cross of a mixture with higher air voids quickly overshadows the increased oxidation and stiffness of the binder (i.e. almost no stiffness in the air void itself). There is merely less binder and more air in the bulk measure in the mixture at higher air void levels. Further discussion of this issue will be considered following the UTSST discussion to that those results may be included as well.

Consideration of the rate of increase for the stiffness of the mixtures (i.e. E^*) in section 9.1.5 presented a summary of the overall stiffening rate of the mixtures relative to one another. In this format, it is clearly shown that for nearly all the evaluated mixtures, the rate of increase in the E^* values decreases with increased air void levels under isothermal aging conditions. It is further determined that the magnitude of the rates were fairly similar for both aging temperatures with the mixtures containing the modified binders. Further it was noted that the mixture characteristics may potentially influence the oxidation and subsequent stiffening of the mixtures. Clearly, the level of air voids or density of the mixture are expected to influence the overall stiffening of the mixtures as a function of oxidation, however the rate of the oxidation growth cannot be ignored in such considerations. The increased rate of oxidation of the mixtures with higher air voids may offset the reduced sensitivity of the measured E^* values as a function of oxidation, however the net effect of these two behaviors is expected to depend upon the actual aging conditions (i.e. not isothermal for pavements in the field).

Rather inconsistent findings were observed on the measured E^* values due to the different oxidation temperature as determined by two mixtures; one with an unmodified and one with the SBS modified binder with different aggregate sources. For the majority of the aging conditions, the higher aging temperature increased the oxidation level of the mixtures. When the measured E^* values were considered as a function of the oxidation level (i.e. carbonyl measurements) rather than a time or duration scale, the results were not as consistent nor the deviations readily explained. Due to the complex interactions between the increased oxidation rates and the reduced sensitively noted with increased air void levels, it is not clear what the overall effect the mixture density will have on the

measured E^* values under non-isothermal aging conditions such as the exposure conditions expected in the field.

In summary, the air void level of the mixtures was found to have a profound influence on the thermal stress induced within the mixtures which led to a substantial decrease in the UTSST modulus values at colder temperatures for mixtures with higher air void levels. The effect was not as substantial with the temperatures of the thermo-viscoelastic properties. However, three of the four mixtures generally indicated increased crack initiation temperatures as well as increased oxidation measures within the same mixtures due to increased air void levels.

The UTSST measures presented in section 9.2.2 indicated that the effect of the air void level was also very prevalent within each of the mixtures. In each respective mixture, at each aging level observed, there was a clear separation with the 4% air void level indicating the highest UTSST modulus values, the 11% air void presenting the lowest measures, with the 7% air void level fell in between. With almost all of the mixtures, the short-term aged zero month specimens with 11% air voids exhibited UTSST modulus values less than the 4% air void specimens after the long-term aging duration despite the oxidation values being nearly double the short-term aged specimens. After the long-term aging, the distinction between the UTSST modulus values was still substantial within each respective mixture. Similar to the E^* ananlysis, the long-term aged mixtures with the 11% air void level showed rather substantial deviation from all the other mixtures.

However, the overall behavior of the mixtures in terms of the UTSST measures at different temperatures indicated a general increase in the stiffness of the mixtures with a

corresponding increase in the brittle components of the binder. The increased brittleness of the mixtures was generally exhibited in the lower temperature ranges of the material characterization (i.e. UTSST modulus relationship) at temperatures where the thermal cracking potential is examined. Some differences were observed between the overall behavior of the unmodified binder compared to the modified, particularly with regard to the development of the brittle behavior corresponding to the level of oxidation measured in the respective mixtures. The evaluation of the influence of the aging temperature noted discrepancies between the UTSST measurements and the determined oxidation level (i.e. CAg measures). However, these results were logically considered to be in support of the differential observations with aging temperature noted in the hardening susceptibility measures presented in section 7.1.6. Both of these evaluations suggested that sometimes increases in the aging temperature may lead to increased brittleness in the binder which may not always be quantified in every evaluation method. Thus, the overall behavior of the mixtures in terms of the UTSST measures at different temperatures indicates a general increase in the stiffness of the mixtures with a corresponding increase in the brittle components of the binder. The increased brittleness of the mixtures was generally exhibited in the lower temperature ranges of the material characterization (i.e. UTSST modulus relationship) at temperatures where the thermal cracking potential is examined. Some differences were observed between the inherent behavior of the unmodified binder compared to the modified binder, particularly with regard to the development of brittleness in the mixtures corresponding to increased levels of oxidation measured in the respective mixtures.

The relative increase in stiffness noted in the E^* measures accompanied with the increased brittleness in the UTSST measures again suggests that the physical quantity of material in a given cross-sectional area of a given mixture will have a profound influence on the sensitivity of the mixture to binder oxidation. As supported by these results, the lower quantity of air voids in the 4% air void mixture makes the overall mixture more sensitive to changes in the binder stiffness. Conversely, the increased air void area in a given cross of a mixture with higher air voids quickly overshadows the increased oxidation and stiffness of the binder (i.e. almost no stiffness in the air void itself). There is merely less binder and more air in the bulk measure in the mixture at higher air void levels. The increased exposure to oxidation attributable to the higher air void level and thus the higher the rate of stiffening within the mixture which was partially exhibited in the UTSST measurements. However, the E^* results indicated nearly the the opposite effect with substantial deviations from the preceding influence on the material behavior with lesser aging conditions.

There are two potential explanations to account for the influence of the air void levels on the results just discussed. The first possible explanation can be summarized by considering the physical nature of the cross-sectional area of the mixtures. It is understood that the lower the air void level, the more tightly pack the aggregate structure and thus the overall mixture (i.e. the less air voids present the more physical material in a given area) provided the other properties of the mixture remain constant (i.e. binder content, aggregate gradation, etc.). As this asphalt binder stiffens with oxidation, the sheer amount of material throughout the specimen can have a substantial influence on the overall stiffness of the conglomerate mixture. In other words, a slight increase in the

oxidation of the 4% air void mixture will ultimately cause a greater net increase in the mixture stiffness compared to an 11% air void mixture, despite the higher oxidation level of the less dense mixture. Essentially, the increased oxidation of the binder itself was not sufficiently large to overcome the reduction in the stiffness due to the large volume of air voids found within a given test specimen of higher air void levels.

This explanation is somewhat supported by the previous evaluation of the mixture aged asphalt binders. The kinetics evaluation of section 7.2.2 demonstrated the increased level of oxidation with increased air void levels of the mixture-aged binders over the same aging conditions. However, the hardening susceptibility plots discussed in section 7.4.2 indicated that the overall HS relationship of the mixture-aged binders was largely independent of the air void level, though the air void level did influence where on the relationship a particular aging condition would be present. Thus the reduced oxidation of the lower air void level mixtures were ultimately more influential than the higher rate of oxidation with the higher air void levels on the measured E^* values of the mixtures in this analysis.

Further, this explanation does not fully account for the clear changes in the upper asymptote of the E^* master curves noted with the mixtures aged for 3 month at 85°C. If this were the true cause of the deviation in behavior, the upper asymptote should not have been reduced, at least not to such an extent. Therefore, there should theoretically be some additional mechanism causing the drastic change in the material properties measured in both the E^* and UTSST measures. Caution is advised when considering such boundaries in the E^*as the potential for extrapolation of the data beyond the measurements can unintentionally occur if such situations are not specifically monitored.

The second potential explanation for these results stems from the physical application of the kinetics modeling methodology. Specifically, the rate of oxidation reactions as were conducted here are typically either limited by the oxygen availability (i.e. oxygen deprivation slowing the reaction) or by the rate of diffusion of oxygen through the binder into the interior of the film thickness. Thus generally making the oxidation reaction either oxygen limited or diffusion limited, for simplicity sake. Without a detailed experimental evaluation designed specifically for one case or the other, it is quite difficult to determine which is aspect is actually controlling the oxidation reaction and thus the aging of the binder. Therefore, without being able to clearly interpret which is the limiting factor in the aging of any of the evaluated mixtures, it becomes distinctly possible that 4 and 11% air void cases may be controlled by different mechanisms, but it cannot be stated for certain either way.

Without specific measures focusing on this aspect, it cannot be determined for sure which is the controlling condition for a given mixture. However, it is important to note that the CA measures and the HS determinations were conducted on extracted and recovered binders from the respective aged mixtures. Evidence was provided in section 3.3 indicating that the actual extraction a recovery procedure was expected not to have a significant influence on these measures, either the chemical structure measured with the FT-IR or the rheological measures on the DSR. However, it most certainly out of necessity blends all of the extracted binder together, thus eliminating the inherent separation of the layers required to evaluate partial penetration or diffusion limitations within the asphalt binder layer itself.

With all of that included in the consideration, it is feasible that the 11% air void mixtures effectively have full oxygen exposure at the interface of a given air void and the asphalt binder film. This may potentially enable the very outer surface of the air void to oxidize at a rapid rate, nearly the same as the pan-aged binders. This rapid oxidation at the surface could potentially create a very stiff boundary which would in turn substantially decrease the rate of oxygen diffusion to the interior of the binder film. This oxidized barrier would serve to essentially protect the interior of the binder film and reduce the level of oxygen exposure; effectively creating diffusion limited system. During the extraction and recover process, nearly all the binder was blended together in the solution, thus yielding the increased CA growth as was observed in section 7.2.2. However, when the binder remained within the mixture, the relatively lesser aged binder would be located between the aggregate particles away from the air voids (i.e. at the aggregate contact points), thereby producing a reduced stiffening effect from the mixture testing (i.e. measured E^* values).

Initially, this suggested occurrence may seem to directly contradict the findings of the pan-aged binders where full exposure is nearly completely assured. However, there is a significant difference in the area of the exposed surface of the pan-aged binders compared to those surrounding the pore (i.e. air void) and binder interface. Considering the cylindrical coordinate system discussed in the methodology section, the surface area of the inner surface of a pore is substantially smaller than that of a fully exposed pan-aged geometry. Therefore on a surface to volume comparative basis, the cylindrical pore system has a significant reduction in the surface area of the exposed surface compared to the volume of binder into which the oxygen would diffuse. Essentially, the concentration

of the oxygen would be far greater at the pore interface compared to the surface area of a fully exposed pan-aged binder sample.

In the case of the 4% air void mixtures, it is conceivable that a quite different set of circumstances is controlling the reaction. Possibly, the replenishment of the oxygen within the pore space of the mixture would not be as fast or complete, thus depleting the overall quantity of available oxygen at the air void (i.e. pore) interface. This would directly decrease the oxidation level at the very interface, which in turn would permit the diffusion rate at that location to remain comparatively higher than the aged and stiffened interface with the 11% air void mixture. Although the overall oxygen level would be reduced, the amount of oxygen that was available would more readily diffuse into the interior regions of the asphalt binder film. In such an environment, the interior of the binder, such as would be present at the aggregate contact points would be at higher oxidation level than the so called protected binder mentioned with the 11% air void mixtures. Possibly, the combined effect of the increased quantity material (i.e. more mixture per cross sectional area due to reduced air void levels) and only minor increases in the oxidation of the binder would result in the higher rate of oxidation with the lower air void levels on the measured E^* values of the mixtures.

Again, validation of these potential explanations of the oxidation rates based upon the air voids in the aged mixtures would require a more focused investigation of these mixtures as well as the specific evaluation of the oxidation level at various locations within a given asphalt binder film. It is highly likely that some combination of the two interactions are responsible for the observed behaviors of the majority of the mixtures evaluated in this study. By similar logic, the aging rate of the 7% air void samples may

potentially be the combined effect of both influences, each to their own relative extent as dictated by the actual conditions controlling the oxidation rate (i.e. either diffusion limitations or oxygen supply starvation).

When these potential explanations are carried over to the UTSST results, the diffusion limited circumstances continue to increase in potential validity. Whether these behaviors are the product of the aging condition, some level of damage or cracking within the structure of the mixture, or some other cause has yet to be determined for these materials and will be recommended for additional evaluation as part of that relevant section of chapter 11. It is possible that an evaluation of the aggregate structure of these mixtures (e.g. two-dimensional imaging analysis of the aggregate orientation, x-ray or CT scans, etc.) may provide some useful justification for the observed behavior of the 11% air void mixtures aged for three months at 85°C. It is logical that some common unknown factor may explain these uncharacteristic behaviors. It is odd that even though the prior aging conditions did not yield the same response to aging between the two mixtures, this particular aging condition gave almost the same response.

Without further investigation it is difficult to decipher, however it is possible that perhaps the binders in these particular mixtures became so aged that they exhibited micro cracks and were thus damaged yielding the much reduced E^* measures noted. This type of cracking was noted with some initial pan-aged binder samples that were aged at 135°C and a few at lower temperatures. To be clear, the majority of the pan-aged binders did not exhibit this type of surface distortion, but a few examples were observed as indicated in the figure. It is fairly evident that there may be some differential aging on the very

exterior surface of this sample, to such an extent that it has physically separated and formed several cracks in the surface.

As an example, Figure 10.1 presents one of the pan-aged binder samples of the PG64-28 asphalt binder that had been aged for 60 days at 50°C that was noted to exhibit the surface cracking during the oxidation process.

Figure 10.1 Example of Cracked Pan-Aged PG64-28 Binder Aged at 50°C for 60 days

The damage was not evident in the testing of the pan-aged materials presumably due to the annealing effect during the heating and remolding processes required for the FT-IR and DSR measurements. However, if this type of damage occurred along the interface between the air void and the binder, it would readily create a stress concentration

sufficient to produce micro cracks very easily. At either range of the physical scale, such damage could readily create weak points that would influence the mechanical measures such as the E* stiffness and certainly the thermal contraction behaviors evaluated in the UTSST measurements.

Further, both the E^* and the UTSST specimens were specifically not annealed or heated above ambient temperature in any way prior to the testing process. In fact, they were kept at colder temperatures (i.e. -18°C), which very well may have increased the amount of damage to these particular specimens prior to testing. Therefore, their influence on the overall behavior of the mixtures at the other aged conditions should be tentatively accepted until further evaluation reveals the underlying cause of these behaviors.

10.4 Concluding Remarks

Over the course of this research effort exploring the influence on many factors on the oxidative aging of asphalt binders, it has become increasingly clear that many of the mechanisms dictating the overall response of asphalt mixtures in service are not very thoroughly understood. Certain aspects have been well studies and the pavement industry is more mature in the comprehension of the material behaviors and physical interactions which may be taking place within the pavement structure.

However, there are certainly many more complex interactions that are not as well understood and are far from being implemented in any sort of practical application. This

is not to state that every piece of fundamental knowledge must be implemented at the level of the practitioner, but the technology and comprehension of such topics should aim to support and further the industry in an effort to better understand the materials and the complex interactions with each other, their environment, the service loads they are subjected to all the while considering the duration of the in-service lifespan of the pavement itself. Neglecting the time component and evaluating material properties at a single or few stages in the overall lifespan of the material, would necessarily force the design and evaluation process to be fully blind to potentially significant components of the overall evaluation effort.

This study has presented indications of substantial material specific behaviors of asphalt binders, that when coupled with complex interactions between the aggregate and the aging environment often produced substantial effects that dramatically influence the performance measured on a given mixture. Certain aspects of these behaviors are fairly well understood, while others have observed even more inexplicable characteristics.

However, this study should if nothing else, establish that many of the performance characteristics that would ultimately dictate the in-service performance of a pavement section may most certainly not be assessed by the individual components alone. The asphalt mixture itself is a complex network of materials, each with their own physical properties that may readily interact with each other on the physical and chemical level to alter the overall performance of the parent materials. As such, assessment of such complicated systems should be evaluated in a careful and comprehensive manner.

11 ADDITIONAL CONSIDERATIONS

The following sections provide further information regarding the several aspects of this study that were not fully developed in the current evaluation. Many of these topics are areas of potential further research that were considered to be points of interest over the duration of this study. Some are concerned with further exploration aimed to fully comprehend and understand inexplicable findings in this study. Additional subjects are merely the next step in this line of research as would appear to be the logical direction based upon the efforts presented previously in this manuscript.

It is fully recognized that there are many ways to analyze the data presented here and by no means should this analysis considered a complete or exhaustive analysis. It is quite clear that many other considerations and evaluation methods applied to this information could be useful and thus warranted. However, specific suggestions are considered in the following sections.

11.1 Asphalt Binder Types

Clearly, the results and conclusions from this study were drawn based upon a limited number of aggregates sources and asphalt binders. Specifically, the main binders used for the mixture aging portion of the evaluations were the PG 64-22 and the PG 64-28, which were both quite similar so far as the base asphalt binder composition was concerned. The main difference between the two centered around the PG 64-28 being

modified by less than 3% Styrene-butadiene-styrene (SBS) polymer. This is not to say that the PG64-22 binder was the base material that was modified to make the PG 64-28 binder, but they contained the same base asphalts originally.

Therefore, the conclusions drawn from this study should be understood to apply with similar materials. It is possible that some of the many measurements conducted here and thus the conclusions drawn from them may very well result in substantially different behaviors with different materials (e.g. crude oil or aggregate sources). This potential stems from possible differences in unmodified or neat binders with differences in the chemical or compositional makeup, to any adjustment or alternate treatment of the binder. These treatments may include aspects such as polyphosphoric acid (PPA) treatment, simple differences in the polymer materials (e.g. ethylene-vinyl acetate (EVA), styrene butadiene rubber (SBR) latex, or other rubber products, etc.), to any number of the warm mix additives that are becoming more commonplace in the industry.

Thus, any adjustments such as these which may potentially have a significant influence on aging or oxidation performance of the mixtures should have at least initial or simplified evaluations completed to determine similar behaviors to those evaluated here or if significant changes may be present due to any number of the material specific behaviors that have been observed.

11.2 Relationship between Binder Kinetics Parameters

It was originally observed by Dr. Charles Glover and his group at Texas A&M University that a correlation existed between the binders kinetics parameters (i.e. E_a and AP^{α}) as was also observed with the current dataset. In the current state of practice, this correlation is not overly useful since the methodology utilized to determine one parameter directly provides the other. However, further investigation into the correlation between the activation energy and the pre-exponential terms may prove fruitful if alternative methods to determine the activation energy can be identified. As an initial starting point, it has been considered that the Arrhenius shift factors or other measured parameter of similar form may be a potential avenue for exploration in this matter.

As an alternative to replacing the testing methods, accelerated aging methods compared to the current oven aging procedures that would permit the aging and determination of the kinetics parameters in a more time efficient manner. It is understood that there currently may be a select few newly proposed methods that have yet to be proven robust enough for common usage. These are generally to increase either the aging temperature or the pressure for the duration of the oxidation process. However, these new methods should be carefully considered noting the distinct differences in the chemical species that have been identified in such accelerated aging schemes, such as the current pressure aging vessel (PAV) methodology.

11.3 Rheology Measures as a Function of Aging Temperature

Over the course of this investigation, it was observed that the hardening susceptibility (HS) was found to be temperature dependent for some asphalt binders, but not others. As mentioned with the PAV aging in the previous section, there have been measurable differences observed in the chemical structure of the oxidation products due to artificially high aging temperatures. Therefore, it stands to reason that perhaps similar deviations would potentially lead to the discrepancies observed in the rheological measures which were used to develop the HS parameters. If the true mechanism dictating the which binders are temperature dependent and which are not can be identified, the industry would gain a much better understanding of the overall physiochemical interactions leading to the micromechanical material characterization of asphalt materials that have also been researched elsewhere. Ideally, a phenomenological relationship should be possible; however, more in-depth analysis and characterization will be the initiation point of such evaluations.

Relationships such as these would be a great asset in efforts to develop abbreviated aging procedure for kinetics and HS determinations. Proposed methods have included additional cycles of RTFO or PAV aging, at times under different conditions (i.e. temperatures and pressures). However, significant deviation from ambient pressures and in-services temperatures should be utilized with caution until the influence of such variations on the resulting kinetics and HS parameters are fully understood.

11.4 Alternative Forms of Hardening Susceptibility Determinations

The hardening susceptibility parameters in this study were determined utilizing the low shear viscosity (LSV) concept, which is slightly different from true zero shear viscosity (ZSV) measures, but they are similar. The procedure, which is described in more detail in the methodology section, was based upon the development of full dynamic shear modulus (G^*) master curves which were converted to the complex viscosity (η^*). The LSV value was selected as the plateau of the η^* curve, which numerically was selected at the set frequency of 0.001 rad/s. Each of the developed master curves required a considerable amount of testing time, essentially one half to a full day of DSR testing depending upon the binder grade. It would be very advantageous to reduce the required testing time necessary to make these determinations. To this end, Dr. Charles Glover and his group at Texas A&M University have utilized a parameter known as the DSR function, which is of the form of Equation 11.1 (Ruan, et al. 2003).

$$DSRFn = \frac{G'}{\left(\eta'/_{G'}\right)} \qquad \textbf{Equation 11.1}$$

where, G' - dynamic shear storage modulus;
η' - viscous component of dynamic viscosity.

This function was also reformatted, but with additional rheological considerations, to the form of Equation 11.2 which is a format that more readily permits consideration in the black space representation and also presents the more commonly used inputs of G8 and delta (Rowe, 2011).

$$DSRFn_{GR} = G^{*}\omega\left(\cos^{2}\delta / \sin\delta\right) \qquad \textbf{Equation 11.2}$$

where, $DSRFn_{GR}$ – DST function as the Glover-Rowe parameter
G* - complex dynamic shear modulus;
ω - angular frequency;
δ - phase angle.

The so called Glover-Rowe parameter or DSR function has been linked to ductility and other brittleness indications particularly fatigue related distresses. Therefore, it is suggested that these types of parameters also be considered to accompany other performance measures such as the UTSST measures to investigate the low-temperature characterization of asphalt mixtures. However, a substantial portion of additional work on these types of measures should initially be compared to the more traditional measurements used to evaluate the HS of the binders, to evaluate the potential for systematic variations or offsets between the measurement systems. Particularly when the kinetics and HS parameters are utilized in oxidation modeling efforts any deviation on the input parameters will have to be evaluated on a case by case basis.

11.5 Normalized Binder Kinetics and Hardening Susceptibility Measures

It was considered, but not fully developed as part of this research effort; to normalize the mixture-aged binder kinetics and HS parameters to the values of the measured pan-aged binders as the standard of practice. This is expected to be beneficial to the use of this information from the oxidation modeling standpoint. The current models and calculation forms fit the data input produced solely from binder oxidation studies. As an example, it is not clear whether the effect of the mixture air void level should be represented purely through adjustment to the kinetics and HS parameters or if the overall diffusion model would require modification as well. Thus, as an interim evaluation the diffusion model could be left unmodified and the kinetics parameters could be adjusted by simple factors (e.g. the kinetics relationship (k_C) can be multiplied by a factor, say 0.9, and leave the HS unchanged). Hpoweever, this type of adjustment will necessarily require more in-depth analysis of the overall oxidation models than has been conducted in this effort. Therefore, such evaluations have been excluded from this manuscript.

11.6 Aggregate Selection

During the initial planning stages of this research, it was not completely evident what characteristics would prove the most influential to the oxidation parameters being investigated. Over the course of this study, it has become apparent that the particular aggregates selected may not have provided the most statistically powerful range of

material characteristics in terms of the mineralogical and thus the chemical makeup of the aggregate sources, especially when considering the usage of silica sand in several of the mixtures.

As such, it may prove useful to partially investigate additional aggregates with a more focused emphasis on the actual mineral makeup of the aggregate sources. The aggregate sources utilized thus far, were selected to provide a range of sources available throughout the intermountain region of the western United States. Specifically, it appears that the overall silica content (SiO_2) and to a lesser extent the calcium content (CaO) as compared to lower proportions of either chemical group may significantly add to the overall comprehension of the complex interaction between the asphalt binder and the mineral aggregates within a mixture during the oxidation process.

As part of the analyses of the findings presented here, it has been discussed to conduct a full elemental analysis of each of the current aggregate sources to provide a more thorough characterization of the chemical makeup of the material. This would permit the actual quantification of the total silica content and other elements as opposed to the estimation procedure based upon the quantity of certain stockpiles with certain petrographic characterizations.

Another approach to obtain similar information would be to conduct the modified SARA analysis to determine if that may be an effective surrogate for the actual elemental analysis. From the current results, it appears that the modified SARA analysis may provide the effective or apparent interaction between the binder and a given aggregate blend. However, this would be understood to measure the effects of the interaction and would not necessarily provide the fundamental understanding of the specific chemical

interactions were actually taking place. Nevertheless, useable information particularly when considering the relative difference between proposed aggregate and asphalt binder combinations relative to their interactions with one another.

11.7 Quantification of UTSST Brittleness

During the evaluation of the UTSST results, particularly in the lower temperature ranges of the calculated modulus relationships, it was not always completely clear whether or not a lower modulus value was due to a softer material or if it were due to a more brittle material exhibiting some degree of damage or micro cracking thus representing an effective or some type of damaged modulus value. Nevertheless, there were clear distinctions between the various factors being evaluated especially oxidative aging. However, further investigation very well may prove beneficial in the interpretation between apparent softer materials compared to the damaged response of more brittle materials as they undergo thermal loading throughout the test. Presumably, the direct quantification of the damage developed within the mixture will permit the clear distinction between the two characteristic material behaviors.

11.8 Model for UTSST Modulus Relationship

In the current methodology, the UTSST modulus relationship as a function of thermal load (i.e. temperature) does not have a phenomenological or even a robust model form that it can be fitted to. Currently, the overall relationship is fit to a polynomial function, which can be fitted to the data quite nicely, but otherwise provides little in terms of additional information such as meaningful parameters that may be used to characterize the behavior (e.g. 2S2P1D parameters or even the sigmoidal function parameters). If a more appropriate and ideally phenomenological relationship can be developed, interpretation of the material behavior and specifically changes to the behavior can be readily observed. Such models would directly lend to the possibility of three-dimensional plots of the UTSST modulus as a function and temperature, which could be readily shifted as a function of aging (i.e. carbonyl or other similar measures). This capability could directly be utilized in mechanistic evaluations and predictive modeling of the thermal cracking performance of asphalt mixtures.

As an initial suggestion, the form of the Kaelble shift function presents a similar form to that observed in the UTSST modulus. Although, the Kaelble function does not include enough input parameters to appropriately define all of the inflection points noted in the UTSST modulus. However, a review of the development of the Kaelble function indicated that the difference between the original Williams-Landel-Ferry (WLF) shift function and the modified Kaelble function was primarily the additional of another parameter to define the additional inflection point observed in some low temperature shifting relationships. Therefore, it stands to reason that potentially another input

parameter could be added to the appropriate location within the Kaelble function to properly address the three inflection points observed in the UTSST modulus relationship. If not the Kaelble function, then some other appropriate model form may be determined through appropriate efforts.

11.9 Field Validation

Given that this entire investigation was focused primarily on laboratory prepared mixtures and laboratory aged binders. Granted some mixtures and binders were included to prepare for field validation efforts, the evaluation of the field samples (i.e. cores) have not been evaluated to date. This validation should initially include the suggested modifications to the oxidation properties due to the influence of the mixture characteristics and the associated predictive modeling efforts. Provided the appropriate field sections may be identified, there remains a substantial amount of validation work to be done in regards to the oxidation of in-service pavements. The laboratory aging utilized in this study produced some highly oxidized asphalt binders, both from the mixture-aged and pan-aged evaluations. Further efforts should investigate whether or not these oxidation levels can reasonably be expected under practical in-service conditions. Depending on those findings, verification of the similarities between the physical and chemical properties of the field-aged and accelerated laboratory-aged asphalt binders and mixtures becomes of critical interest.

Clearly, further validation efforts should focus on the measured UTSST modulus relationships and the associated thermo-viscoelastic properties seeking to develop correlations and logical explanations of observed in-service thermal cracking performance of asphalt mixtures. The UTSST methodology presents a great deal more information with regard to the low temperature behavior and properties of asphalt mixtures compared to previously available evaluation methods. However, complicated data matrices do not always contribute to a better understanding of the material. But in the case of the UTSST measures, this study has shown that the subtle and inherent changes that occur in asphalt mixtures during their in-service lifetime can be readily quantified. What remains to be developed is to quantitatively identify the specific properties that control the thermal cracking performance of mixtures in actual pavement sections. Once this association is established, then the method may readily be used to assess and ultimately enhance the design of asphalt mixtures specifically in terms of the thermal cracking resistance of the mixture.

12 REFERENCES

AASHTO, 1995. Provisional Test Method, *Standard Specifications for Transportation Materials and Methods of Sampling and Testing*, 15nd Edition, American Association of State Highway and Transportation Officials, Washington D.C., 20001.

AASHTO, 2006. *Standard Specifications for Transportation Materials and Methods of Sampling and Testing*, 26th Edition, American Association of State Highway and Transportation Officials, Washington D.C., 20001.

AASHTO, 2012. *Standard Specifications for Transportation Materials and Methods of Sampling and Testing*, 32nd Edition, American Association of State Highway and Transportation Officials, Washington D.C., 20001.

AASHTO, 2013. *Standard Specifications for Transportation Materials and Methods of Sampling and Testing*, 33rd Edition, American Association of State Highway and Transportation Officials, Washington D.C., 20001.

AASHTOWare, 2013. AASHTOWare Pavement ME Design, American Association of State Highway and Transportation Officials, Washington D.C.

Abu-Elgheit et al., 1960. M.A. Abu-Elgheit, C.K. Hancock, and R.N. Traxler, *Effect of Selected Solvent on the Viscosities and Oxygen Contents of Asphalts,* Analytical Chemistry, Vol. 41, No.6, American Chemical Society.

AbWahab, et al., 1993. Y. AbWahab, D. Sosnovske, C.A. Bell, P. Ryus, *Evaluation of Asphalt-Aggregate Mixture Aging by Dynamic Mechanical Analysis*, In Transportation Research Record: Journal of the Transportation Research Board, No. 1386, Transportation Research Board of the National Academies, Washington D.C.

Airey and Brown, 1998. Gordon D. Airey and Stephen F. Brown, *Rheological Performance of Aged Polymer Modified Bitumens*, Journal of the Association of Asphalt Paving Technologists, AAPT, Vol. 67, Ann Arbor, Michigan.

Al-Azri et al., 2006. Nasser Al-Azri, Sung Hoon Jung, Kevin M. Lunsford, Ann Ferry, Jerry A. Bullin, Richard R. Davison, and Charles J. Glover, *Binder Oxidative Aging in Texas Pavements; Hardening Rates, Hardening Susceptibilities, and Impact of Pavement Depth*, In Transportation Research Record: Journal of the Transportation Research Board, No. 1962, Transportation Research Board of the National Academies, Washington D.C.

Alavi and Hajj, 2014. Mohammad Zia Alavi and Elie Y. Hajj, *Effect of Cooling Rate on the Thermo-Volumetric, Thermo-Viscoelastic, and Fracture Properties of Asphalt Mixtures*, In Press, Proceeding of International Society for Asphalt Pavements, ISAP 2014, Raleigh, North Carolina, June 1-5.

Alavi et al., 2013. Mohammad Zia Alavi, Elie Y. Hajj, Nathan E. Morian, Peter E. Sebaaly, *Low Temperature Characterization of Asphalt Mixtures by Measuring Visco-elastic Properties Under Thermal Loading*, 10th International Symposium on Cold Regions Development, ISCORD 2013: Planning for Sustainable Cold Regions, American Society of Civil Engineers (ASCE).

Alavi et al., 2014. Mohammad Zia Alavi, Mohammad Reza Pouranian, and Elie Y. Hajj, *Prediction of Asphalt Pavement Temperature Profile Using the Finite Control Volume Method (FCVM)*, In Transportation Research Record: Journal of the Transportation Research Board, In Press, Transportation Research Board of the National Academies, Washington D.C.

Anderson et al., 2002. David A. Anderson, Yann M. Le Hir, Jean-Pascal Planche, Didier Martin, *Zero Shear Viscosity of Asphalt Binders*, In Transportation Research Record: Journal of the Transportation Research Board, No. 1810, Transportation Research Board of the National Academies, Washington D.C.

ARA, 2004. Applied Research Associates, Inc., ERES Consultants Division, *Guide for Mechanistic-Empirical Design of New and Rehabilitated Pavement Structures*, Final Report, National Cooperative Highway Research Program Project 1-37A, Transportation Research Board, Washington, D.C.

Arnold et al., 2006. Terry Arnold, Muriel Rozario-Ranasinghe, and Jack Youtcheff, *Determination of Lime in Hot-Mix Asphalt*, Transportation Research Record No. 1962, Transportation Research Board, Washington, D.C.

ASTM, 2010. American Society for Testing and Materials, ASTM International, West Conshohocken, New Jersey.

Bell, 1989. C.A. Bell, *Summary Report on Aging of Asphalt-Aggregate Systems*, Strategic Highway Research Program Report A-305, SR,-OCU-A-003A-89-2, National Research Council, Washington, D.C.

Bell et al., 1994. C.A. Bell, Y. AbWahab, M.E. Cristi, D. Sosnovske, *Selection of Laboratory Aging Procedures for Asphalt-Aggregate Mixtures*, SHRP-A-383, Strategic Highway Research Program, National Research Council, Washington, D.C.

Bell and Sosnovske, 1994. C.A. Bell , D. Sosnovske, *Aging: Binder Validation*, SHRP-A-384, Strategic Highway Research Program, National Research Council, Washington, D.C.

Biro et al., 2008. Szabolcs Biro, Tejash Gandhi, and Serji Amirkhanian, *Determination of zero shear viscosity of warm asphalt binders*, Construction and Building Materials, Vol. 23, Elsevier Ltd.

Bolzan and Huber, 1993. Pablo E. Bolzan and Gerald Huber, *Direct Tension Experiments*, SHRP Report A-641, Strategic Highway Research Program, National Research Council, Washington, D.C.

Bonaquist et al., 2003. Ramon F. Bonaquist, Donald W. Christensen, and William Stump III, *Simple Performance Tester for Superpave Mix Design: First-Article Development and Evaluation*, National Cooperative Highway Research Program, NCHRP Report 513, Transportation Research Board, Washington, D.C.

Burr et al., 1990. Barry L. Burr, Richard R. Davison, Charles J. Glover, and Jerry A. Bullin, *Solvent Removal from Asphalt*, in Transportation Research Record No. 1269, Transportation Research Board, Washington, D.C.

Burr et al., 1991. Barry L. Burr, Richard R. Davison, Howard B. Jemison, Charles J. Glover, and Jerry A. Bullin, *Asphalt Hardening in Extraction Solvents*, in Transportation Research Record No. 1323, Asphalt Mix Materials, Transportation Research Board, Washington, D.C.

Chari, 1988. Commandur T. Chari, *Evaluation of Age Hardening on the Characteristics of Asphalts and Mixtures*, Ph.D. Dissertation, University of Florida.

Christensen, 2003. Richard M. Christensen, *Theory of Viscoelasticity*, Second Edition, Dover Publication Inc., Mineola, New York.

Christensen et al., 2003. Donald W. Christensen, Terhi. K. Pellinen, Ramon F. Bonaquist, *Hirsch Model for Estimating the Modulus of Asphalt Concrete*, Journal of the Association of Asphalt Paving Technologists, Volume 72.

Christensen, 2010. Donald W. Christensen, *A Manual for the Design of Hot Mix Asphalt with Commentary*, NCHRP Report 673, National Cooperative Highway Research Program, Washington, D.C.,

Christensen and Anderson, 1992. Donald W. Christensen and David A. Anderson, *Interpretation of Dynamic Mechanical Test Data for Paving Grade Asphalt Cements*, Journal of the Association of Asphalt Paving Technologists, Vol. 61, Ann Arbor, Michigan.

Christensen and Bonaquist, 2004. Donald W. Christensen and Ramon F. Bonaquist, *Evaluation of Indirect Tensile Test (IDT) Procedures for Low-Temperature Performance of Hot Mix Asphalt*, National Cooperative Highway Research Program, NCHRP Report 530, Transportation Research Board, Washington, D.C.

Cipione et al., 1991. Charles A. Cipione, Richard R. Davison, Barry L. Burr, Charles J. Glover, and Jerry A. Bullin, *Evaluation of Solvents for Extraction of Residual Asphalt from Aggregates*, in Transportation Research Record No. 1323, Asphalt Mix Materials, Transportation Research Board, Washington, D.C.

Coates, 2000. John Coates, *Interpretation of Infrared Spectra, A Practical Approach*, In Encyclopedia of Analytical Chemistry, John Wiley & Sons Ltd, Chichester, United Kingdom.

Corbett, 1969. L. W. Corbett, *Composition of Asphalt Based on Generic Fractionation, Using Solvent Deasphaltening, Elution-Adsorption Chromatography, and Densimetric Characterization*, Analytical Chemistry, Vol. 41, No 4.

Corbett and Petrossi, 1978. L.W. Corbett and U. Petrossi, *Differences in Distillation and Solvent Separated Asphalt Residua*, Industrial & Engineering Chemistry Product Research and Development, Vol. 17 No. 4.

Cortez et al., 2011. Edward M. Cortez,, Elie Y. Hajj, S.M. Zia Alavi, Peter E. Sebaaly, *Investigating Low-Temperature Properties of Cylindrical Superpave Gyratory – Compacted Asphalt Concrete Specimens Using the TSRST*, poster presentation 11-2631, 90th Annual Meeting of the Transportation Research Board, Washington D.C.

Dave, 2009. Eshan V. Dave. *Asphalt Pavement Aging and Temperature Dependent Properties Using Functionally Graded Viscoelastic Model*, Doctoral Dissertation, University of Illinois at Urbana-Champaign.

Demange, 2012. Michel Demange, *Mineralogy for Petrologists, Optics, Chemistry, and Occurrences of Rock-Forming Minerals*, CRC Press, Taylor & Francis Group, Ondon, UK.

Di Benedetto et al., 2004. Herve Di Benedetto, Francois Olard, Cedric Sauzeat, and Brice Delaporte, *Linear viscoelastic behaviour of bituminous materials: from binders to mixes*, Road Materials and Pavements Design, Volume 5, Special Issue, Taylor & Francis.

Elseifi et al., 2008. Mostafa A. Elseifi, Imad L. Al-Qadi, Shin-Hsien Yang, and Samuel H. Carpenter, *Validity of Asphalt Binder Film Thickness Concept in Hot-Mix Asphalt*, in Transportation Research Record No. 2057, Transportation Research Board, Washington, D.C.

Epps et al., 2002. Jon A. Epps, Adam Hand, Steve Seeds, Todd Schulz, Sirous Alavi, Colin Ashmore, Carl L. Monismith, John A Deacon, John T. Harvey, and Rita Leahy, *Recommended Performance-Related Specification for Hot-Mix Asphalt Construction: Results of the WesTrack Project*, NCHRP Report 455, Transportation Research Board, National Academies Press, Washington, D.C.

European Standard, 2012., *CSN EN 12697-46, Bituminous mixtures – Test methods for hot mix asphalt – Part 46: Low temperature cracking and properties by uniaxial tension tests*, CSN European Standards.

Farrar et at., 2012. Michael J. Farrar, William R. Grimes, Changping Sui, Jean-Pascal Planche, Shin-Che Huang, T. Fred Turner, Ronald Glaser, *Thin Film Oxidative Aging and Low Temperature Performance Grading Using Small Plate Dynamic Shear Rheometry: An Alternative to Standard RTFO, PAV, and BBR*, 5th Eurasphalt & Eurobitume Congress, Istanbul, Turkey.

Fernandez, 2003. George C.F. Fernandez, *Data Mining Using SAS Applications*, Chapman & Hall/CRC Press, Boca Raton, Florida.

Ferry, 1980. John D. Ferry, *Viscoelastic Properties of Polymers*, Third Edition, John Wiley & Sons, Inc., Hoboken, New Jersey.

Fortier and Vinson, 1998. R. Fortier, and T.S. Vinson, Low-temperature cracking and aging performance of modified asphalt concrete specimens. *Transportation Research Record*, No.1630, Transportation Research Board of the National Academies, Washington, D.C., pp. 77-86.

Glaser et al., 2012. Ronald Glaser, Jenny Loveridge, Steve Salmans, Bruce Thomas, Jerry Forney, T. Fred Turner, Jean-Pascal Planche, *WRI/FHWA Annual Progress Review, Aging Chemistry and Rheology*, January 26, 2012, Washington, D.C.

Glover and Cui, 2013. Charles J. Glover and Yuanchen Cui, *Exploring the Combined Effects of Asphalt Oxidation Kinetics, Hardening Susceptibility, Oxygen Diffusivity, Pavement Characteristics and Climate on Pavement Durability*, presentation at the 50th Annual Petersen Asphalt Research Conference, July 16, 2013, Laramie, Wyoming.

Glover et al., 2009. Charles J. Glover, Amy Epps Martin, Arif Chowdhury, Rongbin Han, Nikornpon Prapaitrakul, Xin Jin, James Lawrence, *Evaluation of Binder Aging and It's Influence in Aging of Hot Mix Asphalt Concrete: Literature Review and Experimental Design*, Report 0-6009-1, Texas Transportation Institute, College Station, Texas.

Goode and Lufsey, 1965. J. F. Goode and L.A. Lufsey, *Voids, Permeability, Film Thickness Versus Asphalt Hardening*, Journal of the Association of Asphalt Paving Technologists, Vol. 34, Ann Arbor, Michigan.

Gordon and Shaw, 1994. Glen V. Gordon and Montgomery T. Shaw, *Computer Programs for Rheologists*, Hanser – Gardner Publications.

Hajj et al., 2013. Elie Y. Hajj, Mohammad Zia Alavi, Nathan E. Morian, Peter E. Sebaaly, *Effect of Select Warm-mix Additives on Thermo-viscoelastic Properties of Asphalt Mixtures*, Road Materials and Pavement Design, Special Issue: EATA 2013, Volume 14, Supplement 1.

Han, 2011. Rongbin Han, *Improvement to a Transport Model of Asphalt Binder Oxidation in Pavements: Pavement Temperature Modeling, Oxygen Diffusivity in Asphalt Binders and Mastics, and Pavement Air Void Characterization*, Ph.D. Dissertation, Chemical Engineering Department, Texas A&M University, College Station, TX.

Hu and Zhou, 2010. Sheng Hu and Fujie Zhou, *Development of a new interconversion tool for hot mix asphalt (HMA) linear viscoelastic functions*, Canadian Journal of Civil Engineering, Volume 37, No. 8, NRC Research Press, Ottawa, Ontario.

Huang et al., 2002. Shin-Che Huang, J. Claine Petersen, Raymond E. Robertson, and Jan F. Branthaver, *Effect of Hydrated Lime on Long-Term Oxidative Aging Characteristics of Asphalt*, in Transportation Research Record No. 1810, Transportation Research Board, Washington, D.C.

Hubbard and Reeve, 1913. Prevost Hubbard and C.S. Reeve, *The Effect of Exposure on Bitumens*, The Journal of Industrial and Engineering Chemistry, ACS Publications, Washington D.C.

Huet, 1963. C. Huet. *Etude par une méthode d'impédance du comportement viscoélastique des matériaux hydrocarbonés*, Doctoral Thesis, Faculté des Sciences de l'université de Paris.

Ingham, 2010. Jeremy P. Ingham, *Geomaterials Under the Microscope, A Colour Guide*, CRC Press, Taylor & Francis Group, Boca Raton, Florida.

ISU, 2013. Idaho State University, *Thin Section Tutorial*, http://geology.isu.edu/geostac/Field_Exercise/Cassia_mtns/thinsect.html, webpage accessed Nov. 6, 2013.

Jung and Vinson, 1994. D.H. Jung and T.S. Vinson, *Low-Temperature Cracking: Test Selection*, SHRP A-400, Strategic Highway Research Program, Washington, D.C.

Kandhal and Chakraborty, 1996. Prithvi S. Kandhal and Sanjoy Chakraborty, *Effect of Asphalt Film Thickness on Short- and Long-Term Aging of Asphalt Paving Mixtures*, in Transportation Research Record No. 1535, Transportation Research Board, National Research Council, Washington, D.C.

Kanerva et al., 1994. H. Kanerva, T. S. Vinson, and H., Zeng, *Low-Temperature Cracking: Field Validation of Thermal Stress Restrained Specimen Tes*t. SHRP A-401, Strategic Highway Research Program, National Research Council, Washington D.C.

Kuehl, 2000. Robert O. Kuehl, *Design of Experiments: Statistical Principles of Research Design and Analysis*, Second Edition, Duxbury Press, Brooks/Cole Publishing Company, Pacific Grove, California.

Kumar and Goetz, 1977. A. Kumar and W.H. Goetz, *Asphalt Hardening as Affected by Film Thickness, Voids, and Permeability in Asphalt Mixtures*, Journal of the Association of Asphalt Paving Technologists, Vol. 46, Ann Arbor, Michigan.

Kutner et al., 2004. Michael H. Kutner, Christopher J. Nachtheim, and John Neter, *Applied Linear Regression Models*, Fourth Edition, McGraw-Hill/Irwin, New York, New York.

Lau et al., 1992. C.K. Lau, Kevin M. Lunsford, Charles J. Glover, Richard R Davison, Jerry A. Bullin, *Reaction Rates and Hardening Susceptibilities as Determined from Pressure Oxygen Vessel Aging of Asphalts*, in Transportation Research Record No. 1342, Transportation Research Board, National Research Council, Washington, D.C.

Lesueur and Little, 1999. Didier Lesueur and Dallas N. Little, *Effect of Hydrated Lime on Rheology, Fracture, and Aging of Bitumen*, in Transportation Research Record No. 1661, Transportation Research Board, National Research Council, Washington, D.C.

Little and Petersen, 2005. Dallas N. Little and J. Claine Petersen, *Unique Effects of Hydrated Lime Filler on the Performance-Related Properties of Asphalt Cements: Physical and Chemical Interactions Revisited*, Journal of Materials in Civil Engineering, Vol. 17(2).

Liu et al., 1998. M. Liu, M.A. Ferry, Richard R. Davison, Charles J. Glover, and Jerry A. Bullin, *Oxygen Uptake as Correlated to Carbonyl Growth in Aged Asphalts and Asphalt Corbett Fractions*, Industrial & Engineering Chemistry Product Research and Development, Vol. 37.

Lunsford, 1994. Kevin M. Lunsford, *The Effect of Temperature and Pressure on Laboratory Oxidized Asphalt Films with Comparison to Field Aging*, Ph.D. Dissertation, Department of Chemical Engineering, Texas A&M University, College Station TX.

Marasteanu and Anderson, 1999. Mihai O. Marasteanu and David A. Anderson, *Improved model for bitumen rheological characterization*, Paper No. 133, Eurobitume Workshop of Performance Related Properties for Bituminous Binder, Luxembourg.

Marasteanu et al., 2007. Mihai O. Marasteanu, Adam Zofka, Mugur Turos, Xinjun Li, Raul Velasquez, Xue, Li, William Buttlar, Glaucio Paulino, Andrew Braham, Eshan Dave, Joshua Ojo, Hussain Bahia, Christopher Williams, Jason Bausano, Allen Gallistel, and Jim McGraw, *Investigation of Low Temperature Cracking in Asphalt Pavements: National Pooled Fund Study 776*, Minnesota Department of Transportation, MN/RC 2007-43.

Martin et al., 1990. K. L Martin, Richard R. Davison, Charles J. Glover, and Jerry A. Bullin, *Asphalt Aging in Texas Roads and Test Sections*, In Transportation Research Record No. 1269, Transportation Research Board, National Research Council, Washington, D.C.

Masad et al., 1999. Eyad A. Masad, B. Muhunthan, N. Shashidhar, and Ted Harman, *Quantifying Laboratory Compaction Effects on the Internal Structure of Asphalt Concrete*," in Transportation Research Record No. 1681, Journal of the Transportation Research Board, Washington, D.C.

Mezger, 2011. Thomas G. Mezger, *The Rheology Handbook*, 3rd Revised Edition, Vincent Network, Hanover, Germany.

Microsoft, 2013. Microsoft Office Excel Help, website http://office.microsoft.com/en-us/excel-help/add-change-or-remove-a-trendline-in-a-chart-HP010007461.aspx, accessed December 1, 2013.

Minitab, 2006. Minitab software, version 15.1.0.0, Minitab Inc., State College, PA.

Mirza and Witczak, 1995. Muhammad W. Mirza and Matthew W. Witczak, *Development of a Global Aging System for Short and Long Term Aging of Asphalt Cements*, Journal of Association of Asphalt Paving Technologists, Vol. 64, Ann Arbor, Michigan.

Morian et al., 2011. Nathan Morian, Elie Y. Hajj, Charles J. Glover, and Peter E. Sebaaly, *Oxidative Aging of Asphalt Binders in Hot Mix Asphalt Mixtures*, In Transportation Research Record No. 2207, Vol. 1, Journal of the Transportation Research Board, Washington, D.C.

Morian et al., 2013. Nathan Morian, Elie Y. Hajj, and Peter E. Sebaaly, *Significance of Mixture Parameters on Binder Aging in HMA Mixtures*, In Transportation Research Record No. 2370, Vol. 1, Journal of the Transportation Research Board, Washington, D.C.

Morian et al., 2014. Nathan E. Morian, Mohammad Zia Alavi, Elie Y. Hajj, and Peter E. Sebaaly, *Evolution of Thermo-Viscoelastic Properties of Asphalt Mixtures with Oxidative Aging*, In Transportation Research Record, In Press, Journal of the Transportation Research Board, Washington, D.C.

Odian and Blei, 1994. George Odian and Ira Blei, *Schaum's Outlines of Theory and Problems of General, Organic, and Biological Chemistry*, McGraw-Hill, Hightstown, New Jersey.

Olard and Di Benedetto, 2003. Francois Olard and Herve Di Benedetto, *General "2S2P1D" model and relation between the linear viscoelastic behaviors of bituminous binders and mixes*, Road Materials and Pavements Design, Volume 4, Taylor & Francis.

Park and Schapery, 1998. S.W. Park and R.A. Schapery, *Methods of interconversion between linear viscoelastic material functions. Part I – a numerical method based on Prony series*, International Journal of Solids and Structures, Vol. 36, Elsevier Science Ltd., New York, NY.

Petersen, 2009. J. Claine Petersen, *A Review of the Fundamentals of Asphalt Oxidation*, Transportation Research Circular E-C140, Transportation Research Board, Washington, D.C.

Petersen and Glaser, 2011. J. Claine Petersen and Ronald Glaser, *Asphalt Oxidation Mechanisms and the Role of Oxidation Products on Age Hardening Revisited*, Road Materials and Pavement Design, Vol. 12, Issue 4, Taylor & Francis, London, UK.

Petersen and Harnsberger, 1998. J. Claine Petersen and P. Michael Harnsberger, *Asphalt Aging, Dual Oxidation Mechanism and Its Interrelationships with Asphalt Composition and Oxidative Age Hardening*, in Transportation Research Record No. 1638, Journal of the Transportation Research Board, Washington, D.C.

Petersen et al., 1987a. J. Claine Petersen, H. Plancher, and P. Michael Harnsberger, *Lime Treatment of Asphalt to Reduce Age Hardening and Improve Flow Properties*, Journal of the Association of Asphalt Paving Technologists, Vol. 56, Ann Arbor, Michigan.

Petersen et al., 1987b. J. Claine Petersen, H. Plancher, and P. Michael Harnsberger, *Lime Treatment of Asphalts*, Final Report, National Lime Association, Western Research Institute, Laramie, Wyoming.

Pine, 2011. *Aggregate Image Measurement System, Model: AFA2A Operation Manual*, Version 2.07, Pine Instrument Company, Grove City, PA.

Pucci et al., 2004. T. Pucci, A. G. Dumont, and Herve Di Benedetto, *Thermomechanical and Mechanical Behavior of Asphalt Mixtures at Cold Temperature*, Road Materials and Pavement Design, Vol. 5, No.1, Taylor & Francis.

Radovskiy 2003. Boris Radovskiy, *Analytical Formulas for Film Thickness in Compacted Asphalt Mixtures*, in Transportation Research Record No. 1829, Journal of the Transportation Research Board, Washington, D.C.

Reid et al., 1984. R.C. Reid, J.M. Prausnitz, and T.K. Sherwood, *The Properties of Gases and Liquids*, 4th Edition, McGraw-Hill, New York, NY.

RHEA, 2011. *Rhea, Rheology Analysis Software*, version 1.2.1 Abatech, Inc., Blooming Glen, PA.

Robertson et al., 2006. Raymond E. Robertson, Kenneth P. Thomas, P. Michael Harnsberger, Francis P. Miknis, T. Fred Turner, Jan F. Branthaver, Shin-Che Huang, A. Troy Pauli, Daniel A. Netzel, Theresa M. Bomstad, Michael J. Farrar, John F. McKay, and Martin McCann, *Fundamental Properties of Asphalts and Modified Asphalts II, Final Report, Volume I: Interpretive Report*, Contract No. DTFH61-99C-00022, Western Research Institute, Laramie, Wyoming.

Rouse, 1953. Prince E. Rouse, Jr., *A Theory of the Linear Viscoelastic Properties of Dilute Solutions of Coiling Polymers*, Journal of Chemical Physics, Vol. 21, No. 7.

Rowe, 2012. Geoffrey M. Rowe, *Rheology considerations for recycled and recovered binder*, presentation, Pavement Performance Prediction Symposium (P3 Symposium), Laramie, Wyoming.

Rowe and Sharrock, 2011. Geoffrey M. Rowe and Mark J. Sharrock, *Alternate Shift Factor Relationship for Describing the Temperature Dependency of the Viscoelastic Behavior of Asphalt Materials*, Transportation Research Record: Journal of the Transportation Research Board, Vol. 2207, Transportation Research Board of the National Academies, Washington D.C.

Rowe et al., 2001. Geoffrey M. Rowe, Mark J. Sharrock, Mark G. Bouldin, Raj. N. Dongré, *Advanced Techniques to Develop Asphalt Master Curves from the Bending Beam Rheometer*, Petroleum and Coal, Vol. 43, No. 1.

Rowe et al., 2009. Geoffrey M. Rowe, Gaylon Baumgardner, and Mark J. Sharrock, *Functional forms for master curve analysis of bituminous materials*, Advanced Testing and Characterization of Bituminous Materials – Loizos, Partl, Scarpas & Al-Qadi (eds), Taylor & Francis Group, London, UK.

Rowe, 2011. Geoffrey M. Rowe, Discussion. *Evaluation of the Relationship between Asphalt Binder Properties and Non-Load Related Cracking*, Journal of Association of Asphalt Paving Technologists, Vol. 80, Ann Arbor, Michigan.

Rowe et al., 2011. Geoffrey M. Rowe, Gaylon Baumgardner, and Mark J. Sharrock, *Application of Rheological Models to Modified Binders*, presentation, 48th Petersen Asphalt Research Conference, Laramie, Wyoming.

Ruan et al., 2003a. Yonghong Ruan, Richard R. Davison, and Charles J. Glover, *Oxidation and Viscosity Hardening of Polymer-Modified Asphalt*, Energy & Fuels, Vol. 17, American Chemical Society.

Ruan et al., 2003b. Yonghong Ruan, Richard R. Davison, and Charles J. Glover, *An Investigation of Asphalt Durability: Relationships between Ductility and Rheological Properties for Unmodified Asphalts*, Petroleum Science and Technology, Vol. 21, Issue 1- 2, Marcel Drekker, Inc., New York, NY.

Sayegh, 1965. G. Sayegh. *Variation des modules de quelques bitumes purs et bétons bitumineux*, Doctoral Thesis, Faculté des Sciences de l'université de Paris.

Shaw and MacKnight, 2005. Montgomery T. Shaw and William J. MacKnight, *Introduction to Polymer Viscoelasticity*, 3rd Edition, John Wiley & Sons, Inc., Hoboken, New Jersey.

Smith, 2011. Brian C. Smith, *Fundamentals of Fourier Transform Infrared Spectroscopy*, Second Edition, CRC Press, Taylor & Francis Group, Boca Raton, Florida.

SP-1, 1994. Asphalt Institute, *Performance Graded Asphalt Binder Specification and Testing, Superpave Series No.1 (SP-1)*, Asphalt Institute, Lexington, Kentucky.

Sperling, 2006. Leslie H. Sperling, *Introduction to Physical Polymer Science*, Fourth Edition, Wiley Interscience, John Wiley & Sons Inc., Hoboken, New Jersey.

SSPWC, 2006. *Standard Specifications for Public Works Construction*, Regional Transportation Commission of Washoe County, Reno, NV.

Sybilski, 1993. Dariusz Sybilski, *Non-Newtonian viscosity of polymer-modified bitumens*, Materials and Structures, Volume 26, RILEM.

Sybilski, 1996. Dariusz Sybilski, *Zero-Shear Viscosity of Bituminous Binder and Its Relation to Bituminous Mixture's Rutting Resistance*, in Transportation Research Record No. 1535, Transportation Research Board, Washington, D.C.

Ulloa, 2013. Alvaro Ulloa-Calderon, Ph.D. Dissertation, Department of Civil and Environmental Engineering, University of Nevada, Reno.

Von Quintus et al, 1991. Harold L. Von Quintus, James A. Scherocman, C.S. Hughes, T.W. Kennedy, *Asphalt-Aggregate Mixture Analysis System AAMAS*, National Cooperative Research Program Report 338, Transportation Research Board, Washington, D.C.

Wagoner and Braham, 2008. Michael P. Wagoner and Andrew F. Braham, *Anisotropic Behavior of Hot-Mix Asphalt at Low Temperatures*, in Transportation Research Record No. 2057, Transportation Research Board, Washington, D.C.

Williams et al., 1955. Malcolm L. Williams, Robert F. Landel, and John D. Ferry, *The Temperature Dependence of Relaxation Mechanisms in Amorphous Polymers and Other Glass-forming Liquids,* Vol. 77, Journal of American Chemical Society.

Wisneski et at., 1996. M.L. Wisneski, J.M. Chaffin, Richard R. Davison, Jerry A. Bullin, and Charles J. Glover, *Use of Lime in Recycling Asphalt*, in Transportation Research Record No. 1535, Transportation Research Board, Washington, D.C.

Witczak, 2005. Matthew W. Witczak. *Simple Performance Tests: Summary of Recommended Methods and Database*, National Cooperative Highway Research Program, Report 547, Transportation Research Board, Washington, D.C.

Woo et al., 2007a. Won Jun Woo, Edward Ofori-Abebresse, Arif Chowdhury, Jacob M. Hilbrich, Zachary Kraus, Amy Epps Martin, and Charles J. Glover, *Polymer Modified Asphalt Durability in Pavements*, Report No. FHWA/TX-07/0-4688-1, Texas Transportation Institute, College Station, Texas.

Woo et al., 2007b. Won Jun Woo, Jacob M. Hilbrich, and Charles J. Glover, *Loss of Polymer-Modified Binder Durability with Oxidative Aging*, in Transportation Research Record No. 1998, Transportation Research Board, Washington, D.C.

Yusoff et al., 2011. Nur Izzi Md. Yusoff, Emmanuel Chailleux, and Gordon D. Airey, *A Comparative Study of the Influence of Shift Factor Equations on Master Curve Construction*, International Journal of Pavement Research and Technology, Vol. 4, No. 6, Chinese Society of Pavement Engineering.

Zeng et al., 2001. Menglan Zeng, Hussain U. Bahia, Huachen Zhai, R. Michael Anderson, and Pamela Turner, *Rheological Modeling of Modified Asphalt Binders and Mixtures*, Journal of the Association of Asphalt Paving Technologists, Vol. 70, Ann Arbor, Michigan.

Zhang et al., 2012. Yuqing Zhang, Rong Luo, Robert L. Lytton, *Anisotropic Viscoelastic Properties of Undamaged Asphalt Mixtures*, Journal of Transportation Engineering, Volume 138, Issue 1, American Society of Civil Engineers, Reston, Virginia.

13 APPENDIX A:

Draft AASHTO Method

Determining Thermal Cracking Properties of Asphalt Mixtures through Measurement of Thermally Induced Stress and Strain

Standard Method of Test for

Determining Thermal Cracking Properties of Asphalt Mixtures through Measurement of Thermally Induced Stress and Strain

AASHTO Designation: TP XX- (2013)

1. SCOPE

1.1. This method of test is used to determine the thermal viscoelastic and thermal volumetric properties of field cored or laboratory compacted asphalt mixture specimens by measuring the thermally induced stress and strain while being cooled at a constant rate from an initial equilibrium temperature. The Thermal stress and strain can be measured using one of the two methods.

Method A: Uniaxial Thermal Stress and Strain Tester (UTSST)

Method B: Asphalt Thermal Cracking Analyzer (ATCA)

1.2. This standard method covers procedures for preparing and testing asphalt mixtures to measure thermal stress and strain and directly calculate: (1) the coefficient of axial thermal contraction; and (2) the relaxation modulus of asphalt mixture over a range of temperature.

1.3. The procedures described in this standard provide required information for estimation of thermal cracking susceptibility of asphalt mixtures. The procedures apply to test specimens having maximum aggregate size of 19 mm or less.

1.4. This standard can be used for conventional and non-conventional asphalt mixture: hot mixture, mixture with recycled materials, cold mixture, warm mixture, and modified mixture (e.g., polymer-modified).

1.5. This standard can be used to determine the following:

1.5.1.1. Thermal stress buildup of asphalt mixture during a single cooling event.

1.5.1.2. Thermal strain of asphalt mixtures as a function of temperature.

1.5.1.3. Coefficient of axial thermal contraction.

1.5.1.4. Relaxation modulus of asphalt mixture as a function of temperature

1.5.1.5. Thermal viscoelastic properties of asphalt mixture: viscous softening, viscous-glassy transition, glassy hardening, crack initiation, fracture temperature, and fracture stress.

1.6. The values stated in SI units are to be regarded as the standard.

1.7. *This method does not purport to address all of the safety concerns, if any, associated with its use. It is the responsibility of the user of this method to establish appropriate safety and health practices and determine the application of regulatory limitations prior to use.*

2. REFERENCE DOCUMENTS

2.1. *AASHTO Standards*

2.1.1. T166- Standard Method of Test for Bulk Specific Gravity (G_{mb}) of Compacted Hot Mix Asphalt (HMA) Using Saturated Surface-Dry Specimens.
2.1.2. T168- Standard Method of Test for Sampling Bituminous Paving Mixtures.
2.1.3. T209- Standard Method of Test for Theoretical Maximum Specific Gravity (G_{mm}) and Density of Hot Mix Asphalt (HMA).
2.1.4. T269- Standard Method of Test for Percent Air Voids in Compacted Dense and Open Asphalt Mixtures.
2.1.5. T312- Standard Method of Test for Preparing and Determining the Density of Hot Mix Asphalt (HMA) Specimens by Means of the Superpave Gyratory Compactor.
2.1.6. T328- Standard Practice for Reducing Samples of Hot Mix Asphalt (HMA) to Testing Size.
2.1.7. R30- Standard Practice for Mixture Conditioning of Hot-Mix Asphalt (HMA).
2.1.8. PP060-09-UL Standard Practice for Preparation of Cylindrical Performance Test Specimens Using the Superpave Gyratory Compactor (SGC)

2.2. *ASTM Standards*

2.2.1. D 8, Standard Terminology Relating to Materials for Roads and Pavements
2.2.2. D3549- Standard Test Method for Thickness or Height of Compacted Bituminous Paving Mixture Specimens.
2.2.3. D3665-Standard Practice for Random Sampling of Construction Materials.
2.2.4. F1684- Standard Specification for Iron-Nickel and Iron-Nickel-Cobalt Alloys for Low Thermal Expansion Applications.

2.3. *Other Documents*

2.3.1. Chapra, Steven C. and Raymond P. Canale. *Numerical Methods for Engineers*. Fifth Edition, The McGraw-Hill Companies, Inc., New York, NY, 2006.
2.3.2. Sperling, L.H., *Introduction to physical Polymer Science*, Fourth Edition, Wiley Interscience, John Wiley and Sons Inc., New Jersey, 2006

3. TERMINOLOGY

3.1. *Initial starting temperature, $T_{initial}$*- the temperature from which the test starts by cooling the specimens at a constant rate. The asphalt mixture specimens have to be at thermal equilibrium at the initial starting temperature prior to the starting of the test.

3.2. *Cooling rate*- the constant rate at which the temperature of asphalt mixture specimen decreases with time (°C/hr) during the test.

3.3. *Uniaxial Thermal Stress, $\sigma(T)$*- accumulated tensile stress induced in the specimen by decreasing the temperature from $T_{initial}$ at a constant rate while maintaining the overall specimen height/length constant.

3.4. *Uniaxial Thermal strain, $\varepsilon(T)$*- accumulated contraction strain induced in the specimen by decreasing the temperature from $T_{initial}$ when the sample is free to contract axially.

3.5. *Coefficient of axial thermal contraction, $\alpha(T)$*- the fractional change in size in the axial direction associated with a temperature change.

3.6. *Relaxation modulus, $E_r(t, T)$*- the time and temperature dependent modulus of the asphalt mixture. The relaxation modulus can be determined using the synchronized thermal stress and strain resulting from a change in temperature.

3.7. *Micro-cracking*- microscopic damage initiated at a certain temperature in the restrained specimen while cooling which leads to macro-cracking and eventually the fracture of the specimen.

3.8. *Thermal viscoelastic properties*- viscoelastic properties of the asphalt mixture determined from the thermal loading history including the viscous softening, viscous-glassy transition, glassy hardening, and crack initiation properties.

3.9. *Viscous softening stage*- from this stage the relaxation modulus of the asphalt mixture increases rapidly, mostly in a linear fashion, with decreases in temperature.

3.10. *Viscous-glassy transition stage*- at this stage the glassy properties of the asphalt mixture overcome its viscous properties.

3.11. *Glassy hardening stage*- at this stage the behavior of the asphalt mixture is considered glassy.

3.12. *Crack initiation stage*- in this stage micro-cracks occur in the specimen due to the induced thermal stresses when the asphalt mixture is characterized as glassy.

3.13. *Fracture stage*- at this stage the asphalt mixture specimen breaks due to the propagation of micro-cracks by the induced thermal stress.

3.14. Fracture stress- thermal tensile stress at failure.

3.15. Fracture temperature- temperature at failure.

4. SUMMARY OF TEST METHOD AND PRACTICE

4.1. This standard describes the procedure for determining the thermal stress and thermal strain measurements from the restrained and unrestrained asphalt mixture specimens, respectively. The thermal stress and strain can be determined in accordance with *Method A* - Uniaxial Thermal Stress and Strain Tester (UTSST) or *Method B*- Asphalt Thermal Cracking Analyzer (ATCA).

4.2. The induced thermal stress and strain measured data are used to determine: (1) the coefficient of axial thermal contraction; and (2) the relaxation modulus of asphalt mixture and characterizing the thermal viscoelastic properties of the asphalt mixture at different stages of the material behavior.

4.3. The thermal strain is determined by measuring the uniaxial deformation from an asphalt mixture specimen during cooling from an initial equilibrium temperature while it is free to deform without any friction.

4.4. The relaxation modulus is determined from the concurrent measured data of thermal stress and strain data from restrained and unrestrained asphalt mixture specimen, respectively.

4.5. The thermal viscoelastic properties of the asphalt mixture including viscous softening, viscous-glassy transition, glassy hardening, and crack initiation are determined from the relaxation modulus curve in the temperature domain. The fracture stress and fracture temperature are determined from the induced thermal stress curve in the temperature domain.

4.6. A cylindrical (Method A) or prismatic (Method B) asphalt mixture specimen cored or cut either from Superpave gyratory compacted specimen or field cores of specific dimensions, is fixed at the ends to the platens of a test system and it is enclosed within an environmental chamber. A small initial tensile load is applied to the specimen and the specimen is cooled at a given temperature rate. In Method A, thermal contraction along the long axis of the specimen is monitored electronically using Linear Variable Differential Transformers (LVDTs) and the

initial length of the specimen is maintained by automatic adjustment of the platens by the Test System. In Method B, specimen contraction is restricted by a steel loading frame with minimal compliance. The cooling process continues until tensile fracture of the restrained specimen occurs. Concurrently, an unrestrained specimen is set on a frictionless roller stand and contraction along the long axis of the specimen is recorded while cooling using LVDTs. In Method A, unrestrained beam is made by gluing two cylindrical specimens cored from Superpave gyratory compacted specimen or field core specimen. In Method B, unrestrained beam is made by gluing three prismatic beams cut from Superpave gyratory compacted specimen or cylindrical core.

5. SIGNIFICANCE AND USE

5.1. The thermal strain measurements allow for the calculation of the coefficient of axial thermal contraction which can be directly used in the mechanistic-empirical pavement design.

5.2. The thermal stress and strain measurements allow calculations of the relaxation modulus of asphalt mixture in the temperature domain.

5.3. From relaxation modulus versus temperature and thermal stress versus temperature relationships the thermal viscoelastic and fracture properties may be determined for asphalt mixtures.

5.4. The derived relaxation modulus, thermal viscoelastic, and fracture properties may be used in evaluating the low temperature cracking resistance of asphalt mixtures.

6. APPARATUS

6.1. *Method A - Uniaxial Thermal Stress and Strain Tester (UTSST)*– A closed-loop servo-controlled test system, as described in Figure 1, capable of cooling unrestrained and restrained asphalt mixture specimens at a constant rate from an initial starting temperature through failure in the restrained specimen. The system shall be capable of measuring the tensile load in restrained specimen, contraction deformation in unrestrained specimen and the temperature from a control specimen.

6.1.1. *A closed-loop servo-controlled test system*- A system capable of applying or maintaining an applied load based upon the response of the two or more LVDT's attached to the restrained specimen. The test is conducted by allowing no net change in the LVDTs, i.e., the platens must be held at a constant distance from each other. The minimum recommended loading system capacity is 20 kN.

6.1.2. *Restrained specimen mild steel platens*- Two platens per specimen 150±25 mm in diameter or square platens of similar area. The platens should be of sufficient

thickness to prevent significant deflection during sample testing. Typically, platens of 25 mm thick have been used successfully.

6.1.2.1. Each platen should have holes containing set screws of the appropriate diameter to hold the LVDTs and the extension rods on the restrained specimen. These holes should be at a constant radial distance and should align along the same axis (Figure 2).

6.1.2.2. Each platen should also have a pedestal approximately 5 mm height and the same diameter as the specimen oriented along the central axis of the platen.

> **Note 1:** the pedestal shall be machined along with the platen and not be a separate component.

6.1.3. *Environmental chamber*- the environmental chamber shall be equipped with temperature conditioners and controls capable of generating test temperature between 30°C and at least -50°C inside the chamber with a predefined constant rate for cooling.

6.1.4. *Cooling/Heating System* – A cooling/heating system capable of applying temperatures as high as 30°C and as low as -50°C at a constant rate up to 20°C/hr is required. Air flow cooling systems may be utilized for this purpose.

6.1.5. *Thermally stable rods*-rods made of invar (conforming to ASTM F1684, UNS 93050, or UNS 93600) or other material (e.g. certain ceramics) with similarly low coefficient of thermal expansion and contraction of sufficient geometry to permit the necessary measurement and subsequent restraint of the asphalt mixture specimen. For the restrained specimen, each LVDT requires one rod, and for the unrestrained specimen, one rod for each of the two LVDTs is required.

6.1.6. *Deformation Measurement Device*-The unrestrained asphalt mixture specimen is placed on a frictionless roller stand during the test. The rollers should be smooth enough and have free movement to minimize the friction. The asphalt mixture must be free to contract during cooling in order to obtain accurate strain measurements. Two invar rods are glued to the ends of the unrestrained specimen and must be long enough to extend to the outside of the environmental chamber to make contact with the LVDT.

6.1.7. *Data Acquisition System*- The data acquisition system shall be used to record the developed load in the restrained specimen, contraction deformation of unrestrained specimen, and the temperature of control specimen for the duration of the test.

6.1.8. *Specimen Alignment Stand*- A device capable of providing concentric and perpendicular alignment of the platens and restrain the specimen within axial alignment of the platen while the epoxy cures.

6.1.8.1. The alignment stand for the restrained specimen should rigidly affix the platens parallel and concentric with each other and permit the distance between the plates to be readily adjusted. The stand should also provide adjustable support to retain specimen once it is concentrically aligned with the platens. It should also be capable of applying a small load or weight to the top platen to assure complete contact and aid in bonding of the epoxy. Although not the required design, the device provided in Figure 3 has been found adequate for gluing the restrained specimen.

6.1.8.2. The alignment stand for the unrestrained specimen shall be capable of restraining the specimens and the invar rods in axial alignment with each other. While being restrained, the specimens and the invar rods shall be compressed under a small load or weight to permit the adequate bonding of all epoxied surfaces. Although not the required design, the device provided in Figure 4 has been found sufficient for gluing the unrestrained specimens.

6.1.9. *Miscellaneous Apparatus*- Spatula (for proportioning and mixing epoxy components), metals pans, masking tape, and gloves.

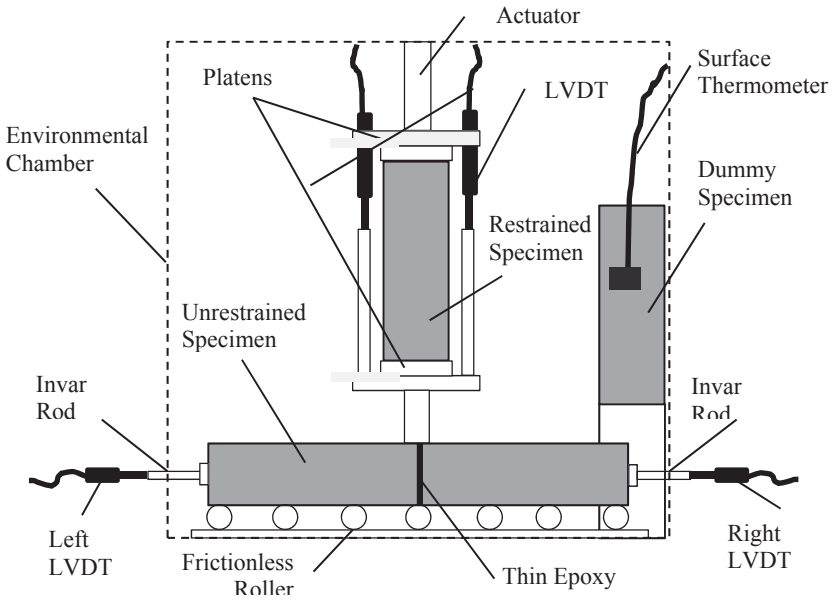

Figure 1: Uniaxial thermal stress and strain tester (UTSST)

Figure 2: Sketch of restrained specimen platens.

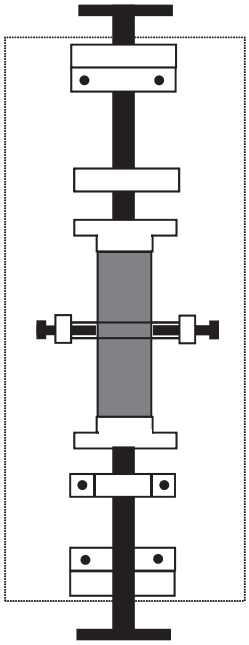

Figure 3: Specimen alignment stand for the restrained specimen

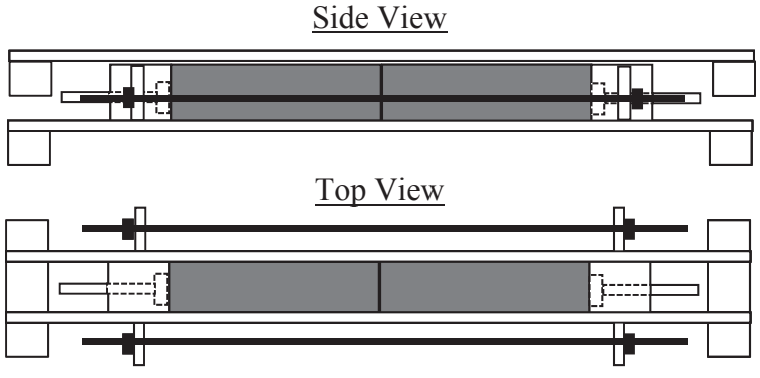

Figure 4: specimen alignment stand for the unrestrained specimen

6.2. *Method B – Asphalt Thermal Cracking Analyzer (ATCA)*– The general setup of the apparatus used in Method B is shown in Figure 5. A steel loading frame capable of withstanding loads of up to 25 kN without compliance is required to restrained one of the samples. A suitable support system using rollers should be used to maintain the weight of the sample beams and prevent sagging, without inducing any movement resistance to the beam samples. Figure 6 shows the recommended frame and support system setup and design. Asphalt mixture temperature is measured using a dummy sample placed at the bottom of the environmental chamber.

6.2.1. *Restrained specimen steel platens*- Two square platens 150±25 mm by 150±25 mm are used to attach restrained beam to loading frame. The platens should be of sufficient thickness to prevent significant deflection during sample testing. Typically, platens of 25 mm thick have been used successfully.

6.2.2. *Environmental Chamber* –the environmental chamber shall be equipped with temperature conditioners and controls capable of generating test temperature between 30°C and at least -50°C inside the chamber with a predefined constant rate for cooling. Openings should be placed to allow for insertion of LVDTs on sample ends as well as fixing restrained beam to the frame. Figure 6 shows the typical setup for the environmental chamber.

6.2.3. *Cooling/Heating System* – A cooling/heating system capable of applying temperatures as high as 30°C and as low as -50°C at a fixed rate of up to 1°C/min is required. Liquid nitrogen, cryogenic gas, and mechanical cooling systems may be utilized for this purpose.

6.2.4. *Thermally stable rods*-rods made of invar as indicated in 6.1.4. Two rods are needed for the unrestrained specimen to properly measure contraction of the sample.

6.2.5. *Frictionless Roller Stand*- To allow for free contraction, the unrestrained beam is placed on a frictionless roller stand. The recommended support stand is shown in Figure 6c.

6.2.6. *Data Acquisition System*- The data acquisition system shall be used to record the thermal load in the restrained specimen, thermal contraction of unrestrained specimen, and the temperature of the dummy specimen.

6.2.7. *Specimen Alignment Stand*- An alignment system capable of providing concentric and perpendicular alignment of the platens and restrain the specimen while the epoxy cures. The recommended gluing setup for Method B is shown in Figure 7.

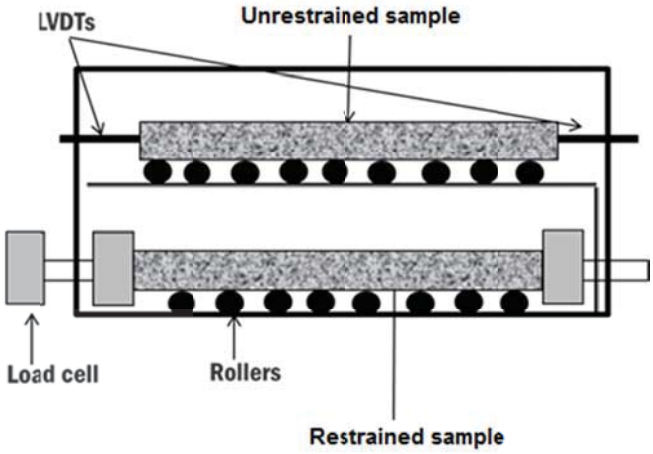

Figure 5: Schematic of the Asphalt Thermal Cracking Analyzer (ATCA) system.

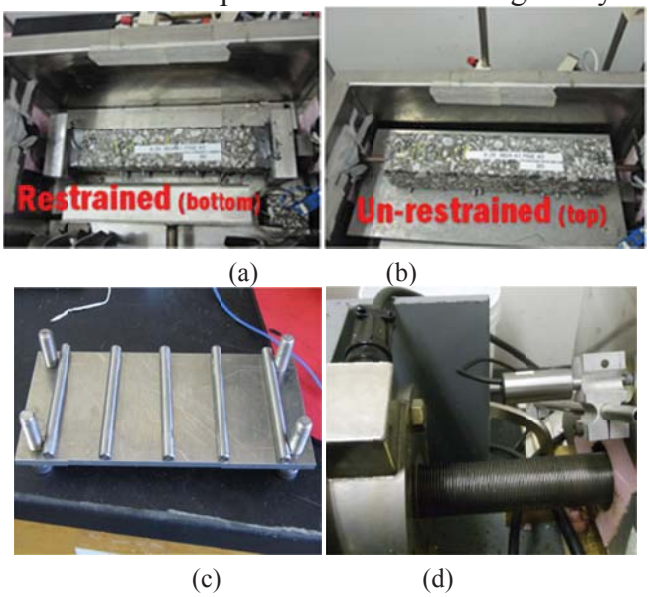

Figure 6: ATCA - (a) Restrained beam setup, (b) unrestrained beam setup, (c) adjustable height beam support platform with rollers, and (d) load cell and LVDT's.

Figure 7: Sample gluing setup for Method B.

7. MATERIALS

7.1. *Epoxy* –Devcon Plastic Steel® Putty (A) 10110 has been found sufficient.

7.2. *Miscellaneous Materials* – 240-grit sandpaper, acetone or other degreaser.

8. HAZARDS

8.1. Follow the safety requirements listed in the manufacturer's safety information sheet when using epoxy, acetone.

9. TEST SPECIMENS

9.1. *Obtain Test Specimens* – Obtain the test specimens for Method A (cylindrical specimens) or Method B (prismatic Specimens).

9.2. *Method A – Uniaxial Thermal Stress and Strain Tester (UTSST):*

9.2.1. *Laboratory Mixed Laboratory Compacted Asphalt Mixture Specimens* – Mix, age, and compact the asphalt mixture specimens according to T312 using the 150 mm diameter molds. Follow the short-term and long-term aging recommendations of R30 for Mixture Mechanical Testing. Specimens should be compacted to obtain a target air void level ±0.5% after trimming to the final dimensions as determined by T269.

9.2.2. *Field Mixed Laboratory Compacted Asphalt Mixture Specimens* – Obtain the asphalt mixture samples in accordance with T168. Reduce the sample to the appropriate specimen sizes adding to T328. Follow the applications section of T312 to compact the specimens using the 150 mm diameter molds. Follow the short-term and long-term aging recommendations of R30 for Mixture Mechanical Testing. Specimens should be compacted to obtain a target air void level ±0.5% after trimming to the final dimensions as determined by T269.

9.2.3. *Field Mixed Field Compacted Asphalt Mixture Specimens* – Obtain mixture cores in accordance with T168, to obtain core samples nominally 150 mm in diameter. Take care to prevent deformation or other disturbance of the samples during storage and transport to the testing location. When the samples are taken from existing pavement obtain them in accordance with ASTM D3665, unless specific locations are under investigation.

9.2.4. *Coring of Test Specimens* – Obtain the test specimens by laying the sample, either SGC sample or field core, on its side and core the test specimen 90° from the axis

of compaction with a wet diamond core bit. Depending upon the nominal maximum aggregate size (NMAS) of the mixture, the cored specimens, after side-coring, shall be 57±5 mm or 45±5 mm in diameter for 19 mm and 12.5 mm NMAS mixtures, respectively. However, the 57 mm samples may also be used for 12.5 mm NMAS mixtures as well.

Trim the length of the side-cut cores using a wet diamond blade so that the ends of the sample are a perpendicular as possible to the sides. The length of the specimens shall be as long as possible, but sufficient to remove the radius ends of from the original sample geometry. The final length of the test specimens should be no shorter than 140 mm.

9.2.5. *Bulk Specific Gravity*– Determine the bulk specific gravity according to T166 and the corresponding air voids in accordance with T269.

9.2.6. *Drying of the Specimens* – Assure the specimens are dry from appreciable moisture after the specific gravity determinations either by air drying in front of high-output fans for several days, or other sufficient means.

9.2.7. *Measurement of Core Specimens* – Determine the dimensions, diameter and height, of the specimens in accordance with ASTM D3549. Use the average diameter to determine the cross-sectional area of the restrained specimen. Use the average height to determine the length of unrestrained specimen. Record the average cross-sectional area to the nearest 1 $mm^2$and the height to the 0.1mm.

9.3. *Method B – Asphalt Thermal Cracking Analyzer (ATCA):*

9.3.1. *Laboratory or Field Compacted* - To produce restrained and unrestrained beams for Method B, four prismatic beams of 50 by 50 mm in cross section and 150 mm long are cut from 170 mm height samples. Two of these beams are sawed in half to produce four 75 mm blocks. By gluing a 75 mm block to each end of the two 150 mm blocks, two 300 mm beams are produced. Follow the short-term and long-term aging recommendations of R30 for Mixture Mechanical Testing. Figure 9 shows how to procure unrestrained and restrained beams for Method B.

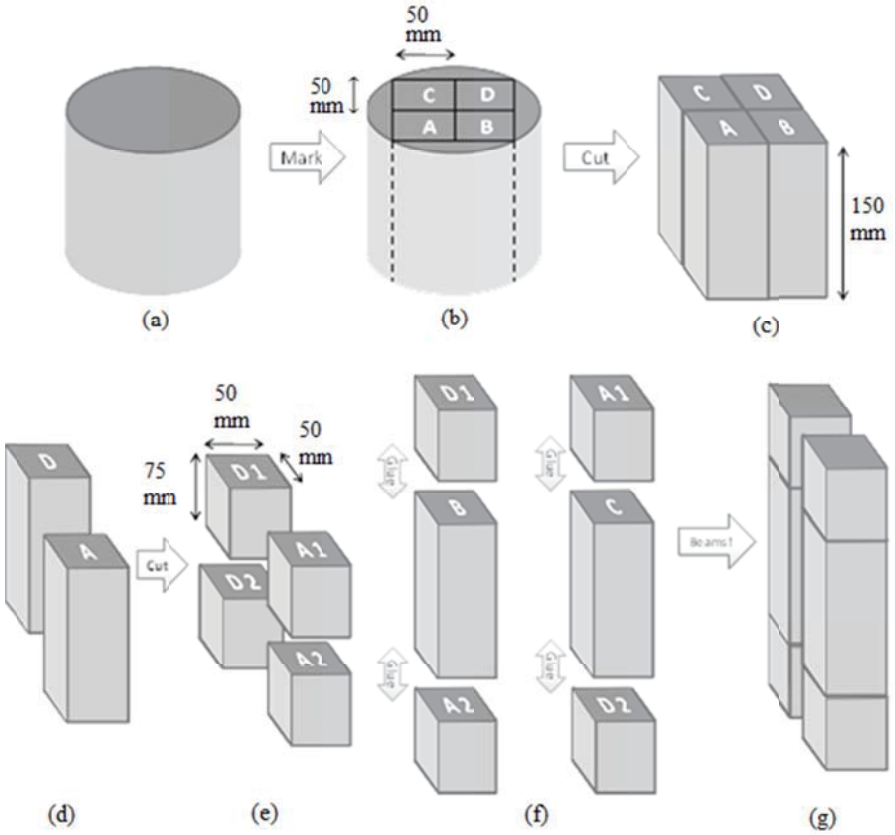

Figure 9: Step by step procedure for producing prismatic asphalt mixture sample (Method B) from cylindrical samples.

10. SPECIMEN PREPARATION

10.1. *Restrained Specimen Preparation (Method A and B)*

10.1.1. *Platen Preparation*– Scrape the epoxy and remain mixtures from the platens with spatulas after heating the plates or as suggested by the epoxy manufacturer to remove residual epoxy. Sand the platen surface with a piece of sandpaper to completely remove any epoxy or specimen-end residue remaining from prior tests and to provide a rough surface for epoxy adhesion. Clean the surface of the platen using acetone or other degreaser to remove all the debris remained on the surface after sanding.

10.1.2. *Restrained Specimen Preparation* – Verify that the specimen has been sufficiently dried and is free from saw slurry, dust, grease, or other debris on the exterior of the specimen that maybe inhibit the bonding of epoxy to the surface. Prior to applying any epoxy, wrap a single layer of masking tape around the circumference of the sample leaving the middle portion and approximately 5 to 10 mm of each end exposed and uncovered. This will be to assure a straight line of epoxy on the sample after gluing. It is recommended to leave a small tab of the

tape wrapped back upon itself to aid in removal of the tape with minimal disturbance of the sample prior the epoxy setting.

10.2. *Epoxy Preparation* – Follow the mixing, proportioning, applying, and curing instructions supplied by the manufacturer for the epoxy being used. If Devcon Plastic Steel® Putty (A) 10110 is used; obtain 25 grams or more of mixed epoxy blended by the recommended mix ratio (typically 9:1 by weight of resin and hardener, respectively). Thoroughly mix the two epoxy components until a uniform color and consistency results.

10.3. *Attaching the Restrained Specimen to Platens (Method A and B)*

10.3.1. Apply 2 to 3 mm thick film of epoxy over a nearly the entire diameter of one end the specimen. Holding the specimen in alignment with the center pedestal on the platen on the non-epoxied end of the specimen, apply the collar to that to assure complete alignment between the sample and the platen. While holding the epoxied end in alignment with the pedestal with ones fingers, apply the axial load to assure complete adhesion of the epoxy on the platens. While maintaining the specimen alignment, apply the sample restraints to restrain the specimen in that position.

10.3.2. Assure that epoxy has been squeezed out between the specimen and the platen pedestal and that not gaps exist around its perimeter. Assure that the alignment of the specimen still coincides with the pedestals. Using the remainder of the epoxy, apply a small band of epoxy around the perimeter of both the specimen and the pedestal on the platen. The epoxy should cover the sample up to the masking tape and the remainder of the pedestal, but need not be a thick mass of epoxy, such as a fillet weld would appear.

10.3.3. With the specimen in alignment and restrained by the alignment stand and while the epoxy is still fresh and pliable, carefully remove the masking tape on the epoxied end of the specimen revealing a clean line of epoxy in the specimen.

10.3.4. Though not required, it is recommended to allow the first epoxied end of the specimen to mostly set, before attempting to affix the other end. It will likely reduce the chance of misalignment due to handling while the epoxy is still fresh.

> **Note 2:** If Devcon 10110 epoxy is used, the permissible set time is approximately 45 minutes to two hours prior to gluing the other end of the specimen.
>
> **Note 3:** Alignment is critical to obtaining meaningful test results. Therefore, the alignment device must sufficiently align the platens and specimen, and support the specimen in a level position while the epoxy cures.

10.3.5. To apply epoxy to the second end of the restrained specimen, make sure the specimen restraints are firmly in place, remove the collar from the non-epoxied end of the specimen, and remove the load or weight to permit separation of the platen and non-epoxied end of the specimen. Assure the specimen does not move and remains in alignment with both platens. Apply a film of epoxy of approximately the same thickness as the first end to the now exposed specimen end, making sure to get complete and uniform coverage of the specimen.

10.3.6. Make contact with the specimen and platen by applying the contact load or weight. Again, make sure the epoxy is squeezed from the between the two with no gaps or voids.

10.3.7. Be sure to align the holes in both the top and bottom platens used to align the LVDTs and the invar rods before the epoxy is set on the second end of the specimen.

10.3.8. Apply the same procedure as the first end, by applying the overlapping band-aid to the end of the specimen and the platen pedestal. Remove the masking tape to provide the clean straight line of epoxy on the sample.

10.4. *Preparation of the Unrestrained Specimen – Method A:*

Verify that the specimens are sufficiently dried and are free from saw slurry, dust, grease, or other debris on the exterior of the specimen that maybe inhibit the bonding of epoxy to the surfaces.

10.4.1. Align the two specimens, the invar extension rods, and their restraints on the bottom rack of the gluing jig such that any gaps between the two specimen will be minimized if they were not cut exactly perpendicular to the sides.

10.4.2. Follow the mixing, proportioning, applying, and curing instructions supplied by the manufacturer for the epoxy being used. If Devcon Plastic Steel® Putty (A) 10110 is used; obtain 25 grams or more of mixed epoxy blended by the recommended mix ratio (typically 9:1 by weight of resin and hardener, respectively). Thoroughly mix the two epoxy components until a uniform color and consistency results.

10.4.3. Apply the minimum required amount of epoxy between the two samples and verify the fit by making sure the epoxy is squeezed out along the entire perimeter of the joint. Adjust as needed before the epoxy sets. Using a card or other means remove as much of the excess epoxy as possible. Attempt not to create the band-air seal as was done in the restrained specimen, but remove all the excess as much as possible.

10.4.4. Follow the mixing, proportioning, applying, and curing instructions supplied by the manufacturer for the epoxy being used. If Devcon Plastic Steel® Putty (A) 10110 is used; obtain 25 grams or more of mixed epoxy blended by the recommended mix ratio (typically 9:1 by weight of resin and hardener, respectively). Thoroughly mix the two epoxy components until a uniform color and consistency results.

10.4.5. Apply enough epoxy to the end of the invar extensions to adequately adhere them to the sample.

10.4.6. Lightly squeeze the component together assure a proper fit and adequate epoxy. Apply the top of the alignment jig to maintain axial alignment of the epoxied components. Adding a small load or weight to the top of the jig for confinement may be necessary to assure proper axial alignment.

10.4.7. Apply the lateral pressure to the retainers on the invar rods to firmly squeeze the components together. Check and verify the fit and alignment of the components. Remove any additional epoxy that may have been extruded between the samples.

10.5. *Preparation of the Unrestrained Specimen – Method B:*

10.5.1. *Attaching Invar Rods to Sample* – Mark the cross section centroid on each end of the beam by using an ink marker to draw diametric lines across the surface. Apply a 2±0.5 gram of fast during epoxy resin to the back surface of each invar rod end-piece and place firmly on the cross point of the diametric lines at each end of the beam. The end-piece may be kept in place using masking tape until epoxy cures. Invar rods are screwed into each end-piece of the beam. It may be necessary to place beam in chamber and screw in invar rods through the openings designed to have LVDTs outside the environmental chamber.

> **Note 4:** The use of invar rods extending out of chamber in Method B is to minimize temperature effects and creep of LVDT during the test procedure.

10.6. *Curing* - Permit both the restrained and unrestrained specimens to remain undisturbed until the epoxy has fully cured. At least 16 hours is recommended for the Devcon 10110 epoxy.

11. CONDITIONING

11.1. *Specimens Pre-Conditioning* – After the epoxy has cured, remove the restrained specimen/platen assembly and invar rods/unrestrained specimen assembly from their respective alignment stands. Condition both assemblies at 20±2°C environment for minimum of 2 hours prior to testing.

12. PREPARATION OF APPARATUS

12.1. *Preparation of the Environmental Chamber –*
Method A: Both the environmental and loading systems can be initialized and warmed up simultaneously.
Method B: The environmental chamber is initialized and warmed up.

12.1.1. Set the environmental chamber to 20°C and permit the chamber and all interior components to come to equilibrium for a minimum of 30 minutes.

12.1.2. *Method A:* Turn on the servo-controlled loading system. If the loading system is servo-hydraulic, initialize the system and run it through a warm-up scheme for a period of approximately 30 minutes or until the hydraulic fluid has been brought to the operating temperature before proceeding.

12.2. *Restrained Specimen-*

12.2.1. *Method A:*

Insert the invar connecting rods into the appropriate holes in the bottom plate and secure with the set screws.

Connect the restrained specimen/platen assembly to the bottom universal joint by screwing the bottom platen to the bottom threaded connecting rod. By controlling the location of the ram attached to the top universal joint, insert the top universal joint connection rod assembly into the top universal joint and secure with the pin as shown in Figure 10a without applying any load to the specimen.

> **Note 5:** Clevis, ball-joint, or other moment reduction devices have been successfully used rather than the universal joints (Figure 10b).

Insert the LVDTs into the appropriate holes in the top platen and lightly secure with set screws.

> **Note 6:** It is quite easy to over tighten the LVDT set screws and destroy the LVDT. As such, care should be taken to avoid damage. It is suggested to obtain set screws that contain a plastic buffer on the bearing surface of the set screw to help minimize damage to the LVDTs.

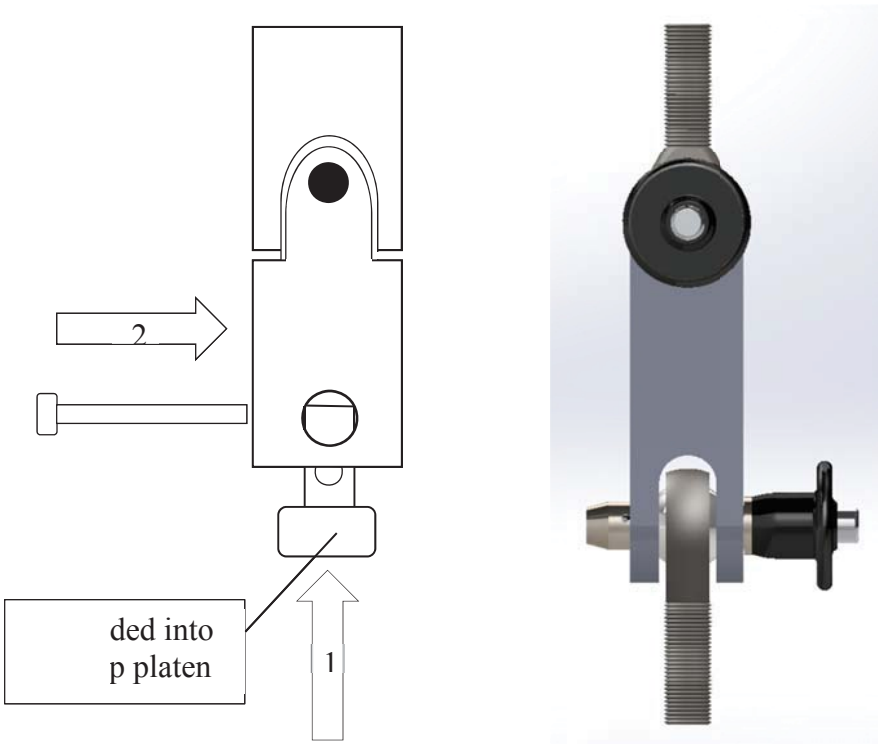

Figure 10: (a) Top universal joint and pin connector, (b) Alternate pin-ball joint connection.

12.2.2. *Method B:*

Restrained sample glued to two steel platens is placed in the environmental chamber and screwed into the steel framed as shown in Figure 6a. Care should be paid in not applying torsion when screwing beam into the steel frame. This can be minimized by using steel stripes as support during placement of the beam.

12.3. *Preparation of the Unrestrained Specimen*

12.3.1. *Method A*

Place the unrestrained specimen on the frictionless roller stand, taking care not to damage the end extension rods while installing them through the environmental chamber walls.

Since the unrestrained specimen for Method A is round it is possible for the specimen to roll laterally during the test if the stand is not perfectly level. To restrict this movement, it is permissible to apply a restrictive band very near the center of the specimen. Care should be taken in the installation, so that the lateral movement is in no way restricted by the band.

Adjust the unrestrained LVDTs such that they come into contact with the extension rods on the specimen. It is preferred to set the LVDTs such that they are depressed to near the full length of their stroke, such that and contraction of the specimen will not exceed the stroke of the LVDTs.

> **Note 5:** It is important that the LVDTs remain outside of the environmental chamber as many of the current manufactured LVDTs will not operate through the temperature range expected during this test, i.e. they may begin to exhibit non-linear behavior due to thermal contraction of the LVDT itself.

12.3.2. *Method B*

Place six roller rods at equally spaced intervals across the placement location of the unrestrained specimen in chamber. Place beam sample on roller rods and align ends with openings of the chamber. Center beam on rollers such that the beam is equally spaced from the side walls of the chamber and invar rod is extended equally from both sides of chamber.

. Place each LVDT on invar rod extruding out of chamber opening in such a manner that the LVDTs be initially compressed to a length of 1±0.2 mm on each side. Insure that assembly holding LVDTs sufficiently tight and secure to eliminate any sliding or shifting of the LVDTs during test.

12.4. Set the control specimen in close proximity to the other specimens within the chamber and close the chamber door.

12.5. Assure the chamber returns to thermal equilibrium without applying any load to the restrained specimen. Verify that the LVDTs on the unrestrained specimen at an acceptable value, so they will remain within their readable range throughout the duration of the test.

13. PROCEDURE

13.1. Start conditioning of the environmental chamber to the initial temperature of 20°C. When the average surface temperature is 20±1°C, apply the initial tensile load to the specimen.

13.2. Apply an initial tensile load of 50±10 N to the specimen immediately before starting the test.

13.3. Start cooling the cabinet at predefined constant cooling rate (X °C per hour).

Note 6: Although the actual maximum cooling rate of an asphalt pavement has been shown to be around 2.7°C per hour or lower, the lowest practical rate has been assumed to be 2.5°C per hour. For evaluations focused on ranking the thermal viscoelastic and fracture performance of different mixes a rate of 10°C per hour has been commonly used. Faster rates may be possible depending upon the cooling equipment available. However, the material response discussed in this standard has not been verified for cooling rates faster than 17.5°C per hour.

13.4. Automatically record the elapsed time, dummy specimen temperature, restrained specimen thermally induced tensile load, and unrestrained specimen thermal deformation as the test progresses at every predefined time step.

13.5. Continue the test until the restrained specimen fails or to a temperature below fracture temperature if additional strain measurements data is required.

14. CALCULATIONS

14.1. This section provides a standard procedure for calculating relaxation modulus and indexes of thermo-viscoelastic and fracture behavior of asphalt mixtures. The thermal relaxation modulus is determined from the thermal stress and strain induced in restrained and unrestrained asphalt mixtures specimens, respectively, obtained using either *Method A* (*UTSST*) or *Method B* (*ATCA*).

14.2. *Calculation of thermal stress*

14.2.1. Obtain the average cross section area of the restrained specimen according to Section 8.5.

14.2.2. Determine the maximum induced thermal load, $F_{n_{Max}}$ by finding the maximum of the recorded thermal tensile load data.

14.2.3. Calculate the thermal stress at each measured temperature by dividing measured induced thermal tensile load at any recorded temperature to the average cross section area of the specimen.

$$\sigma_n(T) = \frac{F_n\,(T)}{A_{ave}} \qquad (1)$$

where:
$\sigma_n(T)$= thermal stress at temperature T;
$F_n\,(T)$= induced thermal tensile load;
A_{ave}= cross section area of the restrained specimen.

14.2.4. Normalized the thermal stress values by subtracting all the calculated stress values (at each temperature) from the initial stress at the start of the test (i.e. time zero).

14.2.5. Smooth the thermal stress versus temperature curve by fitting a polynomial of degree 5 or 6 to the measured values of thermal stress and check for acceptable fit of the polynomial.

14.3. *Calculation of thermal strain*

14.3.1. Obtain the average length of the unrestrained specimen after both specimens are epoxied together in accordance with the procedure found in ASTM D3549.

14.3.2. Normalize the thermal deformation measurements from both left and right ends of the unrestrained specimen, at each recorded temperature, to the initial value at the start of the test (i.e. time zero) by subtracting each value from the initial deformation at time zero.

14.3.3. Calculate the total normalized deformation by summation of normalized thermal deformation from left and right ends of the unrestrained specimen.

$$\Delta_{n_{ave}}(T) = \Delta_n^L(T) + \Delta_n^R(T) \qquad (2)$$

where:
$\Delta_{n_{ave}}(T)$= normalized thermal deformation of the specimen;
$\Delta_n^L(T)$, $\Delta_n^R(T)$ = normalized thermal deformation from the left and right end of unrestrained specimen, respectively.

14.3.4. Compute the normalized thermal strain by dividing the normalized total thermal deformation, at each recorded temperature, to the average length of the specimen.

$$\varepsilon_n(T) = \frac{\Delta_{n_{ave}}(T)}{L_{ave}} \qquad (3)$$

Where:
$\varepsilon_n(T)$ = Normalized thermal strain at temperature of T;
$\Delta_{n_{ave}}(T)$= normalized thermal deformation of the specimen;
L_{ave} = Average length of the unrestrained specimen.

14.3.5. Smooth the thermal strain versus temperature curve by fitting a polynomial of degree 3 or 4 to the measured values of thermal stress and check for acceptable fit of the polynomial.

14.4. *Calculation of coefficient of axial thermal contraction (CTC)*

14.4.1. Calculate the coefficient of axial thermal contraction (CTC) at each temperature by finding the slope of the thermal strain versus temperature curve.

Note 7: The temperature dependency of the coefficient of axial thermal contraction (CTC) can be defined using a binary function. The binary function results in two values for the CTC before and after the glassy temperature of the asphalt mixture.

14.5. *Calculation of relaxation modulus in temperature domain*

14.5.1. The relaxation modulus is determined by back-calculation of Boltzmann's convolution integral which represents the uniaxial constitutive relation for linear viscoelastic materials.

$$\sigma(t) = \int_0^t E_r(t - t') \frac{\partial \varepsilon(t\prime)}{\partial t\prime} dt' \quad (4)$$

where:
$E_r(t)$, relaxation modulus;
$\sigma(t)$, thermal stress;
$\varepsilon(t)$, the thermal strain.

Note 7: Back-calculation is done by representing the Boltzmann equation in discrete form.

14.5.2. Rewriting the Boltzmann equation in discrete form by:

$$\sigma(t_n) = \sum_{i=1}^{n} E(t_n - t_i) \times (\varepsilon(t_i) - \varepsilon(t_{i-1}) \quad (5)$$

Where:
n is a time index start from zero
$\sigma(t_0)$ and $\varepsilon(t_0)$ are set to be zero corresponding to initial test condition.

14.5.3. Calculate relaxation modulus at any temperature by:

$$E(T(t_n)) = \frac{\left(\sigma(t_{n+1}) - \sum_{i=2}^{n+1} E(t_{n+1} - t_i)\left(\varepsilon(t_i) - \varepsilon(t_{i-1})\right)\right)}{\varepsilon(t_1)} \quad (6)$$

Note 8: if the data of thermal strain is not available, the relaxation modulus of asphalt mixture can be estimated by assuming a constant value for thermal coefficient of contraction, α, by:

$$E_r\big(T(t_n)\big) = \frac{\sigma(T(t_n)) - \sigma(T(t_{n-1}))}{\alpha \times (T(t_n) - T(t_{n-1}))} \quad (7)$$

14.6. *Determination of thermal viscoelastic properties*

14.6.1. Compute the first derivative of relaxation modulus with respect to temperature.

$$E_r{}'\big(T(t_i)\big) = \frac{E_r\big(T(t_i)\big) - E_r\big(T(t_{i-1})\big)}{T(t_i) - T(t_{i-1})} \quad (8)$$

14.6.2. Calculate the second derivative of relaxation modulus with respect to temperature.

$$E_r{}''\big(T(t_i)\big) = \frac{E_r{}'\big(T(t_i)\big) - E_r{}'\big(T(t_{i-1})\big)}{T(t_i) - T(t_{i-1})} \quad (9)$$

14.6.3. *Determination of crack initiation properties*.

14.6.3.1. The crack initiation modulus is defined as the maximum value of relaxation modulus. This point is identified when the first derivative of relaxation modulus with respect to temperature is equal to zero.

14.6.3.2. The crack initiation temperature is the temperature that corresponds to the maximum relaxation modulus.

14.6.3.3. The crack initiation stress is defined as the developed thermal stress at the crack initiation temperature.

14.6.4. *Determination of glassy hardening properties*.

14.6.4.1. Glassy hardening modulus is defined as the modulus at the point at which the second derivative of relaxation modulus with respect to temperature is zero on the colder side of the second derivative curve.

13.5.1.1. Glassy hardening temperature is defined as the temperature corresponding to the glassy hardening modulus.

13.5.1.2. Glassy slope determined as the absolute value of first derivative of relaxation modulus with respect to temperature at the point of glassy hardening.

14.6.5. *Determination of viscous-glassy transition properties.*

14.6.5.1. Viscous-glassy transition modulus- the modulus at the point at which the second derivative of relaxation modulus in respect to temperature is maximum.

14.6.5.2. Viscous-glassy transition temperature- the corresponding temperature to the viscous-glassy transition modulus.

14.6.6. *Determination of viscous softening properties.*

14.6.7. Viscous softening modulus- the modulus at the point at which the second derivative of relaxation modulus is zero at the warmer side.

14.6.8. Viscous softening temperature- the corresponding temperature to the viscous softening modulus.

Note 9: viscous softening properties may not be detected based on the testing program described in this standard.

Note 10: the calculations contained in this standard need to be performed on computer. Software to perform the calculation can be written or purchased as a stand-alone program.

15. EXAMPLE OF CALCULATION

15.1. In this example an asphalt mixture has been evaluated to determine thermal viscoelastic properties using data generated with Method A - Uniaxial Thermal Stress and Strain Test (UTSST).

15.2. The test is conducted on a sample of hot asphalt mixture. The initial equilibrium temperature was 20°C and the cooling rate was 10°C per hour.

15.3. Calculate the average diameter of restrained specimen and average length of the unrestrained specimen.
Average diameter of restrained specimen = 57.4 mm
Average length of unrestrained specimen = 279.6 mm

15.4. Calculation of normalized smoothed thermal stress and strain (Figure 11).

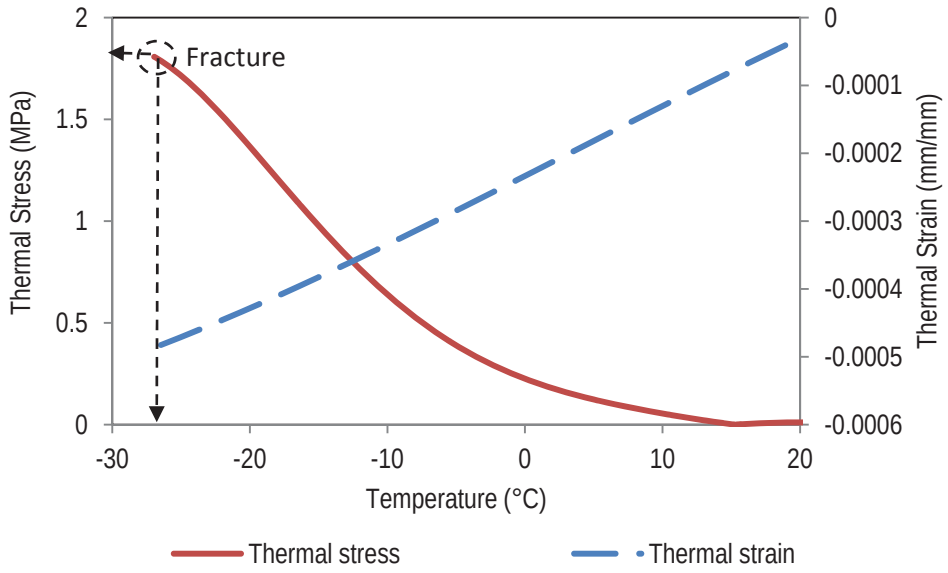

Figure 11: Thermal stress and thermal strain obtained from Method A (UTSST)

15.5. Determination of rate of thermal stress and rate of thermal strain.

15.6. Calculation of relaxation modulus and first and second derivatives with respect to temperature.

15.7. Determination of thermal viscoelastic and strength properties (Figure 12).

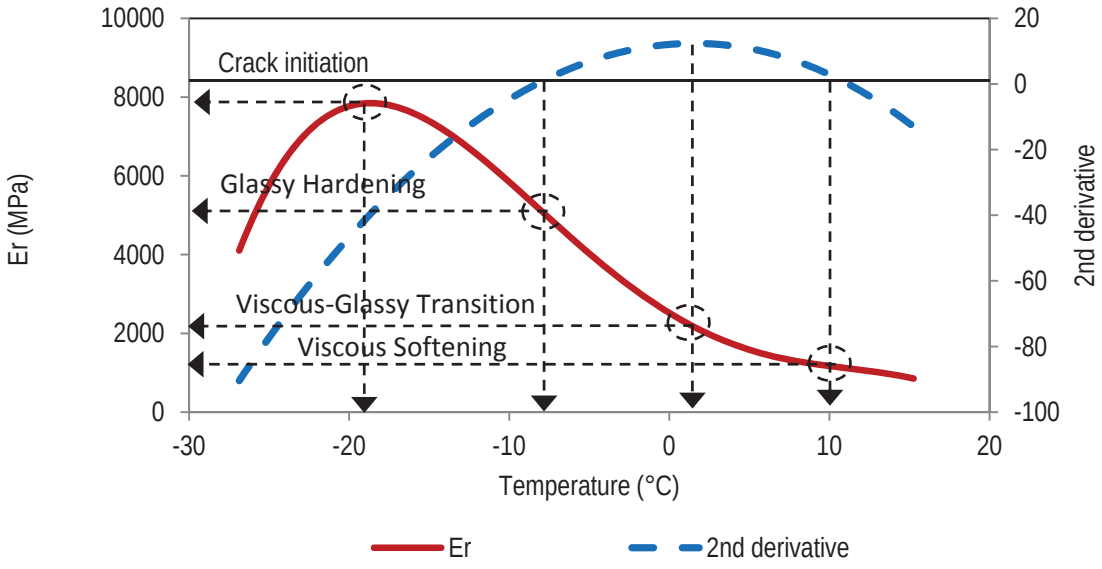

Figure 12: Determination of thermal viscoelastic properties of asphalt mixture

16. REPORT

16.1. *Test Specimen Description* – asphalt binder type, asphalt binder content, aggregate gradation, and air void percentage of test specimen.

16.2. *Test Specimen Aging History*- temperature, pressure and period of aging.

16.3. *Test Method Description*- method (UTSST or ATCA), cooling rate, initial equilibrium temperature, time step.

16.4. Average cross-sectional area of the specimen, nearest 1 mm^2.

16.5. Average length of the unrestrained specimen, nearest 0.1 mm.

16.6. Normalized thermal stress versus temperature curve.

16.7. Normalized thermal strain versus temperature curve.

16.8. Coefficient of axial thermal contraction.

16.9. Relaxation modulus versus temperature curve.

16.10. Thermal induced tensile load, nearest 10 N.

16.11. Fracture temperature, nearest 0.1°C.

16.12. Fracture stress, nearest 50 kPa.

16.13. Crack initiation temperature, nearest 0.1°C.

16.14. Crack initiation modulus, nearest 1 MPa.

16.15. Crack initiation stress, nearest 50 kPa.

16.16. Glassy hardening temperature, nearest 0.1°C.

16.17. Glassy hardening modulus, nearest 1 MPa.

16.18. Glassy hardening slope.

16.19. Viscous-glassy temperature, nearest 0.1°C.

16.20. Viscous-glassy modulus, nearest 1 MPa.

16.21. Viscous softening temperature, nearest 0.1°C.

16.22. Viscous softening modulus, nearest 1 MPa.

16.23. Failure Description – location of break along specimen length, nature of break (angular, flat, broken aggregate, etc.).

17. PRECISION AND BIAS

17.1. *Precision* – The work necessary to determine the precision of this test has not yet been performed.

17.2. *Bias* – No justifiable statement can be made on the bias of this test method due to the lack of availability of a valid reference value available.

14 APPENDIX B:

Outline of Mixture Extraction and Binder Recovery Procedure

1. Sample Preparation

1.1 Heat binder to the proper mixing temperature (2 hours for quart cans, 4 hours for gallon cans, or until fluid enough to mix).

1.2 Mix asphalt binder and aggregates for 5 minutes adding heat to the bottom of the mixing bowl.

1.3 Short term age the mixture loose for 4 hours at 135°C (275°F).

1.4 Adjust the mix temperature to the proper compaction temperature for the mix (typically within 1 hour).

1.5 Compact the specimens in the Superpave Gyratory compactor (SGC) to obtain the correct air void level.

1.6 Obtain the bulk specific gravity of the compacted specimen to verify the appropriate air void level. Note that the uncut SGC air void level may be different that the cut specimen, either dynamic modulus or UTSST geometries. Typically, the cut air voids are between one to two percent lower than the SGC specimens, with the overall average of about 1.5 to 1.7 percent for the mixtures tested in this study.

2. Sample Aging

2.1 Subject the specimens to oven aging in the compacted state in a forced draft oven at 60°C (140°F) for the prescribed duration (0-no aging, 3, 6, and 9 months). A second set of mixtures was also aged at 85°C (185°F) for 0, 1 and 3 months.

2.2 Upon removal of the specimens from the oven, let them cool to room temperature overnight.

2.3 Core and cut the specimens to the correct geometry using wet diamond bit sawing.

2.4 Determine the SSD and under water weights for the bulk specific gravity.

2.5 Dry the specimens for two days ambient conditions in front of a high volume fan.

2.6 Determine the dry weight of the specimens to calculate Gmb.

2.7 Wrap the specimen in plastic wrap and place in -18°C (0°F) freezer at least overnight (for consistency purposes and to prevent further oxidation over longer durations).

3. Dynamic Modulus Testing

3.1 Remove the specimens from the freezer and allow them warm up to room temperature overnight then remove the outer wrapping.

3.2 Glue LVDT tabs on the specimens and place them in 4.4°C (40°F) conditioning chamber overnight (min 12 hours).

3.3 Conduct dynamic modulus, E*, testing with the following temperatures adopted from AASHTO TP62 and NCHRP Report 513. Stabilize the specimens to the respective test temperature as follow:

4.4°C (40°F)	Overnight, then test
21.1°C (70°F)	Min. of 3 hours from 4.4°C
37.8°C (100°F)	Min. of 2 hours from ambient or 21.1°C
54°C (130°F)	Min. of 1 hour from 37.8°C, or min. of 3 hours from ambient temp.

3.4 Remove LVDT tabs and as much associated epoxy from the specimens as possible. Wrap specimens in plastic wrap, and place them in -18°C (0°F) freezer.

4. Extraction

4.1 Remove specimens from the freezer, unwrap the plastic and immediately wrap them tightly in aluminum foil.

4.2 Place specimens in 163°C (325°F) oven for 1 hour and 15 minutes.

4.3 Remove specimens from oven and foil and break down the mixture to individual sized particles (similar to the Rice procedure, AASHTO T209).

4.4 Once cooled to ambient temperature, place in 1 gallon self-sealing (Ziploc®) freezer bags and place them in the -18°C freezer at least overnight.

4.5 Thoroughly mix the specimen, weigh, and record between 700 and 1800 grams of materials into a weighed centrifuge bowl, depending upon the binder content and the amount recovered binder needed.

4.6 Cover the mixture with solvent (85% Toluene and 15%Ethanol, by volume) cover with aluminum foil and let stand for 30 minutes (Soak 1). While the mixture is soaking dry a filter paper ring in an oven at 135 to 163°C (275 to 325°F). Weigh and record the dried filter paper and the high speed centrifuge cup and screen.

4.7 Place the dried filter paper ring, the bowl lid and securing nut, and the centrifuge cover on the assembly. Spin the centrifuge until no solvent is running out of the centrifuge. Stop the centrifuge from spinning using the brake. Retain the solvent/binder mixture for step 4.8.

4.8 Immediately start the high speed (10,000 rpm) centrifuge and let it get up to speed (determined by sound). Make sure the #80 screen is in the funnel and run the solvent/binder through the high speed centrifuge taking care not to overflow the funnel or spill the solution (High Speed 1). Keep the solution covered to reduce exposure to air (oxygen) as much as possible.

4.9 While the high speed centrifuge is running, remove the cover, retaining nut and bowl lid, and the filter paper ring. Carefully scrape any fines adhering to the ring back into the bowl. Scrape the mixture from the sides of the bowl back into the bottom of the bowl. Cover the mix/aggregate with new solvent. Let stand for 20 minutes (Soak 2).

4.10 After the solution has run through the high speed centrifuge once (High Speed 1 from step 4.8), run it through the high speed centrifuge a second time to assure the fines have been removed from the solution (High Speed 2). After High Speed 2, the solution is ready to be recovered by section 5. Again, keep the solution covered to reduce exposure to air (oxygen) as much as possible.

4.11 Repeat steps 4.7 through 4.9 again (Soak 3 and repeat High Speed 1 and 2 for each iteration).

4.12 Leaving the large centrifuge apparatus intact, add approximately 1,000 mL of solvent to the top, which will drain into the bowl. Agitate back and forth, by hand, the large centrifuge bowl at slow speed for about a minute at a time to aid in washing the solvent through the aggregate (but not spinning it fast enough so the solvent is spun out of the bowl). Repeat the hand agitation two to three times over the 20 minute wait period between washings.

4.13 Spin the centrifuge until no solvent is running out of the centrifuge. Stop the centrifuge from spinning using the brake. Again run the solution through the High Speed 1 and 2 as in steps 4.8 and 4.10.

4.14 Repeat steps 4.12 and 4.13 until the solution coming out of the large centrifuge is nearly clear and compare the shade or tint of the solvent to the comparator sample to assure it is at least as clear.

4.15 After all the solution has been run through the High Speed twice run about 50 to 100mL of clear solvent through the High Speed centrifuge retaining it in the sample solvent (i.e. washing out residual binder from the centrifuge).

4.16 Disassemble the large and high speed centrifuges leaving the bowl and High Speed cup in the fume hood until it is dry (about 1 hour or so). Dry both in a forced draft oven at around 110°C (230°F) for at least 2 to 3 hours (overnight is preferred). Make sure the oven is labeled as containing Toluene and should not be opened and that the oven is vented to the exhaust system. Remove the bowl, filter paper, high speed cup and dried aggregate from the oven and allow them to cool at room temperature. Note that the high speed screen should not be placed in the oven, but left exposed in the fume hood so the solvent may evaporate without damaging the screen in the oven. Weigh each of the components and retain the dried aggregate for further testing if desired.

5. Binder Recovery

5.1 After assuring the solvent/binder has been through the High Speed centrifuge twice, place the appropriate amount of solvent (1 Liter or so) in the 3 Liter pear shaped evaporation flask and attach to the Rotovap apparatus.

5.2 Turn the water supply on. Set the bath temperature to 150°C. Apply a vacuum of about 100 to 200 mbar which is set automatically (the monitor should read about 650 to 750 mbar). Rotate the flask at 40 rpm. Immediately turn on the nitrogen supply (approximately 500mL/min.). Drop the evaporation flask so it is slightly submerged in the bath oil.

5.3 Monitor the evaporation flask to make sure the liquid is not at a rolling boil. If it is boiling too much, raise the elevation of the flask out of the bath slightly to prevent flash boiling or bumping of the sample.

5.4 Empty the recovery flask (spherical flask) as often as necessary and add more solvent binder as necessary to keep the process running continuously until all the

solution from one extracted sample is completely in the pear shaped evaporation flask. Add more solution as follows:

5.5 Raise the Rotovap assembly using the joystick control.

5.6 Stop the rotation of the pear shaped evaporation flask.

5.7 Stop the vacuum by pressing the [STOP] button once, and release the vacuum to atmospheric by pressing the [STOP] button a second time.

5.8 Empty the round recovery flask into the appropriate receptacle and replace it.

5.9 Remove the pear shaped evaporation flask using the attachment but as a wedge. Be careful not to break any glassware.

5.10 Add more solution/binder to make a total volume of about 1 Liter in the pear shaped evaporation flask. Replace the evaporation flask and softly locking the retaining nut.

5.11 Press the [START] button to start the vacuum again.

5.12 Start the rotation of the pear shaped evaporation flask, 40 rpm.

5.13 Check the nitrogen flow rate and the vacuum level.

5.14 Once all the solvent has been removed by visual inspection (recovery flask is no longer dripping), make sure there is a very slight layer of vacuum grease on the connection of both the evaporation and recovery flasks.

5.15 Maintain the bath Temperature at 150°C, begin slowly decreasing the vacuum pressure about 200 mbar at a time, waiting for the solvent fog for dissipate in the condenser coil before proceeding with the next drop.

5.16 Sink the evaporation flask as far as practical into the bath without overflowing and spilling.

5.17 Continue steps 5.6 and 5.7 until the vacuum pressure is 0 mbar (the response pressure may be as high as 20 or 30mbar). Note the time when the temperature and vacuum are reached, this is the beginning of the “Recovery Time” designation.

5.18 After the designated recovery time (2 to 4 hours), remove the flask from the rotovap. As quickly as possible to avoid the flask cooling, clean any vacuum grease or other minor contaminants from the inside and outside of the flask with a cotton swab wrapped in a Kimwipe, or similar tool, taking care not to come into contact with the recovered binder. Weigh the cleaned flask and recovered binder.

5.19 To remove the recovered binder from the flask, place a pre-weighed can on a paper covered oven shelf centered in the flask holder. Invert the flask so the binder will drain into the can and heat in the oven at 163°C (325°F) for 20 minutes. After the 20 minute drain down time, remove the flask from above the can and skim the top of the can with an index card or clean paper (to remove any thin films of oil or other contaminants). Place the lid on the can and leave in the over for another minute or two, stir the can with a heated and clean glass rod. Pour a few grams (an asphalt button of approximately 30 mm (1.25 inches) in diameter will be enough) into the smaller can for FT-IR testing.

5.20 Cool the can, purge with nitrogen gas, seal with vinyl (electrical) tape, and label can, prior to placing in the -18°C (0°F) freezer for storage. Clean the flask and all other necessary equipment with the recovered toluene/Ethanol mixture.

15 APPENDIX C:

Summary of Superpave Mix Designs for Laboratory Mixtures

SUPERPAVE VOLUMETRIC MIX DESIGN
(According to AASHTO M323, R30, R35, and T312)

Project: E2d.3.c Thermal Cracking - Mix Characteristics
Project Locat CAL19122

Aggregate Source: Gardner-Buellton, CA
Binder Grade: PG64-22 Paramount Nevada

Mix Design		
Nominal Maximum Aggregate Size, mm		19.0
Property	**Value**	**Requirement**
Design ESALs, millions	10	--
N_{inital}	8	--
N_{design}	100	--
N_{max}	160	--
Optimum Binder Content, %	6.65	--
Hydrated Lime, %	None	--
Liquid Antistrip, %	None	--
Max theoretical specific gravity, G_{mm}	2.250	--
%Gmm at N_{ini}	87.5	≤ 89.0
%Gmm at N_{des}	96.0	96.0
%Gmm at N_{max}	98.4	≤ 98.0
VMA, %	12.6	13.0% Min.
VFA, %	68.2	65-75
Percent Effective Binder P_{be}, %	4.08	--
Dust Proportion, $P_{0.075}/P_{be}$	1.3	0.6-1.2
Unconditioned Tensile Strength on 6" Gyratory Samples, psi	115	--
Conditioned Tensile Strength on 6" Gyratory Samples, psi	77	--
Tensile Strength Ratio, %	67	80 Min.
Unconditioned Tensile Strength on 4" Gyratory Samples, psi		--
Conditioned Tensile Strength on 4" Gyratory Samples, psi		--
Tensile Strength Ratio, %		80 Min.

Aggregate Properties			
Nominal Maximum Aggregate Size, mm			19.0
Aggregate Bulk Specific Gravity, G_{sb}			2.308
Aggregate Effective Specific Gravity, G_{se}			2.460
Sieve Size	**%Passing**	**Control Points**	
		Min	**Max**
37.5 mm (1 1/2")	100.0	--	--
25.0 mm (1")	100.0	100	--
19.0 mm (3/4")	93.7	90	100
12.5 mm (1/2")	79.2	--	90
9.5 mm (3/8")	64.4	--	--
4.75 mm (No. 4)	52.5	--	--
2.36 mm (No. 8)	35.5	23	49
2.00 mm (No. 10)	32.2	--	--
1.18 mm (No. 16)	24.6	--	--
0.6 mm (No. 30)	18.5	--	--
0.425 mm (No. 40)	14.1	--	--
0.3 mm (No. 50)	11.1	--	--
0.15 mm (No. 100)	7.4	--	--
0.075 mm (No. 200)	5.39	2	8
Aggregates	**Material Description**		**Bin %**
Aggr. 1	3/4 inch-Gardner		13.0%
Aggr. 2	1/2 inch-Gardner		25.0%
Aggr. 3	3/8 inch-Gardner		12.0%
Aggr. 4	CF-Gardner		40.0%
Aggr. 5	CF-Bee		0.0%
Aggr. 6	Sand-Gardner		10.0%
Aggr. 7			
Aggr. 8			

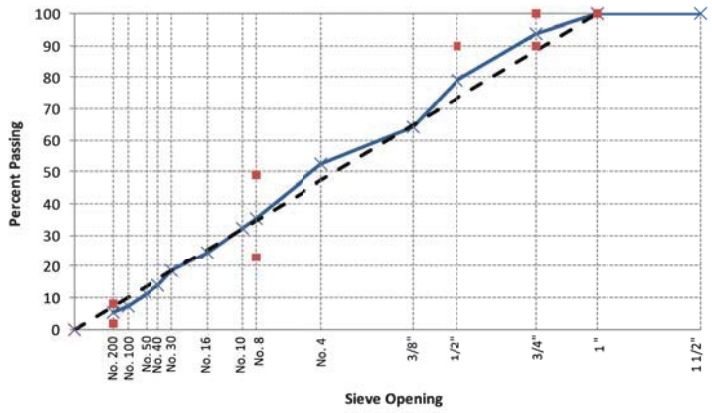

Figure 15.1(a) Mix Design Summary: California Intermediate PG 64-22

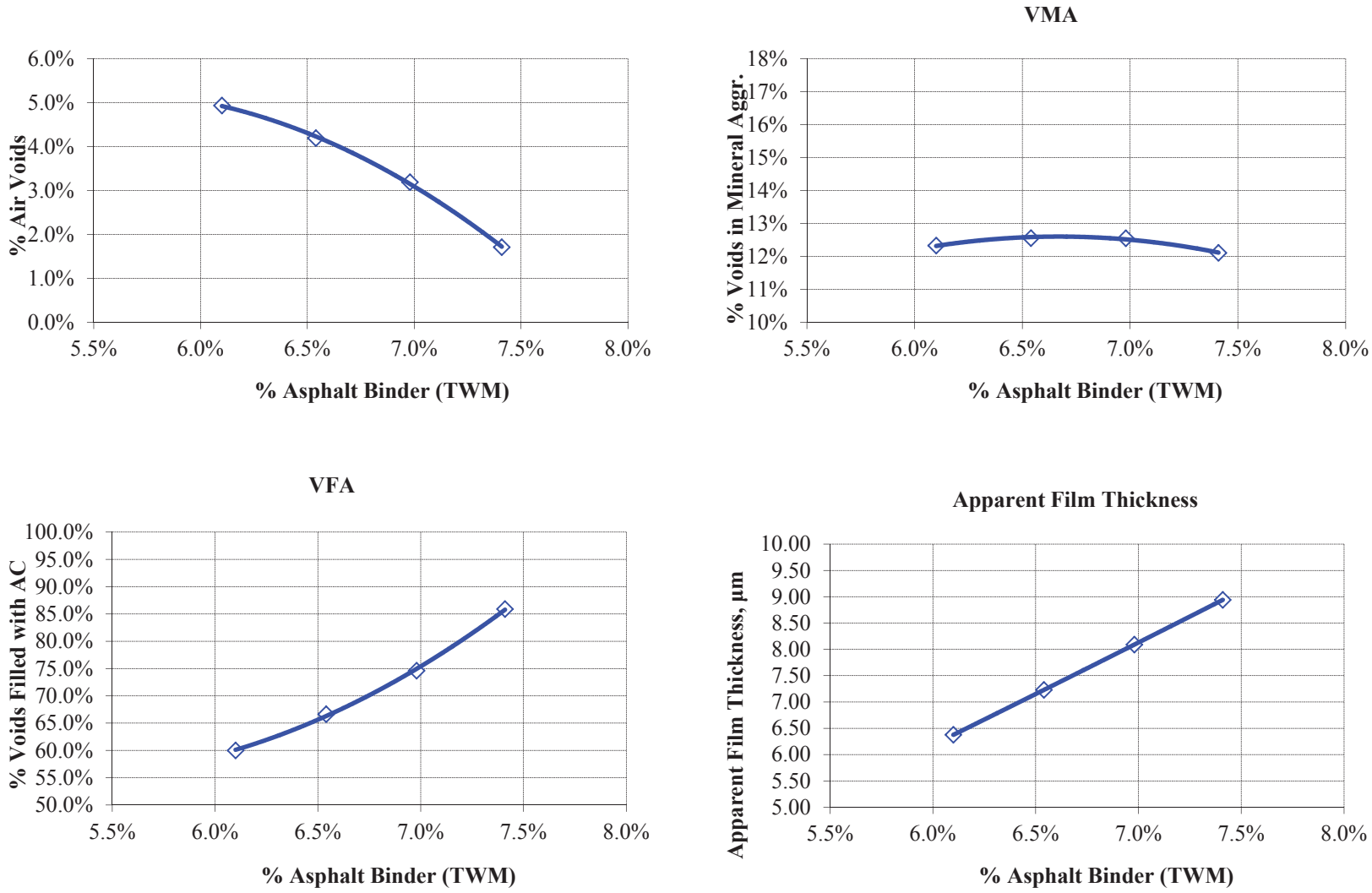

Figure 15.1(b) Mix Design Volumetrics Summary: California Intermediate PG 64-22

SUPERPAVE VOLUMETRIC MIX DESIGN
(According to AASHTO M323, R30, R35, and T312)

Project: E2d.3.c Thermal Cracking - Mix Characteristics
Project Locat CAL19128

Aggregate Source: Gardner-Buellton, CA
Binder Grade: PG64-28 Paramount Nevada

Mix Design		
Nominal Maximum Aggregate Size, mm		19.0
Property	**Value**	**Requirement**
Design ESALs, millions	10	--
N_{inital}	8	--
N_{design}	100	--
N_{max}	160	--
Optimum Binder Content, %	6.10	--
Hydrated Lime, %	None	--
Liquid Antistrip, %	None	--
Max theoretical specific gravity, G_{mm}	2.252	--
%Gmm at N_{ini}	87.1	≤ 89.0
%Gmm at N_{des}	96.0	96.0
%Gmm at N_{max}	97.1	≤ 98.0
VMA, %	12.2	13.0% Min.
VFA, %	67.2	65-75
Percent Effective Binder P_{be}, %	3.89	--
Dust Proportion, $P_{0.075}/P_{be}$	1.4	0.6-1.2
Unconditioned Tensile Strength on 6" Gyratory Samples, psi	127	--
Conditioned Tensile Strength on 6" Gyratory Samples, psi	79	--
Tensile Strength Ratio, %	62	80 Min.
Unconditioned Tensile Strength on 4" Gyratory Samples, psi		--
Conditioned Tensile Strength on 4" Gyratory Samples, psi		--
Tensile Strength Ratio, %		80 Min.

Aggregate Properties			
Nominal Maximum Aggregate Size, mm			19.0
Aggregate Bulk Specific Gravity, G_{sb}			2.312
Aggregate Effective Specific Gravity, G_{se}			2.442
Sieve Size	**%Passing**	**Control Points**	
		Min	**Max**
37.5 mm (1 1/2")	100.0	--	--
25.0 mm (1")	100.0	100	--
19.0 mm (3/4")	93.7	90	100
12.5 mm (1/2")	79.2	--	90
9.5 mm (3/8")	64.4	--	--
4.75 mm (No. 4)	52.5	--	--
2.36 mm (No. 8)	35.5	23	49
2.00 mm (No. 10)	32.2	--	--
1.18 mm (No. 16)	24.6	--	--
0.6 mm (No. 30)	18.5	--	--
0.425 mm (No. 40)	14.1	--	--
0.3 mm (No. 50)	11.1	--	--
0.15 mm (No. 100)	7.4	--	--
0.075 mm (No. 200)	5.39	2	8
Aggregates	**Material Description**		**Bin %**
Aggr. 1	3/4 inch-Gardner		13.0%
Aggr. 2	1/2 inch-Gardner		25.0%
Aggr. 3	3/8 inch-Gardner		12.0%
Aggr. 4	CF-Gardner		40.0%
Aggr. 5	CF-Bee		0.0%
Aggr. 6	Sand-Gardner		10.0%
Aggr. 7			
Aggr. 8			

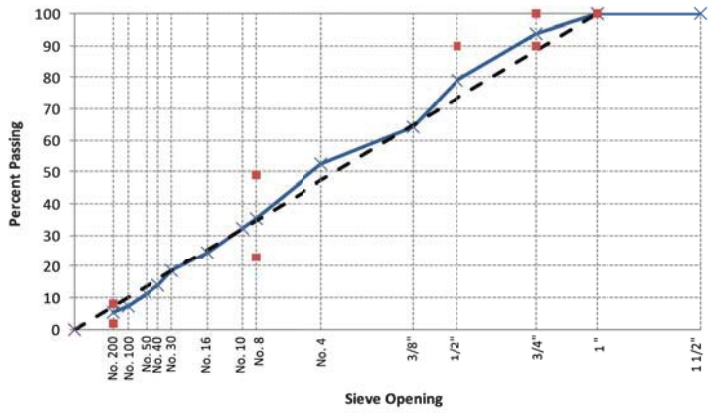

Figure 15.2(a) Mix Design Summary: California Intermediate PG 64-28

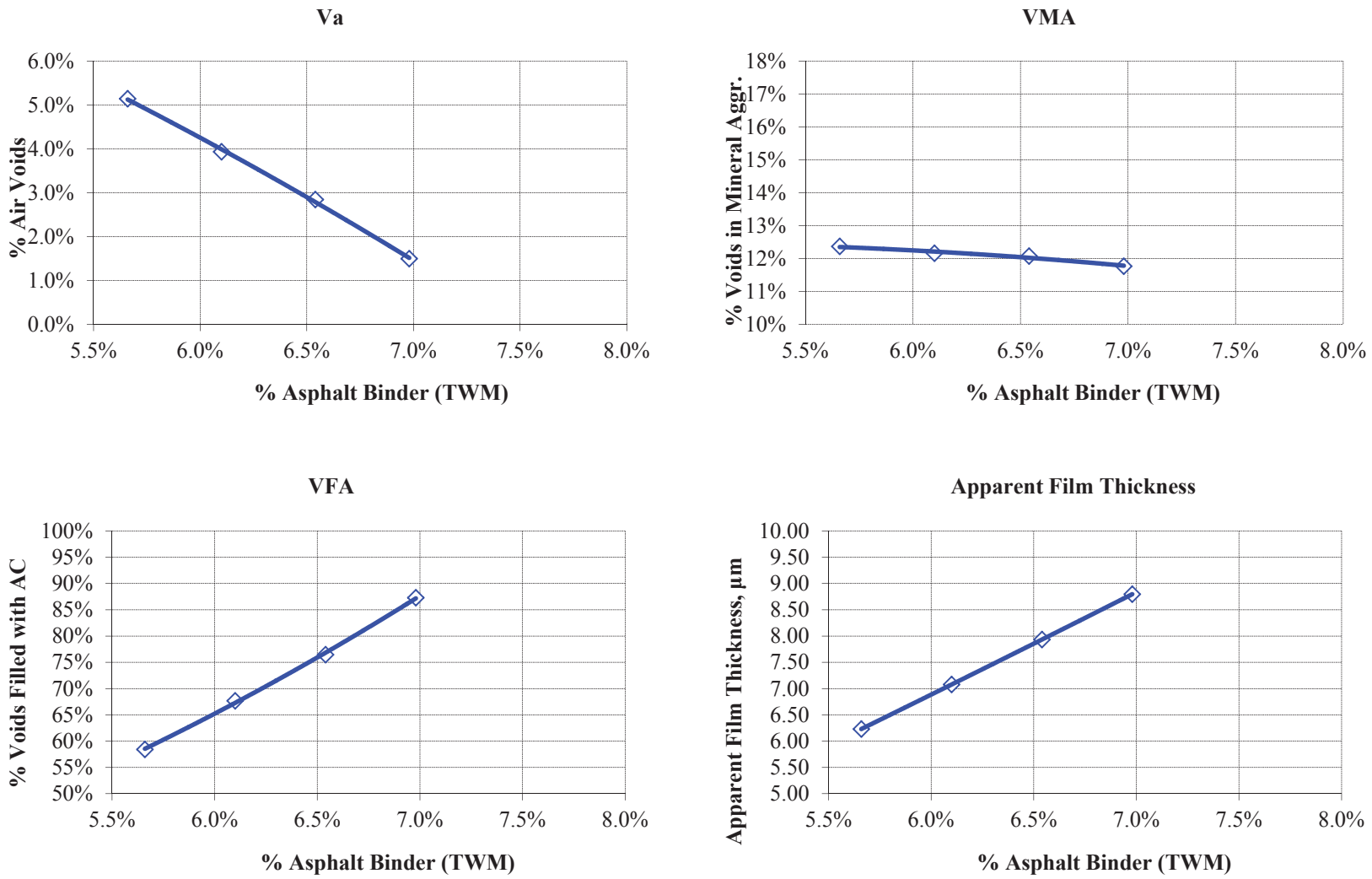

Figure 15.2(b) Mix Design Volumetrics Summary: California Intermediate PG 64-28

SUPERPAVE VOLUMETRIC MIX DESIGN
(According to AASHTO M323, R30, R35, and T312)

Project: E2d.3.c Thermal Cracking - Mix Characteristics
Project Locat CA19F22

Aggregate Source: Buelton, CA
Binder Grade: PG64-22 Paramount Nevada

Mix Design		
Nominal Maximum Aggregate Size, mm		19.0
Property	**Value**	**Requirement**
Design ESALs, millions	10	--
N_{inital}	8	--
N_{design}	100	--
N_{max}	160	--
Optimum Binder Content, %	7.04	--
Hydrated Lime, %	None	--
Liquid Antistrip, %	None	--
Max theoretical specific gravity, G_{mm}	2.222	--
%Gmm at N_{ini}	86.9	≤ 89.0
%Gmm at N_{des}	96.0	96.0
%Gmm at N_{max}	98.9	≤ 98.0
VMA, %	12.9	13.0% Min.
VFA, %	69.3	65-75
Percent Effective Binder P_{be}, %	4.26	--
Dust Proportion, $P_{0.075}/P_{be}$	1.7	0.6-1.2
Unconditioned Tensile Strength on 6" Gyratory Samples, psi		--
Conditioned Tensile Strength on 6" Gyratory Samples, psi		--
Tensile Strength Ratio, %		80 Min.
Unconditioned Tensile Strength on 4" Gyratory Samples, psi		--
Conditioned Tensile Strength on 4" Gyratory Samples, psi		--
Tensile Strength Ratio, %		80 Min.

Aggregate Properties			
Nominal Maximum Aggregate Size, mm			19.0
Aggregate Bulk Specific Gravity, G_{sb}			2.276
Aggregate Effective Specific Gravity, G_{se}			2.438
Sieve Size	**%Passing**	**Control Points**	
		Min	**Max**
37.5 mm (1 1/2")	100.0	--	--
25.0 mm (1")	100.0	100	--
19.0 mm (3/4")	96.1	90	100
12.5 mm (1/2")	90.3	--	90
9.5 mm (3/8")	85.5	--	--
4.75 mm (No. 4)	70.8	--	--
2.36 mm (No. 8)	46.5	23	49
2.00 mm (No. 10)	41.8	--	--
1.18 mm (No. 16)	31.5	--	--
0.6 mm (No. 30)	23.2	--	--
0.425 mm (No. 40)	18.2	--	--
0.3 mm (No. 50)	14.6	--	--
0.15 mm (No. 100)	9.9	--	--
0.075 mm (No. 200)	7.28	2	8
Aggregates	**Material Description**		**Bin %**
Aggr. 1	3/4 inch-Gardner		8.0%
Aggr. 2	1/2 inch-Gardner		6.0%
Aggr. 3	3/8 inch-Gardner		18.0%
Aggr. 4	CF-Gardner		59.0%
Aggr. 5	CF-Bee		0.0%
Aggr. 6	Sand-Gardner		9.0%
Aggr. 7			
Aggr. 8			

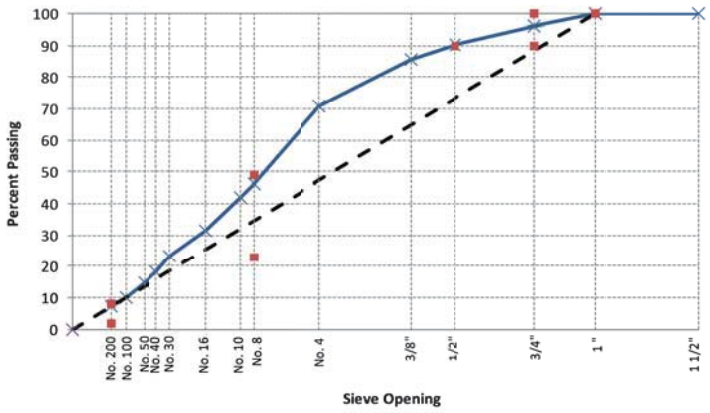

Figure 15.3(a) Mix Design Summary: California Fine PG 64-22

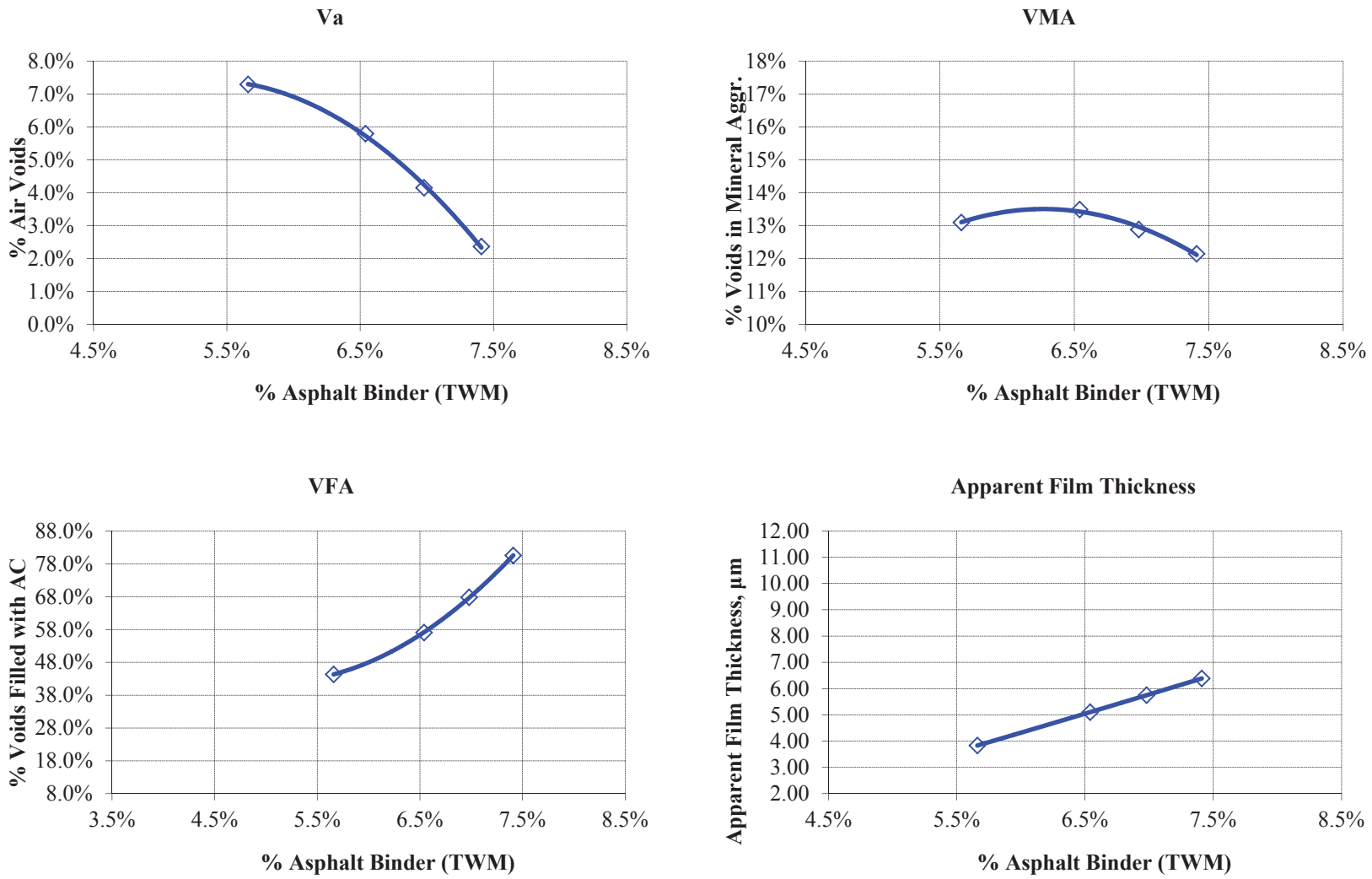

Figure 15.3(b) Mix Design Volumetrics Summary: California Fine PG 64-22

SUPERPAVE VOLUMETRIC MIX DESIGN
(According to AASHTO M323, R30, R35, and T312)

Project: E2d.3.b Thermal Cracking - Agg. Absorption
Project Locat CO19I22

Aggregate Source: Colorado
Binder Grade: PG64-22 Paramount

Mix Design		
Nominal Maximum Aggregate Size, mm		19.0
Property	**Value**	**Requirement**
Design ESALs, millions	10	--
N_{nital}	8	--
N_{design}	100	--
N_{max}	160	--
Optimum Binder Content, %	4.36	--
Hydrated Lime, %	None	--
Liquid Antistrip, %	None	--
Max theoretical specific gravity, G_{mm}	2.500	--
%Gmm at N_{ini}	90.5	≤ 89.0
%Gmm at N_{des}	96.0	96.0
%Gmm at N_{max}	96.5	≤ 98.0
VMA, %	13.0	13.0% Min.
VFA, %	69.3	65-75
Percent Effective Binder P_{be}, %	3.85	--
Dust Proportion, $P_{0.075}/P_{be}$	0.6	0.6-1.2
Unconditioned Tensile Strength on 6" Gyratory Samples, psi	125	--
Conditioned Tensile Strength on 6" Gyratory Samples, psi	62	--
Tensile Strength Ratio, %	49	80 Min.
Unconditioned Tensile Strength on 4" Gyratory Samples, psi		--
Conditioned Tensile Strength on 4" Gyratory Samples, psi		--
Tensile Strength Ratio, %		80 Min.

Aggregate Properties			
Nominal Maximum Aggregate Size, mm			19.0
Aggregate Bulk Specific Gravity, G_{sb}			2.639
Aggregate Effective Specific Gravity, G_{se}			2.676
Sieve Size	**% Passing**	**Control Points**	
		Min	**Max**
37.5 mm (1 1/2")	100.0	--	--
25.0 mm (1")	100.0	100	--
19.0 mm (3/4")	94.6	90	100
12.5 mm (1/2")	66.4	--	90
9.5 mm (3/8")	56.1	--	--
4.75 mm (No. 4)	44.0	--	--
2.36 mm (No. 8)	39.4	23	49
2.00 mm (No. 10)	37.7	--	--
1.18 mm (No. 16)	30.4	--	--
0.6 mm (No. 30)	19.9	--	--
0.425 mm (No. 40)	14.4	--	--
0.3 mm (No. 50)	9.2	--	--
0.15 mm (No. 100)	3.8	--	--
0.075 mm (No. 200)	2.43	2	8
Aggregates	**Material Description**		**Bin %**
Aggr. 1	3/4 inch Morrison		58.0%
Aggr. 2	MC-Crusher Fines		12.0%
Aggr. 3	PV-Processed Sand		0.0%
Aggr. 4	TCS-Conc Sand		30.0%
Aggr. 5			
Aggr. 6			
Aggr. 7			
Aggr. 8			

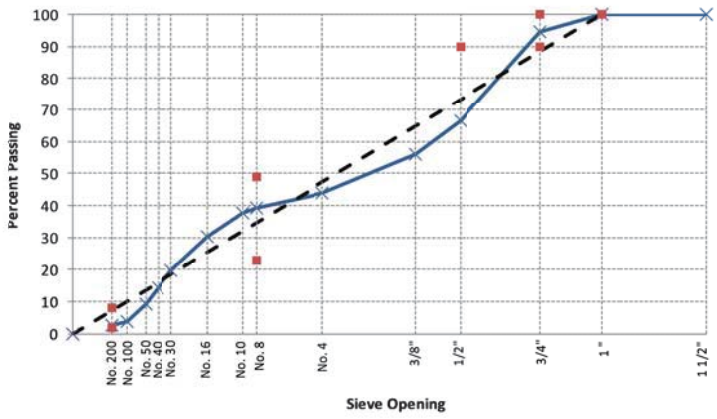

Figure 15.4(a) Mix Design Summary: Colorado Intermediate PG 64-22

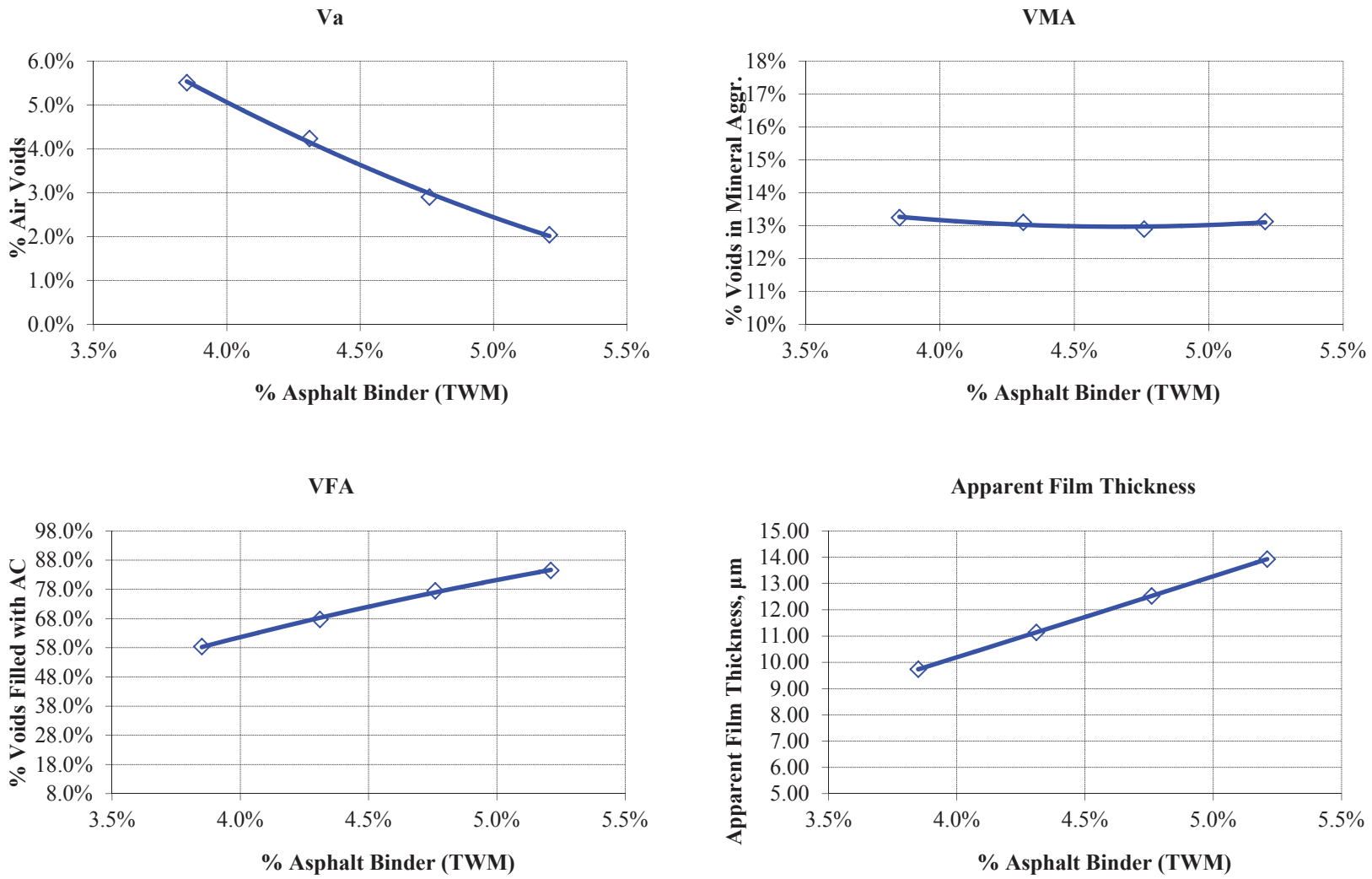

Figure 15.4(b) Mix Design Volumetrics Summary: Colorado Intermediate PG 64-22

SUPERPAVE VOLUMETRIC MIX DESIGN
(According to AASHTO M323, R30, R35, and T312)

Project: E2d.3.b Thermal Cracking - Agg. Absorption
Project Locat CO19I28

Aggregate Source: Colorado
Binder Grade: PG64-28 Paramount

Mix Design		
Nominal Maximum Aggregate Size, mm		19.0
Property	**Value**	**Requirement**
Design ESALs, millions	10	--
N_{inital}	8	--
N_{design}	100	--
N_{max}	160	--
Optimum Binder Content, %	4.40	--
Hydrated Lime, %	None	--
Liquid Antistrip, %	None	--
Max theoretical specific gravity, G_{mm}	2.501	--
%Gmm at N_{ini}	89.8	≤ 89.0
%Gmm at N_{des}	96.0	96.0
%Gmm at N_{max}	97.2	≤ 98.0
VMA, %	13.0	13.0% Min.
VFA, %	69.2	65-75
Percent Effective Binder P_{be}, %	3.81	--
Dust Proportion, $P_{0.075}/P_{be}$	0.6	0.6-1.2
Unconditioned Tensile Strength on 6" Gyratory Samples, psi	89	--
Conditioned Tensile Strength on 6" Gyratory Samples, psi	75	--
Tensile Strength Ratio, %	84	80 Min.
Unconditioned Tensile Strength on 4" Gyratory Samples, psi		--
Conditioned Tensile Strength on 4" Gyratory Samples, psi		--
Tensile Strength Ratio, %		80 Min.

Aggregate Properties			
Nominal Maximum Aggregate Size, mm			19.0
Aggregate Bulk Specific Gravity, G_{sb}			2.639
Aggregate Effective Specific Gravity, G_{se}			2.681
Sieve Size	**% Passing**	**Control Points**	
		Min	**Max**
37.5 mm (1 1/2")	100.0	--	--
25.0 mm (1")	100.0	100	--
19.0 mm (3/4")	94.6	90	100
12.5 mm (1/2")	66.4	--	90
9.5 mm (3/8")	56.1	--	--
4.75 mm (No. 4)	44.0	--	--
2.36 mm (No. 8)	39.4	23	49
2.00 mm (No. 10)	37.7	--	--
1.18 mm (No. 16)	30.4	--	--
0.6 mm (No. 30)	19.9	--	--
0.425 mm (No. 40)	14.4	--	--
0.3 mm (No. 50)	9.2	--	--
0.15 mm (No. 100)	3.8	--	--
0.075 mm (No. 200)	2.43	2	8
Aggregates	**Material Description**		**Bin %**
Aggr. 1	3/4 inch Morrison		58.0%
Aggr. 2	MC-Crusher Fines		12.0%
Aggr. 3	PV-Processed Sand		0.0%
Aggr. 4	TCS-Conc Sand		30.0%
Aggr. 5			
Aggr. 6			
Aggr. 7			
Aggr. 8			

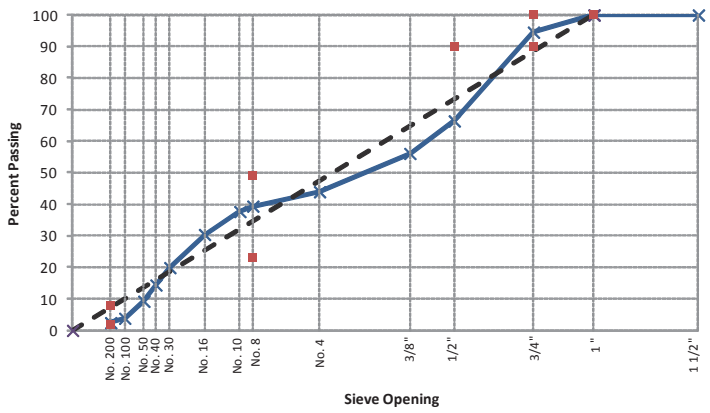

Figure 15.5(a) Mix Design Summary: Colorado Intermediate PG 64-28

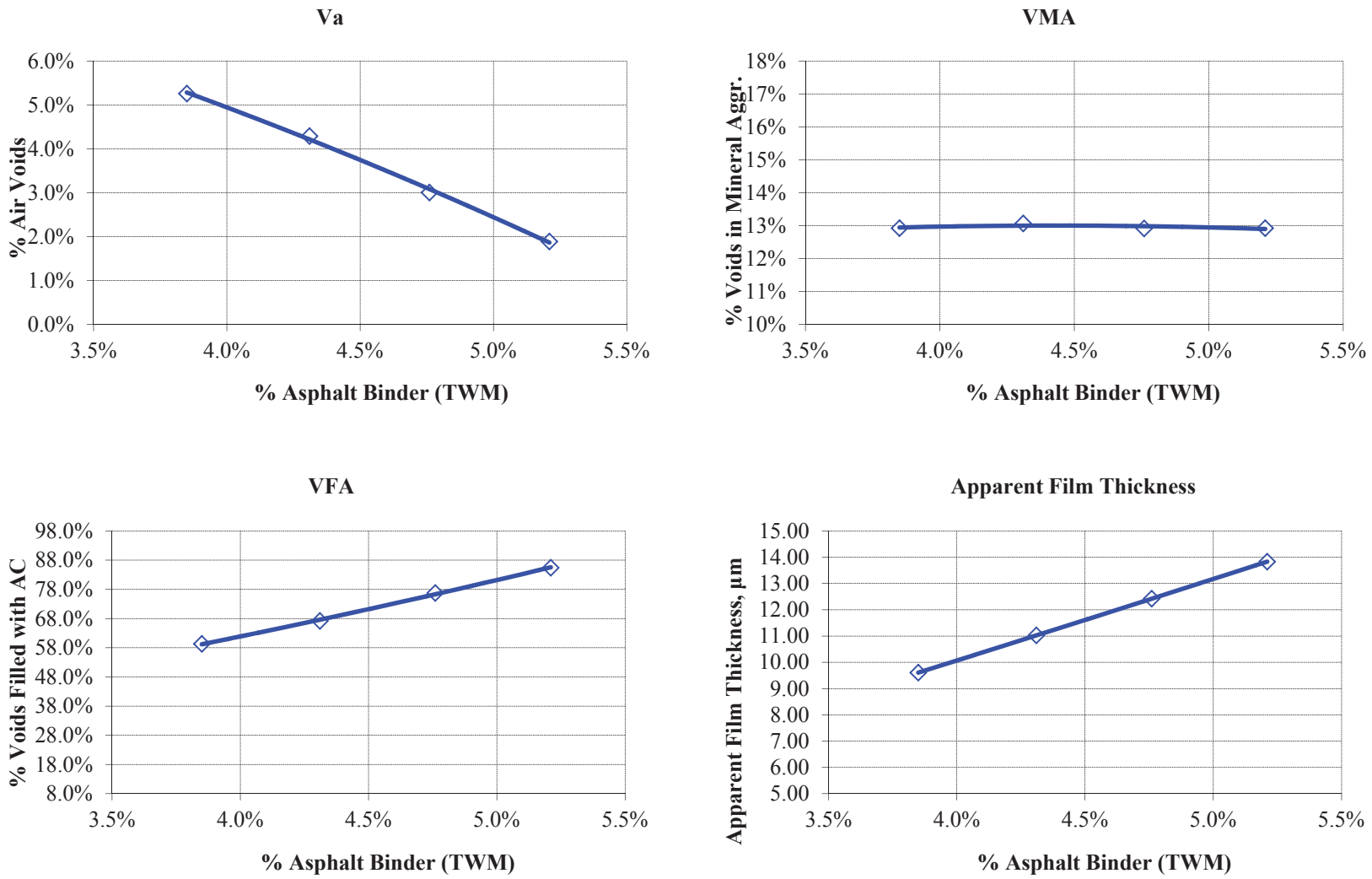

Figure 15.5(b) Mix Design Volumetrics Summary: Colorado Intermediate PG 64-28

SUPERPAVE VOLUMETRIC MIX DESIGN
(According to AASHTO M323, R30, R35, and T312)

Project: E2d.3.b Thermal Cracking - Agg. Absorption
Project Locat NV19122

Aggregate Source: Lockwood, NV
Binder Grade: PG64-22 Paramount

Mix Design		
Nominal Maximum Aggregate Size, mm		19.0
Property	**Value**	**Requirement**
Design ESALs, millions	10	--
N_{inital}	8	--
N_{design}	100	--
N_{max}	160	--
Optimum Binder Content, %	5.18	--
Hydrated Lime, %	None	--
Liquid Antistrip, %	None	--
Max theoretical specific gravity, G_{mm}	2.442	--
%Gmm at N_{ini}	88.1	≤ 89.0
%Gmm at N_{des}	96.0	96.0
%Gmm at N_{max}	97.7	≤ 98.0
VMA, %	13.1	13.0% Min.
VFA, %	69.6	65-75
Percent Effective Binder P_{be}, %	3.97	--
Dust Proportion, $P_{0.075}/P_{be}$	1.0	0.6-1.2
Unconditioned Tensile Strength on 6" Gyratory Samples, psi	114	--
Conditioned Tensile Strength on 6" Gyratory Samples, psi	92	--
Tensile Strength Ratio, %	80	80 Min.
Unconditioned Tensile Strength on 4" Gyratory Samples, psi		--
Conditioned Tensile Strength on 4" Gyratory Samples, psi		--
Tensile Strength Ratio, %		80 Min.

Aggregate Properties			
Nominal Maximum Aggregate Size, mm			19.0
Aggregate Bulk Specific Gravity, G_{sb}			2.557
Aggregate Effective Specific Gravity, G_{se}			2.641
Sieve Size	**%Passing**	**Control Points**	
		Min	**Max**
37.5 mm (1 1/2")	100.0	--	--
25.0 mm (1")	100.0	100	--
19.0 mm (3/4")	99.9	90	100
12.5 mm (1/2")	88.6	--	90
9.5 mm (3/8")	74.4	--	--
4.75 mm (No. 4)	46.9	--	--
2.36 mm (No. 8)	34.2	23	49
2.00 mm (No. 10)	32.6	--	--
1.18 mm (No. 16)	28.5	--	--
0.6 mm (No. 30)	22.8	--	--
0.425 mm (No. 40)	18.2	--	--
0.3 mm (No. 50)	13.0	--	--
0.15 mm (No. 100)	6.4	--	--
0.075 mm (No. 200)	4.02	2	8
Aggregates	**Material Description**		**Bin %**
Aggr. 1	3/4 inch		20.0%
Aggr. 2	1/2 inch		15.0%
Aggr. 3	3/8 inch		24.0%
Aggr. 4	Crushed Dust		21.0%
Aggr. 5	Wadsworth Sand		20.0%
Aggr. 6	Hydrated Lime		0.0%
Aggr. 7			
Aggr. 8			

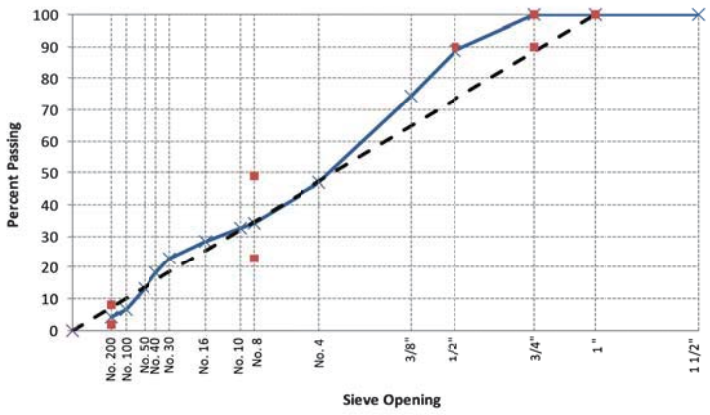

Figure 15.6(a) Mix Design Summary: Nevada Intermediate PG 64-22

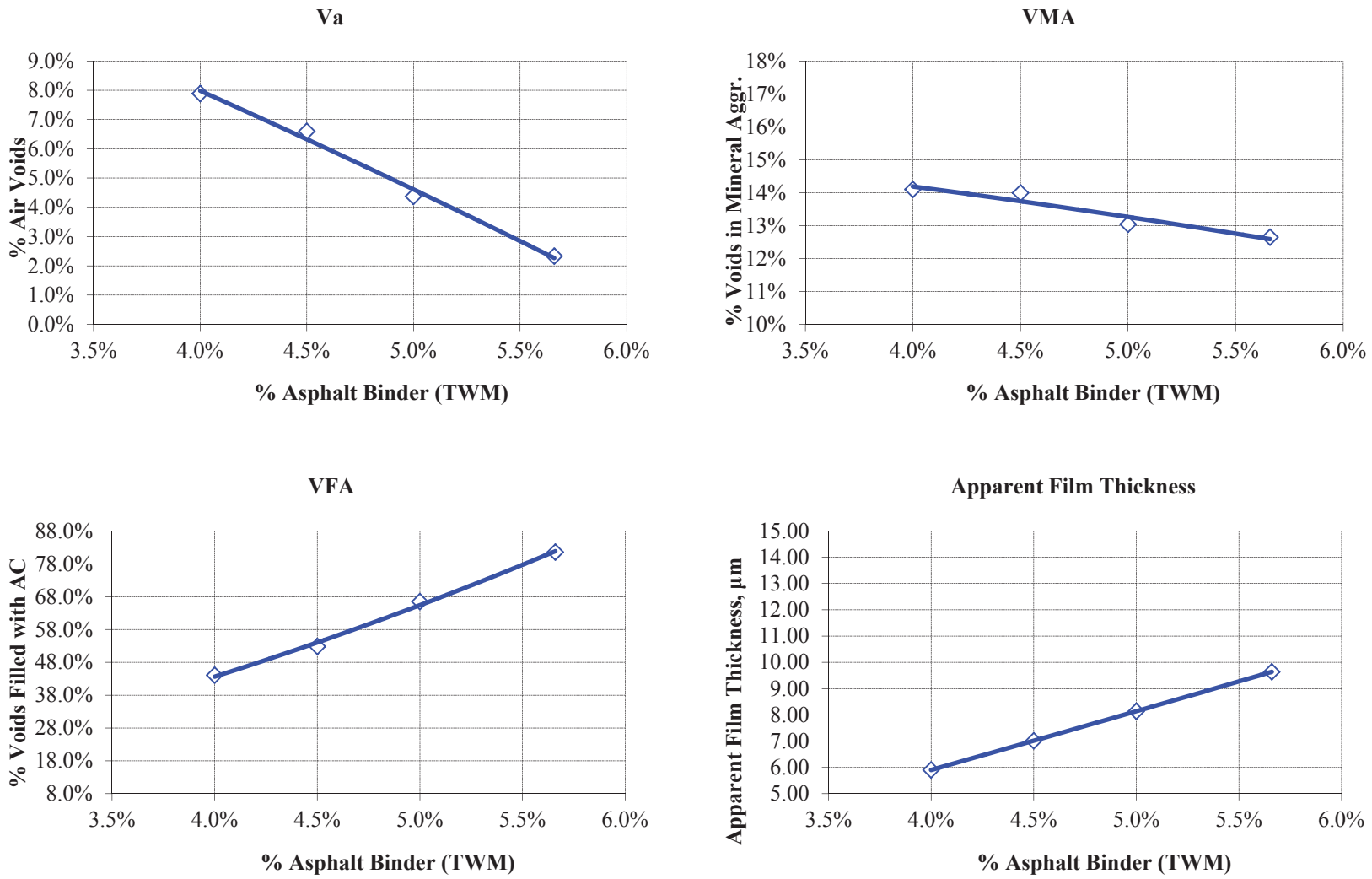

Figure 15.6(b) Mix Design Volumetrics Summary: Nevada Intermediate PG 64-22

SUPERPAVE VOLUMETRIC MIX DESIGN
(According to AASHTO M323, R30, R35, and T312)

Project: E2d.3.b Thermal Cracking - Agg. Absorption
Project Locat NV19128

Aggregate Source: Lockwood, NV
Binder Grade: PG64-28 Paramount

Mix Design		
Nominal Maximum Aggregate Size, mm		19.0
Property	**Value**	**Requirement**
Design ESALs, millions	10	--
N_{inital}	8	--
N_{design}	100	--
N_{max}	160	--
Optimum Binder Content, %	5.11	--
Hydrated Lime, %	None	--
Liquid Antistrip, %	None	--
Max theoretical specific gravity, G_{mm}	2.434	--
%Gmm at N_{ini}	88.1	≤ 89.0
%Gmm at N_{des}	96.0	96.0
%Gmm at N_{max}	96.3	≤ 98.0
VMA, %	13.3	13.0% Min.
VFA, %	69.8	65-75
Percent Effective Binder P_{be}, %	4.05	--
Dust Proportion, $P_{0.075}/P_{be}$	1.0	0.6-1.2
Unconditioned Tensile Strength on 6" Gyratory Samples, psi	96	--
Conditioned Tensile Strength on 6" Gyratory Samples, psi	85	--
Tensile Strength Ratio, %	89	80 Min.
Unconditioned Tensile Strength on 4" Gyratory Samples, psi		--
Conditioned Tensile Strength on 4" Gyratory Samples, psi		--
Tensile Strength Ratio, %		80 Min.

Aggregate Properties			
Nominal Maximum Aggregate Size, mm			19.0
Aggregate Bulk Specific Gravity, G_{sb}			2.557
Aggregate Effective Specific Gravity, G_{se}			2.631
Sieve Size	**%Passing**	**Control Points**	
		Min	**Max**
37.5 mm (1 1/2")	100.0	--	--
25.0 mm (1")	100.0	100	--
19.0 mm (3/4")	99.9	90	100
12.5 mm (1/2")	88.6	--	90
9.5 mm (3/8")	74.4	--	--
4.75 mm (No. 4)	46.9	--	--
2.36 mm (No. 8)	34.2	23	49
2.00 mm (No. 10)	32.6	--	--
1.18 mm (No. 16)	28.5	--	--
0.6 mm (No. 30)	22.8	--	--
0.425 mm (No. 40)	18.2	--	--
0.3 mm (No. 50)	13.0	--	--
0.15 mm (No. 100)	6.4	--	--
0.075 mm (No. 200)	4.02	2	8
Aggregates	**Material Description**		**Bin %**
Aggr. 1	3/4 inch		20.0%
Aggr. 2	1/2 inch		15.0%
Aggr. 3	3/8 inch		24.0%
Aggr. 4	Crushed Dust		21.0%
Aggr. 5	Wadsworth Sand		20.0%
Aggr. 6	Hydrated Lime		0.0%
Aggr. 7			
Aggr. 8			

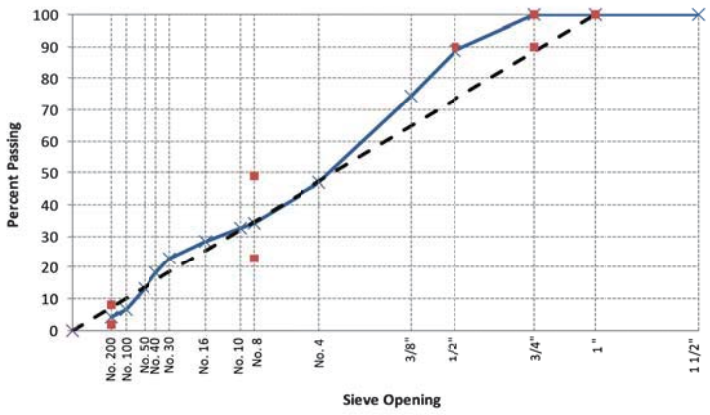

Figure 15.7(a) Mix Design Summary: Nevada Intermediate PG 64-28

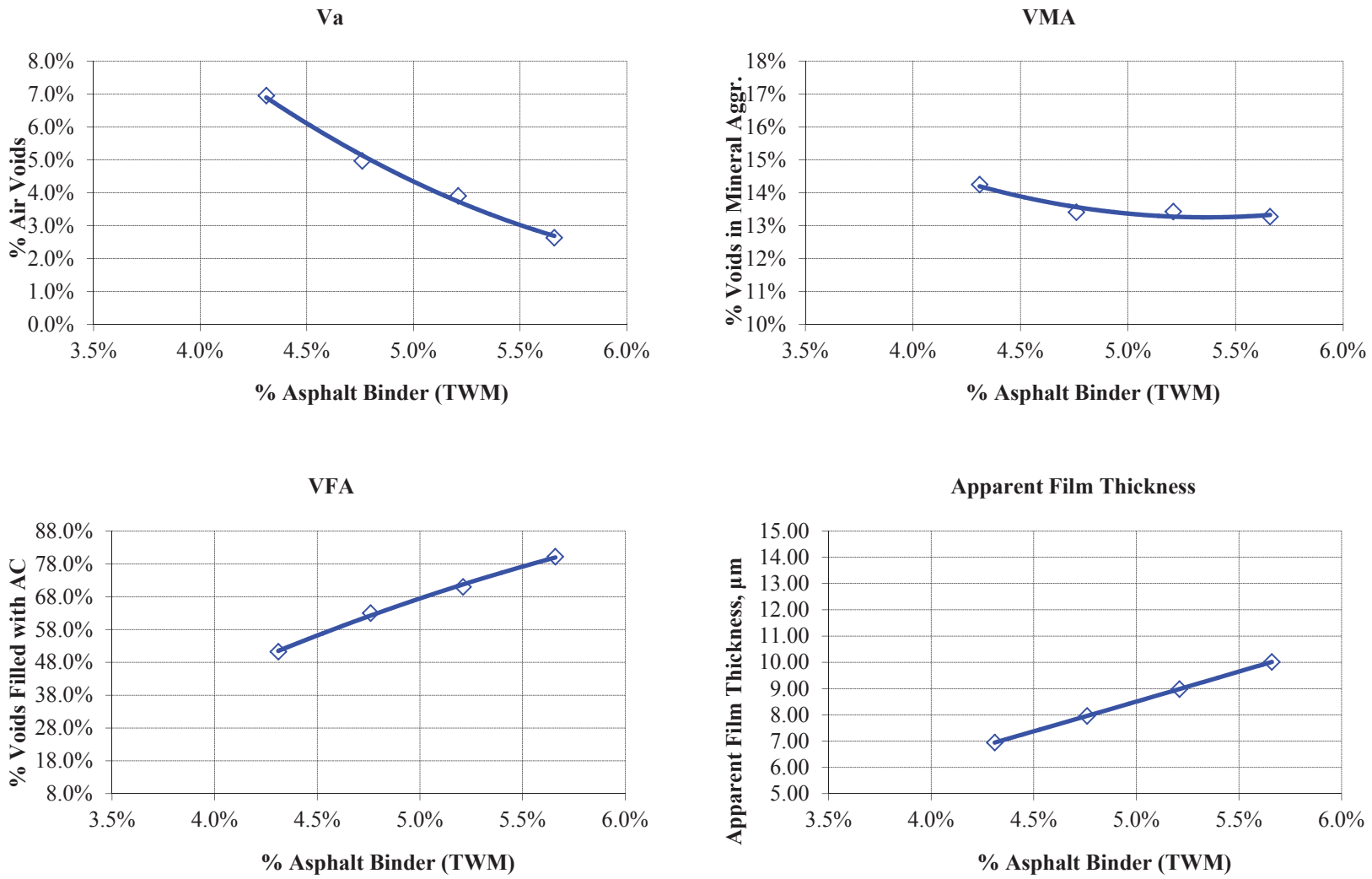

Figure 15.7(b) Mix Design Volumetrics Summary: Nevada Intermediate PG64-28

SUPERPAVE VOLUMETRIC MIX DESIGN
(According to AASHTO M323, R30, R35, and T312)

Project: E2d.3.c Thermal Cracking - Mix Characteristics
Project Locat NV19F28

Aggregate Source: Loclwood, NV
Binder Grade: PG64-28 Paramount

Mix Design		
Nominal Maximum Aggregate Size, mm		19.0
Property	**Value**	**Requirement**
Design ESALs, millions	10	--
N_{inital}	8	--
N_{design}	100	--
N_{max}	160	--
Optimum Binder Content, %	5.45	--
Hydrated Lime, %	None	--
Liquid Antistrip, %	None	--
Max theoretical specific gravity, G_{mm}	2.426	--
%Gmm at N_{ini}	89.0	≤ 89.0
%Gmm at N_{des}	96.0	96.0
%Gmm at N_{max}	97.5	≤ 98.0
VMA, %	14.1	13.0% Min.
VFA, %	71.7	65-75
Percent Effective Binder P_{be}, %	4.42	--
Dust Proportion, $P_{0.075}/P_{be}$	1.1	0.6-1.2
Unconditioned Tensile Strength on 6" Gyratory Samples, psi	105	--
Conditioned Tensile Strength on 6" Gyratory Samples, psi	85	--
Tensile Strength Ratio, %	81	80 Min.
Unconditioned Tensile Strength on 4" Gyratory Samples, psi		--
Conditioned Tensile Strength on 4" Gyratory Samples, psi		--
Tensile Strength Ratio, %		80 Min.

Aggregate Properties			
Nominal Maximum Aggregate Size, mm			19.0
Aggregate Bulk Specific Gravity, G_{sb}			2.564
Aggregate Effective Specific Gravity, G_{se}			2.637
Sieve Size	**%Passing**	**Control Points**	
		Min	**Max**
37.5 mm (1 1/2")	100.0	--	--
25.0 mm (1")	100.0	100	--
19.0 mm (3/4")	99.9	90	100
12.5 mm (1/2")	89.9	--	90
9.5 mm (3/8")	81.2	--	--
4.75 mm (No. 4)	57.1	--	--
2.36 mm (No. 8)	42.3	23	49
2.00 mm (No. 10)	40.3	--	--
1.18 mm (No. 16)	35.1	--	--
0.6 mm (No. 30)	28.0	--	--
0.425 mm (No. 40)	22.3	--	--
0.3 mm (No. 50)	15.9	--	--
0.15 mm (No. 100)	7.9	--	--
0.075 mm (No. 200)	4.89	2	8
Aggregates	**Material Description**		**Bin %**
Aggr. 1	3/4 inch		17.7%
Aggr. 2	1/2 inch		5.5%
Aggr. 3	3/8 inch		25.6%
Aggr. 4	Crushed Dust		26.8%
Aggr. 5	Wadsworth Sand		24.4%
Aggr. 6	Hydrated Lime		0.0%
Aggr. 7			
Aggr. 8			

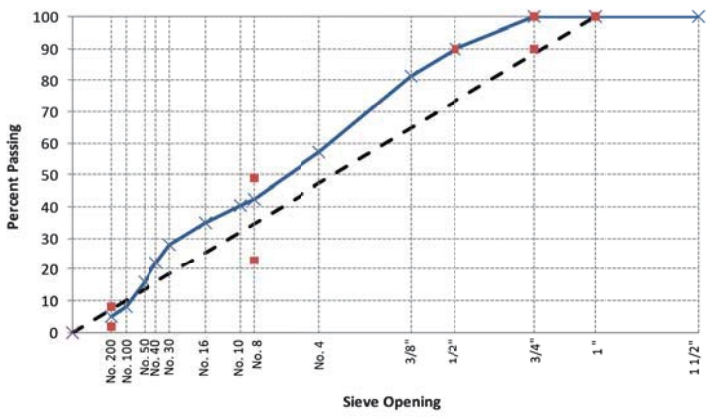

Figure 15.8(a) Mix Design Summary: Nevada Fine PG 64-28

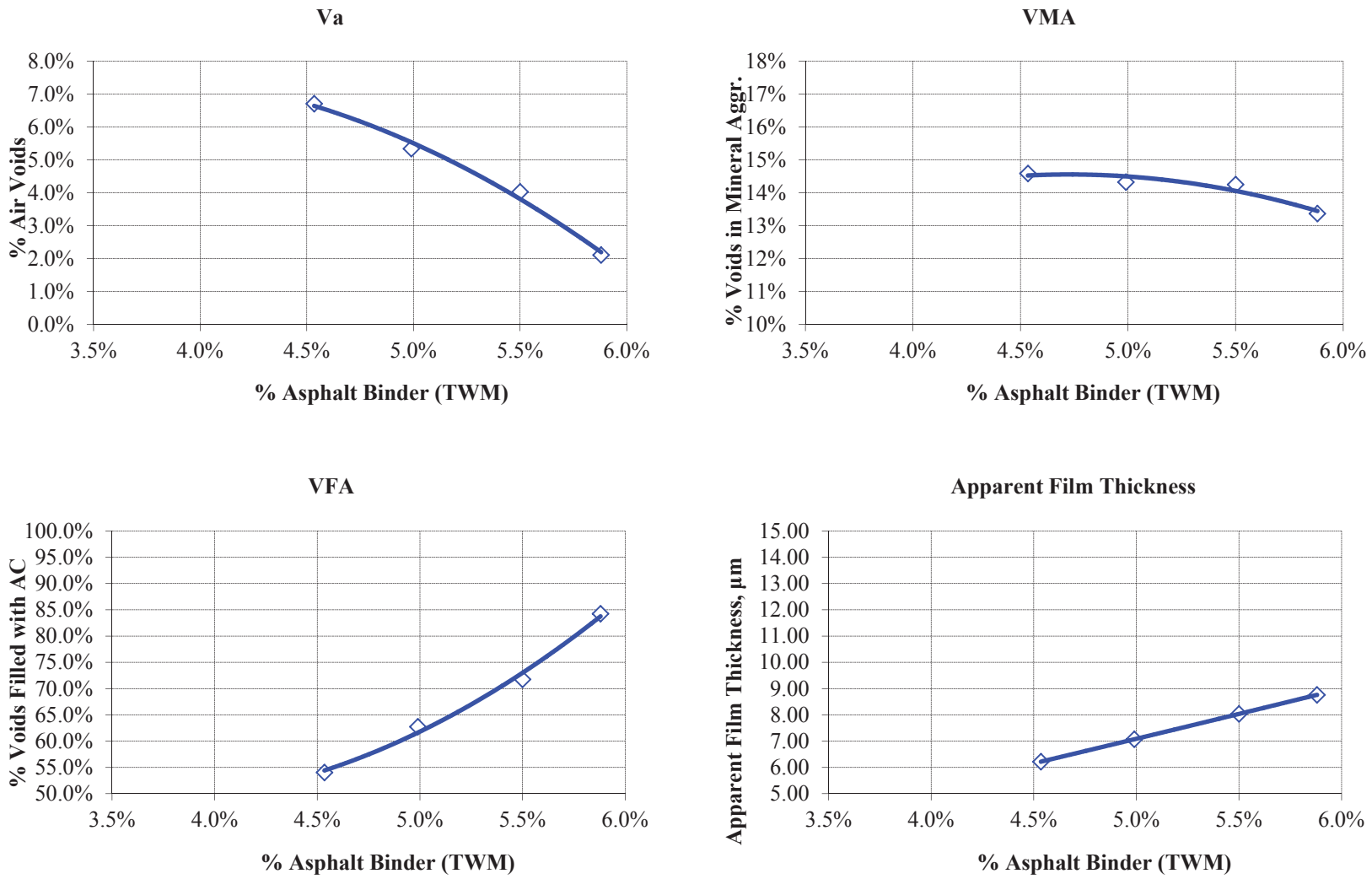

Figure 15.8(b) Mix Design Volumetrics Summary: Nevada Fine PG 64-28

SUPERPAVE VOLUMETRIC MIX DESIGN
(According to AASHTO M323, R30, R35, and T312)

Project: E2d.3.c Thermal Cracking - Mix Characteristics
Project Locat UT12.5128

Aggregate Source: Utah
Binder Grade: PG64-28 Paramount

Mix Design		
Nominal Maximum Aggregate Size, mm		12.5
Property	**Value**	**Requirement**
Design ESALs, millions	10	--
N_{nital}	8	--
N_{design}	100	--
N_{max}	160	--
Optimum Binder Content, %	4.97	--
Hydrated Lime, %	None	--
Liquid Antistrip, %	None	--
Max theoretical specific gravity, G_{mm}	2.483	--
%Gmm at N_{ini}	87.9	≤ 89.0
%Gmm at N_{des}	96.0	96.0
%Gmm at N_{max}	96.2	≤ 98.0
VMA, %	14.5	14.0% Min.
VFA, %	72.3	65-75
Percent Effective Binder P_{be}, %	4.51	--
Dust Proportion, $P_{0.075}/P_{be}$	0.5	0.6-1.2
Unconditioned Tensile Strength on 6" Gyratory Samples, psi	82	--
Conditioned Tensile Strength on 6" Gyratory Samples, psi	82	--
Tensile Strength Ratio, %	100	80 Min.
Unconditioned Tensile Strength on 4" Gyratory Samples, psi		--
Conditioned Tensile Strength on 4" Gyratory Samples, psi		--
Tensile Strength Ratio, %		80 Min.

Aggregate Properties			
Nominal Maximum Aggregate Size, mm			12.5
Aggregate Bulk Specific Gravity, G_{sb}			2.649
Aggregate Effective Specific Gravity, G_{se}			2.683
Sieve Size	**% Passing**	**Control Points**	
		Min	**Max**
37.5 mm (1 1/2")	100.0	--	--
25.0 mm (1")	100.0	--	--
19.0 mm (3/4")	100.0	100	--
12.5 mm (1/2")	95.7	90	100
9.5 mm (3/8")	89.1	--	90
4.75 mm (No. 4)	55.9	--	--
2.36 mm (No. 8)	28.3	28	58
2.00 mm (No. 10)	26.7	--	--
1.18 mm (No. 16)	24.7	--	--
0.6 mm (No. 30)	20.8	--	--
0.425 mm (No. 40)	16.6	--	--
0.3 mm (No. 50)	11.4	--	--
0.15 mm (No. 100)	4.6	--	--
0.075 mm (No. 200)	2.47	2	10
Aggregates	**Material Description**		**Bin %**
Aggr. 1	3/4"		9.5%
Aggr. 2	7/16"		23.6%
Aggr. 3	1/4"		40.4%
Aggr. 4	T3		4.3%
Aggr. 5	Wadsworth		22.2%
Aggr. 6			
Aggr. 7			
Aggr. 8			

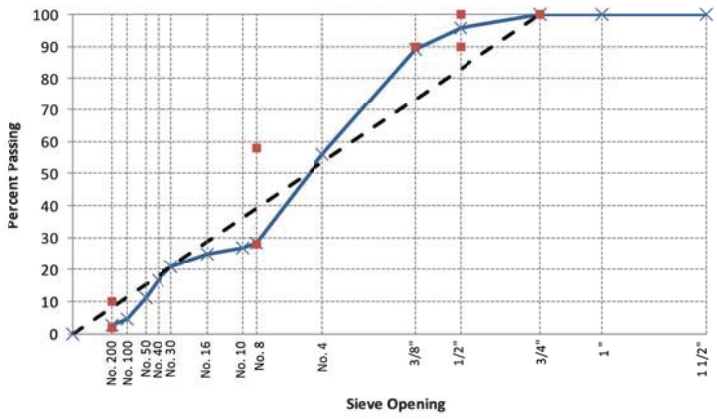

Figure 15.9(a) Mix Design Summary: Utah Intermediate PG 64-28

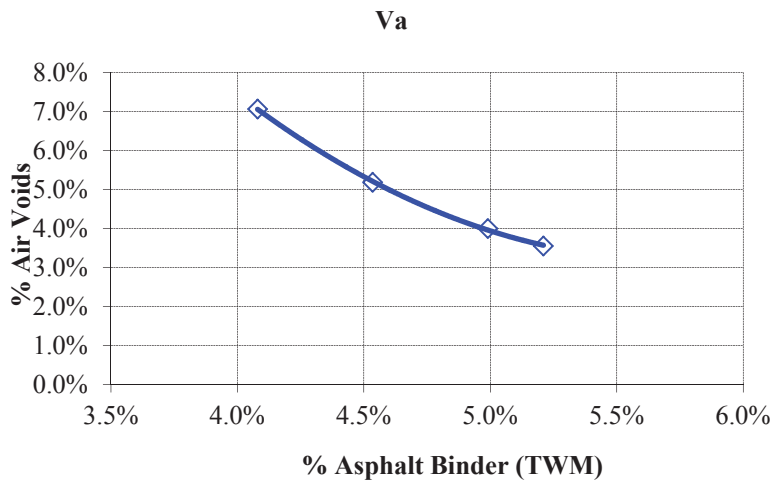

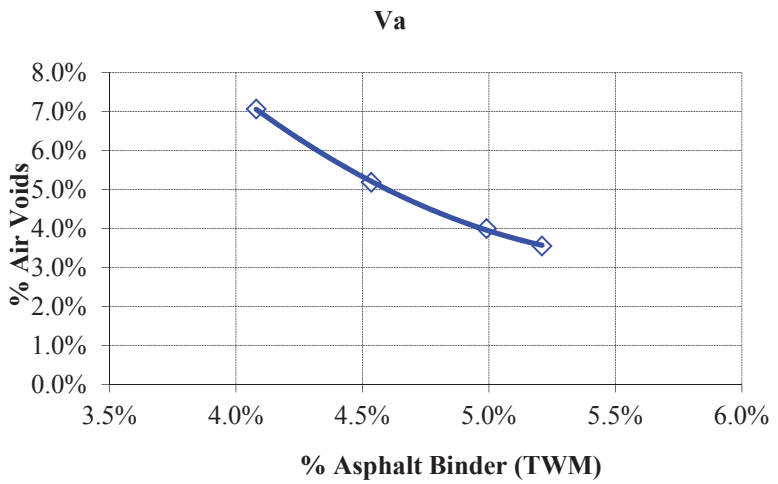

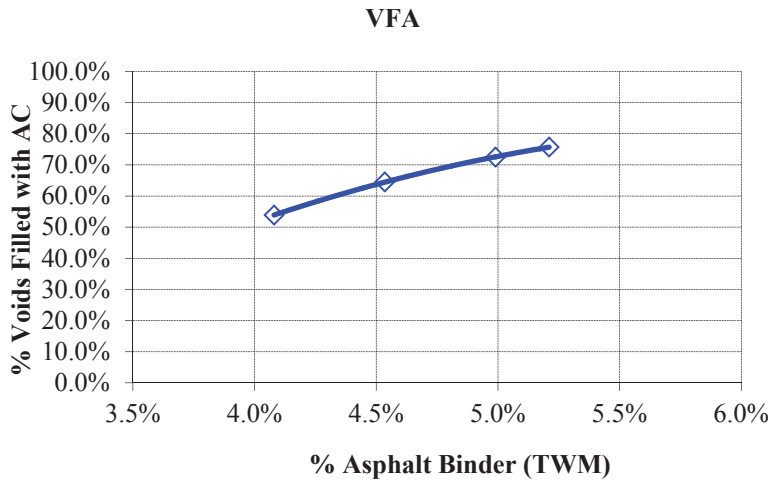

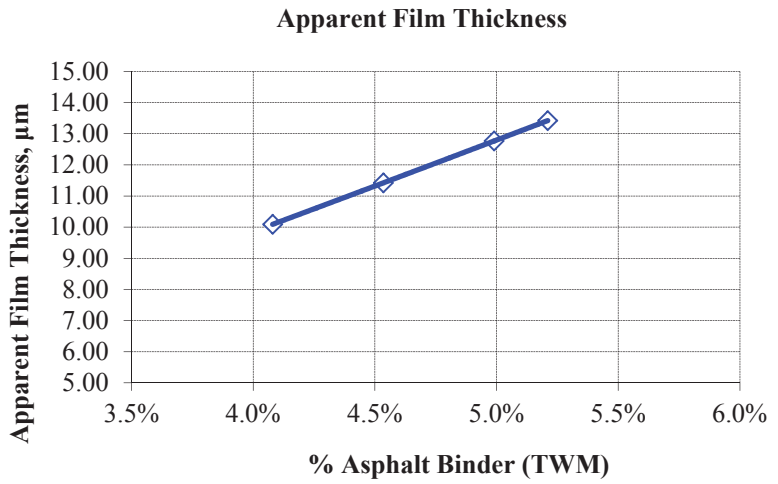

Figure 15.9(b) Mix Design Volumetrics Summary: Utah Intermediate PG 64-28

SUPERPAVE VOLUMETRIC MIX DESIGN
(According to AASHTO M323, R30, R35, and T312)

Project: E2d.3.c Thermal Cracking - Mix Characteristics
Project Locat UT12.5F28

Aggregate Source: Utal
Binder Grade: PG64-28 Paramount

Mix Design		
Nominal Maximum Aggregate Size, mm		12.5
Property	**Value**	**Requirement**
Design ESALs, millions	10	--
N_{inital}	8	--
N_{design}	100	--
N_{max}	160	--
Optimum Binder Content, %	5.57	--
Hydrated Lime, %	None	--
Liquid Antistrip, %	None	--
Max theoretical specific gravity, G_{mm}	2.455	--
%Gmm at N_{ini}	90.1	≤ 89.0
%Gmm at N_{des}	96.0	96.0
%Gmm at N_{max}	96.1	≤ 98.0
VMA, %	14.9	14.0% Min.
VFA, %	73.2	65-75
Percent Effective Binder P_{be}, %	4.75	--
Dust Proportion, $P_{0.075}/P_{be}$	0.6	0.6-1.2
Unconditioned Tensile Strength on 6" Gyratory Samples, psi	90	--
Conditioned Tensile Strength on 6" Gyratory Samples, psi	84	--
Tensile Strength Ratio, %	93	80 Min.
Unconditioned Tensile Strength on 4" Gyratory Samples, psi		--
Conditioned Tensile Strength on 4" Gyratory Samples, psi		--
Tensile Strength Ratio, %		80 Min.

Aggregate Properties			
Nominal Maximum Aggregate Size, mm			12.5
Aggregate Bulk Specific Gravity, G_{sb}			2.616
Aggregate Effective Specific Gravity, G_{se}			2.675
Sieve Size	**%Passing**	**Control Points**	
		Min	**Max**
37.5 mm (1 1/2")	100.0	--	--
25.0 mm (1")	100.0	--	--
19.0 mm (3/4")	100.0	100	--
12.5 mm (1/2")	94.8	90	100
9.5 mm (3/8")	87.9	--	90
4.75 mm (No. 4)	61.9	--	--
2.36 mm (No. 8)	42.1	28	58
2.00 mm (No. 10)	40.8	--	--
1.18 mm (No. 16)	38.2	--	--
0.6 mm (No. 30)	32.2	--	--
0.425 mm (No. 40)	25.4	--	--
0.3 mm (No. 50)	17.2	--	--
0.15 mm (No. 100)	6.6	--	--
0.075 mm (No. 200)	3.02	2	10
Aggregates	**Material Description**		**Bin %**
Aggr. 1	3/4"		11.5%
Aggr. 2	7/16"		18.2%
Aggr. 3	1/4"		26.4%
Aggr. 4	T3		9.0%
Aggr. 5	Wadsworth		34.9%
Aggr. 6			
Aggr. 7			
Aggr. 8			

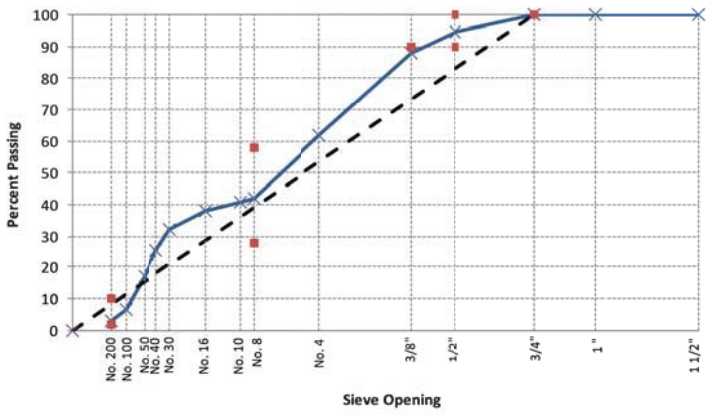

Figure 15.10(a) Mix Design Summary: Utah Fine PG 64-28

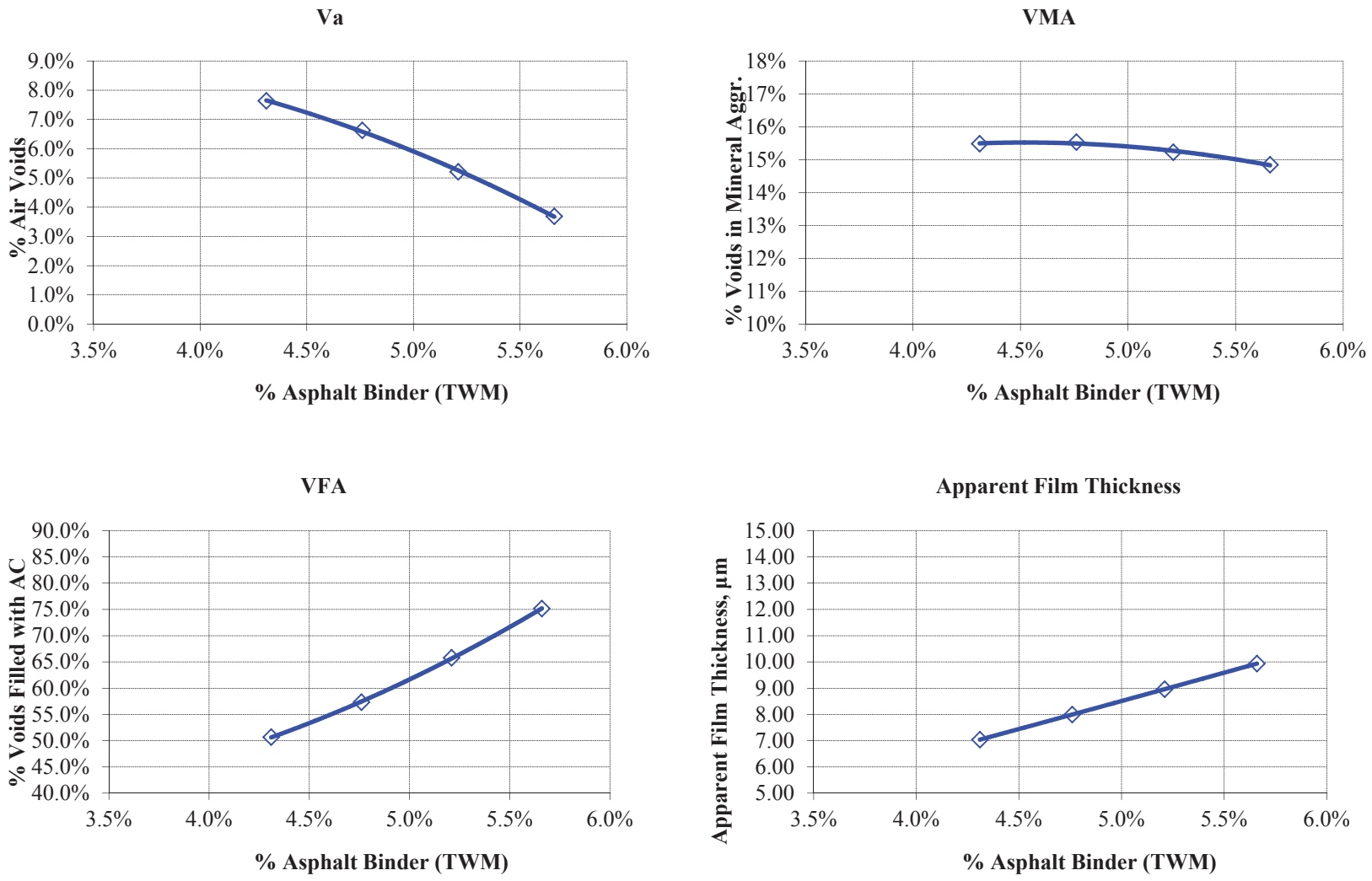

Figure 15.10(b) Mix Design Volumetrics Summary: Utah Fine PG 64-28

16 APPENDIX D:

Summary of Established Mix Designs for Field Mixtures

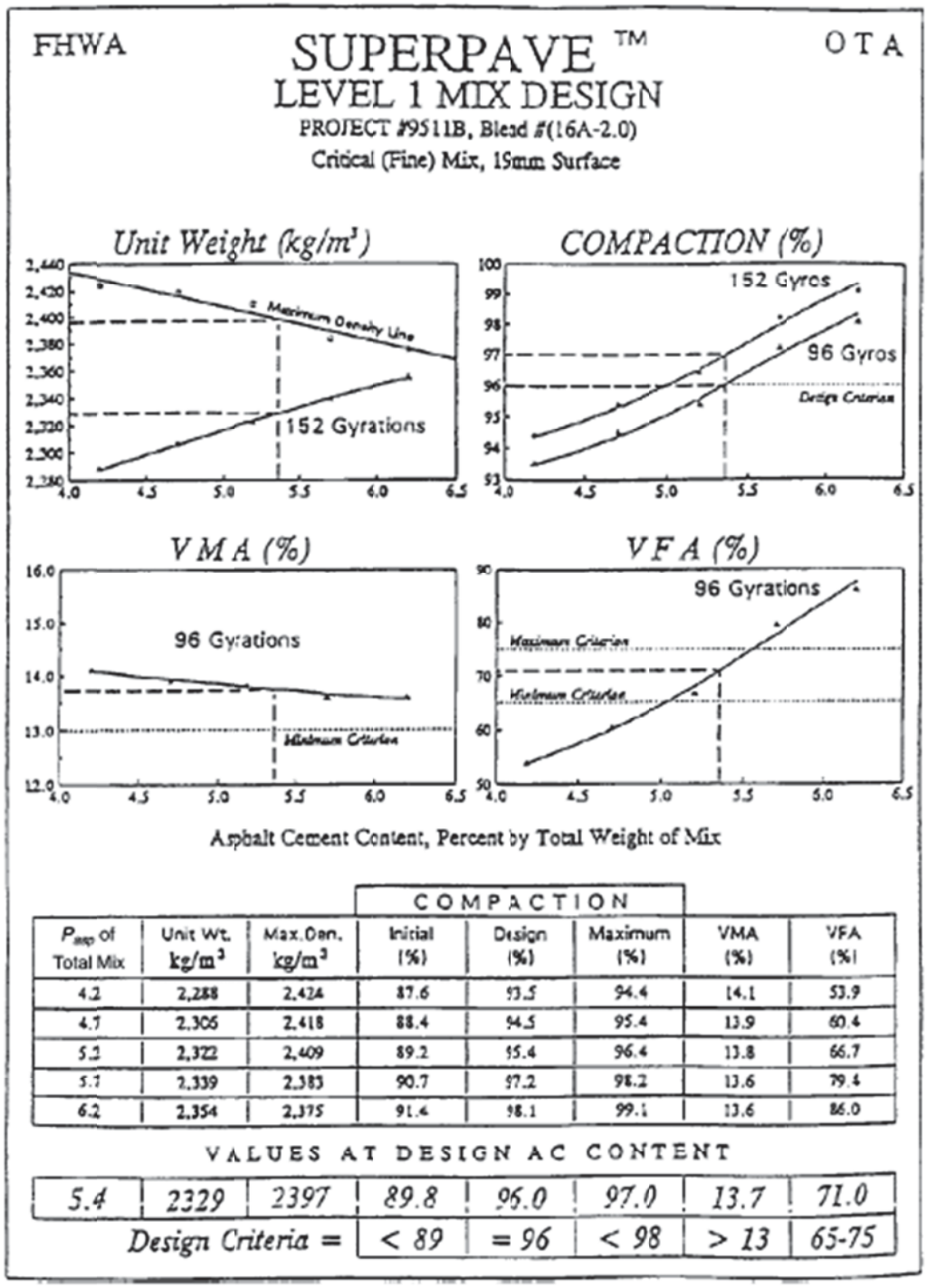

			COMPACTION				
P_{ep} of Total Mix	Unit Wt. kg/m³	Max.Den. kg/m³	Initial (%)	Design (%)	Maximum (%)	VMA (%)	VFA (%)
4.2	2,288	2,424	87.6	93.5	94.4	14.1	53.9
4.7	2,305	2,418	88.4	94.5	95.4	13.9	60.4
5.2	2,322	2,409	89.2	95.4	96.4	13.8	66.7
5.7	2,339	2,383	90.7	97.2	98.2	13.6	79.4
6.2	2,354	2,375	91.4	98.1	99.1	13.6	86.0

VALUES AT DESIGN AC CONTENT

5.4	2329	2397	89.8	96.0	97.0	13.7	71.0
Design Criteria =			< 89	= 96	< 98	> 13	65-75

Figure 16.1 Mix Design Summary: WesTrack Fine, 1995 West Coast Refinery PG 64-22 (Epps et al., 2002)

Project:	WesTrack Rehab
Mixture ID:	F
Other:	Lockwood at Patrick (June 7, 1997 sampling)
Date:	June 12, 1997
Technician:	TO

P_{asp}	% Gmmd	V_{air}	% VMA	% VFA	% Gmmi	% Gmmm	F/A
4.0							
4.5	93.8	6.2	14.6	57.6	84.4	95.2	1.56
5.0	95.1	4.9	14.6	66.8	85.5	96.6	1.35
5.5	95.8	4.2	14.9	72.0	86.5	97.2	1.23
6.0	96.3	3.7	15.4	75.9	87.6	97.6	1.12
6.5	97.0	3.0	15.9	81.5	87.3	98.3	1.01
7.0							

Properties at optimum asphalt content

P_{asp}	% Gmmd	V_{air}	% VMA	% VFA	% Gmmi	% Gmmm	F/A
5.65	96.0	4.0	15	73	86.6	97.5	1.18

Figure 16.2 Mix Design Summary: WesTrack Coarse, 1997 Idaho Asphalt PG 64-22 (Epps et al., 2002)

GRANITE CONSTRUCTION COMPANY SINCE 1922

April 1, 2006

Asphalt Concrete Mix Design : Type II 75 Blow AC - 20 with Lime

Aggregate Source: Lockwood Quarry

Design Criteria: Orange Book / Asphalt Institute MS-2

The following is a summary of laboratory testing and Mix Design criteria for a Type II Hot Mix Asphalt Concrete. All material and mix design procedures were performed in our AMRL accredited Lockwood Materials Laboratory by WAQTC / NAQTC qualified technicians in accordance with the above referenced Standard Specifications and Marshall mix design method as specified in the most recent version of the Asphalt Institute Manual Series 2 (MS – 2).

During production of this material, process control testing will be conducted to determine if mix properties meet acceptance criteria. Past experience has shown that differences in mix properties may exist between laboratory generated specimens for mix design purposes, and actual plant produced material. Adjustments to plant bin percentages and asphalt set point may be necessary during production to achieve job mix formula targets and or in-place specification requirements.

MIX PROPERTIES

Asphalt Cement:	Paramount Nevada AC - 20
Specific Gravity of Asphalt Cement:	1.0323
Aggregate Proportions:	18% ¾" HMA 16% ½" HMA 15% 3/8"HMA 41% Rock Dust 10% Wade Sand
Anti-Strip Agent:	Hydrated Lime @ 1 ½% Dry Weight of Aggregate
Number of Compaction Blows:	75 Automatic Hammer
Compaction Temperature:	295 Degrees Fahrenheit
Mixing Temperature:	310 Degrees Fahrenheit

Nevada Operations

Reply to the following office

☐Sparks - Main Office
1900 Glendale • P.O. Box 2087
Sparks, NV 89432-2087
775) 358-8708 • FAX (775) 358-0378

☐Las Vegas Office
4055 E. Post Rd. • P.O Box 95715
Las Vegas, NV 89190
(702) 696-1090 • FAX (702) 696-1091

☐Carson City Office
5855 Sheep Drive
Carson City, NV 89701-1442
(775) 884-4100 • FAX (775) 884-3334

Figure 16.3(a) Mix Design Summary: Moana Lane Extension PG 64-22

08/24/2005 19:23 7823420254 GRANITE CONSTRUCTION PAGE 8

Page 2

Optimum Asphalt Content:	4.9 % Total Weight of Mix 5.2 % Dry Weight of Aggregate
Marshall Stability:	4025 lbs.
Marshall Flow (0.01 inches):	13.8
Total Air Voids:	4.0 %
Voids in Mineral Aggregate:	13.3
Voids Filled With Asphalt	70.0 %
Unit Weight:	147.8 PCF

Attached are the results of laboratory testing of the aggregates and asphalt concrete design.

Respectfully Submitted,
Granite Construction Company

John C. Elkins
Engineering Services Manager

Reviewed By:

Adam J. Hand, PE, PhD
Quality System Engineer

PROFESSIONAL ENGINEER STATE OF NEVADA
ADAM J.T. HAND
Exp: 6/30/07
CIVIL
No. 15765

Date: April 1, 2006
Granite Construction Company
Type II 75 Blow AC - 20 with Lime
Lookwood Quarry
Paramount Nevada Asphalt

Figure 16.3(b) Mix Design Summary: Moana Lane Extension PG 64-22, continued

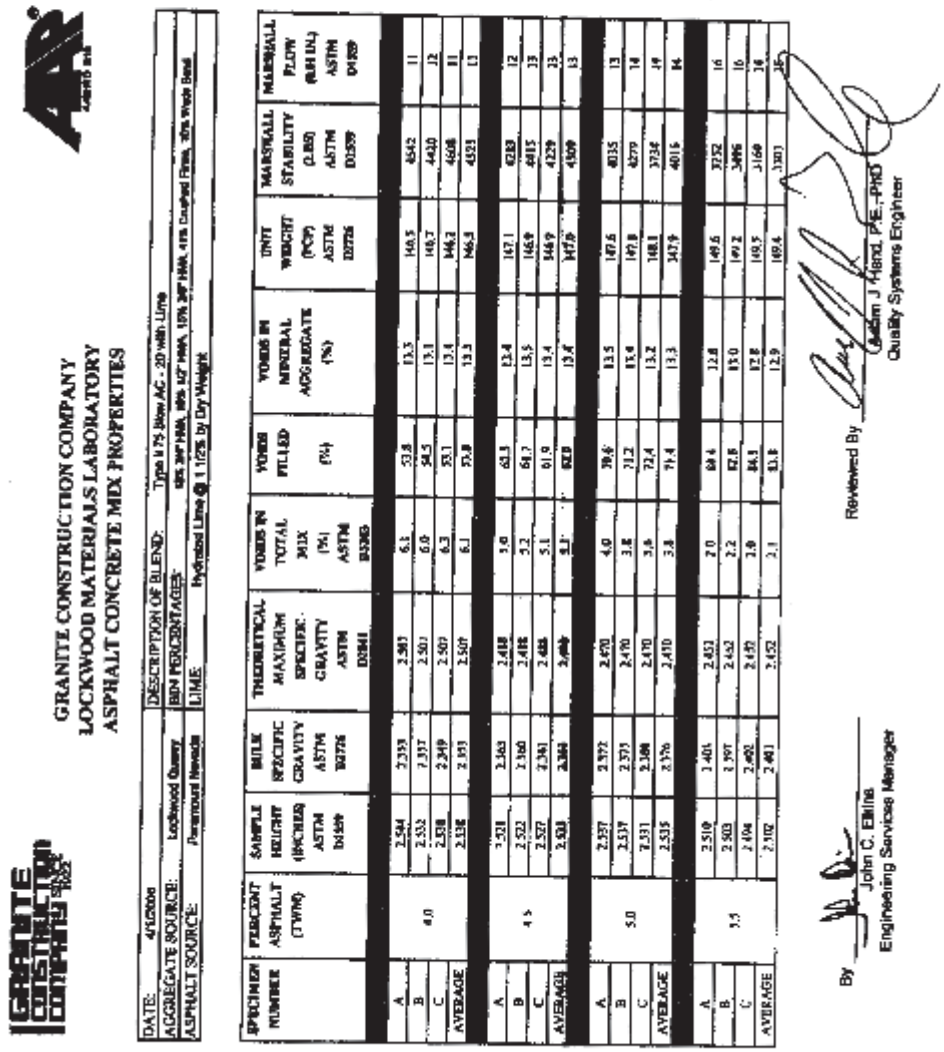

GRANITE CONSTRUCTION COMPANY
LOCKWOOD MATERIALS LABORATORY
ASPHALT CONCRETE MIX PROPERTIES

DATE: 4/12/2006 DESCRIPTION OF BLEND: Type II PG Blow AC - 20 with Lime
AGGREGATE SOURCE: Lockwood Quarry BIN PERCENTAGES: 62% 3/4" HMA, 8% 1/2" HMA, 10% 3/8" HMA, 11% Crushed Fines, 10% Wash Sand
ASPHALT SOURCE: Paramount Nevada LIME: Hydrated Lime @ 1 1/2% by Dry Weight

SPECIMEN NUMBER	PERCENT ASPHALT (TWW)	SAMPLE HEIGHT (INCHES) ASTM D3549	BULK SPECIFIC GRAVITY ASTM D2726	THEORETICAL MAXIMUM SPECIFIC GRAVITY ASTM D2041	VOIDS IN TOTAL MIX (%) ASTM D3203	VOIDS FILLED (%)	VOIDS IN MINERAL AGGREGATE (%)	UNIT WEIGHT (PCF) ASTM D2726	MARSHALL STABILITY (LBS) ASTM D1559	MARSHALL FLOW (0.01 IN.) ASTM D1559
A	4.0	2.544	2.353	2.567	6.1	53.8	13.3	146.5	4542	11
B		2.532	2.357	2.563	6.6	54.5	13.1	146.7	4430	12
C		2.538	2.349	2.563	6.3	53.1	13.4	146.3	4668	11
AVERAGE		2.538	2.353	2.564	6.1	53.8	13.3	146.5	4521	13
A	4.5	2.521	2.363	2.488	5.0	63.3	13.4	147.1	4283	12
B		2.522	2.360	2.488	5.2	61.7	13.5	146.9	4415	13
C		2.527	2.361	2.488	5.1	61.9	13.4	146.9	4229	13
AVERAGE		2.523	2.361	2.488	5.1	62.3	13.4	147.0	4309	13
A	5.0	2.537	2.372	2.470	4.0	70.6	13.5	147.6	4035	13
B		2.537	2.373	2.470	3.8	71.2	13.4	147.8	4279	14
C		2.531	2.368	2.470	3.8	72.4	13.2	148.1	3734	19
AVERAGE		2.535	2.376	2.470	3.8	71.4	13.3	147.8	4016	14
A	5.5	2.510	2.401	2.452	2.0	84.4	12.8	149.6	3732	16
B		2.503	2.397	2.452	2.2	82.8	13.0	149.2	3496	16
C		2.494	2.402	2.452	2.0	84.1	12.8	149.5	3160	16
AVERAGE		2.502	2.401	2.452	2.1	83.8	12.9	149.4	3463	16

By _____
John C. Elling
Engineering Services Manager

Reviewed By _____
Gudrun J Hand, P.E., PhD
Quality Systems Engineer

Figure 16.3(c) Mix Design Summary: Moana Lane Extension PG 64-22, continued

08/24/2006 19:23 7023420254 GRANITE CONSTRUCTION PAGE 05

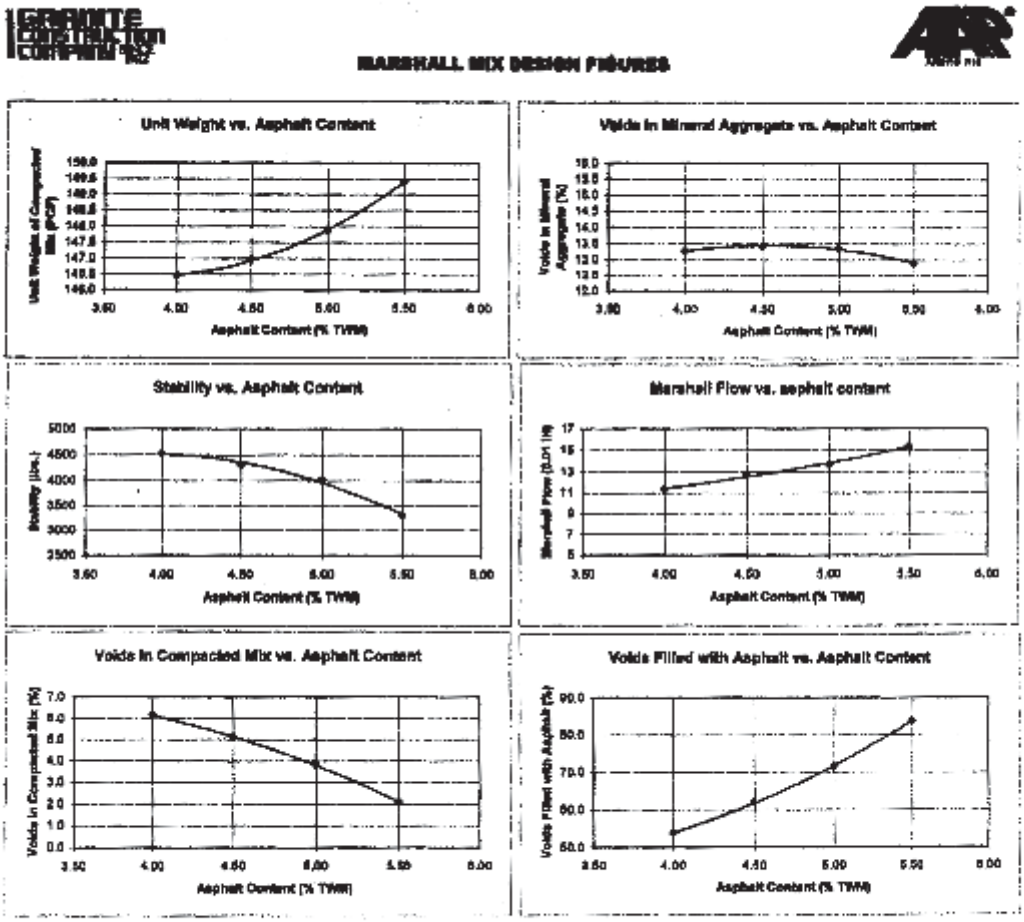

4/1/2006
Granite Construction Company
Aggregate Source: Lockwood Quarry
Asphalt Source: Paramount Nevada
Mix Type: Type II 75 Blow AC - 20 with Lime

Figure 16.3(d) Mix Design Summary: Moana Lane Extension PG 64-22, continued

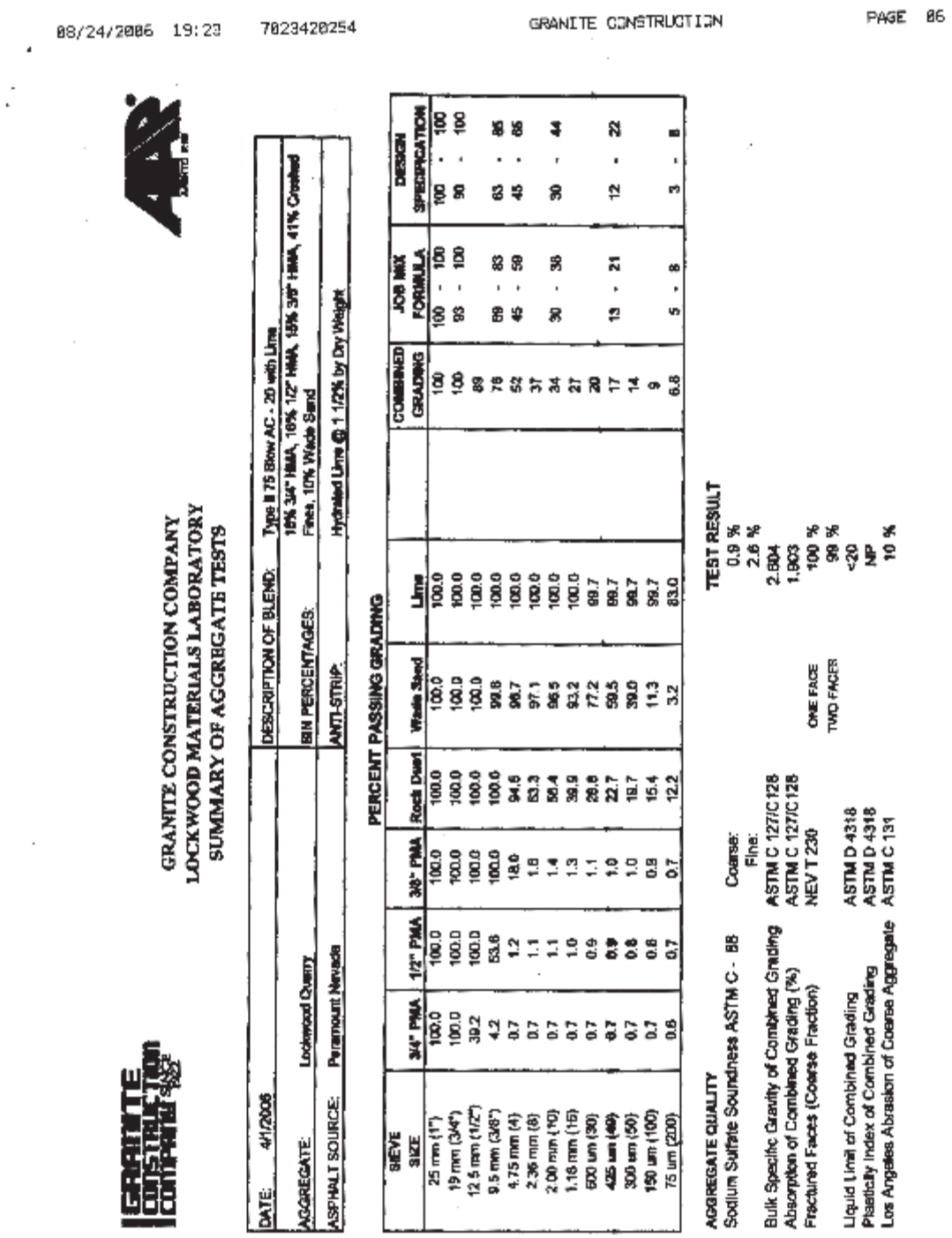

08/24/2006 19:23 7023420254 GRANITE CONSTRUCTION PAGE 06

GRANITE CONSTRUCTION COMPANY
LOCKWOOD MATERIALS LABORATORY
SUMMARY OF AGGREGATE TESTS

DATE:	4/1/2006	DESCRIPTION OF BLEND:	Type II 75 Blow AC - 20 with Lime
AGGREGATE:	Lockwood Quarry	BIN PERCENTAGES:	16% 3/4" HMA, 16% 1/2" HMA, 15% 3/8" HMA, 41% Crushed Fines, 10% Wade Sand
ASPHALT SOURCE:	Paramount Nevada	ANTI-STRIP:	Hydrated Lime @ 1 1/2% by Dry Weight

PERCENT PASSING GRADING

SIEVE SIZE	3/4" PMA	1/2" PMA	3/8" PMA	Rock Dust	Wade Sand	Lime		COMBINED GRADING	JOB MIX FORMULA	DESIGN SPECIFICATION
25 mm (1")	100.0	100.0	100.0	100.0	100.0	100.0		100	100 - 100	100 - 100
19 mm (3/4")	100.0	100.0	100.0	100.0	100.0	100.0		100	93 - 100	90 - 100
12.5 mm (1/2")	39.2	100.0	100.0	100.0	100.0	100.0		89		
9.5 mm (3/8")	4.2	53.6	100.0	100.0	99.8	100.0		76	69 - 83	63 - 85
4.75 mm (4)	0.7	1.2	18.0	94.6	96.7	100.0		52	45 - 59	45 - 65
2.36 mm (8)	0.7	1.1	1.8	63.3	97.1	100.0		37		
2.00 mm (10)	0.7	1.1	1.4	60.4	96.5	100.0		34	30 - 38	30 - 44
1.18 mm (16)	0.7	1.0	1.3	39.9	93.2	100.0		27		
600 um (30)	0.7	0.9	1.1	28.8	77.2	99.7		20		
425 um (40)	0.7	0.9	1.0	22.7	59.5	99.7		17	13 - 21	12 - 22
300 um (50)	0.7	0.8	1.0	18.7	39.0	98.7		14		
150 um (100)	0.7	0.8	0.9	15.4	11.3	98.7		9		
75 um (200)	0.6	0.7	0.7	12.2	3.2	83.0		6.8	5 - 8	3 - 8

AGGREGATE QUALITY		TEST RESULT	
Sodium Sulfate Soundness ASTM C - 88	Coarse:	0.9 %	
	Fine:	2.6 %	
Bulk Specific Gravity of Combined Grading	ASTM C 127/C128	2.604	
Absorption of Combined Grading (%)	ASTM C 127/C128	1.903	
Fractured Faces (Coarse Fraction)	NEV T 230	ONE FACE	100 %
		TWO FACER	99 %
Liquid Limit of Combined Grading	ASTM D 4318	<20	
Plasticity Index of Combined Grading	ASTM D 4318	NP	
Los Angeles Abrasion of Coarse Aggregate	ASTM C 131	10 %	

Figure 16.3(e) Mix Design Summary: Moana Lane Extension PG 64-22, continued

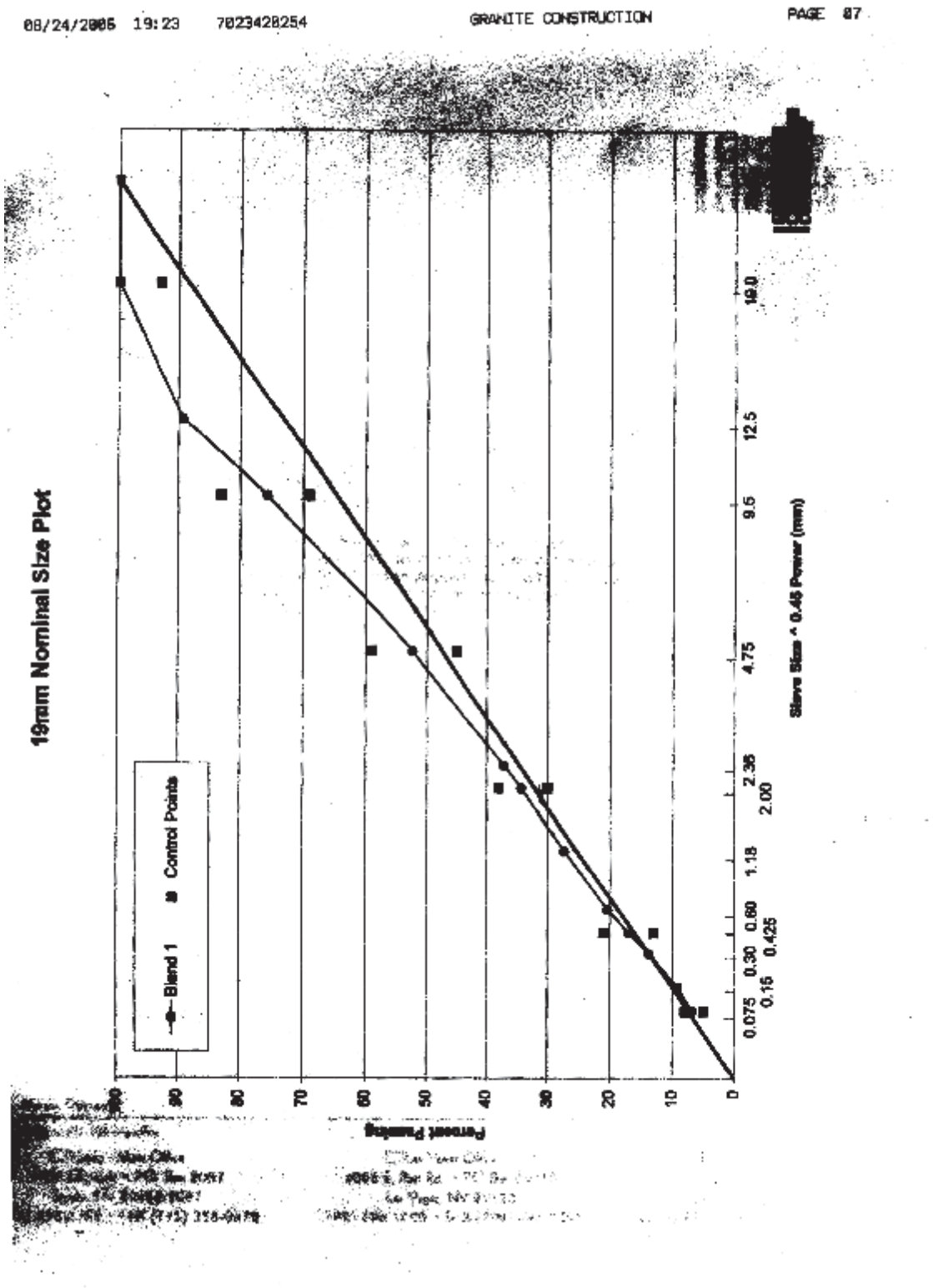

Figure 16.3(f) Mix Design Summary: Moana Lane Extension PG 64-22, continued

GRANITE CONSTRUCTION COMPANY SINCE 1922

April 1, 2006

Asphalt Concrete Mix Design : Type II 75 Blow PG 64-28NV with Lime

Aggregate Source: Lockwood Quarry

Design Criteria: Orange Book / Asphalt Institute MS-2

The following is a summary of laboratory testing and Mix Design criteria for a Type II Hot Mix Asphalt Concrete. All material and mix design procedures were performed in our AMRL accredited Lockwood Materials Laboratory by WAQTC / NAQTC qualified technicians in accordance with the above referenced Standard Specifications and Marshall mix design method as specified in the most recent version of the Asphalt Institute Manual Series 2 (MS – 2).

During production of this material, process control testing will be conducted to determine if mix properties meet acceptance criteria. Past experience has shown that differences in mix properties may exist between laboratory generated specimens for mix design purposes, and actual plant produced material. Adjustments to plant bin percentages and asphalt set point may be necessary during production to achieve job mix formula targets and or in-place specification requirements.

MIX PROPERTIES

Asphalt Cement:	Paramount Nevada PG 64-28NV
Specific Gravity of Asphalt Cement:	1.018
Aggregate Proportions:	18% ¾" HMA 16% ½" HMA 15% 3/8" HMA 41% Rock Dust 10% Wade Sand
Anti-Strip Agent:	Hydrated Lime @ 1 ½% Dry Weight of Aggregate
Number of Compaction Blows:	75 Automatic Hammer
Compaction Temperature:	300 Degrees Fahrenheit
Mixing Temperature:	315 Degrees Fahrenheit

Nevada Operations

Reply to the following office

☐Sparks - Main Office
1950 Glendale • P.O. Box 2087
Sparks, NV 89432-2067
(775) 358-8799 • FAX (775) 358-0378

☐Las Vegas Office
4055 E. Post Rd • P.O. Box 96715
Las Vegas, NV 89120
(702) 696-1090 • FAX (702) 696-1091

☐Carson City Office
5855 Sheze Drive
Carson City, NV 89701-1442
(775) 884-4100 • FAX (775) 884-33

Figure 16.4(a) Mix Design Summary: Moana Lane Extension PG 64-28

Optimum Asphalt Content:	4.8 % Total Weight of Mix 5.0 % Dry Weight of Aggregate
Marshall Stability:	3800 lbs.
Marshall Flow (0.01 inches):	13.0
Total Air Voids:	4.0 %
Voids in Mineral Aggregate:	13.0
Voids Filled With Asphalt	69.0 %
Unit Weight:	148.4 PCF

Attached are the results of laboratory testing of the aggregates and asphalt concrete design.

Respectfully Submitted,
Granite Construction Company

John C. Elkins
Engineering Services Manager

Reviewed By:

Adam J. Hand, PE, PhD
Quality System Engineer

PROFESSIONAL ENGINEER-STATE OF NEVADA
ADAM J.T. HAND
No. 15763
CIVIL

Date: April 1, 2006
Granite Construction Company
Type II 75 Blow PG 64-28NV with Lime
Lockwood Quarry
Paramount Nevada Asphalt

Figure 16.4(b) Mix Design Summary: Moana Lane Extension PG 64-28, continued

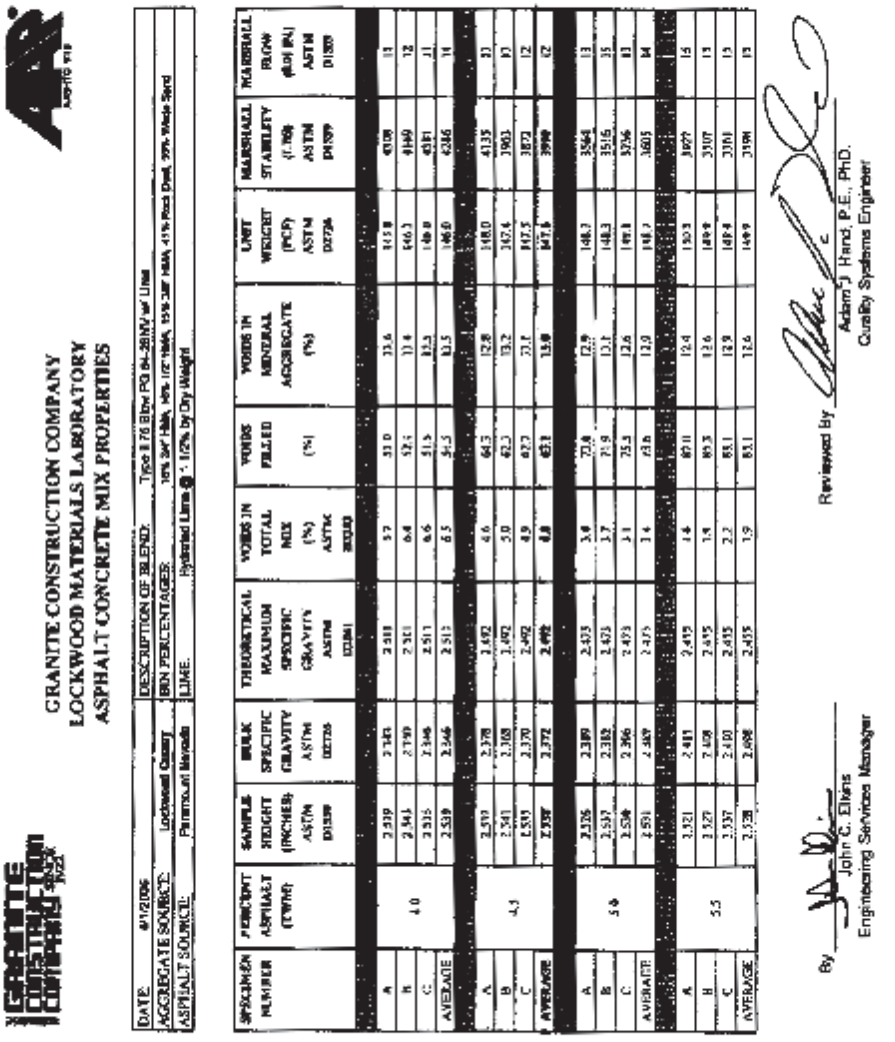

GRANITE CONSTRUCTION COMPANY
LOCKWOOD MATERIALS LABORATORY
ASPHALT CONCRETE MIX PROPERTIES

DATE: 8/1/2006 DESCRIPTION OF BLEND: Type II 76 Blow PG 64-28NV w/ Lime

AGGREGATE SOURCE: Lockwood Quarry BIN PERCENTAGES: 16% 3/4" Rock, 16% 1/2" Rock, 15% 3/8" Rock, 41% Rock Dust, 9% White Sand

ASPHALT SOURCE: Paramount Nevada LIME: Hydrated Lime @ 1.12% by Dry Weight

SPECIMEN NUMBER	PERCENT ASPHALT (TOTAL)	SAMPLE HEIGHT (INCHES) ASTM D3549	BULK SPECIFIC GRAVITY ASTM D2726	THEORETICAL MAXIMUM SPECIFIC GRAVITY ASTM D2041	VOIDS IN TOTAL MIX (%) ASTM D3203	VOIDS FILLED (%)	VOIDS IN MINERAL AGGREGATE (%)	UNIT WEIGHT (PCF) ASTM D2726	MARSHALL STABILITY (LBS) ASTM D1559	MARSHALL FLOW (0.01 IN.) ASTM D1559
A	4.0	2.539	2.345	2.511	6.7	51.0	13.6	146.3	4108	13
B		2.541	2.350	2.511	6.4	52.5	13.4	146.5	4149	12
C		2.535	2.346	2.511	6.6	51.5	13.5	146.0	4181	11
AVERAGE		2.538	2.346	2.511	6.5	51.5	13.5	146.0	4146	12
A	4.5	2.537	2.378	2.492	4.6	64.3	12.8	148.0	4135	13
B		2.541	2.368	2.492	5.0	62.3	13.2	147.4	3963	13
C		2.539	2.370	2.492	4.9	62.9	13.1	147.5	3873	12
AVERAGE		2.539	2.372	2.492	4.8	63.1	13.0	147.6	3990	12
A	5.0	2.535	2.389	2.473	3.4	73.4	12.9	148.7	3564	13
B		2.537	2.382	2.473	3.7	71.9	13.1	148.3	3515	15
C		2.536	2.386	2.473	3.5	72.5	12.6	148.6	3756	13
AVERAGE		2.536	2.486	2.473	3.5	72.6	12.9	148.7	3605	14
A	5.5	2.521	2.401	2.459	2.4	85.0	12.4	150.3	3677	15
B		2.527	2.408	2.459	2.1	85.3	12.6	149.9	3507	15
C		2.527	2.400	2.459	2.2	85.1	12.9	149.4	3761	15
AVERAGE		2.525	2.403	2.459	1.9	85.1	12.6	149.9	3598	15

By _____
John C. Elkins
Engineering Services Manager

Reviewed by _____
Adam J. Hand, P.E., PhD.
Quality Systems Engineer

Figure 16.4(c) Mix Design Summary: Moana Lane Extension PG 64-28, continued

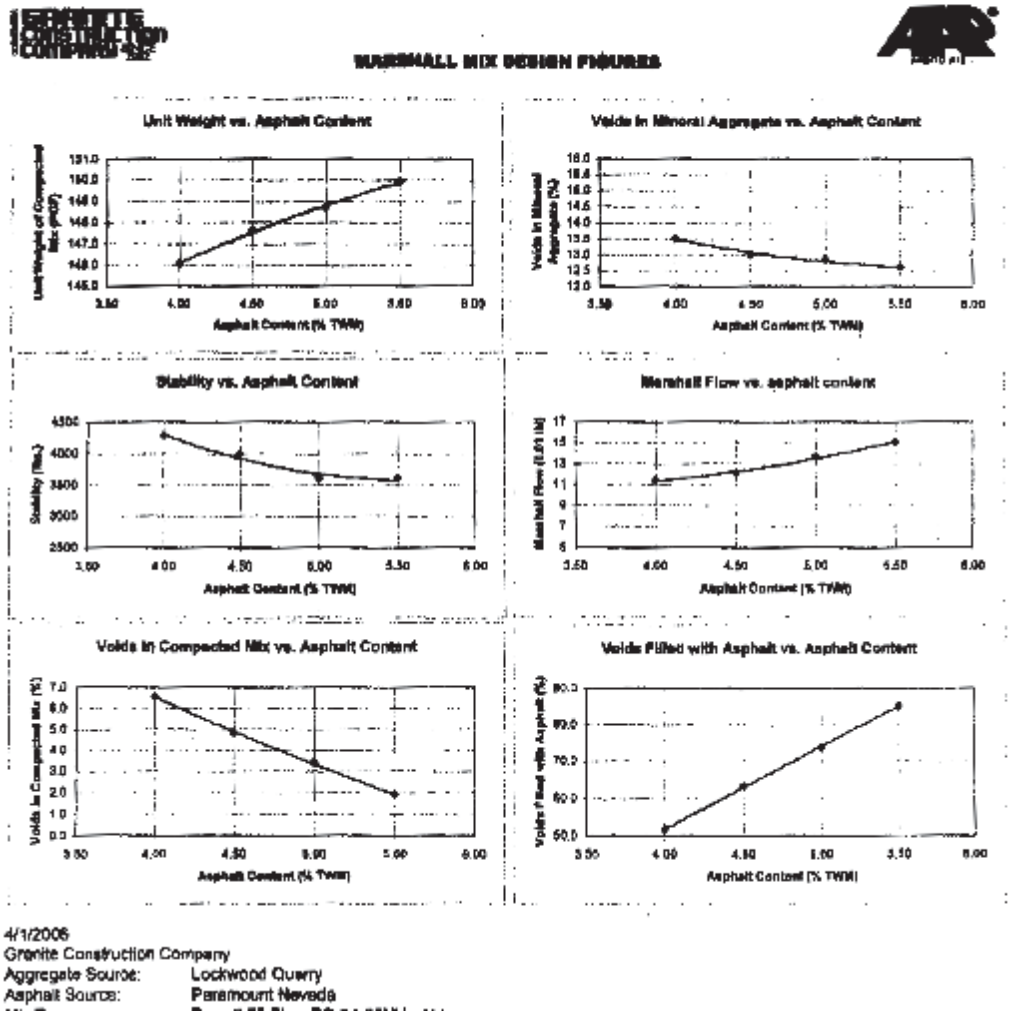

4/1/2006
Granite Construction Company
Aggregate Source: Lockwood Quarry
Asphalt Source: Paramount Nevada

Figure 16.4(d) Mix Design Summary: Moana Lane Extension PG64-28, continued

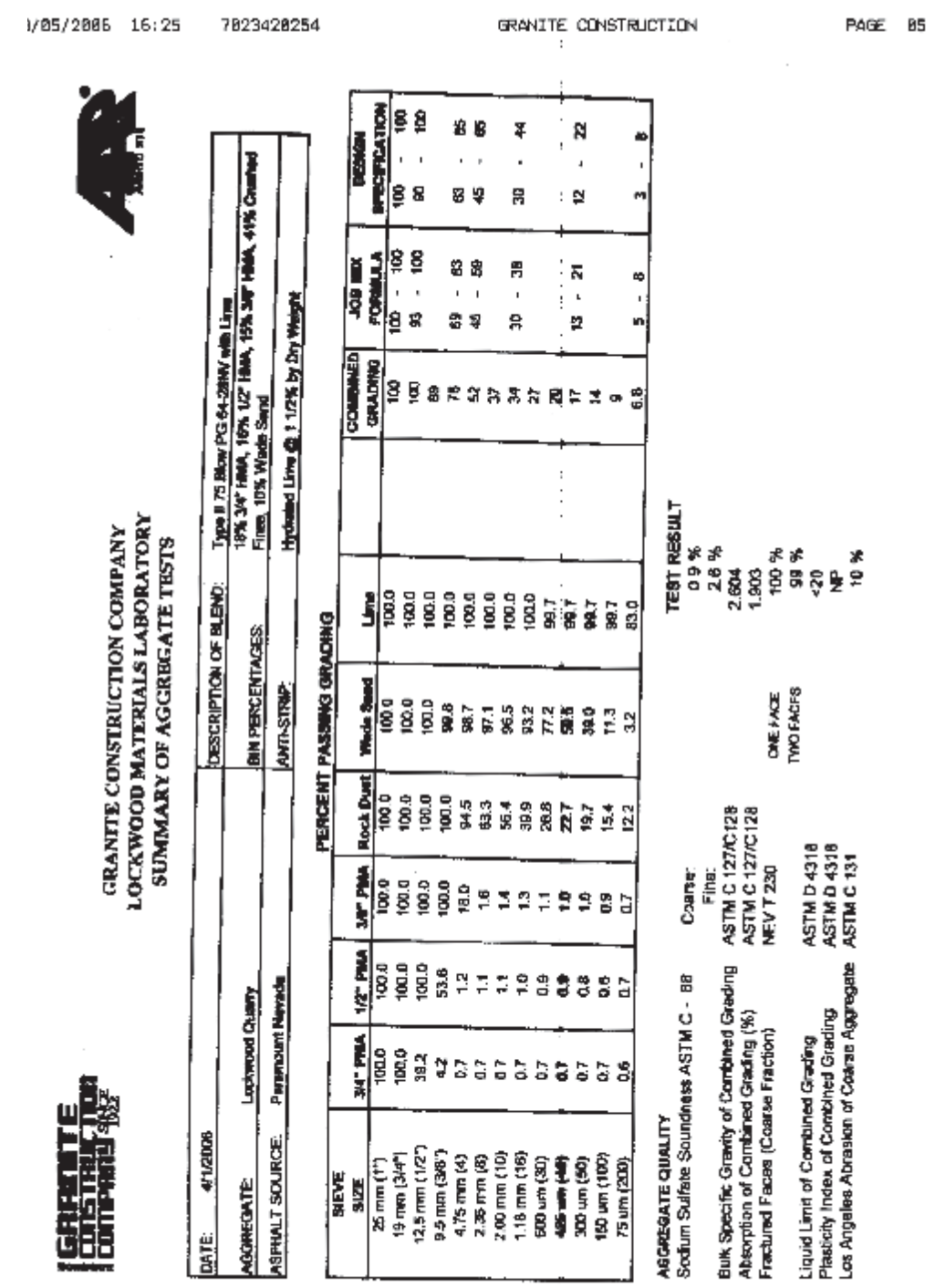

1/05/2006 16:25 7023420254 GRANITE CONSTRUCTION PAGE 05

GRANITE CONSTRUCTION COMPANY
LOCKWOOD MATERIALS LABORATORY
SUMMARY OF AGGREGATE TESTS

DATE:	4/1/2006	DESCRIPTION OF BLEND:	Type II 75 Blow PG 64-28NV with Lime
AGGREGATE:	Lockwood Quarry	BIN PERCENTAGES:	18% 3/4" HMA, 16% 1/2" HMA, 15% 3/8" HMA, 41% Crushed Fines, 10% Wade Sand
ASPHALT SOURCE:	Paramount Nevada	ANTI-STRIP:	Hydrated Lime @ 1 1/2% by Dry Weight

PERCENT PASSING GRADING

SIEVE SIZE	3/4" PMA	1/2" PMA	3/8" PMA	Rock Dust	Wade Sand	Lime		COMBINED GRADING	JOB MIX FORMULA	DESIGN SPECIFICATION
25 mm (1")	100.0	100.0	100.0	100.0	100.0	100.0		100	100 - 100	100 - 100
19 mm (3/4")	100.0	100.0	100.0	100.0	100.0	100.0		100	93 - 100	90 - 100
12.5 mm (1/2")	38.2	100.0	100.0	100.0	100.0	100.0		89		
9.5 mm (3/8")	4.2	53.6	100.0	100.0	99.8	100.0		78	69 - 83	63 - 85
4.75 mm (4)	0.7	1.2	18.0	94.5	98.7	100.0		52	46 - 59	45 - 65
2.36 mm (8)	0.7	1.1	1.6	83.3	97.1	100.0		37		
2.00 mm (10)	0.7	1.1	1.4	56.4	96.5	100.0		34	30 - 38	30 - 44
1.18 mm (16)	0.7	1.0	1.3	39.9	93.2	100.0		27		
600 um (30)	0.7	0.9	1.1	28.8	77.2	99.7		20		
425 um (40)	0.7	0.9	1.0	22.7	58.5	99.7		17	13 - 21	12 - 22
300 um (50)	0.7	0.8	1.0	19.7	39.0	99.7		14		
150 um (100)	0.7	0.6	0.9	15.4	11.3	99.7		9		
75 um (200)	0.6	0.7	0.7	12.2	3.2	83.0		6.8	5 - 8	3 - 8

AGGREGATE QUALITY			TEST RESULT
Sodium Sulfate Soundness ASTM C - 88	Coarse:		0.9 %
	Fine:		2.8 %
Bulk Specific Gravity of Combined Grading	ASTM C 127/C128		2.604
Absorption of Combined Grading (%)	ASTM C 127/C128		1.903
Fractured Faces (Coarse Fraction)	NEVT 230	ONE FACE	100 %
		TWO FACES	99 %
Liquid Limit of Combined Grading	ASTM D 4318		<20
Plasticity Index of Combined Grading	ASTM D 4318		NP
Los Angeles Abrasion of Coarse Aggregate	ASTM C 131		10 %

Figure 16.4(e) Mix Design Summary: Moana Lane Extension PG 64-28, continued

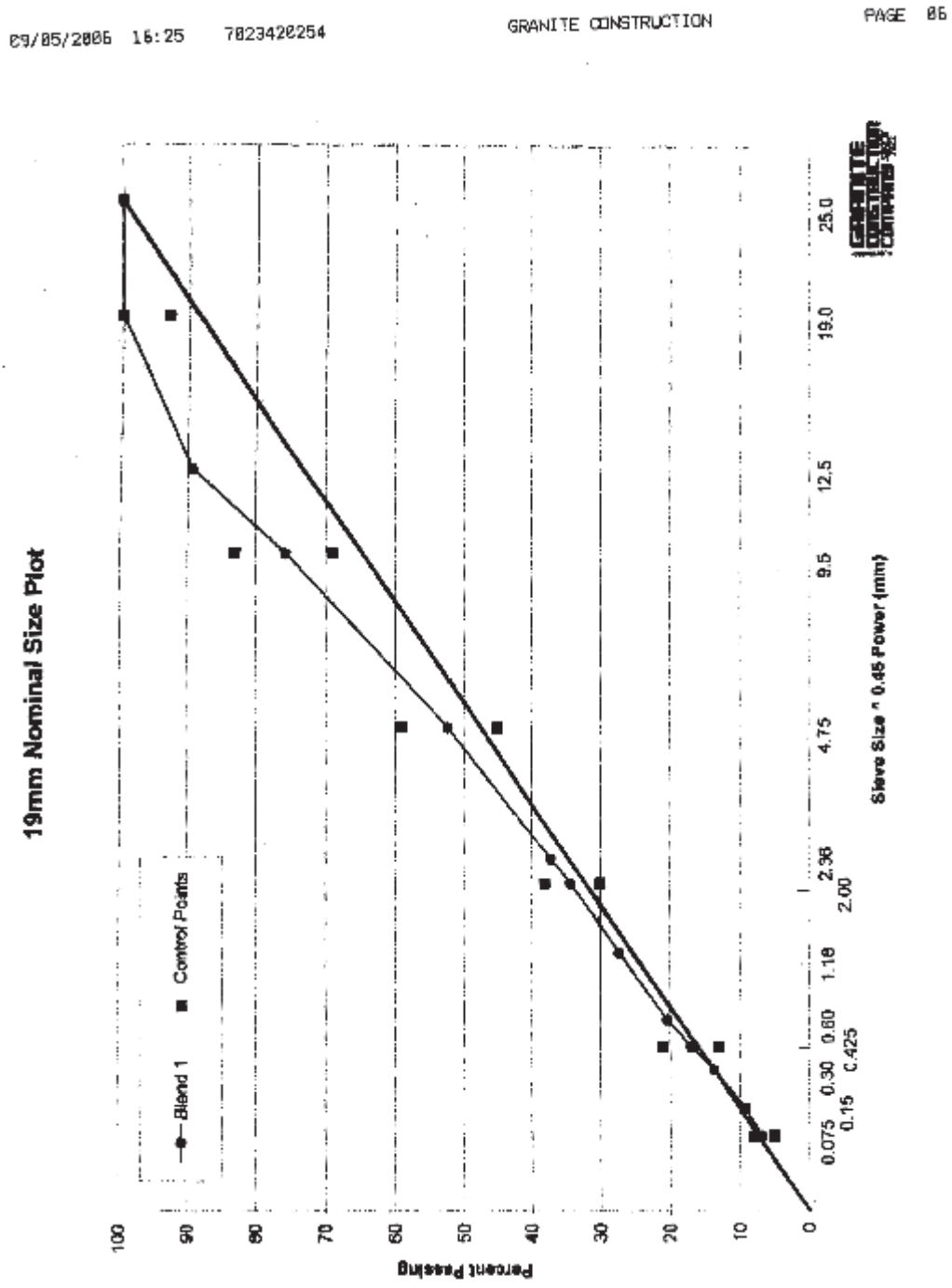

Figure 16.4(f) Mix Design Summary: Moana Lane Extension PG 64-28, continued

April 1, 2008

GRANITE CONSTRUCTION COMPANY SINCE 1922

AAP AASHTO R18

Asphalt Concrete Mix Design : Type II 75 Blow Paramount PG 64-28NV 4 Void w/ Lime

Aggregate Source: Lockwood Quarry

Design Criteria: Orange Book / Asphalt Institute MS-2

The following is a summary of laboratory testing and Mix Design criteria for a Type II Hot Mix Asphalt Concrete. All material and mix design procedures were performed in our AMRL accredited Lockwood Materials Laboratory by NAQTC qualified technicians in accordance with the above referenced Standard Specificatiors and Marshall mix design method as specified in the most recent version of the Asphalt Institute Manual Series 2 (MS – 2).

During production of this material, process control testing will be conducted to determine if mix properties meet acceptance criteria. Past experience has shown that differences in mix properties may exist between laboratory generated specimens for mix design purposes, and actual plant produced material. Adjustments to plant bin percentages and asphalt set point may be necessary during production to achieve job mix formula targets and or in-place specification requirements.

MIX PROPERTIES

Asphalt Cement:	Paramount Nevada PG 64 –28NV
Specific Gravity of Asphalt Cement:	1.016
Aggregate Proportions:	18% ¾" Lockwood PMA 13% ½" Lockwood PMA 26% 3/8" Lockwood PMA 31% Lockwood Rock Dust 12% Wade Sand
Anti-Strip Agent:	Hydrated Lime @ 1 ½% Dry Weight of Aggregate
Number of Compaction Blows:	75 Automatic Hammer
Compaction Temperature:	305 Degrees Fahrenheit
Mixing Temperature:	325 Degrees Fahrenheit

Nevada Operations

Reply to the following office

☐ Northern Nevada Operations
1900 Glendale • P.O. Box 2087
Sparks, NV 89432-2087
(775) 358-8792 • FAX (775) 358-0372

☐ Southern Nevada Operations
2031 Palco Road
Henderson, NV 89015
(702) 696-1090 • FAX (702) 696-1091

Figure 16.5(a) Mix Design Summary: Sparks Boulevard PG 64-28

Optimum Asphalt Content:	4.8 % Total Weight of Mix 5.0 % Dry Weight of Aggregate
Marshall Stability:	3312 lbs.
Marshall Flow (0.01 inches):	12
Total Air Voids:	4.0 %
Voids in Mineral Aggregate:	13.7 %
Voids Filled With Asphalt	70.9 %
Unit Weight:	144.8 PCF

Attached are the results of laboratory testing of the aggregates and asphalt concrete design.

Respectfully Submitted,
Granite Construction Company

John C. Elkins
Engineering Services Manager

Reviewed By:

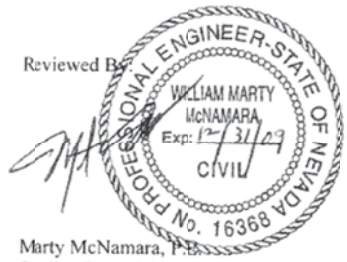

Marty McNamara, P.E.
Quality Control Engineer

Date: 4/1/2008
Granite Construction Company
Type II 75Blow PG 64-28NV 4Void with Lime
Lockwood Quarry
Paramount Nevada Asphalt

Figure 16.5(b) Mix Design Summary: Sparks Boulevard PG 64-28, continued

GRANITE CONSTRUCTION COMPANY SINCE 1922

GRANITE CONSTRUCTION COMPANY
LOCKWOOD MATERIALS LABORATORY
ASPHALT CONCRETE MIX PROPERTIES

DATE:	4/1/2008	DESCRIPTION OF BLEND:	Type II 75 Blow Paramount PG 64-28NV with Lime
AGGREGATE SOURCE:	Lockwood	BIN PERCENTAGES:	3/4 = 17.8, 1/2 = 12.8, 3/8 = 25.5, Rock Dust = 30.5, Wade Sand = 11.0, Lime = 1.5
ASPHALT SOURCE:	Paramount Nevada	LIME:	Hydrated Lime @ 1.1/2% by Dry Weight

SPECIMEN NUMBER	PERCENT ASPHALT (TWM)	SAMPLE HEIGHT (INCHES) ASTM D1559	BULK SPECIFIC GRAVITY ASTM D2726	THEORETICAL MAXIMUM SPECIFIC GRAVITY ASTM D2041	VOIDS IN TOTAL MIX (%) ASTM D3203	VOIDS FILLED (%)	VOIDS IN MINERAL AGGREGATE (%)	UNIT WEIGHT (PCF) ASTM D2726	MARSHALL STABILITY (LBS) ASTM D1559	MARSHALL FLOW (0.01 IN.) ASTM D1559
A	4.0	2.519	2.369	2.454	6.6	58.7	14.2	142.7	3938	10
B		2.523	2.390	2.454	6.7	58.4	14.3	142.5	3722	11
C		2.518	2.392	2.454	6.6	58.7	14.2	142.7	3576	10
AVERAGE		2.520	2.291	2.454	6.6	58.6	14.3	142.6	3745	10
A	4.5	2.517	2.312	2.436	5.1	63.5	13.9	143.9	3631	11
B		2.517	2.319	2.436	4.8	65.0	13.7	144.3	3742	11
C		2.528	2.315	2.436	5.0	64.1	13.8	144.1	3549	12
AVERAGE		2.521	2.315	2.436	5.0	64.2	13.8	144.1	3641	11
A	5.0	2.517	2.335	2.418	3.4	74.6	13.5	145.8	3454	12
B		2.514	2.329	2.418	3.7	73.2	13.8	145.0	3037	12
C		2.493	2.321	2.418	4.0	71.4	14.0	144.5	3054	11
AVERAGE		2.507	2.328	2.418	3.7	73.1	13.8	144.9	3182	12
A	5.5	2.504	2.350	2.401	2.1	84.3	13.4	146.3	2816	11
B		2.517	2.357	2.401	1.8	86.2	13.2	146.7	3709	12
C		2.490	2.358	2.401	1.8	86.5	13.1	146.8	2943	13
AVERAGE		2.504	2.353	2.401	1.9	85.7	13.2	146.6	2820	13
A	6.0	2.517	2.362	2.383	0.9	93.3	13.5	147.0	2801	13
B		2.493	2.368	2.383	0.6	95.1	13.2	147.4	2716	13
C		2.499	2.365	2.383	0.8	94.2	13.3	147.2	2409	13
AVERAGE		2.503	2.365	2.383	0.8	94.2	13.3	147.2	2642	14

By _____
John C. Elkins
Engineering Services Manager

Reviewed By _____
Marty McNamara, P.E.
Quality Control Engineer

Figure 16.5(c) Mix Design Summary: Sparks Boulevard PG 64-28, continued

GRANITE CONSTRUCTION COMPANY SINCE 1922

MARSHALL MIX DESIGN FIGURES

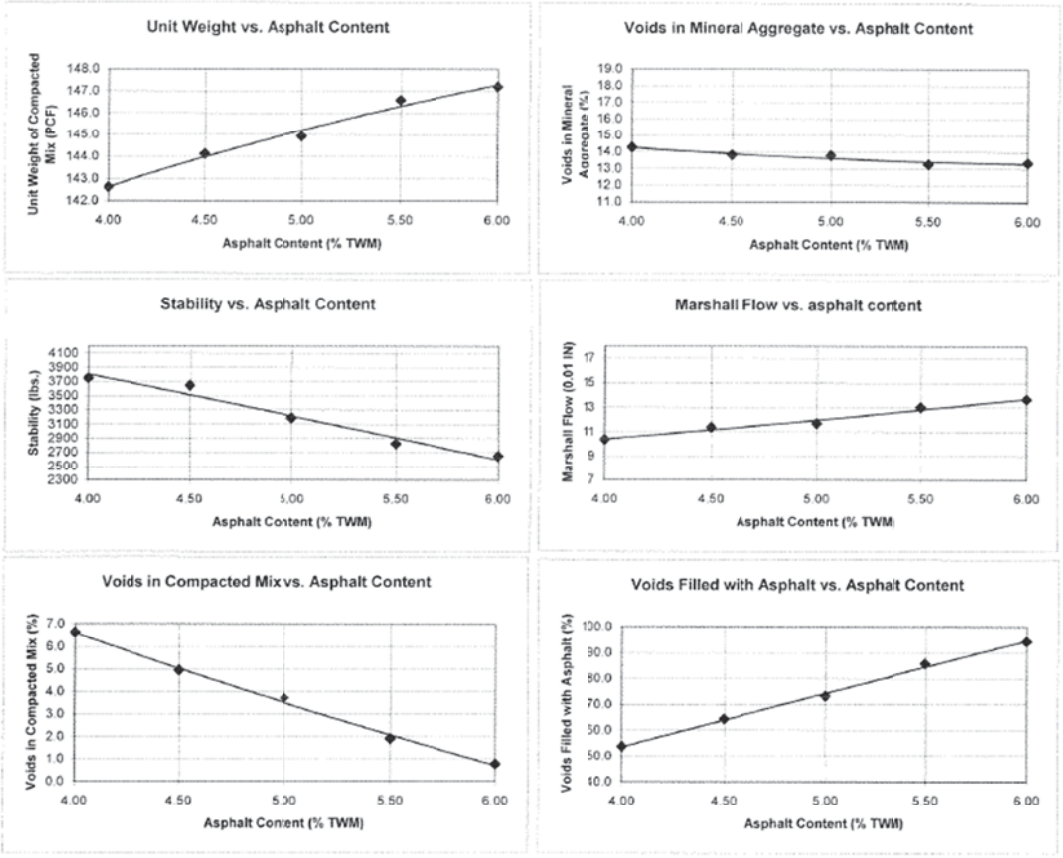

4/1/2008
Granite Construction Company
Aggregate Source: Lockwood
Asphalt Source: Paramount Nevada
Mix Type: Type II 75 Blow Paramount PG 64-28NV with Lime

Figure 16.5(d) Mix Design Summary: Sparks Boulevard PG 64-28, continued

GRANITE CONSTRUCTION COMPANY SINCE 1922

AASHTO R18

GRANITE CONSTRUCTION COMPANY
LOCKWOOD MATERIALS LABORATORY
SUMMARY OF AGGREGATE TESTS

DATE:	4/1/2008	DESCRIPTION OF BLEND:	Type II 75 Blow Paramount PG 64-28NV with Lime
AGGREGATE:	Lockwood	BIN PERCENTAGES:	3/4 = 17.8, 1/2 = 12.8, 3/8 = 25.5, Rock Dust = 30.5, Wade Sand = 11.9, Lime = 1.5
ASPHALT SOURCE:	Paramount Nevada	ANTI-STRIP:	Hydrated Lime @ 1 1/2% by Dry Weight

PERCENT PASSING GRADING

SIEVE SIZE	3/4" PMA	1/2" PMA	3/8" PMA	Rock Dust	Wade Sand	Hydrated Lime		COMBINED GRADING	JOB MIX FORMULA	DESIGN SPECIFICATION
25 mm (1")	100.0	100.0	100.0	100.0	100.0	100.0		100	100	100
19 mm (3/4")	100.0	100.0	100.0	100.0	100.0	100.0		100	93 - 100	90 - 100
12.5 mm (1/2")	38.1	100.0	100.0	100.0	100.0	100.0		89		
9.5 mm (3/8")	6.7	50.0	99.9	100.0	100.0	100.0		77	70 - 84	63 - 85
4.75 mm (4)	0.9	1.0	19.0	97.4	98.5	100.0		48	45 - 55	45 - 65
2.36 mm (8)	0.7	1.0	1.2	72.3	96.4	100.0		36		
2.00 mm (10)	0.7	0.7	1.0	63.8	95.6	100.0		33	30 - 37	30 - 44
1.18 mm (16)	0.7	0.6	0.8	44.8	91.4	100.0		26		
600 um (30)	0.7	0.6	0.8	29.7	72.1	99.7		20		
425 um (40)	0.7	0.6	0.8	25.0	52.4	99.7		16	12 - 20	12 - 22
300 um (50)	0.7	0.6	0.7	21.3	32.1	99.7		12		
150 um (100)	0.6	0.6	0.7	16.8	8.3	99.7		8		
75 um (200)	0.5	0.5	0.5	13.5	2.4	83.0		5.9	3.9 - 7.9	3 - 8

AGGREGATE QUALITY			TEST RESULT
Sodium Sulfate Soundness ASTM C - 88	Coarse:		2 %
	Fine:		3 %
Bulk Specific Gravity of Combined Grading	ASTM C 127/C128		2.565
Absorption of Combined Grading (%)	ASTM C 127/C128		1.963
Fractured Faces (Coarse Fraction)	ASTM D5821	ONE FACE	100 %
		TWO FACES	99 %
Liquid Limit of Combined Grading	ASTM D 4318		<20
Plasticity Index of Combined Grading	ASTM D 4318		NP
Los Angeles Abrasion of Coarse Aggregate	ASTM C 131		14 %

Figure 16.5(e) Mix Design Summary: Sparks Boulevard PG 64-28, continued

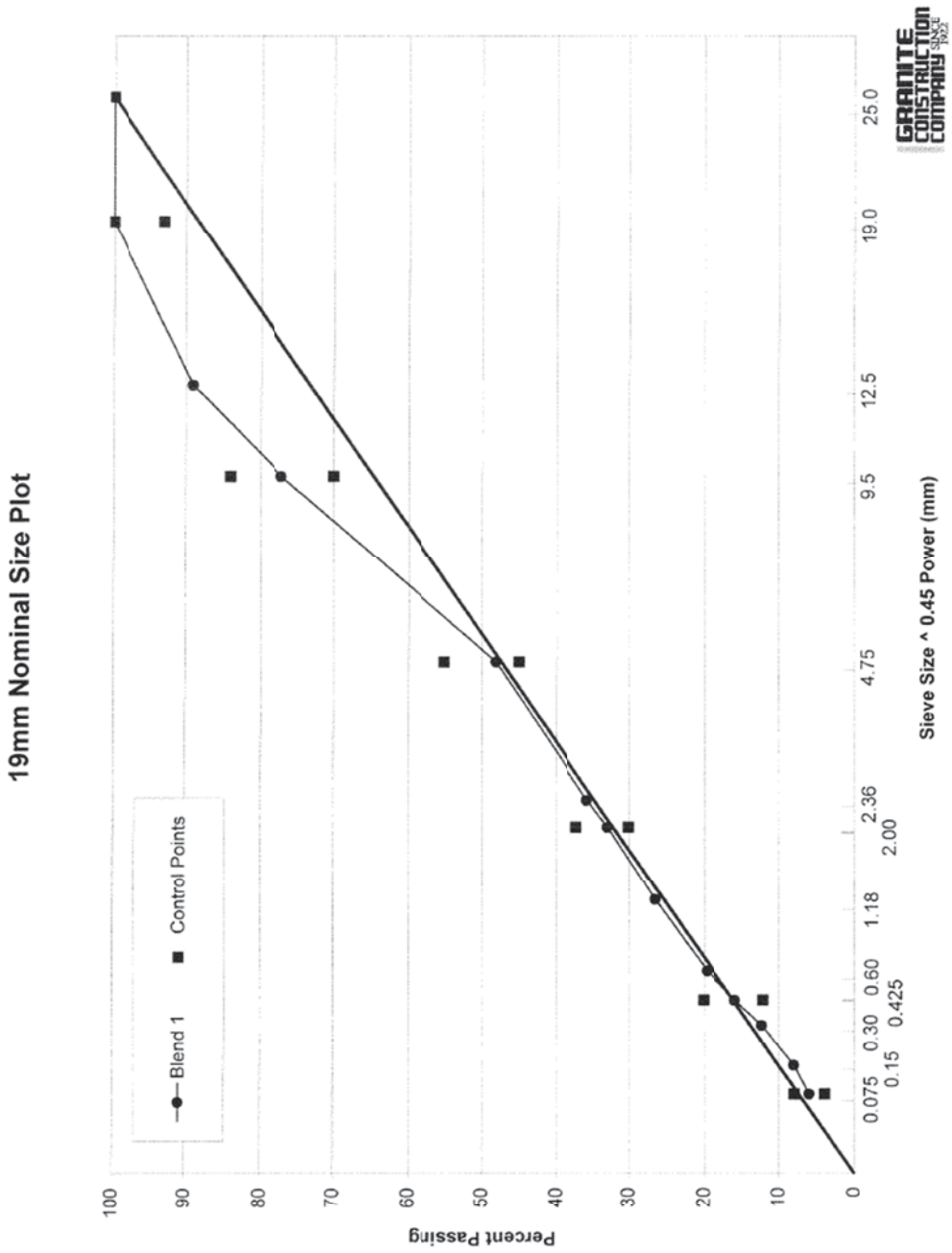

Figure 16.5(f) Mix Design Summary: Sparks Boulevard PG 64-28, continued

PARAMOUNT-NEVADA
ASPHALT COMPANY, LLC

425 Logan Lane
P.O. Box 2247
Fernley, NV 89408
Office (775) 8356366
Fax (775) 835-6144

Product: ***PG64-28NV Asphalt Cement***
Code: #153
Date: 1/29/2008

Purchaser: Granite
Destination: n/a
Transporter: n/a
Truck No: n/a
Bill of Lading No: n/a
Contract No: Yearly plant Mix Design
Purchase Order No: n/a

MEETS SPECIFICATIONS: *Nevada 703,03.05 NDOT*

CERTIFICATE OF COMPLIANCE

TESTS	NEV#	AASHTO #	SPEC	RESULT
Test on Original Asphalt:				
Viscosity, 135°C (275°F), Pa.s		T316	3.00 Max	0.72
DSR, G*/sind, 64°C @ 10 rad/s, kPa		T315	1.00 min	1.51
Flash Point, C.O.C., °F	T716	T48	450 min	550+
Ductility, 4°C (39.2°F), 5cn/min, cm	T746		50 min	53
Toughness, inch-lbs	T745		110 min	150
Tenacity, inch-lbs	T745		75 min	135
Specific Gravity, 77/77°F		T228	----	1.0162
Specific Gravity, 60/60°F		T228	----	1.0222
API Gravity, 60°F		T228	----	6.9
Sieve Test, Particles Retained	T730		0	0
Test on Residue from Rolling Thin Film Oven:	T728	T240	----	
DSR, G*/sind, 64°C @ 10 rad/s, kPa		T315	2.20 min	3.11
Ductility, 4°C (39.2°F), 5cn/min, cm	T746	T51	25 min	30
Loss on Heating, wt. %		T240	1.0 max	0.450
Tests on Residue from Pressure Aging Vessel @100°C				
DSR, G*/sind, 22°C @ 10 rad/s, kPa		T315	5000 max	1530
Creep Stiffness, S, -18°C @ 60s, Mpa		T313	300 max	135
Creep Stiffness, m-value, -18°C @ 60s, Mpa		T313	0.300 min	0.328
Direct Tension, Failure Strain, @ -18°C @ 1.0 mm/min, %		T314	1.00 min	N/A

We hereby certify that the above material was sampled and tested according to the applicable ASTM and AASHTO standards and that it complies with all specifications.
This certification is valid for 30 days from the day of issued

Certified By:
Paramount-Nevada Asphalt Company, L.L.C.

Figure 16.5(g) Mix Design Summary: Sparks Boulevard PG 64-28, continued

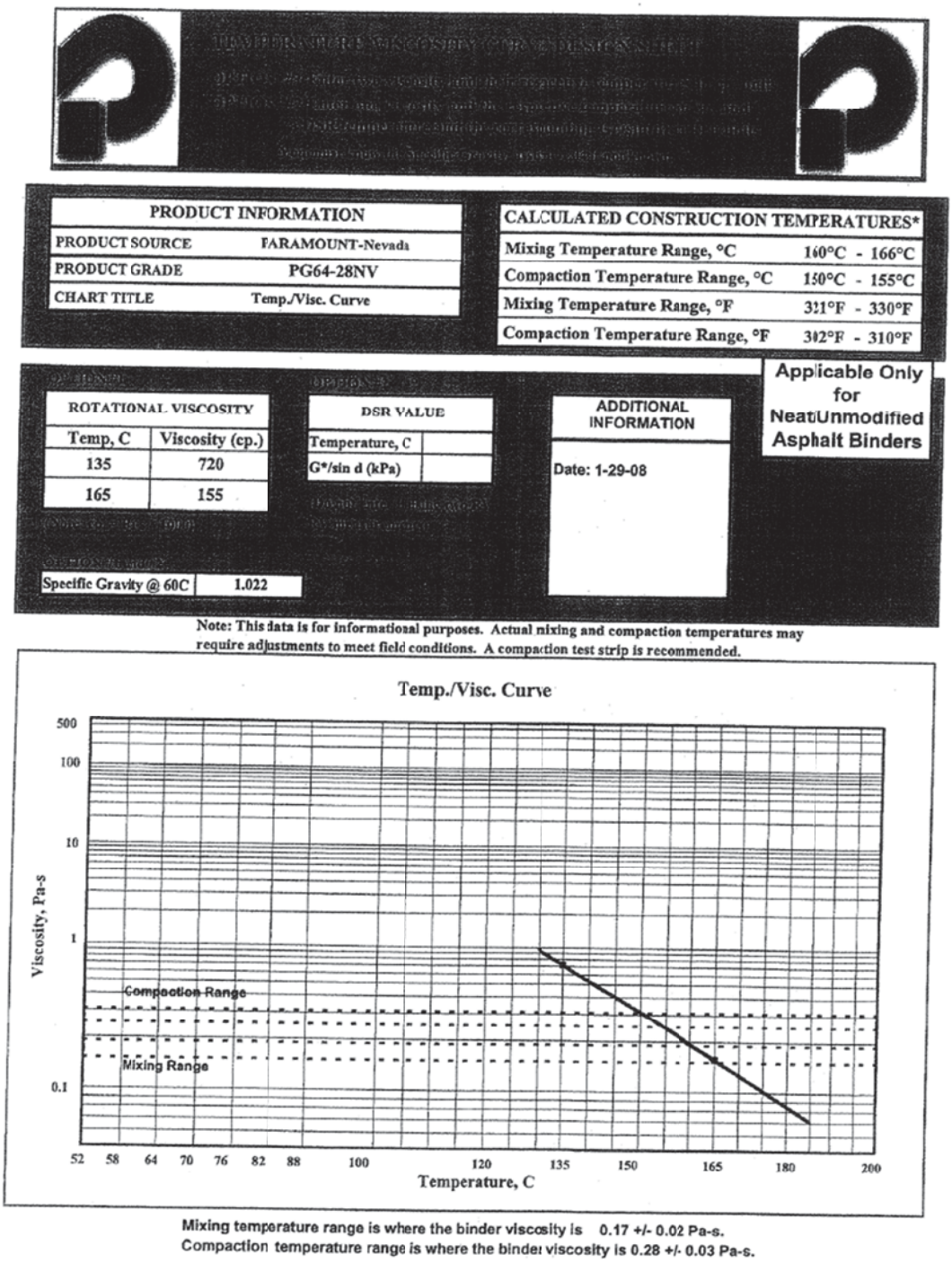

PRODUCT INFORMATION	
PRODUCT SOURCE	FARAMOUNT-Nevada
PRODUCT GRADE	PG64-28NV
CHART TITLE	Temp./Visc. Curve

CALCULATED CONSTRUCTION TEMPERATURES*	
Mixing Temperature Range, °C	160°C - 166°C
Compaction Temperature Range, °C	150°C - 155°C
Mixing Temperature Range, °F	321°F - 330°F
Compaction Temperature Range, °F	302°F - 310°F

ROTATIONAL VISCOSITY	
Temp, C	Viscosity (cp.)
135	720
165	155

DSR VALUE	
Temperature, C	
G*/sin d (kPa)	

ADDITIONAL INFORMATION

Date: 1-29-08

Applicable Only for NeatUnmodified Asphalt Binders

Specific Gravity @ 60C	1.022

Note: This data is for informational purposes. Actual mixing and compaction temperatures may require adjustments to meet field conditions. A compaction test strip is recommended.

Mixing temperature range is where the binder viscosity is 0.17 +/- 0.02 Pa-s.
Compaction temperature range is where the binder viscosity is 0.28 +/- 0.03 Pa-s.

Figure 16.5(h) Mix Design Summary: Sparks Boulevard PG 64-28, continued

Chemical Lime
A Lhoist Group Company

CERTIFICATE OF COMPLIANCE

To: **GRANITE CONSTRUCTION**
P.O. BOX 2007
SPARKS, NV 89432

Job: **HOT PLANT**
LOCKWOOD, NV

Control Nbr 10245377
Shipped 11/19/07

This is to certify that this commercially produced **HYDRATED LIME** manufactured by the CHEMICAL LIME COMPANY conforms to the chemical and physical requirements of ASTM Designation: C-1097, Type N Hydrate.

Very truly yours,

Ray Cawthorne, CMfgE
Terminal Manager
Stockton, CA

Chemical Lime Company
4303 South McKinley Avenue
Stockton, California 95206
Phone: (800) 284-6048 (209) 982-4112
Fax: (209) 982-1485

Figure 16.5(i) Mix Design Summary: Sparks Boulevard PG 64-28, continued

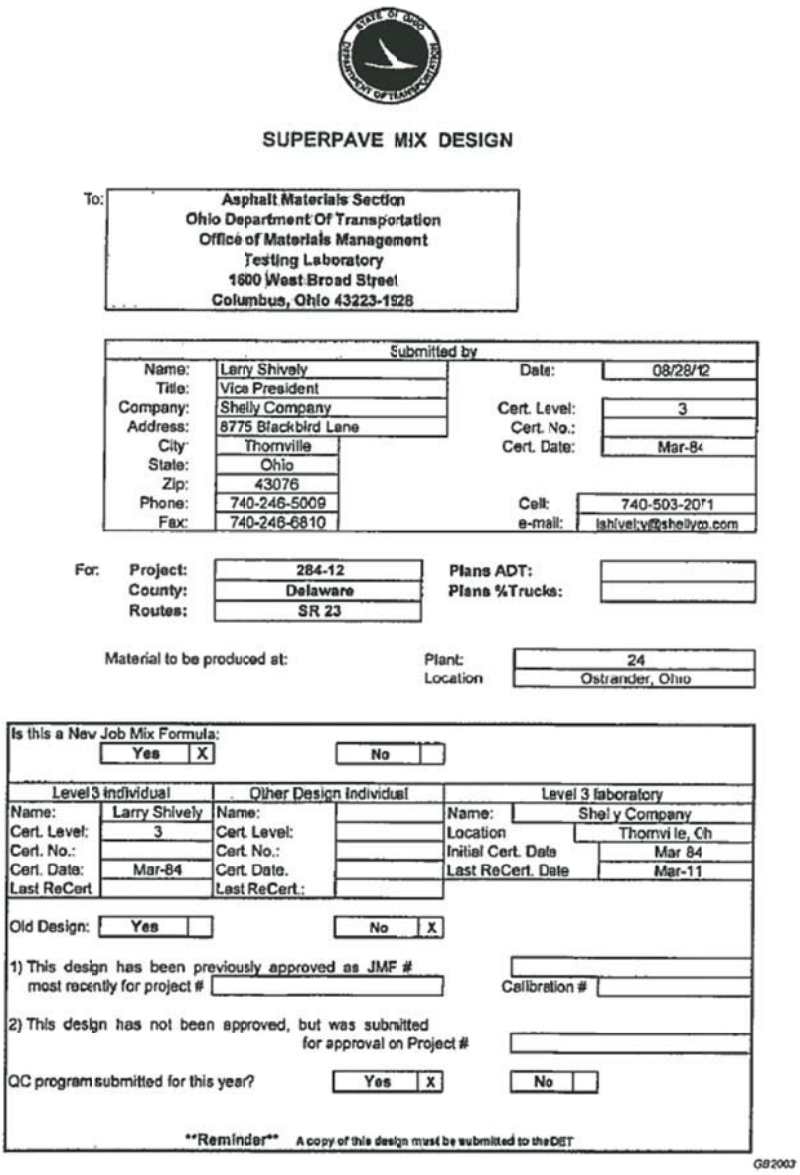

SUPERPAVE MIX DESIGN

To: Asphalt Materials Section
Ohio Department Of Transportation
Office of Materials Management
Testing Laboratory
1600 West Broad Street
Columbus, Ohio 43223-1928

Submitted by			
Name:	Larry Shively	Date:	08/28/12
Title:	Vice President		
Company:	Shelly Company	Cert. Level:	3
Address:	8775 Blackbird Lane	Cert. No.:	
City:	Thornville	Cert. Date:	Mar-84
State:	Ohio		
Zip:	43076		
Phone:	740-246-5009	Cell:	740-503-2071
Fax:	740-246-6810	e-mail:	lshively@shellyco.com

For:			
Project:	284-12	Plans ADT:	
County:	Delaware	Plans %Trucks:	
Routes:	SR 23		

Material to be produced at: Plant: 24
Location: Ostrander, Ohio

Is this a New Job Mix Formula: Yes [X] No [ ]

Level 3 individual		Other Design individual		Level 3 laboratory	
Name:	Larry Shively	Name:		Name:	Shely Company
Cert. Level:	3	Cert. Level:		Location	Thornville, Oh
Cert. No.:		Cert. No.:		Initial Cert. Date	Mar 84
Cert. Date:	Mar-84	Cert. Date.		Last ReCert. Date	Mar-11
Last ReCert		Last ReCert.:			

Old Design: Yes [ ] No [X]

1) This design has been previously approved as JMF # ____ most recently for project # ____ Calibration # ____

2) This design has not been approved, but was submitted for approval on Project # ____

QC program submitted for this year? Yes [X] No [ ]

Reminder A copy of this design must be submitted to the OET

GB2003

Figure 16.6(a) Mix Design Summary: Ohio Test Section PG 70-22

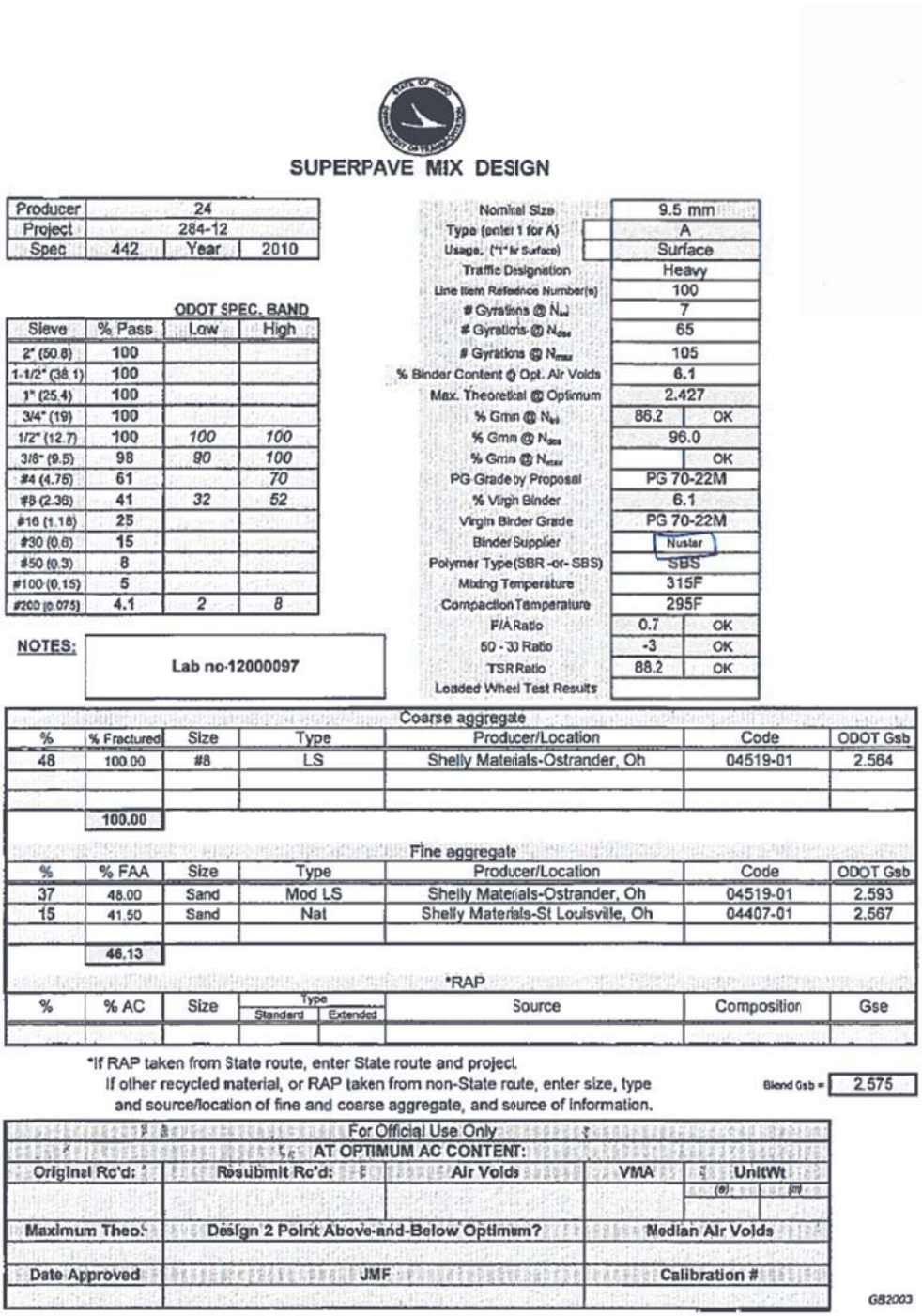

SUPERPAVE MIX DESIGN

Producer	24		
Project	284-12		
Spec	442	Year	2010

Nominal Size	9.5 mm		
Type (enter 1 for A)	A		
Usage: ("1" for Surface)	Surface		
Traffic Designation	Heavy		
Line Item Reference Number(s)	100		
# Gyrations @ N_{ini}	7		
# Gyrations @ N_{des}	65		
# Gyrations @ N_{max}	105		
% Binder Content @ Opt. Air Voids	6.1		
Max. Theoretical @ Optimum	2.427		
% Gmm @ N_{ini}	86.2	OK	
% Gmm @ N_{des}	96.0		
% Gmm @ N_{max}		OK	
PG Grade by Proposal	PG 70-22M		
% Virgin Binder	6.1		
Virgin Binder Grade	PG 70-22M		
Binder Supplier	Nustar		
Polymer Type(SBR -or- SBS)	SBS		
Mixing Temperature	315F		
Compaction Temperature	295F		
F/A Ratio	0.7	OK	
50 - 30 Ratio	-3	OK	
TSR Ratio	88.2	OK	
Loaded Wheel Test Results			

Sieve	% Pass	ODOT SPEC. BAND Low	High
2" (50.8)	100		
1-1/2" (38.1)	100		
1" (25.4)	100		
3/4" (19)	100		
1/2" (12.7)	100	100	100
3/8" (9.5)	98	90	100
#4 (4.75)	61		70
#8 (2.36)	41	32	52
#16 (1.18)	25		
#30 (0.6)	15		
#50 (0.3)	8		
#100 (0.15)	5		
#200 (0.075)	4.1	2	8

NOTES:

Lab no-12000097

Coarse aggregate

%	% Fractured	Size	Type	Producer/Location	Code	ODOT Gsb
48	100.00	#8	LS	Shelly Materials-Ostrander, Oh	04519-01	2.564
	100.00					

Fine aggregate

%	% FAA	Size	Type	Producer/Location	Code	ODOT Gsb
37	48.00	Sand	Mod LS	Shelly Materials-Ostrander, Oh	04519-01	2.593
15	41.50	Sand	Nat	Shelly Materials-St Louisville, Oh	04407-01	2.567
	46.13					

*RAP

%	% AC	Size	Type: Standard	Type: Extended	Source	Composition	Gse

*If RAP taken from State route, enter State route and project.
If other recycled material, or RAP taken from non-State route, enter size, type and source/location of fine and coarse aggregate, and source of information.

Blend Gsb = 2.575

For Official Use Only

AT OPTIMUM AC CONTENT:

Original Rc'd:	Resubmit Rc'd:	Air Voids	VMA	UnitWt (e)	UnitWt (in)
Maximum Theo:	Design 2 Point Above-and-Below Optimum?		Median Air Voids		
Date Approved	JMF		Calibration #		

GB2003

Figure 16.6(b) Mix Design Summary: Ohio Test Section PG 70-22, continued

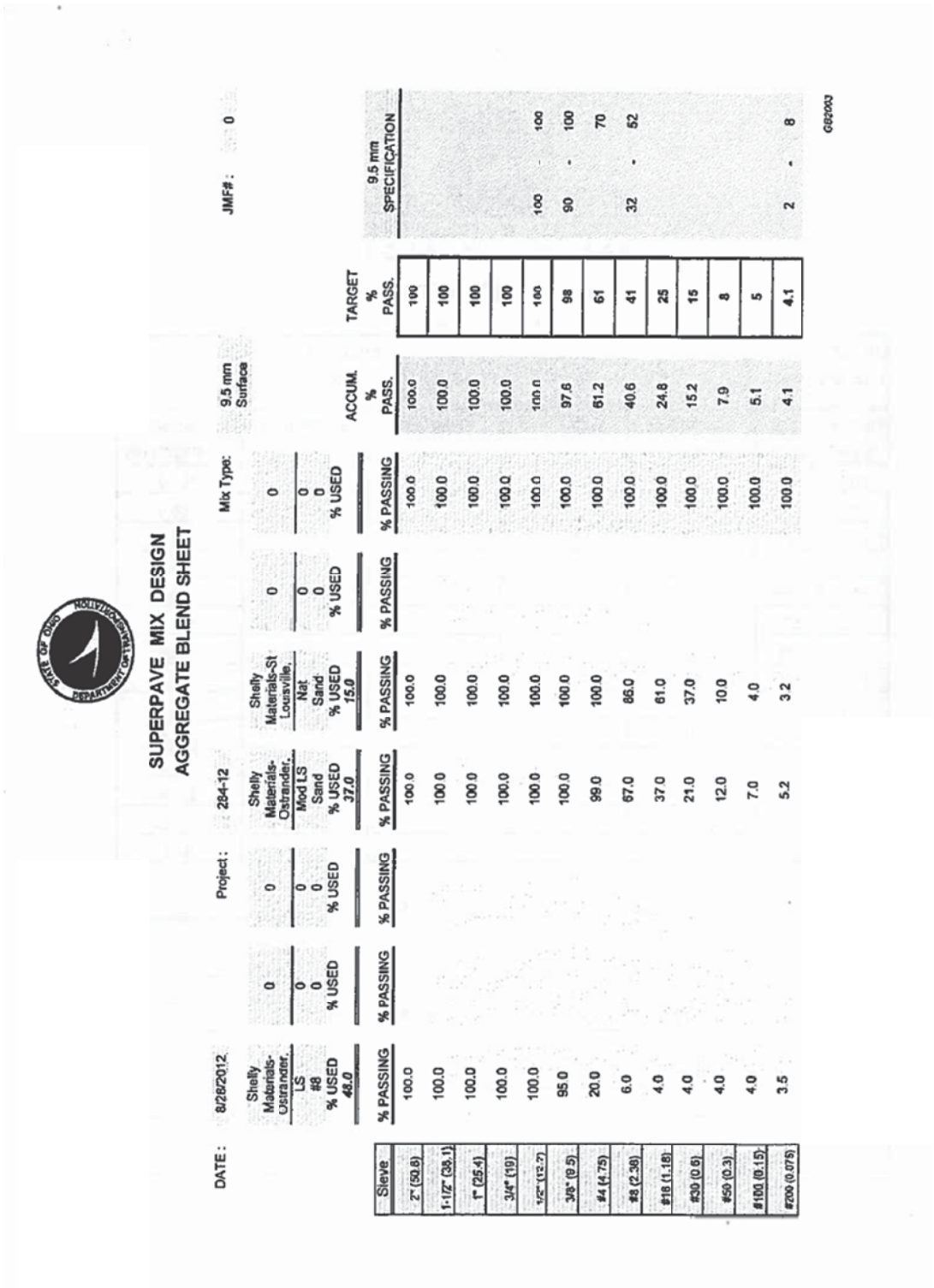

SUPERPAVE MIX DESIGN
AGGREGATE BLEND SHEET

DATE : 8/28/2012 Project : 284-12 Mix Type: 9.5 mm Surface JMF# : 0

Sieve	Shelly Materials-Ustrander. LS #8 48.0 % USED	% PASSING	0 0 0 % USED	% PASSING	Shelly Materials-Ostrander. Mod LS Sand 37.0 % USED	% PASSING	Shelly Materials-St Lousville. Nat Sand 15.0 % USED	% PASSING	0 0 0 % USED	% PASSING	ACCUM. % PASS.	TARGET % PASS.	9.5 mm SPECIFICATION
2" (50.8)	100.0				100.0		100.0				100.0	100	
1-1/2" (38.1)	100.0				100.0		100.0				100.0	100	
1" (25.4)	100.0				100.0		100.0				100.0	100	
3/4" (19)	100.0				100.0		100.0				100.0	100	
1/2" (12.7)	100.0				100.0		100.0				100.0	100	100
3/8" (9.5)	95.0				100.0		100.0				97.6	98	90 - 100
#4 (4.75)	20.0				99.0		100.0				61.2	61	70
#8 (2.36)	6.0				67.0		86.0				40.6	41	32 - 52
#16 (1.18)	4.0				37.0		61.0				24.8	25	
#30 (0.6)	4.0				21.0		37.0				15.2	15	
#50 (0.3)	4.0				12.0		10.0				7.9	8	
#100 (0.15)	4.0				7.0		4.0				5.1	5	
#200 (0.075)	3.5				5.2		3.2				4.1	4.1	2 - 8

GB2003

Figure 16.6(c) Mix Design Summary: Ohio Test Section PG 70-22, continued

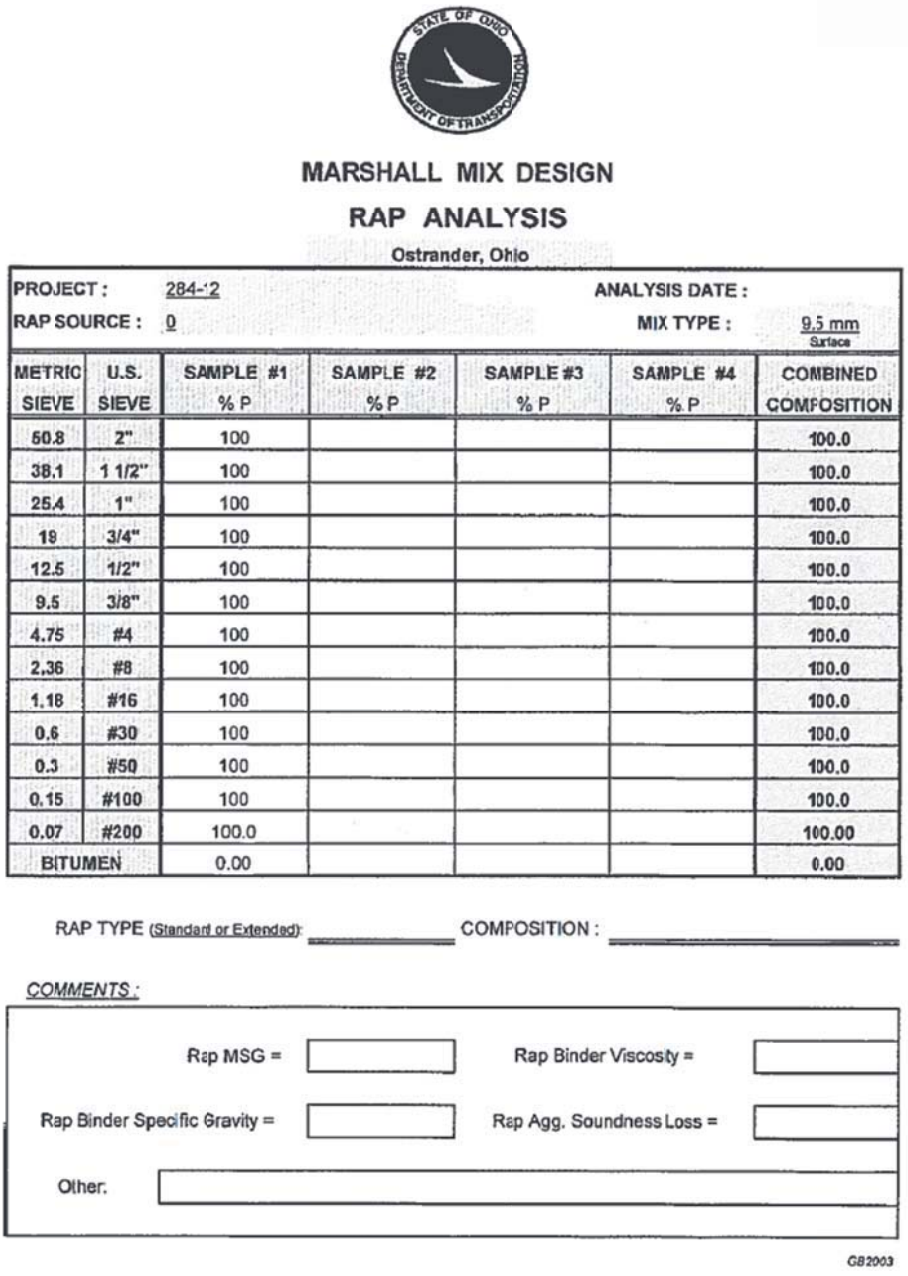

MARSHALL MIX DESIGN

RAP ANALYSIS

Ostrander, Ohio

PROJECT : 284-'2 ANALYSIS DATE :

RAP SOURCE : 0 MIX TYPE : 9.5 mm Surface

METRIC SIEVE	U.S. SIEVE	SAMPLE #1 % P	SAMPLE #2 % P	SAMPLE #3 % P	SAMPLE #4 % P	COMBINED COMPOSITION
50.8	2"	100				100.0
38.1	1 1/2"	100				100.0
25.4	1"	100				100.0
19	3/4"	100				100.0
12.5	1/2"	100				100.0
9.5	3/8"	100				100.0
4.75	#4	100				100.0
2.36	#8	100				100.0
1.18	#16	100				100.0
0.6	#30	100				100.0
0.3	#50	100				100.0
0.15	#100	100				100.0
0.07	#200	100.0				100.00
BITUMEN		0.00				0.00

RAP TYPE (Standard or Extended): _____ COMPOSITION : _____

COMMENTS :

Rap MSG = Rap Binder Viscosity =

Rap Binder Specific Gravity = Rap Agg. Soundness Loss =

Other:

GB2003

Figure 16.6(d) Mix Design Summary: Ohio Test Section PG 70-22, continued

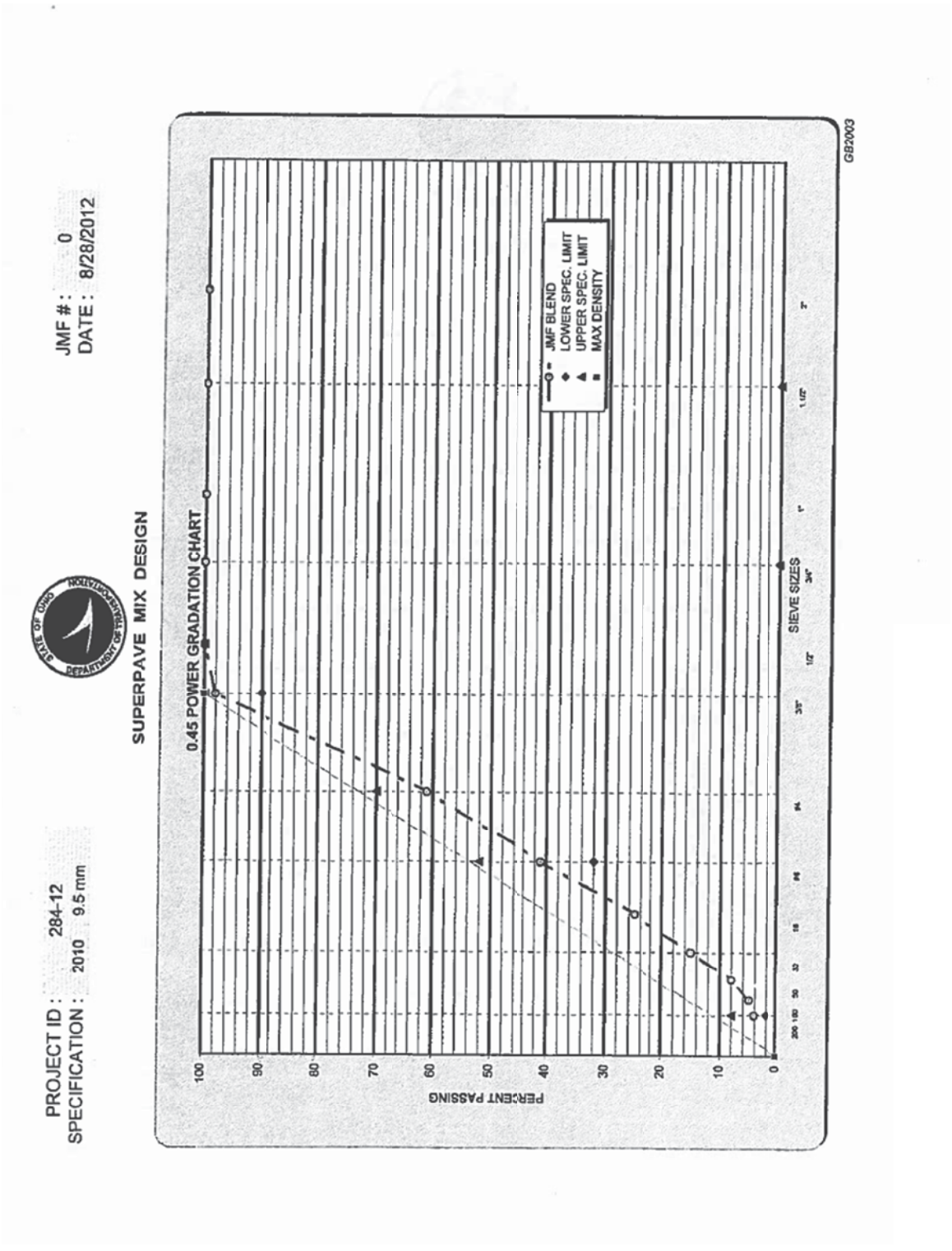

Figure 16.6(e) Mix Design Summary: Ohio Test Section PG 70-22, continued

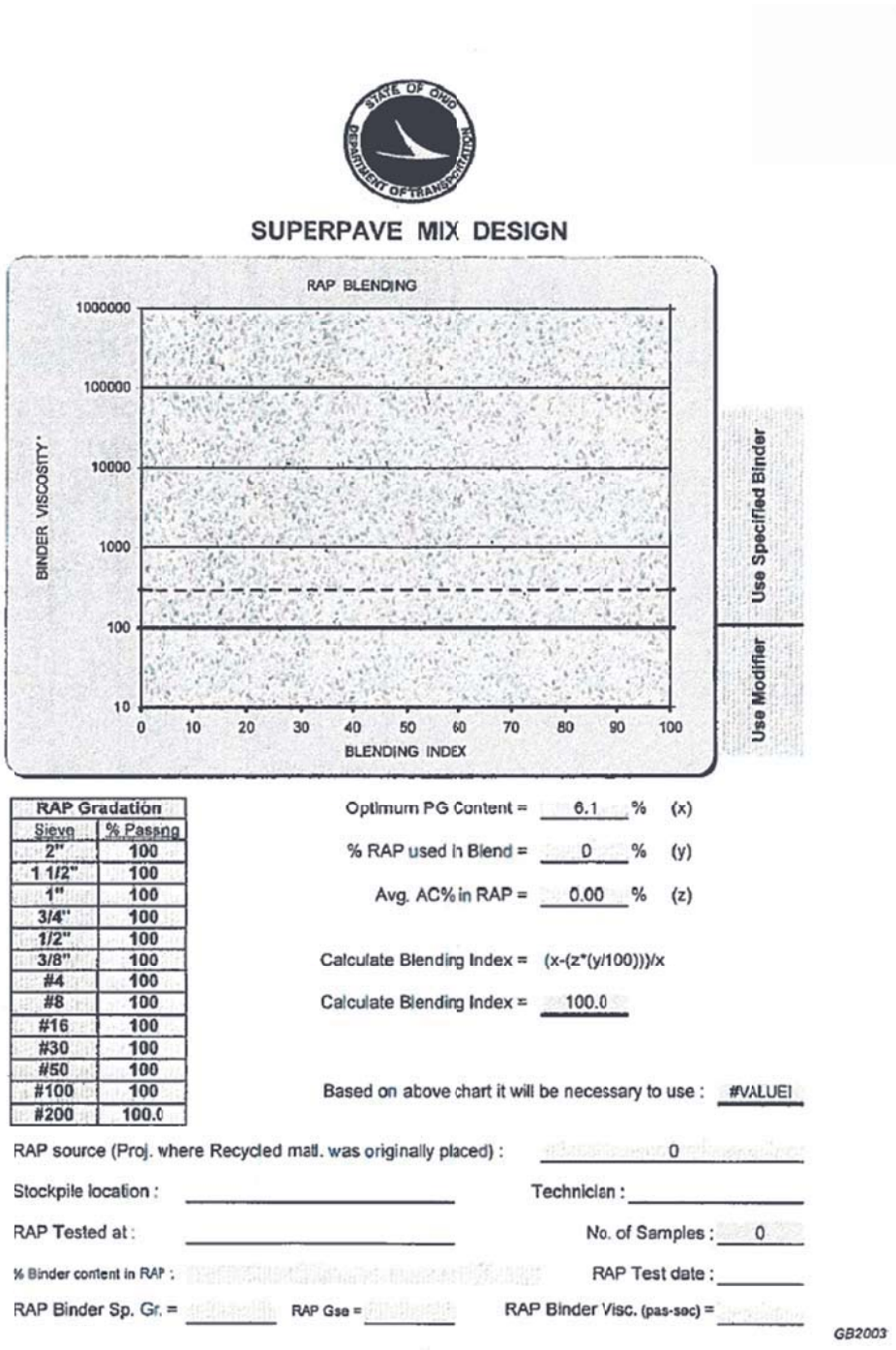

Figure 16.6(f) Mix Design Summary: Ohio Test Section PG 70-22, continued

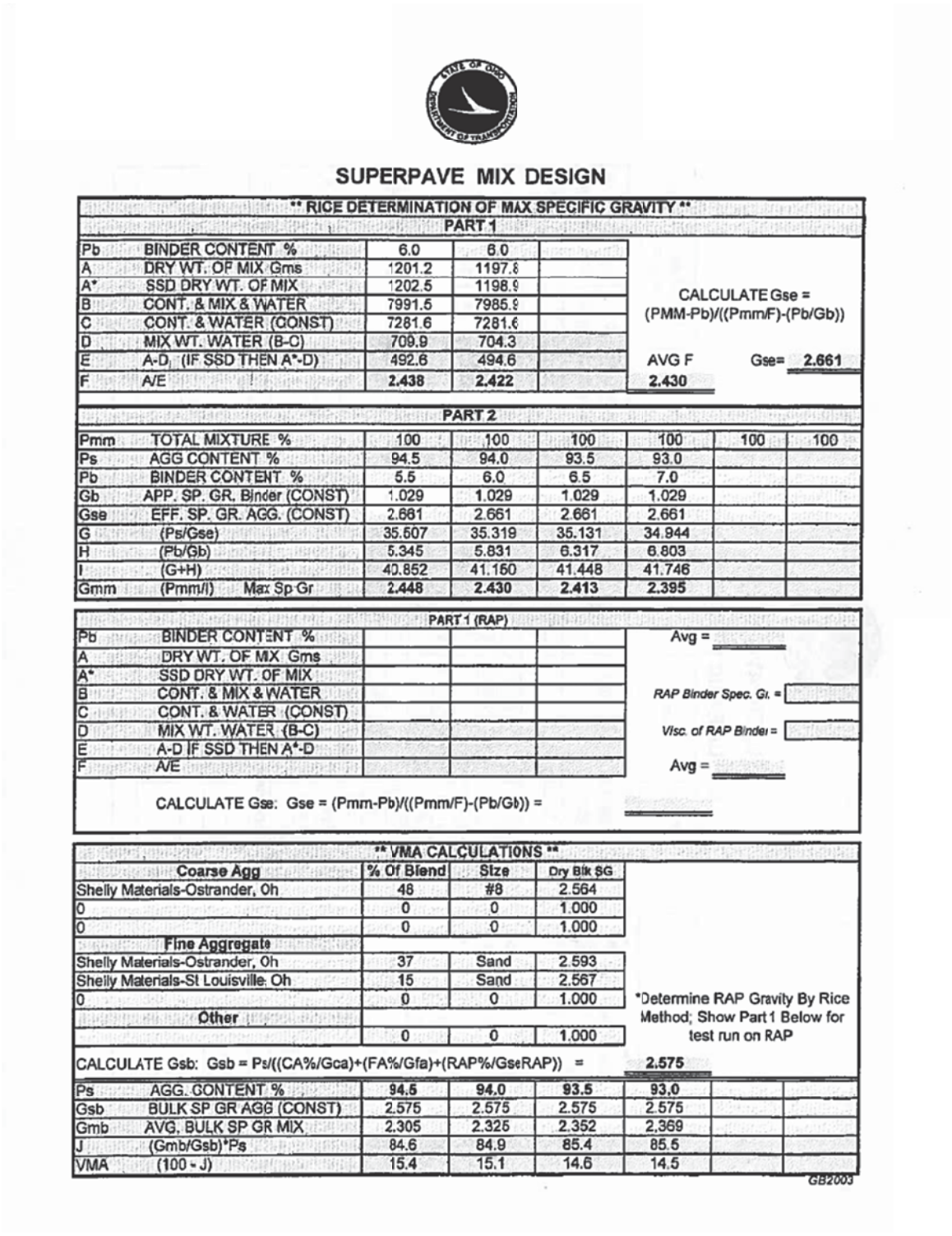

SUPERPAVE MIX DESIGN

**** RICE DETERMINATION OF MAX SPECIFIC GRAVITY ****

PART 1

Pb	BINDER CONTENT %	6.0	6.0		CALCULATE Gse = (PMM-Pb)/((Pmm/F)-(Pb/Gb))
A	DRY WT. OF MIX Gms	1201.2	1197.8		
A*	SSD DRY WT. OF MIX	1202.5	1198.9		
B	CONT. & MIX & WATER	7991.5	7985.9		
C	CONT. & WATER (CONST)	7281.6	7281.6		
D	MIX WT. WATER (B-C)	709.9	704.3		
E	A-D, (IF SSD THEN A*-D)	492.6	494.6		AVG F Gse= 2.661
F	A/E	2.438	2.422		2.430

PART 2

Pmm	TOTAL MIXTURE %	100	100	100	100	100	100
Ps	AGG CONTENT %	94.5	94.0	93.5	93.0		
Pb	BINDER CONTENT %	5.5	6.0	6.5	7.0		
Gb	APP. SP. GR. Binder (CONST)	1.029	1.029	1.029	1.029		
Gse	EFF. SP. GR. AGG. (CONST)	2.661	2.661	2.661	2.661		
G	(Ps/Gse)	35.507	35.319	35.131	34.944		
H	(Pb/Gb)	5.345	5.831	6.317	6.803		
I	(G+H)	40.852	41.150	41.448	41.746		
Gmm	(Pmm/I) Max Sp Gr	2.448	2.430	2.413	2.395		

PART 1 (RAP)

Pb	BINDER CONTENT %				Avg =
A	DRY WT. OF MIX Gms				
A*	SSD DRY WT. OF MIX				
B	CONT. & MIX & WATER				RAP Binder Spec. Gr. =
C	CONT. & WATER (CONST)				
D	MIX WT. WATER (B-C)				Visc. of RAP Binder =
E	A-D IF SSD THEN A*-D				
F	A/E				Avg =

CALCULATE Gse: Gse = (Pmm-Pb)/((Pmm/F)-(Pb/Gb)) =

**** VMA CALCULATIONS ****

Coarse Agg	% Of Blend	Size	Dry Blk SG	
Shelly Materials-Ostrander, Oh	48	#8	2.564	
0	0	0	1.000	
0	0	0	1.000	
Fine Aggregate				
Shelly Materials-Ostrander, Oh	37	Sand	2.593	
Shelly Materials-St Louisville Oh	15	Sand	2.567	
0	0	0	1.000	*Determine RAP Gravity By Rice Method; Show Part 1 Below for test run on RAP
Other				
	0	0	1.000	

CALCULATE Gsb: Gsb = Ps/((CA%/Gca)+(FA%/Gfa)+(RAP%/GseRAP)) = 2.575

Ps	AGG. CONTENT %	94.5	94.0	93.5	93.0		
Gsb	BULK SP GR AGG (CONST)	2.575	2.575	2.575	2.575		
Gmb	AVG. BULK SP GR MIX	2.305	2.325	2.352	2.369		
J	(Gmb/Gsb)*Ps	84.6	84.9	85.4	85.5		
VMA	(100 - J)	15.4	15.1	14.6	14.5		

GB2003

Figure 16.6(g) Mix Design Summary: Ohio Test Section PG 70-22, continued

SUPERPAVE MIX DESIGN

VOLUMETRIC MIX DESIGN DATA

JMF #	0	Mix Type:	9.5 mm	Design Force Applied:	65 Gyrations	Compaction Temperature	295F

Sample No.	Binder %	Thickness inches	Weight (g) In Air	Weight (g) SSD	Weight (g) In Water	Vol. Cc	Gmb	Gmm	% Binder by Volume	Voids (Percent) Total Mix	Voids (Percent) Filled	VMA	Unit Wt lb/ft³	Unit Wt kg/m³
A	B	C	D	R	E	F	G	H	I	J	K	L	M	N
						(R-E)	(D/F)		(BxGy/ Gb	100-100(G/H)	(I-J)/I		Gx62.4	Mx16.02
A	5.5	120.9	4829.6	4844.7	2752.7	2092.0	2.309							
B	5.5	120.8	4813.6	4831.7	2740.3	2091.4	2.302							
Average of 5.5% Binder Specimens							2.305	2.448	12.3	5.8	62.2	15.4	143.8	2304
A	6.0	119.5	4803.1	4810.3	2742.5	2067.8	2.323							
B	6.0	118.8	4790.6	4796.5	2737.2	2059.3	2.326							
Average of 6.0% Binder Specimens							2.325	2.430	13.6	4.3	71.3	15.1	145.1	2323
A	6.5	117.9	4826.8	4828.9	2783.1	2045.8	2.359							
B	6.5	118.6	4831.4	4834.9	2773.7	2061.2	2.344							
Average of 6.5% Binder Specimens							2.352	2.413	14.9	2.5	82.7	14.6	146.7	2351
A	7.0	117.5	4842.6	4845.3	2801.9	2043.4	2.370							
B	7.0	117.2	4835.1	4837.9	2795.4	2042.5	2.367							
Average of 7.0% Binder Specimens							2.369	2.395	16.1	1.1	92.2	14.6	147.8	2367
A														
B														

GB2003

Figure 16.6(h) Mix Design Summary: Ohio Test Section PG 70-22, continued

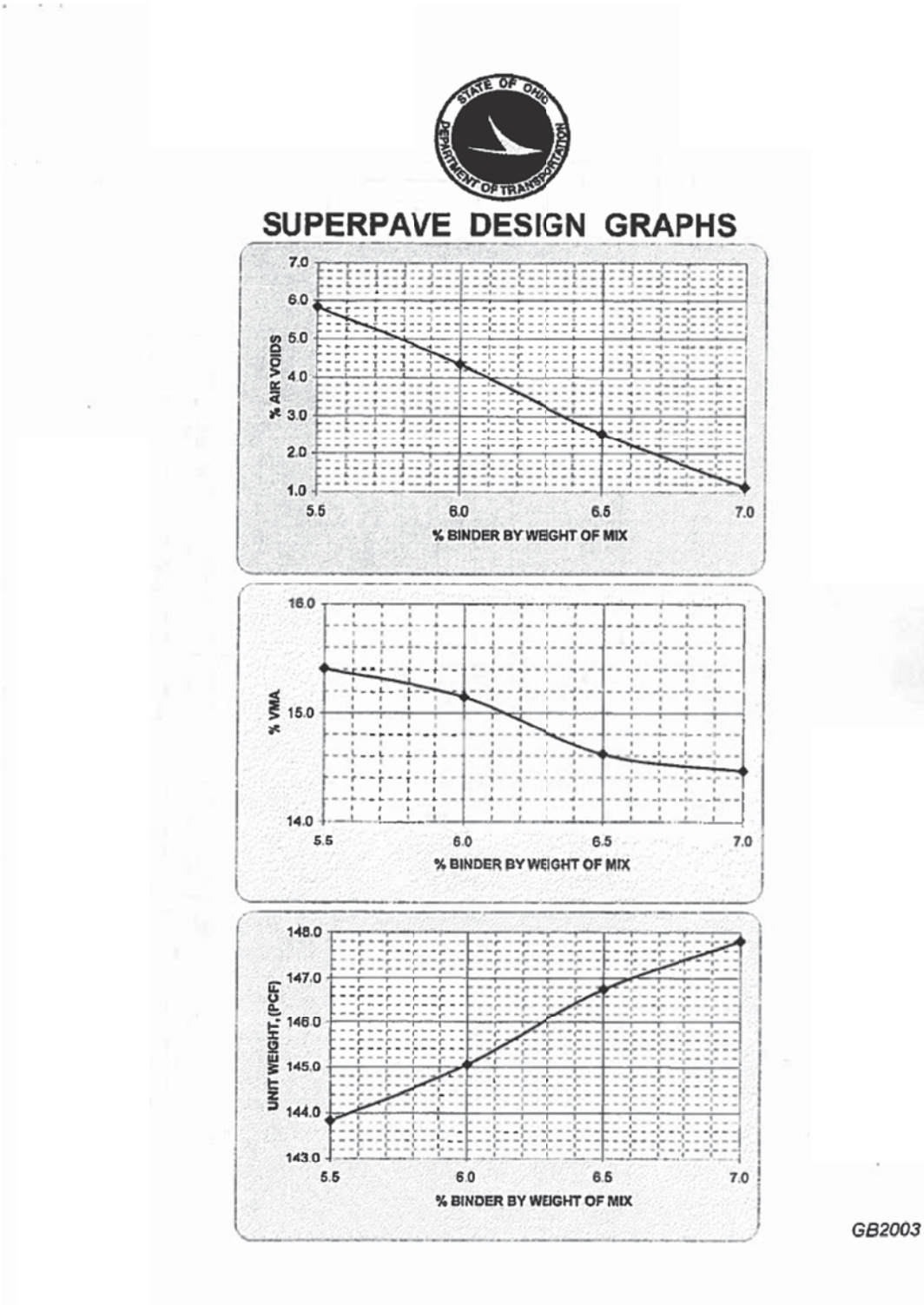

Figure 16.6(i) Mix Design Summary: Ohio Test Section PG 70-22, continued

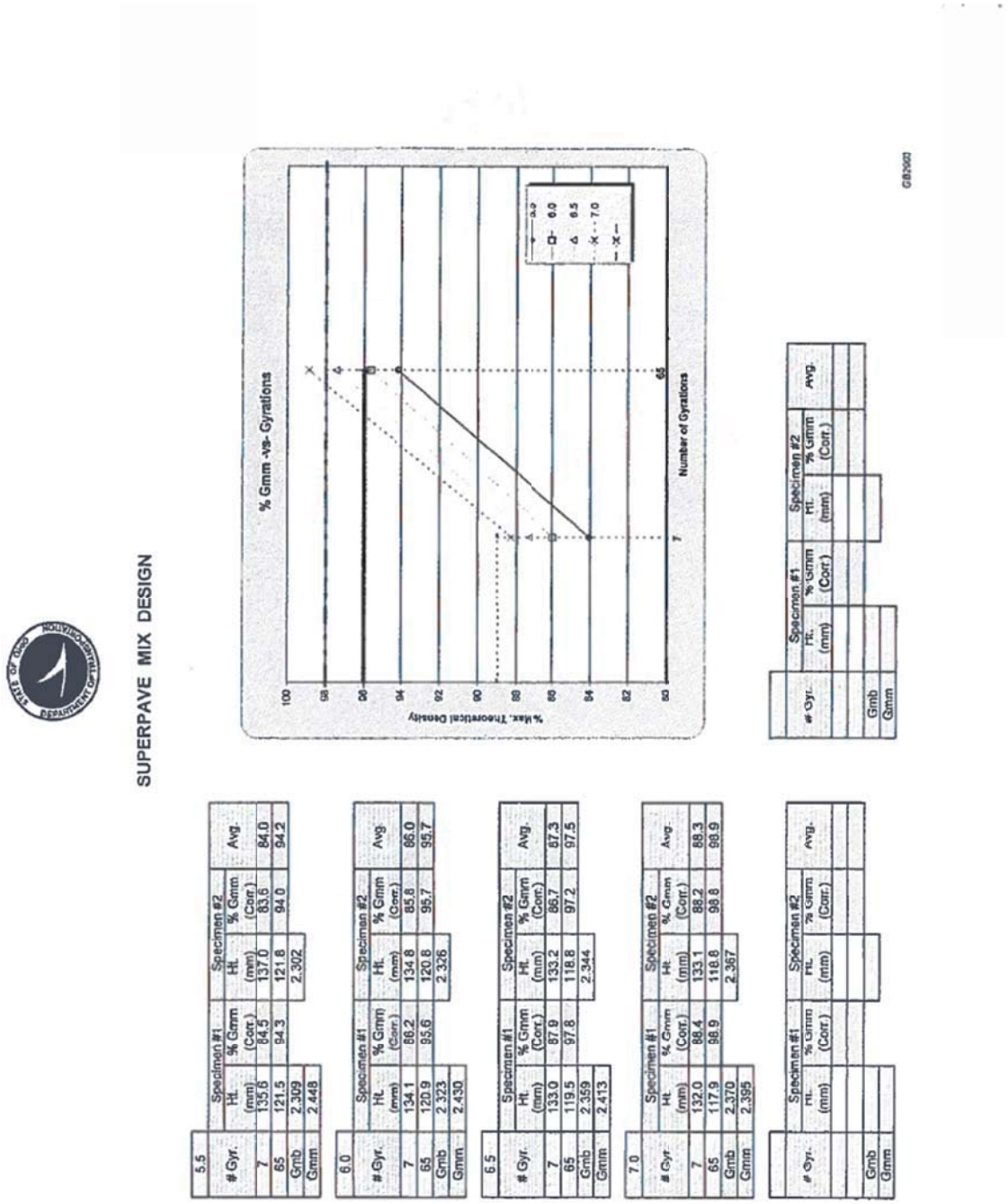

Figure 16.6(j) Mix Design Summary: Ohio Test Section PG 70-22, continued

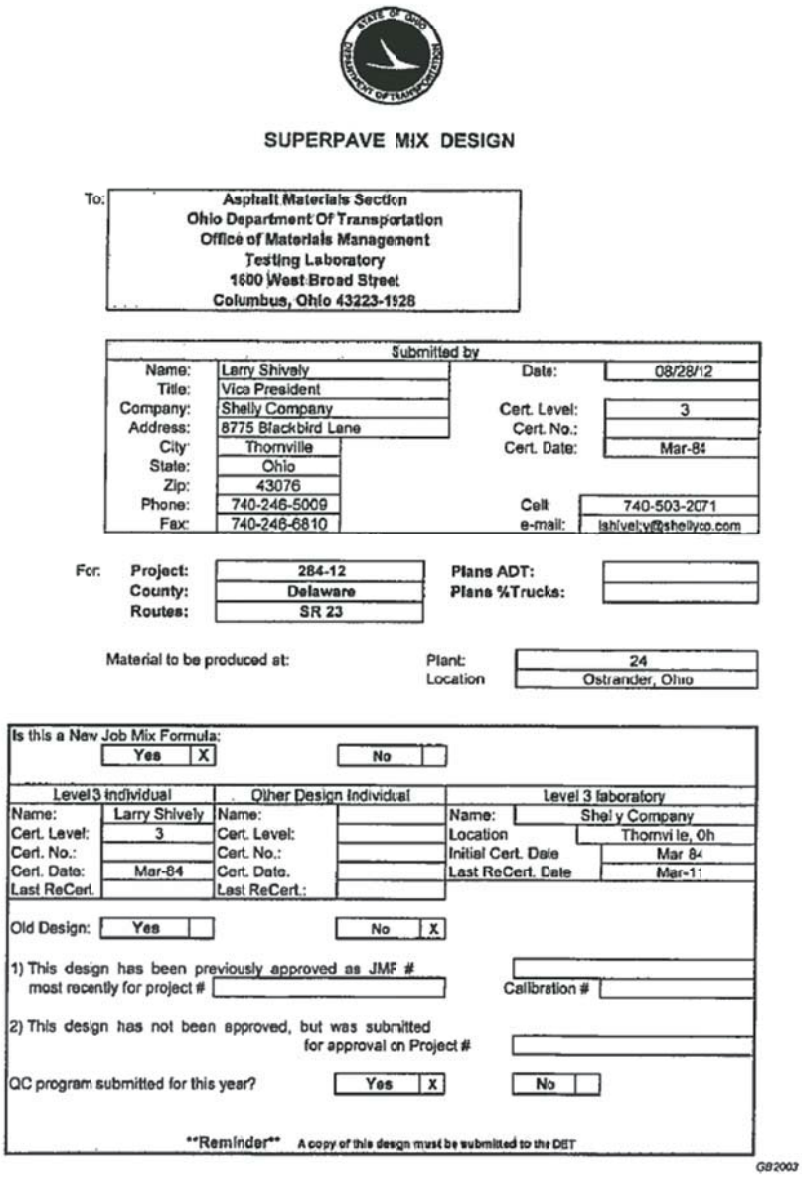

SUPERPAVE MIX DESIGN

To: Asphalt Materials Section
Ohio Department Of Transportation
Office of Materials Management
Testing Laboratory
1600 West Broad Street
Columbus, Ohio 43223-1528

Submitted by

Name:	Larry Shively	Date:	08/28/12
Title:	Vice President		
Company:	Shelly Company	Cert. Level:	3
Address:	8775 Blackbird Lane	Cert. No.:	
City:	Thornville	Cert. Date:	Mar-84
State:	Ohio		
Zip:	43076		
Phone:	740-246-5009	Cell	740-503-2071
Fax:	740-246-6810	e-mail:	lshively@shellyco.com

For: Project: 284-12 Plans ADT:
County: Delaware Plans %Trucks:
Routes: SR 23

Material to be produced at: Plant: 24
Location: Ostrander, Ohio

Is this a New Job Mix Formula: Yes X No

Level3 individual		Other Design Individual		Level 3 laboratory	
Name:	Larry Shively	Name:		Name:	Shelly Company
Cert. Level:	3	Cert. Level:		Location	Thornville, Oh
Cert. No.:		Cert. No.:		Initial Cert. Date	Mar 84
Cert. Date:	Mar-84	Cert. Date.		Last ReCert. Date	Mar-11
Last ReCert.		Last ReCert.:			

Old Design: Yes No X

1) This design has been previously approved as JMF # most recently for project # Calibration #

2) This design has not been approved, but was submitted for approval on Project #

QC program submitted for this year? Yes X No

Reminder A copy of this design must be submitted to the DET

GB2003

Figure 16.6(k) Mix Design Summary: Ohio Test Section PG 70-22, continued

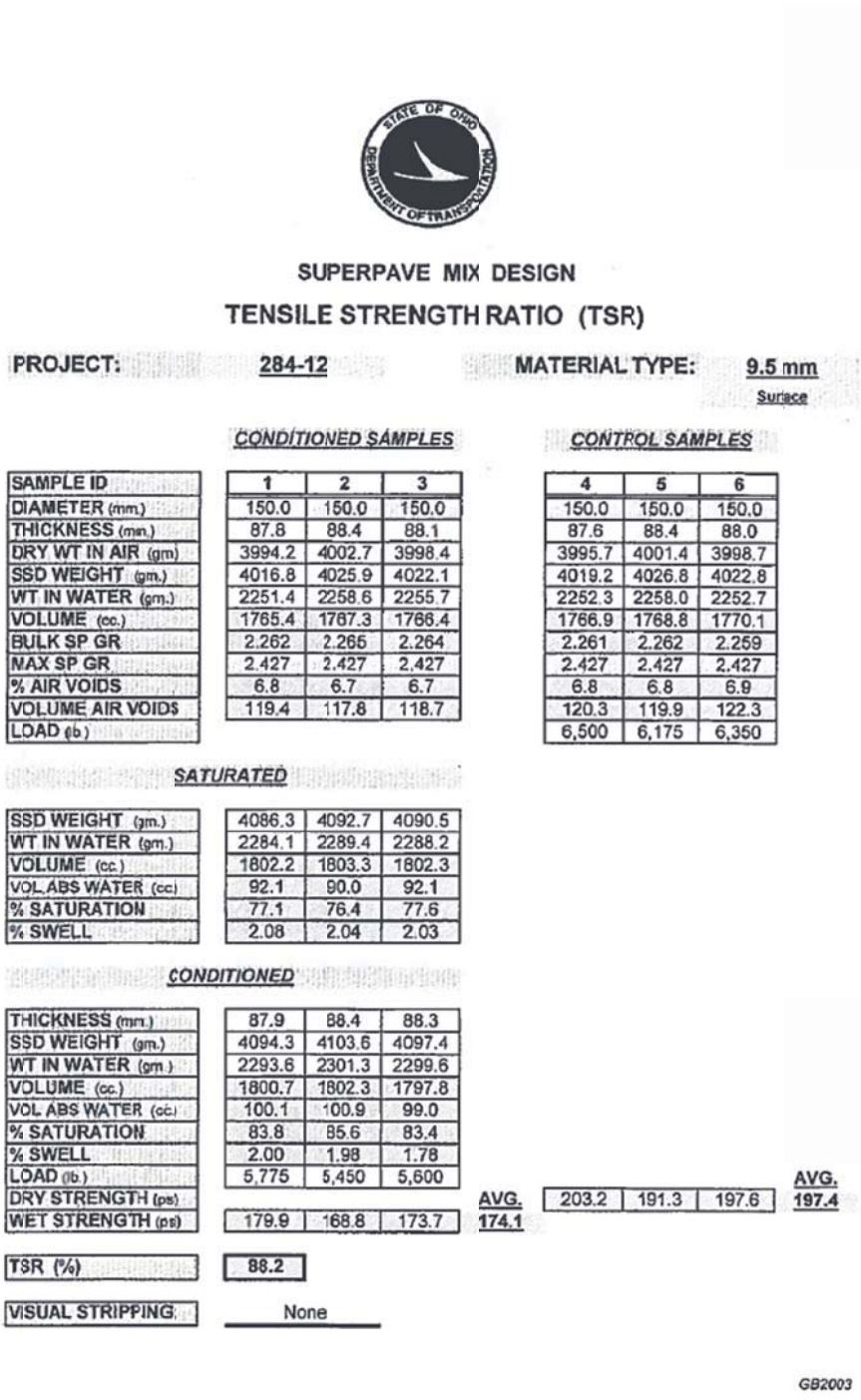

SUPERPAVE MIX DESIGN

TENSILE STRENGTH RATIO (TSR)

PROJECT: 284-12 MATERIAL TYPE: 9.5 mm Surface

	CONDITIONED SAMPLES			CONTROL SAMPLES			
SAMPLE ID	1	2	3	4	5	6	
DIAMETER (mm.)	150.0	150.0	150.0	150.0	150.0	150.0	
THICKNESS (mm.)	87.8	88.4	88.1	87.6	88.4	88.0	
DRY WT IN AIR (gm)	3994.2	4002.7	3998.4	3995.7	4001.4	3998.7	
SSD WEIGHT (gm.)	4016.8	4025.9	4022.1	4019.2	4026.8	4022.8	
WT IN WATER (gm.)	2251.4	2258.6	2255.7	2252.3	2258.0	2252.7	
VOLUME (cc.)	1765.4	1767.3	1766.4	1766.9	1768.8	1770.1	
BULK SP GR	2.262	2.265	2.264	2.261	2.262	2.259	
MAX SP GR	2.427	2.427	2.427	2.427	2.427	2.427	
% AIR VOIDS	6.8	6.7	6.7	6.8	6.8	6.9	
VOLUME AIR VOIDS	119.4	117.8	118.7	120.3	119.9	122.3	
LOAD (lb.)				6,500	6,175	6,350	

SATURATED			
SSD WEIGHT (gm.)	4086.3	4092.7	4090.5
WT IN WATER (gm.)	2284.1	2289.4	2288.2
VOLUME (cc.)	1802.2	1803.3	1802.3
VOL ABS WATER (cc.)	92.1	90.0	92.1
% SATURATION	77.1	76.4	77.6
% SWELL	2.08	2.04	2.03

CONDITIONED							
THICKNESS (mm.)	87.9	88.4	88.3				
SSD WEIGHT (gm.)	4094.3	4103.6	4097.4				
WT IN WATER (gm.)	2293.6	2301.3	2299.6				
VOLUME (cc.)	1800.7	1802.3	1797.8				
VOL ABS WATER (cc.)	100.1	100.9	99.0				
% SATURATION	83.8	85.6	83.4				
% SWELL	2.00	1.98	1.78				
LOAD (lb.)	5,775	5,450	5,600				
DRY STRENGTH (psi)				AVG.	203.2	191.3	197.6	AVG. 197.4
WET STRENGTH (psi)	179.9	168.8	173.7	174.1			

TSR (%)	88.2
VISUAL STRIPPING	None

GB2003

Figure 16.6(l) Mix Design Summary: Ohio Test Section PG 70-22, continued

17 APPENDIX E:

Photographs of Representative Laboratory Prepared Mixtures

(a) 4% Va (b) 7% Va (c) 11% Va

Figure 17.1 Mixture Photographs: California Intermediate PG 64-22 7.44%TWM Uncut, Dynamic Modulus, UTSST Specimens

(a) 7% Va (b) 7% Va (c) 7% Va

Figure 17.2 Mixture Photographs: California Intermediate PG 64-28 7.51% TWM Uncut, Dynamic Modulus, UTSST Specimens

(a) 7% Va (b) 7% Va (c) 7% Va

Figure 17.3 Mixture Photographs: California Fine PG 64-22 9.14% TWM Uncut, Dynamic Modulus, UTSST Specimens

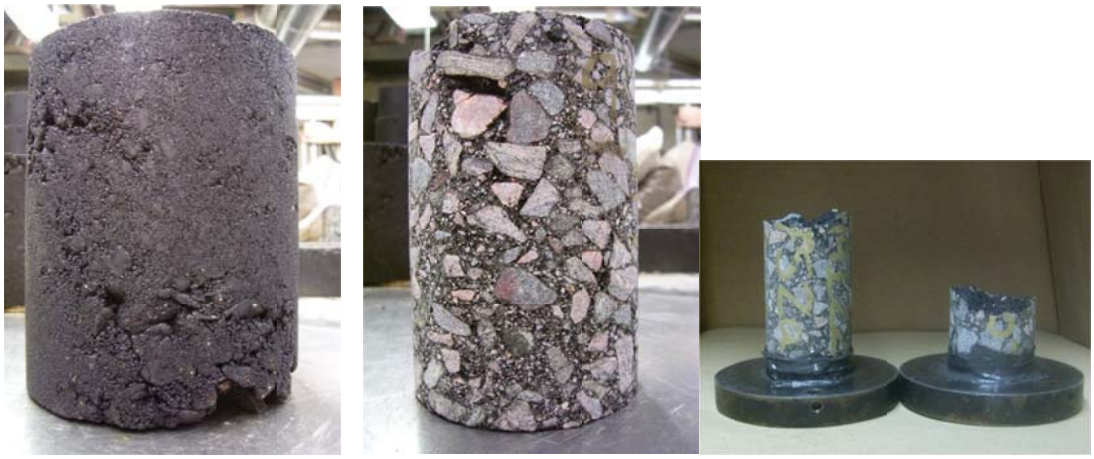

(a) 7% Va **(b) 7% Va** **(c) 7% Va**

Figure 17.4 Mixture Photographs: Colorado Intermediate PG 64-22 3.61% TWM Uncut, Dynamic Modulus, UTSST Specimens

(a) 7% Va **(b) 7% Va** **(c) 7% Va**

Figure 17.5 Mixture Photographs: Colorado Intermediate PG 64-22 4.5% TWM Uncut, Dynamic Modulus, UTSST Specimens

(a) 7% Va **(b) 7% Va** **(c) 7% Va**

Figure 17.6 Mixture Photographs: Colorado Intermediate PG 64-28 3.65% TWM Uncut, Dynamic Modulus, UTSST Specimens

(a) 7% Va **(b) 7% Va** **(c) 7% Va**

Figure 17.7 Mixture Photographs: Colorado Intermediate PG 64-28 4.5% TWM Uncut, Dynamic Modulus, UTSST Specimens

(a) 7% Va **(b) 7% Va** **(c) 7% Va**

Figure 17.8 Mixture Photographs: Nevada Intermediate PG 64-22 4.5% TWM Uncut, Dynamic Modulus, UTSST Specimens

(a) 7% Va **(b) 7% Va** **(c) 7% Va**

Figure 17.9 Mixture Photographs: Nevada Intermediate PG 64-22 5.38% TWM Uncut, Dynamic Modulus, UTSST Specimens

(a) 4% Va (b) 7% Va (c) 11% Va

Figure 17.10 Mixture Photographs: Nevada Intermediate PG 64-28 5.22%TWM Uncut, Dynamic Modulus, UTSST Specimens

(a) 7% Va (b) 7% Va (c) 7% Va

Figure 17.11 Mixture Photographs: Nevada Intermediate PG 64-28 4.5%TWM Uncut, Dynamic Modulus, UTSST Specimens

(a) 7% Va (b) 7% Va (c) 7% Va

Figure 17.12 Mixture Photographs: Nevada Fine PG 64-28 6.0%TWM Uncut, Dynamic Modulus, UTSST Specimens

(a) 4% Va **(b) 7% Va** **(c) 11% Va**

Figure 17.13 Mixture Photographs: Utah Intermediate PG 64-28 3.79%TWM Uncut, Dynamic Modulus, UTSST Specimens

(a) 7% Va (b) 7% Va (c) 7% Va

Figure 17.14 Mixture Photographs: Utah Fine PG 64-28 5.22%TWM Uncut, Dynamic Modulus, UTSST Specimens

(a) 7% Va (b) 7% Va (c) 7% Va

Figure 17.15 Mixture Photographs: WesTrack 1995 Fine PG 64-22 5.2%TWM Uncut, Dynamic Modulus, UTSST Specimens

(a) 4% Va (b) 7% Va (c) 11% Va

Figure 17.16 Mixture Photographs: WesTrack 1997 Coarse PG 64-22 5.1%TWM Uncut, Dynamic Modulus, UTSST Specimens

18 APPENDIX F:

Photographs of Aggregate Gradations and Petrographic Thin Sections

Figure 18.1 Gardner, California: Blended Aggregate Photograph

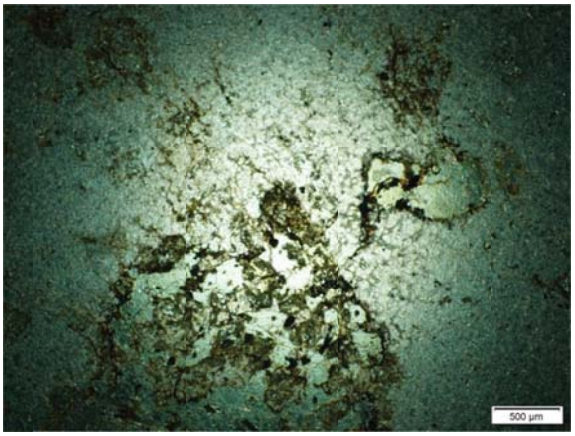

0° angle

Figure 18.2 Gardner, California: Mudstone Example Thin Section Under Plane-PolarizedLight, 2x magnification

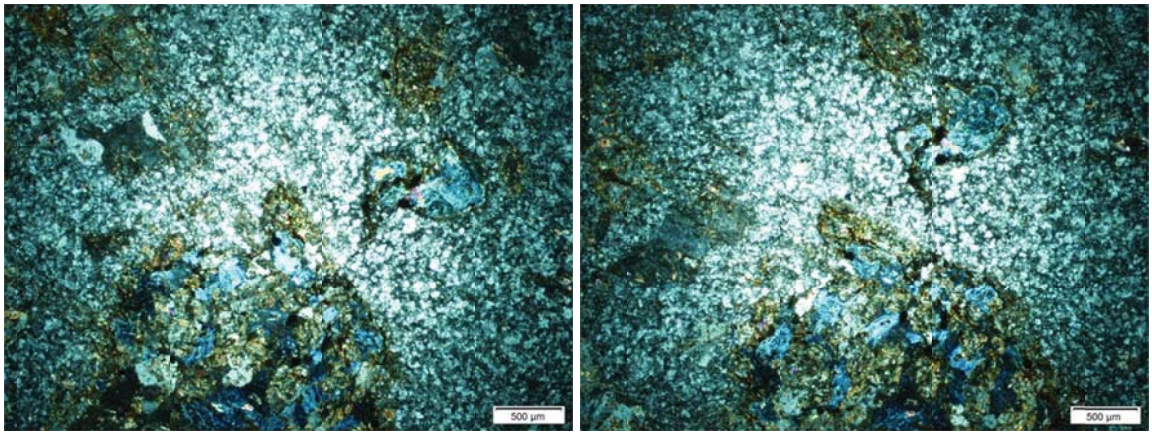

0° angle **30° angle**

Figure 18.3 Gardner, California: Mudstone Example Thin Section Under Cross-Polarized Light, 2x magnification

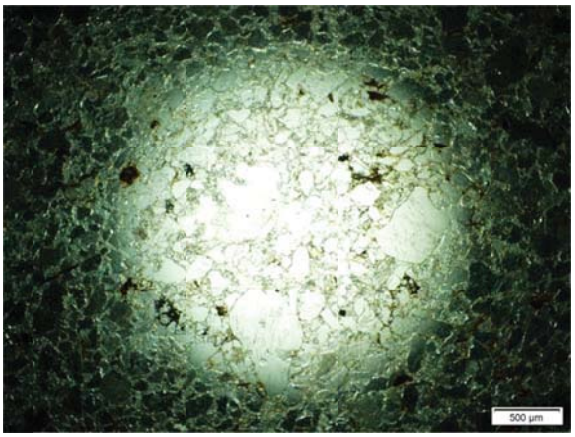

0° angle

Figure 18.4 Gardner, California: Sandstone Example Thin Section Under Plane-PolarizedLight, 2x magnification

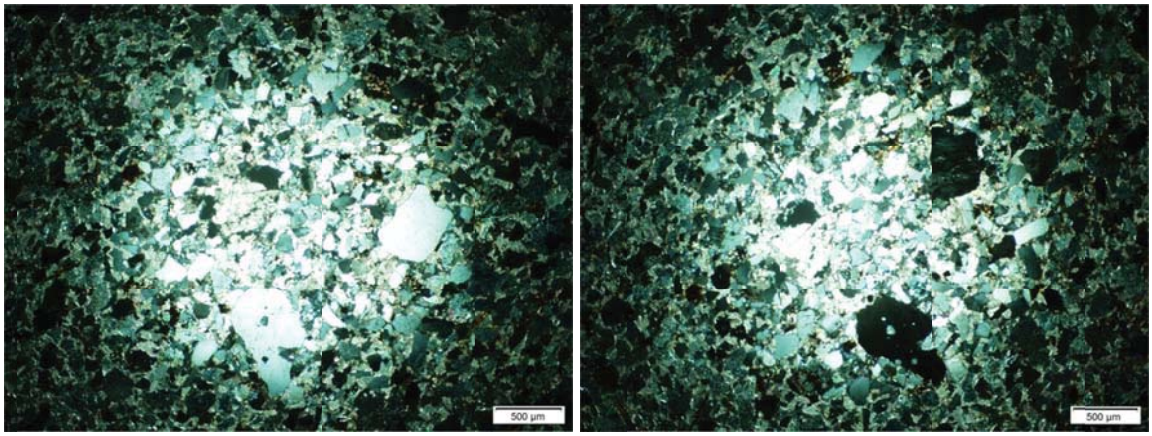

0° angle **37° angle**

Figure 18.5 Gardner, California: Sandstone Example Thin Section Under Cross-Polarized Light, 2x magnification

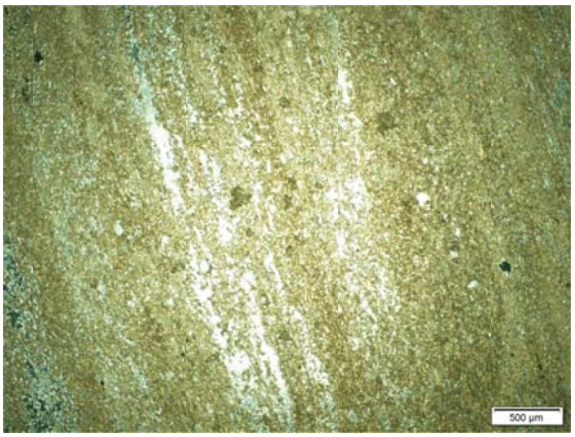

0° angle

Figure 18.6 Gardner, California: Gneiss Example A Thin Section Under Plane-Polarized Light, 2x magnification

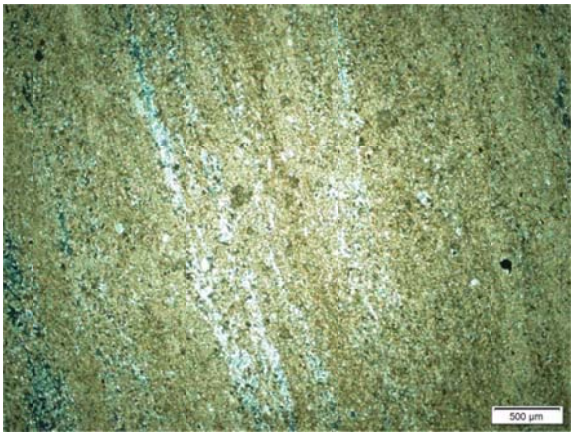

0° angle

Figure 18.7 Gardner, California: Gneiss Example A Thin Section Under Cross-Polarized Light, 2x magnification

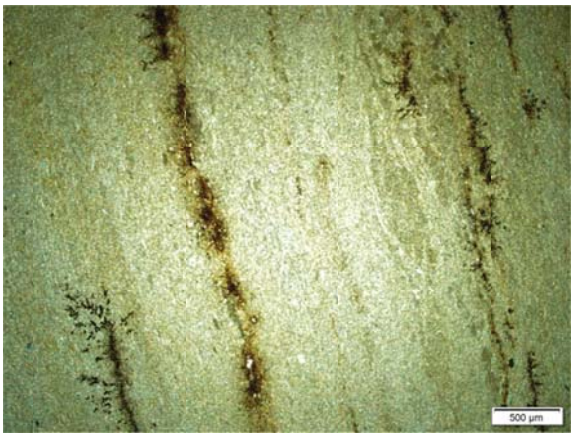

0° angle

Figure 18.8 Gardner, California: Gneiss Example B Thin Section Under Plane-Polarized Light, 2x magnification

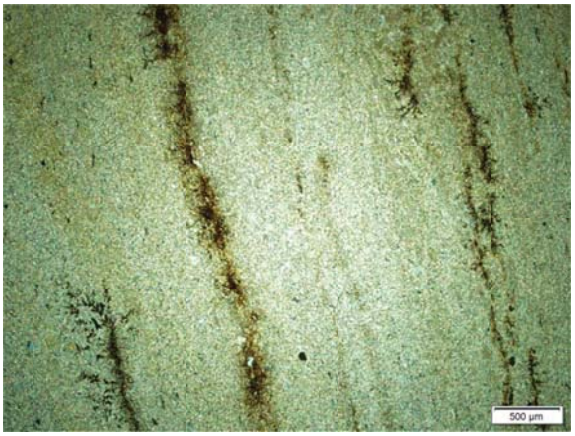

0° angle

Figure 18.9 Gardner, California: Gneiss Example B Thin Section Under Cross-Polarized Light, 2x magnification

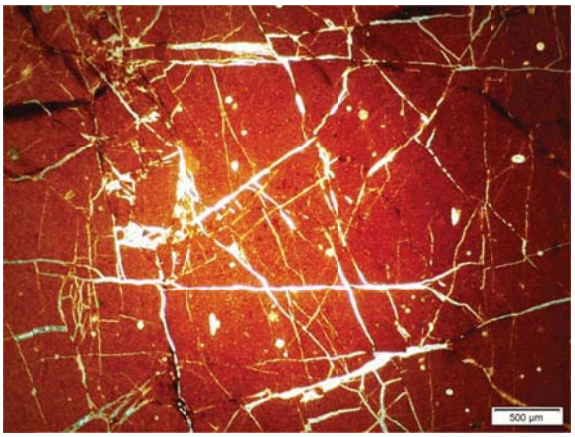

0° angle

Figure 18.10 Gardner, California: Chert Example A Thin Section Under Plane-Polarized Light, 2x magnification

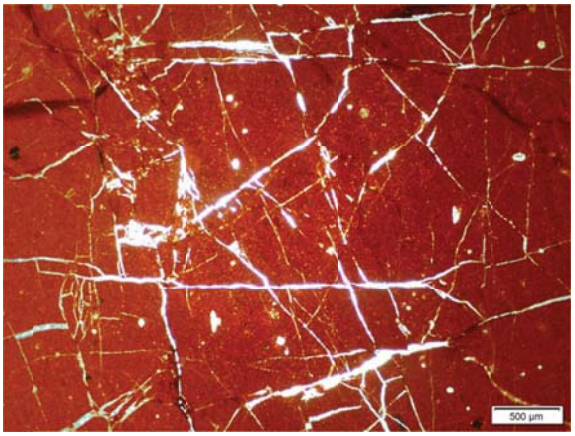

0° angle

Figure 18.11 Gardner, California: Chert Example A Thin Section Under Cross-Polarized Light, 2x magnification

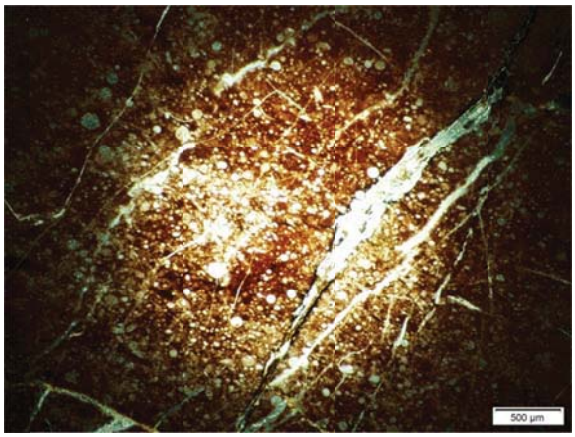

0° angle

Figure 18.12 Gardner, California: Chert Example B Thin Section Under Plane-Polarized Light, 2x magnification

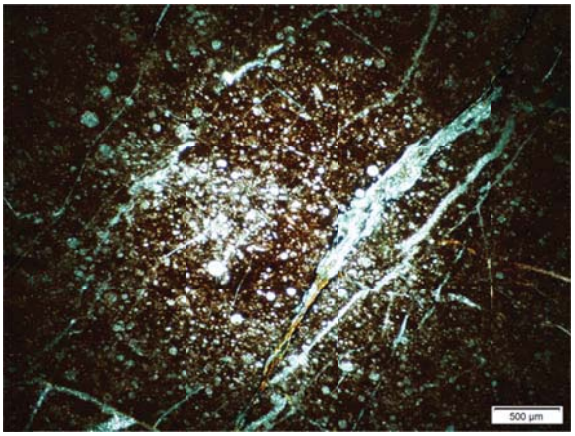

0° angle

Figure 18.13 Gardner, California: Chert Example B Thin Section Under Cross-Polarized Light, 2x magnification

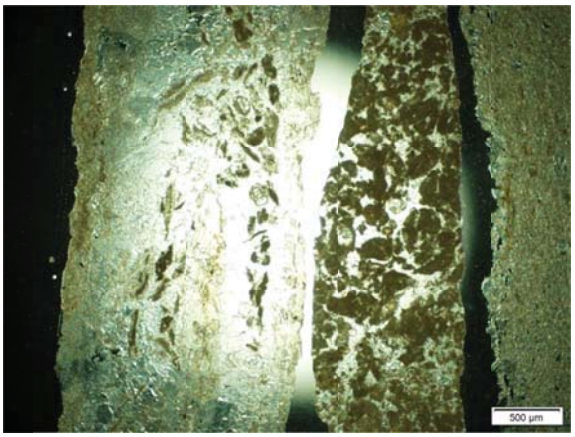

0° angle

Figure 18.14 Bee Rock, California: Limestone Example A Thin Section Under Plane-Polarized Light, 2x magnification

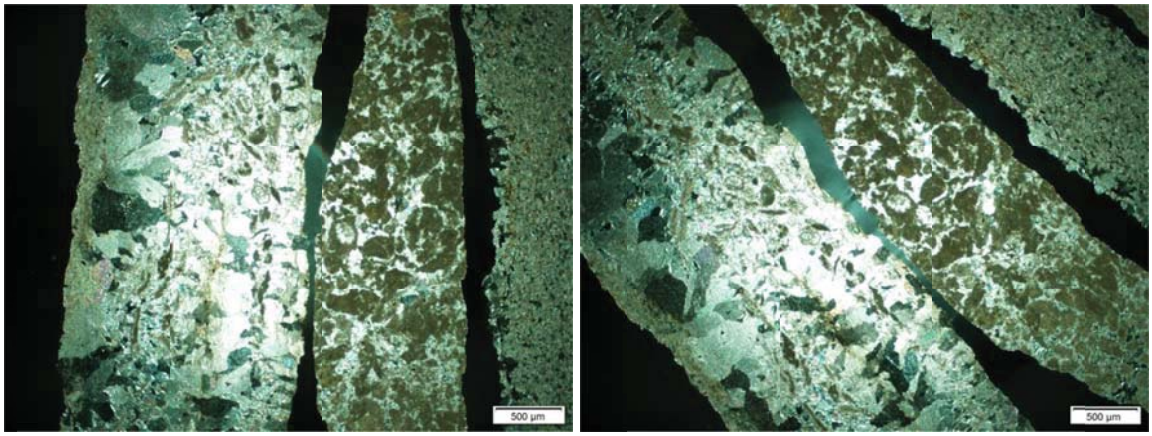

0° angle **45° angle**

Figure 18.15 Bee Rock, California: Limestone Example A Thin Section Under Cross-Polarized Light, 2x magnification

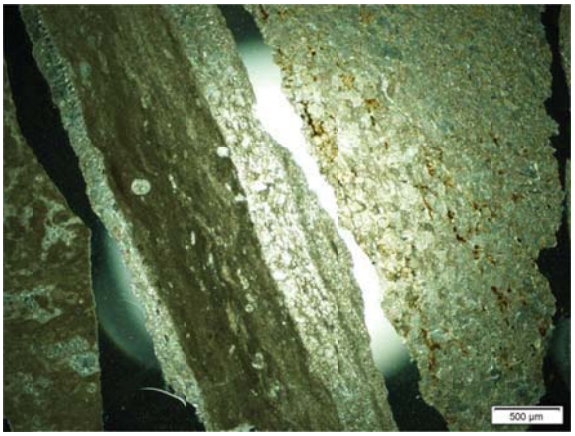

0° angle

Figure 18.16 Bee Rock, California: Limestone Example B Thin Section Under Plane-Polarized Light, 2x magnification

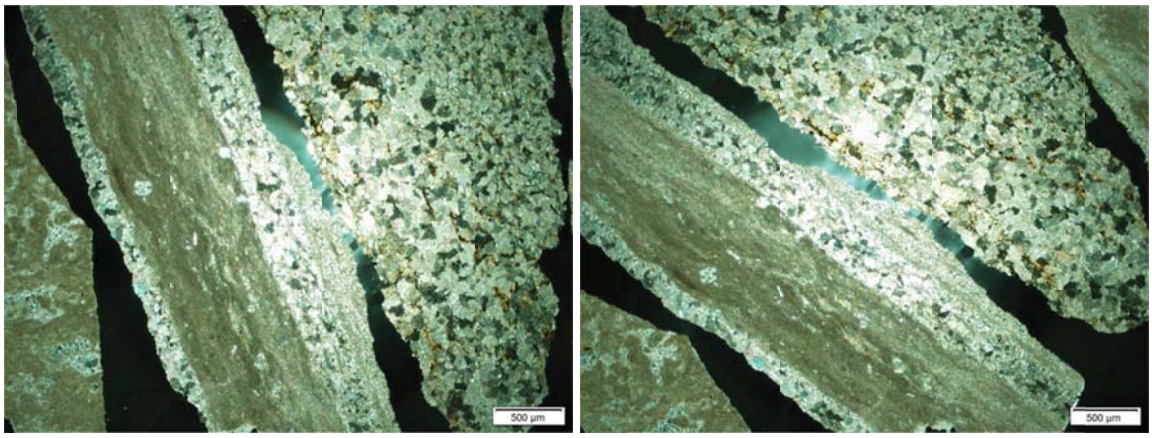

0° angle **30° angle**

Figure 18.17 Bee Rock, California: Limestone Example B Thin Section Under Cross-Polarized Light, 2x magnification

Figure 18.18 Morrison, Colorado: Blended Aggregate Photograph

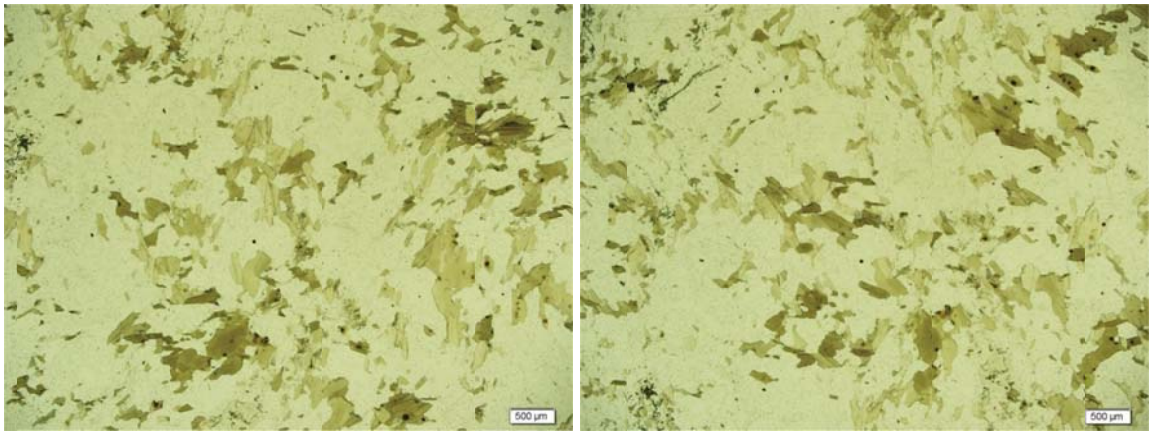

0° angle **32° angle**

Figure 18.19 Morrison, Colorado: Mica Schist Example Thin Section Under Plane-Polarized Light, 2x magnification

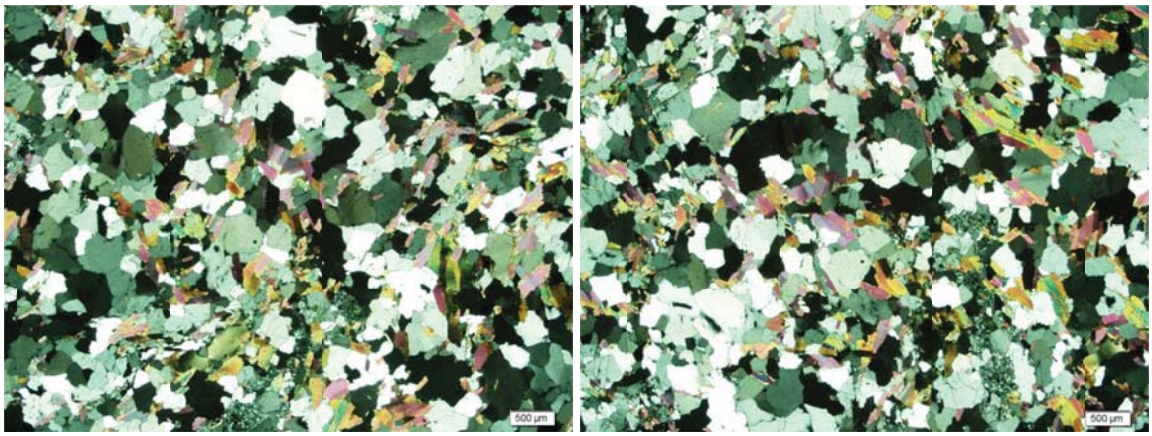

0° angle **32° angle**

Figure 18.20 Morrison, Colorado: Mica Schist Example Thin Section Under Cross-Polarized Light, 2x magnification

0° angle

Figure 18.21 Morrison, Colorado: Mica Gneiss Example Thin Section Under Plane-Polarized Light, 2x magnification

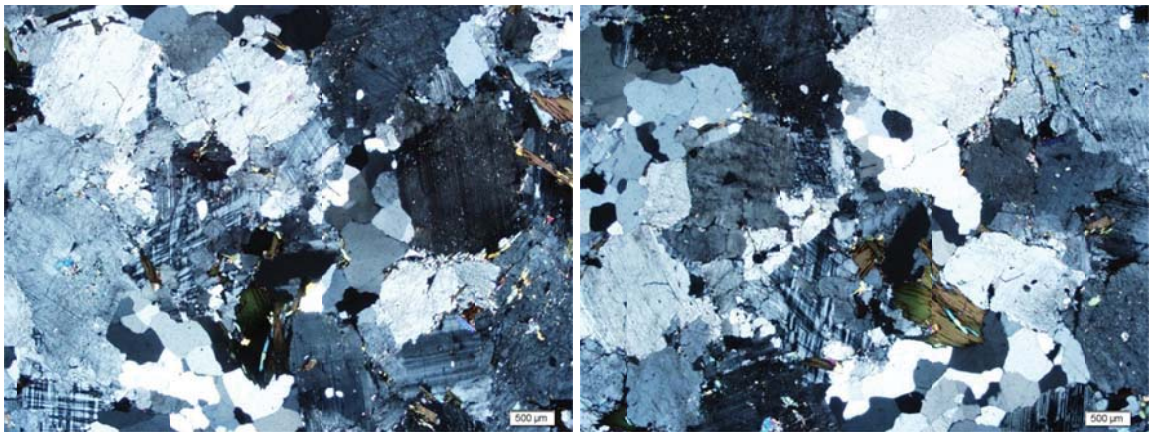

0° angle **53° angle**

Figure 18.22 Morrison, Colorado: Mica Gneiss Example Thin Section Under Cross-Polarized Light, 2x magnification

Figure 18.23 Morrison, Colorado: Muscovite (Mica Gneiss) Thin Section Under Cross-Polarized Light, 10x magnification

0° angle

Figure 18.24 Morrison, Colorado: Quartz Example Thin Section Under Plane-Polarized Light, 2x magnification

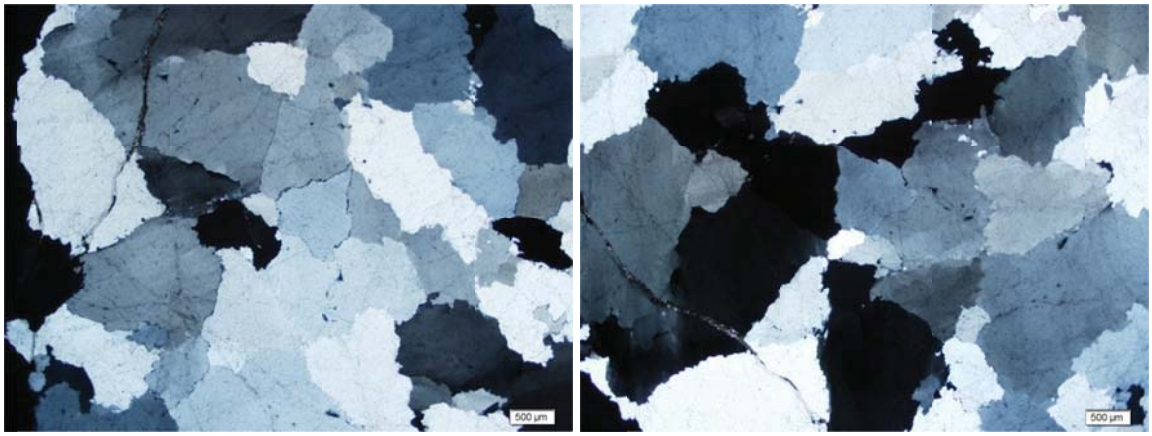

0° angle **61° angle**

Figure 18.25 Morrison, Colorado: Quartz Example Thin Section Under Cross-Polarized Light, 2x magnification

Figure 18.26 Lockwood, Nevada: Blended Aggregate Photograph

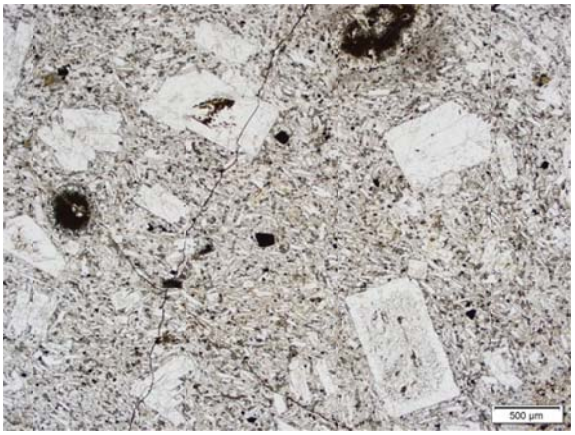

0° angle

Figure 18.27 Lockwood, Nevada: Basalt, Andesite, Rhyolite Example Thin Section Under Plane-Polarized Light, 2x magnification

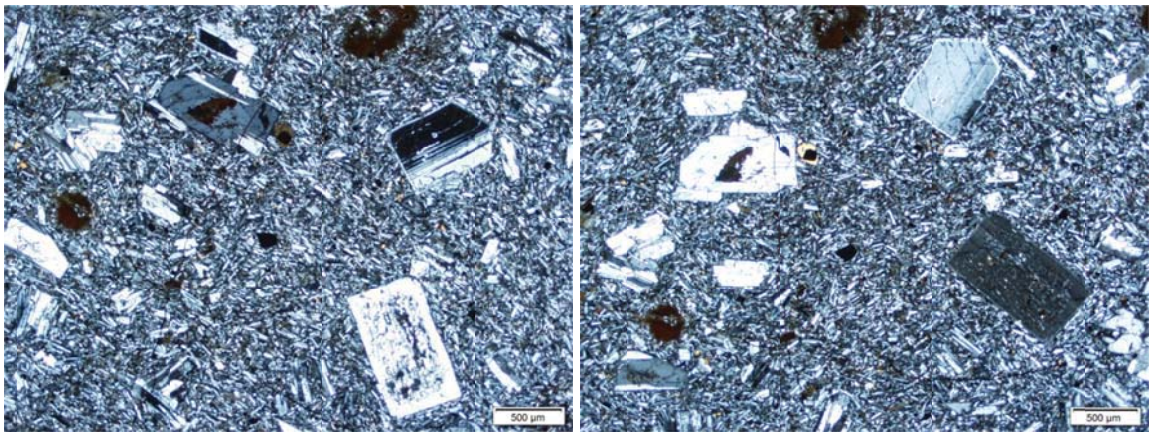

0° angle **30° angle**

Figure 18.28 Lockwood, Nevada: Basalt, Andesite, Rhyolite Example Thin Section Under Cross-Polarized Light, 2x magnification

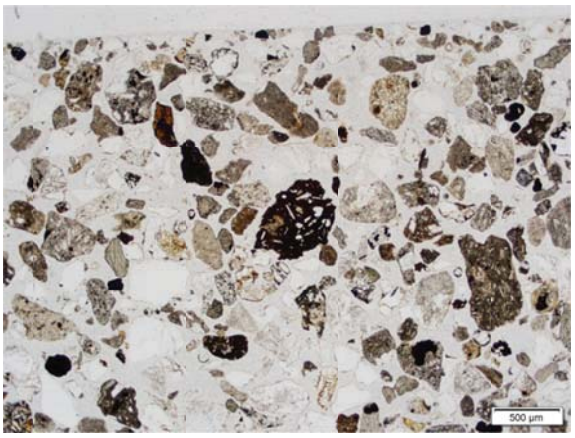

0° angle

Figure 18.29 Wadsworth, Nevada: Quartz, Lithic Clasts, Feldspar Example A Thin Section Under Plane-Polarized Light, 2x magnification

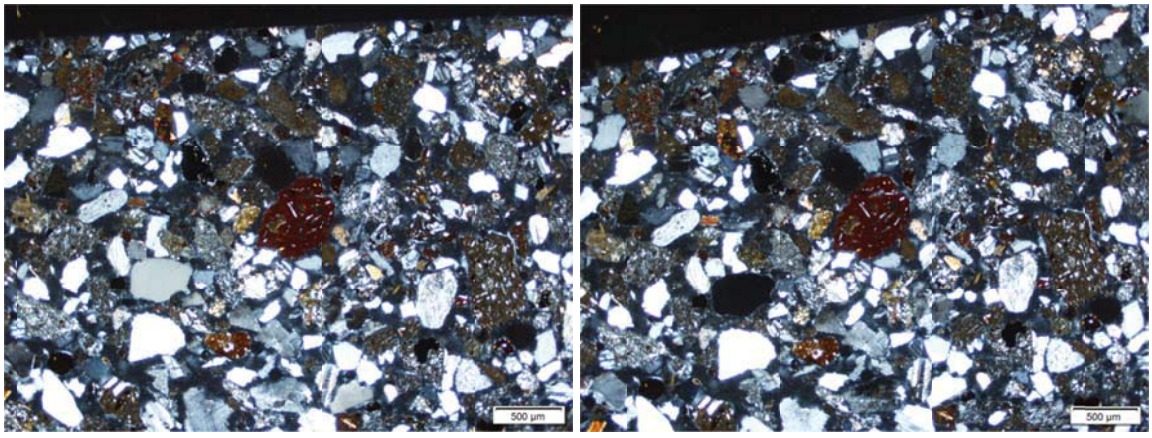

0° angle **7.5° angle**

Figure 18.30 Wadsworth, Nevada: Quartz, Lithic Clasts, Feldspar Example A Thin Section Under Cross-Polarized Light, 2x magnification

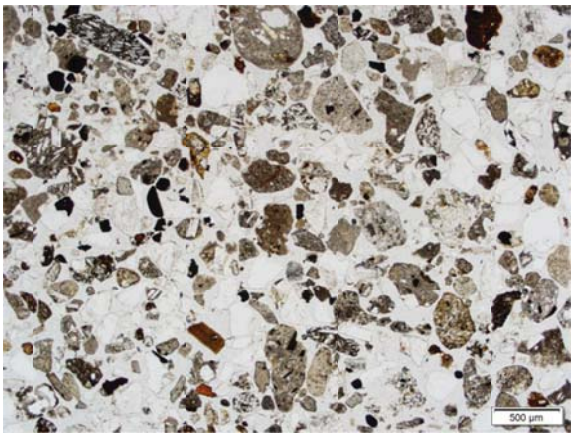

0° angle

Figure 18.31 Wadsworth, Nevada: Quartz, Lithic Clasts, Feldspar Example B Thin Section Under Plane-Polarized Light, 2x magnification

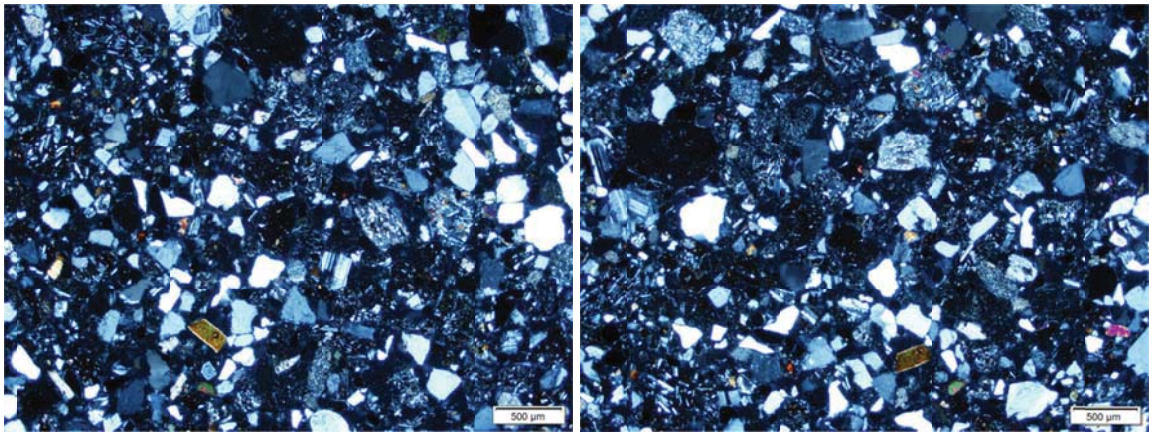

0° angle **60° angle**

Figure 18.32 Wadsworth, Nevada: Quartz, Lithic Clasts, Feldspar Example B Thin Section Under Cross-Polarized Light, 2x magnification

Figure 18.33 Utah: Blended Aggregate Photograph

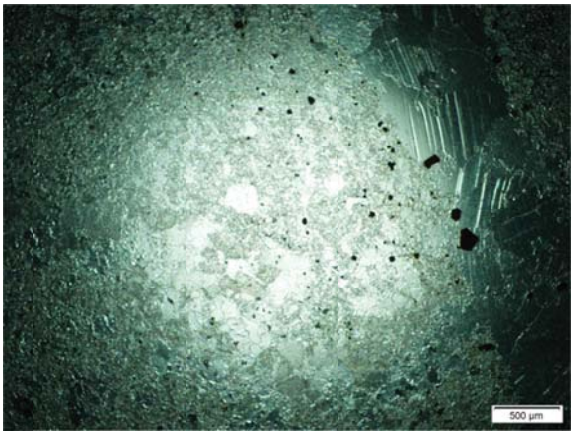

0° angle

Figure 18.34 Utah: Quarzite Example A Thin Section Under Plane-Polarized Light, 2x magnification

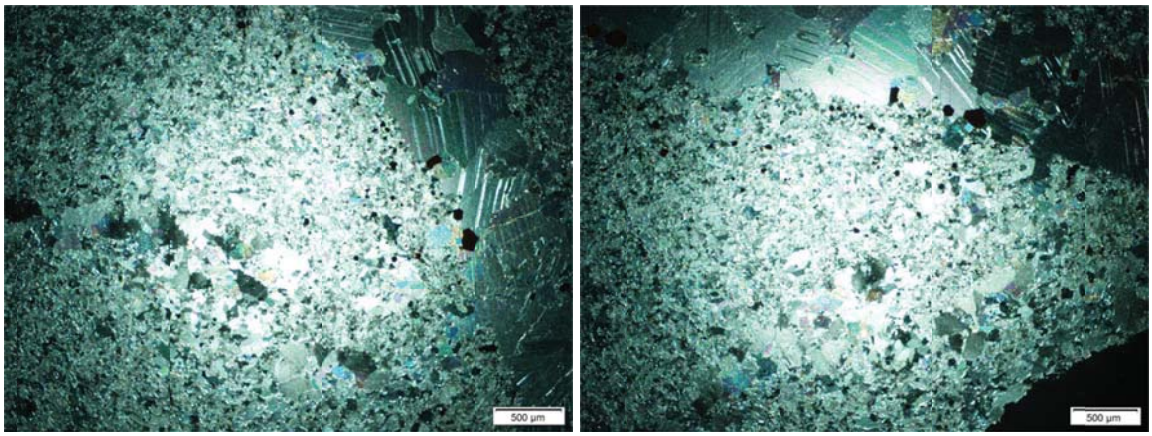

0° angle **50° angle**

Figure 18.35 Utah: Quarzite Example A Thin Section Under Cross-Polarized Light, 2x magnification

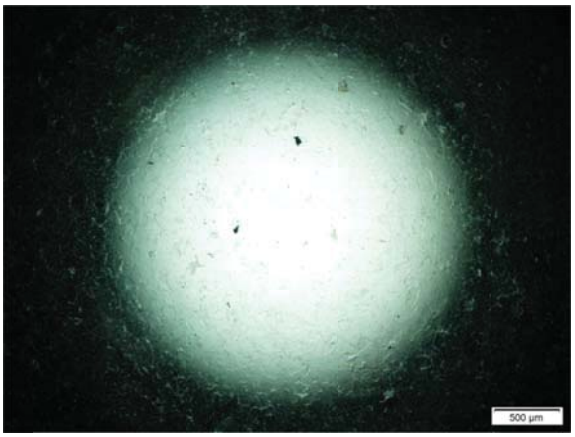

0° angle

Figure 18.36 Utah: Quarzite Example B Thin Section Under Plane-Polarized Light, 2x magnification

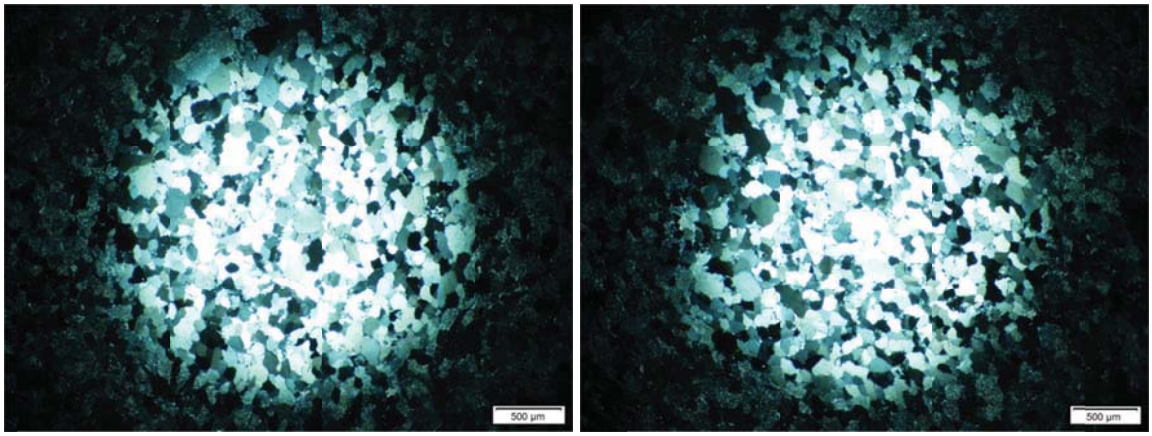

0° angle **35° angle**

Figure 18.37 Utah: Quarzite Example B Thin Section Under Cross-Polarized Light, 2x magnification

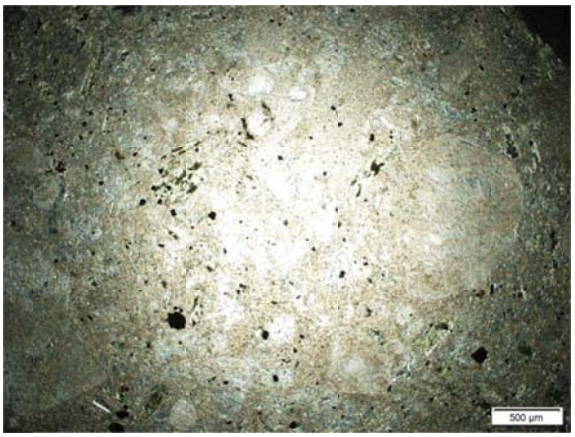

0° angle

Figure 18.38 Utah: Limestone Example A Thin Section Under Plane-Polarized Light, 2x magnification

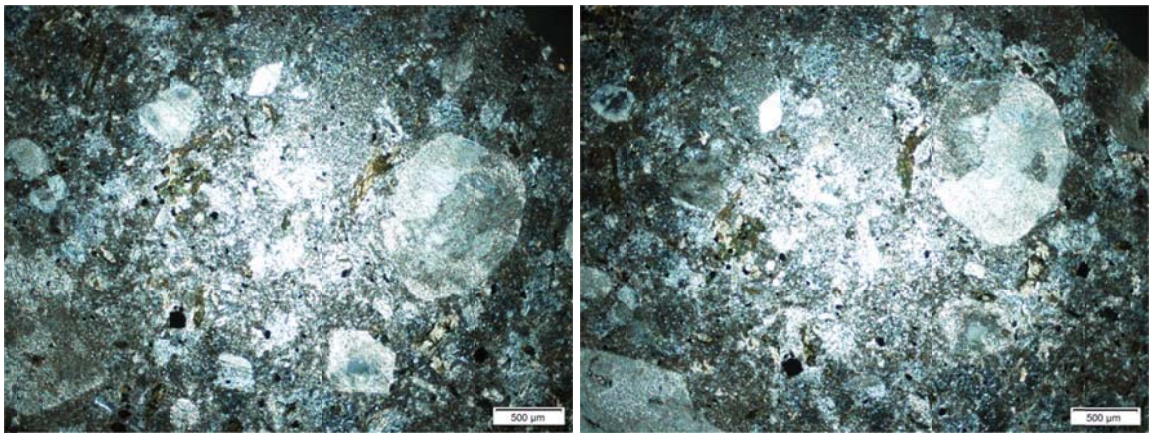

0° angle **25° angle**

Figure 18.39 Utah: Limestone Example A Thin Section Under Cross-Polarized Light, 2x magnification

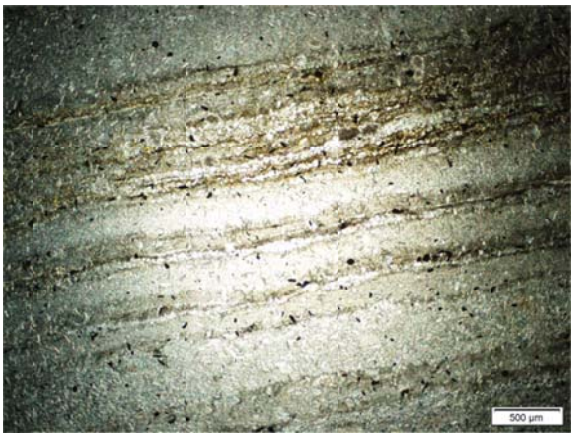

0° angle

Figure 18.40 Utah: Limestone Example B Thin Section Under Plane-Polarized Light, 2x magnification

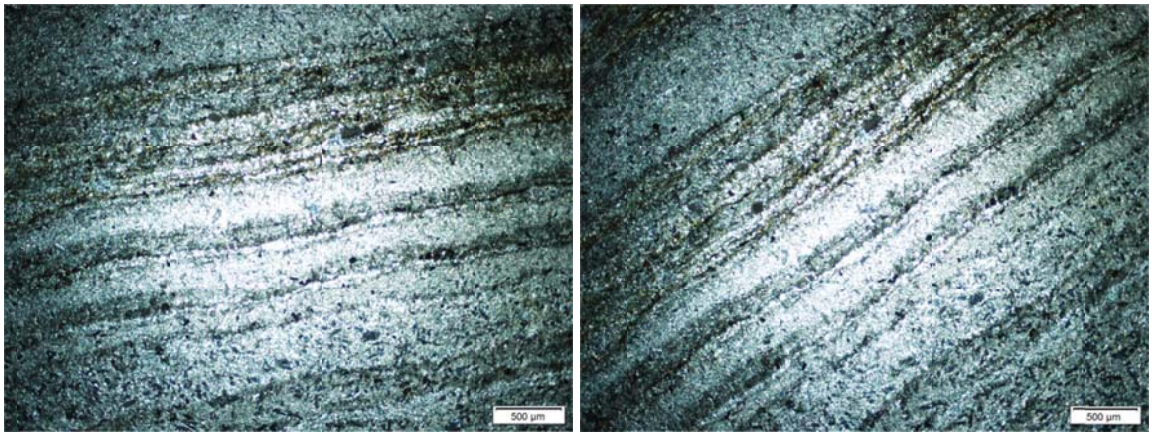

0° angle **25° angle**

Figure 18.41 Utah: Limestone Example B Thin Section Under Cross-Polarized Light, 2x magnification

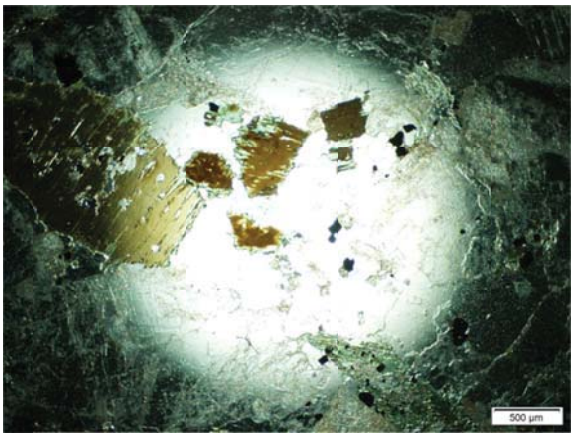

0° angle

Figure 18.42 Utah: Granodiorite Example A Thin Section Under Plane-Polarized Light, 2x magnification

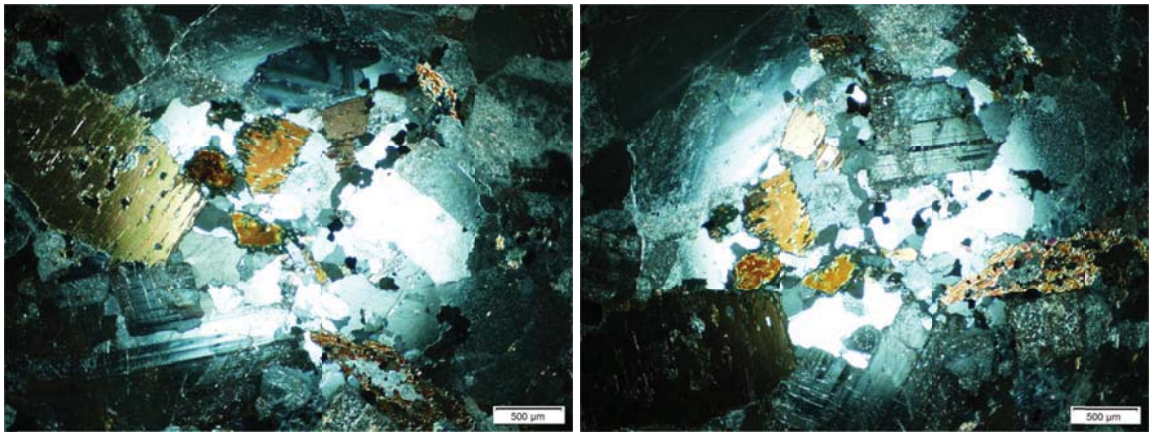

0° angle **50° angle**

Figure 18.43 Utah: Granodiorite Example A Thin Section Under Cross-Polarized Light, 2x magnification

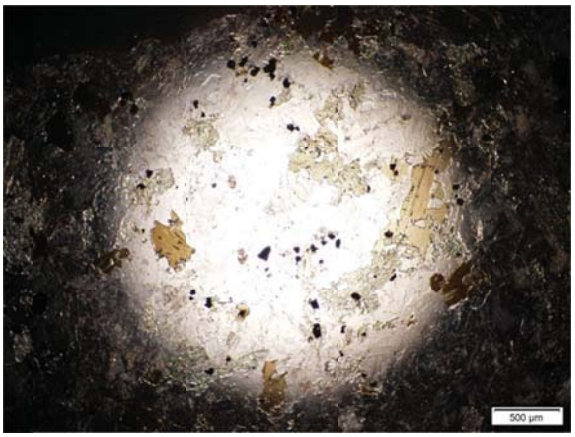

0° angle

Figure 18.44 Utah: Granodiorite Example B Thin Section Under Plane-Polarized Light, 2x magnification

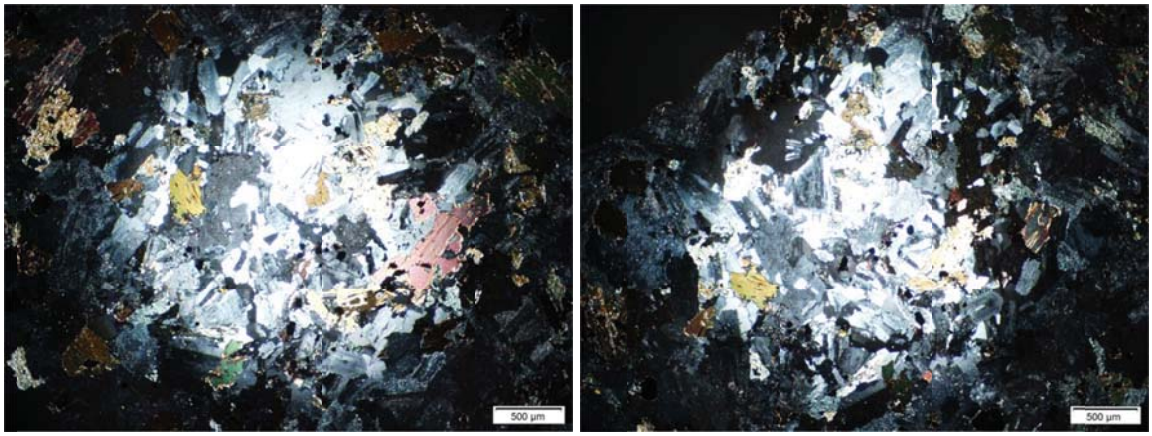

0° angle **40° angle**

Figure 18.45 Utah: Granodiorite Example B Thin Section Under Cross-Polarized Light, 2x magnification

0° angle

Figure 18.46 Utah: Basalt Example A Thin Section Under Plane-Polarized Light, 2x magnification

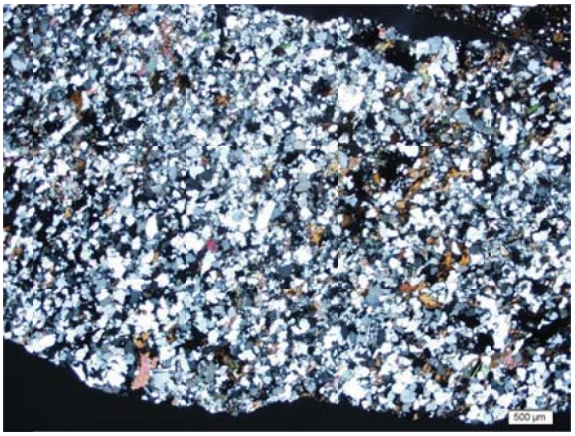

0° angle

Figure 18.47 Utah: Basalt Example A Thin Section Under Cross-Polarized Light, 2x magnification

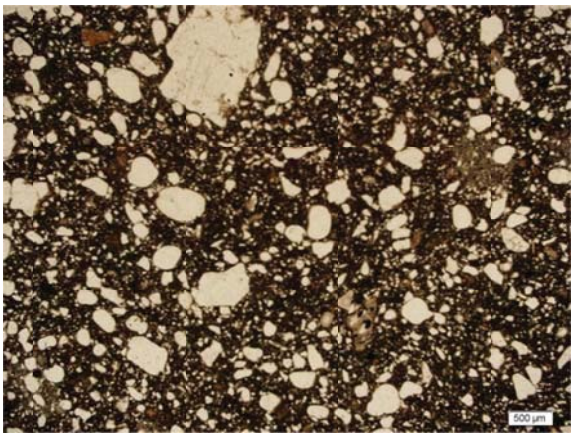

0° angle

Figure 18.48 Utah: Basalt Example B Thin Section Under Plane-Polarized Light, 2x magnification

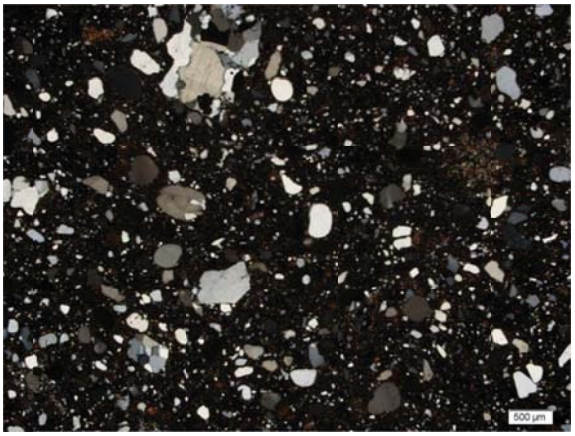

0° angle

Figure 18.49 Utah: Basalt Example B Thin Section Under Cross-Polarized Light, 2x magnification

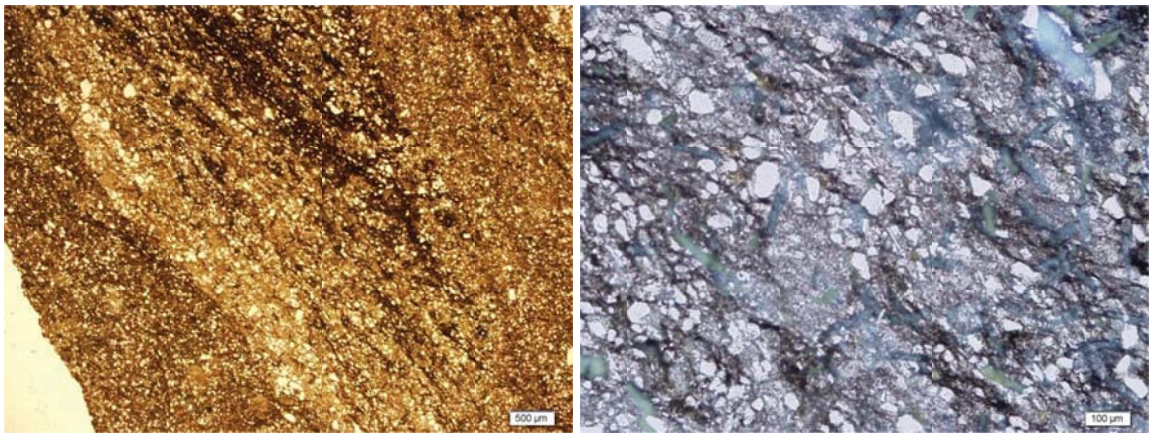

2x magnification **10x magnification**

Figure 18.50 Utah: Basalt Example C Thin Section Under Plane-Polarized Light

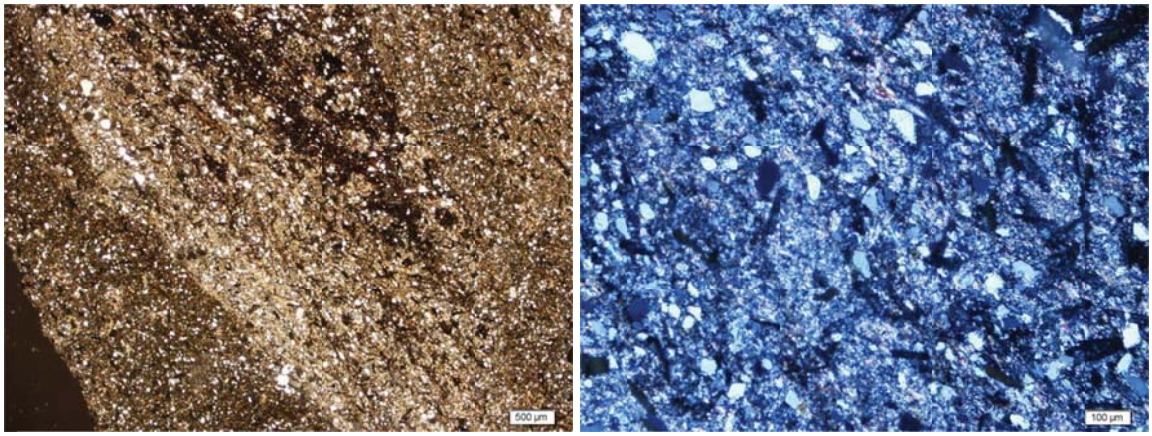

2x magnification **10x magnification**

Figure 18.51 Utah: Basalt Example C Thin Section Under Cross-Polarized Light

Figure 18.52 WesTrack 1995: Blended Aggregate Photograph

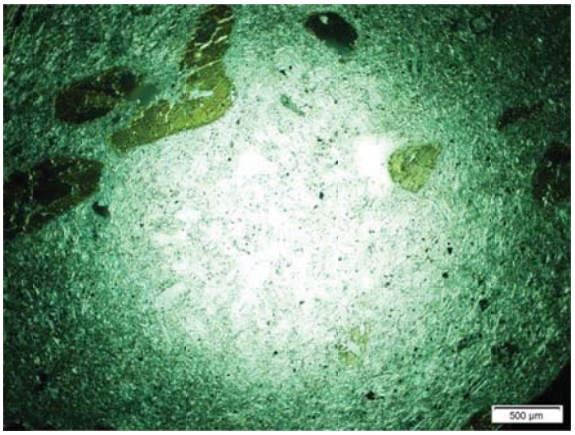

0° angle

Figure 18.53 WesTrack 1995: Basalt to Andesite Example A Thin Section Under Plane-Polarized Light, 2x magnification

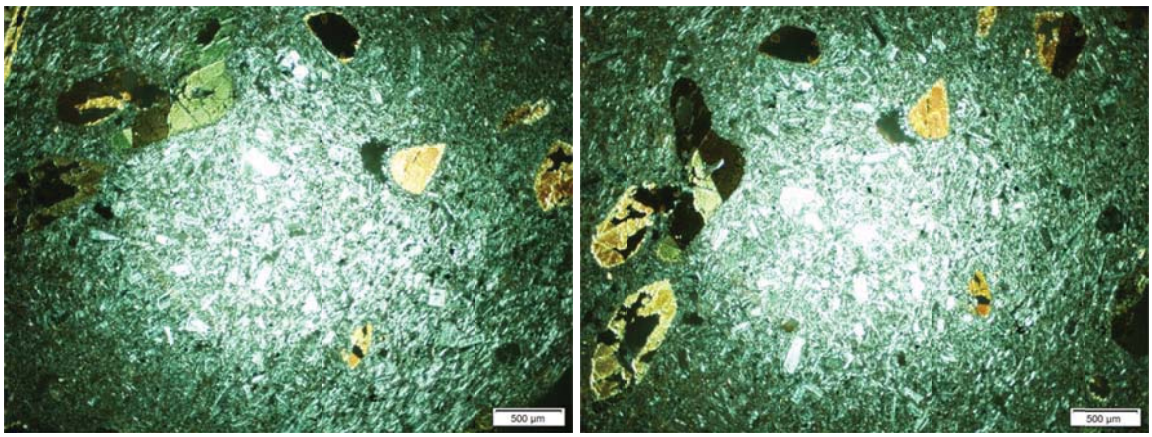

0° angle **32° angle**

Figure 18.54 WesTrack 1995: Basalt to Andesite Example A Thin Section Under Cross-Polarized Light, 2x magnification

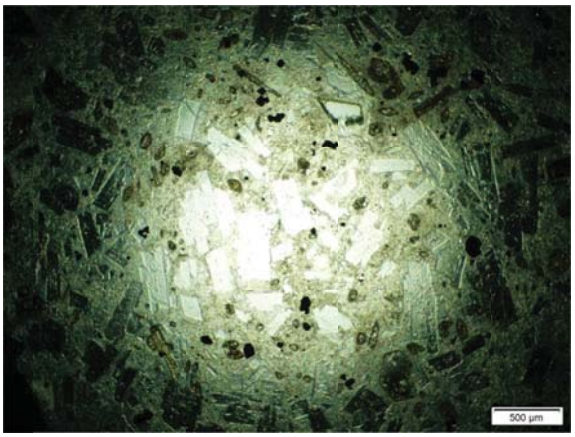

0° angle

Figure 18.55 WesTrack 1995: Basalt to Andesite Example B Thin Section Under Plane-Polarized Light, 2x magnification

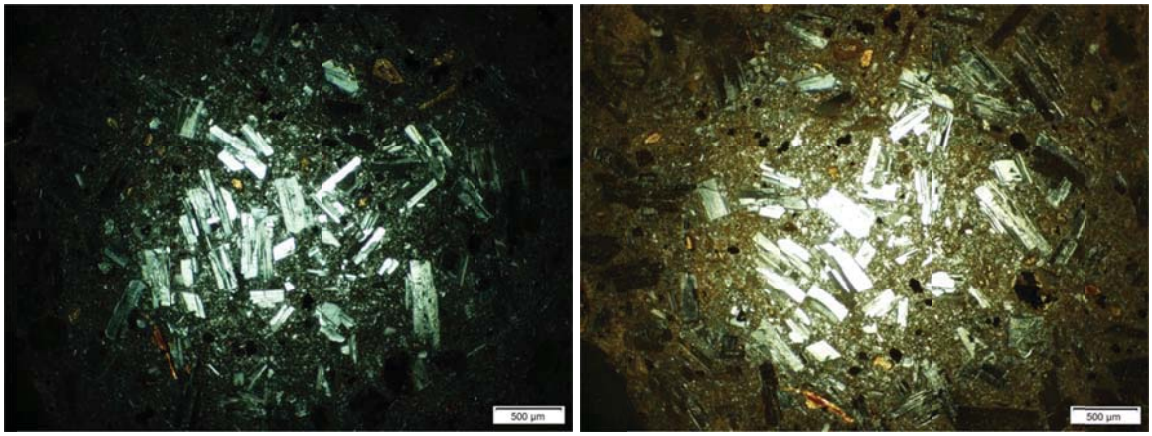

0° angle **32° angle**

Figure 18.56 WesTrack 1995: Basalt to Andesite Example B Thin Section Under Cross-Polarized Light, 2x magnification

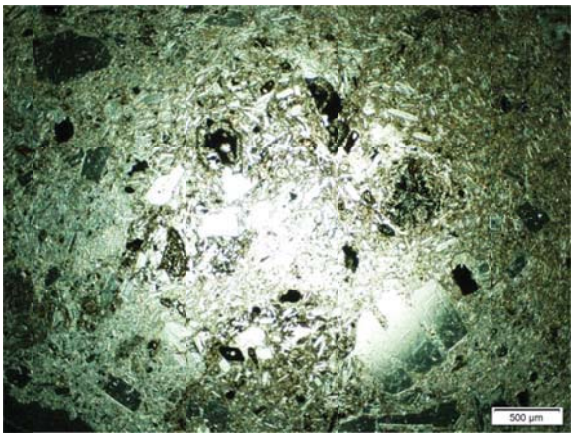

0° angle

Figure 18.57 WesTrack 1995: Basalt to Andesite Example C Thin Section Under Plane-Polarized Light, 2x magnification

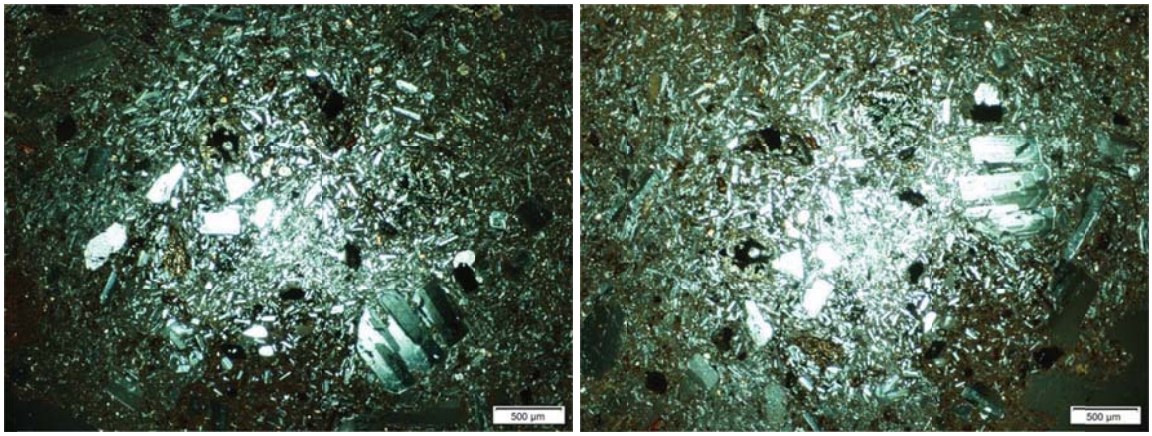

0° angle **60° angle**

Figure 18.58 WesTrack 1995: Basalt to Andesite Example C Thin Section Under Cross-Polarized Light, 2x magnification

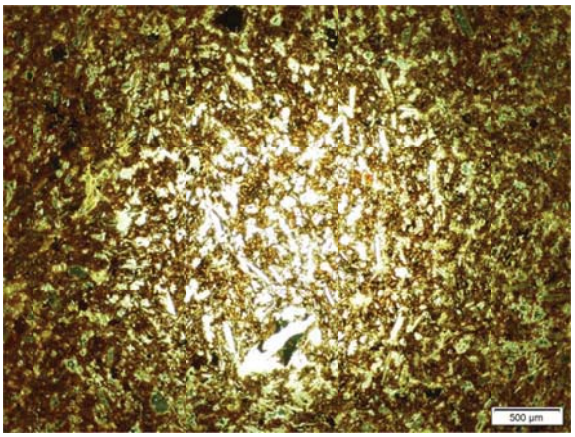

0° angle

Figure 18.59 WesTrack 1995: Rhyolite Example Thin Section Under Plane-Polarized Light, 2x magnification

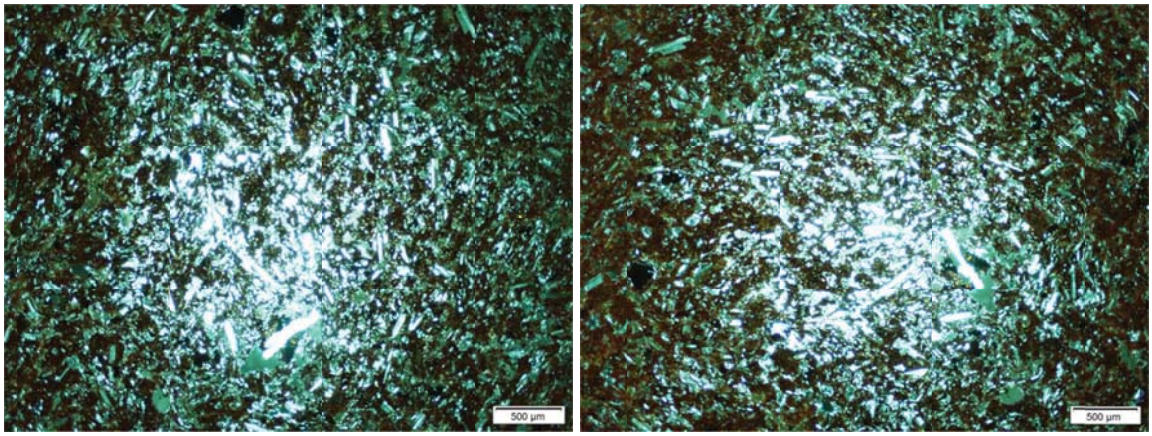

0° angle **83° angle**

Figure 18.60 WesTrack 1995: Rhyolite Example Thin Section Under Cross-Polarized Light, 2x magnification

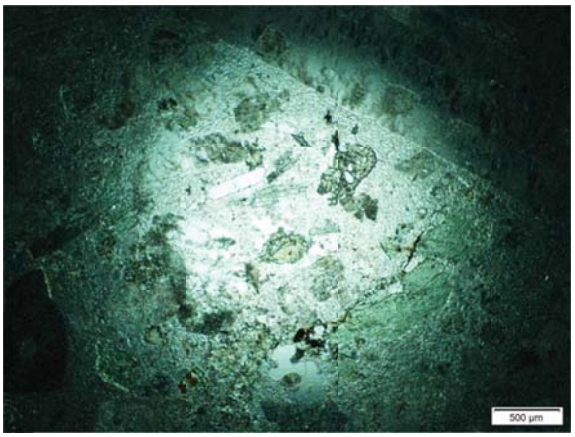

0° angle

Figure 18.61 WesTrack 1995: Granite Example A Thin Section Under Plane-Polarized Light, 2x magnification

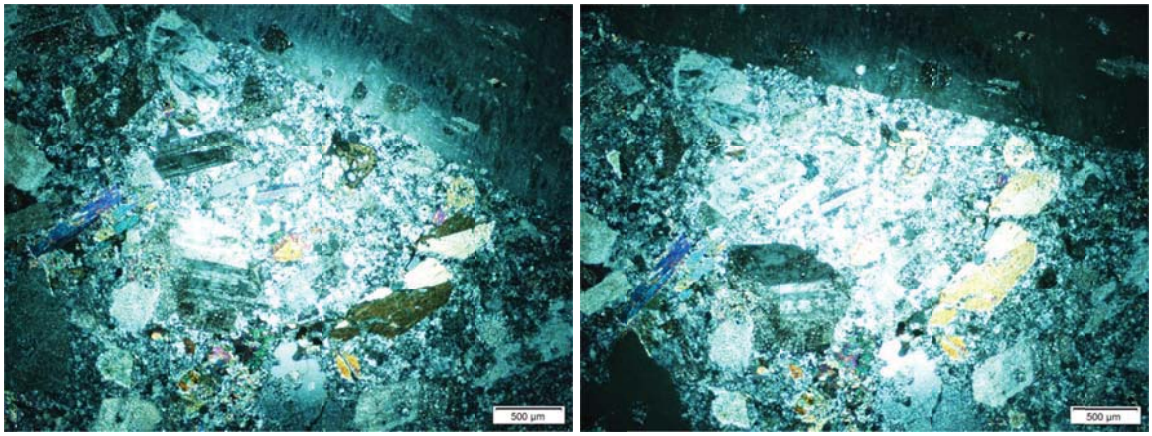

0° angle **15° angle**

Figure 18.62 WesTrack 1995: Granite Example A Thin Section Under Cross-Polarized Light, 2x magnification

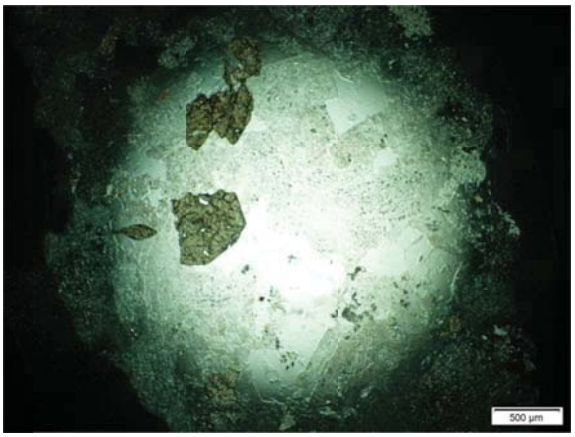

0° angle

Figure 18.63 WesTrack 1995: Granite Example B Thin Section Under Plane-Polarized Light, 2x magnification

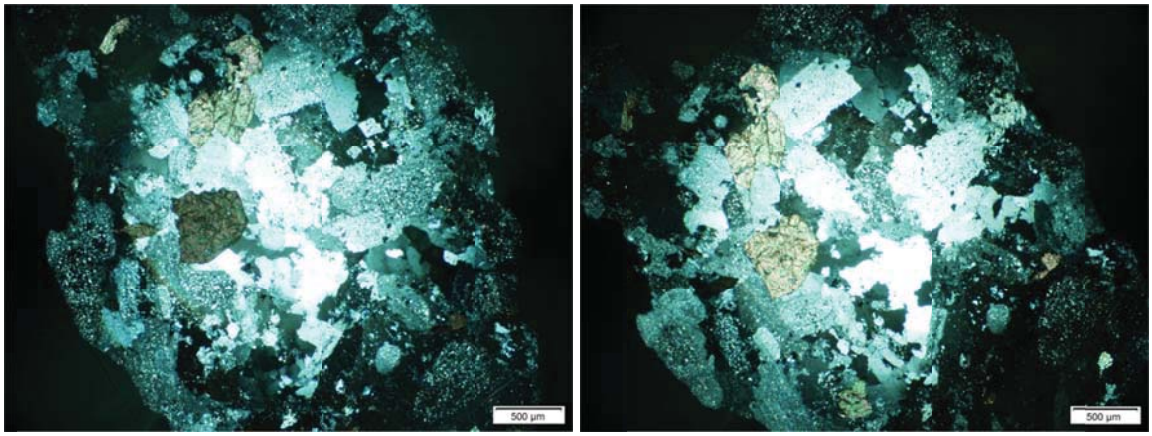

0° angle **20° angle**

Figure 18.64 WesTrack 1995: Granite Example B Thin Section Under Cross-Polarized Light, 2x magnification

Figure 18.65 WesTrack 1997: Blended Aggregate Photograph

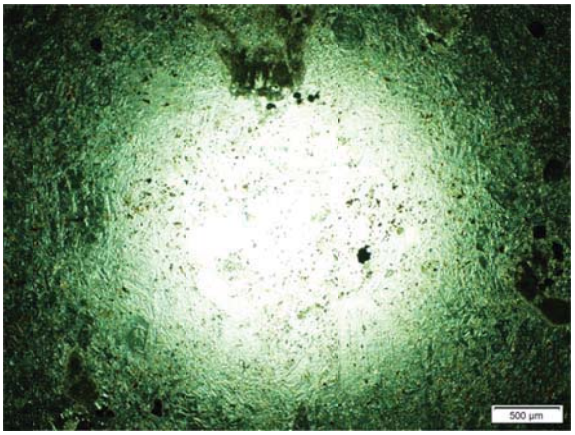

0° angle

Figure 18.66 WesTrack 1997: Basalt to Andesite Example A Thin Section Under Plane-Polarized Light, 2x magnification

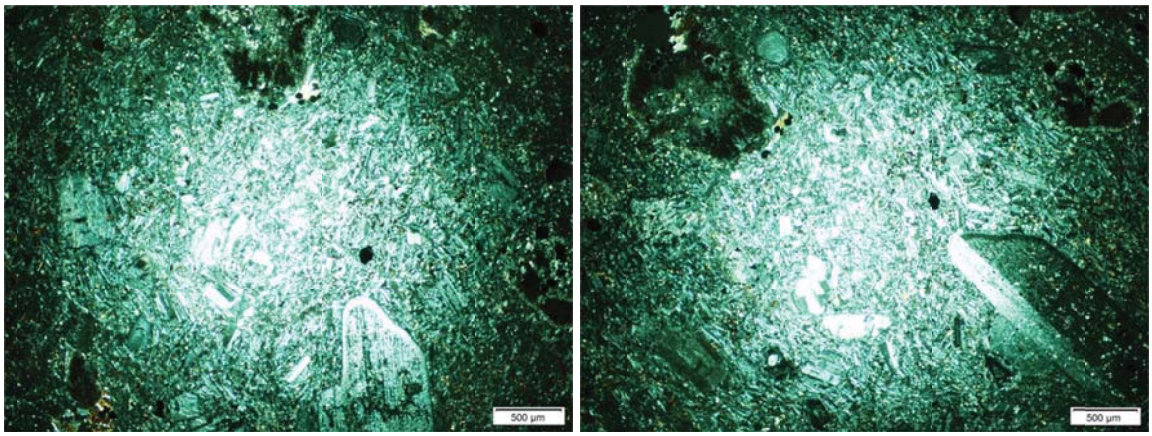

0° angle **42° angle**

Figure 18.67 WesTrack 1997: Basalt to Andesite Example A Thin Section Under Cross-Polarized Light, 2x magnification

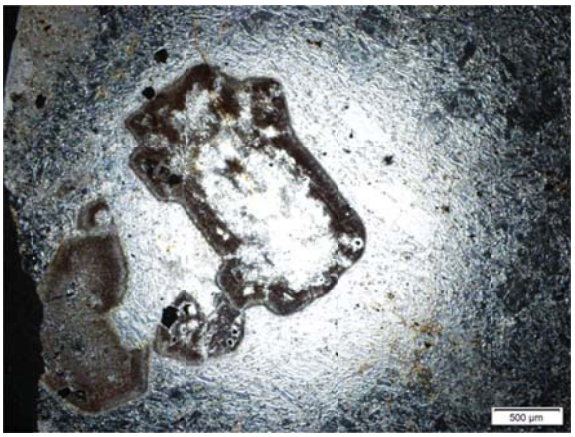

0° angle

Figure 18.68 WesTrack 1997: Basalt to Andesite Example B Thin Section Under Plane-Polarized Light, 2x magnification

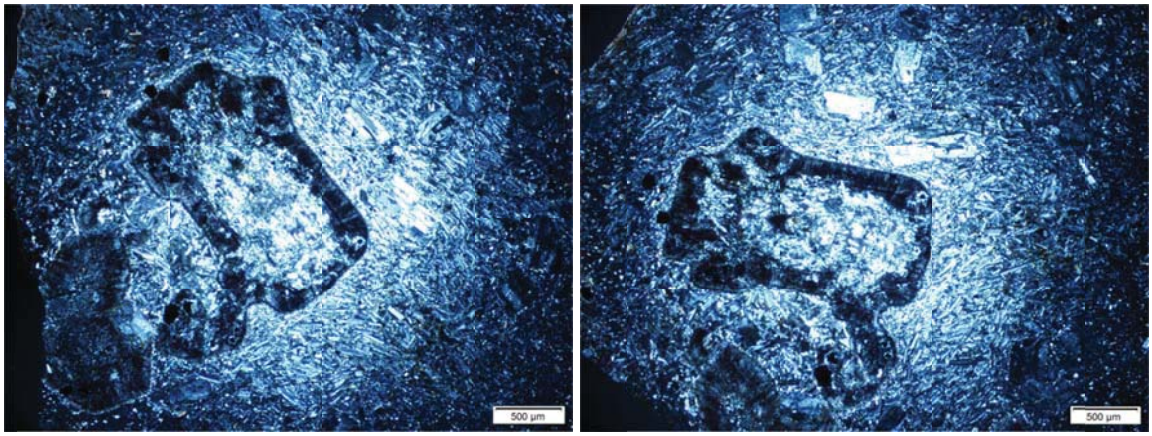

0° angle **40° angle**

Figure 18.69 WesTrack 1997: Basalt to Andesite Example B Thin Section Under Cross-Polarized Light, 2x magnification

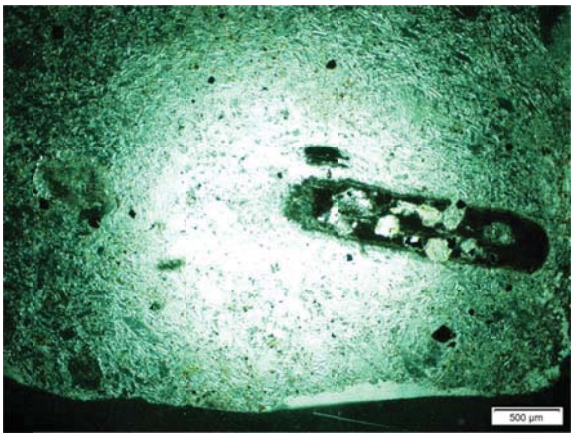

0° angle

Figure 18.70 WesTrack 1997: Basalt to Andesite Example C Thin Section Under Plane-Polarized Light, 2x magnification

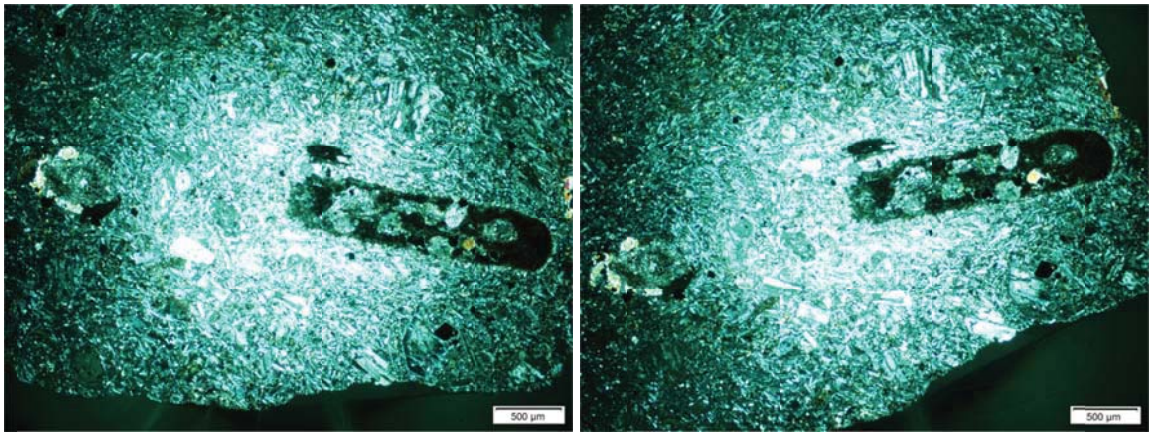

0° angle **22° angle**

Figure 18.71 WesTrack 1997: Basalt to Andesite Example C Thin Section Under Cross-Polarized Light, 2x magnification

19 APPENDIX G:

Summary Figures of Carbonyl Area Measures on Pan-Aged Binders

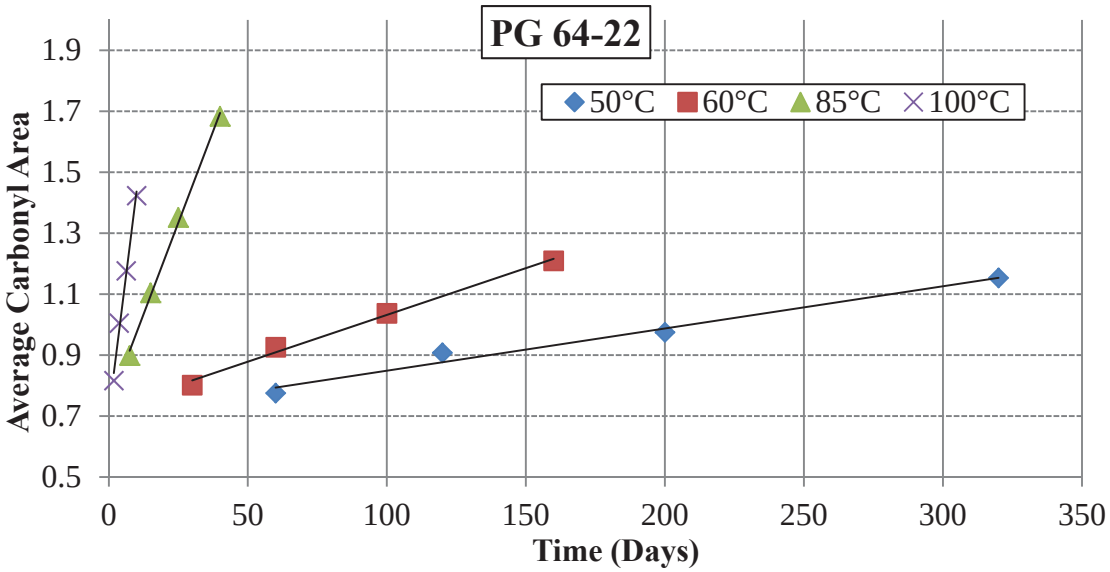

Figure 19.1 Carbonyl Measurement Summary Paramount PG 64-22

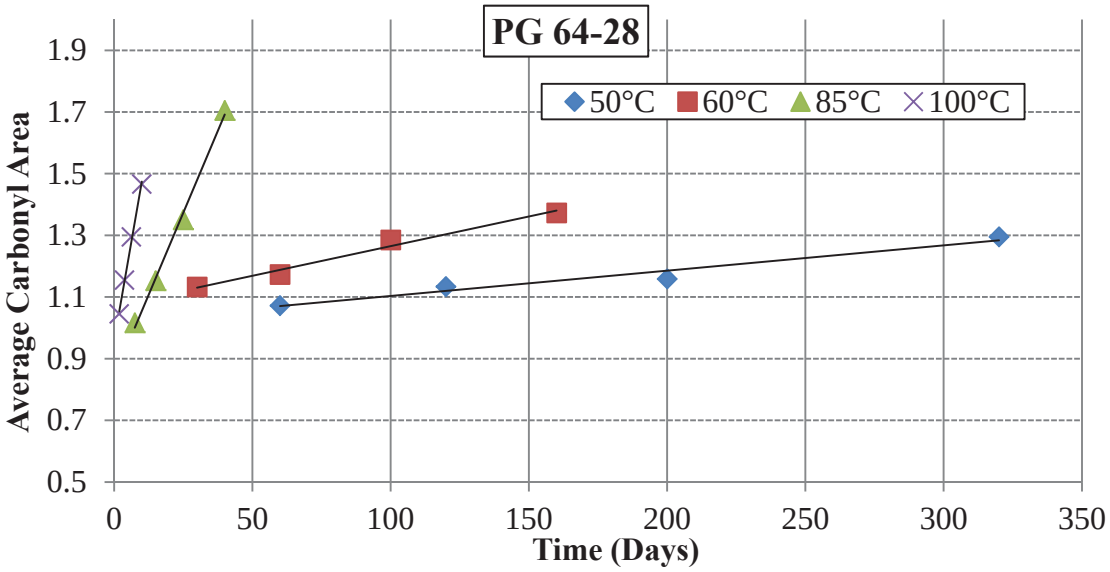

Figure 19.2 Carbonyl Measurement Summary Paramount PG 64-28

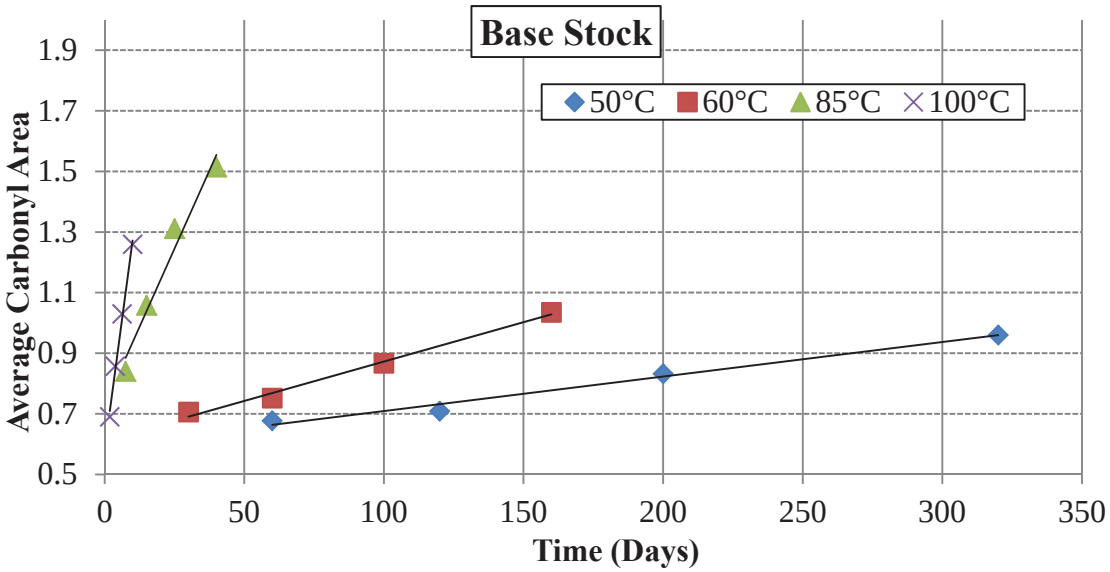

Figure 19.3 Carbonyl Measurement Summary Paramount Base Stock

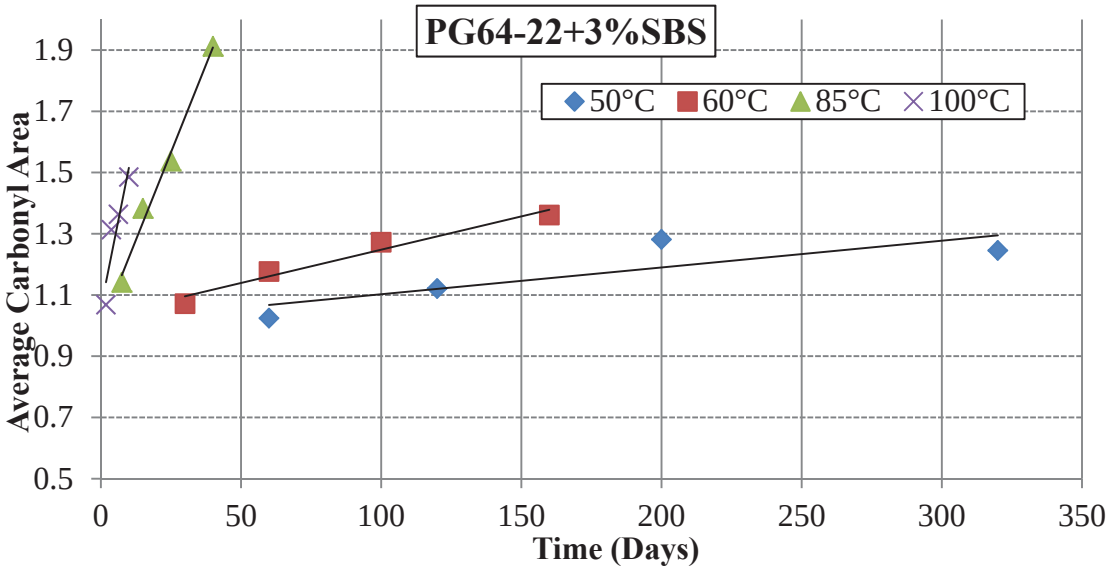

Figure 19.4 Carbonyl Measurement Summary Paramount PG 64-22+3% SBS

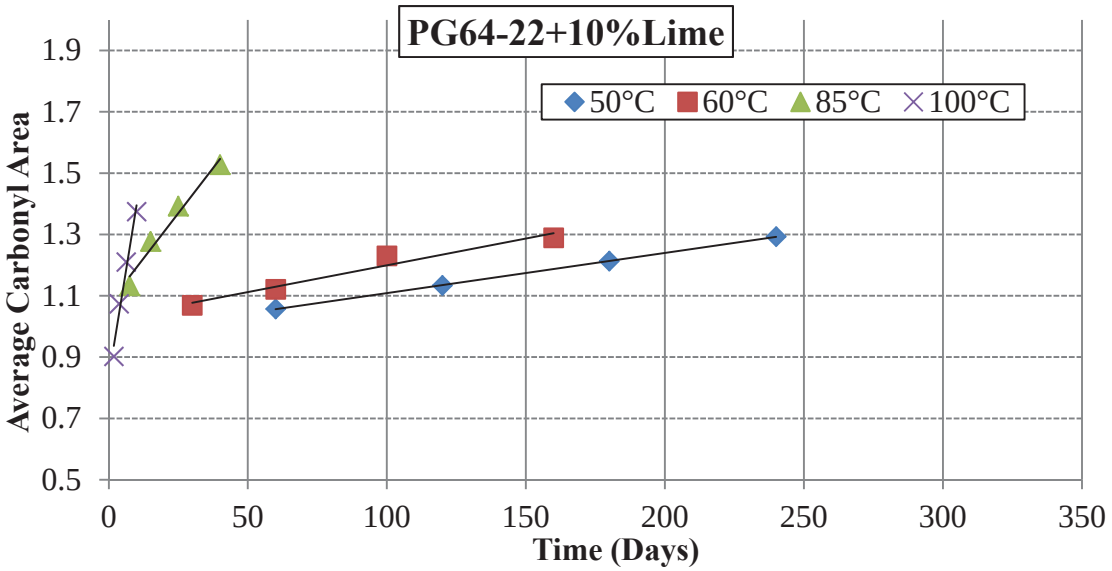

Figure 19.5 Carbonyl Measurement Summary Paramount PG 64-22+10% Lime

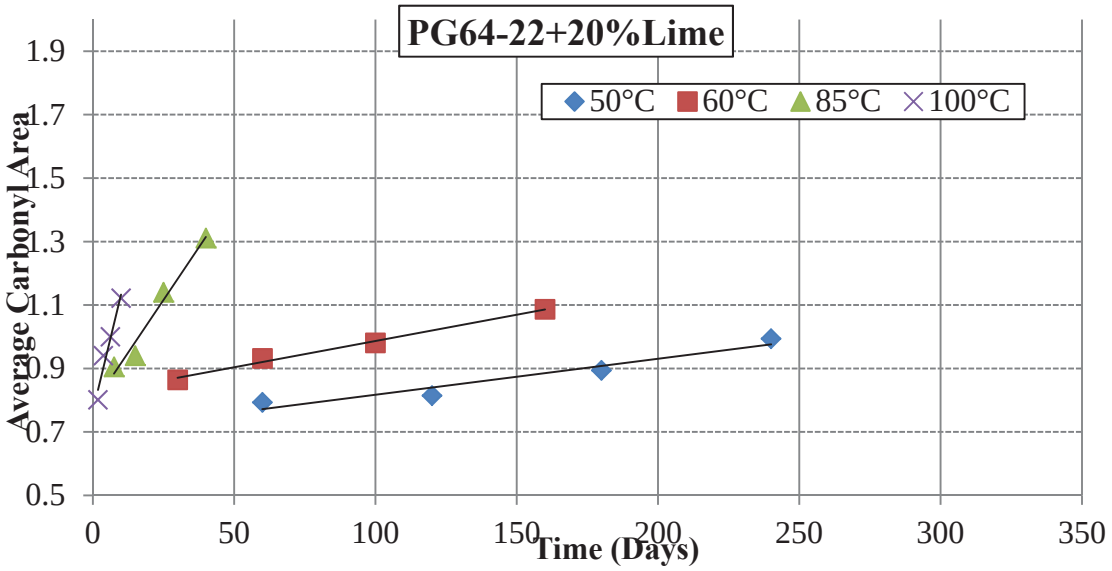

Figure 19.6 Carbonyl Measurement Summary Paramount PG 64-22+20% Lime

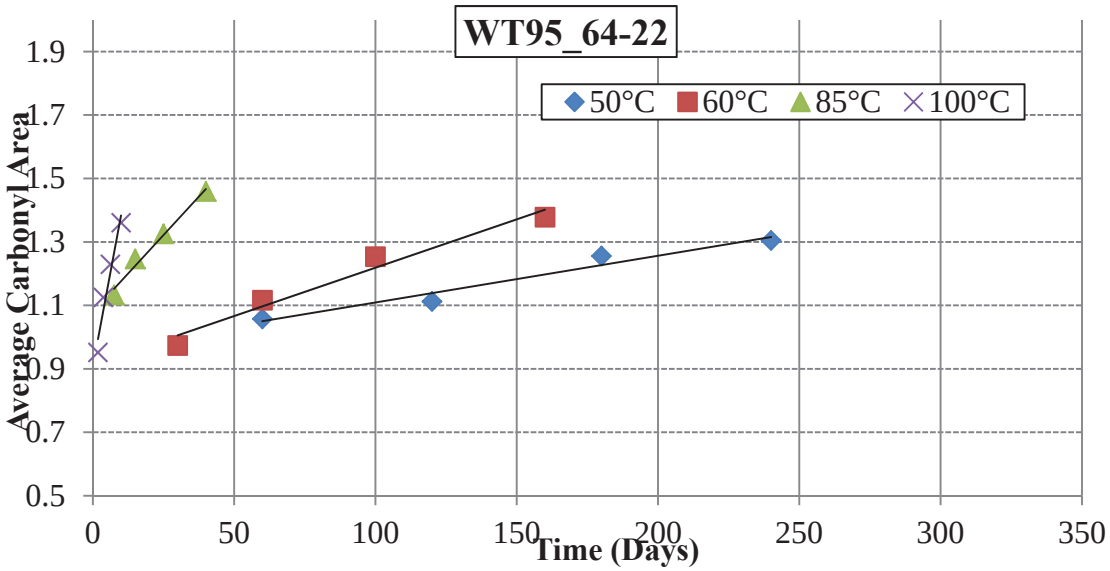

Figure 19.7 Carbonyl Measurement Summary WesTrack 1995 PG 64-22

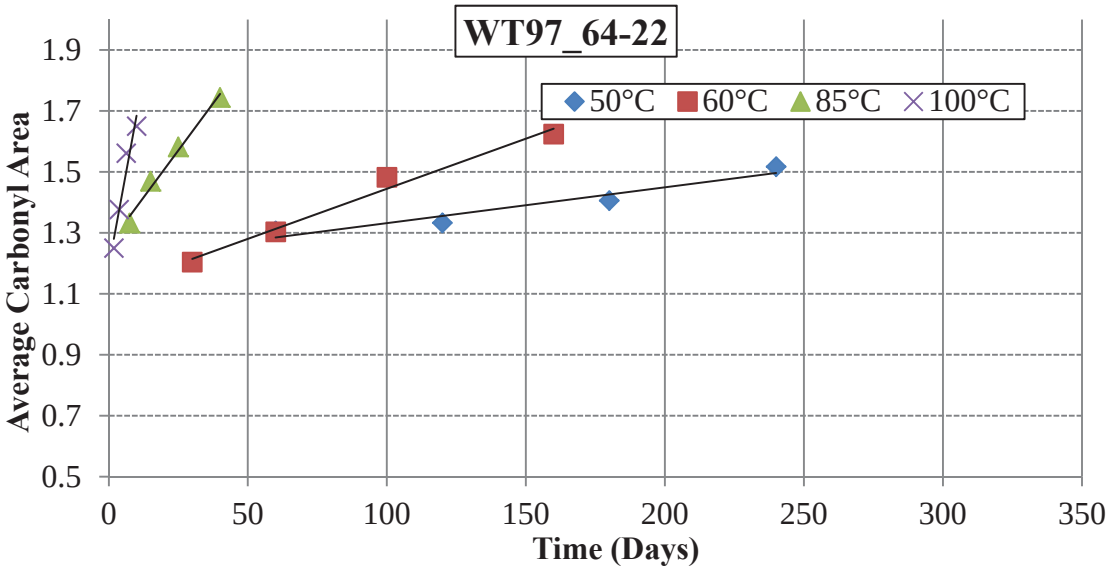

Figure 19.8 Carbonyl Measurement Summary WesTrack 1997 PG 64-22

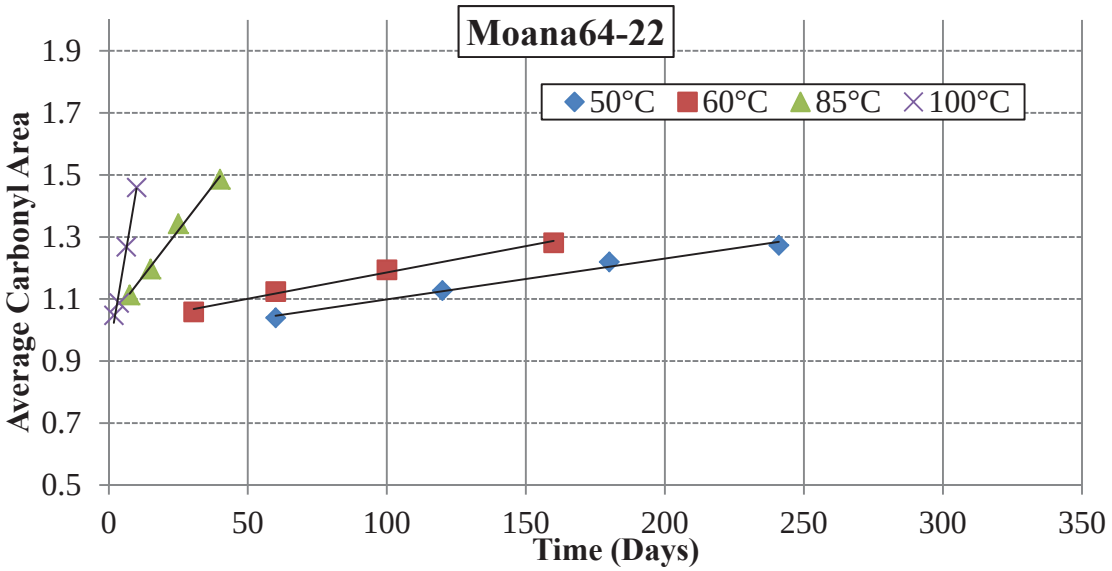

Figure 19.9 Carbonyl Measurement Summary Moana Lane, Paramount PG 64-22

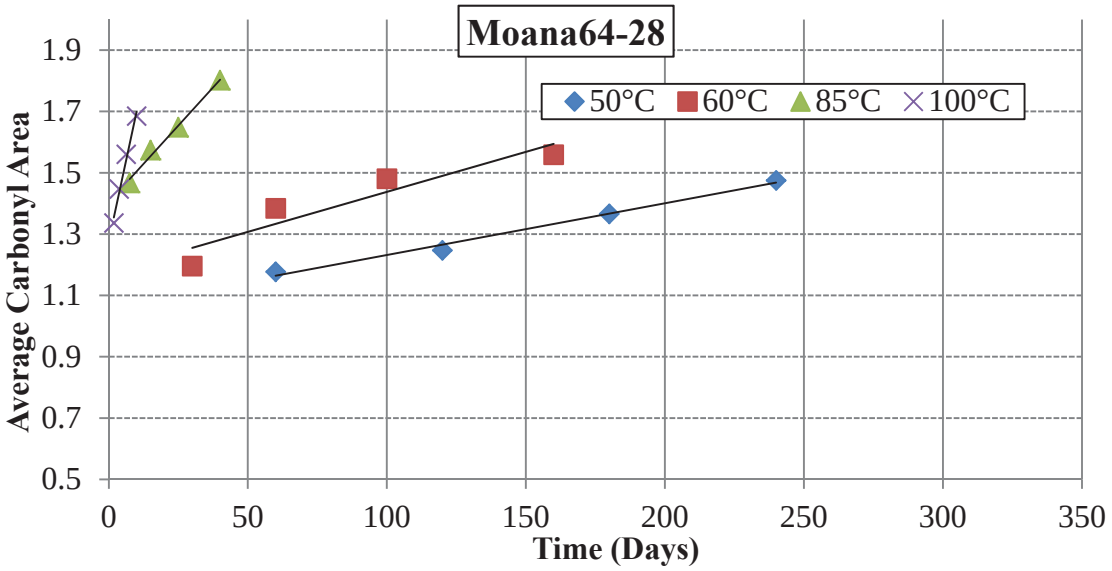

Figure 19.10 Carbonyl Measurement Summary Moana Lane, Paramount PG 64-28

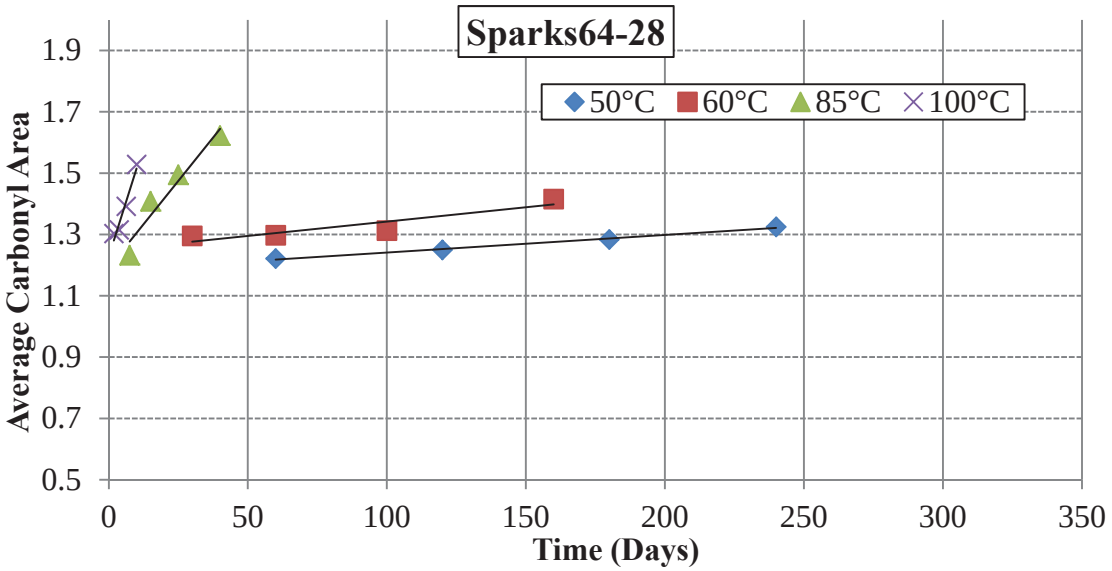

Figure 19.11 Carbonyl Measurement Summary Sparks Blvd., Paramount PG 64-28

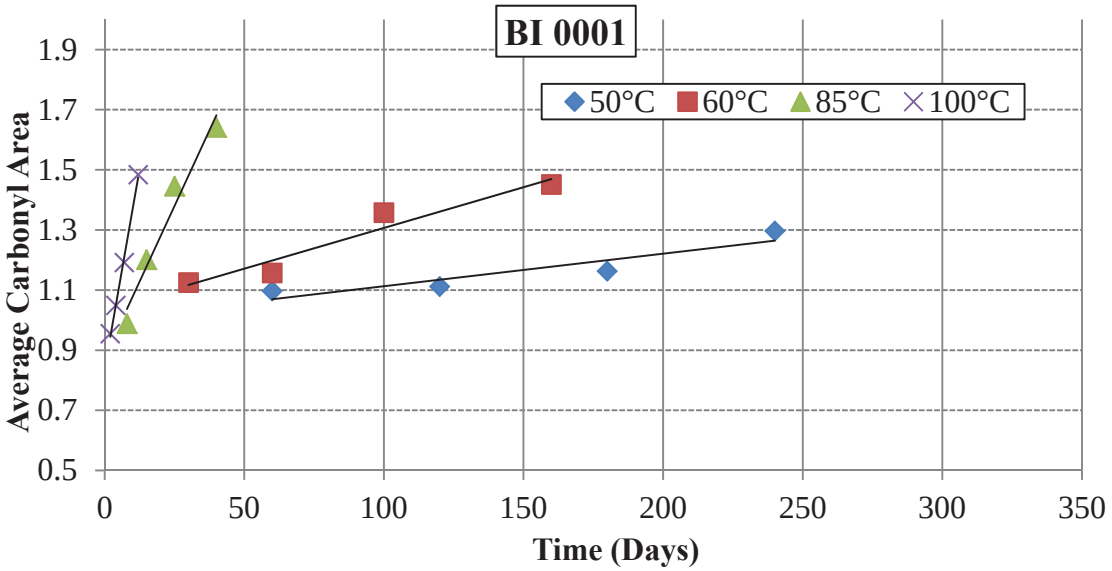

Figure 19.12 Carbonyl Measurement Summary BI 0001, Venezuelan PG 67-22

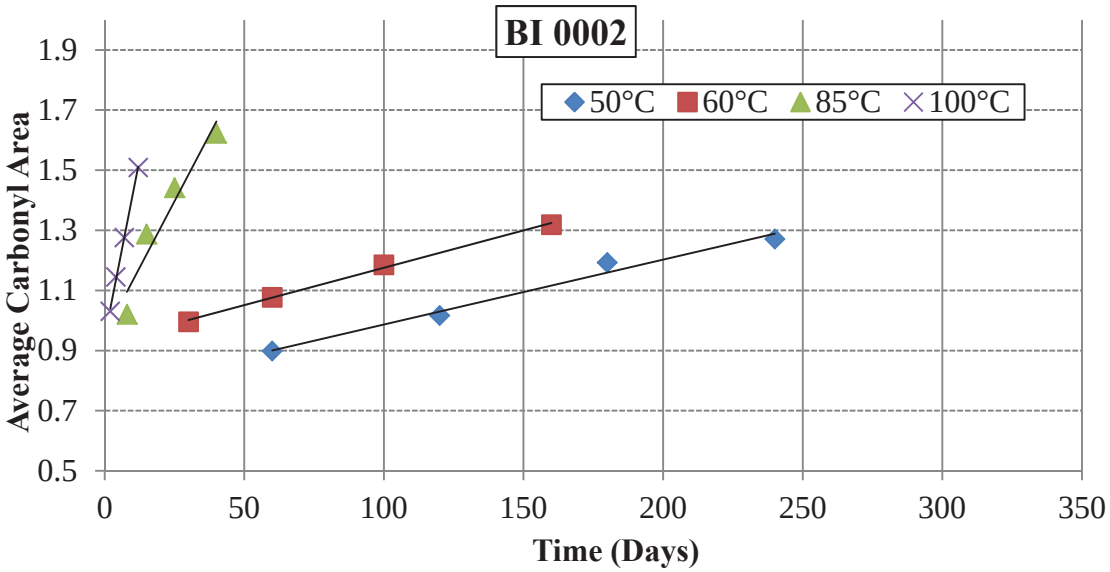

Figure 19.13 Carbonyl Measurement Summary BI 0002, Valero PG 64-16

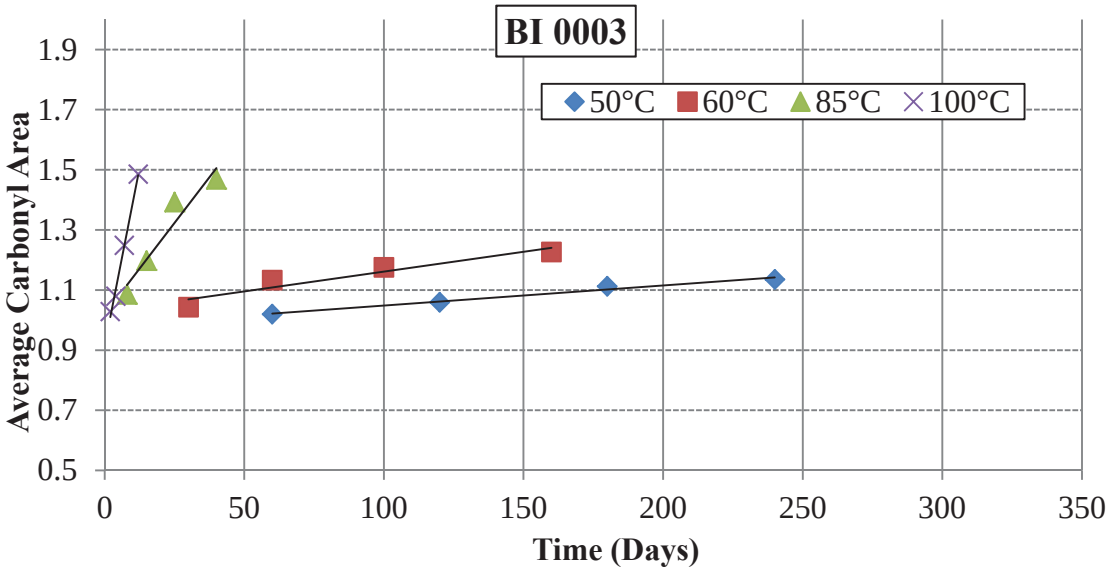

Figure 19.14 Carbonyl Measurement Summary BI 0003, Holly Frontier PG 58-28

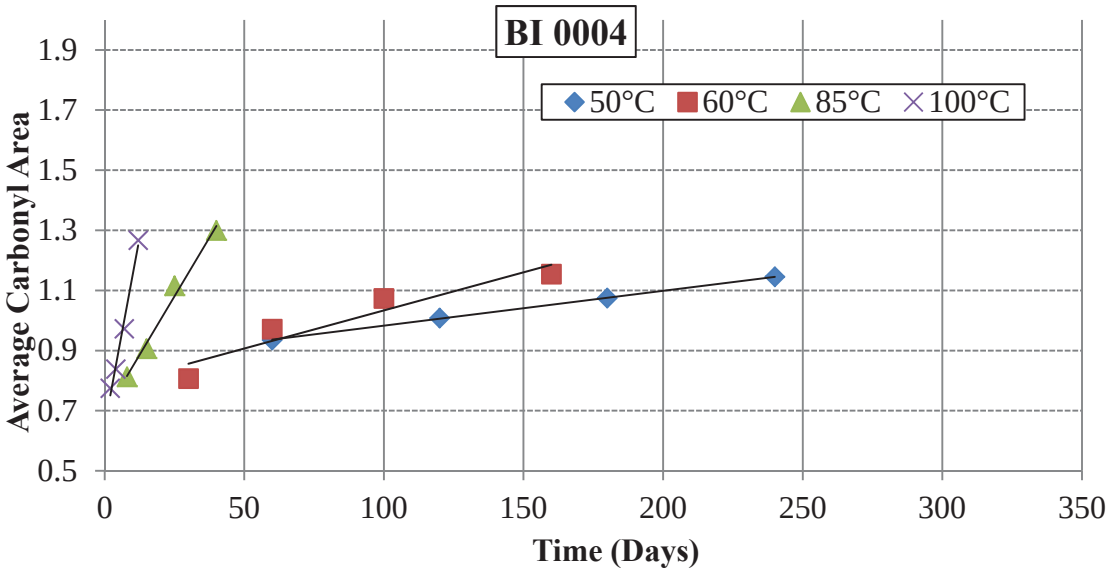

Figure 19.15 Carbonyl Measurement Summary BI 0004, Shelly Materials PG 70-22

20 APPENDIX H:

Summary of Dynamic Shear Modulus and Black Space Plots for Pan-Aged Asphalt Binders

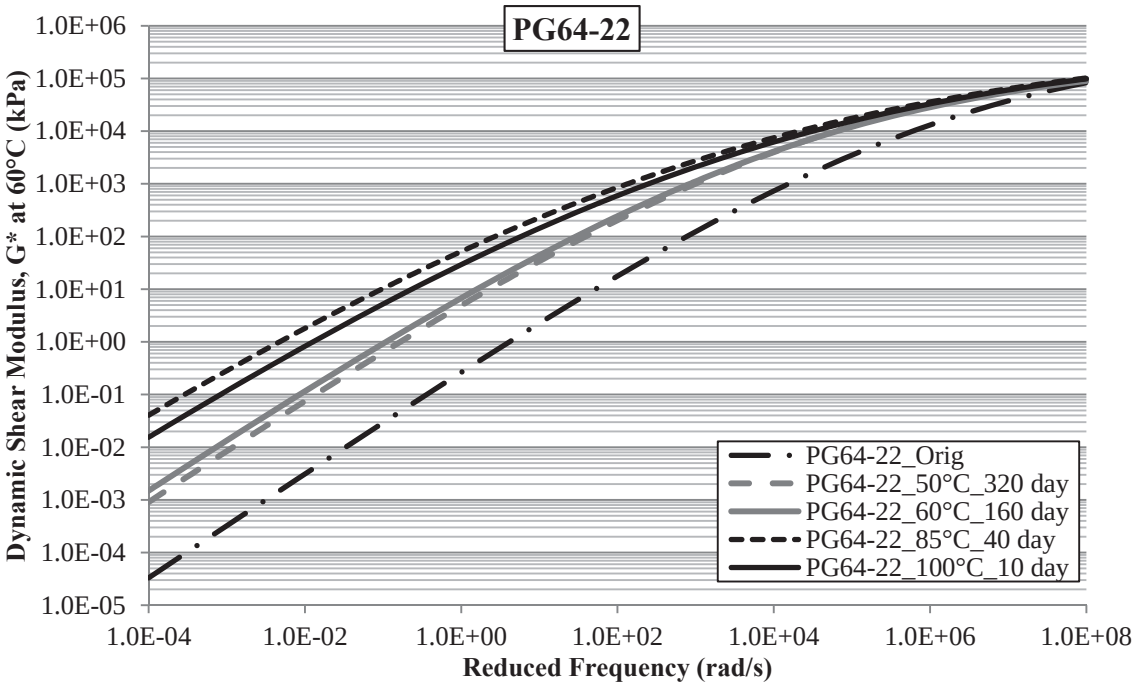

Figure 20.1 Summary of PG 64-22 Dynamic Shear Modulus Master Curves

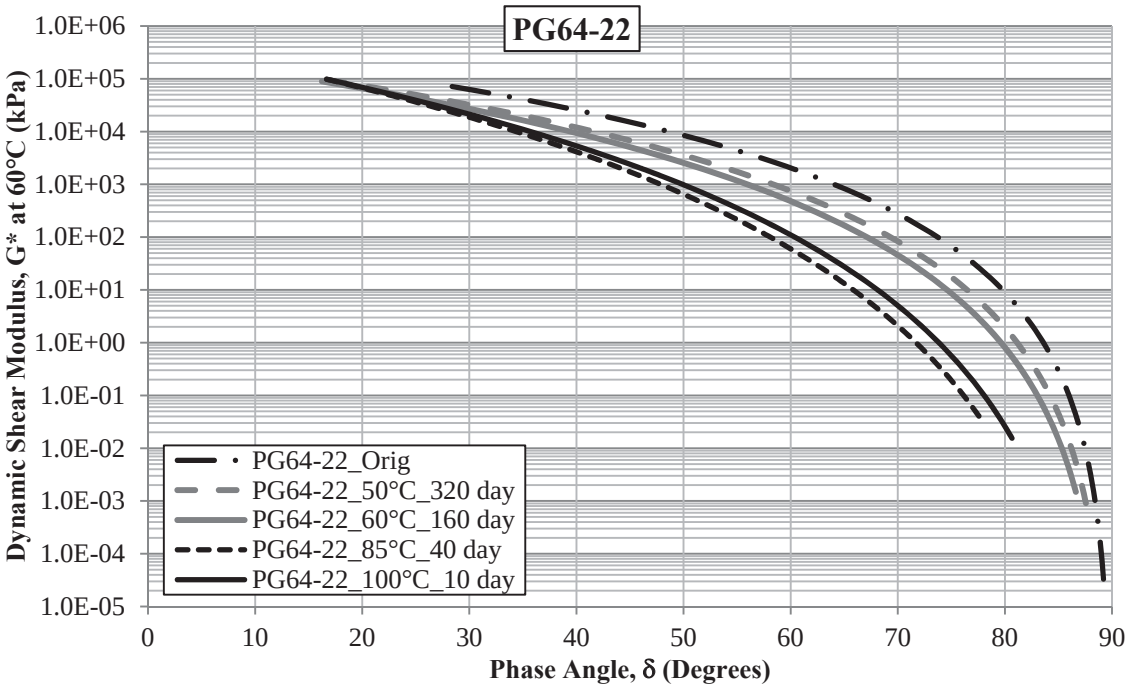

Figure 20.2 Summary of PG 64-22 Black Space Plots

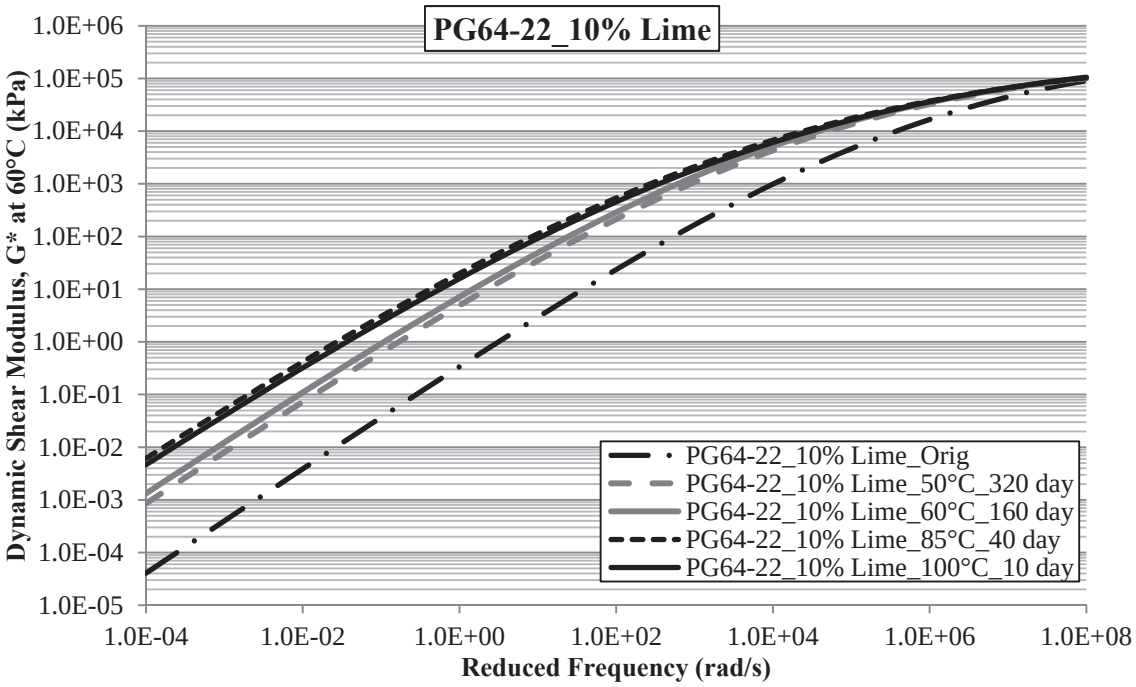

Figure 20.3 Summary of PG 64-22 + 10% Lime Dynamic Shear Modulus Master Curves

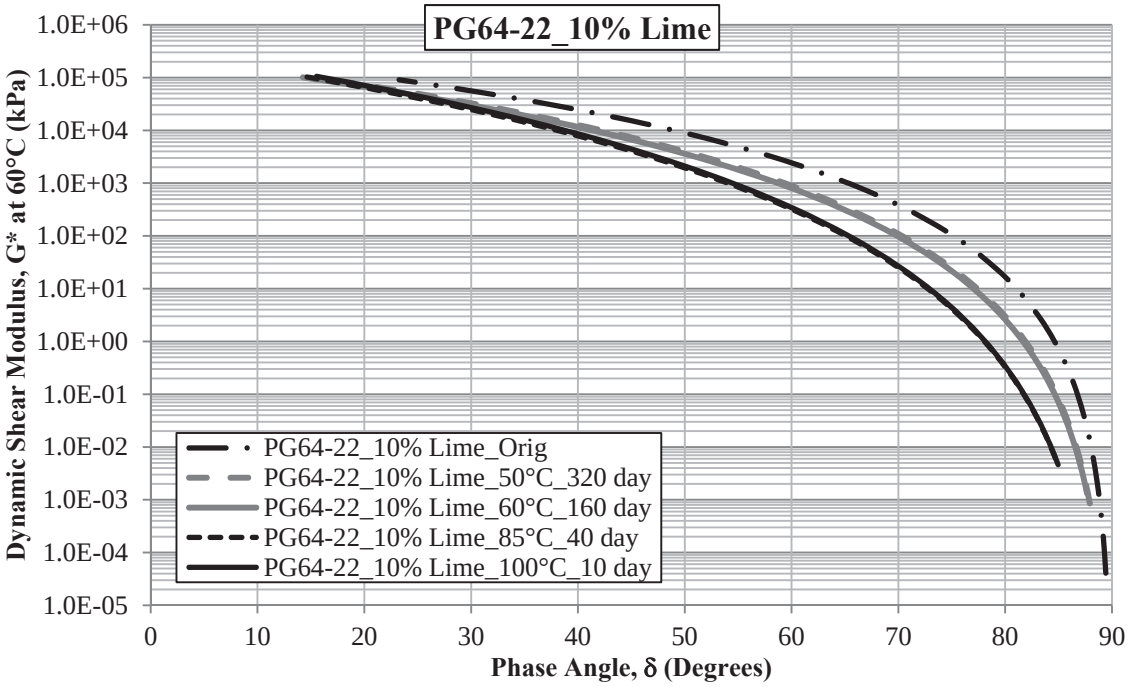

Figure 20.4 Summary of PG 64-22 + 10% Lime Black Space Plots

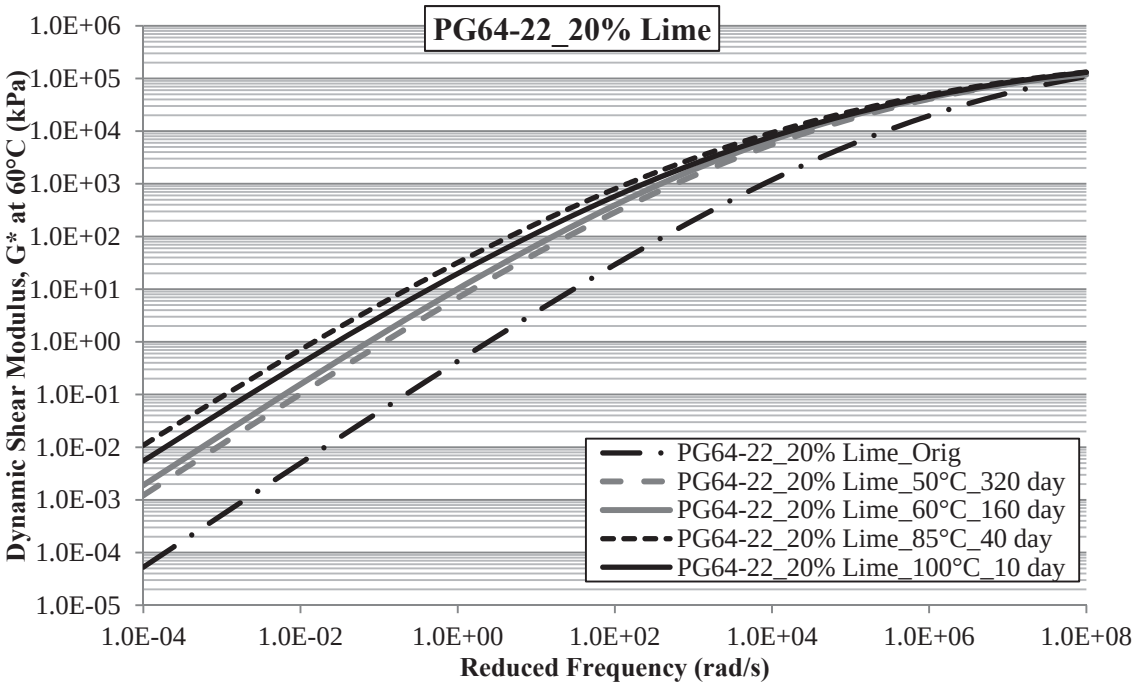

Figure 20.5 Summary of PG 64-22 + 20% Lime Dynamic Shear Modulus Master Curves

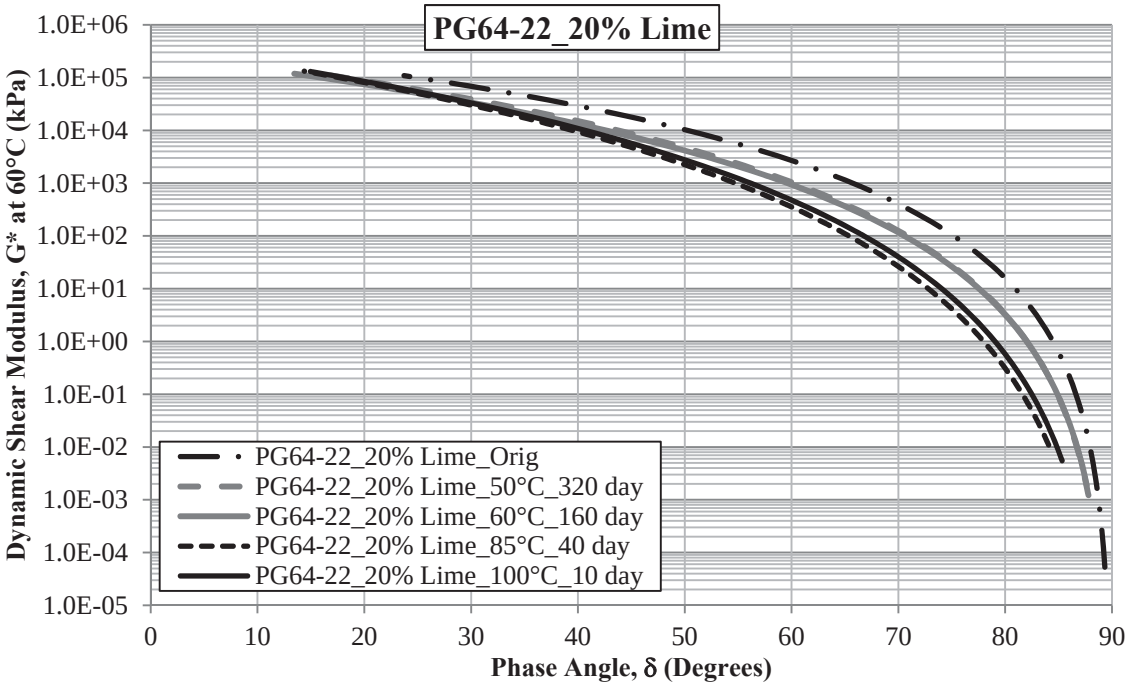

Figure 20.6 Summary of PG 64-22 + 20% Lime Black Space Plots

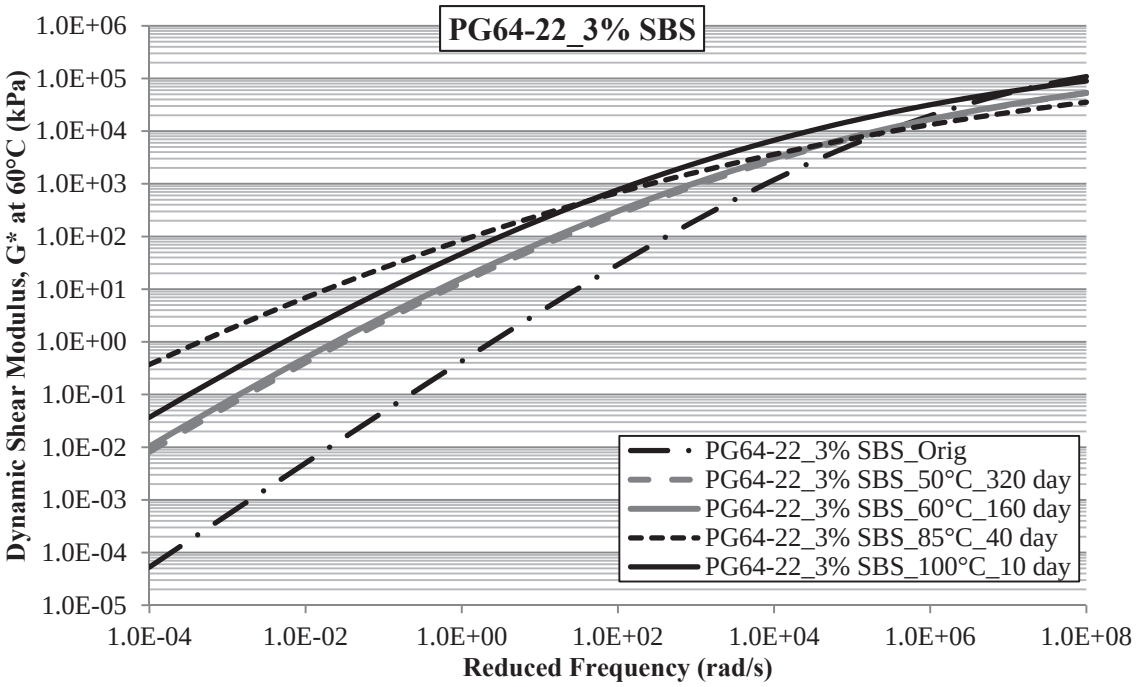

Figure 20.7 Summary of PG 64-22 + 3% SBS Dynamic Shear Modulus Master Curves

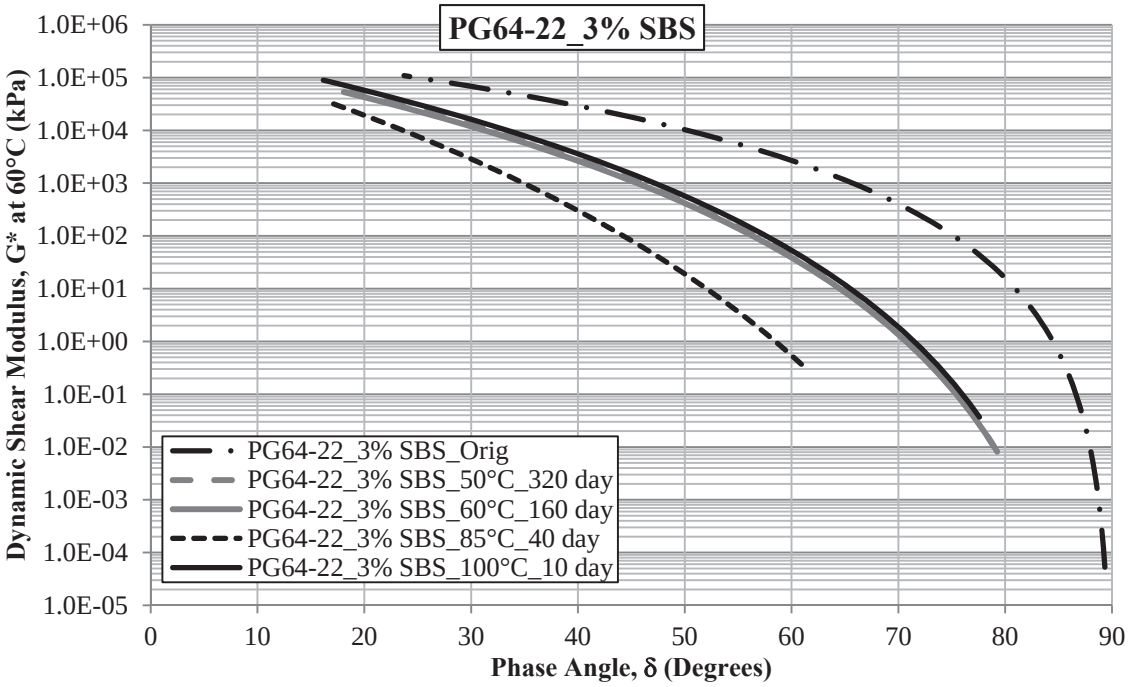

Figure 20.8 Summary of PG 64-22 + 3% SBS Black Space Plots

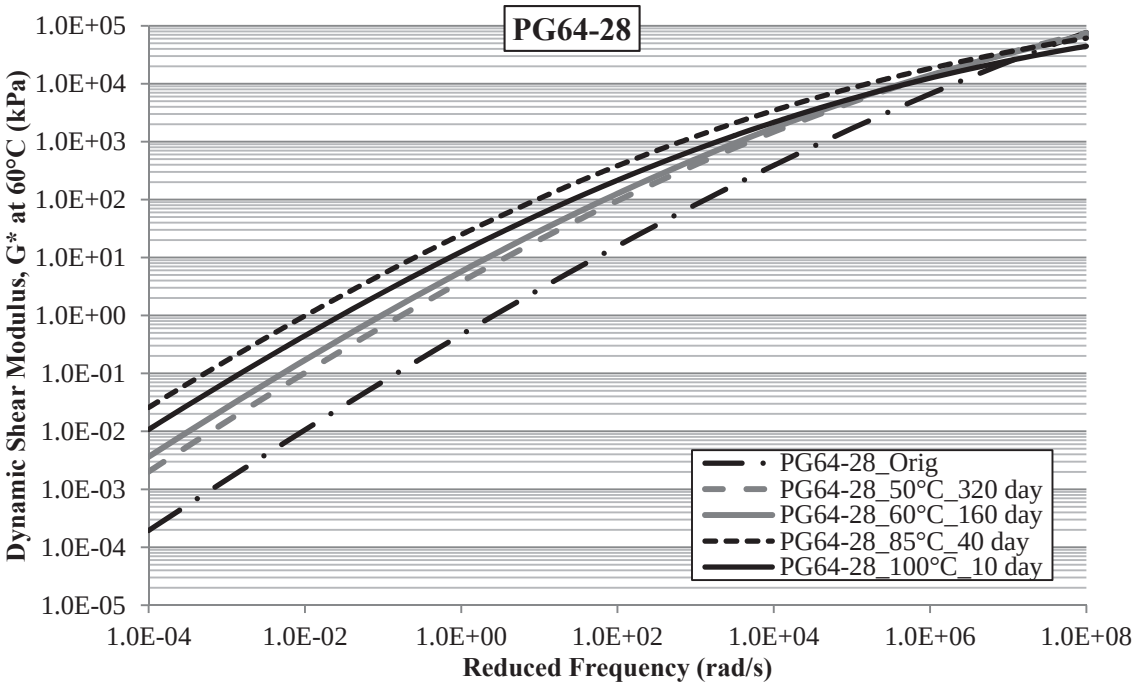

Figure 20.9 Summary of PG 64-28
Dynamic Shear Modulus Master Curves

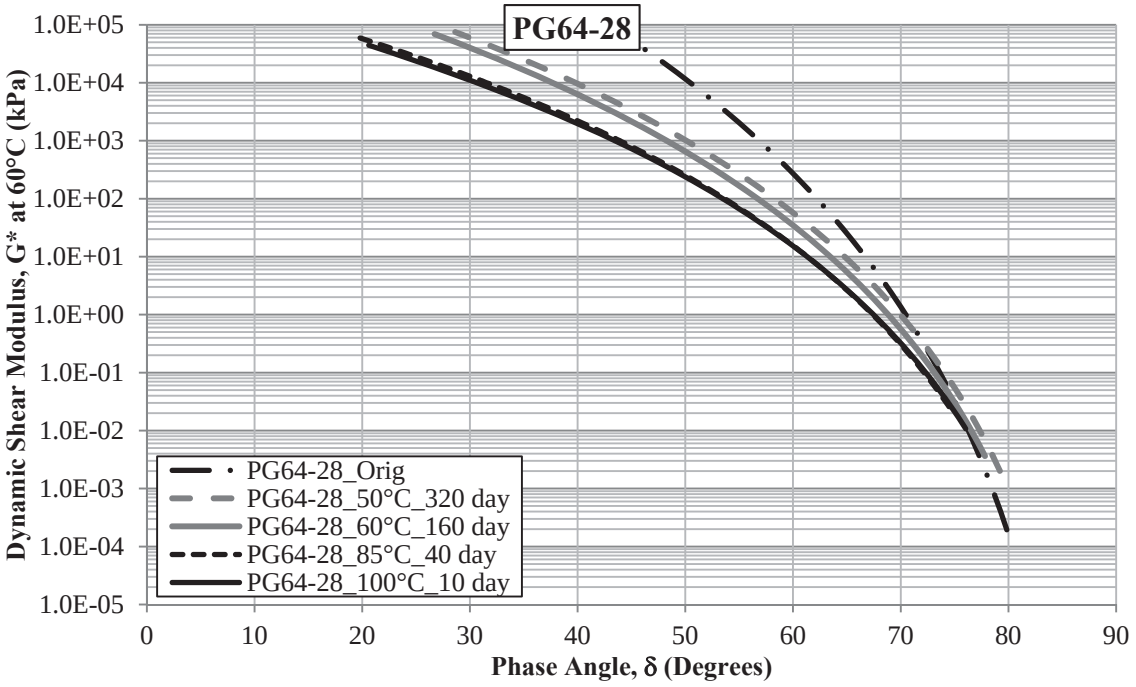

Figure 20.10 Summary of PG 64-28 Black Space Plots

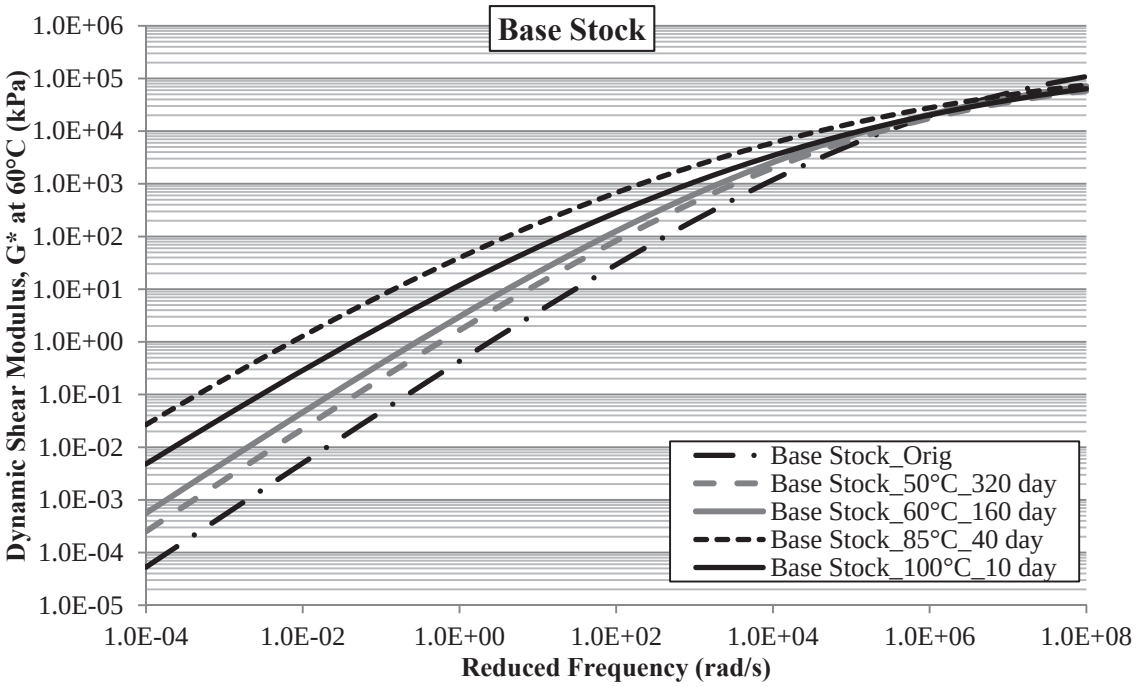

Figure 20.11 Summary of the Base Stock Dynamic Shear Modulus Master Curves

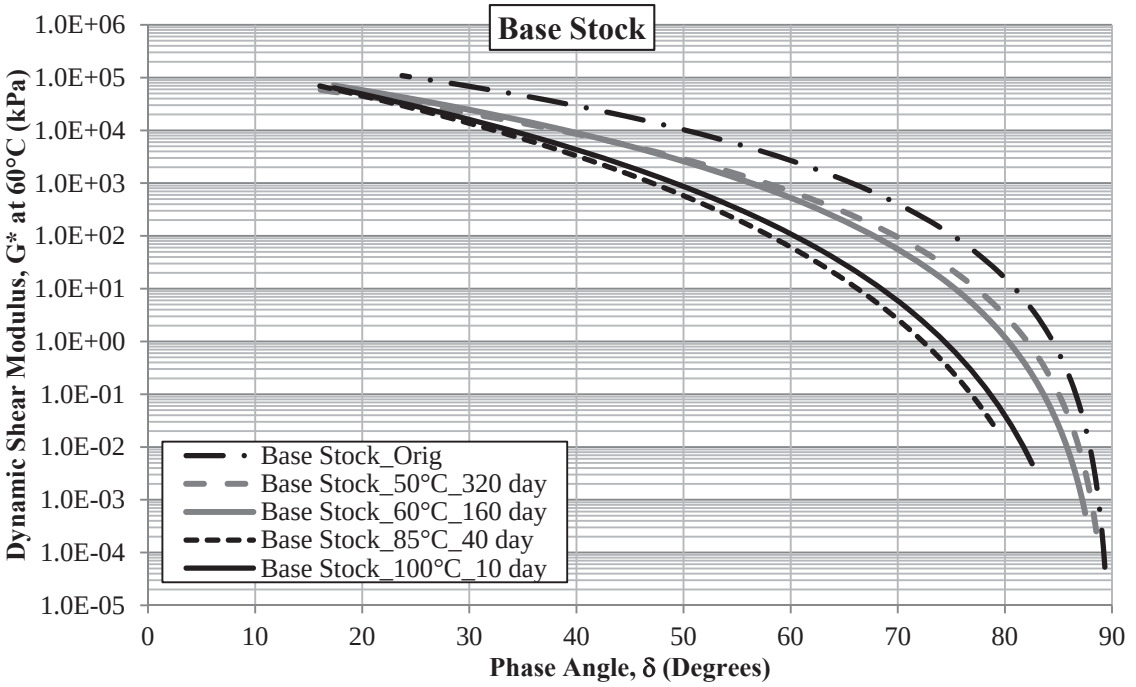

Figure 20.12 Summary of the Base Stock Black Space Plots

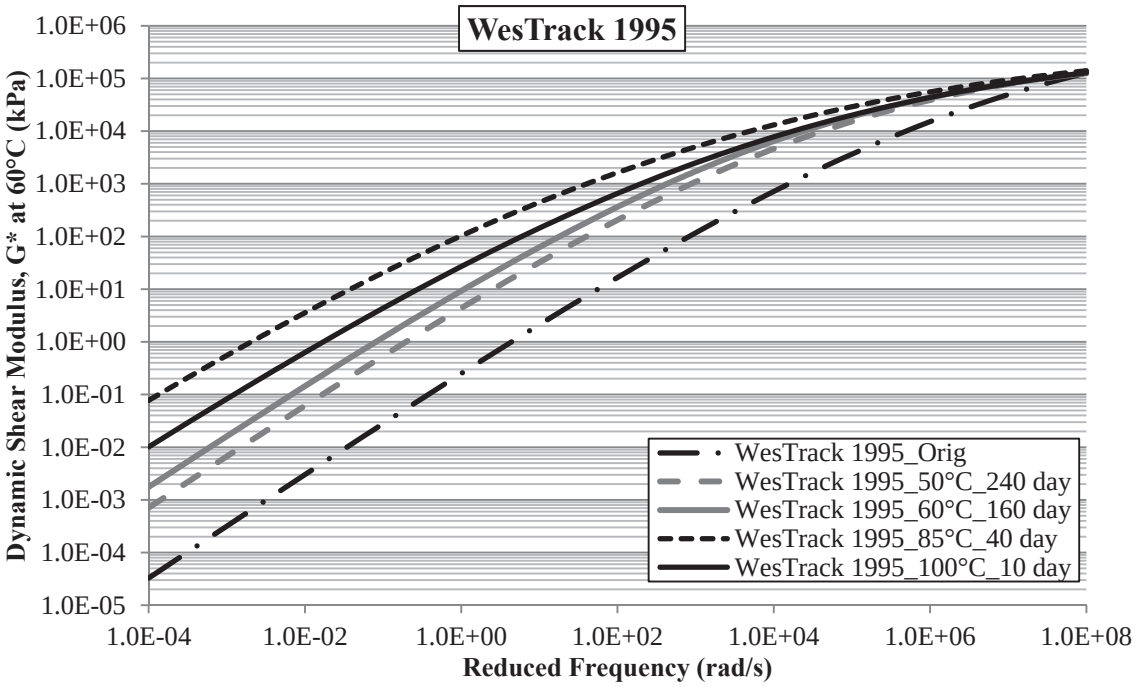

Figure 20.13 Summary of WesTrack 1995 Dynamic Shear Modulus Master Curves

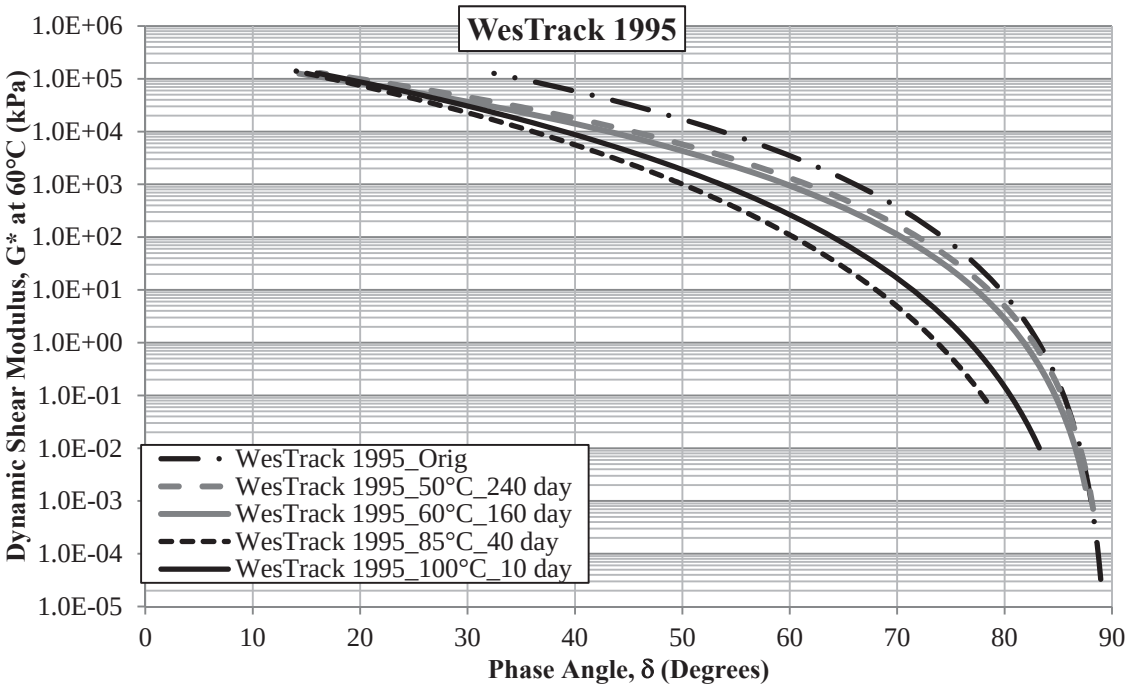

Figure 20.14 Summary of WesTrack 1995 Black Space Plots

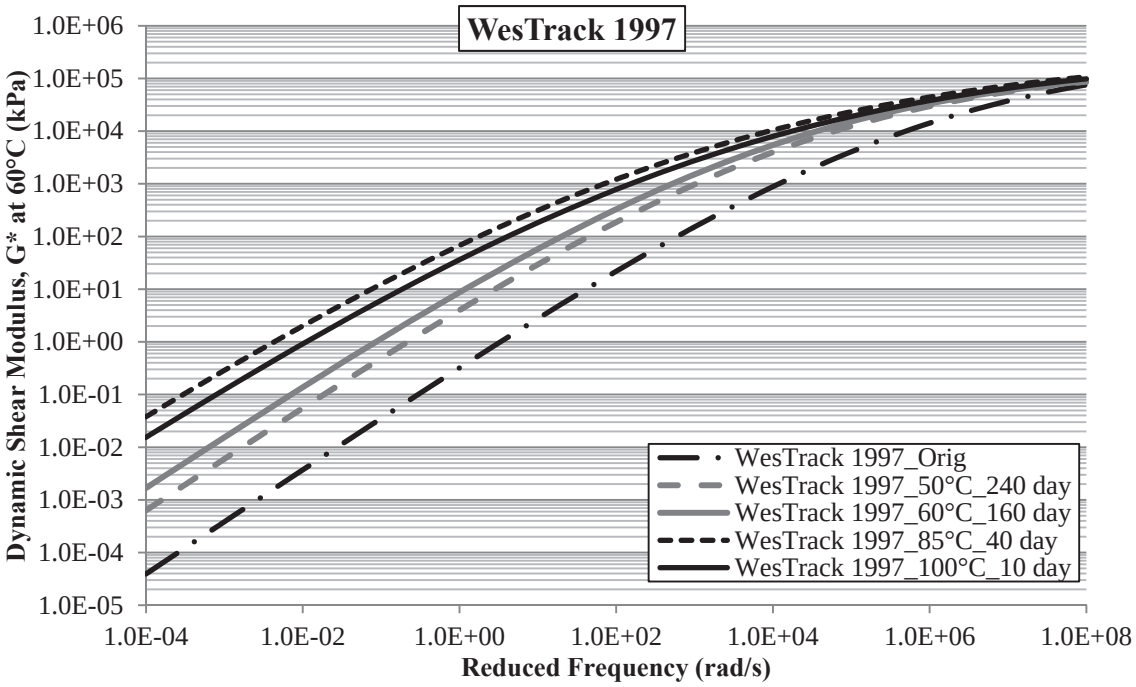

Figure 20.15 Summary of WesTrack 1997 Dynamic Shear Modulus Master Curves

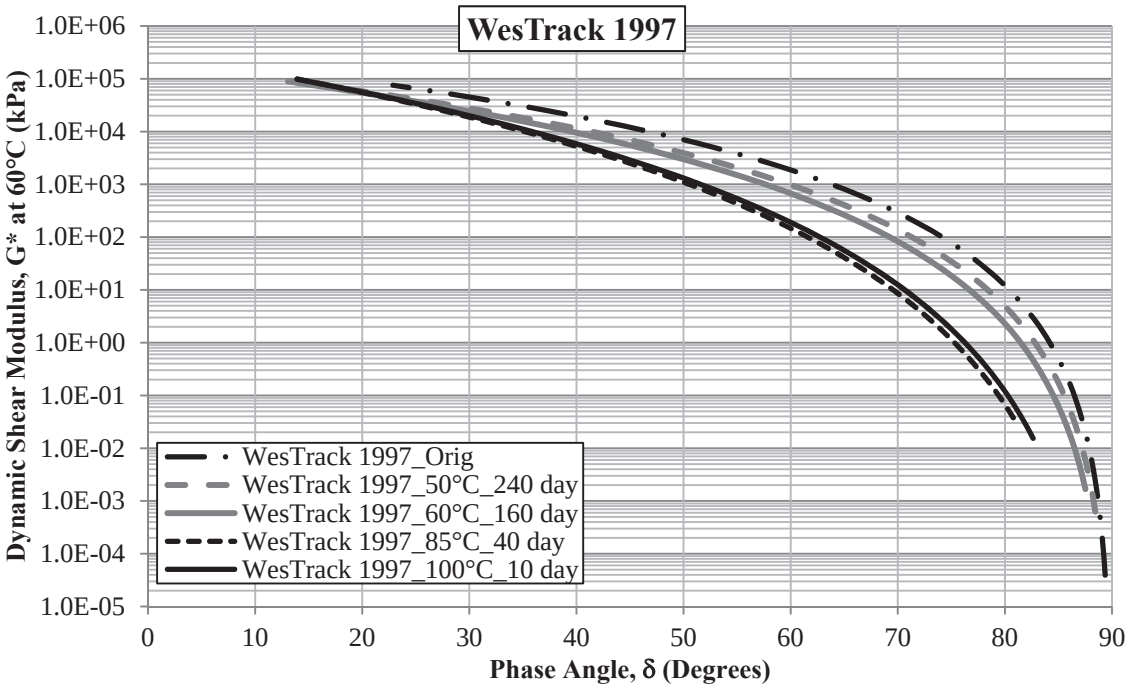

Figure 20.16 Summary of WesTrack 1997 Black Space Plots

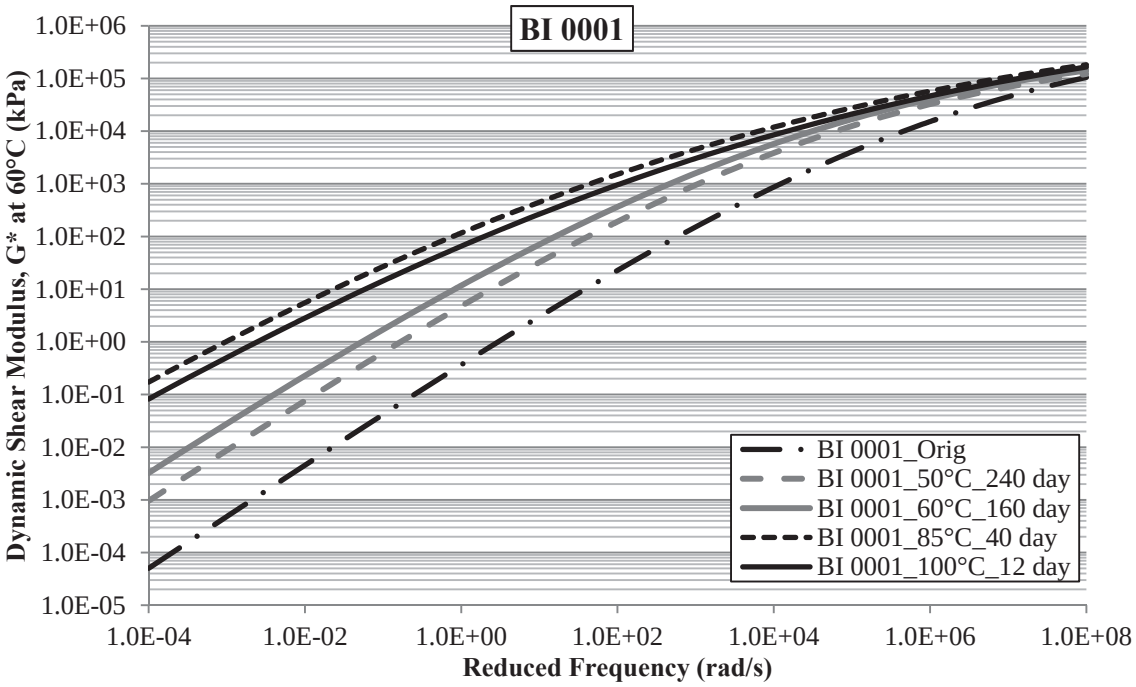

Figure 20.17 Summary of ARC Core BI 0001 Dynamic Shear Modulus Master Curves

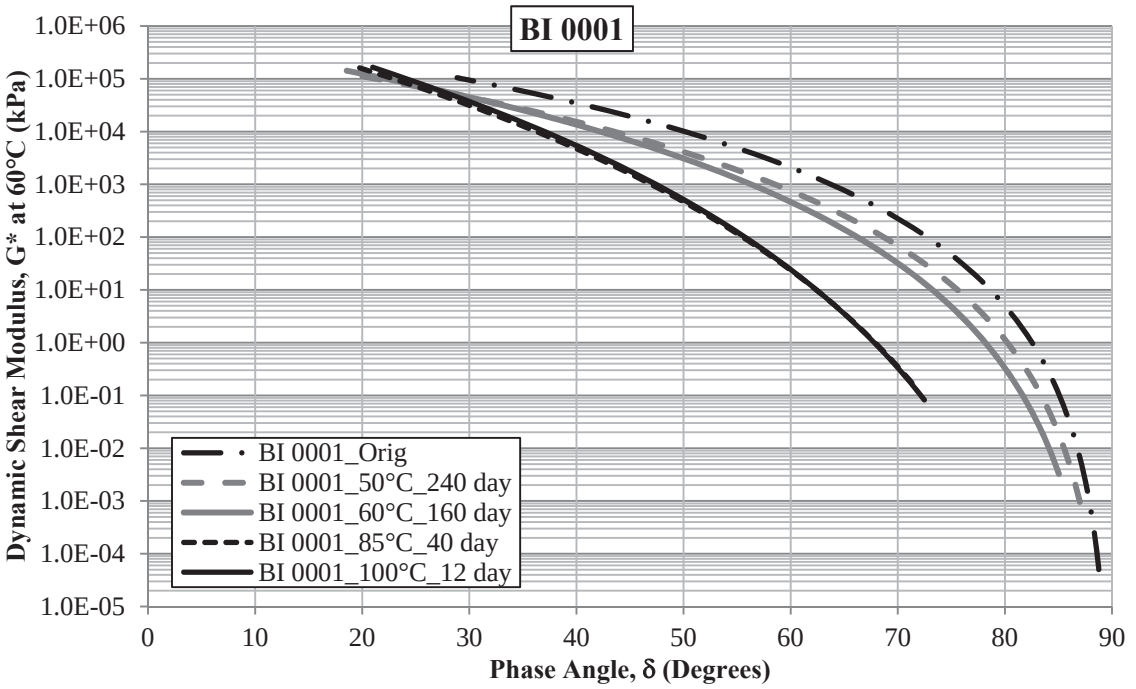

Figure 20.18 Summary of ARC Core BI 0001 Black Space Plots

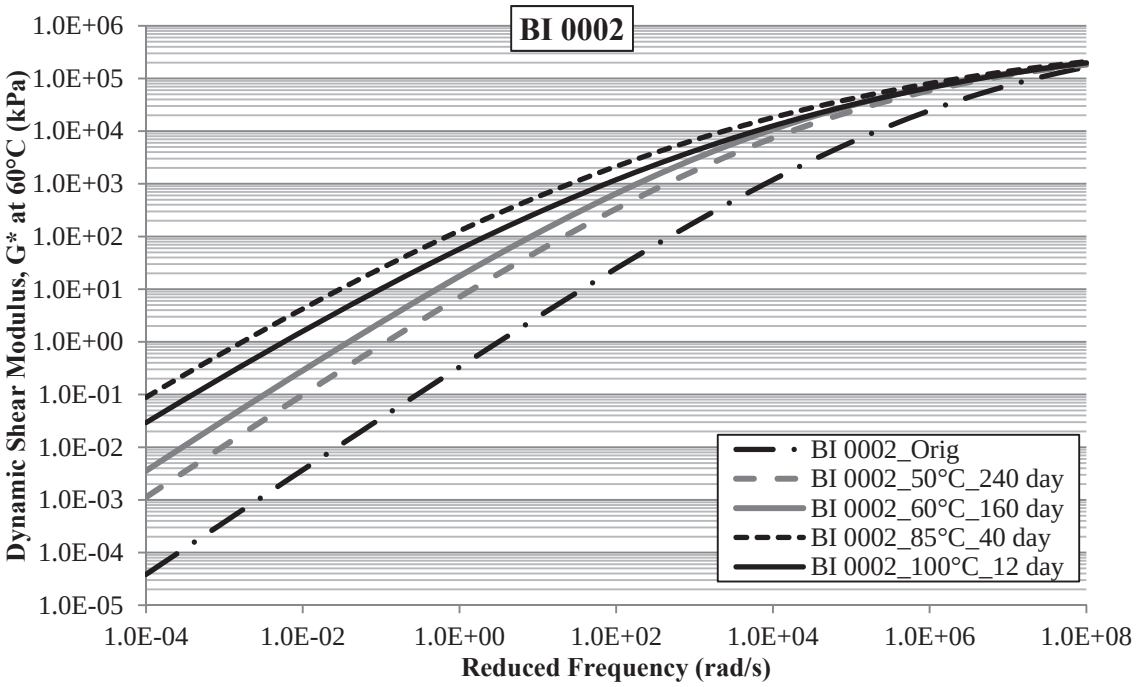

Figure 20.19 Summary of ARC Core BI 0002
Dynamic Shear Modulus Master Curves

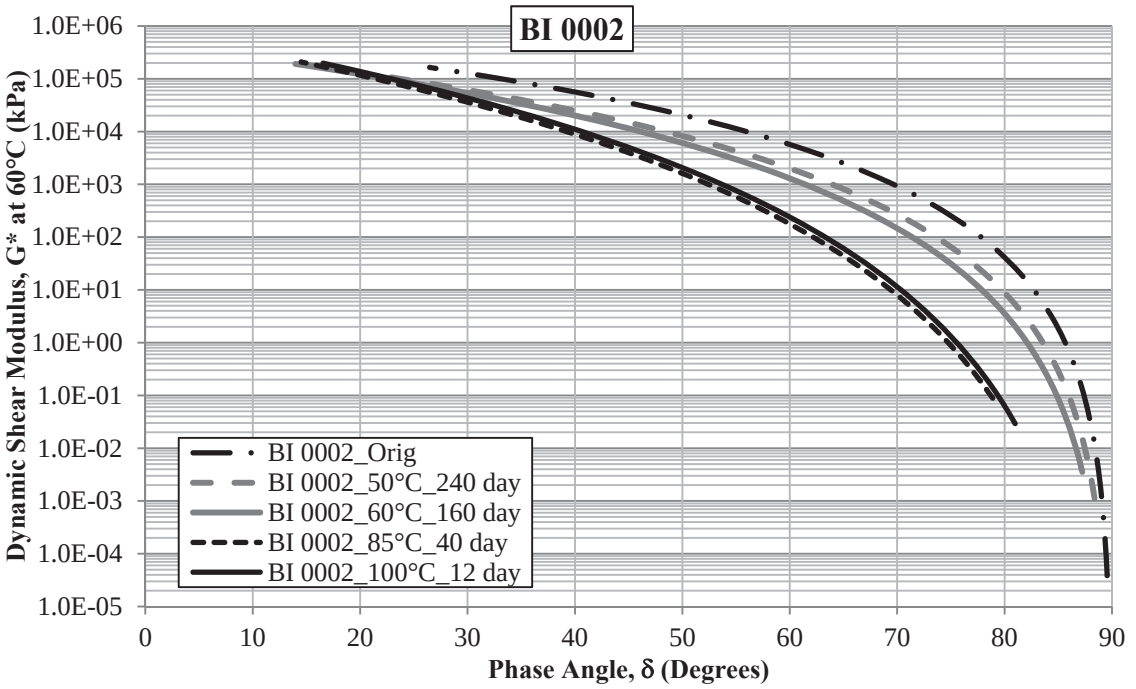

Figure 20.20 Summary of ARC Core BI 0002 Black Space Plots

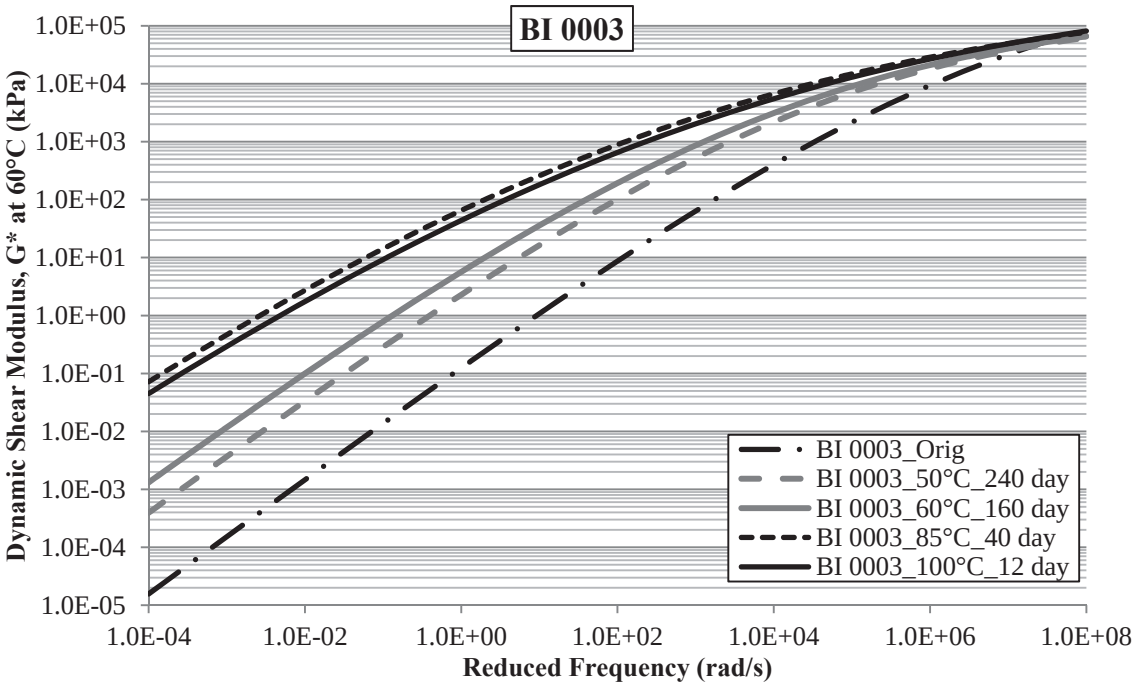

Figure 20.21 Summary of ARC Core BI 0003 Dynamic Shear Modulus Master Curves

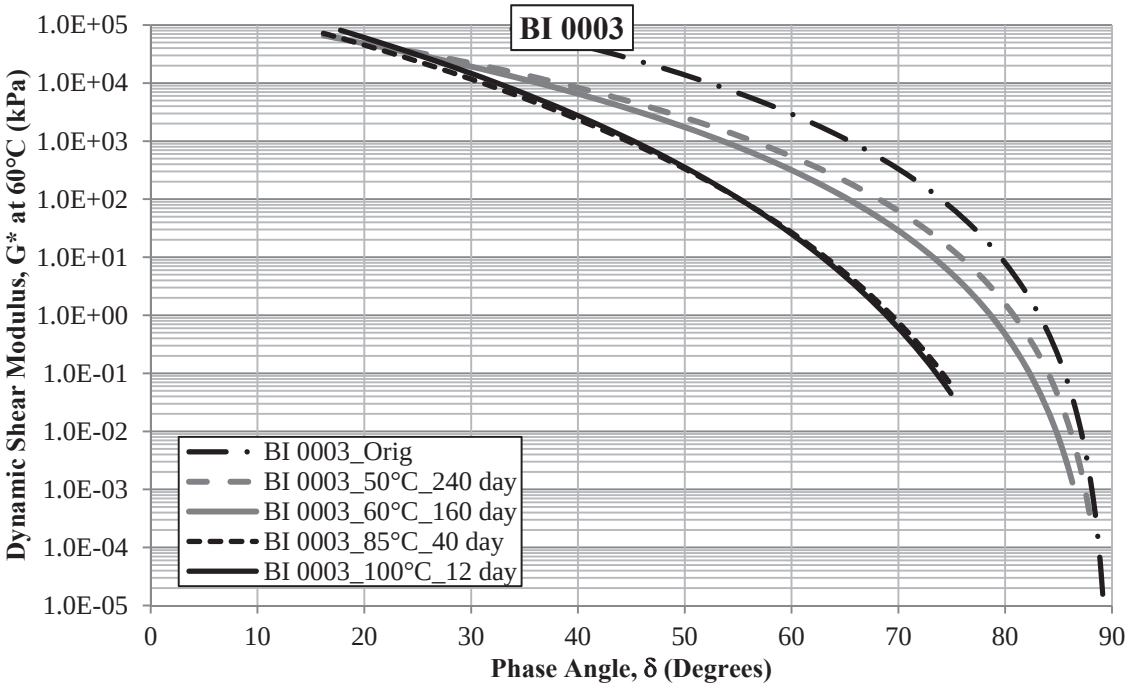

Figure 20.22 Summary of ARC Core BI 0003 Black Space Plots

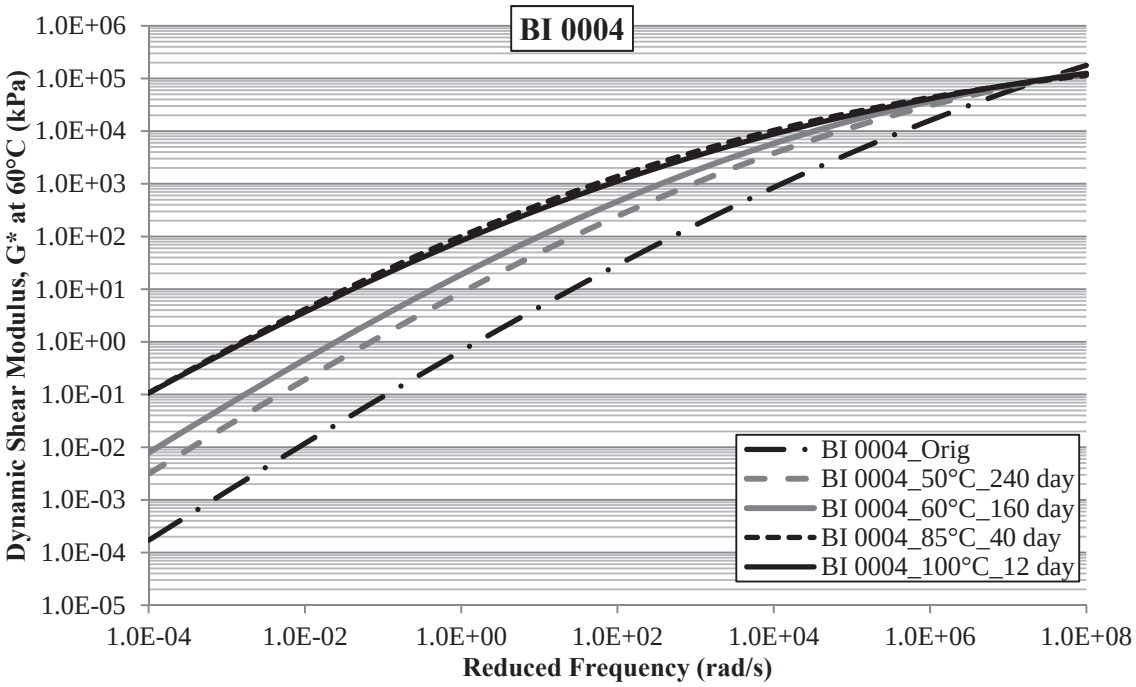

Figure 20.23 Summary of ARC Core BI 0004 Dynamic Shear Modulus Master Curves

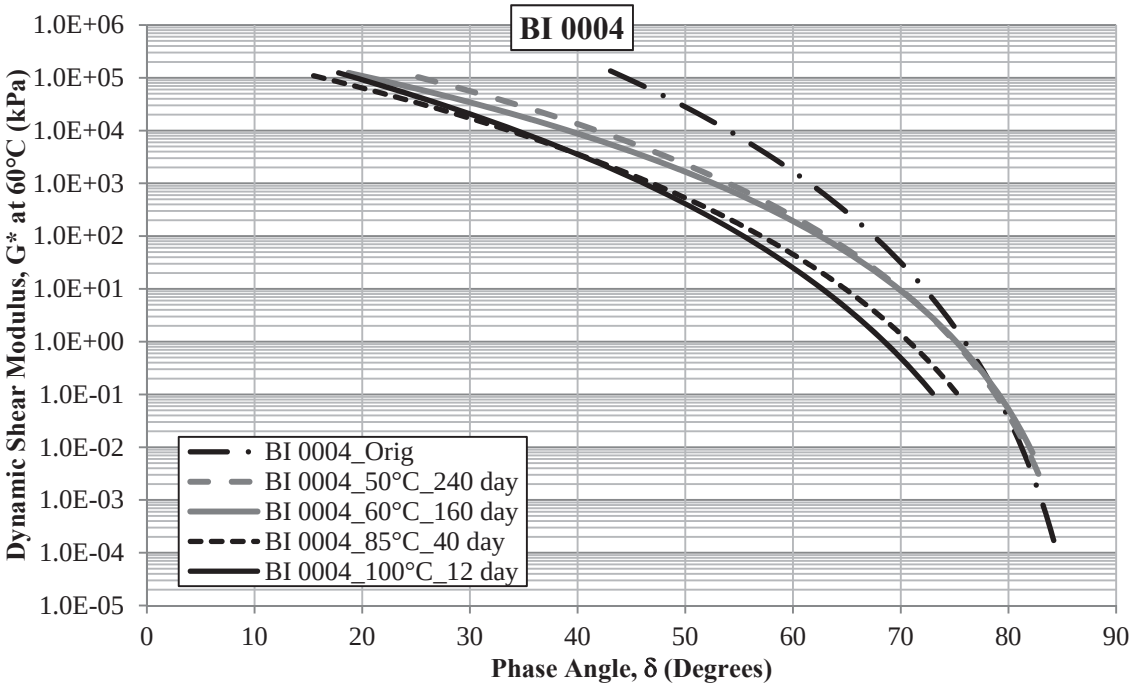

Figure 20.24 Summary of ARC Core BI 0004 Black Space Plots

21 APPENDIX I:

Summary of Pan-Aged Asphalt Binder Master Curve Function Parameters

Table 21.1 Dynamic Shear Modulus and Shift Function Parameters
PG 64-22

Aging Conditions		CAS Parameters				WLF		Kaelble			
Temp.	Dur. (days)	G_0 (kPa)	ω_0 (rad/s)	β	κ	C_1	C_2	C_1	C_2	T_k (°C)	T_r (°C)
Orig.	**Orig.**	464,309	1,338,497	0.2026	1	9.22	141.0	13.41	97.0	16	60
50°C	**60**	270,216	124,156	0.2010	1	12.14	160.0	16.74	116.0	16	60
	120	272,113	81,728	0.1981	1	12.89	164.1	17.61	120.1	16	60
	180	229,721	46,548	0.1978	1	12.67	160.6	17.46	116.6	16	60
	240	290,137	27,470	0.1844	1	13.32	164.6	18.18	120.6	16	60
60°C	**30**	284,877	102,869	0.1931	1	12.96	166.0	17.63	122.0	16	60
	60	266,653	61,161	0.1910	1	13.90	171.1	18.71	127.1	16	60
	100	317,641	35,275	0.1760	1	12.98	164.2	17.74	120.2	16	60
	160	284,168	15,228	0.1722	1	15.02	177.2	19.99	133.2	16	60
85°C	**7.5**	323,621	49,170	0.1758	1	13.21	167.4	17.92	123.4	16	60
	15	294,404	14,016	0.1662	1	14.16	171.2	17.94	125.5	20	60
	25	355,409	3,451	0.1485	1	15.21	178.0	19.05	132.2	20	60
	40	537,274	387	0.1208	1	16.45	185.0	19.44	134.5	22	60
100°C	**1.83**	319,573	97,974	0.1824	1	12.02	159.3	16.61	115.3	16	60
	3.75	288,022	28,905	0.1727	1	13.36	167.3	18.13	126.3	16	60
	6.25	344,205	7,887	0.1544	1	13.63	167.8	16.54	118.2	22	60
	10	465,890	1,311	0.1316	1	16.10	183.9	19.99	138.0	20	60

Table 21.2 Dynamic Shear Modulus and Shift Function Parameters
PG 64-22 + 10% Lime

Aging Conditions		CAS Parameters				WLF		Kaelble			
Temp.	Dur. (days)	G_0 (kPa)	ω_0 (rad/s)	β	κ	C_1	C_2	C_1	C_2	T_k (°C)	T_r (°C)
Orig.	**Orig.**	352,780	840,761	0.2206	1	9.01	139.7	13.15	95.7	16	60
50°C	**60**	250,483	100,728	0.2083	1	11.66	154.7	16.30	110.7	16	60
	120	269,769	66,888	0.2032	1	12.03	156.0	16.75	112.0	16	60
	180	263,364	48,522	0.1979	1	12.34	157.0	17.15	113.0	16	60
	240	267,635	27,668	0.1927	1	12.74	160.0	17.58	116.0	16	60
60°C	**30**	239,239	82,266	0.2090	1	11.72	155.0	16.37	110.9	16	60
	60	238,238	51,842	0.2015	1	12.54	159. 6	17.31	115.6	16	60
	100	259,340	28,301	0.1936	1	13.72	167.7	18.59	123.7	16	60
	160	249,074	16,372	0.1916	1	14.16	169.9	19.11	125.9	16	60
85°C	**7.5**	263,009	51,781	0.1940	1	12.16	157.9	16.86	113.9	16	60
	15	264,342	19,299	0.1859	1	12.87	160.7	17.73	116.7	16	60
	25	297,306	10,859	0.1748	1	14.05	169.2	18.99	125.2	16	60
	40	312,861	3,486	0.1596	1	14.74	171.4	17.78	121.6	22	60
100°C	**1.83**	283,740	102,113	0.1954	1	11.55	154.4	16.16	110.4	16	60
	3.75	292,947	40,029	0.1831	1	12.30	158.4	17.03	114.4	16	60
	6.25	299,136	19,929	0.1753	1	13.46	166.0	18.32	122.0	16	60
	10	347,824	5,209	0.1589	1	14.15	168.6	18.00	123.0	20	60

Table 21.3 Dynamic Shear Modulus and Shift Function Parameters
PG 64-22 + 20% Lime

Aging Conditions		CAS Parameters				WLF		Kaelble			
Temp.	Dur. (days)	G_0 (kPa)	ω_0 (rad/s)	β	κ	C_1	C_2	C_1	C_2	T_k (°C)	T_r (°C)
Orig.	**Orig.**	453,463	826,683	0.2143	1	9.16	141.2	13.31	97.2	16	60
50°C	**60**	318,081	90,459	0.2040	1	11.28	151.8	15.89	107.8	16	60
	120	297,920	56,781	0.2078	1	12.06	156.3	16.78	112.3	16	60
	180	282,213	38,807	0.2045	1	12.25	156.1	17.06	112.1	16	60
	240	324,940	23,356	0.1912	1	12.46	157.5	17.29	113.5	16	60
60°C	**30**	278,922	71,892	0.2094	1	11.65	154.7	16.29	110.7	16	60
	60	298,765	40,033	0.1988	1	12.71	161.1	17.48	117.1	16	60
	100	286,680	24,207	0.1960	1	12.46	159.5	16.37	114.1	20	60
	160	273,712	12,564	0.1937	1	13.90	167.6	18.85	123.6	16	60
85°C	**7.5**	329,863	49,070	0.1921	1	11.95	156.2	16.63	112.2	16	60
	15	297,084	18,645	0.1892	1	13.59	167.0	18.45	123.0	16	60
	25	321,587	6,748	0.1703	1	13.64	165.9	16.59	116.4	22	60
	40	404,361	2,396	0.1560	1	14.87	172.9	19.95	128.9	16	60
100°C	**1.83**	336,643	76,919	0.1945	1	11.46	153.9	16.05	109. 9	16	60
	3.75	326,921	37,287	0.1851	1	12.48	160.7	17.19	116. 7	16	60
	6.25	318,999	21,851	0.1859	1	12.91	162.5	17.70	118.5	16	60
	10	396,565	5,203	0.1635	1	13.47	164.6	18.38	120.6	16	60

Table 21.4 Dynamic Shear Modulus and Shift Function Parameters
PG 64-22 + 3% SBS

Aging Conditions		CAS Parameters				WLF		Kaelble			
Temp.	**Dur. (days)**	G_0 (kPa)	ω_0 (rad/s)	β	κ	C_1	C_2	C_1	C_2	T_k (°C)	T_r (°C)
Orig.	**Orig.**	453,463	826,683	0.2143	1	9.16	141.2	13.31	97.2	16	60
50°C	**60**	289,671	9,477	0.1330	1	13.17	160.5	15.20	104.0	23	60
	120	404,025	6,422	0.1266	1	15.08	175.7	15.76	108.3	24	60
	180	373,934	2,388	0.1206	1	13.81	162.9	16.60	112.8	23	60
	240	368,555	1,573	0.1206	1	16.26	182.1	17.32	116.2	23	60
60°C	**30**	581,970	9,562	0.1184	1	12.97	160.5	15.21	106.3	23	60
	60	577,342	3,873	0.1162	1	14.68	172.4	16.33	112.1	23	60
	100	330,504	1,239	0.1218	1	13.98	163.0	17.21	116.5	23	60
	160	339,695	1,114	0.1210	1	14.07	165.1	17.85	122.0	22	60
85°C	**7.5**	368,526	2,174	0.1166	1	15.65	177.7	16.47	109.7	23	60
	15	365,959	376	0.1106	1	13.17	157.7	18.48	128.8	22	60
	25	394,158	29	0.0991	1	12.55	145.0	23.21	155.5	16	60
	40	431,910	1	0.0809	1	18.96	188.6	16.12	95.8	26	60
100°C	**1.83**	762,749	5,800	0.1092	1	13.09	160.8	15.41	107.3	23	60
	3.75	636,264	104	0.0960	1	14.09	164.6	19.27	133.9	22	60
	6.25	382,495	2,411	0.1384	1	14.67	173.5	18.27	125.6	20	60
	10	457,458	364	0.1213	1	15.24	176.2	21.17	140.2	16	60

Table 21.5 Dynamic Shear Modulus and Shift Function Parameters
PG 64-28

Aging Conditions		CAS Parameters				WLF		Kaelble			
Temp.	Dur. (day)	G_0 (kPa)	ω_0 (rad/s)	β	κ	C_1	C_2	C_1	C_2	T_k (°C)	T_r (°C)
Orig.	**Orig.**	462,042,400	49,760,230	0.0766	1	18.15	264.5	9.88	82.8	22	60
50°C	**60**	3,098,367,000	2,490,158	0.0561	1	10.37	148.4	15.97	117.5	16	60
	120	61,857,630	390,235	0.0755	1	11.16	153.7	13.37	99.2	22	60
	180	13,278,400	107,240	0.0857	1	11.41	155.0	15.78	109.4	16	60
	240	3,491,122	48,031	0.0997	1	12.72	164.1	17.43	120.6	16	60
60°C	**30**[a]	72,724,710	0	0.0132	1	10.87	153.0	15.25	109.0	16	60
	60	20,055,280	118,086	0.0813	1	11.24	153.6	14.70	107.8	20	60
	100	5,806,557	40,552	0.0911	1	12.08	159.0	17.31	121.2	16	60
	160	2,489,733	15,591	0.0983	1	13.34	167.5	18.40	126.4	16	60
85°C	**7.5**	15,862,320	95,827	0.0820	1	11.53	157.5	16.42	117.8	16	60
	15	3,750,338	15,672	0.0914	1	12.90	166.4	18.07	127.7	16	60
	25	1,293,880	3,662	0.1007	1	14.61	179.6	20.10	143.0	16	60
	40	659,902	407	0.1031	1	16.70	194.3	22.76	161.3	16	60
100°C	**1.83**	17,412,510,000	8,226,034	0.0513	1	10.78	155.1	13.90	98.3	16	60
	3.75	10,769,920	59,891	0.0838	1	12.51	166.2	16.94	121.3	16	60
	6.25	3,451,797	11,175	0.0896	1	13.05	168.9	18.75	136.2	16	60
	10	525,147	980	0.1052	1	12.82	161.2	20.81	148.3	16	60

a – G* master curve was determined by Rhea software to not sufficiently fit the CAS model parameters, thus were fit to a standard logistic curve function.

Table 21.6 Dynamic Shear Modulus and Shift Function Parameters
Base Stock

Aging Conditions		CAS Parameters				WLF		Kaelble			
Temp.	Dur. (day)	G_0 (kPa)	ω_0 (rad/s)	β	κ	C_1	C_2	C_1	C_2	T_k (°C)	T_r (°C)
Orig.	**Orig.**	453,463	826,683	0.2143	1	9.16	141.2	13.31	97.2	16	60
50°C	**60**	185,641	315,710	0.2167	1	11.26	157.9	15.61	113.9	16	60
	120	137,936	150,051	0.2183	1	11.26	156.2	15.68	112.2	16	60
	180	197,645	112,530	0.1999	1	12.90	167.6	17.49	123.6	16	60
	240	154,208	56,258	0.2034	1	13.03	165.9	17.73	121.9	16	60
60°C	**30**	221,199	185,949	0.2090	1	11.77	161.6	16.17	117.6	16	60
	60	200,593	139,876	0.1983	1	12.38	164.6	16.89	120.6	16	60
	100	203,260	79,389	0.1892	1	12.55	164.3	17.14	120.3	16	60
	160	232,604	35,531	0.1805	1	15.59	186.2	20.41	142.2	16	60
85°C	**7.5**	211,515	130,317	0.1887	1	12.68	168.4	17.17	124.4	16	60
	15	210,644	33,466	0.1754	1	14.79	181.7	19.52	137.7	16	60
	25	268,241	6,928	0.1512	1	16.69	194.6	21.57	150.6	16	60
	40	319,654	427	0.1284	1	19.72	213.6	23.61	167.3	20	60
100°C	**1.83**	160,885	199,323	0.2021	1	11.21	158.4	15.52	114.4	16	60
	3.75	204,932	92,859	0.1843	1	12.89	169.4	17.41	125.4	16	60
	6.25	196,620	25,406	0.1725	1	12.67	165.0	17.28	121.0	16	60
	10	299,035	3,332	0.1388	1	17.42	200.2	22.33	156.2	16	60

Table 21.7 Dynamic Shear Modulus and Shift Function Parameters
WesTrack 1995

Aging Conditions		CAS Parameters				WLF		Kaelble			
Temp.	Dur. (days)	G_0 (kPa)	ω_0 (rad/s)	β	κ	C_1	C_2	C_1	C_2	T_k (°C)	T_r (°C)
Orig.	**Orig.**	453,463	4,257,647	0.1815	1	9.96	143.1	14.38	99.1	16	60
50°C	**60**	185,641	163,042	0.2112	1	12.22	155.3	17.05	111.3	16	60
	120	137,936	56,386	0.2075	1	11.43	148.4	15.18	103.2	20	60
	180	197,645	60,952	0.2005	1	13.87	165.0	18.91	121.0	16	60
	240	154,208	45,353	0.1965	1	14.76	170.8	19.89	126.8	16	60
60°C	**30**	221,199	144,822	0.2023	1	13.16	162.1	18.06	118.1	16	60
	60	200,593	63,035	0.1966	1	13.78	164.4	18.82	120.4	16	60
	100	203,260	39,007	0.1888	1	14.99	171.9	20.14	127.9	16	60
	160	232,604	15,333	0.1895	1	16.41	180.3	20.48	134.4	20	60
85°C	**7.5**	211,515	101,222	0.1871	1	13.66	166.5	18.57	122.5	16	60
	15	210,644	19,316	0.1767	1	16.21	181.8	21.39	137.8	16	60
	25	268,241	3,455	0.1546	1	18.44	196.1	23.78	152.1	16	60
	40	319,654	228	0.1300	1	20.70	208.8	26.22	164.8	16	60
100°C	**1.83**	160,885	246,937	0.1940	1	12.16	156.8	16.91	112.8	16	60
	3.75	204,932	69,472	0.1798	1	14.23	170.0	19.21	126.0	16	60
	6.25	196,620	6,982	0.1680	1	14.43	169.7	17.43	120.0	22	60
	10	299,035	2,812	0.1463	1	17.63	190.1	22.95	146.1	16	60

Table 21.8 Dynamic Shear Modulus and Shift Function Parameters
WesTrack 1997

Aging Conditions		CAS Parameters				WLF		Kaelble			
Temp.	Dur. (days)	G_0 (kPa)	ω_0 (rad/s)	β	κ	C_1	C_2	C_1	C_2	T_k (°C)	T_r (°C)
Orig.	**Orig.**	453,463	714,306	0.2179	1	8.30	129.1	12.60	85.0	16	60
50°C	**60**	185,641	91,878	0.2135	1	11.10	147.9	15.80	103.9	16	60
	120	137,936	79,023	0.2103	1	13.07	159.6	16.92	114.2	20	60
	180	197,645	37,796	0.2082	1	12.52	156.6	17.42	112.6	16	60
	240	154,208	28,512	0.2074	1	13.05	159.6	16.89	114.1	20	60
60°C	**30**	221,199	71,105	0.2121	1	11.49	150.2	16.25	106.2	16	60
	60	200,593	39,441	0.2000	1	12.20	153.9	16.00	108.6	20	60
	100	203,260	21,831	0.1971	1	13.49	163.0	17.35	117.5	20	60
	160	232,604	10,320	0.1930	1	14.01	165.4	17.05	115.8	22	60
85°C	**7.5**	211,515	34,693	0.2005	1	11.82	151.4	14.78	102.5	22	60
	15	210,644	10,762	0.1796	1	14.18	167.2	18.09	121.6	20	60
	25	268,241	2,064	0.1683	1	14.56	167.9	17.62	118.0	22	60
	40	319,654	398	0.1429	1	17.31	187.5	20.38	136.9	22	60
100°C	**1.83**	160,885	79,958	0.1998	1	11.26	149.8	15.95	105.8	16	60
	3.75	204,932	26,304	0.1871	1	12.71	159.2	17.57	115.2	16	60
	6.25	196,620	15,159	0.1628	1	15.73	179.0	20.85	135.0	16	60
	10	299,035	1,110	0.1490	1	15.18	174.2	18.21	124.2	22	60

Table 21.9 Dynamic Shear Modulus and Shift Function Parameters
BI 0001 Venezuelan

Aging Conditions		CAS Parameters				WLF		Kaelble			
Temp.	Dur. (days)	G_0 (kPa)	ω_0 (rad/s)	β	κ	C_1	C_2	C_1	C_2	T_k (°C)	T_r (°C)
Orig.	Orig.	875,693	1,615,470	0.1820	1	9.05	143.3	13.06	99.3	16	60
50°C	4	676,105	644,148	0.1798	1	9.39	144.1	13.52	100.1	16	60
	8	775,290	583,513	0.1742	1	10.33	152.5	14.53	108.5	16	60
	15	574,127	362,564	0.1817	1	10.40	151.7	14.65	107.7	16	60
	30	468,654	229,822	0.1859	1	10.63	151.6	14.97	107.6	16	60
	60	650,561	200,181	0.1737	1	11.31	156.5	15.73	112.5	16	60
	120	615,140	120,877	0.1714	1	11.14	152.8	15.64	108.8	16	60
	180	550,571	73,455	0.1718	1	11.34	152.9	15.93	108.9	16	60
	240	492,249	42,021	0.1695	1	11.23	149.8	15.90	105.8	16	60
60°C	2	843,680	748,414	0.1723	1	9.47	144.6	13.62	100.6	16	60
	4	804,570	579,134	0.1738	1	10.12	150.4	14.31	106.4	16	60
	8	804,004	398,761	0.1693	1	10.56	152.7	14.83	108.7	16	60
	15	761,501	299,267	0.1683	1	10.98	154.7	15.34	110.7	16	60
	30	778,793	178,696	0.1648	1	11.08	154.6	15.48	110.6	16	60
	60	569,608	77,580	0.1681	1	11.64	156.7	16.18	112.7	16	60
	100	738,628	45,243	0.1560	1	12.56	162.4	17.23	118.4	20	60
	160	651,351	13,794	0.1517	1	12.83	160.6	17.67	116.6	16	60
85°C	0.5	642,587	662,264	0.1799	1	9.40	144.2	13.53	100.2	16	60
	1	667,894	524,168	0.1766	1	10.25	150.7	14.48	106.7	16	60
	2	780,392	413,181	0.1698	1	9.65	145.6	13.84	101.6	16	60
	4	742,896	198,455	0.1642	1	11.44	158.1	15.86	114.1	16	60
	8	789,364	113,215	0.1554	1	12.00	160.4	16.53	116.4	16	60
	15	935,892	29,199	0.1417	1	13.32	168.7	17.92	124.7	16	60
	25	1,480,005	2,757	0.1173	1	15.34	182.0	20.24	138.0	16	60
	40	2,107,450	109	0.0964	1	16.48	184.8	21.63	140.8	23	60
100°C	0.083	1,149,070	1,452,501	0.1714	1	9.36	146.0	13.39	102.0	16	60
	0.25	1,352,143	1,132,206	0.1620	1	9.55	145.8	13.68	101.8	16	60
	0.5	927,658	684,209	0.1675	1	9.58	145.5	13.74	101.5	16	60
	1	685,563	306,965	0.1688	1	10.11	148.0	14.39	104.0	16	60
	2	685,940	161,531	0.1626	1	10.75	152.7	15.10	108.7	16	60
	4	1,052,857	47,528	0.1392	1	11.99	159.0	16.57	115.0	16	60
	7	1,223,435	8,220	0.1230	1	12.41	160.0	17.12	116.0	16	60
	12	2,739,525	336	0.0945	1	14.55	172.7	18.39	127.1	16	60

Table 21.10 Dynamic Shear Modulus and Shift Function Parameters
BI 0002 Valero

Aging Conditions		CAS Parameters				WLF		Kaelble			
Temp.	Dur. (days)	G_0 (kPa)	ω_0 (rad/s)	β	κ	C_1	C_2	C_1	C_2	T_k (°C)	T_r (°C)
Orig.	Orig.	782,229	1,983,077	0.2232	1	9.52	139.2	13.92	95.2	16	60
50°C	4	613,829	880,417	0.2222	1	10.36	144.4	14.90	100.4	16	60
	8	604,873	621,912	0.2168	1	10.73	146.6	15.33	102.6	16	60
	15	612,092	500,974	0.2137	1	11.05	148.5	15.70	104.5	16	60
	30	525,770	259,247	0.2140	1	11.74	152.4	16.51	108.4	16	60
	60	474,711	145,385	0.2129	1	12.25	154.1	17.15	110.1	16	60
	120	467,371	84,810	0.2093	1	13.13	159.6	18.13	115.6	16	60
	180	476,810	53,655	0.2038	1	14.04	164.5	19.17	120.5	16	60
	240	452,545	36,677	0.2027	1	14.17	164.3	19.36	120.3	16	60
60°C	2	830,962	1,133,463	0.2097	1	10.52	146.7	15.03	102.7	16	60
	4	581,287	585,044	0.2115	1	10.19	142.0	14.77	98.0	16	60
	8	512,218	386,753	0.2172	1	11.12	148.5	15.81	104.5	16	60
	15	518,549	275,533	0.2117	1	11.82	153.1	16.59	109.1	16	60
	30	497,188	125,175	0.2051	1	12.67	157.7	17.57	113.7	16	60
	60	475,311	62,757	0.2002	1	13.64	162.7	17.55	117.2	16	60
	100	446,457	29,624	0.1995	1	14.99	170.9	20.18	126.9	20	60
	160	473,532	11,237	0.1862	1	15.49	171.9	20.81	127.9	16	60
85°C	0.5	695,908	1,069,163	0.2165	1	10.11	142.8	14.62	98.8	16	60
	1	663,057	826,863	0.2157	1	10.46	145.0	15.01	101.0	16	60
	2	646,826	489,088	0.2059	1	10.72	146.3	15.33	102.3	16	60
	4	563,861	231,596	0.2019	1	11.55	151.3	16.28	107.3	16	60
	8	559,432	91,559	0.1887	1	12.61	157.3	17.50	113.3	16	60
	15	539,182	19,927	0.1753	1	14.85	171.2	19.99	127.2	16	60
	25	526,656	4,311	0.1610	1	17.77	192.4	20.15	137.8	16	60
	40	801,227	329	0.1306	1	19.56	199.3	25.10	155.3	23	60
100°C	0.083	731,504	1,411,427	0.2177	1	9.85	141.1	14.31	97.1	16	60
	0.25	791,473	1,168,323	0.2118	1	10.10	143.4	14.56	99.4	16	60
	0.5	868,580	1,072,308	0.2048	1	10.79	148.7	15.33	104.7	16	60
	1	624,526	517,946	0.2103	1	11.09	149.7	15.70	105.7	16	60
	2	729,994	279,451	0.1923	1	12.31	158.2	17.06	114.2	16	60
	4	648,195	79,164	0.1797	1	13.04	160.9	17.94	116.9	16	60
	7	723,619	22,823	0.1612	1	14.21	167.6	19.26	123.6	16	60
	12	908,037	1,404	0.1334	1	18.25	193.0	23.64	149.0	16	60

Table 21.11 Dynamic Shear Modulus and Shift Function Parameters
BI 0003 Holly Frontier

Aging Conditions		CAS Parameters				WLF		Kaelble			
Temp.	Dur. (days)	G_0 (kPa)	ω_0 (rad/s)	β	κ	C_1	C_2	C_1	C_2	T_k (°C)	T_r (°C)
Orig.	Orig.	1,083,623	6,552,617	0.1859	1	8.96	143.1	12.94	99.1	16	60
50°C	4	379,715	1,152,835	0.1999	1	10.44	153.7	14.63	109.7	16	60
	8	289,325	722,040	0.2058	1	10.47	152.3	14.72	108.3	16	60
	15	244,392	438,378	0.2049	1	10.77	153.1	15.11	109.1	16	60
	30	240,510	309,589	0.2038	1	11.26	156.3	15.68	112.3	16	60
	60	178,637	158,802	0.2077	1	11.90	158.9	16.46	114.9	16	60
	120	196,288	92,465	0.1943	1	13.26	168.2	17.96	124.2	16	60
	180	242,726	74,815	0.1853	1	14.42	176.6	19.20	132.6	16	60
	240	190,717	42,588	0.1876	1	14.30	173.7	19.15	129.7	16	60
60°C	2	382,683	1,208,279	0.1980	1	10.16	151.2	14.33	107.2	16	60
	4	257,358	625,139	0.2062	1	9.62	144.6	13.83	100.6	16	60
	8	186,847	334,493	0.2127	1	10.67	152.2	15.02	108.2	16	60
	15	191,626	230,377	0.2069	1	11.57	158.2	16.03	114.2	16	60
	30	221,475	157,247	0.1959	1	12.78	166.7	17.37	122.7	16	60
	60	189,211	63,006	0.1910	1	13.98	172.8	18.75	128.8	16	60
	100	219,312	32,675	0.1784	1	16.20	189.3	21.10	145.3	16	60
	160	213,176	12,591	0.1687	1	17.60	196.5	22.68	152.5	16	60
85°C	0.5	413,290	1,510,912	0.2001	1	9.97	150.0	14.11	106.0	16	60
	1	311,648	863,006	0.2033	1	10.13	150.2	14.33	106.2	16	60
	2	344,203	551,628	0.1912	1	11.11	157.5	15.41	113.5	16	60
	4	213,641	201,680	0.2020	1	11.83	160.3	16.30	116.3	16	60
	8	233,317	72,384	0.1811	1	13.74	173.5	18.41	129.5	16	60
	15	251,486	14,415	0.1596	1	17.16	196.4	22.11	152.4	16	60
	25	294,548	2,253	0.1392	1	18.14	199.4	20.92	147.0	16	60
	40	410,077	111	0.1140	1	20.31	210.9	23.10	157.5	22	60
100°C	0.083	1,341,609	6,038,489	0.1751	1	10.46	157.1	14.52	113.1	16	60
	0.25	476,473	1,777,386	0.1959	1	9.87	149.5	13.99	105.5	16	60
	0.5	388,722	1,143,124	0.1958	1	10.59	155.3	14.78	111.3	16	60
	1	257,374	465,781	0.2024	1	10.92	156.9	15.18	112.9	16	60
	2	239,099	170,639	0.1882	1	12.56	167.1	17.05	123.1	16	60
	4	252,963	55,081	0.1717	1	13.89	174.8	18.56	130.8	16	60
	7	352,897	7,960	0.1429	1	17.67	201.4	22.61	157.4	16	60
	12	613,612	252	0.1088	1	19.62	211.1	24.78	167.1	16	60

Table 21.12 Dynamic Shear Modulus and Shift Function Parameters
BI 0004 Shelly

Aging Conditions		CAS Parameters				WLF		Kaelble			
Temp.	Dur. (day)	G_0 (kPa)	ω_0 (rad/s)	β	κ	C_1	C_2	C_1	C_2	T_k (°C)	T_r (°C)
Orig.	Orig.	79,084,020	24,093,270	0.1021	1	9.96	151.5	14.44	112.2	16	60
50°C	4	29,282,810	3,227,769	0.1010	1	11.17	158.6	15.80	118.5	16	60
	8	15,419,490	1,515,903	0.1054	1	11.55	161.3	16.27	121.5	16	60
	15	14,054,150	761,117	0.1025	1	11.92	164.3	17.34	131.8	16	60
	30	9,641,205	427,161	0.1055	1	12.72	167.1	16.88	119.1	16	60
	60	4,845,614	144,098	0.1099	1	13.06	168.5	18.02	128.0	16	60
	120	2,706,760	67,486	0.1192	1	13.55	171.1	18.22	126.9	16	60
	180	1,714,019	44,070	0.1267	1	13.65	167.1	18.06	118.6	16	60
	240	1,372,145	22,735	0.1268	1	13.96	168.6	18.76	123.2	16	60
60°C	2	47,805,760	5,029,695	0.0981	1	11.17	159.4	15.41	115.2	16	60
	4	21,608,840	1,966,486	0.1021	1	11.45	160.7	16.37	123.2	16	60
	8	12,501,980	698,515	0.1037	1	12.38	168.3	17.25	129.4	16	60
	15	6,979,553	269,664	0.1071	1	12.61	167.3	17.70	129.5	16	60
	30	3,730,576	102,788	0.1137	1	13.34	169.8	18.31	128.8	16	60
	60	2,253,350	36,878	0.1172	1	13.65	169.0	18.63	126.7	16	60
	100	1,512,822	14,357	0.1214	1	14.51	173.7	19.22	127.7	16	60
	160	710,867	4,614	0.1338	1	15.93	181.3	18.71	129.2	16	60
85°C	0.5	55,231,290	6,023,100	0.0974	1	10.98	158.4	15.68	119.8	22	60
	1	24,360,420	2,116,152	0.1021	1	11.75	163.9	16.29	122.4	16	60
	2	11,472,710	584,810	0.1036	1	12.46	168.2	17.17	127.4	16	60
	4	7,416,126	194,031	0.1054	1	13.73	172.7	18.32	133.9	16	60
	8	3,297,701	42,978	0.1104	1	13.97	174.5	18.81	131.7	16	60
	15	1,410,789	6,628	0.1159	1	15.13	181.8	20.80	145.9	16	60
	25	974,944	2,151	0.1189	1	16.04	184.8	21.62	146.1	16	60
	40	552,113	110	0.1167	1	20.32	211.1	23.02	156.9	16	60
100°C	0.083	216,952,600	23,353,420	0.0880	1	10.81	158.4	15.54	120.9	16	60
	0.25	51,853,430	6,530,375	0.0993	1	11.08	160.6	16.03	125.4	16	60
	0.5	16,527,230	1,777,746	0.1060	1	11.41	161.2	15.98	120.3	16	60
	1	16,567,840	697,729	0.0996	1	11.82	163.3	17.24	130.7	16	60
	2	6,078,298	158,580	0.1065	1	13.40	174.5	18.43	135.7	16	60
	4	2,599,296	16,758	0.1093	1	14.95	182.7	20.37	145.3	16	60
	7	1,654,897	3,057	0.1077	1	16.16	187.9	21.41	146.8	16	60
	12	1,051,157	130	0.1032	1	19.78	211.8	24.70	165.4	16	60

22 APPENDIX J:

Hardening Susceptibility Relationships of Pan-Aged Binders Based Upon Carbonyl Area

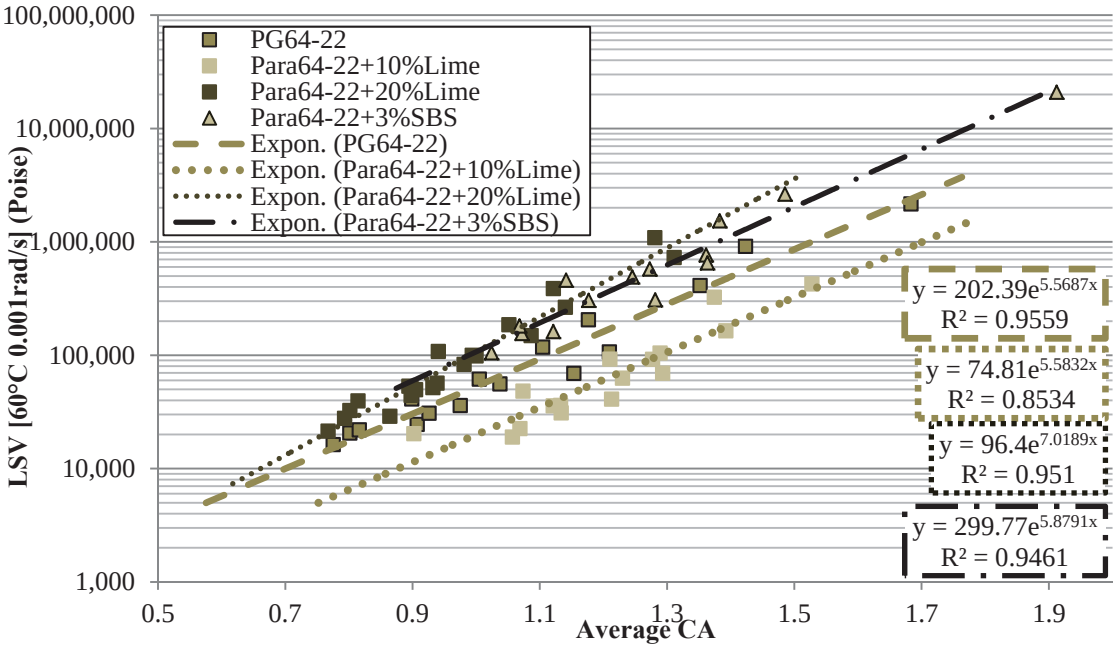

Figure 22.1 Hardening Susceptibility Relationships for PG 64-22 and Associated Binders

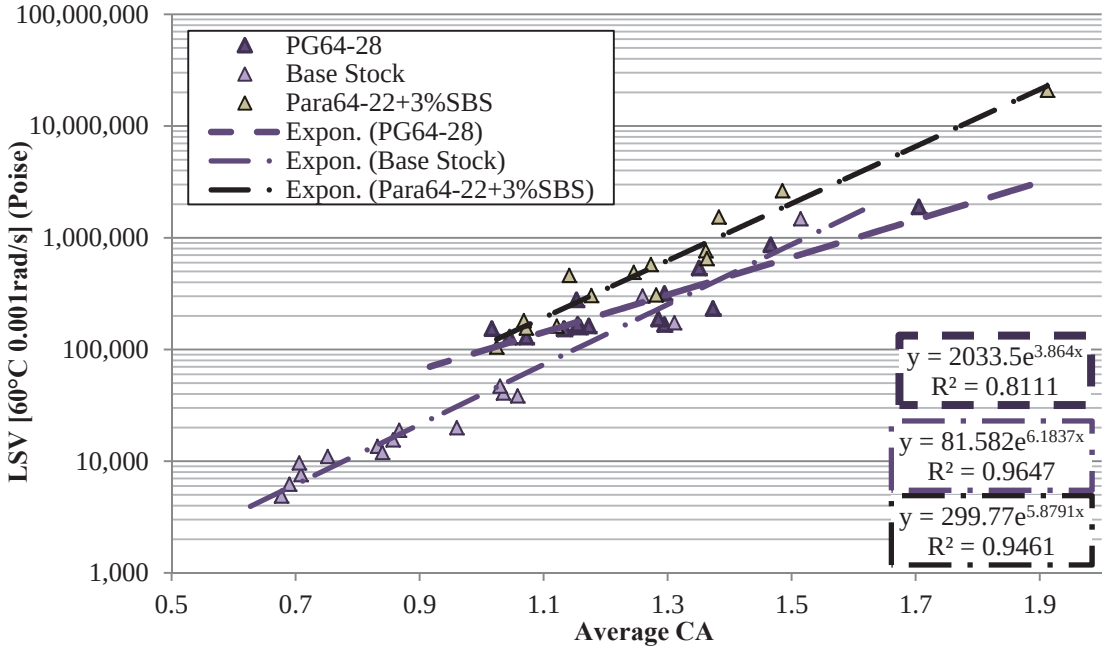

Figure 22.2 Hardening Susceptibility Relationships for PG 64-28 and Associated Binders

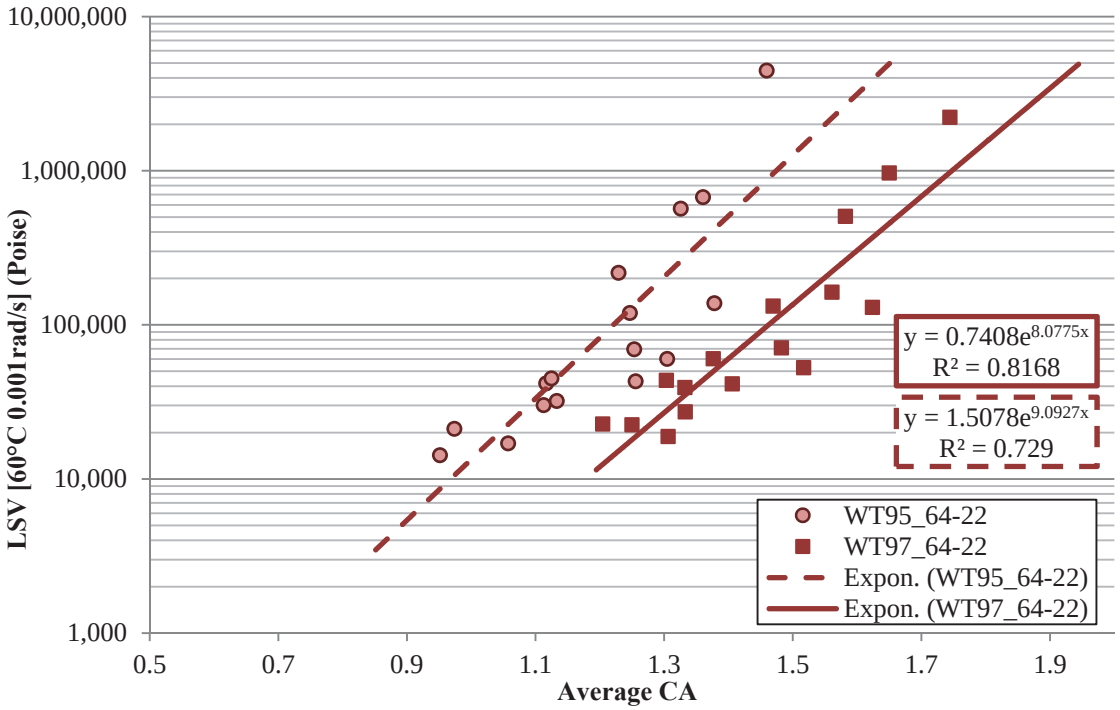

Figure 22.3 Hardening Susceptibility Relationships for WesTrack PG 64-22 Binders

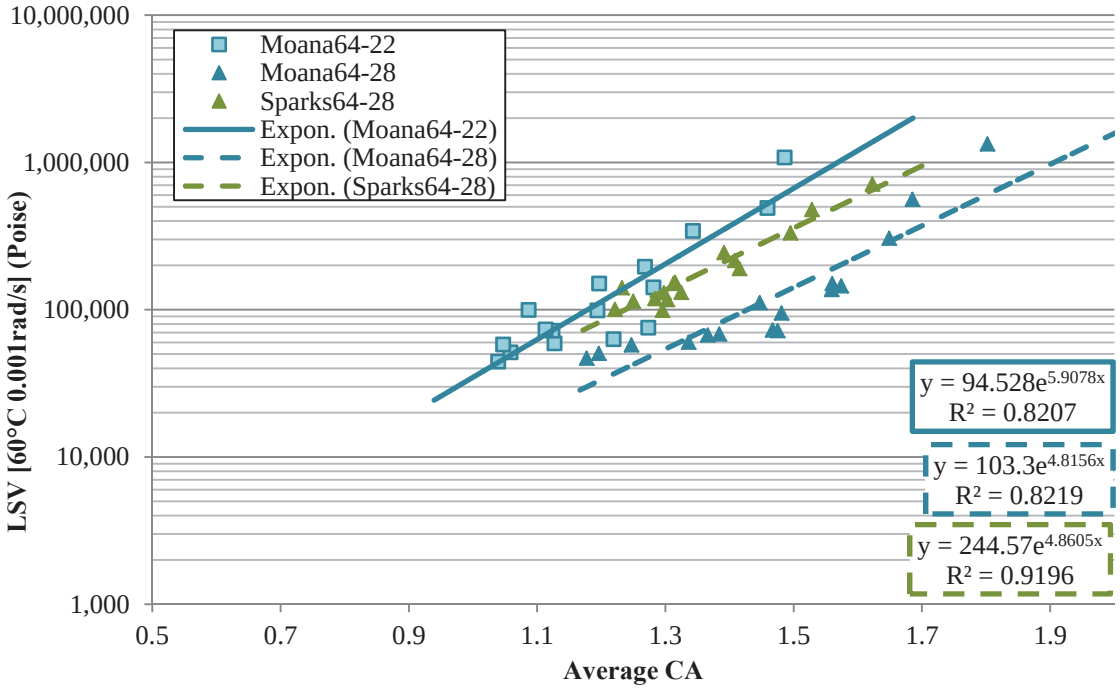

Figure 22.4 Hardening Susceptibility Relationships for Moana Lane and Sparks Blvd. Binders

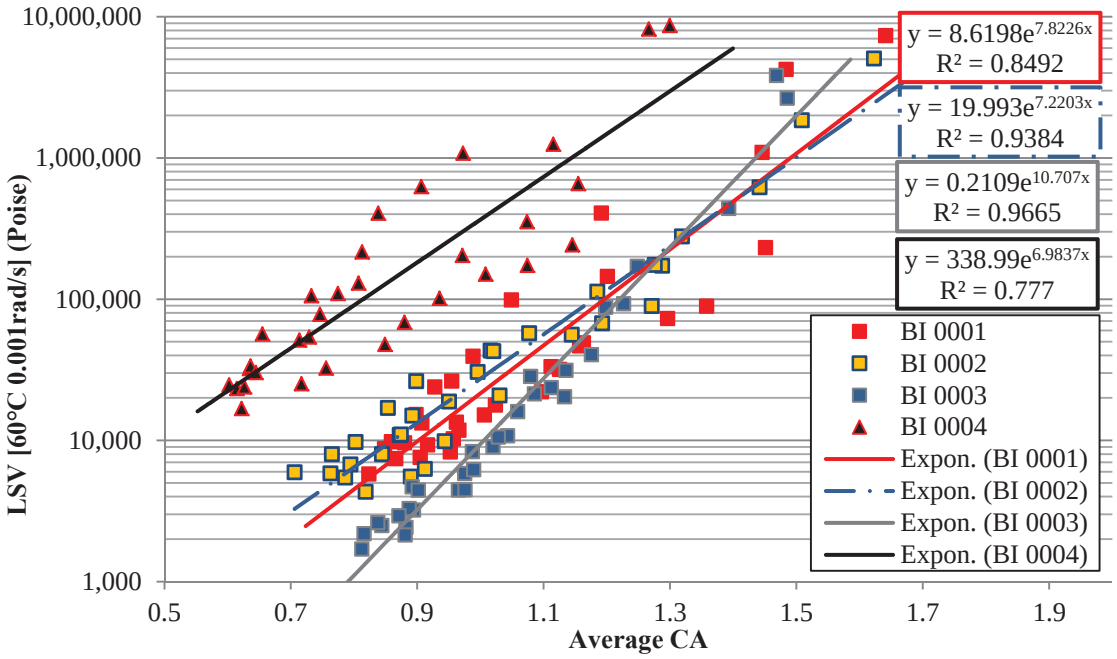

Figure 22.5 Hardening Susceptibility Relationships for ARC Core Binders

Table 22.1 Hardening Susceptibility Parameters of Pan-Aged Binders

Asphalt Binder ID	Hardening Susceptibility[a], HS	Intercept[a], m_{Tank}	Intercept[a], m
PG64-22	5.5687	8.0722	5.3102
PG64-22 +10% Lime	5.5832	8.2762	4.3150
PG64-22 +20% Lime	7.0189	8.7424	4.5685
PG64-22 + 3% SBS	5.8791	10.2769	5.7030
PG64-28	3.8640	10.3359	7.6175
Base Stock	6.1837	7.0823	4.4016
WT95-22	9.0927	7.7727	0.4107
WT97-22	8.0775	4.9988	-0.3000
Moana 22	5.9078	9.5351	4.5489
Moana 28	4.8156	7.6739	4.6376
Sparks 28	4.8605	10.8436	5.4995
BI 0001 PG67-22	7.8226	6.6990	2.1541
BI 0002 PG64-16	7.2203	7.7825	2.9954
BI 0003 PG58-28	10.707	6.5774	-1.5564
BI 0004 PG70-22	6.9837	9.8975	5.8260

a – Reported values are based upon η_0^* reported in Poise.

23 APPENDIX K:

Summary of Dynamic Shear Modulus and Black Space Plots for Mixture-Aged Asphalt Binders

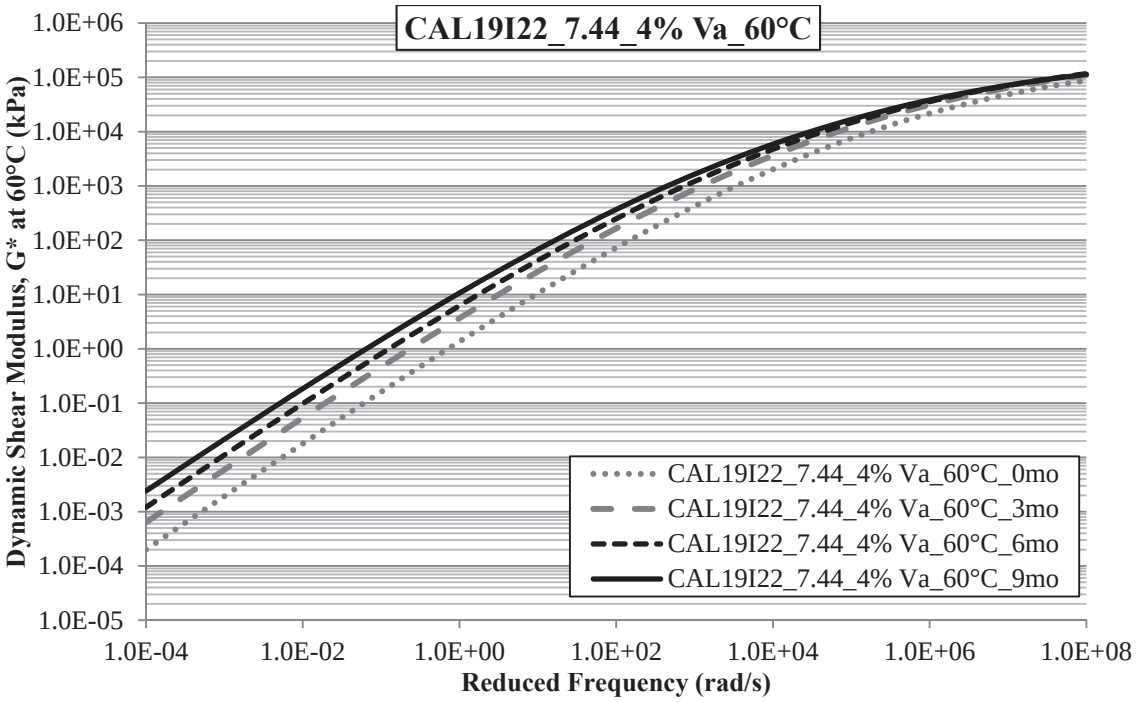

Figure 23.1 Summary of CAL19I22_7.44_4% Va Aged at 60°C Dynamic Shear Modulus Master Curves

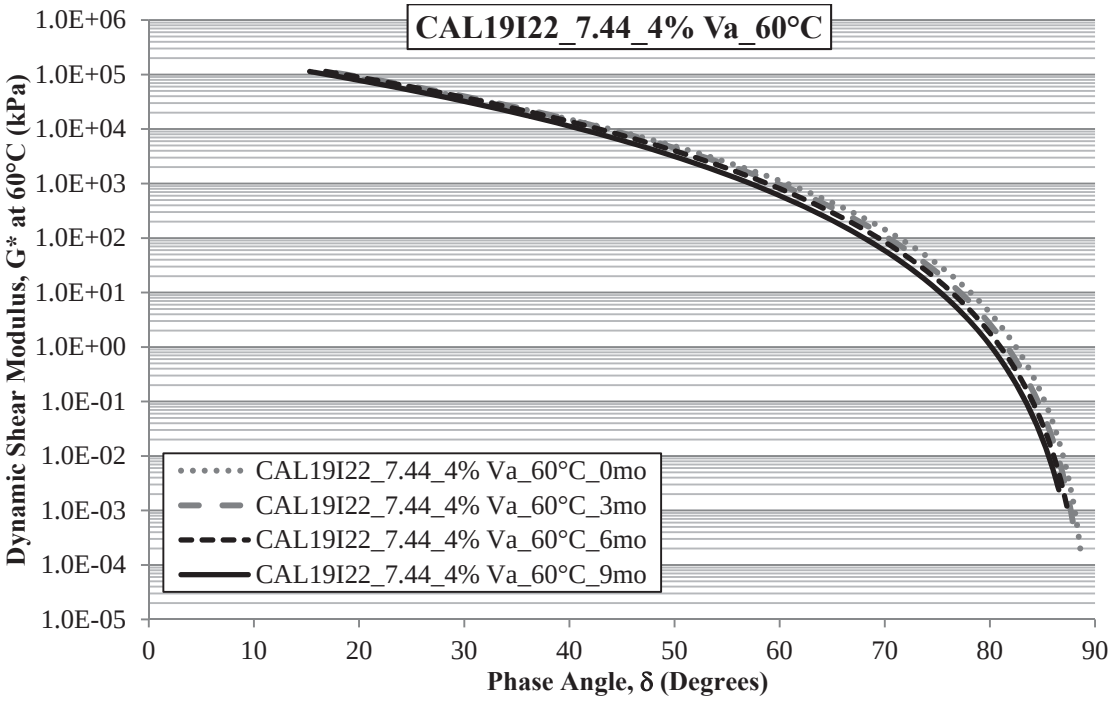

Figure 23.2 Summary of CAL19I22_7.44_4% Va Aged at 60°C Black Space Plots

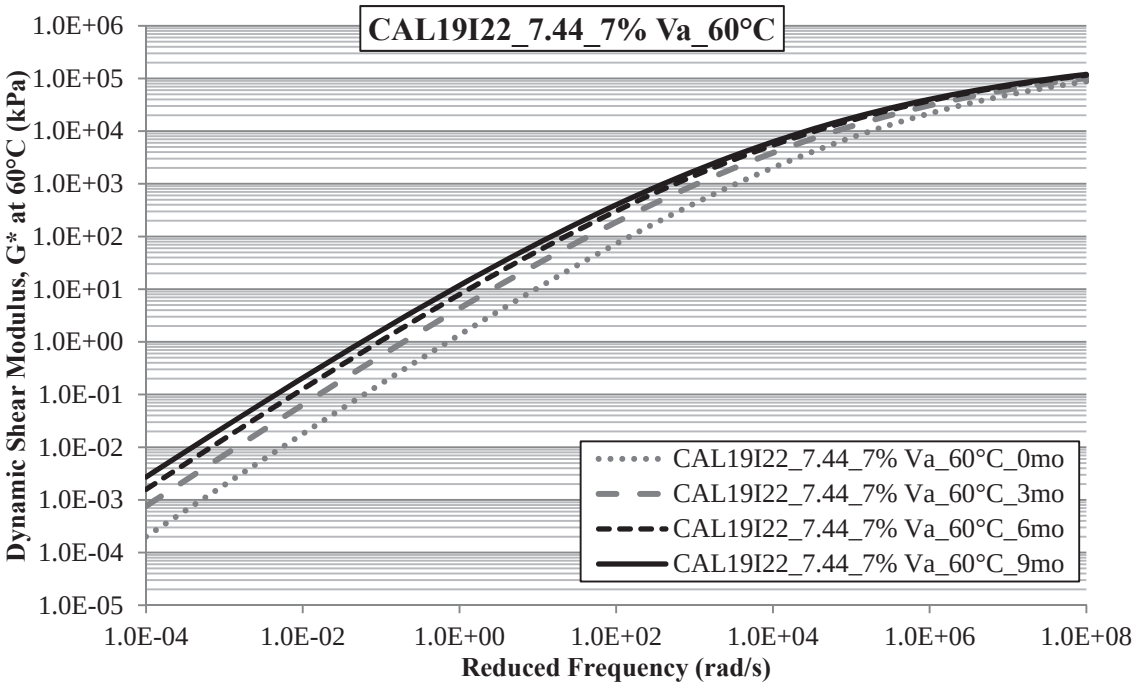

Figure 23.3 Summary of CAL19I22_7.44_7% Va Aged at 60°C Dynamic Shear Modulus Master Curves

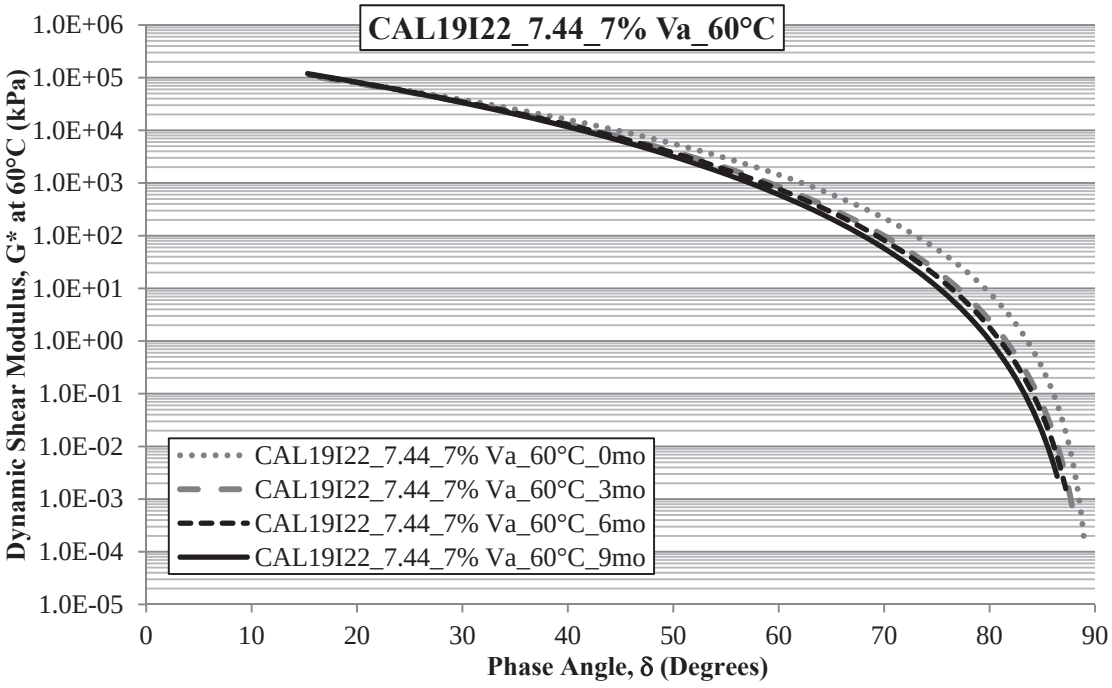

Figure 23.4 Summary of CAL19I22_7.44_7% Va Aged at 60°C Black Space Plots

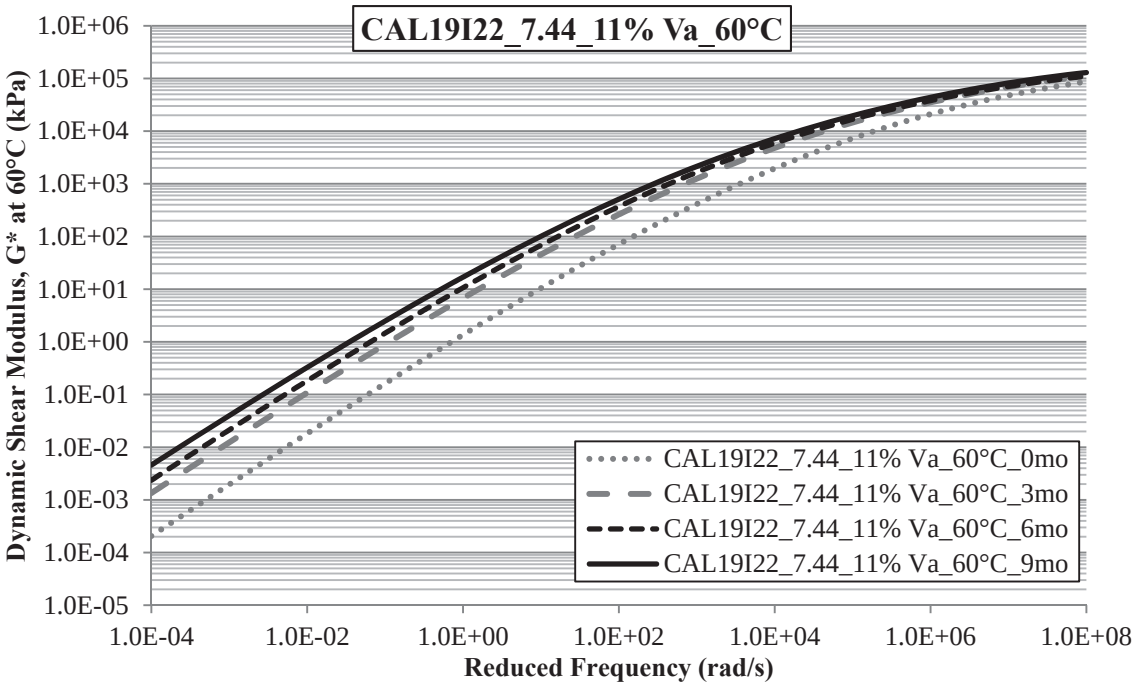

Figure 23.5 Summary of CAL19I22_7.44_11% Va Aged at 60°C Dynamic Shear Modulus Master Curves

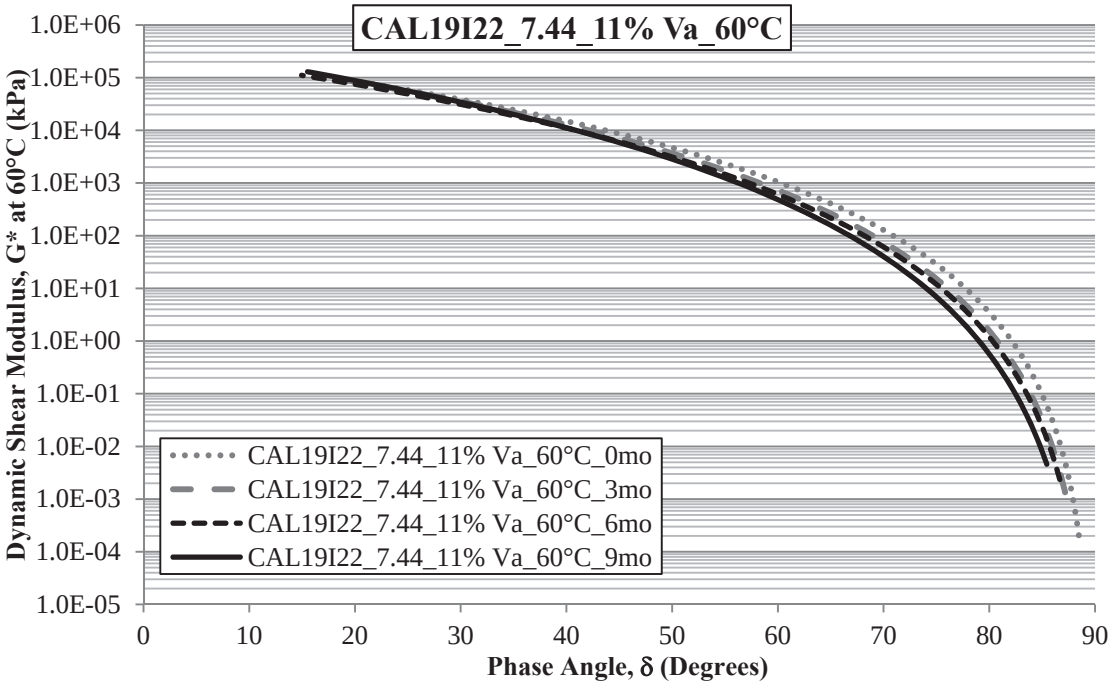

Figure 23.6 Summary of CAL19I22_7.44_11% Va Aged at 60°C Black Space Plots

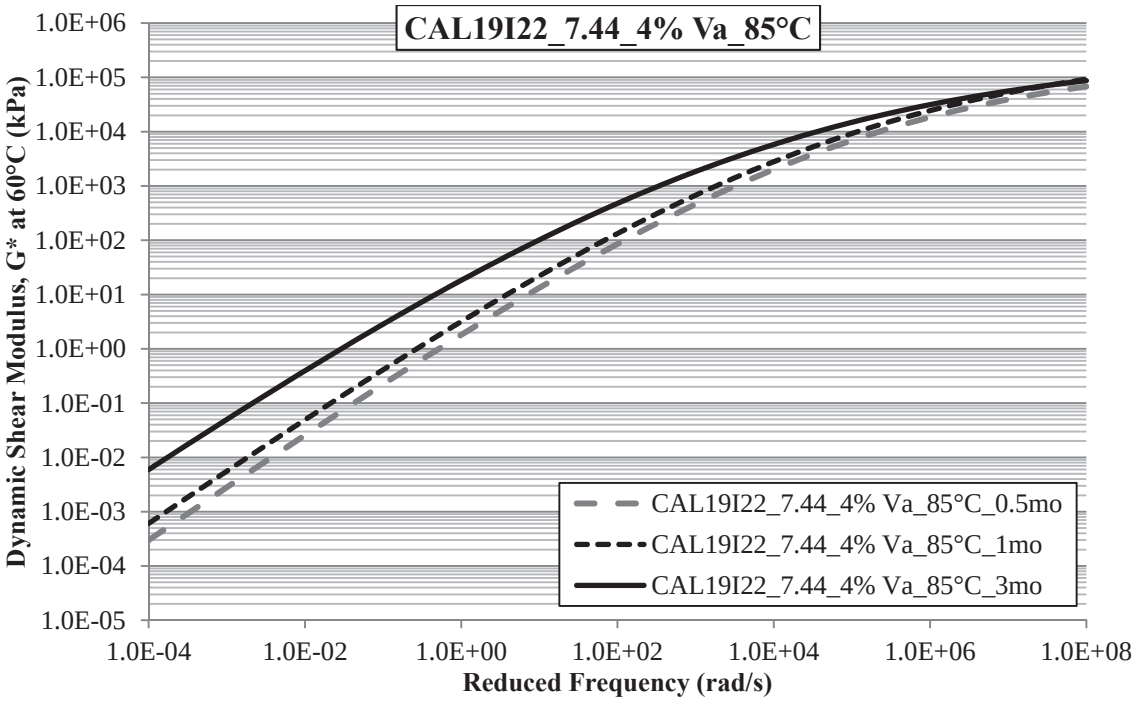

Figure 23.7 Summary of CAL19I22_7.44_4% Va Aged at 85°C Dynamic Shear Modulus Master Curves

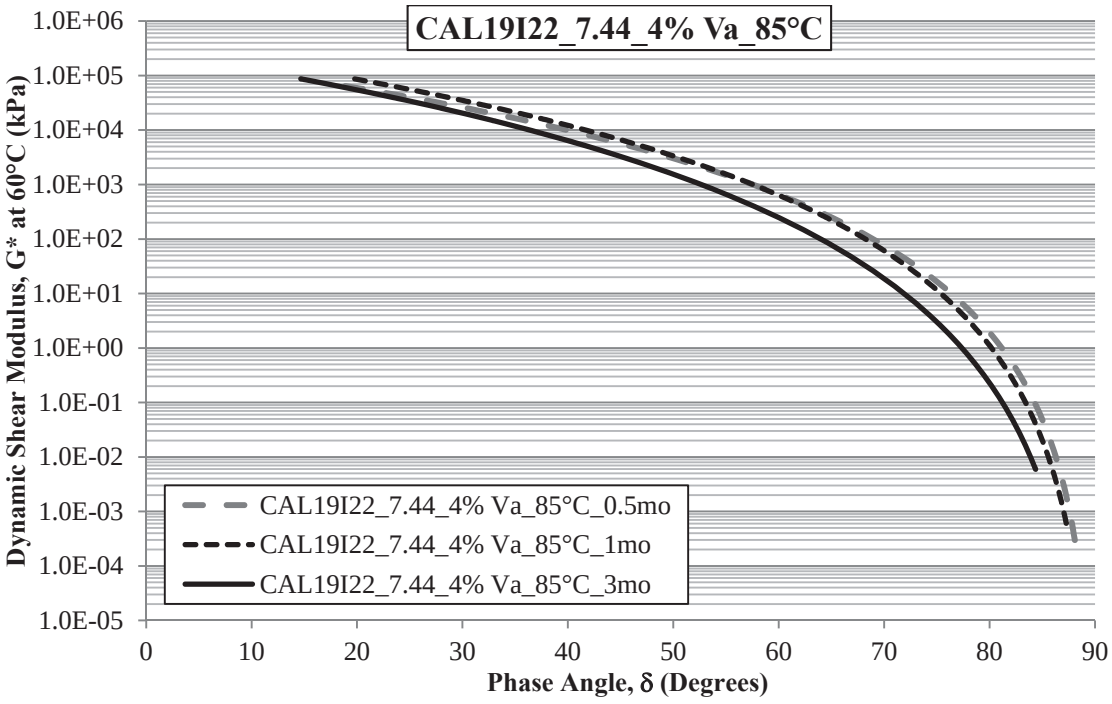

Figure 23.8 Summary of CAL19I22_7.44_4% Va Aged at 85°C Black Space Plots

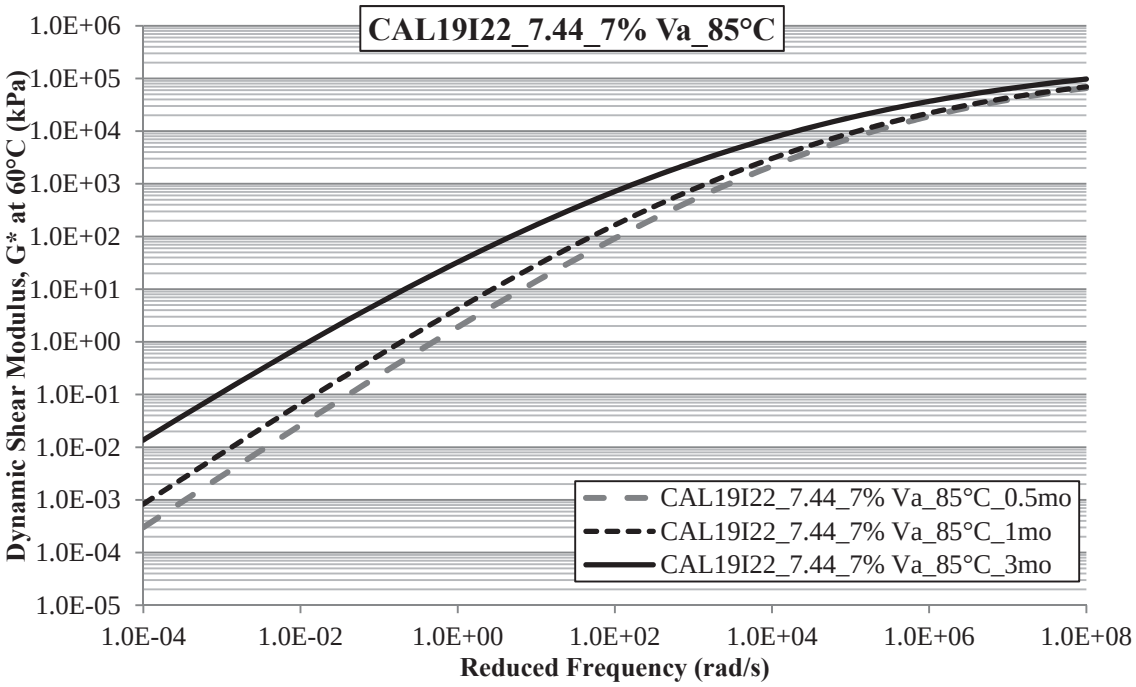

Figure 23.9 Summary of CAL19I22_7.44_7% Va Aged at 85°C Dynamic Shear Modulus Master Curves

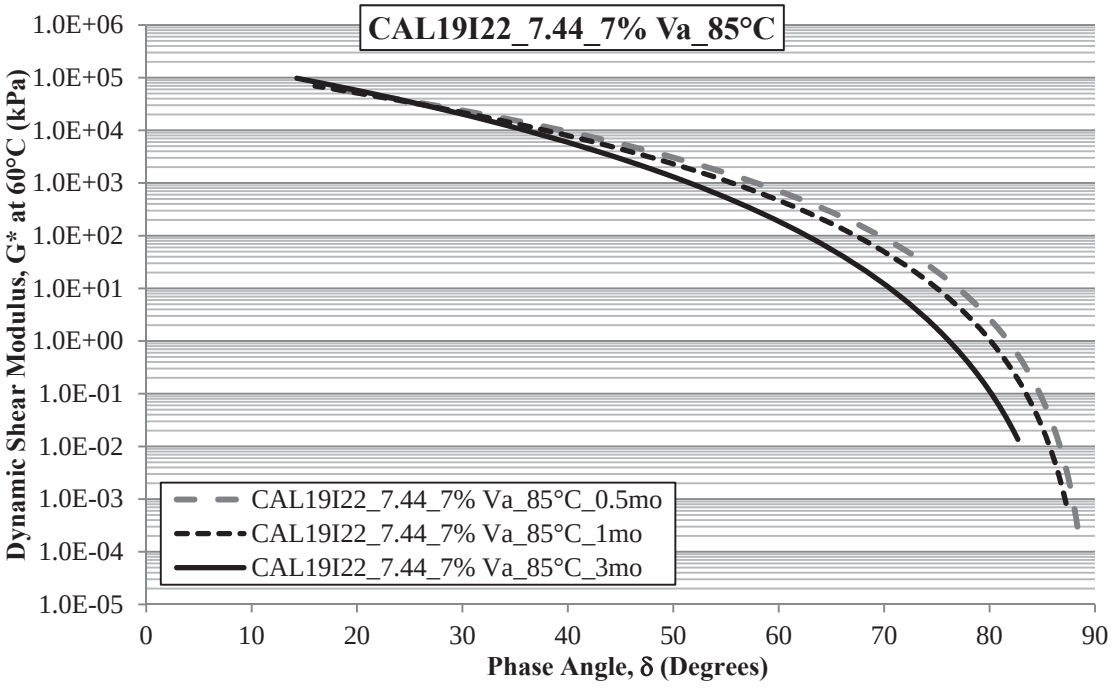

Figure 23.10 Summary of CAL19I22_7.44_7% Va Aged at 85°C Black Space Plots

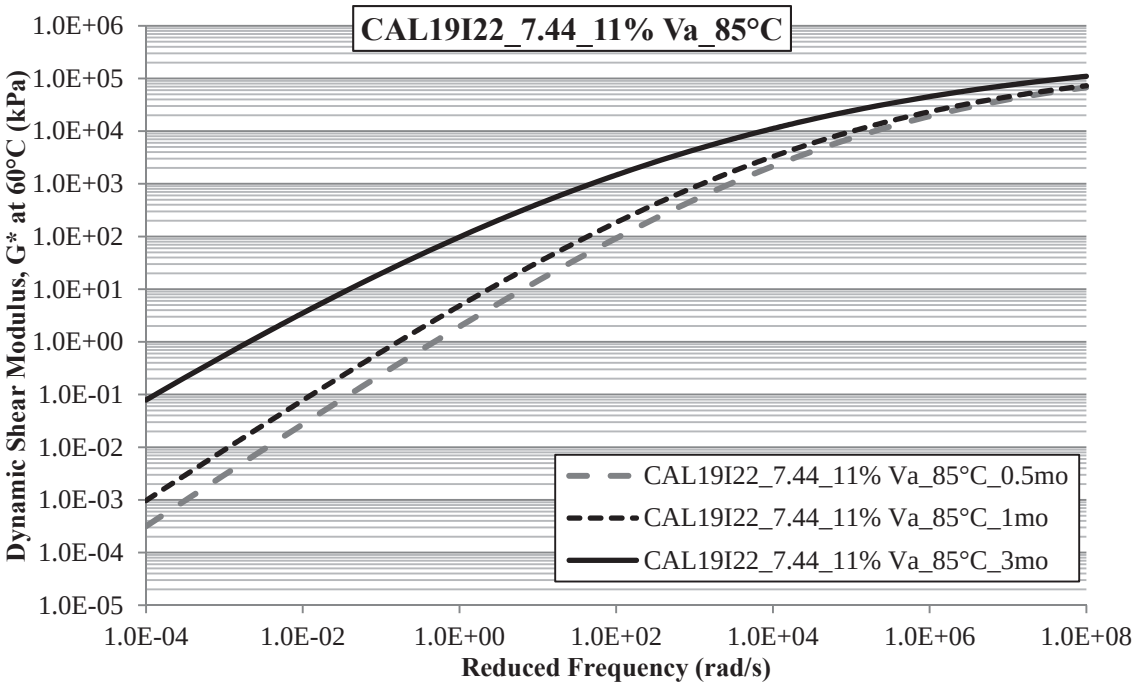

Figure 23.11 Summary of CAL19I22_7.44_11% Va Aged at 85°C Dynamic Shear Modulus Master Curves

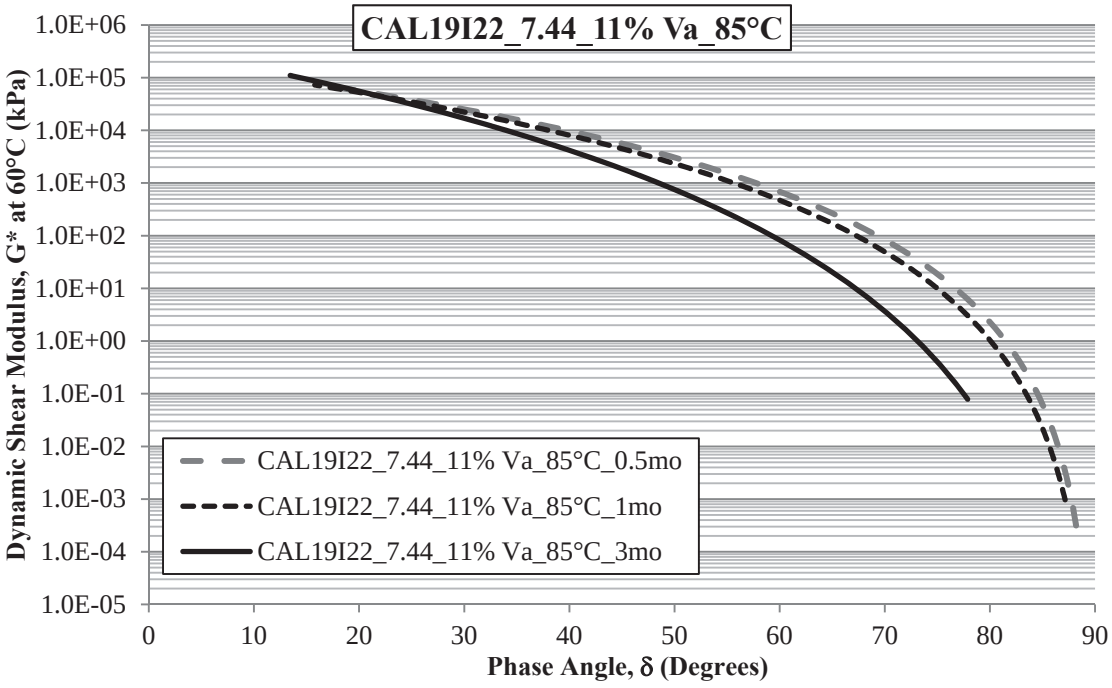

Figure 23.12 Summary of CAL19I22_7.44_11% Va Aged at 85°C Black Space Plots

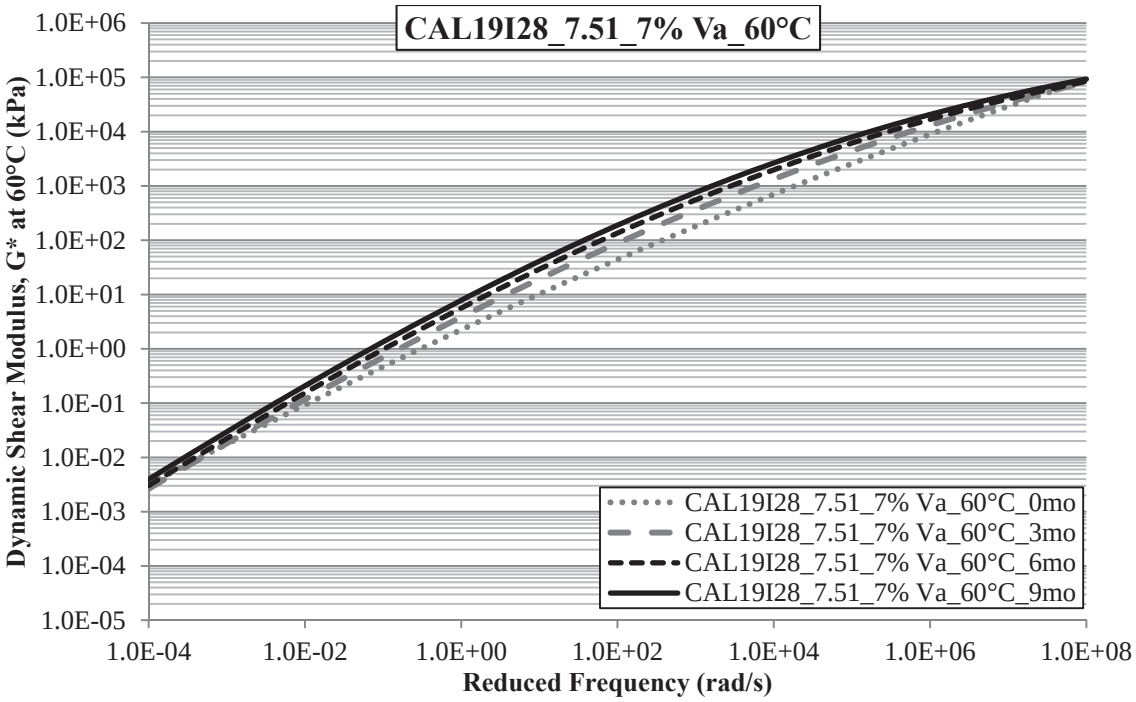

Figure 23.13 Summary of CAL19I28_7.51_7% Va Aged at 60°C Dynamic Shear Modulus Master Curves

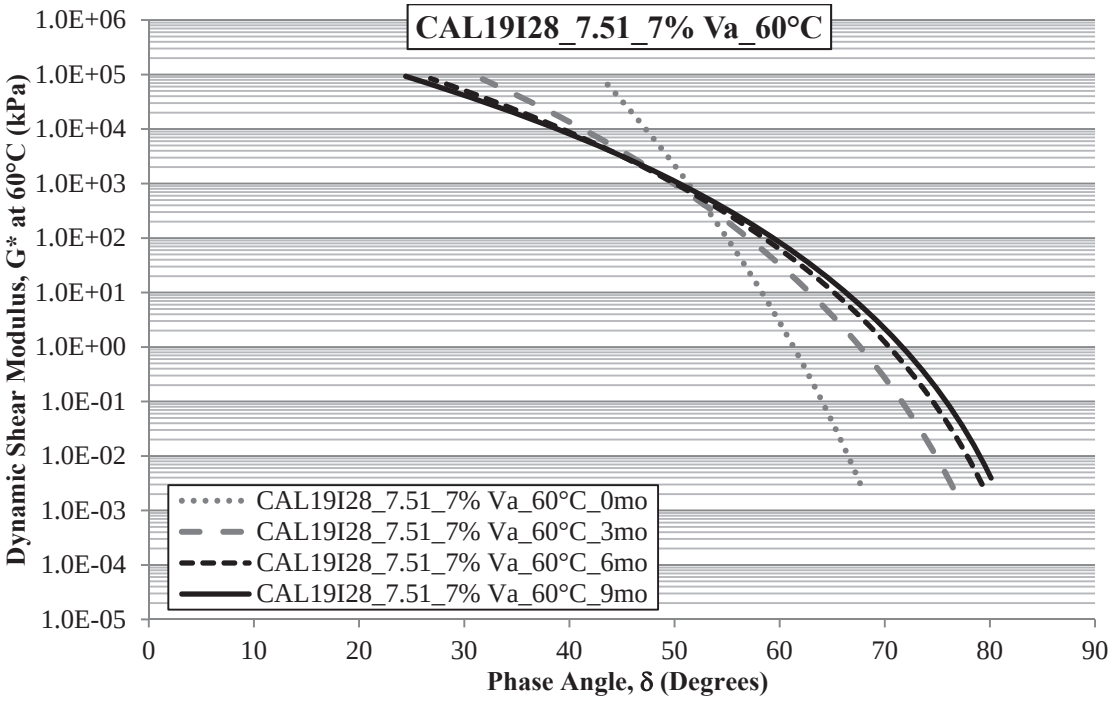

Figure 23.14 Summary of CAL19I28_7.51_7% Va Aged at 60°C Black Space Plots

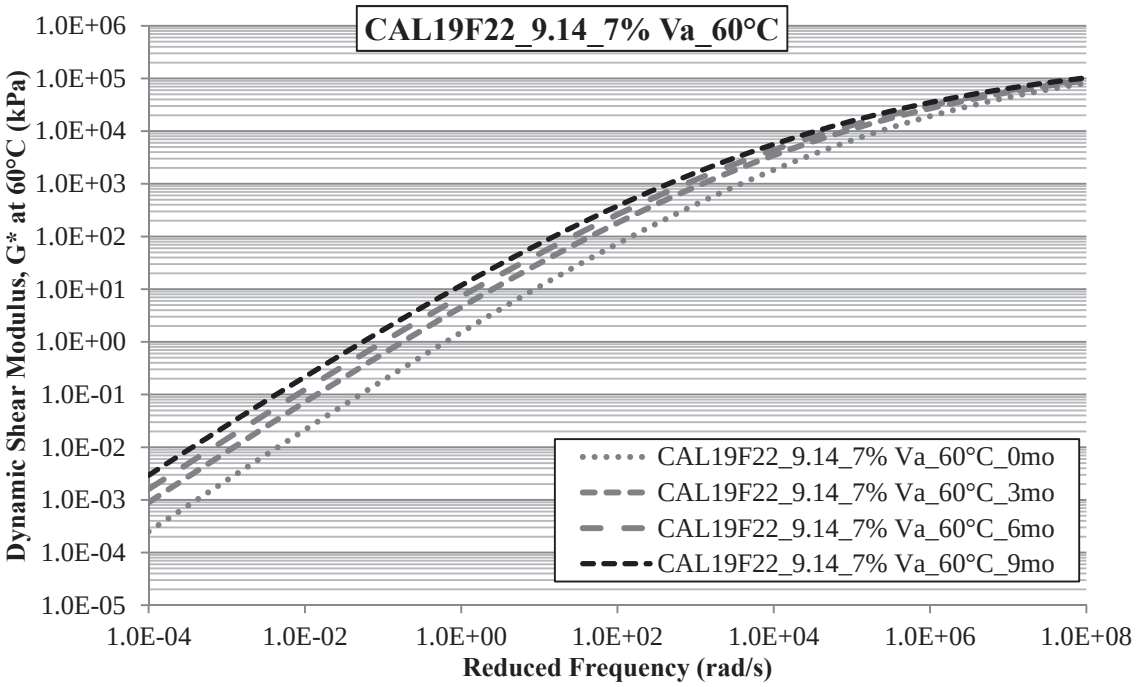

Figure 23.15 Summary of CAL19F22_9.14_7% Va Aged at 60°C Dynamic Shear Modulus Master Curves

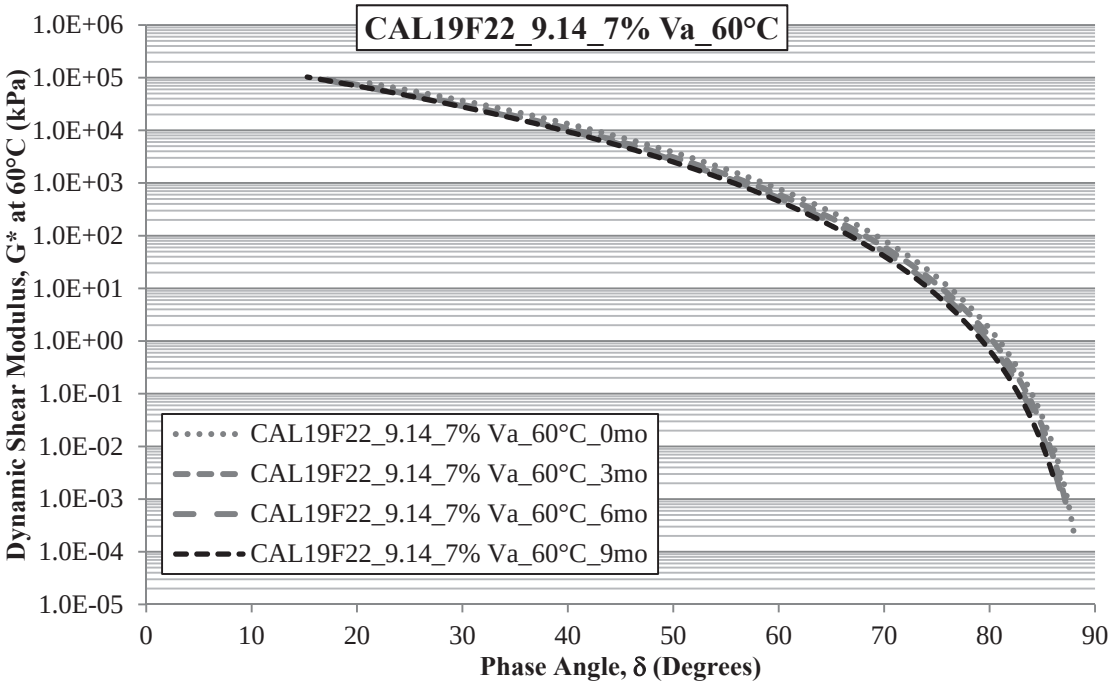

Figure 23.16 Summary of CAL19F22_9.14_7% Va Aged at 60°C Black Space Plots

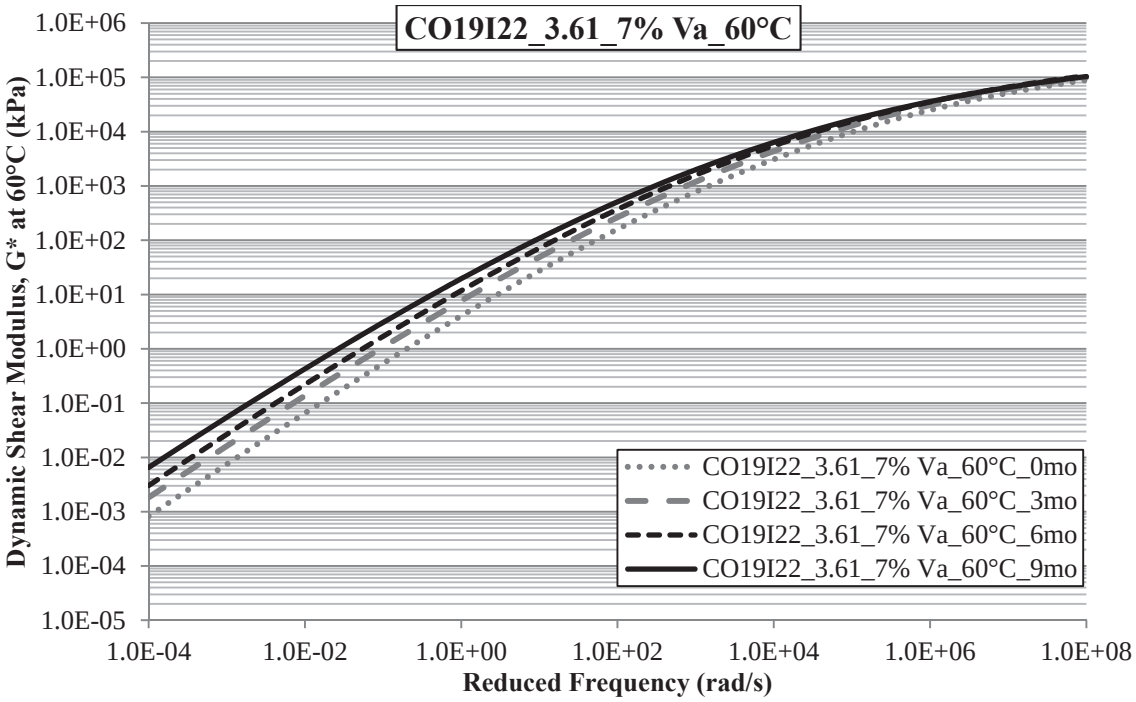

Figure 23.17 Summary of CO19I22_3.61_7% Va Aged at 60°C Dynamic Shear Modulus Master Curves

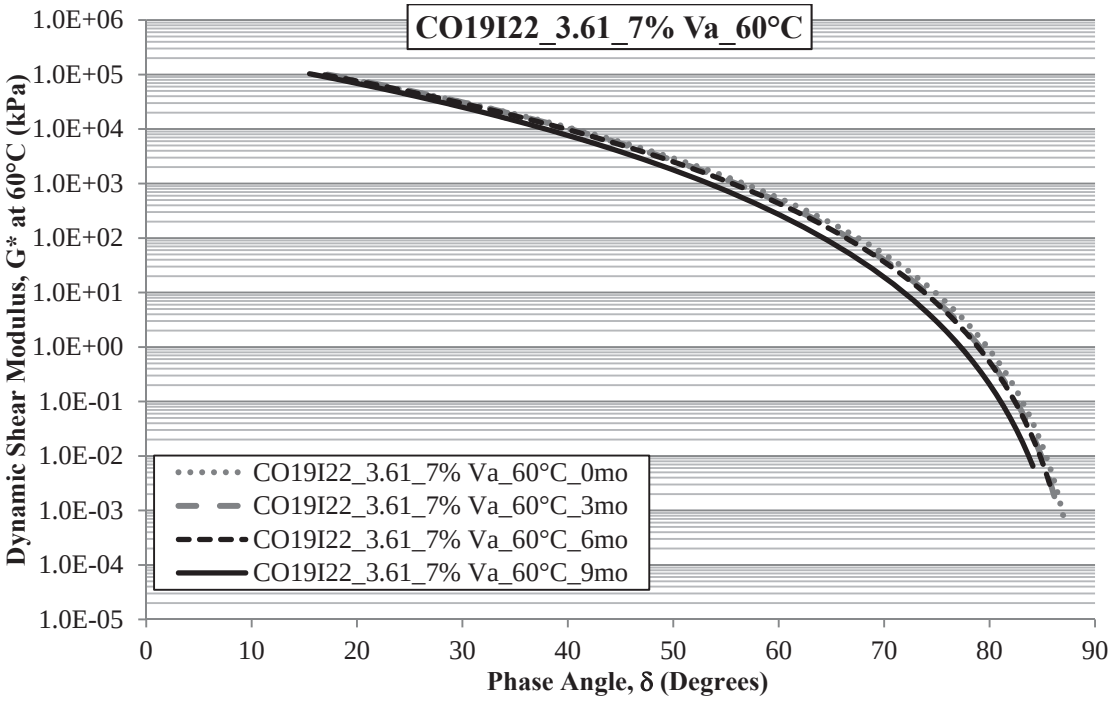

Figure 23.18 Summary of CO19I22_3.61_7% Va Aged at 60°C Black Space Plots

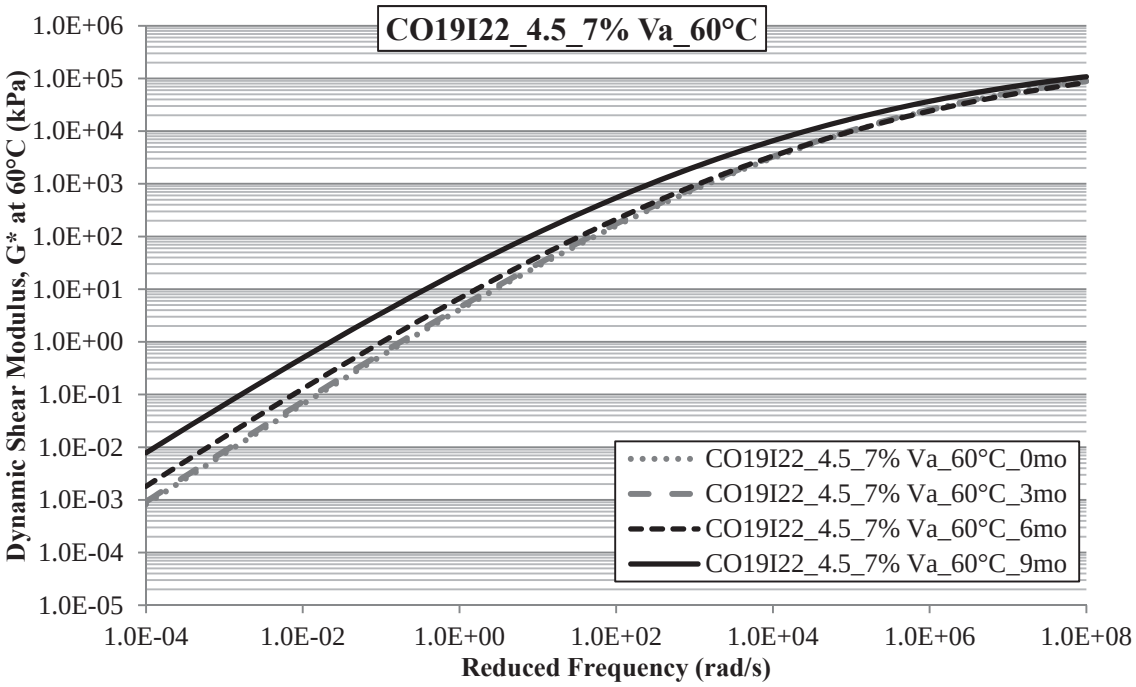

Figure 23.19 Summary of CO19I22_4.5_7% Va Aged at 60°C Dynamic Shear Modulus Master Curves

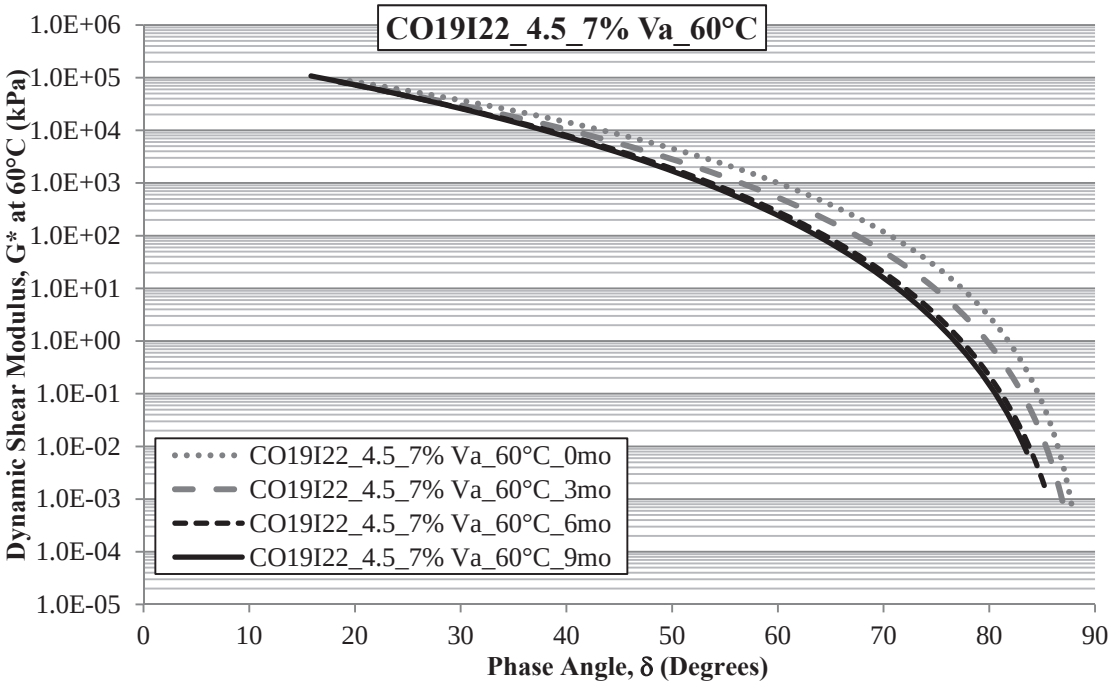

Figure 23.20 Summary of CO19I22_4.5_7% Va Aged at 60°C Black Space Plots

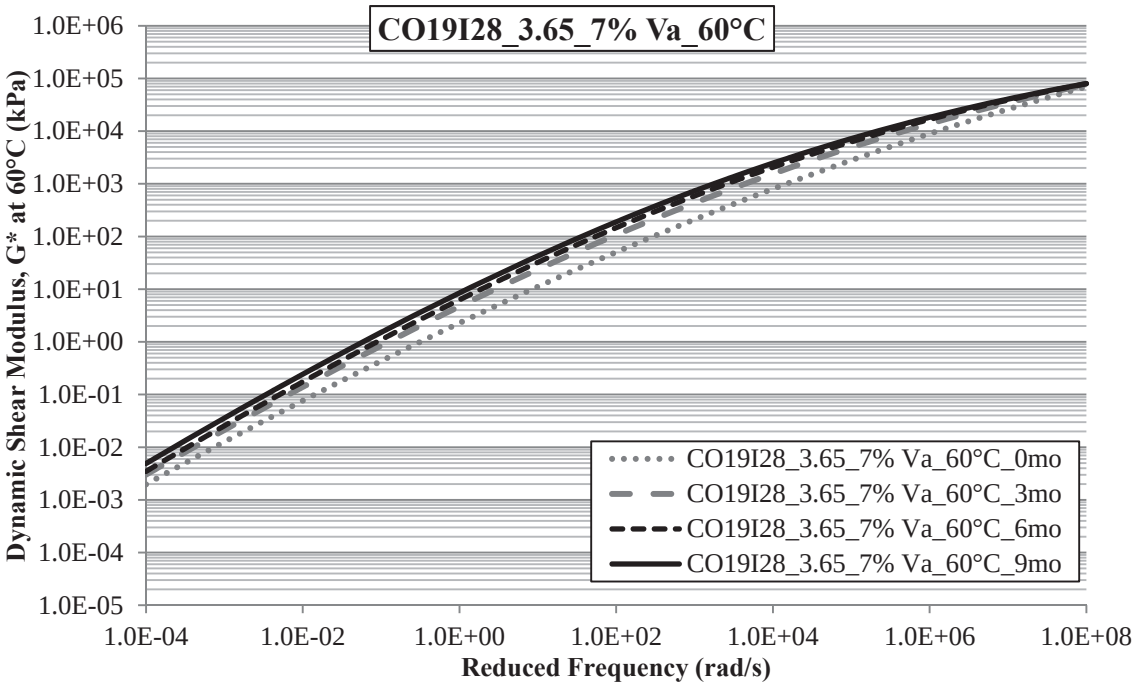

Figure 23.21 Summary of CO19I28_3.65_7% Va Aged at 60°C Dynamic Shear Modulus Master Curves

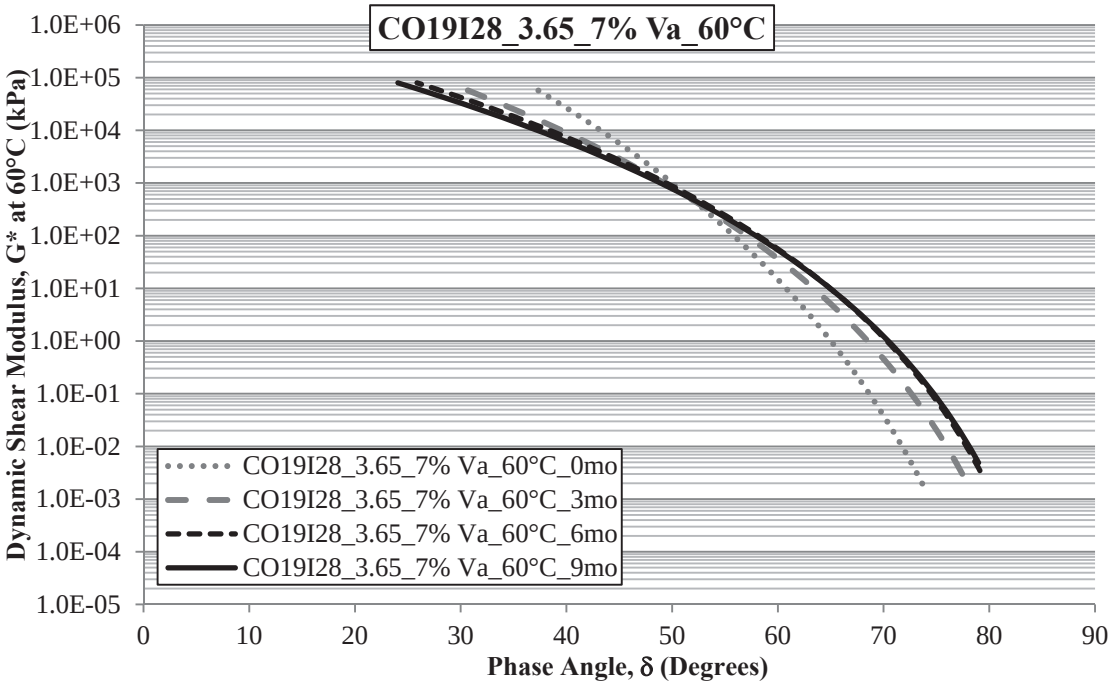

Figure 23.22 Summary of CO19I28_3.65_7% Va Aged at 60°C Black Space Plots

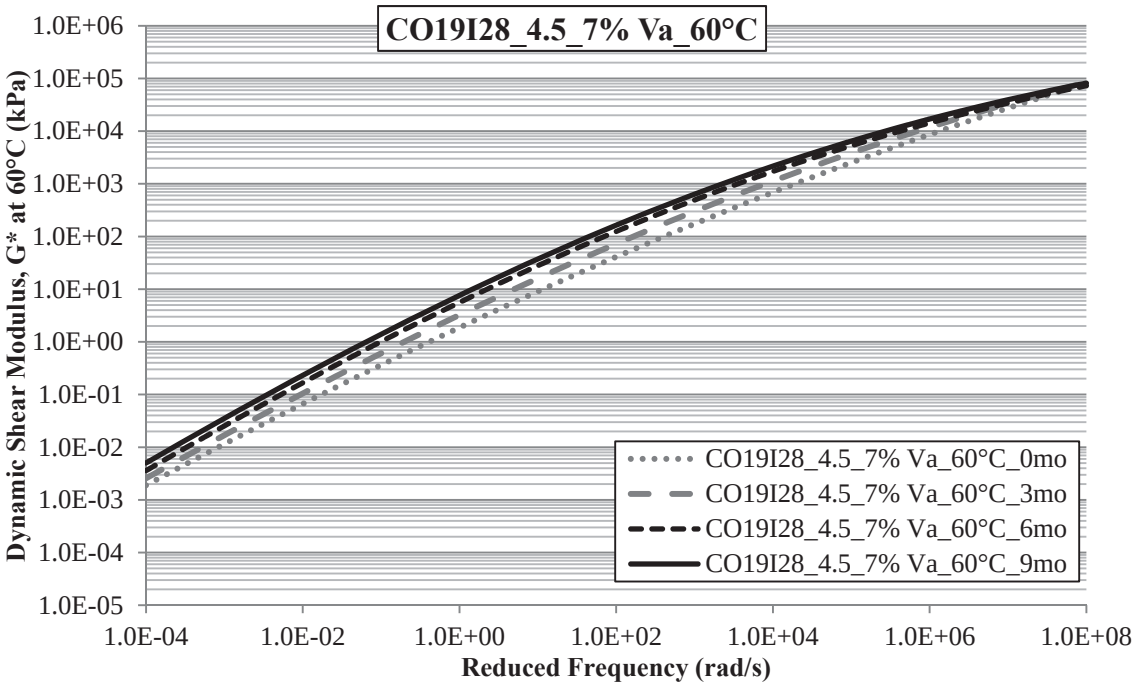

Figure 23.23 Summary of CO19I28_4.5_7% Va Aged at 60°C Dynamic Shear Modulus Master Curves

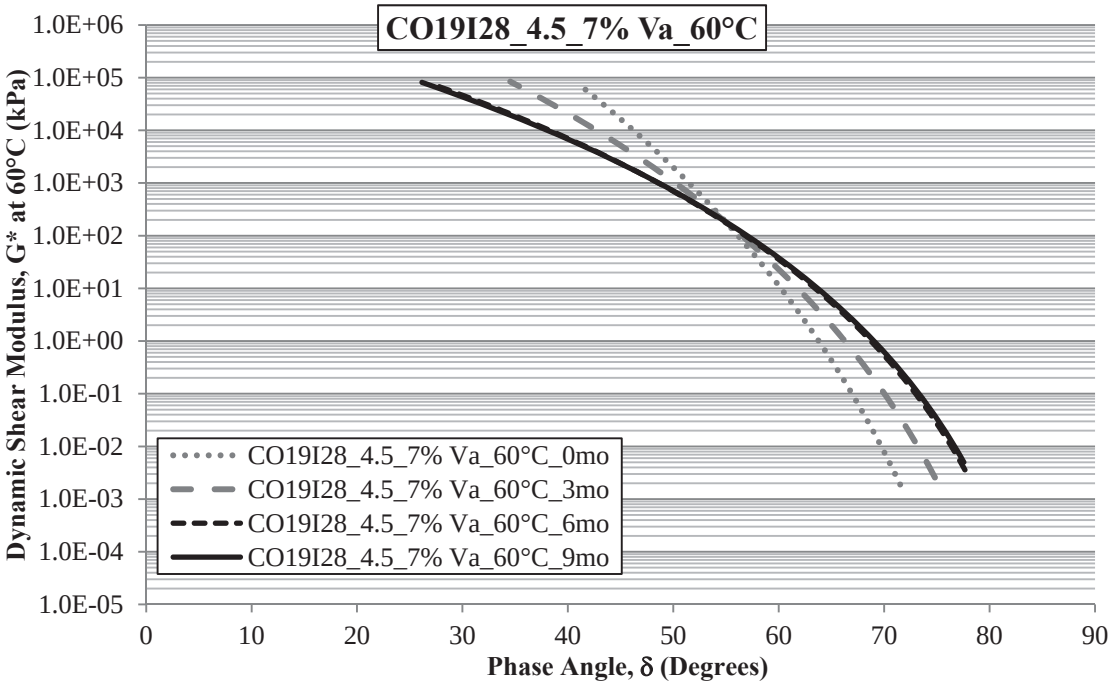

Figure 23.24 Summary of CO19I28_4.5_7% Va Aged at 60°C Black Space Plots

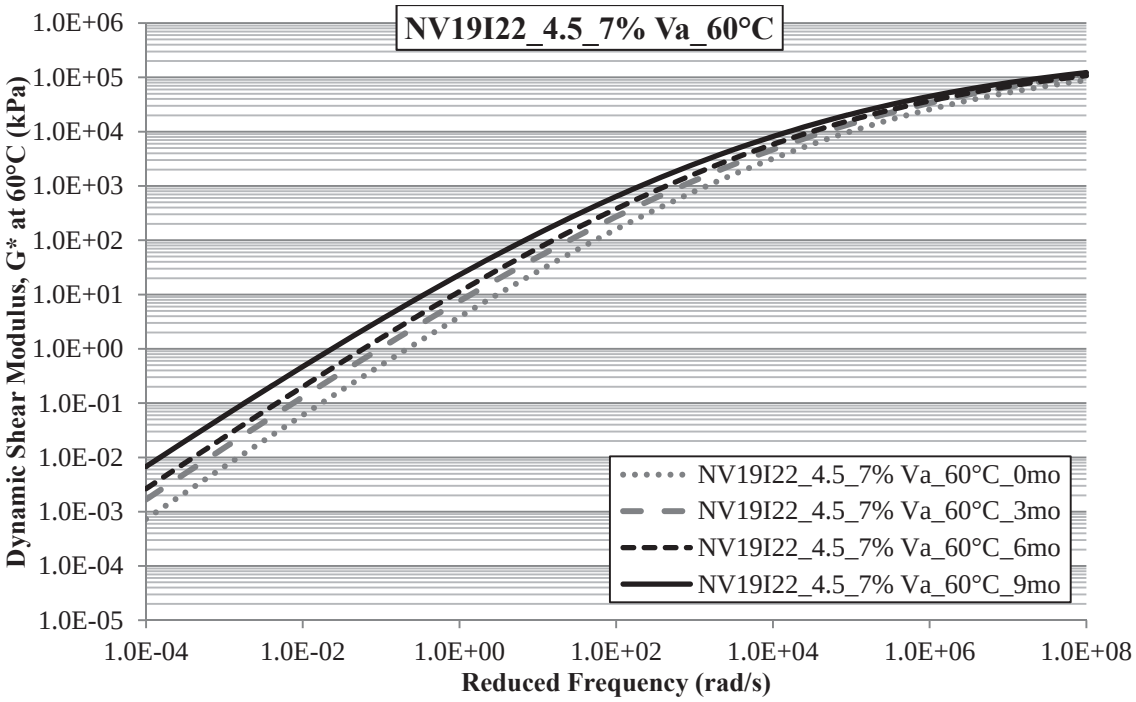

Figure 23.25 Summary of NV19I22_4.5_7% Va Aged at 60°C Dynamic Shear Modulus Master Curves

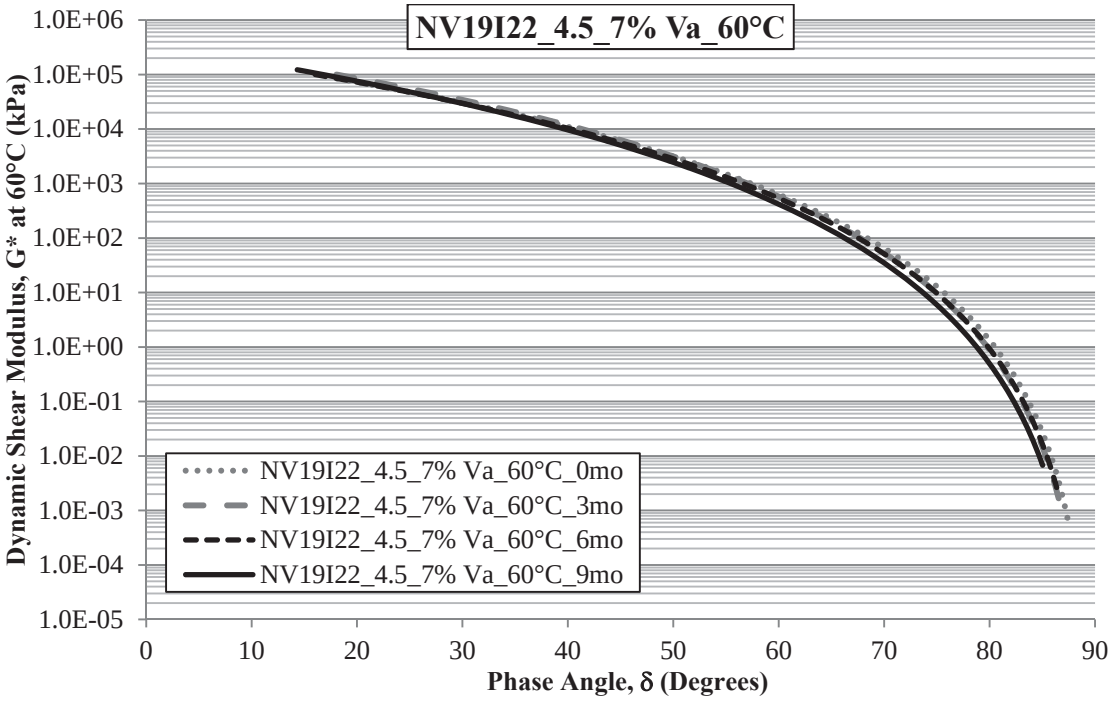

Figure 23.26 Summary of NV19I22_4.5_7% Va Aged at 60°C Black Space Plots

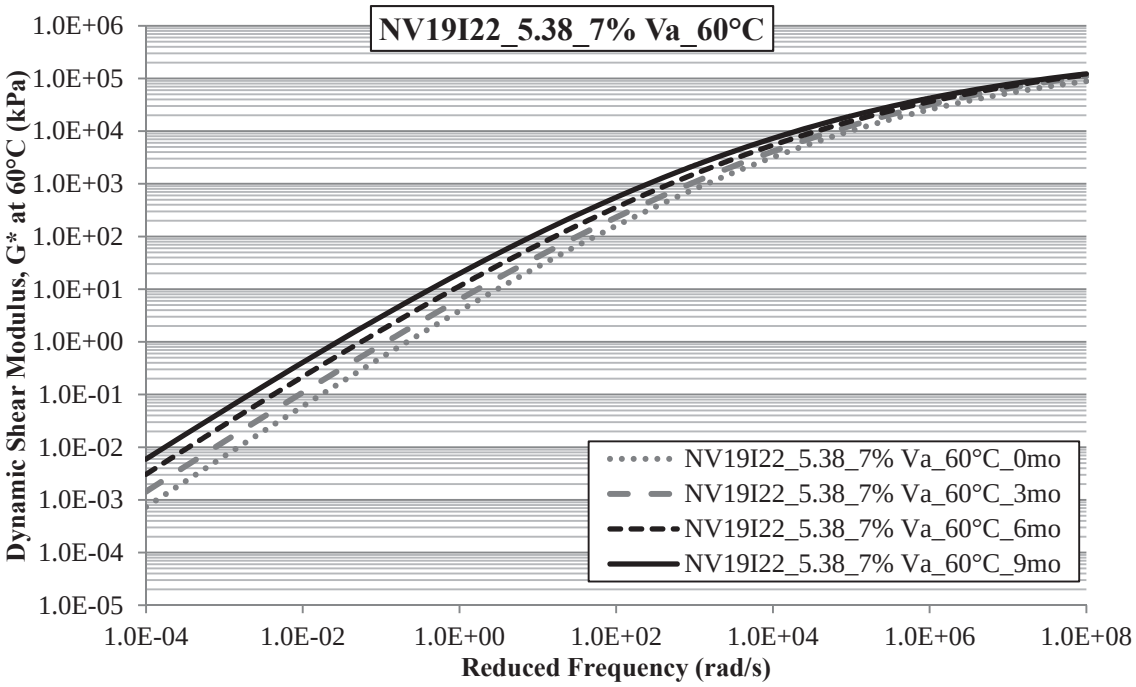

Figure 23.27 Summary of NV19I22_5.38_7% Va Aged at 60°C Dynamic Shear Modulus Master Curves

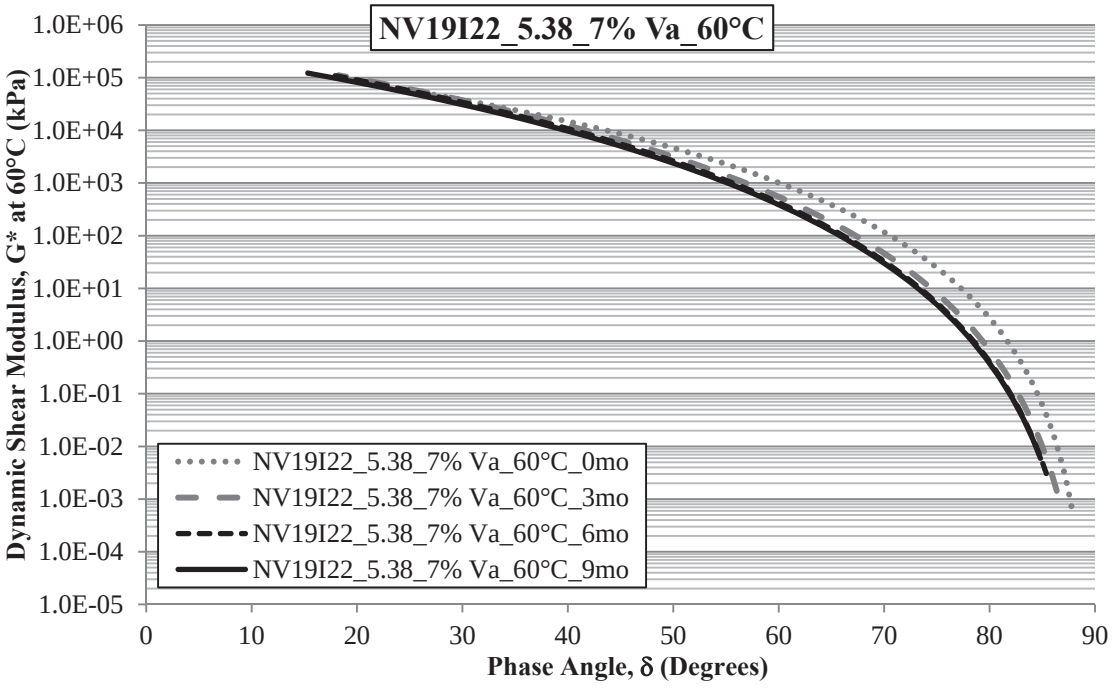

Figure 23.28 Summary of NV19I22_5.38_7% Va Aged at 60°C Black Space Plots

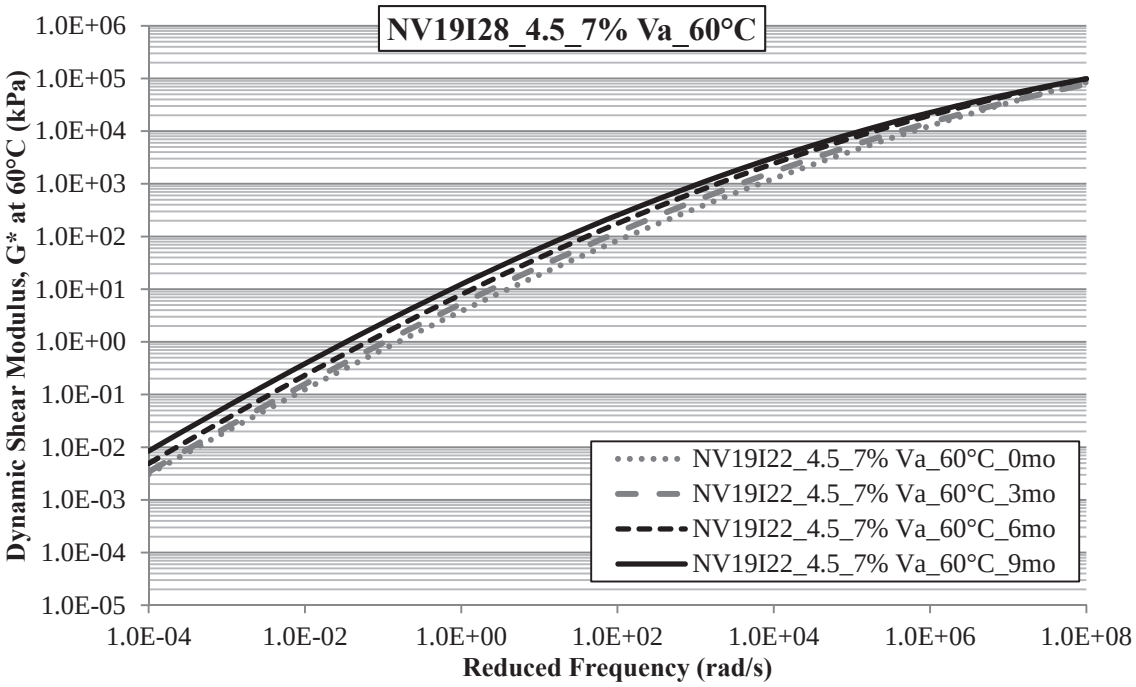

Figure 23.29 Summary of NV19I28_4.5_7% Va Aged at 60°C Dynamic Shear Modulus Master Curves

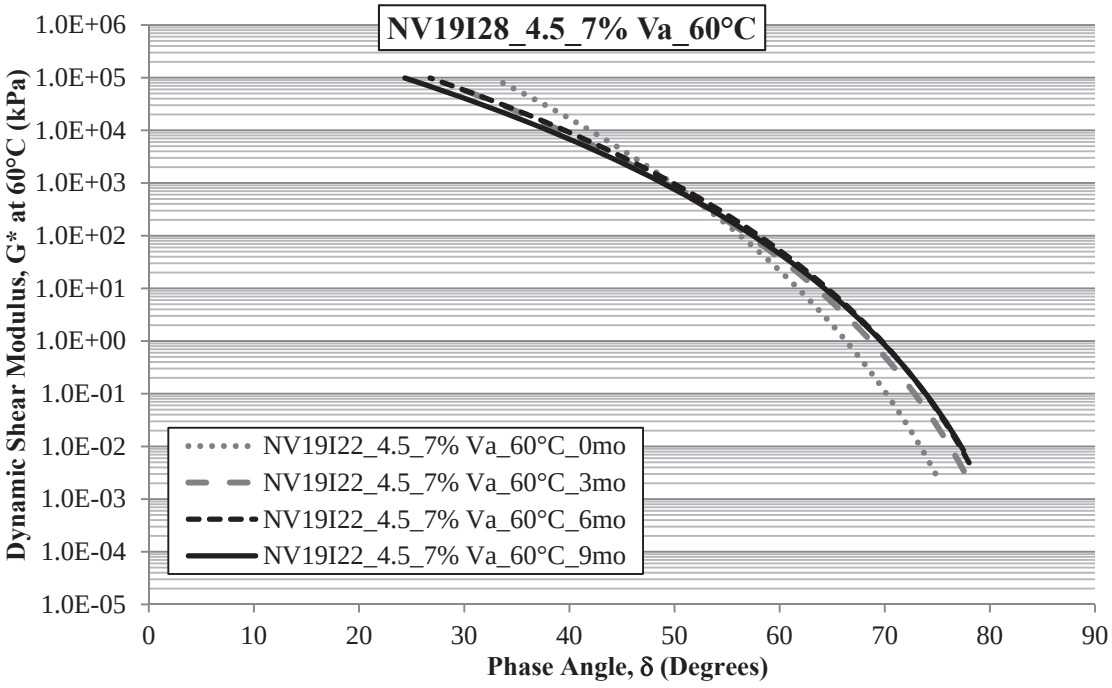

Figure 23.30 Summary of NV19I28_4.5_7% Va Aged at 60°C Black Space Plots

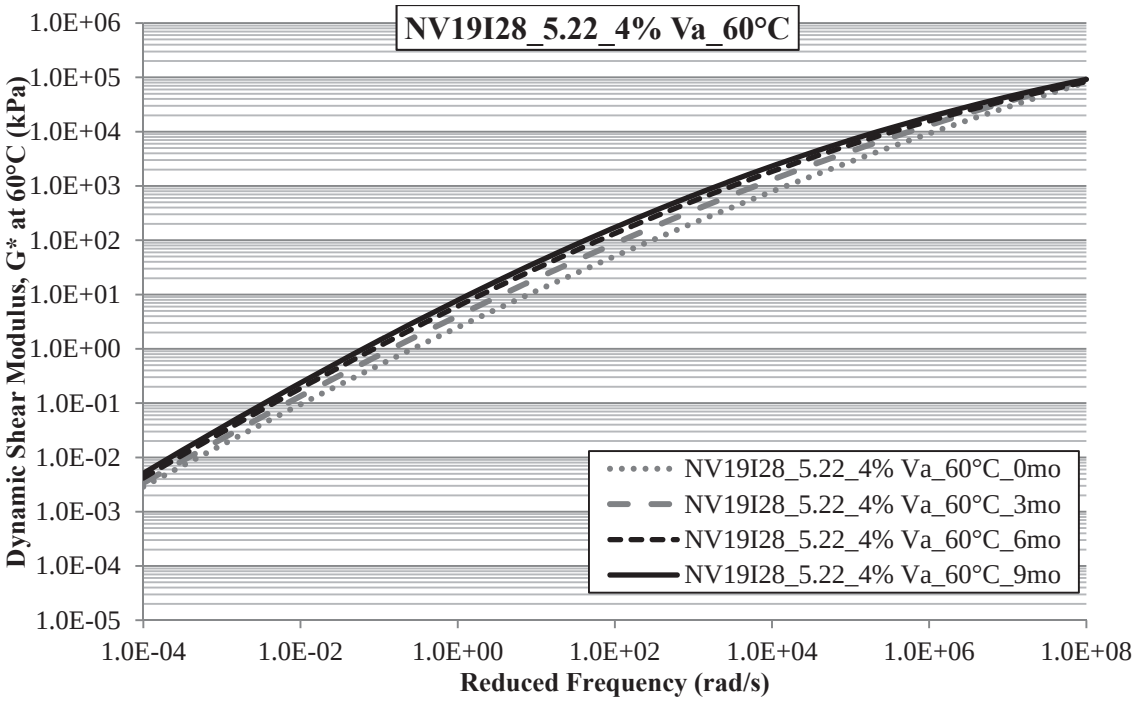

Figure 23.31 Summary of NV19I28_5.22_4% Va Aged at 60°C Dynamic Shear Modulus Master Curves

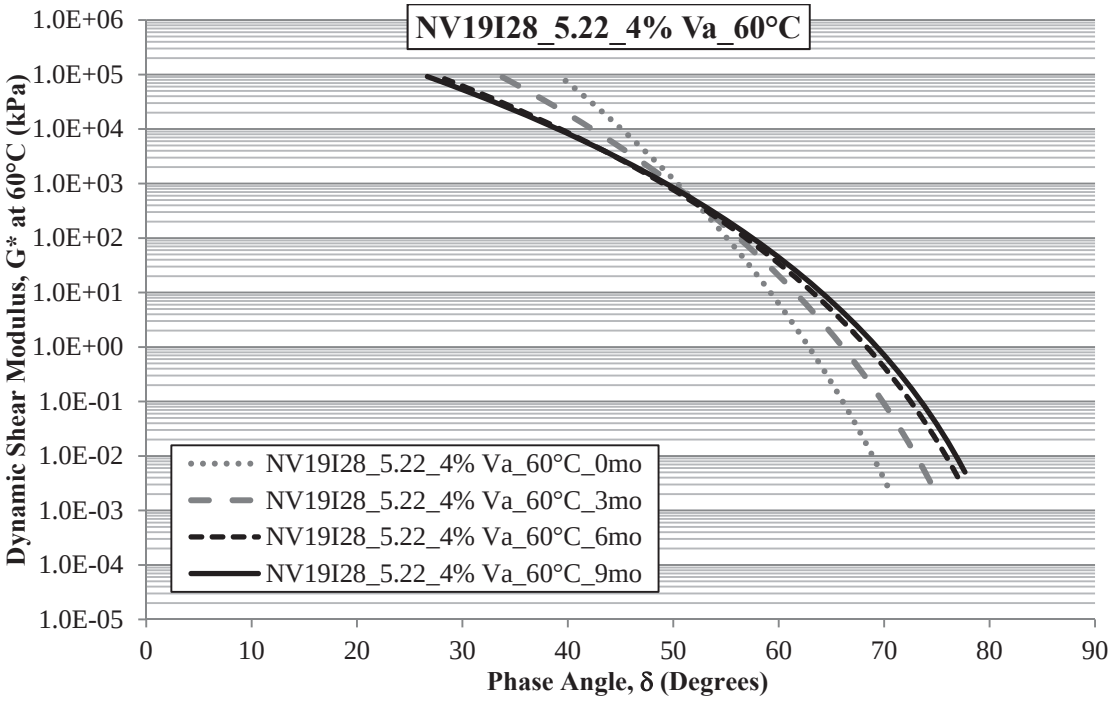

Figure 23.32 Summary of NV19I28_5.22_4% Va Aged at 60°C Black Space Plots

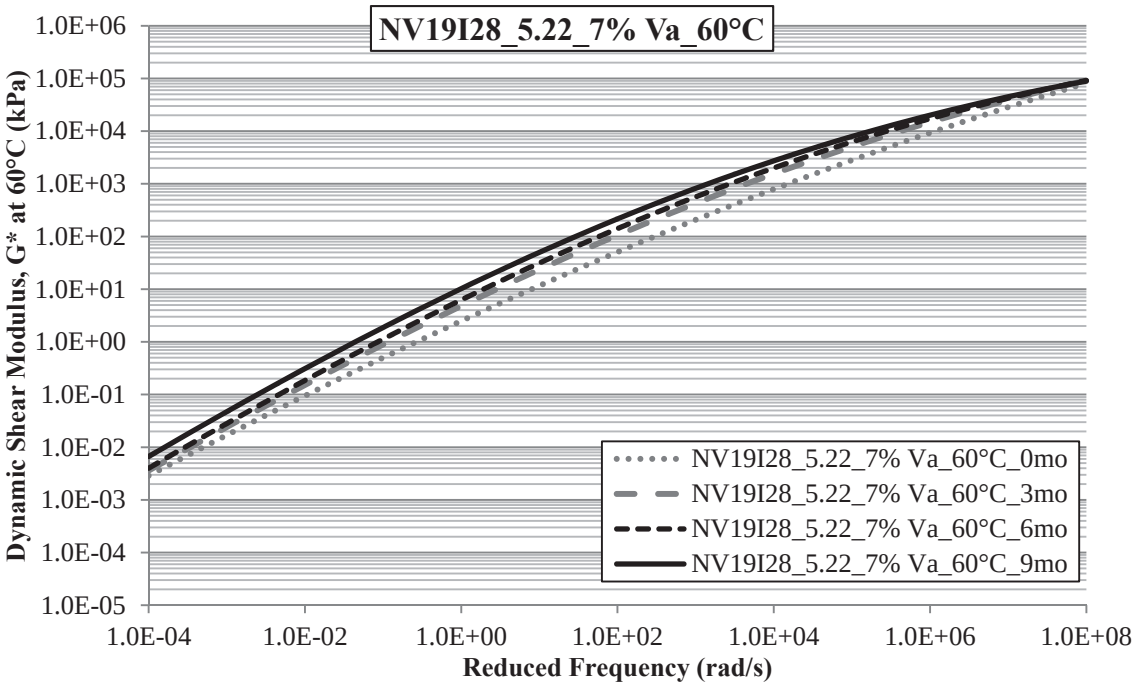

Figure 23.33 Summary of NV19I28_5.22_7% Va Aged at 60°C Dynamic Shear Modulus Master Curves

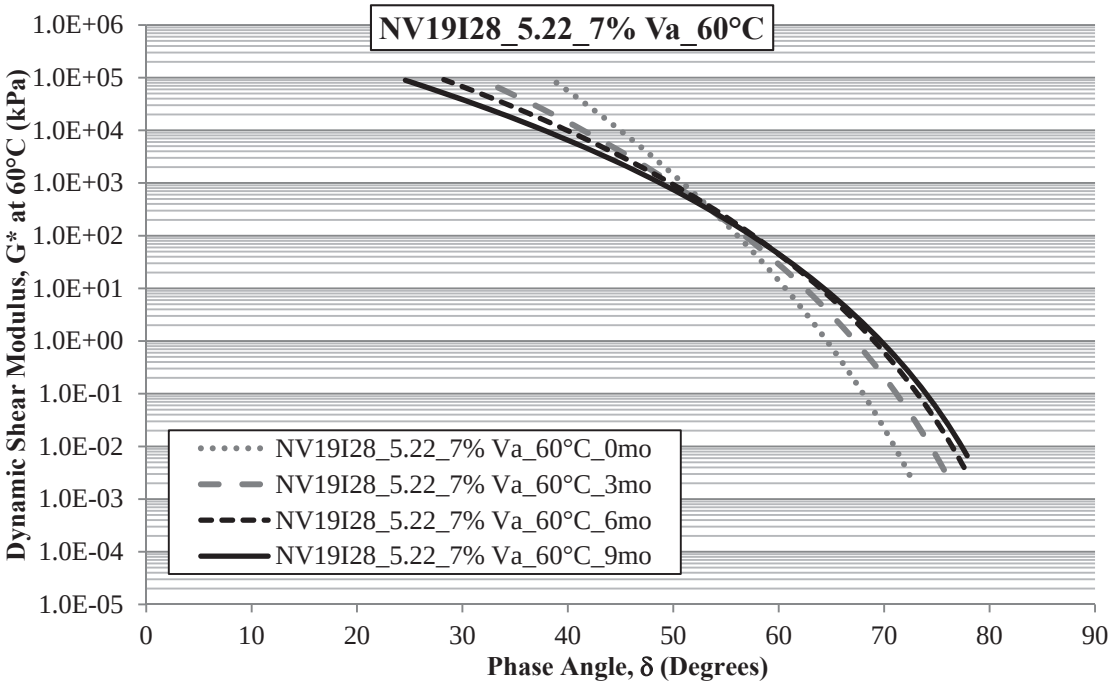

Figure 23.34 Summary of NV19I28_5.22_7% Va Aged at 60°C Black Space Plots

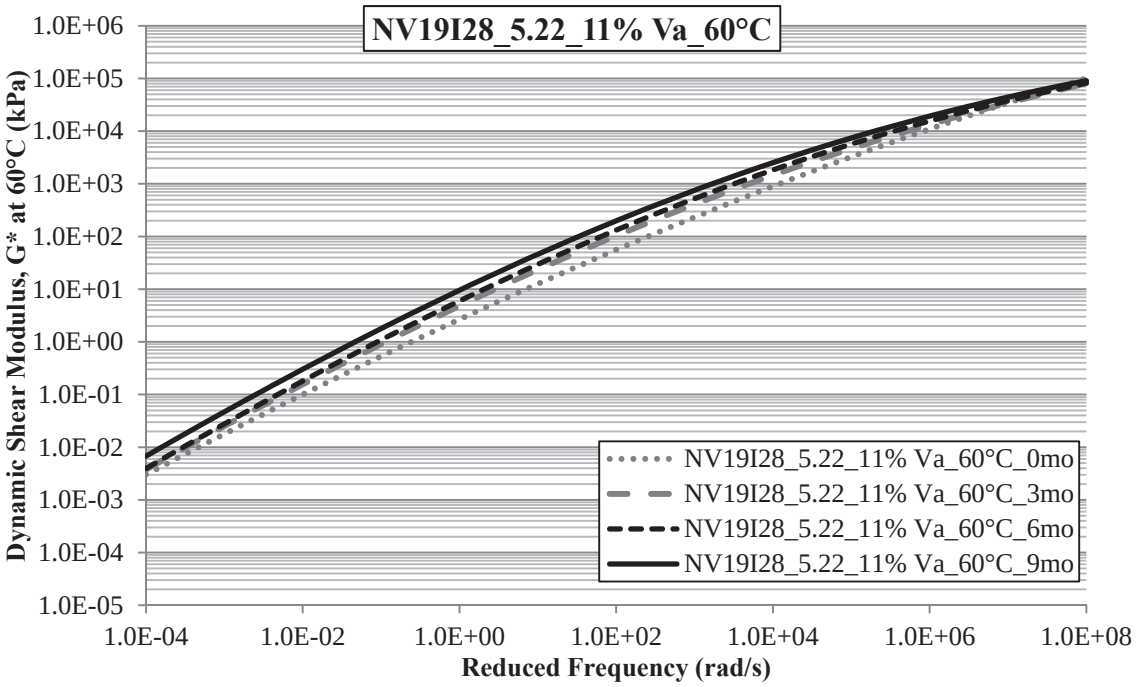

Figure 23.35 Summary of NV19I28_5.22_11% Va Aged at 60°C Dynamic Shear Modulus Master Curves

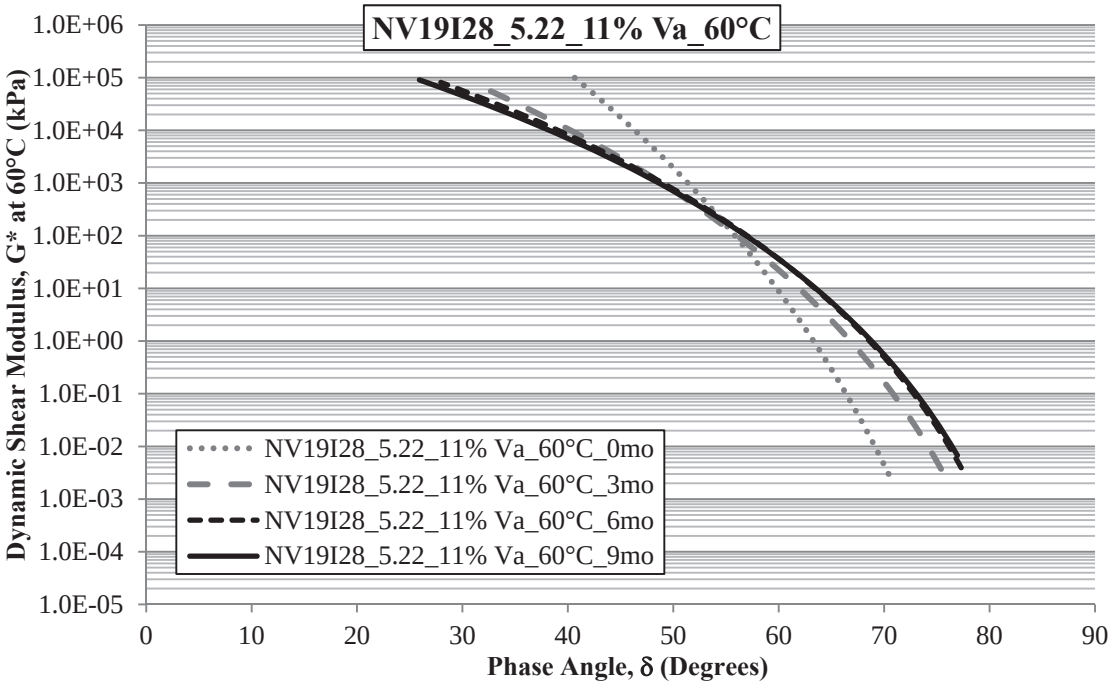

Figure 23.36 Summary of NV19I28_5.22_11% Va Aged at 60°C Black Space Plots

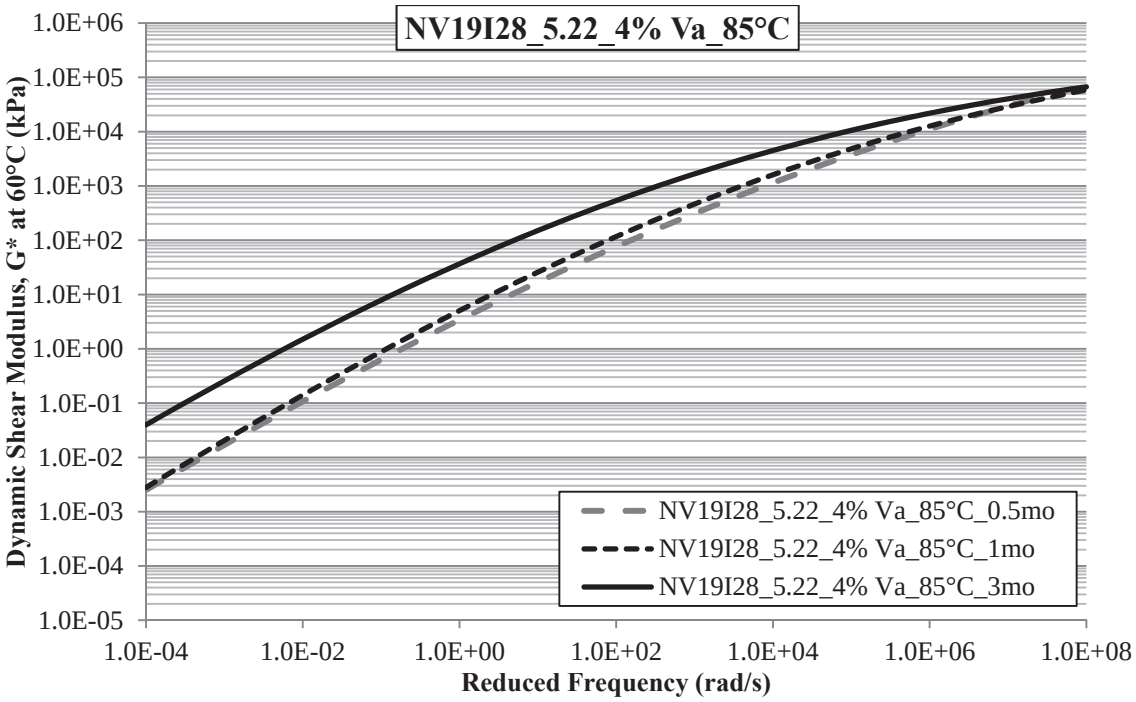

Figure 23.37 Summary of NV19I28_5.22_4% Va Aged at 85°C Dynamic Shear Modulus Master Curves

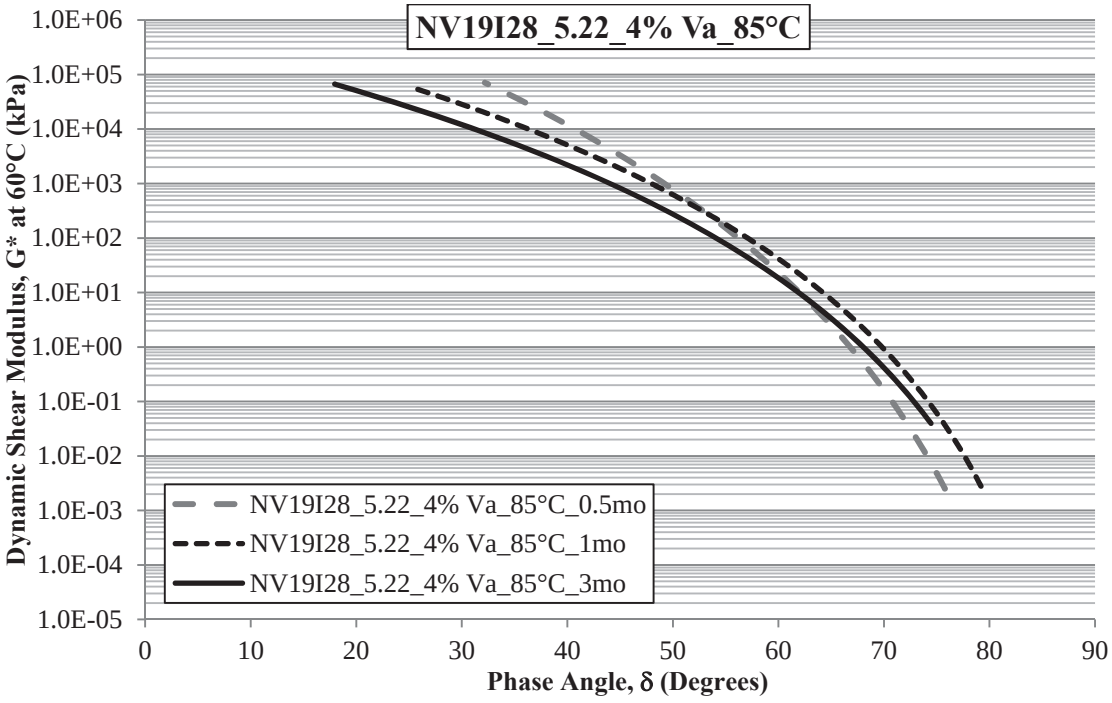

Figure 23.38 Summary of NV19I28_5.22_4% Va Aged at 85°C Black Space Plots

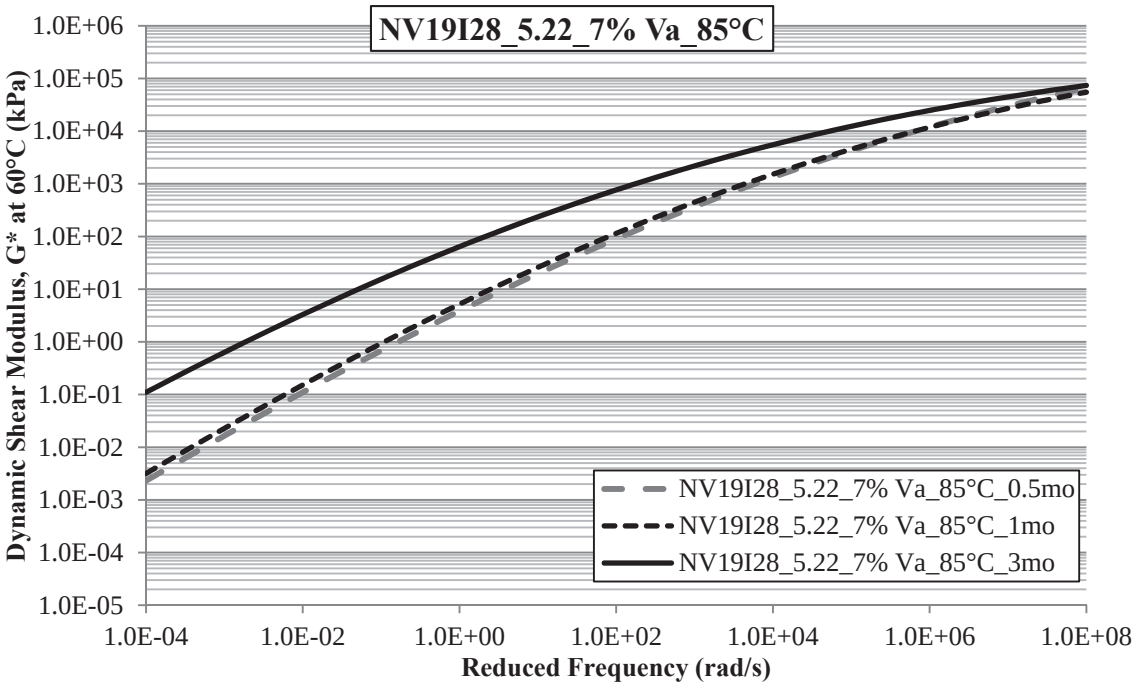

Figure 23.39 Summary of NV19I28_5.22_7% Va Aged at 85°C Dynamic Shear Modulus Master Curves

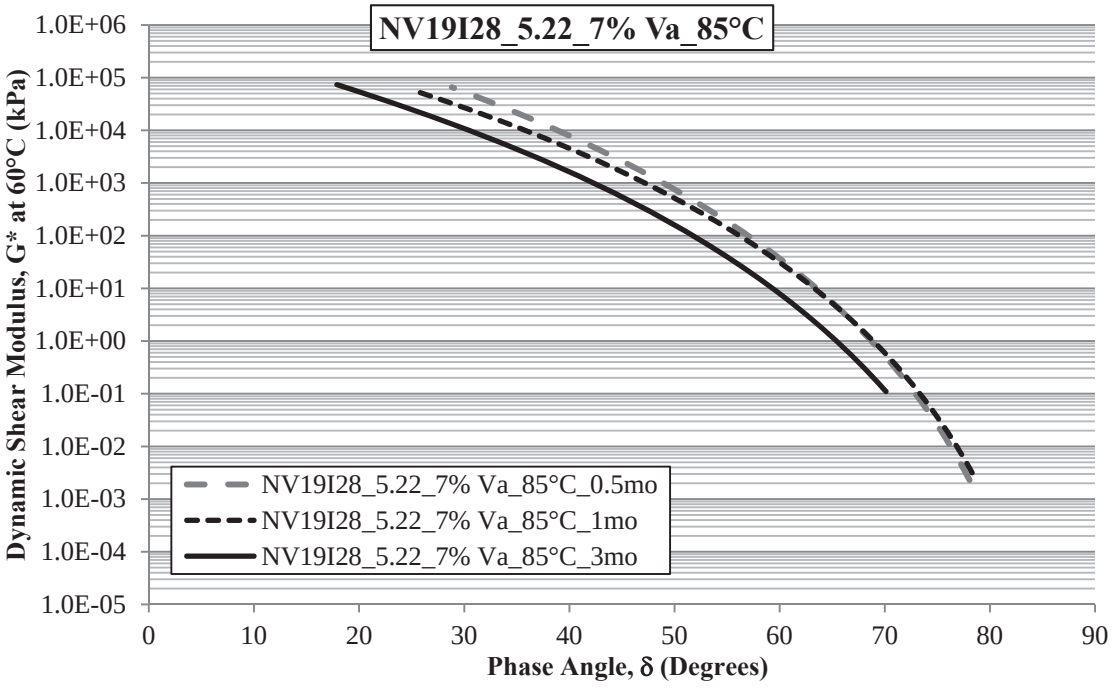

Figure 23.40 Summary of NV19I28_5.22_7% Va Aged at 85°C Black Space Plots

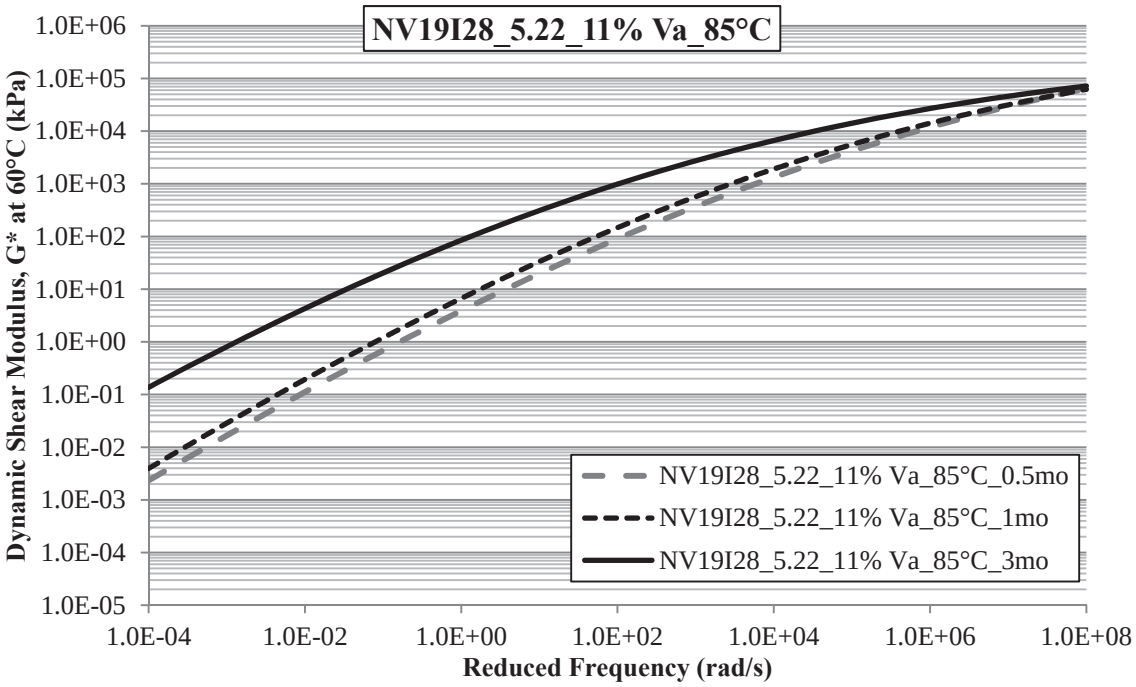

Figure 23.41 Summary of NV19I28_5.22_11% Va Aged at 85°C Dynamic Shear Modulus Master Curves

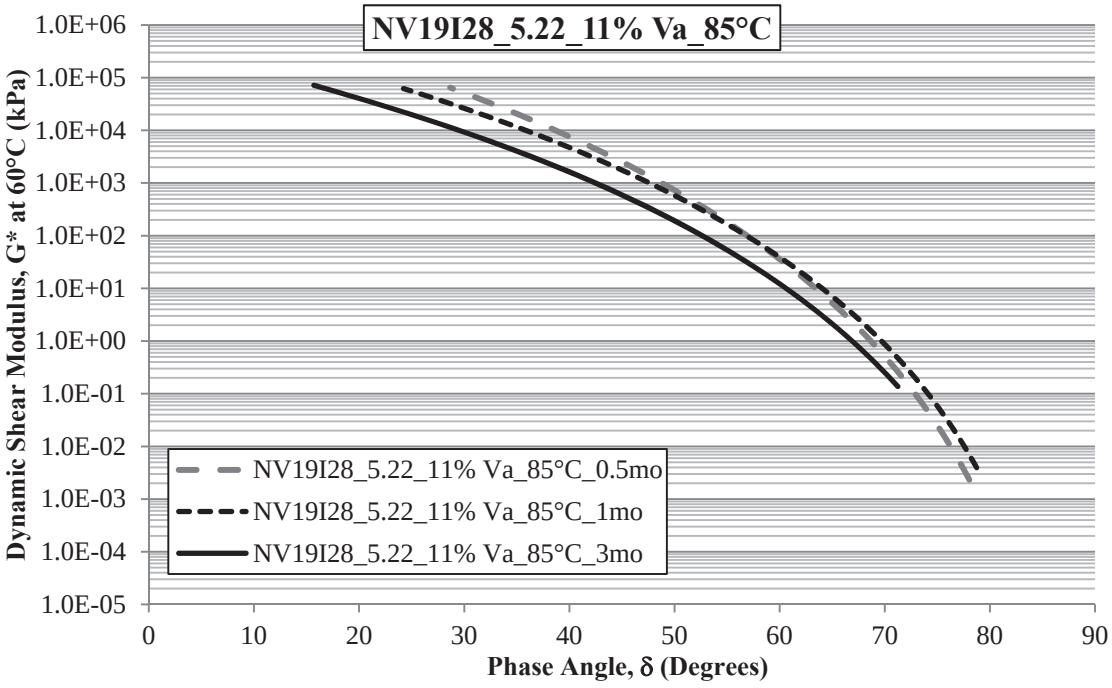

Figure 23.42 Summary of NV19I28_5.22_11% Va Aged at 85°C Black Space Plots

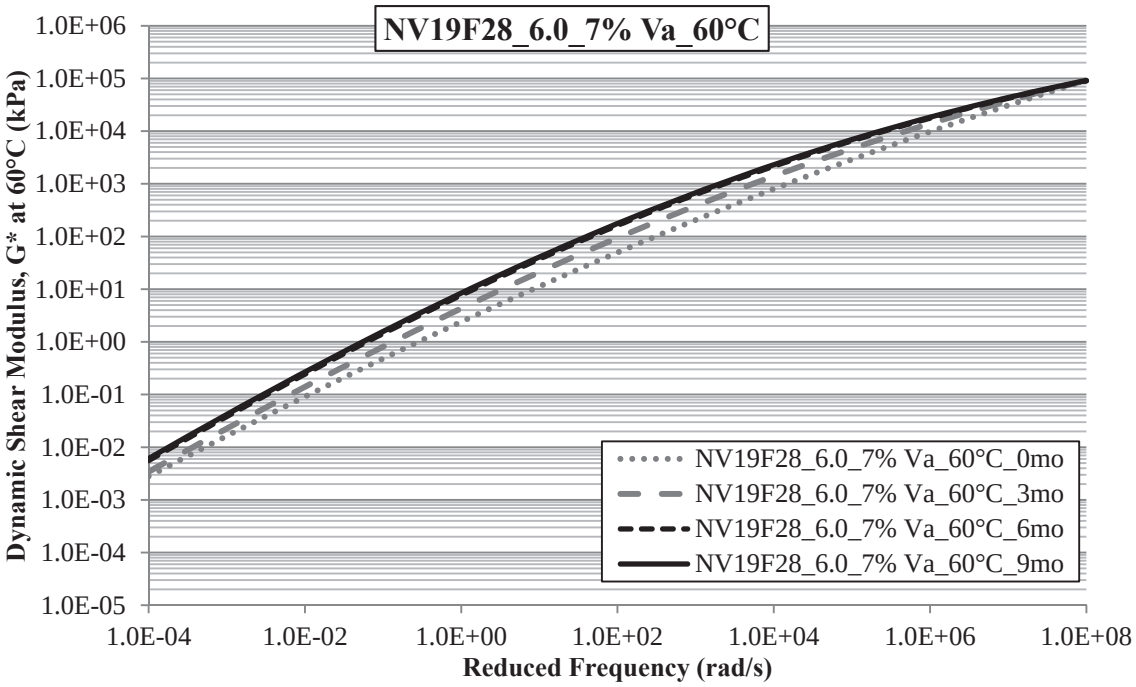

Figure 23.43 Summary of NV19F28_6.0_7% Va Aged at 60°C Dynamic Shear Modulus Master Curves

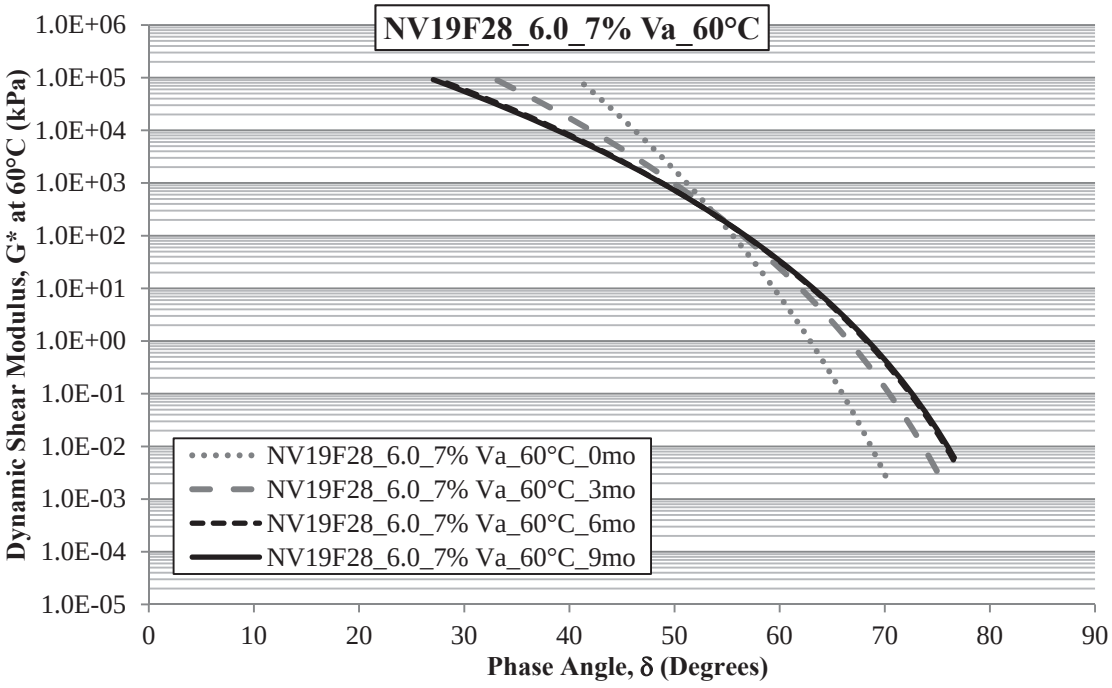

Figure 23.44 Summary of NV19F28_6.0_7% Va Aged at 60°C Black Space Plots

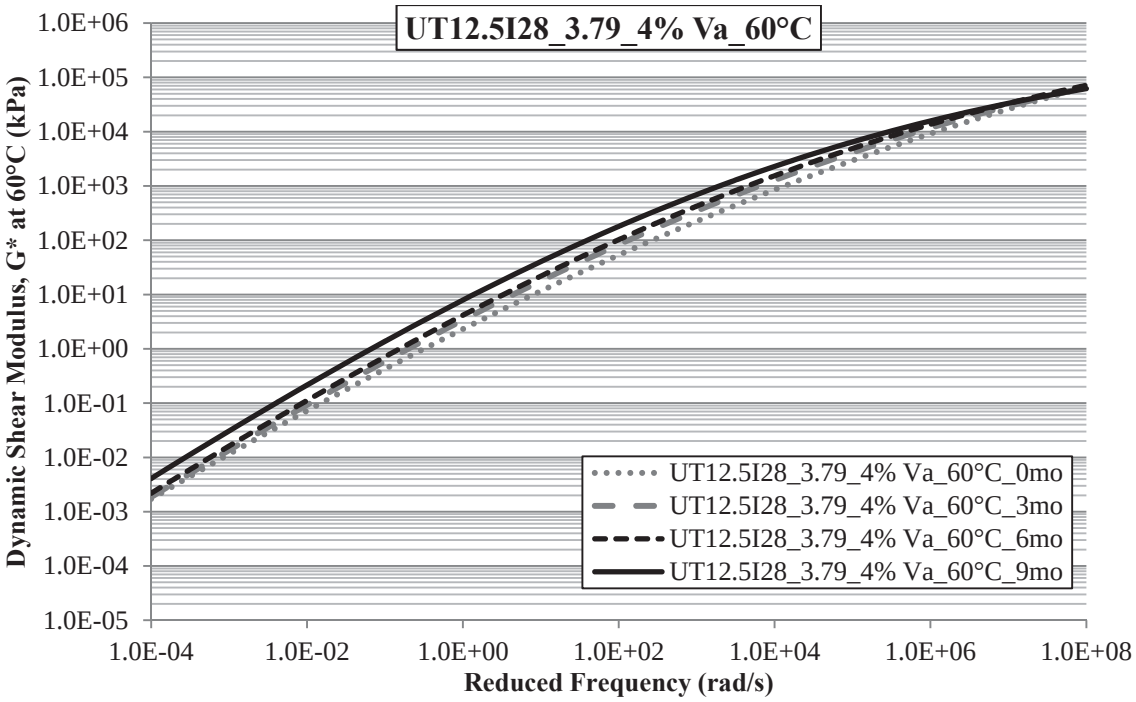

Figure 23.45 Summary of UT12.5I28_3.79_4% Va Aged at 60°C Dynamic Shear Modulus Master Curves

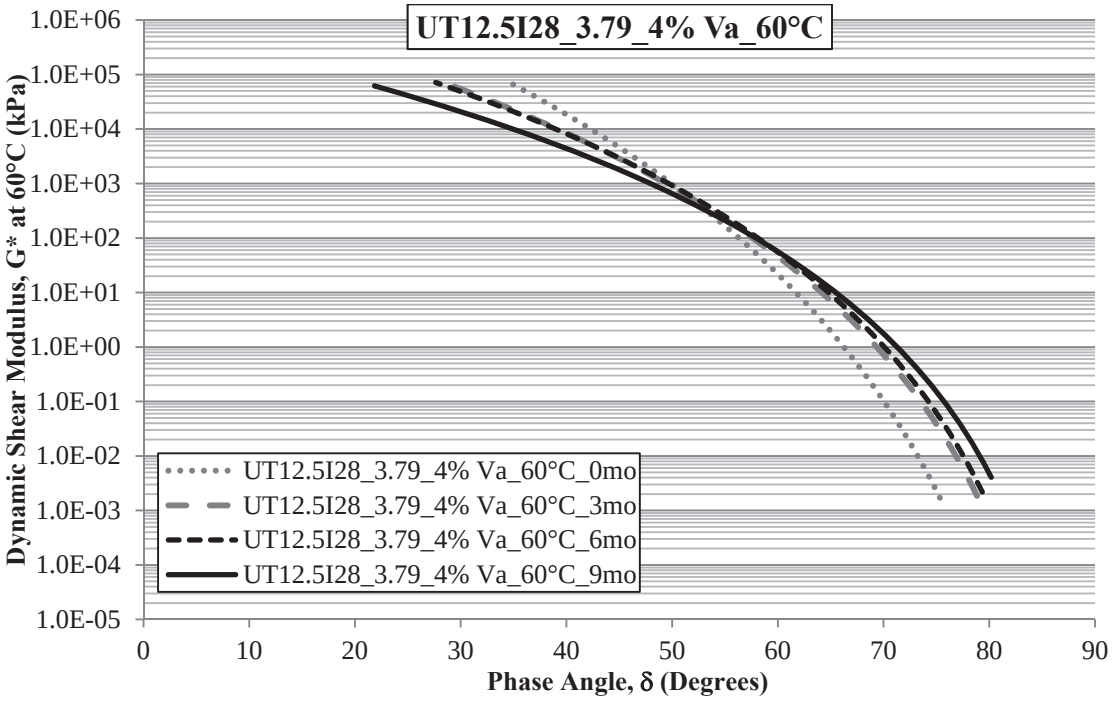

Figure 23.46 Summary of UT12.5I28_3.79_4% Va Aged at 60°C Black Space Plots

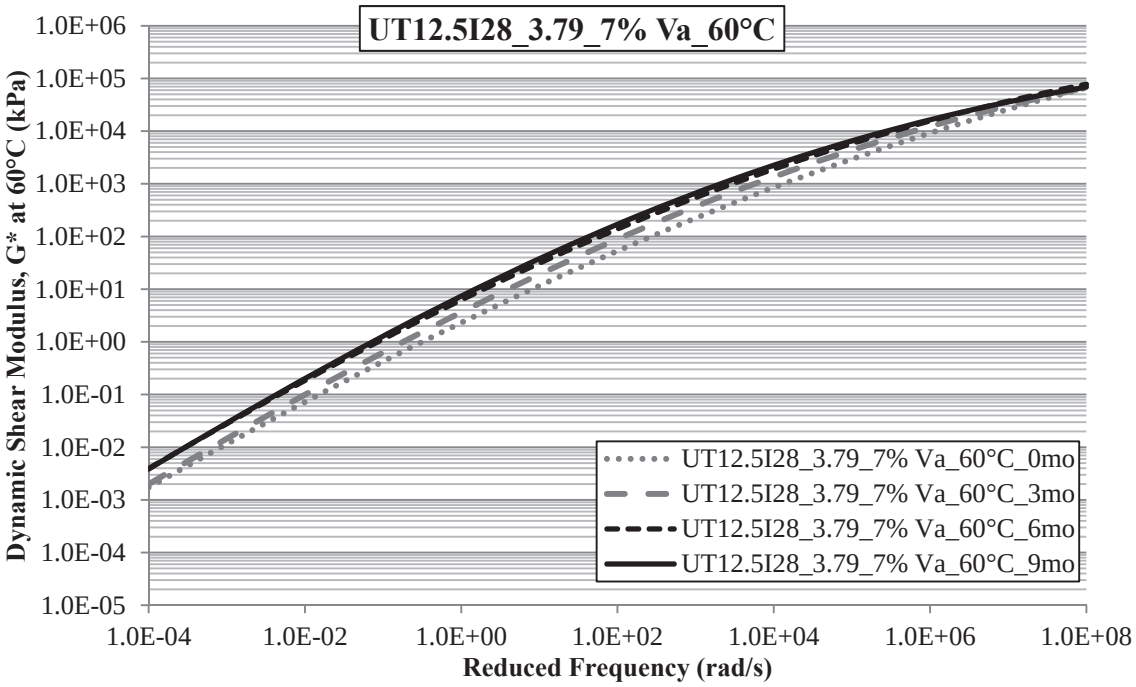

Figure 23.47 Summary of UT12.5I28_3.79_7% Va Aged at 60°C Dynamic Shear Modulus Master Curves

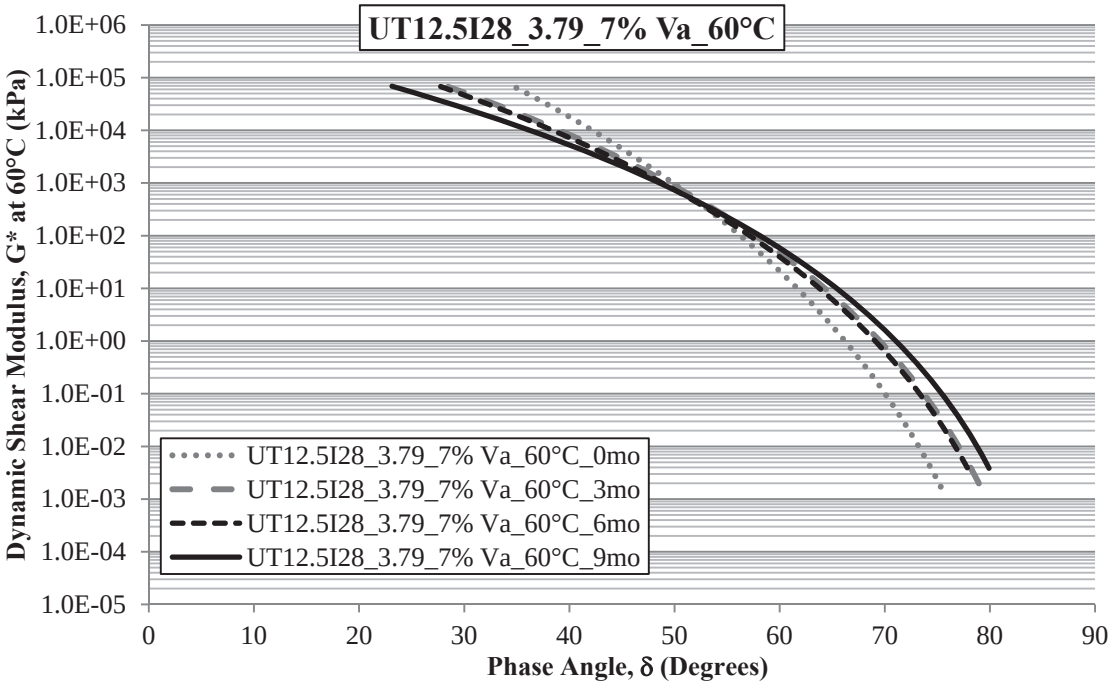

Figure 23.48 Summary of UT12.5I28_3.79_7% Va Aged at 60°C Black Space Plots

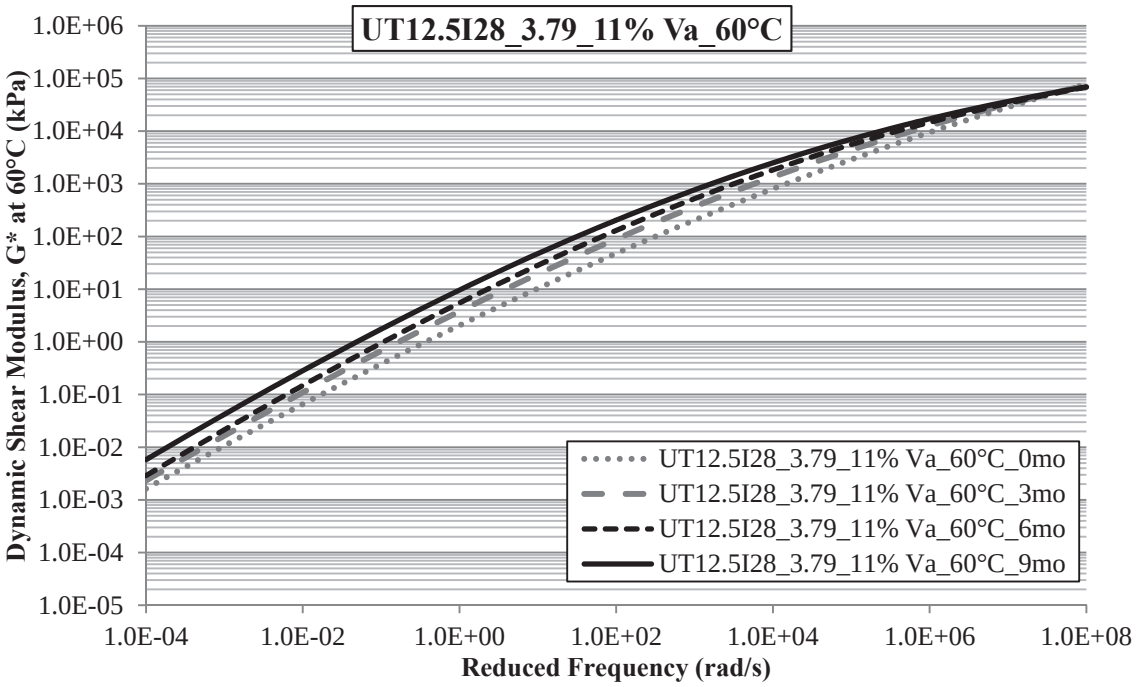

Figure 23.49 Summary of UT12.5I28_3.79_11% Va Aged at 60°C Dynamic Shear Modulus Master Curves

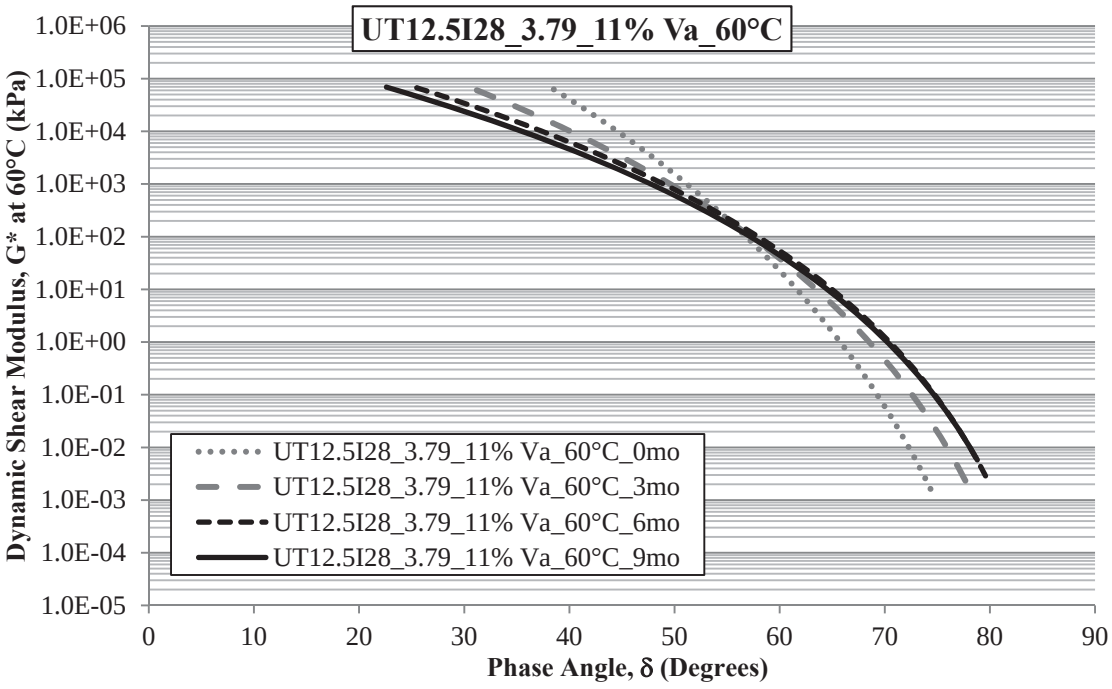

Figure 23.50 Summary of UT12.5I28_3.79_11% Va Aged at 60°C Black Space Plots

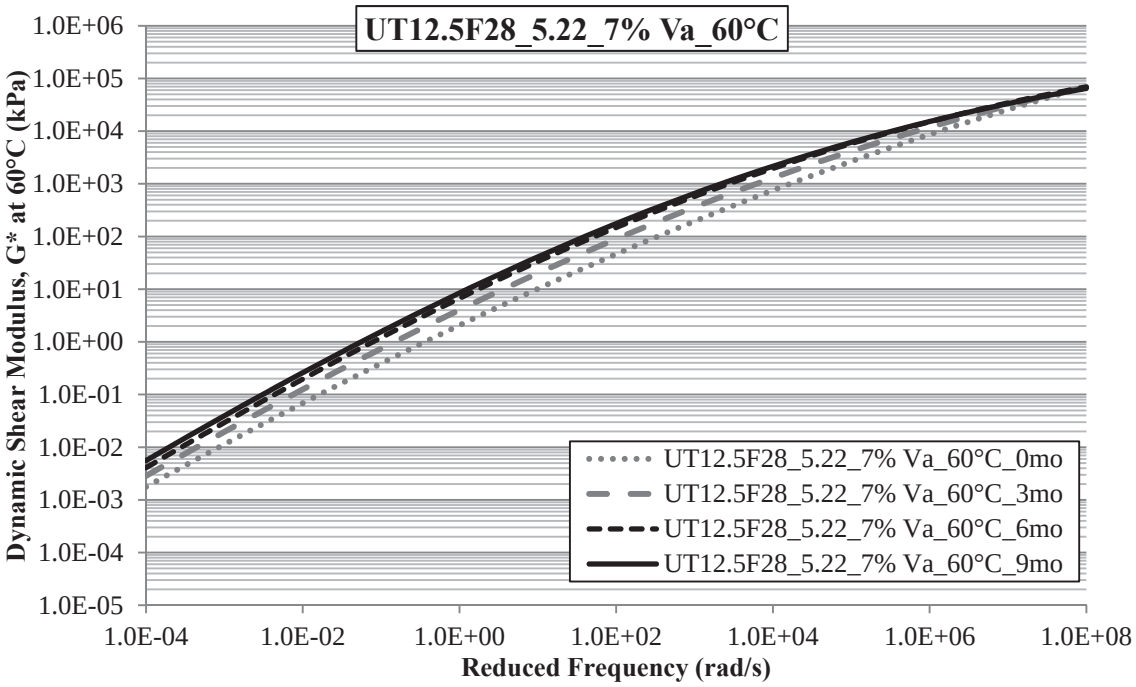

Figure 23.51 Summary of UT12.5F28_5.22_7% Va Aged at 60°C Dynamic Shear Modulus Master Curves

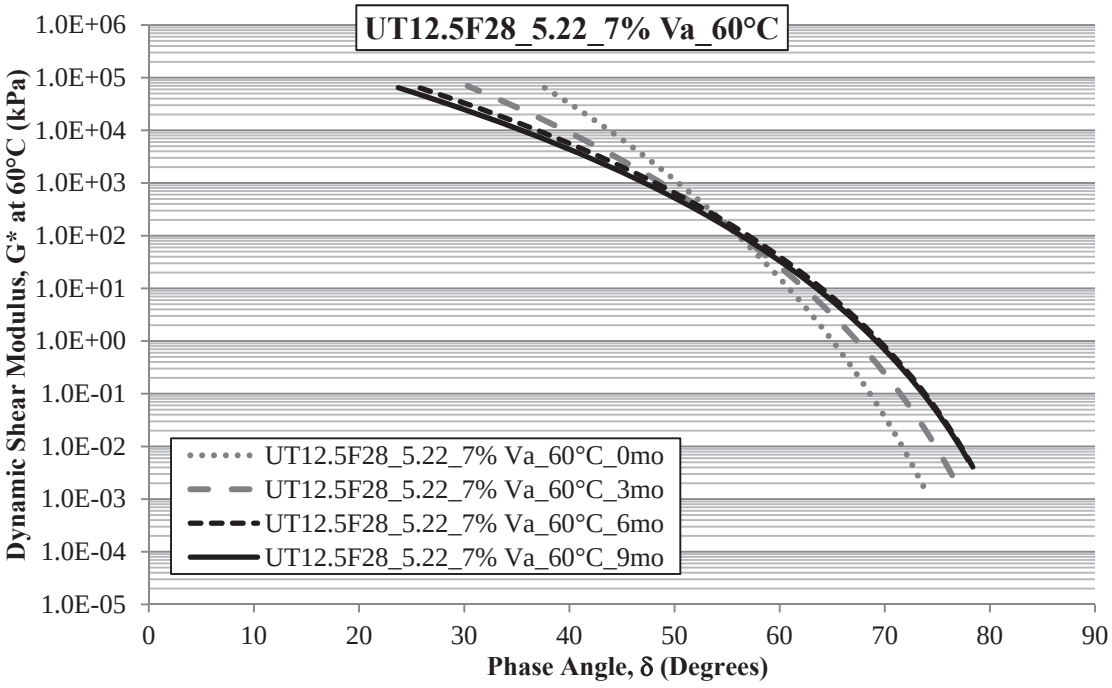

Figure 23.52 Summary of UT12.5F28_5.22_7% Va Aged at 60°C Black Space Plots

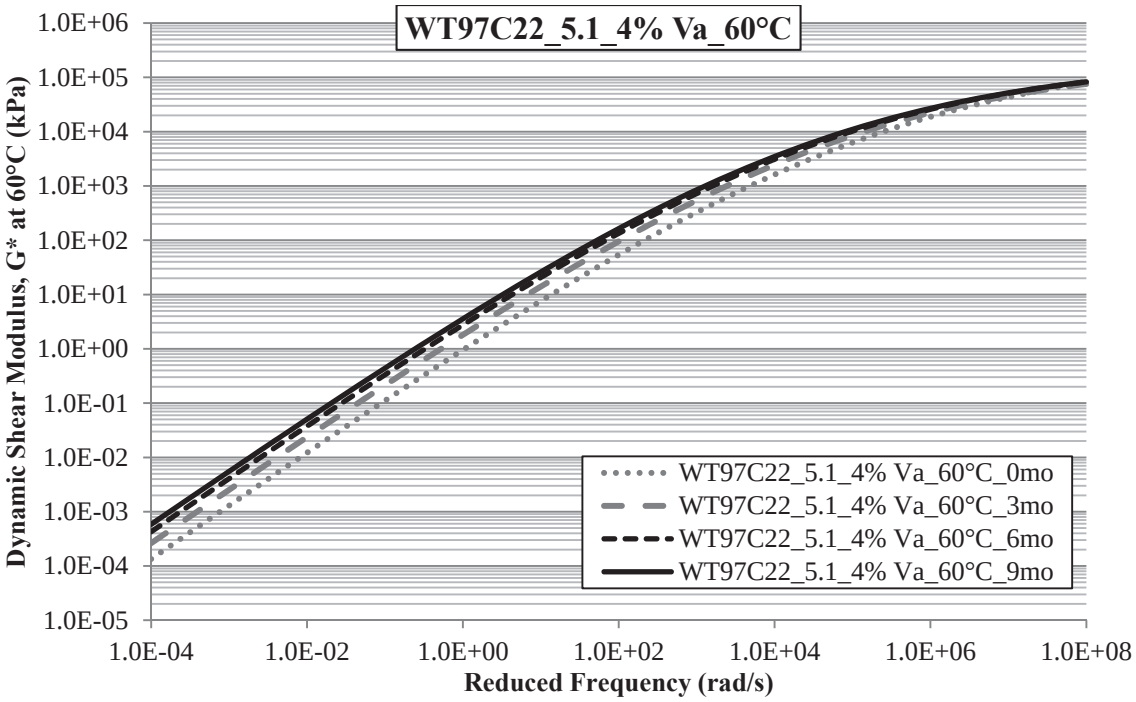

Figure 23.53 Summary of WT97C22_5.1_4% Va Aged at 60°C Dynamic Shear Modulus Master Curves

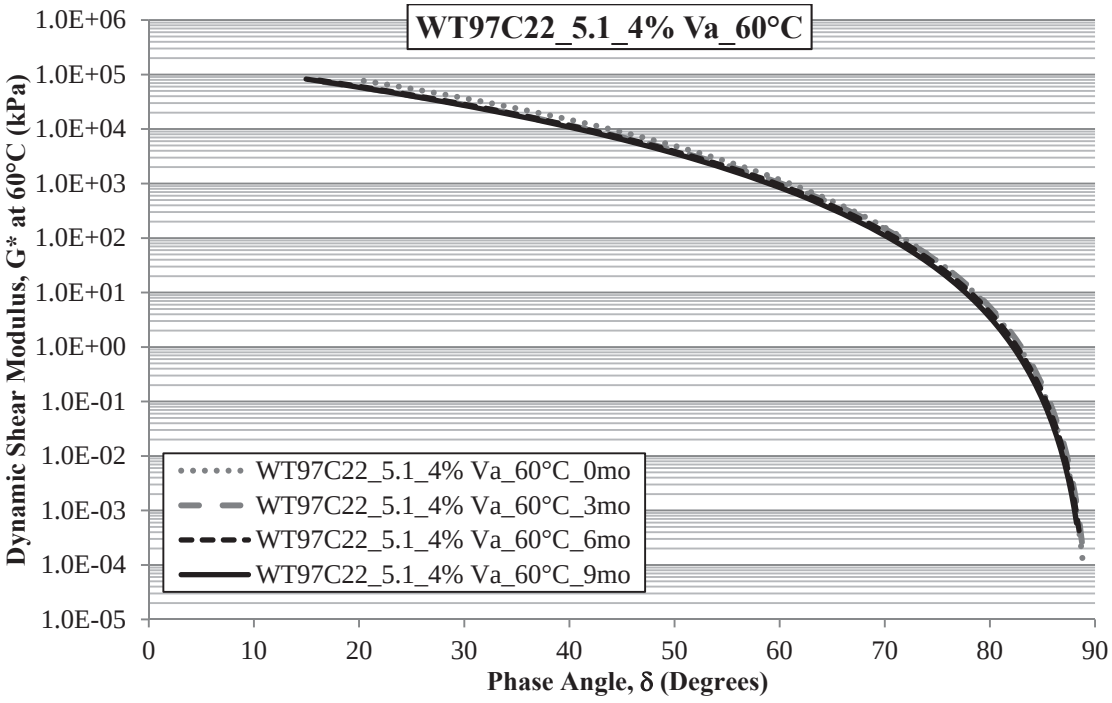

Figure 23.54 Summary of WT97C22_5.1_4% Va Aged at 60°C Black Space Plots

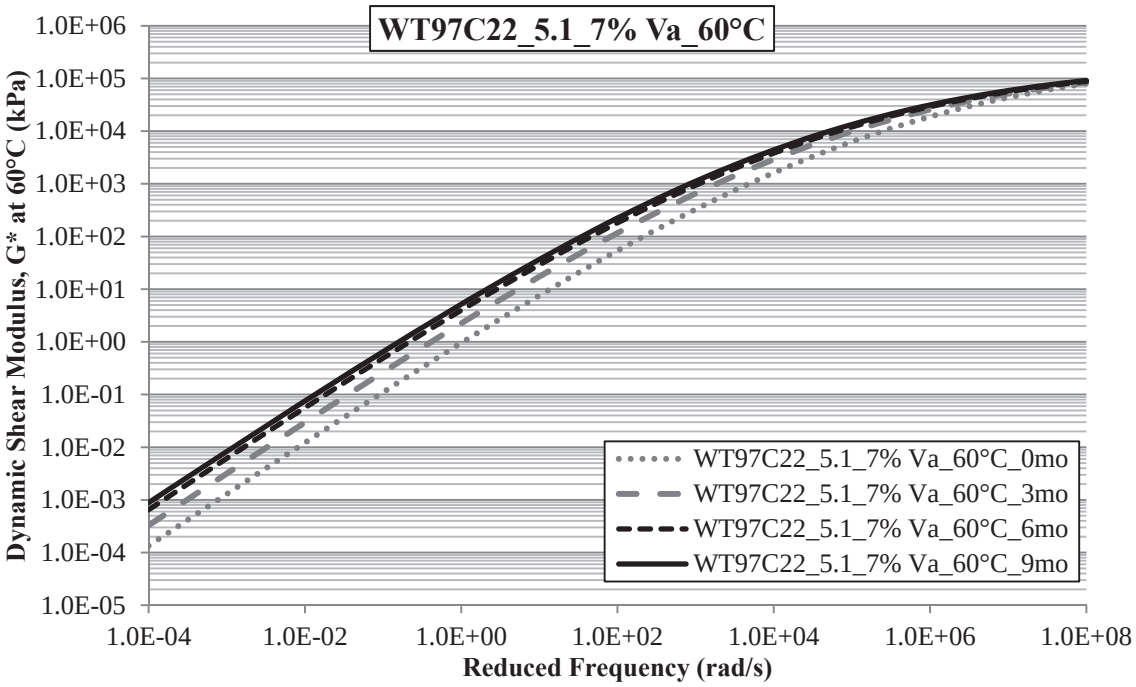

Figure 23.55 Summary of WT97C22_5.1_7% Va Aged at 60°C Dynamic Shear Modulus Master Curves

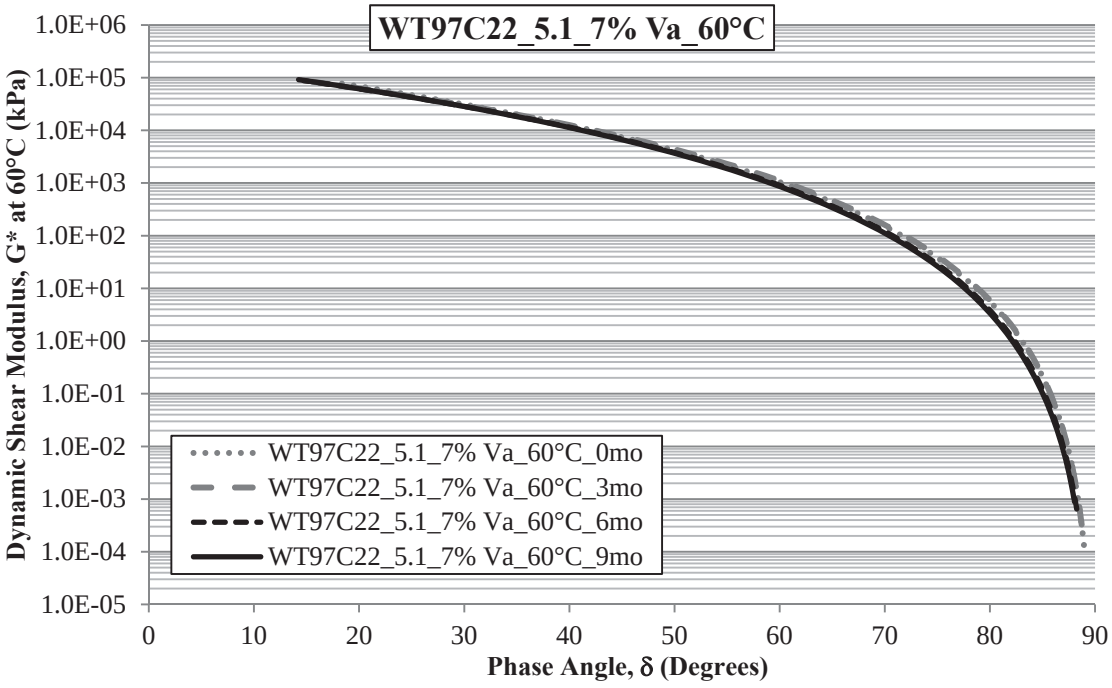

Figure 23.56 Summary of WT97C22_5.1_7% Va Aged at 60°C Black Space Plots

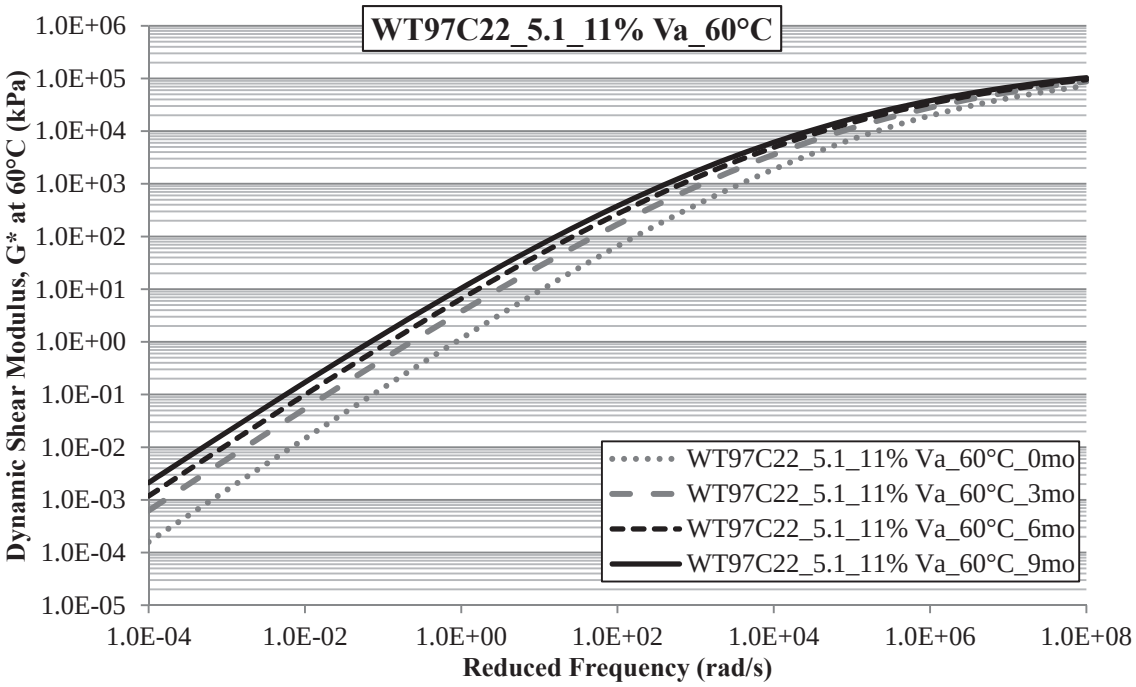

Figure 23.57 Summary of WT97C22_5.1_11% Va Aged at 60°C Dynamic Shear Modulus Master Curves

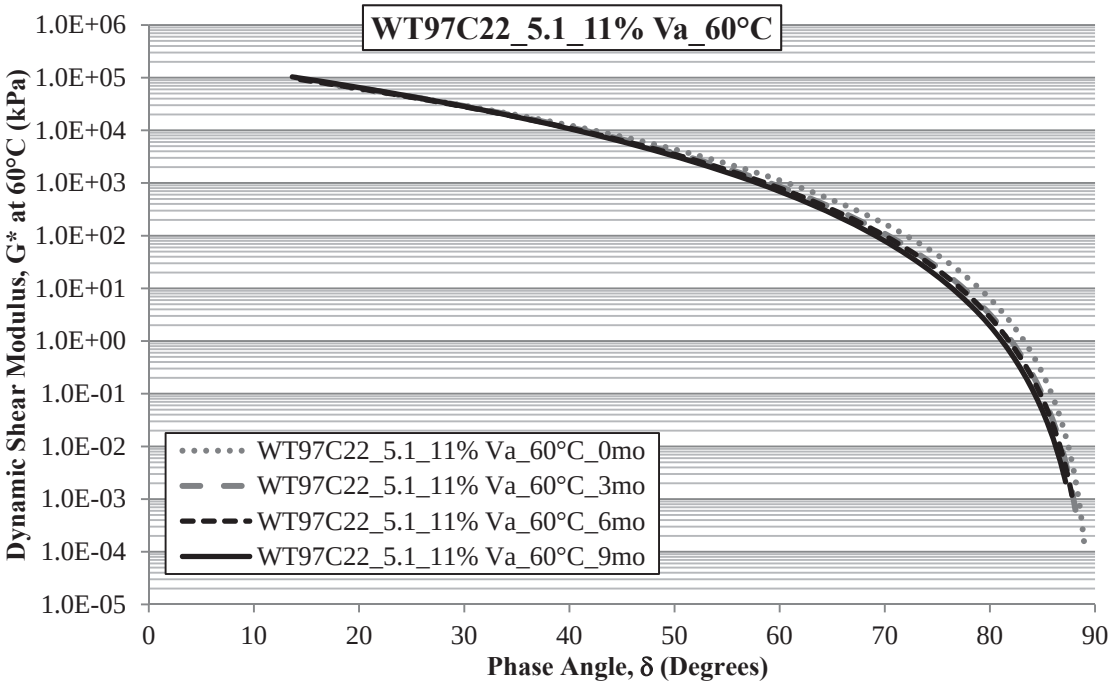

Figure 23.58 Summary of WT97C22_5.1_11% Va Aged at 60°C Black Space Plots

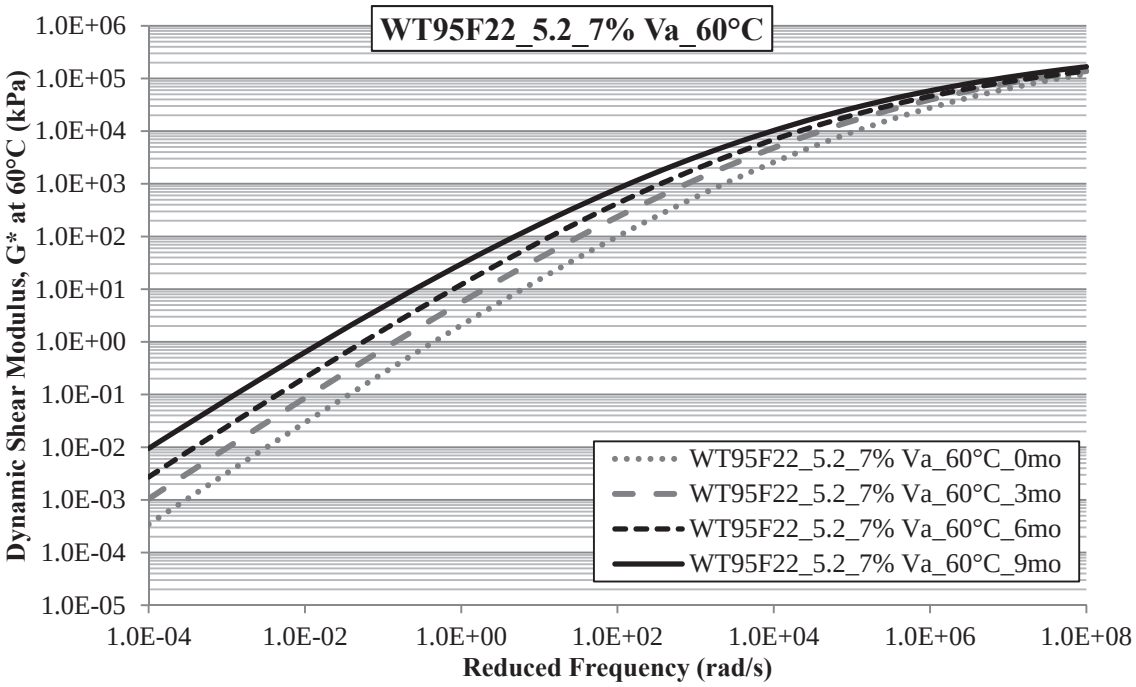

Figure 23.59 Summary of WT95F22_5.2_7% Va Aged at 60°C Dynamic Shear Modulus Master Curves

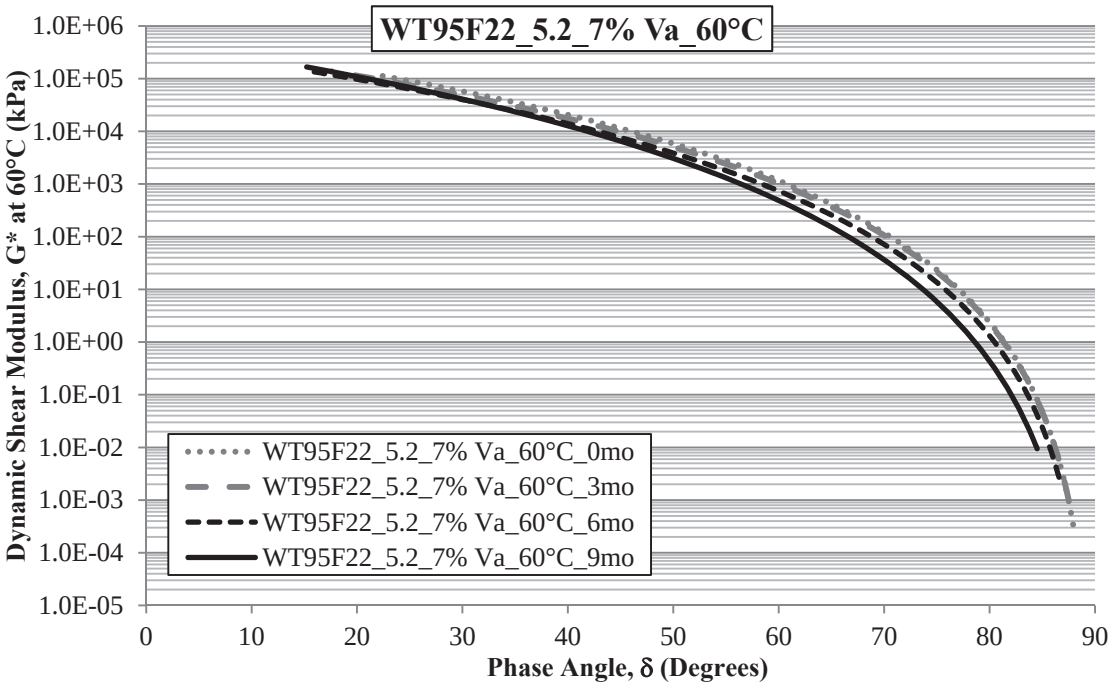

Figure 23.60 Summary of WT95F22_5.2_7% Va Aged at 60°C Black Space Plots

24 APPENDIX L:

Summary of Mixture-Aged Asphalt Binder Master Curve Function Parameters

Table 24.1 Dynamic Shear Modulus and Shift Function Parameters for California Mixtures

Aging Conditions			CAS Parameters				WLF		Kaelble			
ID	Air Void	Dur. (mo)	G_0 (kPa)	ω_0 (rad/s)	β	κ	C_1	C_2	C_1	C_2	T_k (°C)	T_r (°C)
CAL19I22_7.44_60°C	4%	0	298,069	136,880	0.1969	1	9.65	138.3	14.15	94.3	16	60
		3	350,886	48,597	0.1862	1	12.27	159.4	16.95	115.4	16	60
		6	361,221	25,369	0.1800	1	12.50	158.5	17.31	114.5	16	60
		9	332,078	11,040	0.1740	1	13.90	167.8	18.84	123.8	16	60
	7%	0	285,059	164,668	0.2080	1	9.70	139.1	14.19	95.1	16	60
		3	296,234	34,130	0.1879	1	12.06	155.7	16.80	111.7	16	60
		6	323,567	17,215	0.1817	1	12.96	161.8	17.79	117.8	16	60
		9	352,150	10,223	0.1724	1	13.93	168.7	18.85	124.7	16	60
	11%	0	316,009	140,237	0.1925	1	9.85	140.1	14.37	96.1	16	60
		3	341,674	21,168	0.1788	1	12.78	160.0	17.63	116.0	16	60
		6	310,693	10,614	0.1763	1	13.64	165.1	17.47	119.6	20	60
		9	414,035	6,546	0.1628	1	14.59	171.9	19.61	127.9	16	60
CAL19I22_7.44_85°C	4%	0.5	224,772	67,089	0.1883	1	10.40	144.3	13.95	99.2	20	60
		1	364,454	50,262	0.1730	1	11.84	155.6	14.65	106.2	22	60
		3	270,126	3,007	0.1571	1	13.51	166.7	17.26	121.1	20	60
	7%	0.5	186,953	56,369	0.1970	1	10.81	147.7	15.40	103.7	16	60
		1	205,818	20,800	0.1805	1	11.76	153.6	14.63	104.6	22	60
		3	313,318	1,291	0.1480	1	15.58	179.5	18.54	129.3	22	60
	11%	0.5	205,427	58,511	0.1927	1	10.83	147.8	15.42	103.8	16	60
		1	212,166	18,266	0.1798	1	11.48	151.5	14.36	102.7	22	60
		3	380,991	159	0.1303	1	17.25	189.8	20.23	139.0	22	60
CAL19I28_7.51_60°C	7%	0	2.92x10^11[a]	12,658,980	0.0433	1	10.47	152.3	14.80	109.3	16	60
		3	14,037,470	77,701	0.0847	1	12.14	162.8	16.64	118.8	16	60
		6	2,588,957	24,959	0.1033	1	13.38	171.7	17.99	127.7	16	60
		9	1,593,590	14,258	0.1115	1	13.87	173.8	18.58	129.8	16	60
CAL19F22_9.14_60°C	7%	0	349,615	122,200	0.1798	1	10.08	141.6	14.63	97.6	16	60
		3	303,394	28,284	0.1767	1	12.42	158.0	17.21	114.0	16	60
		6	301,340	15,110	0.1726	1	12.78	159.0	16.56	113.6	20	60
		9	309,797	8,044	0.1684	1	13.19	162.0	17.00	116.6	20	60

a - G_0 = 292,216,100,000 (kPa)

Table 24.2 Dynamic Shear Modulus and Shift Function Parameters for Colorado Mixtures Aged at 60°C

Aging Conditions			CAS Parameters				WLF		Kaelble			
ID	Pb, % TWM	Dur. (mo)	G_0 (kPa)	ω_0 (rad/s)	β	κ	C_1	C_2	C_1	C_2	T_k (°C)	T_r (°C)
CO19I22_7% Va	3.61	0	333,426	33,121	0.1711	1	11.82	154.2	16.5	110.16	16	60
		3	363,110	15,225	0.1648	1	13.08	163.3	16.8	117.84	20	60
		6	352,835	8,633	0.1639	1	14.58	173.2	19.5	129.19	16	60
		9	356,039	3,502	0.1530	1	14.01	167.3	17.9	121.69	20	60
	4.5	0	307,617	69,785	0.1803	1	11.88	156.6	16.5	112.61	16	60
		3	318,248	28,062	0.1717	1	12.86	161.8	17.7	117.79	16	60
		6	373,621	14,392	0.1531	1	12.40	159.8	16.1	114.34	20	60
		9	397,146	3,072	0.1485	1	14.68	172.9	18.5	127.22	20	60
CO19I28_7% Va	3.65	0	149,156,300	398,696	0.0681	1	10.96	154.9	15.3	110.87	16	60
		3	5,150,954	33,655	0.0926	1	12.79	167.6	17.3	123.6	16	60
		6	2,036,526	17,065	0.1046	1	13.84	173.6	18.5	129.57	16	60
		9	1,430,231	8,680	0.1078	1	14.14	175.0	18.9	131.02	16	60
	4.5	0	4.15x10^9[a]	3,539,446	0.0557	1	10.62	153.3	14.9	109.32	16	60
		3	54,148,780	178,569	0.0749	1	11.85	161.3	16.3	117.25	16	60
		6	3,093,568	18,691	0.0966	1	12.98	168.0	17.6	124.01	16	60
		9	2,659,256	11,688	0.0985	1	13.64	172.2	18.3	128.19	16	60

a - G_0 = 4,147,283,000 (kPa)

Table 24.3 Dynamic Shear Modulus and Shift Function Parameters for Nevada Mixtures

Aging Conditions			CAS Parameters				WLF		Kaelble			
ID	Air Void	Dur. (mo)	G_0 (kPa)	ω_0 (rad/s)	β	κ	C_1	C_2	C_1	C_2	T_k (°C)	T_r (°C)
NV19I22_4.5_60°C	7%	0	296,786	34,228	0.1785	1	11.35	150.8	14.99	105.6	20	60
		3	374,354	17,717	0.1696	1	12.55	160.8	17.28	116.8	16	60
		6	311,255	9,263	0.1727	1	14.28	170.9	19.23	126.9	16	60
		9	354,932	3,691	0.1630	1	14.76	173.1	19.79	129.1	16	60
NV19I22_5.38_60°C	7%	0	326,988	68,500	0.1803	1	11.45	151.4	15.20	107.1	20	60
		3	440,703	23,850	0.1642	1	13.88	171.4	18.68	127.4	16	60
		6	443,659	10,377	0.1580	1	14.19	172.1	19.07	128.1	16	60
		9	396,859	4,596	0.1585	1	14.74	174.6	19.71	130.6	16	60
NV19I28_4.5_60°C	7%	0	35,347,810	103,963	0.0768	1	12.20	165.1	17.11	126.1	16	60
		3	4,254,831	25,654	0.0944	1	12.80	167.8	17.35	123.8	16	60
		6	3,484,786	16,750	0.0989	1	13.86	174.4	18.54	130.4	16	60
		9	2,183,083	5,941	0.1019	1	14.56	179.1	19.30	135.1	16	60
NV19I28_5.22_60°C	4%	0	3,318,178,000	1,251,776	0.0547	1	10.57	150.8	15.8	116.1	16	60
		3	48,365,800	111,750	0.0748	1	11.95	163.1	17.8	135.0	16	60
		6	4,959,424	21,895	0.0924	1	12.86	167.0	18.0	128.5	16	60
		9	3,340,913	14,561	0.0979	1	13.90	174.5	18.4	128.4	16	60
	7%	0	905,630,000	1,131,378	0.0611	1	11.48	164.1	18.4	150.5	16	60
		3	18,155,520	61,307	0.0822	1	12.37	165.8	16.8	121.8	16	60
		6	4,907,393	25,523	0.0946	1	13.32	169.9	18.0	125.9	16	60
		9	1,994,736	7,300	0.1027	1	14.41	176.8	19.2	132.9	16	60
	11%	0	7,666,950,000	2,561,775	0.0534	1	10.11	145.4	17.1	129.7	16	60
		3	12,841,770	40,229	0.0828	1	11.64	155.8	18.0	130.1	16	60
		6	4,197,622	21,170	0.0942	1	13.30	170.3	18.5	131.7	16	60
		9	3,010,803	8,814	0.0970	1	13.80	174.2	19.2	134.7	16	60
NV19I28_5.22_85°C	4%	0.5	15,937,970	77,292	0.0817	1	12.06	162.5	18.40	138.1	16	60
		1	1,294,424	13,904	0.1062	1	13.09	169.7	18.76	136.8	16	60
		3	536,082	229	0.1070	1	17.72	199.9	20.50	148.2	22	60
	7%	0.5	3,795,025	36,893	0.0952	1	11.57	156.4	18.72	139.8	16	60
		1	1,404,573	11,402	0.1025	1	14.65	183.0	18.45	130.6	16	60
		3	739,772	50	0.0961	1	17.87	203.7	25.26	182.9	16	60
	11%	0.5	3,595,222	34,466	0.0954	1	12.19	161.1	17.83	128.0	16	60
		1	1,177,274	8,474	0.1065	1	13.28	169.6	19.36	139.9	16	60
		3	448,350	35	0.1046	1	18.40	203.4	22.56	163.8	22	60
NV19F28_6.0_60°C	7%	0	1.01x10^13[a]	2,955,253	0.0521	1	10.38	150.1	15.1	111.1	16	60
		3	32,459,600,000	90,413	0.0779	1	11.68	158.1	17.3	125.2	16	60
		6	4,771,319,000	14,788	0.0923	1	13.27	13.3	18.7	133.7	16	60
		9	4,159,577,000	12,213	0.0937	1	13.54	13.5	19.1	136.7	16	60

a - G_0 = 10,079,480,000,000 (kPa)

Table 24.4 Dynamic Shear Modulus and Shift Function Parameters for Utah Mixtures

Aging Conditions			CAS Parameters				WLF		Kaelble			
ID	Air Void	Dur. (mo)	G_0 (kPa)	ω_0 (rad/s)	β	κ	C_1	C_2	C_1	C_2	T_k (°C)	T_r (°C)
UT12.5I28_3.79_60°C	4%	0	43,815,510	242,205	0.0757	1	10.50	149.7	18.08	140.6	16	60
		3	3,427,682	47,572	0.0979	1	11.79	159.6	17.76	131.1	16	60
		6	2,605,692	34,594	0.1021	1	13.15	170.8	17.88	128.4	16	60
		9	665,319	6,085	0.1172	1	13.44	169.6	18.98	133.9	16	60
	7%	0	44,584,950	229,310	0.0759	1	11.01	153.5	17.69	133.7	16	60
		3	3,114,874	41,768	0.0991	1	12.01	160.6	17.92	131.0	16	60
		6	2,908,207	16,821	0.0981	1	13.00	166.5	18.51	131.1	16	60
		9	944,629	8,578	0.1133	1	14.35	176.7	18.53	127.0	16	60
	11%	0	225,845,400	840,846	0.0682	1	10.78	154.1	17.65	138.2	16	60
		3	6,303,807	53,880	0.0915	1	12.65	165.9	17.87	128.6	16	60
		6	1,481,826	16,348	0.1075	1	12.97	166.9	18.56	132.5	16	60
		9	954,799	4,927	0.1101	1	14.52	176.8	19.18	131.2	16	60
UT12.5F28 5.22_60°C	7%	0	212,844,500	601,062	0.0669	1	10.57	151.2	16.65	126.3	16	60
		3	7,802,383	41,609	0.0870	1	10.79	149.1	18.54	138.9	16	60
		6	1,680,128	10,762	0.1032	1	13.52	171.0	19.10	135.9	16	60
		9	1,205,733	5,450	0.1046	1	13.54	167.9	18.11	134.6	22	60

Table 24.5 Dynamic Shear Modulus and Shift Function Parameters for WesTrack Mixtures

Aging Conditions			CAS Parameters				WLF		Kaelble			
ID	Air Void	Dur. (mo)	G_0 (kPa)	ω_0 (rad/s)	β	κ	C_1	C_2	C_1	C_2	T_k (°C)	T_r (°C)
WT97C22_5.1_60°C	4%	0	276,891	192,474	0.2012	1	9.65	136.3	13.24	91.3	20	60
		3	193,823	69,010	0.2095	1	10.72	143.9	14.39	98.7	20	60
		6	208,433	44,968	0.2039	1	11.35	148.4	15.08	103.2	20	60
		9	204,967	31,805	0.2002	1	11.62	149.8	14.56	100.8	22	60
	7%	0	214,021	136,088	0.2110	1	9.95	139.9	13.52	94.9	20	60
		3	206,444	58,496	0.2102	1	10.95	145.3	13.88	96.7	22	60
		6	213,691	29,819	0.2011	1	11.89	151.9	16.65	107.9	16	60
		9	218,562	22,055	0.1985	1	12.49	156.2	15.46	107.1	22	60
	11%	0	198,101	117,397	0.2125	1	10.19	141.6	13.77	96.6	20	60
		3	226,926	32,563	0.1968	1	11.53	149.2	14.49	100.5	22	60
		6	225,025	16,711	0.1948	1	12.93	158.7	15.94	109.5	22	60
		9	249,834	9,922	0.1867	1	13.84	165.9	16.84	116.3	22	60
WT95F28 5.2_60°C	7%	0	565,125	143,737	0.1775	1	12.53	158.5	15.45	109.3	22	60
		3	462,982	37,650	0.1795	1	14.43	169.7	19.48	125.7	16	60
		6	414,178	12,158	0.1735	1	15.66	176.4	19.67	130.6	20	60
		9	544,796	3,849	0.1565	1	18.37	195.8	23.70	151.8	16	60

25 APPENDIX M:

Summary Dynamic Modulus Master Curves of Asphalt Mixtures

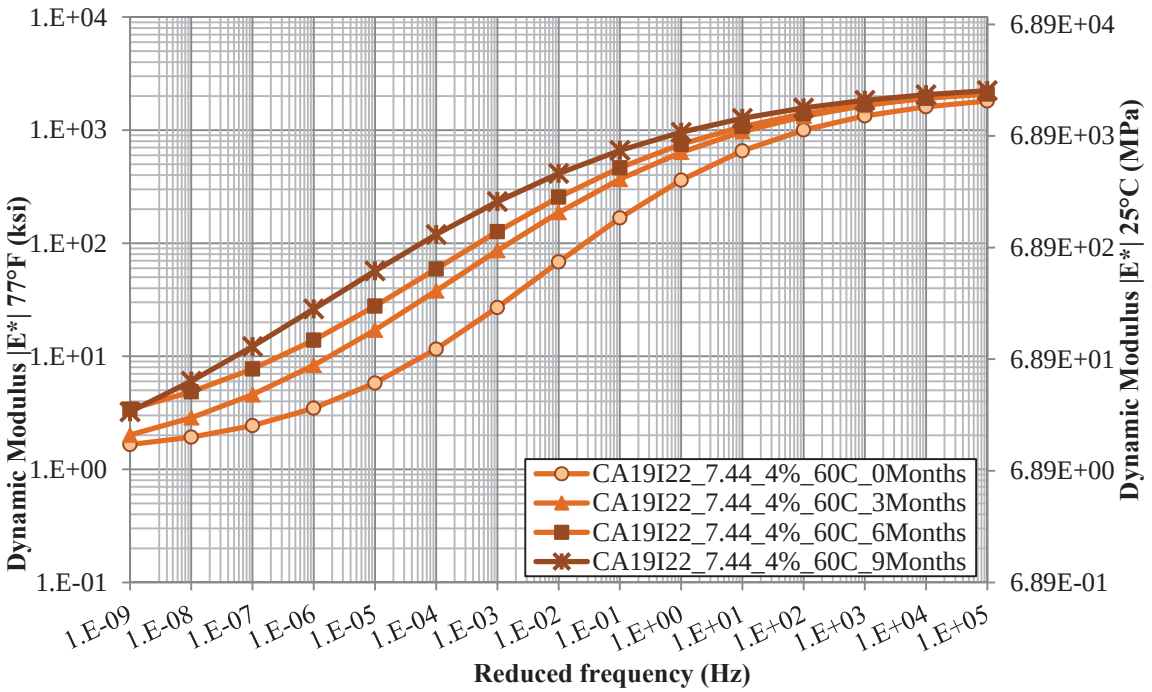

Figure 25.1 Summary of CAL19I22_7.44_4% Va Aged at 60°C Dynamic Modulus Master Curves

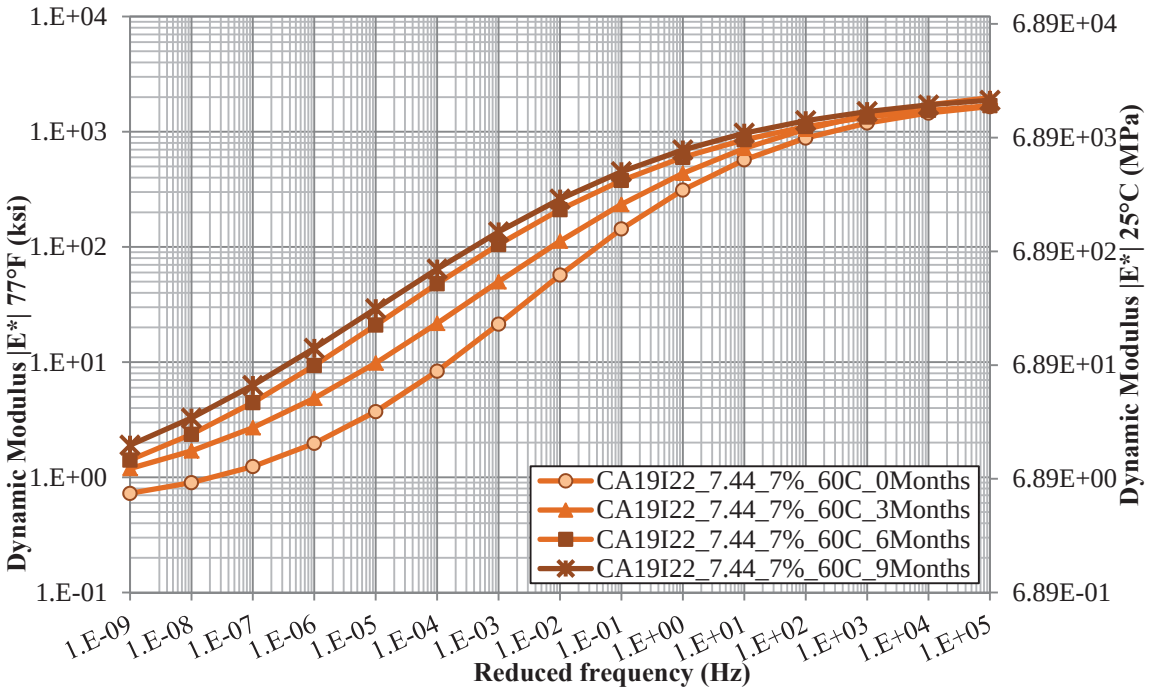

Figure 25.2 Summary of CAL19I22_7.44_7% Va Aged at 60°C Dynamic Modulus Master Curves

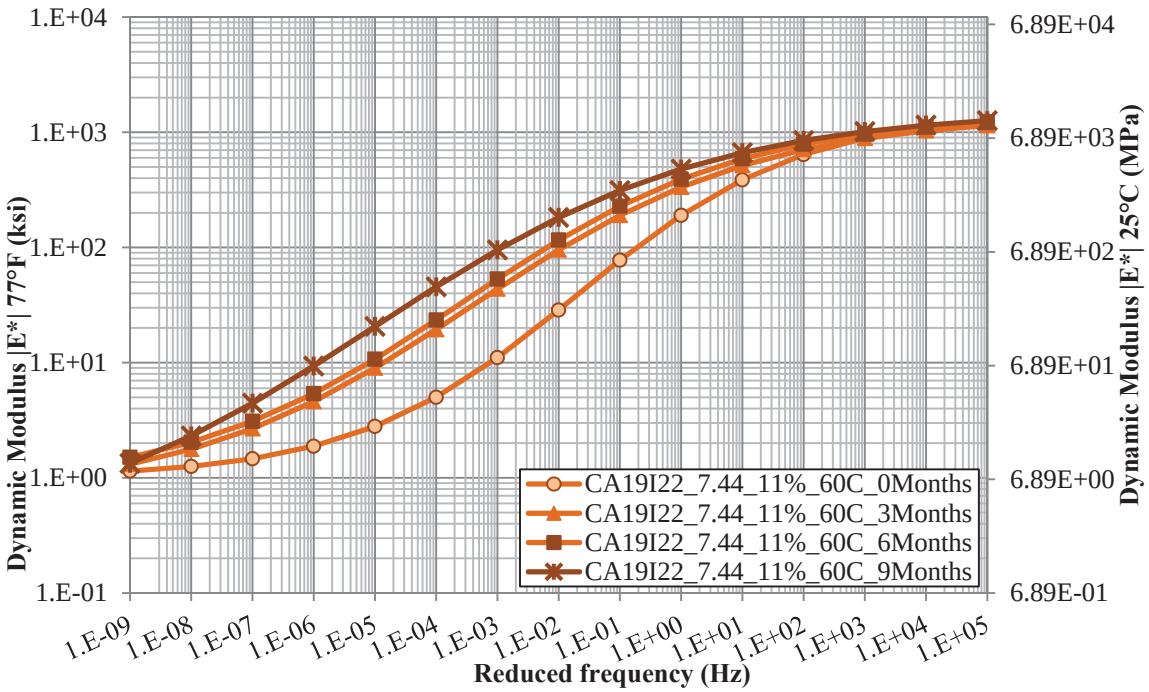

Figure 25.3 Summary of CAL19I22_7.44_11% Va Aged at 60°C Dynamic Modulus Master Curves

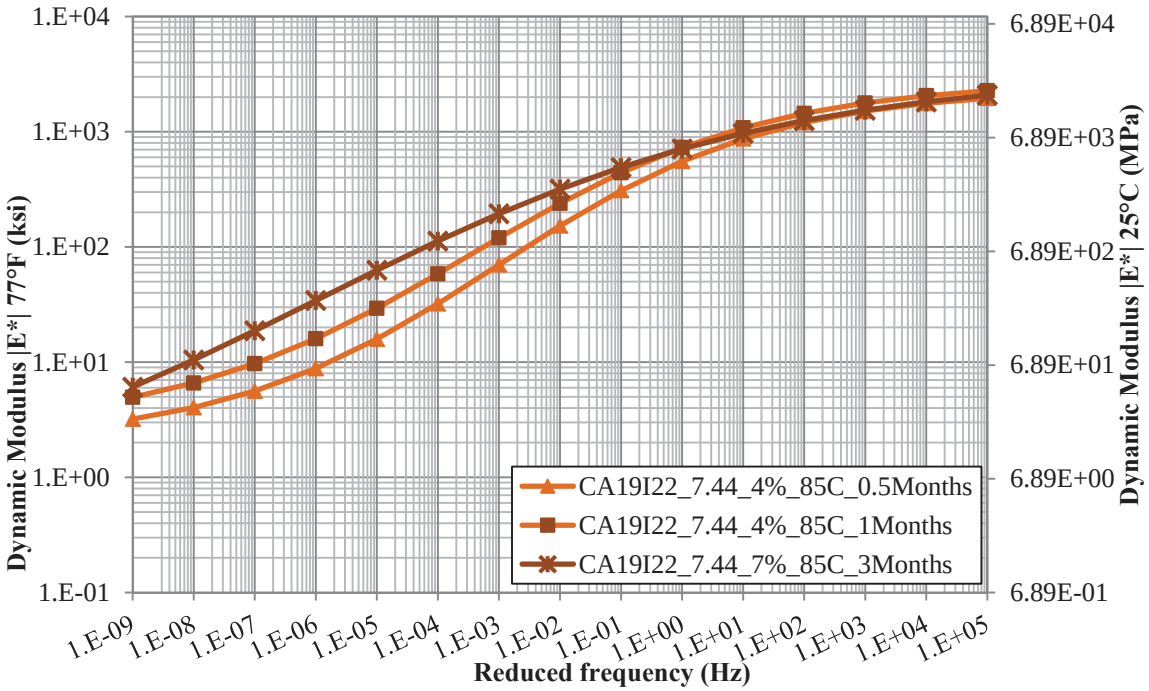

Figure 25.4 Summary of CAL19I22_7.44_4% Va Aged at 85°C Dynamic Modulus Master Curves

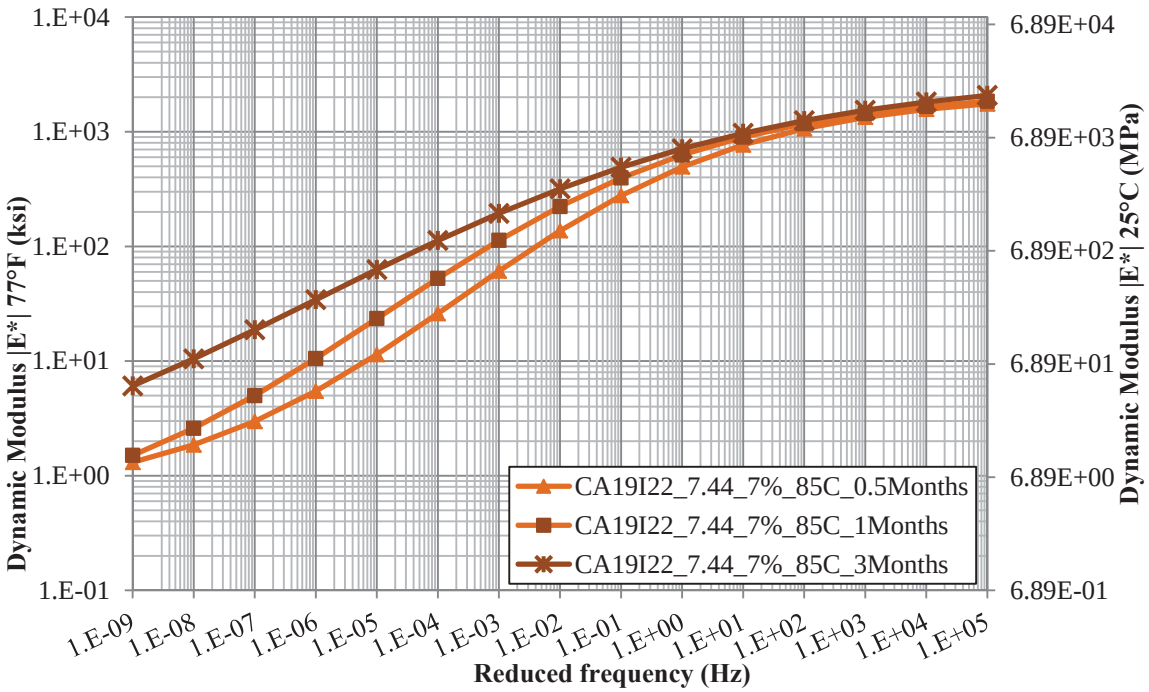

Figure 25.5 Summary of CAL19I22_7.44_7% Va Aged at 85°C Dynamic Modulus Master Curves

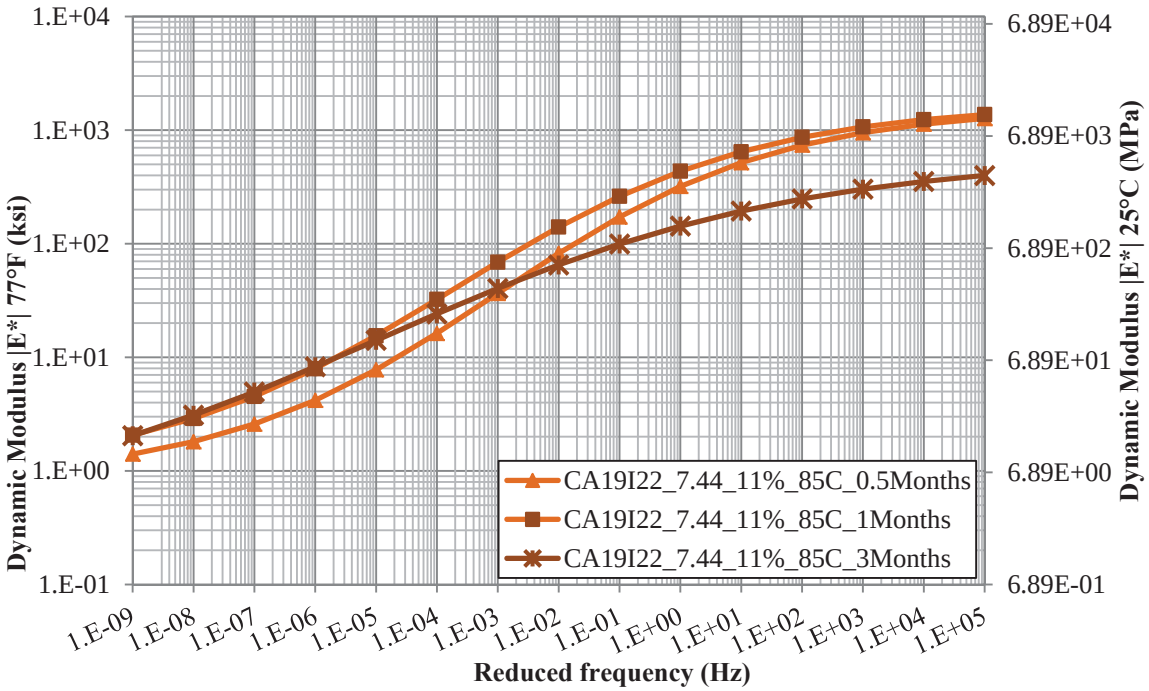

Figure 25.6 Summary of CAL19I22_7.44_11% Va Aged at 85°C Dynamic Modulus Master Curves

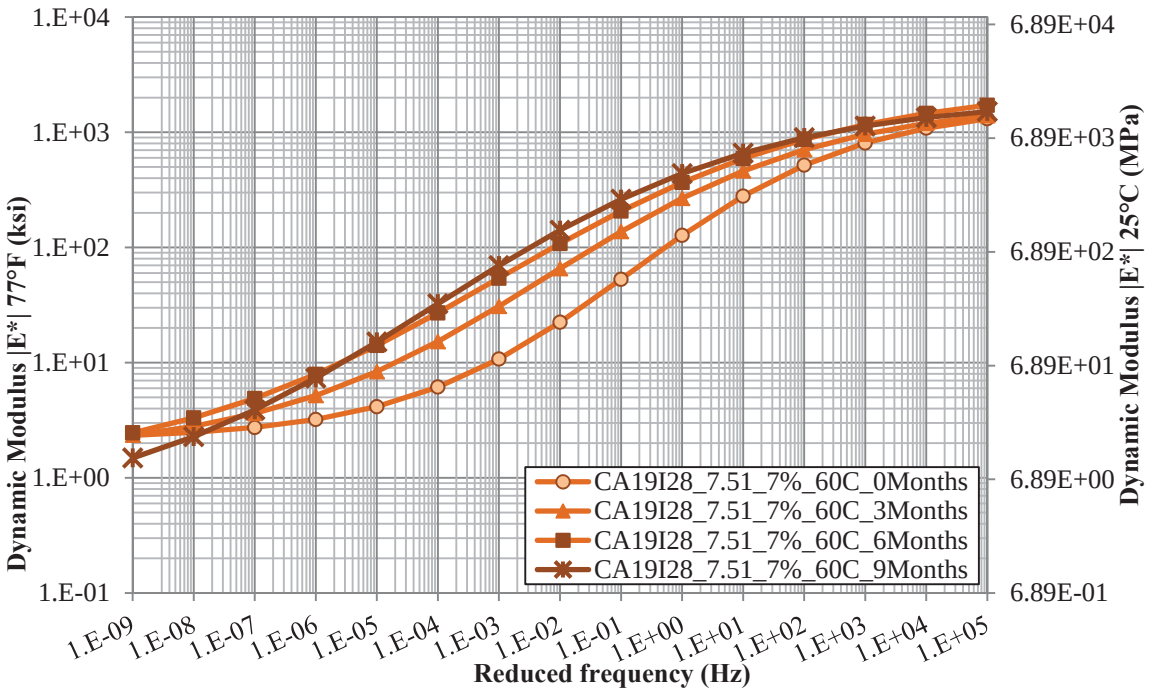

Figure 25.7 Summary of CAL19I28_7.51_7% Va Aged at 60°C Dynamic Modulus Master Curves

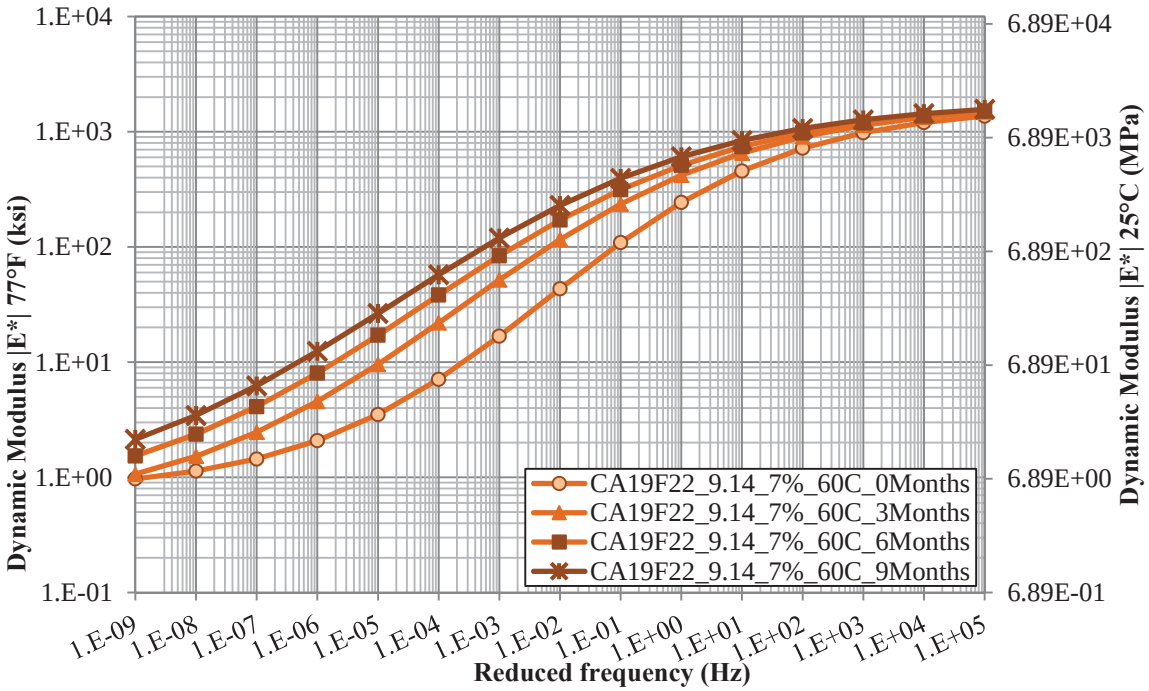

Figure 25.8 Summary of CAL19F22_9.14_7% Va Aged at 60°C Dynamic Modulus Master Curves

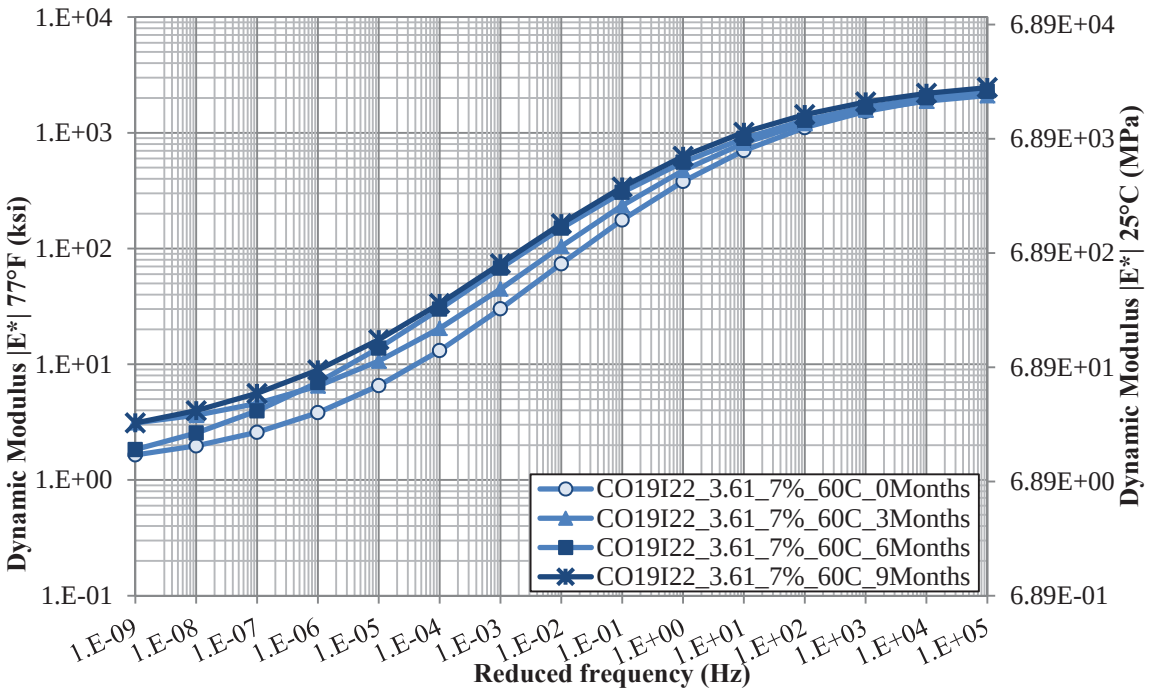

Figure 25.9 Summary of CO19I22_3.61_7% Va Aged at 60°C Dynamic Modulus Master Curves

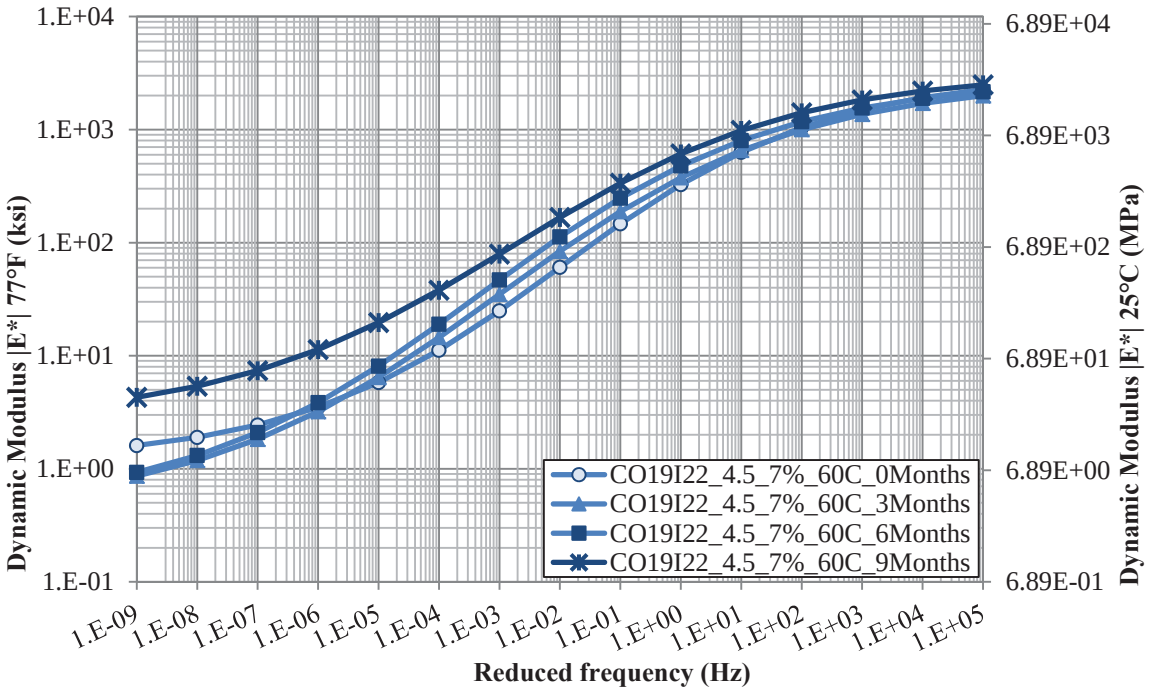

Figure 25.10 Summary of CO19I22_4.5_7% Va Aged at 60°C Dynamic Modulus Master Curves

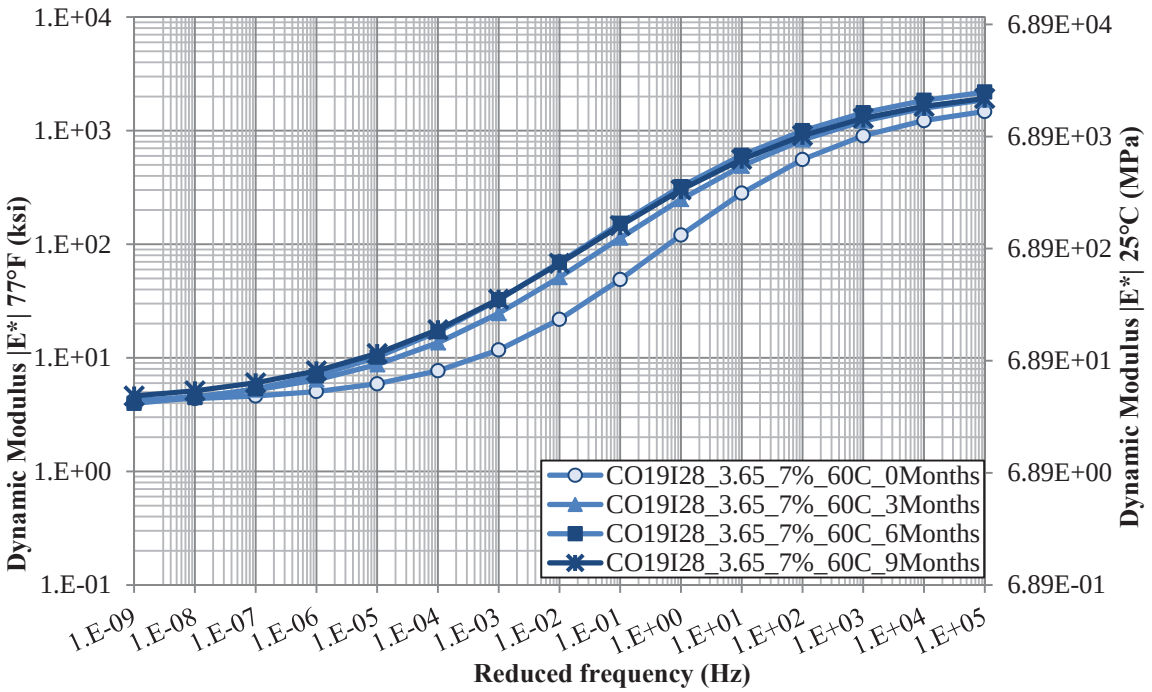

Figure 25.11 Summary of CO19I28_3.65_7% Va Aged at 60°C Dynamic Modulus Master Curves

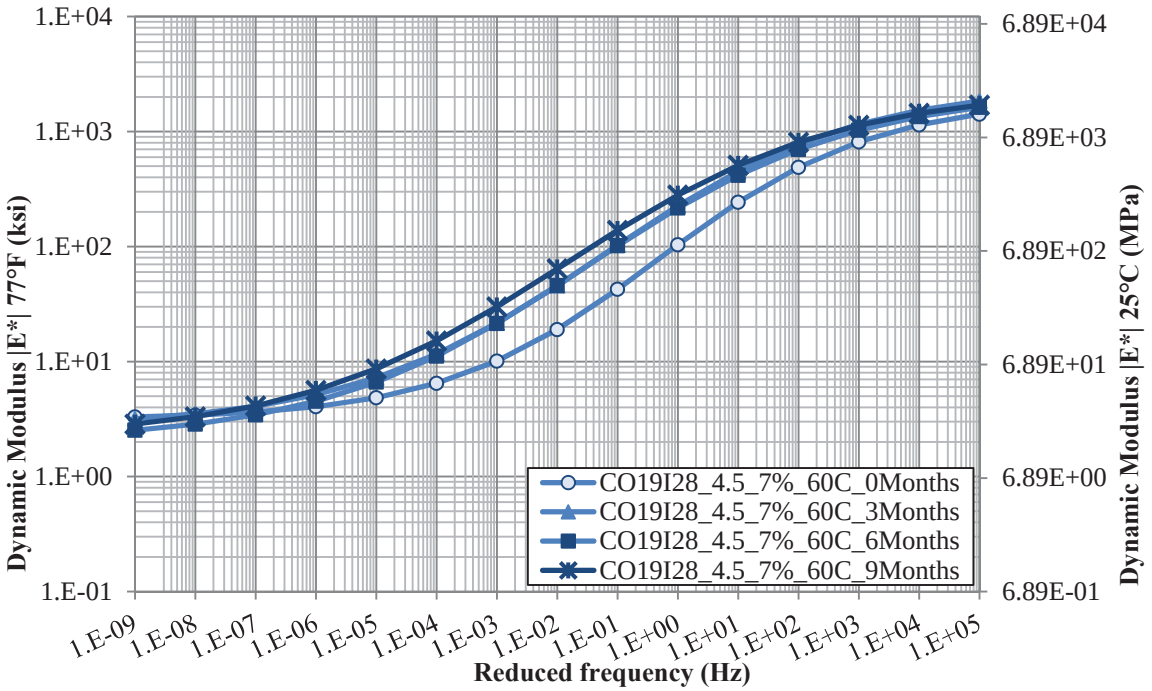

Figure 25.12 Summary of CO19I28_4.5_7% Va Aged at 60°C Dynamic Modulus Master Curves

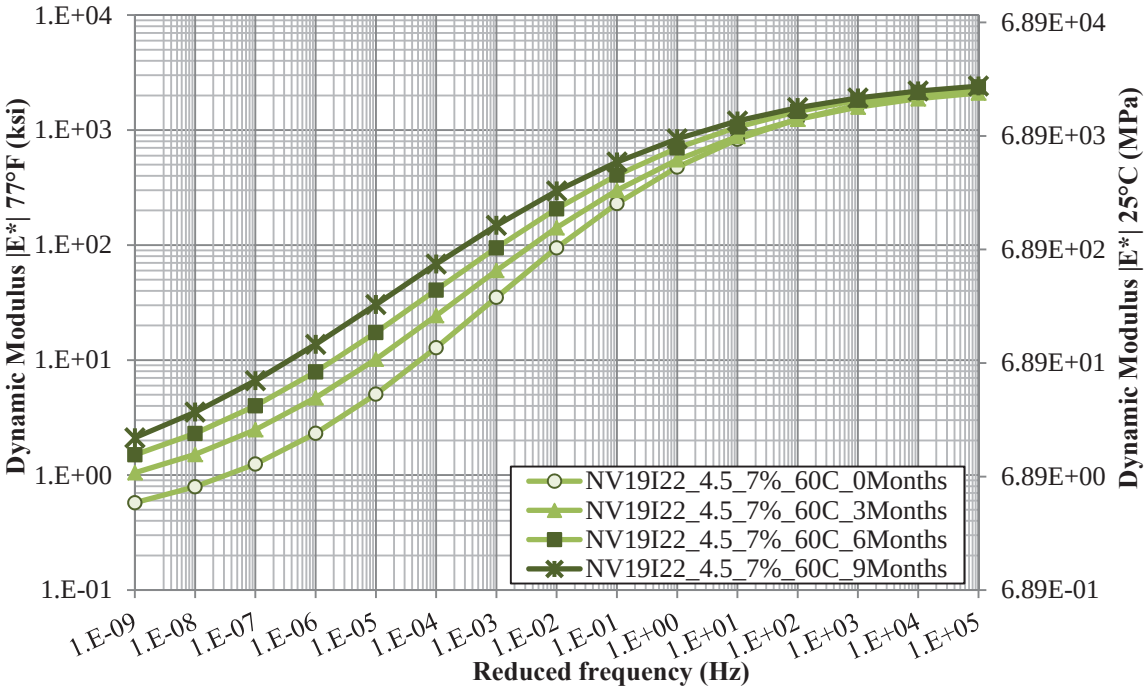

Figure 25.13 Summary of NV19I22_4.5_7% Va Aged at 60°C Dynamic Modulus Master Curves

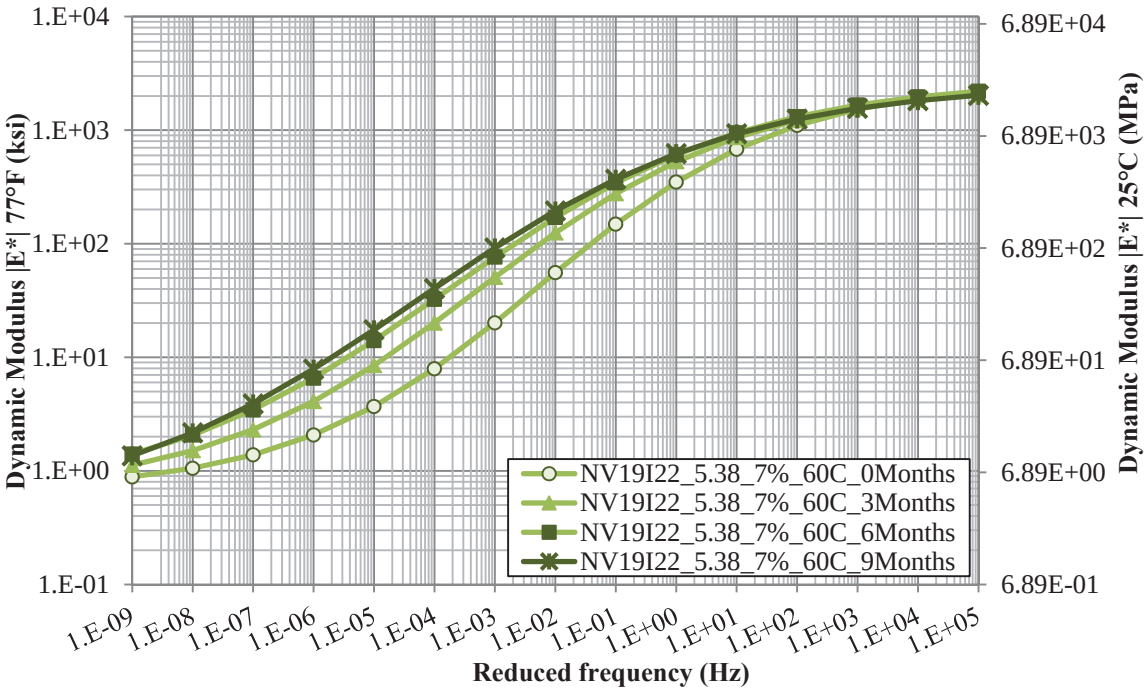

Figure 25.14 Summary of NV19I22_5.38_7% Va Aged at 60°C Dynamic Modulus Master Curves

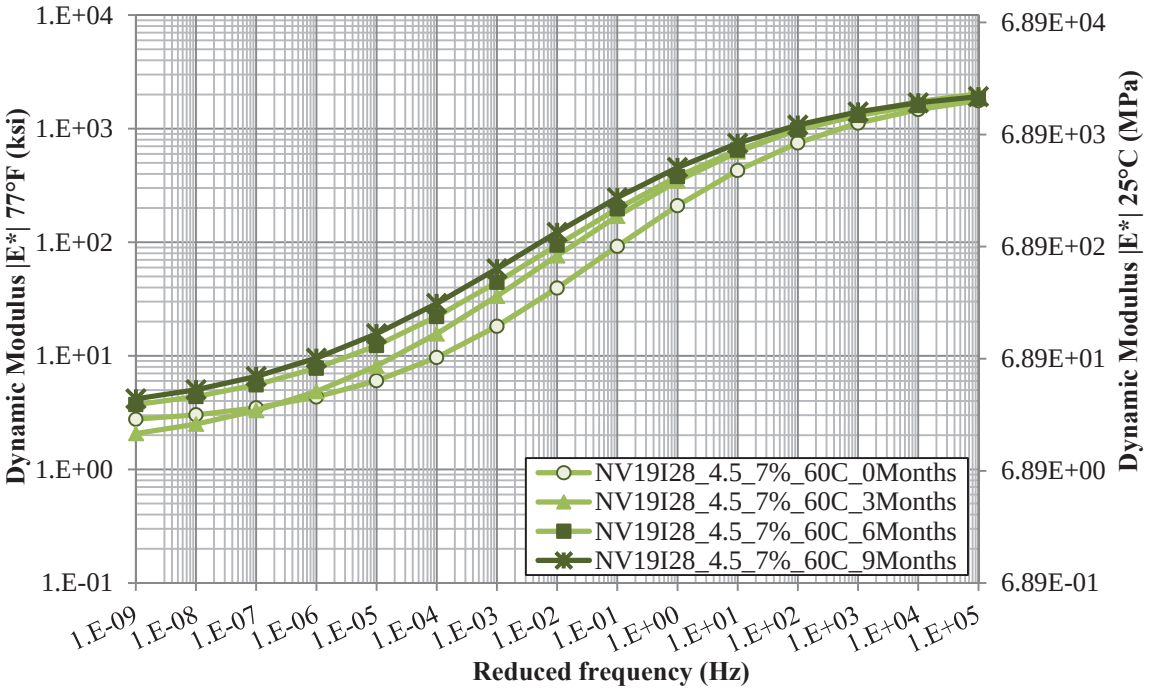

Figure 25.15 Summary of NV19I28_4.5_7% Va Aged at 60°C Dynamic Modulus Master Curves

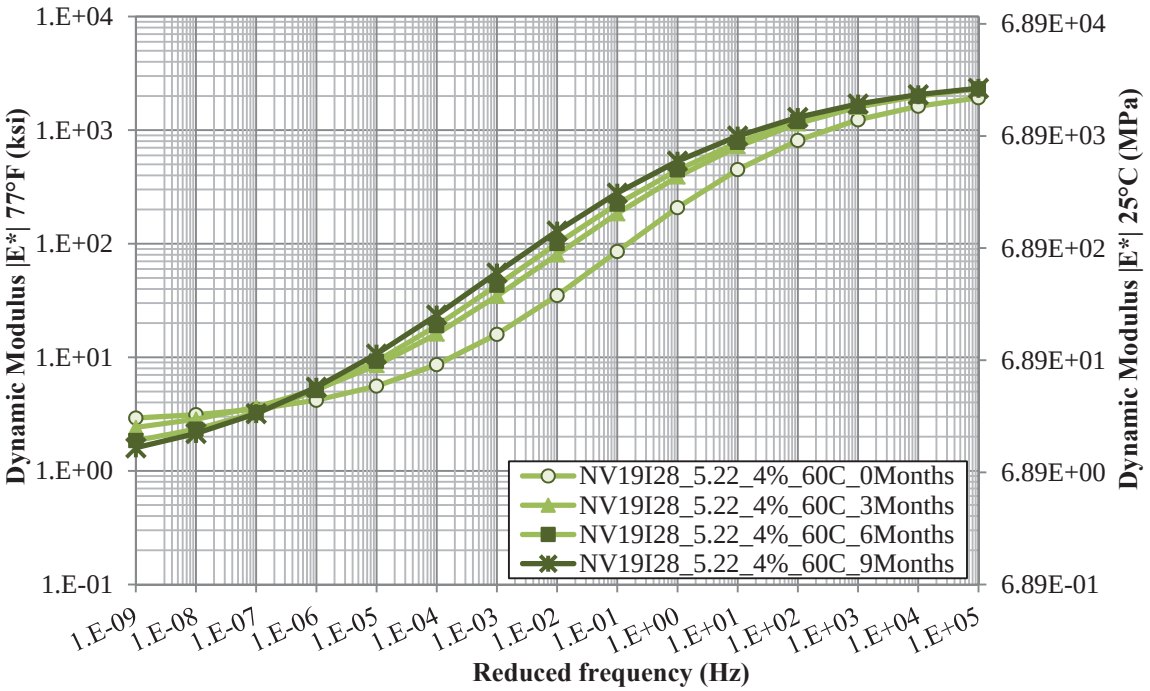

Figure 25.16 Summary of NV19I28_5.22_4% Va Aged at 60°C Dynamic Modulus Master Curves

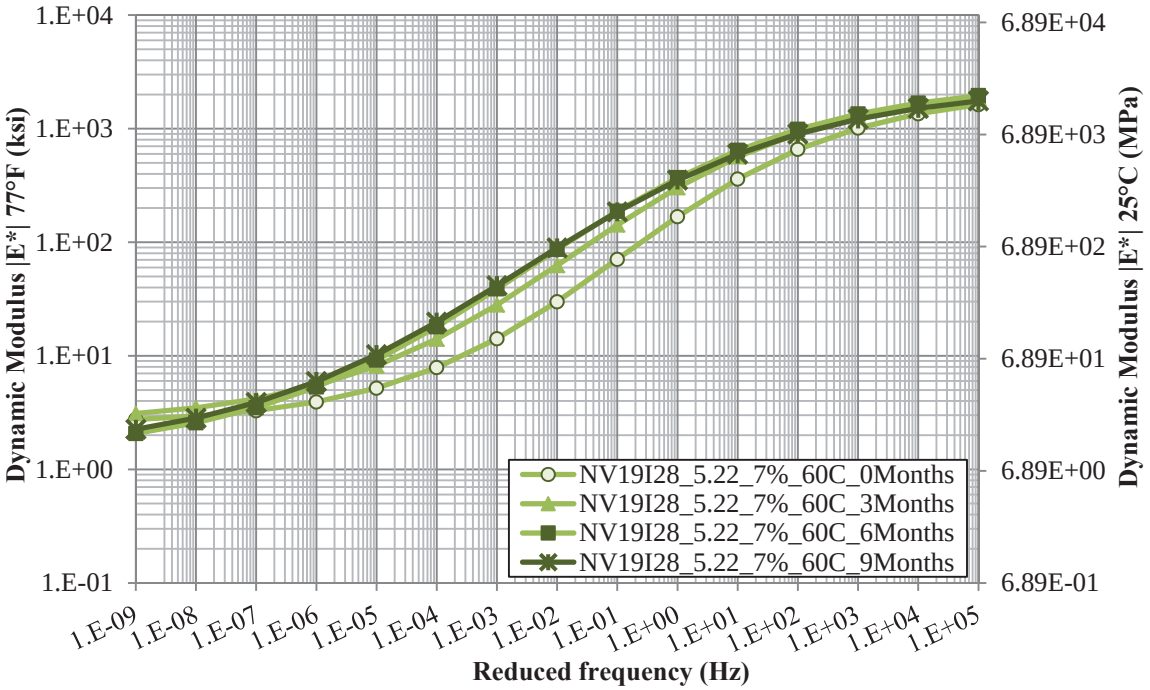

Figure 25.17 Summary of NV19I28_5.22_7% Va Aged at 60°C Dynamic Modulus Master Curves

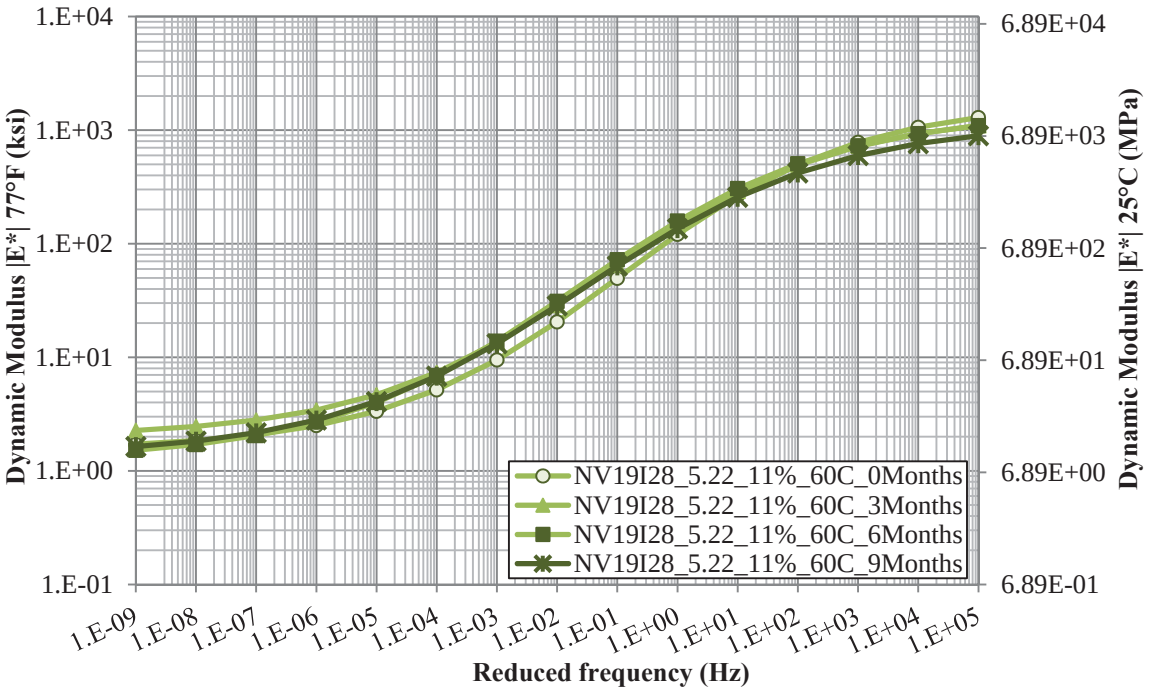

Figure 25.18 Summary of NV19I28_5.22_11% Va Aged at 60°C Dynamic Modulus Master Curves

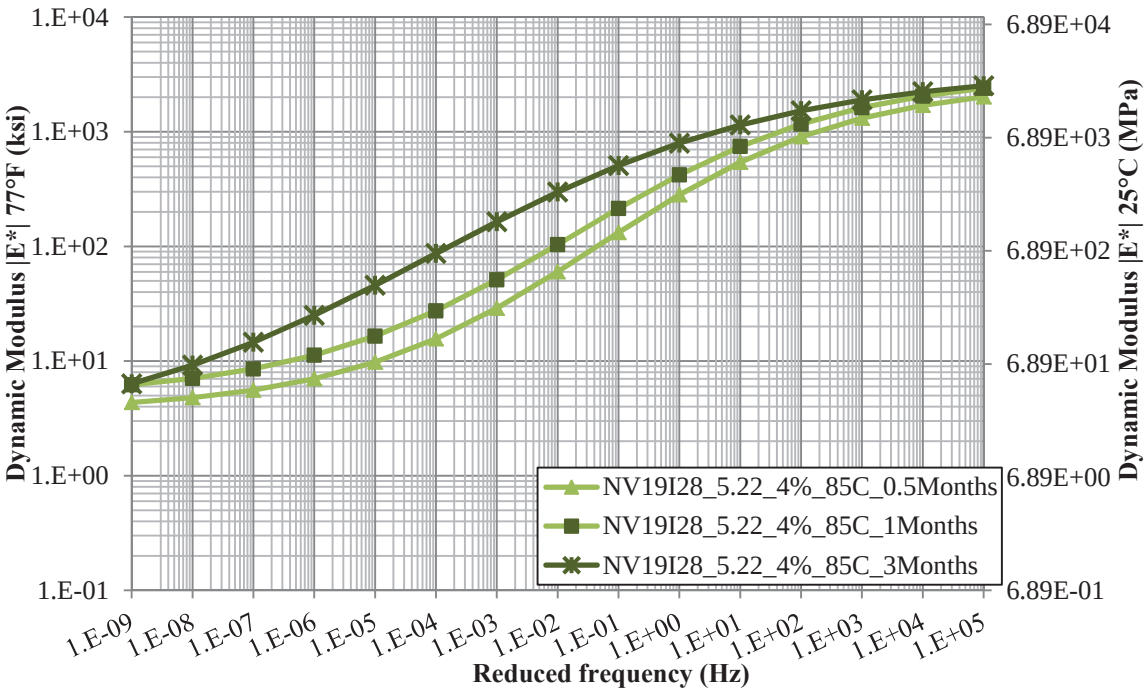

Figure 25.19 Summary of NV19I28_5.22_4% Va Aged at 85°C Dynamic Modulus Master Curves

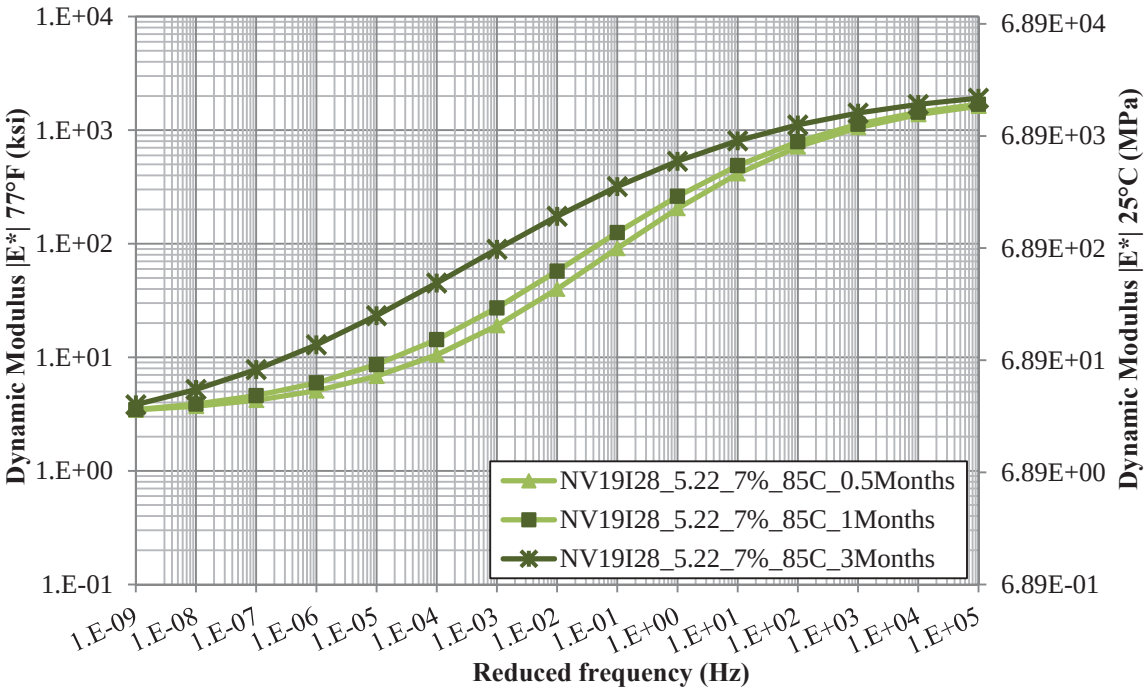

Figure 25.20 Summary of NV19I28_5.22_7% Va Aged at 85°C Dynamic Modulus Master Curves

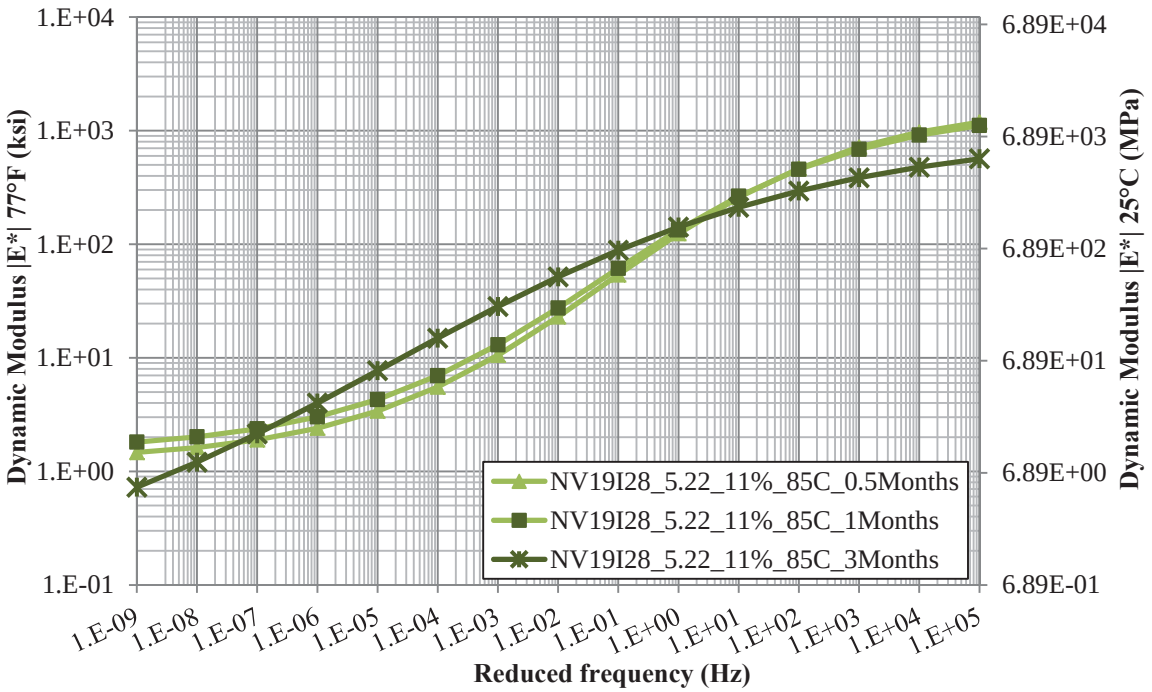

Figure 25.21 Summary of NV19I28_5.22_11% Va Aged at 85°C Dynamic Modulus Master Curves

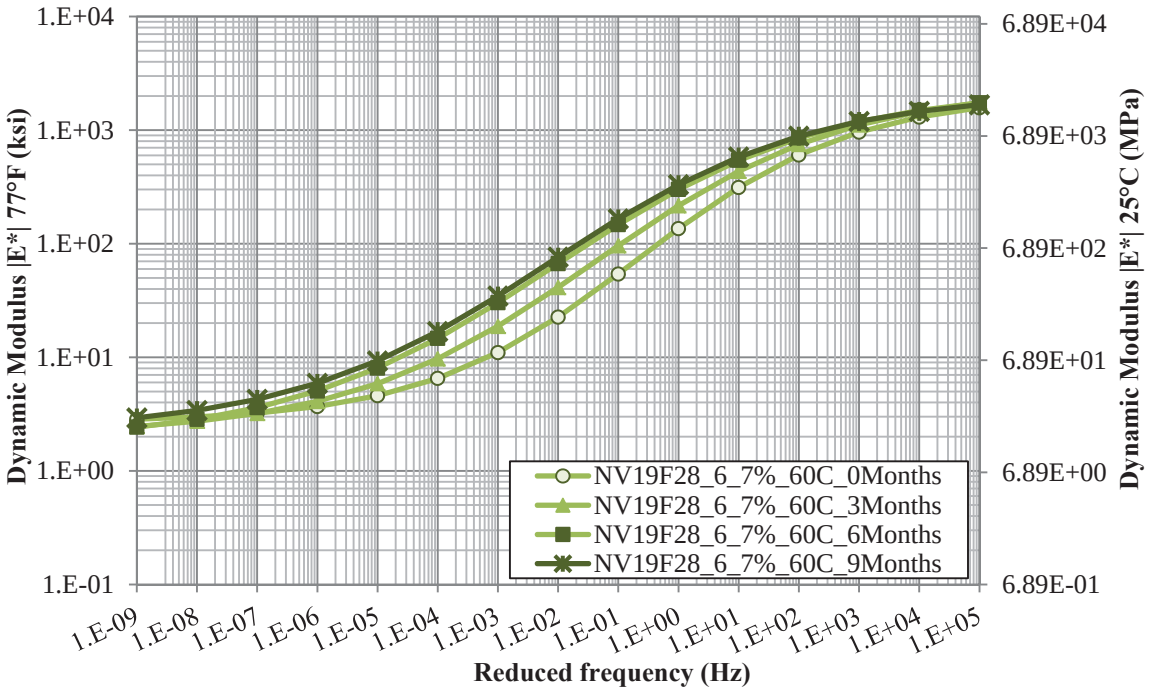

Figure 25.22 Summary of NV19F28_6.0_7% Va Aged at 60°C Dynamic Modulus Master Curves

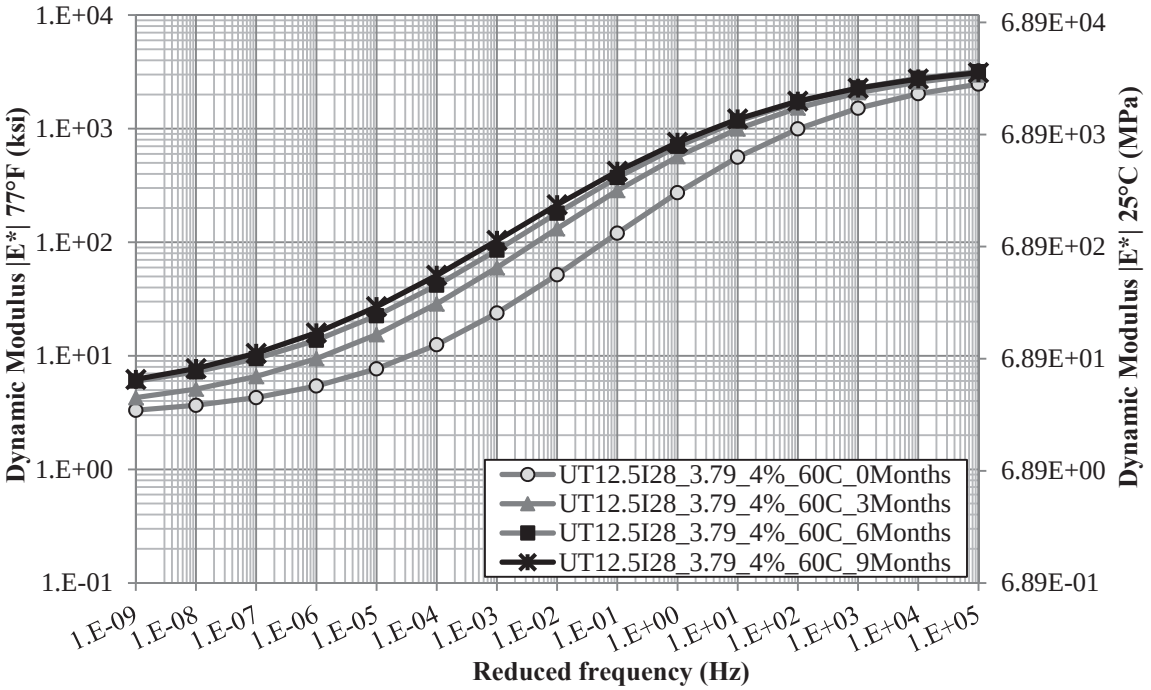

Figure 25.23 Summary of UT12.5I28_3.79_4% Va Aged at 60°C Dynamic Modulus Master Curves

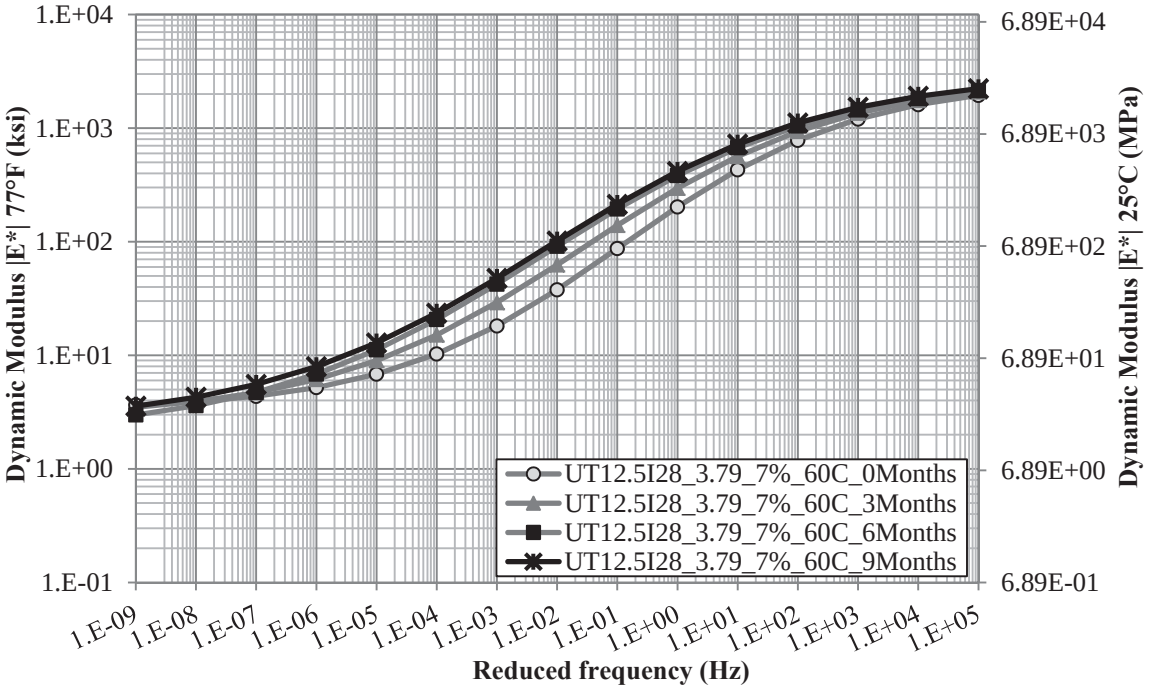

Figure 25.24 Summary of UT12.5I28_3.79_7% Va Aged at 60°C Dynamic Modulus Master Curves

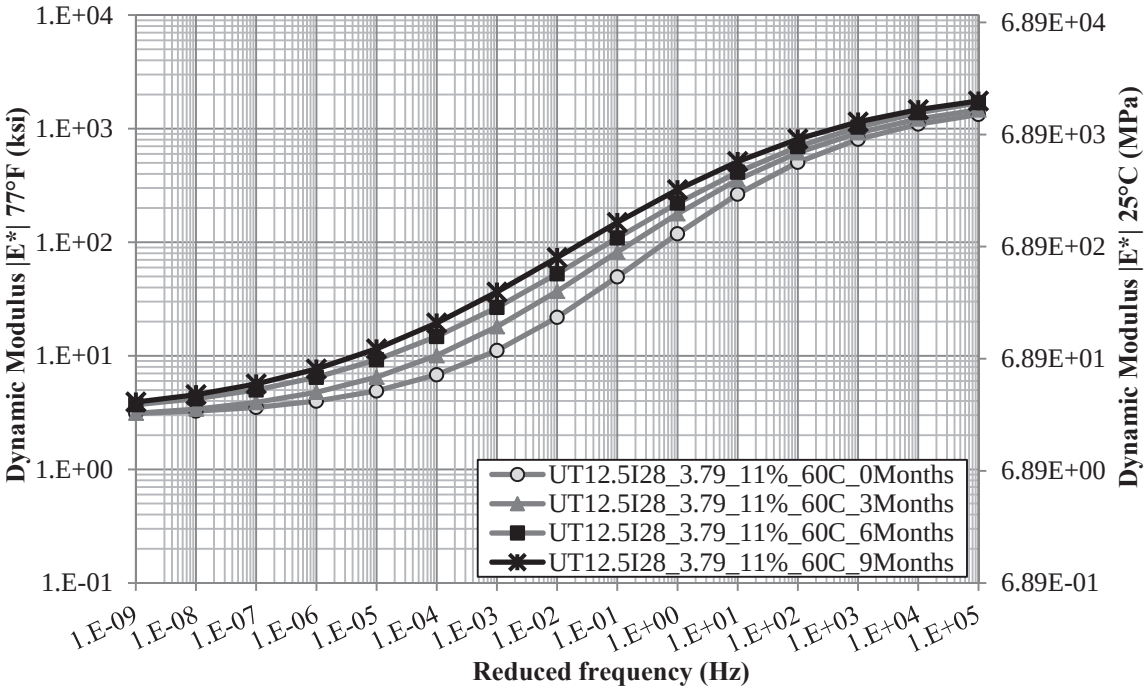

Figure 25.25 Summary of UT12.5I28_3.79_11% Va Aged at 60°C Dynamic Modulus Master Curves

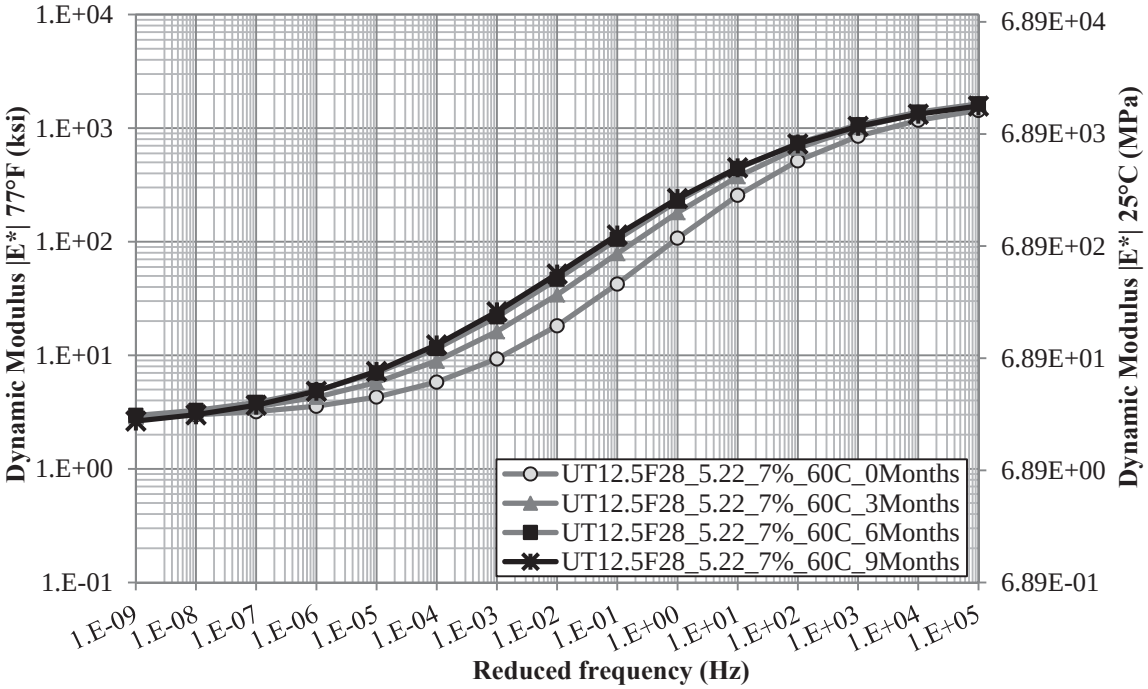

Figure 25.26 Summary of UT12.5F28_5.22_7% Va Aged at 60°C Dynamic Modulus Master Curves

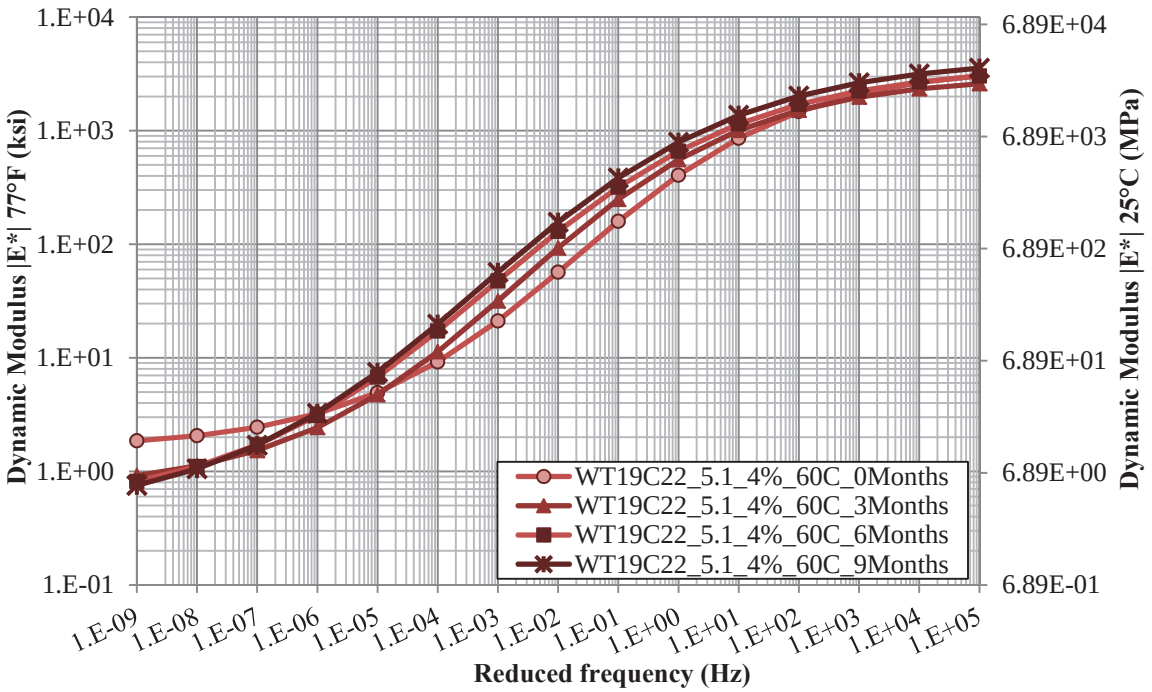

Figure 25.27 Summary of WT97C22_5.1_4% Va Aged at 60°C Dynamic Modulus Master Curves

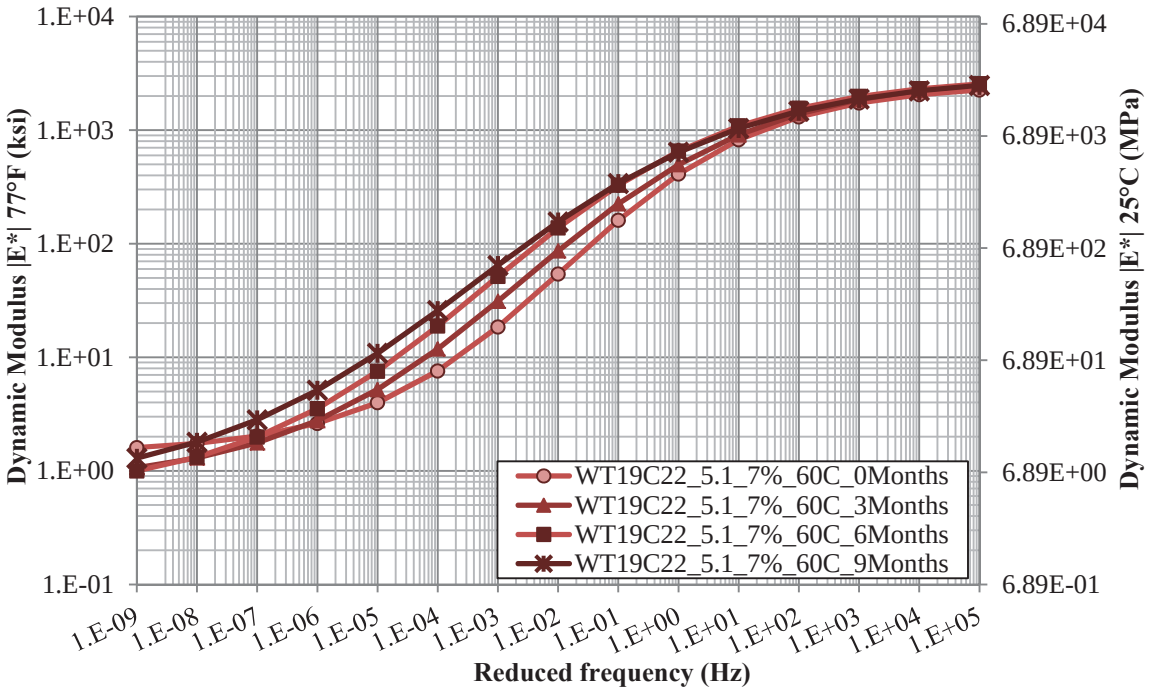

Figure 25.28 Summary of WT97C22_5.1_7% Va Aged at 60°C Dynamic Modulus Master Curves

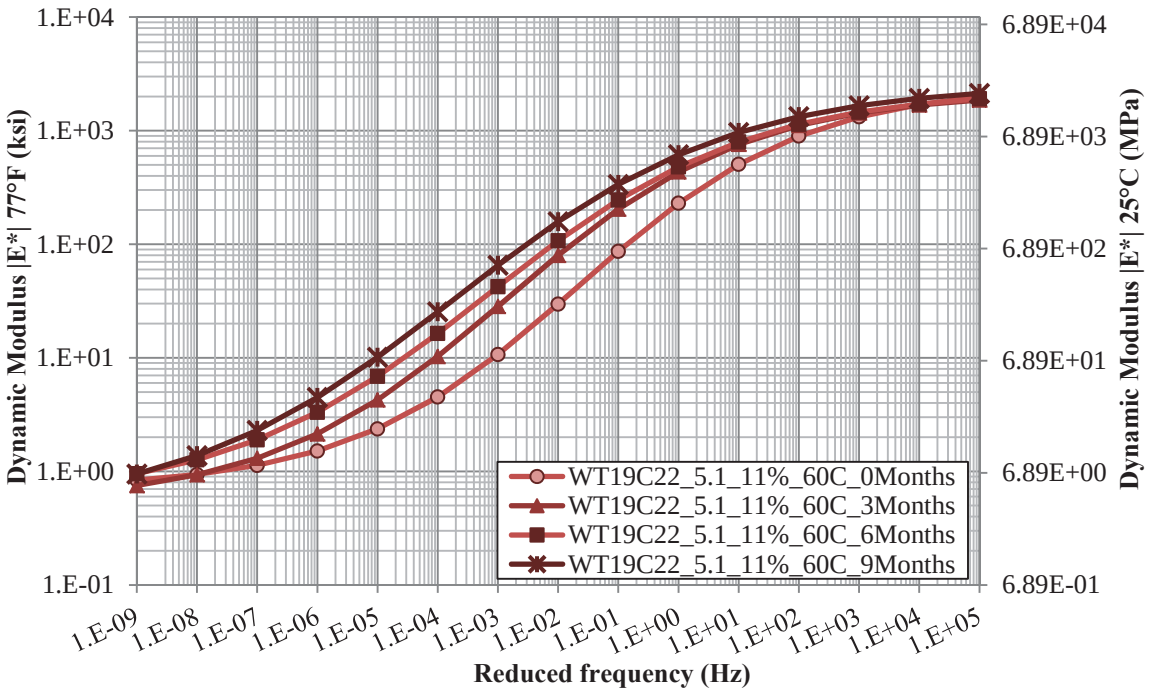

Figure 25.29 Summary of WT97C22_5.1_11% Va Aged at 60°C Dynamic Modulus Master Curves

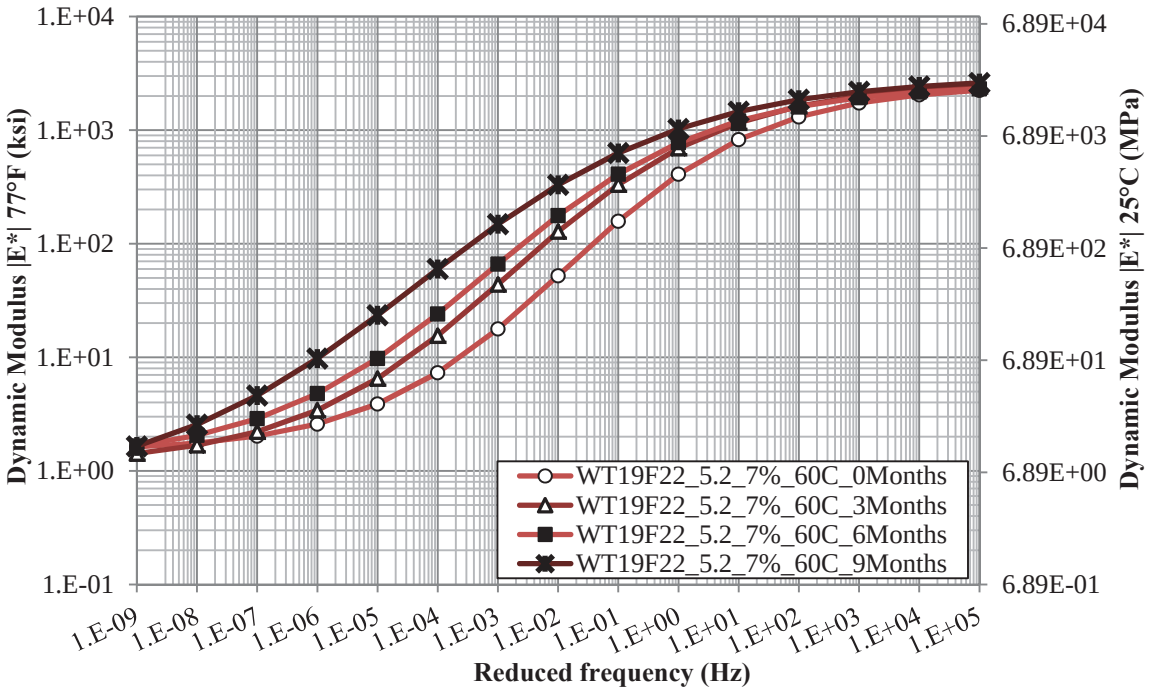

Figure 25.30 Summary of WT95F22_5.2_7% Va Aged at 60°C Dynamic Modulus Master Curves

26 APPENDIX N:

Summary of Mixture Dynamic Modulus Master Curve Function Parameters

Table 26.1 Dynamic Modulus and Shift Function Parameters for California Mixtures

Aging Conditions			Standard Logistic Sigmoid Parameters				Second-Order Polynomial Shift Function			
ID	Air Void	Dur. (mo)	δ (ksi)	α (ksi)	γ	β	a	b	c	T_r (°F)
CAL19I22_7.44_60°C	4%	0	0.1148	3.2240	0.5039	-1.3772	2.64E-04	-0.1065	6.172	70
		3	-0.0449	3.4691	0.4129	-1.7320	2.36E-04	-0.1080	6.414	70
		6	0.1827	3.2113	0.4164	-1.8509	2.31E-04	-0.1063	6.321	70
		9	-0.4256	3.8628	0.3503	-2.1671	2.39E-04	-0.1092	6.547	70
	7%	0	-0.3044	3.6195	0.4740	-1.4159	1.79E-04	-0.0968	5.995	70
		3	-0.2969	3.7324	0.3890	-1.4961	1.21E-04	-0.0853	5.361	70
		6	-0.4718	3.7899	0.3804	-1.9938	3.09E-04	-0.1194	6.841	70
		9	-0.4295	3.7989	0.3665	-2.0270	2.29E-04	-0.1085	6.448	70
	11%	0	0.0029	3.1699	0.5504	-1.2154	2.42E-04	-0.1051	6.148	70
		3	-0.1584	3.3049	0.4280	-1.6535	3.14E-04	-0.1198	6.909	70
		6	-0.0918	3.2497	0.4400	-1.7967	2.60E-04	-0.1117	6.522	70
		9	-0.5861	3.7798	0.3678	-2.0457	2.35E-04	-0.1085	6.432	70
CAL19I22_7.44_85°C	4%	0.5	0.3116	3.0603	0.4494	-1.5884	2.68E-04	-0.1088	6.263	70
		1	0.4163	3.0280	0.4142	-1.6537	2.60E-04	-0.1111	6.500	70
		3	0.3904	3.0460	0.3636	-1.8852	2.37E-04	-0.1024	6.051	70
	7%	0.5	-0.2228	3.5602	0.4178	-1.7228	2.31E-04	-0.1051	6.219	70
		1	-0.5466	3.9213	0.3603	-1.9434	2.40E-04	-0.1106	6.575	70
		3	-0.4413	3.9586	0.2668	-1.7513	2.37E-04	-0.1028	5.934	70
	11%	0.5	-0.0734	3.2729	0.4369	-1.5326	2.62E-04	-0.1114	6.520	70
		1	-0.0312	3.2622	0.4039	-1.7156	2.36E-04	-0.1080	6.394	70
		3	-0.4362	3.2033	0.2928	-1.5301	3.30E-04	-0.0952	5.082	70
CAL19I28_7.51_60°C	7%	0	0.3310	2.9117	0.5313	-0.6967	2.78E-04	-0.1058	6.023	70
		3	0.2151	3.0581	0.4323	-1.1702	2.31E-04	-0.1020	5.997	70
		6	0.0432	3.3669	0.3616	-1.2671	1.56E-04	-0.0913	5.626	70
		9	-0.3429	3.6473	0.3678	-1.6907	2.42E-04	-0.1086	6.428	70
CAL19F22_9.14_60°C	7%	0	-0.1244	3.3519	0.4962	-1.3417	2.17E-04	-0.1016	6.037	70
		3	-0.3217	3.5903	0.4159	-1.7315	2.39E-04	-0.1076	6.354	70
		6	-0.2965	3.5670	0.3926	-1.8924	2.20E-04	-0.1070	6.392	70
		9	-0.2407	3.5185	0.3835	-1.9972	2.08E-04	-0.1072	6.528	70

Table 26.2 Dynamic Modulus and Shift Function Parameters for Colorado Mixtures Aged at 60°C

Aging Conditions			Standard Logistic Sigmoid Parameters				Second-Order Polynomial Shift Function			
ID	Air Void	Dur. (mo)	δ (ksi)	α (ksi)	γ	β	a	b	c	T_r (°F)
CO19I22_7% Va	3.61	0	0.0753	3.3791	0.4647	-1.2726	2.25E-04	-0.1029	6.110	70
		3	0.3816	3.0200	0.4903	-1.3886	2.71E-04	-0.1079	6.208	70
		6	-0.0721	3.5511	0.4010	-1.5484	2.53E-04	-0.1083	6.337	70
		9	0.2798	3.2076	0.4370	-1.5397	3.06E-04	-0.1168	6.619	70
	4.5	0	0.0737	3.4134	0.4590	-1.1382	2.73E-04	-0.1088	6.285	70
		3	-0.3774	3.8199	0.4045	-1.4177	2.18E-04	-0.1022	6.103	70
		6	-0.3679	3.8223	0.4121	-1.5746	2.26E-04	-0.1049	6.233	70
		9	0.4265	3.0778	0.4250	-1.4141	2.39E-04	-0.1047	6.114	70
CO19I28_7% Va	3.65	0	0.6136	2.6624	0.5942	-0.4757	2.41E-04	-0.0976	5.632	70
		3	0.5657	2.8301	0.4966	-0.8388	3.00E-04	-0.1096	6.179	70
		6	0.5090	2.9650	0.4655	-0.9640	2.49E-04	-0.1031	5.954	70
		9	0.5855	2.8222	0.4738	-0.9392	2.75E-04	-0.1076	6.177	70
	4.5	0	0.4969	2.7883	0.5611	-0.4329	2.97E-04	-0.1041	5.803	70
		3	0.4311	2.9766	0.4776	-0.7996	2.04E-04	-0.0947	5.669	70
		6	0.3053	3.0560	0.4553	-0.8749	2.22E-04	-0.0972	5.750	70
		9	0.3364	3.0281	0.4467	-1.0564	3.14E-04	-0.1169	6.646	70

Table 26.3 Dynamic Modulus and Shift Function Parameters for Nevada Mixtures

Aging Conditions			Standard Logistic Sigmoid Parameters				Second-Order Polynomial Shift Function			
ID	Air Void	Dur. (mo)	δ (ksi)	α (ksi)	γ	β	a	b	c	T_r (°F)
NV19I22_ 4.5_60°C	7%	0	-0.5168	3.9740	0.4448	-1.6398	2.91E-04	-0.1112	6.324	70
		3	-0.3328	3.7543	0.4193	-1.7156	2.22E-04	-0.1045	6.235	70
		6	-0.2845	3.7624	0.3964	-1.8010	2.77E-04	-0.1149	6.687	70
		9	-0.3125	3.7939	0.3733	-1.9452	1.78E-04	-0.1010	6.224	70
NV19I22_ 5.38_60°C	7%	0	-0.1792	3.6162	0.4923	-1.3792	2.94E-04	-0.1118	6.326	70
		3	-0.2039	3.6006	0.4497	-1.6884	2.54E-04	-0.1110	6.550	70
		6	-0.2506	3.6968	0.4041	-1.7196	2.30E-04	-0.1073	6.410	70
		9	-0.4026	3.8148	0.3839	-1.8427	2.74E-04	-0.1161	6.795	70
NV19I28_ 4.5_60°C	7%	0	0.3795	2.9975	0.4959	-0.8494	2.40E-04	-0.0988	5.702	70
		3	0.1518	3.2908	0.4356	-1.1921	2.32E-04	-0.1020	5.979	70
		6	0.4372	2.9386	0.4481	-1.1954	2.55E-04	-0.1044	6.062	70
		9	0.4622	2.9238	0.4400	-1.3281	2.55E-04	-0.1076	6.265	70
NV19I28_5.22_60°C	4%	0	0.4222	2.9772	0.5324	-0.7971	2.41E-04	-0.1011	5.912	70
		3	0.2496	3.2432	0.4561	-1.1802	2.47E-04	-0.1050	6.123	70
		6	0.0599	3.4270	0.4309	-1.3239	2.72E-04	-0.1113	6.505	70
		9	-0.0655	3.5457	0.4235	-1.5359	2.71E-04	-0.1100	6.335	70
	7%	0	0.3951	2.9437	0.5202	-0.7347	2.17E-04	-0.0953	5.591	70
		3	0.4086	2.9637	0.4868	-1.0780	2.17E-04	-0.0997	5.911	70
		6	0.1219	3.3018	0.4248	-1.2593	2.55E-04	-0.1094	6.419	70
		9	0.1387	3.2423	0.4122	-1.2648	2.60E-04	-0.1080	6.280	70
	11 %	0	0.1869	3.0616	0.5144	-0.7175	2.21E-04	-0.0970	5.713	70
		3	0.3022	2.8548	0.5073	-0.8713	2.68E-04	-0.1022	5.794	70
		6	0.0938	3.0679	0.4798	-0.9811	2.47E-04	-0.1007	5.880	70
		9	0.1323	2.9397	0.4789	-1.0010	2.99E-04	-0.1088	6.094	70
NV19I28_5.22_85°C	4%	0.5	0.5690	2.8650	0.4808	-0.8750	2.49E-04	-0.1025	5.946	70
		1	0.6901	2.8191	0.4500	-0.9939	2.94E-04	-0.1120	6.407	70
		3	0.3083	3.2276	0.3464	-1.5912	2.02E-04	-0.1031	6.207	70
	7%	0.5	0.4855	2.8431	0.5110	-0.8183	2.47E-04	-0.0996	5.749	70
		1	0.4535	2.9002	0.4706	-0.9658	2.48E-04	-0.1031	5.990	70
		3	0.2348	3.1736	0.3769	-1.4865	2.71E-04	-0.1145	6.703	70
	11 %	0.5	0.0927	3.1392	0.4765	-0.8033	2.42E-04	-0.0995	5.726	70
		1	0.1762	3.0241	0.4647	-0.8331	3.03E-04	-0.1106	6.216	70
		3	-1.0871	4.0839	0.2823	-1.5005	3.17E-04	-0.1153	6.441	70
NV19F28_ 6.0_60°C	7%	0	0.4275	2.8870	0.5587	-0.6371	2.67E-04	-0.1026	5.829	70
		3	0.3172	3.0596	0.4833	-0.8934	2.57E-04	-0.1041	6.005	70
		6	0.2535	3.1132	0.4493	-1.1555	2.28E-04	-0.1018	5.959	70
		9	0.3509	2.9775	0.4656	-1.2095	2.92E-04	-0.1107	6.319	70

Table 26.4 Dynamic Modulus and Shift Function Parameters for Utah Mixtures

Aging Conditions			Standard Logistic Sigmoid Parameters				Second-Order Polynomial Shift Function			
ID	Air Void	Dur. (mo)	δ (ksi)	α (ksi)	γ	β	a	b	c	T_r (°F)
UT12.5I28_3.79_60°C	4%	0	0.4472	3.0952	0.4780	-0.7952	2.31E-04	-0.0985	5.784	70
		3	0.4869	3.1054	0.4459	-1.1976	2.07E-04	-0.0986	5.907	70
		6	0.6168	2.9972	0.4369	-1.2810	2.74E-04	-0.1093	6.291	70
		9	0.5870	3.0202	0.4184	-1.3368	1.78E-04	-0.0953	5.834	70
	7%	0	0.5173	2.9027	0.5150	-0.7056	1.91E-04	-0.0917	5.481	70
		3	0.4507	3.0052	0.4650	-0.9450	2.55E-04	-0.1034	5.965	70
		6	0.3081	3.1623	0.4255	-1.1368	2.85E-04	-0.1079	6.157	70
		9	0.3941	3.0878	0.4295	-1.1205	2.31E-04	-0.1001	5.938	70
	11%	0	0.4662	2.7829	0.5493	-0.5523	2.41E-04	-0.0974	5.640	70
		3	0.4328	2.8729	0.4857	-0.7824	2.69E-04	-0.1033	5.870	70
		6	0.4658	2.9445	0.4311	-0.7394	3.23E-04	-0.1145	6.501	70
		9	0.4607	2.9396	0.4237	-0.9800	2.89E-04	-0.1089	6.152	70
UT12.5F28 5.22_60°C	7%	0	0.4396	2.8379	0.5731	-0.4599	2.53E-04	-0.0991	5.755	70
		3	0.4057	2.9379	0.5031	-0.7871	2.62E-04	-0.1041	5.955	70
		6	0.3952	2.9460	0.4813	-0.9383	2.76E-04	-0.1087	6.218	70
		9	0.3209	3.0063	0.4603	-1.0063	2.53E-04	-0.1048	6.074	70

Table 26.5 Dynamic Modulus and Shift Function Parameters for WesTrack Mixtures

Aging Conditions			Standard Logistic Sigmoid Parameters				Second-Order Polynomial Shift Function			
ID	Air Void	Dur. (mo)	δ (ksi)	α (ksi)	γ	β	a	b	c	T_r (°F)
WT97C22_5.1_60°C	4%	0	0.2027	3.3732	0.5361	-1.1841	2.45E-04	-0.1042	6.063	70
		3	-0.1717	3.6542	0.5148	-1.6329	2.53E-04	-0.1059	6.147	70
		6	-0.3387	3.9124	0.4570	-1.6608	2.46E-04	-0.1084	6.389	70
		9	-0.4085	4.0523	0.4524	-1.7437	2.88E-04	-0.1153	6.606	70
	7%	0	0.1588	3.2468	0.5962	-1.4191	2.24E-04	-0.1026	6.085	70
		3	-0.1155	3.5989	0.4949	-1.5191	2.48E-04	-0.1084	6.384	70
		6	-0.2179	3.6989	0.4766	-1.7624	2.38E-04	-0.1075	6.354	70
		9	-0.1810	3.6677	0.4360	-1.7108	2.24E-04	-0.1052	6.245	70
	11%	0	-0.1489	3.5486	0.5276	-1.1325	2.44E-04	-0.1030	6.014	70
		3	-0.2796	3.6180	0.5034	-1.6848	2.02E-04	-0.1026	6.184	70
		6	-0.2522	3.6154	0.4601	-1.6712	2.44E-04	-0.1077	6.389	70
		9	-0.3624	3.7722	0.4374	-1.8528	2.20E-04	-0.1062	6.350	70
WT95F28 5.2_60°C	7%	0	0.1688	3.2313	0.6064	-1.4290	2.32E-04	-0.1035	6.101	70
		3	0.0508	3.3777	0.5584	-1.8294	2.44E-04	-0.1098	6.526	70
		6	0.0769	3.3278	0.5340	-1.9486	2.00E-04	-0.1044	6.386	70
		9	-0.1851	3.6556	0.4481	-2.1599	1.54E-04	-0.1013	6.395	70

27 APPENDIX O:

Summary of Uniaxial Thermal Stress and Strain Measurements of Aged Asphalt Mixtures

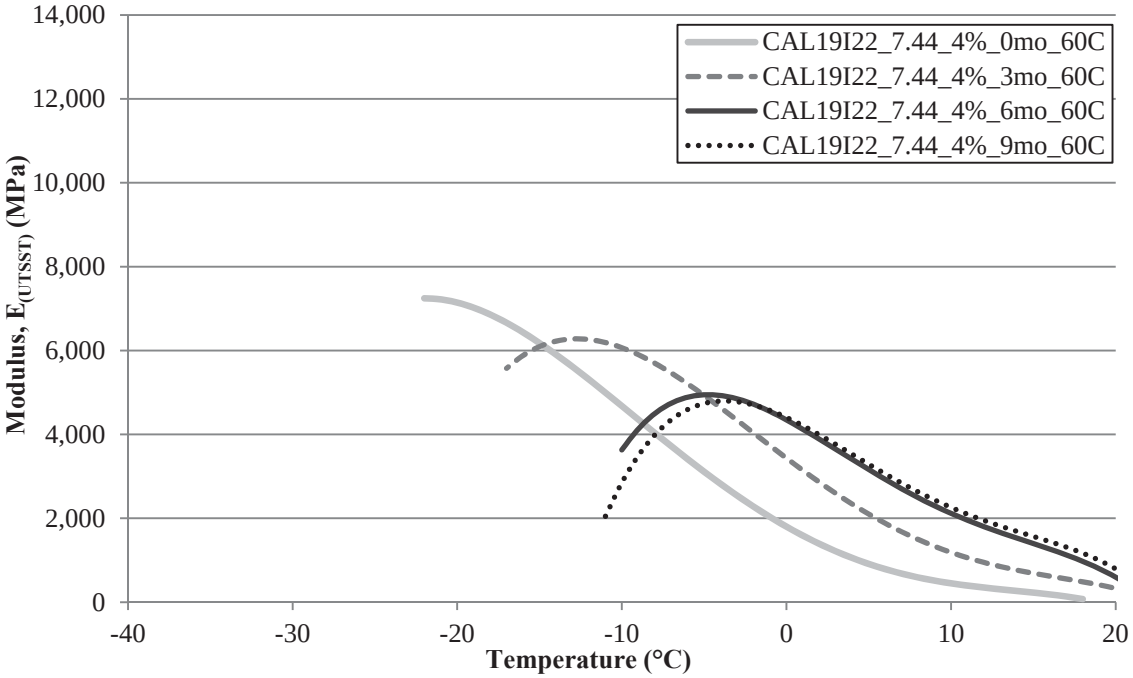

Figure 27.1 Summary of CAL19I22_7.44_4% Va Aged at 60°C UTSST Modulus Curves

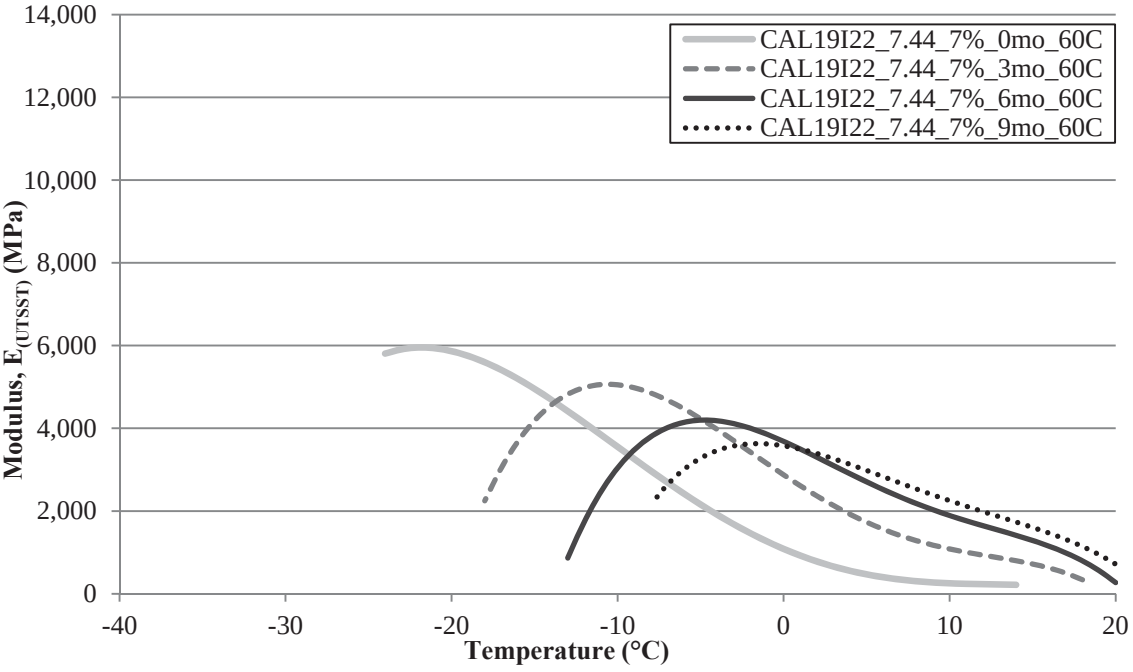

Figure 27.2 Summary of CAL19I22_7.44_7% Va Aged at 60°C UTSST Modulus Curves

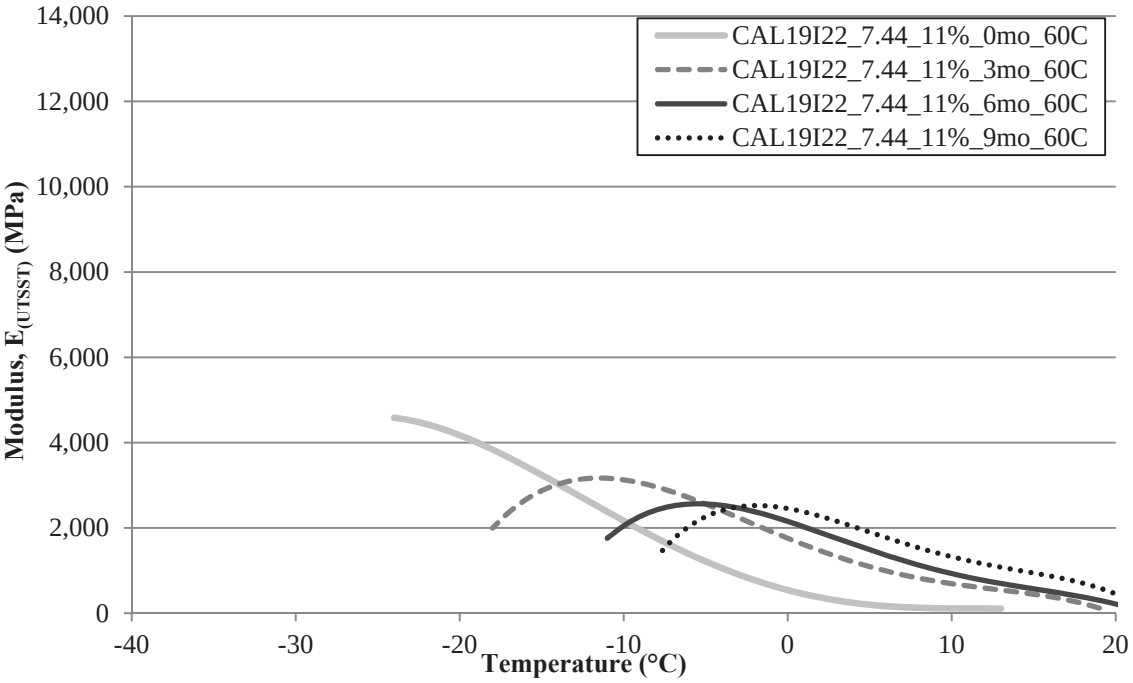

Figure 27.3 Summary of CAL19I22_7.44_11% Va Aged at 60°C UTSST Modulus Curves

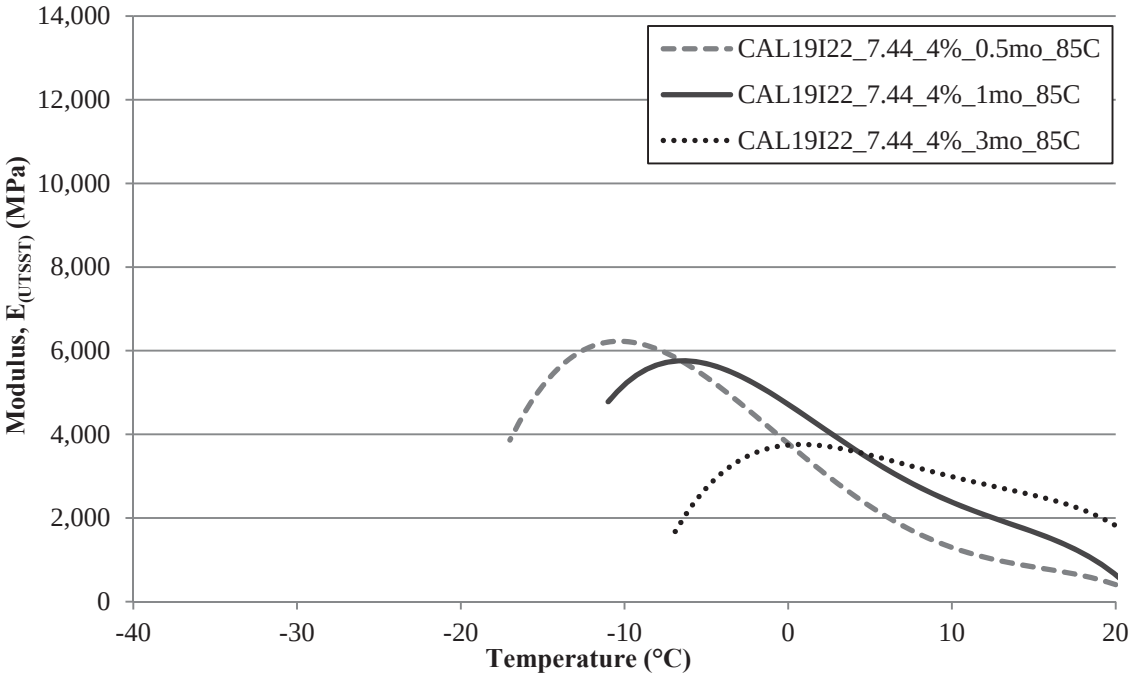

Figure 27.4 Summary of CAL19I22_7.44_4% Va Aged at 85°C UTSST Modulus Curves

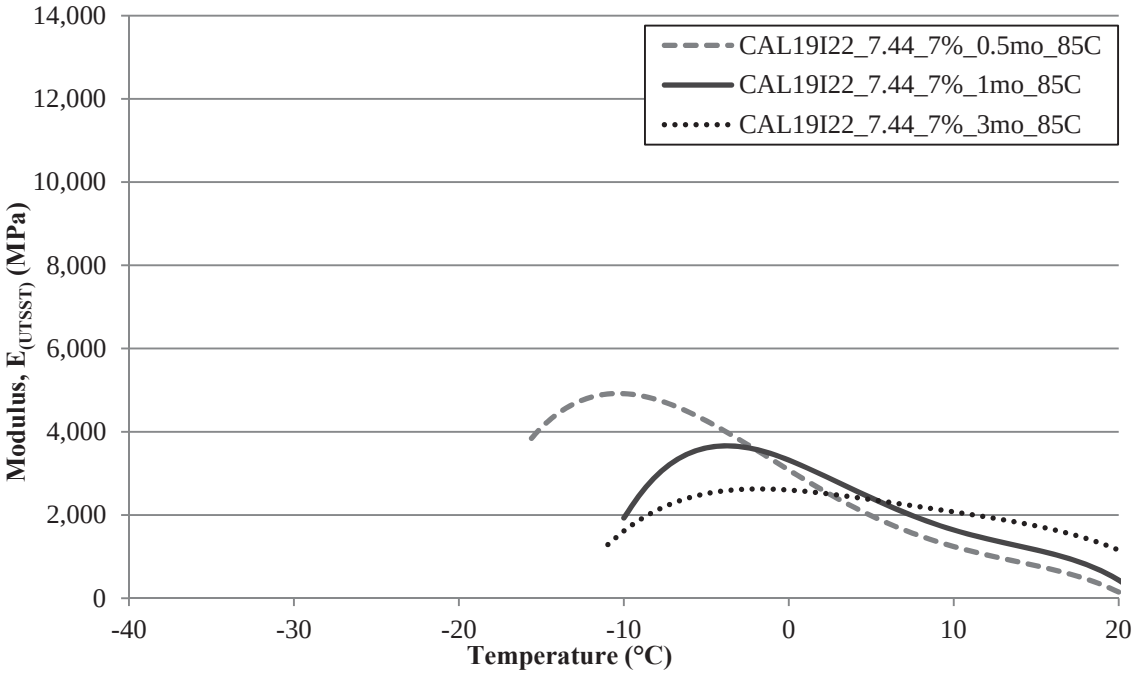

Figure 27.5 Summary of CAL19I22_7.44_7% Va Aged at 85°C UTSST Modulus Curves

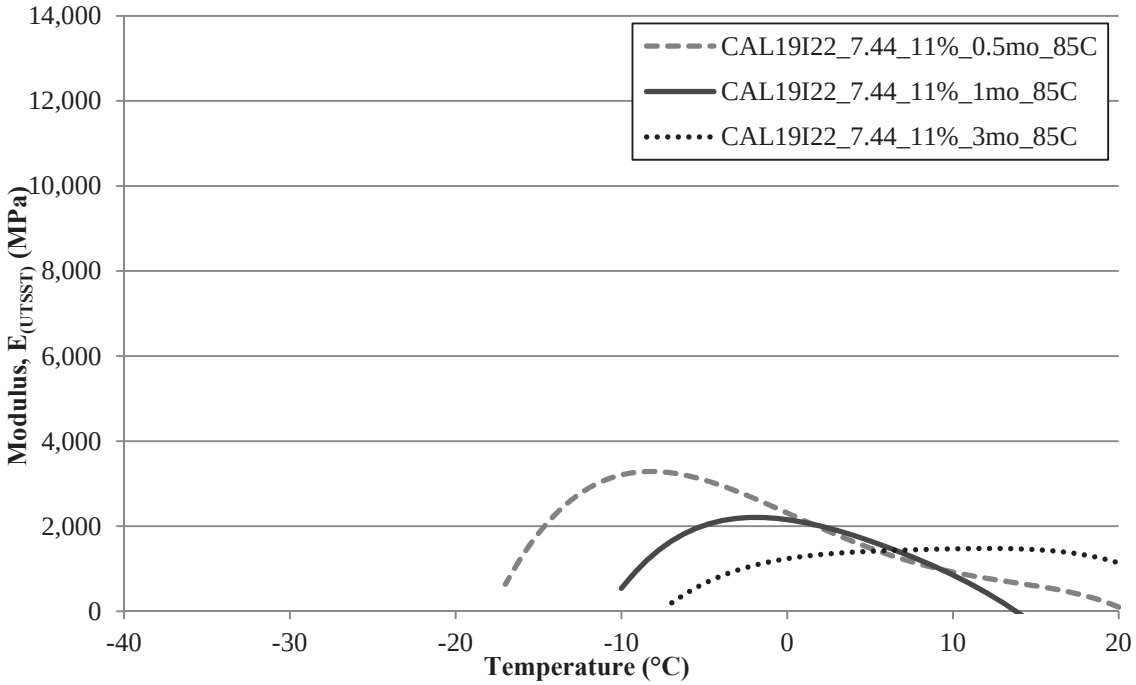

Figure 27.6 Summary of CAL19I22_7.44_11% Va Aged at 85°C UTSST Modulus Curves

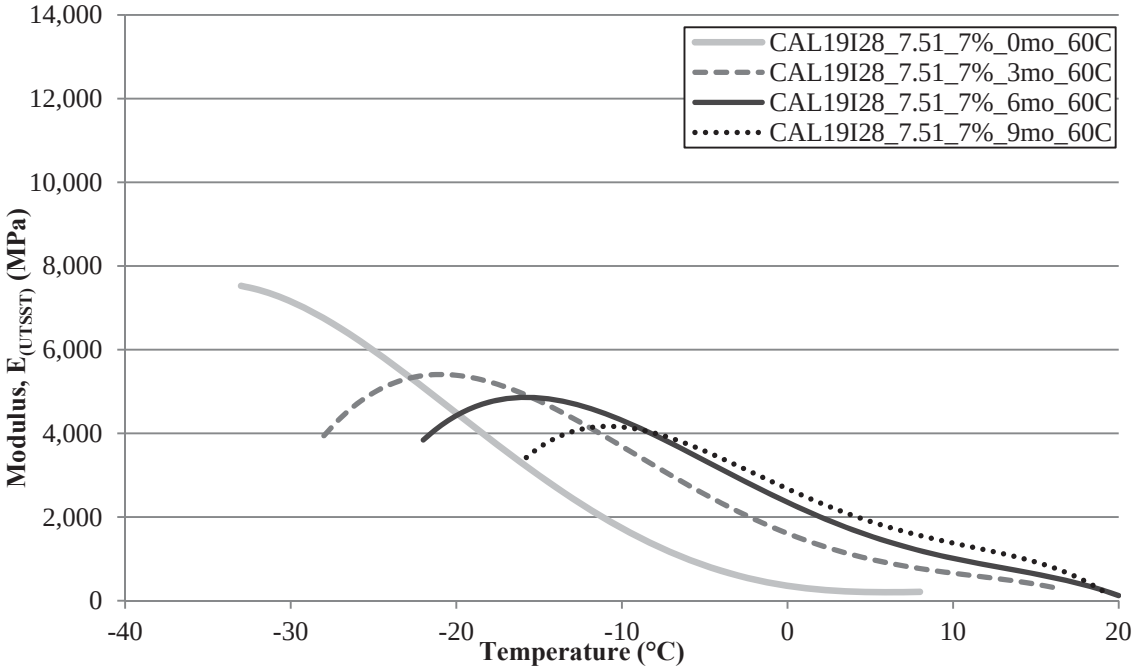

Figure 27.7 Summary of CAL19I28_7.51_7% Va Aged at 60°C UTSST Modulus Curves

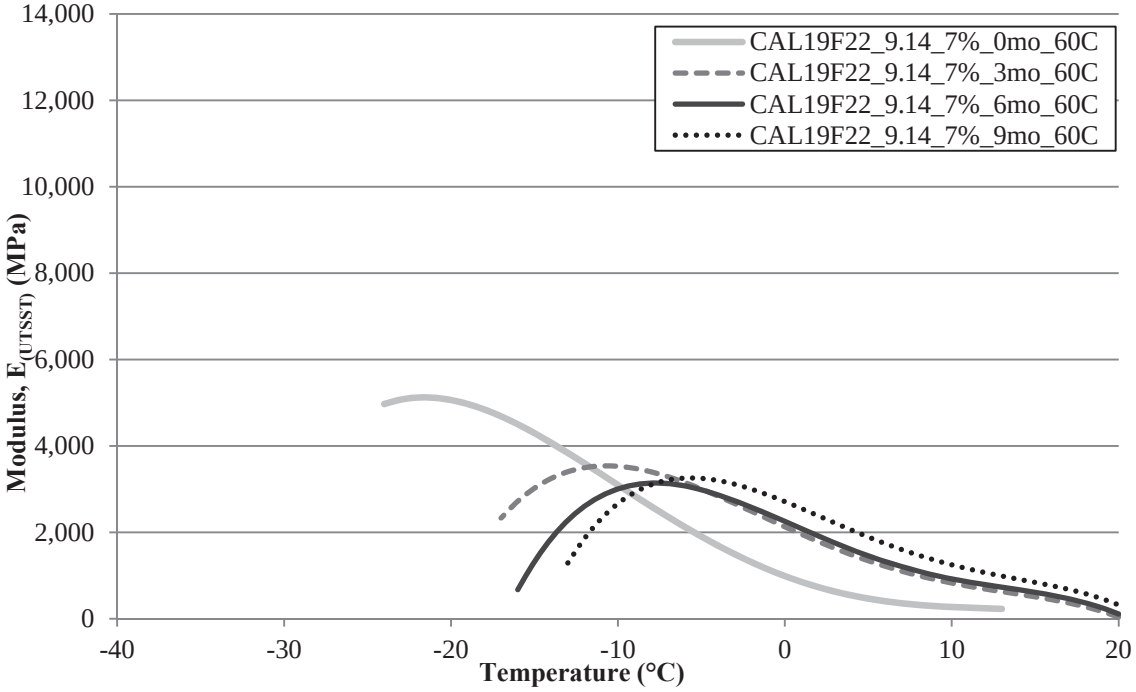

Figure 27.8 Summary of CAL19F22_9.14_7% Va Aged at 60°C UTSST Modulus Curves

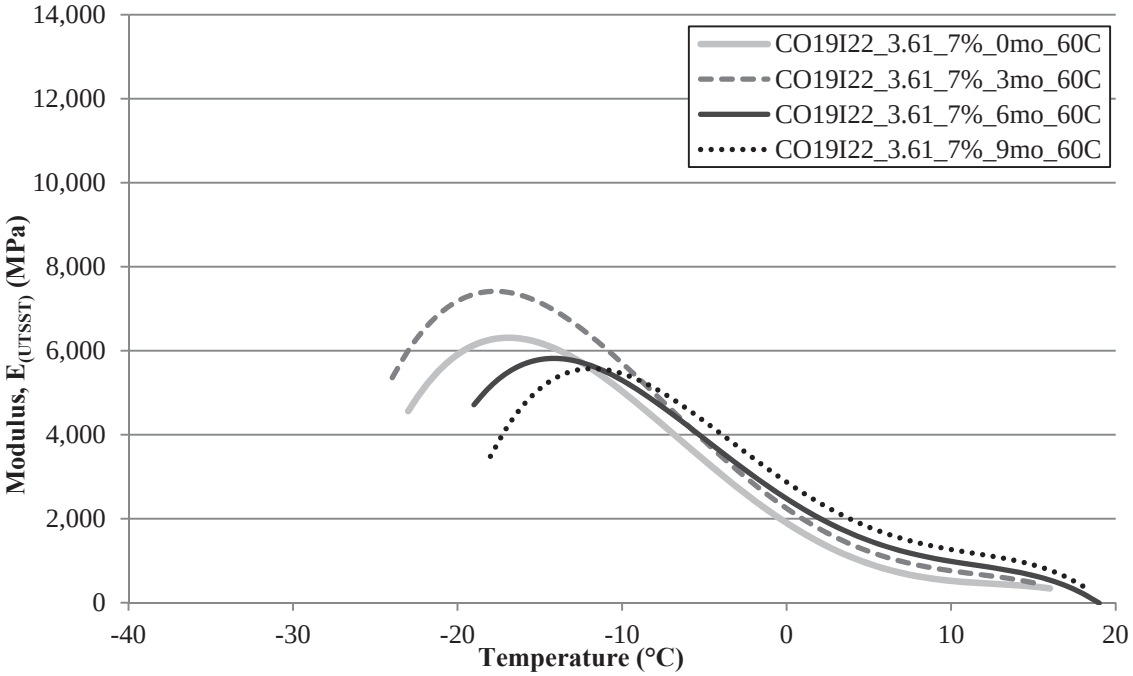

Figure 27.9 Summary of CO19I22_3.61_7% Va Aged at 60°C UTSST Modulus Curves

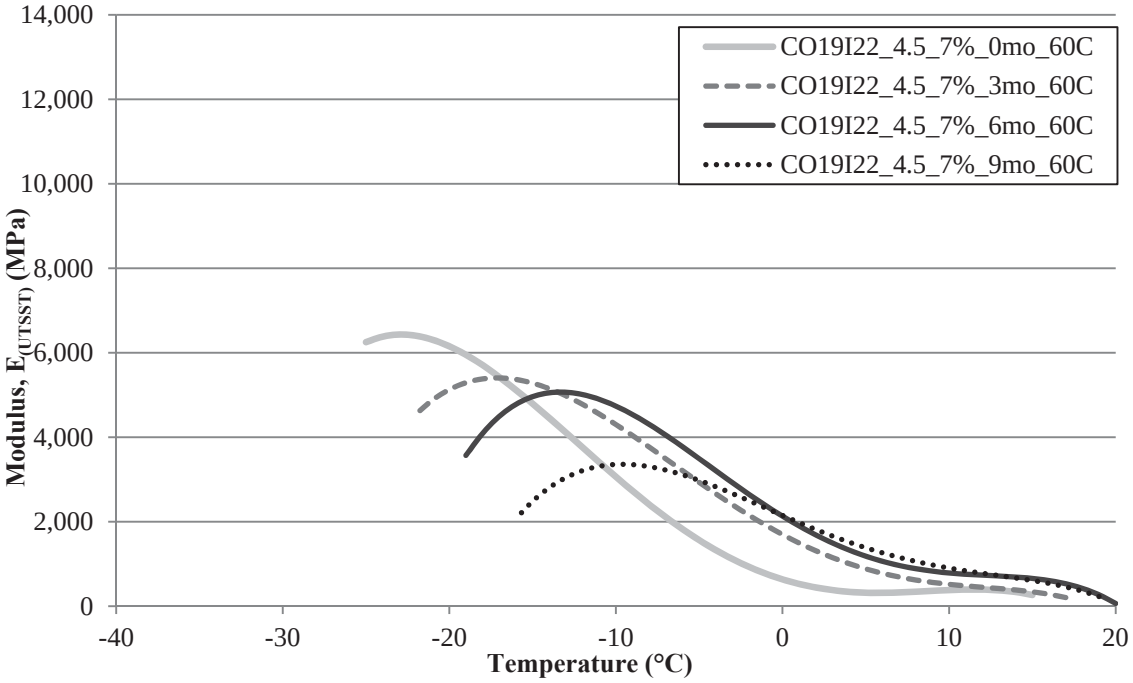

Figure 27.10 Summary of CO19I22_4.5_7% Va Aged at 60°C UTSST Modulus Curves

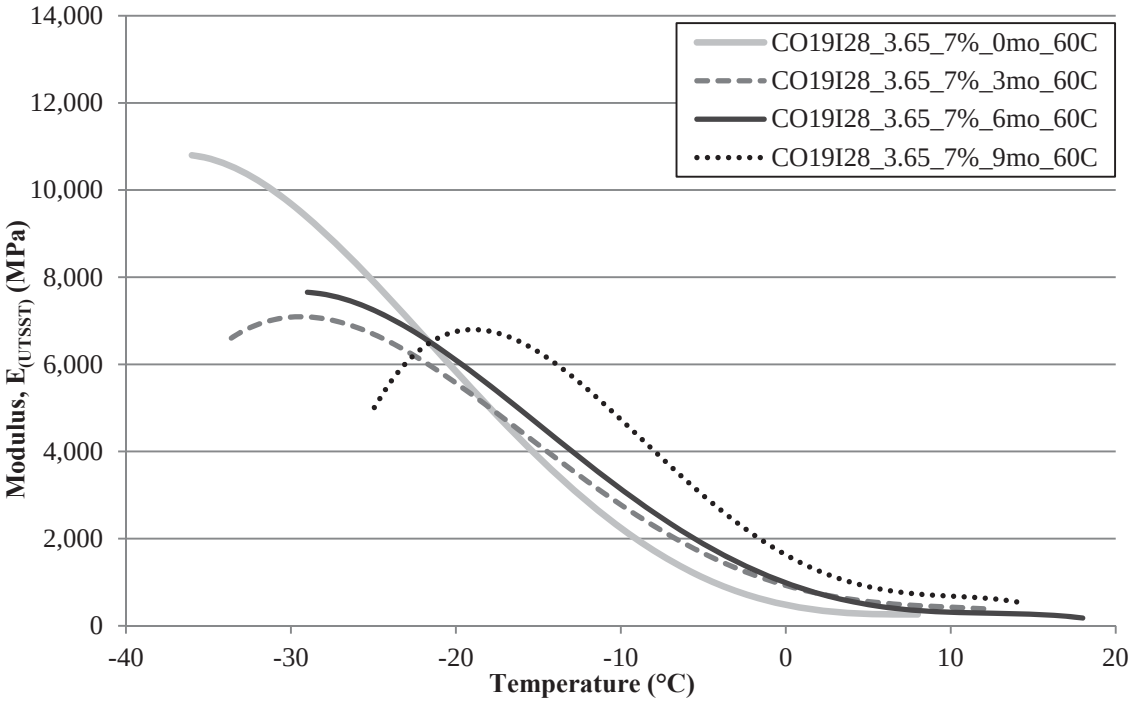

Figure 27.11 Summary of CO19I28_3.65_7% Va Aged at 60°C UTSST Modulus Curves

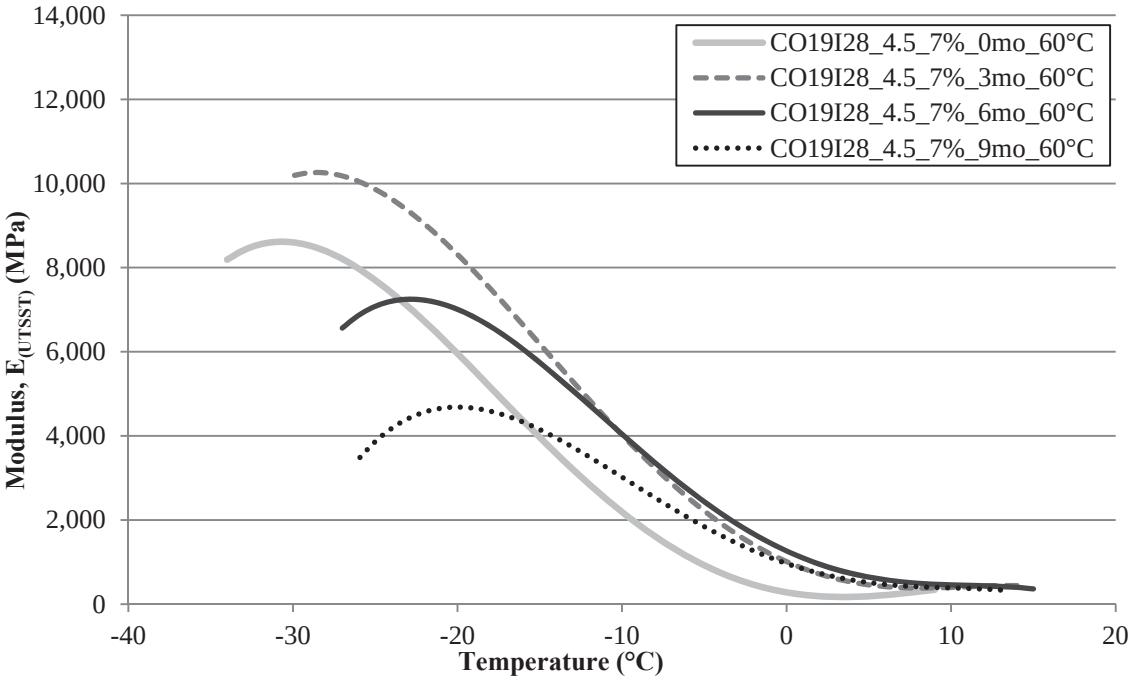

Figure 27.12 Summary of CO19I28_4.5_7% Va Aged at 60°C UTSST Modulus Curves

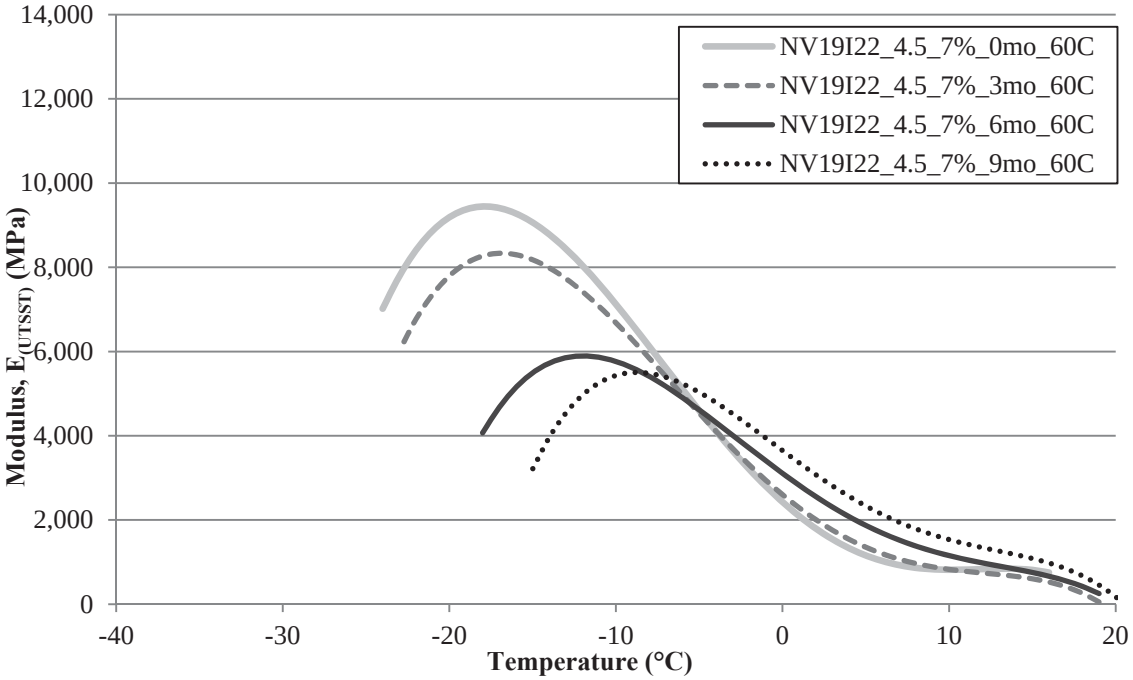

Figure 27.13 Summary of NV19I22_4.5_7% Va Aged at 60°C UTSST Modulus Curves

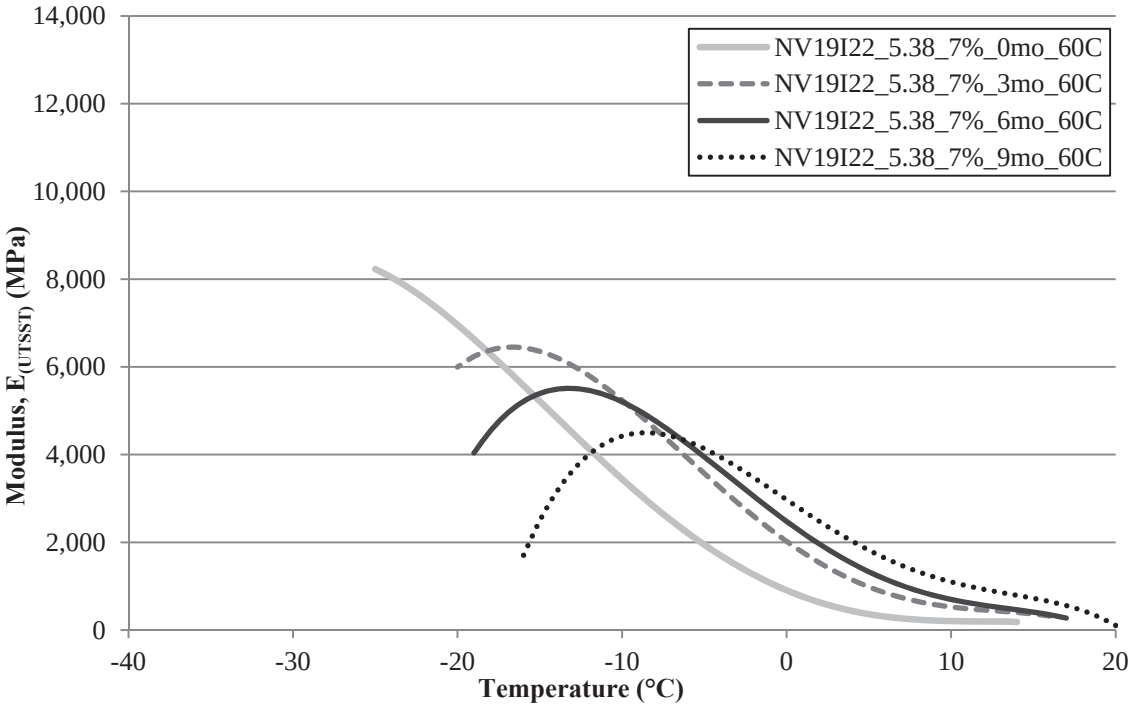

Figure 27.14 Summary of NV19I22_5.38_7% Va Aged at 60°C UTSST Modulus Curves

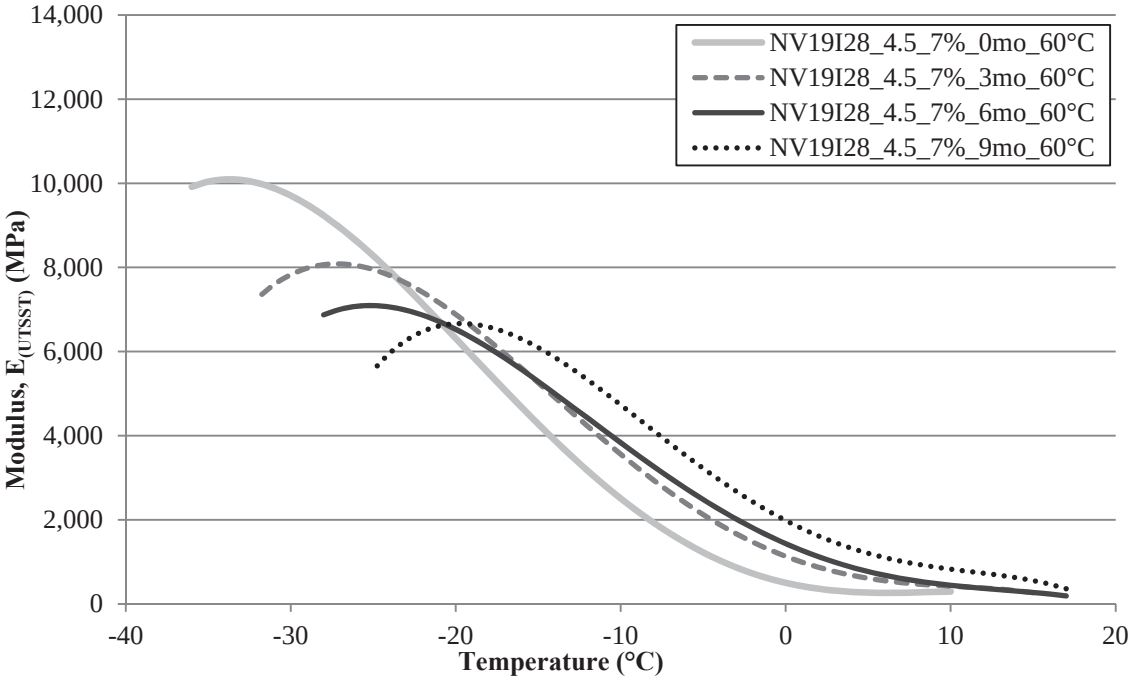

Figure 27.15 Summary of NV19I28_4.5_7% Va Aged at 60°C UTSST Modulus Curves

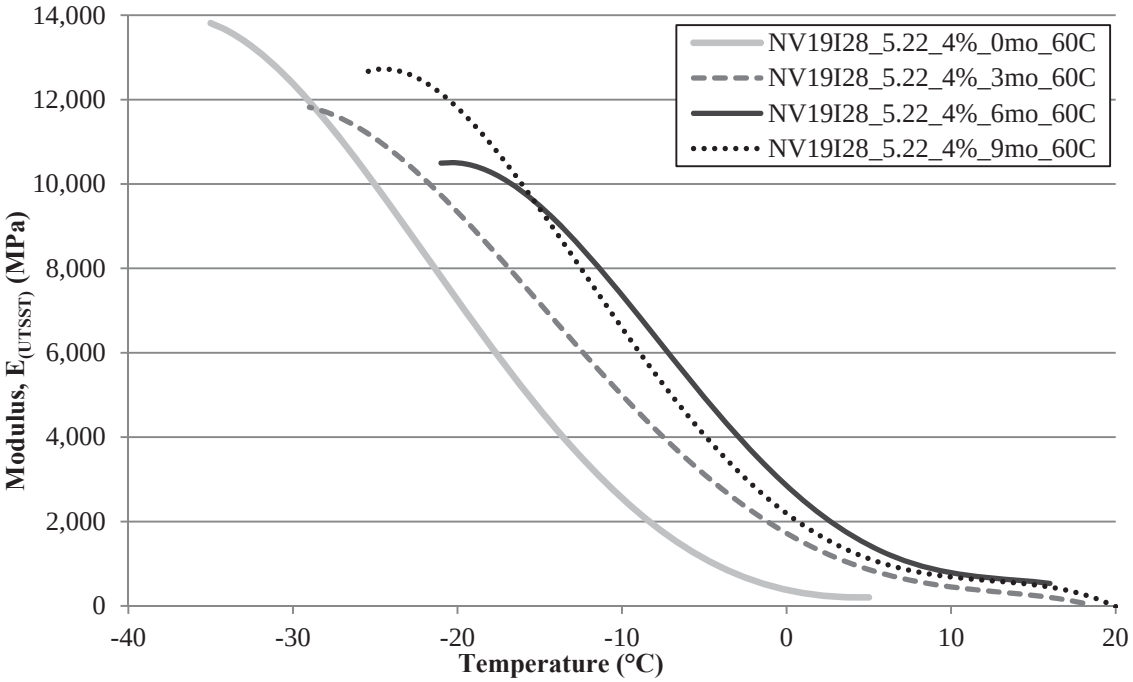

Figure 27.16 Summary of NV19I28_5.22_4% Va Aged at 60°C UTSST Modulus Curves

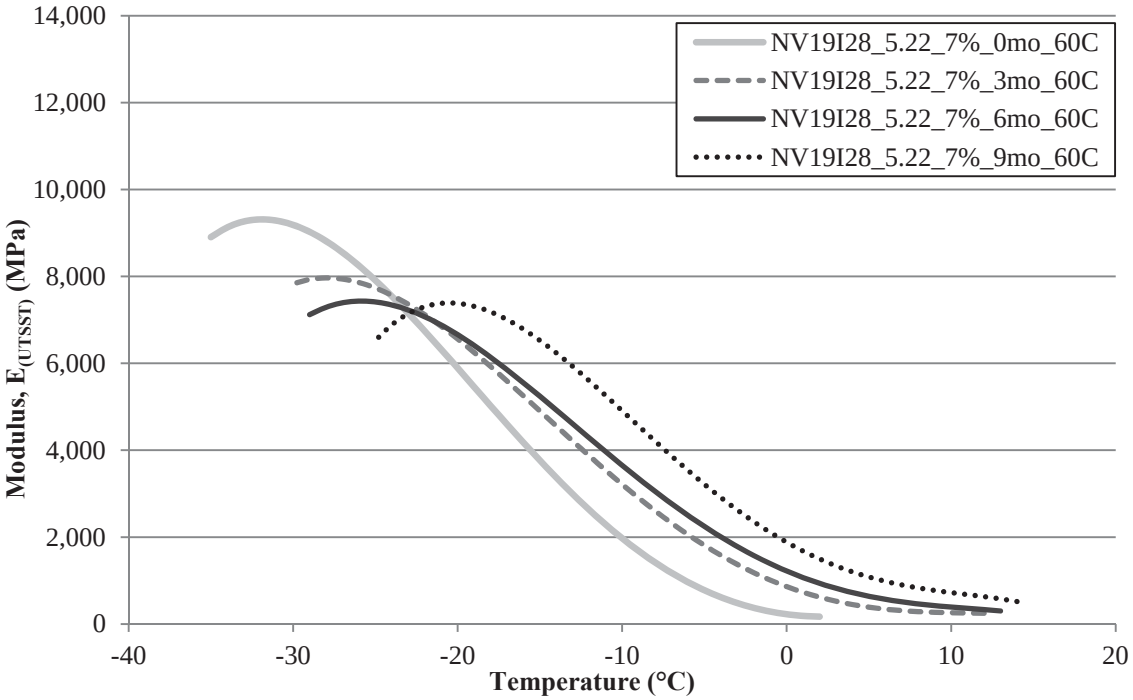

Figure 27.17 Summary of NV19I28_5.22_7% Va Aged at 60°C UTSST Modulus Curves

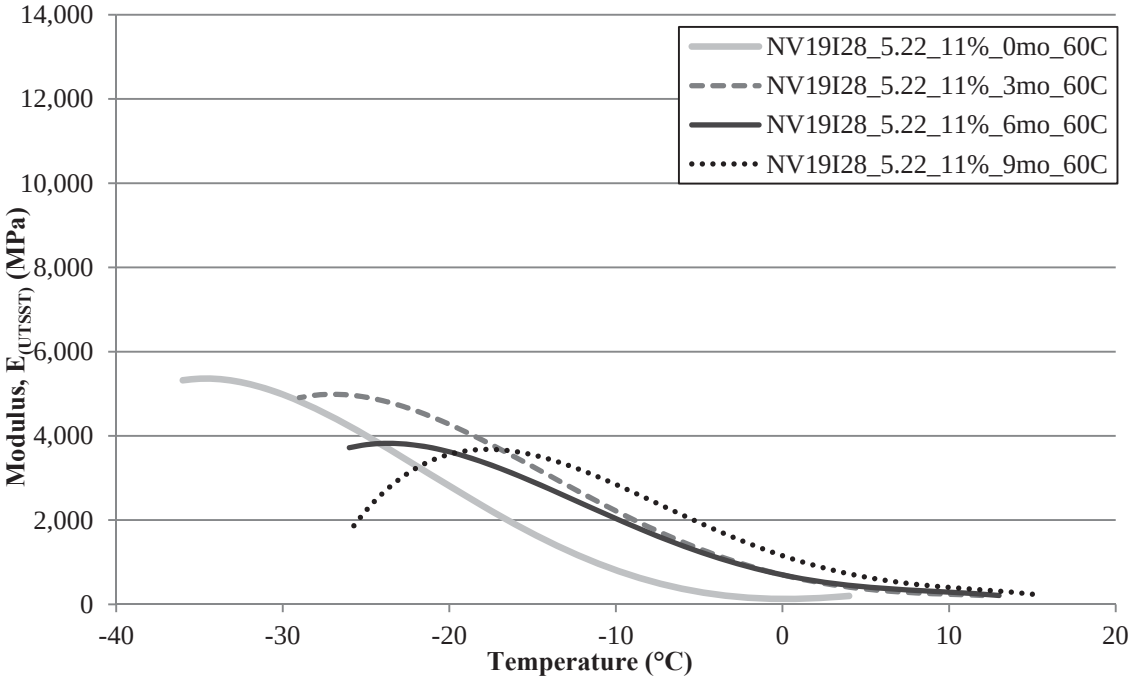

Figure 27.18 Summary of NV19I28_5.22_11% Va Aged at 60°C UTSST Modulus Curves

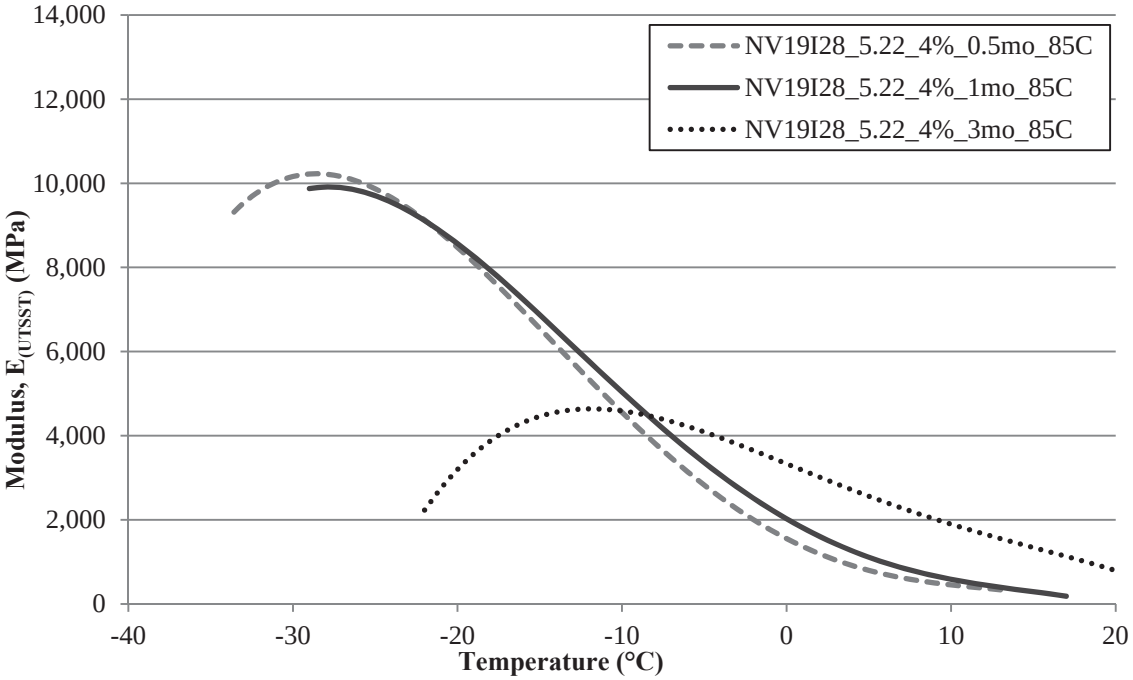

Figure 27.19 Summary of NV19I28_5.22_4% Va Aged at 85°C UTSST Modulus Curves

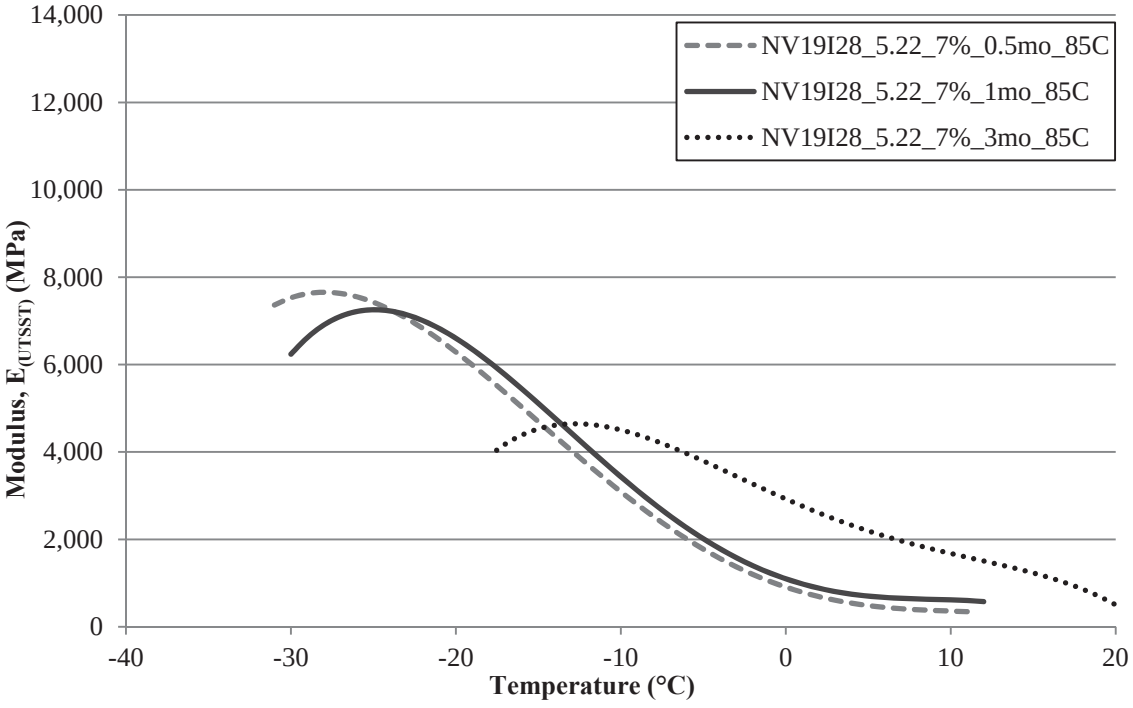

Figure 27.20 Summary of NV19I28_5.22_7% Va Aged at 85°C UTSST Modulus Curves

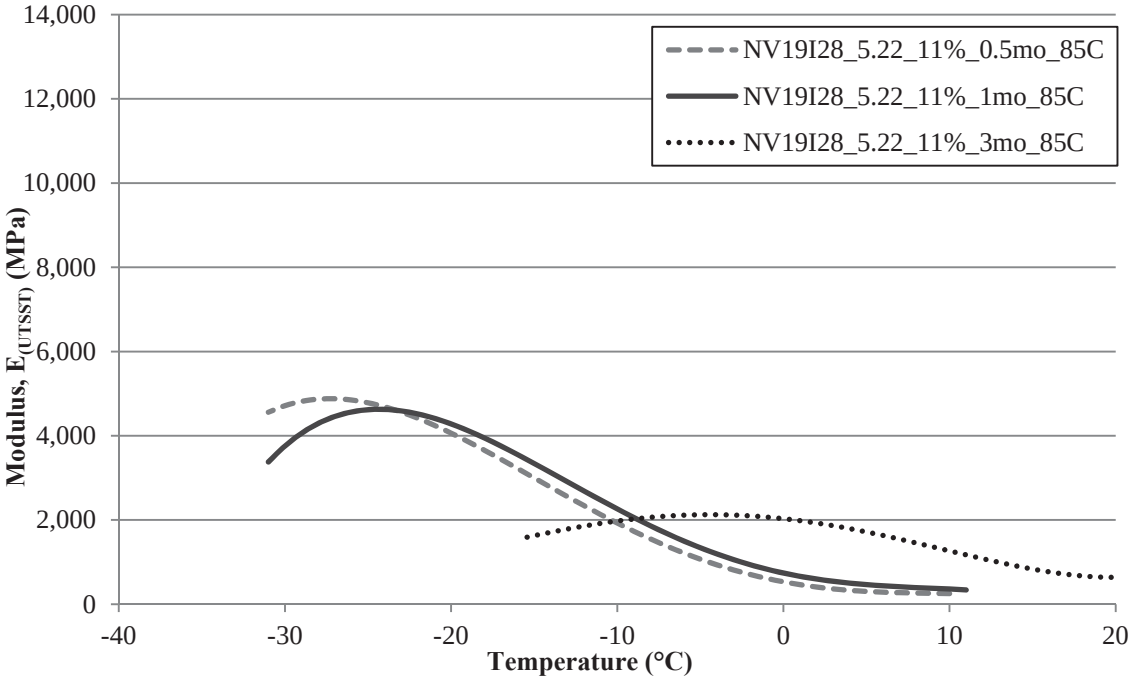

Figure 27.21 Summary of NV19I28_5.22_11% Va Aged at 85°C UTSST Modulus Curves

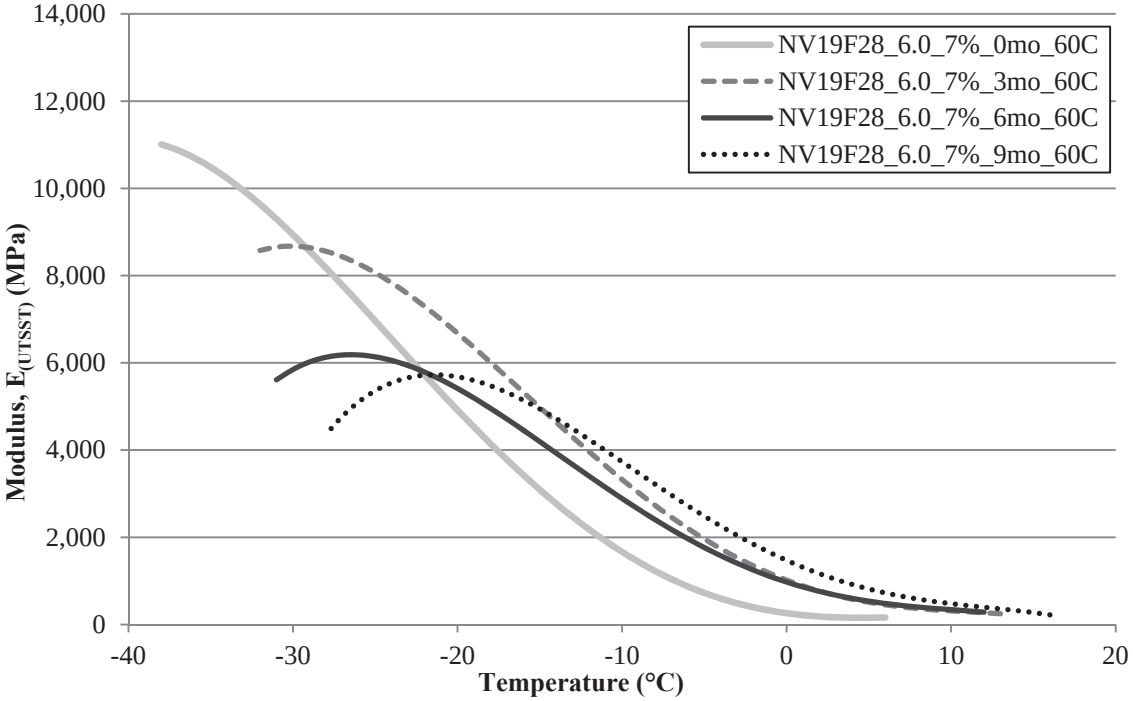

Figure 27.22 Summary of NV19F28_6.0_7% Va Aged at 60°C UTSST Modulus Curves

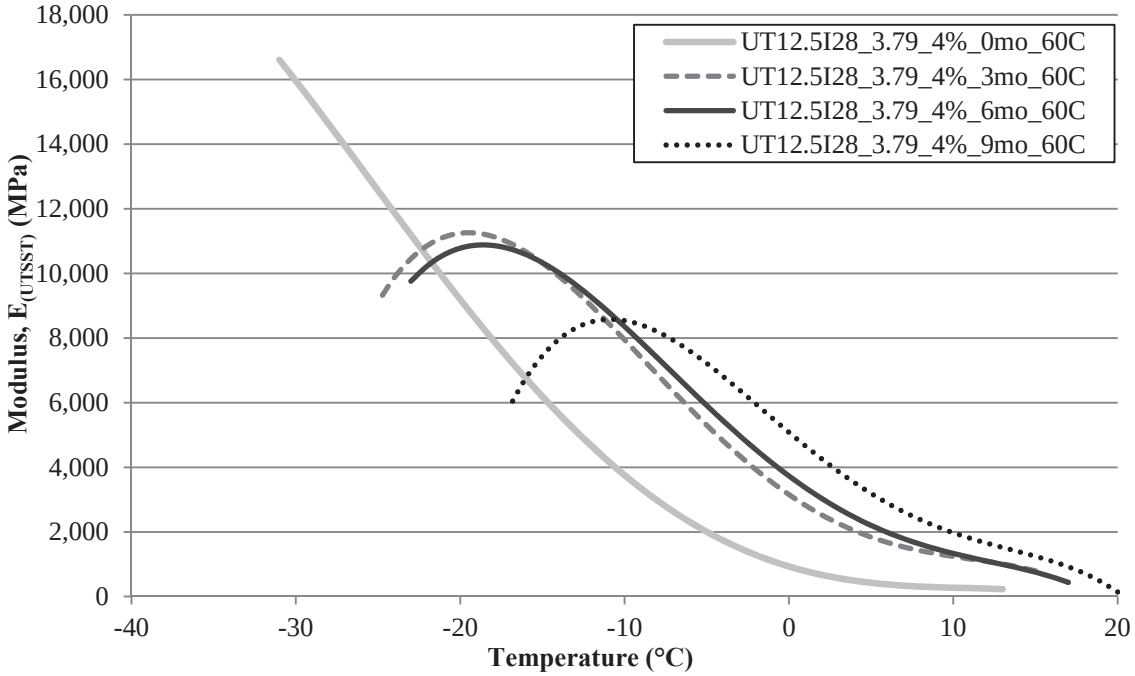

Figure 27.23 Summary of UT12.5I28_3.79_4% Va Aged at 60°C UTSST Modulus Curves

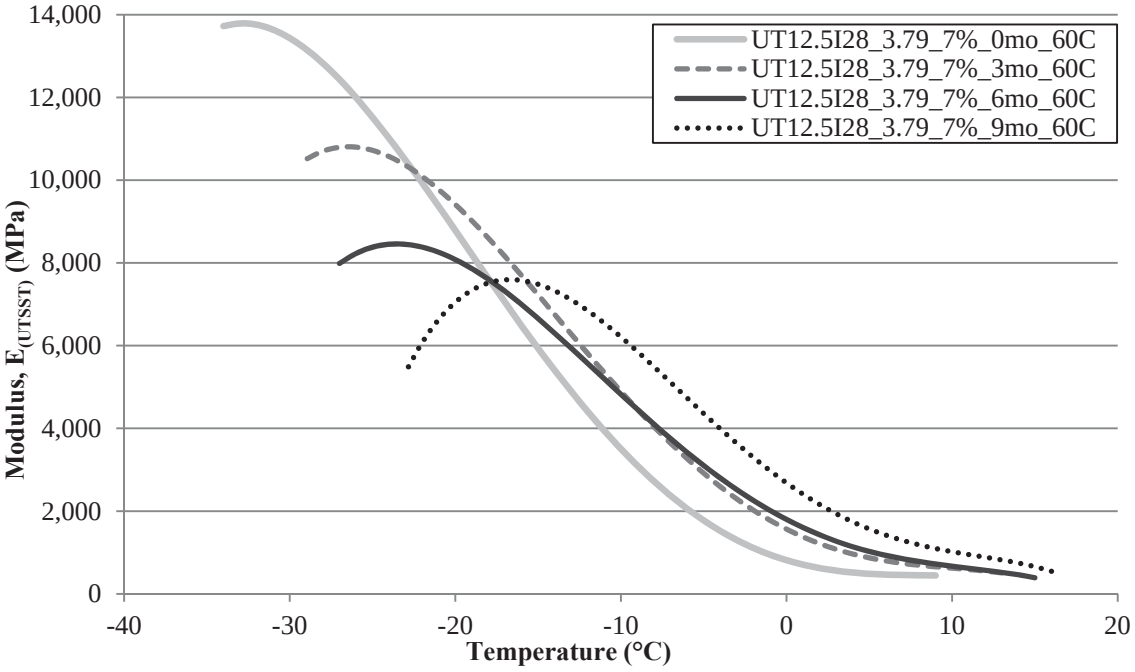

Figure 27.24 Summary of UT12.5I28_3.79_7% Va Aged at 60°C UTSST Modulus Curves

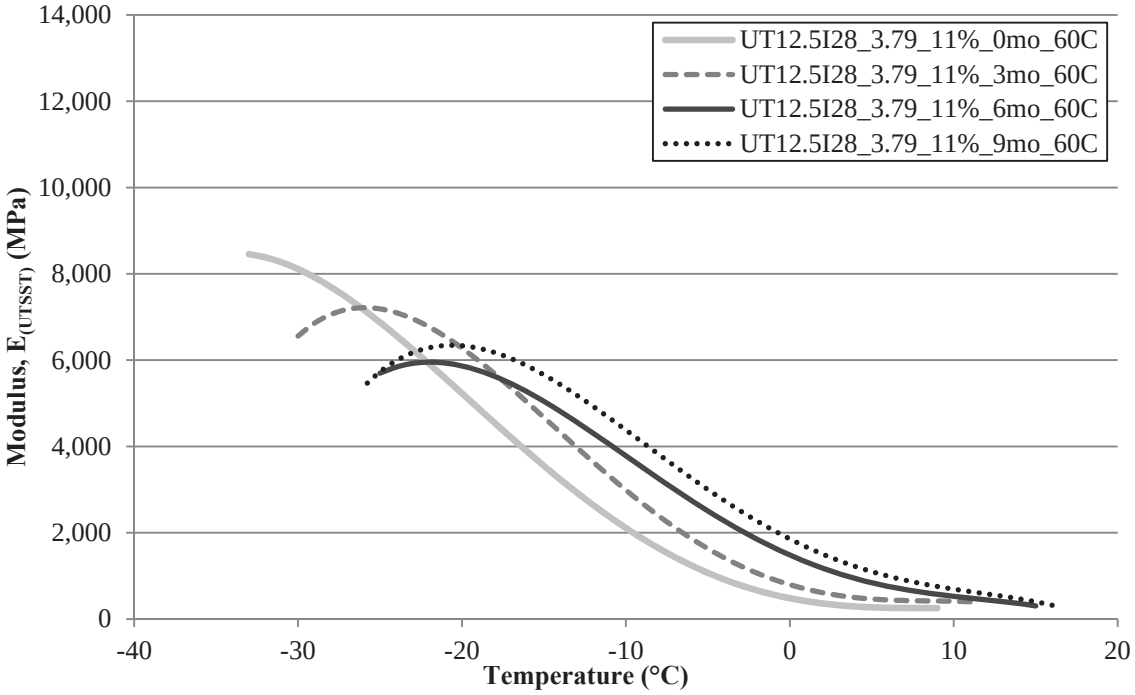

Figure 27.25 Summary of UT12.5I28_3.79_11% Va Aged at 60°C UTSST Modulus Curves

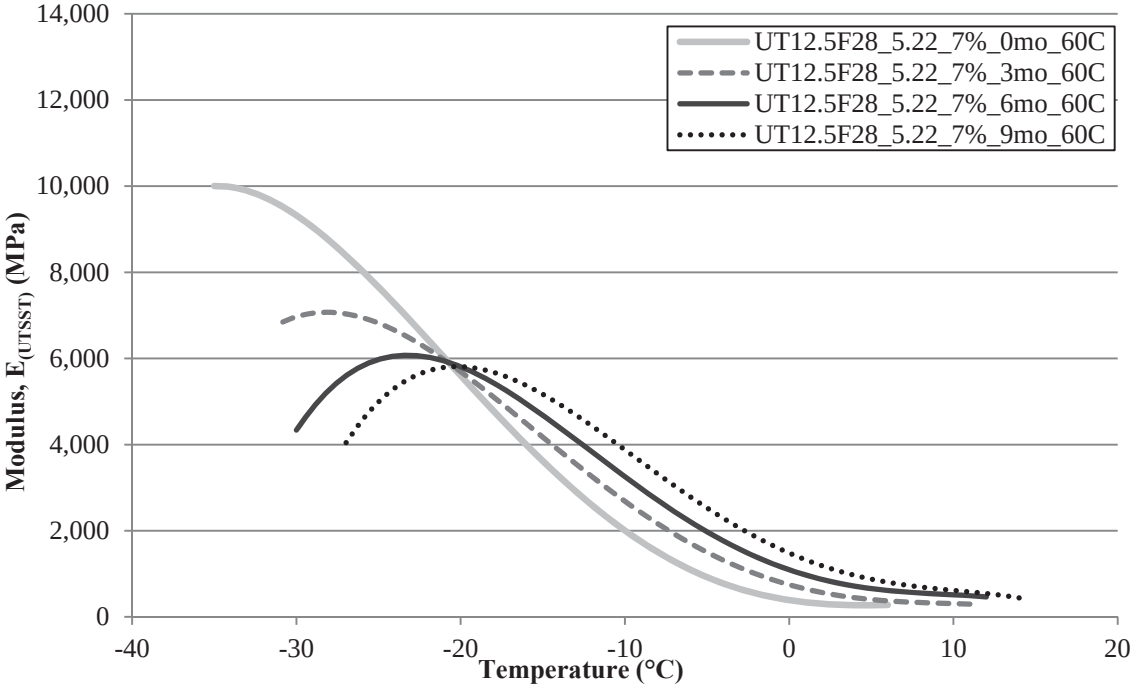

Figure 27.26 Summary of UT12.5F28_5.22_7% Va Aged at 60°C UTSST Modulus Curves

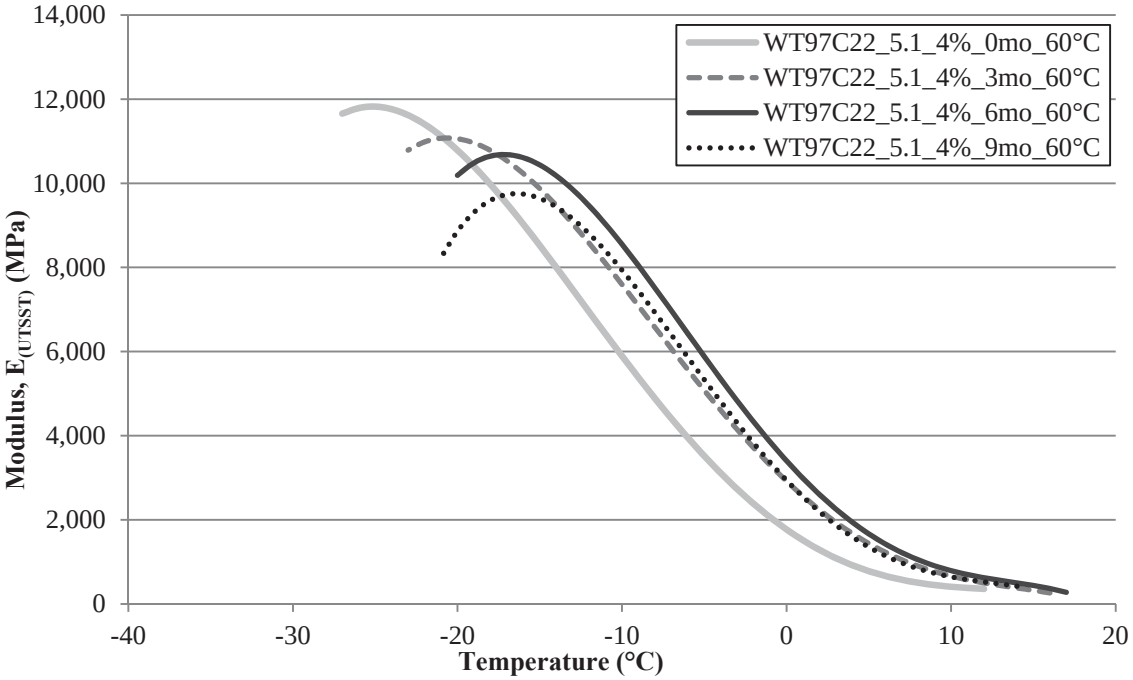

Figure 27.27 Summary of WT97C22_5.1_4% Va Aged at 60°C UTSST Modulus Curves

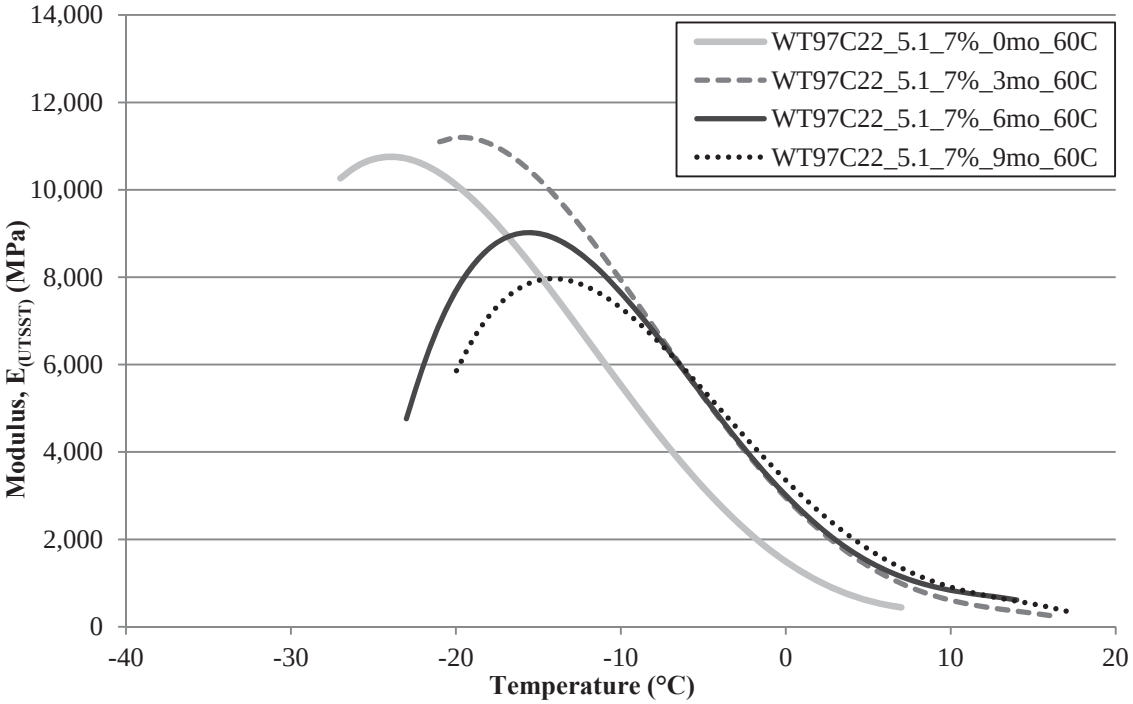

Figure 27.28 Summary of WT97C22_5.1_7% Va Aged at 60°C UTSST Modulus Curves

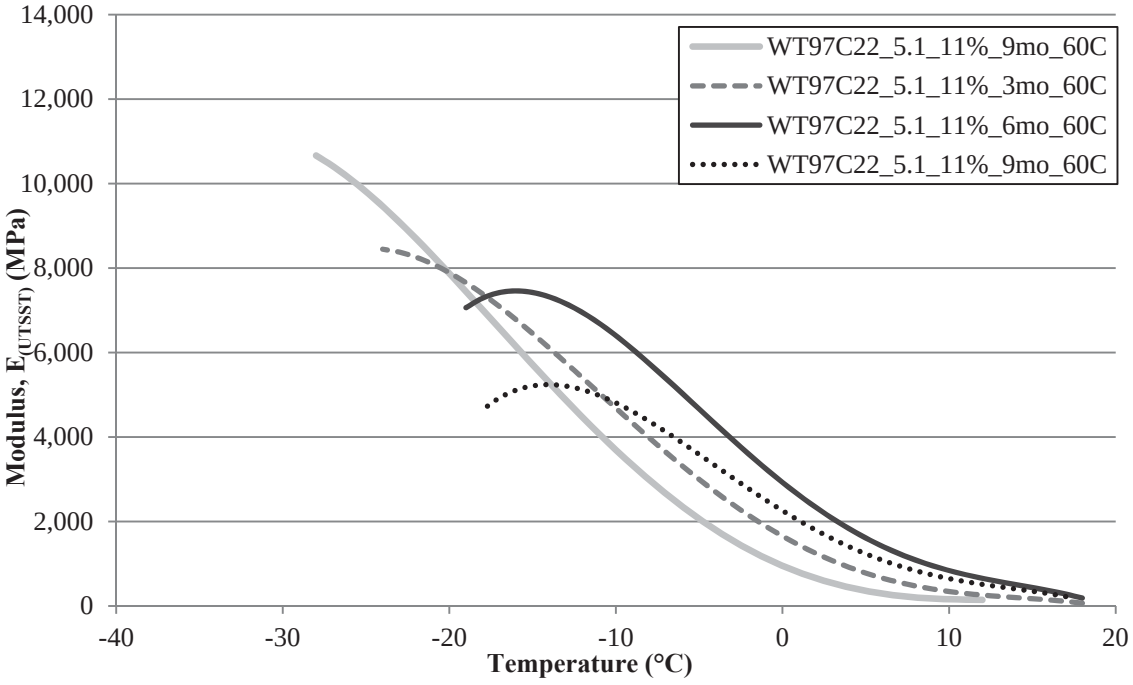

Figure 27.29 Summary of WT97C22_5.1_11% Va Aged at 60°C UTSST Modulus Curves

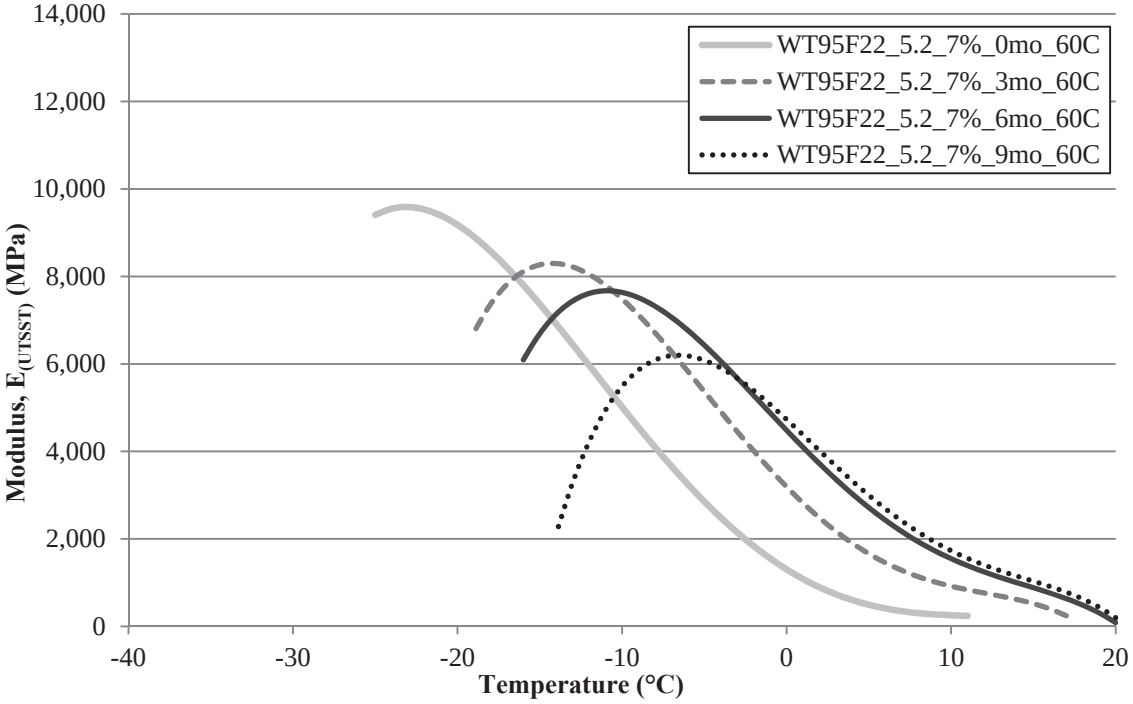

Figure 27.30 Summary of WT95F22_5.2_7% Va Aged at 60°C UTSST Modulus Curves

28 APPENDIX P:

Summary of Thermo-Viscoelastic Property Measurements of Aged Asphalt Mixtures

Table 28.1 Thermo-Viscoelastic Properties for California Mixtures

Aging Conditions			$E_{(UTSST)}$ Modulus (MPa)				UTSST Temperatures (°C)				
ID	Air Void	Dur. (mo)	C. I.	G. H.	V. G. T.	V. S.	Fr.	C. I.	G. H.	V. G. T.	V. S.
CAL19I22_7.44_60°C	4%	0	7,173	4,489	1,220	266	-21.2	-20.4	-9.4	3.0	14.5
		3	6,280	4,043	1,590	579	-16.5	-12.7	-2.0	7.5	16.6
		6	4,951	3,580	2,306	1,437	-10.5	-4.8	3.2	8.9	14.7
		9	4,798	3,525	2,344	1,584	-10.4	-3.8	4.0	9.5	14.9
	7%	0	6,089	3,680	885	225	-23.3	-22.3	-10.4	1.2	12.2
		3	5,083	3,416	1,626	886	-18.2	-10.7	-2.0	5.6	12.7
		6	4,201	3,133	2,156	1,504	-13.2	-4.8	2.8	8.1	13.3
		9	3,631	2,654	2,209	1,683	-7.7	-1.5	7.5	9.4	13.7
	11%	0	2,904	1,957	990	494	-23.9	-23.6	-12.7	-0.3	11.5
		3	3,191	2,147	1,039	538	-18.3	-11.4	-2.3	5.5	13.0
		6	2,572	1,793	1,026	546	-11.4	-5.4	2.8	9.0	15.5
		9	2,525	1,913	1,354	984	-8.2	-1.9	4.9	9.7	14.4
CAL19I22_7.44_85°C	4%	0.5	6,226	4,074	1,693	792	-17.1	-10.3	-0.9	7.6	15.6
		1	5,758	4,202	2,757	1,851	-15.3	-6.4	1.9	7.9	13.6
		3	3,759	3,285	2,970	2,706	-7.2	0.8	7.2	10.3	13.2
	7%	0.5	4,921	3,350	1,725	882	-16.8	-10.4	-1.1	6.5	13.8
		1	3,907	2,869	1,861	1,267	-12.1	-4.5	2.9	8.4	13.8
		3	2,626	2,195	-- [a]	-- [a]	-11.2	-1.8	8.0	-- [a]	-- [a]
	11%	0.5	3,336	2,278	1,179	655	-16.2	-8.5	0.2	7.4	14.0
		1	2,272	1,699	1,225	860	-9.0	-2.3	5.1	9.7	14.3
		3	1,476	1,452	-- [a]	-- [a]	-7.8	12.1	8.2	-- [a]	-- [a]
CAL19I28_7.51_60°C	7%	0	7,355	4,854	983	182	-32.9	-31.3	-21.3	-6.0	7.5
		3	5,410	3,510	1,428	592	-28.2	-20.9	-9.2	1.2	11.4
		6	4,864	3,257	1,600	763	-21.9	-15.8	-4.5	4.6	13.3
		9	4,223	3,074	1,941	1,279	-19.6	-11.0	-2.1	4.7	11.2
CAL19F22_9.14_60°C	7%	0	5,186	3,190	882	249	-24.3	-21.8	-10.4	0.8	11.5
		3	3,538	2,396	1,200	589	-16.3	-10.7	-1.5	6.1	13.6
		6	3,158	2,197	1,207	691	-16.6	-7.9	0.3	7.0	13.7
		9	3,257	2,340	1,428	895	-12.4	-5.7	2.3	8.4	14.3

a – Certain behaviors were not observed on all tested specimens.

Fr. – Fracture
G. H. – Glassy Hardening
V. S. – Viscous Softening
C. I. – Crack Initiation
V. G. T. – Viscous-Glassy Transition

Table 28.2 UTSST Stress Measures for California Mixtures

Aging Conditions				UTSST Stress (kPa)				
ID	Air Void	Dur. (mo.)	Average Carbonyl Growth ($CA-CA_{Tank}$)	Fracture (Fr.)	Crack Initiation (C. I.)	Glassy Hardening (G. H.)	Viscous-Glassy Transition (V. G. T.)	Viscous Softening (V. S.)
CAL19I22_7.44_60°C	4%	0	0.232	2,798	2,658	1,003	181	13
		3	0.445	2,721	2,178	842	249	42
		6	0.504	2,241	1,677	825	419	156
		9	0.643	2,233	1,568	774	398	158
	7%	0	0.200	2,389	2,236	722	121	9
		3	0.444	2,359	1,584	683	262	73
		6	0.593	2,156	1,449	726	384	162
		9	0.699	1,627	1,183	521	390	200
	11%	0	0.299	1,642	1,609	556	71	2
		3	0.506	1,608	1,132	494	192	52
		6	0.689	1,126	828	387	174	51
		9	0.833	1,096	768	405	226	102
CAL19I22_7.44_85°C	4%	0.5	0.383	2,616	1,796	730	246	60
		1	0.499	2,576	1,699	818	410	161
		3	0.854	1,705	1,178	704	507	338
	7%	0.5	0.363	2,427	1,736	761	305	83
		1	0.598	1,780	1,220	618	321	135
		3	1.006	1,382	1,008	505	-- [a]	-- [a]
	11%	0.5	0.504	1,569	1,046	451	177	50
		1	0.684	959	683	343	194	87
		3	1.151	683	241	353	-- [a]	-- [a]
CAL19I28_7.51_60°C	7%	0	0.347	3,136	2,854	1,234	141	1
		3	0.523	2,790	2,004	799	254	48
		6	0.705	2,410	1,783	736	271	65
		9	0.870	2,134	1,487	738	365	140
CAL19F22_9.14_60°C	7%	0	0.347	2,583	2,233	766	152	12
		3	0.523	2,084	1,539	673	264	68
		6	0.705	1,906	1,310	614	272	88
		9	0.870	1,850	1,309	637	307	113

a – Certain behaviors were not observed on all tested specimens.

Table 28.3 Thermo-Viscoelastic Properties for Colorado Mixtures Aged at 60°C

Aging Conditions			$E_{(UTSST)}$ Modulus (MPa)				UTSST Temperatures (°C)				
ID	Air Void	Dur. (mo)	C. I.	G. H.	V. G. T	V. S.	Fr.	C. I.	G. H.	V. G. T.	V. S.
CO19I22_7% Va	3.61	0	6,559	4,048	1,199	449	-22.3	-17.3	-6.8	3.3	12.5
		3	7,469	4,745	1,673	661	-23.0	-17.9	-7.4	2.4	11.9
		6	5,821	3,878	1,743	882	-19.5	-14.1	-4.9	3.4	11.7
		9	5,587	3,826	1,881	1,123	-17.9	-11.8	-3.2	4.4	11.8
	4.5	0	5,593	3,518	1,133	503	-25.1	-22.9	-12.4	-1.6	9.0
		3	5,406	3,388	1,091	422	-19.0	-17.0	-6.6	3.4	12.6
		6	5,079	3,311	1,290	730	-19.6	-13.4	-4.4	4.3	12.6
		9	3,359	2,328	1,258	725	-16.4	-9.6	-1.0	6.0	13.0
CO19I28_7% Va	3.65	0	10,753	6,457	1,322	263	-35.4	-35.3	-21.5	-6.2	7.9
		3	7,094	4,384	1,263	434	-36.1	-29.4	-15.8	-2.6	9.6
		6	7,619	4,635	1,092	289	-28.3	-28.2	-15.0	-0.7	12.4
		9	7,178	4,526	1,478	693	-26.3	-19.8	-9.4	0.7	10.4
	4.5	0	8,616	5,021	787	204	-33.1	-30.6	-17.7	-4.3	5.5
		3	10,263	6,063	1,175	417	-30.7	-28.5	-14.7	-0.9	11.0
		6	7,253	4,472	1,242	448	-28.5	-22.8	-11.2	0.1	11.1
		9	4,693	2,939	912	386	-25.0	-20.0	-9.7	0.4	10.2

Fr. – Fracture
C. I. – Crack Initiation
G. H. – Glassy Hardening
V. G. T. – Viscous-Glassy Transition
V. S. – Viscous Softening

Table 28.4 UTSST Stress Measures for Colorado Mixtures

Aging Conditions				UTSST Stress (kPa)				
ID	Air Void	Dur. (mo.)	Average Carbonyl Growth ($CA-CA_{Tank}$)	Fracture (Fr.)	Crack Initiation (C. I.)	Glassy Hardening (G. H.)	Viscous-Glassy Transition (V. G. T.)	Viscous Softening (V. S.)
CO19I22_7% Va	3.61	0	0.511	1,625	1,192	422	106	21.6
		3	0.677	2,457	1,878	715	200	33.0
		6	0.860	2,038	1,528	675	257	67.2
		9	1.024	1,830	1,319	615	260	84.6
	4.5	0	0.440	2,247	1,931	642	110	4.0
		3	0.618	1,802	1,570	575	147	24.7
		6	0.762	1,998	1,421	613	230	77.0
		9	1.062	1,572	1,097	506	220	69.9
CO19I28_7% Va	3.65	0	0.485	3,125	3,110	1,036	125	0.8
		3	0.740	3,058	2,273	798	172	17.3
		6	0.841	2,281	2,270	795	128	8.9
		9	0.999	2,592	1,856	718	207	40.2
	4.5	0	0.309	2,953	2,530	714	58	0.5
		3	0.516	3,473	3,042	917	152	35.6
		6	0.697	3,153	2,332	827	192	35.3
		9	0.865	2,046	1,527	566	144	20.7

Table 28.5 Thermo-Viscoelastic Properties for Nevada Mixtures

Aging Conditions			$E_{(UTSST)}$ Modulus (MPa)				UTSST Temperatures (°C)				
ID	Air Void	Dur. (mo)	C. I.	G. H.	V. G. T	V. S.	Fr.	C. I.	G. H.	V. G. T.	V. S.
NV19I22_4.5_60°C	7%	0	9,448	5,723	1,461	847	-24.2	-17.9	-7.2	3.3	11.5
		3	8,334	5,250	1,732	736	-23.6	-16.9	-6.6	3.1	12.2
		6	5,943	3,957	1,786	857	-17.2	-12.1	-2.8	5.4	13.5
		9	5,503	3,848	2,096	1,264	-15.4	-8.8	-0.7	6.2	12.9
NV19I22_5.38_60°C	7%	0	8,284	5,104	1,088	198	-25.4	-25.3	-14.7	-1.1	11.8
		3	6,463	4,002	1,185	433	-19.5	-16.7	-6.3	3.8	12.9
		6	5,569	3,531	1,267	481	-18.8	-13.3	-3.5	5.4	13.7
		9	4,498	3,051	1,496	806	-16.3	-8.6	-0.3	6.9	13.8
NV19I28_4.5_60°C	7%	0	10,146	6,043	1,162	292	-34.8	-32.8	-19.3	-4.7	8.8
		3	8,086	4,996	1,395	412	-32.1	-27.2	-14.2	-1.6	10.7
		6	7,093	4,400	1,342	336	-25.3	-25.2	-11.9	0.6	13.1
		9	6,719	4,371	1,714	758	-26.1	-19.7	-8.8	1.4	11.4
NV19I28_5.22_60°C	4%	0	13,649	8,284	1,470	219	-34.4	-34.3	-21.9	-6.5	5.2
		3	11,794	7,183	1,808	333	-28.9	-28.8	-15.0	-0.4	12.9
		6	10,514	6,306	1,634	651	-27.2	-20.5	-7.8	4.1	13.2
		9	12,819	7,797	1,898	461	-27.2	-23.3	-10.4	2.4	15.4
	7%	0	9,435	5,549	921	184	-35.4	-32.1	-19.2	-5.8	1.9
		3	7,974	4,816	1,126	259	-29.7	-27.8	-14.8	-1.7	10.9
		6	7,433	4,597	1,317	359	-29.3	-25.8	-13.0	-0.6	11.3
		9	7,395	4,726	1,707	676	-26.2	-20.5	-9.5	0.9	11.0
	11%	0	5,119	3,157	874	220	-36.5	-35.1	-21.4	-7.2	4.1
		3	4,993	3,081	862	227	-28.8	-27.3	-14.4	-1.8	10.5
		6	3,825	2,412	791	302	-28.5	-23.6	-12.1	-1.0	10.1
		9	3,679	2,367	892	353	-26.6	-17.7	-7.3	2.2	11.7
NV19I28_5.22_85°C	4%	0.5	10,190	6,225	1,684	376	-27.6	-27.5	-14.2	-0.6	12.1
		1	9,743	6,121	1,815	312	-25.4	-25.3	-13.0	1.0	14.6
		3	4,638	3,307	2,190	1,296	-23.0	-11.8	0.2	7.7	15.4
	7%	0.5	7,657	4,678	1,233	354	-30.6	-28.0	-15.0	-2.2	10.0
		1	7,259	4,501	1,306	582	-30.5	-24.9	-13.2	-1.6	9.3
		3	4,676	3,391	2,179	1,427	-24.7	-12.5	-2.4	4.9	12.4
	11%	0.5	4,884	2,992	792	263	-32.3	-27.3	-15.0	-2.8	9.0
		1	4,630	2,931	963	389	-31.7	-24.3	-13.1	-2.2	8.8
		3	2,879	2,843	2,843	646	-39.6	-39.6	-39.5	-39.5	20.9
NV19F28_6.0_60°C	7%	0	10,723	6,785	1,260	156	-36.2	-36.1	-24.6	-8.2	5.5
		3	8,677	5,274	1,335	292	-31.1	-30.1	-15.8	-2.0	11.2
		6	6,190	3,852	1,178	331	-30.5	-26.5	-13.7	-1.6	10.5
		9	5,728	3,618	1,240	385	-28.4	-21.4	-9.5	1.5	12.4

Fr. – Fracture
C. I. – Crack Initiation
G. H. – Glassy Hardening
V. G. T. – Viscous-Glassy Transition
V. S. – Viscous Softening

Table 28.6 UTSST Stress Measures for Nevada Mixtures

Aging Conditions				UTSST Stress (kPa)				
ID	Air Void	Dur. (mo)	Average Carbonyl Growth ($CA-CA_{Tank}$)	Fracture (Fr.)	Crack Initiation (C. I.)	Glassy Hardening (G. H.)	Viscous-Glassy Transition (V. G. T.)	Viscous Softening (V. S.)
NV19I22_ 4.5_60°C	7%	0	0.417	2,570	1,711	547	114	17.0
		3	0.610	2,658	1,853	693	191	38.7
		6	0.744	2,095	1,587	683	252	64.1
		9	0.942	1,927	1,374	664	305	106.5
NV19I22_ 5.38_60°C	7%	0	0.389	2,983	2,965	1,112	135	5.3
		3	0.606	2,047	1,706	599	141	23.6
		6	0.764	2,086	1,510	562	154	25.1
		9	0.873	1,778	1,208	543	219	64.4
NV19I28_ 4.5_60°C	7%	0	0.479	3,082	2,795	894	108	5.1
		3	0.633	3,186	2,506	875	183	20.5
		6	0.786	2,307	2,286	815	185	22.5
		9	0.934	2,444	1,801	742	243	55.0
NV19I28_5.22_60°C	4%	0	0.302	4,147	4,126	1,458	129	0.5
		3	0.495	3,804	3,786	1,314	207	11.6
		6	0.577	3,942	2,680	812	154	25.5
		9	0.742	3,986	3,175	1,201	293	47.2
	7%	0	0.303	3,233	2,695	796	61	0.3
		3	0.512	2,888	2,592	847	131	6.3
		6	0.647	2,959	2,469	858	173	11.0
		9	0.803	2,683	2,001	777	222	33.4
	11%	0	0.352	2,056	1,904	590	54	0.2
		3	0.487	1,741	1,606	558	110	6.1
		6	0.623	1,516	1,196	454	119	16.1
		9	0.857	1,625	1,106	439	131	21.9
NV19I28_5.22_85°C	4%	0.5	0.644	3,299	3,283	1,142	206	12.8
		1	0.767	3,130	3,115	1,238	243	14.1
		3	1.190	2,262	1,654	771	384	119.6
	7%	0.5	0.700	3,039	2,641	899	166	6.6
		1	0.844	2,627	1,972	710	169	22.2
		3	1.452	2,011	1,461	744	392	157.4
	11%	0.5	0.724	1,875	1,446	499	97	5.5
		1	0.861	1,953	1,398	538	144	18.3
		3	1.543	1,120	1,118	1,115	1,115	1.8
NV19F28_ 6.0_60°C	7%	0	0.288	3,823	3,805	1,276	118	0.5
		3	0.469	3,389	3,214	1,061	179	10.2
		6	0.697	3,053	2,500	905	201	14.4
		9	0.774	3,035	2,208	828	213	25.4

Table 28.7 Thermo-Viscoelastic Properties for Utah Mixtures

Aging Conditions			$E_{(UTSST)}$ Modulus (MPa)				UTSST Temperatures (°C)				
ID	**Air Void**	**Dur. (mo)**	**C. I.**	**G. H.**	**V. G. T**	**V. S.**	**Fr.**	**C. I.**	**G. H.**	**V. G. T.**	**V. S.**
UT12.5I28_3.79_60°C	**4%**	**0**	16,862	13,636	3,415	264	-32.0	-31.9	-26.0	-9.1	10.9
		3	11,262	7,260	2,737	1,139	-24.7	-19.5	-8.7	1.3	11.3
		6	10,948	7,043	2,782	1,060	-23.2	-18.8	-7.4	2.8	12.4
		9	8,807	5,949	2,893	1,416	-17.2	-11.5	-2.1	5.9	13.8
	7%	**0**	14,341	8,815	2,040	465	-33.4	-32.4	-20.1	-6.0	8.2
		3	10,810	6,681	1,940	625	-30.6	-26.4	-13.8	-1.7	10.0
		6	8,476	5,354	1,796	618	-27.8	-23.5	-11.4	0.0	11.1
		9	7,596	4,970	2,020	893	-23.4	-16.7	-6.6	2.6	11.9
	11%	**0**	8,469	5,122	1,123	262	-33.4	-33.0	-19.7	-5.3	8.6
		3	7,217	4,454	1,204	423	-31.7	-25.9	-14.4	-2.8	8.9
		6	5,956	3,760	1,289	454	-24.7	-21.9	-9.9	1.3	11.9
		9	6,344	4,078	1,553	593	-26.8	-20.6	-8.9	1.7	11.8
UT12.5F28_ 5.22_60°C	**7%**	**0**	10,032	6,196	1,308	275	-35.5	-33.1	-21.3	-7.0	6.3
		3	7,084	4,346	1,117	295	-33.3	-28.1	-15.5	-2.9	9.8
		6	6,123	3,869	1,269	526	-30.4	-23.5	-12.2	-1.3	9.4
		9	5,824	3,750	1,390	597	-26.8	-20.3	-9.5	0.6	10.6

Fr. – Fracture
C. I. – Crack Initiation
G. H. – Glassy Hardening
V. G. T. – Viscous-Glassy Transition
V. S. – Viscous Softening

Table 28.8 UTSST Stress Measures for Utah Mixtures

Aging Conditions				UTSST Stress (kPa)				
ID	**Air Void**	**Dur. (mo)**	**Average Carbonyl Growth ($CA-CA_{Tank}$)**	**Fracture (Fr.)**	**Crack Initiation (C. I.)**	**Glassy Hardening (G. H.)**	**Viscous-Glassy Transition (V. G. T.)**	**Viscous Softening (V. S.)**
UT12.5I28_3.79_60°C	**4%**	**0**	0.463	4,565	4,540	3,012	463	8
		3	0.552	3,794	2,894	1,164	366	76
		6	0.652	3,771	2,996	1,148	338	57
		9	0.917	2,873	2,123	920	347	86
	7%	**0**	0.436	3,662	3,462	1,260	190	3
		3	0.611	3,743	3,026	1,071	233	23
		6	0.782	3,141	2,524	936	240	33
		9	0.874	2,549	1,835	763	257	57
	11%	**0**	0.411	2,648	2,594	884	126	3
		3	0.656	2,404	1,781	637	137	14
		6	0.849	2,060	1,758	650	168	23
		9	1.051	2,275	1,684	647	187	30
UT12.5F28_5.22_60°C	**7%**	**0**	0.348	3,752	3,322	1,238	161	1
		3	0.491	3,378	2,653	922	169	8
		6	0.759	3,091	2,234	852	226	30
		9	0.889	2,748	2,018	811	248	45

Table 28.9 Thermo-Viscoelastic Properties for WesTrack Mixtures

Aging Conditions			$E_{(UTSST)}$ Modulus (MPa)				UTSST Temperatures (°C)				
ID	**Air Void**	**Dur. (mo)**	**C. I.**	**G. H.**	**V. G. T**	**V. S.**	**Fr.**	**C. I.**	**G. H.**	**V. G. T.**	**V. S.**
WT97C22_5.1_60°C	**4%**	**0**	11,807	7,194	1,762	361	-25.3	-24.6	-12.4	0.1	11.6
		3	10,988	6,791	1,893	364	-19.7	-19.6	-8.4	3.1	14.3
		6	10,686	6,582	1,954	522	-19.4	-17.2	-6.3	4.0	13.7
		9	9,760	6,021	1,745	484	-20.6	-16.5	-6.3	3.4	12.9
	7%	**0**	10,758	6,458	1,421	362	-26.2	-23.9	-11.8	0.3	10.0
		3	11,196	6,869	1,850	353	-19.8	-19.7	-8.0	3.2	14.1
		6	9,034	5,672	1,835	704	-22.7	-15.7	-5.8	3.6	12.3
		9	7,983	5,033	1,749	586	-18.3	-14.1	-4.1	5.1	14.0
	11%	**0**	8,512	5,281	1,351	224	-26.3	-26.2	-17.2	-2.3	12.2
		3	8,167	5,167	1,229	173	-21.4	-21.4	-11.4	2.2	15.0
		6	7,490	4,738	1,670	474	-17.4	-16.1	-5.2	4.7	14.7
		9	5,241	3,374	1,264	406	-15.9	-14.0	-4.2	4.8	13.9
WT95F28 5.2_60°C	**7%**	**0**	9,672	5,848	1,378	251	-24.2	-23.2	-11.7	-0.3	11.1
		3	8,299	5,290	1,954	748	-19.7	-14.3	-4.8	3.8	12.2
		6	7,677	5,053	2,221	904	-14.1	-10.9	-1.4	6.8	14.9
		9	6,459	4,363	2,157	1,051	-12.8	-7.1	1.2	8.0	14.8

Fr. – Fracture
C. I. – Crack Initiation
G. H. – Glassy Hardening
V. G. T. – Viscous-Glassy Transition
V. S. – Viscous Softening

Table 28.10 UTSST Stress Measures for WesTrack Mixtures

Aging Conditions				UTSST Stress (kPa)				
ID	**Air Void**	**Dur. (mo)**	**Average Carbonyl Growth ($CA-CA_{Tank}$)**	**Fracture (Fr.)**	**Crack Initiation (C. I.)**	**Glassy Hardening (G. H.)**	**Viscous-Glassy Transition (V. G. T.)**	**Viscous Softening (V. S.)**
WT97C22_5.1_60°C	**4%**	**0**	0.208	4,023	3,863	1,324	209	7.5
		3	0.334	3,383	3,364	1,218	222	10.8
		6	0.444	3,384	2,924	1,002	209	17.9
		9	0.485	3,488	2,708	941	193	12.8
	7%	**0**	0.230	3,435	2,993	939	122	1.0
		3	0.331	3,010	2,978	1,009	179	8.8
		6	0.455	3,319	2,270	821	196	19.5
		9	0.556	2,772	2,146	796	209	29.5
	11 %	**0**	0.314	2,325	2,311	1,047	122	1.0
		3	0.548	2,260	2,247	920	133	6.5
		6	0.669	2,119	1,955	729	188	21.6
		9	0.741	1,677	1,483	588	167	22.7
WT95F28 5.2_60°C	**7%**	**0**	0.554	2,976	2,674	902	140	0.8
		3	0.745	2,823	2,053	783	221	29.4
		6	0.841	2,485	2,024	829	278	53.9
		9	0.890	2,313	1,665	724	279	71.4

29 APPENDIX Q

Summary of Thermo-Viscoelastic Property Measurements of Aged Asphalt Mixtures

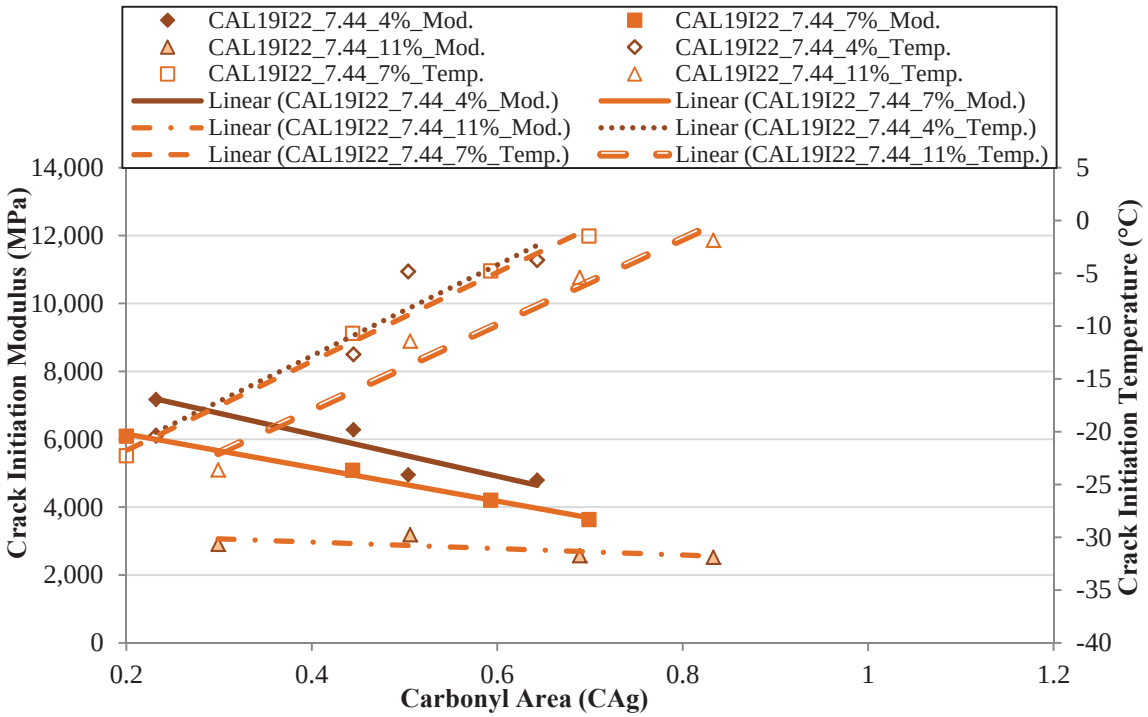

Figure 29.1 Crack Initiation Modulus Values for the CAL19I22_7.44 Mixtures Aged at 60°C with Different Air Void Levels

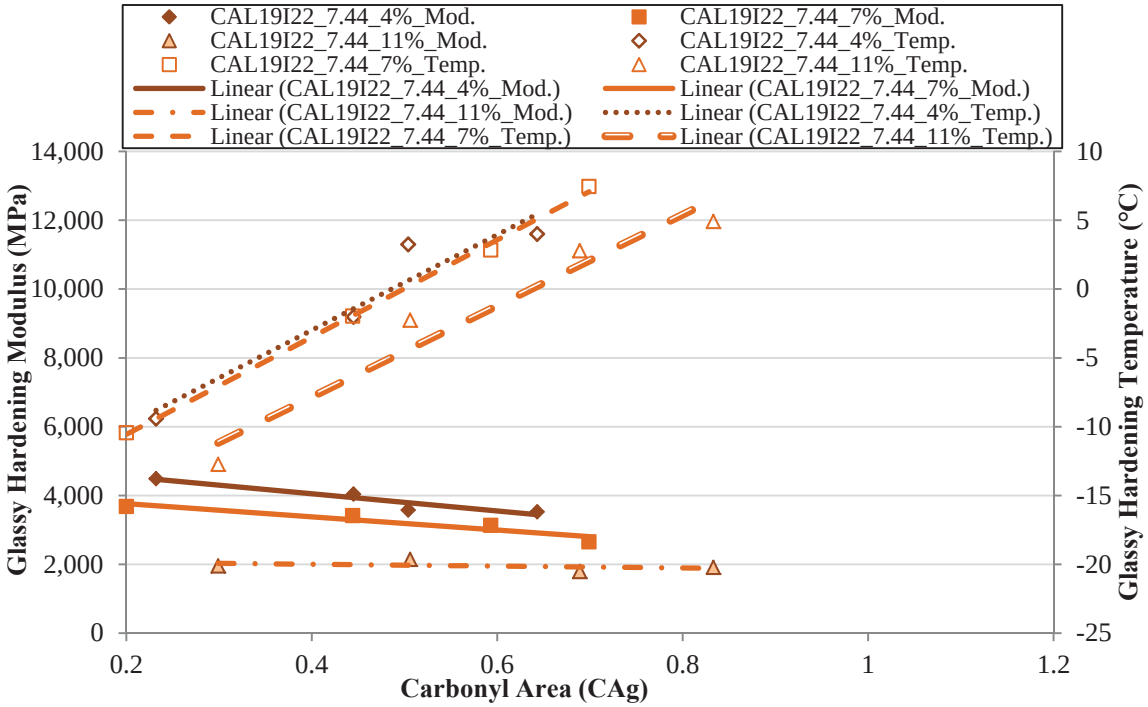

Figure 29.2 Glassy Hardening Modulus Values for the CAL19I22_7.44 Mixtures Aged at 60°C with Different Air Voids

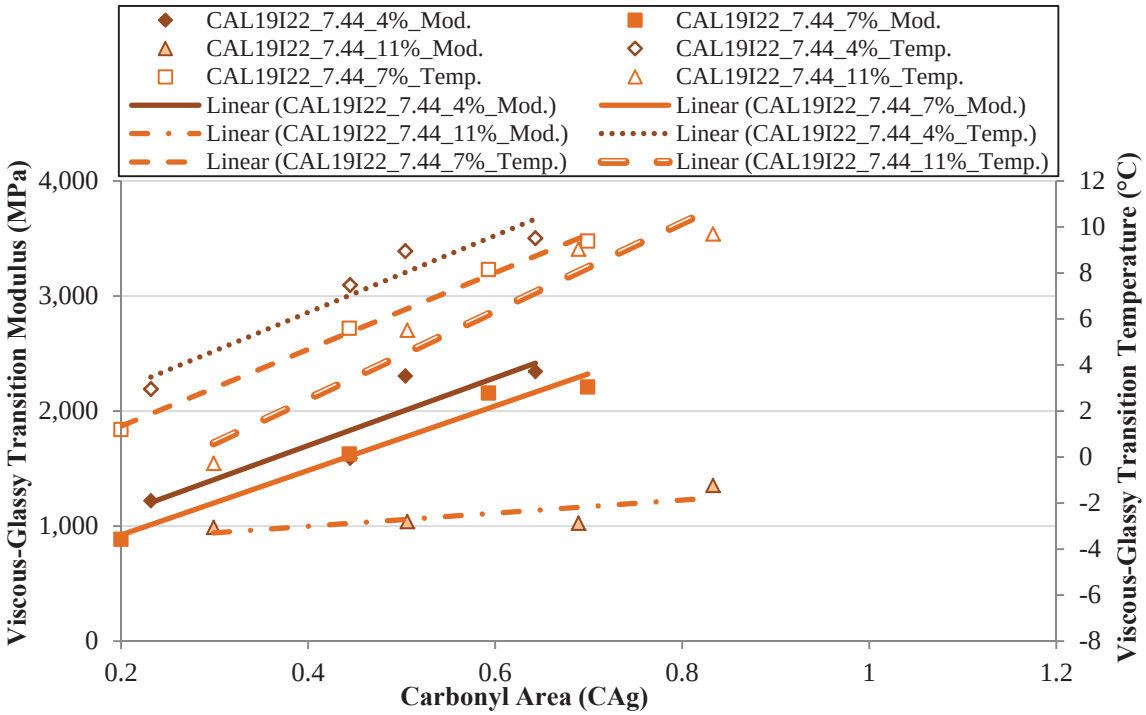

Figure 29.3 Viscous-Glassy Transition Modulus Values for the CAL19I22_7.44 Mixtures Aged at 60°C with Different Air Voids

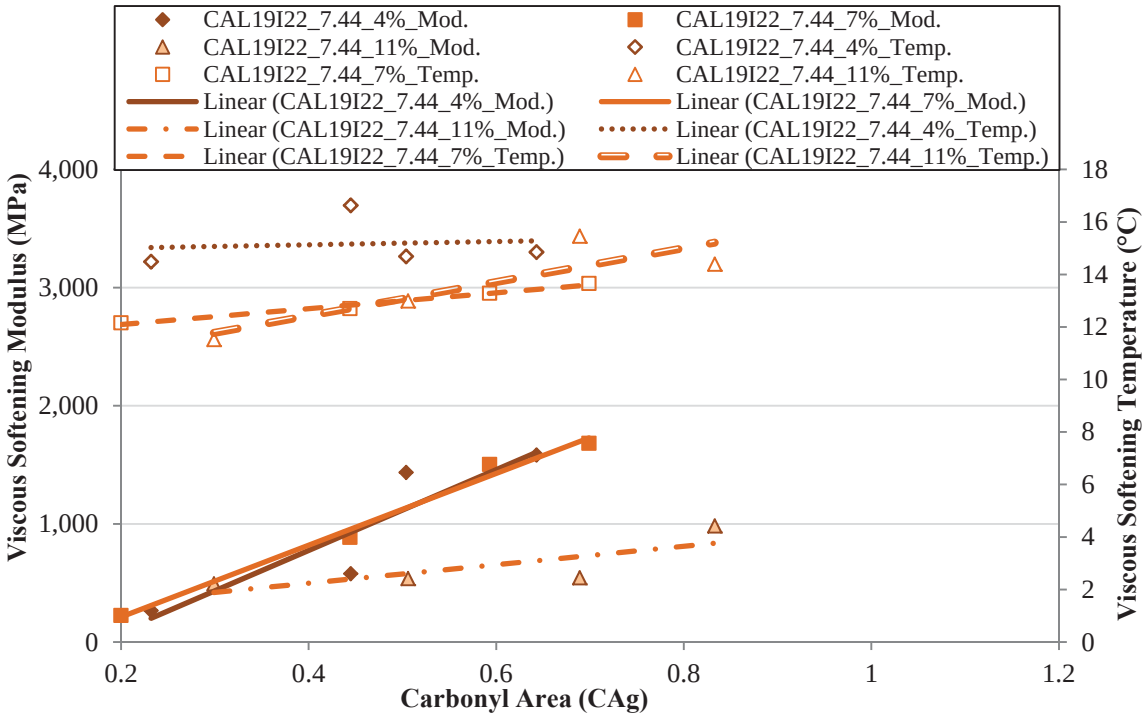

Figure 29.4 Viscous Softening Modulus Values for the CAL19I22_7.44 Mixtures Aged at 60°C with Different Air Void Levels

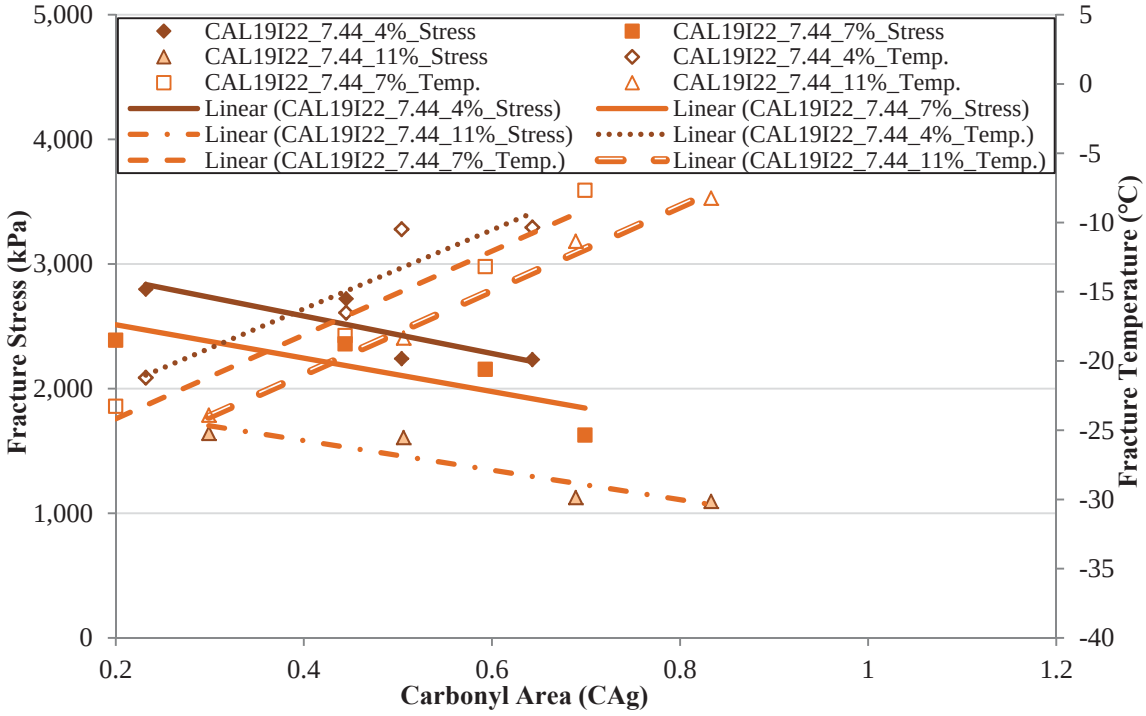

Figure 29.5 Fracture Stress Measurements for the CAL19I22_7.44 Mixtures Aged at 60°C with Different Air Void Levels

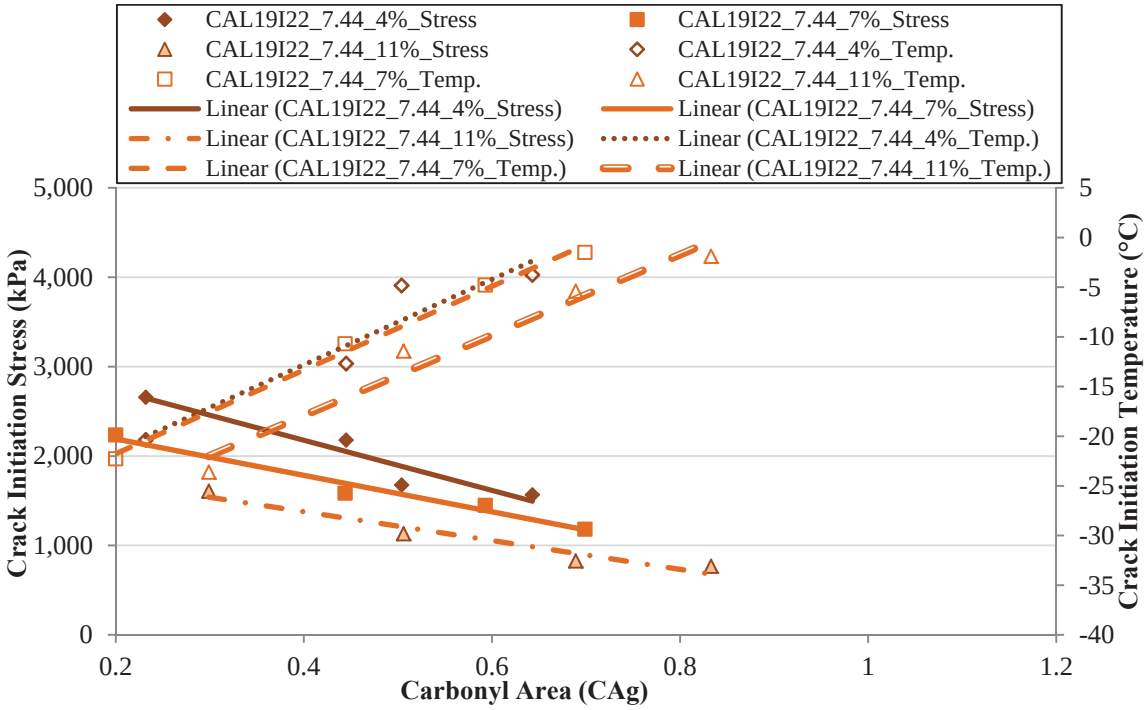

Figure 29.6 Crack Initiation Stress Measurements for the CAL19I22_7.44 Mixtures Aged at 60°C with Different Air Voids

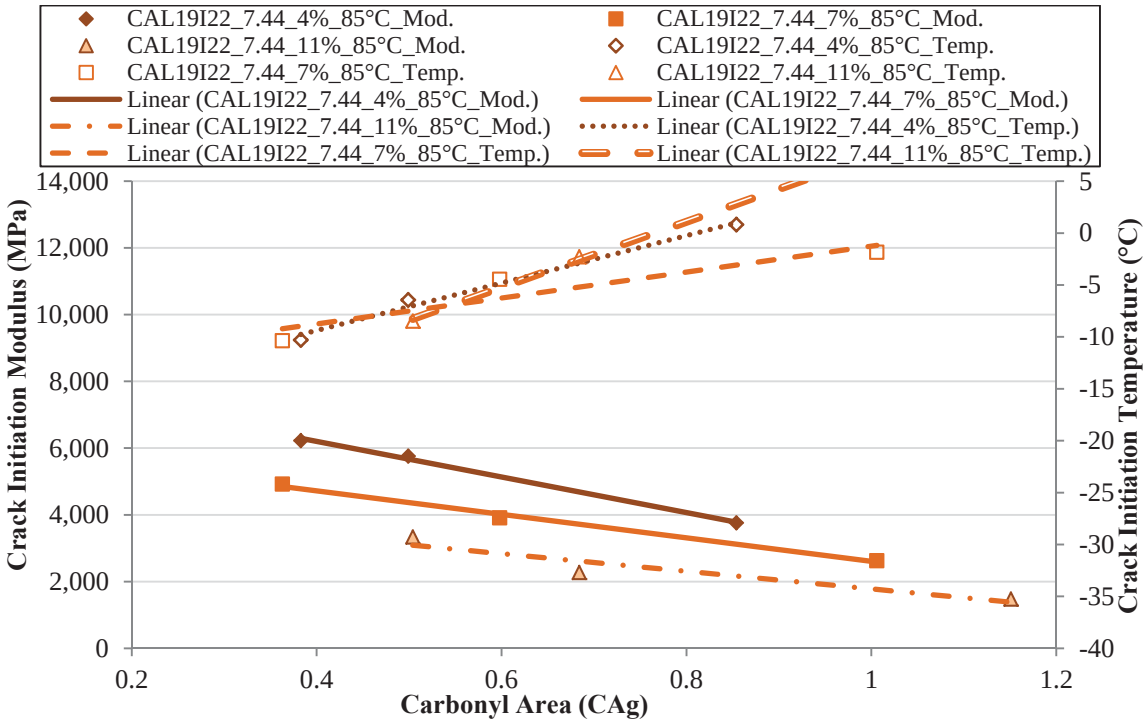

Figure 29.7 Crack Initiation Modulus Values for the CAL19I22_7.44 Mixtures Aged at 85°C with Different Air Void Levels

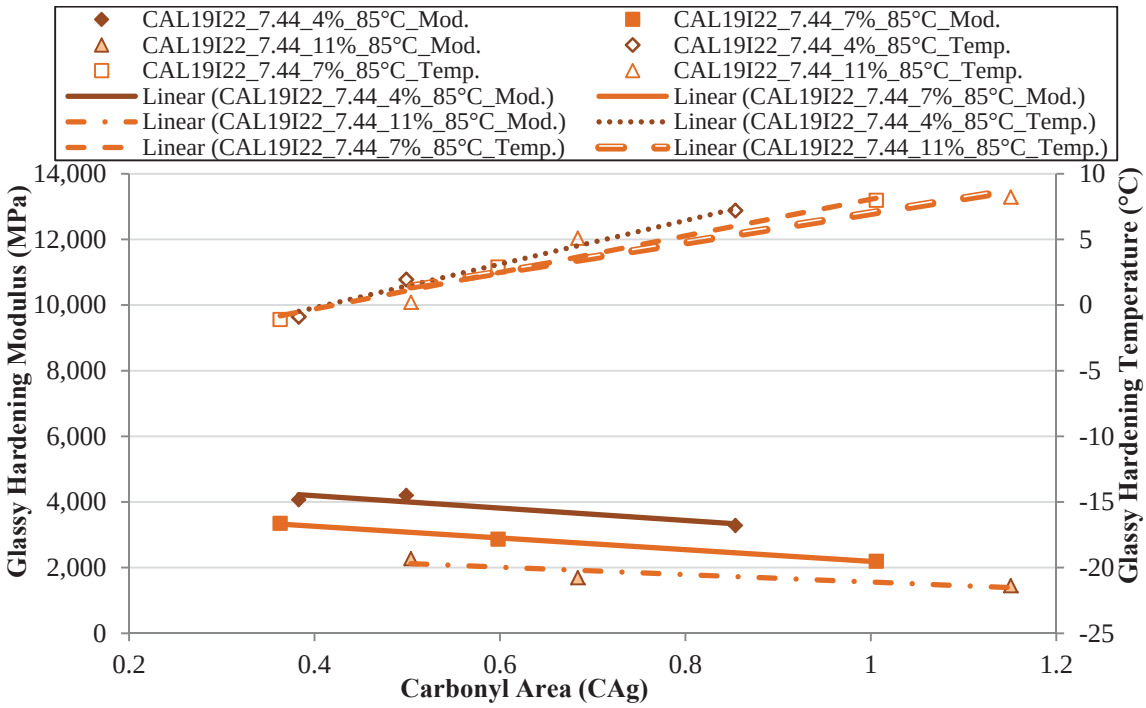

Figure 29.8 Glassy Hardening Modulus Values for the CAL19I22_7.44 Mixtures Aged at 85°C with Different Air Voids

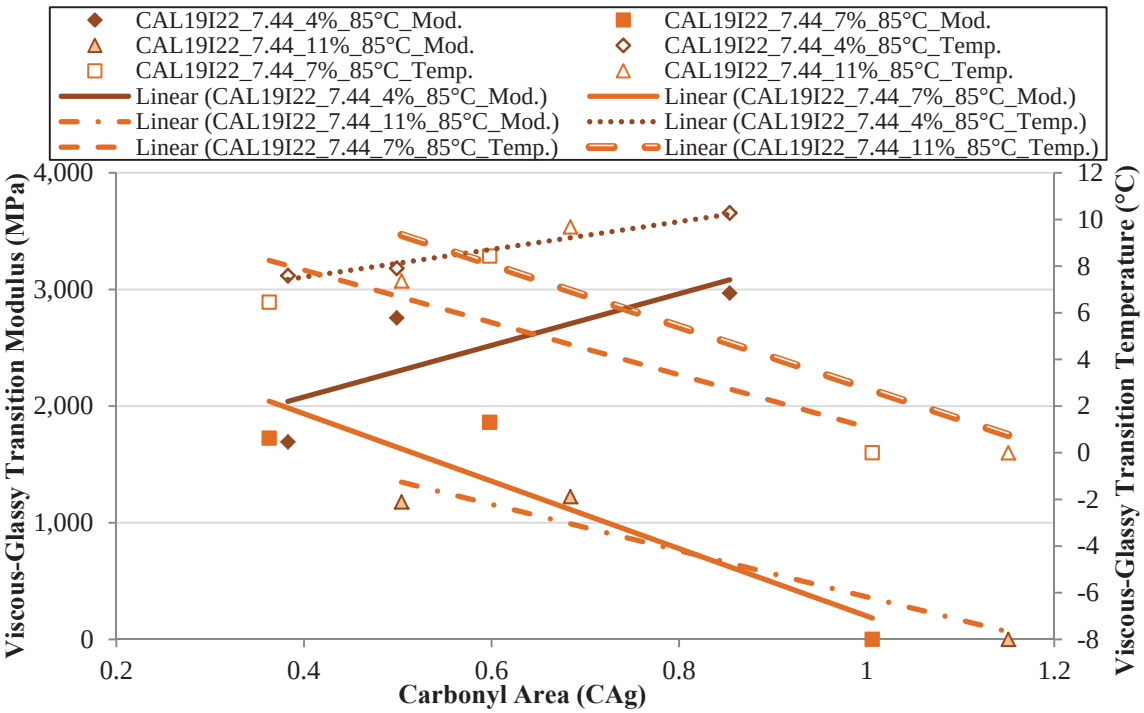

Figure 29.9 Viscous-Glassy Transition Modulus Values for the CAL19I22_7.44 Mixtures Aged at 85°C with Different Air Voids

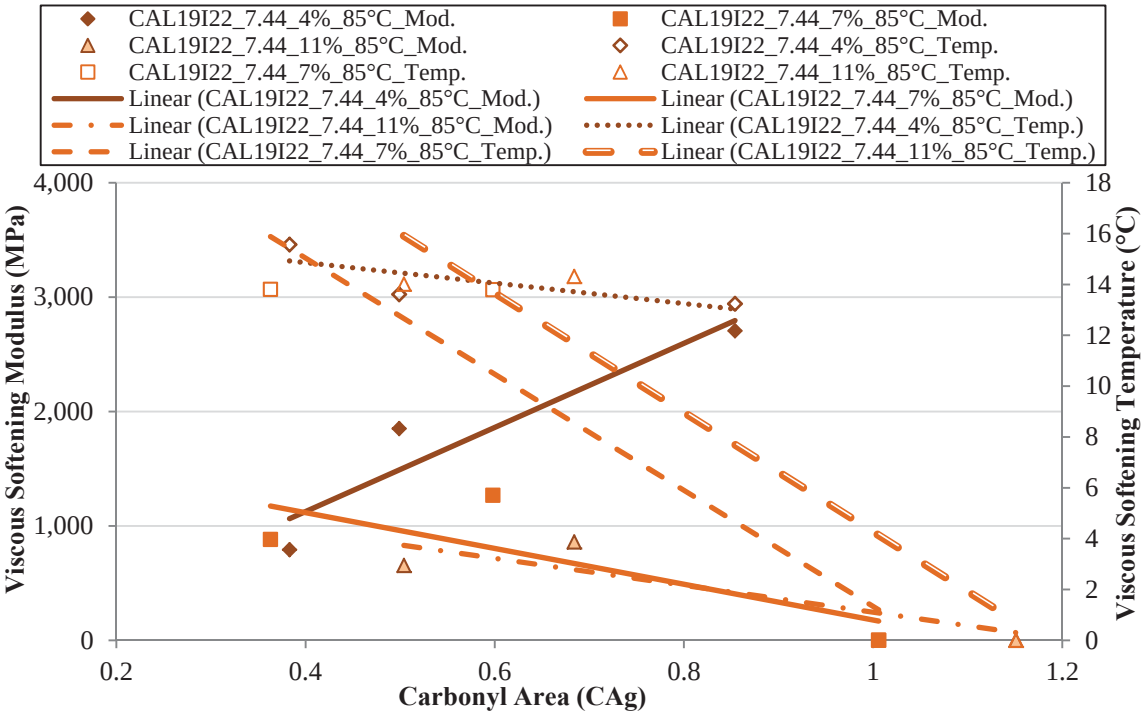

Figure 29.10 Viscous Softening Modulus Values for the CAL19I22_7.44 Mixtures Aged at 85°C with Different Air Voids

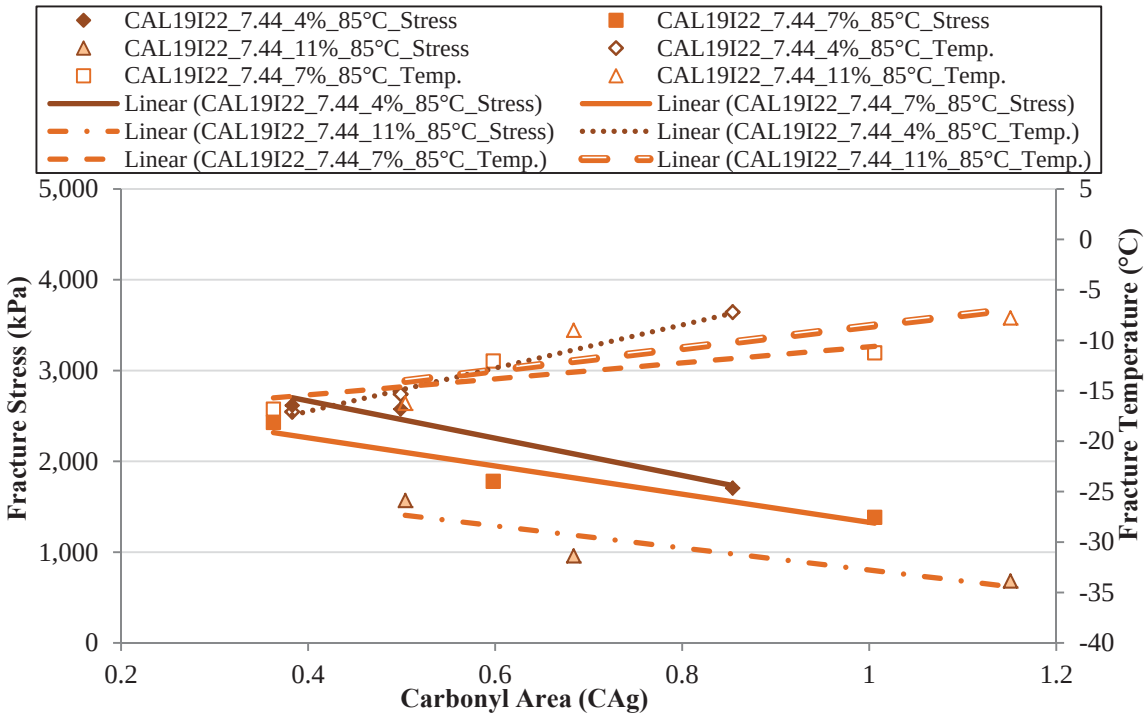

Figure 29.11 Fracture Stress Measurements for the CAL19I22_7.44 Mixtures Aged at 85°C with Different Air Void Levels

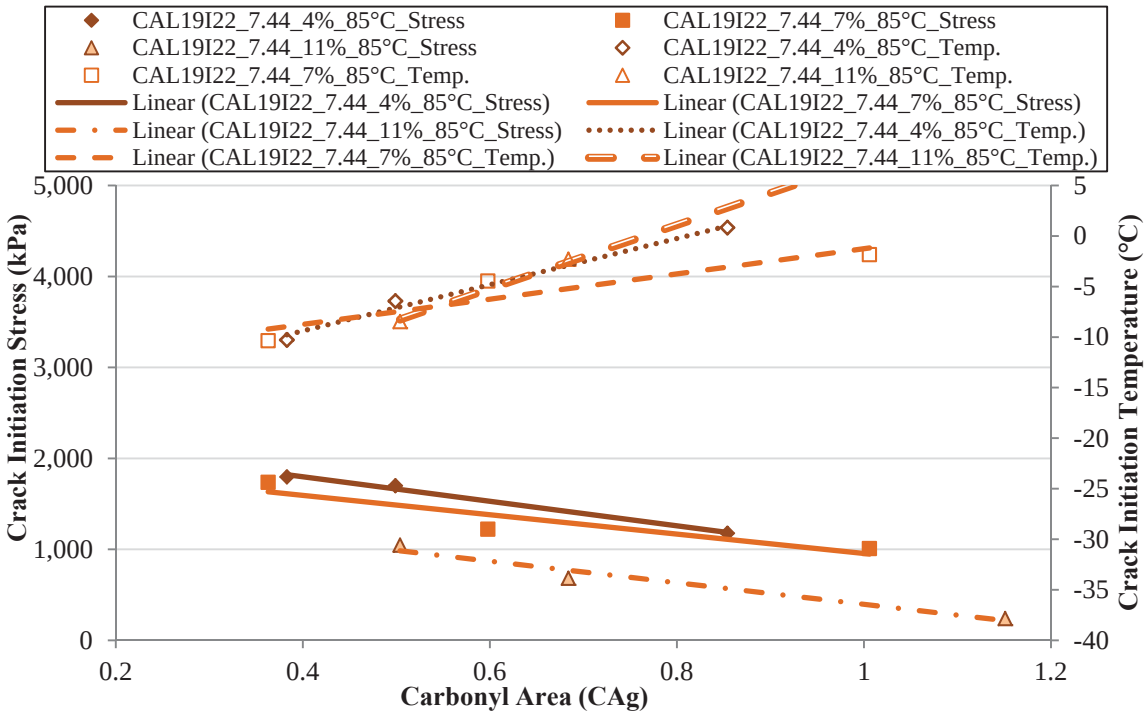

Figure 29.12 Crack Initiation Stress Measurements for the CAL19I22_7.44 Mixtures Aged at 85°C with Different Air Voids

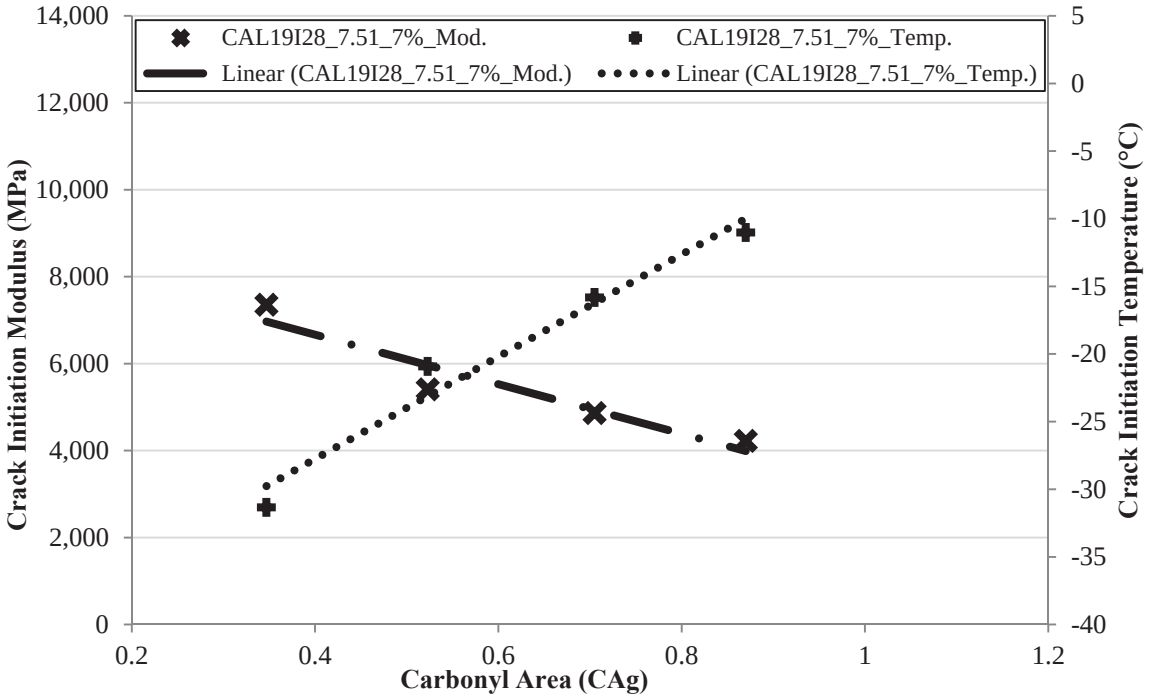

Figure 29.13 Crack Initiation Modulus Values for the CAL19I28_7.51_7% Va Mixtures Aged at 60°C

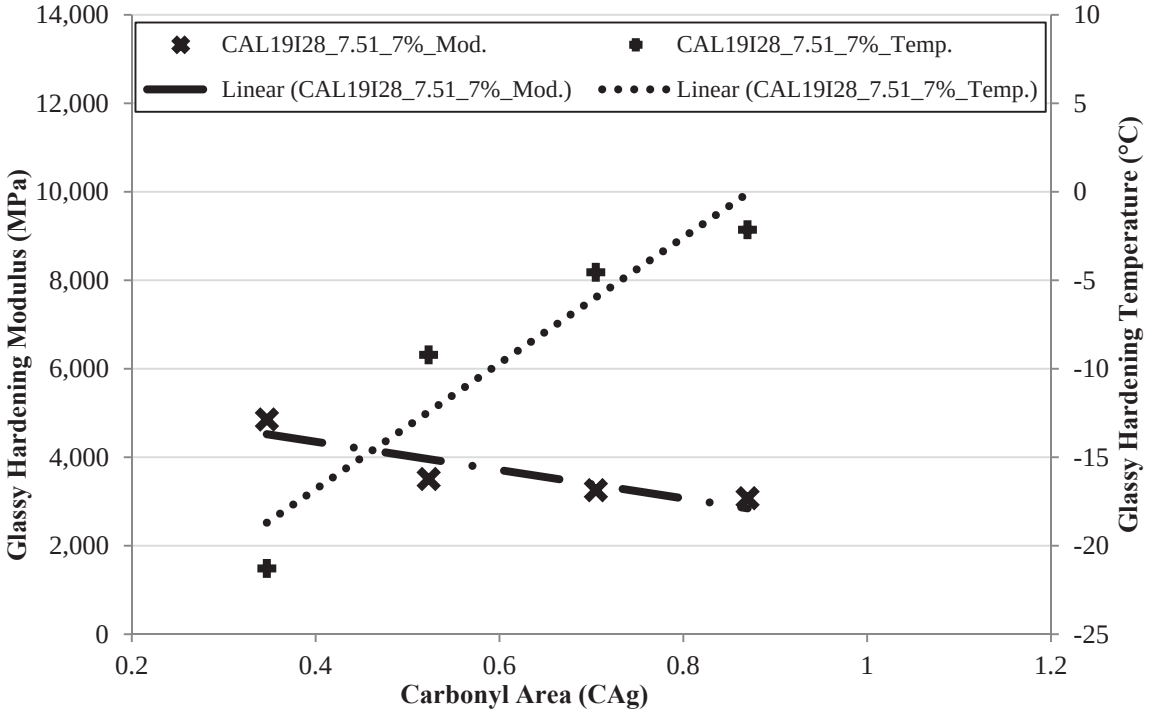

Figure 29.14 Glassy Hardening Modulus Values for the CAL19I28_7.51_7% Va Mixtures Aged at 60°C

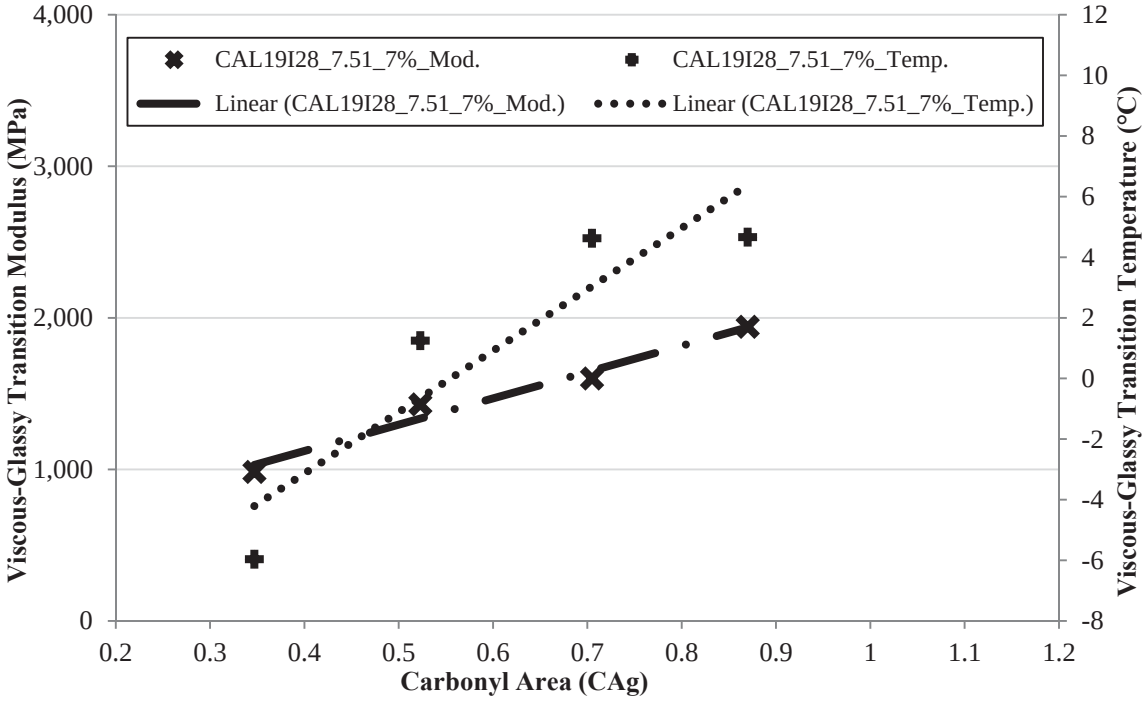

Figure 29.15 Viscous-Glassy Transition Modulus Values for the CAL19I28_7.51_7% Va Mixtures Aged at 60°C

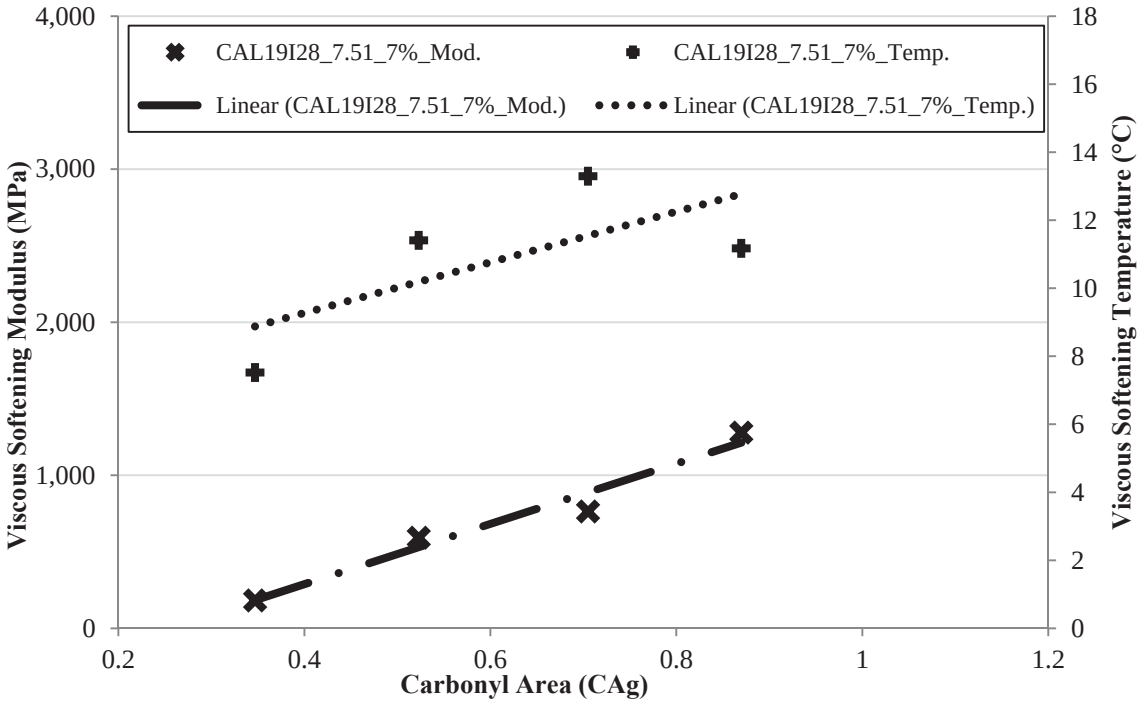

Figure 29.16 Viscous Softening Modulus Values for the CAL19I28_7.51_7% Va Mixtures Aged at 60°C

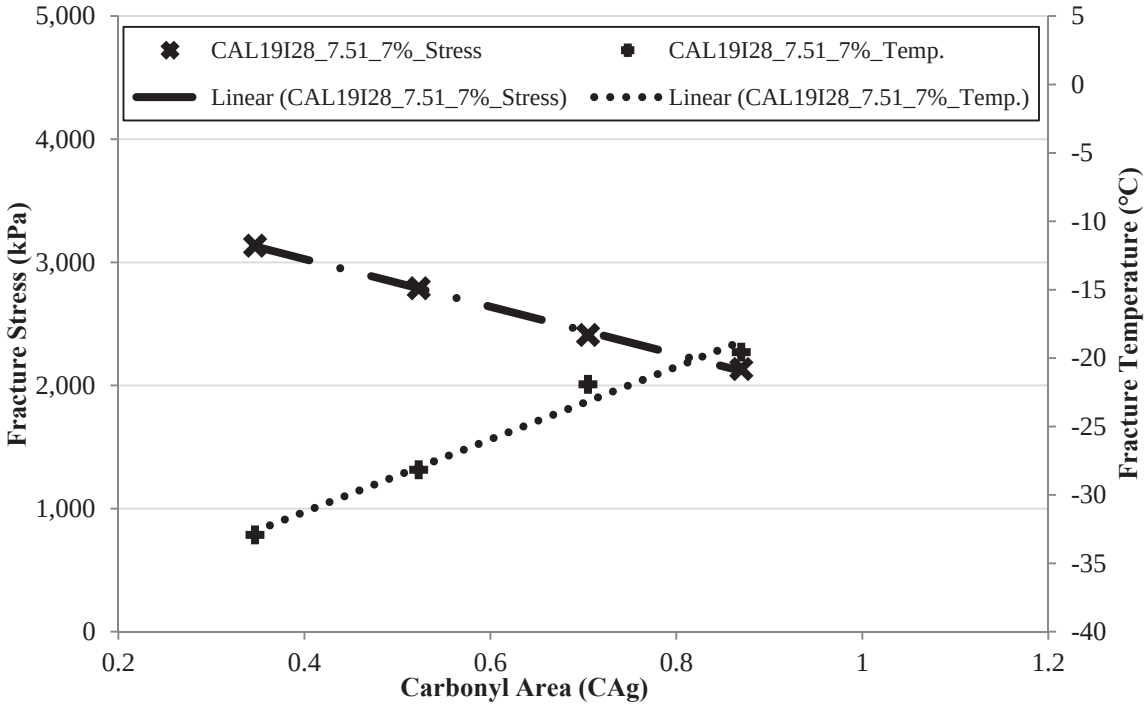

Figure 29.17 Fracture Stress Measurements for the CAL19I28_7.51_7% Va Mixtures Aged at 60°C

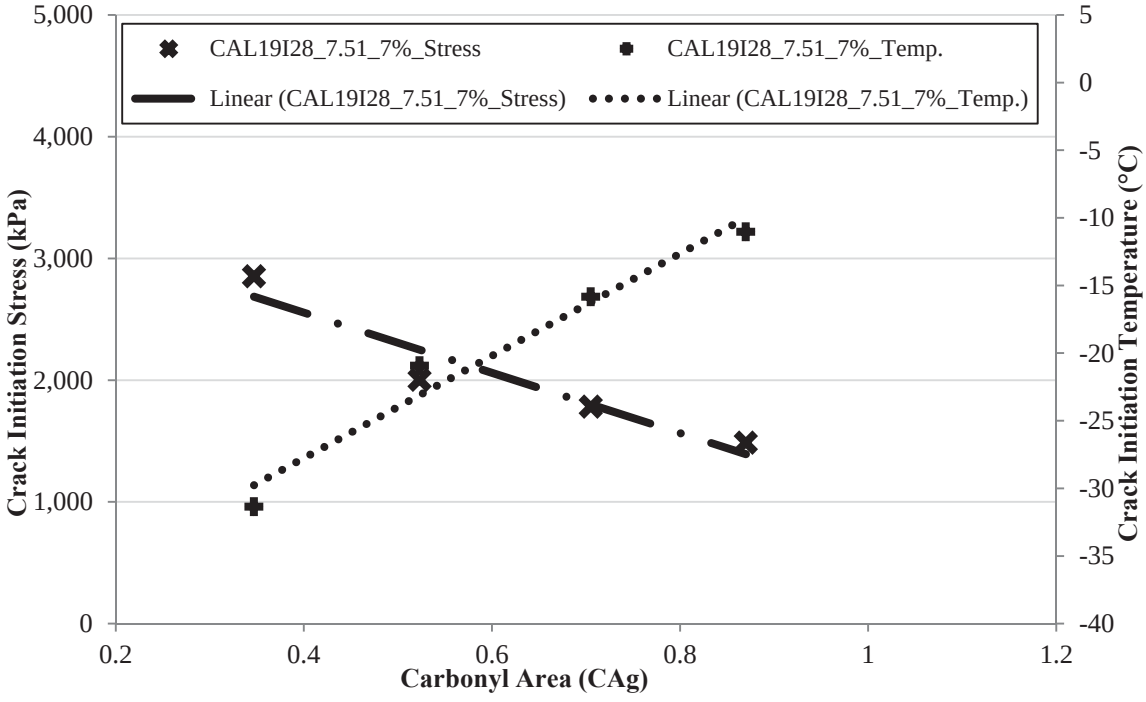

Figure 29.18 Crack Initiation Stress Measurements for the CAL19I28_7.51_7% Va Mixtures Aged at 60°C

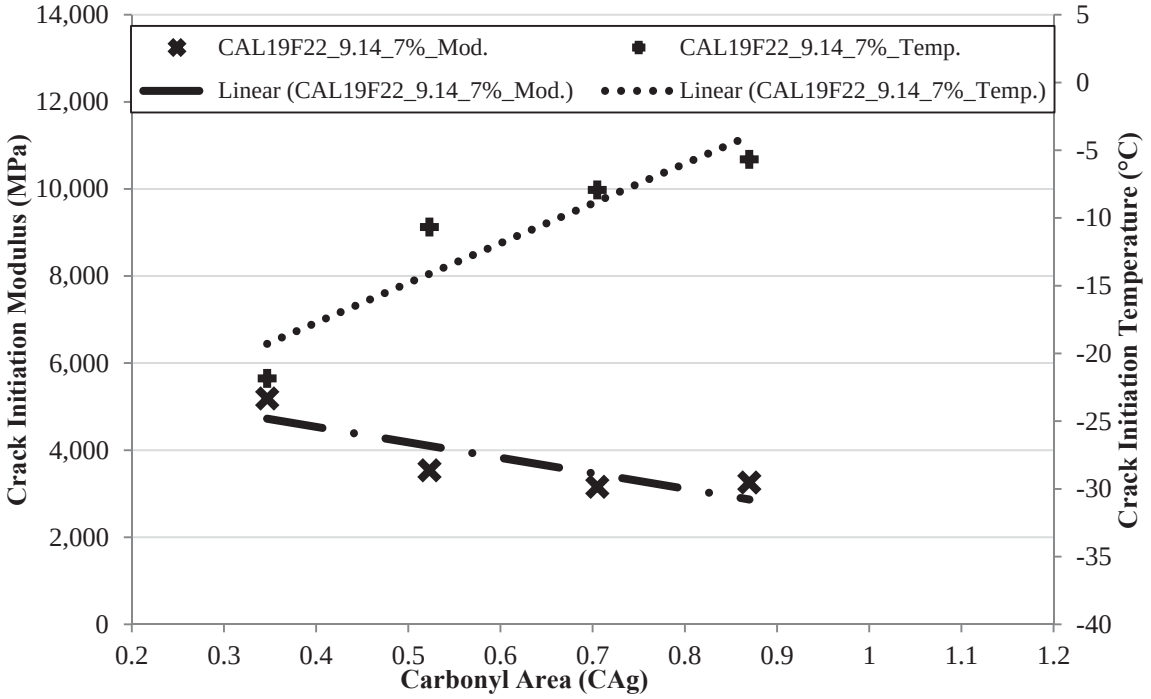

Figure 29.19 Crack Initiation Modulus Values for the CAL19F22_9.14_7% Va Aged at 60°C

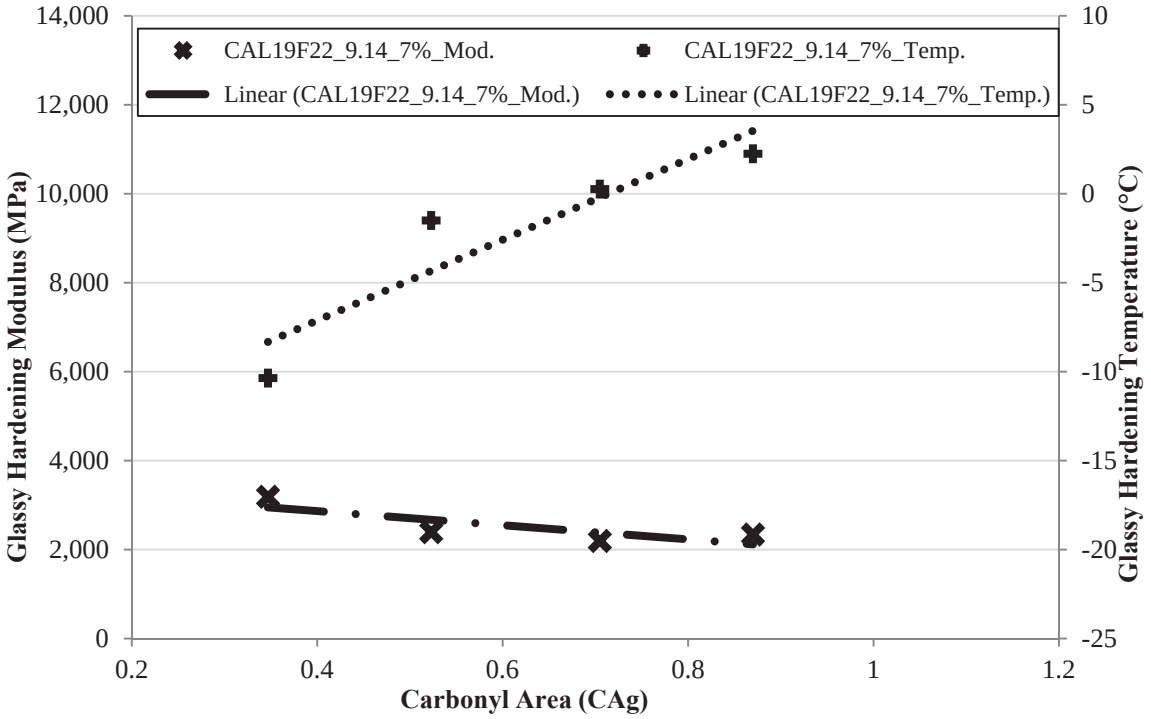

Figure 29.20 Glassy Hardening Modulus Values for the CAL19F22_9.14_7% Va Aged at 60°C

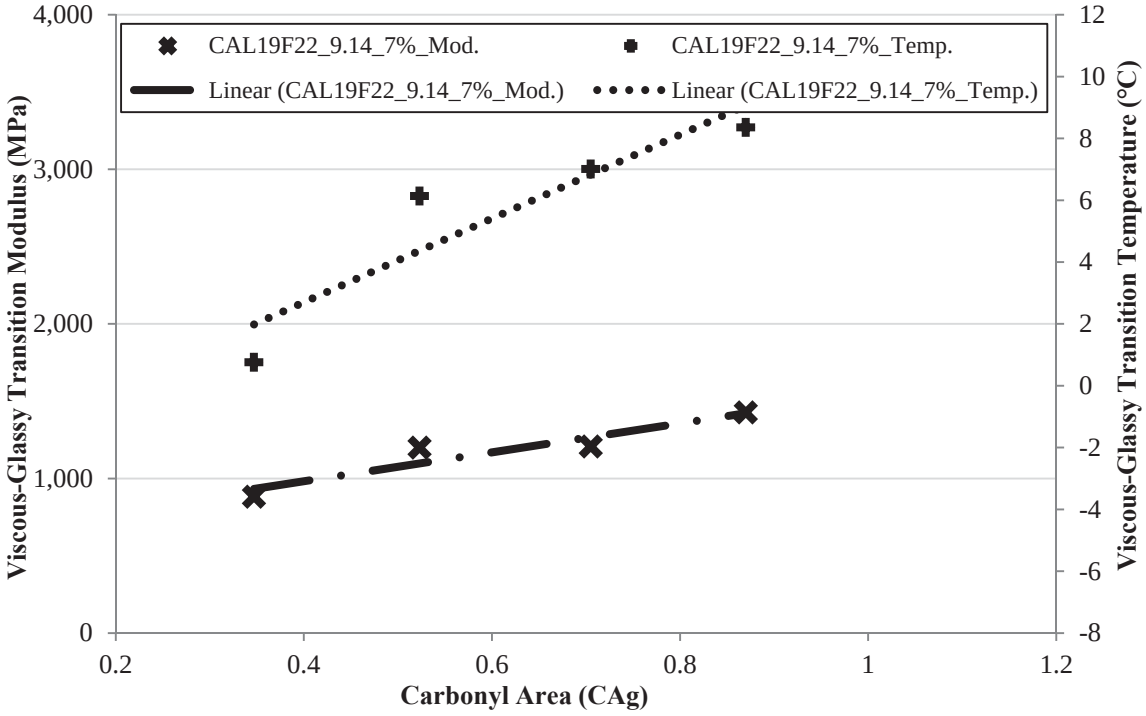

Figure 29.21 Viscous-Glassy Transition Modulus Values for the CAL19F22_9.14_7% Va Aged at 60°C

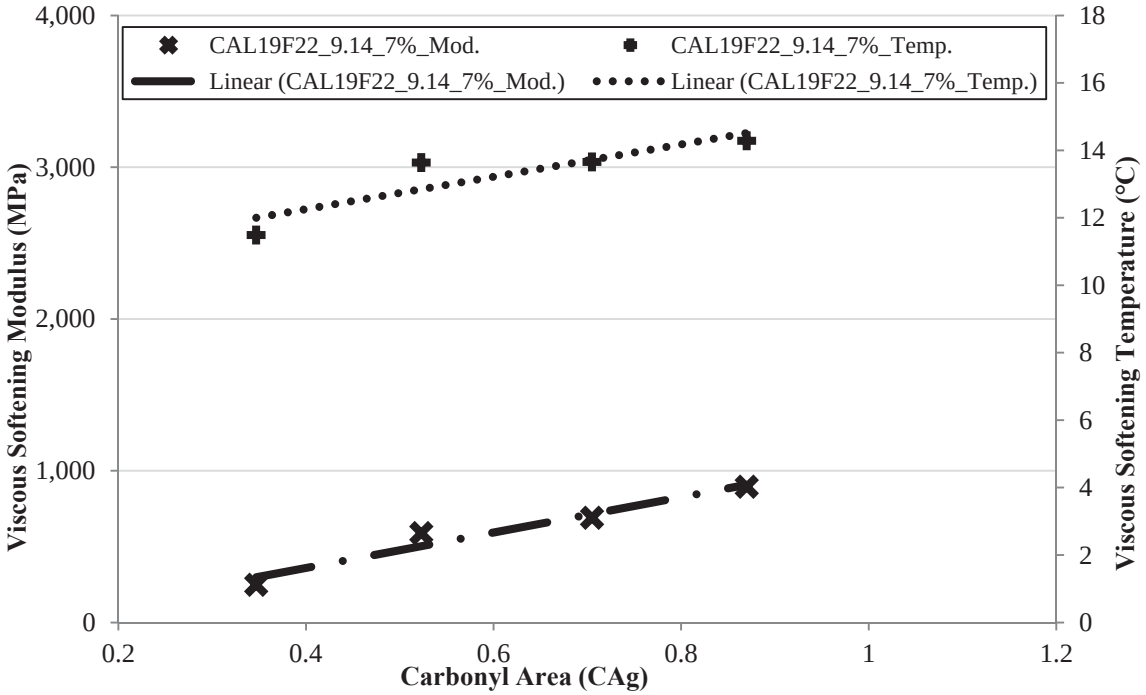

Figure 29.22 Viscous Softening Modulus Values for the CAL19F22_9.14_7% Va Aged at 60°C

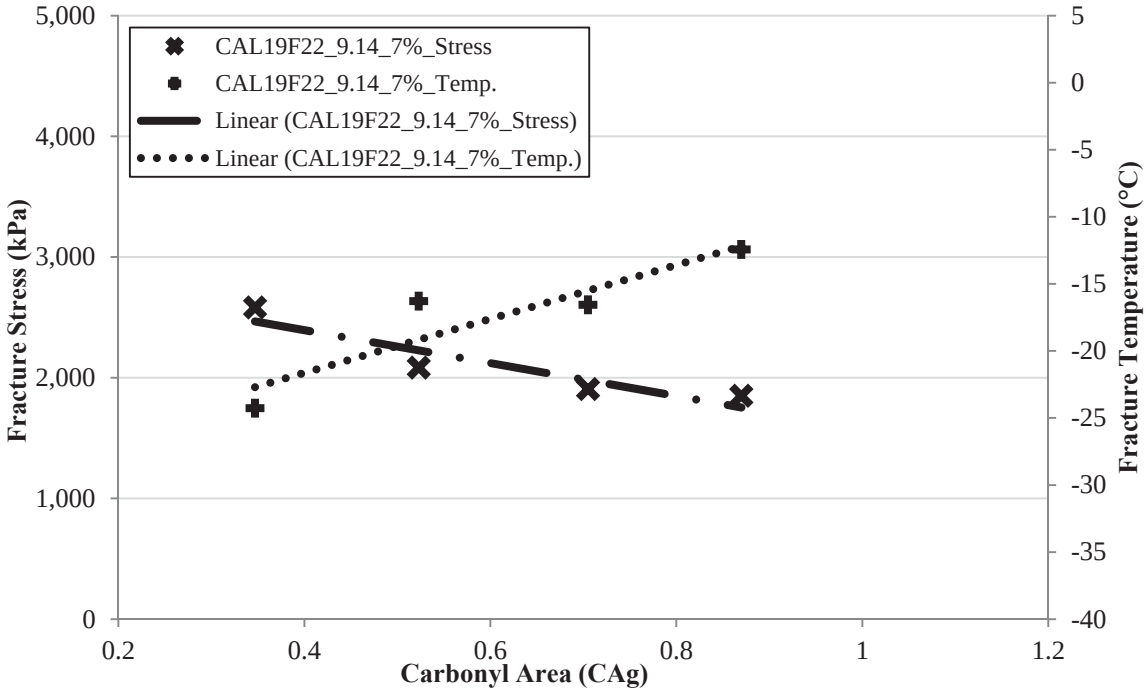

Figure 29.23 Fracture Stress Measurements for the CAL19F22_9.14_7% Va Aged at 60°C

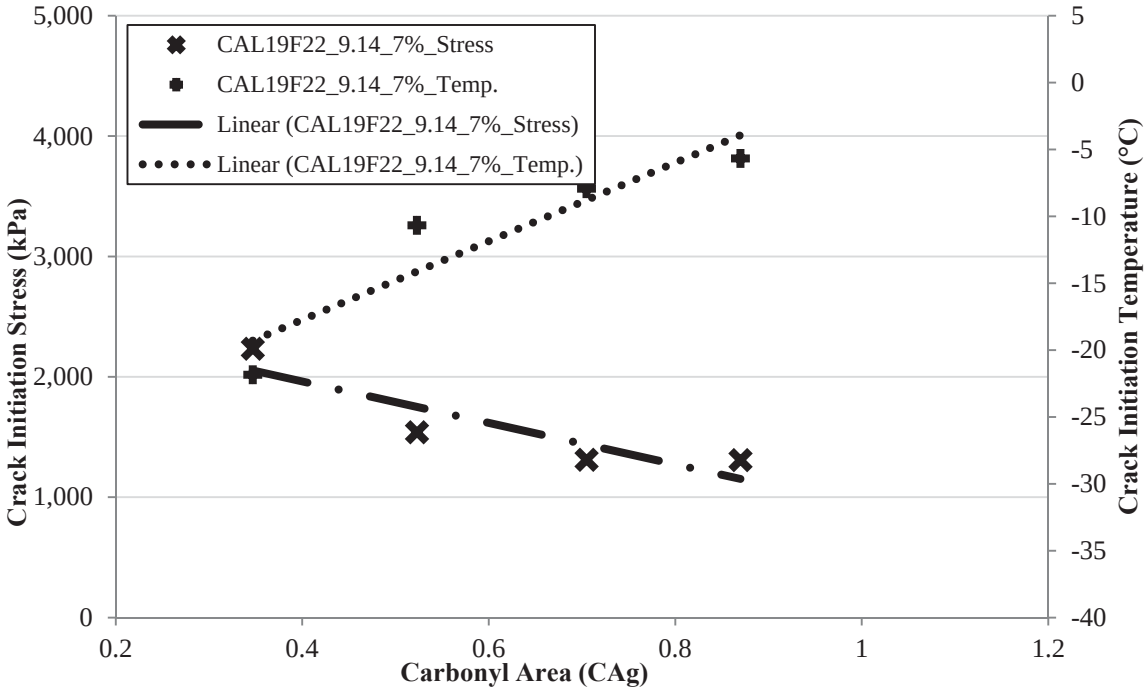

Figure 29.24 Crack Initiation Stress Measurements for the CAL19F22_9.14_7% Va Aged at 60°C

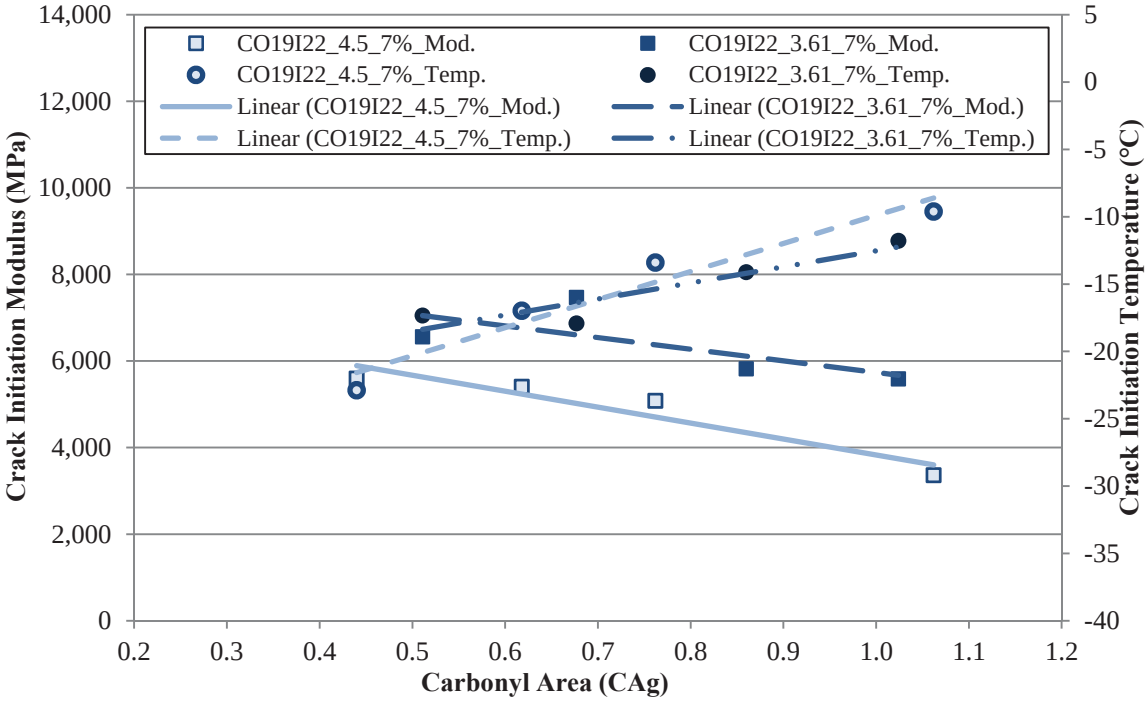

Figure 29.25 Crack Initiation Modulus Values for the CO19I22_7% Va Mixtures Aged at 60°C with Different Binder Contents

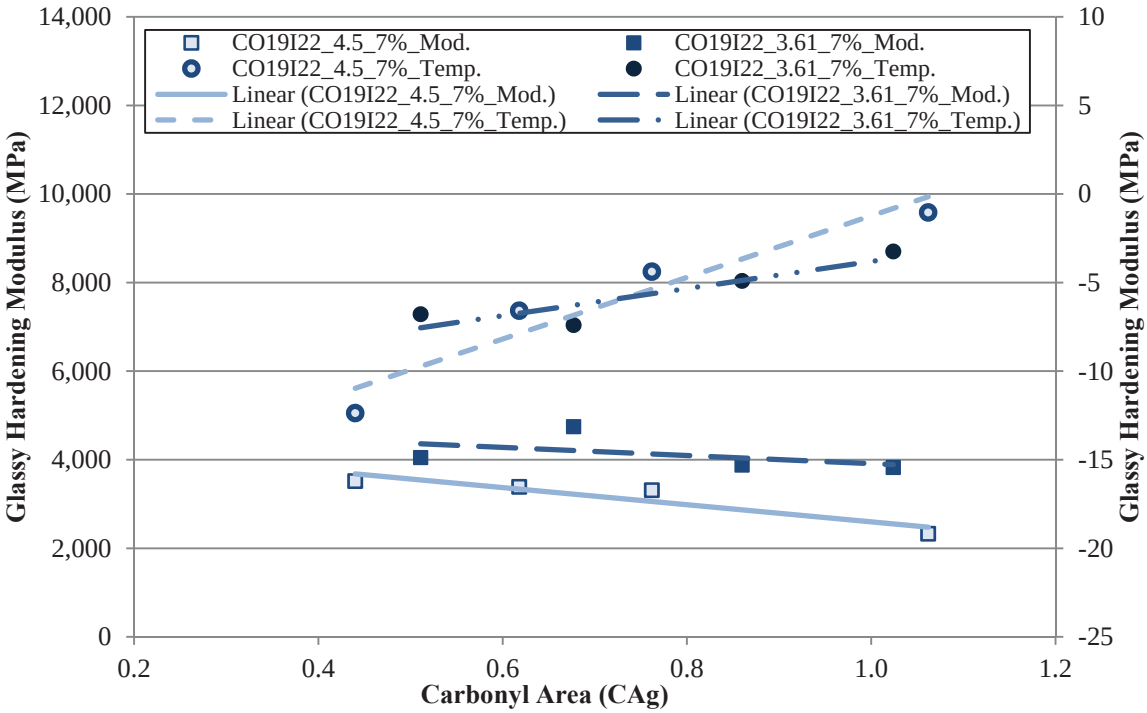

Figure 29.26 Glassy Hardening Modulus Values for the CO19I22_7% Va Mixtures Aged at 60°C with Different Binder Contents

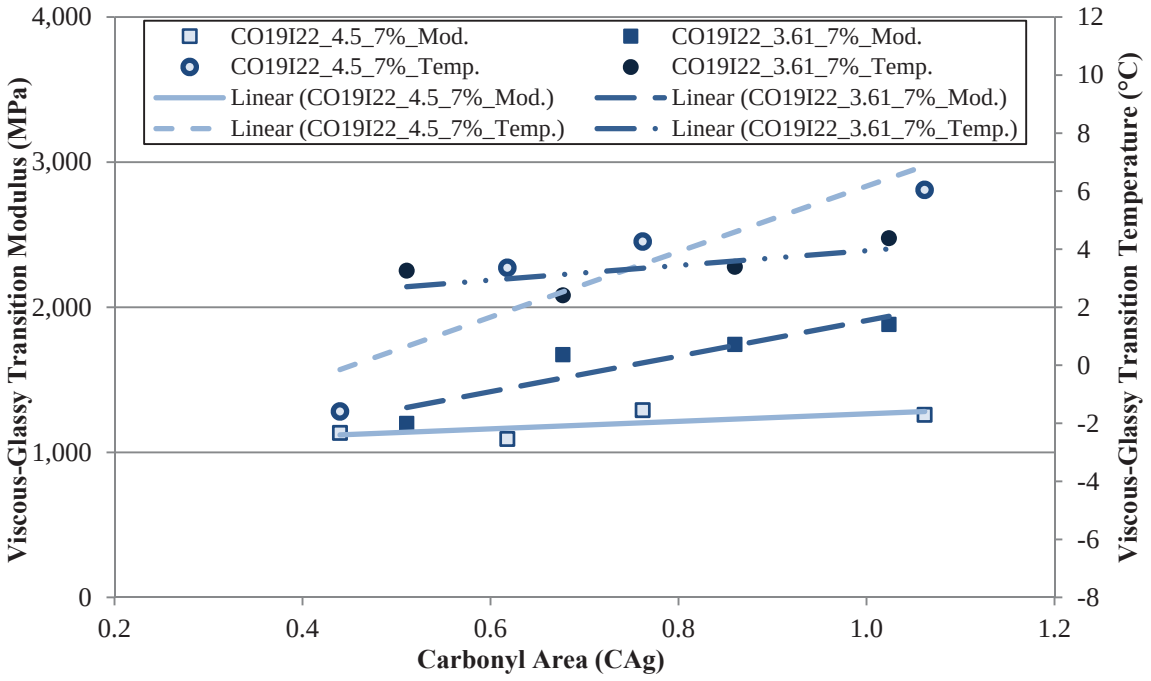

Figure 29.27 Viscous-Glassy Transition Modulus Values for the CO19I22_7% Va Mixtures Aged at 60°C with Different Binder Contents

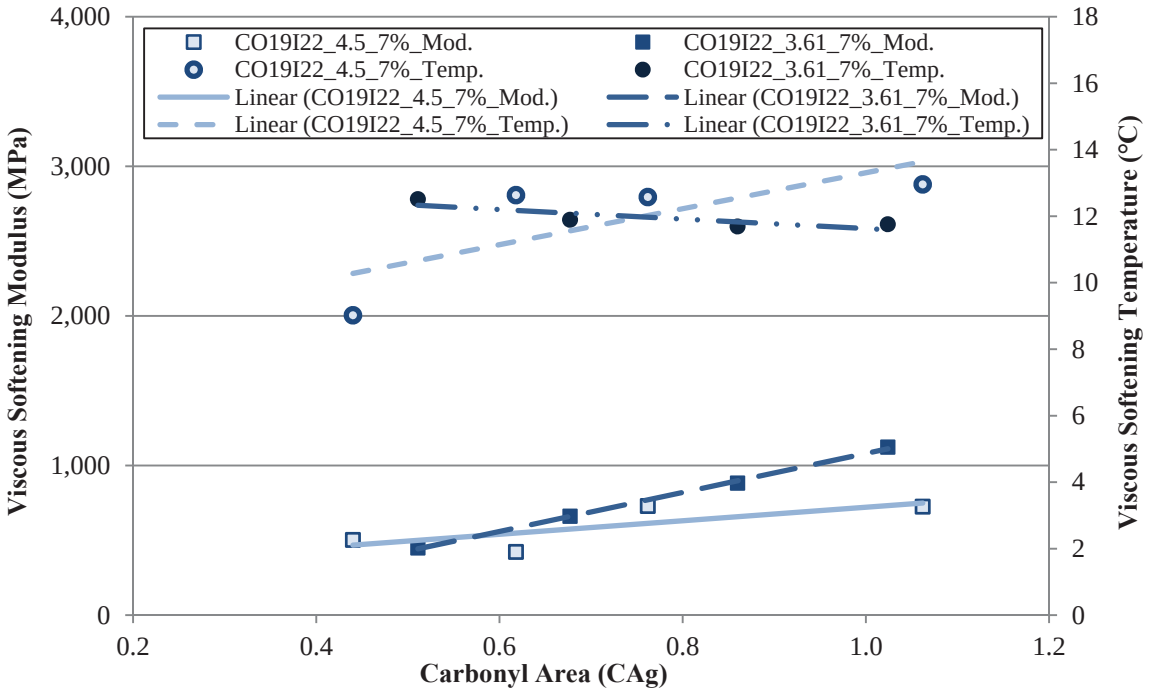

Figure 29.28 Viscous Softening Modulus Values for the CO19I22_7% Va Mixtures Aged at 60°C with Different Binder Contents

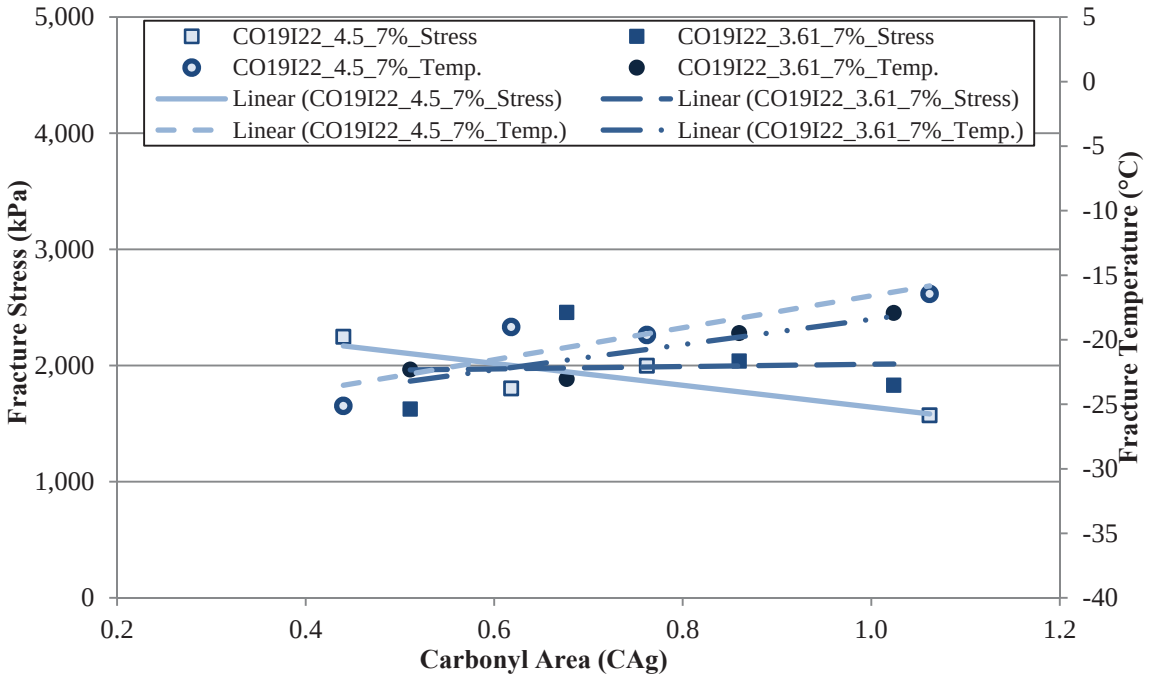

Figure 29.29 Fracture Stress Measurements for the CO19I22_7% Va Mixtures Aged at 60°C with Different Binder Contents

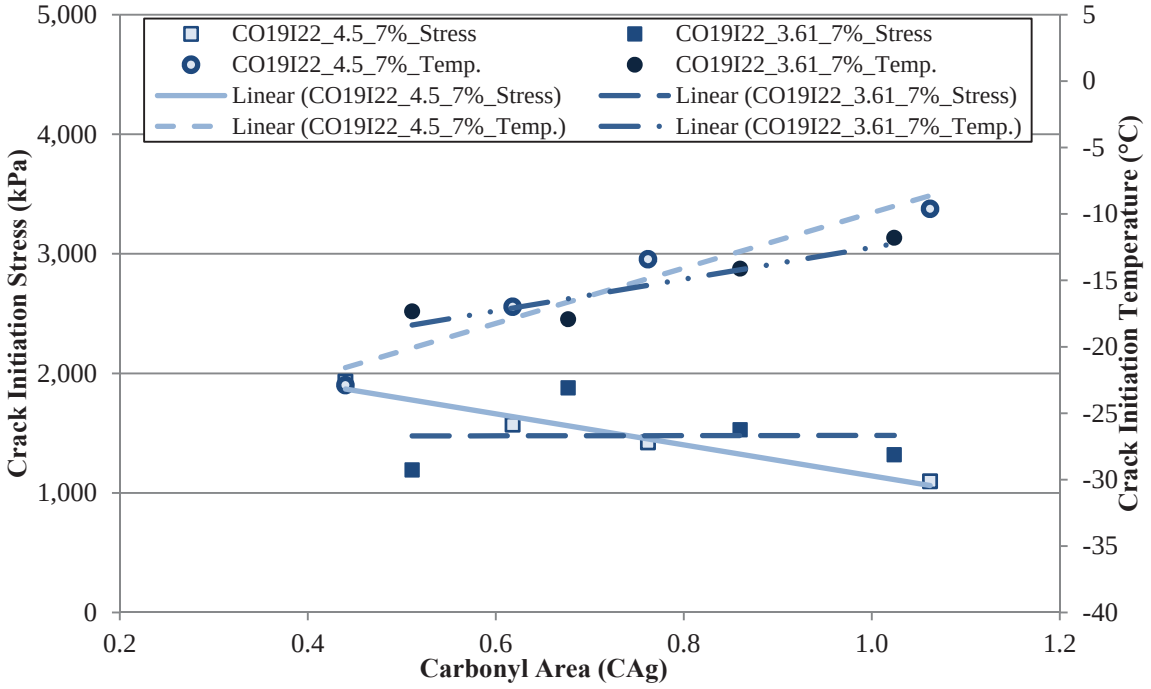

Figure 29.30 Crack Initiation Stress Measurements for the CO19I22_7% Va Mixtures Aged at 60°C with Different Binder Contents

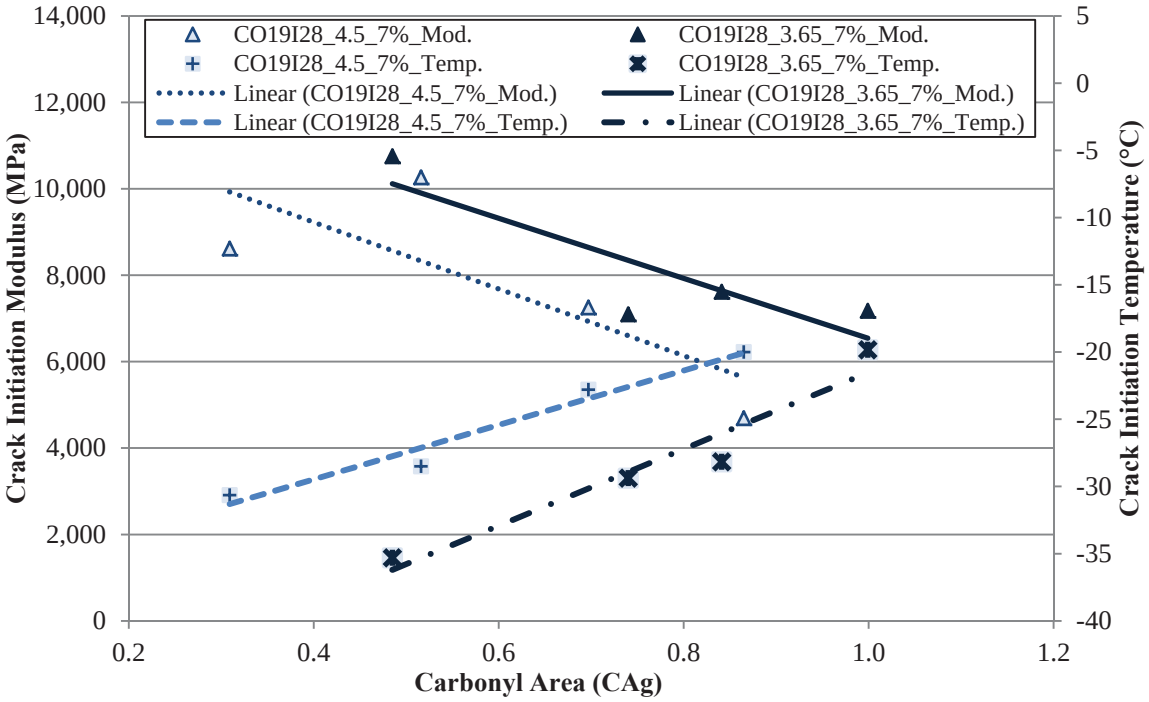

Figure 29.31 Crack Initiation Modulus Values for the CO19I28_7% Va Aged at 60°C with Different Binder Contents

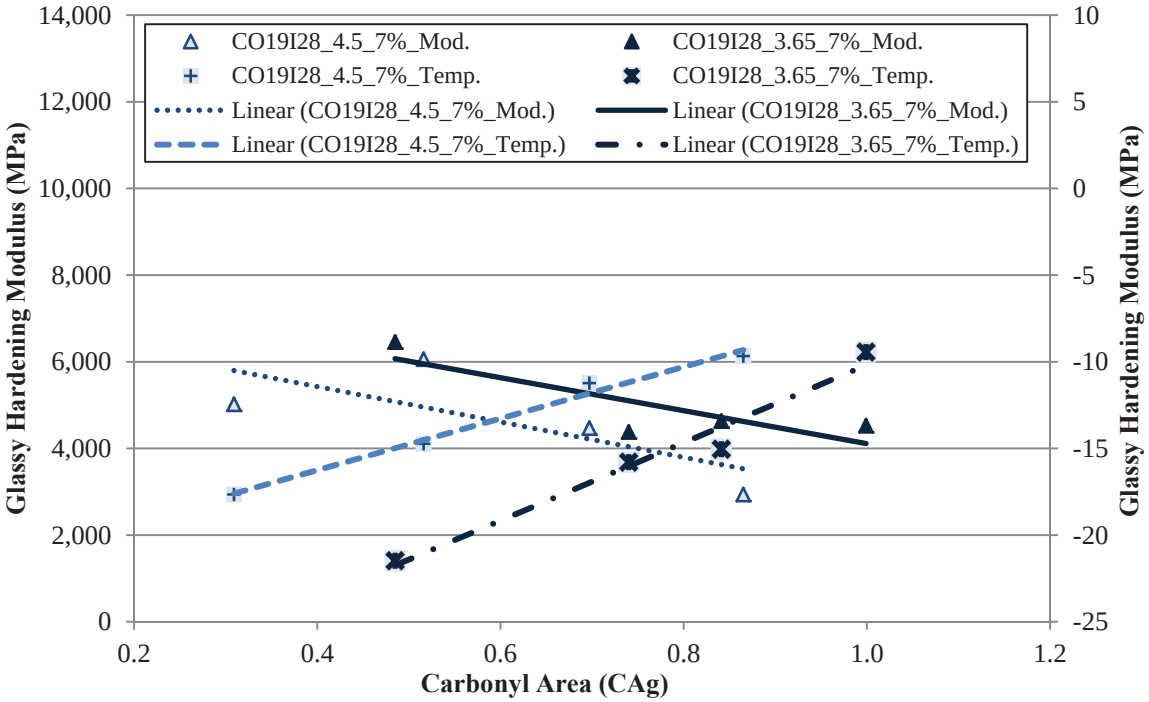

Figure 29.32 Glassy Hardening Modulus Values for the CO19I28_7% Va Aged at 60°C with Different Binder Contents

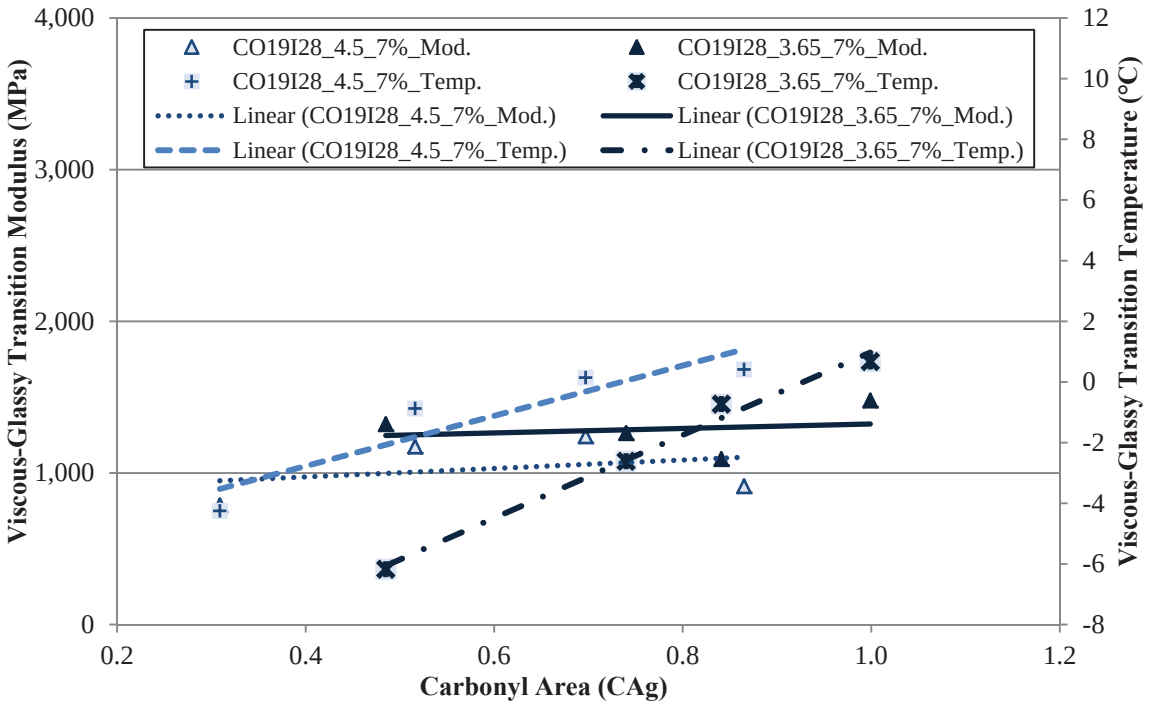

Figure 29.33 Viscous-Glassy Transition Modulus Values for the CO19I28_7% Va Aged at 60°C with Different Binder Contents

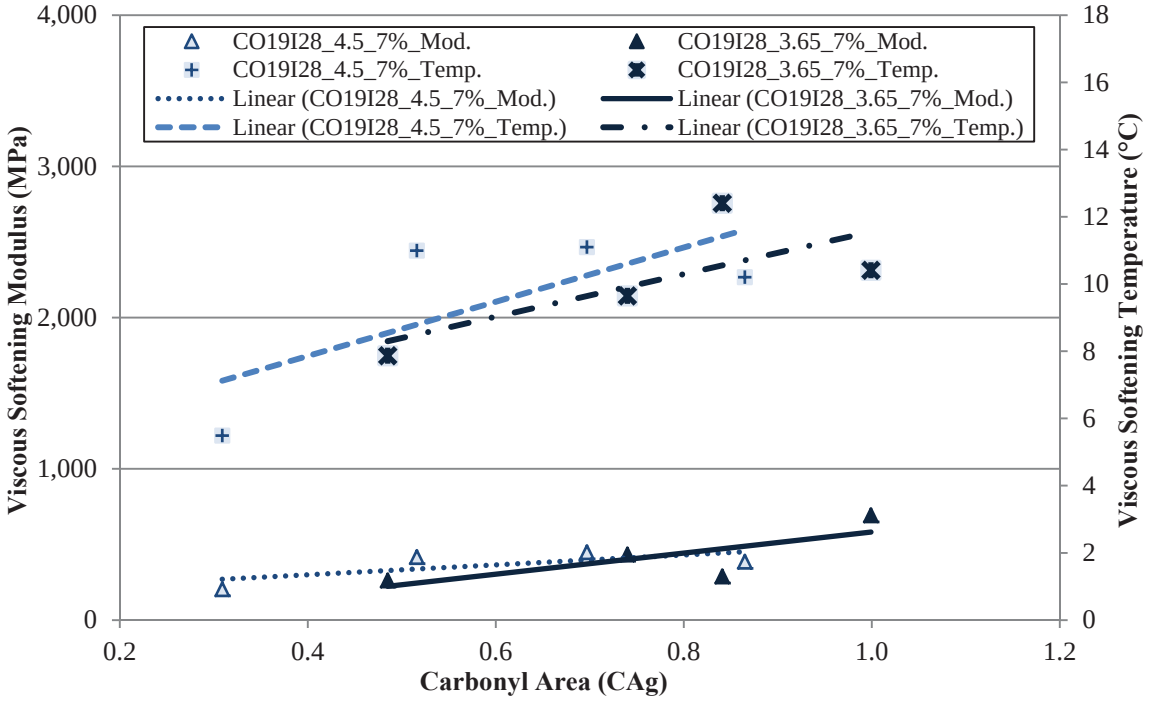

Figure 29.34 Viscous Softening Modulus Values for the CO19I28_7% Va Aged at 60°C with Different Binder Contents

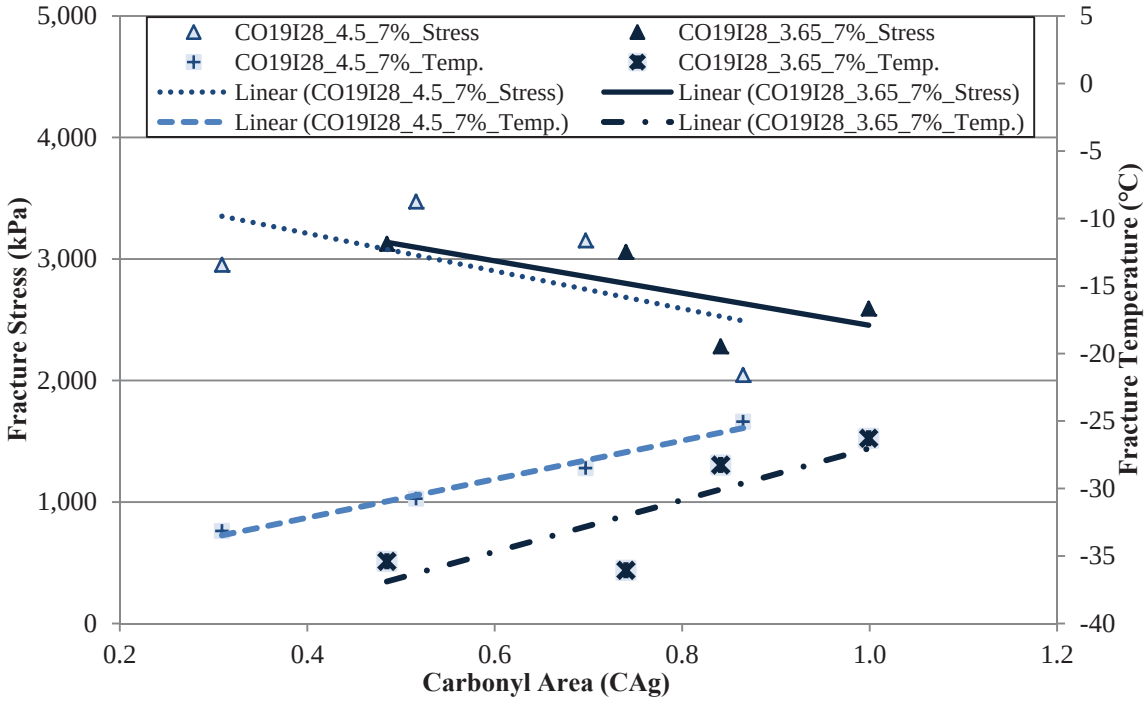

Figure 29.35 Fracture Stress Measurements for the CO19I28_7% Va Aged at 60°C with Different Binder Contents

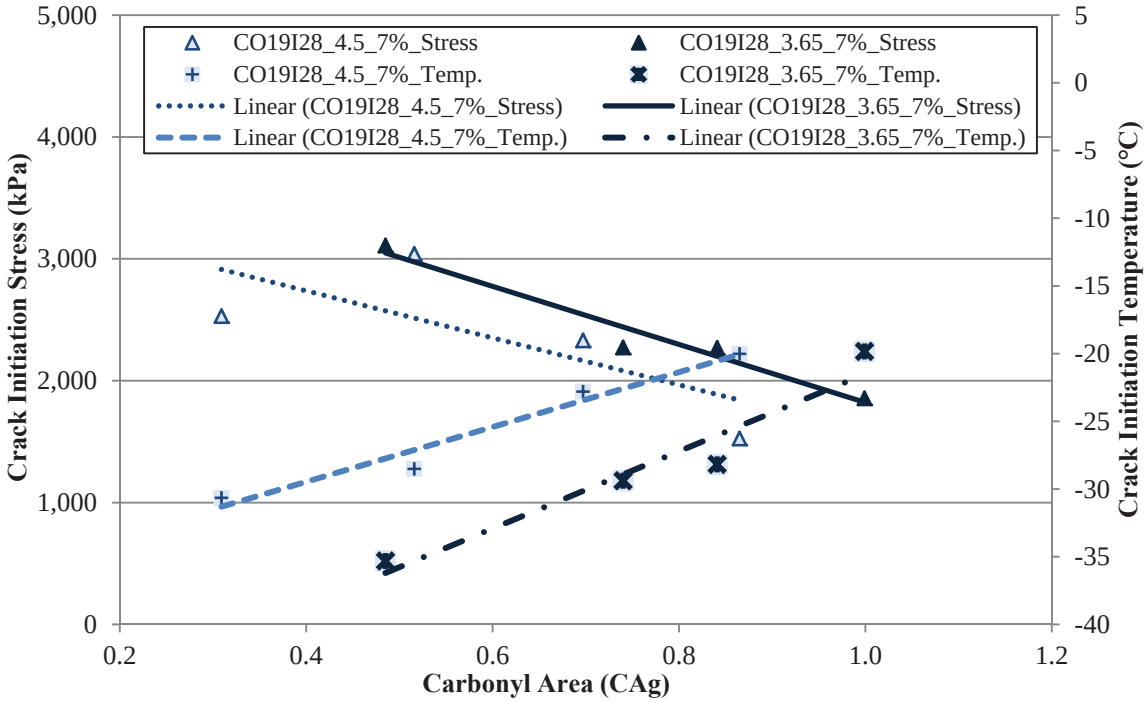

Figure 29.36 Crack Initiation Stress Measurements for the CO19I28_7% Va Aged at 60°C with Different Binder Contents

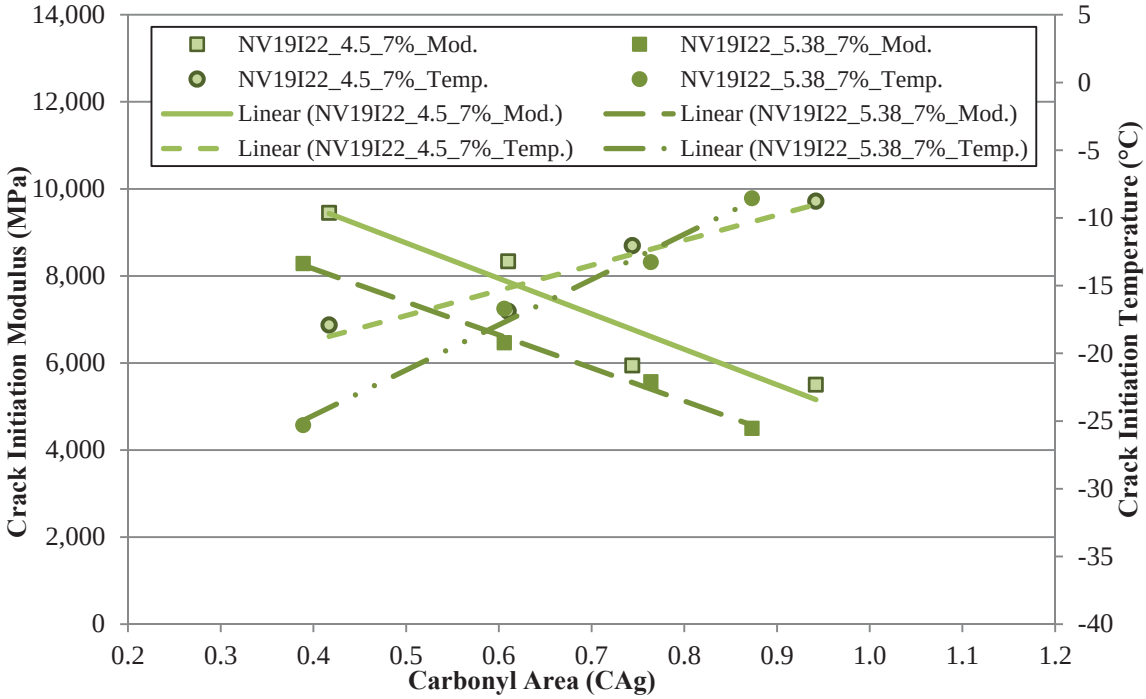

Figure 29.37 Crack Initiation Modulus Values for the NV19I22_7% Va Mixtures Aged at 60°C with Different Binder Contents

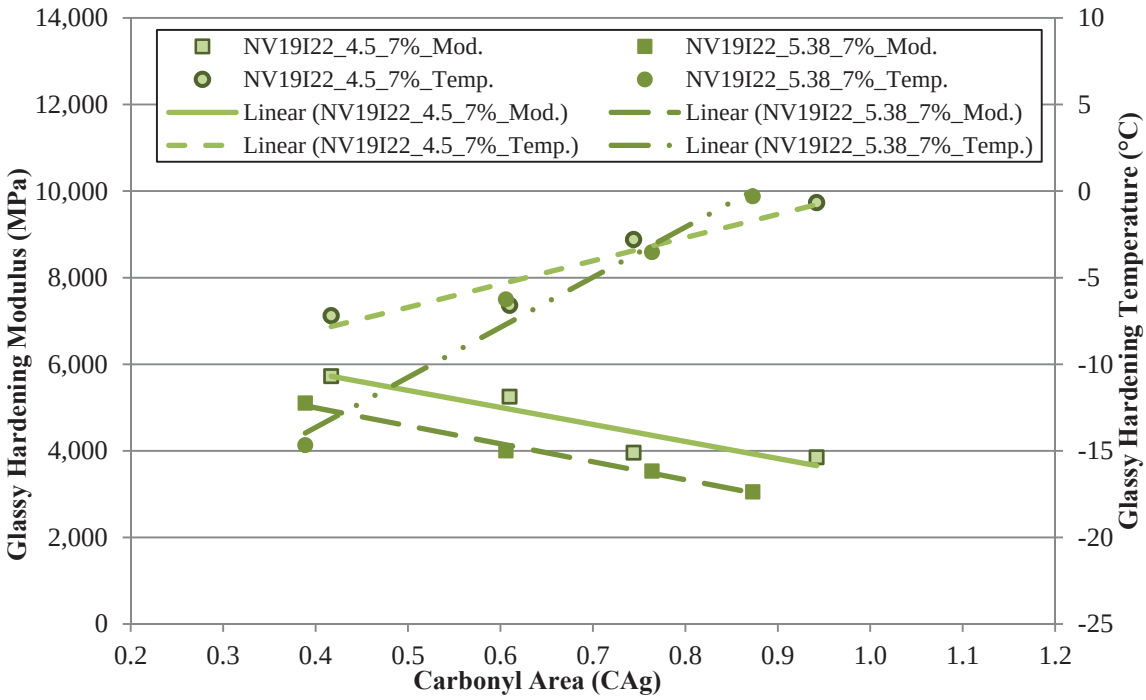

Figure 29.38 Glassy Hardening Modulus Values for the NV19I22_7% Va Mixtures Aged at 60° C with Different Binder Contents

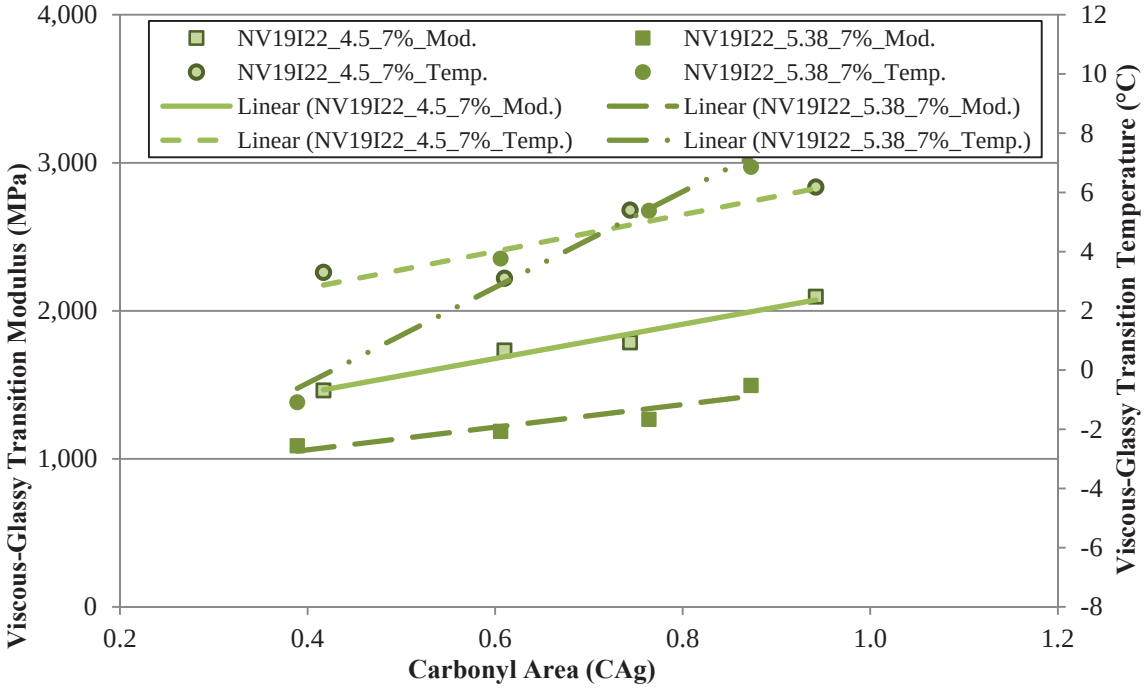

Figure 29.39 Viscous-Glassy Transition Modulus Values for NV19I22_7% Va Mixtures Aged at 60°C with Different Binder Contents

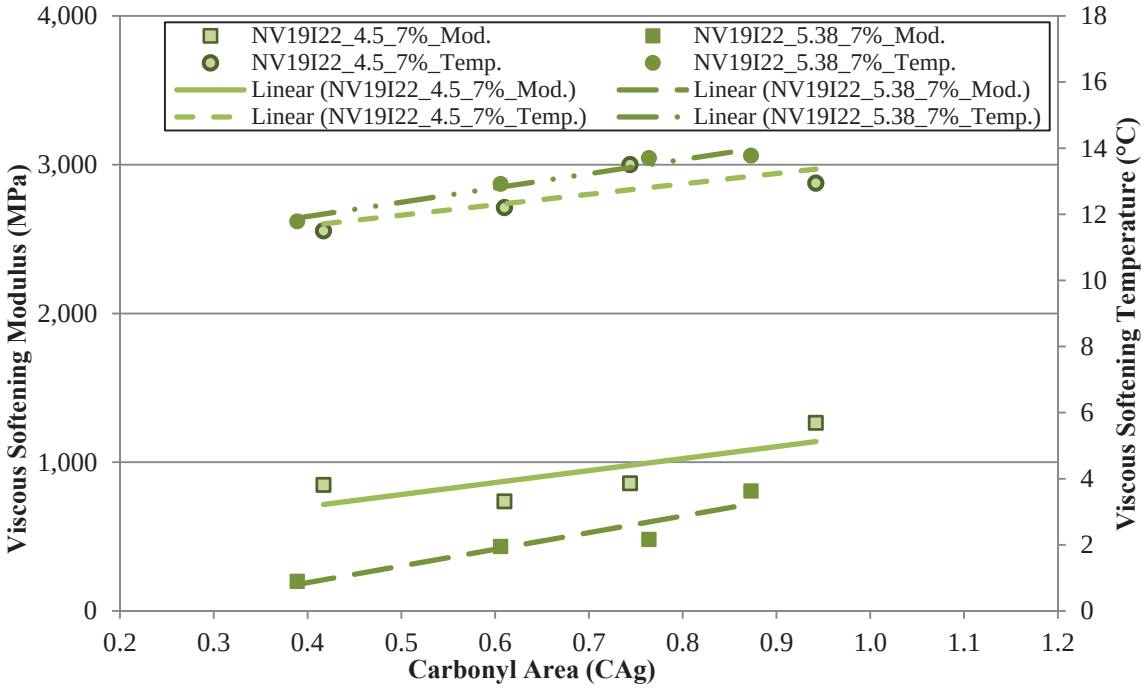

Figure 29.40 Viscous Softening Modulus Values for the NV19I22_7% Va Mixtures Aged at 60° C with Different Binder Contents

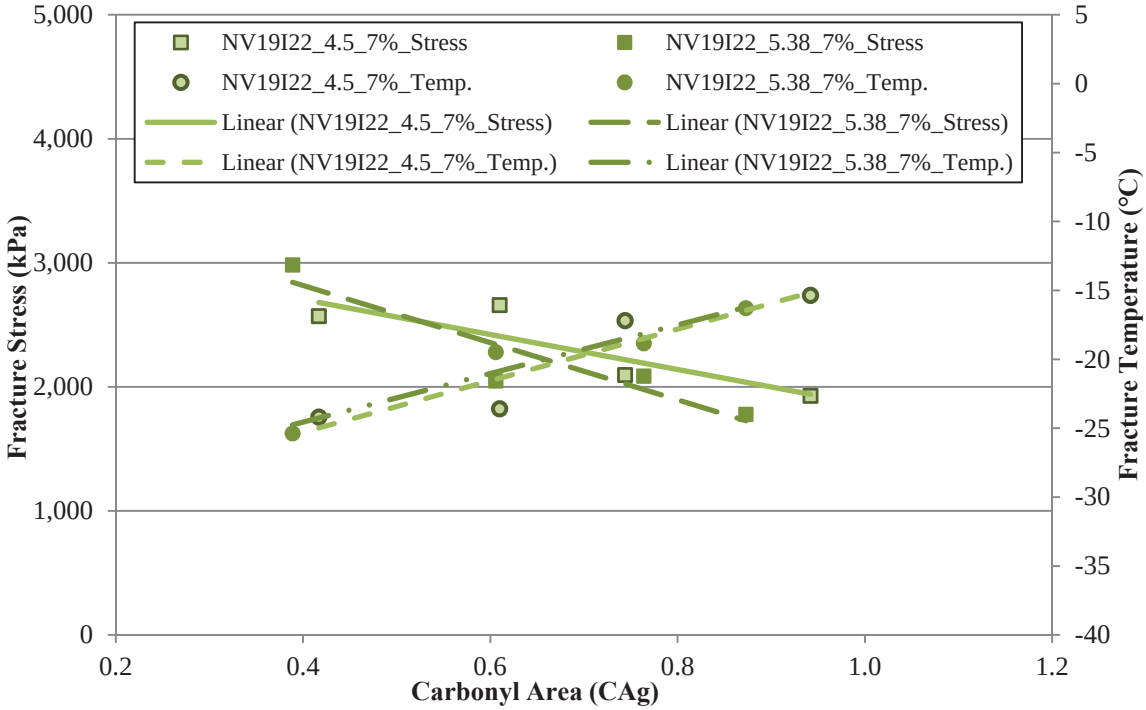

Figure 29.41 Fracture Stress Measurements for the NV19I22_7% Va Mixtures Aged at 60° C with Different Binder Contents

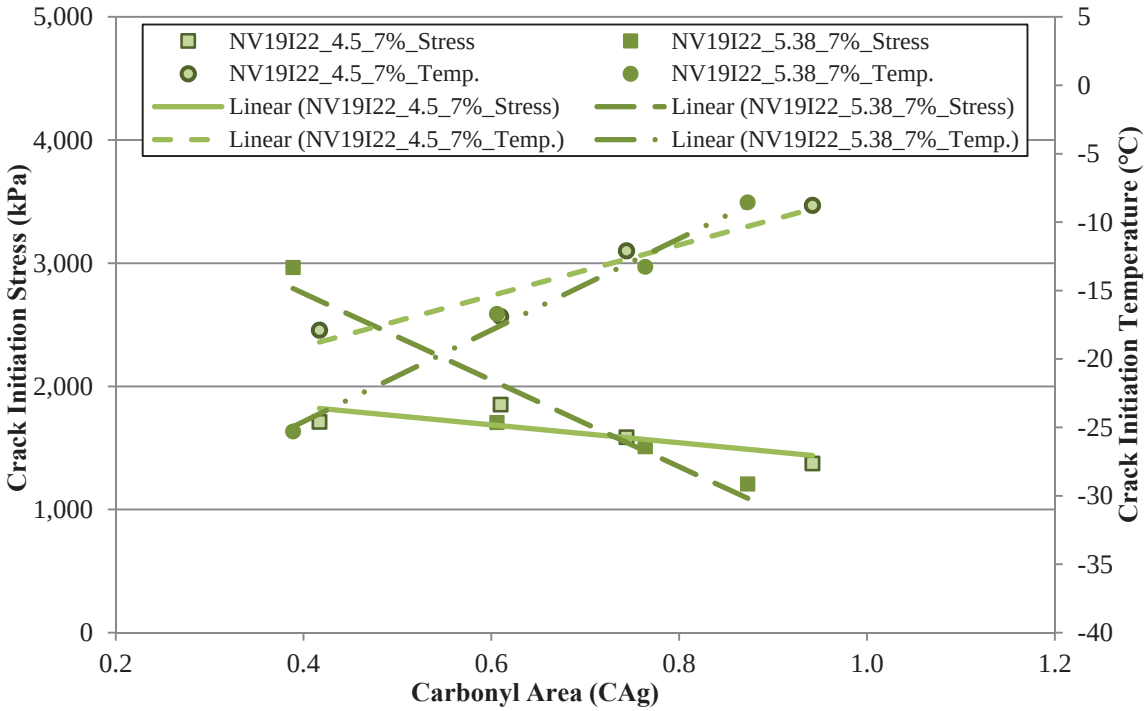

Figure 29.42 Crack Initiation Stress Measurements for NV19I22_7% Va Mixtures Aged at 60°C with Different Binder Contents

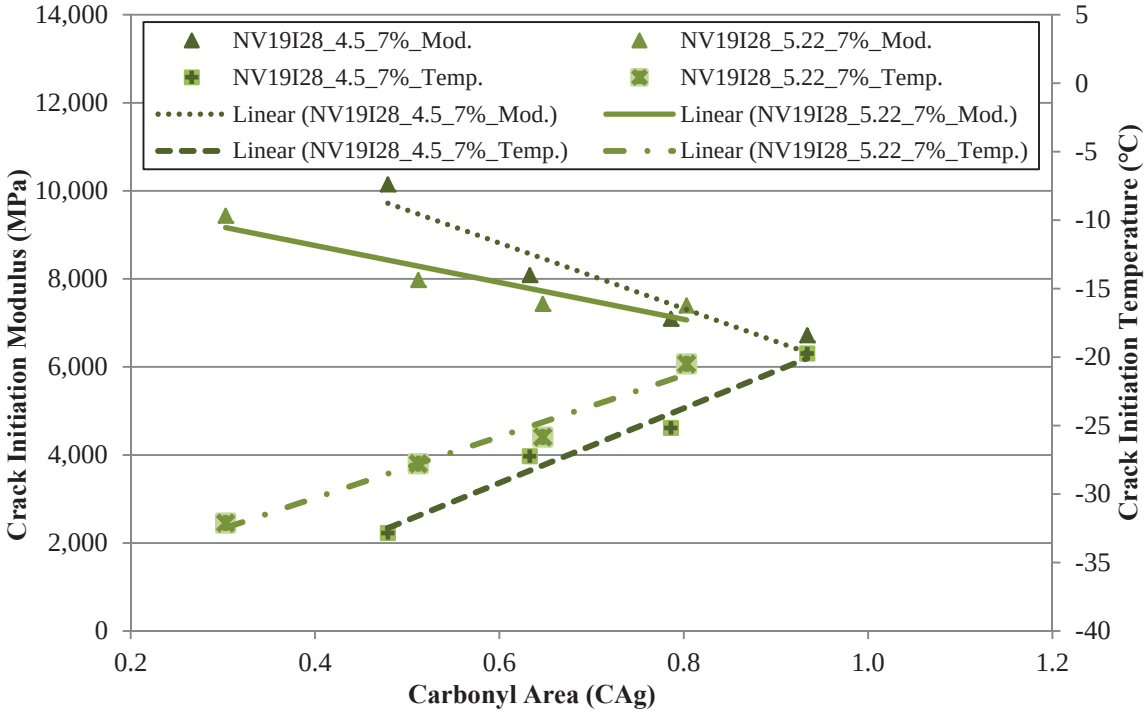

Figure 29.43 Crack Initiation Modulus Values for the NV19I28_7% Va Aged at 60°C with Different Binder Contents

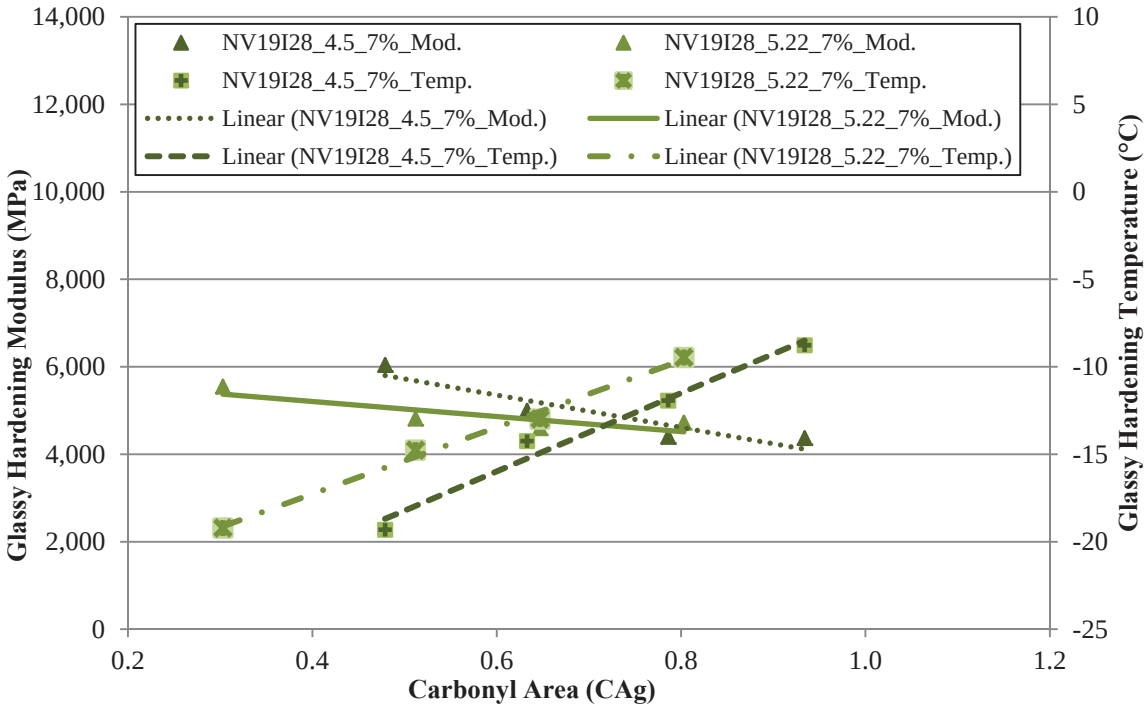

Figure 29.44 Glassy Hardening Modulus Values for the NV19I28_7% Va Aged at 60°C with Different Binder Contents

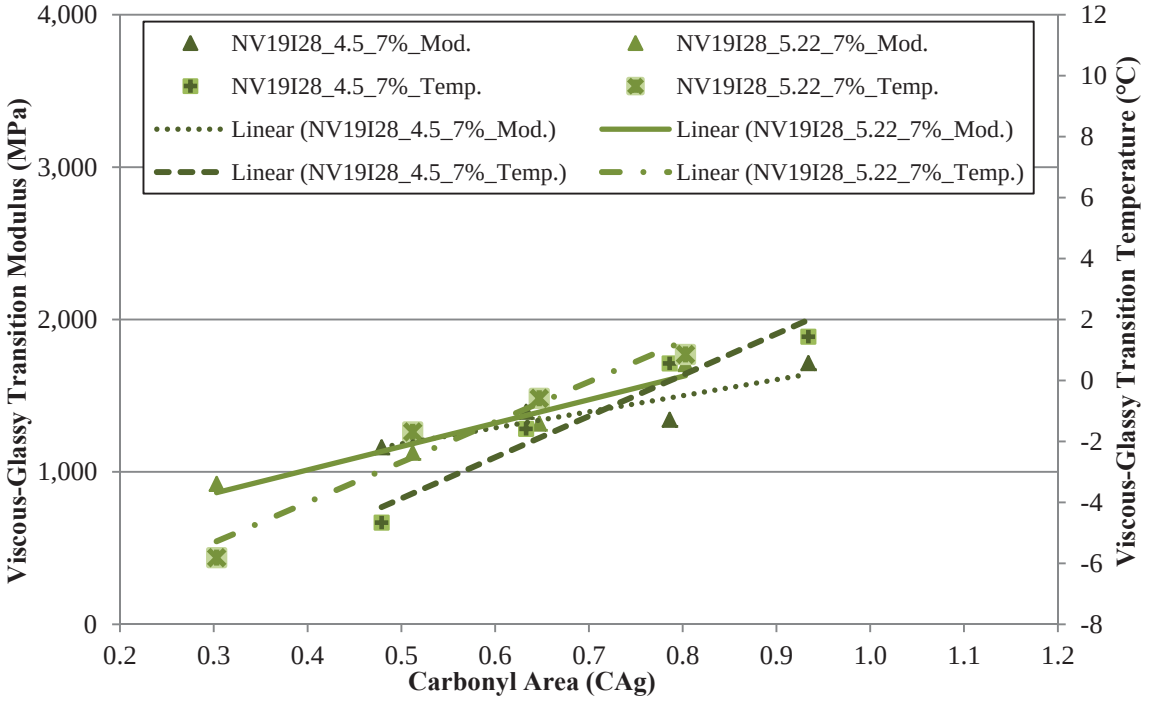

Figure 29.45 Viscous-Glassy Transition Modulus Values for the NV19I28_7% Va Aged at 60°C with Different Binder Contents

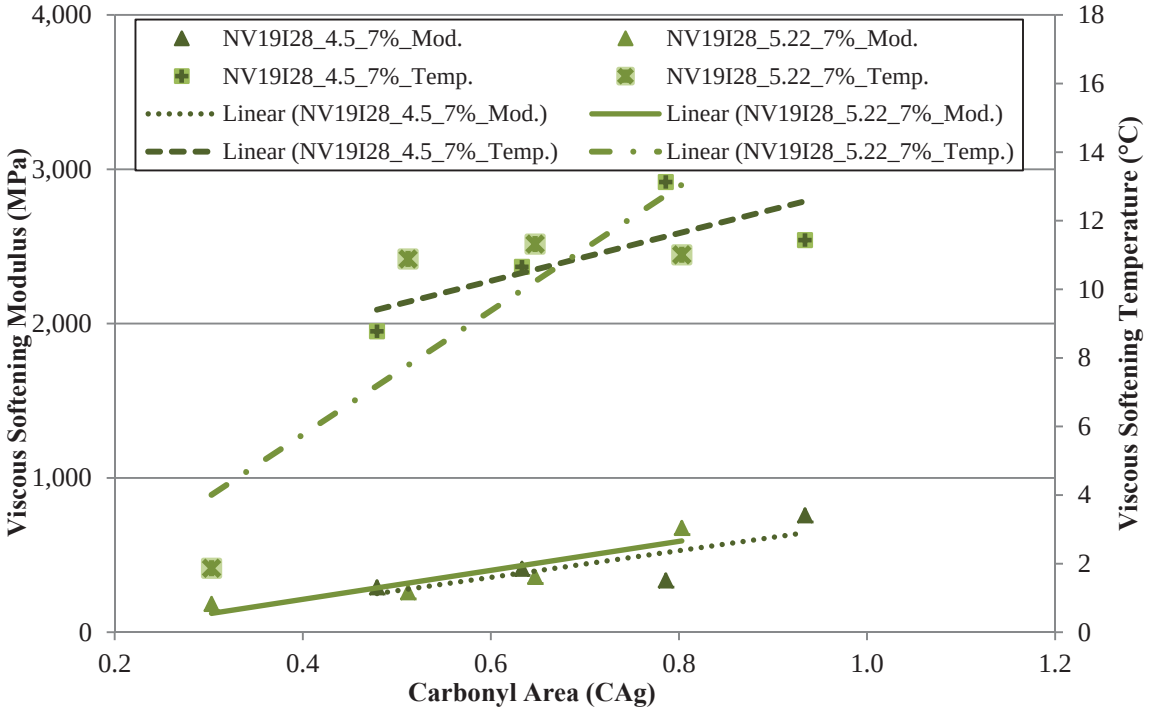

Figure 29.46 Viscous Softening Modulus Values for the NV19I28_7% Va Aged at 60°C with Different Binder Contents

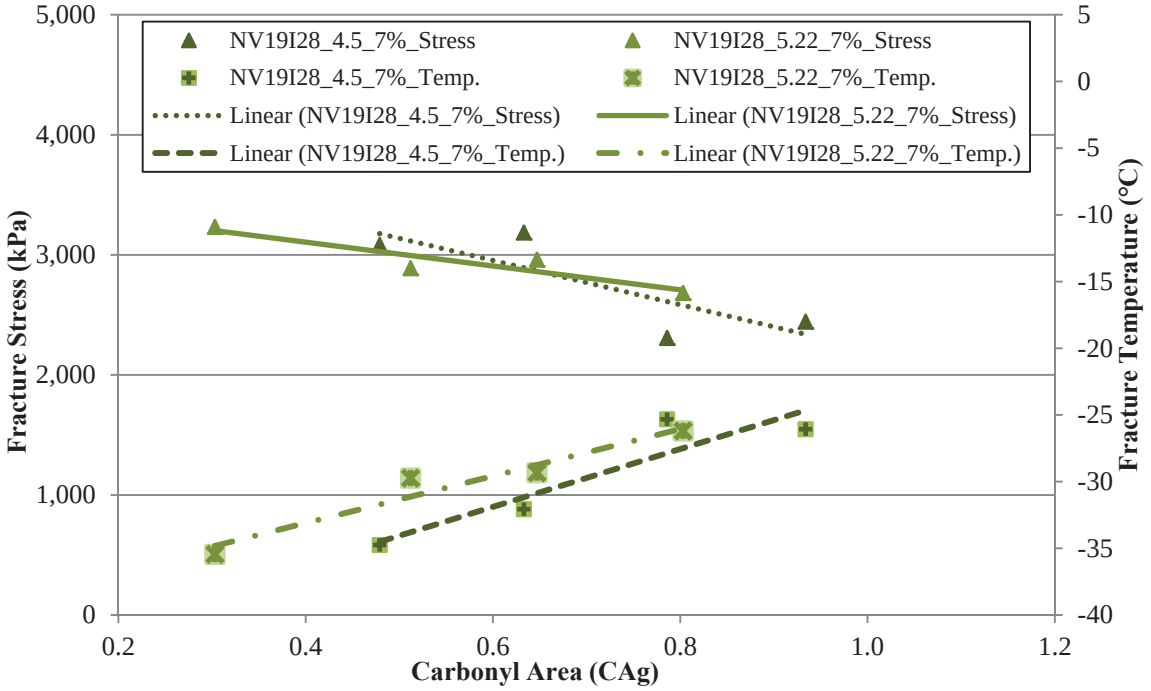

Figure 29.47 Fracture Stress Measurements for the NV19I28_7% Va Aged at 60°C with Different Binder Contents

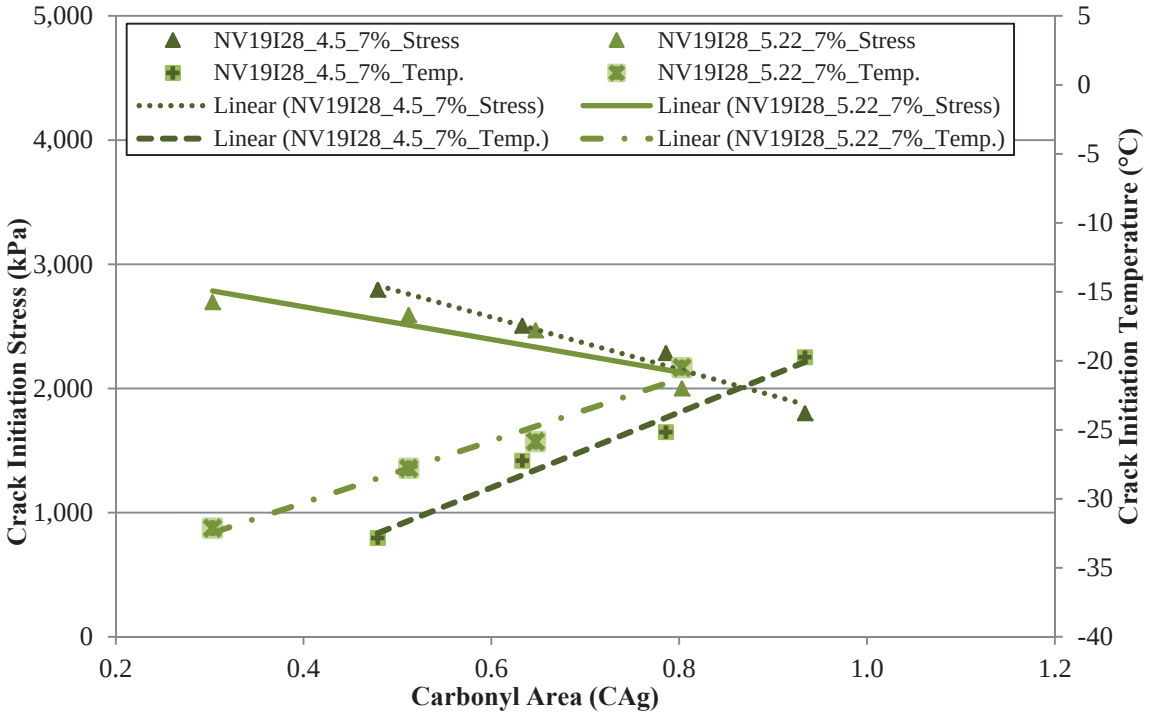

Figure 29.48 Crack Initiation Stress Measurements for the NV19I28_7% Va Aged at 60°C with Different Binder Contents

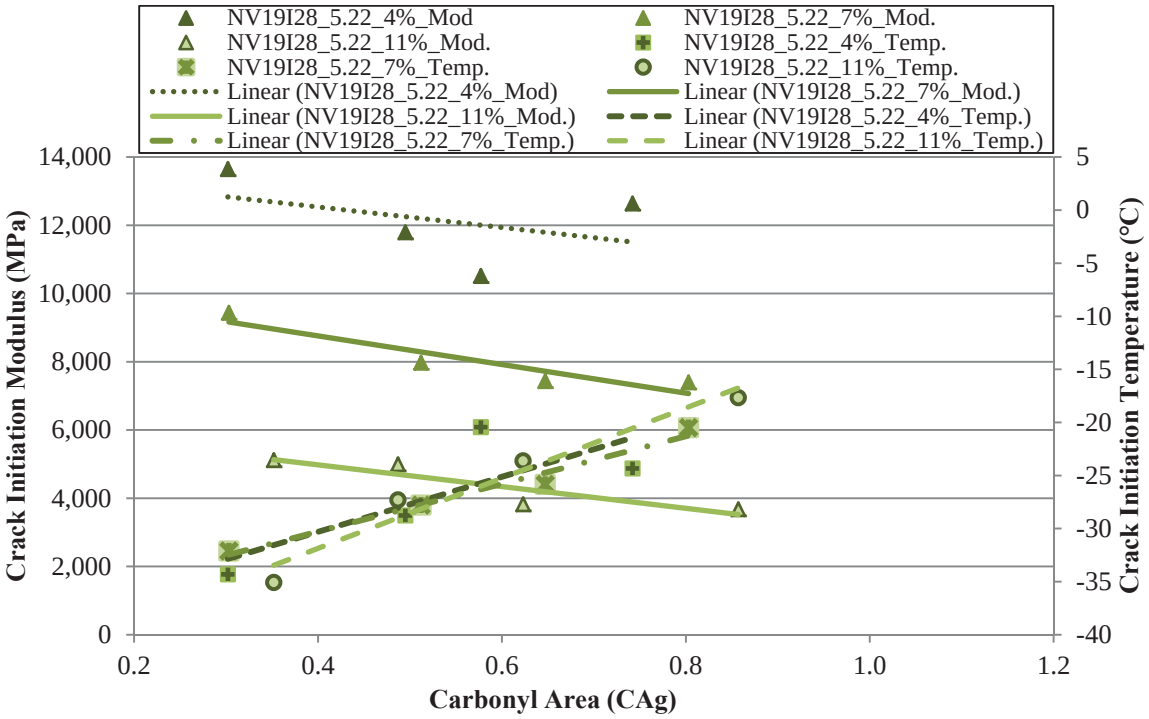

Figure 29.49 Crack Initiation Modulus Values for the NV19I28_5.22 Mixtures Aged at 60°C with Different Air Void Levels

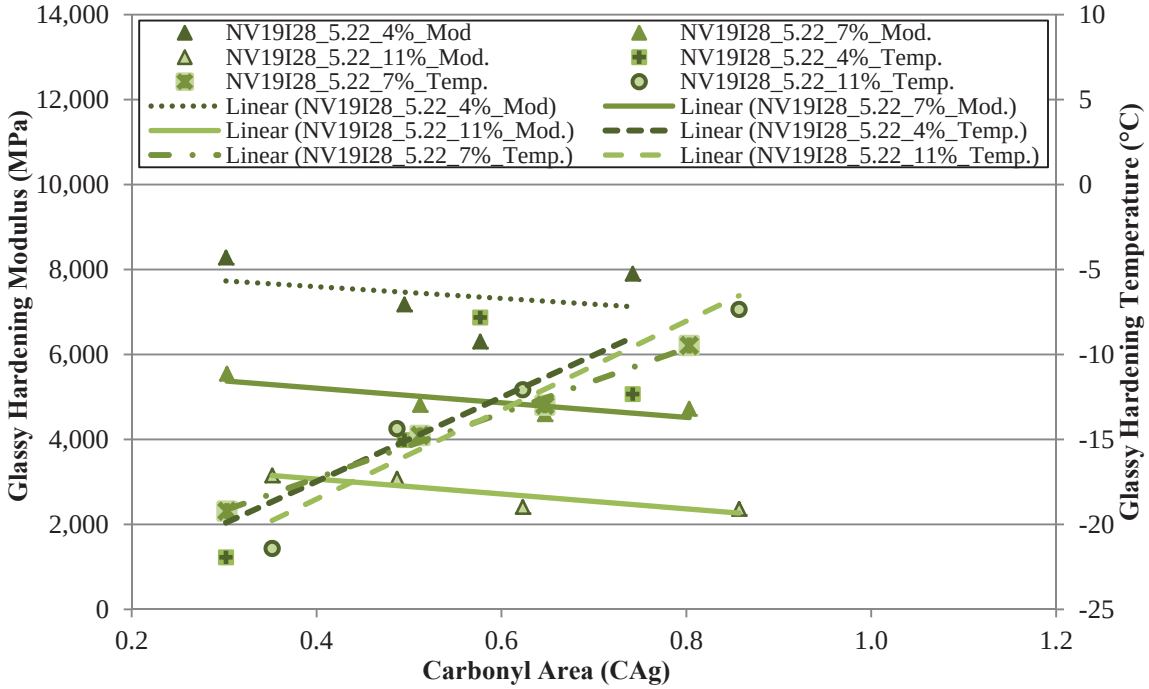

Figure 29.50 Glassy Hardening Modulus Values for the NV19I28_5.22 Mixtures Aged at 60°C with Different Air Void Levels

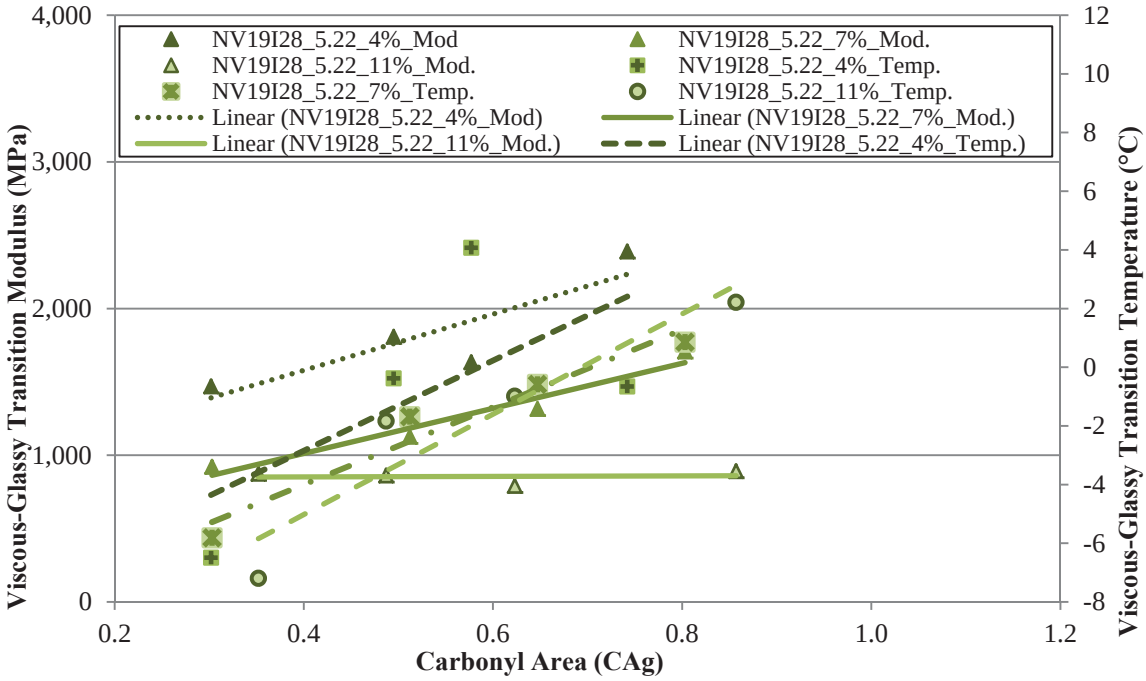

Figure 29.51 Viscous-Glassy Transition Modulus Values for the NV19I28_5.22 Mixtures Aged at 60°C with Different Air Void Levels

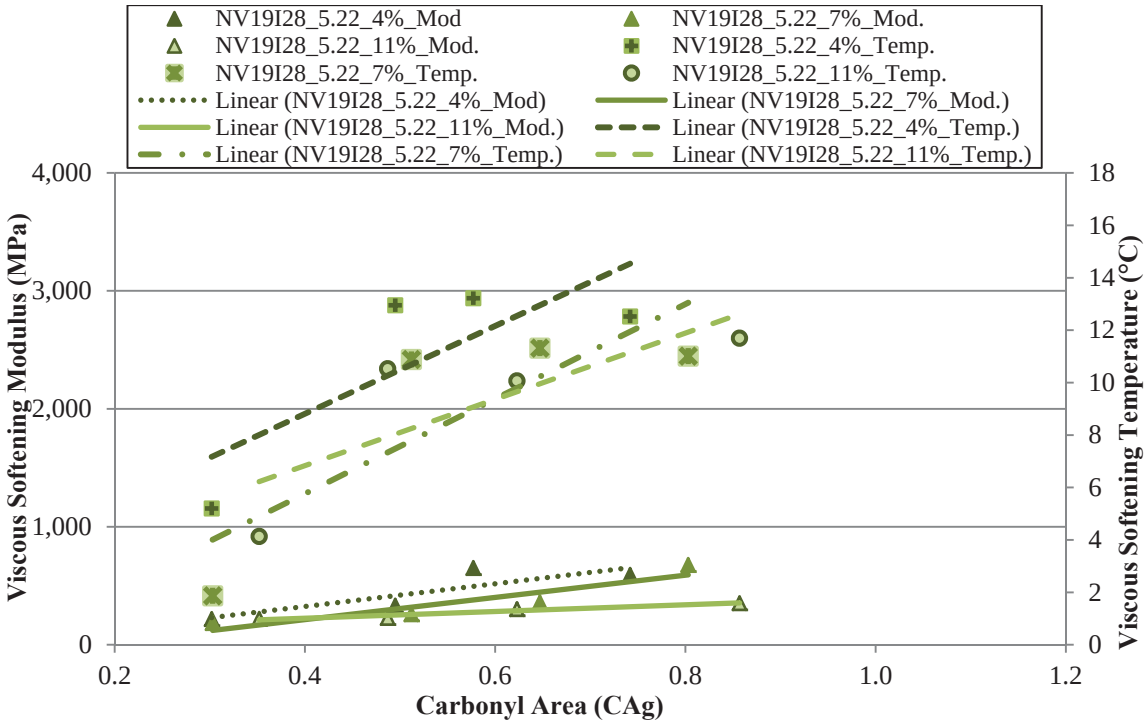

Figure 29.52 Viscous Softening Modulus Values for the NV19I28_5.22 Mixtures Aged at 60°C with Different Air Void Levels

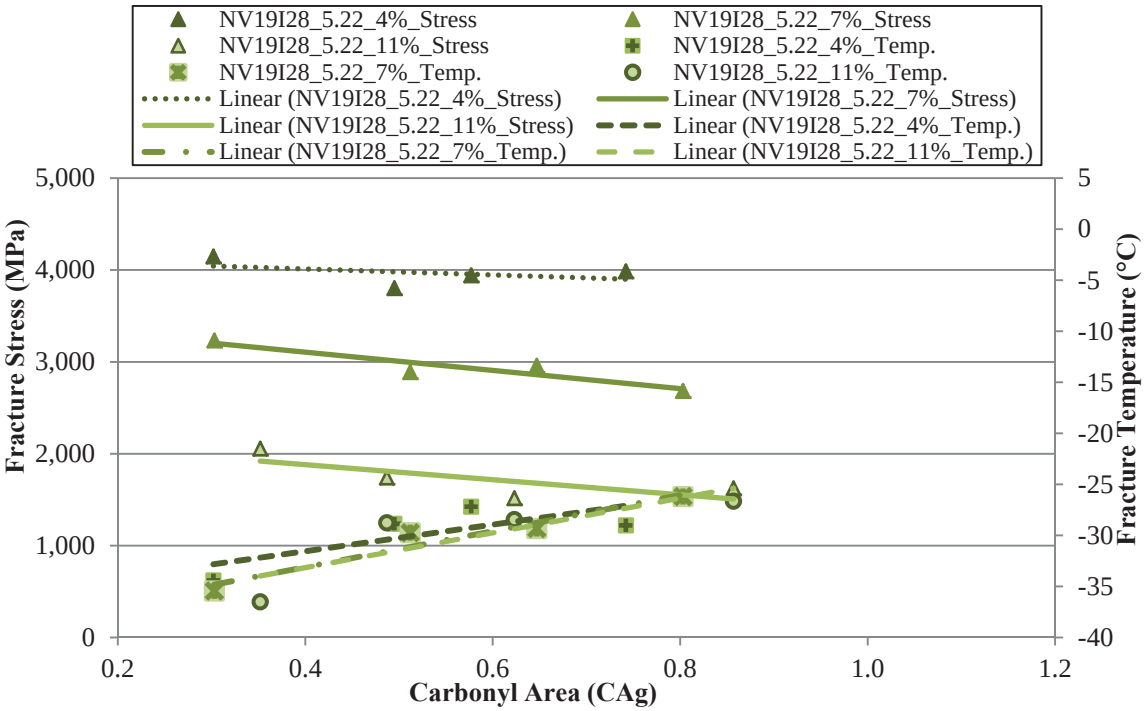

Figure 29.53 Fracture Stress Measurements for the NV19I28_5.22 Mixtures Aged at 60°C with Different Air Void Levels

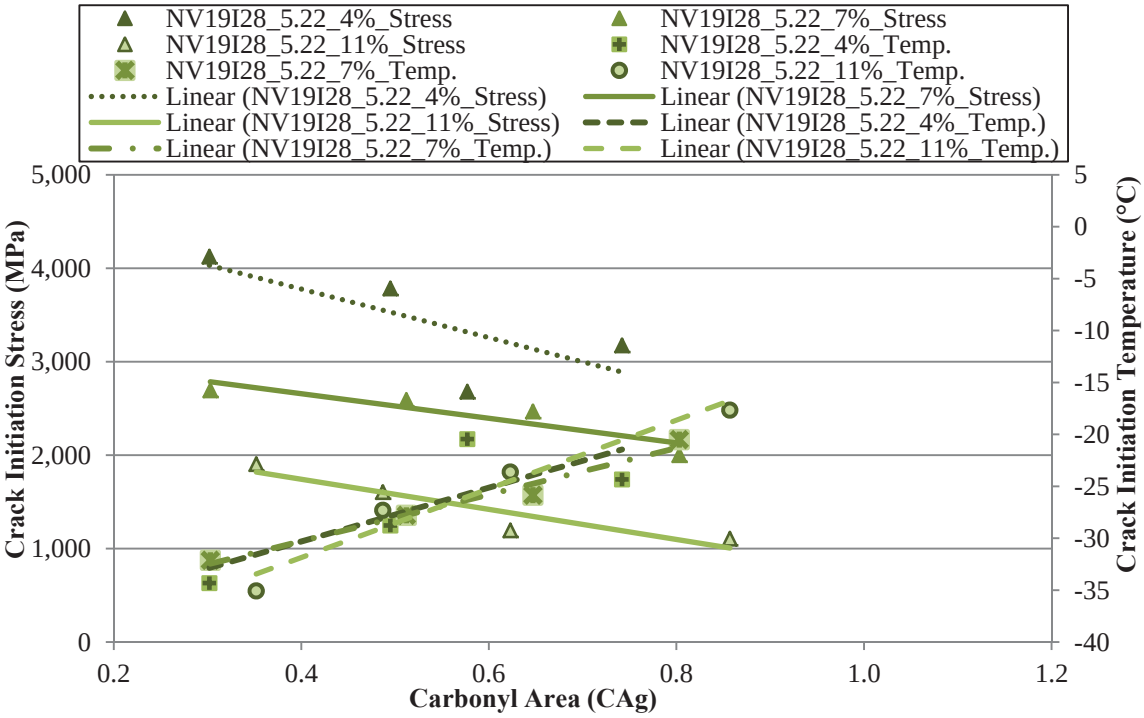

Figure 29.54 Crack Initiation Stress Measurements for the NV19I28_5.22 Mixtures Aged at 60°C with Different Air Void Levels

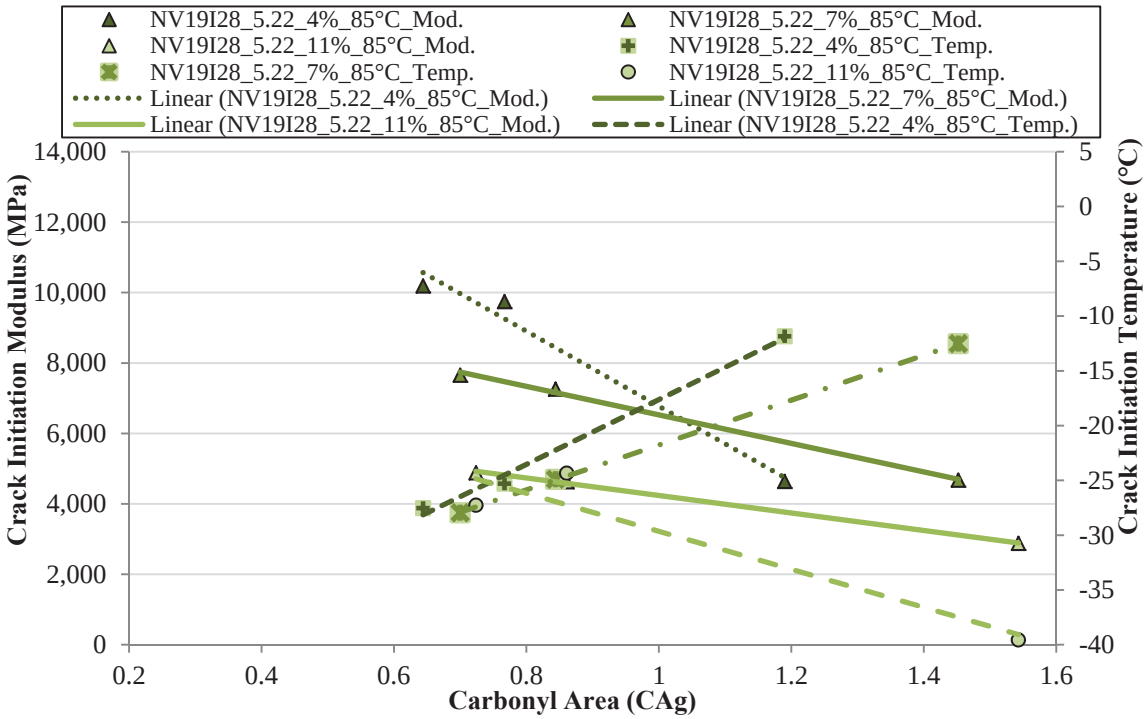

Figure 29.55 Crack Initiation Modulus Values for the NV19I28_5.22 Mixtures Aged at 85°C with Different Air Void Levels

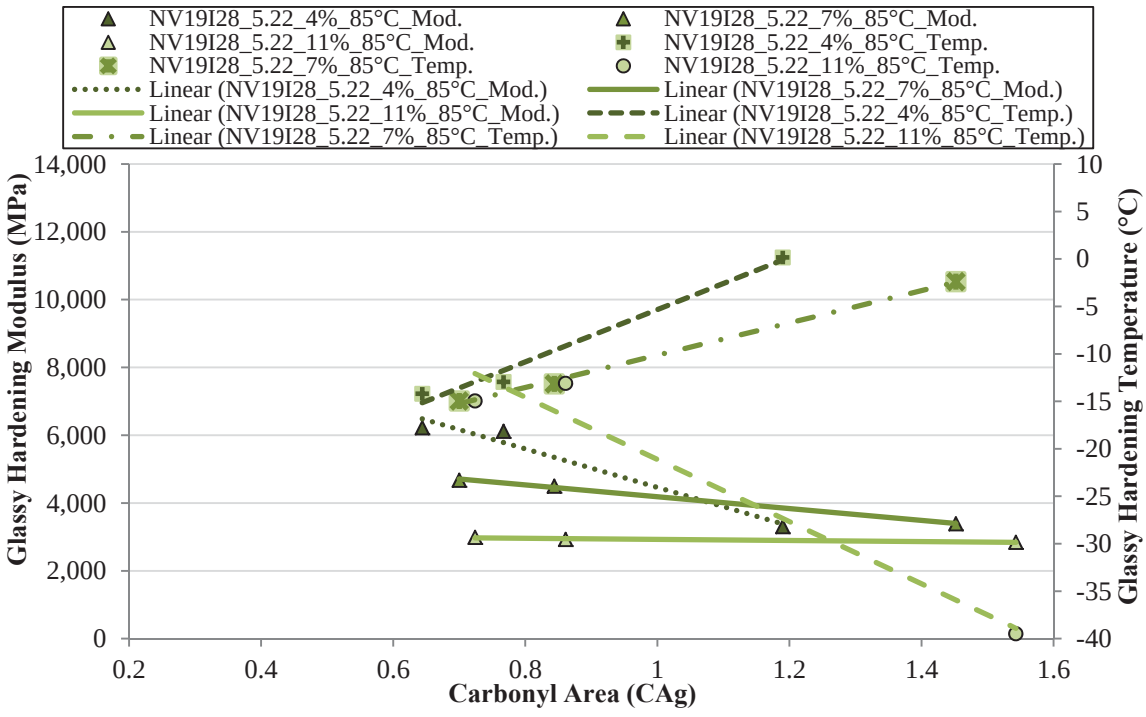

Figure 29.56 Glassy Hardening Modulus Values for the NV19I28_5.22 Mixtures Aged at 85°C with Different Air Void Levels

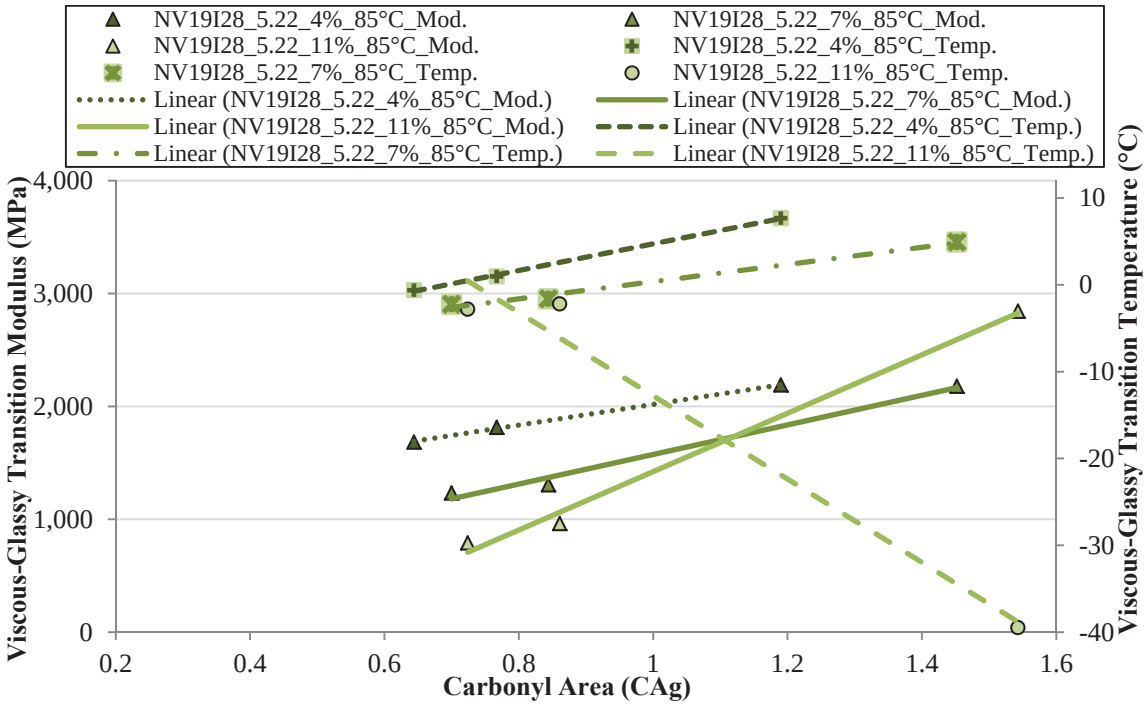

Figure 29.57 Viscous-Glassy Transition Modulus Values for the NV19I28_5.22 Mixtures Aged at 85°C with Different Air Void Levels

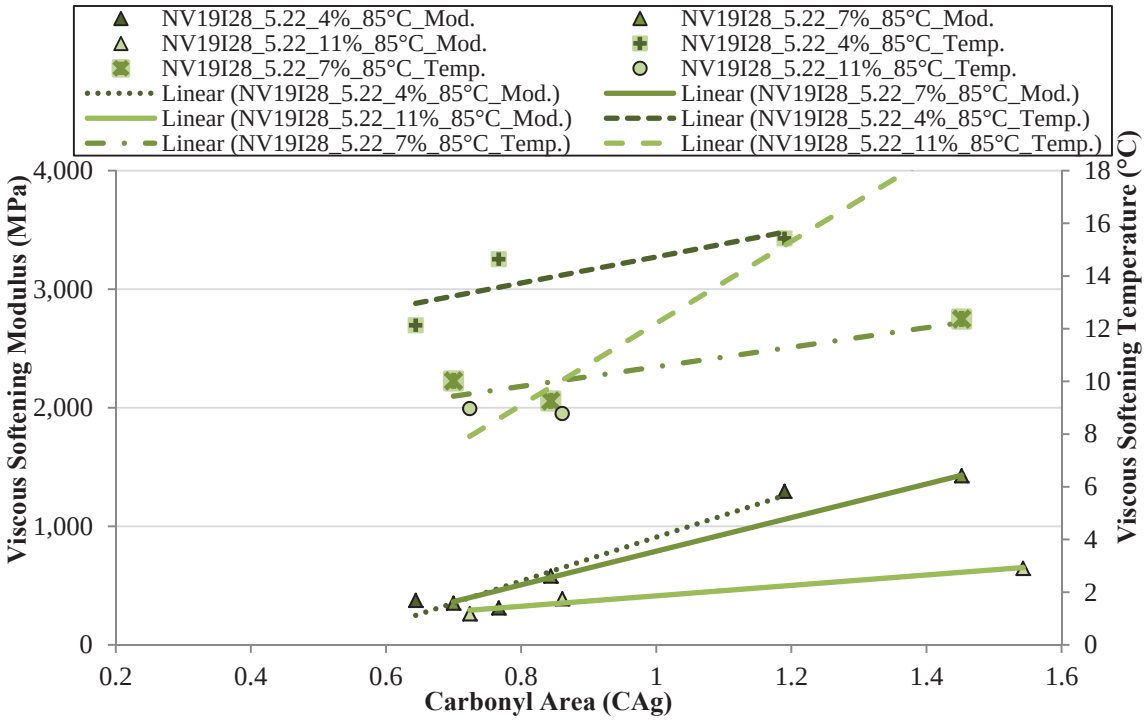

Figure 29.58 Viscous Softening Modulus Values for the NV19I28_5.22 Mixtures Aged at 85°C with Different Air Void Levels

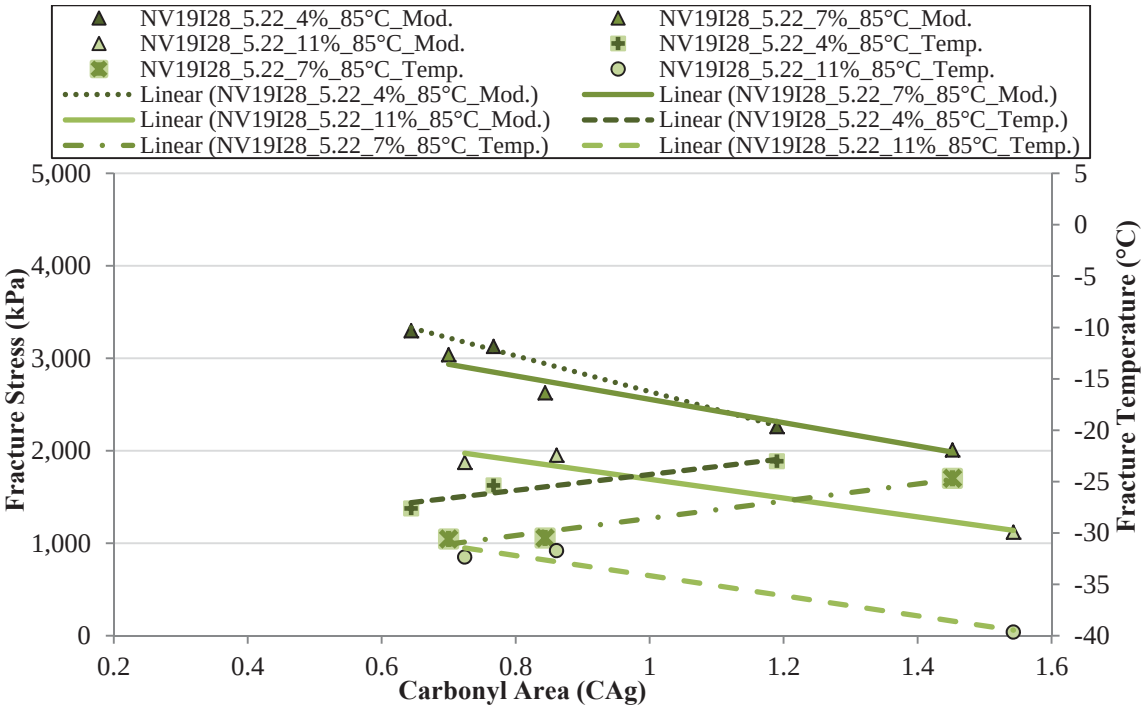

Figure 29.59 Fracture Stress Measurements for the NV19I28_5.22 Mixtures Aged at 85°C with Different Air Void Levels

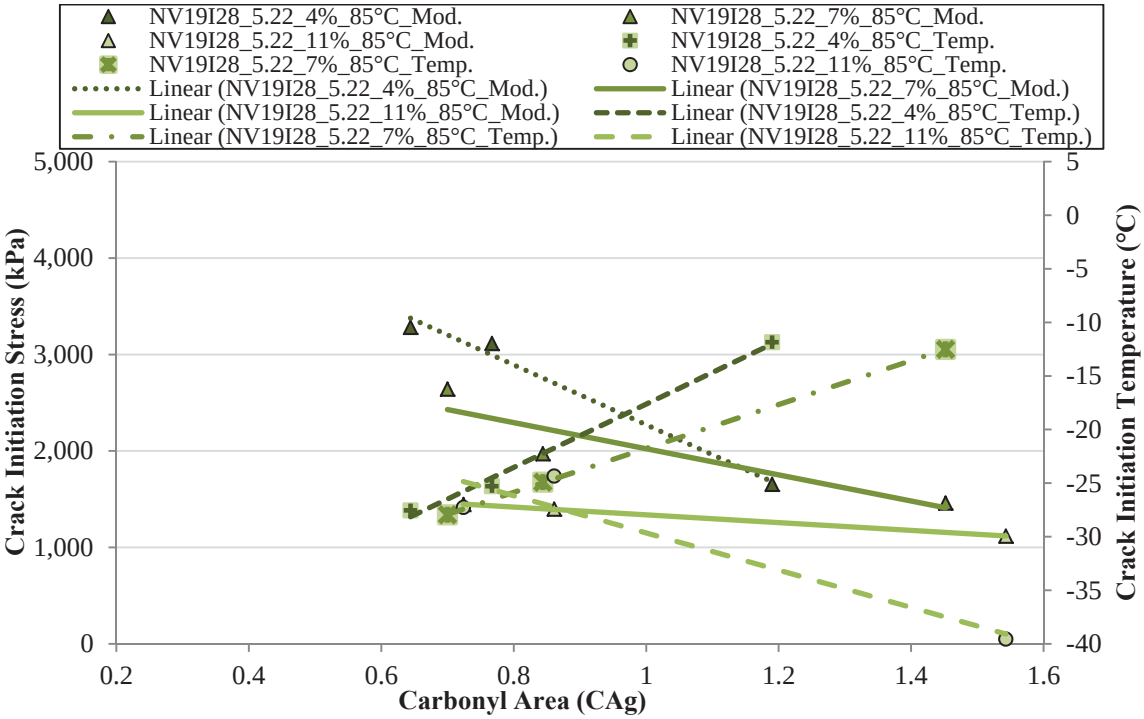

Figure 29.60 Crack Initiation Stress Measurements for the NV19I28_5.22 Mixtures Aged at 85°C with Different Air Void Levels

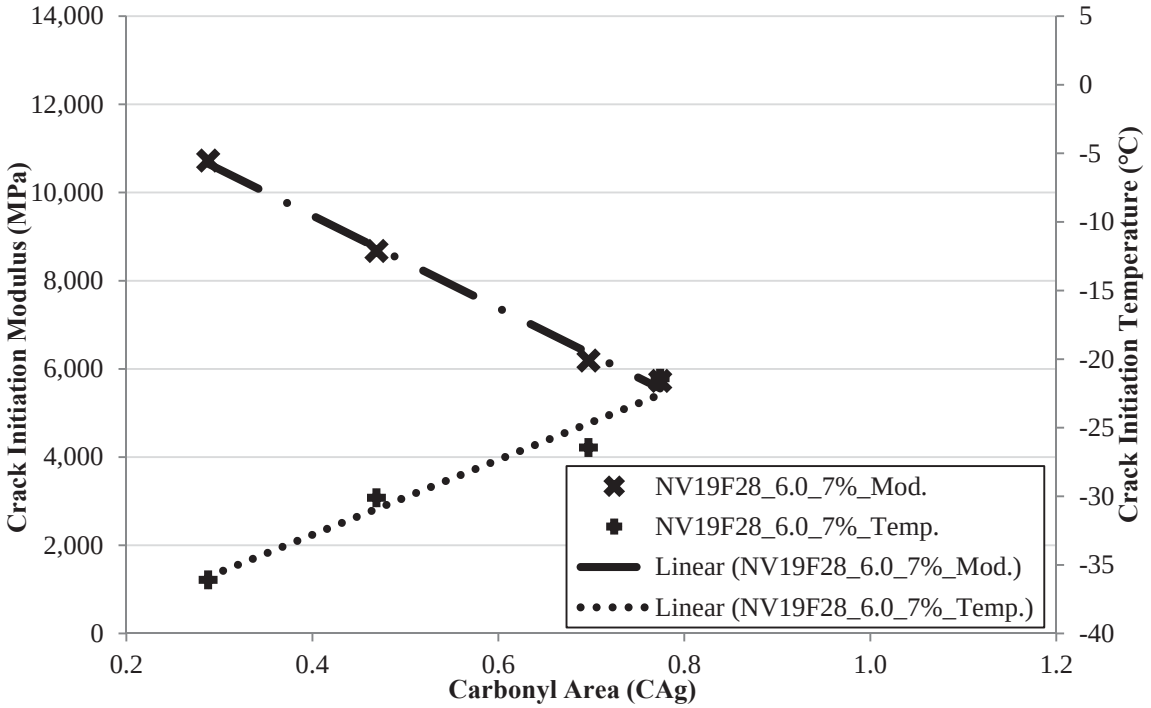

Figure 29.61 Crack Initiation Modulus Values for the NV19F28_6.0_7% Va Mixtures Aged at 60°C

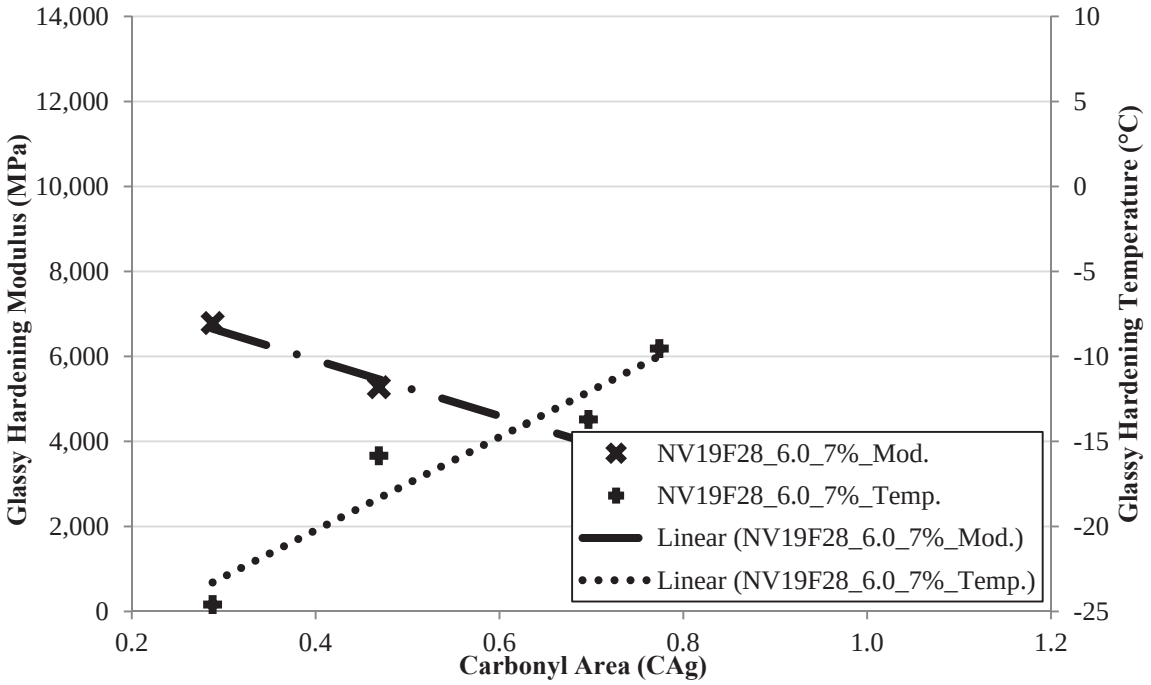

Figure 29.62 Glassy Hardening Modulus Values for the NV19F28_6.0_7% Va Mixtures Aged at 60°C

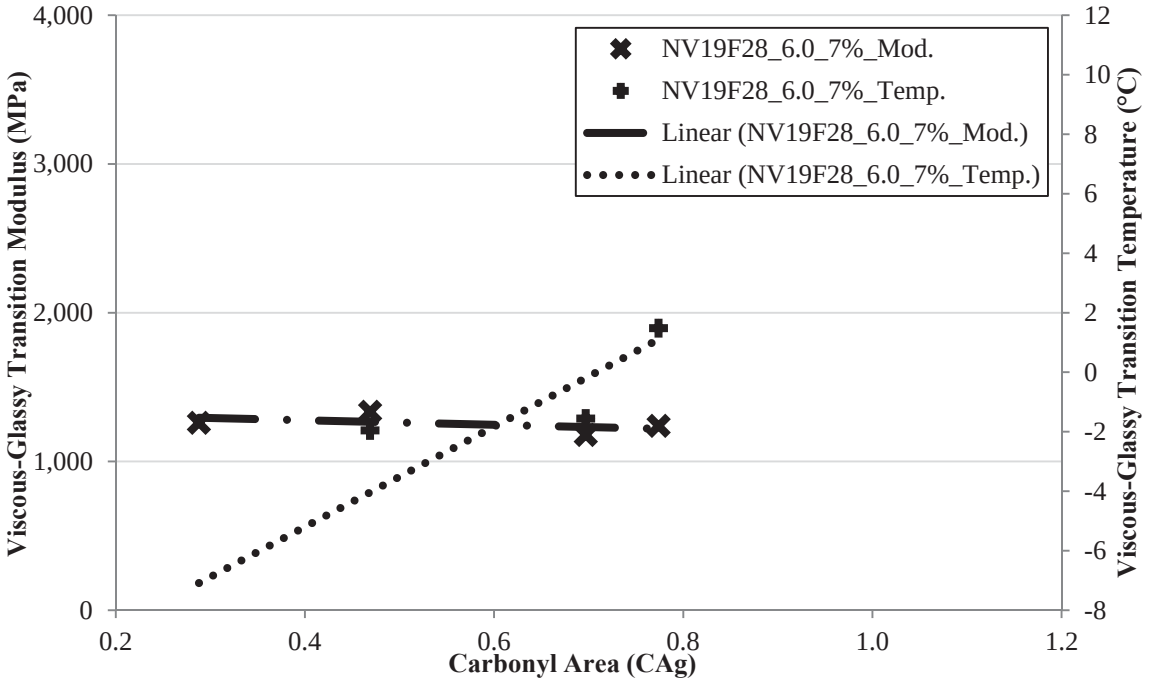

Figure 29.63 Viscous-Glassy Transition Modulus Values for the NV19F28_6.0_7% Va Mixtures Aged at 60°C

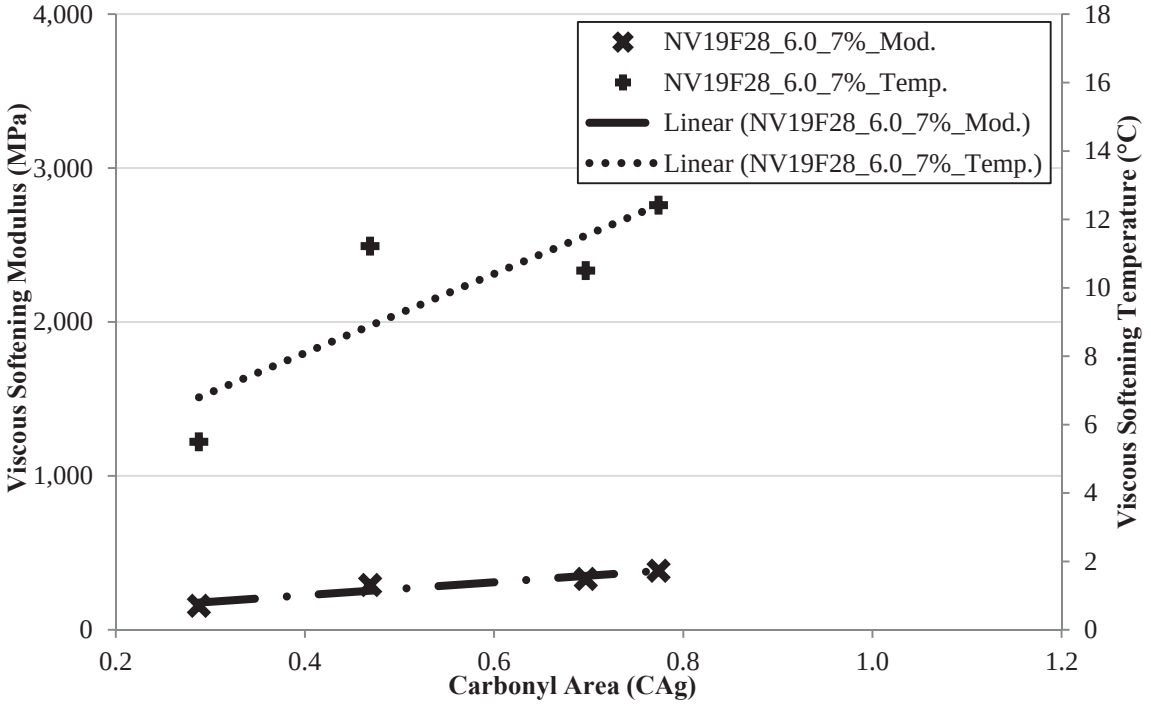

Figure 29.64 Viscous Softening Modulus Values for the NV19F28_6.0_7% Va Mixtures Aged at 60°C

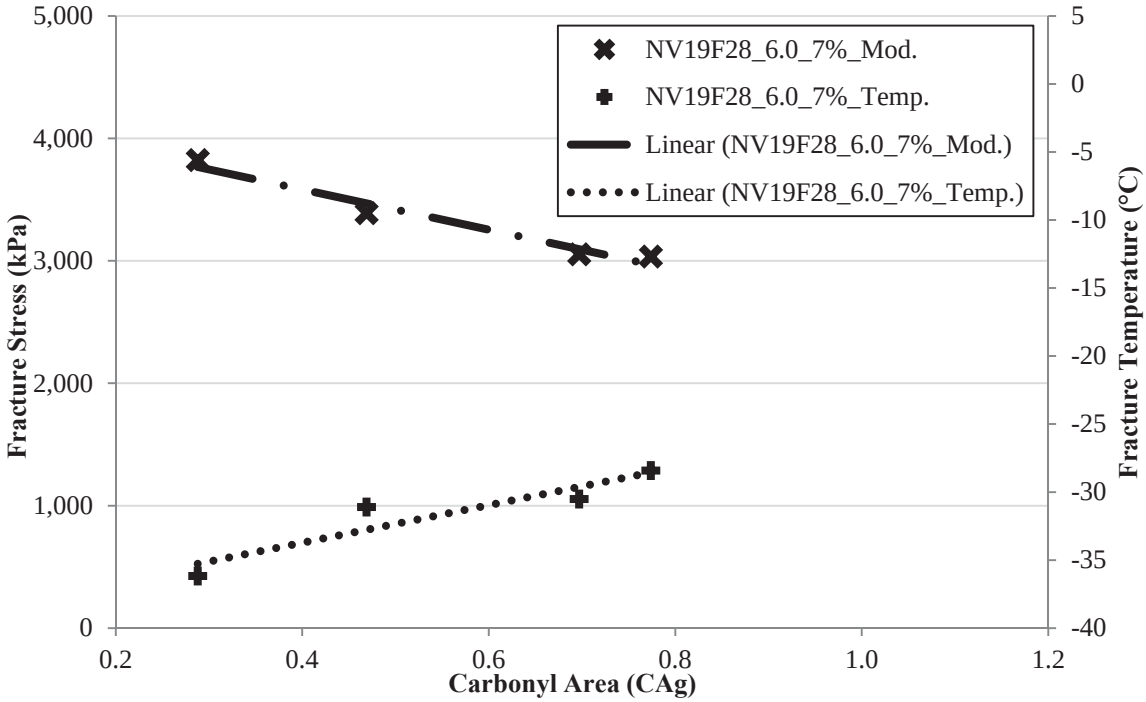

Figure 29.65 Fracture Stress Measurements for the NV19F28_6.0_7% Va Mixtures Aged at 60°C

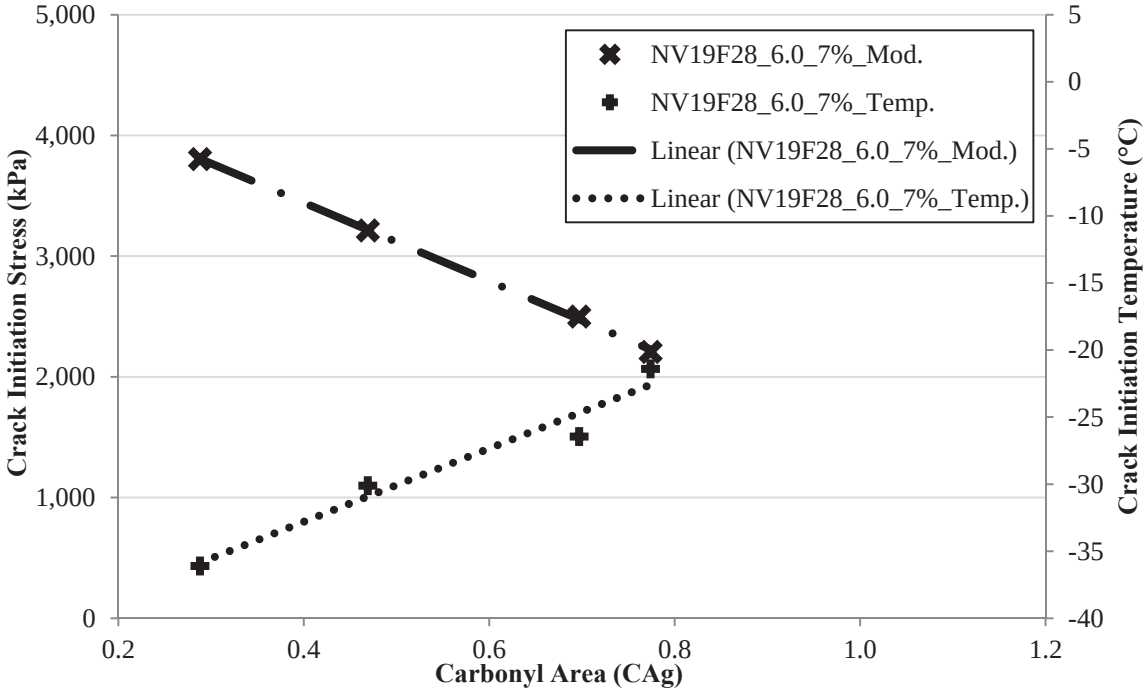

Figure 29.66 Crack Initiation Stress Measurements for the NV19F28_6.0_7% Va Mixtures Aged at 60°C

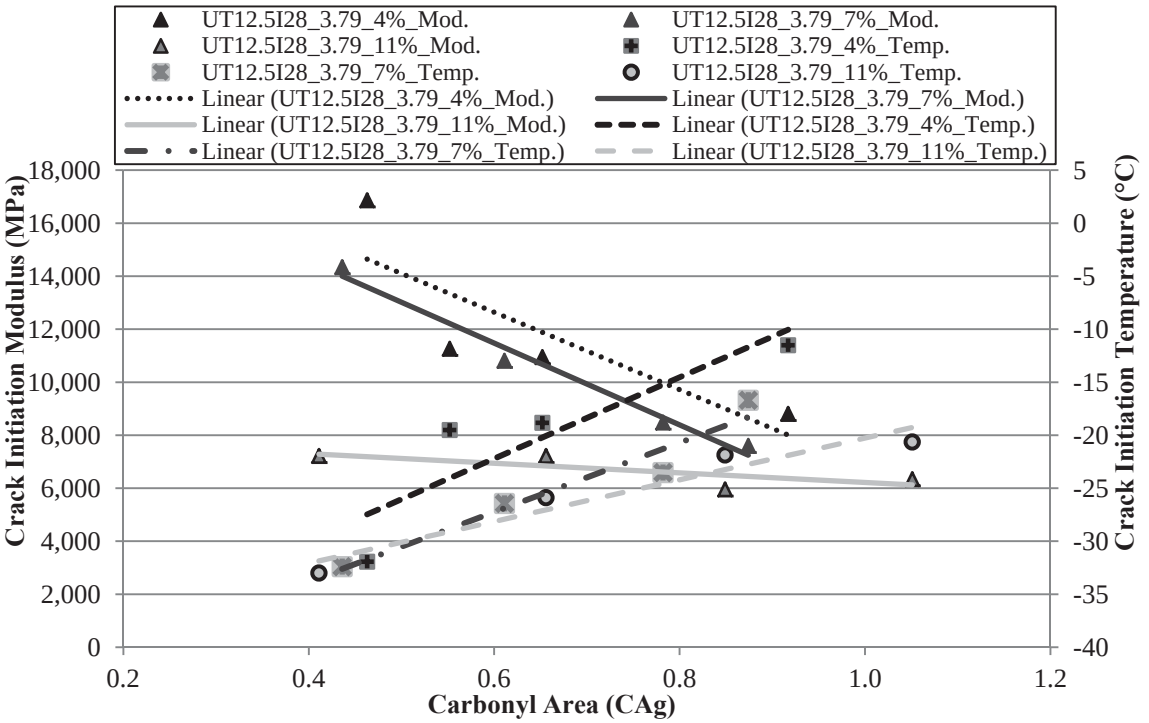

Figure 29.67 Crack Initiation Modulus Values for the UT12.5I28_3.79 Mixtures Aged at 60°C with Different Air Voids

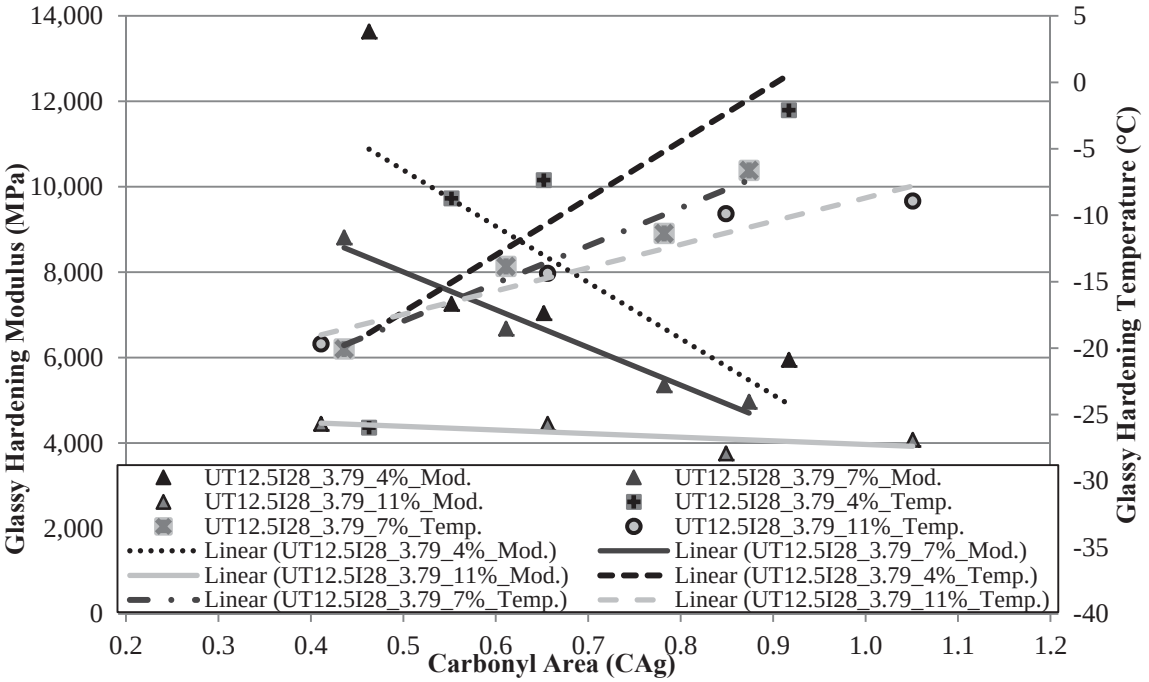

Figure 29.68 Glassy Hardening Modulus Values for the UT12.5I28_3.79 Mixtures Aged at 60°C with Different Air Voids

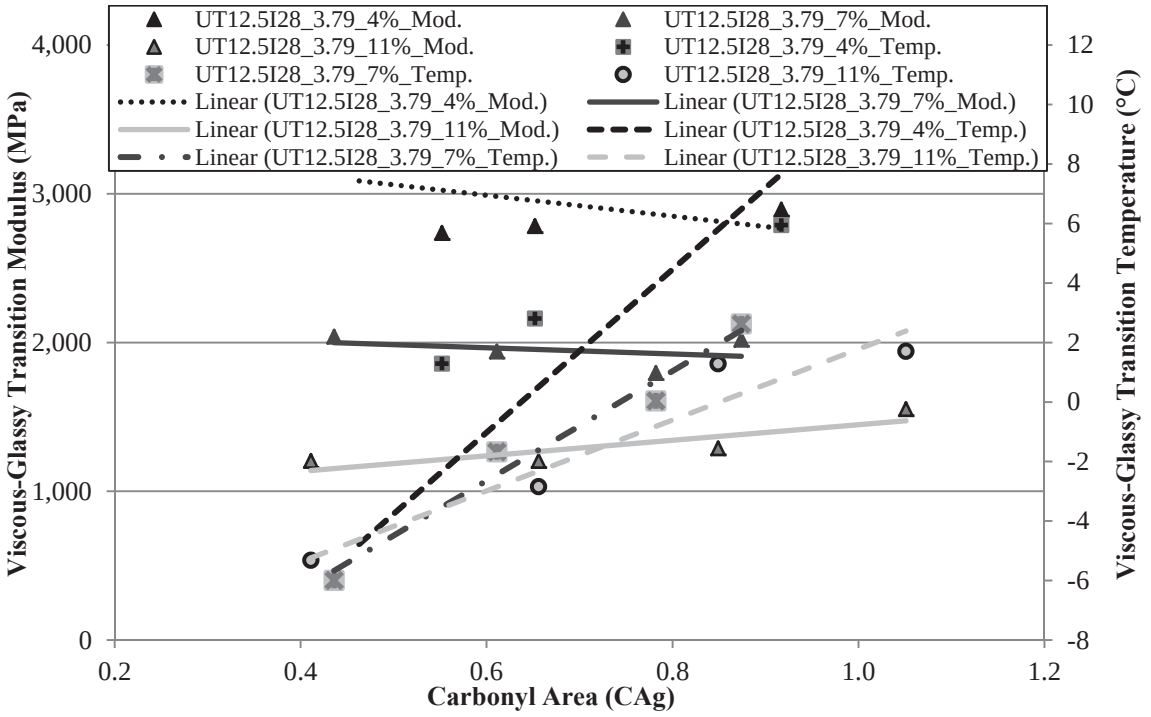

Figure 29.69 Viscous-Glassy Transition Modulus Values for the UT12.5I28_3.79 Mixtures Aged at 60°C with Different Air Voids

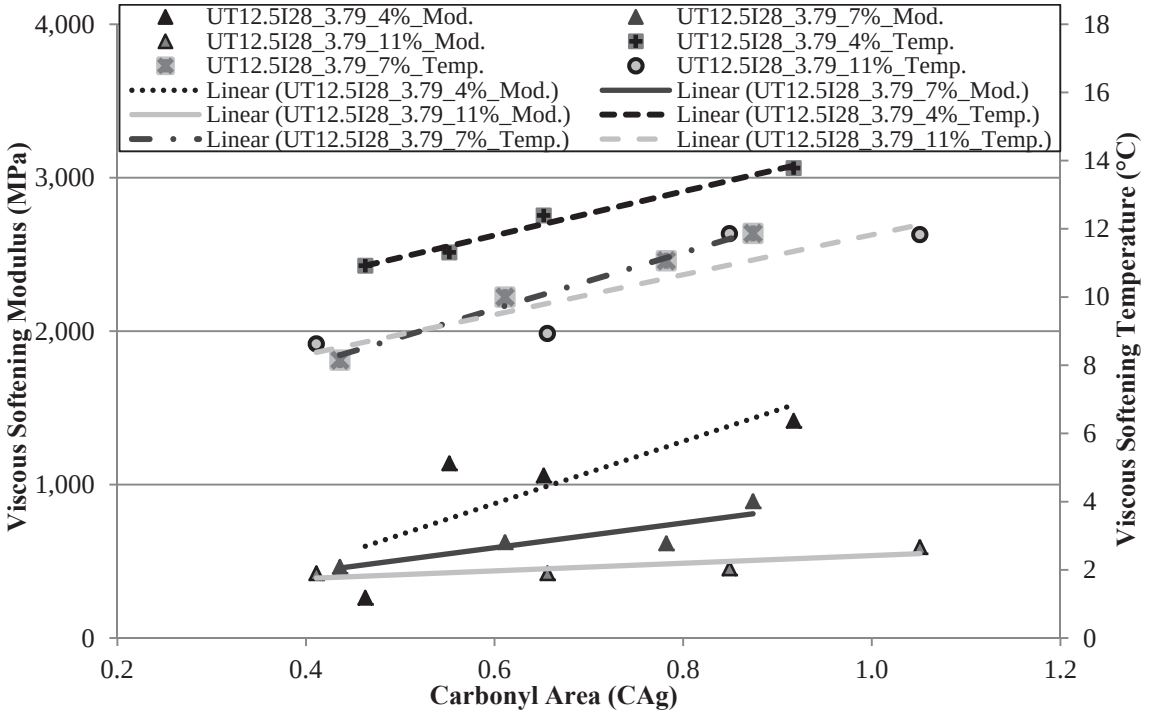

Figure 29.70 Viscous Softening Modulus Values for the UT12.5I28_3.79 Mixtures Aged at 60°C with Different Air Voids

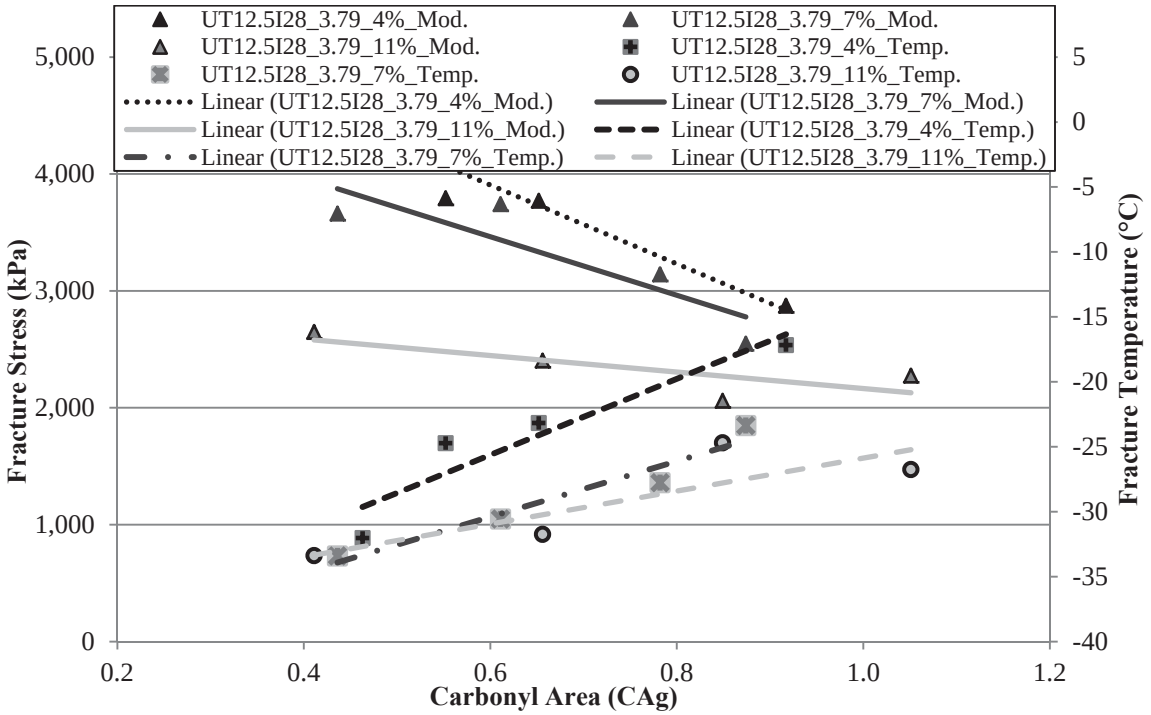

Figure 29.71 Fracture Stress Measurements for the UT12.5I28_3.79 Mixtures Aged at 60°C with Different Air Voids

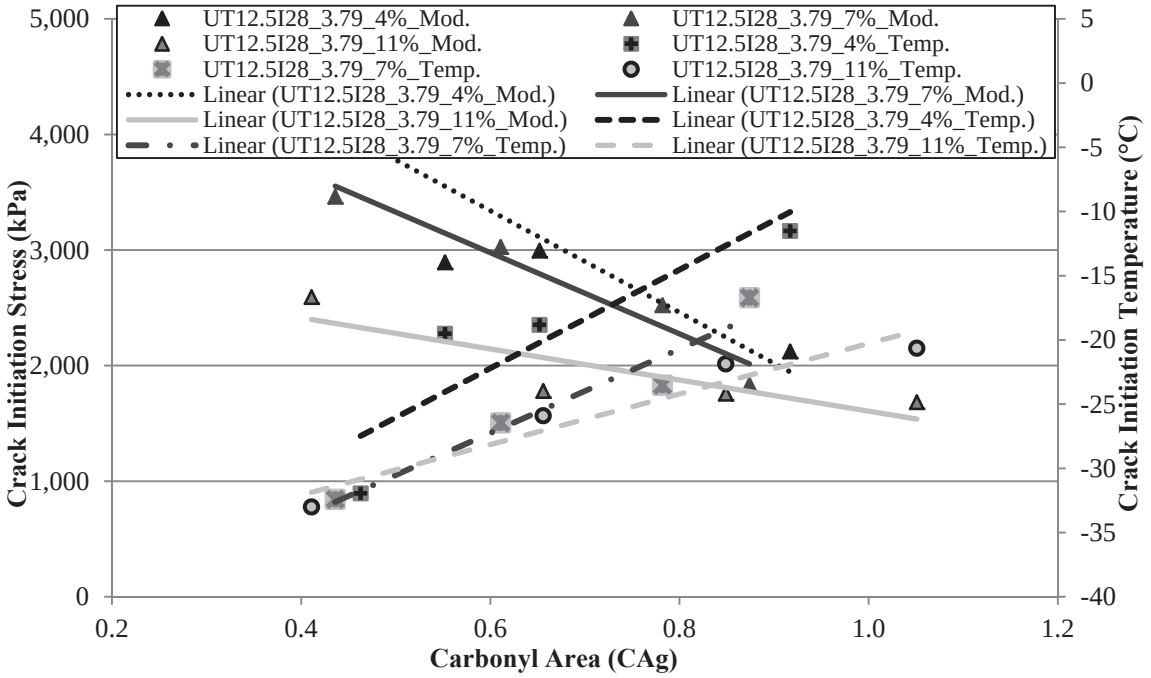

Figure 29.72 Crack Initiation Stress Measurements for the UT12.5I28_3.79 Mixtures Aged at 60°C with Different Air Voids

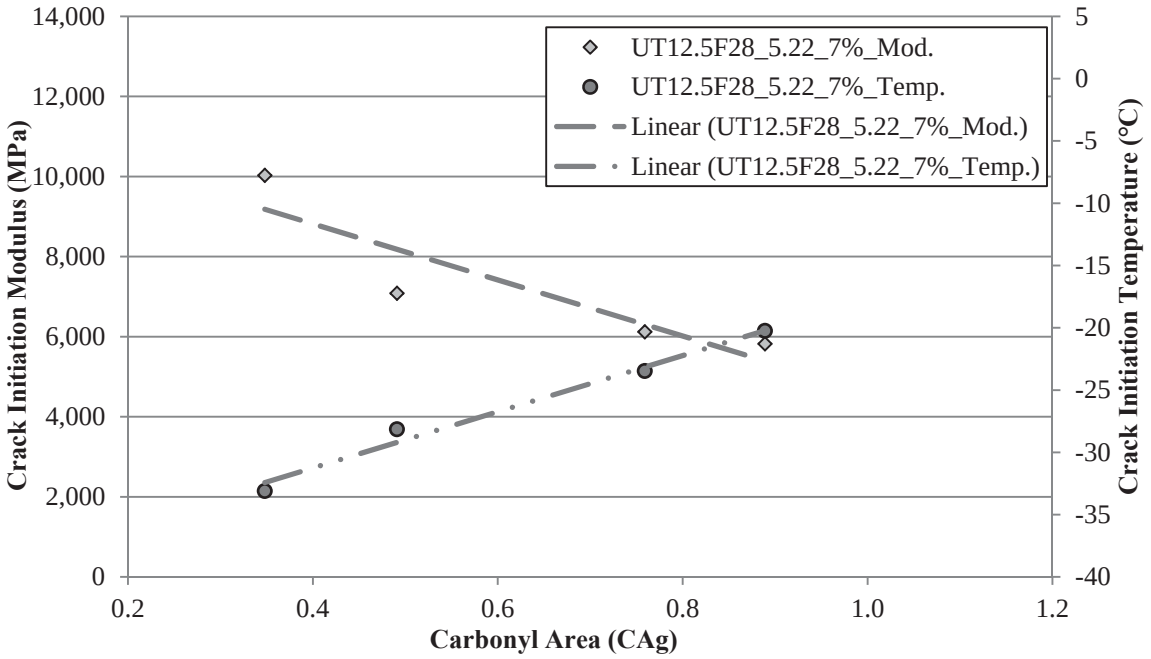

Figure 29.73 Crack Initiation Modulus Values for the UT12.5F28_5.22_7% Va Mixtures Aged at 60°C

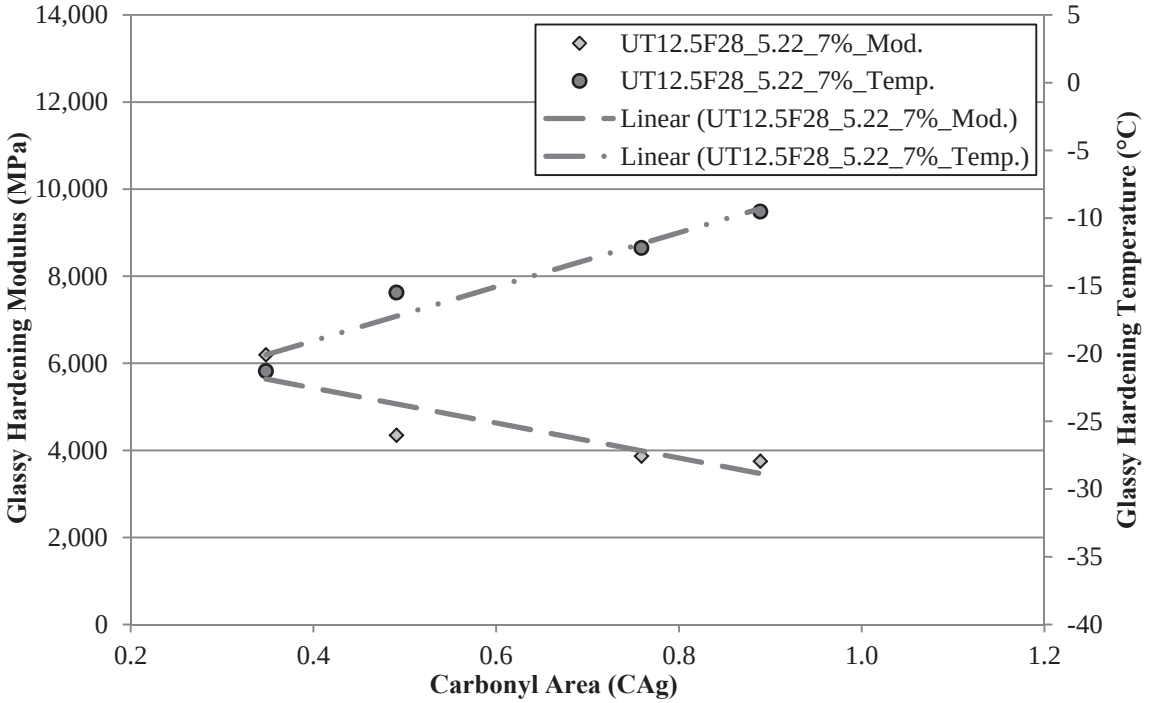

Figure 29.74 Glassy Hardening Modulus Values for the UT12.5F28_5.22_7% Va Mixtures Aged at 60°C

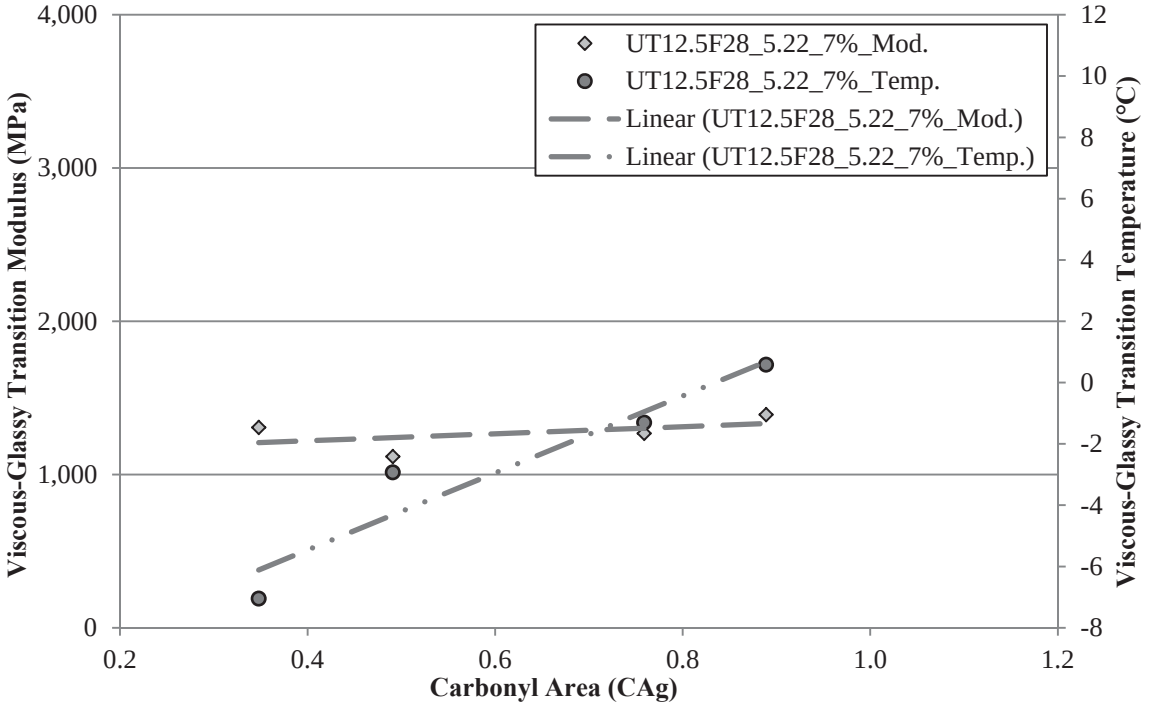

Figure 29.75 Viscous-Glassy Transition Modulus Values for the UT12.5F28_5.22_7% Va Mixtures Aged at 60°C

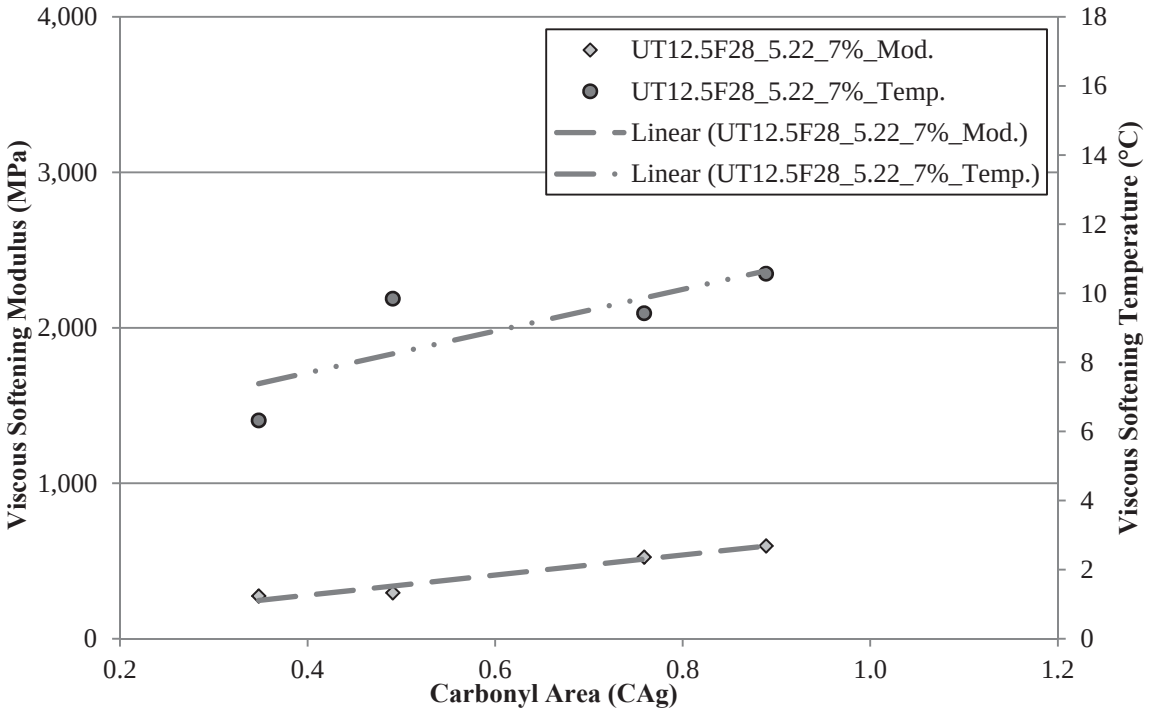

Figure 29.76 Viscous Softening Modulus Values for the UT12.5F28_5.22_7% Va Mixtures Aged at 60°C

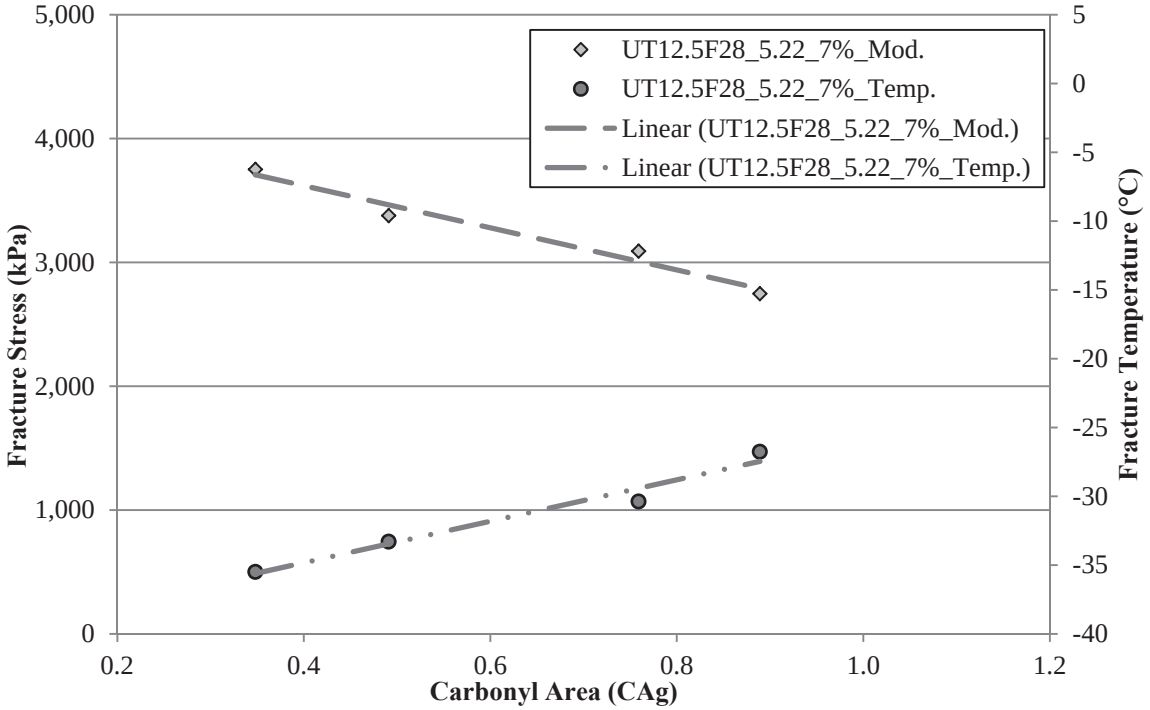

Figure 29.77 Fracture Stress Measurements for the UT12.5F28_5.22_7% Va Mixtures Aged at 60°C

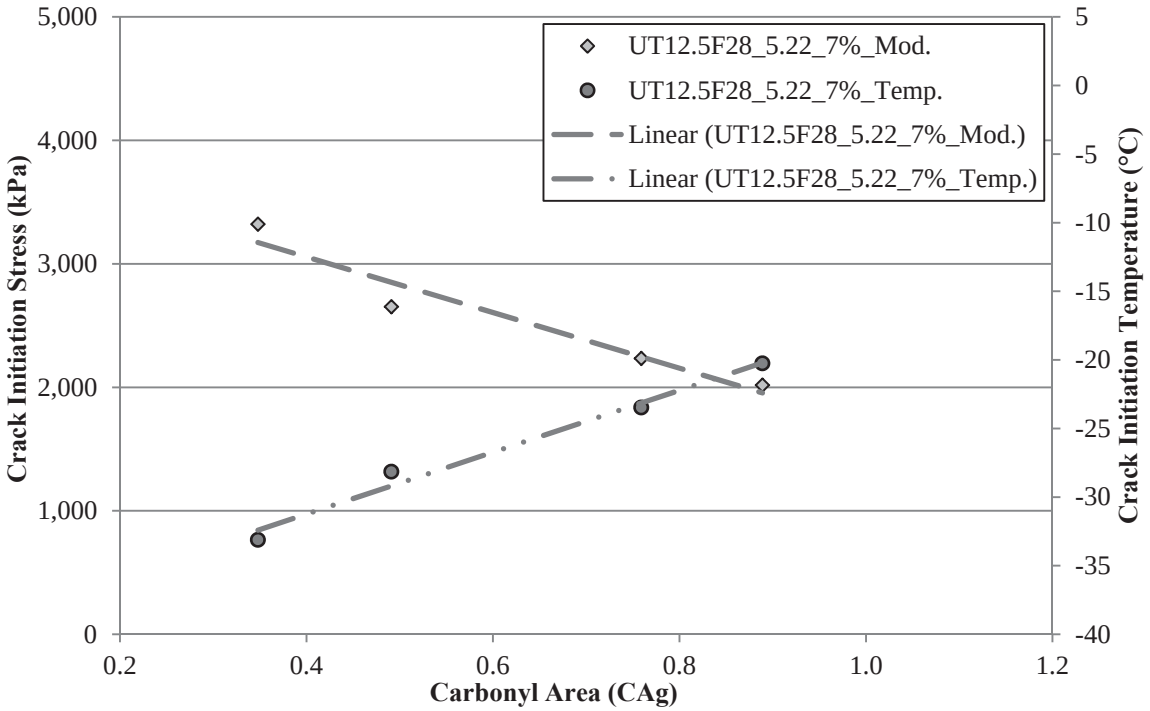

Figure 29.78 Crack Initiation Stress Measurements for the UT12.5F28_5.22_7% Va Mixtures Aged at 60°C

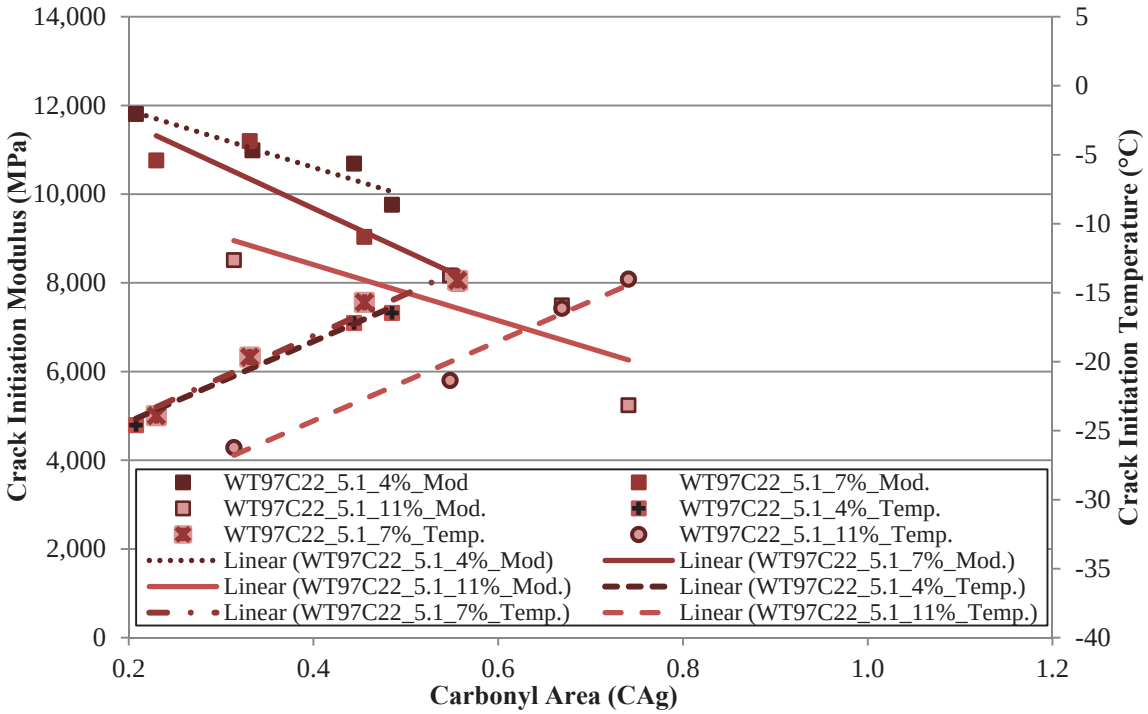

Figure 29.79 Crack Initiation Modulus Values for the WT97C22_5.1 Mixtures Aged at 60°C with Different Air Void Levels

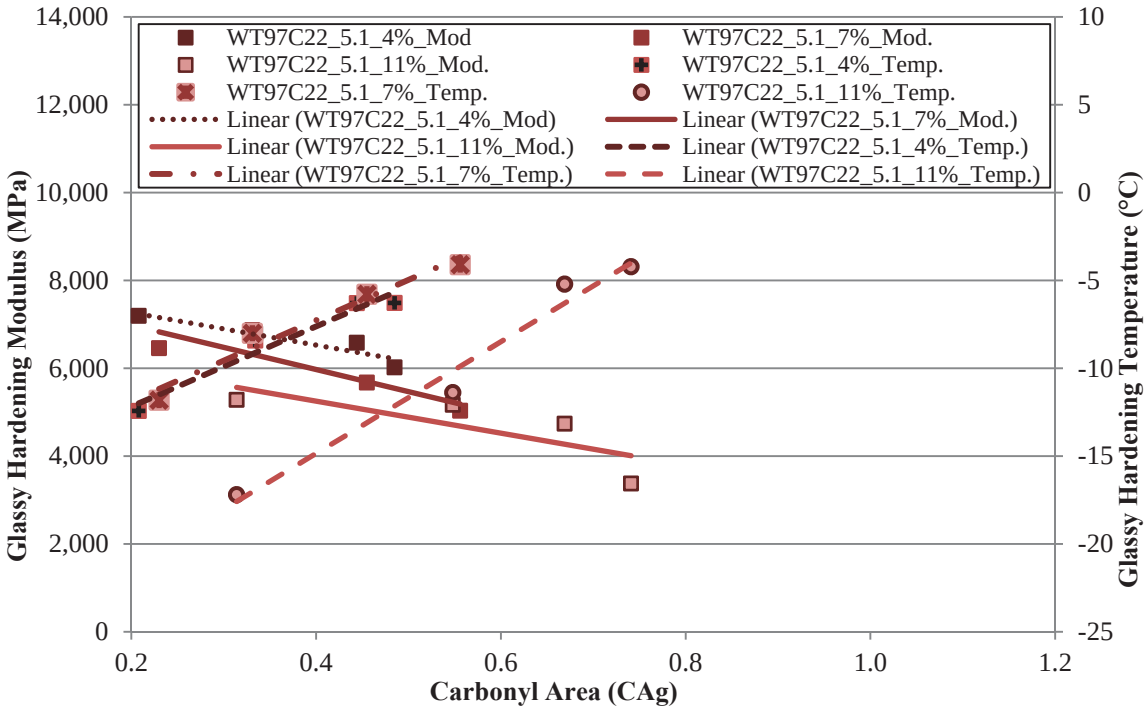

Figure 29.80 Glassy Hardening Modulus Values for the WT97C22_5.1 Mixtures Aged at 60°C with Different Air Void Levels

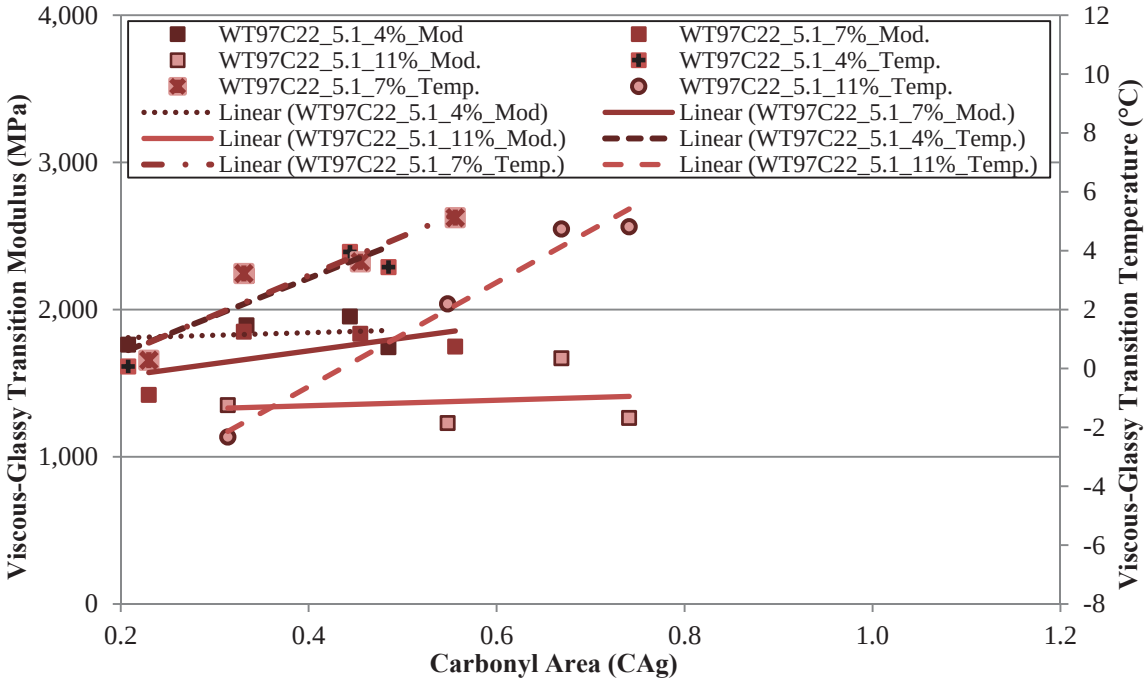

Figure 29.81 Viscous-Glassy Transition Modulus Values for the WT97C22_5.1 Mixtures Aged at 60°C with Different Air Void Levels

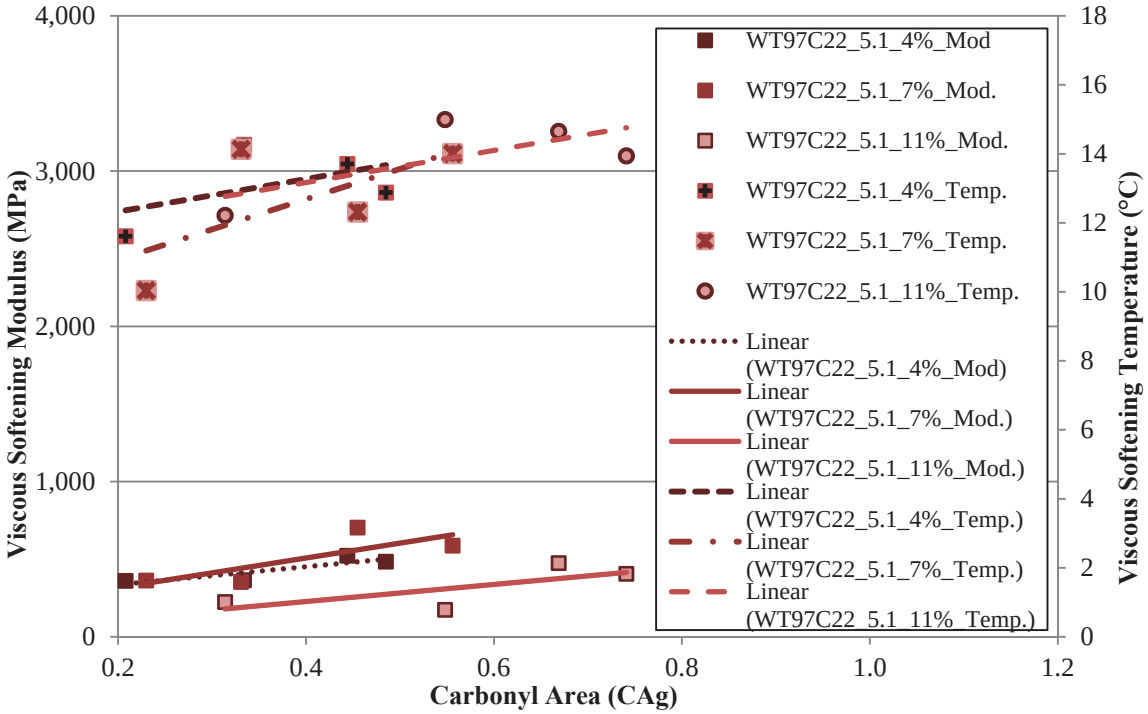

Figure 29.82 Viscous Softening Modulus Values for the WT97C22_5.1 Mixtures Aged at 60°C with Different Air Void Levels

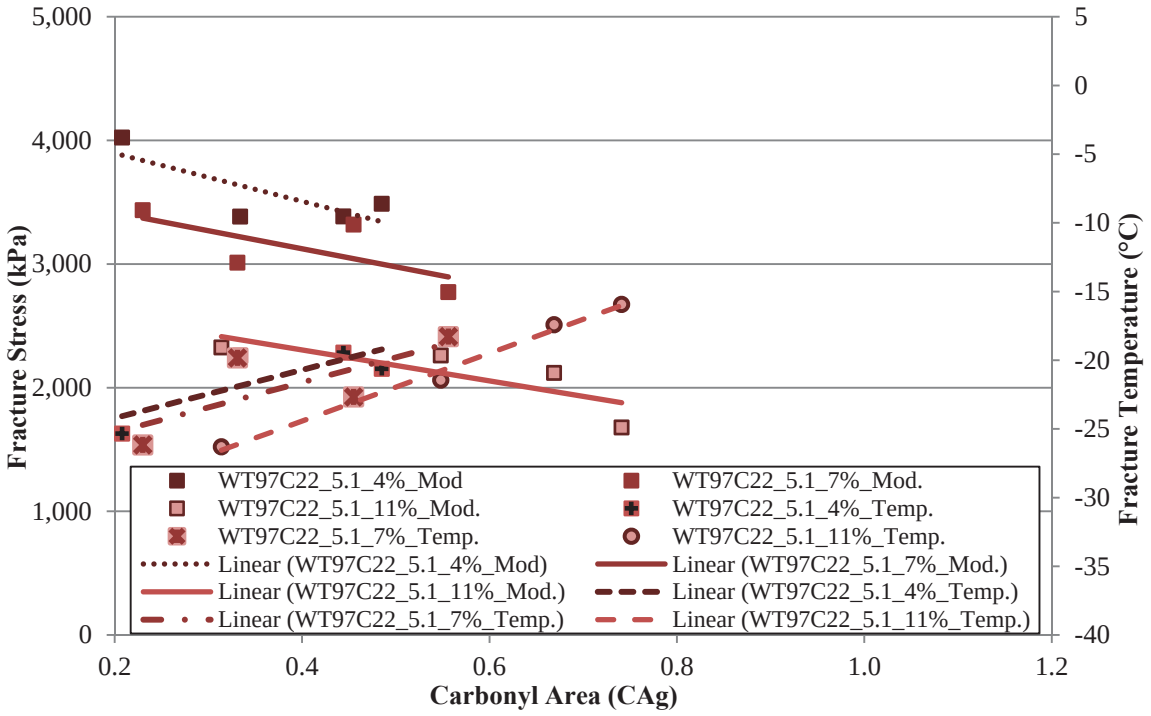

Figure 29.83 Fracture Stress Measurements for the WT97C22_5.1 Mixtures Aged at 60°C with Different Air Void Levels

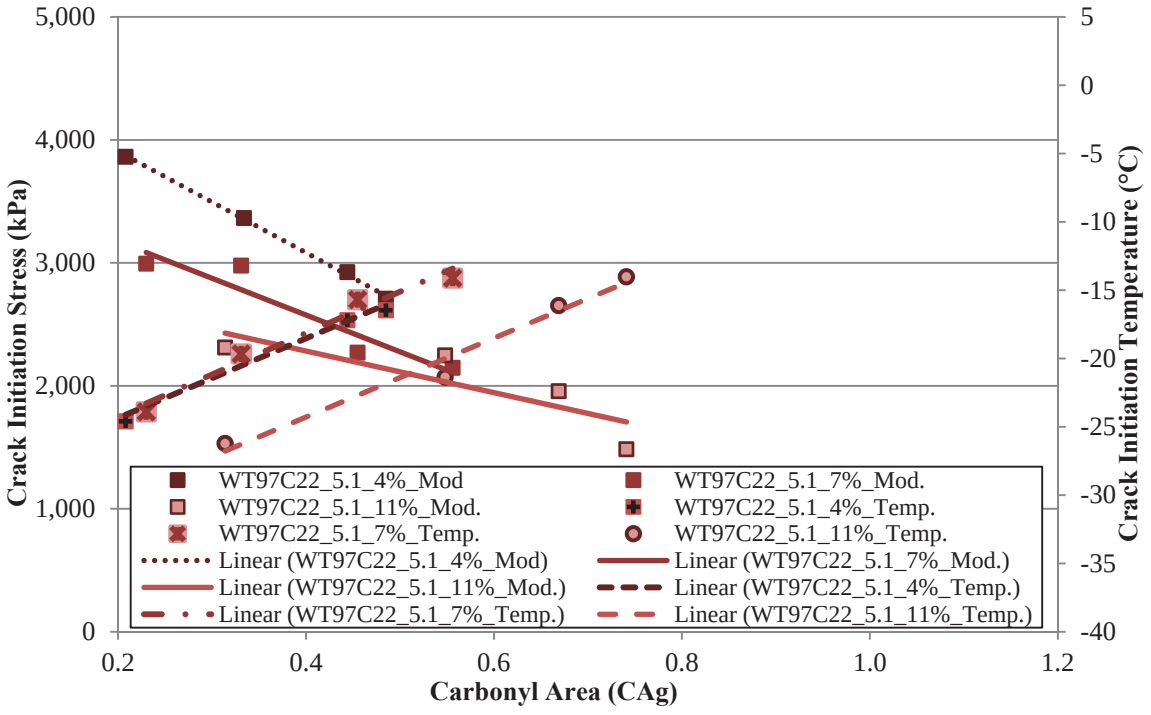

Figure 29.84 Crack Initiation Stress Measurements for the WT97C22_5.1 Mixtures Aged at 60°C with Different Air Void Levels

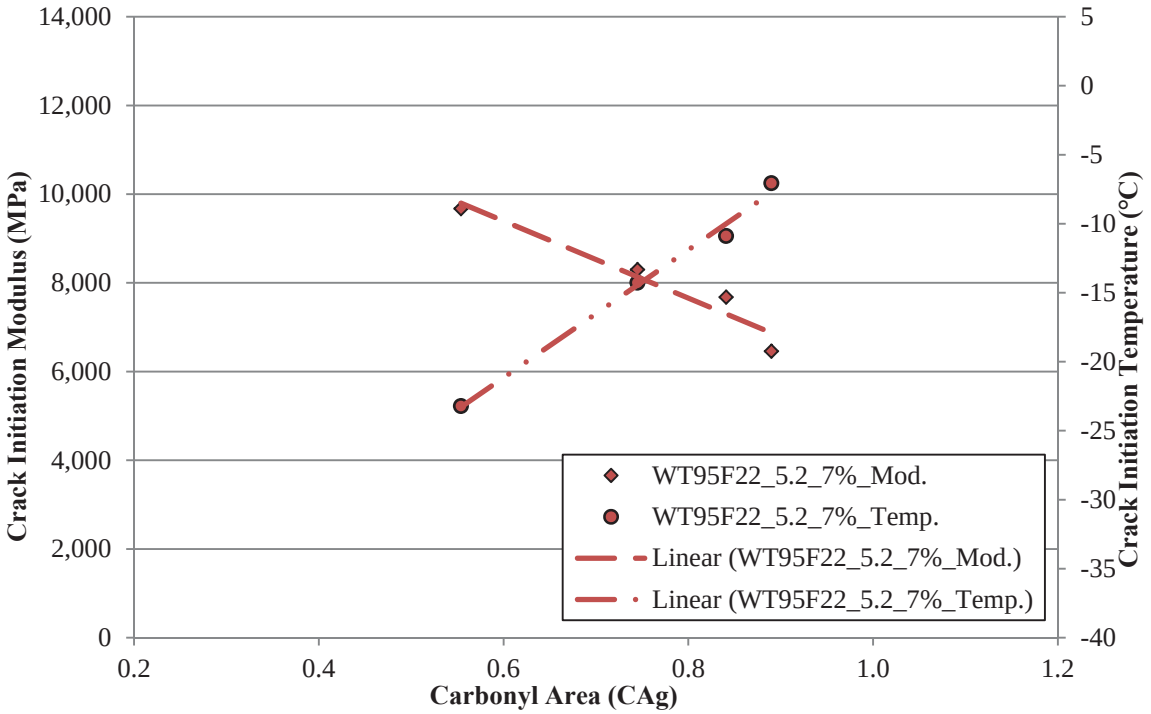

Figure 29.85 Crack Initiation Modulus Values for the WT95F22_5.2_7% Va Mixtures Aged at 60°C

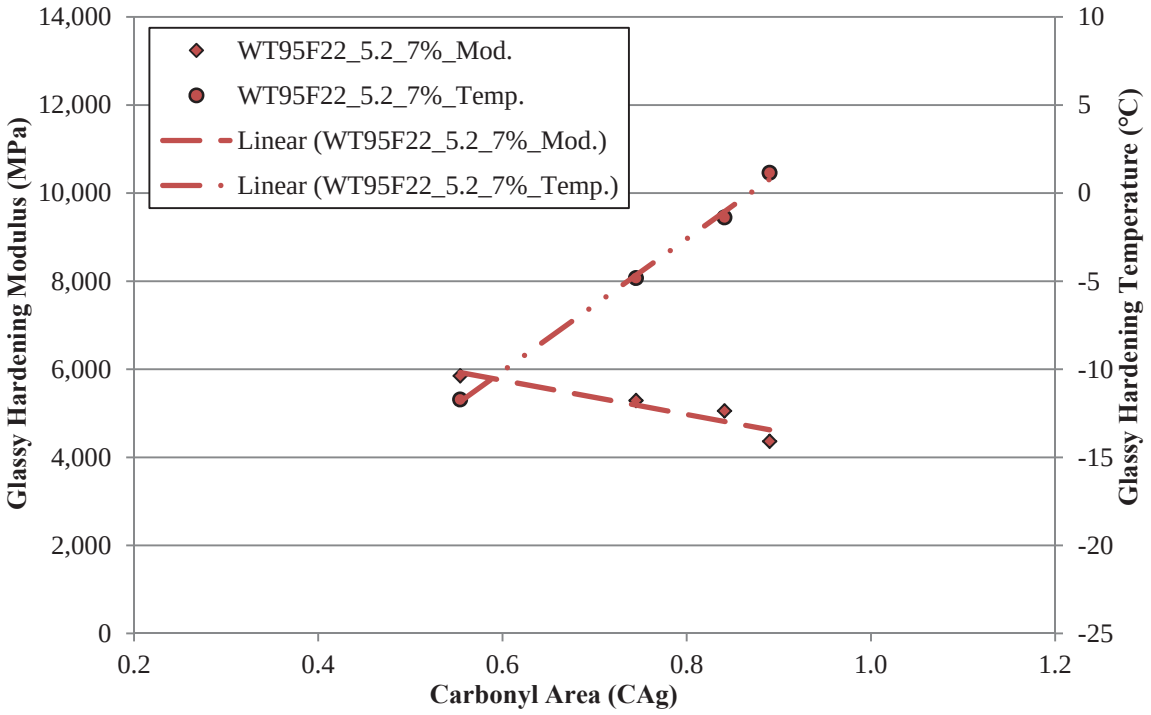

Figure 29.86 Glassy Hardening Modulus Values for the WT95F22_5.2_7% Va Mixtures Aged at 60°C

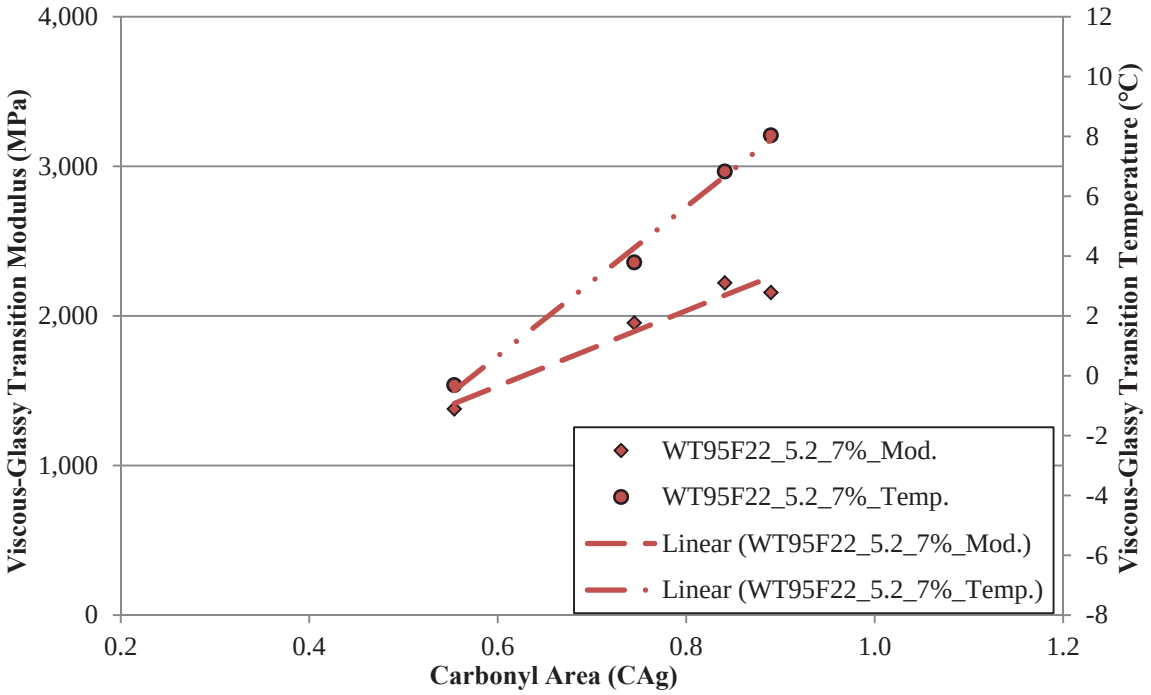

Figure 29.87 Viscous-Glassy Transition Modulus Values for the WT95F22_5.2_7% Va Mixtures Aged at 60°C

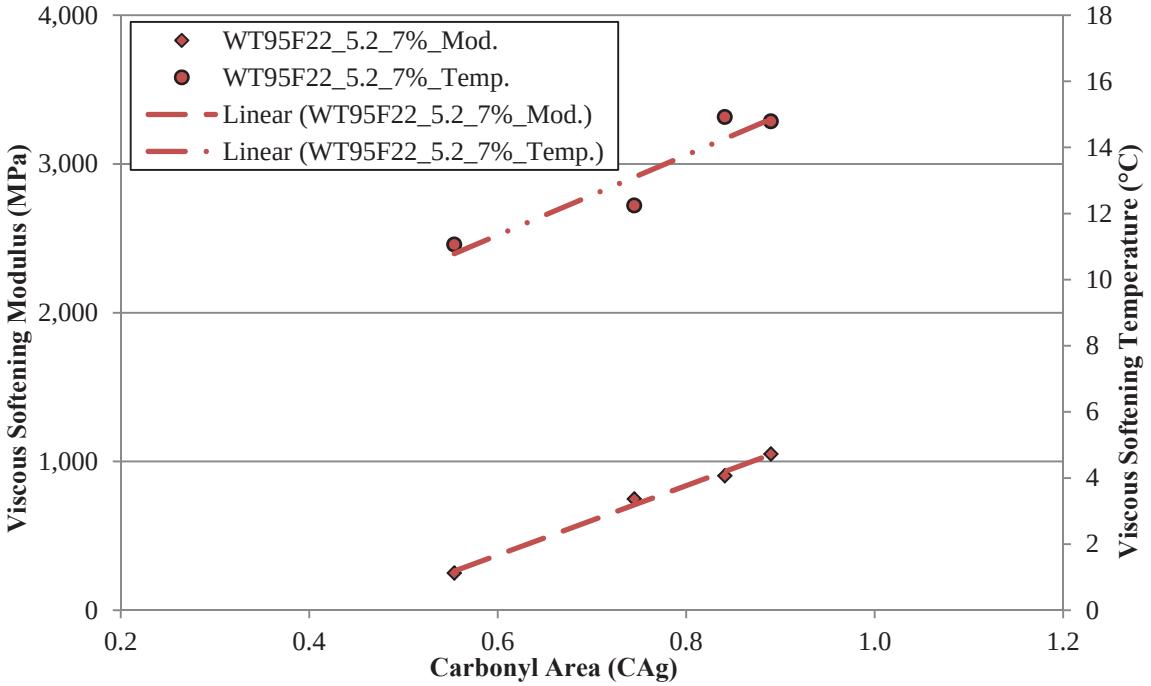

Figure 29.88 Viscous Softening Modulus Values for the WT95F22_5.2_7% Va Mixtures Aged at 60°C

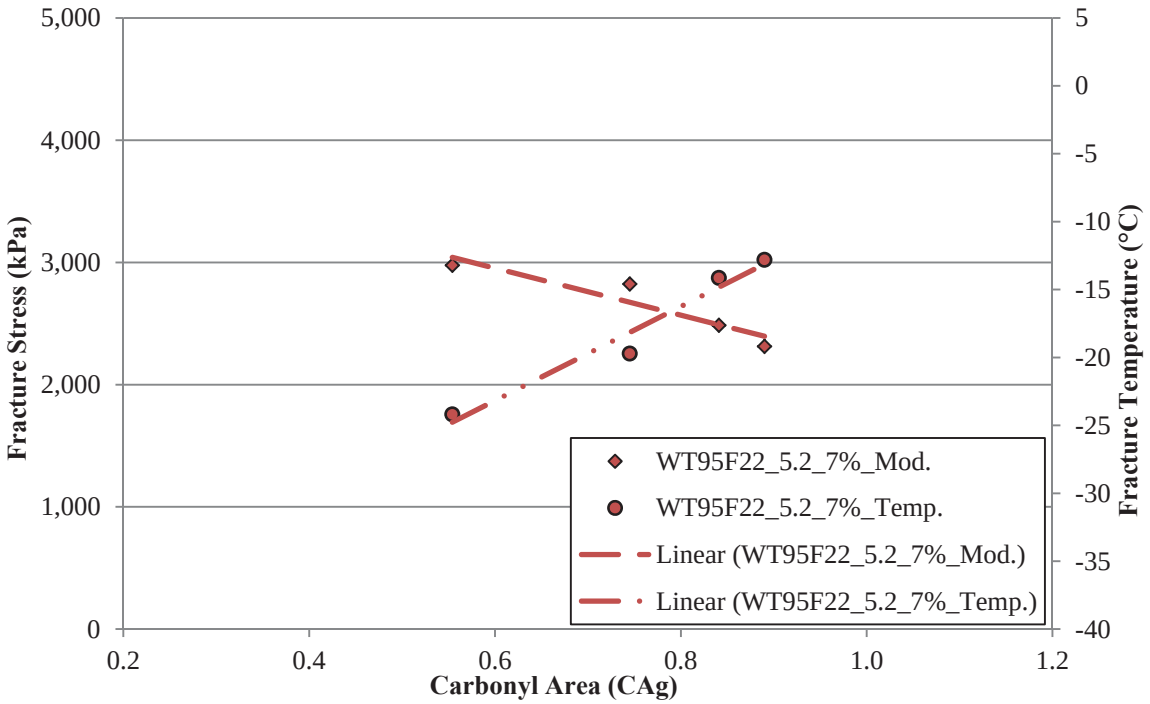

Figure 29.89 Fracture Stress Measurements for the WT95F22_5.2_7% Mixtures Aged at 60°C

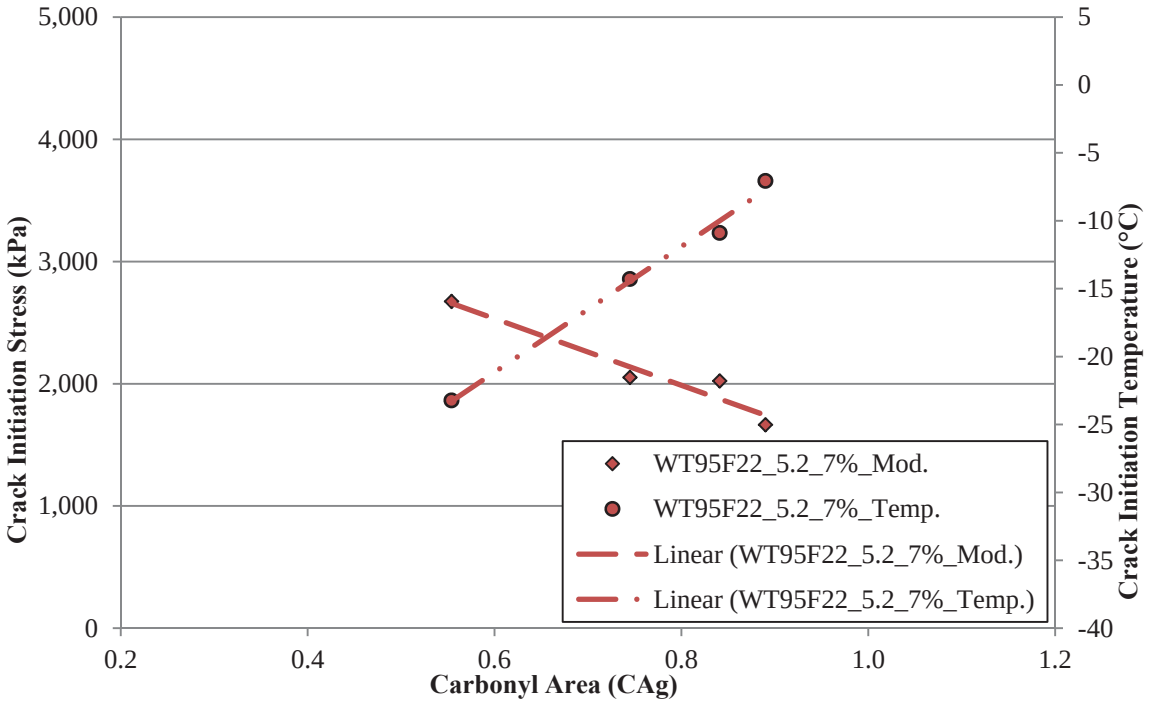

Figure 29.90 Crack Initiation Stress Measurements for the WT95F22_5.2_7% Mixtures Aged at 60°C